Virchows Arch (2002) 440:3–11
DOI 10.1007/s00428-001-0577-6

REVIEW ARTICLE

**Antonio Lopez-Beltran · Liang Cheng
Lennart Andersson · Maurizio Brausi
Anna de Matteis · Rodolfo Montironi
Isabell Sesterhenn · Theodorus van der Kwast
Catherine Mazerolles**

Preneoplastic non-papillary lesions and conditions of the urinary bladder: an update based on the Ancona International Consultation

Received: 23 October 2001 / Accepted: 23 October 2001 / Published online: 6 December 2001
© Springer-Verlag 2001

Abstract *Background and aims*: This paper summarizes the work done by the members of the Committee no. 2 at the *International Consultation on the Diagnosis of Non-Invasive Urothelial Neoplasms* held in Ancona, Italy (11–12 May 2001). The committee members discussed and reached consensus regarding the optimal contemporary diagnosis and classification of the preneoplastic non-papillary lesions of the urothelium. An important objective was to promote a precise terminology and to use it consistently in daily practice in pathology and urology. *Results and conclusions*: The result of the meeting is represented by a refined classification of the non-papillary intraepithelial lesions and conditions of the urothelium. This classification includes epithelial abnormalities (reactive urothelial atypia and flat urothelial hyperplasia), presumed preneoplastic lesions and conditions (keratinizing squamous and glandular metaplasia, and malignancy-associated cellular changes), as well as preneoplastic (dysplasia) and neoplastic non-invasive (carcinoma in situ) lesions. Each of these lesions is defined with strict morphological criteria in order to provide more accurate information to urologists in managing patients.

Keywords Urothelium · Flat hyperplasia · Reactive changes · Urothelial dysplasia · Carcinoma in situ · Urothelial metaplasia

A. Lopez-Beltran (✉)
Department of Pathology, Cordoba University Medical School, Facultad de Medicina, Avda. Menendez Pidal s/n, 14004 Cordoba, Spain
e-mail: em1lobea@uco.es
Tel.: +34-957-218993, Fax: +34-957-218229

L. Cheng
Division of Surgical Pathology, Indiana University Medical Center, Indianapolis, USA

L. Andersson
WHO Center for Urologic Tumors, Karolinska Hospital, Stockholm, Sweden

M. Brausi
Urology Service, Estense-Sant'Agostino Hospital, Modena, Italy

A. de Matteis
Department of Experimental Medicine and Pathology, Policlinico Umberto 1, Roma, Italy

R. Montironi
Institute of Pathological Anatomy and Histopathology, University of Ancona School of Medicine, Torrette di Ancona, Italy

I. Sesterhenn
Division of Genitourinary Pathology, AFIP, Washington, DC, USA

T. van der Kwast
Department of Pathology, Erasmus University, Rotterdam, The Netherlands

C. Mazerolles
Laboratoire d'Anatomie Pathologique, Hôpital Purpan, Toulouse, France

Introduction

Great advance has been made in the molecular genetic and biomarker characterization of bladder cancer in recent years. Although several molecular alterations have been associated with intraepithelial lesions such as dysplasia and carcinoma in situ (CIS), their use in a routine clinical setting remains controversial [54]. The methodology to perform these tests and the cut-off points to interpret the results need to be standardized [54]. Therapy for these lesions and their related bladder tumors must rely presently on pathological and clinical factors [46]. The members of the committee no. 2 concentrated their work on defining what might be meant by "premalignant" (flat) lesions in relation to different forms of urothelial neoplasms, on characterizing their morphological features, and on comparing these with previous descriptions. An important objective is to provide a precise terminology for consistent use in the daily practice of pathology and urology [18]. These terms are intended to describe a histological spectrum of architectural and cytological abnormalities which culminate in the unequivocally malignant (CIS). Also, morphological

Table 1 Working classification of preneoplastic non-papillary intraepithelial lesions and conditions of the urothelium: the Ancona proposal

Epithelial abnormality
Reactive urothelial atypia
Flat urothelial hyperplasia
Presumed preneoplastic lesions and conditions
Metaplasia of the urinary bladder
Keratinizing squamous metaplasia
Glandular metaplasia
Malignancy-associated cellular changes (cytological abnormality not recognizable by light microscopy)
Preneoplastic lesion
Dysplasia
Neoplastic non-invasive lesion
Carcinoma in situ

aspects of other "presumed" preneoplastic lesions related to the development of squamous cell carcinoma and adenocarcinoma are discussed. A full list of such intraepithelial lesions is given in Table 1. The morphological appearance of some of the lesions listed in this table is shown in Fig. 1.

At this time, the biological potential of these lesions in individual patients cannot be accurately predicted, although the degree of risk for an adverse outcome is very likely to be proportional to the degree of architectural alterations and cytological changes [46]. Future knowledge in this area might be enhanced by better definitions of terms and more accurate application of words such as early lesion, precursor, premalignant, atypia, and dysplasia, and by increased understanding of the biological and molecular processes underlying phenotypic changes.

"Benign" epithelial abnormalities

Urothelial reactive atypia (atypia, reactive atypia, reactive changes)

Urothelial abnormalities whose architectural and cytological changes are of lesser degree than in dysplasia (see below) have often been termed atypia [44]. The term atypia is, by its very nature, non-specific, and the intra- and inter-observer variation in its recognition and interpretation has been great [46]. However, the term of atypia is still in use in many institutions.

Two similar categories of atypia have been recently recognized [3, 22, 43]. Both of them are placed among the "benign" urothelial abnormalities:

- Reactive atypia. This is characterized by mild nuclear abnormalities occurring in acutely or chronically inflamed urothelium. The nuclei display uniform enlargement and a vesicular appearance together with prominent nucleoli. The cells are often larger than normal, with more abundant cytoplasm. These features occasionally impart a squamoid appearance. Inflammatory cells in the lamina propria with extension to the urothelium are invariably present. In most cases, there is a history of instrumentation, stones, or previous therapy [49].
- Atypia of unknown (uncertain) significance. This variety shows nuclear changes similar to those seen in reactive atypia. The degree of nuclear pleomorphism and/or hyperchromasia is greater than in the latter, and dysplasia cannot always be ruled out with certainty [3, 46]. Inflammation in the lamina propria with urothelial extension is also present. However, the cellular changes seem to be disproportionate to the degree of inflammation. Atypia of unknown (uncertain) significance is often seen in patients with a previous diagnosis of urothelial neoplasms. Progression to urothelial carcinoma has not been documented. There is no evidence supporting a premalignant nature in such lesions.

Flat urothelial hyperplasia (simple hyperplasia)

Histologically, urothelial hyperplasia is usually focal, consisting of an increase in the number of cell layers, usually ten or more (but at least more than seven). There are few or no significant cytological abnormalities, although slight nuclear enlargement may be focally present [7, 8]. Hyperplasia may occasionally be associated with dysplasia or carcinoma in situ in the adjacent mucosa. Morphological evidence of maturation from base to surface is generally evident [7]. Urothelial compression artifact, and tangential sectioning of the mucosa with pseudopapillary growth (lacking a true vascular core) may rarely resemble flat urothelial hyperplasia.

Flat urothelial hyperplasia is an epithelial abnormality associated with a wide variety of inflammatory disorders, lithiasis, papillary hyperplasia, and low-grade papillary tumors [16, 58]. A recent report found that 71% of cases of urothelial hyperplasia had the same chromosome 9 deletions that exist in low-grade papillary carcinoma [5]. In contrast, 17p13 deletion was found in 8% of urothelial hyperplasias and low-grade carcinomas [27]. In that particular study, the same chromosomal anomalies were present in the adjacent "normal-looking" epithelium [27]. Current evidence on the neoplastic potential of urothelial hyperplasia is at present inconclusive.

Urothelial hyperplasia has been considered the source of papillary neoplasia, and the lesions were more likely to be associated with low-grade tumors [31, 32, 55]. As mentioned earlier, current evidence on the neoplastic potential of urothelial hyperplasia is at present inconclusive.

Malignancy-associated changes

Malignancy-associated changes refer to abnormalities in the epithelial cells that are not usually distinguishable by routine light microscopic examination. With the use of image analysis subtle morphological nuclear abnormalities that are not readily seen by the human eyes have been

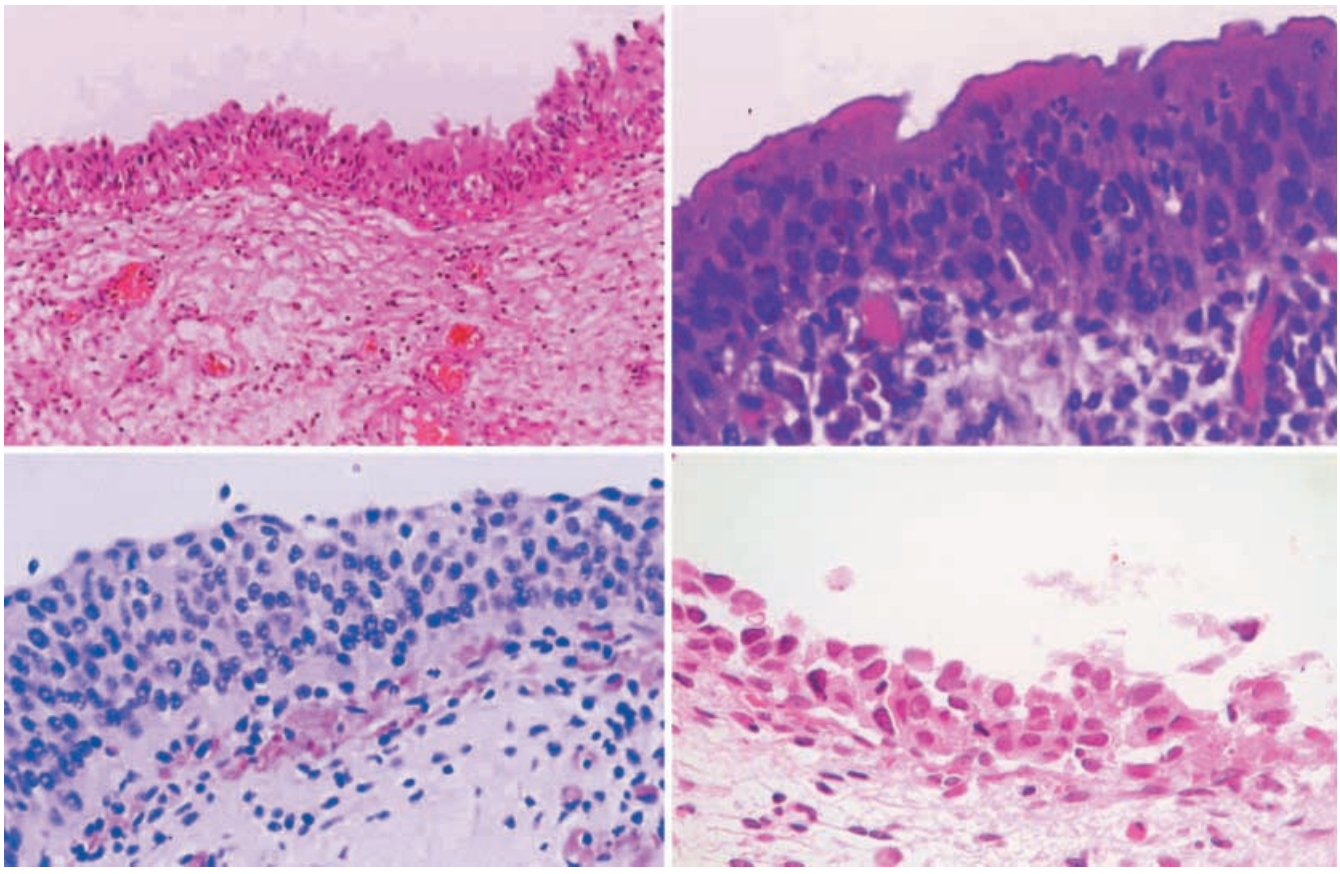

Fig. 1 Representative images of normal (*upper left*) and reactive urothelium (*upper right*), urothelial dysplasia (*lower left*), and carcinoma in situ (*lower right*)

demonstrated in urinary bladders harboring preneoplastic and neoplastic lesions. Recent studies showed that 50% of the histologically normal urothelium adjacent to superficial urothelial carcinoma has genetic anomalies on chromosome 9, similar to the anomalies found in the coexistent carcinoma [4, 5]. In addition, non-diploid histograms occur in 4.2–53.5% of normal-looking urothelium adjacent to bladder tumors (L. Andersson, personal communication). These genetic alterations suggest a neoplastic potential for flat urothelial lesions, regardless of whether or not cytological atypia is histologically present [5, 27, 48]. This suggests that additional preneoplastic conditions/lesions not recognizable by light microscopy may be clinically relevant [42, 57]. Some of these findings might represent "precancerous conditions," e.g., a state associated with a significantly increased risk of cancer.

Additional epithelial abnormalities (endophytic)

Von Brunn nests and cystitis cystica, even though listed under epithelial abnormalities, are benign endophytic conditions that usually do not represent a problem from the diagnostic point of view. Their epithelial lining might show features of reactive atypia, dysplasia, and carcinoma in situ identical to those of the flat urothelium.

The opinion of the committee members is that there is a host of urothelial "benign" epithelial abnormalities. Some of them represent benign lesions whose morphological identification and interpretation do not pose a particular problem from the diagnostic point of view. Others are either part of the morphological spectrum of the non-papillary neoplasia or reactive lesions whose histological appearance cannot be easily distinguished from that of dysplasia. In such situations morphometric, immunohistochemical, and molecular techniques should be of great help. In addition, the committee members formally discourage the use of the term atypia (urothelial atypia) without any further specification to encompass reactive atypia. Reactive urothelial atypia is more appropriate. The introduction of the term atypia of unknown significance does not add any value in practice. In those rare cases of "reactive urothelial atypia" in which the pathologist is unsure whether the changes are reactive or truly dysplastic, a conservative approach is indicated, with repeated cystoscopy and biopsy after the inflammation has subsided.

Urothelial dysplasia

Epithelial changes that have some but not all of the features of CIS are most commonly termed dysplasia. Synonyms include: low-grade intraurothelial neoplasia,

Table 2 Comparative parameters of bladder intraurothelial lesions: the Ancona proposal

	Reactive urothelial atypia	Flat urothelial hyperplasia	Urothelial dysplasia	Urothelial carcinoma in situ
Cell layers	Variable	>7cells	Variable	Variable
Polarization	Slightly abnormal	Normal	Slightly abnormal	Abnormal
Cytoplasm	Vacuolated	Homogeneous	Homogeneous	Homogeneous
Nuclei:cytoplasm ratio	Normal or slightly increased	Normal or slightly increased	Slightly increased	Increased
Position of nuclei	Normal	Normal	Mild anysonucleosis	Moderate to severe anysonucleosis
Borders of nuclei	Regular/smooth	Regular/smooth	Notches/creases	Pleomorphic
Chromatin	Fine/dusty	Fine	Slight hyperchromasia	Coarse/hyperchromatic
Distribution of chromatin	Even	Even	Even	Uneven
Nucleoli	Large	Small or absent	Small or absent	Large/prominent
Mitotic figures	Variable	Absent	Rare and basal	Plentiful
Denudation	Variable	No	No	Variable
CK20	Surface	Surface	Variable	Variable

atypical hyperplasia, intraepithelial neoplasia grades I to II, intraurothelial neoplasia grades I to II, dysplasia grades I to II, and mild-moderate dysplasia [7, 8]. These are among the synonymous terms proposed during the last 25 years, none widely adopted. The difficulty in standardizing nomenclature for urothelial cytological abnormalities is compounded by the lack of reproducibility in classification and grading [11, 14, 44].

The morphology of dysplasia generally is of cohesive cells, with umbrella cells usually present, characterized by mild nuclear/nucleolar changes that focally include irregular nuclear crowding and slight hyperchromasia. Anysonucleosis is generally present; there may be an increased number of cell layers; nucleoli may be prominent; mitotic figures when present are generally basally located. The overall appearance is that of the urothelium of grade-1 (WHO 1973) papillary urothelial carcinoma. Most cellular abnormalities in dysplasia are restricted to the basal and intermediate layers. Nuclear and architectural features are considered most useful in distinguishing reactive atypia and dysplasia. Cytokeratin 20 and high molecular weight cytokeratin immunoreactivity might be objective markers of dysplasia in selected cases [26, 28] (Table 2).

A common practice in many institutions is to classify dysplasia as mild, moderate, or severe, emulating a current practice in cervical cancer. CIS and high-grade dysplasia are considered synonymous by most investigators. There are no apparent distinguishing histological features, and there is a high level of agreement for these lesions. In the urothelium, separation of epithelial changes with fewer cytological and architectural abnormalities than in CIS, such as low-grade dysplasia or intermediate-grade (moderate) dysplasia, is often difficult; the morphological continuum does not provide any absolute features that allow unequivocal separation [47]. Lesions with fewer changes that are still considered dysplastic and not reactive are considered dysplasia without qualifiers (Table 2). We have the greatest difficulty when trying to separate the lowest grade of dysplasia (so-called intraurothelial neoplasia grade 1) and reactive changes, and usually we group these lesions under the term reactive urothelial atypia, recognizing that their biological significance is probably very low. When morphometry and image analysis were used, it was seen that dysplasia has a pattern similar to that of papillary carcinoma of grade 1 (WHO 1973) [42].

- Primary dysplasia. It occurs in the absence of other urothelial tumors. Its incidence in the general population is largely unknown because of a lack of screening. Only a few studies provide clinical information on patients with primary dysplasia [49]. These patients are predominantly middle-aged men with irritative bladder symptoms with or without hematuria. Low-grade dysplasia is not cystoscopically visible, although occasionally the urothelium may appear raised and irregular or mildly erythematous. In a retrospective study of 15 patients with primary dysplasia, Zuk et al. [61] showed that 2 patients (13%) progressed to CIS, while 13 had an uneventful course.
- Secondary dysplasia. Dysplasia is usually seen histologically in patients with bladder neoplasia. The incidence of dysplasia in patients with bladder neoplasia varies from 22% to 86% and approaches 100% in patients with invasive carcinoma. Dysplasia in patients with noninvasive transitional cell carcinoma (TCC) appears to be a marker for progression [59]. Althausen et al. [2] observed that, of the 30% of patients with superficial TCC who developed muscle invasion 5 years after the diagnosis, most had dysplasia or CIS in the flat urothelium adjacent to the primary tumor. Of the patients with dysplasia elsewhere in the bladder mucosa, 36% eventually developed muscle invasive tumors, whereas only 7% of patients with normal urothelium developed muscle invasion. Smith et al. reported recurrence in 73% of patients with superficial neoplasia and concomitant dysplasia, compared with 43% without dysplasia. Dysplasia in the mucosa adjacent to papillary urothelial carcinoma is associated with an increased risk of recurrence (73% versus 43%). Meanwhile, isolated urothelial dysplasia had a 19% progression [11, 14]. As many as 24% of random biopsies from patients with Ta and T1 carcinoma show epithelial abnormalities that include dysplasia and CIS. As mentioned before, when morphometry

and image analysis were used, it was seen that dysplasia has a pattern which is similar to that of papillary carcinoma grade I (WHO 1973) [41, 42].

The members of the committee reached the consensus that dysplasia is a true premalignant lesion of the urothelium, and most of the evidence indicates that sometimes it will progress (see below). We prefer to use the term dysplasia, not otherwise specified, to describe the morphological spectrum of dysplastic lesions of the urothelium. Most committee members do not use the term "atypia" as a synonym for dysplasia.

Urothelial carcinoma in situ

Carcinoma in situ (synonyms: high-grade intraurothelial neoplasia, severe dysplasia, grade-III CIS, high-grade dysplasia, grade-III intraurothelial neoplasia) refers to a flat noninvasive neoplastic change of the urothelium with substantial architectural and cytological abnormalities, the latter being indistinguishable from those of carcinoma [1].

The morphological diagnosis of CIS requires the presence of severe cytological atypia (nuclear anaplasia); full-thickness change is not essential, although it is usually present. The cells of CIS may form a layer that is only one cell layer thick, of normal thickness (up to 7 cells), or the thickness of hyperplasia (greater than 7 cells). Prominent disorganization of cells is characteristic, with loss of polarity and cohesiveness. Superficial (umbrella) cells may be present except in areas of full thickness abnormality. The tumor cells tend to be large and pleomorphic, with moderate to abundant cytoplasm, although they are sometimes small with a high nucleus to cytoplasmic ratio. The chromatin tends to be coarse and clumped [52].

Morphometrically, the cells in CIS display an increase in nuclear area, nuclear perimeter, and maximum nuclear diameter. Nucleoli are usually large and prominent in at least some of the cells, and may be multiple. Mitotic figures that may be atypical are often seen in the uppermost layers of urothelium [7, 8]. The adjacent mucosa often contains lesser degrees of cytological abnormality. Tissue edema, vascular ectasia, and proliferation of small capillaries are frequent in the lamina propria in cases of CIS, and, although some extravasated erythrocytes can be found, hemorrhage is not common.

Interobserver agreement with CIS is high. A number of histological patterns have been described:

- Small cell CIS
- Large cell CIS
- "Denuding cystitis" and "clinging" CIS
- Undermining (lepidic) growth
- Pagetoid CIS
- CIS involving Von Brunn nests
- CIS involving prostatic urethra or ureter

Cell size in the small cell CIS pattern is unrelated to neuroendocrine differentiation. In such cases, the cytoplasm is scant and nuclei are enlarged and hyperchromatic, with coarse unevenly distributed chromatin; scattered prominent nucleoli are distorted and angulated. Striking cellular discohesion in some cases results in few ("clinging CIS") or no recognizable epithelial cells on the surface, a condition referred to as denuding cystitis of CIS [21, 33]. In denuded areas, CIS may only be present in Von Brunn nests, a useful clue in the diagnosis of residual CIS [40]. Rarely, CIS exhibits pagetoid growth [37, 51], characterized by large single cells or small clusters of cells within otherwise normal urothelium in the bladder, ureter, urethra, or within prostatic ducts, but also pagetoid cells can be present within squamous metaplasia of the urinary bladder [36]. This variant of CIS is frequently overlooked and may be responsible for unsuspected recurrent disease after surgery. Individual cells in pagetoid spread have enlarged nuclei with coarse chromatin.

CIS may be primary or secondary:

- Primary CIS. Primary or isolated CIS accounts for less than 10% of cases of CIS, and 1% of bladder tumors. It occurs in the absence of other urothelial tumors, almost exclusively in men over 50 years. Symptoms typically include dysuria, nocturia, and sterile pyuria, and the clinical presentation may closely mimic interstitial cystitis. Primary CIS is asymptomatic in approximately 25% of patients [12]. It may be present throughout the bladder but usually involves the trigone, floor, and neck. CIS is multifocal in over 50% of patients at the time of diagnosis. Mapping studies of cystectomy specimens show extensive CIS, with involvement of the prostatic urethra and the ureter in as many as 67% and 57% of cases, respectively.
- Secondary CIS is more common than primary CIS, accounting for 90% of cases. It is so named because of prior or synchronous association with a urothelial tumor, including noninvasive or invasive urothelial carcinoma. The frequency of CIS increases with the grade and stage of the associated neoplasm. As many as 24% of random biopsies from patients with Ta and T1 carcinoma show epithelial abnormalities that include dysplasia and CIS [12, 14].

In most instances, CIS is multifocal, appearing cystoscopically as erythematous, velvety, or granular patches, although it may be visually undetectable. Urothelial CIS has a high likelihood of progressing to invasive carcinoma if left untreated [9]. The mean interval from diagnosis to progression is 5 years. Patients with primary CIS treated by radical cystectomy have an up to 100% 5-year survival, and a progression-free and a cancer-specific survival of 63% and 79% at 10 years, respectively. Primary CIS has a lower risk of progression (28% versus 59%) and death (7% versus 45%)) than secondary CIS [29]. Factors predictive of a high risk of progression include multifocality, coexistent bladder neoplasm, prostatic urethral involvement, and recurrence after treatment.

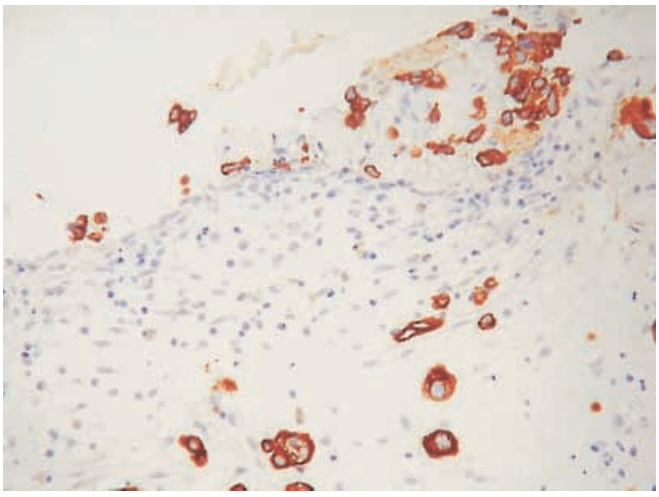

Fig. 2 Carcinoma in situ with early invasion. The latter pattern is identified using immunohistochemistry with antibodies against cytokeratins AE1–AE3

Understanding of the clinical importance and biological potential of CIS is greater than that of dysplasia because CIS may be symptomatic and may be detected at cystoscopy. In patients in whom CIS is concomitant with or subsequent to noninvasive bladder carcinoma, the incidence of progression to muscle invasive is 42–83%. Patients with multifocal and extensive disease are more likely to progress (78%) compared with only 8% in patients with a single, focal CIS [12, 14].

CIS with microinvasion

In bladder carcinoma in situ, a careful search should be made for the presence of invasion. Microinvasive carcinoma of the urinary bladder (CISmic) is defined as invasion into the lamina propria to a depth ranging 2–5 mm from the basement membrane [24, 39]. Microinvasion often appears as cords of direct extension (tentacular), single cells, or single cells and clusters of cells with retraction artifact that may be mimic vascular invasion. Stromal response may be present but is usually absent. The neoplastic cells may be interspersed among and masked by cells of chronic inflammation. In these situations the committee recommends that immunohistochemistry with antibodies against CEA or cytokeratins (such as AE1–AE3) be applied to identify the invading cells (Fig. 2).

That CISmic is a clinically relevant lesion can be appreciated from reports of totally embedded cystectomy specimens that have revealed extensive CIS involving at least 25% of the bladder, 34% of which displayed microinvasion. In addition, 5.8% of these patients had lymph-node metastases and died of disease [24, 25].

The committee members suggest that for the surgical pathology report pathologists should simply indicate urothelial CIS with no further mention of the morphological pattern. Still, awareness of the histological diversity of CIS will facilitate the diagnosis of this important flat lesion of the urothelium [38, 39]. Concerning CIS with microinvasion, the consensus reached in the meeting is that the microinvasive component into the lamina propria should be constituted of no more than 20 invading cells, measured from the stroma-epithelial interface.

Pathways in the natural history of urothelial bladder cancer

Early clinical observations regarding the field effect theory on bladder cancer tumorigenesis suggested that sites of preneoplastic changes could follow several distinct clinical courses. Areas of dysplasia may remain simply dysplastic.

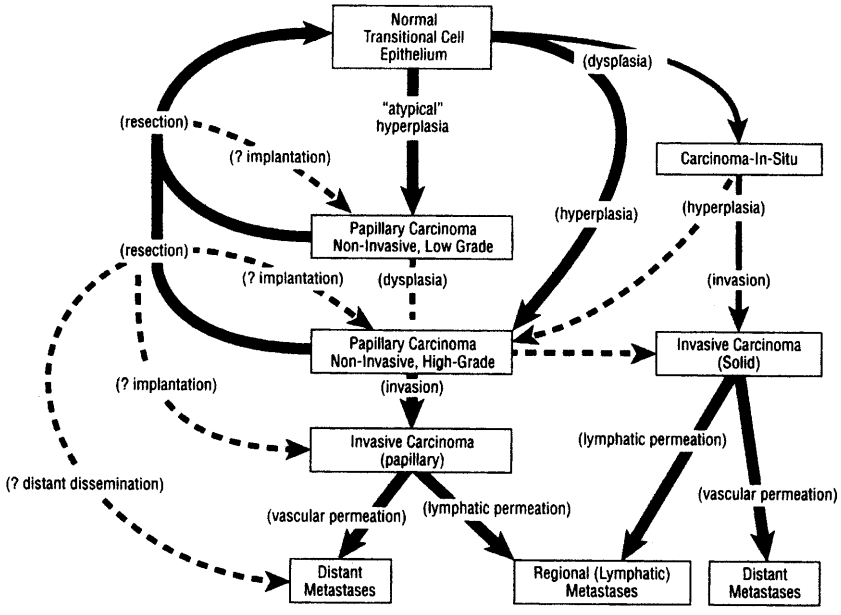

Fig. 3 Proposed pathway for bladder tumor development. Note that superficial and invasive pathways are distinct, with divergence early in the process of tumorigenesis [from Semin Urol (1993) 11:177–192]

Alternatively, the urinary epithelium can progress either to superficial bladder neoplasms, characterized by recurrence but rarely life threatening progression, or along the path toward invasion with its well-recognized risk of mortality. Evidence in support of these disparate pathways comes from the low progression rate of the majority of superficial bladder tumors, coupled with the fact that many invasive neoplasms present as invasive tumors when initially diagnosed. A model of a pathway, based on clinical evidence, detailing these distinctions in urothelial tumor biology is illustrated in Fig. 3.

Mimics of urothelial flat neoplasia

Several inflammatory conditions of the urinary bladder, some of them related to the effects of treatment, may cause urothelial atypia leading to overdiagnosis of urothelial dysplasia and carcinoma in situ [7, 35]. In addition, mucosa damaged by inflammation may become ulcerated, with adjacent regenerating atypical urothelium showing a pattern of pseudoepitheliomatous hyperplasia which is more common after radiation therapy [7].

Intravesical chemotherapy (e.g., mitomycin C, thio-TEPA) and treatment with BCG, commonly used to treat urothelial carcinoma in situ, often induce marked atypia of the urothelium. Chemotherapeutic agents used in the treatment of systemic non-urologic diseases (e.g., alkylating agents such as cyclophosphamide or busulfan) may injure the urothelium with subsequent severe regenerative atypia. It can be very difficult to confidently distinguish this atypia from carcinoma in situ, even for an experienced observer [35].

As seen in radiation injury, the urothelial atypia often has a degenerative appearance with smudged, hyperchromatic, multilobulated nuclei; nuclear and cytoplasmic vacuolization; and a ballooning of the cytoplasm to produce a low nuclear to cytoplasmic ratio. The atypia associated with intravesical chemotherapy may be predominantly found in the superficial layer of the urothelium. Chemotherapy can cause a widespread denudation of the urothelium with a variably retained single cell layer of very atypical large cells, mimicking the clinging pattern of CIS [35]. The atypical urothelium is commonly accompanied by an inflamed, edematous, sometimes hemorrhagic lamina propria that may have atypical stromal cells (giant cell cystitis). In BCG-treated bladders, it is important to keep in mind that residual CIS might be present only in Von Brunn nests. In rare cases, polyoma virus (BK virus) infection can mimic flat intraepithelial lesions in immunodepressed patients [35].

The common view of the members of committee no. 2 is that pathologists must exercise caution when evaluating urothelial atypia following treatment with chemotherapy or pelvic irradiation. In most cases, knowledge of the prior treatment can be crucial in arriving at the correct diagnosis. If the distinction between treatment-induced atypia and dysplasia/carcinoma in situ is uncertain, a conservative approach with repeat cystoscopy and biopsy, preferably after inflammation has subsided, is indicated.

Preneoplastic conditions and lesions other than urothelial

Metaplasia in the bladder reflects a response to chronic irritation. There are two basic forms of metaplasia: squamous and glandular. These two types of metaplasia may co-exist.

Keratinizing squamous metaplasia

This occurs in response to chronic irritative stimuli. It is considered a preneoplastic condition which has the potential to develop into squamous cell carcinoma with intraepithelial dysplastic changes and carcinoma in situ (or high-grade squamous intraepithelial neoplasia) as intermediate steps. These intermediate steps are similar, from the morphological point of view, to those usually seen in the uterine cervix. Usually such lesions are of the flat type, i.e., the lesions do not appear to be elevated above the surrounding unaffected mucosa. The urologist can identify them by the whitish discoloration due to keratin accumulation or to associated changes in the lamina propria. In rare cases the keratinizing squamous epithelium can have an exophytic pattern similar in morphology, nature, and behavior to viral lesions of the ano-genital region. This exophytic pattern of squamous metaplasia, also called squamous cell papilloma, might be related to the development of verrucous (squamous cell) carcinoma.

A study of 78 patients with keratinizing squamous metaplasia showed that 22% had synchronous squamous carcinoma, and an additional 20% developed carcinoma when followed up for as long as 30 years [6]. Squamous metaplasia frequently precedes squamous cell carcinoma in areas in which schistosomiasis is endemic [30].

Nonkeratinizing squamous epithelium often shows prominent glycogenation [50] and may resemble vaginal epithelium [53]. It is present in the trigone in 75–86% of women [34], is considered to be a normal finding, and should not be labeled metaplasia [17].

Glandular metaplasia

Glandular metaplasia is characterized by the presence of epithelial cells of colonic type with a goblet cell appearance (or rarely that of Paneth's, argentaffin, or argyrophil cells) within the surface epithelium (flat pattern) or/and in association with cystitis cystica (endophytic pattern). The development of adenocarcinoma from these cells has been documented in the long-term follow-up of very few patients. Still, such lesions have been considered examples of preneoplastic conditions.

Mucin-secreting metaplasia that shows a striking resemblance to intestinal mucosa, including a crypt-like

Table 3 Therapies causing "cellular atypia" in the urothelium

Systemic cyclophosphamide
Necrosis of the urothelium
Large, bizarre nuclei with coarse chromatin
Atypical form of regeneration
Small-to-medium-sized nucleoli
Reactivation of polyoma virus infection owing to systemic cyclophosphamide therapy
External beam radiotherapy
Intravesical therapy
Immunotherapy: bacillus Calmette-Guerin, interferon-α, others
Chemotherapy: thiotepa, mitomycin C, others
Denudation of the surface epithelium
Profound effects on the surface umbrella urothelial cells
Less significant abnormalities in the deeper layers of the urothelium
Nuclear and cytoplasmic vacuolization
Low nuclear-to-cytoplasmic ratio

architecture, has been designated intestinal metaplasia. The diffuse form of this metaplasia is associated with an increased risk of development of adenocarcinoma [20]. The appearance of cellular atypia, manifested by nuclear pleomorphism and prominent nucleoli, is considered indicative of malignant change – that is to say, glandular dysplasia and adenocarcinoma in situ may be considered intermediate steps between mucous metaplasia and invasive adenocarcinoma [10, 19, 56]. Intestinal-type mucinous metaplasia may include focal or diffuse areas of the type of intestinal metaplasia consisting of goblet cells or colonic-type glands (Table 3).

Glandular metaplasia may have an exophytic pattern usually called villous adenoma. Morphologically it has a villous or a tubulo-villous architecture with fronds lined by tall, pseudo-stratified, colonic-type epithelium whose nuclei are dark, elongated and in a basal position. Prominent nucleoli or stromal invasion indicate malignant change. Probably this represents another pathological route to adenocarcinoma through the intermediate step of adenoma, similar to the adenoma-carcinoma sequence observed in colon cancer [13, 15, 60]. Few examples of villous and tubular adenomas exist in the bladder, and none of those that have been reported have had an adverse outcome.

The opinion of the committee members is that squamous and glandular metaplasia are benign lesions and, as such, they have to be regarded by the clinicians. However, since cancer has been observed either in the follow-up of some patients or in association with these lesions, they can be considered examples of preneoplastic conditions. Squamous and glandular metaplasia become preneoplastic lesions when cells changes occur of the type described above.

Conclusions

This paper gives details on the following topics related to the preneoplastic non-papillary lesions and conditions of the epithelial lining the bladder, urethra, ureters, and renal pelves:

- Morphological (i.e., architectural and cytological) criteria
- Classification and grading schemes
- Patterns of early invasion and clinical significance of lamina propria invasion
- Relationship between flat and exophytic neoplasms
- Malignancy-associated changes and urothelial neoplasia
- Mimics of urothelial flat neoplasia: criteria for differential diagnosis
- Preneoplastic conditions and lesions other than urothelial

Standardized classification and grading of such lesions has now been achieved internationally. Uniformity of pathological reporting should improve the comparability of different studies and therapies, and provide more accurate information to urologists in managing patients.

References

1. Adsay NV, Sakr WA, Grignon DJ (1997) Flat-type transitional cell carcinoma in situ. Pathol Case Rev 2:115–121
2. Althusen AF, Prout GRJ, Dal JJ (1976) Noninvasive papillary carcinoma of the bladder associated with carcinoma in situ. J Urol 116:575–580
3. Amin MB, Young RH (1997) Intraepithelial lesions of the urinary bladder with a discussion of the histogenesis of urothelial neoplasia. Semin Diagn Pathol 14:84–97
4. Baithun SI, Naase M, Blanes A, Diaz-Cano SJ (2001) Molecular and kinetic features of transitional cell carcinomas of the bladder: biological and clinical implications. Virchows Arch 438:289–297
5. Baud E, Catilina P, Boitux JP, Bignon YJ (1998) Human bladder cancers and normal bladder mucosa present the same hot spot of heterozygous chromosome-9 deletion. In J Cancer 77:821–824
6. Benson RC, Swanson SK, Farrow GM (1984) Relationship of leucoplakia to urothelial malignancy. J Urol 131:507–511
7. Bostwick DG, Lopez-Beltran A (1999) Bladder biopsy interpretation. United Pathologists Press, New York
8. Bostwick DG, Ramnani D, Cheng L (1999) Diagnosis and grading of bladder cancer and associated lesions. Urol Clin North Am 26:493–507
9. Brawn PN (1982) The origen of invasive carcinoma of the bladder. Cancer 50:515–520
10. Chan TY, Epstein JI (2001) In situ adenocarcinoma of the bladder. Am J Surg Pathol 25:892–899
11. Cheng L, Cheville JC, Neumann RM, Bostwick DG (1999) Natural history of urothelial dysplasia of the bladder. Am J Surg Pathol 23:443–447
12. Cheng L, Cheville JC, Neumann RM, Leibovich BC, Egan KS, Spotts BE, Bostwick DG (1999) Survival of patients with carcinoma in situ of the urinary bladder. Cancer 85:2469–2474
13. Cheng L, Montironi R, Bostwick DG (1999) Villous adenoma of the urinary tract:a report of 23 cases, including 8 with coexisting adenocarcinoma. Am J Surg Pathol 23:764–771
14. Cheng L, Cheville JC, Neumann RM, Bostwick DG (2000) Flat intraepithelial lesions of the urinary bladder. Cancer 88: 625–631
15. Cheng L, Cheville JC, Sebo TJ, Eble JN, Bostwick DG (2000) Atypical nephrogenic metaplasia of the urinary tract: a precursor lesion? Cancer 8:853–861
16. Chow NH, Cairns P, Eisenberger CF, Schoenberg MP, Taylor DC, Epstein JI, Sidransky D (2000) Papillary urothelial hyperplasia is a clonal precursor to papillary transitional cell bladder carcinoma. Int J Cancer 89:514–518

17. Cifuentes L (1947) Epithelium of vaginal type in the female trigone: the clinical problem of trigonitis. J Urol 57:1028–1037
18. Cohen SM, Shirai T, Steineck G (2000) Epidemiology and etiology of premalignant and malignant urothelial changes. Scand J Urol Nephrol Suppl 205:105–115
19. Corica FA, Husmann DA, Churchill BM, Young RH, Pacelli A, Lopez-Beltran A, Bostwick DG (1997) Intestinal metaplasia is not a strong risk factor for bladder cancer: study of 53 cases with long-term follow up. Urology 50:427–431
20. Elem B, Alam SZ (1984) Total intestinal metaplasia with focal adenocarcinoma in a schistosoma-infested defunctioned urinary bladder. Br J Urol 56:331–343
21. Elliot GB, Moloney PJ, Anderson GH (1973) Denuding cystitis and in situ urothelial carcinoma. Arch Pathol 96:91–94
22. Epstein JI, Amin MB, Reuter V, Mostofi FK (1998) The world health organisation/international society of urological pathology consensus classification of urothelial (transitional cell) neoplasms of the urinary bladder. Am J Surg Pathol 22: 1435–1448
23. Farrow GM (1992) Pathology of carcinoma in situ of the urinary bladder and related lesions. J Cell Biochem 161:39–43
24. Farrow GM, Utz DC (1982) Observations on microinvasive transitional cell carcinoma of the urinary bladder. Clin Oncol 1:609–615
25. Farrow GM, Utz DC, Rife CC (1977) Clinical observations on 69 cases of in situ carcinoma of the urinary bladder. Cancer Res 37:2794–2802
26. Harnden P, Eardley I, Joyce AD, Southgate J (1996) Cytokeratin 20 as an objective marker of urothelial dysplasia. Br J Urol 78:870–875
27. Hartmann A, Moser K, Kriegmair M, Hofstetter A, Hofstaedter F, Knuechel R (1999) Frequent genetic alterations in simple urothelial hyperplasias of the bladder in patients with papillary urothelial carcinoma. Am J Pathol 154:721–727
28. Helpap B, Köllermann J (2000) Assesment of basal cell status and proliferative patterns in flat and papillary urothelial lesions: a contribution of the new WHO classification of urothelial tumors of the urinary bladder. Hum Pathol 31:745–750
29. Hudson MA, Herr HW (1995) Carcinoma in situ of the bladder. J Urol 153:564–572
30. Khafagy MM, El Bolkainy MN, Mansour MA (1972) Carcinoma of the Bilharzial urinary bladder: a study of the associated mucosal lesions in 86 cases. Cancer 30:150–159
31. Koss L (1975) Tumors of the urinary bladder: atlas of tumor pathology, vol. 16. AFIP, Washington
32. Koss LG (1979) Mapping of the urinary bladder: its impact on the concepts of bladder cancer. Hum Pathol 10:533–548
33. Levi AW, Potter SR, Schoenberg MP, Epstein JI (2001) Clinical significance of denuded urothelium in bladder biopsy. J Urol 166:457–460
34. Long ED, Shepherd RT (1983) The incidence and significance of vaginal metaplasia of the bladder trigone in adult women. Br J Urol 55:189–194
35. Lopez-Beltran A (1999) Bladder treatment. Immunotherapy and chemotherapy. Urol Clin North Am 26:535–554
36. Lopez-Beltran A, Bollito E, Luque RJ, Montironi R (2001) A practical approach to bladder sampling and diagnostic reporting of pathological findings. Pathologica 93:698-700
37. Lopez-Beltran A, Moreno A, Luque RJ, Carmona E, Bollito E, Montironi R (2001) The pagetoid variant of bladder urothelial carcinoma in situ. A clinicopathologic study of 11 cases. Virchows Arch (in press)
38. McKenney JK, Desai S, Cohen C, Amin MB (2001) Discriminatory immunohistochemical staining of urothelial carcinoma in situ and non-neoplastic urothelium. An anlysis of cytokeratin 20, p53, and CD44 antigens. Am J Surg Pathol 25: 1074–1078
39. McKenney JK, Gomez JA, Desai S, Lee MW, Amin MB (2001) Morphologic expressions of urothelial carcinoma in situ. A detailed evaluation of its histologic patterns with emphasis on carcinoma in situ with microinvasion. Am J Surg Pathol 25:356–362
40. Melicow M, Hollowell J (1952) Intra-urothelial cancer: carcinoma in situ, Bowen's disease of the urinary system: discusssion of 30 cases. J Urol 68:763–771
41. Milord RA, Lecksell K, Epstein JI (2001) An objective morphologic parameter to aid in the diagnosis of flat urothelial carcinoma in situ. Hum Pathol 32:997–1002
42. Montironi R, Filho AL, Santinelli A,Mazzuchelli R, Pomante R, Colanzi P, Scarpelli M (2000) Nuclear changes in the normal-looking columnar epithelium adjacent to and distant from prostatic intraepithelial neoplasia and prostate cancer: morphometric analysis in whole-mount sections. Virchows Arch 437:625–634
43. Mostofi FK, Davis CJ, Sesterhenn IA (1999) Histological typing of urinary bladder tumors. WHO International Histological Classification of Tumors, 2nd edn, Springer, Berlin Heidelberg New York
44. Mostofi FK, Sesterhenn IA (1984) Pathology of epithelial tumors and carcinoma in situ of bladder: bladder cancer. Progress Clin Biol Res 162A:55–74
45. Murphy WM, Beckwith JB, Farrow GM (1994) Tumors of the kidney, bladder and related urinary structures. AFIP, Washington
46. Murphy WM, Busch C, Algaba F (2000) Intraepithelial lesions of the urinary bladder: morphologic considerations Scand J Urol Nephrol Suppl 205:67–81
47. Murphy WM, Soloway MS (1982) Urothelial dysplasia. J Urol 127:849–854
48. Muto S, Horie S, Takahashi S, Tomita K, Kitamura T (2000) Genetic and epigenetic alterations in normal epithelium in patients with metachronous bladder cancer. Cancer Res 60: 4021–4025
49. Nagy GH, Frable WJ, Murphy WM (eds) (1982) The classification of premalignant urothelial abnormalities. Pathol Ann 17: 219–233
50. Ney C, Ehrlich JC (1955) Squamous epithelium in the trigone of the human female urinary bladder with a note on cystoscopic observations during estrogen therapy. J Urol 73:809–819
51. Orozco RE, Zwaag RV, Murphy WM (1993) The pagetoid variant of urothelial carcinoma in situ. Hum Pathol 24: 1199–1202
52. Orozco RE, Martin AA, Murphy WM (1994) Carcinoma in situ of the urinary bladder: clues to host involvement in human carcinogenesis. Cancer 76:115–122
53. Packham DA (1971) The epithelial lining of the female trigone and urethra. Br J Urol 43:201–205
54. Reuter VE (1999) Bladder risk and prognostic factors: a pathologist's perspective. Urol Clin North Am 26:481–492
55. Sarma KP (1981) Genesis of papillary tumors: histological and micorangiographic study. Br J Urol 53:228–236
56. Shaw JL, Gislason GJ, Imbriglia JE (1958) Transition of cystitis glandularis to primary adenocarcinoma of the bladder. J Urol 79:815–821
57. Smith G, Elton RA, Beynon LL (1983) Prognostic significance of biopsy results of normal looking mucosa in cases of superficial bladder cancer. Br J Urol 55:665–669
58. Taylor DC, Bhagavan DS, Larsen MP (1996) Papillary urothelial hyperplasia: a precursor to papillary neoplasm. Am J Surg Pathol 20:1481–1488
59. Wolf H, Hojgaard K (1980) Urothelial dysplasia in random mucosal biopsies from patients with bladder tumors. Scan J Urol Nephrol 14:37–41
60. Young RH, Parkhurst EC (1984) Mucinous adenocarcinoma of the bladder: case associated with extensive intestinal metaplasia of the urothelium in a patient with nonfunctioning bladder for 12 years. Urology 24:192–195
61. Zuk RJ, Rogers HS, Martin JE (1988) Clinicopathological importance of primary dysplasia of the bladder. J Clin Pathol 41:1277–1280

Virchows Arch (2002) 440:12–15
DOI 10.1007/s004280100491

ORIGINAL ARTICLE

Sumika Okamoto · Masanori Hisaoka
Jeanne M. Meis-Kindblom · Lars-Gunnar Kindblom
Hiroshi Hashimoto

Juxta-articular myxoma and intramuscular myxoma are two distinct entities

Activating Gsα mutation at Arg 201 codon does not occur in juxta-articular myxoma

Received: 20 March 2001 / Accepted: 5 June 2001 / Published online: 26 July 2001
© Springer-Verlag 2001

Abstract Juxta-articular myxoma is a rare myxoid tumor of soft tissue that bears a close histologic resemblance to intramuscular myxoma but is distinguished from the latter by its clinical setting and behavior. Activating missense mutations at the Arg 201 codon of the Gsα gene ultimately leading to increased levels of cyclic adenosine monophosphate have been implicated in McCune-Albright syndrome and sporadic fibrous dysplasia of bone. Recently, we have demonstrated that the same Gsα mutations occur in intramuscular myxomas associated with fibrous dysplasia of bone (Mazabraud's syndrome) as well as in sporadic intramuscular myxoma. The overlapping histologic appearances of juxta-articular myxoma and intramuscular myxoma prompted us to investigate whether there is a relationship between the two entities. We studied this possibility by looking for Gsα mutations in juxta-articular myxoma using polymerase chain reaction (PCR) to amplify appropriate genomic DNA fragments extracted from formalin-fixed, paraffin-embedded specimens of five juxta-articular myxomas, followed by single-strand conformation polymorphism analysis. Using these techniques, no aberrant bands were detected in any of the five juxta-articular myxomas, indicating that they lack Gsα mutations. Moreover, DNA sequencing of the PCR products of two JAMs showed no abnormalities. We conclude that juxta-articular myxomas, in contrast to intramuscular myxomas, do not involve Arg 201 mutations of the Gsα gene, indicating that they represent distinct entities with different underlying molecular mechanisms.

Keywords Gsα · Juxta-articular myxoma · Intramuscular myxoma · Myxoid soft tissue tumors · PCR-SSCP

S. Okamoto · M. Hisaoka · H. Hashimoto (✉)
Department of Pathology and Oncology, School of Medicine,
University of Occupational and Environmental Health,
1-1 Iseigaoka, Yahatanishi-ku, Kitakyushu 807-8555, Japan
e-mail: hiroshi@med.uoeh-u.ac.jp
Tel.: +81-93-6917239, Fax: +81-93-6920189

J.M. Meis-Kindblom · L.-G. Kindblom
Department of Pathology,
Gothenburg Musculoskeletal Tumor Center,
Sahlgrenska University Hospital, Gothenburg University,
Gothenburg, Sweden

Introduction

Myxomas of soft tissue are localized proliferations of sparsely distributed spindle cells with fibroblastic features embedded in an abundant myxoid matrix. Although they share similar histologic features, they are generally subclassified into intramuscular, superficial-cutaneous, and juxta-articular types depending on their clinical setting [10].

Juxta-articular myxoma (JAM) is a recently described and relatively rare lesion of uncertain pathogenesis which commonly occurs in the vicinity of the knee joint in adult men. They are often associated with a history of trauma or osteoarthritis and may attain a considerable size, thereby arousing suspicion of a sarcoma. Although benign, JAM has a tendency to recur, sometimes repeatedly, after local excision [18].

Intramuscular myxoma (IM) is a benign lesion that occurs sporadically, in association with Mazabraud's syndrome (multiple IM and polyostotic fibrous dysplasia), or occasionally in the context of McCune-Albright syndrome [9, 11, 16, 28]. The underlying abnormality in the two latter conditions is a mosaic distribution of cells with a somatic mutation of the Gsα gene encoding the α subunit of the stimulatory G protein (Gsα) [23, 24, 25, 27]. Abnormal Gsα protein, which is derived from activating missense mutations at the Arg201 codon of the Gsα gene, causes continuous activation of adenylyl cyclase and increased levels of cyclic adenosine monophosphate (cAMP), leading to diverse biological consequences due to its regulatory effects on signaling path-

ways involved in cell proliferation, differentiation, and apoptosis [7, 14]. We recently identified missense mutations at the Arg201 codon of the Gsα gene in both sporadic IM and IM associated with Mazabraud's syndrome, and we suggested that these mutations are important in the development of IM [20].

The histological similarities between JAM and IM prompted us to investigate whether Gsα gene mutations could also be involved in the pathogenesis of JAM. We therefore studied this possibility using polymerase chain reaction–single-strand conformation polymorphism (PCR–SSCP) analysis.

Materials and methods

Five cases of formalin-fixed, paraffin-embedded JAM were retrieved from the files of the Department of Pathology and Oncology, School of Medicine, University of Occupational and Environmental Health (cases 1 and 2), and the Department of Pathology, Gothenburg Musculoskeletal Tumor Center, Sahlgrenska University Hospital (cases 3–5). A case of IM with known Gsα mutation was included as a positive control in our molecular analysis.

PCR–SSCP assay

After deparaffinization and treatment with proteinase K (0.75 mg/ml) for 3 days, genomic DNA was extracted from five 4-µm-thick sections of each case using a DNA extraction kit (Sepagene, Sankojunyaku, Tokyo, Japan). Exon 8 of the Gsα gene was amplified by means of PCR using a primer set flanking a 115-bp fragment, as previously described by Candeliere et al. [2]. The forward primer was 5′-CCATTGACCTCAATTTTGTTTCAG-3′ and the reverse primer was 5′-GGTAACAGTTGGCTTACTGGAAGTTG-3′. The reaction mixture was composed of 100 ng genomic DNA, 12.5 pmol each primer, 200 µM dNTP, and 2.5 U *Pfu* DNA polymerase (native Pfu, Stratagene, La Jolla, Calif.) in a standard reaction buffer (10 mM Tris-HCl, 50 mM KCl, 1.5 mM $MgCl_2$ and 0.001% gelatin). PCR consisted of 40 cycles of denaturation for 45 s at 94°C, annealing for 45 s at 60°C, and strand elongation for 45 s at 72°C. The PCR product was screened by means of SSCP analysis using 3 µl PCR product in sample-denaturing buffer [99% formamide, 5 mM Tris-HCl, 0.5 mM ethylene diamine tetraacetic acid (EDTA), 0.05% xylene cyanol and 0.05% bromophenol blue]. After denaturation at 95°C for 5 min, the samples were placed onto a pre-cast polyacrylamide ready-to-run gel (GeneGel Excel 12.5/24, Pharmacia Biotech, Uppsala, Sweden) at 15°C for 90 min with a Peltier temperature-regulated electrophoresis unit (Genephor, Pharmacia Biotech). To visualize nucleic acids in the gel, a silver staining kit (Bio-Rad, Hercules, Calif.) was used. DNA sequencing of the PCR products was performed on two chosen samples to confirm the amplification of exon 8 of the Gsα gene. The PCR products were cloned into a pCR2.1 vector (Invitrogen, San Diego, Calif.) by TA ligation and sequenced using an automated sequencer (ALFexpress, Pharmacia Biotech, Uppsala, Sweden).

Results

The clinicopathological features of the five cases are summarized in Table 1. All five patients were men and their ages ranged from 35 years to 67 years (median 56 years; mean 53 years). Four of five lesions occurred in the vicinity of the knee and one in the foot. Tumor sizes ranged from 2.5 cm to 4.0 cm (mean 3 cm) in maximum dimension. One patient had rheumatoid arthritis (case 1) and another had osteoarthritis (case 2); their JAM were incidental findings during total arthroplasty and synovectomy, respectively. There have been no local recurrences in any of the cases (follow-up 2.5–5 years, median 3 years).

Microscopically, all five JAMs were multilobular with delicate, fibrous septa and they contained variable amounts of collagen. Three cases had irregular, ganglion cyst-like spaces (Fig. 1A). In all cases, there were sparsely distributed spindle-shaped or stellate-shaped fibroblast-like cells in an abundant myxoid matrix with few vessels (Fig. 1B). No hypercellular or pleomorphic areas were identified in any of the cases. A diffuse growth pattern with ill-defined boundaries containing entrapped adipose tissue was seen in cases 2 and 4. Alcian blue staining confirmed the presence of abundant acid mucopolysaccharides in the myxoid matrix of all five cases.

In the PCR analysis, all five samples yielded one major band of the predicted size for exon 8 of the Gsα gene. No aberrant bands were seen in the SSCP analysis using the PCR products (Fig. 2). DNA sequencing of the PCR products of two randomly chosen samples with a normal band on SSCP showed neither point mutations nor any other alterations in this region of the Gsα gene. Thus, the analyzed DNA in all five JAMs did not contain Arg 201 mutations of the Gsα gene.

Discussion

JAM occurs primarily in the periarticular subcutaneous adipose tissue and may involve the adjacent dermis, joint capsule, tendons, and rarely skeletal muscle [10]. The histological findings of JAM are quite similar to those of IM, but there are certain clinical and morphological differences between them. JAM affects men more often than women, tends to recur after incomplete excision, and is often associated with trauma to the joint or degenerative joint disease [18]. One patient in this study had

Table 1 Clinicopathologic features of juxta-articular myxomas

Case	Age (years)/sex	Site	Size (cm)	Clinical features
1	67/Male	Knee	2.5×2.5×1	Rheumatoid arthritis
2	57/Male	Knee	2.5×2×2	Osteoarthritis
3	35/Male	Knee	2.5×2.5×1	Ganglion cyst clinically suspected
4	56/Male	Knee	4×3×1.5	Ganglion cyst clinically suspected
5	51/Male	Foot (between 1st and 2nd toes)	3×2×1	Discomfort, 2 years

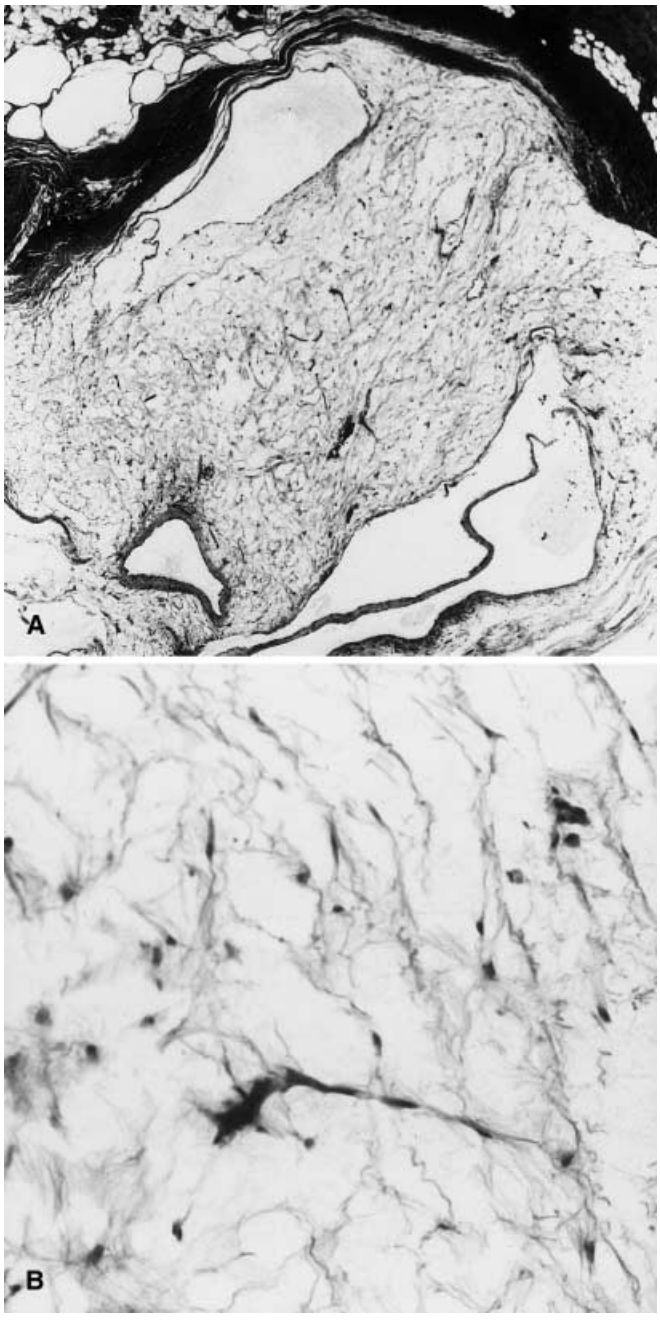

Fig. 1 **A** Low-power view of juxta-articular myxoma in the knee showing several irregular cystic spaces and involvement of the adjacent fibroadipose tissue (case 2). Original magnification, ×6.6. **B** Constituent fibroblast-like cells having small pyknotic nuclei and delicate cytoplasmic processes suspended in a myxoid matrix. Original magnification, ×50

rheumatoid arthritis and another had osteoarthritis. Although cystic foci are not uncommon in IM, most JAM has pronounced cystic changes that may at times be indistinguishable from a ganglion cyst.

In this study, we have demonstrated that in addition to differences in clinical setting and behavior, there are also molecular differences between JAM and IM. In contrast to our previous findings of Gsα gene mutations in IM

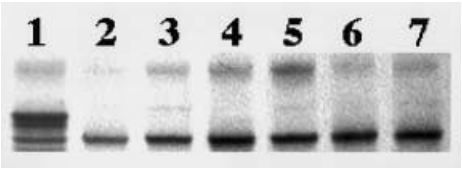

Fig. 2 Single-strand conformation polymorphism analysis of exon 8 of the Gsα gene. No aberrant bands are seen in each case of juxta-articular myxoma. *Lane 1* intramuscular myxoma (positive control); *lanes 2–6* cases 1–5; *lane 7* normal peripheral blood mononuclear cells (negative control)

[20], we did not detect mutations at the Arg 201 codon of the Gsα gene in any of the five JAM examined using PCR-SSCP analysis. We believe that our PCR-SSCP analysis is sensitive enough to detect point mutations in the amplified Gsα gene, since detection of Gsα gene mutation has been successful using similar techniques in other studies [8]. Moreover, sequencing of the PCR products in two cases did not reveal any point mutations or other alterations. Our results therefore indicate that, unlike IM, Arg 201 mutations of the Gsα gene are not associated with the development of JAM. They further suggest that JAM and IM are two distinct entities with different underlying molecular mechanisms involved in their development.

In a recent cytogenetic analysis of JAM, Sciot and associates found two abnormal cell populations, inv (2)(p15q36) and +7, t (8; 22)(q11–12; q12–13), indicating that JAM are true neoplasms and not merely reactive [22]. To the best of our knowledge, there is only one study reporting the cytogenetic findings of IM; one case had trisomy 18 and another a normal karyotype [19]. Clonal chromosomal changes in 20q12-q13.2, where the Gsα gene is located [21], have not been reported in either JAM or IM. Thus, further investigation is necessary to elucidate the pathogenesis of both JAM and IM.

Interestingly, Gsα mutations have also been investigated in other types of “myxomas”, including cardiac myxoma and odontogenic myxoma or myxoma of the jaw. Both of these entities have histologic and, in the case of cardiac myxomas, immunophenotypic characteristics that distinguish them from JAM and IM. Cardiac myxoma is encountered sporadically or as part of the Carney complex, an autosomal dominant syndrome characterized by cutaneous and cardiac myxomas, endocrine hyperactivity, and spotty pigmentations. The Carney complex gene defect has recently been mapped to chromosome 17q24 and identified as the tumor suppressor gene PRKAR1A that encodes the type-A regulatory subunit of protein kinase A. Cardiac myxomas associated with this syndrome have revealed a number of functionally null mutations of this gene [5, 13]. DeMarco et al. detected no Gsα mutations in sporadic cardiac myxomas or other tumors occurring in patients with Carney complex, suggesting that activating Gsα mutations play no role in their development [6]. The results further indicate that cardiac myxomas are clearly distinct from JAM and IM.

Odontogenic myxoma, which is primarily a bone tumor, occurs in the mandible or maxilla [10]. This tumor may occasionally extend into the adjacent soft tissues of the face forming a myxoid mass, but it differs histologically from other soft tissue myxomas, including JAM, by a higher degree of cellularity and pleomorphism as well as increased numbers of mitoses. Boson et al. detected no Gsα mutations in odontogenic myxomas [1]. This finding further indicates that odontogenic myxoma is clearly distinct from JAM and IM.

Myxoma of bone in extra-gnathic sites is extremely rare. To our knowledge, only eight cases have been reported in the English-language literature, with three cases in the femur [17], one in the humerus [26], one in the phalanx of a toe [12], and three in the skull and orbit [3, 4, 15]. Interestingly, seven of the eight myxomas of bone occurred in women. Two femoral myxomas involved the articular surface of the bone, raising the possibility that they may represent JAM. To date, there have been no investigations regarding Gsα gene mutations in primary myxomas of bone in extra-gnathic sites.

In conclusion, the results of our study indicate that Gsα mutations at the Arg 201 codon do not occur in JAM, although they do in IM, which is histologically quite similar. Thus, the two entities are probably not related and other mechanisms may well be involved in the pathogenesis of JAM.

Acknowledgements This work was supported by grants from the Ministry of Education, Science, Sports and Culture (12770102 and 12670184) and the Fukuoka Cancer Society, Japan, 2000.

References

1. Boson WL, Gomez RS, Araujo L, Kalapothakis E, Friedman E, De Marco L (1998) Odontogenic myxomas are not associated with activating mutations of the Gsα gene. Anticancer Res 18:4415–4418
2. Candeliere GA, Roughley PJ, Glorieux FH (1997) Polymerase chain reaction-based technique for the selective enrichment and analysis of mosaic arg201 mutations in Gsα from patients with fibrous dysplasia of bone. Bone 21:201–206
3. Candy EJ, Miller MR, Carson BS (1991) Myxoma of bone involving the orbit (letter). Arch Opthalmol 109:919–920
4. Carabi S, Engel P, Bonding P (1989) Myxoid tumours in the temporal bone. J Laryngol Otol 103:1206–1209
5. Casey M, Vaughan CJ, He J, Hatcher CJ, Winter JM, Weremowicz S, Montgomery K, Kucherlapati R, Morton CC, Basson CT (2000) Mutations in the protein kinase A R1alpha regulatory subunit cause familial cardiac myxomas and Carney complex. J Clin Invest 106:R31–R38
6. De Marco L, Stratakis CA, Boson WL, et al (1996) Sporadic cardiac myxomas and tumors from patients with Carney complex are not associated with activating mutations of the Gs alpha gene. Hum Genet 98:185–188
7. Dhanasekaran N, Tsim St, Dermott JM, Onesime D (1998) Regulation of cell proliferation by G proteins. Oncogene 17: 1383–1394
8. Drews RT, Gravel RA, Collu R (1992) Identification of G protein a subunit mutations in human growth hormone (GH)- and GH/prolactin-secreting pituitary tumors by single-strand conformation polymorphism (SSCP) analysis. Mol Cell Endocrinol 87:125–129
9. Enzinger FM (1965) Intramuscular myxoma. A review and follow up study of 34 cases. Am J Clin Pathol 43:104–113
10. Enzinger FM, Weiss S (1995) Soft tissue tumors, 3rd edn. St Louis, Mosby, pp 1045–1055
11. Hashimoto H, Tsuneyoshi M, Daimaru Y, Enjoji M, Shinohara N (1986) Intramuscular myxoma. A clinicopathologic, immunohistochemical, and electron microscopic study. Cancer 58:740–747
12. Hill JA, Victor TA, Dawson WJ, Milgran JW (1978) Myxoma of the toe: a case report. J Bone Joint Surg Am 60:128–130
13. Kirschner LS, Sandrini F, Monbo J, Lin JP, Carney JA, Stratakis CA (2000) Genetic heterogeneity and spectrum of mutations of the PRKAR1A gene in patients with the Carney complex. Hum Mol Genet 9:3037–3046
14. Landis CA, Masters SB, Spada A, Pace AM, Bourne HR, Vallar L (1989) GTPase inhibiting mutations activate the α chain of Gs and stimulate adenylyl cyclase in human pituitary tumours. Nature 340:692–696
15. Maiuri F, Corriero G, Galicchio B, Angrisani P, Bonavolonta G (1988) Myxoma of the skull and orbit. Neurochirurgia 31:136–138
16. Mazabraud A, Semat P, Roze R (1967) A propos de l'association de fibromyxomes des tissus mous a la dysplasie fibreuse des os. La Presse Med 75:2223–2228
17. McClure DK, Dahlin DC (1977) Myxoma of bone: report of three cases. Mayo Clin Proc 52:249–253
18. Meis JM, Enzinger FM (1992) Juxta-articular myxoma: a clinical and pathologic study of 65 cases. Hum Pathol 23:639–646
19. Meis-Kindblom JM, Sjogren H, Kindblom L-G, Peydro-Mellquist A, Roijer E, Aman P, Stenman G (2001) Cytogenetic and molecular genetic analyses of liposarcoma and its soft tissue simulators: recognition of new variants and differential diagnosis. Virchows Arch (in press)
20. Okamoto S, Hisaoka M, Ushijima M, Nakahara S, Toyoshima S, Hashimoto H (2000) Activating Gsα mutation in intramuscular myxomas with and without fibrous dysplasia of bone. Virchows Arch 437:133–137
21. Rao VV, Schnittger S, Hansmann I (1991) G protein Gs alpha (GNAS1), the probable candidate gene for Albright hereditary osteodystrophy, is assigned to human chromosome 20q12-q13.2. Genomics 10:257–261
22. Sciot R, Dal Cin P, Samson I, van den Berghe H, Van Damme Boudewijn (1999) Clonal chromosomal changes in juxta-articular myxoma. Virchows Arch 434:177–180
23. Shenker A, Weinstein LS, Sweet DE, Spiegel AM (1994) An activating Gsα mutation is present in fibrous dysplasia of bone in the McCune-Albright syndrome. J Clin Endocrinol Metab 79:750–755
24. Shenker A, Chanson P, Weinstein LS, Chi P, Spiegel AM, Lomri A, Marie PJ (1995) Oteoblastic cells derived from isolated lesions of fibrous dysplasia contain activating somatic mutations of the Gsα gene. Hum Mol Genet 4:1675–1676
25. Singer FR (1997) Commentary: fibrous dysplasia of bone. The bone lesion unmasked. Am J Pathol 151:1511–1515
26. Sundaram M, Janney C, McDonald DJ (2000) Myxoma of the humerus: an exceptional site of origin. Skeletal Radiol 29: 57–60
27. Weinstein LS, Shenker A, Gejman PV, Merino MJ, Friedman E, Spiegel AM (1991) Activating mutations of the stimulatory G protein in the McCune-Albright syndrome. N Eng J Med 325:1688–1695
28. Wirth WA, Leavitt D, Enzinger FM (1971) Multiple intramuscular myxomas. Another extraskeletal manifestation of fibrous dysplasia. Cancer 27:1167–1173

Virchows Arch (2002) 440:16–21
DOI 10.1007/s004280100487

ORIGINAL ARTICLE

Joana Paredes · Fernanda Milanezi · Leda Viegas
Isabel Amendoeira · Fernando Schmitt

P-cadherin expression is associated with high-grade ductal carcinoma in situ of the breast

Received: 5 January 2001 / Accepted: 29 April 2001 / Published online: 3 July 2001
© Springer-Verlag 2001

Abstract Cadherins are calcium-dependent cell–cell adhesion glycoproteins, separated into several subclasses with distinct adhesive specificities and tissue distribution, which play an important role in many cellular events. We analyse the expression of E-, N- and P-cadherin in a series of ductal carcinoma in situ (DCIS) of the breast, since this disease represents a heterogeneous group, with different risks of progression to invasive breast carcinoma. We also studied the correlation between cadherin expression and DCIS classification systems, namely the Van Nuys and the Holland et al. classification, this latter based on cytonuclear differentiation and cell polarity. Our results showed that, regardless the classification applied, P-cadherin expression is strongly associated with high histological grade of DCIS (P=0.0047) and lack of estrogen receptors (P=0.0008). The use of Holland et al. classification showed a significant correlation between P-cadherin expression and decreased cell polarity (P=0.01). In conclusion, P-cadherin expression seems to be more relevant in DCIS pathogenesis than the altered expression of any other cadherin, including the decrease of E-cadherin expression.

Keywords Cadherins · Ductal carcinoma in situ of the breast · P-cadherin · E-cadherin · Cell polarity

J. Paredes · F. Milanezi · F. Schmitt (✉)
The Institute of Pathology and Molecular Immunology
of Porto University (IPATIMUP), Rua Roberto Frias s/n,
4200 Porto, Portugal
e-mail: fernando.schmitt@ipatimup.pt
Tel.: +351-22-5570700, Fax: +351-22-5570799

L. Viegas
The Medical Sciences Faculty of Santos, Lusiada Foundation,
Santos, São Paulo, Brazil

I. Amendoeira
The Department of Pathology, Hospital de São João,
Porto, Portugal

Introduction

Cadherins are a family of glycoproteins expressed on the cell surface, which act as intercellular adhesion molecules by calcium-dependent homophilic binding [9, 38]. Their structural and functional integrity play a role in cell sorting during embryogenesis and in the maintenance of adult tissue architecture [9, 38]. Intracellularly, these transmembrane molecules form complexes with several proteins [41] and cytoskeleton components that constitute the intercellular adherens junctions and mediate signal-transduction mechanisms to control cellular events, including cell polarity, differentiation, growth and migration [18, 42].

The classical cadherins, namely epithelial (E-), neural (N-) and placental (P-) cadherin, originally described by their tissue specificity, have been used as markers in the identification of benign tissues and some neoplastic processes [11, 12, 13, 26, 37, 38, 41]. Nowadays, the study of cadherins has been focused on their possible role in carcinogenic pathways. In normal adult breast, E-cadherin is expressed in both luminal epithelial cells and myoepithelial cells, whereas P-cadherin is present only in myoepithelial cells [25, 28, 32]. The expression of N-cadherin is not found in normal breast tissue [11, 17, 29, 36].

The role of E-cadherin in breast cancer has been explored in the last few years and its lack or decreased expression has been correlated with tumour grade, invasiveness and prognosis [4, 5, 7, 34, 39], especially in lobular carcinomas, which have a high frequency of mutations in the E-cadherin gene [2, 3, 22].

N- and P-cadherin expression in breast carcinoma is still poorly understood. Recent studies have shown that N-cadherin in breast cancer cell lines contributes to a diffuse phenotype and promotes motility, invasion and metastasis [14, 24]. P-cadherin, however, can be expressed in a subset of breast cancers [25, 28]. Recently, Peralta Soler et al. observed P-cadherin expression in invasive ductal carcinomas with higher histological grade and poor survival, suggesting that this protein could constitute a prognostic marker [27].

Ductal carcinoma in situ (DCIS) represents a heterogeneous group of lesions which is manifested in clinical and radiological presentation, histological appearance, expression of biological markers and, most significantly, in biological behaviour, with different risks of progression to invasive breast carcinoma [19, 33]. The several classification systems in use reflect the heterogeneity of these lesions. Van Nuys classification, a combination of nuclear grade and necrosis evaluation, seems to predict clinical recurrence [35]. Holland et al. proposed a different system of classification based on cytonuclear morphology and architectural differentiation (cellular polarisation) [15], and this latter criterion could be correlated with cadherins expression, since one of the major functions of them is to maintain the epithelial cell polarity.

We analysed the expression of E-, N- and P-cadherin in a series of DCISs of the breast and its correlation with other biological markers in attempt to study the possible role of cadherins in the different histotypes of DCIS.

Materials and methods

Tumour specimens

Formalin-fixed, paraffin-embedded blocks of 73 ductal carcinomas in situ of the breast were retrieved from the histopathology files of our institutes. All cases were reviewed on haematoxylin and eosin stained sections by three pathologists (F.S., F.M., L.V.). Histological typing and grading were performed in accordance with two types of DCIS classification: the Van Nuys classification, presented by Silverstein et al. [35], and the classification proposed by Holland et al. [15]. The Van Nuys classification, which consists of a combination of tumour nuclear grade and extent of necrosis, defines three distinct recognisable groups: (i) non-high grade DCIS without comedo-type necrosis, (ii) non-high grade DCIS with comedo-type necrosis and (iii) high grade DCIS with or without comedo-type necrosis [35]. Holland's proposal, based on nuclear morphology and cell polarisation (architecture), divides DCIS cases into well differentiated (type I) and poorly differentiated (type III) tumours. Cases with an intermediate differentiation are included in type-II DCIS [15].

All relevant data were available for analysis, including age, tumour size, estrogen receptor status, and p53, c-erbB-2 and cyclin D1 expression. The mean age of the patients at diagnosis was 55 years (range 32–78 years). The size of the tumours ranged from 4.5 mm to 125.0 mm (mean 31.8 mm±28.9 mm).

Immunohistochemistry

Three-micron-thick sections were immunostained with monoclonal antibodies against E-cadherin (HECD-1, 1:200, Zymed Laboratory, San Francisco, Calif.), P-cadherin (clone 56, 1:50, Transduction Laboratories, Lexington, Ky.) and N-cadherin (clone 3B9, 1:400, Zymed Laboratory). Immunostainings were performed using the avidin–biotin–peroxidase (ABC) complex. Antigen retrieval was carried out by microwave treatment in a 0.05% detergent solution for E- and N-cadherin antibodies, and with 10 mM citrate buffer, pH 6.0 (Dako Corporation, Carpinteria, Calif.) for P-cadherin antibody. After cooling at room temperature, the sections were immersed in 3% hydrogen peroxide (H_2O_2) and methanol to block endogenous peroxidase activity. Non-specific staining was eliminated by incubation with normal rabbit serum (Dako), and the specific monoclonal antibodies were incubated overnight at 4°C in a humid chamber. After washing the slides, sections were incubated with a 1:200 dilution of biotin-labelled secondary antibody followed by ABC complex (avidin, 1:100 and biotin-labelled peroxidase, 1:100). These reagents were purchased from Dako. Subsequently, sections were stained with a solution of 3,3-diaminobenzidine tetrahydrochloride (DAB) with H_2O_2 in Tris-HCl buffer, pH 7.6 (LabVision Corporation, Fremont, Calif.), counterstained with Mayer's haematoxylin, dehydrated, and mounted.

Positive and negative controls were included in all series for all the antibodies used. Paraffin sections of normal skin tissue were used as positive control for E-cadherin, normal breast tissue for P-cadherin and cardiac muscle for N-cadherin. Immunohistochemical results were not assessed in ten cases (six for E-cadherin and four for P-cadherin), since there was no more tumour material available.

Quantification of immunostaining

The DCIS presenting cells with an unequivocal membranous staining for the three cadherins tested were scored as positive. Cells with cytoplasmic expression alone were not considered. The assessment of immunohistochemical results was based on a semiquantitative evaluation proposed by Han et al. [12], which does not include the intensity of staining. The cases were separated into four groups according to the percentage of immunopositive cells: 0, <10%; 1, 10–25%; 2, 26–50%; 3, >50%. The expression of cadherin was considered positive if staining was identified in at least 10% of the cells in the expected cell–cell membrane location.

Statistical analysis

For statistical analysis, contingency tables and chi-square test were done using StatView 5.0 (SAS Institute Inc., Cary, N.C.) to estimate the relationship between staining patterns of the different antibodies used. Two values were considered significantly different when $P<0.05$.

Results

Of the 73 cases that were reviewed and graduated by Van Nuys classification, 10 (13.7%) were classified as grade-I, 18 (24.7%) as grade-II and 45 (61.6%) as grade-III tumours. Using Holland et al. classification, 10 cases were considered well-differentiated tumours (13.7%), 13 were intermediately differentiated (17.8%) and 50 cases were included in the poorly differentiated group (68.5%).

P-cadherin was positive in 23 (33.3%) cases and negative in 46 (66.7%) cases of DCIS. Distribution of P-cadherin in tumour cells showed membranous staining frequently associated with cytoplasmic expression (Fig. 1). Myoepithelial cells were always positive for P-cadherin in normal ducts and in ducts containing in situ carcinoma.

Regardless of the classification applied, P-cadherin expression showed a strong correlation with high histological grade, since this protein was essentially present in grade-III (poorly differentiated) tumours, while grade-I (well differentiated) cases were all negative for P-cadherin (Table 1 and Table 2). We correlated separately the expression of each cadherin with the two parameters used in Holland's system: cytonuclear and architectural differentiation (cellular polarisation). Our results showed that expression of P-cadherin is related to loss of cell polarity ($P=0.01$), as well as with nuclei pleomorphism ($P=0.0072$; Table 3 and Table 4).

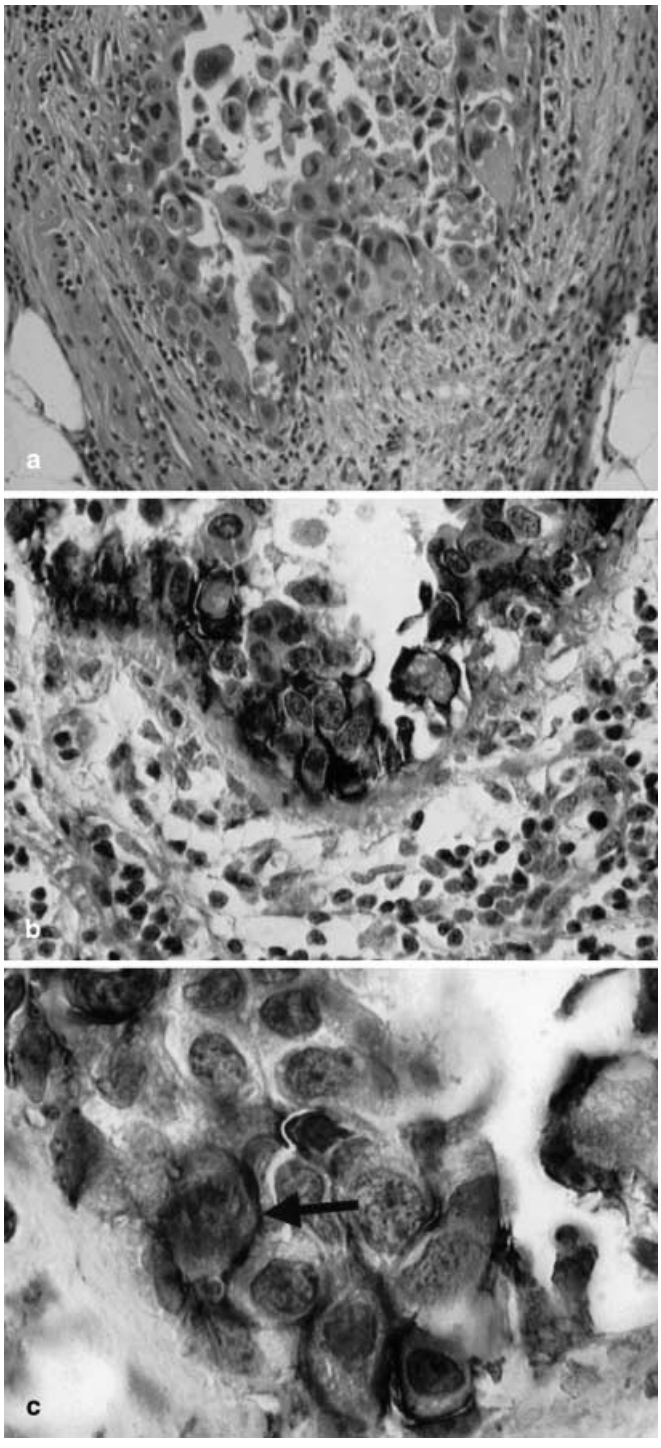

Fig. 1 **a** Ductal carcinoma in situ (DCIS) of the breast with high histological grade (poorly differentiated). Haematoxylin and eosin ×200. **b** Strong expression of P-cadherin in a poorly differentiated DCIS of the breast; ×400. **c** Higher magnification of P-cadherin membranous staining; ×1000 (*black arrow*)

Statistical analysis of the data revealed an inverse correlation between P-cadherin expression and estrogen receptor status: 60.9% of P-cadherin positive cases were estrogen receptor negative (Table 5). The chi-square test showed that this difference was statistically significant (P=0.0008).

The comparison between cases with positive and negative P-cadherin expression was performed for p53, c-erbB-2 and cyclin D1: 86.9% of the cases c-erbB-2 positive have demonstrated P-cadherin positivity (P=0.015); the expression of p53 was also higher in P-cadherin positive cases than in negative cases (P=0.0544), but no significant correlation was found with cyclin D1. Some difference in tumour size was found between cases with P-cadherin positive (41.9 mm±34.2 mm) and P-cadherin negative (28.3mm±26.0 mm) tumours, although it was not statistically significant (P=0.0871).

Most of the cases were positive for E-cadherin (89.4%), showing a clear and strong membranous staining of the neoplastic epithelial cells, particularly along their lateral and basal membranes (Fig. 2). In contrast to P-cadherin, expression of E-cadherin was lower in high-grade DCIS: 71.4% of E-cadherin negative cases were grade-III tumours.

N-cadherin was only found in 12.3% of the tumours, and its expression was restricted to a small population of cells, which presented a faint membranous staining, always associated with a strong expression in the cytoplasm. There was no correlation between N-cadherin expression and histological grade or any other parameter studied.

Discussion

The present study shows that P-cadherin expression is strongly associated with high histological grade of DCIS and with loss of ER, as already reported by two other studies in invasive ductal carcinoma [25, 27]. Moreover, almost all P-cadherin-positive cases were also positive to c-erbB-2, and some have presented p53 immunoreactivity. All these biological conditions were already reported as correlated with poor differentiation in DCIS [19, 33].

Our results also demonstrated a relationship between P-cadherin expression and loss of tumour cell polarity, one of the parameters of the DCIS classification proposed by Holland et al. [15]. Cell polarity is an indicator and a determinant of cellular differentiation, and adhesion molecules provide the spatial structure to the establishment of a polarised epithelium [6, 21]. The progression of the normal polarised epithelial phenotype to the malignant invasive phenotype could be attributed in part to a loss of intercellular adhesion mediated by E-cadherin, with a resulting increase in cell motility and loss of cell polarity. Recent studies have suggested that, in breast epithelia, other mechanisms should be able to establish apical/basal domains at the morphological level [8, 39], which probably are downregulated in some cases of DCIS, inducing loss of cell polarity without loss of E-cadherin expression. P-cadherin could be one of the proteins responsible for loss of cell polarity, since it mediates weaker and unstable cell–cell contacts that are easily broken and reformed [43], which could not maintain the differentiated epithelia. In this context, P-cadherin

Table 1 Correlation between P-, E- and N-cadherin expression and Van Nuys classification [31]

	P-cadherin		E-cadherin		N-cadherin	
	Positive	Negative	Positive	Negative	Positive	Negative
Total	23	46	59	7	9	64
GI	0 (0%)	10 (21.8%)	9 (15.3%)	1 (14.3%)	2 (22.2%)	9 (14.1%)
GII	3 (13.0%)	14 (30.4%)	16 (27.1%)	1 (14.3%)	1 (11.1%)	16 (25.0%)
GIII	20 (87.0%)	22 (47.8%)	34 (57.6%)	5 (71.4%)	6 (66.7%)	39 (60.9%)
P value	0.0047	0.7387	0.5933			

Table 2 Correlation between P-, E- and N-cadherin expression and the classification proposed by Holland et al. [15]. *Wd* well-differentiated tumours, *Id* intermediately differentiated tumours, *Pd* poorly differentiated tumours

	P-cadherin		E-cadherin		N-cadherin	
	Positive	Negative	Positive	Negative	Positive	Negative
Total	23	46	59	7	9	64
Wd	0 (0%)	9 (19.6%)	8 (13.6%)	1 (14.3%)	2 (22.2%)	8 (12.5%)
Id	2 (8.7%)	11 (23.9%)	12 (20.3%)	1 (14.3%)	1 (11.1%)	12 (18.8%)
Pd	21 (91.3%)	26 (56.5%)	39 (66.1%)	5 (71.4%)	6 (66.7%)	44 (68.7%)
P value	0.0105	0.9298	0.6676			

Table 3 Correlation between P-, E- and N-cadherin expression and cytonuclear pleomorphism (size, outline, chromatin, nucleoli, mitoses)

	P-cadherin		E-cadherin		N-cadherin	
	Positive	Negative	Positive	Negative	Positive	Negative
Total	23	46	59	7	9	64
Monomorphic	1 (4.3%)	8 (17.4%)	9 (15.3%)	1 (14.3%)	2 (22.2%)	8 (12.5%)
Pleomorphic	2 (8.7%)	16 (34.8%)	16 (27.1%)	1 (14.3%)	1 (11.1%)	17 (26.6%)
Marked pleomorphic	20 (86.9%)	22 (47.8%)	34 (57.6%)	5 (71.4%)	6 (66.7%)	39 (60.9%)
P value	0.0072	0.7387	0.509			

Table 4 Correlation between P-, E- and N-cadherin expression and the architectural differentiation (cell polarisation)

	P-cadherin		E-cadherin		N-cadherin	
	Positive	Negative	Positive	Negative	Positive	Negative
Total	23	46	59	7	9	64
Absent	18 (78.3%)	21 (45.6%)	35 (59.3%)	2 (28.6%)	4 (44.4%)	38 (59.4%)
Present	5 (21.7%)	25 (54.4%)	24 (40.7%)	5 (71.4%)	5 (55.6%)	26 (40.6%)
P value	0.01	0.1212	0.3962			

Table 5 Correlation between P-cadherin expression and size of the tumour, estrogen receptor status, and c-erbB-2, p53 and cyclin D1 positive expression

	P-cad+	P-cad–	*P* value	E-cad+	E-cad–	*P* value	N-cad+	N-cad–	*P* value
Size (mm)	41.9±34.2 (20)	28.3±26.0 (43)	0.0871	35.1±30.2 (55)	13.2±9.4 (6)	0.086	17.5±13.8 (8)	31.7±29.5 (54)	0.1869
ER	39.1% (9/23)	80.0% (36/45)	0.0008	67.2% (39/58)	85.7% (6/7)	0.3172	66.7% (6/9)	68.3% (43/63)	0.9239
c-erb-B2	86.9% (20/23)	57.7% (26/45)	0.015	67.8% (40/59)	50.0% (3/6)	0.3801	77.8% (7/9)	65.1% (41/63)	0.4497
P53	39.1% (9/23)	17.7% (8/45)	0.0544	20.3% (12/59)	28.6% (2/7)	0.6144	44.4% (4/9)	22.2% (14/63)	0.1498
Cyclin D1	82.6% (19/23)	80.4% (37/46)	0.8277	76.3% (45/59)	100% (7/7)	0.1465	88.9% (8/9)	78.1% (50/64)	0.4543
Total	23	46		59	7		9	64	

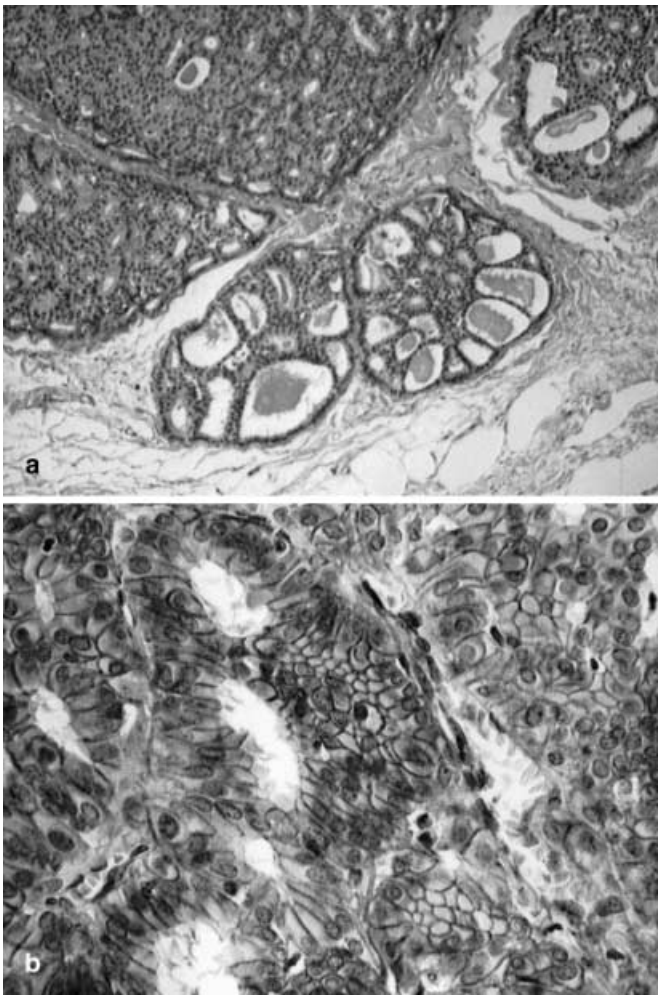

Fig. 2 **a** Ductal carcinoma in situ (DCIS) of the breast with low histological grade (well differentiated). Haematoxylin and eosin ×200. **b** Cell-membrane pattern of E-cadherin expression in a well-differentiated DCIS of the breast; ×400

aberrant expression in E-cadherin positive cells could interfere with the normal adhesion system.

In addition, the results provide evidence that P-cadherin is probably involved in early steps of breast carcinogenesis, activating mechanisms responsible for cell proliferation, which is higher in cells of poorly differentiated DCIS [23]. In fact, P-cadherin constitutes a molecule that is always present in normal cells with high proliferation rate, like the basal layers of stratified epithelia.

The expression of P-cadherin by breast cancer cells has been explained by several hypotheses. Palacios et al. suggested that its expression in breast carcinomas could indicate a proliferative ability acquired by tumour cells with high mitotic index, to respond to E-cadherin downregulation and to maintain cancer cells nests [25]. An alternative is that P-cadherin could be a member of an oncofetal protein family, since it is highly present in embryogenesis stages and weakly and focally expressed in the adult tissues [25]. More recently, Soler et al. advanced that the expression of P-cadherin by tumour cells could be related to a histogenetic origin in cap cells or in the acquisition of a phenotype with characteristics similar to this type of cell [27]. Cap cells constitute a single layer of growing cells located at the tip of the end buds during the development of mammary glands and represent a stem cell population in the adult breast, specialised in paving the way for ductal elongation as well as serving as precursors to myoepithelial cells [30]. The higher proliferation rate of cap cells, the absence of ER expression and the ability to differentiate into myoepithelial cells suggest that they could be responsible for development of some types of breast cancer cells [27, 30, 31].

The association between E-cadherin expression and DCIS histological grade was not statistically significant. In contrast with lobular carcinoma in situ (LCIS), where E-cadherin alterations [mutations and loss of heterozygosity (LOH)] are frequently present indicating that this is an early event in lobular neoplasia [40], only 7 of our 73 cases of DCIS were negative for E-cadherin. Some authors have recorded a correlation between reduced expression of E-cadherin and the grade of malignancy of DCIS [10], but most of them have failed to find any relationship [1, 22]. Recent studies have demonstrated that E-cadherin immunostaining could be a valuable tool in the distinction between DCIS and LCIS, since the former are usually E-cadherin positive [16, 20]. With regard to N-cadherin expression in breast DCIS, it failed to correlate with histological grade or any other factor, as reported recently in invasive cases [27].

The distinct patterns of P-, E- and N-cadherin expression observed in this study suggest a differential role for these cadherins in DCIS. We conclude that P-cadherin expression in DCIS is associated with a high histological grade, probably due to loss of cell polarisation and increase of proliferation, and it seems to be more relevant in DCIS pathogenesis than the altered expression of any other cadherin, including the decrease of E-cadherin expression.

References

1. Bánkfalvi À, Terpe H-J, Breukelmann D, Bier B, Rempe D, Pschadka G, Krech R, Lellè R-J, Boecker W (1999) Immunophenotypic and prognostic analysis of E-cadherin and β-catenin expression during breast carcinogenesis and tumour progression: a comparative study with CD44. Histopathology 34:25–34
2. Berx G, Cleton-Jansen AM, Nollet F, de Leeuw WJ, van de Vijver M, Cornelisse C, van Roy F (1995) E-cadherin is a tumour/invasion suppressor gene mutated in human lobular breast cancers. EMBO J 14:6107–6115
3. Berx G, Cleton-Jansen AM, Strumane K, de Leeuw WJ, Nollet F, van Roy F, Cornelisse C (1996) E-cadherin is inactivated in a majority of invasive human lobular breast cancers by truncation mutations throughout its extracellular domain. Oncogene 13:1919–1925
4. Bukholm IK, Nesland JM, Karesen R, Jacobsen U, Borresen-Dale AL (1998) E-cadherin and alpha-, beta-, and gamma-catenin protein expression in relation to metastasis in human breast carcinoma. J Pathol 185:262–266

5. Bukholm IK, Nesland JM, Borresen-Dale AL (2000) Re-expression of E-cadherin, alpha-catenin and beta-catenin, but not of gamma-catenin, in metastatic tissue from breast cancer patients. J Pathol 190:15–19
6. Fish EM, Molitoris BA (1994) Alterations in epithelial polarity and the pathogenesis of disease states. N Engl J Med 330: 1580–1588
7. Gamallo C, Palacios J, Suarez A et al (1993) Correlation of E-cadherin expression with differentiation grade and histological type in breast carcinoma. Am J Pathol 142:987–993
8. Gonzalez MA, Pinder SE, Wencyk PM, Bell JA, Elston CW, Nicholson RI, Robertson JFR, Blamey RW, Ellis IO (1999) An immunohistochemical examination of the expression of E-cadherin, α- and β/γ-catenins, and α2- and β1-integrins in invasive breast cancer. J Pathol 187:523–529
9. Grunwald GB (1993) The structural and functional analysis of cadherin calcium-dependent cell adhesion molecules. Curr Opin Cell Biol 5:797–805
10. Gupta SK, Douglas-Jones AG, Jasani B, Morgan JM, Pignatelli M, Mansel RE (1997) E-cadherin (E-cad) expression in duct carcinoma in situ (DCIS) of the breast. Virchows Arch 430:23–28
11. Han AC, Peralta-Soler A, Knudsen KA, Wheelock MJ, Johnson KR, Salazar H (1997) Differential expression of N-cadherin in pleural mesotheliomas and E-cadherin in lung adenocarcinomas in formalin-fixed, paraffin-embedded tissues. Hum Pathol 28:641–645
12. Han AC, Soler AP, Knudsen KA, Salazar H (1999) Distinct cadherin profiles in special variant carcinomas and other tumors of the breast. Hum Pathol 30:1035–1039
13. Han AC, Soler AP, Tang CK, Knudsen KA, Salazar H (2000) Nuclear localization of E-cadherin expression in Merkel cell carcinoma. Arch Pathol Lab Med 124:1147–1151
14. Hazan RB, Phillips GR, Qiao RF, Norton L, Aaronson SA (2000) Exogenous expression of N-cadherin in breast cancer cells induces cell migration, invasion, and metastasis. J Cell Biol 148:779–790
15. Holland R, Peterse JL, Millis RR, Eusebi V, Faverly D, van de Vijver MJ, Zafrani B (1994) Ductal carcinoma in situ: a proposal for a new classification. Semin Diagn Pathol 11:167–180
16. Jacobs TW, Pliss N, Kouria G, Schnitt SJ (2001) Carcinoma in situ of the breast with indeterminate features: role of E-cadherin staining in categorization. Am J Surg Pathol 25:229–236
17. Knudsen KA, Myers L, McElwee SA (1990) A role for the Ca2(+)-dependent adhesion molecule, N-cadherin, in myoblast interaction during myogenesis. Exp Cell Res 188:175–184
18. Larue L, Antos C, Butz S, Huber O, Delmas V, Dominis M, Kemler R (1996) A role for cadherins in tissue formation. Development 122:3185–3194
19. Leal CB, Schmitt FC, Bento MJ, Maia NC, Lopes CS (1995) Ductal carcinoma in situ of the breast. Cancer 75:2123–2131
20. Maluf HM, Swanson PE, Koerner FC (2001) Solid low-grade in situ carcinoma of the breast: role of associated lesions and E-cadherin in differential diagnosis. Am J Surg Pathol 25: 237–244
21. Molitoris BA, Nelson WJ (1990) Alterations in the establishment and maintenance of epithelial cell polarity as a basis for disease process. J Clin Invest 85:3–9
22. Moll R, Mitze M, Frixen UH, Birchmeier W (1993) Differential loss of E-cadherin expression in infiltrating ductal and lobular breast carcinomas. Am J Pathol 143:1731–1742
23. Mommers EC, van Diest PJ, Leonhart AM, Meijer CJ, Baak JP (1999) Balance of cell proliferation and apoptosis in breast carcinogenesis. Breast Cancer Res Treat 58:163–169
24. Nieman MT, Prudoff RS, Johnson KR, Wheelock MJ (1999) N-cadherin promotes motility in human breast cancer cells regardless of their E-cadherin expression. J Cell Biol 147: 631–643
25. Palacios J, Benito N, Pizarro A, Suarez A, Espada J, Cano A, Gamallo C (1995) Anomalous expression of P-cadherin in breast carcinoma. Correlation with E-cadherin expression and pathological features. Am J Pathol 146:605–612
26. Peralta Soler A, Knudsen KA, Jaurand MC, Johnson KR, Wheelock MJ, Klein-Szanto AJ, Salazar H (1995) The differential expression of N-cadherin and E-cadherin distinguishes pleural mesotheliomas from lung adenocarcinomas. Hum Pathol 26:1363–1369
27. Peralta Soler A, Knudsen KA, Salazar H, Han AC, Keshgegian AA (1999) P-cadherin expression in breast carcinoma indicates poor survival. Cancer 86:1263–1272
28. Rasbridge SA, Gillett CE, Sampson SA, Walsh FS, Millis RR (1993) Epithelial (E-) and placental (P-) cadherin cell adhesion molecule expression in breast carcinoma. J Pathol 169: 245–250
29. Redies C, Engelhart K, Takeichi M (1993) Differential expression of N- and R-cadherin in functional neuronal systems and other structures of the developing chicken brain. J Comp Neurol 333:398–416
30. Sapino A, Macri L, Gugliotta P, Pacchioni D, Liu YJ, Medina D, Bussolati G (1993) Immunophenotypic properties and estrogen dependency of budding cell structures in the developing mouse mammary gland. Differentiation 55:13–18
31. Sapino A, Macri L, Tonda L, Bussolati G (1993) Oxytocin enhances myoepithelial cell differentiation and proliferation in the mouse mammary gland. Endocrinology 133:838–842
32. Shimoyama Y, Hirohashi S, Hirano S, Noguchi M, Shimosato Y, Takeichi M, Abe O (1989) Cadherin cell-adhesion molecules in human epithelial tissues and carcinomas. Cancer Res 49:2128–2133
33. Schmitt FC, Figueiredo P, Lacerda M (1995) Expression of c-erbB-2 protein and DNA ploidy in breast carcinogenesis. Arch Pathol Lab Med 119:815–820
34. Siitonen SM, Kononen JT, Helin HJ, Rantala IS, Holli KA, Isola JJ (1996) Reduced E-cadherin expression is associated with invasiveness and unfavorable prognosis in breast cancer. Am J Clin Pathol 105:394–402
35. Silverstein MJ, Lagios MD, Craig PH, Waisman JR, Lewinsky BS, Colburn WJ, Poller DN (1996) A prognostic index for ductal carcinoma in situ of the breast. Cancer 77:2267–2274
36. Soler AP, Knudsen KA (1994) N-cadherin involvement in cardiac myocyte interaction and myofibrillogenesis. Dev Biol 162:9–17
37. Soler AP, Knudsen KA, Tecson-Miguel A, McBrearty FX, Han AC, Salazar H (1997) Expression of E-cadherin and N-cadherin in surface epithelial-stromal tumors of the ovary distinguishes mucinous from serous and endometrioid tumors. Hum Pathol 28:734–739
38. Takeichi M (1990) Cadherins: a molecular family important in selective cell-cell adhesion. Annu Rev Biochem 59:237–252
39. Tan DS, Potts HW, Leong AC, Gillett CE, Skilton D, Harris WH, Liebmann RD, Hanby AM (1999) The biological and prognostic significance of cell polarity and E-cadherin in grade I infiltrating ductal carcinoma of the breast. J Pathol 189:20–27
40. Vos CBJ, Cleton-Jansen AM, Berx G et al (1997) E-cadherin inactivation in lobular carcinoma in situ of the breast: an early event in tumorigenesis. Br J Cancer 76:1131–1133
41. Wheelock MJ, Knudsen KA (1991) Cadherins and associated proteins. In Vivo:505–513
42. Wollner DA, Krzeminski KA, Nelson WJ (1992) Remodelling the cell surface distribution of membrane proteins during the development of epithelial cell polarity. J Cell Biol 116: 889–899
43. Wu JC, Gregory CW, De Philip RM (1993) P-cadherin and E-cadherin are co-expressed in MDCK cells. Biochem Biophys Res Commun 195:1329–1335

Virchows Arch (2002) 440:22–28
DOI 10.1007/s004280100480

ORIGINAL ARTICLE

Daniela Massi · Alessandro Franchi
Lorenzo Borgognoni · Milena Paglierani
Umberto Maria Reali · Marco Santucci

Tumor angiogenesis as a prognostic factor in thick cutaneous malignant melanoma

A quantitative morphologic analysis

Received: 29 January 2001 / Accepted: 10 May 2001 / Published online: 17 July 2001
© Springer-Verlag 2001

Abstract The prognostic value of the extent of neovascularization in cutaneous melanoma is a highly controversial issue. The aim of the current study was to evaluate whether the morphometric analysis of tumor vascularity may be helpful in predicting the clinical outcome of patients with thick cutaneous melanomas. A series of 15 patients with melanoma (>3 mm in thickness) who did not experience disease progression after long-term follow-up (10 years) and 30 matched controls who underwent recurrence and/or metastases were selected for the study. Microvessels were immunohistochemically stained with anti-CD31 antibody. Several parameters, including vessel number, vascular density, vessel area, equivalent circle diameter, perimeter, shape factor, compactness, and the number of vascular ramifications per 100 vessel sections, were quantitatively assessed by a computer-aided semi-automatic image analysis system. Mean vessel area was 341.69 μm^2 in cases without progression and 512.55 μm^2 in the progressed melanomas (P=0.008, Mann-Whitney U test). The mean equivalent circle diameter was 18.95 μm in non-progressed melanomas and 22.57 μm in progressed melanomas (P=0.009). The mean number of ramifications was 0.8 in cases without progression and 1.9 in the controls (P=0.03). Microvessel count and vascular density were higher in progressed cases (17.37 vs. 11.73 and 28.94/mm^2 vs. 19.55/mm^2, respectively), but the difference did not reach statistical significance (P=0.06). Our results suggest that neovascularization is a critical event in the progression of thick melanoma. Its prognostic significance is better assessed by quantification of vessel area, equivalent circle diameter, and microvessel branching, whereas microvessel count and vascular density do not provide significant prognostic information.

Keywords Angiogenesis · Neovascularization · Image analysis · Morphometry · Melanoma · Prognosis

D. Massi · A. Franchi · M. Paglierani · M. Santucci (✉)
Dipartimento di Patologia Umana ed Oncologia,
Università degli Studi di Firenze, Viale G.B. Morgagni, 85,
50134 Florence, Italy
e-mail: Marco.Santucci@unifi.it
Tel.: +39-055-432144, Fax: +39-055-4379868

L. Borgognoni · U.M. Reali
U.O. di Chirurgia Plastica e Ricostruttiva,
Azienda Sanitaria di Firenze, Florence, Italy

Introduction

It has been well established that the growth of a solid tumor requires the development of a tumor microvascular network [10]. In addition, increasing formation of new blood vessels is assumed to be associated with a tumor's aggressiveness and unfavorable prognosis [13, 23, 24]. This notion has been confirmed by the finding that a high intratumoral microvessel density correlates directly with metastasis and inversely with patient survival in breast, prostate, head-and-neck, non-small-cell lung carcinomas, and in a variety of other solid tumors. As regards cutaneous melanoma, this correlation is less straightforward and data available thus far are still uncertain. In earlier studies, it was suggested that increased tumor vascularity, as determined by percentage of vascular area at the tumor base, has prognostic significance in lesions of intermediate thickness [21], and these results were subsequently confirmed by others [18]. Moreover, the extent of vascularization, expressed as mean vessel number, was found to be predictive of metastasis and death in thin (≤0.75 mm) melanomas [12]. It has also been reported that angiogenesis may have a key role in the process of metastasis of thin melanomas exhibiting extensive histopathological regression [2, 3]. Yet, more recent studies provided evidences against the prognostic value of tumor vascularity in cutaneous melanoma [5, 14]. Conceivably, such contradictory results are due to heterogeneous patients' databases and are possibly related to the differences and objective difficulties in quantifying vascularization in terms of the methodologies used to stain and to count the microvessels. In this regard,

most studies have evaluated vascular structures by manual counting, whereas few investigators have attempted to obtain more objective and reliable results by using image analysis for quantification.

Thick cutaneous melanomas (>3 mm) are in general associated with a poor clinical outcome; however, some patients survive far longer than expected [1, 15, 20]. Because thickness cannot serve as the only predictor of disease course in the individual patient, further studies aimed at identification of other variables which might be prognostically helpful are clearly needed.

The goal of the current study was to investigate the prognostic value of angiogenesis in thick (>3 mm) cutaneous melanoma by comparing two groups of patients with diverse outcomes. Besides microvessel density, several additional morphometric parameters related to the size and shape of each intratumoral vascular profile were evaluated by a semi-automatic computer-aided image analysis system.

Materials and methods

Selection of patients and specimens

From 1975 to 1994, 982 consecutive patients with primary cutaneous malignant melanoma were treated at the Division of Plastic and Reconstructive Surgery, Azienda Sanitaria Firenze. Among them, 195 (19.8%) melanomas >3 mm in thickness were evaluated. The patients' charts were analyzed for age at diagnosis, sex, and location of the tumor. Histopathological slides were reviewed for the following parameters: histological type and level of invasion, respectively, assigned and categorized according to the guidelines of Clark et al. [7]; tumor thickness, determined according to the method suggested by Breslow [4]; histological regression, presence of ulceration, vascular invasion, presence of microscopic satellites, tumor invasive front (labeled as pushing or infiltrating) [15], and mitotic rate/mm^2, determined by the method of Schmoeckel and Braun-Falco [19] and using the cut-off values proposed by Clark et al. [8].

Patients lost to follow-up or with no histological material available for revision were dropped from the study. Among the 140 cases that could be evaluated, a total of 15 patients with melanoma (>3 mm in thickness) who did not experience disease progression after long-term follow-up (10 years) were enrolled in the study. There were seven men and eight women; the median age was 56 years (range 35 to 67 years). Tumor thickness ranged from 3.1 to 8 mm (mean 4.3 mm; median 3.3 mm); the other clinicopathological features are summarized in Table 1. Living patients were followed for from 118 to 205 months, with a median of 154 months. Thirty patients with invasive melanomas >3 mm in thickness who underwent disease progression, i.e., cutaneous recurrence and/or distant metastasis, were selected as control group. The control subjects were matched to the cases, when possible, by 5-year age groups, sex, histotype, and tumor thickness. Among the progressed melanomas, only two cases showed recurrences at the site of the previous excision, and in both cases skin recurrences were followed by metastases to regional lymph nodes. The other patients experienced lymph node and/or distant metastases, the most common sites being lung, central nervous system, liver, and bone. Follow-up for living patients ranged from 55 and 144 months, with a median of 94 months.

Table 1 Clinicopathologic features of the whole series (*SSM* superficial spreading melanoma, *NM* nodular melanoma, *ALM* acral lentiginous melanoma)

Parameter	Cases (*n*=15)		Controls (*n*=30)		*P*
	(*n*)	(%)	(*n*)	(%)	
Sex					0.8
Male	7	46.6	15	50.0	
Female	8	53.4	15	50.0	
Site					0.6
Head and neck	2	13.3	4	13.3	
Upper extremity	2	13.3	1	3.3	
Trunk	7	46.7	14	46.6	
Lower extremity	3	20.0	9	30.0	
Volar/subungueal	1	6.7	2	6.8	
Histotype					0.7
SSM	10	66.7	17	56.6	
NM	4	26.6	11	36.6	
ALM	1	6.7	2	6.8	
Level					0.7
III	1	6.7	3	10	
IV	14	93.3	26	86.7	
V	0	0.0	1	3.3	
Regression					0.1
Absent	0	0.0	4	13.3	
Present	15	100	26	86.7	
Ulceration					0.3
Absent	6	40.0	8	26.7	
Present	9	60.0	22	73.3	
Vascular invasion					0.7
Absent	14	93.3	27	90.0	
Present	1	6.7	3	10.0	
Microsatellites					1.0
Absent	14	93.3	28	93.3	
Present	1	6.7	2	6.7	
Invasive front					0.2
Pushing	12	80.0	19	63.4	
Infiltrating	3	20.0	11	36.6	
Mitotic rate/mm^2					0.5
0.1–6	7	46.6	11	36.6	
>6	8	53.4	19	63.4	

Immunohistochemistry

Immunohistochemical studies were performed on representative tumor tissue blocks of formalin-fixed, paraffin-embedded tissue. For the identification of microvessels, after digestion with protease XIV (Sigma Chemical Co., St. Louis, MO), the tissue sections were stained with a monoclonal antibody against CD31 antigen (clone JC/70A, Dako Corporation, Carpinteria, CA) at 1:20 dilution in PBS pH 7.4, for 60 min at room temperature. Primary antibody bound to antigen was detected with a standard streptavidin-biotin-peroxidase technique (Lab Vision Kit, Fremont, CA) and visualized with 3-amino-9-ethylcarbazole (Lab Vision) as chromogen. A light Mayer's hematoxylin was used as nuclear counterstain. Negative controls were performed by replacing the primary antibody with non-immune mouse serum. The immunohistochemically stained sections were evaluated without previous knowledge of the clinical outcome of each patient.

Evaluation of microvessel density and image analysis

For each melanoma case, we selected the histological slide in which the Breslow thickness was measured. In the corresponding CD31-stained slide, the area with the highest density of distinct CD31-positive vascular profiles, was determined at low power (×40). In this "angiogenic hot spot" the number of profiles was evaluated with a ×10 objective and ×10 ocular, (average size 601,793.4 μm^2 per field) (Fig. 1). Because melanomas showed a

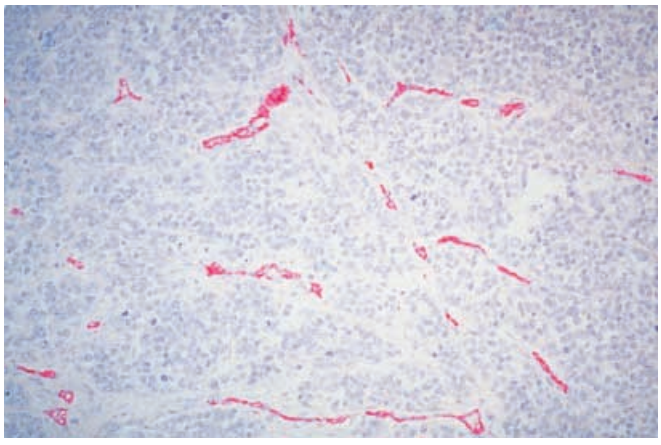

Fig. 1 Thick cutaneous melanoma showing numerous microvessels within the tumor mass. Each microvessel is highlighted by staining endothelial cells with anti-CD31 antibody (original magnification ×100)

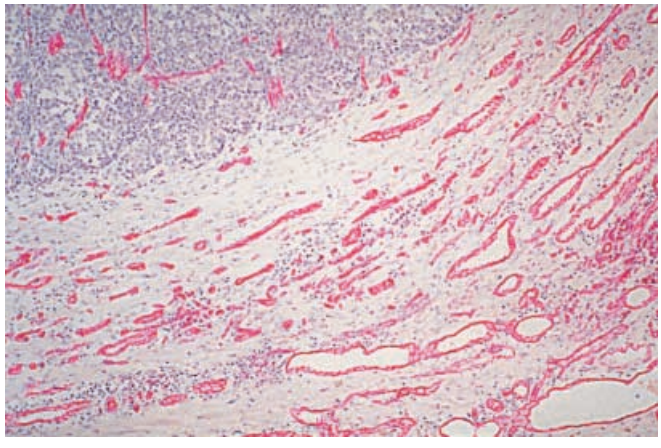

Fig. 2 The areas of clear-cut histological regression, preferentially located in the dermis underneath the tumor base, were not considered in the evaluation of tumor's microvessels (original magnification ×100)

heterogeneous distribution of blood vessels, an attempt was made to select the area of highest vascularization within the tumor mass at the advancing edge and to avoid the areas of clear-cut histological regression, preferentially located in the dermis underneath the tumor base (Fig. 2). Areas of the tumor adjacent to zones of ulceration and necrosis were also avoided. The presence of blood cells or fibrin without any detectable endothelial cell was not sufficient to define a microvessel. Any endothelial cell cluster consisting of two or more cells as well as large microvessels were included in the microvessel count. Branching structures were counted as one, unless there was a break in the continuity of the vessel, in which case it was counted as two distinct vessels. In each selected field, the outline of each individual stained vessel was identified and traced. For each case, the following morphometric microvascular parameters were estimated by a computer-aided image analysis system consisting of an image analyzer system (Quantimet, Leica Ltd., Cambridge, UK) coupled with a Leica DM LB microscope (Leica Qwin 2.32 software, Leica Ltd., Cambridge, UK):

1. Microvessel number, defined as the number of separate vascular profiles in a field
2. Vascular density, defined as the number of vessels per mm^2

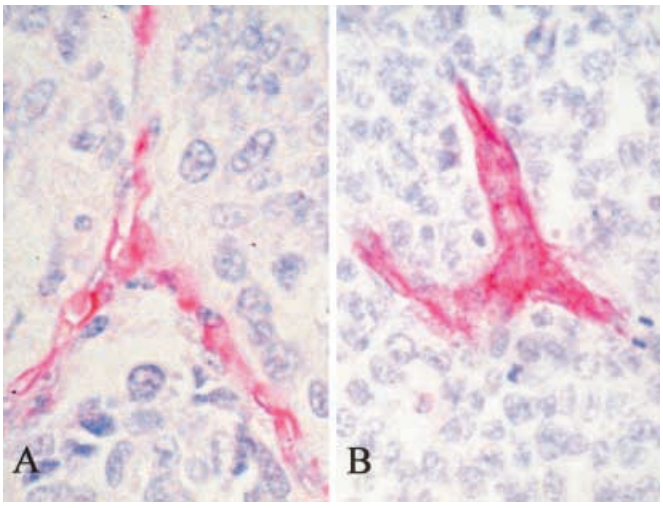

Fig. 3 **A** A new branch emerges from a parent vessel, forming a microvascular bifurcation (original magnification ×400); **B** Another Y-shaped microvessel bifurcation is seen within a highly vascularized area of a thick melanoma (original magnification ×400)

3. Equivalent circle diameter (μm), defined as $2\sqrt{(area/\pi)}$
4. Perimeter (μm)
5. Convex perimeter (μm)
6. Vessel area of each microvessel (μm^2)
7. Total vessel area (μm^2), corresponding to the sum of areas of all vascular profiles
8. Percentage of field area, defined as the percentage of positively stained vascular areas in a field
9. Compactness, expressed as $perimeter^2/area$
10. Shape factor, defined as $4\pi \times area/perimeter^2$, resulting in values between 0 and 1, closer to 1 meaning more circular
11. Vessel branching, expressed as the number of vascular ramifications per 100 vessel sections (Fig. 3).

Statistical analysis

The relationship between clinical and pathological variables was assayed by the two-tailed Fisher's exact test or by the two-tailed Pearson's chi-squared method. Differences in the mean values of tested parameters were evaluated by the Mann-Whitney U test. Disease-free and cause-specific survival rates were calculated according to the Kaplan-Meier method and their differences were evaluated by the log rank test. A *P* value less than 0.05 was considered statistically significant. Data analysis was performed with the SPSS statistical package, release 5.0.1 (SPSS Inc., Chicago, IL).

Results

The two patients groups did not differ with reference to mean age, sex, and tumor thickness. Because of the difficulty in collecting cases with long follow-up, not all of the pairs were perfectly matched by anatomical site and level. However, there were no significant differences between cases and controls as concerns these variables as well as the other histopathological parameters evaluated (Table 1). With regard to tumor vascularity, the most relevant results of the morphometric analysis are summarized in Table 2. Significant differences between the two groups were found as concerns vessel area,

Table 2 Distribution of microvascular parameters in the whole series. Mean values ± standard deviations

Parameter	Cases (*n*=15)	Controls (*n*=30)	*P*
Vessel number	11.73±6.05	17.37±11.53	0.06
Vascular density (mm^2)	19.55±10.08	28.94±19.22	0.06
Equivalent circle diameter (μm)	18.95±3.61	22.57±5.49	0.009
Perimeter (μm)	101.33±31.65	115.89±34.06	0.13
Convex perimeter (μm)	94.85±30.06	107.60±31.53	0.14
Vessel area (μm^2)	341.69±152.01	512.55±299.93	0.008
Total vessel area (μm^2)	4,113.39±2,688.85	8,668.76±6,408.19	0.01
Percentage of field area	0.68±0.44	1.43±1.06	0.01
Compactness	34.60±12.0	32.73±9.83	0.66
Shape factor	0.50±0.09	0.51±0.09	0.69
Vessel branching	0.8±1.08	1.9±1.84	0.03

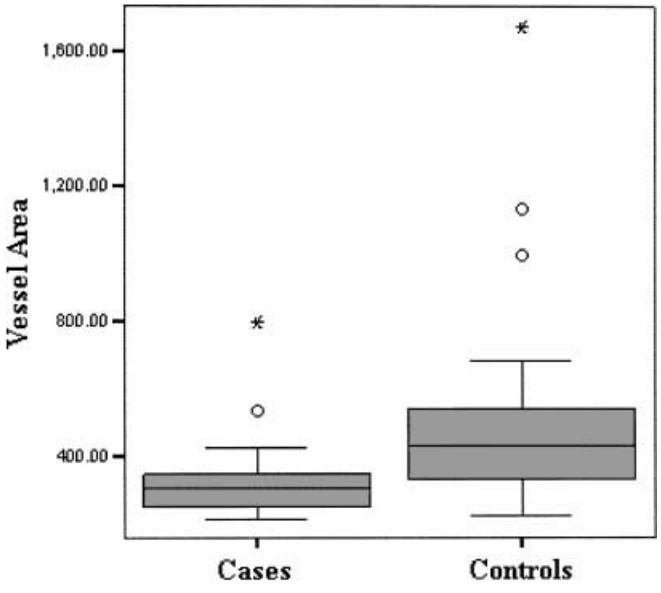

Fig. 4 Box plot for vessel area. Statistically significant lower values of mean vessel area were observed in melanomas without progression in comparison with the progressed melanomas (*P*=0.008). Box and whisker plot displaying median and interquartile range (*shaded area*) and largest and smallest values that are not outliers (*whiskers*). The box plot also includes two categories of cases with outlying values. Those values more than three box-lengths from the upper or lower edge of the box are called extreme values and are denoted by "*". Cases with values that are between 1.5 and 3 box lengths from the upper and lower edge of the box are called outliers and are designated with "°"

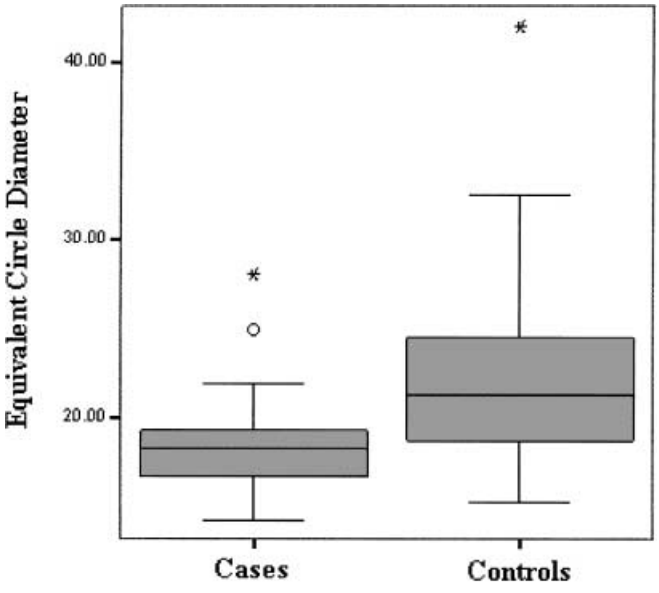

Fig. 5 Box plot for equivalent circle diameter. Statistically significant lower values of equivalent circle diameter was observed in non-progressed melanomas in comparison with progressed melanomas (*P*=0.009)

equivalent circle diameter, and number of ramifications, whereas statistical analysis revealed no significant differences regarding the distribution of the other parameters evaluated, including vessel number, vascular density, perimeter, convex perimeter, compactness, and shape factor. Figure 4 shows that statistically significant lower values of mean vessel area were observed in melanomas without progression in comparison with the progressed melanomas (*P*=0.008). Figure 5 shows that statistically significant lower values of equivalent circle diameter were observed in non-progressed melanomas in comparison with progressed melanomas (*P*=0.009). The prognostic significance of the various parameters was also assessed using the Kaplan-Meier method, which revealed a reduced disease-free survival in the subgroup of cases presenting with a higher mean vessel area (*P*=0.009) (Fig. 6). Similarly, a reduced disease-free survival was demonstrated in the subgroup of cases showing a higher equivalent circle diameter (*P*=0.003) (Fig. 7) and a higher number of vessel ramifications (*P*=0.02). When performing such analyses, the median value of each microvessel parameter was taken into consideration as a cut-off point for transforming the continuous variables into categorical values, and hence for splitting the whole series of patients into two groups. In the whole series, the presence of vascular invasion by neoplastic cells was significantly correlated with both the number of microvessels (*P*=0.01) and vascular density (*P*=0.01). No statistically significant correlation was found between microvascular parameters and other clinicopathological features investigated. In addition, no correlation was found between microvascular parameters and cause-specific survival.

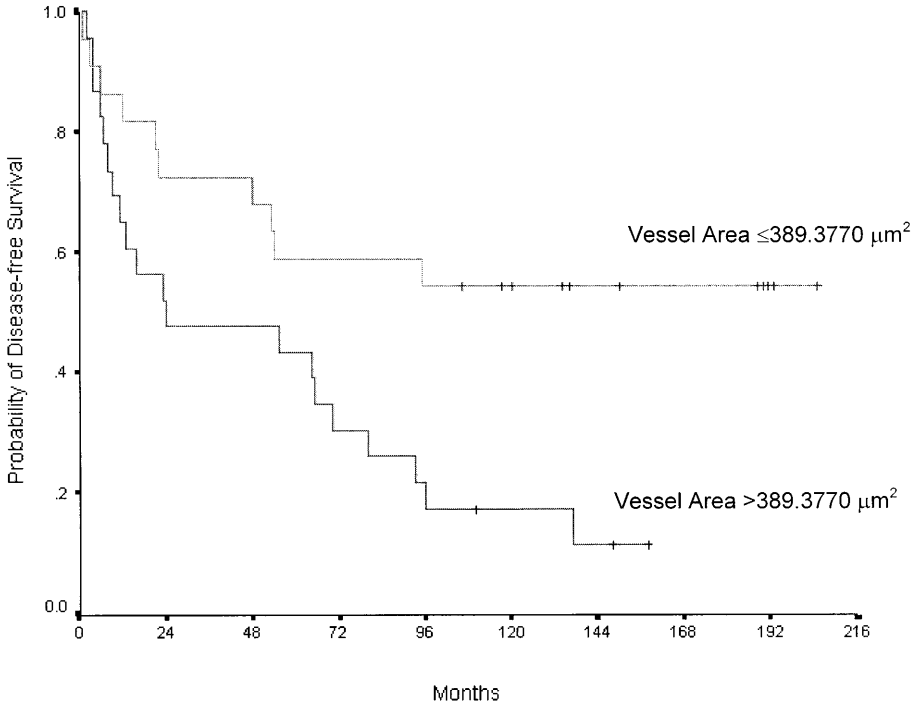

Fig. 6 Probability of disease-free survival by vessel area (P=<0.009). The median value (389.3770 μm²) was used as a cut-off to split the patients into two groups of tumors of high and low-microvessel area

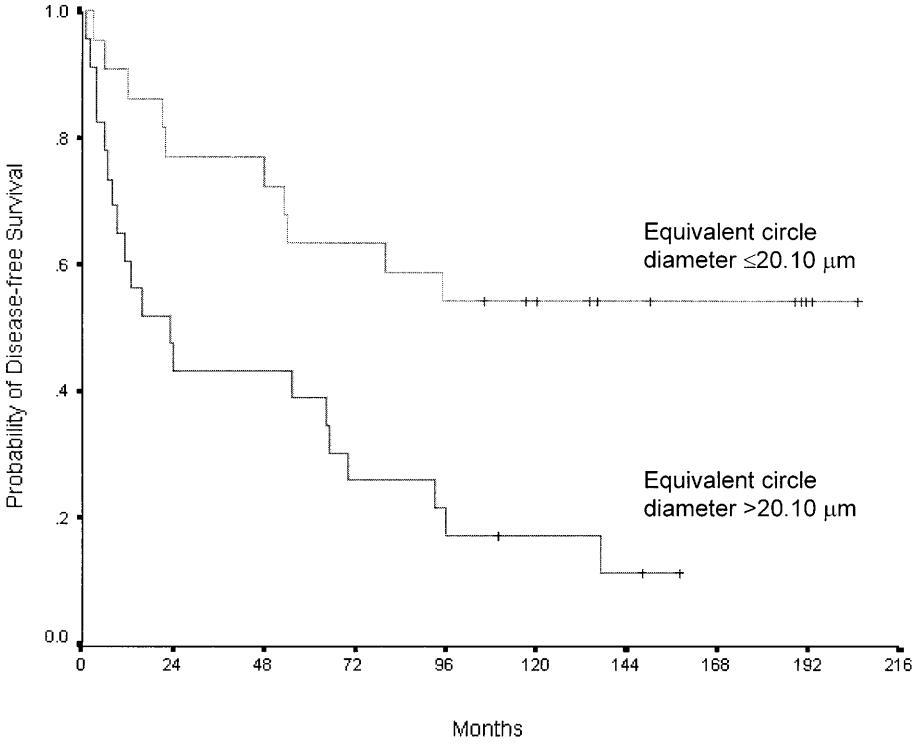

Fig. 7 Probability of disease-free survival by equivalent circle diameter (P=<0.003). The median value (20.10 μm) was used as a cut-off to split the patients into two groups of tumors with vessels of high and low-equivalent circle diameter

Discussion

To the best of our knowledge, the current study is the first in the literature to assess the prognostic significance of several morphometric parameters related to microvasculature in a large series of thick cutaneous malignant melanomas (>3 mm). Among these parameters, we found that the evaluation of the area occupied by microvessels provides significant prognostic information in terms of a melanoma's metastatic propensity. In fact, mean vessel area, total vessel area, percentage of field area, and equivalent circle diameter had significantly lower values in melanomas not undergoing disease progression in comparison with progressed melanomas. These results are in line with the original observations by Srivastava et al., who reported that percentage of vessel

area at the base of the tumor had prognostic significance in intermediate thickness melanomas [21]. It is conceivable that an increase in the microvessel size increases the overall vascular surface area and thereby the chance for tumor cells to enter in the circulation and to spread to distant body sites. Box plots comparing the values of vessel area and equivalent circle diameter, as shown in Figs 4 and 5, suggest that, although the highest values in the progressed melanomas exceeded the corresponding values of the non-progressed cases, a wide overlap still exists in the populations.

In our study, progressed melanomas had higher values of microvessel count and vascular density in comparison to the non-progressed cases, but the difference did not reach statistical significance, possibly due to the relatively small number of cases evaluated. The lack of correlation between microvessel count and microvessel density and prognosis in melanoma patients has been previously noted by others [5, 12]. Among them, Graham et al. demonstrated that there was no significant difference in the mean vessel number between thick melanomas (≥5.5 mm) that metastasized and resulted in death and matched melanoma cases that did not [12]. In our study we found a statistically significant association between microvessel number or microvessel density and vascular invasion. This finding is not surprising since these parameters are biologically related. As concerns the relationship between melanoma vascularity and thickness, in our study vascularity was not correlated to thickness, in agreement with previous observations by others [3, 6, 21].

To identify blood vessels, we employed anti-CD31 antibody, which has shown good specificity [16, 17, 22] and is currently regarded more sensitive than anti-FVIII-RAg and anti-CD34 for identifying endothelial cells. It should be pointed out that anti-CD31 antibody coats endothelial cells of both blood and lymphatic vessels. Hence, it is not possible to state with certainty to what extent lymphangiogenesis occurred and was involved in the process of melanoma dissemination. Indeed, it is well known that cutaneous melanoma has an initial preference for lymphatic spread. In this regard, however, de Waal et al., employing an immunostaining protocol which differentially highlights blood and lymphatic vessels, demonstrated that in thick melanoma an increase in blood vessels density is present whereas lymphatic density remains essentially unaltered [9].

When evaluating neovascularization in melanomas, an important issue to be discussed is that of regression. In fact, new blood vessel formation in the dermis is a known component of the regression response to cutaneous melanoma, as is a variable admixtures of lymphohistiocytes and melanophages, as well as a disruption of tumor cells with segmental replacement by fibrosis. There is no doubt that the presence of angiogenesis typically associated with the stromal response may account for the variable association reported in different studies between vascular counts and prognosis in cutaneous melanoma. For this reason, an attempt was made to select the area of highest vascularization within the tumor mass at the advancing edge and to avoid the areas of clear-cut histological regression, preferentially located in the dermis underneath the tumor base.

Interestingly, a statistically significant difference between cases and controls was observed as regards the presence of vascular branching in that melanomas not experiencing recurrences and/or metastases showed a lower number of vascular ramifications in comparison with progressed melanomas. The issue of the possible prognostic significance of microvascular branching as an expression of the complexity of the microvascular network has never been previously evaluated in thick cutaneous melanomas. As a possible explanation for our findings, it may be hypothesized that either a tumor with a metastatic potential induces the structure of a complex vascular pattern or there is an increased probability of vessel invasion and metastasis through a more complex microvascular network.

The results herein reported support the notion that neovascularization is a crucial event in the progression of thick melanoma. Although the evidence is largely experimental, it has been suggested that neovascularization could increase the vascular area that is the target of the invasive neoplastic cells, thus facilitating the metastatic process. In addition, endothelial cells could facilitate the growth of the primary neoplasm and increase its proliferative rate [10, 11]. This process could be enhanced by the “leaky” nature of newly formed blood vessels, making the vascular invasion step easier to accomplish.

In conclusion, our study has validated the hypothesis that neovascularity is an essential requirement for melanoma progression. The higher vascularization exhibited by tumors that recurred and/or metastasized could have potentially important clinical applications. However, in the individual patient, the quantitative assessment of neovascularity will have to be weighted with other prognostic indicators with the goal to separate those patients with a dismal prognosis from those with tumors of a more indolent clinical behavior.

References

1. Balch CM, Soong S, Shaw HM, McCarthy WH (1992) An analysis of prognostic factors in 8500 patients with cutaneous melanoma. In: Balch CM (ed) Cutaneous melanoma. Lippincott, Philadelphia, pp 165–187
2. Barnhill RL, Levy MA (1993) Regressing thin cutaneous malignant melanomas (≤1.0 mm) are associated with angiogenesis. Am J Pathol 143:99–104
3. Barnhill RL, Fandrey K, Levy MA, Mihm MC Jr, Hyman B (1992) Angiogenesis and tumor progression of melanoma. Quantification of vascularity in melanocytic nevi and cutaneous malignant melanoma. Lab Invest 67:331–337
4. Breslow A (1970) Thickness, cross-sectional area and depth of invasion in the prognosis of cutaneous melanoma. Ann Surg 172:902–908
5. Busam KJ, Berwick M, Blessing K, Fandrey K, Kang S, Karaoli T, Fine J, Cochran AJ, White WL, Rivers J, Elder DE, Wen DRP, Heyman BH, Barnhill RL (1995) Tumor vascularity is not a prognostic factor for malignant melanoma of the skin. Am J Pathol 147:1049–1056

6. Carnochan P, Briggs JC, Westbury G, Davies AJS (1991) The vascularity of cutaneous melanoma: a quantitative histological study of lesions 0.85–1.25 mm in thickness. Br J Cancer 64:102–107
7. Clark WH Jr, Fromm L, Bernardino EA, Mihm MC (1969) The histogenesis and biologic behaviour of primary human malignant melanomas of the skin. Cancer Res 29:705–727
8. Clark WH Jr, Elder DE, DuPont G IV, Braitman LE, Trock BJ, Schultz D, Synnestvedt M, Halpern AC (1989) Model predicting survival in stage I melanoma based on tumor progression. J Natl Cancer Inst 81:1893–1904
9. De Waal RMW, van Altena MC, Erhard H, Weidle UH, Nooijen PTGA, Ruiter DJ (1997) Lack of lymphangiogenesis in human primary cutaneous melanoma. Consequences for the mechanism of lymphatic dissemination. Am J Pathol 150:1951–1957
10. Folkman J (1990) What is the evidence that tumors are angiogenesis dependent? J Natl Cancer Inst 82:4–6
11. Folkman J, Watson K, Ingber D, Hanahan D (1989) Induction of angiogenesis during the transition from hyperplasia to neoplasia. Nature 339:58–61
12. Graham CH, Rivers J, Kerbel RS, Stankiewicz KS, White WL (1994) Extent of vascularization as a prognostic indicator in thin (<0.76 mm) malignant melanomas. Am J Pathol 145:510–514
13. Liotta LA, Steeg PS, Stetler-Stevenson WG (1991) Cancer metastasis and angiogenesis: an imbalance of positive and negative regulation. Cell 64:327–336
14. Llmonen S, Kariniemi AL, Vlaykova T, Muhonen T, Pyrhonen S, Asko-Seljavaara S (1999) Prognostic value of tumor vascularity in primary melanoma. Melanoma Res 9:273–278
15. Massi D, Borgognoni L, Franchi A, Martini L, Reali UM, Santucci M (2000) Thick cutaneous malignant melanoma: a reappraisal of prognostic factors. Melanoma Res 10:153–164
16. Miettinen M, Lindenmayer AE, Chaubal A (1994) Endothelial cell markers CD31, CD34, and BNH9 antibody to H- and Y-antigens: evaluation of their specificity and sensitivity in the diagnosis of vascular tumors in comparison with von Willebrand factor. Mod Pathol 7:82–90
17. Parums DV, Cordell JL, Micklem K, Heryet AR, Gatter KC, Mason DY (1990) JC70: a new monoclonal antibody that detects vascular endothelium associated antigen on routinely processed tissue sections. J Clin Pathol 43:752–757
18. Rongioletti F, Miracco C, Gambini C, Pastorino A, Tosi P, Rebora A (1996) Tumor vascularity as a prognostic indicator in intermediate-thickness (0.76–4 mm) cutaneous melanoma. Am J Dermatopathol 18:474–477
19. Schmoeckel C, Braun-Falco O (1978) Prognostic index in malignant melanoma. Arch Dermatol 114:871–873
20. Schneebaum S, Briele HA, Walker MJ, Greager J, Wood DK, Ronan SG, Patel MK, Das Gupta TK (1987) Cutaneous thick melanoma. Prognosis and treatment. Arch Surg 122:707–711
21. Srivastava A, Laidler P, Davies RP, Horgan K, Hughes LE (1988) The prognostic significance of tumor vascularity in intermediate-thickness (0.76–4.0 mm thick) skin melanoma. Am J Pathol 113:419–423
22. Vermeulen PB, Gasparini G, Fox SB, Toi M, Martin L, McCulloch P, Pezzella F, Viale G, Weidner N, Harris AL, Dirix LY (1996) Quantification of angiogenesis in solid human tumours: an international consensus on the methodology and criteria of evaluation. Eur J Cancer 32:2474–2484
23. Weidner N (1995) Intratumoral microvessel density as a prognostic factor in cancer. Am J Pathol 147:9–19
24. Weidner N (1998) Tumoural vascularity as a prognostic factor in cancer patients: the evidence continues to grow. J Pathol 184:119–122

Virchows Arch (2002) 440:29–35
DOI 10.1007/s004280100481

ORIGINAL ARTICLE

A. Skálová · M. Michal · R. H. W. Simpson · I. Stárek
J. Přádná · M. Pfaltz

Sclerosing polycystic adenosis of parotid gland with dysplasia and ductal carcinoma in situ

Report of three cases with immunohistochemical and ultrastructural examination

Received: 20 December 2000 / Accepted: 14 May 2001 / Published online: 30 June 2001
© Springer-Verlag 2001

Abstract We describe three cases of sclerosing polycystic adenosis (SPA) of the parotid gland, a salivary condition analogous to fibrocystic disease of the breast. For the first time, immunoreactivity for oestrogen and progesterone receptors was demonstrated, suggesting a possible participation of hormone stimulation in its pathogenesis. In addition, all our cases showed foci of dysplasia of the ductal epithelium, which in one case was severe enough to amount to carcinoma in situ. This feature that has not previously been reported in SPA.

Keywords Salivary gland · Sclerosing polycystic adenosis · Sialadenopathy · Dysplasia · Ductal carcinoma in situ

Introduction

Several neoplasms of the major salivary glands bear a strong histopathological resemblance to breast tumours, but, although similar, they are not quite identical. Most notably, salivary duct carcinoma is morphologically identical to mammary ductal carcinoma with invasive and in situ components, the latter often taking the form of comedocarcinoma [15]. Biologically, however, it is closer to prostatic adenocarcinoma as it is usually negative for oestrogen receptors and positive for androgen receptors [10]. Salivary epithelial–myoepithelial carcinoma [8, 18] is morphologically identical to adenomyoepithelioma of the breast [14], although the former is a true malignancy often with invasion and with a low but definite metastatic potential, whereas the breast lesion is benign with a tendency to recur; evolution of a high-grade malignancy has been described in both [1, 16]. Adenoid cystic carcinoma and pleomorphic adenoma are found in both organs, and collagenous spherulosis too has been described in the breast [3], and salivary glands, particularly in some types of myoepithelial cell-derived salivary tumours [11, 17]. Acinic cell carcinoma of the breast represents another example of this interesting phenomenon [5, 13].

Strangely, the most common breast condition, benign fibrocystic disease, was not thought to have a salivary counterpart, but recently sclerosing polycystic adenosis (SPA) was described as a distinctive pseudoneoplastic lesion of the major glands [7, 21] and it has many histological similarities to its mammary counterpart. Here, we describe three cases of SPA with focal epithelial dysplasia that ranged from mild atypia to low-grade ductal carcinoma in situ. This is a feature that has not previously been reported in SPA.

A. Skálová (✉) · M. Michal
Department of Pathology,
Medical Faculty of Charles University,
dr. E. Beneše 13, 305 99 Plzeň, Czech Republic
e-mail: skalova@fnplzen.cz
Tel.: +420-19-7402545, Fax: +420-19-7421561

R.H.W. Simpson
Department of Pathology,
Royal Devon and Exeter Hospital, Exeter, UK

I. Stárek
Department of Otorhinolaryngology,
Medical Faculty, Palacký University,
Olomouc, Czech Republic

J. Přádná
Department of Pathology,
District Hospital České Budějovice, Czech Republic

M. Pfaltz
Institute of Clinical Pathology,
University Hospital of Zürich, Switzerland

Materials and methods

The specimens were fixed in 10% formalin, embedded in paraffin and routinely stained with haematoxylin and eosin. Additional histochemical studies included periodic acid-Schiff (PAS), with and without prior diastase digestion, and mucicarmine stains. For electron microscopy, formalin-fixed wet tumour tissue samples of case 1 were washed in phosphate buffer, fixed briefly in 4% paraformaldehyde, postfixed in 1% osmium tetraoxide, and embedded in epoxy resin (Durcupan-Epon). Sections 1-µm thick were stained with uranyl acetate and lead citrate, and examined under an electron microscope.

Table 1 Antibodies used for immunohistochemical studies. *GCDFP-15* gross cystic fluid disease protein, *EMA* epithelial membrane antigen, *CEA* carcinoembryonal antigen, *MIA* anti-mitochondrial antigen

Antibodies	Clone	Dilution	Source
AE1/AE3		1:500	Boehringer Manheim
CAM 5.2		1:50	Becton-Dickinson, Mountain View
Muscle-specific actin	HHF-35	1:3000	Dako A/S, Glostrup, Denmark
Smooth muscle actin	1A4	1:1000	Dako A/S
Calponin		1:200	Dako A/S
MIA	113–1	1:100	Biogenex, San Ramon, Calif.
GCDFP-15 (BRST2)	D6 clone	1:2000	Signet Laboratories, Mass.
CD68	PGM1	1:100	Dako A/S
CD68	KP1	1:40	Dako A/S
CEA		1:800	Dako A/S
EMA		1:1000	Dako A/S
Oestrogen receptor		1:150	Novocastra, Newcastle upon Tyne, UK
Progesterone receptor		1:150	Novocastra
Ki67	MIB1	1:100	Immunotech, Marseille
Collagen type IV	CIV22	1:50	Dako A/S
S-100 protein	Polyclonal	1:100	Dako A/S
Anti-HER-2/neu Ab-17	Clone e2–4001and 3B5	1:2000	NeoMarkers, Fremont, Calif.

Immunohistochemical studies were performed on deparaffinized, formalin-fixed sections. The antibodies used are listed in Table 1. Specifically for the MIB1 antibody, and for oestrogen and progesterone receptor analyses, sections 4-µm thick were cut from the specimens and placed on slides coated with 3-aminopropyltriethoxy-silane (Sigma, St. Louis, Mo.). An antigen-unmasking technique, with which the sections were microwaved in an oven twice, each for 5 min at 700 W in citrate buffer (pH 6.0) was employed prior to incubation with the primary antibodies. The bound antibodies were visualised using the supersensitive streptavidin–biotin–peroxidase complex (Novocastra, Newcastle upon Tyne, UK), with 3,3-diaminobenzidine (Sigma) as chromogen.

Case reports

Clinical findings

Case 1

A 31-year-old woman was admitted to hospital for a slowly growing tender mass in her right parotid gland region, which she had noticed over the preceding 2 years. Grossly, the lesion measured 3×2.5×2 cm; it was hard in consistency, partly cystic, and freely mobile. A malignant parotid tumour was suspected clinically and a lateral superficial conservative parotidectomy was performed, sparing the facial nerve. The postoperative course was uneventful. No recurrence or other complaints have been experienced during a 3-year follow-up period, and the patient remains alive and well.

Case 2

A 27-year-old woman presented with a slowly growing painless retro-mandibular mass approximately 4.5×3×1.5 cm in size. The lesion was surgically removed from the right parotid gland. It was well circumscribed, firm in consistency, and measured 1.5 cm in maximum diameter. No abnormality was found in six adjacent cervical lymph nodes. The postoperative course was uneventful, and 4 years after surgery there are no signs of recurrence. This lesion was previously reported as *Case 3* in a series of sclerosing polycystic sialadenopathy by Donath et al. [7].

Case 3

A 9-year-old girl first presented to hospital with a mass at the angle of the left mandible, which had been present for 18 months. This was sometimes painful, particularly at night when lying on it in bed. On examination, there was a left parotid mass, 5 cm in diameter. It was spherical and slightly mobile but was not adherent to the skin or bone. Microscopic examination showed "calcular atrophy with sialadenitis". Six years later, a nodule was noted under the surgical scar. It was excised and reported as a pleomorphic adenoma. Thirteen years after that, she presented again with a "massive recurrence", although this has not yet been biopsied. Case 3 was taken from the consultation files, and sections were seen from both the original biopsy and the recurrence. Further tissue was not available for immunohistochemistry.

Microscopic findings

Histological examination in each of the three cases showed a well-circumscribed, partly encapsulated tumour with a peripheral rim of normal salivary gland tissue. Microscopically, the lesions were very similar; they demonstrated an abundant sclerotic collagenous stroma within which were ductal and acinar lobules composed of ectatic ducts, as well as smaller tubular and acinar structures arranged in a vaguely nodular pattern. The collagenous stroma was mostly hypocellular with focal lymphocytic infiltration and occasional lymphocytes encroaching upon the duct epithelium (Fig. 1). Many ducts were cystically dilated and the epithelium comprised flattened cuboidal cells (Fig. 1), but other ducts were lined by hyperplastic epithelium with intraluminal papillary projections. At higher power, smaller ducts and acini were seen to be composed mostly of large cells with abundant eosinophilic, amphophilic or clear cytoplasm. Many ducts contained large eosinophilic cells with abundant cytoplasm with rounded intraluminal projections suggestive of apocrine metaplasia (Fig. 2). The epithelial cells with apocrine morphology merged in places with vacuolated foam cells suggesting sebaceous differentiation (Fig. 2). A few ducts contained aggregates of foam cells within the lumina, and the same vacuolated cells were also observed focally within the collagenous stroma. A spectrum of vacuolated, foam, apocrine, mucous and acinic granular cells was often seen within the same duct or lobule (Fig. 3). Squamous metaplasia of the duc-

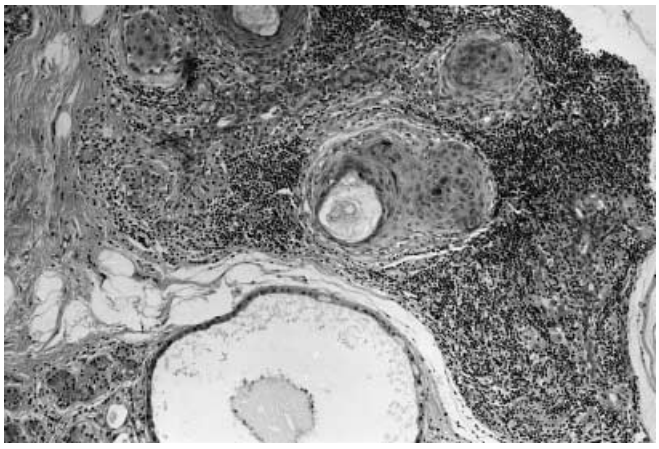

Fig. 1 The lesion is composed of tubular and acinar structures embedded in abundant sclerotic collagenous stroma with focal lymphocytic infiltration. Many ducts are cystically dilated and lined by flattened cuboidal epithelium. Haematoxylin-eosin, ×36

tal epithelium was identified in places. A very typical finding was partial preservation of some lobules, and these were composed of abnormal salivary serous acini consisting of large granular acinar cells with cytoplasm filled with numerous eosinophilic granules and globules. These were of various sizes, but often large, and they stained strongly with PAS (Fig. 4), as well as being faintly positive for mucicarmine. Among these foci of acinar differentiation, there were also cells with water-clear and vacuolated cytoplasm (Fig. 4).

Fig. 2 Dilated ducts are lined by apocrine cells. Epithelial cells with apocrine morphology merge in places with foamy and vacuolated cells resembling sebaceous differentiation. Haematoxylin-eosin, ×180

Fig. 3 A spectrum of vacuolated, foam, apocrine, mucous and acinic granular cells is seen within the same lobule. Heamatoxylin-eosin, ×360

Fig. 4 Irregular serous acini consisting of large acinic cells with abundant granular cytoplasm. Haematoxylin-eosin, ×180

Fig. 5 Focally, the ducts contain – in addition to foamy cells – hyperplastic intraluminal epithelium forming interconnecting bridges in a cribriform pattern. Haematoxylin-eosin, ×180

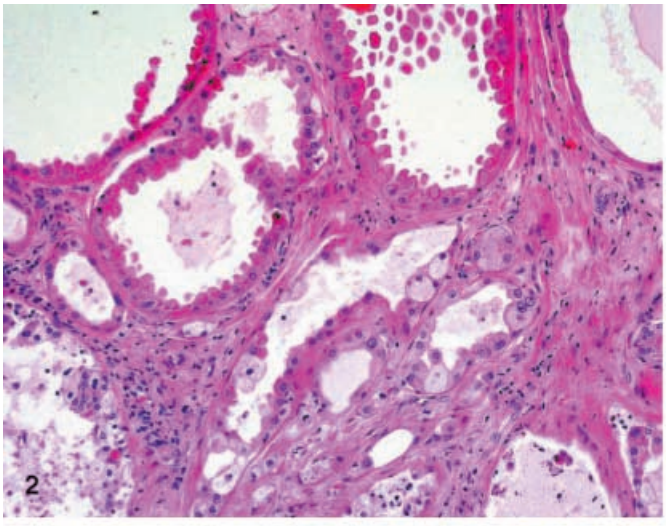

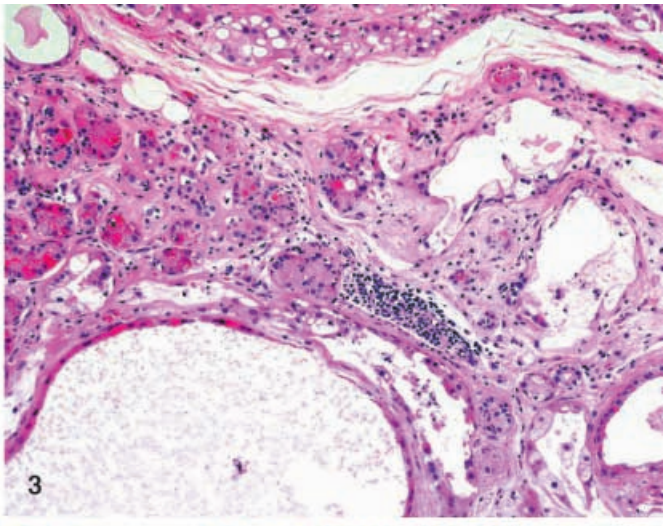

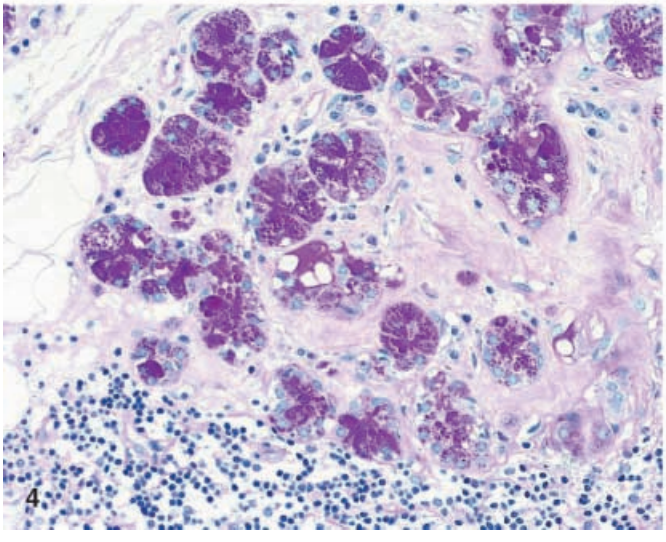

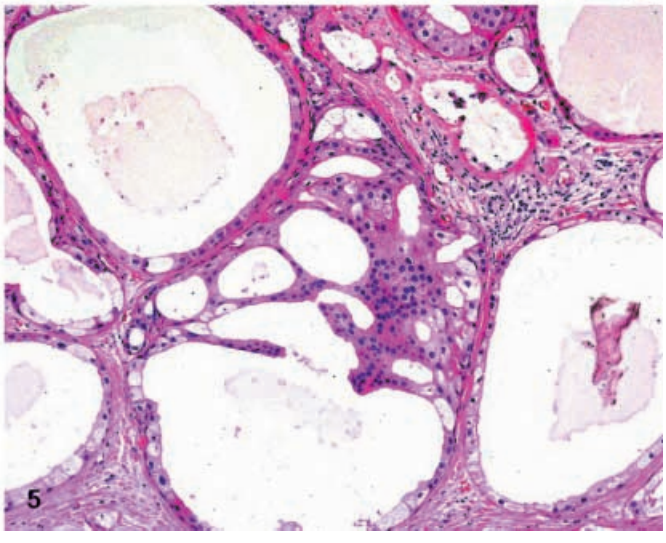

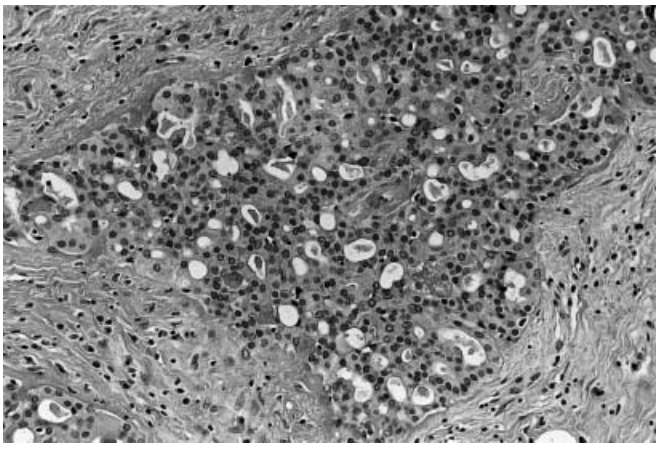

Fig. 6 Focal ductal in situ carcinoma pattern within the solid nest. Haematoxylin-eosin, ×180

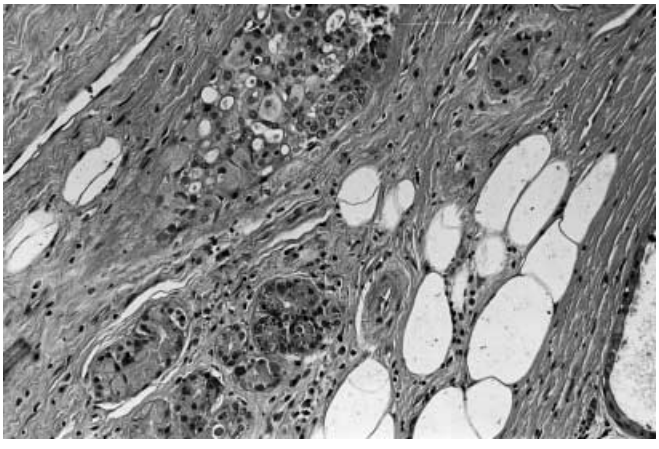

Fig. 7 Dysplastic cells in tiny aggregates and duct are embedded in collagenous stroma, thus suggesting invasive growth pattern. Haematoxylin-eosin, ×180

In all three cases, there were dilated ducts composed of hyperplastic intraluminal epithelium that formed interconnecting bridges in a cribriform pattern (Fig. 5). Within these solid and cribriform foci, the epithelial cells had eosinophilic or vacuolated cytoplasm and nuclei of different shapes and sizes. The nuclear atypia ranged from mild (cases 2 and 3) to severe (case 1) with changes focally amounting to ductal carcinoma in situ of low grade (Fig. 6). Tiny cell aggregates and small ducts composed of dysplastic cells were embedded within the collagenous stroma thus resembling an invasive growth pattern (Fig. 7). Furthermore, there was compression of the stroma to produce bundles of spindle cells mimicking nerves and perineural infiltration.

Immunohistochemical staining

Sections from cases 1 and 2 only were available for study. They showed that the ductal and acinar structures reacted uniformly for cytokeratins, as did the vacuolated and apocrine cells of the ductal lining epithelium. The foam cells that filled some lumina and formed stromal aggregates reacted with both anti-CD68 antibodies, but not cytokeratins. Epithelial membrane antigen (EMA) was positive in ductal and apocrine epithelium, while acinar cells were negative. Foam cells that were in contact with lining ductal epithelium were strongly positive for EMA, while intraluminal and stromal foam cells were negative. S-100 protein decorated most proliferating ductal cells and foci of dysplastic epithelium, but apocrine cells, the epithelial lining of ectatic ducts and foam cells did not react. Antimitochondrial antigen 113-1 was expressed in many eosinophilic ductal cells, including a few foam cells lining the ducts. GCDFP-15 was detected in the acinar cells with coarse eosinophilic granules, and also in the epithelium with apocrine-like "decapitation secretion" and in intraductal foam cells; other cells of the lesion were negative. Staining for carcinoembryonal antigen (CEA), and for oncoprotein HER2/neu/cerbB-2 was negative. Most epithelial cells of the cystic ducts, some foam cells lining the ducts, and the cells within the dysplastic foci expressed strong nuclear immunoreactivity for progesterone receptors (about 80%) while staining for oestrogen receptors was detected in about 20% of ductal cells in dysplastic foci only. Most ectatic ducts and serous acini were surrounded by continuous layers of myoepithelial cells that were decorated with S-100 protein, actin and calponin antibodies. Ducts filled with hyperplastic and dysplastic epithelium were mostly surrounded by intact layers of myoepithelial cells. Collagen type IV stained continuous basement membranes subjacent to ectatic and hyperplastic ductal structures, while no staining for collagen type IV was seen close to serous acini. Proliferative activity was low with the MIB1 index about 1%.

Electron microscopic examination

The ultrastructural appearance was variable. Most epithelial cells demonstrated features of secretory cells, and desmosomes were visible between adjacent epithelial cells (Fig. 8A, B). The cells displayed abundant round to oval secretory granules of various size and electron density. The cytoplasm of some cells was packed with large numbers of electron-dense secretory granules consistent

Fig. 8 **A** The secretory cell displays abundant structures of rough endoplasmic reticulum and many round to oval secretory granules of various size and electron density (×4000). **B** The cell shows mucous granules of varying morphology. Note large pale granules with a reticular or particulate content, dense granules, and an assortment of "bull's eye" granules with a central or eccentric core (*arrow*) set in a light or dense matrix (×4000). **C** The apocrine cell has the free surface covered by short widely spaced microvilli and the apical pole of the cytoplasm is filled with numerous electron-lucent secretory granules and empty vesicles (×4000). **D** Ballooned cells exhibit extensive vacuolisation of the cytoplasm (×4000) ▶

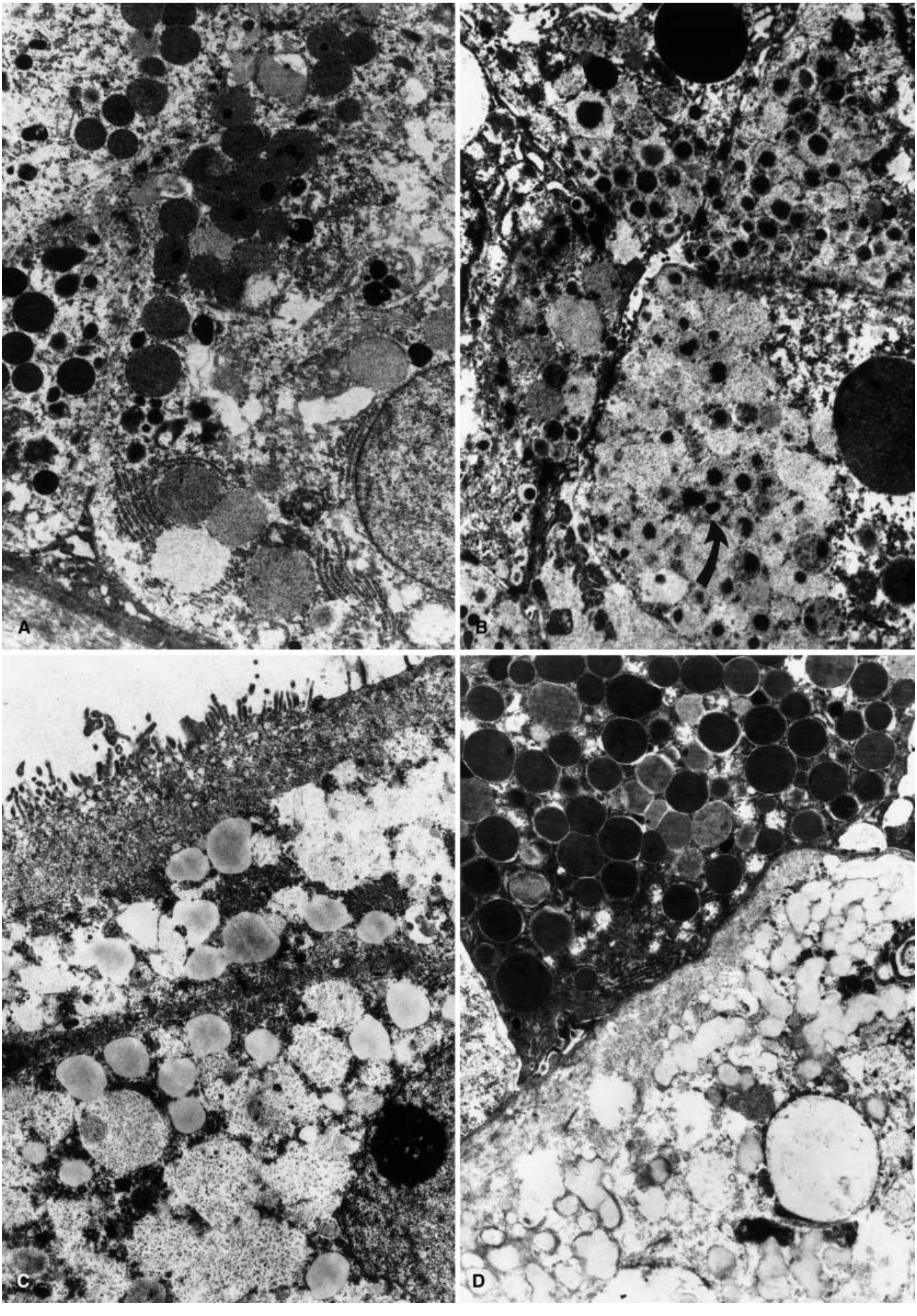
A
B
C
D

with zymogen granules (Fig. 8A), whilst others contained both electron-dense and lucent granules (Fig. 8B). The latter granules often demonstrated indefinite margins and irregular shapes, and many displayed a "bull's-eye" morphology (Fig. 8B). Rough endoplasmic reticulum was frequently prominent within the space between secretory granules (Fig. 8A). The apocrine cells had their free surfaces covered by short widely spaced microvilli and the apical pole of the cytoplasm was filled with numerous electron lucent secretory granules and empty vesicles (Fig. 8C). Ballooned cells exhibited extensive vacuolisation of the cytoplasm (Fig. 8D).

Discussion

Several non-neoplastic diseases and reactive lesions of the salivary glands can mimic malignant neoplasms, both clinically and histopathologically. For example, extensive squamous metaplasia in Warthin's tumour may be misinterpreted as squamous or mucoepidermoid carcinoma [6], and reactive changes in oncocytomas caused by fine needle aspiration injury can resemble acinic cell carcinoma [20]. SPA was first described by Smith et al. in 1996 as a slowly growing mass in the parotid gland suggestive of a neoplasm [21]. Most cases of SPA were initially misdiagnosed as tumours, such as mucoepidermoid and acinic cell carcinomas, cystadenocarcinoma, and pleomorphic adenoma. Similarly, the clinical impression in all our cases of SPA was a salivary gland neoplasm. The initial histopathological interpretation in case 1 was a low-grade cystadenocarcinoma with apocrine differentiation and in case 2 low-grade carcinoma most likely of mucoepidermoid type. Case 3 was diagnosed as pleomorphic adenoma, but, when it recurred, mucoepidermoid carcinoma was suspected.

SPA is quite rare; 21 cases have been published so far [2, 7, 21] and most histopathologists are not familiar with this lesion. Therefore, the lesion can represent a distinctive differential diagnostic problem. Major microscopic clues to a correct diagnosis include maintenance of the lobular architecture of the gland, ductal ectasia, scar-like hyalinised fibrous sclerosis, and a spectrum of foam, apocrine, granular, and mucous cells, in addition to the presence of tubuloacinar structures composed of large acinar cells with prominent brightly eosinophilic granules. In contrast, intraductal hyperplasia, particularly if associated with dysplasia as in our cases, may lead one to suspect a neoplastic process, but clues to the benign nature of SPA are that it is well-circumscribed, lacks an invasive growth pattern, and that mitotic/proliferative activity is low.

A particularly interesting finding in both our cases and previous studies of SPA is an overlapping spectrum of apocrine, vacuolated, foamy and sebaceous-like cells. The foam cells were observed floating free within the cystic lumina, clustered in the periductal stroma or in continuity with the epithelial lining of the glandular structures. An identical spectrum of cells showing apocrine morphology and abundant finely vacuolated cytoplasm (foam cells) is frequently found in most benign lesions of the breast, particularly in those associated with apocrine cystic changes and duct ectasia [4]. The origin of mammary foam cells has long been debated, and many morphological and immunohistochemical studies have supported either a histiocytic or an epithelial nature. Recently, Damiani et al. [4] used immunohistochemistry and in situ hybridisation to demonstrate a spectrum of phenotypes in mammary foam cells, from epithelial-apocrine cells to macrophage-derived phagocytic cells. This phenomenon of overlapping between epithelial-apocrine, epithelial-oncocytic, and macrophagic phenotype may be more common than is now realised. In the salivary glands, we have demonstrated a similar combination of oncocytic, apocrine and foam cells in a series of oncocytic myoepitheliomas [19]. The most probable explanation is related to the well-known propensity of myoepithelial and ductal cells in mammary and salivary gland tissues to undergo metaplastic changes.

Electron microscopic examination confirmed secretory activity in most epithelial cells of the lesion. Neoplastic cells had abundant cytoplasm filled by electron-dense granules of various sizes consistent with zymogen granules. Moreover, the serous acini of SPA did not show histologically architectural and cytological features of normal salivary gland acini. They resembled acinic cell carcinoma differentiation with histological features strongly reminiscent of those seen in cases of acinic cell carcinoma of the breast [5, 13]. The electron-lucent granules with indefinite margins and irregular shapes are most probably identical to the empty vesicles, observed in studies of normal and neoplastic apocrine epithelium [9, 12].

The pathogenesis of SPA is uncertain. Most histological features, such as duct ectasia, sclerotic fibrosis, intraluminal epithelial proliferation, acinic cell hyperplasia, and metaplastic changes of the epithelium, point to a reactive postinflammatory process, and a pathogenetic relationship with juvenile recurrent chronic parotitis has been suggested [2]. However, microscopic resemblance to fibrocystic disease of the breast, and expression of oestrogen and progesterone receptors suggest that SPA of the salivary glands and fibrocystic disease of the breast may share a similar aetiological basis.

In our cases, we found a variable degree of dysplastic changes within the epithelium that ranged between mild atypia (cases 2 and 3) to focally severe dysplasia (case 1): the latter conformed to the established criteria of ductal carcinoma in situ in the breast. The presence of hyperplastic intraluminal ductal epithelium with minimal nuclear atypia was briefly mentioned by Smith et al. [21], but dysplasia such as in our cases has not so far been described in SPA. We have seen foci of dysplasia in all our cases, and the lesions illustrated in Fig. 2 and Fig. 5 by Smith et al. [21] are at least suspicious of cribriform pattern of carcinoma in situ very similar to our lesions. Two of our patients remained well without any

signs of disease within limited follow-up periods of 4 years and 3 years after surgery, whilst the third still has recurrent disease. Also there were two recurring cases in the report of Smith et al. [21] and two recurrences in that of Batsakis et al. [2]. It is noteworthy that recurrences occurred after 4.5 years and 9 years after excision in the series by Smith et al. [21] and after 6 years in our patient, while the mean follow-up period in recurrence-free patients from both previous series [2, 21] is only 30 months. We believe that the recurrence rate and occurrence of malignancy in the lesions called SPA is more frequent than expected before and we are convinced that SPA is a neoplastic lesion with a low-grade malignancy potential.

In conclusion, regardless of the causative mechanism, sclerosing polycystic adenosis of major salivary glands is a distinctive histopathological lesion that may simulate malignant tumours, both clinically and microscopically, and, despite possibly alarming features, such as epithelial hyperplasia and dysplasia, SPA seems to have a favourable outcome. However, reports of cases of SPA are still few, and more are needed to evaluate the biological nature of the lesion.

Acknowledgements The authors are most grateful to Dr. John Callaghan of Galway, Ireland, for information on case 3. We thank Dr. Hůlková and Professor Elleder (Department of Pathology, Medical Faculty of Charles University in Prague) for performing the immunohistochemistry with PGM1 and to Dr. Mukenšnabl for photographic assistance. We also very much appreciate the technical assistance with the electron microscopy by Mr. Dostál.

References

1. Alos A, Carrillo R, Ramos J, Baez JM, Mallofre C, Fernandez PL, Cardesa A (1999) High-grade carcinoma component in epithelial-myoepithelial carcinoma of salivary glands: clinicopathological, immunohistochemical and flow-cytometric study of three cases. Virchows Arch 434:291–299
2. Batsakis JG (1996) Sclerosing polycystic adenosis: newly recognized salivary gland lesion – a form of chronic sialadenitis? Adv Anat Pathol 3:298–304
3. Clement PB, Young RH, Azzopardi JG (1987) Collagenous spherulosis of the breast. Am J Surg Pathol 11:411–417
4. Damiani S, Cattani MG, Buonamici L, Eusebi V (1998) Mammary foam cells. Characterization by immunohistochemistry and in situ hybridization. Virchows Arch 432:433–440
5. Damiani S, Pasquinelli G, Lamovec J, Peterse JL, Eusebi V (2000) Acinic cell carcinoma of the breast: an imunohistochemical and ultrastructural study. Virchows Arch 437:74–81
6. Di Palma S, Simpson RHW, Skálová A, Michal M (1999) Metaplastic (infarcted) Warthin's tumour of the parotid gland: a possible consequence of fine needle aspiration biopsy. Histopathology 35:432–438
7. Donath K, Seifert G (1997) Sclerosierende polycystische Sialadenopathie. Eine seltene nichttumorose Erkrankung. Pathologe 18:368–373
8. Donath K, Seifert G, Schmintz R (1972) Zur Diagnose und Ultrastructur des tubularen Speichelgangcarcinoms. Epithelial-myoepitheliales Schaltstuckcarcinom. Virchows Arch A 356: 16–32
9. Eusebi V, Damiani S, Losi L, Millis RR (1997) Apocrine differentiation in breast epithelium. Adv Anat Pathol 4:139–155
10. Fan CY, Wang J, Barnes EL (2000) Expression of androgen receptor and prostatic specific markers in salivary duct carcinoma. An imunohistochemical analysis of 13 cases and review of the literature. Am J Surg Pathol 24:579–586
11. Michal M, Skálová A (1990) Collagenous spherulosis. A comment on its histogenesis. Pathol Res Pract 186:365–370
12. Pier WJ Jr, Garancis JC, Kuzma JF (1970) The ultrastructure of apocrine cells in intracystic papilloma and fibrocystic disease of the breast. Arch Pathol 89:446–452
13. Roncaroli F, Lamovec J, Zidar A, Eusebi V (1996) Acinic cell-like carcinoma of the breast. Virchows Arch A 429:69–74
14. Seifert G (1998) Are adenomyoepithelioma of the breast and epithelial-myoepithelial carcinoma of the salivary glands identical tumors? Virchows Arch 433:285–287
15. Simpson RHW, Clarke TJ, Sarsfield PTL, Babajews AV (1991) Salivary duct adenocarcinoma. Histopathology 18:229–235
16. Simpson RHW, Cope N, Skálová A, Michal M (1998) Malignant adenomyoepithelioma of the breast with mixed osteogenic, spindle cell, and carcinomatous differentiation. Am J Surg Pathol 22:631–636
17. Skálová A, Leivo I (1992) Extracellular collagenous spherulosis in salivary gland tumors. Arch Pathol Lab Med 116:649–653
18. Skálová A, Michal M (1990) Epimyoepithelial carcinoma of parotid gland. Zentralbl Allg Pathol Pathol Anat 136:715–718
19. Skálová A, Michal M, Ryška A, Simpson RHW, Kinkor Z, Walter J, Leivo I (1999) Oncocytic myoepithelioma and pleomorphic adenoma of the salivary glands. Virchows Arch 434:537–546
20. Skálová A, Stárek I, Michal M, Leivo I (1999) Malignancy-simulating change in parotid gland oncocytoma following fine needle aspiration. Report of three cases. Pathol Res Pract 195: 399–405
21. Smith BC, Ellis GL, Slater LJ, Foss RD (1996) Sclerosing polycystic adenosis of major salivary glands. A clinicopathologic analysis of nine cases. Am J Surg Pathol 20:161–170

Virchows Arch (2002) 440:36–44
DOI 10.1007/s004280100482

ORIGINAL ARTICLE

Brian Eyden · S. Sankar Banerjee

Spindle-cell squamous carcinoma exhibiting myofibroblastic differentiation

A study of two cases showing fibronexus junctions

Received: 5 December 2000 / Accepted: 14 May 2001 / Published online: 20 July 2001
© Springer-Verlag 2001

Abstract The features of two spindle-cell carcinomas of the dermis are described with special reference to the presence of fibronexus junctions in tumour cells. The cases were of a 78-year-old man with a left eye-lid tumour and a 78-year-old woman with a naso-labial fold tumour, who had been given radiotherapy 13 years earlier for a clinically diagnosed basal cell carcinoma. Both specimens were slightly ulcerated and polypoid. Histologically, invasive tumour consisted of interlacing fascicles of plump spindled and oval cells, which were positive for several anti-cytokeratin antibodies, epithelial membrane antigen, vimentin and smooth-muscle and muscle-specific actins. Ultrastructurally, tumour cells in both cases contained rough endoplasmic reticulum (prominent in case 1), tonofibrils, desmosomes and smooth-muscle type myofilaments with focal densities. Fibronexus junctions were also present, which correlated with positive staining for fibronectin. This is the first documentation of the fibronexus in epithelial tissue in vivo, and the first unambiguous demonstration in a spindle-cell carcinoma. It extends the known distribution of the fibronexus and expands the ultrastructural spectrum of squamous carcinoma.

Keywords Fibronexus · Spindle-cell · Squamous-cell-carcinoma · Myofibroblast · Electron microscopy

Introduction

Spindle-cell carcinoma is a variant of carcinoma in which epithelial features such as desmosomes and tonofibrils [3, 17, 25, 26, 30, 32, 34, 35, 39, 44, 47, 50, 57, 59, 61, 64, 66] may be co-expressed with organelles more usually associated with mesenchymal cells, i.e., abundant rough endoplasmic reticulum (rER) [1, 11, 14, 18, 21, 22, 28, 31, 36, 37, 38, 43, 45, 55, 56, 62, 63, 64, 65] and the myofilaments with focal densities typical of smooth-muscle cells [1, 2, 14, 16, 19, 24, 28, 37, 40]. rER and myofilaments, in addition to being found separately in fibroblasts and smooth-muscle cells, are co-localised in the myofibroblast. This cell also possesses the cell-to-matrix specialisation known as the fibronexus, which is so well developed and so frequently expressed on the surfaces of myofibroblasts in granulation tissue and tumour stroma [5, 6, 49] that it has been regarded as an important ultrastructural marker for these cells and their tumours [5, 6, 8, 9, 10, 15, 54, 58].

As with so many diagnostically useful organelles, however, the fibronexus is not entirely specific for the myofibroblast: structures with varying similarity to well-developed fibronexus junctions have been seen in several mesenchymal cells and lesions [4, 23, 27, 33, 42, 46, 51, 52, 53, 60]. The present paper provides evidence for the first unambiguously documented example of fibronexus junctions in an epithelial tissue in vivo and specifically a spindle-cell carcinoma, and discusses the significance of this wider distribution of the fibronexus.

B. Eyden (✉) · S.S. Banerjee
Department of Histopathology, Christie Hospital NHS Trust, Manchester M20 4BX, United Kingdom
e-mail: Brian.Eyden@christie-tr.nwest.nhs.uk
Tel.: +44-161-4463292, Fax: +44-161-4463300

Materials and methods

Both lesions were fixed in phosphate-buffered histological formalin, and tissue was available for light and electron microscopy. After fixation, tumour tissue was dehydrated in ethanol and embedded in paraffin wax. Sections cut at 4 μm were stained with haematoxylin and eosin. Immunohistochemical studies were performed using the streptavidin-peroxidase complex technique with diaminobenzidine as chromogen. The antibodies used are listed in Table 1. Appropriate positive and negative controls were used throughout. For electron microscopy, tissue was retrieved from histological formalin, osmicated, stained en bloc with uranyl acetate, dehydrated in ethanol, and embedded in agar 100 epoxy resin. Ultrathin sections were stained with uranyl acetate and lead citrate, and examined in a JEOL JEM-1220 electron microscope.

Table 1 Immunohistochemical reagents, dilutions and commercial sources

Antibody	Dilution	Commercial source
MNF116[a]	1/80	Dako, Ely, UK
AE1/3[a]	1/200	Biogenex, Upton-on-Severn, UK
CK1[a]	1/20	Dako, Ely, UK
34βE12[a]	1/50	Dako, Ely, UK
CAM5.2[a]	1/20	Becton-Dickinson, Oxford, UK
Anti-cytokeratin-14	1/400	Sigma, Poole, UK
Anti-EMA[b]	1/50	Dako, Ely, UK
Anti-vimentin	1/1000	Sigma, Poole, UK
Anti-SMA[c]	1/2000	Sigma, Poole, UK
HHF-35[d]	1/40	Menarini Diagnostics, Wokingham, UK
Anti-desmin	1/50	Dako, Ely, UK
Anti-S100 protein	1/1000	Dako, Ely, UK
Anti-fibronectin	1/600	Dako, Ely, UK

[a] Anti-cytokeratin
[b] Epithelial-membrane antigen
[c] α-Smooth-muscle actin
[d] Muscle-specific actin

Table 2 Immunohistochemistry results

Antibody	Case 1	Case 2
MNF116[a]	+	+
AE1/3[a]	+	+
CK1[a]	+ focal	+
34βE12[a]	+	+
CAM5.2[a]	–	+ focal
Anti-cytokeratin-14[b]	–	–
Anti-EMAc	+ focal	+ focal
Anti-vimentin	+	+
Anti-SMA[d]	+	+
HHF-35[e]	+	+
Anti-desmin	–	–
Anti-S100 protein	–	–
Anti-fibronectin	+	+

[a] Anti-cytokeratin
[b] Given the phenotypic overlap between squamous and myoepithelial cells (both can have desmosomes, tonofibrils and myofilaments), cytokeratin 14 was included in the panel as a discriminating marker for myoepithelial differentiation [41]
[c] Epithelial-membrane antigen
[d] α-Smooth-muscle actin
[e] Muscle-specific actin

Results

Clinical and gross findings

Case 1

A 78-year-old man presented with a rapidly enlarging lesion of the left eye-lid, which had been present for about 10 weeks and which had shown bleeding after minor trauma. The lesion was completely excised, and tissue blocked out for light and electron microscopy. Four months post-operatively, the patient developed a right temporo-parietal infarct and died a further 5 months later.

Case 2

A 64-year-old woman presented with a slowly growing lesion of the naso-labial fold. Clinically, it was thought to be a basal cell carcinoma, and the patient was given radiotherapy. A small inactive lesion persisted, but after 13 years it began to increase in size. This lesion was excised from the right nasal margin and adjacent cheek, and tissue was blocked out for light and electron microscopy. The patient has remained free of disease for 6 months since surgery. Both tumours were slightly ulcerated and polypoid, and both measured 1.5 cm in maximum diameter.

Light microscopy

Histologically, both specimens were dermal tumours, occupying the full thickness of the dermis with extension into the subcutis in places (Fig. 1A). The dermis adjacent to the tumours showed marked solar elastosis, and a multifocal basal cell carcinoma was present on one side of the spindle cell carcinoma in case 2. Both tumours exhibited more or less similar features. The overlying epidermis was extensively ulcerated, and the intact epidermis at the lateral margins of the tumours showed changes of intraepidermal (in-situ) squamous carcinoma. Focally, the in-situ component merged with invasive tumour. The latter consisted of interlacing fascicles of plump spindled and oval cells containing elongated vesicular or hyperchromatic nuclei with small nucleoli and moderately abundant eosinophilic cytoplasm (Fig. 1B). Nuclei appeared moderately pleomorphic in places in case 2. Nine to ten mitoses per 10 high-power fields were detected. A vague storiform pattern was seen in case 1 in a few areas. The stroma of these tumours exhibited varying degrees of collagenisation, this feature being more marked in case 2. Some foci of myxoid and acantholytic, pseudoangiomatoid change were also detected. Neither tumour showed any basaloid features or evidence of eccrine differentiation. There were scattered acute and chronic inflammatory cells throughout the neoplasms. Both contained foci of necrosis, which was more marked in case 2. The immunohistochemical results are given in Table 2. All anti-cytokeratin antibodies

Fig. 1 Light microscopy (case 1). **A**, **B** Haematoxylin and eosin. **A** Cellular tumour merging (*) with epidermis, ×60. **B** Spindled tumour cells organised loosely into fascicles, ×240. Immunohistochemistry for cytokeratin (**C**), smooth-muscle actin (**D**) and fibronectin (**E**). **C** Clusters of tumour cells are intensely stained for cytokeratin, ×240. **D** Tumour cells are lightly stained for smooth-muscle actin in a mainly linear pattern near cell surfaces (*arrows*). The *asterisk* indicates a strongly stained vessel, ×240. **E** Antibody to fibronectin shows intracellular immunoreactivity (*arrowheads*) as well as a linear pattern consistent with the staining of cell processes or fibronectin fibrils (*arrows*), ×380 ▶

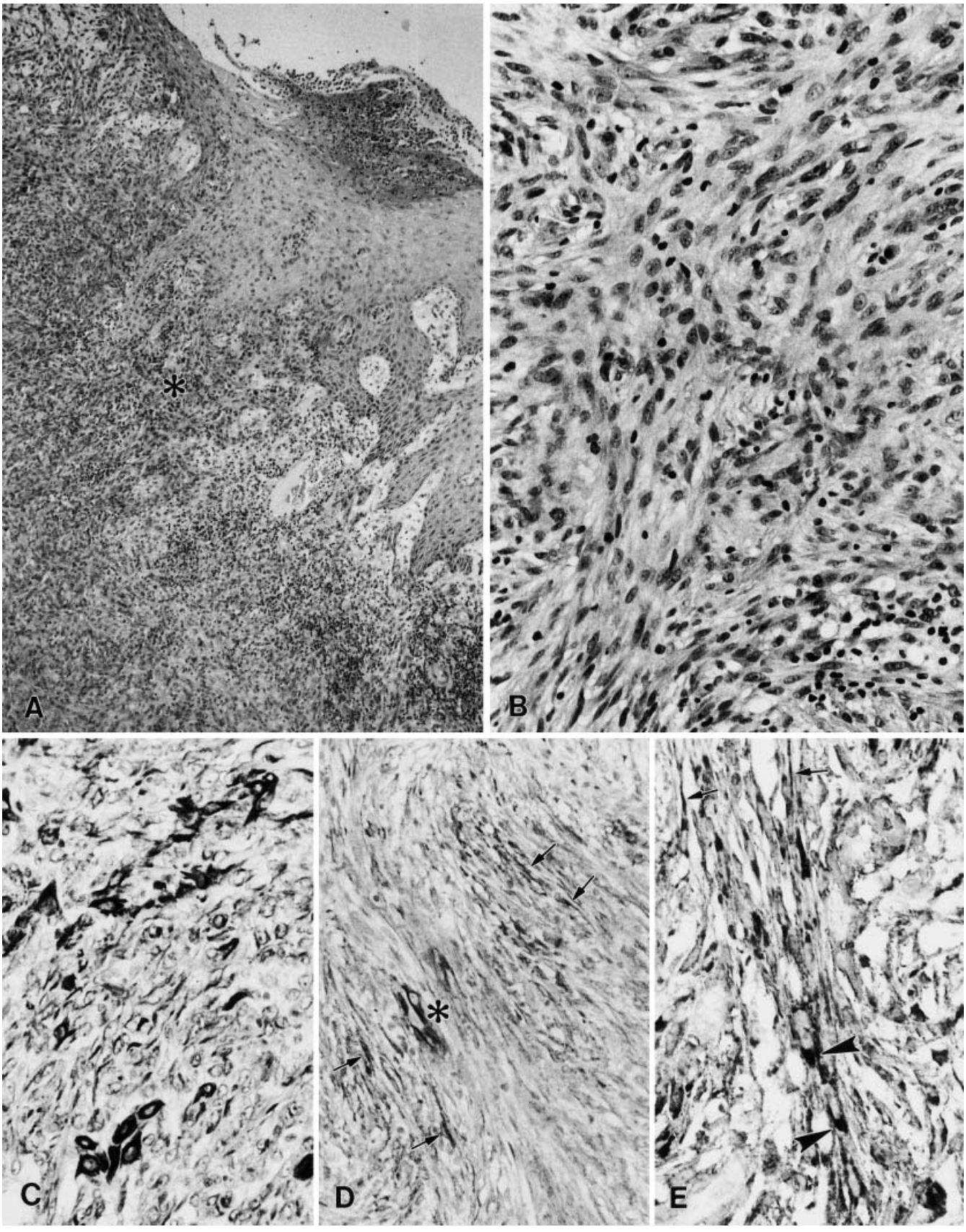

Fig. 1 Legend see page 37

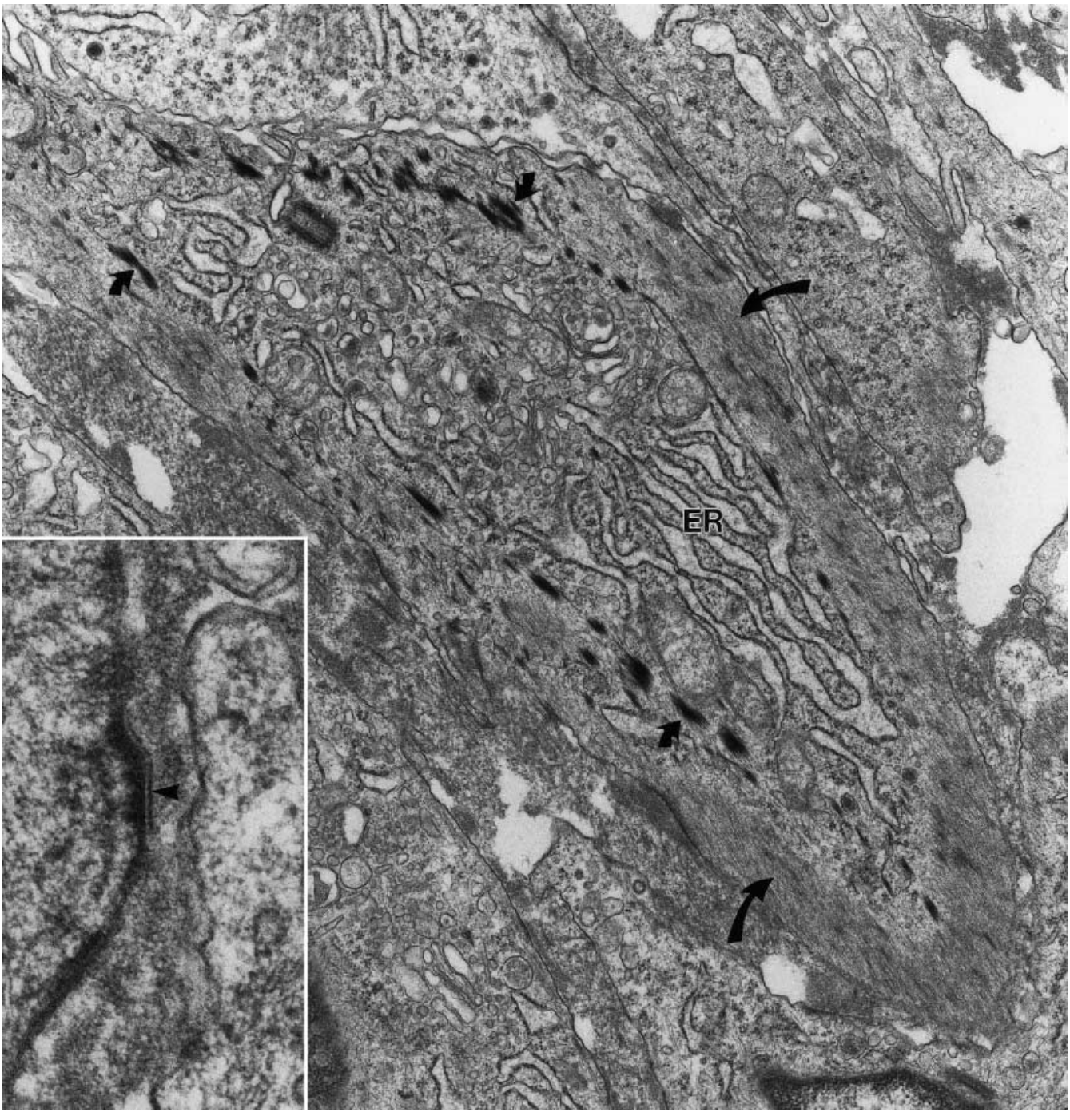

Fig. 2 Case 1. Broad tumour cell process showing rough endoplasmic reticulum (*ER*), well-developed tonofibrils (*short curved arrows*) and peripheral myofilaments (*long curved arrows*), ×20,000. *Inset* Hemi-desmosome showing thin sub-basal plate (*arrowhead*), ×95,000

except for cytokeratin 14, which was negative, stained clusters of tumour cells intensely (Fig. 1C), while α-smooth-muscle actin showed light staining often in a linear pattern (Fig. 1D). Fibronectin stained cytoplasm and slender processes or strands (Fig. 1E).

Electron microscopy

Ultrastructural appearances in the two cases were similar, although the tumour of case 1 showed better preservation. Tumour cells had rounded, oval, somewhat elongated or irregular nuclear profiles and abundant cytoplasm, the latter appearing as broad processes arising from the perinuclear area. Cytoplasm contained rER cisternae, which were more prominent in case 1 (Fig. 2), some of which were expanded by a putative secretory material. Moderate numbers of tonofibrils and well-formed desmosomes were present (Fig. 2 and Fig. 3).

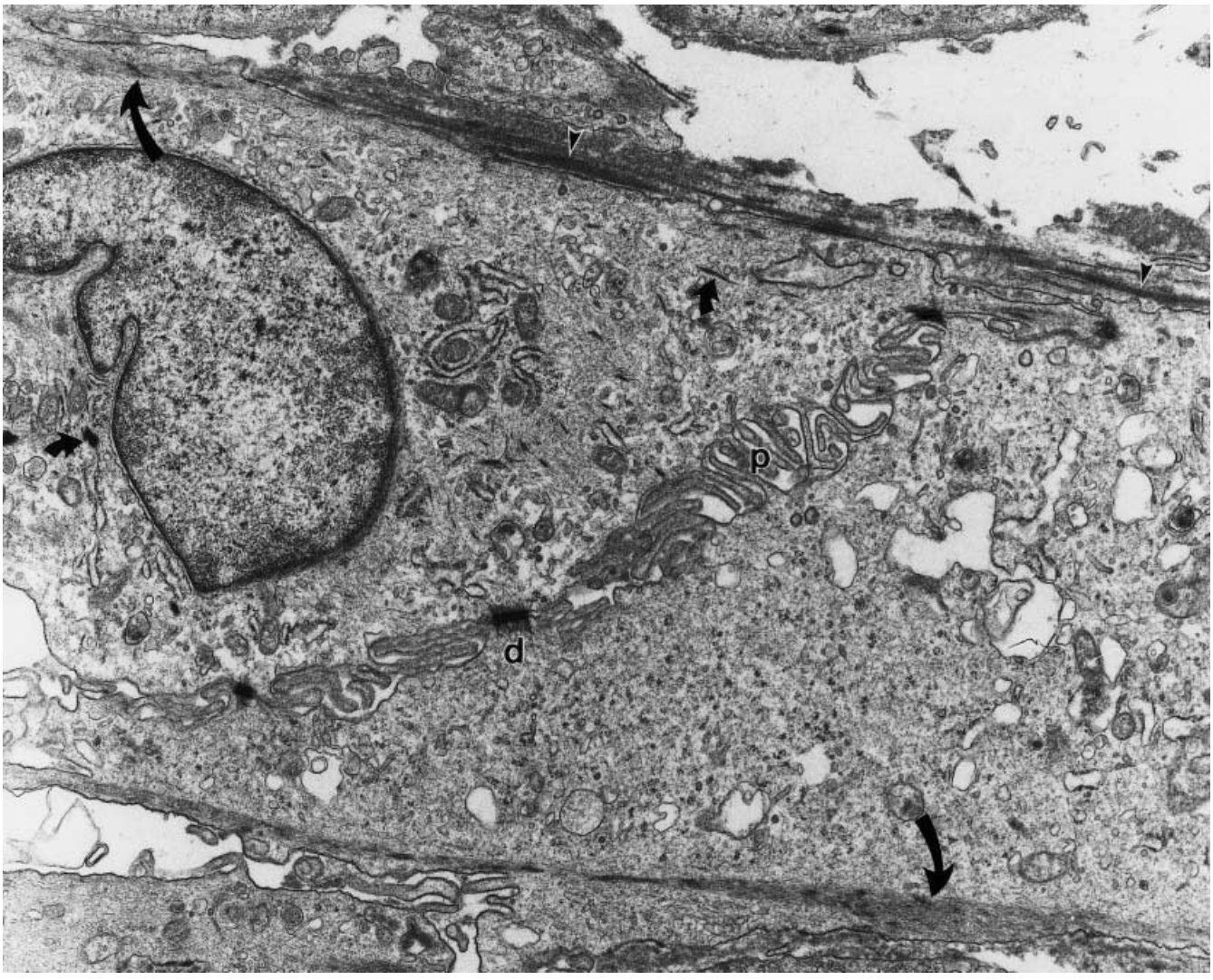

Fig. 3 Case 1. Tumour cells showing slender, lateral cell processes (*p*), desmosomes (*d*), myofilaments (*long curved arrows*) and modestly developed tonofibrils (*short curved arrows*). In the upper part of the figure there are rigid-looking filamentous fibrils (*arrowheads*) associated with the cell surface, ×13,000

The tonofibrils were electron dense and were somewhat more modestly developed in case 2 (Fig. 5C). Bundles of smooth-muscle-type myofilaments with focal densities were readily identified, frequently in a subplasmalemmal position (Fig. 2, Fig. 3, Fig. 5A).

In case 1, prominent, dense fibrillar material was present in the intercellular space and on cell surfaces (Fig. 3), and in some instances this was recognisable as fibronectin fibrils of the fibronexus (Fig. 4). The fibronectin fibrils had a rather straight profile, a longitudinal, finely filamentous substructure and were co-linear with bundles of intracellular myofilaments. In case 2, the dense intercellular material was replaced by abundant, closely packed collagen fibrils, and the fibronectin fibrils were less well developed (Fig. 5A, B). The fibronectin fibrils/fibronexus junctions were on the surfaces of cells, which, by their overall morphology and size, and presence of epithelial features, were undoubtedly tumour cells.

Cells having abundant rER, peripheral myofilaments with focal densities and fibronexus junctions but without epithelial features were also to be seen sparsely distributed amongst tumour cells and were identifiable as reactive stromal myofibroblasts.

Discussion

Carcinomas consisting exclusively or largely of spindled cells, although only forming a small minority of all carcinomas, have nonetheless been widely studied. The features most commonly encountered – cytokeratin demonstrated by immunohistochemistry, and tonofilaments and desmosomes by electron microscopy [3, 17, 25, 26, 30, 32, 34, 35, 39, 44, 47, 50, 56, 57, 61, 64, 66] – permit distinction from a non-epithelial spindle-cell malignancy. In addition to showing epithelial features, however, some spindle-cell carcinomas show organelles that are more typical of mesenchymal cells, and the term spindle-cell carcinoma with “mesenchymal metaplasia” has been

Fig. 4 Case 1. Fibronexus at the surface of a tumour cell showing cell processes of the kind illustrated in Fig. 2. Note that the myofilaments (*long curved arrows*) and fibronectin fibrils (*arrowheads*) are in line ("co-linear") and appear to contact one another at a shelf-like region of the cell surface (*short arrow*), ×39,000

used [16]. Such organelles include rER [1, 11, 14, 18, 21, 22, 28, 31, 36, 37, 38, 43, 45, 55, 56, 62, 63, 64, 65] and the myofilaments with focal densities typical of smooth-muscle cells [1, 2, 14, 16, 19, 24, 29, 37, 40]. The observations in our cases, which are recorded here for the first time in an in vivo epithelial tissue and in particular the neoplastic cells of a spindle-cell squamous carcinoma, relate to the presence of fibronexus junctions. These are characterised by the convergence of intracellular smooth-muscle myofilaments and extracellular fibronectin filaments [5, 6, 49, 51], and are regarded functionally as cell-to-matrix junctions. These tumours, therefore, can be regarded as showing signs of myofibroblastic "metaplasia", hitherto a novel form of differentiation in spindle-cell squamous carcinoma.

While the fibronexus is very largely associated with myofibroblasts, it is not entirely specific for these cells. They have been seen in malignant fibrous histiocytoma [33], which is perhaps not surprising, since these tumours are essentially fibroblastic, and fibroblasts are regarded as having the capability of readily transforming into myofibroblasts under appropriate conditions of stimulation [48]. For example, they appear in the course of culturing fibroblasts in vitro [42, 51, 52], which appear to transform into myofibroblasts as they transdifferentiate and attach to new substrata. Other well-developed fibronexuses have been observed in rat endothelium [23, 53], while a structure resembling a fibronectin fibril has been observed in bovine arteriosclerotic aortic smooth muscle [27]. In a small number of other mesenchymal cells, less well defined structures, nevertheless reminiscent of the fibronexus, have been described: aortic smooth-muscle [4, 5], scleral spur cell of the eye [60], mesenchymal stromal cells around the seminiferous tubule [20], and mesenchymal tumour cells of multicystic peritoneal mesothelioma [46]. Most of these cells, tissues or lesions can be seen to have an underlying, pre-existing differentiation, for example, smooth-muscle or endothelial, and it seems appropriate, therefore, to regard the presence of fibronexus junctions in these cells as consistent with myofibroblastic metaplasia.

While the present observations are the first unambiguous demonstration of fibronexus junctions in a spindle-cell squamous carcinoma, we recognise that the involvement of myofibroblasts has been suggested before in these carcinomas, by Harris [16] and Zarbo et al. [66]. Zarbo et al. [66] reported the presence of myofibroblasts in a paper without micrographic illustration, and in neither paper was it made entirely clear whether the myofibroblasts were reactive stromal myofibroblasts or tumour cells. Harris [16] illustrated a cell containing myofilaments and exhibiting a microtendon, indicating that it was a myofibroblast, although it lacked the tonofilaments of an unambiguous tumour cell.

As indicated above, myofibroblastic metaplasia, defined primarily by fibronexus junctions superimposed upon a pre-existing non-myofibroblastic phenotype, so far appears to be a rare phenomenon, restricted to a small number of cells. By contrast, smooth-muscle metaplasia, characterised by the presence of smooth-muscle myofilaments in cells that are demonstrably non-smooth-muscle in nature, is much more common with an occurrence in a

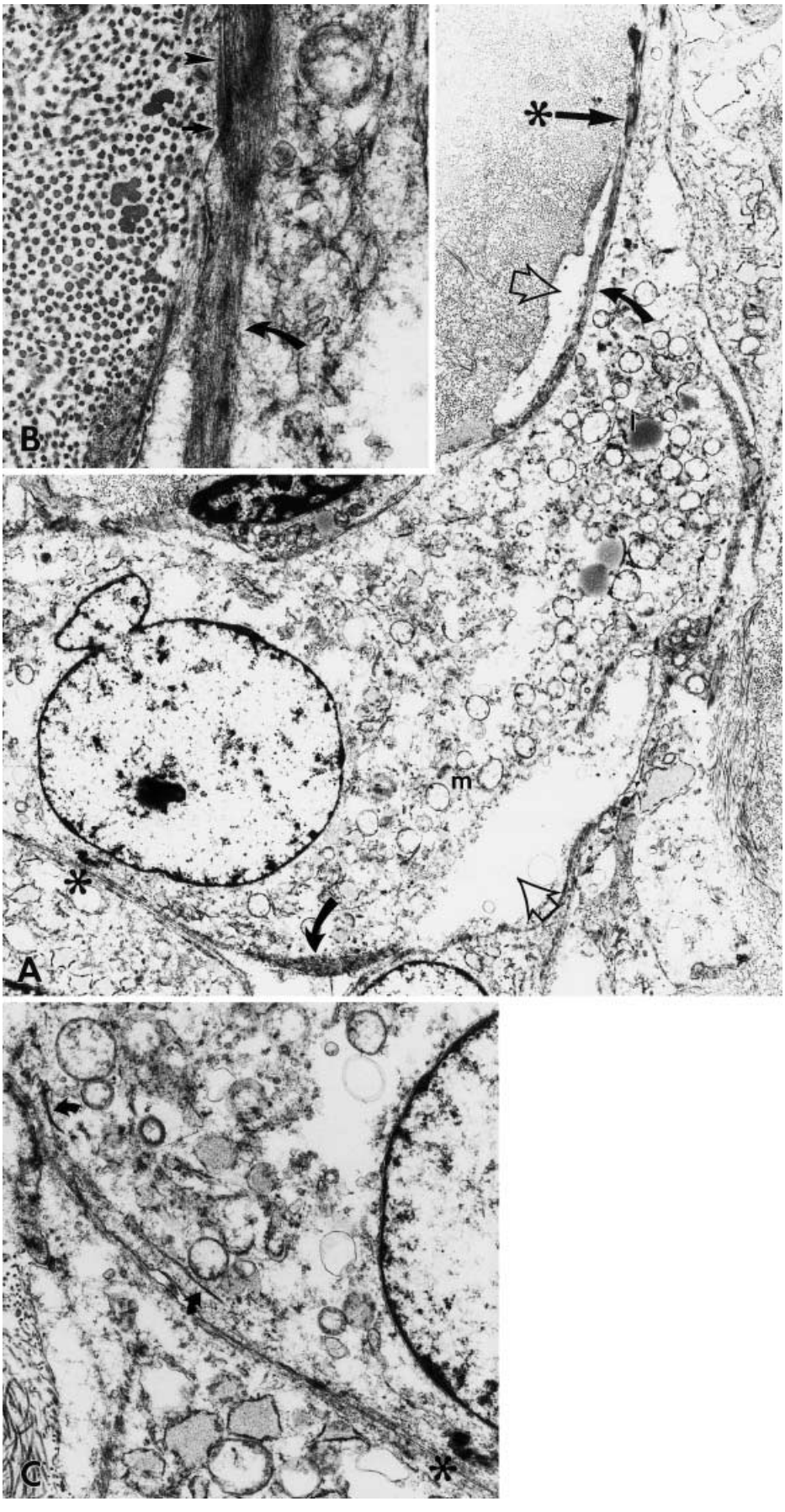

Fig. 5 Case 2. **A** A large tumour cell with prominent cytoplasm containing many washed-out mitochondria (*m*) and one or two lipid droplets (*l*). Subplasmalemmal bands of myofilaments are present (*curved arrows*), showing artefactual retraction from the plasma membrane and producing a focus of clear structureless cytoplasm (*empty arrowhead*). The *asterisked arrow* points to a fibronexus, which is detailed in **B**, while the *asterisk* on its own indicates an area of cytoplasm, which is detailed in **C** and which contains small tonofibrils, ×7500. **B** A band of myofilaments (*large curved arrow*) with focal densities meets a plaque at a shelf of the cell surface (*small arrow*), from which projects a slender fibronectin fibril (*arrowhead*). Note the co-linearity of the fibronectin fibril and the myofilaments, ×36,000. **C** This area of cytoplasm contains two dense tonofibrils (*curved arrows*). Both are modestly developed, and one (*upper left*) has a classically curving profile, ×17,000

wide range of epithelial, mesenchymal and other cells [7, 13, 48]. It seems, therefore, that while the development of smooth-muscle myofilaments is a common phenomenon accompanying or consequent upon trauma or inherent cellular abnormality such as neoplasia [7], myofibroblastic metaplasia appears to be a much rarer process. Further work, however, is needed to ascertain whether this is indeed the case, or is a result of inadequate recognition of the fibronexus [12].

References

1. Battifora H (1976) Spindle cell carcinoma. Ultrastructural evidence of squamous origin and collagen production by the tumor cells. Cancer 37:2275–2282
2. Carcangiu ML, Steeper T, Zampi G, Rosai J (1985) Anaplastic thyroid carcinoma. A study of 70 cases. Am J Clin Pathol 83:135–158
3. Cohen BH, Green WR, Iliff NT, Taxy JB, Schwab LT, de la Cruz Z (1980) Spindle cell carcinoma of the conjunctiva. Arch Ophthalmol 98:1809–1813
4. Dingemans KP, Teeling P, Lagenduijk JH, Becker AE (2000) Extracellular matrix of the human aortic media: an ultrastructural histochemical and immunohistochemical study of the adult aortic media. Anat Rec 258:1–14
5. Eyden BP (1993) Brief review of the fibronexus and its significance for myofibroblastic differentiation and tumor diagnosis. Ultrastruct Pathol 17:611–622
6. Eyden B (2001) The fibronexus in reactive and tumoral myofibroblasts: further characterisation by electron microscopy. Histol Histopathol 16:57–70
7. Eyden B (2000) Smooth-muscle-type myofilaments and actin in reactive and neoplastic nonmuscle cells. Ultrastruct Pathol 24:347–352
8. Eyden BP, Christensen L (1993) Leiomyosarcoma versus myofibrosarcoma: observations and terminology. Ultrastruct Pathol 17:231–239
9. Eyden BP, Banerjee SS, Harris M, Mene A (1991) A study of spindle cell sarcomas showing myofibroblastic differentiation. Ultrastruct Pathol 15:367–378
10. Eyden BP, Christensen L, Tagore V, Harris M (1992) Myofibrosarcoma of subcutaneous soft tissue of the cheek. J Submicrosc Cytol Pathol 24:307–313
11. Feldman PS, Barr RJ (1976) Ultrastructure of spindle cell squamous carcinoma. J Cutan Pathol 3:17–24
12. Fletcher CDM (1999) Myofibroblastic sarcoma. Author's reply. Am J Surg Pathol 23:1433–1435
13. Gabbiani G, Csank-Brassert J, Schneeberger JC, Kapanci Y, Trenchev P, Holborow EJ (1976) Contractile proteins in human cancer cells. Immunofluorescent and electron microscopic study. Am J Pathol 83:457–474
14. Gersell DJ, Katzenstein AL (1981) Spindle cell carcinoma of the breast. A clinicopathologic and ultrastructural study. Hum Pathol 12:550–561
15. Gocht A, Bosmuller HC, Bassler R, Tavassoli FA, Moinfar F, Katenkamp D, Schirrmacher K, Luders P, Saeger W (1999) Breast tumors with myofibroblastic differentiation: clinicopathological observations in myofibroblastoma and myofibrosarcoma. Pathol Res Pract 195:1–10
16. Harris M (1982) Spindle cell squamous carcinoma: ultrastructural observations. Histopathology 6:197–210
17. Hellquist H, Olofsson J (1989) Spindle cell carcinoma of the larynx. APMIS 97:1103–1113
18. Hill JA, Battifora HA, Milgram JW (1978) Spindle cell carcinoma arising in chronic osteomyelitis. A case report and reassessment of the literature. Bull Hosp Joint Dis 39:187–195
19. Hirose T, Sano T, Abe J, Hizawa K, Mori T (1987) Spindle cell carcinoma of the uterus. Acta Pathol Jpn 37:997–1002
20. Holstein AF, Maekawa M, Nagano T, Davidoff MS (1996) Myofibroblasts in the lamina propria of human seminiferous tubules are dynamic structures of heterogeneous phenotype. Arch Histol Cytol 59:109–125
21. Horova M (1985) Spindle-cell squamous carcinoma (pseudosarcoma) of the breast. Zentralbl Allg Pathol 130:423–427
22. Huntington AC, Langloss JM, Hidayat AA (1990) Spindle cell carcinoma of the conjunctiva. An immunohistochemical and ultrastructural study of six cases. Ophthalmology 97:711–717
23. Hüttner I, Walker C, Gabbiani G (1985) Aortic endothelial cell during regeneration. Remodeling of cell junctions, stress fibers, and stress fiber-membrane attachment domains. Lab Invest 53:287–302
24. Johannessen JV, Gould VE, Jao W (1978) The fine structure of human thyroid cancer. Hum Pathol 9:385–400
25. Kalogeropoulos NK, Antonakopoulos GN, Agapitos MB, Papacharalampous NX (1985) Spindle cell carcinoma (pseudosarcoma) of the anus: a light, electron microscopic and immunocytochemical study of a case. Histopathology 9:987–994
26. Katholm M, Krogdahl A, Hainau B, Bretlau P (1984) Spindle cell carcinoma of the larynx. Acta Otolaryngol Stockh 98:163–166
27. Knieriem HJ (1976) Electron-microscopic study of bovine arteriosclerotic lesions. Am J Pathol 50:1035–1065
28. Leifer C, Miller AS, Putong PB, Min BH (1974) Spindle-cell carcinoma of the oral mucosa. A light and electron microscopic study of apparent sarcomatous metastasis to cervical lymph nodes. Cancer 34:597–605
29. Lichtiger B, Mackay B, Tessmer CF (1970) Spindle-cell variant of squamous carcinoma. A light and electron microscopic study of 13 cases. Cancer 26:1311–1320
30. Lloreta J, Corominas JM, Munne A, Dominguez D, Bielsa O, Gelabert A, Serrano S (1998) Low-grade spindle cell carcinoma of the kidney. Ultrastruct Pathol 22:83–90
31. Manglani KS, Manaligod JR, Ray B (1980) Spindle cell carcinoma of the glans penis: a light and electron microscopic study. Cancer 46:2266–2272
32. Matsui K, Kitagawa M (1991) Spindle cell carcinoma of the lung. A clinicopathologic study of three cases. Cancer 67:2361–2367
33. Meek WD (1994) Fibronexus in a case of malignant fibrous histiocytoma. Ultrastruct Pathol 18:365–370
34. Meijer JW, Ramaekers FC, Manni JJ, Slooff JJ, Aldeweireldt J, Vooys GP (1988) Intermediate filament proteins in spindle cell carcinoma of the larynx and tongue. Acta Otolaryngol Stockh 106:306–313
35. Middlehurst RJ, Blackburn CW, Sloan P (1990) Spindle-cell carcinoma. Br J Oral Maxillofacial Surg 28:114–116
36. Murata M, Soga T, Tajima K, Saito K, Komeda Y, Ioshii SO, Shiraishi T, Sakakura T, Yatani R (1994) Sarcomatoid carcinoma of the urinary tract. Pathol Int 44:138–144
37. Nakayama Y, Iwasaki H, Iwanaga S, Nakamura H, Shiroshita T, Kikuchi M, Jozaki H, Hashimoto M, Ikeda S (1997) Spindle cell carcinoma of the breast: a case report and an immunohistochemical study including p53 and Ki-67 expression. Pathol Int 47:404–411
38. Nesland JM, Holm R, Johannessen JV (1986) Case 5: spindle cell tumor in the breast. Ultrastruct Pathol 10:415–419
39. Ng CS, Suen MWM, Mok SD, Li AKC (1988) Spindle cell carcinoma of bile duct origin. Histopathology 12:329–340
40. Ni C, Liu S-L, Zhong C-S (1989) Spindle cell carcinoma of cornea and conjunctiva with pseudosarcomatous metaplasia. Light microscopic, electron microscopic and immunohistochemical findings in 2 patients. Chinese Med J 102:387–391
41. Ogawa Y, Toyosawa S, Ishida T, Ijuhin N (2000) Keratin 14 immunoreactive cells in pleomorphic adenomas and adenoid cystic carcinomas of salivary glands. Virchows Arch 437:58–68
42. Perdue JF (1973) The distribution, ultrastructure, and chemistry of microfilaments in cultured chick embryo fibroblasts. J Cell Biol 58:265–283

43. Potsic WP, Raney RB Jr, Buck BE, Fischer SW (1979) Juvenile spindle cell carcinoma. Otolaryngol Head Neck Surg 87:573–577
44. Rabkin D, Singh J, Hussain A, Parnes SM, Silver SM (1995) Spindle cell carcinoma of the pyriform sinus: a case report. Ear Nose Throat J 74:574–577
45. Ro JY, Chen JL, Lee JS, Sahin AA, Ordóñez NG, Ayala AG (1992) Sarcomatoid carcinoma of the lung. Cancer 69:376–386
46. Santucci M, Biancalani M, Dini S (1989) Multicystic peritoneal mesothelioma. A fine structure study with special reference to the spectrum of phenotypic differentiation exhibited by mesothelial cells. J Submicrosc Cytol Pathol 21:749–764
47. Schantz HD, Ramzy I, Tio FO, Buhaug J (1985) Metastatic spindle-cell carcinoma. Cytologic features and differential diagnosis. Acta Cytol 29:435–441
48. Schmitt-Gräff A, Desmoulière A, Gabbiani G (1994) Heterogeneity of myofibroblast phenotype features: an example of fibroblast cell plasticity. Virchows Arch 425:3–24
49. Schürch W, Seemayer TA, Gabbiani G (1998) The myofibroblast: a quarter century after its discovery (editorial). Am J Surg Pathol 22:141–147
50. Sheridan R, Robbins S, d'Avis JC, Collins GL (1986) Spindle cell carcinoma of the breast: case report and review. J Surg Oncol 32:189–192
51. Singer II (1979) The fibronexus: a transmembrane association of fibronectin-containing fibers and bundles of 5 nm microfilaments in hamster and human fibroblasts. Cell 16:675–685
52. Singer II (1989) Fibronectin-cytoskeleton relationships. In: Mosher DF (ed) Fibronectin. Academic Press, San Diego, pp 139–161
53. Skalli O, Gabbiani G (1988) The biology of the myofibroblast. Relationship to wound contraction and fibrocontractive diseases. In: Clark RAF, Henson PM (eds) The molecular and cellular biology of wound repair. Plenum Press, New York, pp 373–402
54. Smith DM, Mahmoud HH, Jenkins JJ3rd, Rao B, Hopkins KP, Parham DM (1995) Myofibrosarcoma of the head and neck in children. Pediatr Pathol Lab Med 15:403–418
55. Someren A, Karcioglu Z, Clairmont AA Jr (1976) Polypoid spindle-cell carcinoma (pleomorphic carcinoma). Report of a case occurring on tongue and review of the literature. Oral Surg Oral Med Oral Pathol 42:474–489
56. Suster S, Robinson MJ (1989) Spindle cell carcinoma of the renal pelvis. Immunohistochemical and ultrastructural study of a case demonstrating coexpression of keratin and vimentin intermediate filaments. Arch Pathol Lab Med 113:404–408
57. Suster S, Huszar M, Herczeg E (1987) Spindle cell squamous carcinoma of the lung. Immunocytochemical and ultrastructural study of a case. Histopathology 11:871–878
58. Taccagni G, Rovere E, Masullo M, Christensen L, Eyden B (1997) Myofibrosarcoma of the breast: review of the literature on myofibroblastic tumors and criteria for defining myofibroblastic differentiation. Am J Surg Pathol 21:489–496
59. Takata T, Ito H, Ogawa I, Miyauchi M, Ijuhin N, Nikai H (1991) Spindle cell squamous carcinoma of the oral region. An immunohistochemical and ultrastructural study on the histogenesis and differential diagnosis with a clinicopathological analysis of six cases. Virchows Arch 419:177–182
60. Tamm E, Flügel C, Stefani FH, Rohen JW (1992) Contractile cells in the human scleral spur. Exp Eye Res 54:531–543
61. Torenbeek R, Blomjous CEM, de Bruin PC, Newling DWW, Meijer CJLM (1994) Sarcomatoid carcinoma of the urinary bladder. Clinicopathologic analysis of 18 cases with immunohistochemical and electron microscopic findings. Am J Surg Pathol 18:241–249
62. Tsubota YT, Kawaguchi T, Hoso T, Nishino E, Travis WD (1992) A combined small cell and spindle cell carcinoma of the lung. Report of a unique case with immunohistochemical and ultrastructural studies. Am J Surg Pathol 16:1108–1115
63. Visscher DW, Talerman A, Rivera LR, Mazur MT (1989) Adenocarcinoma of the rete testis with a spindle cell component. A possible metaplastic carcinoma. Cancer 64:770–775
64. Wargotz ES, Deos PH, Norris HJ (1989) Metaplastic carcinomas of the breast. II. Spindle cell carcinoma. Hum Pathol 20:732–740
65. Yamana K, Nakano R, Kinoshita T, Morimatsu M, Nakashima T (1984) Ultrastructure of anaplastic carcinoma (spindle and giant cell type) with large calcification in the thyroid gland. Acta Pathol Jpn 34:585–592
66. Zarbo RJ, Crissman JD, Venkat H, Weiss MA (1986) Spindle-cell carcinoma of the upper aerodigestive tract mucosa. An immunohistochemical and ultrastructural study of 18 biphasic tumors and comparison with seven monophasic spindle-cell tumors. Am J Surg Pathol 10:741–753

Virchows Arch (2002) 440:45–49
DOI 10.1007/s004280100486

ORIGINAL ARTICLE

Hernán García Rivello · Patricia Cabeza Meckert
Amelia Gallo · Luis Palacios · Rubén P. Laguens

DNA content and expression of cell cycle proteins in caterpillar nuclei from fetal human cardiac myocytes

Received: 6 September 2000 / Accepted: 9 April 2001 / Published online: 28 July 2001
© Springer-Verlag 2001

Abstract Caterpillar nuclei (CN) are characterized by their peculiar morphology, with chromatin distributed in clusters and running along the longitudinal axis of the nucleus. They can be observed in normal hearts of fetuses as well as in hearts of children and adults with rheumatic heart disease. This study has demonstrated by means of ploidy studies with digital image analysis that in the fetal heart (20.5±1.8 weeks) the CN (diploid = 5.6±8.4%; tetraploid = 46.2±24.2%; hypertetraploid = 46.9±26.3%) present higher DNA content than non-caterpillar myocyte nuclei (diploid = 89.4±6.2%; tetraploid = 10.0±4.1%; hypertetraploid = 1.5±1.3%) (P=0.000001, 0.00013, and 0.000038, respectively). Expression of proliferation cell nuclear antigen (PCNA; 30.6±11.7% in CN and 13.4±7.3% in non-caterpillar myocyte nuclei; P=0.0115) and cyclin B1 (2.8±3.8% and 12.6±15.6%, respectively; P=n.s.) was also positive in these nuclei. In conclusion, these results suggest that there exists a relationship between CN morphology and myocyte replication phenomena.

Keywords Caterpillar nuclei · Cyclin B1 · Fetal heart · Nuclear ploidy · PCNA

H. García Rivello · R.P. Laguens (✉)
Cátedra de Patología "B",
Facultad de Ciencias Médicas and CONICET,
Universidad Nacional de La Plata,
60 y 120, La Plata, Prov. de Buenos Aires, Argentina
e-mail: laguens@netverk.com.ar
Tel.: +54-11-43781315, Fax: +54-11-43781315

P. Cabeza Meckert · L. Palacios · R.P. Laguens
División Patología, ICyCC Fundación Favaloro and CIC,
Av Belgrano 1746, C1093AAS,
Ciudad de Buenos Aires, Argentina

A. Gallo
Servicio de Anatomía Patológica, Hospital Italiano,
Gascón 450, C1181, Ciudad de Buenos Aires, Argentina

Introduction

At the beginning of the century Von Oppel reported for the first time the presence of caterpillar nuclei (CN) in the rabbit myocardium as a reaction to implantation of a needle [19]. He observed that the muscle fibers in the puncture canal showed hypertrophic nuclei with the chromatin distributed in granules or clusters with a "serrated stripe" or condensed in a "single thread running in the long axis" of the nucleus. Anitschkow made a similar observation some years later and focused on the peculiar chromatin condensation of such muscle fibers, which came to be known as "Anitschkow cells or myocytes", characteristic of the Aschoff bodies in rheumatic heart disease [1].

Anitschkow cells and CN were popular subjects in the literature of the first half of the last century, but these are topics seldom discussed in the past 50 years. The origin and significance of the heart CN have not been established, but on account of their presence in the fetal life, when the heart growth is due to hyperplasia, it has been speculated that their presence may be related to myocyte replication phenomena [14]. In order to find out whether CN present evidence of DNA replication, we decided to study the ploidy status and activity of proliferation cell nuclear antigen (PCNA; a protein expressed during late G1, S, G2 and M phases of the cell cycle) and cyclin B1 in CN and compare them with those in the non-caterpillar myocyte nuclei.

Materials and methods

Tissue fixation and sampling

For the present study, we employed the hearts of ten human fetuses with minimal or no maceration, gestational age 17–23 weeks, established by the predicted menstrual age, Sheppard's tables for fetal weight [5] and by fetal foot length [12]. This gestational age was chosen because of the high proliferative index of the heart during that time. As controls, we employed four hearts collected from a full-term newborn and 1-, 5- and 7-month-old babies. Hearts showed no evidence of myocardial infection.

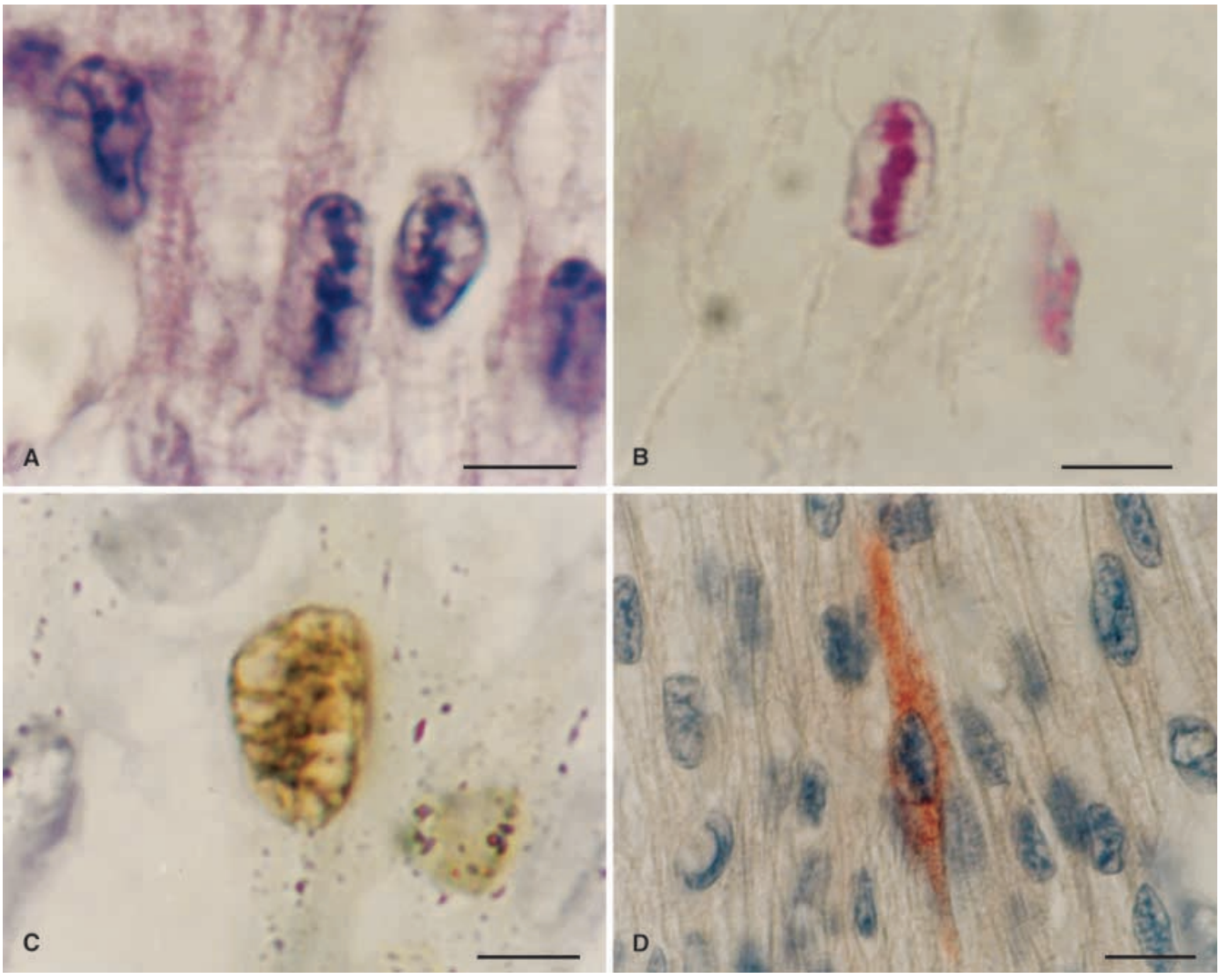

Fig. 1 Morphology of myocytes with caterpillar nuclei (CN): **A** hematoxylin-eosin and **B** Feulgen stain of CN showing the central condensation of chromatin (×1000; *bar* 5 µm); **C** proliferation cell nuclear antigen (PCNA) stain of a CN (diaminobenzidine, ×1000; *bar* 5 µm); **D** the presence of cyclin B1 can be observed in the cytoplasm of a fetal myocyte with CN [aminoethyl carbazole (AEC), ×400; *bar* 10 µm]

Gestational age, sex, weight, fetal dimensions and clinical data are summarized in Table 1. The hearts were removed, sectioned in halves, fixed in 10% buffered formalin and embedded in paraffin. Several 3-µm thick tissue sections from the left ventricular free wall and interventricular septum were stained with hematoxylin-eosin and Feulgen's (Fig. 1a, b) and for immunohistochemical studies.

This study was performed in accordance with the ethics standards of the 1964 Declaration of Helsinki. Parents gave their informed consent prior to the inclusion in the study.

Quantitative analysis of the incidence of CN in myocardial cells

The frequency of CN in myocytes was established in tissue sections stained with hematoxylin-eosin on 40 microscopic fields examined at a 400× magnification.

Determination of DNA content

Nuclear DNA content of individual nuclei was determined by means of densitometry with a digital analysis system (Vidas-Kontron-Zeiss, Germany) with DNA Vidas software in the Feulgen stained-tissue sections. This method is based on the interaction between Schiff's reagent and the aldehyde groups of the deoxyribose molecules, previously unmasked by acid hydrolysis. In order to maximize nuclear detail, the staining process was optimized at 55 min [10]. For evaluation of DNA content by static cytomorphometry, myocytes transversally sectioned were measured in 3-µm tissue sections; only cells containing a centrally located nucleus, longitudinally oriented, and located equidistant to the cell boundaries were analyzed. Nuclei that appeared to be overlapping or not clearly defined were excluded from the study [7, 13].

The ploidy status of 300 non-caterpillar myocytes and 40–60 CN for each case was determined using the interstitial cells as diploid reference cells. In addition, the DNA content of the CN was studied employing the DNA content of non-caterpillar myocyte nuclei content as the baseline 2c reference value.

Determination of PCNA and cyclin B1

Immunohistochemical staining was performed using mouse monoclonal antibodies to PCNA (clone PC10, 1:50; Dakopatts, Denmark) and cyclin B1 (clone 7A9, 1:30; Novocastra, UK). The de-

Table 1 Summary of fetal dimensions and clinical data. Age is expressed as gestational age in weeks

Case	Age (weeks)	Sex	Weight (g)	Crown–rump (cm)	Crown–heel (cm)	Foot length (mm)	Pathology	Manner of delivery
1	17	Female	235	14.1	21.5	26.3	Anencephaly	Vaginal
2	18	Male	220	13.5	21.1	25.1	Deciduitis	Vaginal
3	21	Male	490	17.2	25.2	33.5	Holoprosencephaly	Vaginal
4	21	Male	510	16.8	25.3	34	Anencephaly	Vaginal
5	21	Male	245	14.2	20.1	32.5	Anencephaly	Vaginal
6	21	Male	515	20.4	30	37.3	Chorioamnionitis	Vaginal
7	21	Male	400	18.2	26.2	35	Chorioamnionitis	Vaginal
8	21	Female	280	15.3	21.1	32.6	Chorioamnionitis	Vaginal
9	23	Female	570	16.2	26.5	43.9	Chorioamnionitis	Vaginal
10	21	Female	365	13.6	20.8	37.1	Chorioamnionitis	Vaginal

Table 2 Incidence, ploidy status and proliferation cell nuclear antigen (PCNA) activity of caterpillar nuclei (CN). Age is expressed as gestational age in weeks for stillborns and days or months for liveborns. *%CN* CN per 1000, *Ploidy* DNA content, *2c* percentage of diploid nuclei, *4c* percentage of tetraploid nuclei, *>4c* percentage of hypertetraploid nuclei, *PCNA* expression of PCNA as a percentage in non-caterpillar myocytes, *PCNA CN* expression of PCNA as a percentage in myocytes with CN

Case	Age	% CN	Ploidy			Ploidy (CN)			PCNA	PCNA (CN)
			2c	4c	>4c	2c	4c>	4c		
1	17 weeks	0.5	98.2	1.4	0.4	0	0	100	10.3	13.4
2	18 weeks	6.6	80.3	14	5.7	10	10	80	19.5	45.4
3	21 weeks	0.4	95.2	4.2	0.3	0	56	44	25.6	33.9
4	21 weeks	1.1	85.1	13	1.9	21.5	44	34.5	21.5	44.4
5	21 weeks	0.4	94.7	5.2	0.1	0	57	43	1.68	46.1
6	21 weeks	1.5	89.1	9.1	1.8	0	61.2	38.8	10.6	30
7	21 weeks	5.6	93.1	4.8	2.1	6.9	72.1	21	4.5	16.6
8	21 weeks	6.7	85.4	11.2	3.4	13.9	45	41.1	13.7	28.
9	23 weeks	1	90.7	8.8	0.5	0	44.4	55.6	12.9	24
10	21 weeks	2.7	85.5	14.1	0.8	16.6	72.4	11	13.9	24.2
Mean	20.5	2.7	89.4	10.05	1.56	5.68	46.2	46.9	13.4	30,6
SD	1.81	2.6	6.28	4.17	1.37	8.43	24.2	26.3	7.3	11.7
11	1 day	0.2	85.59	13.56	0.85				3.1	
12	1 month	0	92.04	7.96	0				2	
13	5 months	0	99.2	0.8	0				0.9	
14	7 months	0	96.2	2.9	0.9				1.2	

tection was performed with the immunoperoxidase technique based on a biotin–streptavidin system (Multilink Biogenex, San Ramon, Calif.). The proportion of positively stained caterpillar and non-caterpillar myocyte nuclei was determined in the left ventricle and interventricular septum at ×400 for each case.

Desmin, α-sarcomeric actin and α-smooth muscle specific actin staining

To demonstrate that PCNA and cyclin B1 labeling and caterpillar morphology occurred in myocyte nuclei, sections from a limited number of samples were stained with monoclonal antibodies to desmin (1:100; Biogenex, Calif.), α-sarcomeric actin (alpha-Sr-1, 1:30; Dakopatts, Denmark) and α-smooth muscle specific actin (1A4, 1:40; Dakopatts). The detection was performed with the immunoperoxidase technique (Multilink Biogenex) in conformity with the manufacturer's recommendations.

Statistical analysis

Measurements are presented as mean ± SD. Significance for comparisons among groups was determined using an analysis of variance (ANOVA) method. Analyses were performed using Statistica for Windows (release 4.2) statistical software. Values of $P<0.05$ were considered to be significant.

Results

Proportion of CN

CN were identified in the hematoxylin-eosin and Feulgen-stained histologic sections by their peculiar morphology (Fig. 1a, b). In the 17- to 23-week-old fetuses, the proportion of CN was variable, ranging from 4 to 67 for 1000 non-caterpillar nuclei. In the newborn and infant hearts, the presence of CN was exceptional (Table 2).

Demonstration of the muscular origin of caterpillar nuclei

Samples were stained with the following antibodies: anti-desmin antibody, an intermediate filament [15] expressed in cardiac, skeletal and smooth muscle; anti-α-sarcomeric actin, a sarcomere-specific protein [9], and anti-α smooth-muscle-specific actin (negative in myocytes with CN). CN were present in cells expressing α-sarcomeric actin and desmin.

Ploidy status of non-caterpillar myocyte nuclei and CN

Table 1 shows that most of the non-caterpillar myocyte nuclei in the 17- to 23-week-old fetuses were 2c, with a small proportion of 4c, probably corresponding to cells in the G2/M stage of the cell cycle. With the exception of one case, the proportion of hypertetraploid nuclei was very low (case 2).

In the newborn and infant hearts, the proportion of 2c nuclei was even larger than in the younger fetuses and almost no tetraploid nuclei were observed (Table 2). In the fetal hearts, over 94% of CN had a DNA content higher than 2c, half of them showed tetraploid values and the remaining half were hypertetraploid (Table 2).

The difference between the ploidy status of the myocyte nuclei with conventional morphology and the CN was statistically significant (2c P=0.000001; 4c P=0.00013; >4c P=0.000038).

Expression of PCNA and cyclin B1

PCNA labeling was observed in 13.4±7.3% (mean±SD) of non-caterpillar myocyte nuclei. There was no difference between the left ventricular wall and the interventricular septum. Myocytes with CN morphology showed 30.6±11.7% of PCNA-stained nuclei (P=0.00096; Fig. 1c).

The expression of a G2/M marker, cyclin B1, showed a cytoplasmic stain in 12.6±15.6% of myocytes. In myocytes with CN, 2.8±3.8% were positive (P=n.s.) for cyclin B1 (Fig. 1d).

Discussion

The peculiar morphology of CN can be observed in normal hearts of fetuses and to a lower extent in full-term infants [18] as well as in hearts of children and adults with rheumatic heart disease [16, 17]. Most studies on the origin of CN were carried out in the pre-immunohistochemical era and their myocytic origin was controversial. On the basis of cell size, shape and presence of cross striations, most reports agreed that CN belong mainly to myocytes. The biological meaning of CN in myocytes has not been established.

The presence of CN in normal hearts with high proliferative activity and in young patients with cardiac rheumatic disease favors the idea that CN may be related to myocyte proliferation. This possibility led us to study the expression of some proteins (PCNA, cyclin B1) essential for controlling cell-cycle progression in myocytes with CN.

The PCNA protein expression is a useful immunohistochemical method for determining the proliferative activity of cell populations, although there exist certain restrictions on its interpretation since it is not a cellular cycle-specific marker: PCNA expresses itself in replicative cells and in those with DNA repair processes [2]. The high percentage of caterpillar nuclei (30%) expressing PCNA indicates that this peculiar morphology is related to an increase in DNA synthesis and proliferative activity.

The B1 protein affects the G2 to M transition and it is, therefore, restricted to a specific period of the cell cycle. The type-B cyclins associate with Cdk1 and these complexes are the mitosis-specific kinases [4, 11]. The high level of expression in cytoplasm (and in a lesser extent in nuclei) of fetal myocytes and in a percentage of CN demonstrate that these cells are in an active process of proliferation.

The ploidy studies of CN presented largely tetraploid and hypertetraploid values, which indicate intense DNA synthesis and probably a marginal polyploidization phenomenon in the fetal heart. DNA hyperploidy values have been communicated in previous studies with a low rate of normal myocyte nuclei [20].

CN can also be a morphologic expression of an alternative mechanism for the formation of polyploid nuclei, which can include endomitosis or endoreduplication [8]. Endoreduplication represents a cell cycle that omits the mitotic phase; whereas, in endomitosis, mitosis takes place within the nuclear envelope without the formation of a mitotic spindle. The central localization of the chromatin thread in the largest diameter of the nucleus can also be suggestive of an intranuclear metaphasic plate, as is the case in other eukaryotic cells [21]. In Fig. 1c, a PCNA-stained CN shows a pattern characteristic of chromosomes arranged in a metaphasic plate. Other authors suggested the possibility that CN represent a postmitotic chromatin organization [3] or a morphological expression of a response to hypoxic cardiac injury [6]. Irrespective of these hypothetical interpretations, our results, showing that CN contain an increased amount of DNA and express PCNA, a regulator of the cell cycle, support the opinion that this peculiar morphological change is related to myocyte replicative mechanisms.

It is very difficult to provide evidence of the exact position of these cells in the cell cycle in tissues obtained from human necropsies. On the basis of the expression of PCNA in a large proportion of CN, the occasional positivity of cyclin B1 and the high ploidy status, we can speculate that CN may belong to cells undergoing endomitosis. Further studies using fresh tissues would be required to determine whether the cell cycle proteins are involved in the genesis of CN.

Acknowledgements The authors wish to thank Mrs P. C. Fioravanti for the revision of this manuscript.

References

1. Anitschkow N (1913) Experimentelle untersuchungen uber die Neubildung des granulatiosgewebes im Herzmuskel. Beitr Pathol Anat Allg Pathol 55:373–415
2. Basi G, Draetta G (1995) The cdc2 kinase: structure, activation, and its role at mitosis in vertebrate cells. In: Hutchinson C, Glover DM (eds) Cell cycle control. Oxford University Press, Oxford, pp 194–195

3. Bol'shakova GB (1984) Characteristics of the appearance of Anichkov's cells in the myocardium. Biull Eksp Biol Med 97: 358–360
4. Brooks G, Poolman RA, Li JM (1998) Arresting developments in the cardiac myocyte cell cycle: role of cyclin-dependent kinase inhibitors. Cardiovasc Res 39:301–311
5. Callen M (ed) (1991) Appendix: table of normal weight by Shepard's formula. In: Ecografía en obstetricia y ginecología. Panamericana, Buenos Aires, p 350
6. Favara BE, Moores H (1987) Anitschkow nuclear structure: a study of pediatric hearts. Pediatr Pathol 7:151–164
7. Freed JA (1999) Improved correction of quantitative nuclear DNA (ploidy) measurements in tissue sections. Anal Quant Cytol Histol 21:103–112
8. Ghosh S, Paweletz N (1993) Mitosis: dissociability of its events. In: Jeon K (ed) A survey of cell biology, Int Rev Cytol 144. Academic Press, pp 217–258
9. Hayakawa K, Ono S, Nagaoka R, Saitoh O, Obinata T (1996) Differential assembly of cytoskeletal and sarcomeric actins in developing skeletal muscle cells in vitro. Zoolog Sci 13:509–517
10. Huhn KM, Palcic B, Wilson JE, McManus BM (1995) Cytometric analysis of ventricular myocyte nuclei in idiopathic dilated cardiomyopathy: a tool for evaluation of disease progression? Eur Heart J 16[Suppl O]:97–99
11. MacLellan WR, Schneider M (1999) The cardiac cell cycle. In: Harvey R, Rosenthal N (eds) Heart development. Academic Press, Canada, pp 405–414
12. Macpherson T (1994). A model: perinatal autopsy protocol. Armed Forces Institute of Pathology, Washington, pp 50–54
13. Matturri L, Biondo B, Colombo B, Lavezzi AM, Rossi L (1997) Significance of the DNA synthesis in hypertrophic cardiomyopathies. Basic Res Cardiol 92:85–89
14. Murphy GE, Becker CG (1966) Occurrence of caterpillar nuclei within normal immature and normal appearing and altered mature heart muscle cells and the evolution of Anitschkow cells from the latter. Am J Pathol 48:931–957
15. Nag AC, Huffaker SK (1998) Distribution and organization of desmin in cultured adult cardiac muscle cells: reflection on function. J Muscle Res Cell Motil 19:887–895
16. Schoen F (1999) The heart. In: Cotran R, Kumar V, Collins T (eds) Robbins Pathologic basis of disease. Saunders, Philadelphia, pp 570–572
17. Tanaka H, Kobayashi H, Kano S, Kawaguchi S, Uwabe Y, Nagata N (1995) Autopsy of a patient with rheumatic fever, who initially presented with acute respiratory failure. Nihon Kyobu Shikkan Gakkai Zasshi 33:678–681
18. Valdes-Dapena M (1957) The heart. In: An atlas of fetal and neonatal histology. Lippincott, Philadelphia, USA, pp 11–20
19. Von Oppel W (1901) Ueber Veranderungen des myocards unter der einwirkung von Fremdkorpen. Virchow Arch 164:406–436
20. Zerbini C, Weinberg DS, Perez-Atayde AR (1992) DNA ploidy analysis of myocardial hyperplasia. Hum Pathol 23: 1427–1430
21. Zybina EV, Zybina TG (1996) Polytene chromosomes in mammalian cells. Int Rev Cytol 165:53–119

Virchows Arch (2002) 440:50–62
DOI 10.1007/s004280100463

ORIGINAL ARTICLE

**Lucie Bačáková · Věra Lisá · Lucie Kubínová
Jiří Wilhelm · Jana Novotná · Adam Eckhart
Jan Herget**

Ultraviolet light-irradiated collagen III modulates expression of cytoskeletal and surface adhesion molecules in rat aortic smooth muscle cells in vitro

Received: 30 November 2000 / Accepted: 26 March 2001 / Published online: 21 June 2001
© Springer-Verlag 2001

Abstract Systemic and pulmonary hypertension is characterised by structural reconstruction of the vascular wall which includes hypertrophy and hyperplasia of vascular smooth muscle cells (VSMCs) and fibroproduction. We hypothesise that these changes are stimulated by non-enzymatic modification of collagen molecules in the injured vascular wall by radicals. We exposed collagen III to ultraviolet (UV) light irradiation which, as indicated by fluorescence and electrophoretic analyses, resulted in its fragmentation. Both irradiated and control unmodified collagen were adsorbed on culture dishes and seeded with VSMCs derived from the rat thoracic aorta. During the first week after seeding, the cells on the modified collagen attained significantly higher population density (by 15–83%), higher mitotic index (by 31–135%) and higher BrdU labelling index (by 32%). However, these cells were less resistant to spontaneous and trypsin-mediated detachment from the growth support. As revealed using enzyme-linked immunosorbent assay in 3-day-old cultures, the cells growing on the irradiated collagen exhibited a lower concentration of beta-1 integrins (–10%, measured per milligram of protein), vinculin (–18%), talin (–6%) and vimentin (–15%). Immunofluorescence staining showed that these molecules were distributed more diffusely and less organised into focal adhesion plaques or cytoskeletal fibres. The concentration of two adhesion molecules of immunoglobulin type, ICAM-1 and VCAM-1, was increased by 11% and 16%, respectively. The concentration of alpha-v integrins and alpha-actin was unchanged; the latter, however, formed fewer distinct microfilament bundles in cells on the modified collagen. Our results suggest that the VSMCs growing on UV-modified collagen are more prone to escape the growth control mediated by cell-extracellular matrix contact and can bind the cells of the immune system.

Keywords Integrins · Focal adhesion proteins · Alpha-actin · Vimentin · Immunoglobulins

L. Bačáková (✉) · V. Lisá · L. Kubínová
Institute of Physiology,
Academy of Sciences of the Czech Republic,
Vídeňská 1083, CZ-142 20 Prague 4-Krč, Czech Republic
e-mail: lucy@sun2.biomed.cas.cz
Tel.: +420-2-4752521, Fax: +420-2-4752488

J. Wilhelm · J. Novotná
Department of Biochemistry of 2nd Medical School,
Charles University, Prague, Czech Republic

A. Eckhart · J. Herget
Department of Physiology of 2nd Medical School,
Charles University, Prague, Czech Republic

Introduction

Structural remodelling of the vascular wall plays an important role in the pathogenesis of atherosclerosis and chronic systemic or pulmonary hypertension. In these disorders, the synthesis of extracellular matrix by vascular smooth muscle cells (VSMCs) is enhanced, qualitatively changed, and resembles that in foetal arteries [14, 31, 33]. In addition, other molecules, physiologically absent in the vessel wall, such as lipoproteins, cholesterol, albumin, fibrinogen, fibrin, thrombin or haemoglobin, penetrate from the blood into the vessel wall through a dysfunctional endothelial barrier [1, 7, 27, 30, 37]. Extracellular molecules can be further modified, e.g. degraded by proteolytic enzymes, non-enzymatically glycosylated or oxidised by radicals [2, 7, 8, 16, 18, 22, 25, 27]. We hypothesise that altered extracellular matrix can activate the growth of VSMCs which, together with increased amount of extracellular matrix proteins, results in stiffer vessels with a narrower lumen and higher resistance to blood flow.

We reported previously that VSMCs isolated from rat aorta and cultured on type I collagen modified by oxidative effects of ultraviolet (UV) irradiation proliferated more rapidly than those on native collagen I [4]. At the same time, these cells were more prone to detachment from the modified collagen by trypsin. It was not clear

whether the weak cell adhesion was due to a lower resistance of the UV-irradiated collagen to proteolytic degradation or to a lower binding of cells to this collagen. Therefore, in this study performed on collagen III, i.e. another important extracellular matrix protein of the vessel wall, we focused not only on the proliferation capacity of VSMCs cultured on this substrate modified by UV irradiation, but also on the content and distribution of several molecules taking part in cell-matrix adhesion, such as β_1 and α_v integrins, vinculin, talin and α-isoform of actin, which also represents a marker of VSMC differentiation [2, 3, 11, 14]. In addition, we investigated the content and arrangement of vimentin, a sensitive indicator of oxidative injury [10, 29, 36]. Finally, we evaluated the expression of two surface adhesion molecules of the immunoglobulin superfamily [intercellular adhesion molecule 1 (ICAM-1) and vascular cell adhesion molecule 1 (VCAM-1)], which can be induced by extracellular matrix alterations and are important for binding cells of the immune system and their penetration into the vascular wall [1, 6].

Materials and methods

Preparation and characterisation of UV-irradiated collagen III

Collagen of type III derived from calf skin (gift from Prof. Adam, Institute of Rheumatology, Prague, CR) was dissolved in 0.16 M CH_3COOK (pH 3.1) to the concentration of 1 mg/ml and exposed to UV radiation generated by a mercury lamp (0.5 mW/cm^2) for 120 min as described previously [4]. The modifications induced by UV irradiation were characterised by fluorescence measurements arranged in tri-dimensional spectral arrays. The spectra were measured on a Perkin-Elmer LS-5 spectrofluorometer and the spectral arrays were created using software developed in our laboratory. The excitation spectra were used because they reveal the chemical changes in the protein molecule. We measured the spectra between 280 nm and 400 nm for emission starting at 330 nm and increasing up to 470 nm with a step of 10 nm. The changes in the collagen structure were further investigated using sodium dodecyl sulfate polyacrylamide gel electrophoresis (SDS-PAGE). Electrophoresis was performed on 7.5% polyacrylamide gels under reducing conditions with 5% β-mercaptoethanol using Mini-Protean system (Bio-rad [20]) and stained with silver [35].

Growth curves and adhesion capacity of VSMCs on UV-irradiated collagen

Two millilitres of solution of either irradiated or control unmodified collagen (10 µg/ml in 0.016 M CH_3COOH) were applied on polystyrene Petri dishes (Gama, Ceske Budejovice, CR; diameter 5 cm) and dried in a laminar flow box. The VSMCs were obtained using an explantation method from the intima-media complex of the thoracic aorta of four 8-week-old male Wistar-Kyoto rats [3, 4, 5]. In passages 7 to 10, they were seeded on the collagen samples at the initial density of 30,000 cells per dish (i.e. 1529 cells per cm^2) in 3 ml Dulbecco's Minimum Essential Medium (Institute of Sera and Vaccines, Prague, CR), supplemented with 10% of fetal calf serum (Sebak GmbH, Aidenbach, Germany) and 40 µg/ml gentamicin (LEK, Ljubljana, Slovenia). The cultures were incubated at 37°C and 95% humidity in air atmosphere containing 5% CO_2. When most of the cells were attached and spread on the growth support and the first mitotic figures were observed, the culture medium containing non-adherent cells was removed and replaced with 4 ml of fresh medium. The cells were then grown without medium change for 10 days to determine their growth curves. During the first 4 days after inoculation, the adhered cells were counted under a phase-contrast microscope equipped with a calibrated ocular grid. This method, however, was not suitable at later culture intervals (day 7 and day 10) when the cell population density was higher and multilayered areas were also present. Therefore, the VSMCs were harvested using 0.1% trypsin (Sigma, St. Louis, Mo.) in phosphate-buffered saline (PBS, pH 7.35, 37°C) and counted in the Bürker's haemocytometer. During trypsinisation, the morphology of cells was monitored by means of phase-contrast microscopy at 3-min intervals, and the time needed for the complete detachment of cells from the collagen was measured by a modification of previously described methods [4, 5]. The resistance of cells to the detachment by trypsin was measured also in 3- and 4-day-old cultures. In addition, the spontaneous detachment of cells was evaluated by counting cells floating into the culture medium in the Bürker's haemocytometer on days 3, 4, 7 and 10 after seeding [3].

Doubling time, mitotic index, cell volume

The doubling time (DT) was calculated as $DT=(t-t_o)\log 2/\log Nt-\log Nt_o$, where t_o and t represent earlier and later time intervals after seeding, respectively, and Nt_o and Nt the number of cells at these intervals.

The mitotic index (i.e. percentage of cells in mitosis from all cells in the population adhered to the growth support) was evaluated using phase contrast microscopy in 2-h to 102-h-old cultures fixed with 70% ethanol and stained with 1% toluidine blue. In each culture, at least 200 cells were evaluated.

Cell volume was determined in cells in suspension, where the cell shape could be considered as spherical. Three-day-old cultures were detached using trypsin, re-suspended in PBS and their diameters (d) were measured under a phase-contrast microscope (Axioplan, Opton, Germany) using an ocular microscale. The volume of cells (V) was calculated as $V=4/3\pi(d/2)^3$.

5-Bromo-2-deoxy-uridine labelling index

Three days after seeding, the cells were incubated with 40 µM 5-bromo-2′-deoxy-uridine (BrdU; Sigma; 30 min, 37°C), washed with PBS, fixed with a pre-cooled (–20°C) 70% ethanol for 15 min, and their DNA was partially denatured by treatment with 3 N HCl (20 min, room temperature). The samples were then washed in 0.1 M sodium tetraborate (pH 8.5, 10 min) and non-specific binding sites were blocked using 3% bovine foetal serum in PBS with 0.3% Triton X-100 (Sigma) for 30 min. The newly synthesised DNA was immunolabelled with an anti-BrdU mouse monoclonal antibody (Exbio, Prague, CR; dilution 1:10). Biotin-conjugated goat anti-mouse IgG (Fab specific, Sigma; dilution 1:300) and ExtrAvidin-Peroxidase (Sigma; dilution 1:100) were used in consequent steps. All three chemicals were diluted in PBS with 3% bovine foetal serum and 0.3% Triton X-100 and applied for 60 min at room temperature. 3,3′-Diaminobenzidine (Sigma) was used as chromogen; the colour was intensified by $NiCl_2$ (5 min). The cells were counterstained with light green and the percentage of BrdU-labelled nuclei was assessed using phase-contrast microscopy.

Protein content in cells and enzyme-linked immunosorbent assay

On day 3 after seeding, the cells were harvested by mild trypsinisation (0.1% trypsin in PBS, pH 7.35, 37°C), re-suspended in distilled water (5×10^6 cells/ml) and treated with an Ultrasonic Homogeniser (Cole-Parmer Instrument Co., Chicago, Ill.). For better exposure of epitopes of vinculin and talin, the cell homogenates were incubated with 0.1% Triton-X100 in PBS or 0.1% Zwittergent 3–14 (Calbiochem, La Jolla, Calif.) in 20 mM KCl at 4°C overnight. Protein content was determined using Lowry's method [21]. Aliquots of the homogenates corresponding to 1–50 µg pro-

Table 1 Primary antibodies used for immunofluorescence staining and enzyme-linked immunosorbent assay (ELISA). *Immf* immunofluorescence, *RT* room temperature

Antibody against	Made in	Source	Method	Dilution	Incubation
Human β_1 integrin chain	Rabbit	Chemicon[a]	Immf. ELISA	1:50–1:100 1:100–1:200	4°C overnight RT 1 h
Human α_v integrin chain	Rabbit	Chemicon[a]	Immf. ELISA	1:50–1:100 1:100–1:200	4°C overnight RT 1 h
Human vinculin	Mouse	Serotec[b]	Immf. ELISA	1:50–1:100 1:100–1:200	4°C overnight RT 1 h
Human talin	Mouse	Sigma[c]	Immf. ELISA	1:50–1:100 1:100–1:200	4°C overnight RT 1 h
Human α-actin (clone 1A4)	Mouse	Sigma[c]	Immf. ELISA	1:200 1:500–1:1000	RT 1 h RT 1 h
Human vimentin	Mouse	Exbio[d]	Immf. ELISA	1:25–1:50 1:200–1:400	RT 1 h RT 1 h
Human ICAM-1	Mouse	Exbio[d]	Immf. ELISA	1:100 1:500–1:1000	4°C overnight RT 1 h
Human VCAM-1	Mouse	Exbio[d]	Immf. ELISA	1:100 1:1000–1:2000	4°C overnight RT 1 h

[a] Chemicon International Inc., Temecula, Calif.
[b] Serotec Ltd., Oxford, England
[c] Sigma, St. Louis, Mo.
[d] Exbio, Prague, CR

tein were diluted in 50 µl water and adsorbed onto 200-µl wells of 96-well microtitre plates (Gama Co., Ceske Budejovice, CR, or Maxisorp, Nunc, Roskilde, Denmark) at 4°C overnight. After washing twice with PBS (100 µl/well), the non-specific binding sites were blocked by 0.02% gelatin in PBS (60 min, 100 µl/well). The primary antibodies listed in Table 1 were diluted in 3% bovine foetal serum in PBS and applied in an amount of 50 µl/well for 60 min at room temperature. As a secondary antibody, a peroxidase-conjugated goat anti-rabbit affinity-purified antibody (Chemicon International Inc., Temecula, Calif.; dilution from 1:10000 to 1:40000) was used after staining with polyclonal anti-β_1 integrin antisera or anti-α_v antibody. After staining with monoclonal primary antibodies, a peroxidase-conjugated goat anti-mouse $F(ab')_2$ IgG fragment (Sigma; dilution from 1:1000 to 1:2000) was applied. Both secondary antibodies were diluted in 3% bovine serum in PBS and applied for 45 min at room temperature (50 µl/well). After double washing in PBS/0.1% Triton X-100 solution, the orthophenylendiamine reaction (Sigma) was performed using 0.05% H_2O_2 in 0.1 M phosphate buffer (pH 6.0, dark place, 100 µl/well). The reaction was stopped after 10–25 min by 2 M H_2SO_4 (50 µl/well). The absorbances were measured at 492 nm in the Titertek Multiskan MCC/340 (Finland). The values obtained in cells grown on UV-irradiated collagen were expressed as a percentage of those measured in control cell samples taken from the unmodified collagen. The molecules exhibiting the highest changes in their content were evaluated again in cells in 7-day and 10-day-old cultures.

Immunofluorescence staining

On day 3 after seeding, the cells fixed by methanol (–20°C, 10 min, for staining of β_1 and α_v integrins, vinculin, talin, α-actin, ICAM-1 and VCAM-1) or unfixed (for vimentin) were pre-treated with 3% bovine serum in PBS containing 0.1% Triton X-100 for 30 min at room temperature and incubated with primary antibodies given in Table 1. As the secondary antibodies, we used fluorescein isothiocyanate (FITC)-conjugated goat anti-mouse or goat anti-rabbit IgG (Sigma; dilution 1:200). The antibodies were diluted in PBS supplemented with 3% bovine serum or, in the case of intracellular antigens, also by 0.1% Triton X-100. The cells were mounted in PBS/glycerine (9:1) and observed under an Opton Axioplan epifluorescence microscope or a Bio-Rad MRC600 confocal laser scanning microscope using an oil immersion 60× objective (numerical aperture=1.4) and excitation wavelength 488 nm. The molecules with the most markedly altered distribution were stained also in cells 7 days and 10 days after seeding.

Results

Biochemical characterisation of UV-irradiated collagen type III

The magnitude of the UV irradiation-induced collagen modification was assessed by measuring its tri-dimensional fluorescence spectral arrays. Fig. 1A shows the spectra in a control sample and Fig. 1B spectra after 2 h of UV irradiation. It is apparent that the only alteration in the spectra of collagen type III caused by irradiation is a decrease in the intensity of tyrosine fluorescence. This decrease reflects a magnitude of collagen damage and suggests that approximately one-half of the tyrosine residues has been destroyed.

As the tri-dimensional spectral arrays represent a kind of "fingerprint", the lack of other differences between control and irradiated collagen-III samples indicates a low level of modification of amino acid side chains. It contrasts with our previous findings in collagen type I, where new fluorophores were observed after UV irradiation [4]. SDS-PAGE, illustrated in Fig. 2, revealed fractionation of the irradiated collagen type-III molecules. The asterisks in lane 2 indicate low-molecular weight fragments produced during the UV irradiation. Thus, in collagen type III the oxidative damage induced by UV irradiation includes destruction of tyrosine and fragmentation of the peptide chain.

Adhesion, proliferation, morphology and detachment of VSMCs on UV modified collagen III

Two hours after seeding, almost all cells (i.e., from 90% to 100%) seeded on both control and irradiated collagen samples were attached and flattened. Their initial population densities were similar, i.e. 1460±30 cells/cm^2 and 1470±25 cells/cm^2 on control and modified collagen, re-

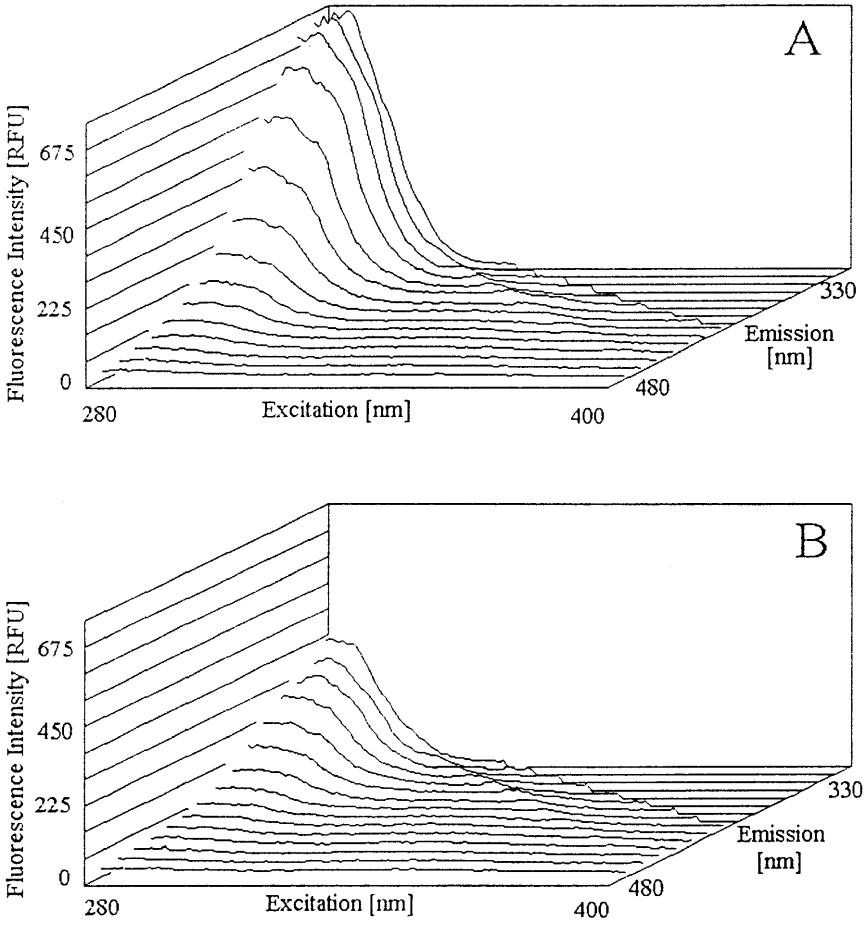

Fig. 1 Excitation spectral arrays of control and ultraviolet (UV)-irradiated collagen III. **A** Spectra of native collagen III. **B** Spectra after 120 min UV irradiation. In both instances, the same collagen concentration of 1 mg/ml was used. The decrease in peak height in irradiated collagen represents destruction of tyrosine residues

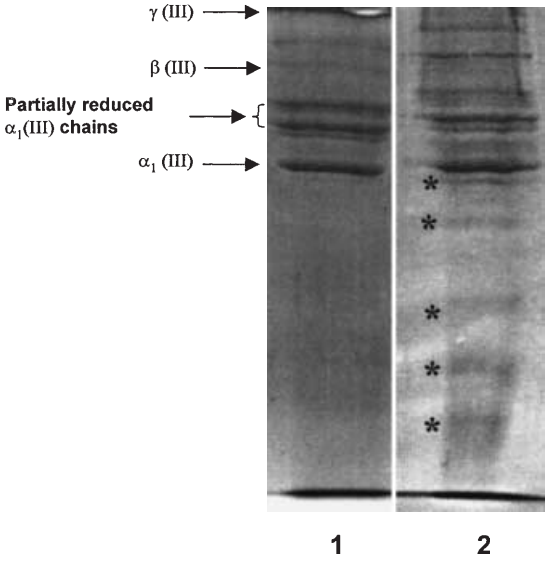

Fig. 2 Electrophoretic profile of collagen type III (*1*) and ultraviolet-irradiated collagen type III (*2*). Electrophoresis was run under reduced conditions with 5% of 2-mercaptoethanol in 7.5% polyacrylamide gel. *γ*: γ fraction (α chain polymers), *β*: β fraction (α chain dimers), *α1*: individual chains of collagen type III

Table 2 Growth parameters of vascular smooth muscle cells cultured on ultraviolet (UV) light-irradiated collagen III. Mean±SEM from 4–8 experiments (3–7 cultures for each experiment)

Parameter	Unmodified collagen	Significance	UV-irradiated collagen
Mitotic index (%)			
2 h	0.21±0.21	n.s.	0.39±0.22
6 h	1.68±0.46	$P \leq 0.02$	3.96±0.56
25 h	3.30±0.54	$P \leq 0.05$	5.17±0.36
72 h	4.66±0.30	$P \leq 0.01$	7.17±0.58
102 h	4.63±0.36	$P \leq 0.05$	6.10±0.47
BrdU labelling index (%)			
72 h	47.78±3.08	$P \leq 0.01$	62.89±2.41
Doubling time (h)			
2–6 h	37.1±5.4*	$P \leq 0.05$	18.4±5.0
6–25 h	34.8±6.0*	$P \leq 0.05$	18.3±1.5
25–72 h	24.9±1.1	n.s.	21.9±0.7
72–102 h	24.0±3.2	n.s.	25.3±1.8
102–168 h	34.1±4.2	n.s.	38.9±3.4
168–240 h	71.0±9.2	n.s.	93.6±17.0
Cell volume (μm^3)			
72 h	1252.2±16.4	n.s.	1203.6±33.5
Protein content (mg/10^6 cells)			
72 h	0.215±0.55	n.s.	0.196±0.34

* In these cases, doubling time was measurable in only 25–50% of cultures. Evaluated using Student's *t*-test for unpaired data

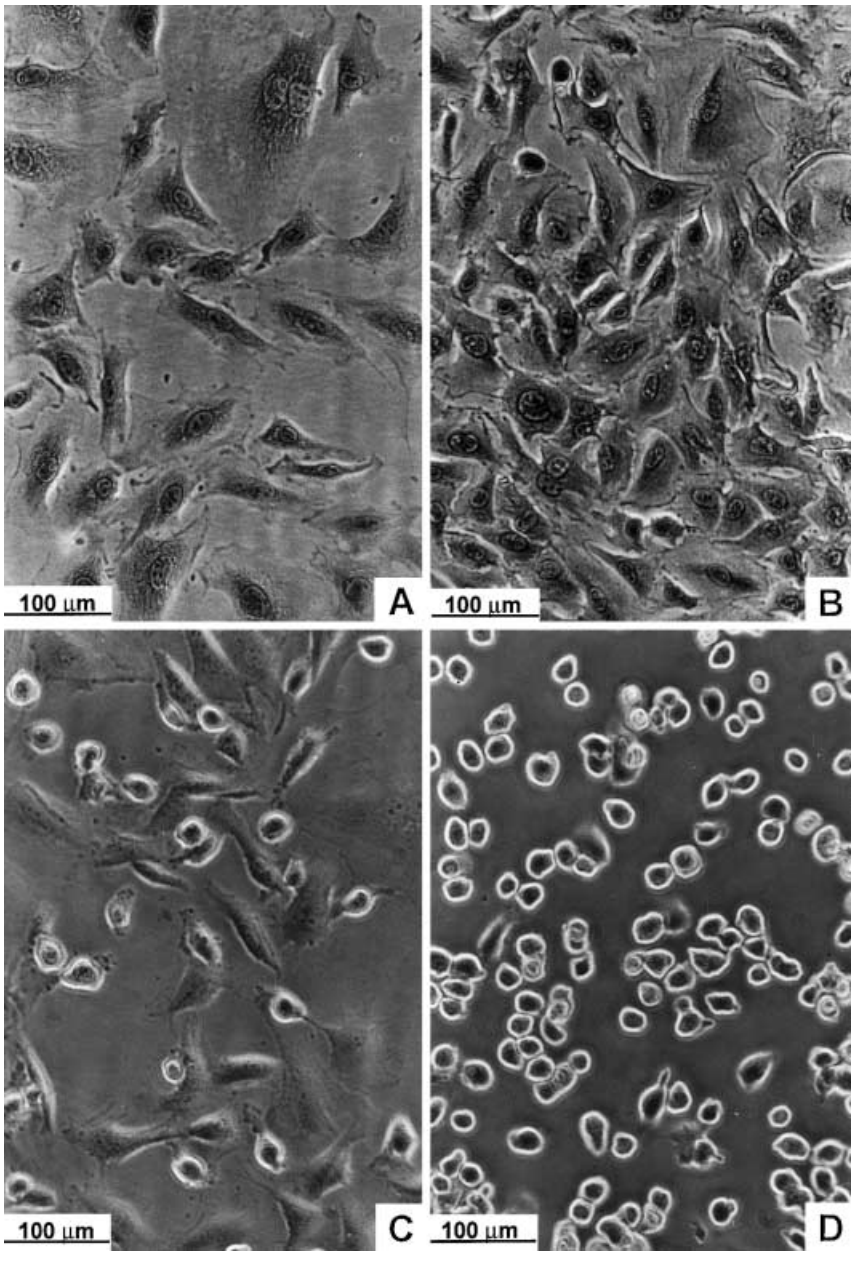

Fig. 3 Morphology of vascular smooth muscle cells on unmodified (**A**, **C**) and ultraviolet-irradiated collagen (**B**, **D**). Adherent cells on day 4 after seeding (**A**, **B**; fixed by methanol, stained with toluidine blue). Living cells after 5-min treatment with 0.1 trypsin (**C**, **D**). Original magnification 200×

spectively. Also, the first mitotic figures appeared at this time. At 6 h after seeding, their percentage (i.e., the mitotic index) became significantly higher in cultures on the irradiated collagen (+135%, Table 2). During the following 96 h, this difference gradually decreased to only +31% but still remained significant. Also, the percentage of cells synthesising DNA (i.e. BrdU labelling index), measured at 72 h after seeding, was significantly higher (by 32%) in cells on the UV-modified collagen.

As a consequence of the higher cell division activity, a shorter doubling time of cells growing on the irradiated collagen was expected. However, this difference was apparent only during the first 25 h after seeding and then disappeared (Table 2). This could be due, at least partly, to a higher spontaneous detachment of cells from the irradiated collagen, as indicated by a higher number of cells floating in the culture medium (Table 3). If the doubling time from 25 h to 72 h was calculated not only in the adherent part of the population, but also the cells released during this time interval from the growth support and floating in the culture medium were included, this time became significantly shorter in cells on the irradiated collagen (20.7±0.6 h vs 24.3±1.0 h on control collagen, $P<0.05$). Also the resistance of cells on the UV-modified collagen to detachment by trypsin was significantly lower (Table 3), although most cells on both collagen samples were of similar morphology and contacted the growth support by areas of similar size (Fig. 3A, B).

Despite the higher tendency to lose contact with the growth support, the cells growing on the irradiated collagen attained a significantly higher population density between 6 h and 102 h after seeding (Table 2, Fig. 4). This

Table 3 Spontaneous and trypsin-mediated detachment of vascular smooth muscle cells from ultraviolet (UV) light-irradiated collagen III. Mean±SEM from 4 experiments (2–4 cultures for each experiment). Evaluated using Student's *t*-test for unpaired data

Parameter	Unmodified collagen	Significance	UV-irradiated collagen
Number of cells floating in the culture medium (%)			
72 h	3.5±0.8	$P \leq 0.01$	8.8±1.0
103 h	3.2±0.6	$P \leq 0.02$	6.6±0.8
168 h	2.8±0.8	n.s.	4.6±0.6
240 h	2.6±0.4	n.s.	3.5±0.4
Time required for the complete detachment of cells by 0.1% trypsin (min)			
72 h	16.5±0.9	$P \leq 0.001$	7.5±0.9
103 h	16.5±0.9	$P \leq 0.01$	8.3±1.4
168 h	18.0±1.2	$P \leq 0.01$	12.8±1.8
240 h	18.0±1.2	$P \leq 0.05$	14.3±0.8

difference reached a maximum in 72-h-old cultures (+83%) and then diminished. On day 7 and day 10 after seeding, the cells on both control and modified collagen samples differed significantly only in their resistance to detachment by trypsin. The cells on both collagen samples showed also similar volume and total protein content, even in the period of proliferation differences (Table 2). As revealed by the changes of pH of the medium monitored by phenol red, the cells on both unmodified and irradiated collagen appeared viable and well metabolising, but the pH did not reach extremely low values (i.e. yellow colour of the medium) during the whole 10-day culture period. During the whole period, the cells of both experimental groups usually grew exponentially without reaching the maximum population density and entering the stationary phase of growth (Fig. 4).

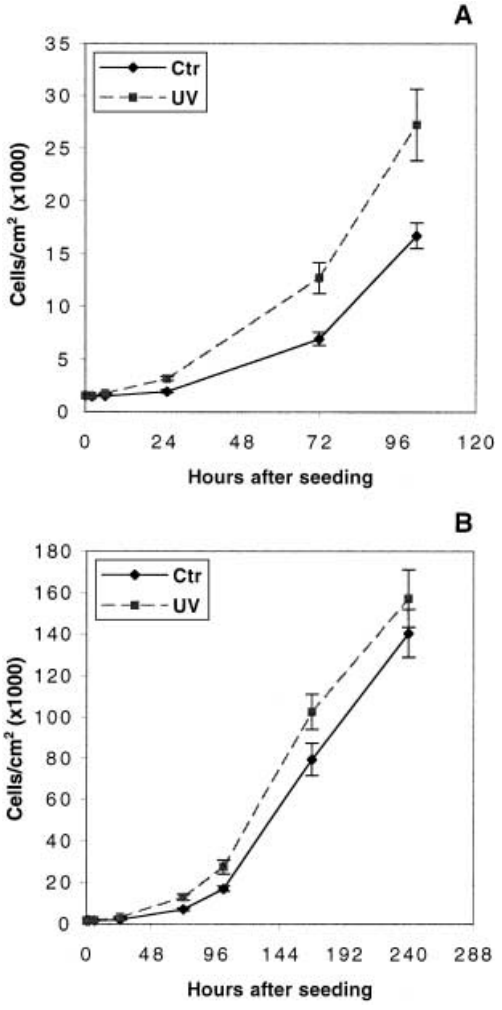

Fig. 4 Growth curves of vascular smooth muscle cells on unmodified (*Ctr*) and ultraviolet-irradiated (*UV*) collagen III. **A** The initial part of the curves obtained by counting cells at lower population densities under a phase-contrast microscope with ocular grid. **B** Whole growth curves completed by counting cells at higher population densities in Bürker haemocytometer after their trypsinisation. The data are given as mean±SEM from four experiments (3–7 cultures for each one) and evaluated using the Student's *t*-test for unpaired data (6–25 h, $P \leq 0.01$; 72 h, $P \leq 0.02$; 96 h, $P \leq 0.05$)

Content and arrangement of adhesion and cytoskeletal molecules in VSMCs on UV-irradiated collagen III

On day 3 after seeding, the enzyme-linked immunosorbent assay (ELISA) revealed that the concentrations of β_1 integrins, focal adhesion proteins talin and vinculin and cytoskeletal protein vimentin were relatively but significantly lower in VSMCs growing on UV-irradiated collagen (by 6–18%, $P<0.05$, Fig. 5A). The concentrations of α_v integrins and α-actin appeared to be unchanged in these cells, but the concentration of ICAM-1 and VCAM-1 was significantly higher by 11% and 16%, respectively ($P<0.05$). The immunofluorescence staining showed that in cells on control collagen, the β_1 integrin molecules are clustered to abundant fine streak-like focal contacts with parallel orientation, whereas in VSMCs on UV-modified collagen they are distributed more randomly (Fig. 6A, B). Similarly, in VSMCs on unmodified collagen, both talin and vinculin molecules were organised into numerous and clearly stained focal adhesion plaques, whereas on UV-irradiated collagen, they were distributed more diffusely and their concentration in focal adhesion sites appeared to be lower (Fig. 7A–D). The arrangement of α_v integrins was similar in cells on both native and irradiated collagen (Fig. 6C, D). However, the number of cells with distinct well-developed α-actin-containing microfilament bundles (Fig. 7E) was lower on the modified collagen (43.8±4.7% compared with 56.8±3.8% of cells on control collagen, $P<0.05$). On this collagen, the cells with finer and less intensely stained α-actin microfilaments (Fig. 7F) or even cells with granular distribution of α-actin prevailed (by 13.0±4.2%). Similarly, in 49.7±4.7% of cells on the unmodified collagen, the vimentin was organised into filaments forming abundant mesh-like network filling the whole cytoplasm (Fig. 7G), whereas on the irradiated collagen, it was only

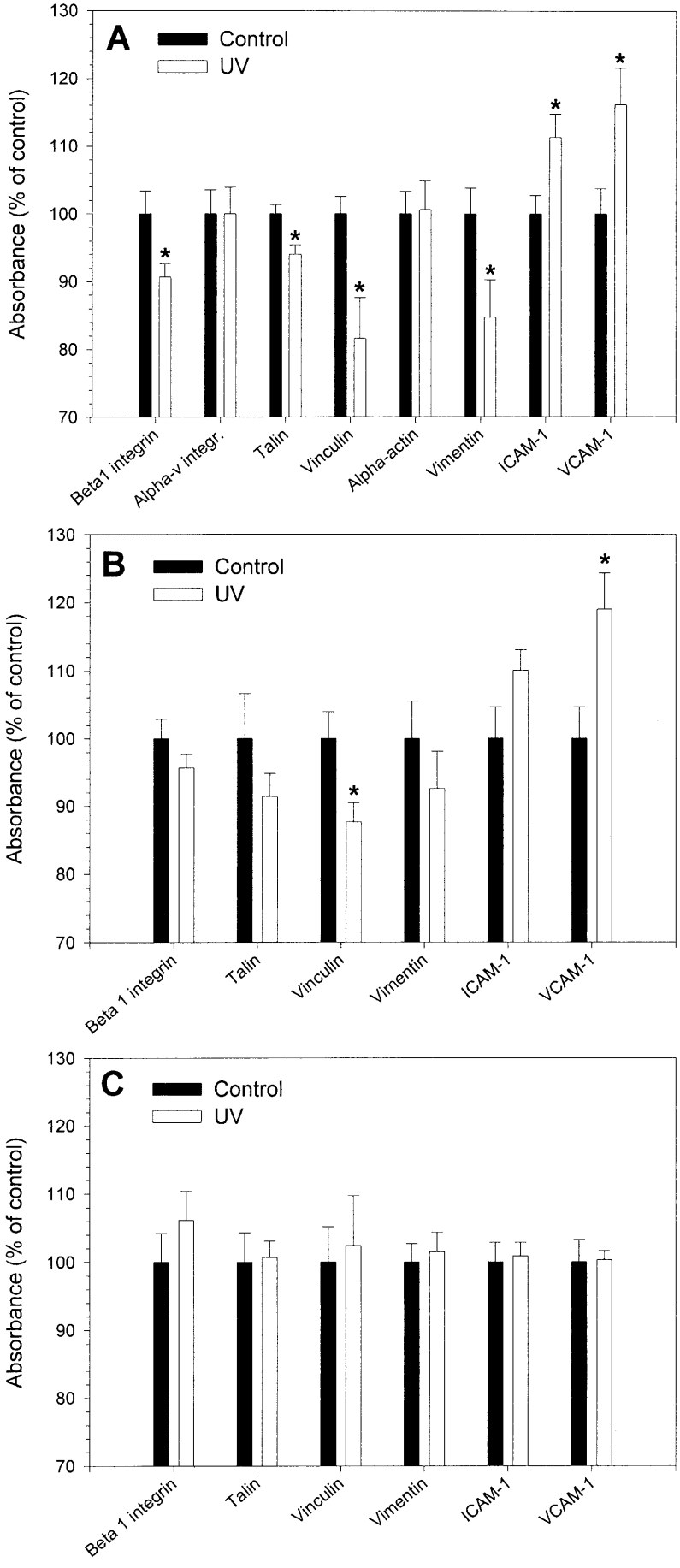

Fig. 5 Content of adhesion and cytoskeletal molecules in the vascular smooth muscle cells growing on unmodified (*Control*) or ultraviolet-irradiated (*UV*) collagen III. Measured using enzyme-linked immunosorbent assay (per milligram of protein) on day 3 after seeding (**A**); the molecules with the most markedly changed content evaluated also on day 7 (**B**) and day 10 (**C**). Absorbances of cell samples from the ultraviolet-irradiated collagen are expressed as a percentage of values obtained from control cells grown on unmodified collagen. Mean±SEM from six experiments; Student's *t*-test for unpaired data, $*P \leq 0.05$ compared with the control

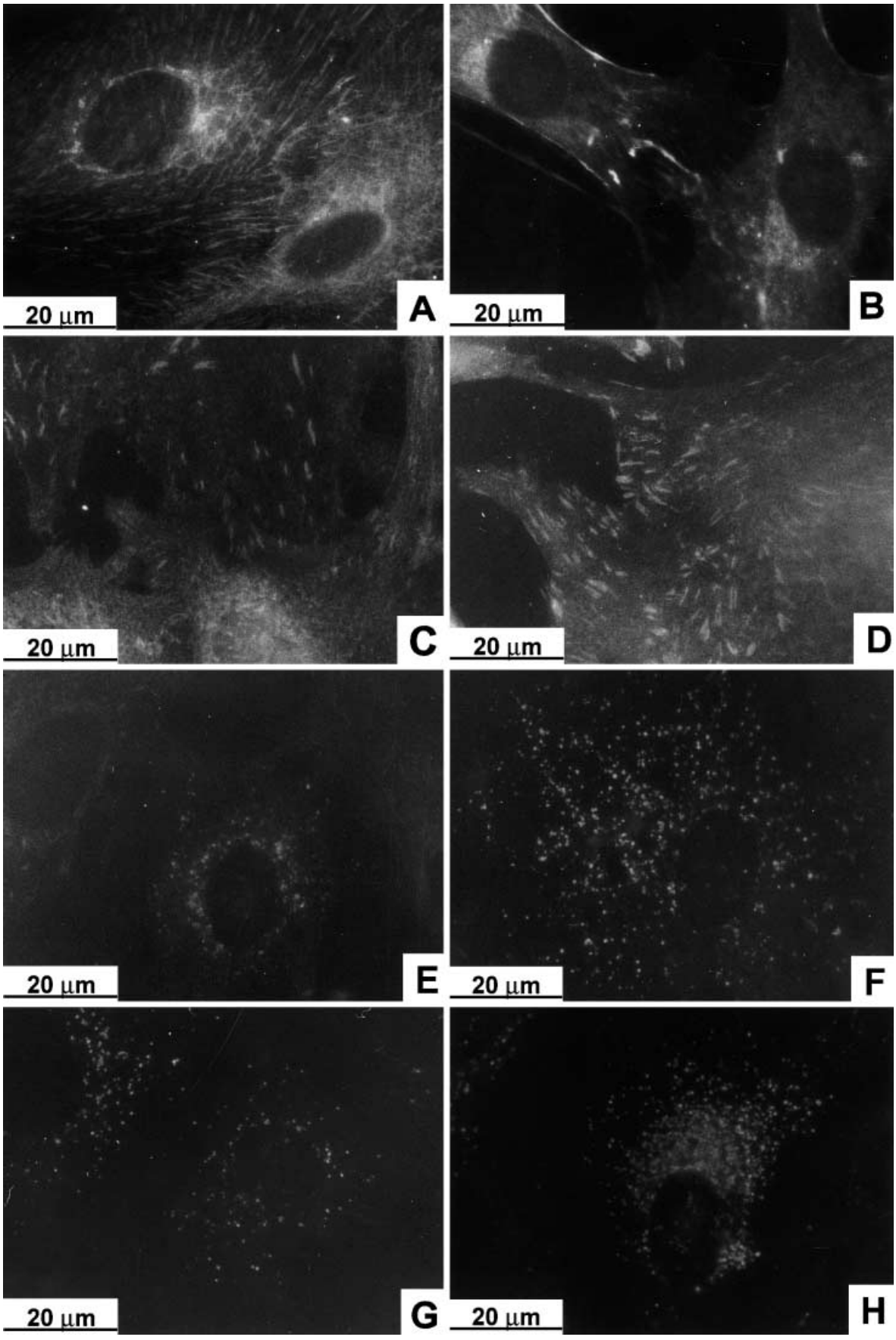

Fig. 6 Legend see page 58

in 29.3±3.5% of cells ($P<0.02$). In most cells on this collagen sample, the vimentin was distributed more diffusely and found mainly in the perinuclear region (Fig. 7H). The immunoglobulin molecules, ICAM-1 and VCAM-1, formed more apparent and numerous dot-like structures in cells on irradiated collagen (Fig. 6E–H).

Towards day 10 after seeding, the differences in content and distribution of surface adhesion and cytoskeletal molecules gradually disappeared. On day 7, only the concentration of vinculin was significantly lower and the concentration of VCAM-1 was higher in cells on the irradiated collagen (Fig. 5B). On day 10, the concentrations of all proteins studied became similar to their control values (Fig. 5C). Also the arrangement of these molecules in cells was almost normalised on day 10; only the β_1 integrins and vinculin were often clustered in more coarse and more irregular focal adhesion plaques (Fig. 8A–D).

Discussion

In agreement with our previous study on UV-irradiated collagen type I [4], we have demonstrated here that also on type-III collagen exposed to UV light the VSMCs proliferated more intensely than on control unmodified collagen. This is documented by a higher DNA synthetic and mitotic activity, resulting in higher cell population densities. The doubling time of the VSMC population adhering to the UV-irradiated collagen was significantly shorter only in the earliest period of culture. Also the differences in population densities of cells growing on both control and tested collagen samples gradually diminished, and, on day 7, they usually disappeared. This could be explained by the higher spontaneous detachment of these cells found in the present study. This detachment could be due to cell death or simply to a lower adhesion strength of normal viable cells (due, for example, to a lower number of bonds between collagen and cells). Our findings of normal gross morphology, metabolism and even higher proliferation capacity of VSMCs on the UV-irradiated collagen, coupled with a lower expression of some adhesion and cytoskeletal molecules, rather suggest the latter possibility. Similar results were obtained when the adhesion of VSMCs derived from male and female rats was compared. The male-derived cells were more prone to spontaneous detachment, but the percentage of dead cells in the floating part of the population was lower [3].

An alternative explanation of the decreasing proliferation differences between VSMCs on control and modified collagen could be a gradual degradation of the modified collagen by VSMCs and its replacement by their own newly synthesised extracellular matrix [14, 31, 33]. Also the autocrine production of growth factors in VSMCs in vitro [12, 19] and their accumulation in the culture medium could mask the stimulatory effect of modified collagen on VSMC proliferation. A similar decrease in cell number differences with the time in culture was also seen when the growth of VSMCs on different types of collagen and plastic dishes was compared [31].

What mechanisms increase the VSMC proliferation on the UV-modified collagen type III? Two types of changes of collagen structure may be expected after UV irradiation: oxidation of the side chains and fragmentation of the collagen molecule. Our fluorescence and electrophoresis analyses presented here showed that the second alternative is more pronounced. Both oxidation and fragmentation of the collagen molecule could stimulate the proliferation of VSMCs by lowering their adhesion to the growth support. In cells growing on the UV-irradiated collagen in the present study, we observed a lower concentration and more random distribution of β_1 integrins, receptors for collagen, as well as focal adhesion proteins talin and vinculin. Also, α-actin-containing microfilaments, which associate with focal adhesion plaques, were less developed. This could be a cellular response to a lower number of functional binding sites for cells on the modified substrate [8, 9, 22, 23]. The lower expression and redistribution of adhesion-mediating molecules in cells on the UV-modified collagen was associated with a lower strength of cell adhesion, indicated by a higher spontaneous and trypsin-mediated detachment of cells. It is known that maximum proliferation rate and migration speed of cells occur at intermediate adhesion strength. Too high a binding capacity of integrin receptors, their grouping in too large and numerous focal contacts and their strong association with well developed actin stress fibres can impair division and migration of cells [13, 26, 28]. In other words, the adhesive capacity of cells cultured on control collagen was probably out of the optimal range for cell proliferation relative to conditions on the UV-irradiated collagen. It has been shown previously that the normal mature molecules of collagen I or III suppress proliferation and migration of VSMCs and other cell types and enhance their differentiation [24, 31]. Similar findings were reported also for other vascular extracellular matrix molecules, such as fibronectin, vitronectin, laminin, elastin and glycosaminoglycans in vitro as well as in situ. Large polymeric and mature molecules usually promote adhesion, quiescence

◀ **Fig. 6** Immunofluorescence staining of surface adhesion molecules of integrin and immunoglobulin superfamilies in 3-day-old cultures of vascular smooth muscle cells (VSMCs) grown on control unmodified (**A**, **C**, **E**, **G**) or ultraviolet-irradiated (**B**, **D**, **F**, **H**) collagen. Integrins β_1 (**A**, **B**), integrins α_v (**C**, **D**), intercellular adhesion molecule 1 (ICAM-1; **E**, **F**) and vascular cell adhesion molecule 1 (VCAM-1; **G**, **H**). Zeiss Axioplan epifluorescence microscope, original magnification 1000×

Fig. 7 Immunofluorescence staining of proteins of membrane and cytoplasmatic cytoskeleton in 3-day-old cultures of vascular smooth muscle cells grown on control unmodified (**A**, **C**, **E**, **G**) or ultraviolet-irradiated (**B**, **D**, **F**, **H**) collagen. Talin (**A**, **B**), vinculin (**C**, **D**), α-actin (**E**, **F**) and vimentin (**G**, **H**). Confocal laser scanning microscope, original magnification 560× ▶

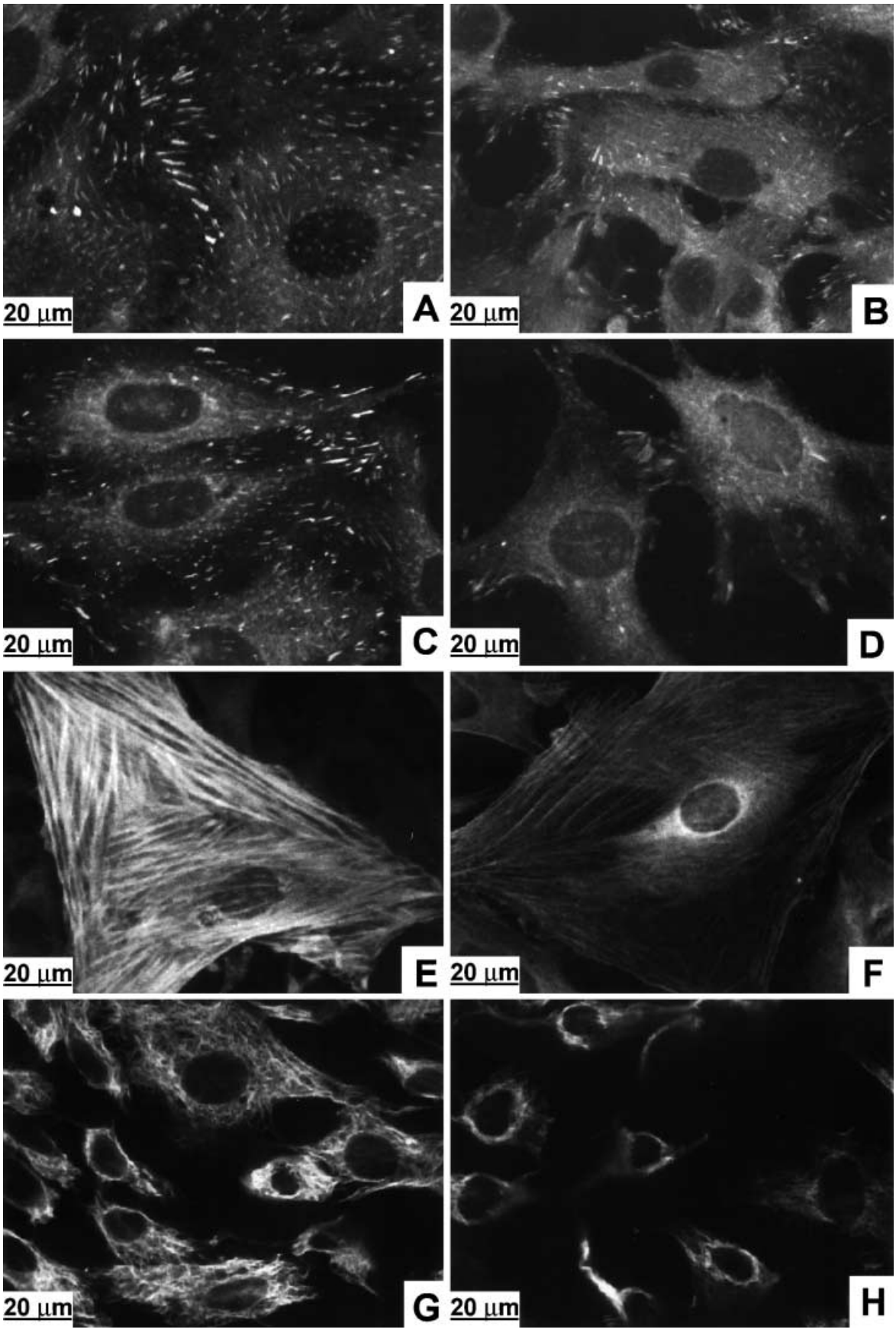
20 μm
A
20 μm
B
20 μm
C
20 μm
D
20 μm
E
20 μm
F
20 μm
G
20 μm
H

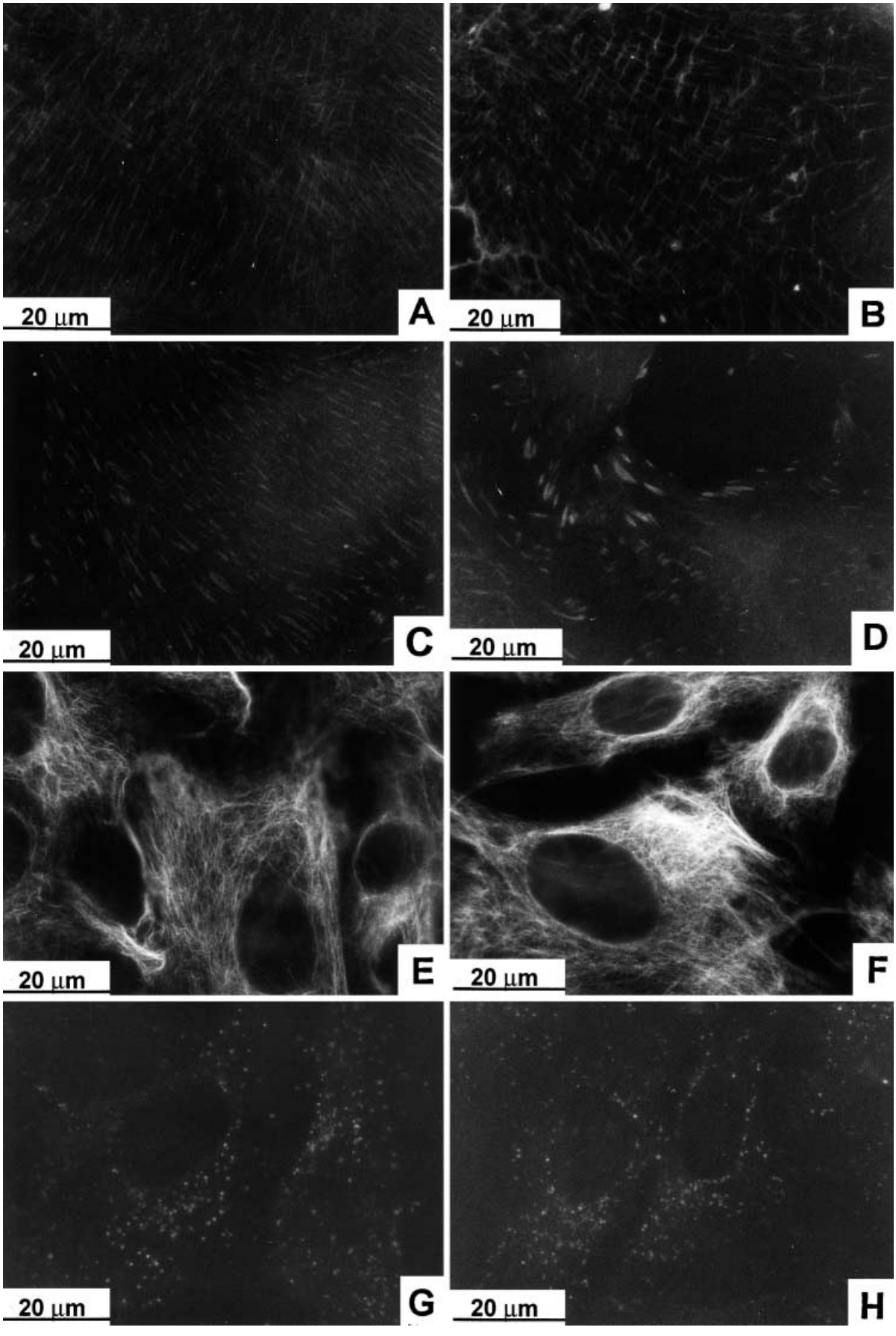
20 μm
A
20 μm
B
20 μm
C
20 μm
D
20 μm
E
20 μm
F
20 μm
G
20 μm
H

and differentiation of VSMCs, whereas their physical and chemical modifications, e.g. fragmentation and glycation, or their immature mono- or oligomeric forms allow migration and proliferation of these cells [14, 15, 17, 33]. Our finding of less developed fibrillar, or even granular forms of α-actin, an important marker of VSMC differentiation [3, 11, 14], in VSMCs on UV-modified collagen is in accordance with this concept and suggests a higher tendency of these cells to so-called "phenotypic modulation", i.e. transition from the "contractile" to the "synthetic" state [2, 3, 14].

The cells in the present study could interact with the collagen growth support not only directly but also through adsorption of proteins from the serum supplement of the culture medium, e.g. vitronectin. The content of α_v integrins, main receptors for this glycoprotein, and their clustering into focal adhesion plaques were similar in cells on both control and modified collagen. However, both groups of cells could differ in expression of individual members of this integrin superfamily – for example $\alpha_v\beta_3$, an important molecule supporting the proliferation of VSMCs [34, 37] – which remains to be investigated in VSMCs growing on the modified collagen.

The concentration of vimentin was significantly lower in 3-day-old cells on UV-modified collagen and its organisation into cytoskeleton disrupted. This can be explained by degradation of vimentin molecules or by its qualitative changes lowering its reactivity to monoclonal antibodies, similarly as observed in cultured vascular cells or synoviocytes exposed to oxyhemoglobin or hydrogen peroxide [10, 29, 36]. In situ conditions, the altered vimentin cytoskeleton can be associated with a lower resistance of vascular cells to the shear stress and blood pressure [32].

A pathophysiologically important finding of our present study is the increased concentration ICAM-1 and VCAM-1, surface adhesion molecules of immunoglobulin superfamily and receptors for cells of the immune system, on VSMCs cultured on UV-irradiated collagen. The increase in expression of these molecules was described in cultures of vascular endothelial cells exposed to oxidised low-density lipoproteins [1] or HeLa cells affected by reactive oxygen intermediates produced by ionising irradiation [6]. The increase of ICAM-1 and VCAM-1 in our study was relatively small. However, it was shown that even a weak increase in expression of these molecules on endothelial cells resulted in a significant increase in number of monocytes bound to these cells [1].

Degradation and oxidation of collagen molecules occur in vivo under various vascular pathological states, such as hypertension and atherosclerosis. In comparison with the direct UV light-induced collagen modifications in the present study, the pathological changes of the collagen in situ are usually indirect and cell mediated, i.e. caused by proteolytic enzymes and free radicals produced in macrophages, leucocytes, thrombocytes, endothelial cells as well as VSMCs [7, 16]. The collagen degradation products in situ may differ from those in the present experiments, e.g. in their size, amino acid composition, spatial conformation as well as in the site of the possible oxidation of the collagen molecule. In addition, collagen III in situ as an interstitial extracellular matrix molecule does not directly contact the VSMC, at least at the onset of the vascular damage. Collagen III and VSMCs are separated by basal lamina molecules, such as laminin, collagen IV or heparan sulphate proteoglycans, which maintain the non-proliferative, differentiated state of VSMCs [14, 33]. Even the blood serum, which penetrates through the dysfunctional endothelial barrier in vascular lesions, can exert some inhibitory effects on the collagen oxidation [18]. Despite the limitations of our described in vitro model, it can be concluded that the collagen of type III modified by UV irradiation increases the proliferation of vascular smooth muscle cells in culture. The increased proliferation is accompanied by a lower strength of adhesion of VSMCs. It is due to the lower β_1 integrin–collagen binding, lower content of focal adhesion proteins talin and vinculin, and alterations of cytoskeleton rather than to increased susceptibility of the UV-modified collagen to trypsin digestion only. At the same time, the VSMCs possess an increased concentration of surface adhesion molecules of immunoglobulin type ICAM-1 and VCAM-1.

Thus, under in situ conditions, the VSMCs surrounded by altered collagen could be more prone to escape the growth control by cell–extracellular matrix contact and to attract cells of the immune system into the vessel wall. It should be pointed out that, in our present in vitro study, the damage of the collagen was only short-term and single, whereas, in the vascular wall in situ, repeated and long-lasting damage to the collagen and other extracellular matrix proteins can be expected. This may result in even more profound changes in the VSMC behaviour. Therefore, our study may help to explain a possible link between the oxidative modification and degradation of matrix proteins and thickening of the vessel wall by hyperplasia of smooth muscle cells in vascular diseases.

Acknowledgements This work was supported by a grant No. 188/98/C from the Grant Agency of the Charles University and a grant No. 305/97/S070 from the Grant Agency of the Czech Republic and by the Centre for Experimental Cardiovascular Reearch, Prague. We also thank Mrs. Ivana Zajanova for her excellent technical assistance. Mr. Peter Photos (Biophys. Eng. Lab., University of Pennsylvania, Philadelphia, USA) is gratefully acknowledged for language revision of the manuscript.

◀ **Fig. 8** Immunofluorescence staining of selected adhesion and cytoskeletal molecules (i.e. most markedly changed on day 3) in 10-day-old cultures of vascular smooth muscle cells grown on control unmodified (**A**, **C**, **E**, **G**) or ultraviolet-irradiated (**B**, **D**, **F**, **H**) collagen. Integrins β_1 (**A**, **B**), vinculin (**C**, **D**), vimentin (**E**, **F**) and vascular cell adhesion molecule 1 (VCAM-1; **G**, **H**). Zeiss Axioplan epifluorescence microscope, original magnification 1000×

References

1. Amberger A, Maczek C, Jurgens G, Michaelis D, Schett G, Trieb K, Eberl T, Jindal S, Xu QB, Wick G (1997) Co-expression of ICAM-1, VCAM-1, ELAM-1 and Hsp60 in human arterial and venous endothelial cells in response to cytokines and oxidized low-density lipoproteins. Cell Stress Chaperon 2:94–103
2. Arisawa S, Arisawa T, Ohashi M, Nitta Y, Ikeya T, Asai J (1996) Effects of the hydroxyl radical on fibroblast-mediated collagen remodelling in vitro. Clin Exp Pharmacol Physiol 23:222–228
3. Bacakova L, Mares V, Lisa V, Bottone MG, Pellicciari C, Kocourek F (1997) Sex-related differences in the migration and proliferation of rat aortic smooth muscle cells in short and long term culture. In Vitro Cell Dev Biol Anim 33:410–413
4. Bacakova L, Wilhelm J, Herget J, Novotna J, Eckhart A (1997) Oxidized collagen stimulates proliferation of vascular smooth muscle cells. Exp Mol Pathol 64:185–194
5. Bacakova L, Mares V, Bottone MG, Pellicciari C, Lisa V, Svorcik V (2000) Fluorine ion-implanted polystyrene improves growth and viability of vascular smooth muscle cells in culture. J Biomed Mater Res 49:369–379
6. Baeuml H, Behrends U, Peter RU, Mueller S, Kammerbauer C, Caughman SW, Degitz K (1997) Ionizing radiation induces, via generation of reactive oxygen intermediates, intercellular adhesion molecule-1 (ICAM-1) gene transcription and NF kappa B-like binding activity in the ICAM-1 transcriptional regulatory region. Free Rad Res 27:127–142
7. Belkhiri A, Richards C, Whaley M, Mcqueen SA, Orr FW (1997) Increased expression of activated matrix metalloproteinase-2 by human endothelial cells after sublethal H_2O_2 exposure. Lab Invest 77:533–539
8. Bobbink IWG, de Boer HC, Telelenburg WLH, Banga J-D, de Groot PG (1997) Effect of extracellular matrix glycation on endothelial cell adhesion and spreading. Involvement of vitronectin. Diabetes 46:87–93
9. Carragher NO, Levkau B, Ross R, Raines EW (1999) Degraded collagen fragments promote rapid disassembly of smooth muscle focal adhesions that correlates with cleavage of pp125(FAK), paxillin, and talin. J Cell Biol 147:619–630
10. Comair YG, Schipper HM, Brem S (1993) The prevention of oxyhemoglobin-induced endothelial and smooth muscle cytoskeletal injury by deferoxamine. Neurosurgery 32:58–64
11. Damiani E, Sugiyama T, Shimamura K, Greci L, Matsuda Y (1998) Altered expression of α-actin, smooth muscle myosin heavy chain-1 and calponin in cultured smooth muscle cells by oxidized low-density lipoproteins. FEBS Lett 425:123–125
12. Delafontaine P, Ku L (1997) Reactive oxygen species stimulate insulin-like growth factor I synthesis in vascular smooth muscle cells. Cardiovasc Res 33:216–222
13. Friedl P, Zänker KS, Bröcker E-B (1998) Cell migration strategies in 3-D extracellular matrix: differences in morphology, cell matrix interactions, and integrin function. Microsc Res Tech 43:369–378
14. Glukhova MA, Koteliansky VE (1995) Integrins, cytoskeletal and extracellular matrix proteins in developing smooth muscle cells of human aorta. In: Schwartz SM, Mecham RP (eds) The vascular smooth muscle cell. Molecular and biological responses to the extracellular matrix. Academic Press, San Diego, pp 37–79
15. Grant MB, Caballero S, Bush DM, Spoerri PE (1998) Fibronectin fragments modulate human retinal capillary cell proliferation and migration. Diabetes 47:1335–1340
16. Hampl V, Herget J (2000) Role of nitric oxide in the pathogenesis of chronic pulmonary hypertension. Physiol Rev 80: 1337–1372
17. Hein M, Fischer J, Kim DK, Hein L, Pratt RE (1996) Vascular smooth muscle cell phenotype influences glycosaminoglycan composition and growth effects of extracellular matrix. J Vasc Res 33:433–441
18. Kalant N, McCormick S (1992) Inhibition by serum components of oxidation and collagen-binding of low-density lipoprotein. Biochim Biophys Acta 1128:211–219
19. Krettek A, Fager G, Lindmark H, Simonson C, Lustig F (1997) Effect of phenotype on the transcription of the genes for platelet-derived growth factor (PDGF) isoforms in human smooth muscle cells, monocyte-derived macrophages, and endothelial cells in vitro. Arterioscler Thromb Vasc Biol 17: 2897–2903
20. Laemmli VK (1970) Cleavage of structural proteins during the assembly of the head of bacteriophage. Nature 227:680–685
21. Lowry OH, Rosebrough NJ, Farr AL, Randall RJ (1951) Protein measurement with the Folin phenol reagent. J Biol Chem 193:265–275
22. Mattana J, Margiloff L, Singhal PC (1997). Metal-catalyzed oxidation of extracellular matrix proteins disrupts integrin-mediated adhesion of mesangial cells. Biochem Biophys Res Commun 233:50–55
23. Messent AJ, Tuckwell DS, Knauper V, Humphries MJ, Murphy G, Gavrilovic J (1998) Effects of collagenase-cleavage of type I collagen on alpha2beta1 integrin-mediated cell adhesion. J Cell Sci 111:1127–1135
24. Miralem T, Whiteside CI, Templeton DM (1996) Collagen type I enhances endothelin-mediated contraction and induces nonproliferating phenotype in mesangial cells. Am J Physiol 270:F960–F970
25. Novotna J, Herget J (1998) Exposure to chronic hypoxia induces qualitative collagen changes in the walls of peripheral pulmonary arteries. Life Sci 62:1–12
26. Palecek SP, Loftus JC, Ginsberg MH, Lauffenburger DA, Horwitz AF (1997) Integrin-ligand binding properties govern cell migration speed through cell-substratum adhesiveness. Nature 385:537–540
27. Peiro C, Angulo J, Rodriguezmanas L, Llergo JL, Vallejo S, Cercas E, Sanchezferrer CF (1998) Vascular smooth muscle cell hypertrophy induced by glycosylated human oxyhaemoglobin. Br J Pharmacol 125:637–644
28. Podesta F, Roth T, Ferrara F, Cagliero E, Lorenzi M (1997) Cytoskeletal changes induced by excess extracellular matrix impair endothelial cell replication. Diabetologia 40:879–886
29. Rogers KR, Morris CJ, Blake DR (1991) Oxidation of thiol in the vimentin cytoskeleton. Biochem J 275:789–791
30. Ruef J, Rao GN, Li FZ, Bode C, Patterson C, Bhatnagar A, Runge MS (1998) Induction of rat aortic smooth muscle cell growth by the lipid peroxidation product 4-hydroxy-2-nonenal. Circulation 97:1071–1078
31. Sakata N, Kawamura K, Takebayashi S (1990) Effects of collagen matrix on proliferation and differentiation of vascular smooth muscle cells in vitro. Exp Mol Pathol 52:179–191
32. Schnittler H-J, Schmandra T, Drenckhahn D (1998) Correlation of endothelial vimentin content with haemodynamic parameters. Histochem Cell Biol 110:161–67
33. Stenmark KR, Mecham RP (1997) Cellular and molecular mechanisms of pulmonary vascular remodeling. Annu Rev Physiol 59:89–144
34. Stouffer GA, Hu ZY, Sajid M, Li HS, Jin GF, Nakada MT, Hanson SR, Runge MS (1998) Beta(3) integrins are upregulated after vascular injury and modulate thrombospondin- and thrombin-induced proliferation of cultured smooth muscle cells. Circulation 97:907–915
35. Swain M, Ross NW (1995) A silver stain control for proteins yielding high resolution and transparent background in sodium dodecyl sulfate-polyacrylamide gels. Electrophoresis 16:948–951
36. Valen G, Sonden A, Vaage J, Malm E, Kjellström BT (1999) Hydrogen peroxide induces endothelial cell atypia and cytoskeleton depolymerization. Free Rad Biol Med 26:1480–1488
37. Yee KO, Rooney MM, Giachelli CM, Lord ST, Schwartz SM (1998) Role of β1 and β3 integrins in human smooth muscle cell adhesion to and contraction of fibrin clots in vitro. Circ Res 83:241–251

Virchows Arch (2002) 440:63–69
DOI 10.1007/s004280100490

ORIGINAL ARTICLE

**Anne Jörns · Markus Tiedge · Ehud Ziv
Eleazar Shafrir · Sigurd Lenzen**

Gradual loss of pancreatic beta-cell insulin, glucokinase and GLUT2 glucose transporter immunoreactivities during the time course of nutritionally induced type-2 diabetes in *Psammomys obesus* (sand rat)

Received: 9 April 2001 / Accepted: 5 June 2001 / Published online: 12 July 2001
© Springer-Verlag 2001

Abstract The *Psammomys obesus* (sand rat) is a well-established model of nutritionally induced non-insulin-dependent type-2 diabetes. When fed a high-energy (HE) diet, the diabetes-prone animals develop hyperinsulinaemia and hyperglycaemia. Within 1 week, all animals become hyperinsulinaemic. However, a loss of immunostaining for insulin as well as for the GLUT2 glucose transporter in the plasma membrane and the glucokinase in the cytoplasm of the pancreatic beta cells became evident only when the animals subsequently developed hyperglycaemia. After 1 week of HE diet feeding, the pancreatic beta-cell volume was reduced by one-third in hyperglycaemic *Psammomys*. Insulin immunostaining as well as GLUT2 glucose transporter immunostaining in the plasma membrane and glucokinase immunostaining in the cytoplasm were reduced by more than 50%. After 3 weeks of HE diet feeding, all changes observed after 1 week were even more pronounced, with reductions in the range of 70–95%. The reduction of the total beta-cell volume of the pancreas due to beta-cell death and the diminution of insulin content of the remaining beta cells in the islets during the HE diet feeding was accompanied by a parallel fall of the pancreas insulin content. For all changes observed, there was a significant correlation with the increase of the blood glucose concentration ($r>0.9$) but not with the increase of the plasma insulin concentration ($r>0.2$). Thus, increasing glycaemia appears to be the factor responsible for the deterioration of the pancreatic beta-cell function and the resulting loss of the insulin secretory capacity in *Psammomys*. The final result of this development is an irreversible diabetic state due to the feeding of the HE diet.

Keywords *Psammomys obesus* · Pancreatic beta cell · Insulin · Glucokinase · GLUT2 glucose transporter · Type-2 diabetes mellitus

A. Jörns (✉)
Centre of Anatomy, Hannover Medical School,
30623 Hannover, Germany

E. Ziv
Diabetes Research Unit, Hadassah-Hebrew University,
Jerusalem, Israel

E. Shafrir
Department of Biochemistry, Hadassah University Hospital,
Jerusalem, Israel

M. Tiedge · S. Lenzen
Institute of Clinical Biochemistry, Hannover Medical School,
Hannover, Germany

Introduction

The *Psammomys obesus* (sand rat) is a desert gerbil with well-established, nutritionally induced non-insulin-dependent type-2 diabetes characterised by insulin resistance, hyperglycaemia and obesity when fed a high-energy (HE) diet [10, 18, 22]. Morphological studies of the *Psammomys* pancreas have shown an initial massive degranulation [2, 12, 14] and a loss of insulin immunostaining [1, 2] of the pancreatic beta cells followed by vacuolisation and finally destruction in the course of the development of the diabetic state [1, 12, 14]. It may be possible that changes in glucokinase, the low-affinity glucose-phosphorylating enzyme, which is the so-called glucose sensor of the pancreatic beta cell responsible for glucose-induced insulin secretion [11, 13], together with changes in the GLUT2 glucose transporter may be responsible for the deterioration of the insulin secretory capacity of the beta cell.

Compared with other animal models of type-2 diabetes, the *Psammomys* has the advantage that the diabetic state develops stepwise in well-classified stages [10, 18, 22]. Within the development of the metabolic disturbances, hyperinsulinaemia appears prior to hyperglycaemia in the animals. This makes it possible to correlate changes in the insulin immunostaining with those of the GLUT2 glucose transporter localisation in the plasma membrane and the glucokinase distribution pattern in the cytoplasm of the pancreatic beta cells, which occur in the different stages of diabetes manifestation. In particu-

lar, it should be possible to decide whether immunocytochemical changes develop in parallel to the development of hyperglycaemia or to hyperinsulinaemia.

We have therefore studied the effects of hyperglycaemia and hyperinsulinaemia on the pancreatic beta cells of the *Psammomys* during the time course of a HE diet. In quantitative analyses, we studied immunocytochemically the changes in insulin staining as well as the expression of the GLUT2 glucose transporter and the glucokinase in the different stages during diabetes development.

Materials and methods

Animals

Pancreatic tissue was obtained from 12- to 14-week-old *Psammomys obesus* (170–230 g b.w.) kept under normal laboratory conditions [1]. One group of *Psammomys* was kept on a low-energy (LE) diet (2.38 Kcal/g; Koffolk, Petach, Tikva, Israel; blood glucose 5.7±0.2 mM) [1]. Another group of *Psammomys* was fed a HE diet (2.93 Kcal/g; Weizmann Institute, Rehovot, Israel) [1]. Blood glucose was determined photometrically, pancreas insulin content radioimmunologically.

For light microscopy, small tissue specimens from the splenic and duodenal parts of the pancreas were freeze dried (–35°C for 72 h), fixed with vapour-phase para-formaldehyde and embedded in Araldite as described in detail elsewhere [8]. Alternatively, larger tissue specimens were fixed by immersion in 4% para-formaldehyde in phosphate buffer and finally embedded in paraffin. For electron microscopy, additional specimens of the pancreases from all experimental groups were fixed with 2% glutaraldehyde and 2% para-formaldehyde and finally embedded in Epon [7].

Immunohistochemistry

Antisera and specificity controls

Polyclonal antisera against insulin (Novo, Bagsvaerd, Denmark), diluted 1:1000–1:3000, against rat GLUT2 glucose transporter (WAK-Chemie, Bad Homburg, Germany), diluted 1:5000–1:10,000, against glucagon (Milab, Malmö, Sweden), diluted 1:10,000–1:20,000, against somatostatin (Dr. Etzrodt, Ulm, Germany), diluted 1:8000, and against pancreatic polypeptide (Dr. Chance, Indianapolis, Ind.), diluted 1:8000 were used. For immunohistochemical staining of glucokinase, we used a polyclonal, affinity-purified antibody raised in rabbits in our laboratory against rat recombinant liver glucokinase at a dilution of 1:25–1:100. Specificity has been confirmed using Western-blot analyses [21]. Antisera against insulin, GLUT2 and glucokinase showed specific immunostaining in *Psammomys* pancreas tissue samples, thus confirming previous results on method and antibody specificities obtained with mouse and rat tissue antisera against insulin, GLUT2 and glucokinase [7, 8, 20].

Immunohistochemical protocol

Serial semi-thin sections (0.5 µm) and paraffin sections (4 µm) were immunostained using the avidin–biotin-complex (ABC) method [4]. Following the fast removal of the resin and overnight incubation with the first antibody, biotinylated goat anti-rabbit Ig G (1:100, 30 min) as second antibody and a mixture of avidin-peroxidase (1:100) and biotin (1:1000, 30 min) (Jackson Immuno Research, West Grove, Ill.) as the third antibody were used. Peroxidase was visualised using 0.7 mM diaminobenzidine and 0.002% hydrogen peroxide in phosphate-buffered saline (PBS), pH 7.3.

A special characteristic of the *Psammomys* pancreas was a particularly large proportion of islets in the pancreatic sections. An average of 4–5 islets were visible per semi-thin section and 10–15 islets per paraffin section. Series of a total of 670 semi-thin and paraffin sections were immunostained sequentially for insulin, GLUT2 glucose transporter and glucokinase and additionally for islet hormones. The sections were viewed using bright-field illumination or phase contrast with a Zeiss Photomicroscope II (Zeiss, Oberkochen, Germany). The thin sections were viewed under an electron microscope EM 9 S2 (Zeiss).

Analysis of sections

In order to verify the changes in the immunoreactivities of insulin, glucokinase and the GLUT2 glucose transporter after 1 week or 3 weeks on a HE diet compared with the control, sections were densitometrically or morphometrically quantified using a computer-assisted method as described previously [8, 9]. The relative beta-cell volume was obtained by calculating the ratio between the area occupied by the insulin-positive cells and the area of the total tissue section. The total beta-cell volume per pancreas was obtained by multiplying this ratio by the total pancreas weight divided by its density. The results are presented as mean values ±SEM and were tested for statistical significance using the Student's *t*-test.

Results

Control pancreas of *Psammomys*

In the pancreas from fed normoglycaemic and normoinsulinaemic control *Psammomys* (Table 1) kept on a LE diet, pancreatic beta cells in islets and at extra-islet sites displayed dense insulin immunoreactivity (Fig. 1A). Pancreatic beta cells exhibited insulin immunostaining all over the cytoplasm. In parallel, beta cells expressed a dense glucokinase staining in the cytoplasm without variations in intercellular distribution (Fig. 1B). The GLUT2 glucose transporter immunoreactivity was restricted to the plasma membrane of the beta cells with small gaps in domains close to the intra-islet capillary system (Fig. 1C).

Pancreas of the *Psammomys* exhibiting normoglycaemia and hyperinsulinaemia after 1 week on HE diet

After 1 week on a HE diet, some *Psammomys* were still normoglycaemic though they had developed hyperinsulinaemia (Table 1). In the pancreases of these animals, the average beta-cell volume was marginally reduced (Table 1). The beta cells in the islets were surrounded by a rim of 1–2 layers of other endocrine cells, mainly α-cells and some δ-cells and PP-cells, as under control conditions. The small reduction of the beta-cell volume of the pancreas and density of the beta-cell insulin immunostaining was accompanied by a reduction of the total pancreas insulin content of around one-third (Table 1). Ultrastructurally, the beta cells showed minimal signs of degranulation. In parallel to the reduction in in-

Table 1 Quantitative analysis of insulin, glucokinase and GLUT2 glucose transporter immunostaining in the beta cells of pancreases from *Psammomys*. The beta cells in the pancreases were analysed at different metabolic stages during development of the diabetic metabolic state. The changes in islet areas and in densities of insulin, glucokinase and GLUT2 glucose transporter staining were determined 1 week or 3 weeks after starting the high energy (HE) diet. The changes in the immunological staining were compared with those of total pancreas insulin content and blood glucose and plasma insulin concentrations. Values are presented as means±SEM

Experimental condition (time on HE diet)	No. of experiments	Blood glucose (mmol/l)	Plasma insulin (ng/ml)	Total beta-cell volume per pancreas (mm^3/pancreas)	Total insulin content per pancreas (U/g wet weight)	Density of beta-cell insulin staining (grey values/μm^2 beta-cell area)	Density of beta-cell glucokinase staining (grey values/μm^2 beta cell area)	Density of GLUT2 staining on beta cell membrane (% staining of membrane)
Control	4	5.7±0.2	4.3±1.3	2.6±0.2	5.8±0.6	254±9	182±2	84±3
After 1 week on HE diet: normoglycaemia hyperinsulinaemia	4	6.5±0.5	32.8±6.4**	2.1±0.1 (–19%)	3.6±0.5* (–36%)	212±17 (–16%)	161±4* (–11%)	62±4 (–26%)
After 1 week on HE diet: hyperglycaemia hyperinsulinaemia	5	15.5±0.8*	45.1±10.9**	1.6±0.2* (–38%)	1.7±0.3** (–71%)	84±21** (–67%)	72±3** (–60%)	24±6** (–71%)
After 3 weeks on HE diet: hyperglycaemia hyperinsulinaemia	4	22.3±1.5*	54.0±17.4**	0.8±0.2** (–70%)	0.4±0.1** (–93%)	51±14** (–80%)	52±3** (–71%)	5±1** (–94%)

*<0.05, **<0.01 compared with the control state

sulin immunostaining of the beta cells (Fig. 2A), the glucokinase immunostaining in the cytoplasm (Fig. 2B) as well as the GLUT2 glucose transporter (Fig. 2C) immunostaining in the plasma membrane were marginally reduced (Table 1).

Pancreas of the *Psammomys* exhibiting hyperglycaemia and hyperinsulinaemia after 1 week on HE diet

Another group of the *Psammomys* had developed both hyperglycaemia and hyperinsulinaemia after 1 week on a HE diet (Table 1). In this group, the changes were more pronounced than in the animals that were still normoglycaemic 1 week after the HE diet (Table 1). The average beta-cell volume in the pancreases was reduced by one-third (Table 1). Also, these beta cells in the islets were still surrounded by a rim of 1–2 layers of other endocrine cells, mainly α-cells and some δ-cells and PP-cells, as under control conditions.

In addition, the insulin immunostaining of the surviving beta cells was significantly reduced (Fig. 3A and Table 1). The decrease of both the beta-cell volume and the beta-cell insulin staining was responsible for a reduction of total pancreas insulin content by more than two-thirds (Table 1). Ultrastructurally, the beta cells showed signs of massive degranulation. Likewise, glucokinase immunostaining in the cytoplasm (Fig. 3B) as well as the GLUT2 glucose transporter (Fig. 3C) immunostaining in the plasma membrane were reduced by more than 50% (Table 1).

Pancreas of the *Psammomys* exhibiting hyperglycaemia and hyperinsulinaemia after 3 weeks on a HE diet

Also after 3 weeks on a HE diet, the *Psammomys* remained hyperinsulinaemic, but they were grossly hyperglycaemic (Table 1). In this group, the changes were more pronounced than in the animals after a 1-week HE diet (Table 1).

The average beta-cell volume in the pancreases was reduced by more than 70% (Table 1). The beta cells in the islets were surrounded by an incomplete rim of other endocrine cells, mainly α-cells and some δ-cells and PP-cells. The insulin immunostaining of the surviving beta cells was reduced by 80% (Fig. 4A and Table 1). This large decrease of both the beta-cell volume and the beta-cell insulin staining led to a more than 90% reduction of total pancreas insulin content (Table 1). Likewise, glucokinase immunostaining in the cytoplasm (Fig. 4B) and GLUT2 glucose transporter (Fig. 4C) immunostaining in the plasma membrane were reduced to a comparable extent (Table 1). Insulin and glucokinase immunoreactive staining were mostly restricted to the submembrane space of the cytoplasm. Ultrastructurally, the beta cells were virtually completely degranulated.

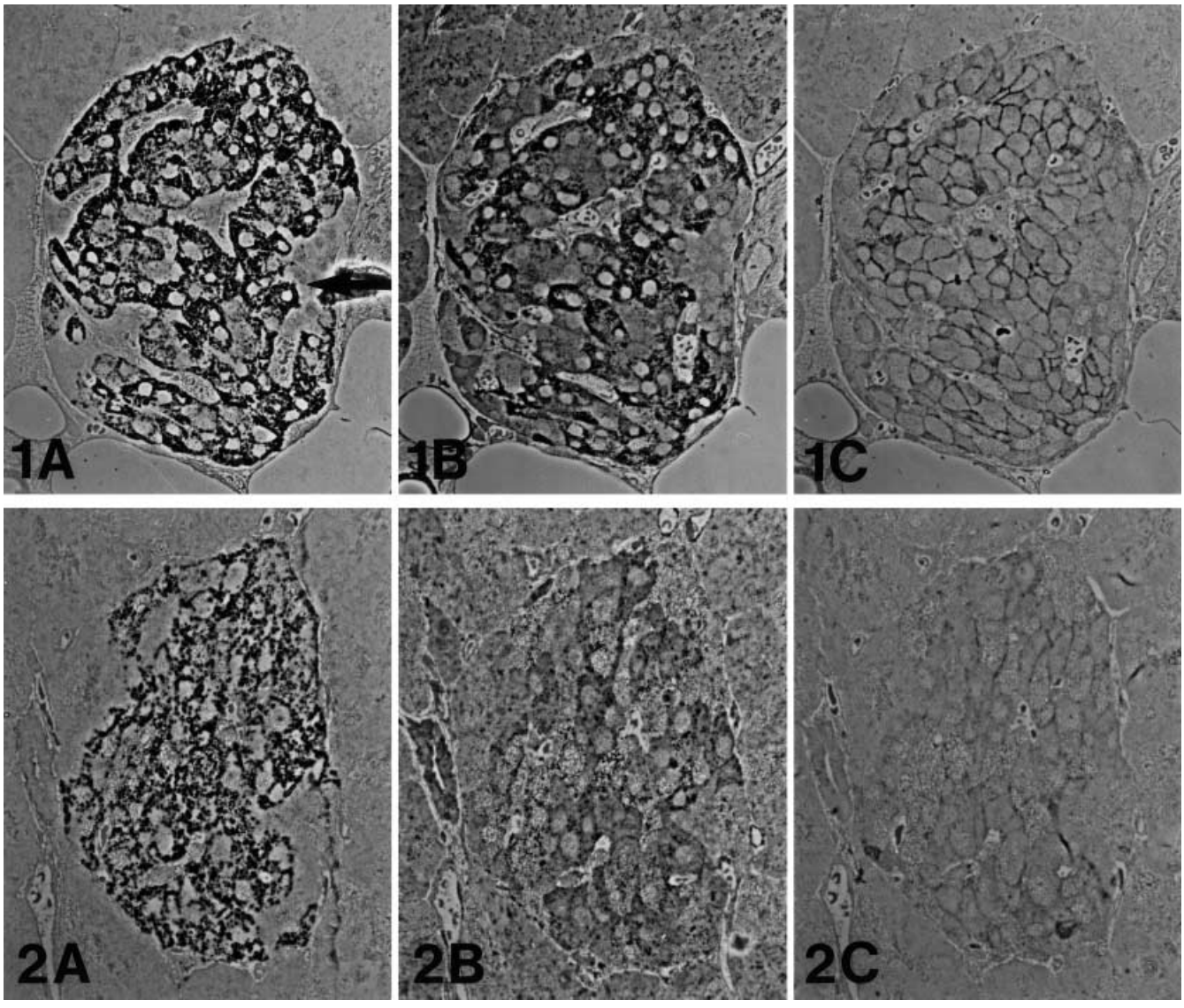

Fig. 1 Control pancreas of the *Psammomys*. Semi-thin sections immunostained for insulin (**A**), glucokinase (**B**) and GLUT2 glucose transporter (**C**). Pancreatic beta cells display a dense insulin and glucokinase immunoreactivity in the cytoplasm (*arrow*). The GLUT2 glucose transporter is restricted to the plasma membrane. ×300

Fig. 2 Pancreas of the *Psammomys* exhibiting normoglycaemia and hyperinsulinaemia after 1 week on a high-energy (HE) diet. Semi-thin sections immunostained for insulin (**A**), glucokinase (**B**), and GLUT2 glucose transporter (**C**). Compared with the immunostaining under control conditions (Fig. 1), the insulin immunoreactivity in beta cells within the islet is moderately reduced and the glucokinase immunostaining is fainter than under control conditions. Also, the GLUT2 glucose transporter exhibits large gaps in the immunostaining of the plasma membrane. ×400

Analysis of the time course of correlation between blood glucose and plasma insulin changes and morphological changes in *Psammomys* rat pancreatic beta cells

While all control *Psammomys* on a LE diet were normoglycaemic and normoinsulinaemic, after 3 weeks on a HE diet, the animals were all hyperglycaemic and hyperinsulinaemic. After 1 week on a HE diet, however, the extent of hyperglycaemia was variable, though all animals were already hyperinsulinaemic (Table 1). Thus, it is not surprising that there was a significant correlation between the extent of hyperglycaemia and the reduction of the total pancreas beta cell volume (r=0.96) and the total pancreas insulin content (r=0.95) as well as the reduction of immunostaining for insulin (r=0.95), glucokinase (r=0.92) and GLUT2 glucose transporter (r=0.85) in the nine animals studied (Table 1). However, for none of these parameters was there significant correlation with the plasma insulin concentration (all r values were <0.2).

Analysis of pancreatic beta-cell destruction in response to HE diet feeding

Ultrastructurally different signs of necrotic destruction of pancreatic beta cells, such as the rupture of cell mem-

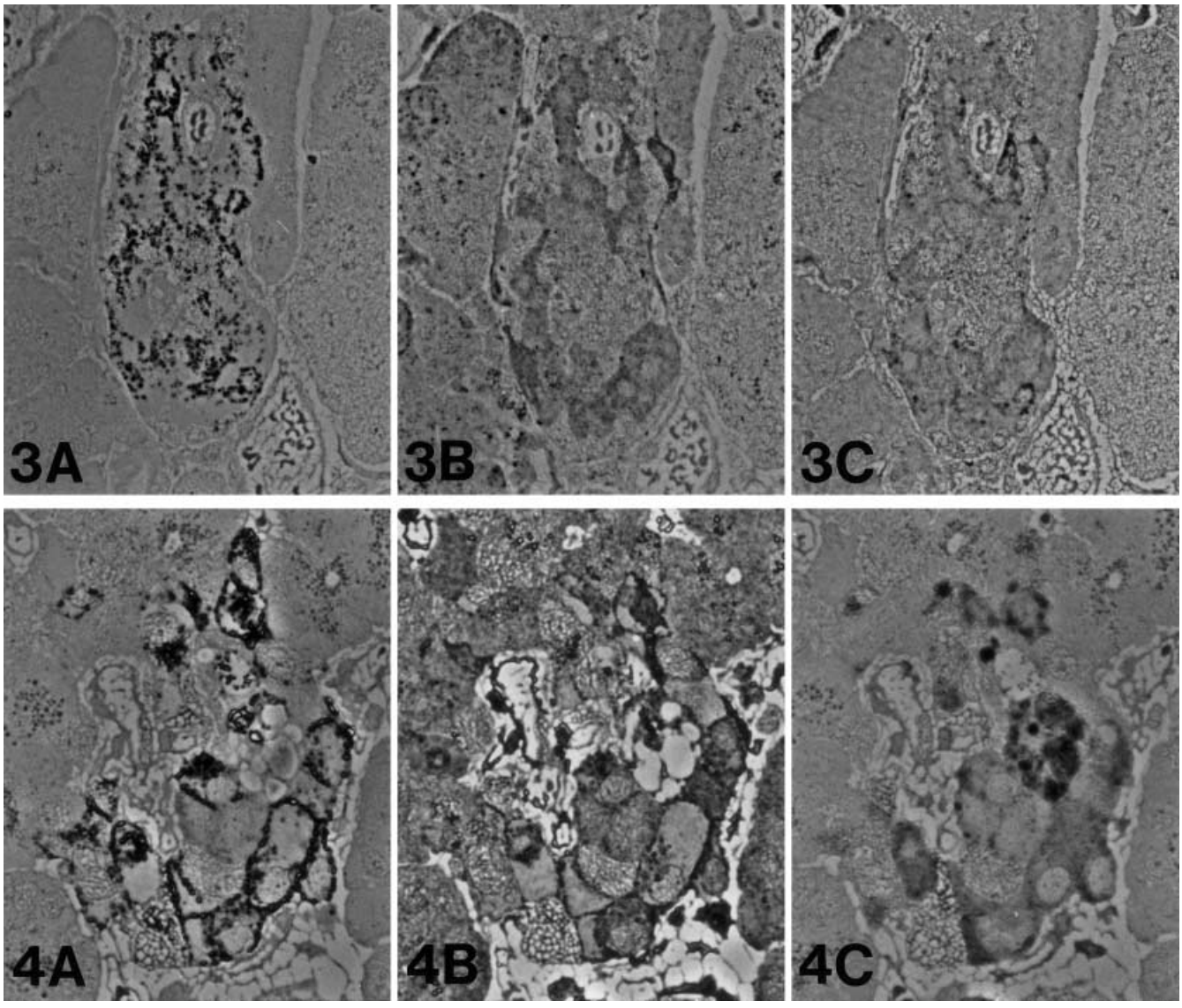

Fig. 3 Pancreas of the *Psammomys* exhibiting hyperglycaemia and hyperinsulinaemia after 1 week on a high-energy (HE) diet. Semi-thin sections immunostained for insulin (**A**), glucokinase (**B**), and GLUT2 glucose transporter (**C**). The immunoreactivities of insulin, glucokinase and GLUT2 glucose transporter are decreased much more than with beta cells after 1 week on a HE diet and normoglycaemia. Only a few beta cells exhibit a detectable insulin, glucokinase immunostaining in the cytoplasm. Sometimes the GLUT2 glucose transporter is completely lost in the plasma membrane of beta cells. ×500

Fig. 4 Pancreas of the *Psammomys* exhibiting hyperglycaemia and hyperinsulinaemia after 3 weeks on a high-energy (HE) diet. Semi-thin sections immunostained for insulin (**A**), glucokinase (**B**), and GLUT2 glucose transporter (**C**). The few remaining beta cells exhibit a faint to lost immunostaining for insulin and glucokinase with vacuoles. The GLUT2 glucose transporter is present in the cytoplasm of the beta cells but is not localised in the plasma membrane. ×800

branes and a massive vacuolisation in the cytoplasm, were evident. These findings were accompanied by swollen mitochondria and dilated cisternae of the Golgi complex and of the rough endoplasmic reticulum in the cytoplasm of the beta cells (Fig. 5). In contrast, most of the secretory granules showed an intact core region. The described changes were particularly evident in the pancreases after 3 weeks on a HE diet while, after 1 week on a HE diet, the beta cells were massively degranulated but showed still an intact ultrastructure. Signs of apoptosis were not observed. The other endocrine cell types showed no ultrastructural lesions.

Discussion

The *Psammomys obesus* is a well-established type-2 diabetes model. It develops non-insulin-dependent diabetes mellitus when fed a HE diet [10, 18]. Compared with other animal models of type-2 diabetes, the *Psammomys* has the advantage that the diabetic state develops step-

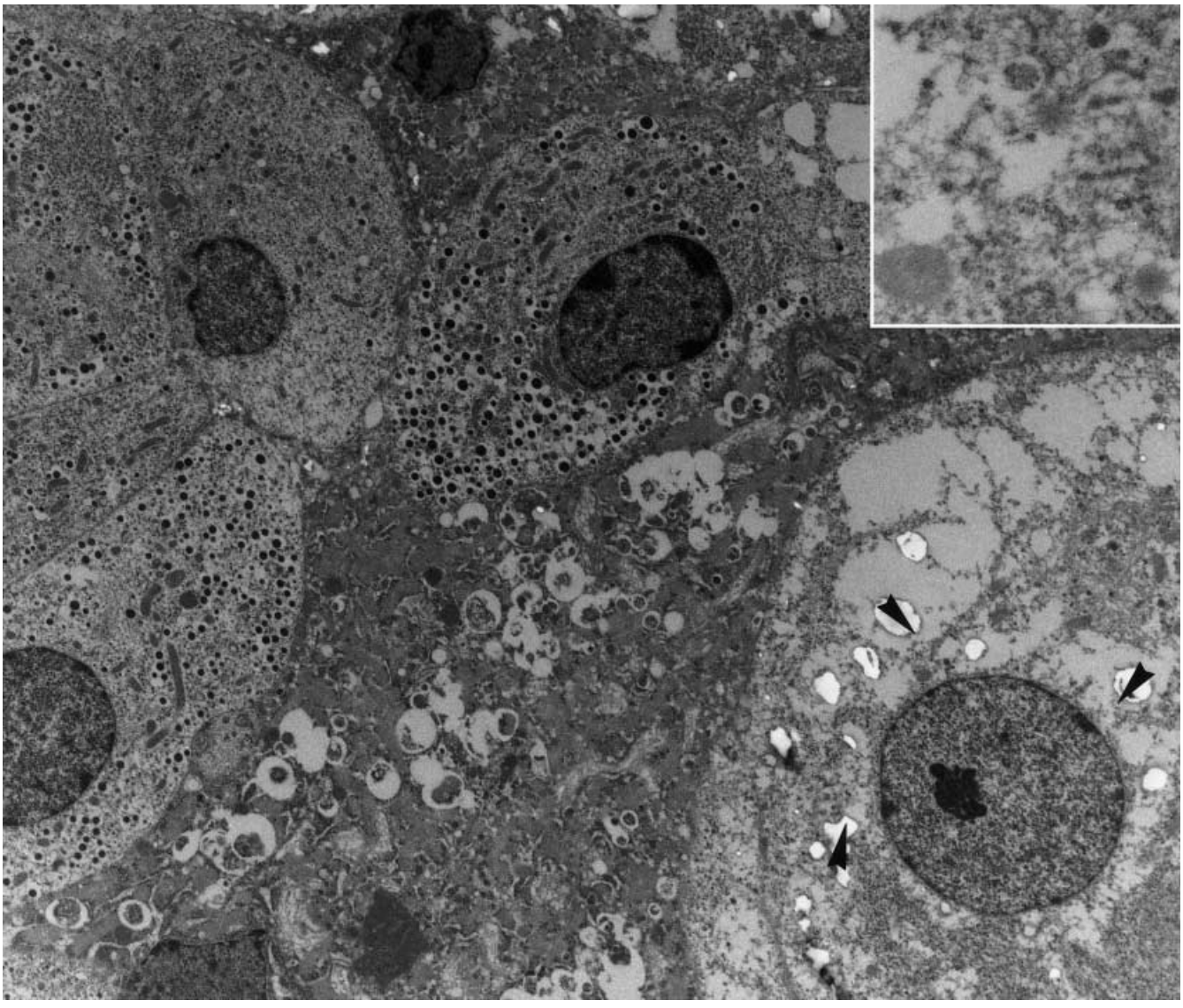

Fig. 5 Pancreatic islet cells from a diabetic *Psammomys* after 3 weeks on a high-energy (HE) diet. Ultrastructurally, the depicted beta cells show the typical signs of necrosis with a rupture of cell membranes and vacuolisation in the cytoplasm and an intact structure of the nucleus (*arrowheads*). Other surrounding endocrine cells remain intact with a high number of secretory granules (×4500). *Inset* higher magnification of the organelles in the necrotic beta cell (×24000)

wise in well-defined stages in which the animals show initially hyperinsulinaemia and, thereafter, only hyperglycaemia [10, 18, 22]. This makes it possible to correlate morphological changes of the endocrine pancreas with either developing hyperinsulinaemia or hyperglycaemia.

The present results show that the feeding of a HE diet induces a gradual loss of pancreatic beta-cell function in parallel to the deterioration of glucose tolerance in these animals [10, 18, 22]. The gradual decrease of total pancreas insulin content is the hallmark of the progressive decline of the endocrine function of the pancreas. This fall of the pancreas insulin content is the result of an additive dual effect, namely a reduction of the total beta-cell volume of the pancreas due to beta-cell death and a diminution of insulin content of the beta cells in the islets, as documented by the decrease of the insulin immunostaining of the surviving beta cells in the islets (Table 1). Necrosis rather than apoptosis is the main mechanism of beta-cell death (Fig. 5) in the different stages of HE diet-induced diabetes development in this animal model analysed in the present study, confirming previous observations [1].

Like in rat [5, 6, 16, 17] and hamster [7] models of type-2 diabetes, the loss of GLUT2 glucose transporter gene [6] and protein [5, 7, 16, 17] expression was observed in parallel to the loss of insulin storage capacity during diabetes development in the *Psammomys*. Likewise, we could demonstrate a loss of the immunostaining also for glucokinase, which plays a central role in the pancreatic beta cell for the physiological regulation of glucose-induced insulin secretion [11, 13]. The loss of the GLUT2 glucose transporter and the glucokinase expres-

sion paralleled the loss of insulin immunostaining but developed more quickly than the decrease of the average beta-cell volume of the pancreas (Table 1). This shows that the deterioration of the pancreatic beta-cell function can be regarded as a result of the loss of these two central structures of the glucose recognition apparatus of the pancreatic beta cell with the disappearance of the beta cells in the islets as the final result of this process of a gradual loss of the pancreatic beta-cell function.

The present study clearly shows that the HE diet-induced pancreatic beta-cell dysfunction in the *Psammomys* is the consequence of a developing hyperglycaemia. Hyperinsulinaemia is not responsible for the observed deterioration of the pancreatic beta-cell function. There is no direct evidence for an involvement of "glucose toxicity" in the death of the beta cells. An attempt to prevent a possible toxic action of glycation end products and of nitrous oxide using the inhibitor aminoguanidine was not effective in protecting the beta cells [3]. Therefore, we conclude that the gradual loss of the insulin biosynthetic and secretory capacity of the beta cells is apparently the result of a beta-cell exhaustion due to a permanent state of hypersecretion in a compensatory attempt to counteract hyperglycaemia [18, 22]. The observed beta-cell lesions in pancreases removed from severely hyperglycaemic animals [1, 3] are in agreement with this conclusion. The same conclusion has been drawn most recently also from in vitro studies [15].

The fact that the reversal of hyperglycaemia through treatment with vanadium salts [19] or a return to a LE diet can reverse the effects of HE diet feeding [18, 22] strongly support the view that it is the elevation of glucose which is highly detrimental to the normal function of the pancreatic beta cell during diabetic hyperglycaemia.

Acknowledgement The skilful technical assistance of F. Hurkuck is gratefully acknowledged.

References

1. Bar-On H, Ben-Sasson R, Ziv E, Arar N, Shafrir E (1999) Irreversibility of nutritionally induced NIDDM in *Psammomys obesus* is related to beta-cell apoptosis. Pancreas 18:259–265
2. Bendayan M, Malide D, Ziv E, Levy E, Ben-Sasson R, Kalman R, Bar-On H, Chretien M, Seidah N (1995) Immunocytochemical investigation of insulin secretion by pancreatic beta-cells in control and diabetic Psammomys obesus. J Histochem Cytochem 43:771–784
3. Donath MY, Gross DJ, Cerasi E, Kaiser N (1999) Hyperglycemia-induced beta-cell apoptosis in pancreatic islets of *Psammomys obesus* during development of diabetes. Diabetes 48: 738–744
4. Hsu SM, Raine L, Fanger H (1981) Use of avidin-biotin-peroxidase complex (ABC) in immunoperoxidase techniques: a comparison between ABC and unlabeled antibody (PAP) procedures. J Histochem Cytochem 29:577–580
5. Johnson JH, Ogawa A, Chen L, Orci L, Newgard CB, Alam T, Unger RH (1990) Underexpression of beta cell high Km glucose transporters in noninsulin-dependent diabetes. Science 250:546–549
6. Jonas JC, Sharma A, Hasenkamp W, Ilkova H, Patane G, Laybutt R, Bonner-Weir S, Weir GC (1999) Chronic hyperglycemia triggers loss of pancreatic beta cell differentiation in an animal model of diabetes. J Biol Chem 274:14112–14121
7. Jörns A, Tiedge M, Sickel E, Lenzen S (1996) Loss of GLUT2 glucose transporter expression in pancreatic beta cells from diabetic Chinese hamsters. Virchows Arch 428:177–185
8. Jörns A, Tiedge M, Lenzen S (1999) Nutrient-dependent distribution of insulin and glucokinase immunoreactivities in rat pancreatic beta cells. Virchows Arch 434:75–82
9. Jörns A, Klempnauer J, Tiedge M, Lenzen S (2001) Recovery of pancreatic beta-cells in response to long-term normoglycemia after pancreas or islet transplantation in severely diabetic adult rats. Pancreas (in press)
10. Kalderon B, Gutman A, Levy E, Shafrir E, Adler JH (1986) Characterization of stages in development of obesity-diabetes syndrome in sand rat (*Psammomys obesus*). Diabetes 35: 717–724
11. Lenzen S, Panten U (1988) Signal recognition by pancreatic B-cells. Biochem Pharmacol 37:371–378
12. Like AA, Miki E (1967) Diabetic syndrome in sand rats. IV. Morphologic changes in islet tissue. Diabetologia 3:143–166
13. Meglasson MD, Matschinsky FM (1986) Pancreatic islet glucose metabolism and regulation of insulin secretion. Diabetes Metab Rev 2:163–214
14. Miki E, Like AA, Soeldner JS, Steinke J, Cahill GF (1966) Acute ketotic-type diabetic syndrome in sand rats (*Psammomys obesus*) with special reference to the pancreas. Metabolism 15:749–760
15. Nesher R, Gross DJ, Donath MY, Cerasi E, Kaiser N (1999) Interaction between genetic and dietary factors determines beta-cell function in *Psammomys obesus*, an animal model of type 2 diabetes. Diabetes 48:731–737
16. Ohneda M, Johnson JH, Inman LR, Chen L, Suzuki K, Goto Y, Alam T, Ravazzola M, Orci L, Unger RH (1993) GLUT2 expression and function in beta-cells of GK rats with NIDDM. Dissociation between reductions in glucose transport and glucose-stimulated insulin secretion. Diabetes 42:1065–1072
17. Orci L, Ravazzola M, Baetens D, Inman L, Amherdt M, Peterson RG, Newgard CB, Johnson JH, Unger RH (1990) Evidence that down-regulation of beta-cell glucose transporters in non-insulin-dependent diabetes may be the cause of diabetic hyperglycemia. Proc Natl Acad Sci U S A 87:9953–9957
18. Shafrir E, Ziv E (1998) Cellular mechanism of nutritionally induced insulin resistance: the desert rodent *Psammomys obesus* and other animals in which insulin resistance leads to detrimental outcome. J Basic Clin Physiol Pharmacol 9:347–385
19. Shafrir E, Spielman S, Nachliel I, Khamaisi M, Bar-On H, Ziv E (2001) Treatment of diabetes with vanadium salts: general overview and amelioration of nutritionally induced diabetes in the *Psammomys obesus* gerbil. Diabetes Metab Res Rev 17: 55–66
20. Thorens B, Sarkar HK, Kaback HR, Lodish HF (1988) Cloning and functional expression in bacteria of a novel glucose transporter present in liver, intestine, kidney, and beta-pancreatic islet cells. Cell 55:281–290
21. Tiedge M, Steffeck H, Elsner M, Lenzen S (1999) Metabolic regulation, activity state, and intracellular binding of glucokinase in insulin-secreting cells. Diabetes 48:514–523
22. Ziv E, Shafrir E (1995) *Psammomys obesus*: nutritionally induced NIDDM-like syndrome on a "thrifty gene" background. In: Shafrir E (ed) Lessons from animal diabetes, vol. 5. Smith-Gordon, London, pp 285–300

Virchows Arch (2002) 440:70–76
DOI 10.1007/s004280100508

ORIGINAL ARTICLE

Michael Scarpatetti · Oleksiy Tsybrovskyy
Helmut H. Popper

Cytokeratin typing as an aid in the differential diagnosis of primary versus metastatic lung carcinomas, and comparison with normal lung

Received: 15 January 2001 / Accepted: 18 June 2001 / Published online: 13 September 2001
© Springer-Verlag 2001

Abstract Due to more efficient chemotherapy protocols, the number of second and even third primary carcinomas is steadily increasing. To denominate the possible origin of a carcinoma, different markers are available as an aid, e.g. hormones, proteins and lipoproteins, secretion products and cytoskeletal proteins. Cytokeratins (CKs) have gained new popularity; however, they have not been extensively evaluated in lung tumours. In our study we evaluated the staining patterns of CK polypeptides 4–8, 10, 13, 14, and 17–20 and high molecular weight (HMW) CK polypeptides in routinely processed primary lung carcinomas and lung metastases of diverse origin. As expected, immunohistochemical investigation gave no clear-cut results, but, with statistical analysis, lung adenocarcinomas could be separated from metastatic adenocarcinomas using CK 5 and 18 and HMW CK (specificity 92.5%, sensitivity 62.5%). The different origin of the metastases could often be detected using CK 18 and CK 20. Lung clear cell carcinomas and large cell carcinomas with clear cell areas could be distinguished from metastatic renal clear cell carcinomas by the CK 7 staining reaction. Squamous cell carcinomas of the lung and metastatic squamous cell carcinomas of the larynx, pharynx and oesophagus could not reliably be separated in part due to the few number of cases available. CK polypeptide typing is thus an additional aid in the differential diagnosis of lung carcinomas versus carcinomas metastatic to the lung.

Keywords Cytokeratin polypeptides · Lung carcinoma · Lung metastasis · Lung epithelia

M. Scarpatetti (✉) · O. Tsybrovskyy · H.H. Popper
Institute of Pathology, Lab. Environmental and Respiratory Pathology, School of Medicine, University of Graz, Auenbruggerplatz 25, 8036 Graz, Austria
e-mail: michael.scarpatetti@kfunigraz.ac.at
Tel.: +43-316-3804450, Fax: +43-316-3853432

Introduction

Due to better cancer-treatment protocols, the incidence of second and even third primary cancers of the lung has obviously increased. Because treatment is quite different for primary tumour or lung metastases, it is always necessary for pathologists to make that distinction. Sometimes this is an easy task that is achievable without any special staining. In other cases unique markers can be used to differentiate metastatic carcinomas from primary lung carcinomas, e.g. thyroglobulin to distinguish between metastatic papillary thyroid carcinoma and papillary adenocarcinoma of the lung. In cases like metastatic squamous cell carcinomas of the larynx or oesophagus, it might be impossible to discern them from primary squamous cell carcinomas of the lung.

Cytokeratin (CK) polypeptides are the major cytoskeletal proteins in epithelial cells. Usually two peptides are joined together, one acidic and one alkaline [3]. For more than a decade, it has been well known that different epithelia have unique sets of CK polypeptides. However, this has never been evaluated at the cellular level, especially not in the lung, nor has there been an investigation reported on CK composition in peripheral versus central bronchial epithelia.

Therefore, we studied the immunohistochemical expression of CK polypeptides in normal lung epithelia from the central bronchi to the alveolar periphery and also compared their expression in primary non-small cell carcinomas of the lung and lung metastases from carcinomas of the colon, breast, stomach, prostate, oral cavity, larynx and oesophagus, and kidney. The aim was to find subsets of CKs that might be used as an aid in the differential diagnosis of second primary versus metastatic carcinomas.

Materials and methods

Lung metastases and primary carcinomas of the lung were retrieved from the archives for lung pathology. Only metastases

Table 1 List of antibodies and the protocols used

Cytokeratin	Clone	Processing	Dilution	Antigen retrieval
CK 4	MON 3015	Manual	1:2	MW 30'160 W
CK 5	MON 3029	Ventana	1:20	Pronase 8'
CK 5, 8	ICN 10521	Ventana	1:10	Pronase 8'
CK 6	BMS 65190	Manual	Neat	MW 30'160 W
CK 7	Dako M7019	Ventana	1:200	Pronase 8'
CK 8	Progen 61031	Ventana	1:100	Pronase 8'
CK 10	Dako M 7002	Ventana	1:200	None
CK 10, 13	Dako M7003	Ventana	1:100	MW 30'160 W
CK 14	Novo.NCL LL002	Ventana	1:50	MW 30'160 W
CK 17	Dako M7046	Ventana	1:20	MW 30'160 W
CK 18	Boehringer8143385	Ventana	1:10	Pronase 18'
CK 19	Dako M7010	Ventana	1:10	MW 30'160 watts
CK 20	Dako M888	Ventana	1:200	Pronase 8'
High molecular weight 34βE12	Dako M630	Ventana	1:50	Pronase 8'

Table 2 Cytokeratin (CK) polypeptide reactions in primary lung and metastatic adenocarcinomas

	CK 4	CK 5	CK 6	CK 7	CK 8	CK 10	CK 13	CK 14	CK 17	CK 18	CK 19	CK 20	High molecular weight CK
Primary lung adenocarcinomas	1/16	10/16	7/16	15/16	15/16	0/16	2/16	1/16	6/16	14/16	15/16	4/16	8/16
Lung metastases from colonic carcinomas	8/21	21/21	12/21	8/21	18/21	0/21	9/21	4/21	4/21	9/21	18/21	16/21	3/21
Lung metastases from breast carcinomas	4/19	17/19	10/19	18/19	14/19	0/19	1/19	5/19	5/19	11/19	17/19	0/19	6/18*
Lung metastases from prostate carcinomas	2/8	7/8	2/8	4/8	6/8	0/8	0/8	1/8	3/8	6/8	8/8	0/8	1/8
Lung metastases from gastric carcinomas	0/5	5/5	3/5	5/5	3/5	0/5	1/5	2/5	0/5	0/5	3/5	0/5	1/5
Fisher's exact test primary vs metastatic carcinoma, *P* value	0.16	0.004	0.78	0.05	0.27	–	0.72	0.27	0.33	0.008	0.67	0.76	0.03
χ^2 test for metastatic tumours only, *P* value	0.17	0.22	0.62	0.002	0.39	–	0.001	0.60	0.31	0.03	0.14	<0.0005	0.61

* No more material was available

with a proven location of the primary tumour and only proven cases of primary lung carcinomas were selected. The specimen consisted of open and transbronchial biopsies, as well as lobectomies. Neither material from needle biopsies nor material from autopsies was used. A total of 111 different cases were investigated; these were composed of 82 carcinomas metastatic to the lung and 29 primary non-small cell lung carcinomas. In the metastases group, we investigated 21 adenocarcinomas of the colon, 19 adenocarcinomas of the breast, 8 adenocarcinomas of the prostate and 5 adenocarcinomas of the stomach. Two metastatic squamous cell carcinomas originated from the larynx, six from the oesophagus, and three from the oral cavity and hypopharynx. We also investigated 18 lung metastases from renal clear cell carcinomas. The primary lung carcinomas were divided into 16 adenocarcinomas: seven squamous cell carcinomas and six large cell carcinomas with predominant clear cell areas, including three pure clear cell carcinomas of the lung.

The tissue was routinely fixed in neutral buffered formaldehyde, paraffin embedded, cut into 5-µm thin sections and then incubated with commercially available antibodies to CK polypeptides, using our modified immunohistochemical protocols (Table 1). A reaction was regarded as positive when at least 5% of tumour cells were stained. We did not further grade staining intensity or the amount of positive tumour cells, due to the limitations in small bronchial biopsies.

Statistical analysis was performed using SPSS software (SPSS, Chicago, Ill.). In univariate cross-tabulation statistics, two-sided Fisher's exact test or Chi-square test was used where appropriate. We also performed multivariate analysis using binomial and multinomial logistic regression to identify the most useful combination of CK polypeptides for distinguishing the tumour groups.

Results

General statements

Most primary lung adenocarcinomas did react with antibodies to CK 5, 7, 8, 18 and 19; only a few reacted with antibodies to CK 6, 17, and 20 and HMW CK; and nearly all had no reaction with antibodies to CK 4, 10, 13 and 14 (Table 2). Metastatic colonic adenocarcinomas reacted with antibodies to CK 5, 6, 8, 19 and 20. Fewer reactions were noticed with antibodies to CK 4, 7, 13, and 18, and only a weak or no reaction with antibodies to CK 10, 14, and 17 and HMW CK (Table 2). Breast adenocarcinoma metastases reacted with antibodies to CK 5–8, 18 and 19; we also noticed fewer reactions for CK 4, 14, and 17 and HMW CK (only 18 of 19 cases could be stained because of tissue limits). Very few or no reactions were seen with antibodies to CK 10, 13 and 20 (Table 2, Fig. 1). The metastases of prostate adenocarcinomas reacted with antibodies to CK 5, 7, 8, 18 and 19. Only a minority

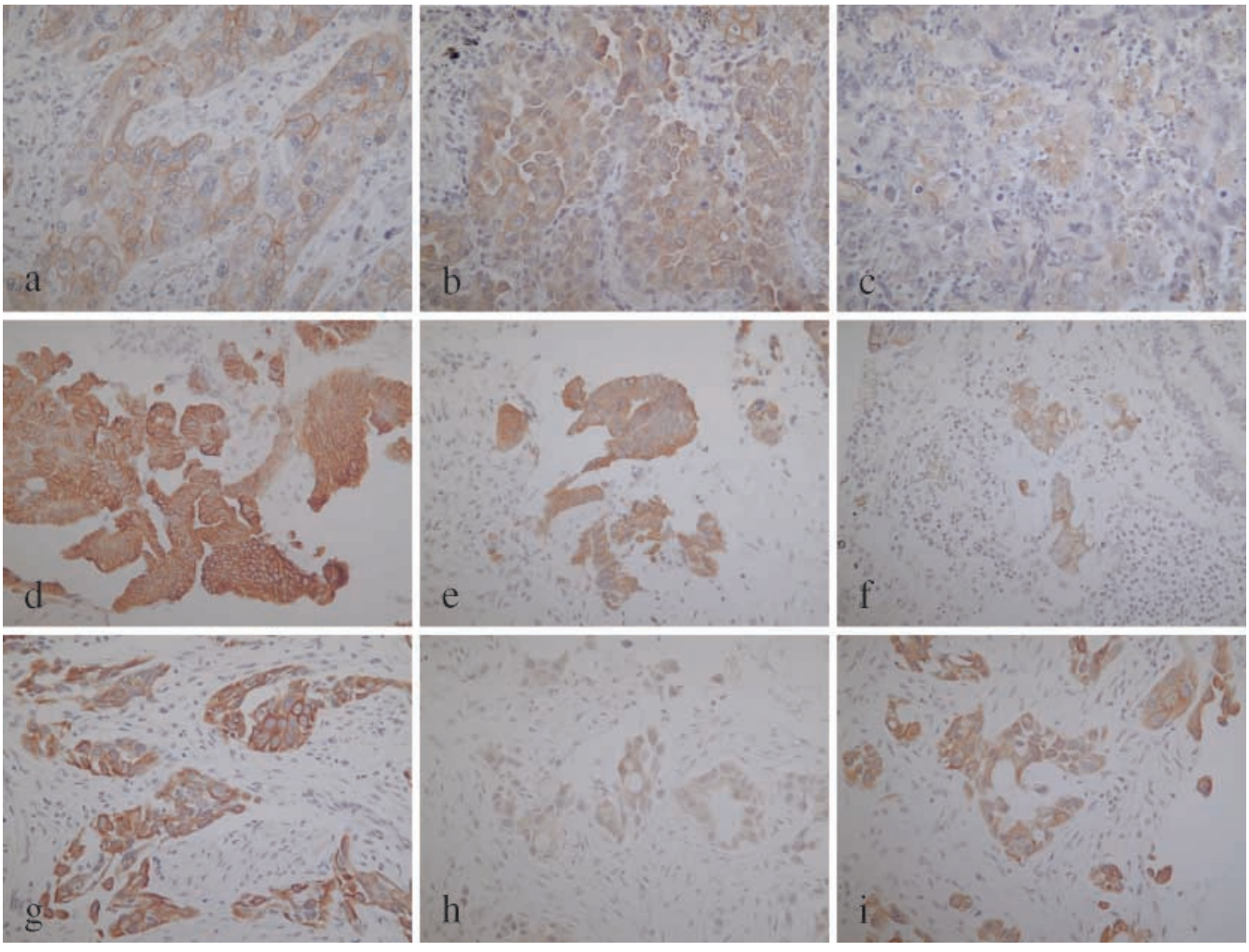

Fig. 1 Immunohistochemical reactions of antibodies to cytokeratins 5 and 18 and high molecular weight cytokeratin in primary lung adenocarcinoma (**a**, **b**, **c**), in colon carcinoma metastases (**d**, **e**, **f**) and in breast carcinoma metastases (**g**, **h**, **i**)

reacted with antibodies to CK 4, 6, 14, and 17 and HMW CK. No reactions were seen for CK 10, 13 and 20 (Table 2). Metastatic gastric adenocarcinomas reacted with antibodies to CK 5–8 and 19. Only weak reactions were seen with antibodies to CK 13 and 14 and HMW CK, and no reactions for CK 4, 10, 17, 18 and 20 were seen.

Primary lung adenocarcinomas versus metastatic adenocarcinomas of the lung

Statistically significant differences between primary and metastatic tumours were detected for CK 5, 7, and 18 and HMW CK (Table 2). Nearly all metastases were positive for CK 5, whereas 6 of 16 primary lung adenocarcinomas were negative. By contrast, almost all primary adenocarcinomas reacted with CK 7, whereas many metastatic tumours, especially those originating from the colon and prostate, showed only few reactions. The reaction rate for CK 18 and HMW CK was also considerably higher in primary lung carcinomas than in metastatic tumours.

By logistic regression analysis, we developed a discriminatory model based on a combination of CK 5 and 18 and HMW CK, which allowed the best discrimination between primary lung carcinoma and metastatic adenocarcinomas of the lung. Regression coefficients were 3.293 (CK 5), –2.581 (CK 18) and –2.306 (HMW CK), with a standard error of the regression coefficient of 0.945, 1.113 and 0.831, respectively (P=0.006, 0.003 and 0.005, respectively, which are statistically highly significant). Univariate tests for these CKs were also significant (Table 2). The coefficients for CK 18 and HMW CK were negative, indicating the higher expression of these CKs in primary lung carcinomas; by contrast, the positive coefficient for CK 5 indicated higher expression in metastatic tumours. The good agreement between uni- and multivariate statistics further proves that the model created is precise and not over-fitted.

Discrimination of metastatic adenocarcinomas of the lung

Differences among metastatic tumours were statistically significant for CK 7, 13, 18 and 20. The significant

Table 3 Cytokeratin (CK) polypeptide reactions in primary lung clear cell carcinomas and metastatic renal clear cell carcinomas

	CK 4	CK 5	CK 6	CK 7	CK 8	CK 10	CK 13	CK 14	CK 17	CK 18	CK 19	CK 20	High molecular weight CK
Large cell, clear cell lung carcinoma	0/6	4/6	2/6	5/6	1/6	0/6	0/6	0/6	2/6	4/6	4/6	0/6	2/6
Renal metastases	6/18	12/18	5/18	1/18	11/18	0/18	3/18	3/18	2/18	5/18	12/18	3/18	0/18
Fisher's exact test, *P*	0.28	1.0	1.0	0.001	0.16	–	0.55	0.55	0.25	0.15	1.0	0.55	0.054

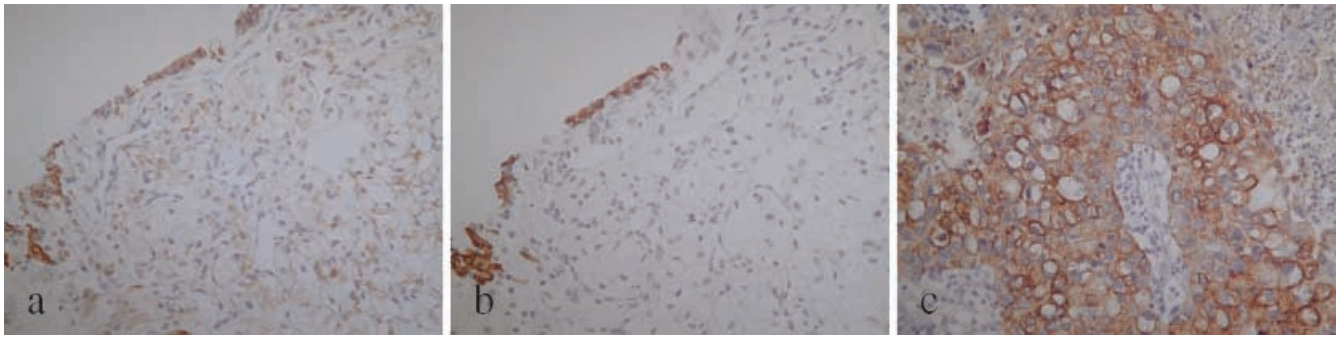

Fig. 2 Immunohistochemical reactions of antibodies to pan-cytokeratin (CK) and CK 7 in a metastasis of a renal cell carcinoma (**a**, **b**), and reactions to CK 7 in a primary large cell and clear cell carcinoma of the lung (**c**)

result for CK 7 was due to the few reactions with antibodies to CK 7 in colonic and prostatic adenocarcinoma metastases, whereas almost all metastases from breast and stomach carcinomas, respectively, did react. CK 13 was often positive in colonic carcinoma metastases, whereas all other metastases were most often negative. A relatively high proportion of prostate carcinoma metastases reacted with CK 18 antibodies, whereas all metastases from gastric cancer did not. Finally, HMW CK was more often positive in breast cancer metastases than in metastases from other locations.

Using multinomial logistic regression, we identified the best combination of CK polypeptides to differentiate metastatic tumours with different locations of the primary tumour. Preliminary analysis showed that, apart from a minor difference in CK 7 expression, there were no systematic differences in CK polypeptides profiles between breast and prostate adenocarcinoma metastases ($P>0.05$). For CK 7, the Fisher's exact test was significant ($P=0.017$). However, it was still not possible to accurately discriminate between these tumours (prostate carcinoma: sensitivity 50%, specificity 94.5%, overall accuracy 81.5%), although this type of differential diagnosis is clinically irrelevant because breast cancer in men is extremely rare. Therefore, for the sake of subsequent analysis, these tumours were merged into one group.

The model selected for discrimination of metastatic carcinomas was based on a combination of CK 18 and CK 20. The significance values for the regression coefficients were less than 0.0005 for CK 20 and equal to 0.001 for CK 18.

Metastatic clear cell carcinomas of the kidney versus large cell clear cell carcinoma of the lung

As can be seen in Table 3, the only highly significant result was noticed for CK 7. Only 1 of 18 metastatic renal clear cell carcinomas reacted positively with antibodies to CK 7, whereas 83% (5 of 6) primary large- and clear cell carcinomas of the lung were positive for CK 7 (Fig. 2). In addition, the test result for HMW CK was marginally significant. In multivariate analysis, however, HMW CK was not significant anymore ($P=0.11$), so only CK 7 was used to discriminate primary versus metastatic tumours. Efficiency indices relating to the primary lung clear and large cell carcinomas were as follows: sensitivity 83.3%; specificity 94.4%; positive predictive value 83.3%; and negative predictive value 94.4%. We also noticed a reaction with antibodies for CK 20 in 17% (3 of 18) of our renal cell carcinoma metastases (Table 3). In contrast to clear cell carcinomas of the kidney, pulmonary clear cell carcinomas never showed co-expression of vimentin and CK (unpublished observation, H. Popper).

Squamous cell carcinomas: primary versus metastatic

Primary squamous cell carcinomas of the lung stained positively with antibodies for CK 7 (43%), 17 (86%), 18 (71%) and 20 (14%). In contrast, metastases from larynx carcinomas did not react with antibodies for CK 17, 18 and 20, but were positive in 50% for CK 7. Metastases from oesophageal carcinomas showed a similar positivity for CK 7, but less positivity for CK 17 and CK 18 than that from lung squamous cell carcinomas. No reactivity for CK 17 and CK 18 was found in squamous cell carcinomas of the oral cavity and the hypopharynx. Our statistical results are documented in Table 4; however, they must be interpreted with respect to the few cases available.

Table 4 Cytokeratin (CK) polypeptide reactions in primary squamous cell carcinomas (SCCs) and SCC metastases

Tumour	CK 4	CK 5	CK 6	CK 7	CK 8	CK 10	CK 13	CK 14	CK 17	CK 18	CK 19	CK 20	High molecular weight CK
Primary lung SCC	2/7	7/7	7/7	3/7	4/7	1/7	4/7	7/7	6/7	5/7	5/7	1/7	7/7
Lung metastases from larynx SCC	0/2	2/2	2/2	1/2	2/2	0/2	2/2	2/2	0/2	0/2	2/2	0/2	2/2
Lung metastases from tongue SCC	1/2	2/2	2/2	0/2	1/2	0/2	1/2	2/2	1/2	1/2	1/2	0/2	2/2
Lung metastases from hypopharynx SCC	0/1	1/1	1/1	0/1	1/1	0/1	1/1	1/1	0/1	1/1	1/1	0/1	1/1
Lung metastases from oesophagus SCC	2/6	6/6	5/6	4/6	3/6	0/6	1/6	5/6	3/6	2/6	4/6	0/6	4/6
Overall Chi-square test, *P*	0.78	–	0.71	0.46	0.67	0.80	0.21	0.71	0.17	0.29	0.78	0.80	0.34
Fisher's exact test primary vs metastatic lung tumours, *P*	1.0	–	1.0	1.0	1.0	0.39	1.0	1.0	0.07	0.34	1.0	0.39	0.49

Normal lung epithelia

Primarily we tried to attribute different CK subsets to different cell types. However, ciliated, goblet and secretory columnar cells in large bronchi all shared the same CK composition, as did Clara cells, ciliated and secretory columnar cells in peripheral bronchioli. The same was seen for basal and reserve cells in their respective location. There was a difference when central and peripheral epithelia were compared: peripheral bronchiolar epithelia were all negative for CK 4, 6 and 20, whereas epithelia of large bronchi were positive for these CKs in differing amounts. With CK 20 antibodies, we noticed a positive stain in 20% of centrally located columnar cells and in 80% of the bronchial gland cells. There was no reactivity for CK 10, centrally or peripherally; with CK 13, we noticed focal positivity in central bronchi, especially in the bronchial glands, and in the periphery only in pneumocyte types I and II. Within central bronchi, the differentiated columnar cells were positive for CK 7, whereas basal and reserve cells were negative. In the alveolar periphery, the most striking finding was CK 17 positivity in pneumocyte II, which was not found in bronchiolar epithelia.

Discussion

Adenocarcinomas

According to the results of logistic regression analysis, three CK polypeptides turned out to be important with respect to a differential diagnosis: CK 5, CK 18 and HMW CK. Based on the analysis of the model coefficients, we worked out a discrimination set-up for primary and metastatic carcinomas (Scheme 1). Using this scheme, we noticed for primary lung carcinomas a sensitivity of 62.5%, a specificity of 92.5%, a positive predictive value of 71.4% and a negative predictive value of 89.1%. Previous studies reporting on CK 7 and CK 20 patterns [11, 13, 14, 15] stated that CK 20 positivity would exclude primary lung adenocarcinoma. However,

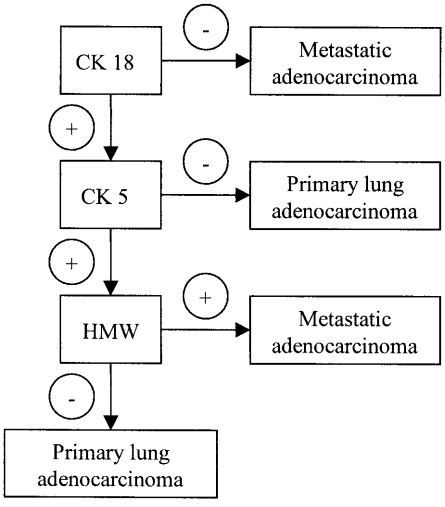

Scheme 1 A discrimination set-up for primary and metastatic carcinomas

4 of 16 lung adenocarcinomas in our study showed positive reactivity for CK 20, which was also seen by Savera et al. [15] and other investigators [8, 11, 12, 14]. Our four cases were centrally located. This correlated well with our findings of positively stained columnar and bronchial gland cells in normal mucosa of large bronchi and might explain the CK 20 positivity. CK 7 positivity, discussed in various articles [6, 13, 14, 15, 17, 18], was not that helpful in our series. Most pulmonary adenocarcinomas and metastases from breast adenocarcinomas and all metastases from gastric adenocarcinomas reacted, but there was also a substantial amount of reacting lung metastases of colonic adenocarcinomas, consistent with the findings of many other authors [2, 4, 7, 20]. In metastatic adenocarcinomas of the prostate, we found CK 7 positivity, which is confirmed by two other studies [12, 18]. Almost all metastatic adenocarcinomas of the prostate did not stain for HMW CK, consistent with the findings of Yang et al. [19]. We noticed in the univariate statistic analysis a significancy with CK 7, but in the

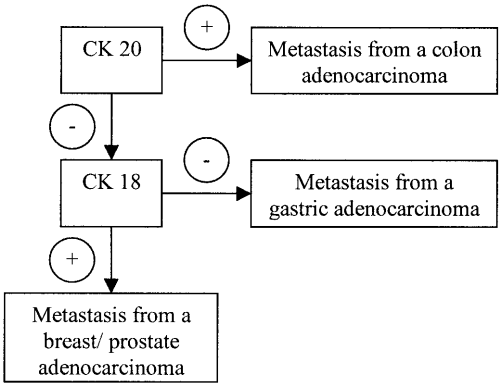

Scheme 2 Classification tree for metastases of different origin

multivariate analysis, it did not bring any further information to that gained by using CK 5 and 18 and HMW CK.

Considering the results of multinomial logistic regression, we developed a classification tree (Scheme 2) for metastases of different origin by using only CK 18 and 20. Using this scheme, the sensitivity for colonic carcinoma metastases was 76.2%, with 100% specificity; the positive predictive value was 100%; and the negative predictive value 86.5%. For breast and prostate carcinoma metastases, we noticed a sensitivity of 63%, a specificity of 88.5%, a positive predictive value of 85% and a negative predictive value of 69.7%. The sensitivity for gastric cancer metastases was 100%, the specificity 75%, the positive predictive value 29.4% (due to the few number of cases) and the negative predictive value 100%.

Renal clear cell carcinomas

Negative CK 7 reactivity was most likely consistent with the diagnosis of metastatic clear cell carcinoma of the kidney, whereas primary large cell carcinomas of the lung (clear cell variant and large cell lung carcinomas with clear cell areas) predominantly showed CK 7 positivity (Table 3). Obviously there is some overlap: 1 of our 18 cases of metastatic renal cell carcinomas reacted positively for CK 7. In their cases, Ramaekers et al. [13] noticed no reaction of renal cell carcinomas with antibodies for CK 7, with a few exceptions. These findings were confirmed by Blobel et al. [1] and Moll et al. [10]. Recognising CK 7 of Moll's catalogue, Gown and Vogel [5] showed that renal adenocarcinomas had a positive reaction to the antibody 35βH11. Also Shah et al. [16] found one autopsy renal cell carcinoma positive for CK 7 in the primary as well as in the metastasis. Savera et al. [15] noticed positivity in 59% (10 of 17) of their primary renal clear cell carcinomas, but no reaction in the investigated metastases.

With antibodies to CK 20, we noticed positivity in 17% (3 of 18) of our renal cell carcinoma metastases, which was, however, not significantly higher than in primary lung carcinomas. Moll et al. [11] had only one case (1 of 25) of primary renal cell carcinoma (clear cell type) that focally positively stained for CK 20. Savera et al. [15] also noticed positivity for CK 20 in 12% (2 of 17) of primary renal clear cell carcinomas. No reaction was noticed in two investigated metastases. We think that a distinction between renal metastasis and lung primary should be possible in most cases by using CK 7 antibodies.

Squamous cell carcinomas

We did not observe any statistically significant differences in the staining pattern of primary squamous cell carcinomas and the metastatic squamous cell carcinomas of the lung (Table 4). We also did not notice a significant difference among the metastases. This might also be due to the small number of cases investigated. The only CK that might be of some value for differentiating primary versus metastatic lung carcinoma is CK 17. In primary lung carcinomas, CK 17 expression seems to be higher than in most metastatic tumours (the Fisher's exact test for this finding is marginally significant). We found three of six oesophageal carcinoma metastases positively stained. Miettinen et al. [9] noticed no reaction in normal oesophagus epithelium for CK 17 but found significant reactivity in oesophageal carcinomas, as well as in laryngeal carcinomas. However, neither in laryngeal, oral cavity, nor hypopharynx carcinomas was the number of cases large enough to give a definite answer.

Normal lung epithelia

Bronchial epithelia and bronchiolar epithelia did not share an identical distribution of their respective CK polypeptides. The different CK composition in bronchial and bronchiolar cells was unexpected but might reflect steps in the embryogenesis and function. Large bronchi are conducting airways, and their main function is stability in allowing undisturbed airflow. Bronchioli, especially respiratory bronchioli, are flexible structures, which must follow lung expansion and collapse during breathing; parts of them are also integrated into gas exchange. The differences of CK polypeptide composition might reflect these differences in function and stability. Another interesting fact is the unique CK 17 positivity of pneumocyte type II. It would not be surprising, therefore, if bronchioloalveolar adenocarcinomas of predominant Clara and pneumocyte types might also be positive for CK 17.

Cytokeratin typing, in addition to other markers, can aid in the differential diagnosis of metastatic versus primary non-small cell carcinomas of the lung. Finding the primary site of the tumour reduces the time period until the patient can be treated and the cost of diagnosis. Our results suggest antibodies to CK 5, 18 and 20 and HMW CK are fairly efficient for the discrimination between primary non-small cell lung carcinomas and metastatic adenocarcinomas of the lung of different ori-

gin. CK 7 appears to be very useful in distinguishing primary large- and clear cell lung carcinomas and metastases from renal cell carcinomas. We admit, however, that some of our results might be too data-driven and should therefore be tested in a larger series of tumours.

Besides CKs, other markers – thyroid transcription factor 1, different mucins, hormones, cell-specific proteins such as surfactant apoprotein and Clara cell proteins, and many others – can also be used in combination to detect the primary site of a carcinoma. Also, tissue- or carcinoma-specific genetic alteration may be important. However, this is beyond the scope of this investigation.

References

1. Blobel G, Moll R, Franke W, Vogt I (1984) Cytokeratins in normal lung and lung carcinomas. Virchows Arch 45:407–429
2. Bruderman I, Cohen R, Leitner O, Ronah R, Guber A, Griffel B, Geiger B (1990) Immunocytochemical characterisation of lung tumors in fine needle aspiration. Cancer 66:1817–1827
3. Cooper D, Schermer A, Sun T (1985) Biology of disease. Lab Invest 3:243–256
4. Flint A, Lloyd R (1992) Pulmonary metastases of colonic carcinoma. Arch Pathol Lab Med 116:39–42
5. Gown A, Vogel A (1984) Monoclonal antibodies to human intermediate filament proteins. Am J Pathol 114:309–321
6. Lagendijk JH, Mullink H, van Diest PJ, GA, Meijer CJLM (1998) Tracing the origin of adenocarcinomas with unknown primary using IHC: differential diagnosis between colonic and ovarian carcinomas as primary sites. Hum Pathol 29:491–497
7. Loy T, Calaluce R (1994) Utility of cytokeratin immunostaining in separating pulmonary adenocarcinomas from colonic adenocarcinomas. Am J Clin Pathol 102:764–767
8. Miettinen M (1995) Keratin 20: immunohistochemical marker for gastrointestinal, urothelial, and merkel cell carcinomas. Mod Pathol 8:384–388
9. Miettinen M, Nobel M, Tuma B, Kovatich A (1997) Keratin 17, immunohistochemical mapping of its distribution in human epithelial tumors and its potential applications. Appl Immunohistochem 5:152–159
10. Moll R, Franke W, Schiller D, Geiger B, Krepler R (1982) The catalog of human cytokeratins: patterns of expression in normal epithelia, tumors and cultured cells. Cell 31:11–24
11. Moll R, Löwe A, Laufer J, Franke W (1992) Cytokeratin 20 in human carcinomas. Am J Pathol 140:427–447
12. Okada H, Tsubura A, Okamura A, Senzaki H, Naka Y, Komatz Y, Morii S (1992) Keratin profiles in normal /hyperplastic prostates and prostate carcinoma. Virchows Arch 421:157–161
13. Ramaekers F, Niekerk van C, Poels L, Schafsma E, Huismans A, Robben H, Schaart G, Vooijs P (1990) Use of monoclonal antibodies to keratin 7 in the differential diagnosis of adenocarcinomas. Am J Pathol 136:641–655
14. Ritter J, Boucher L, Wick M (1998) Peripheral pulmonary adenocarcinomas with bronchioloalveolar features: immunophenotypes correlate with histologic patterns. Mod Pathol 11: 556–572
15. Savera A, Torres F, Linden M, Bacchi C, Gown A, Zarbo R (1996) Primary versus metastatic pulmonary adenocarcinoma. Appl Immunohistochem 4:86–94
16. Shah KD, Tabibzadeh SS, Gerber MA (1987) Comparison of cytokeratin expression in primary and metastatic carcinomas. Am J Clin Pathol 87:708–715
17. Tan J, Sidhu G, Greco A, Ballard H, Wieczorek R (1998) Villin, cytokeratin 7, and cytokeratin 20 expression in pulmonary adenocarcinoma with ultrastructural evidence of microvilli with rootlets. Hum Pathol 29:390–396
18. Tot T (1999) Adenocarcinomas metastatic to the liver. Cancer 85:171–177
19. Yang XJ, Lecksell K, Godin P, Epstein J (1999) Rare expression of high-molecular-weight cytokeratin in adenocarcinomas of the prostate gland. Am J Surg Pathol 23: 147–152
20. Yeger H, Baumal R, Kahn HJ, Duwe G, Phillips MJ (1986) The use of cytoskeletal characteristics of tumor cells for the diagnosis of colon and breast adenocarcinomas. Am J Clin Pathol 86:697–705

Virchows Arch (2002) 440:77–84
DOI 10.1007/s004280100523

ORIGINAL ARTICLE

Ingrid Stallmach · Petra Zenklusen
Paul Komminoth · Stephan Schmid · Aurel Perren
Malgorzata Roos · Zhao Jianming · Philipp U. Heitz
Madeleine Pfaltz

Loss of heterozygosity at chromosome 6q23–25 correlates with clinical and histologic parameters in salivary gland adenoid cystic carcinoma

Received: 2 April 2001 / Accepted: 26 July 2001 / Published online: 31 October 2001
© Springer-Verlag 2001

Abstract The prognosis of salivary gland adenoid cystic carcinoma (ACC) depends on the clinical stage, the location of the primary tumor, and the histologic growth pattern. ACCs with a cribriform growth pattern have a better prognosis than those with a solid growth pattern; however, clear-cut grading criteria have not yet been established, and therefore prognostic indicators on a molecular level are of special interest. In order to analyze tumor tissue with different growth patterns, cribriform and solid tumor areas of 25 patients were microdissected and separately analyzed for loss of heterozygosity (LOH) at nine polymorphic microsatellite markers located between 6q14 and 6q27. LOH was detected in 19/25 (76%) patients and LOH rates were highest at markers D6S441, D6S310, D6S311 and UTRN, which are located at 6q23–25. Combined analysis of LOH at these four markers shows that in primary tumor subtype foci with cribriform growth pattern LOH is associated with high TNM stages ($P<0.01$), high T stages ($P=0.01$), positive lymph node status ($P=0.03$), an unfavorable disease course ($P=0.02$), and the presence of >10% solid growth pattern ($P=0.05$). In contrast, in primary tumor subtype foci with solid growth pattern, no significant differences in LOH rates were found in patients from prognostically and histologically favorable versus unfavorable patient groups. The frequent occurrence of LOH at 6q23–25 and the correlation of LOH rates with prognostic parameters indicate that a prognostically important tumor suppressor gene is located in this chromosomal area.

Keywords Salivary gland tumor · adenoid cystic carcinoma · loss of heterozygosity · chromosome 6

This work was supported by: Sassella-Stiftung and Wolfermann-Nägeli Stiftung.

I. Stallmach · P. Zenklusen · P. Komminoth · A. Perren
Z. Jianming · P.U. Heitz · M. Pfaltz (✉)
Institute of Clinical Pathology, Department of Pathology, University of Zürich, Schmelzbergstrasse 12, 8091 Zürich, Switzerland
e-mail: madeleine.pfaltz@pty.usz.ch
Tel.: +41-1-2552595, Fax: +41-1-2554551

S. Schmid
Clinic of Otorhinolaryngology, ENT Head and Neck Surgery, University of Zürich, Frauenklinikstrasse 24, 8091 Zürich, Switzerland

M. Roos
Institute of Social and Preventive Medicine, Division of Biostatistics, University of Zürich, Sumatrastrasse 30, 8006 Zürich, Switzerland

Introduction

Adenoid cystic carcinoma (ACC) of the salivary glands is an aggressive neoplasm with a slow growth, resulting in an insidious destruction of the surrounding tissues. The clinical course of these neoplasms is often protracted and characterized by local recurrences and by metastases late in the course of the disease to regional lymph nodes, lungs, and bone. Approximately 60% of all ACCs arise in the parotid and submandibular glands; the remaining affect small intraoral glands, especially those of the palate. Three histologic types of ACC are recognized. The most common histologic type is the classic cribriform or glandular type, which is composed of monomorphic tumor cell islands with punched out spaces resulting in the so-called “Swiss cheese” appearance. In contrast the solid subtype is characterized by sheets of basaloid cells showing nuclear polymorphism, mitotic activity, and foci of necrosis (Fig. 1). The tubular type shows an admixture of small nests of cells and narrow ductal structures separated by fibrous stroma.

The prognosis of ACC depends on the clinical stage, the location of the primary, and the histologic growth pattern. ACCs with a solid growth pattern have a worse prognosis than those with a cribriform or tubular growth pattern; however, the extent of solid component required to classify a tumor as a high-grade lesion is a matter of debate [30, 18, 27, 3]. While some authors claim that only tumors lacking a solid growth pattern have a better

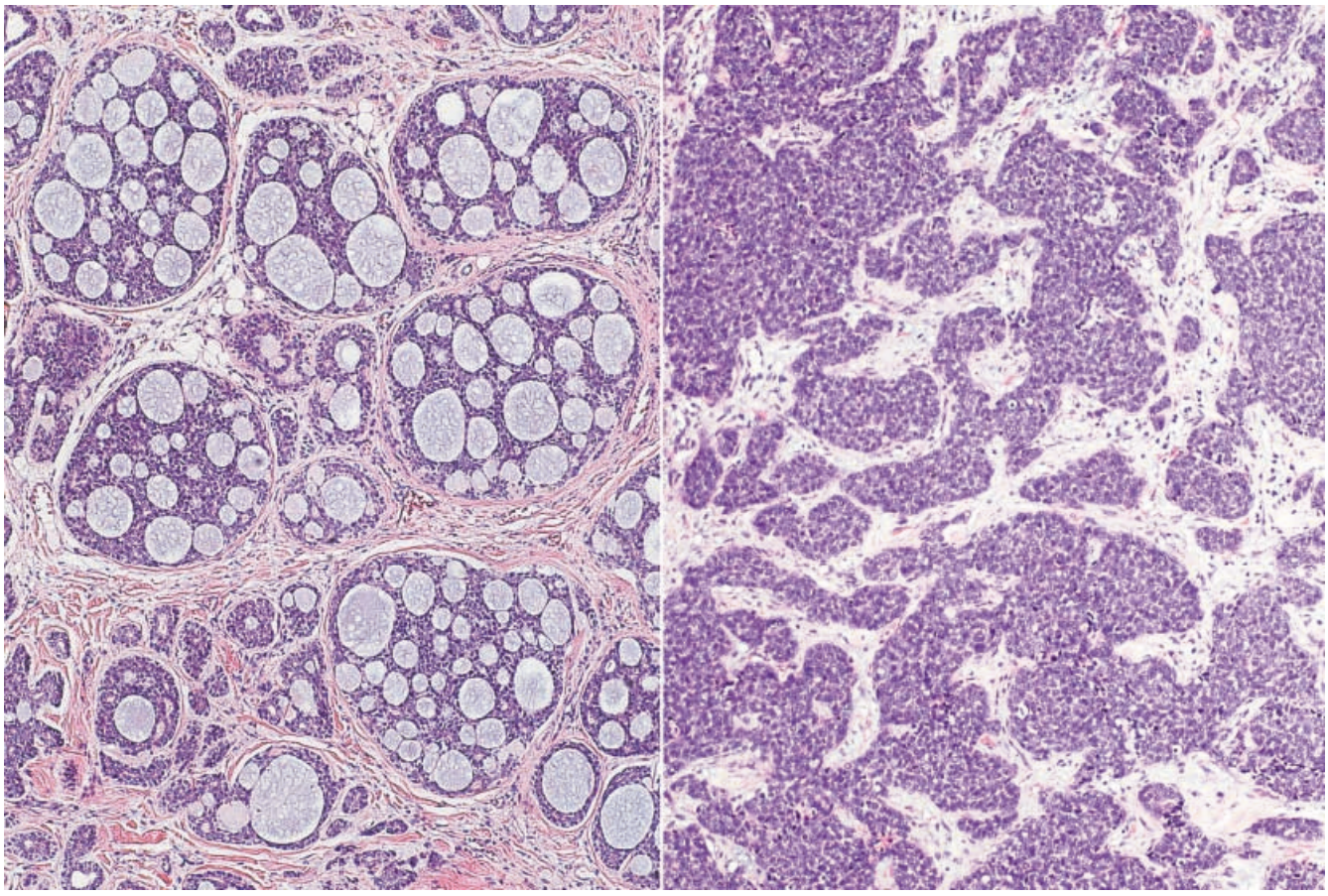

Fig. 1 Histology of adenoid cystic carcinoma. *Left*: Well differentiated tumor with cribriform growth pattern. H&E; ×200. *Right*: Poorly differentiated tumor with solid growth pattern. H&E; ×200

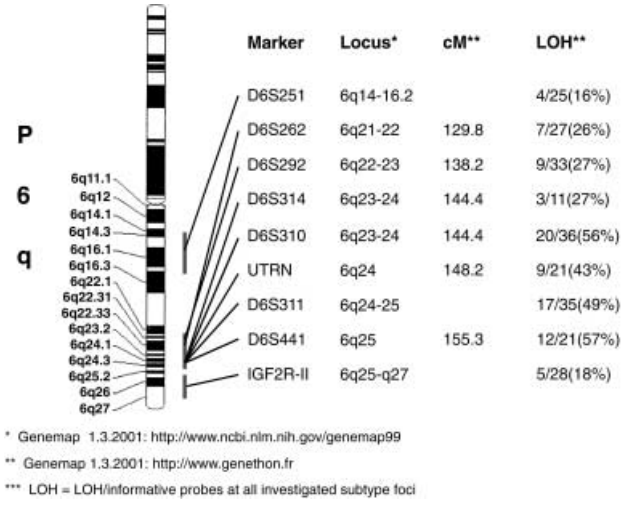

Fig. 2 Microsatellite markers: location and loss of heterozygosity rates

prognosis [30], others studies have documented a less favorable course in patients with more than 10% solid areas [3] and more than 30% solid areas, respectively [18]. Compared to the cribriform subtype, the more aggressive solid subtype is characterized by a relatively high incidence of aneuploidy, a higher dividing cell fraction, and an increase in the number of nucleolar organizer regions (AgNORs) [23, 4, 38]. In addition, overexpression of the tumor suppressor gene *p53* is more frequent in ACCs with a solid growth pattern [40] and in patients with an unfavorable clinical outcome [41]; accordingly, loss of heterozygosity (LOH) rates at the *p53* gene are higher in solid than in cribriform subtype foci of ACCs [39]. Cytogenetic studies of ACCs have revealed recurrent rearrangements of 6q21–24, 9p13–23, and 17p12–13, and the translocation t(6;9)(q21–24; p13–23) seems to be a non-random, primary aberration [29, 8, 15]. Since deletions of 6q are a frequent finding in malignant salivary gland tumors, including ACCs [11, 24], we focused our study on the investigation of this chromosomal arm, and – on the basis of data from previous LOH studies on salivary gland tumors – we selected microsatellite markers located between 6q14 and 6q27 [12, 20] (Fig. 2). So far only little information is available on the molecular events involved in the progression of these neoplasms to a higher histologic grade [39, 40]. The aim of this study was therefore to separately analyze microdissected cribriform and solid foci of both primary and metastastatic ACCs for LOH, a method known to yield valuable data on the localization of possible tumor suppressor genes.

Table 1 Clinical and histologic data. *Alive* alive without disease, *a.w.d.* alive with disease, *d.o.d.* death of disease, *Rec.PT* recurrent primary tumor, *PT* primary tumor

	Sex	PT site	TNM Stage	T Stage	N Stage	Clinical course	Follow-up (months)	% solid growth
1	Female	Parotid gland	I	T2	N0	alive	48	<10%
2	Male	Small oral gland	I	T2	N0	alive	12	<10%
3	Female	Submand. gland	I	T2	N0	alive	24	<10%
4	Male	Parotid gland	I	T1	N0	alive	24	<10%
5	Female	Submand. gland	II	T3	N0	a.w.d.	14	<10%
6	Female	Small oral gland	I	T1	N0	alive	12	<10%
7	Male	Parotid gland	I	T1	N0	d.o.d.	12	10–30%
8	Male	Parotid gland	Rec. PT		N0	alive	72	>30%
9	Female	Parotid gland	Rec. PT		N0	a.w.d.	60	10–30%
10	Male	Parotid gland	II	T3	N0	alive	48	<10%
11	Male	Submand. gland	I	T2	N0	alive	60	<10%
12	Female	Small oral gland.	II	T2	N0	alive	60	<10%
13	Female	Small oral gland.	IV	T4	N0	a.w.d.	1	>30%
14	Female	Submand. gland	II	T3	N0	a.w.d.	60	10–30%
15	Male	Small oral gland	IV	T4	N0	d.o.d.	60	>30%
16	Male	Parotid gland	I	T1	N0	alive	48	10–30%
17	Male	Parotid gland	I	T1	N0	alive	1	10–30%
18	Male	Parotid gland	I	T2	N0	a.w.d.	48	>30%
19	Male	Sublingual gland	IV	T3	N1	alive	60	10–30%
20	Male	Small oral gland	IV	T3	N1	alive	84	10–30%
21	Female	Submand. gland	IV	T3	N1	d.o.d.	12	>30%
22	Male	Parotid gland	IV	T3	N2	d.o.d.	36	10–30%
23	Female	Parotid gland	IV	T3	N2	No data	No data	10–30%
24	Female	Parotid gland	Rec. PT		N1	a.w.d.	36	10–30%
25	Female	Parotid gland	IV	T4	N1	d.o.d.	34	>30%

Material and methods

Patients

Paraffin blocks of 25 patients with ACCs operated between 1991 and 1999 were selected. In five patients metastatic tumor tissue from regional lymph nodes (patients 19, 20, 22, 23) and from the liver (patient 21) was available in addition to the primary tumor. Tissues had been fixed by immersion in 4% formaldehyde, embedded in paraffin and stained with hematoxylin and eosin according to standard procedures. All slides were reclassified according to the classification of Seifert et al. 1991 [25]. Based on the estimated percentage of solid tumor tissue the patients were assigned to the following groups: <10% solid growth pattern (n=9), 10–30% solid growth pattern (n=10), and >30% solid growth pattern (n= 6). Representative blocks with cribriform and solid growth pattern and normal control tissue were selected. One tissue sample of each available histologic growth pattern was microdissected and subsequently investigated per patient. After microdissection the following subtype foci were available: cribriform and solid primary tumor focus (16 patients), cribriform primary tumor focus (four patients), solid primary tumor focus (five patients). In four patients the following metastatic tissue samples were available: cribriform and solid metastatic focus (three patients), cribriform metastatic focus (one patient), and solid metastatic focus (one patient). No tumor tissue with a tubular growth pattern was analyzed, since the prognosis of patients with this growth pattern is similar to the one of patients with cribriform growth pattern; in addition the abundance of fibrous stroma in this subtype may cause technical problems. The average age of patients was 59 (32 to 85), the male:female ratio was 13:12. The tumors were located in the parotid gland (13), submandibular gland (5), sublingual gland (1), and small intraoral salivary glands (6). In three patients (8, 9, 24) only recurrent primaries were available for investigation. The TNM stages were I (10 patients), II (4 patients), and IV (8 patients), the T stages were T1 (5 patients), T2 (6 patients), T3 (8 patients) and T4 (3 patients). 7 patients had regional lymph node metastases. Follow-up data were available from 24 of 25 patients. Thirteen patients were alive without disease, six patients were alive with disease, and five patients had died of disease. The average follow-up period was 39 months (range 1 to 84 months). In patients with a favorable disease course (alive without disease) the average follow-up period was 43 months (range 1–84 months) and in patients with an unfavorable disease course (tumor recurrence or death of disease) the average follow-up period was 34 months (range 1–60 months) (Table 1).

Statistical analysis

For statistical analysis the following patient groups were compared: patients with pT stages 1+2 versus 3+4, patients with TNM stages I+II versus IV, patients with positive versus negative lymph node status, patients with <10% versus >10% solid growth pattern, and patients with <30% versus >30% solid growth pattern. In addition patients with a favorable course (alive without diseases) were compared with patients with an unfavorable course (tumor recurrence or death of disease) (Table 2). For each patient the LOH rate was assessed by dividing the number of LOHs by the total number of informative samples. The Mann-Whitney test was used to analyze the dependence of LOH rates on clinicopathologic parameters. The Wilcoxon signed rank test was used to compare LOH rates in cribriform versus solid primary tumor subtype foci of patients, in which both of these subtype foci were available. A comparison of LOH rates in metastatic versus primary tumor subtype foci was not performed due to the small number of metastases investigated. LOH findings of recurrent primaries (patients 8, 9, 24) were not included in the statistical analysis.

Microdissection and DNA extraction

For microdissection of tumor subtype foci, 20 sections (10 µm thick) were cut, and every fifth slide was stained with hematoxylin-eosin, cover-slipped, and used for microscopic control, whereas the others were used for microdissection. Precisely identified tumor subtype foci and normal control tissue with low amount of

Table 2 Correlation of losses (in n/n informative subtype foci) with clinico-pathologic parameters

	Cribriform primary tumors			Solid primary tumors	
	All markers	D6S310 + D6S311 + D6S441 + UTRN	All other markers: D6S251, D6S262, D6S292, D6S314, IGF2R-II		All markers
TNM stage [b]				TNM stage [c]	
I + II (*n*=12)	17.9% (12/67)	17.2% (5/29)	18.4% (7/38)	I + II (*n*=10)	45.5% (20/44)
IV (*n*= 5)	57.1% (12/21)	83.3% (10/12)	22.2% (2/9)	IV (*n*= 8)	60.0% (24/40)
	P=0.02 [a]	*P=<0.01* [a]	*n.s.* [a]		*n.s.* [a]
T stage [b]				T stage [c]	
1+2 (*n*=10)	14.5% (8/55)	16.0% (4/25)	13.3% (4/30)	1+2 (*n*=7)	50.0% (15/30)
3+4 (*n*= 7)	48.4% (16/33)	68.7% (11/16)	29.4% (5/17)	3+4 (*n*= 11)	52.3% (29/54)
	P=0.02 [a]	*P=0.01* [a]	*n.s.* [a]		*n.s.* [a]
N stage [b]				N stage [c]	
N0 (n=13)	20.2% (14/69)	20.0% (6/30)	20.5% (8/39)	N0 (n=12)	50.0% (28/56)
N1 (n=4)	52.6% (10/19)	81.8% (9/11)	12.5% (1/8)	N1 (n=6)	57.1% (16/28)
	n.s. [a]	*P=0.03* [a]	*n.s.* [a]		*n.s* [a]
Disease course [b, d]				Disease course [c, d]	
favorable (n=12)	14.7% (10/68)	21.2% (7/33)	8.5% (3/35)	favorable (n=8)	33.3% (11/33)
unfavorable (n=4)	76.9% (10/13)	100.0% (4/4)	66.6% (6/9)	unfavorable (n=9)	64.4% (29/45)
	P=<0.01 [a]	*P=0.02* [a]	*n.s.* [a]		*n.s.* [a]
Histology [b]				Histology [c]	
<10% solid (n=9)	15.8% (10/63)	17.8% (5/28)	14.2% (5/35)	<10% solid (n=5)	33.3% (8/24)
>10% solid (n=8)	56.0% (14/25)	76.9% (10/13)	33.3% (4/12)	>10% solid (n=13)	60.0% (36/60)
	n.s. [a]	*P=0.05* [a]	*n.s.* [a]		*n.s.* [a]

[a] Mann-Whitney-test
[b] 3 patients with recurrent primaries and 5 patients without informative cribriform primary tumor foci not included
[c] 3 patients with recurrent primaries and 4 patients without informative solid primary tumor foci not included
[d] 1 patient with missing follow up data not included

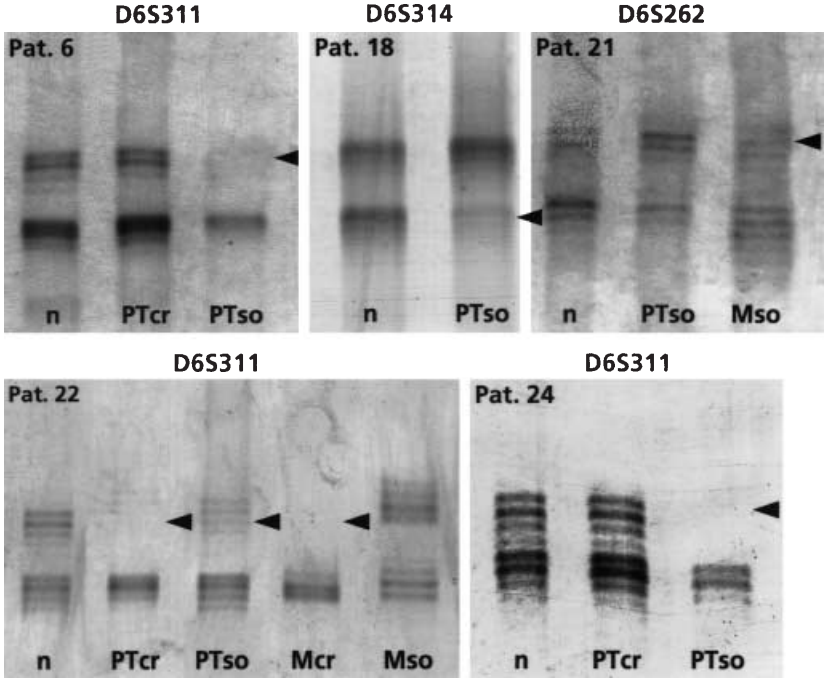

Fig. 3 Examples of allelic imbalance. Silver-stained gels with matched normal (*n*) and tumor (*PTcr* primary tumor cribriform, *PTso* primary tumor solid, *Mcr* metastasis cribriform, *Mso* metastasis solid) DNA are shown. *Arrowheads* show loss of heterozygosity for the respective markers

connective tissue were scraped off under mineral oil (Sigma) using a 24-gauge needle (Terumo Europe, Leuven, Belgium) under a stereomicroscope (Stemi DV4, Zeiss, Germany). The paraffin material was placed in a 1.5-ml Eppendorf tube containing 500 µl of DNA extraction buffer (100 mM Tris, pH 8.0, 5 mM EDTA, 0.5% NPO_4, 0.5% Tween 20) and heated at 55°C until the paraffin was dissolved. After centrifugation for 10 min at 4°C, the floating paraffin was removed and the remnant treated overnight with 50 µg/ml Proteinase K (Sigma, St.Louis, MO, USA) at 55°C. After enzyme inactivation at 94°C for 10 min, the DNA was purified by phenol-chloroform extraction and quantified by spectrophotometry according to standard procedures.

LOH analysis

Normal and tumor DNA were screened for LOH using polymorphic markers mapping between 6q14 and 6q27 (Fig. 2). Primers used for the amplification of microsatellite markers D6S251, D6S262, D6S292, D6S314, D6S310, D6S311, and D6S441 were purchased from Microsynth, Balgach, Switzerland, and primers for UTRN and IGF2R-II were obtained from Research Genetics (Huntsville, Ala., USA). The polymerase chain reaction (PCR) mixtures were prepared in 0.5-ml thin-walled reaction tubes (GeneAmp; Perkin Elmer, Norwalk, CT, USA) and contained 200 ng of template DNA, 0.2 mM of dATP, dTTP, dGTP, and dCTP, respectively, 20 pmol of each sense and antisense primer, 1.5 mM $MgCl_2$, 10 mM Tris-HCl (pH 8.3), 50 mM KCl, and 1 U of Ampli Taq Gold DNA polymerase (Perkin Elmer) in a final volume of 50 µl. PCR was carried out in a programmable thermal cycler (DNA thermal cycler 9600; Perkin Elmer) using an initial denaturation for 420 s at 94°C, 35 to 45 cycles of denaturation for 45 s at 94°C, annealing for 60 s at 50–58°C, and extension for 60 s at 72°C, followed by a final extension at 72°C for 300 s. An amount of 12 µl of each PCR product was diluted 1:1 in blue stop solution (95% formamide, 20 mM EDTA, 0.05% xylene cyanol, 0.05% bromophenol blue), heated at 94°C for 10 min, and loaded onto a 40×30×0.75 cm, 6% denaturating polyacrylamide gel (40:2 acrylamide:bisacrylamide; BioRad, Glattbrugg, Switzerland) containing 7 M urea (Fluka, Buchs, Switzerland). After preheating of the gel for 15 min, electrophoresis was carried out at 80 W for 2 h 15 min (D6S251), 2 h 05 min (D6S262), 2 h 30 min (D6S292), 2 h 20 min (D6S314), 2 h 35 min (D6S310), 2 h 30 min (D6S311), 2 h (D6S441), 2 h (UTRN), and 2 h 10 min (IGF2R-II) respectively, using a programmable electrophoresis power supply (Gibco BRL PS9009; Life Technologies, Basel, Switzerland). After electrophoresis, the DNA was visualized by silver staining as previously described [7]. For LOH analysis, only patients heterozygous for a given DNA sequence were considered informative, whereas the presence of either homozygosity or an unclear distinction between paternal and maternal alleles was considered uninformative. A twofold difference in relative allele intensity ratios between tumor DNA and normal DNA was scored as LOH.

Results

LOH at one or more loci on 6q was found in 19/25 patients (76%). Examples of allelic balance and imbalance are shown in Fig. 3; the extent of allelic loss for each tumor is shown in Table 3. Combined analysis of all investigated subtype foci reveals that LOH is most frequently present at markers D6S441 (57%), D6S310 (56%), D6S311 (49%), and UTRN (43%) (Table 1). Combined analysis of LOH rates at these four markers in cribriform primary tumor subtype foci shows that LOH rates in these subtype foci are higher in patients with high versus low TNM stages (10/12 versus 5/29; $P<0.01$), patients with high versus low T stages (11/16 versus 4/25; $P=0.01$), patients with versus without lymph node metastases (9/11 versus 6/30; $P=0.03$), patients with unfavorable versus favorable course of the disease (4/4 versus 7/33; $P=0.02$), and patients with >10% versus <10% tumor tissue with solid growth pattern (10/13 versus 5/28; $P=0.05$) (Table 2). In contrast, LOH rates at these four markers did not differ significantly in patients with >30% versus <30% solid tumor growth pattern. Combined analysis of the remaining five microsatellite markers (D6S251, D6S262, D6S292, D6S314, and IGF2R-II) shows similar LOH rates in cribriform primary tumor

Table 3 Extent of allelic loss in patients with loss of heterzygosiy (*LOH*) at chromosome 6q. ■ LOH, □ informative with retained alleles, *NI* non informative, *gaps* allelotyping was not successful, *PTcr* primary tumor cribriform, *PTso* primary tumor solid, *Mcr* metastasis cribriform, *Mso* metastasis solid

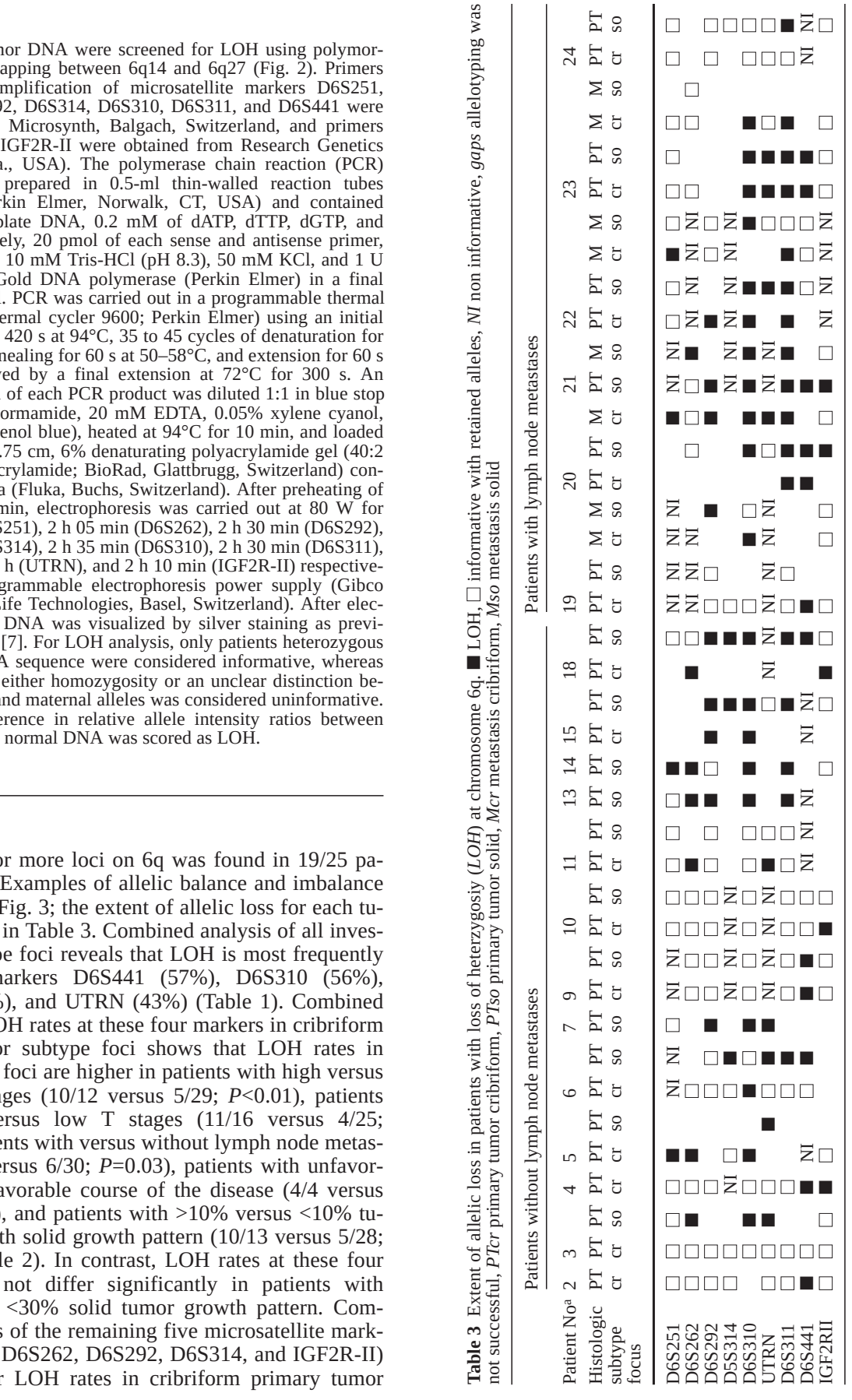

[a] Only patients with LOH at 6q are listed

subtype foci of patients from all prognostically and histologically different patient subgroups. In addition, analysis of solid primary tumor subtype foci also shows similar LOH rates in all different patients subgroups, with combined analysis of all nine microsatellite markers (Table 2), combined analysis of the four markers affected most frequently by LOH, and with combined analysis of the remaining five markers.

Combined analysis of all nine microsatellite markers shows that the total number of LOHs is higher in solid compared to cribriform primary tumor subtype foci (28/60 (47%) versus 21/59 (36%)), but this finding is not statistically significant (P=0.79).

Of the 16 patients in whom both cribriform and solid tumor foci of primaries were available for investigation, identical LOHs were present in cribriform and solid tumor foci at 11/23 informative loci. At 8/23 informative loci LOHs were detected at additional 6q markers in solid compared to cribriform primary tumor foci, and at 4/23 informative loci LOHs present in cribriform primaries were not detected in solid primaries. Of the five patients in whom specimens of metastases were available, identical LOHs were seen in primary and metastatic subtype foci with the same histolgic growth pattern at 7/16 informative loci. Additional lost 6q markers were detected in metastases at 4/16 informative loci, and at 5/16 informative loci LOHs present in primaries could not detected in metastatic subtype foci.

Discussion

In this study LOH at one or more loci on 6q was found in 19/25 patients (76%) and allelic loss was most frequently present at markers D6S441, D6S310, D6S311, and UTRN. Combined analysis of all nine microsatellite markers shows that the total number of LOHs is higher in solid than in cribriform primaries. Although this finding is not statistically significant, it is in accordance with the observation that histologic dedifferentiation goes along with an accumulation of genetic alterations.

The analysis of LOH rates in cribriform primaries is of special interest, since genetic alterations identifiable at an early stage of the disease and in the most frequently occurring cribriform growth pattern might provide prognostically important information. Separate analysis of cribriform primary tumors at the four microsatellite loci with highest percentages of allelic loss (D6S310, D6S311, D6S441, and UTRN) shows that LOH rates in cribriform primary tumors are significantly higher in patients with advanced versus early TNM, T and N stages; in patients with unfavorable versus favorable disease course; and in patients with >10% versus <10% solid growth pattern (Table 2). The fact that patients with advanced T stages have increased LOH rates at 6q23–25 in their cribriform subtype foci indicates that in these patients the 6q deletions correlate with tumor size rather than with tumor grade. Nevertheless, histologic dedifferentiation – assessed by the percentage of solid tumor growth in a given tumor – also seems to go along with an accumulation of LOH at 6q23–25, even in low-grade cribriform primary tumor tissue. Indeed in this study, LOH rates are significantly higher in cribriform tumor tissue of patients with >10% versus <10% solid tumor growth, whereas LOH rates in cribriform primaries of patients with >30% versus <30% solid tumor growth do not differ significantly. Our observation that low LOH rates are restricted to patients with <10% solid growth pattern is interesting with respect to the observations of Szanto et al. [30] and Fordyce et al. [3] that a favorable course is restricted to patients with <10% solid growth pattern.

Comparison of cribriform with solid primary tumor subtype foci from one and the same patient reveals that, in general, LOH loci are either identical in cribriform and solid areas or additional LOHs are present in solid subtype foci, indicating a tendency towards loss of larger parts of 6q with dedifferentiation. However, LOHs present in a cribriform primary are not always detected in the solid primary subtype focus of the same patient. A similar finding can also be observed by comparison of primary tumors with metastases, indicating that both histologic dedifferentiation and progression to metastatic disease are accompanied by the appearance of additional, genetically different tumor cell clones. In addition, although LOH at 6q23–25 seems to play a role both in the development and the progression of ACC, the present study and the one by Queimado et al. [20] show that not all patients with ACC have LOH at these markers; hence, other genetic pathways seem to be involved in the evolution and progression of these neoplasms.

Deletions on chromosome 6q have also been described in other salivary gland carcinomas [20], and they occur in many other neoplasms, including ovarian [2], cervical [13], breast [34], gastric [19], prostate [28], renal cell [10], and urinary bladder carcinomas [22], malignant melanoma [14], and hematopoietic malignancies [31, 6, 26]. The hypothesis that one or several tumor suppressor genes may be located within chromosome 6q are supported by chromosome transfer experiments, which have shown that chromosome 6 can suppress the tumorigenic or metastatic activity of melanoma cell lines [33, 37]. In addition, chromosome 6 can induce senescence when introduced into immortalized cell lines [9].

The microsatellite markers D6S310, D6S441, D6S311, and UTRN, which have shown highest LOH rates in our study, are also frequently affected by LOH in non-Hodgkin lymphoma [6] and in cancer of the breast [5, 16, 32] and the cervix [13]. Interestingly, in a study by Queimado et al. [20] on LOH at 6q in various types of salivary gland carcinomas, none of the tumors – including 6 cases of ACC – showed LOH at D6S311 or D6S441. Several genes have been mapped on the long arm of chromosome 6. Of particular interest with respect to our study is *hZAC*, a gene that encodes a zinc finger protein. This gene localizes to 6q24–25 and has been named according to its functional properties, namely, induction of apoptosis and cell cycle arrest. The expression of this candidate tumor suppr-

esor gene has been shown to be reduced or lost in pituitary adenomas [17] and in carcinoma of the breast [1]. Although *hZAC* has been localized to the region in which we found the highest LOH rates, the relatively poor expression of *hZAC* in normal salivary gland tissue indicates that other pathways also contribute to the development of ACCs [35]. Interestingly, a homologue of *hZAC*, the *PLAG1*, which is located on 8q, is involved in the development of pleomorphic adenoma of the salivary gland [21, 36].

The results of our study show that genetic changes at 6q23–25 may be important in the development and progression of ACC and that LOH rates at this location may provide information of prognostic importance. Of particular interest is the fact that LOH rates correlate with prognostic factors in cribriform subtype foci. On the basis of this finding analysis of a small amount of cribriform tissue may allow an estimation of prognosis, irrespective of the amount of solid tumor tissue present in a given tumor. A more precise identification of prognostically different patient subgroups may also allow a selective application of aggressive treatment procedures, and, on the other hand unnecessary overtreatment may be avoided. In future studies the area of deletion at 6q23–25 should be narrowed down with additional markers by fine deletion mapping, with the aim to identify the suspected tumor suppressor gene. In addition, the application of fluorescence in situ hybridization (FISH) using specific DNA probes might be helpful both in ruling out loss of both alleles and in gaining information on tumor heterogeneity.

References

1. Bilanges B, Verrault A, Rodriguez C, Mazumdar A, Pantoni C, Boekaert J, Theillet C, Spengler C, Journot L (1999) Loss of expression of the candidate tumor suppressor gene ZAC in breast cancer cell lines and primary tumors. Oncogene 18: 3979–3988
2. Colitti CV, Rodabaugh KJ, Welch WR, Berkowitz RS and Mock SC (1998) A novel 4 cM minimal deletion unit on chromosome 6q25.1–25.2 associated with high grade invasive epithelial ovarian carcinomas. Oncogene 16: 555–5559
3. Fordice J, Kershaw C, El-Naggar A, Goepfert H (1999) Adenoid cystic carcinoma of the head and neck. Arch Otolaryngol Head Neck Surg 125: 149–152
4. Franzén G, Nordgard S, Boysen M, Larsen PL, Halvorsen TB, Clausen OP (1995) DNA content in adenoid cystic carcinomas. Head Neck 17: 49–55
5. Fujii H, Zhou W and Gabrielson E (1996) Detection of frequent allelic loss of 6q23-q25.2 in microdissected human breast cancer tissues. Genes Chrom Cancer 16: 35–39
6. Gaidano G, Hauptschein RS, Parsa NZ, Offit K, Rao PH, Lenoir G, Knowles D, Chaganti RSK, Dalla-Favera R (1992) Deletions involving two distinct regions of 6q in B-cell non-Hodgkin lymphoma. Blood 80: 1781–1787
7. Goertz B, Roth J, Speel EJM, Krähenmann A, De Krijger RR, Matias-Guiu X, Muletta-Feurer S, Rüttimann K, Saremaslami P, Heitz PU, Komminoth P (1999) MEN 1 gene mutation analysis of sporadic adrenocortical lesions. Int J Cancer 80: 373–379
8. Highashi K, Jin Y, Yuesheng J, et al (1991) Rearrangement of 9q13 as the primary chromosomal aberration in adenoid cystic carcinoma of the respiratory tract. Genes Chromosomes Cancer 3: 21–23
9. Hubbard-Smith K, Patsalis P, Pardinas JR, Jha KK (1992) Altered chromosome 6 in immortal human fibroblasts. Mol Cell Biol 12: 2273–2281
10. Jiang F, Richter J, Schraml P, Bubendorf L, Gasser T, Sauter G, Mihatsch MJ, Moch H (1998) Chromosomal imbalances in papillary renal cell carcinoma: genetic differences between histological subtypes. Am J Pathol 153: 1467–1473
11. Jin Y, Mertens F, Limon J et al. (1994) Characteristic karyotypic features in lacrimal gland and salivary carcinomas. Br J Cancer 70: 42–47
12. Johns MM, Westra WH, Califano JA, Eisele D, Koch WM, Sifrransky D (1996) Allelotype of salivary gland tumors. Cancer Res 56: 1151–1154
13. Mazurenko N, Attaleb M, Gritsko T, Semjonova L, Pavlova L, Sakharova O, Kisseljov F (1999) High resolution mapping of chromosome 6 deletions in cervical cancer. Oncol Rep 6: 859–863
14. Millikin D, Meese E, Vogelstein B, Witkowski C, Trent J (1991) Loss of heterozygosity for loci on the long arm of chromosome 6 in human malignant melanoma. Cancer Res 51: 5449–5453
15. Nordkwist A, Mark J, Gustafsson H, Bang G, Stenman G (1994) Non-random chromosome rearrangements in adenoid cystic carcinoma of the salivary gland. Genes Chromosome Cancer 10: 115–121
16. Noveillo C, Courjal F, Theillet C (1996) Loss of heterozygosity on the long arm of chromosome 6 in breast cancer: possibly four regions of deletion. Clin Cancer Res 2: 1601–1606
17. Pagotto U, Arzberger T, Theodoropoul M, Gruber Y, Panataloni C, Saeger W, Losa MJ, Journot L, Stalla GK, Spengler D (2000) The expression of the antiproliferative gene ZAC is lost or highly reduced in nonfunctioning pituitary adenomas. Cancer Res 60: 6794–6799
18. Perzin KH, Gullane P, Clairmont AC (1978) Adenoid cystic carcinomas arising in salivary glands. A correlation of histologic features and clinical course. Cancer 42: 265–282
19. Queimado L, Secura R, Pereira AC, Castedo S (1995) Identification of two distinct regions of deletion at 6q in gastric carcinoma. Genes Chromosome Cancer 14: 28–34
20. Queimado L, Reis A, Fonseca I, Martins C, Lovett M, Soares J, Parreira L (1998) A refined localisation of two deleted regions in chromosome 6q associated with salivary gland carcinomas. Oncogene 16: 83–88
21. Queimado L, Lopes C, Du F, Martins C, Bowcock AM, Soares J, Lovett M (1999) Pleomorphic adenoma gene 1 is expressed in cultured benign and malignant salivary gland tumor cells. Lab Invest 79: 583–589
22. Richter J, Beffa L, Wagner U, Schraml P, Gasser TC, Moch H, Mihatsch MJ, Sauter G (1998) Patterns of chromosomal imbalances in advanced urinary bladder cancer detected by comparative genomic hybridization. Am J Pathol 153: 1615–1621
23. Saka T, Yamamoto Y, Takahashi H (1991) Comparative cytofluorometric DNA analysis of pleomorphic adenoma and adenoid cystic carcinoma of the salivary gland. Virchows Arch (C) Cell Pathol 61: 255–261
24. Sandros J, Stenman G, Mark J (1990) Cytogenetic and molecular observations in human and experimental salivary gland tumors. Cancer Genet Cytogenet 44: 153–167
25. Seifert G (1991) Histologic typing of salivary gland tumors, 2nd edn. Springer, Berlin Heidelberg New York, pp 35–36 (WHO International histological classification of tumors)
26. Sherratt T, Morelli C, Boyle JM, Harrison CH (1997) Analysis of chromosome 6 deletions in lymphoid malignancies provides evidence for a region of minimal deletion within a 2-megabase segment of 6q21. Chromosome Res 5: 118–124
27. Spiro RH, Huvos AG (1992) Stage means more than grade in adenoid cystic carcinoma. Am J Surg 164: 623–628
28. Srikantan V, Sesterhenn IA, Davis L, Hankins GR, Avallone FA, Livezey JR, Connelly R, Mostofi FK, McLeod DG, Moul JW, Chandrasekharappa SC, Srivastava S (1999) Allelic loss on chromosome 6q in primary prostate cancer. Int J Cancer 84: 331–335

29. Stenman G, Sandros J, Dahlenfors R, Judberg-Ode M, Mark J (1986) 6q – and loss of the Y chromosome – two common deviations in malignant human salivary gland tumors. Cancer Genet Cytogenet 22: 283–293
30. Szanto PA, Luna MA, Tortoledo ME, White RA (1984) Histologic grading of adenoid cystic carcinoma of the salivary glands. Cancer 54: 1062–1069
31. Takeuchi S, Koike M, Serui T, Bartam CR, Schrappe M, Reither A, Park S, Taub HE, Kubonishi I, Miyoshi I, Koeffler HP (1998) Frequent loss of heterozygosity on the long arm of chromosome 6: identification of two distinct regions of deletion in childhood acute lymphoblastic leukemia. Cancer Res 58: 2618–2623
32. Theile M, Seitz S, Arnold W, Jandrig B, Frege R, Schlag PM, Haensch W, Guski H, Winzer KJ, Barrett JC, Scherneck S (1996) A defined chromosome 6q fragment (at D6S310) harbors a putative tumor suppressor gene for breast cancer. Oncogene 13: 677–685
33. Trent JM, Stanbridge EJ, McBride HL, Meese EU, Casey G, Araujo DE, Witkowski CM, Nagle RB (1990) Tumorigenicity in human melanoma cell lines controlled by introduction of human chromosome 6. Science 247: 568–571
34. Utada Y, Haga S, Kajiwara T, Kasumi F, Sakamoto G, Nakamura Y, Emi M (2000) Mapping of target regions of allelic loss in primary breast cancers to 1-cM intervals on genomic contigs at 6q21 and 6q25.3. Jpn J Cancer Res 91: 293–300
35. Varrault A, Ciani E, Apiou F, Bilanges B, Hoffmann A, Pantaloni C, Bockaert J, Spengler D, Journot L (1998) hZAC encodes a zinc finger protein with antiproliferative properties and maps to a chromosomal region frequently lost in cancer. Proc Natl Acad Sci 95: 8835–8840
36. Voz ML, Agten NS, Van de Ven WJ, Kas K (2000) PLAG1, the main translocation target in pleomorphic adenoma of the salivary glands, is a positive regulator of IGF-II. Cancer Res 60: 106–113
37. Welch DR, Chen P, Miele ME, McGrary CT, Bower JM, Stanbridge EJ, Weissman BE (1994) Microcell-mediated transfer of chromosome 6 into metastatic human C8161 melanoma cells suppresses metastasis but does not inhibit tumorigenicity. Oncogene 9: 255–262
38. Yamamoto Y, Itoh T, Takahashi H (1995) Nucleolar organizer regions in adenoid cystic carcinoma of the salivary glands. Eur Arch Otolaryngol 252: 176–180
39. Yamamoto Y, Virmani AK, Wistuba II, McIntire D, Vuirch F, Albores-Saavedra J, Gazar AF (1996) Loss of heterozygosity and microsatellite alterations in *p53* and *RB* genes in adenoid cystic carcinoma of the salivary glands. Hum Pathol 27: 1204–1210
40. Yamamoto Y, Wistuba II, Kishimoto Y, Virmani AK, Vuitch F, Albores-Saavedra J, Gazdar AF (1998) DNA analysis at p53 locus in adenoid cystic carcinoma: comparison of molecular study and p53 immunostaining. Pathol Int 48: 273–280
41. Zhu QR, White FH, Tipoe GL (1997) p53 oncoprotein accumulation in adenoid cystic carcinoma of parotid and palatine. Pathology 29: 154–158

Virchows Arch (2002) 440:85–93
DOI 10.1007/s004280100540

ORIGINAL ARTICLE

Kyoung-Mee Kim · Min-Joo Kim · Bo-Kyoung Cho
Sang-Wook Choi · Mun-Gan Rhyu

Genetic evidence for the multi-step progression of mixed glandular–neuroendocrine gastric carcinomas

Received: 23 May 2001 / Accepted: 22 August 2001 / Published online: 19 October 2001
© Springer-Verlag 2001

Abstract A mixed glandular–neuroendocrine gastric carcinoma shows discrete, juxtaposed areas of adenocarcinoma and neuroendocrine carcinoma. In order to gain insight into the genetic events and clonality associated with the dual differentiation of a mixed gastric carcinoma, eight cases (two true composite and six neuroendocrine-dominant carcinomas) were examined by analyzing the genome-wide loss of heterozygosity (LOH). Of the eight mixed gastric carcinomas, one true composite and five neuroendocrine-dominant carcinomas showed a primary LOH that was shared by both the glandular and neuroendocrine components and a secondary LOH or mutations that were restricted to the neuroendocrine components. The glandular components contained mixed cell populations with or without primary LOH events, suggesting that a primary LOH arose during adenocarcinoma progression and that the LOH-positive cell served as a precursor for a neuroendocrine carcinoma. The neuroendocrine components were of a homogeneous population with various genetic alterations such as a LOH, *p53* mutations, and microsatellite instability-associated *transforming growth factor (TGF)-β RII* mutation. Therefore, most (six of eight cases) mixed glandular–neuroendocrine gastric carcinomas were likely to have sequentially evolved from a glandular precursor to a genetically heterogeneous adenocarcinoma and then to neuroendocrine differentiation. Two components of the other true composite carcinomas were shown to have reciprocally lost different alleles of identical loci on multiple chromosomes, suggesting that, occasionally (one of eight cases), dual differentiation concurrently arises from a single precursor, possibly as a result of non-disjunctional cell division.

K.-M. Kim
Department of Pathology, College of Medicine,
The Catholic University of Korea, Seoul, Korea

M.-J. Kim · B.-K. Cho · S.-W. Choi · M.-G. Rhyu (✉)
Department of Microbiology, College of Medicine,
The Catholic University of Korea, 505 Banpo-dong, Socho-gu,
Seoul 137-701, Korea
e-mail: rhyumung@cmc.cuk.ac.kr
Tel.: +82-2-5901215, Fax: +82-2-9602534

Keywords Mixed tumor · Neuroendocrine carcinoma · Adenocarcinoma · Chromosomal loss

Introduction

In the stomach, mixed tumors of glandular and neuroendocrine cells have been documented as the continuity of a wide histological spectrum. Neuroendocrine differentiation is dispersed in epithelial tumor cell populations with an estimated frequency ranging from 3% to 34%, depending on the immunohistochemical markers used and the number of specimens examined [12, 22, 27, 30]. In some cases, the neuroendocrine cells occupy the main part of a gastric tumor lesion and an adenocarcinoma is localized in a small portion [2, 16]. The term ‘composite glandular–neuroendocrine carcinoma’ is applied to a rare tumor with discrete, juxtaposed areas of adenocarcinoma and neuroendocrine carcinoma in balanced distribution, even though conclusive criteria on the proportion of the two components cannot be constructed with the current limitations on the cases reported [15]. Such intimate arrangements between the two distinctly differentiated carcinomas raise a question on the possibility of coincidental malignant changes in the two mature cell types or in the common multi-potential stem cells.

There have been a number of isolated reports on mixed glandular–neuroendocrine tumors that arise within the gastrointestinal tract, such as the stomach, colon, and rectum, which normally contain both glandular and neuroendocrine cells [1, 5, 10, 14, 18, 19, 23]. These findings suggest that mixed tumors occur as a consequence of multidirectional differentiation of glandular or neuroendocrine stem cells derived from endoderm [10]. However, it remains unclear whether the glandular and neuroendocrine components expand from two distinct, intimately located precursors or whether they arise from a single progenitor cell. Satellite adenocarcinomas adjacent to the predominant neuroendocrine carcinomas were considered to result from the paracrine effect of growth factors produced by neuroendocrine tumors [3, 20, 21]. In contrast,

histopathologic studies on composite carcinomas using glandular and neuroendocrine markers demonstrated that these two components coexist as an intricate admixture with a transition zone, which is suggestive of dual differentiation of a single ancestor cell [10].

A loss of genetic material detected as an allelic loss or a loss of heterozygosity (LOH) is frequently associated with the initiation and the progression of most solid tumors [13, 32]. Potential causative chromosomal losses that target the tumor suppressor regions and provide a selective growth advantage are observed in the cancer genome in a nonrandom and organ-specific manner. In previous studies, nonrandom tumor-specific losses have been observed on chromosomes 3p, 4q, 5q, 10q, 13q, and 17p in small cell lung cancers, i.e., a pulmonary type of neuroendocrine carcinoma [24], and on 5q, 9p, 13q, 17p, and 18q in gastric adenocarcinomas [4]. In addition, individual cancer genomes frequently harbor varying mixtures of nonrandom and random LOHs, giving rise to highly diverse allelotypes. Therefore, diverse allelotypes separately obtained from glandular and neuroendocrine components are expected to be useful for describing the genetic events or clonality associated with the dual differentiation of a mixed gastric tumor.

In the present study, gastric tumors containing both glandular and neuroendocrine cells in varying proportions were identified according to the well-known microscopic features as putative mixed tumors and then confirmed by immunohistochemistry. The DNAs from the two distinct lesions of the mixed tumors were examined for the genome-wide LOH profiles, microsatellite instability (MSI), and point mutation of the *p53* tumor suppressor gene.

Materials and methods

Pathologic analysis of tissues

The files in the Department of Pathology were reviewed for gastric neuroendocrine tumors with an adenocarcinoma component, and eight cases were selected for the analysis of mixed glandular–neuroendocrine carcinomas. All were surgical cases that allowed extensive sampling of both mixed components and surrounding non-tumor mucosa. The tumors were staged according to the TNM (tumor–node–metastasis) classification [8] and were graded according to the World Health Organization classification [31]. Neuroendocrine differentiation was classified and graded into three types according to the previous criteria proposed by Matsui et al. [17] and Rindi et al. [25], carcinoid (grade 1), atypical carcinoid (grade 2), and poorly differentiated (small cell and large cell) neuroendocrine carcinomas (grade 3).

The formalin-fixed, paraffin-embedded tissue sections stained with hematoxylin and eosin were examined with particular attention to the well-known neuroendocrine tumor microscopic features, such as organoid, trabecular, or rosette-like growth patterns of the undifferentiated small cells (Fig. 1a–d). Large, diffuse sheets of ovoid cells with occasional acini were considered as the dominant histological features of atypical carcinoid and neuroendocrine tumors (Fig. 1e). Serial sections were then stained with periodic acid–Schiff base and Alcian blue for gastric mucin, and the Churukian–Schenk method was employed for argentaffin and argyrophil detection. Immunohistochemistry was carried out using the primary antibodies against a range of glandular (carcinoembryonic antigen, polyclonal, 1:100, Dako, Japan) and neuroendocrine (neuron-specific enolase, polyclonal, 1:50, BioGenex, San Roman, Calif.; chromogranin A, polyclonal, 1:100, Dako; synaptophysin, polyclonal, 1:20, Becton Dickinson, San Jose, Calif.; serotonin, 1:50, Sera-Lab, Crawley-Down, England) markers. The avidin–biotin–peroxidase technique was used with a LSAB 2 kit (Dako) according to the manufacturer's instructions. 3-Amino-9-ethylcarbazole (AEC) was used as substrate for the horseradish peroxidase, and the sections were counterstained with Mayer's hematoxylin. In all immunohistochemical stains, non-tumoral gastric mucosa or colonic carcinoid was used as an internal or external positive control.

Genetic analysis

Homogeneous portions of glandular and neuroendocrine components were selected from the formalin-fixed, paraffin-embedded tissue sections of each mixed gastric carcinoma to obtain a greater than 90% purity in each cell population. Using 20-guage needles under microscopic guidance, the foci with the pure cell contents were manually microdissected from serial 5-µm-thick sections that were stained with hematoxylin and eosin. To extract the genomic DNA, the procured cells were incubated overnight at 37°C in proteinase K-containing tissue-lysis buffer (50 mM Tris HCl, pH 8.5, 0.5% Tween 20, and 0.2 mg/ml proteinase K). Because the digested tissue admixture contained different amounts of DNA with varying qualities, the appropriate volume for the polymerase chain reaction (PCR) was determined based on the resultant band intensities of repeated PCR.

Both highly polymorphic di- or tetranucleotide, and nonpolymorphic mononucleotide markers (Research Genetics, Huntsville, Ala.) that map the entire autosomal arms were used for PCR amplification-based microsatellite analysis. The allelic gain resulting from duplication or amplification of a copy can be confused with an allelic imbalance that is indicative of the loss of a copy. Chromosomes 8q, 13q, 20, 21, and X have shown frequent allelic gain or infrequent allelic loss in previous comparative genomic hybridization studies of lung and stomach cancers [11, 26, 34]. As a result, they were excluded from this LOH study. A total of 44 microsatellite markers, with one or two markers per chromosomal arm, were used for the genome-wide LOH analysis. Four microsatellite markers were examined for chromosome 8p due to infrequent informativeness. The primer pairs for the cancer-related genes were designed to amplify the $(AGC)_{13}$ tract of *E2F-4*, the $(A)_{10}$ tract of *TGF-β RII*, the $(G)_8$ tract of *IGFIIR*, the $(G)_8$ tract of *BAX*, the $(A)_8$ tract of *hMSH3* and the $(C)_8$ tract of *hMSH6*. Template DNA was amplified through 32 PCR cycles with a denaturation step of 94°C for 50 s, an annealing step of 55–60°C for 1 min, and an elongation step of 72°C for 1 min in a total of 10 µl reaction mixture [0.5 µM of each primer, 1.5 mM $MgCl_2$, 0.2 mM of each deoxynucleotide triphosphate, 0.5 U *Taq* DNA polymerase, and 0.5 µl [α-^{32}P]dCTP (3000 Ci/mmol)]. Of the PCR products, 2 µl was diluted with 5 µl of a formamide-dye loading buffer, heated at 80°C for 3 min, and electrophoresed on a 6% polyacrylamide gel containing 7 M urea. After electrophoresis, the gel was dried on filter paper and visualized by means of autoradiography. In order to obtain band intensities close to an optimal range showing a linear correlation between the allelic loss and signal reduction, both the electrophoresis and autoradiography were repeated with different amounts of the matched normal and tumor PCR products.

There appear to be controversial annotations concerning the heterozygosity of amplified microsatellite sequences that commonly produce multiple shadow bands in addition to the main allelic bands. Such equivocal results on the heterozygosity of a microsatellite marker are likely to have been the major source of the inconsistent reports on the LOH status of the cancer genome. In order to clarify the presence of two visible alleles, only the difference between two or more repeats (≤4 bp in dinucleotide microsatellite markers) in the length between the two main allelic bands was considered. The intensity ratio of the two alleles was assessed using both visual and densitometric analyses. Although pure tumor cell contents were used in this analysis, microsatellite markers demonstrated various levels of allelic imbalance in the tumor

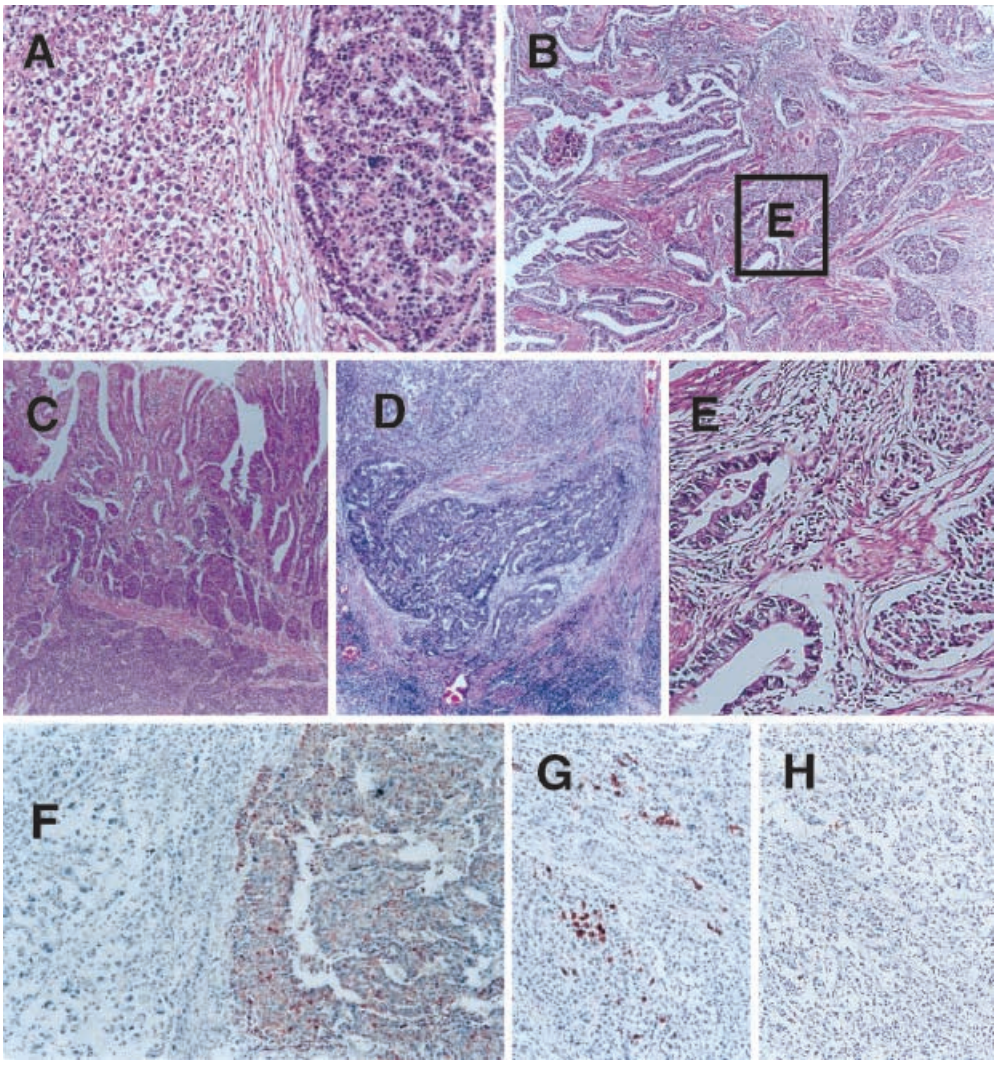

Fig. 1 Representative photomicrographs of glandular-neuroendocrine gastric carcinoma. **a** A true composite tumor showing distinct lesions of poorly differentiated adenocarcinoma with intracytoplasmic mucin droplets and large cell type neuroendocrine carcinoma in close vicinity as observed in a collision-type tumor (case 1). **b** A typical true composite tumor showing an intermingled admixture with a transitional zone of glandular and neuroendocrine components (case 8). **c** Neuroendocrine-dominant form of a mixed tumor with one-upon-another pattern. Each glandular and neuroendocrine component was located in the superficial and deep regions with a transitional zone (case 2). **d** A neuroendocrine-dominant form of a mixed tumor encompasses nests of adenocarcinoma (case 4). Hematoxylin and eosin; magnification ×100. **e** Histologic and cytologic features of dual differentiation existing in an intermingling transitional area between the glandular and neuroendocrine components in **b** is shown at higher magnification, ×400. **f** Synaptophysin immunoreactivity is intense within the neuroendocrine component but absent in the glandular component (case 1). The glandular component consisting of two distinct portions; in one site, chromogranin A-positive cells were interspersed (**g**), but not in the other area (**h**). Magnification ×100

components. The levels of allelic imbalance were calculated by dividing the normal allelic intensity ratio by the tumor allelic intensity ratio. They were graded as a balanced heterozygosity or borderline imbalance when there was a less than 1.5-fold ratio, an incomplete imbalance when the ratio was between 1.5- and 3-fold, and a complete imbalance when it was greater than 3-fold. Representative examples of complete and incomplete LOHs are shown in Fig. 2.

MSI was defined as the presence of band shifts in the target tissue relative to that in the corresponding normal alleles. *p53* mutations were analyzed using direct PCR product sequencing. Exons 5–8 of the *p53* gene were amplified using a Human *p53* Exon 4–9 Amplifier (Clontech, Palo Alto, Calif.) according to the manufacturer's instructions, and sequencing was done using a Sequenase PCR product sequencing Kit (Amersham Pharmacia Biotech, Upsala, Sweden).

Results

A mixed gastric carcinoma with both glandular and neuroendocrine elements was selected by carefully observing serial tissue sections by light microscopy. Eight cases were histologically diagnosed as mixed tumors with definite areas of both glandular and neuroendocrine elements within a single mass. In accordance with the nomenclature and classification proposed by Lewin [15], the term "true composite" was restricted to those lesions in which neuroendocrine and glandular cells occupied more or less equal proportions of the tumor area, i.e., 30–50%. However, when a neuroendocrine carcinoma was observed in the main part and an adenocarcinoma was localized in a focal portion, it was referred to as a neuroendocrine-dominant form in a mixed carcinoma spectrum. Detailed clinicopathologic features of all mixed gastric carcinomas are outlined in Table 1.

Pathologic findings

Two cases contained two distinct cellular components in equal proportions with a side-by-side pattern [5, 35] and were therefore diagnosed as true composite carcinomas (Fig. 1a, b and Table 1). In the remaining six tumors, the neuroendocrine cells were the major component, whereas adenocarcinomas were focally restricted to the superficial region, showing a one-upon-another pattern

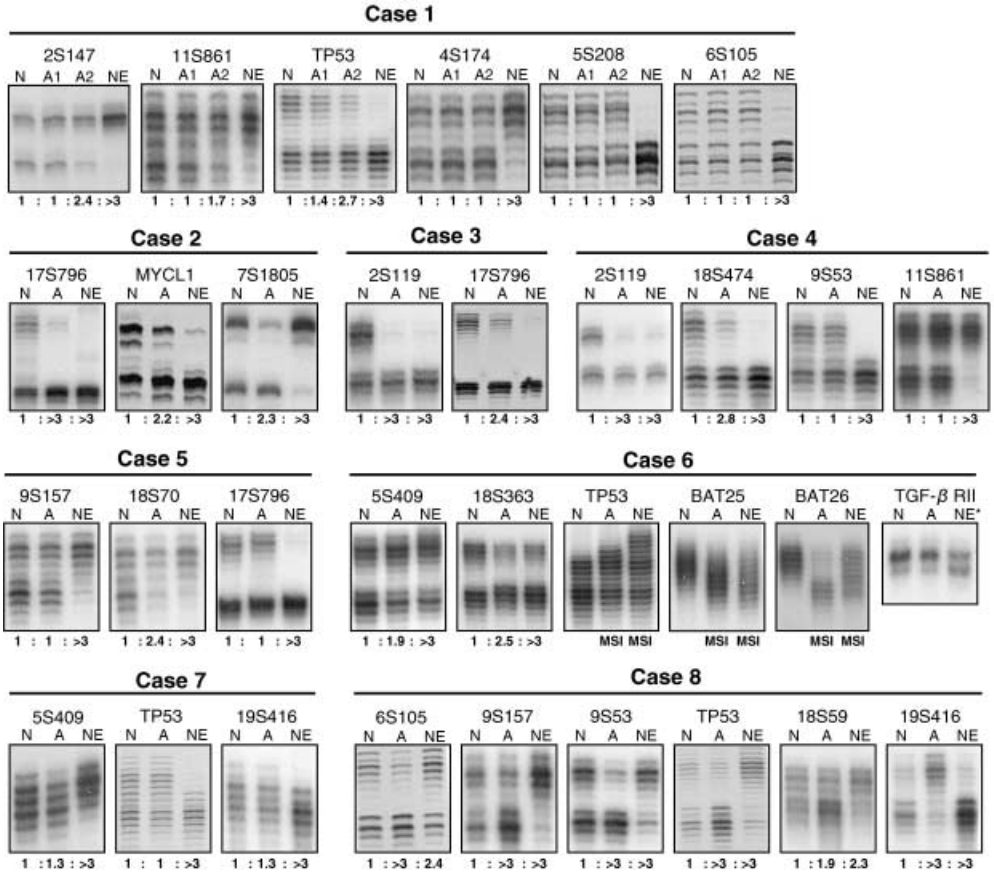

Fig. 2 Representative examples of complete (>3-fold) and incomplete (between 1.5- and 3-fold) allelic imbalances observed in eight cases of mixed glandular–neuroendocrine gastric carcinomas. The value corresponding to the intensity ratio of the two alleles is shown below each lane. The criteria for the complete and incomplete allelic imbalances are described in Materials and methods. *N* normal, *A* adenocarcinoma, *NE* neuroendocrine carcinoma. According to the absence (*A1*) and the presence (*A2*) of scattered chromogranin A reactivity in case 1, two adenocarcinoma sites were microdissected for loss of heterozygosity (LOH) analysis. The A1 site which is non-immunoreactive to chromogranin A (Fig. 1H) contains no LOHs, whereas the chromogranin A-reactive A2 site shows incomplete LOHs on multiple chromosomes. Case 6 shows a microsatellite instability (MSI) and a frameshift mutation in the $(A)_{10}$ tract of the *TGF-β RII* gene restricted to the neuroendocrine component (*asterisk*)

Table 1 Clinicopathologic characteristics of mixed glandular–neuroendocrine gastric carcinomas. *A* antrum, *B* body of the stomach, *NE* neuroendocrine, *WD* well differentiated, *MD* moderately differentiated, *PD* poorly differentiated

Case	Age	Sex	Site	Size (cm)	Stage	Histology		Glandular-NE arrangement	Glandular-NE proportion
						Adenocarcinoma	NE carcinoma		
1	61	Female	A	6	IV	Tubular, MD & PD	Large cell NE	Side by side	Balanced
2	74	Male	A	1.6	I	Tubular, WD & PD	Atypical carcinoid	One upon another	NE dominant
3	81	Male	AB	10.2	IIIa	Tubular, MD	Large cell NE	One upon another	NE dominant
4	77	Male	A	9.5	IIIa	Tubular, MD	Large cell NE	One upon another	NE dominant
5	54	Female	B	1.5	II	Tubular, WD	Carcinoid	One upon another	NE dominant
6	75	Male	A	6.2	IIIa	Papillotubular, MD	Large cell NE	One upon another	NE dominant
7	61	Male	A	2.5	IIIb	Papillotubular, MD	Large cell NE	One upon another	NE dominant
8	67	Male	A	7.5	IIIa	Tubular & mucinous	Large cell NE	Side by side	Balanced

(Fig. 1c, d and Table 1) [5, 9, 17]. One true composite tumor (case 1) demonstrated glandular and neuroendocrine portions that were demarcated by a sharp border in addition to some transition borders and could be designated as collision-like type tumors (Fig. 1a). The other true composite tumor (case 8) and four neuroendocrine-dominant forms (cases 2, 3, 4, and 5) accompanied the adenocarcinomas showing direct continuity from and a transition to typical neuroendocrine carcinomas (Fig. 1b–d). The two remaining cases (cases 6 and 7) of neuroendocrine-dominant carcinoma contained papillotubular adenocarcinomatous foci limited to the surface, which occupied areas that were too small to determine the transitional zone. There were no true collision-type carcinomas found in this study.

Immunohistochemical and special staining demonstrated the dual differentiation characteristics similar to the features of hematoxylin and eosin staining (Fig. 1f–h). The glandular and neuroendocrine components were consistently positive for staining with glandular (periodic acid–Schiff base, Alcian blue, and carcinoembryonic antigen) and with neuroendocrine (Churukian-Schenk, neuron-specific enolase, chromogranin A, and synaptophysin) markers, respectively (Table 2). In some cases, neuroendocrine cells were scattered in the glandular component, and glandular cells were scattered in the

Table 2 Comparison of special stain and immunohistochemistry results between glandular and neuroendocrine carcinoma components. *A* adenocarcinoma portion, *NE* neuroendocrine carcinoma portion, *PAS* periodic acid–Schiff base, *NSE* neuron-specific enolase, *CEA* carcinoembryonic antigen, + positive for immunoreactivity, – negative for immunoreactivity, ± scattered immunoreactive cells, *ND* not determined

Case	1			2		3		4		5		6		7		8	
Components	A1	A2	NE	A	NE	A	NE	A	NE	A	NE	A	NE	A	NE	A	NE
PAS stain	+	+	–	+	–	+	±	+	–	+	–	+	–	+	–	+	–
Alcian blue stain	+	+	–	+	–	+	±	+	–	+	–	–	–	+	–	+	–
Churukian-Schenk	–	–	+	–	–	ND	ND	ND	ND	–	+	–	+	–	–	–	+
NSE	–	–	+	±	+	ND	ND	ND	ND	–	+	–	+	–	+	–	+
Chromogranin A	–	±	+	±	+	–	±	–	+	–	+	–	+	–	+	–	+
Synaptophysin	–	–	+	±	+	–	+	–	+	–	+	–	+	–	+	–	+
CEA	+	+	–	+	–	+	±	+	+	+	+	+	+	+	±	+	–
Serotonin	–	–	–	–	–	ND	ND	ND	ND	–	–	–	–	–	–	–	–

neuroendocrine component. In mixed tumor case 1, the glandular component comprised two distinct sites with respect to chromogranin A special stain; the chromogranin A-positive cells were interspersed throughout one area (Fig. 1g), while no chromogranin A-positive cells were observed in the other (Fig. 1h). Case 3 with immunoreactivity scattered in both the glandular and neuroendocrine markers was diagnosed according to the microscopic features of the undifferentiated small cells, such as large, diffuse sheets of ovoid cells with occasional acini. Among the neuroendocrine markers, chromogranin A (8 of 8), synaptophysin (8 of 8), neuron-specific enolase (6 of 6), and argyrophil (4 of 6) were frequently expressed, whereas the general endocrine markers, the serotonin gastrointestinal hormone, showed poor reactivity in all neuroendocrine components. The analysis depended mainly on conventional histopathology because neuroendocrine carcinomas are characterized by the poor expression of the hormone markers of neuroendocrine differentiation [9, 28, 33]. When most tumor cells showed diffuse and intensive reactivity for general endocrine markers, such tumors were defined as neuroendocrine carcinomas despite the absence of specific hormone expression. Based on the histological patterns and immunoreactivity with the anti-endocrine markers, eight neuroendocrine carcinomas were graded as six large-cell types, one atypical carcinoid, and one carcinoid (Table 1).

Genetic findings

A pair of glandular and neuroendocrine components that were obtained from a given lesion were screened for LOH with a panel of 44 highly informative microsatellite markers covering 18 chromosomes. Because of the limited amount of available DNA, each sample was given a priority in microsatellite analysis at one or more loci per arm, which has been known to be frequently affected in gastric adenocarcinoma, small cell lung cancer, or both [4, 24]. The detailed results of PCR-based microsatellite analysis in the matched glandular and neuroendocrine components of each case are listed in Fig. 3. In five (cases 1–5) of the eight mixed tumors examined, the glandular components exhibited various degrees of complete and incomplete allelic imbalances, when compared with the neuroendocrine component, which invariably showed complete LOHs on the corresponding chromosomes (Fig. 2 and Fig. 3). The neuroendocrine components of the five cases contained complete LOHs on different chromosomes in addition to those on the same chromosomes as glandular components. Conversely, both components of mixed tumor case 6 demonstrated MSI in both the BAT25 and BAT26 markers (Fig. 2) and in 15.4% (glandular) and 19.2% (neuroendocrine) of the polymorphic markers tested, and incomplete LOHs on four chromosomes (Fig. 3). Of the six cancer-related genes including *TGF-β RII*, *IGFRII*, *E2F-4*, *hMSH3*, *hMSH6*, and *BAX*, only *TGF-β RII* showed a frameshift mutation that was restricted to the neuroendocrine component (Fig. 2). As shown in Fig. 3, the LOH profiles of these six mixed gastric carcinomas consisted of the primary LOHs shared by both components and the secondary LOHs (MSI-associated *TGF-β RII* mutation in case 6) localized in the neuroendocrine component.

In two mixed tumor cases, the glandular and neuroendocrine components demonstrated a reciprocal LOH, i.e., different alleles on the identical genetic locus were lost in two distinct components (the D7S1805 and PYGM markers were lost in case 2 and all the LOH-positive markers were lost in case 8, Fig. 3). The differences in the signals between normal DNA and tumor DNA were prominent in most markers. Therefore, the LOHs could be identified by visually inspecting the electrophoretic bands on the gels (Fig. 2). In particular, multiple reciprocal segregation of the alleles on 12 chromosomal arms in case 8 was unlikely to have resulted incidentally from independent events occurring in the two progenitor cells. The presence of multiple reciprocal LOHs strongly suggests that mixed tumor case 8 originated from a single stem cell due to nondisjunctional mitosis.

Mixed tumor case 7 demonstrated multiple complete LOHs on six chromosomal arms in the main neuroendocrine area but none in the focal minute non-neuroendocrine area (Fig. 2 and Fig. 3).

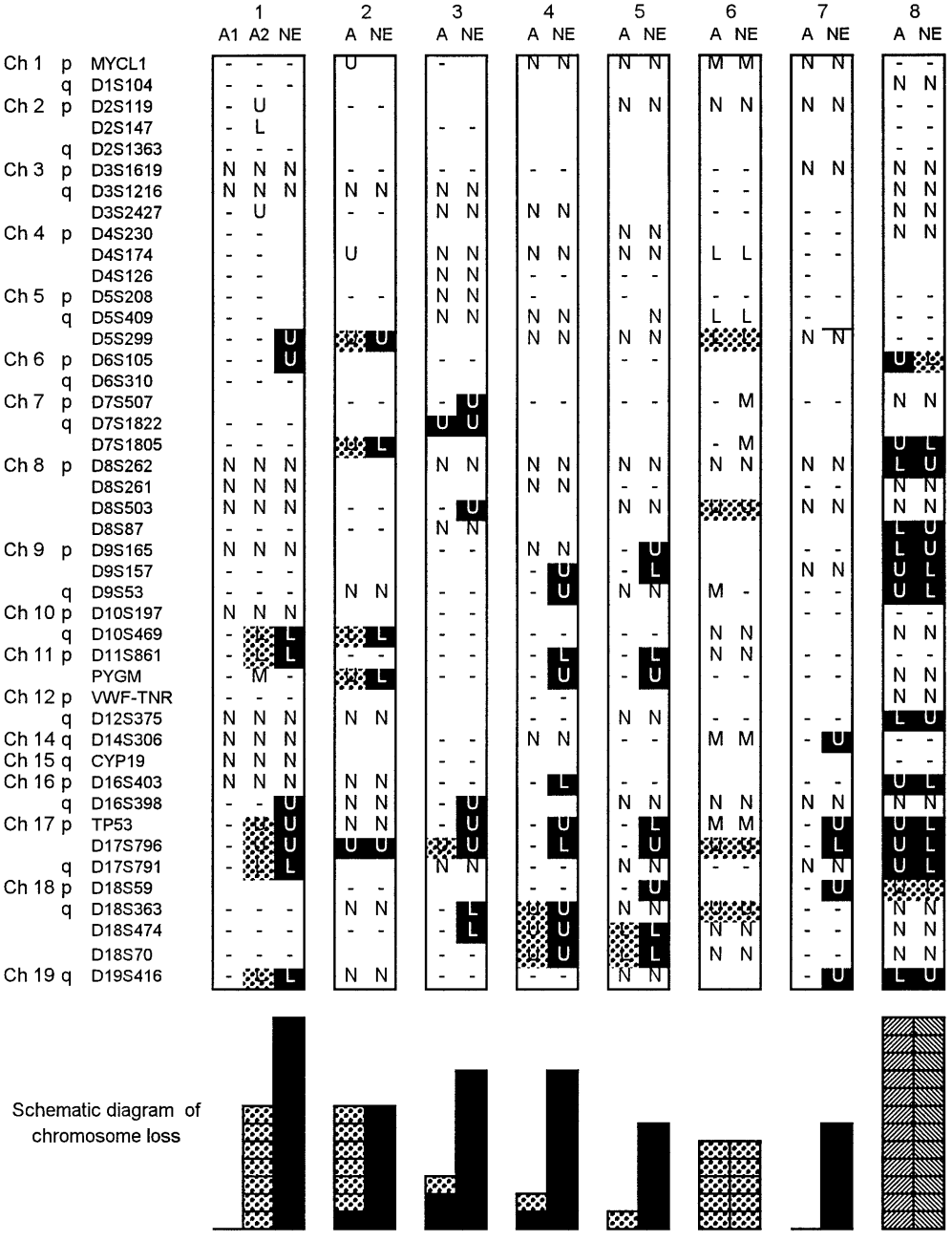

Fig. 3 Genome-wide loss of heterozygosity (LOH) and microsatellite instability (MSI) profiles of eight mixed glandular–neuroendocrine gastric carcinomas. Microsatellite markers are shown on the left. Adenocarcinoma (*A*) and neuroendocrine (*NE*) components of each case are indicated above the figure. Symbols for LOH and MSI data: *L* loss of lower allele, *U* loss of upper allele, *M* microsatellite instability, *N* non-informative, – negative for LOH, *No symbols* not determined. *Gray* and *black boxes* correspond to incomplete and complete LOHs, respectively. The *bottom bars* schematically illustrate the chromosome losses of the matched adenocarcinoma and neuroendocrine components. Each *bar* is constructed by symbols for LOH status of the corresponding chromosome in each component: *gray box* incomplete LOH, *black box* complete LOH, *hatched box in case 8* reciprocal LOH

The missense mutations of the *p53* gene were localized to the neuroendocrine component of two cases: case 1, CGC→CAC at codon 175 of exon 5; case 2, GTG→GGG at codon 173 of exon 5 (Fig. 4).

Discussion

In previous histopathologic analyses, a true composite carcinoma containing glandular and neuroendocrine components in approximately equal proportions was thought to be derived from a single precursor [10]. At the same time, neuroendocrine carcinomas with juxtaposed satellite adenocarcinomas were suggested to have paracrine effects on the surrounding glandular epithelial cells [23, 35]. Six of the eight mixed tumors examined in this investigation exhibited primary genetic alterations that were shared by both glandular and neuroendocrine components and secondary alterations restricted to the neuroendocrine components irrespective of their size. In addition, there was a case with reciprocal LOHs on 12 chromosomal arms in which both a growth advantage and dual differentiation were likely to have risen concurrently at the time of nondisjunctional mitosis of a single progenitor cell. The results in this study suggest that seven of the eight mixed tumors originated from a single precursor, most of which follow a glandular-to-neuroendocrine sequence and not vice versa. The remaining one

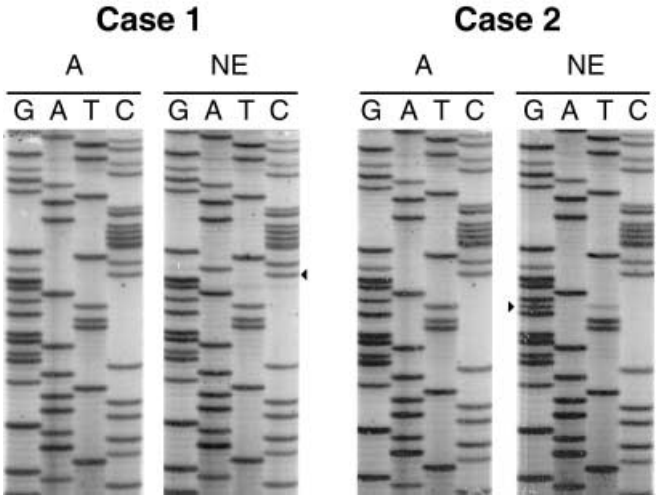

Fig. 4 Sequencing gel electrophoresis of the *p53* tumor suppressor gene. The *arrowheads* indicate bands of mutation sequence. *A* adenocarcinoma, *NE* neuroendocrine carcinoma

neuroendocrine-dominant case with multiple LOHs in the neuroendocrine component but none in the glandular component may also have originated from an adenocarcinoma without detectable genetic alterations. These results are consistent with a previous study on colorectal neuroendocrine carcinomas and associated adenocarcinomas, which demonstrated concordant LOHs on chromosomes 5q, 17p, and 18q in both components [29].

Interestingly, in this microsatellite analysis, the level of allelic imbalance varied in the glandular components when compared with those with complete LOHs in the neuroendocrine components. Although PCR-based microsatellite analysis is a useful tool for identifying an allelic imbalance occurring throughout the cancer genome, common artifacts have been known to result from variable cell contents. However, the glandular components examined in the present study were consistently found to have a pure tumor cell content with a minimal number of normal cells. The DNA extracted from the glandular component also exhibited complete LOHs indicative of high tumor cell purity in addition to incomplete LOHs. Thus, the possibility of contamination by normal cells, which may give rise to various levels of signals that can be misinterpreted as incomplete LOH, can be ruled out. Meanwhile, because the two components coexist as an intricate admixture with a transitional zone, the major neuroendocrine cells invading the non-neuroendocrine components may have an effect on the allelic imbalance of the glandular components. An entirely different LOH status between the glandular and neuroendocrine components was observed on the same chromosomes in all cases, thereby ruling out a likely admixture of two components. In this regard, incomplete allelic imbalances in the glandular components were interpreted as a LOH according to the rationale that adenocarcinomas contained mixed populations of cells with and without a LOH on a given chromosome. The neuroendocrine component of case 8 with multiple reciprocal LOHs also contained incomplete LOHs in two of the 16 LOH-positive markers (Fig. 3), which were thought to be additional alterations independent of the initial multiple LOHs.

In the immunohistochemical and argyrophil staining, although most of the neuroendocrine carcinomas were positive for representative neuroendocrine markers, including chromogranin A, synaptophysin, neuron-specific enolase, and argyrophil, all of them were negative for a specific hormonal substance such as serotonin. These results are compatible with the previous immunohistochemical findings on poorly differentiated neuroendocrine carcinomas of the extrapulmonary sites, such as stomach [9], intestines [33], and vagina [28]. Chromogranin A-positive cells (cases 1 and 2) and neuron-specific enolase- and synaptophysin-positive cells (case 1) were found in the glandular component of a mixed gastric tumor (Table 2), which is in agreement with previous reports [12, 22, 25, 27] showing that neuroendocrine differentiation is dispersed in an ordinary gastric carcinoma. In the true composite tumor case 1 containing a large glandular component, two adenocarcinoma sites that were microdissected according to the presence (Fig. 1g) or the absence (Fig. 1h) of chromogranin A reactivity showed incomplete LOHs and no LOHs, respectively (Fig. 3). This correlation between incomplete LOHs and scattered neuroendocrine differentiation suggests that neuroendocrine cells containing primary LOHs serve as precursors for neuroendocrine carcinomas. However, in previous studies, neuroendocrine cells dispersed throughout adenocarcinomas of the stomach were found to be quiescent with no mitosis [12, 22]. Such neuroendocrine cells were thought to be a fortuitous, non-proliferative outcome of multipotential, mitotic tumor cells. Thus, phenotypcially different cells are unlikely to expand and compose a mixed population. In contrast, when considering the genetic heterogeneity of the glandular components, the mixed populations indicate that genetically distinct and phenotypically similar adenocarcinomatous cells interact to simultaneously proliferate. If this were not the case, LOH-containing tumor cells having a selective growth advantage would comprise a homogeneous population. The clonal expansion of a glandular, but not neuroendocrine, phenotype with different genotypes is likely to result from the autocrine, oncogenic effect of LOH events on a population with the same phenotype (phenotype-dependent autocrine effect).

Alternatively, there appears to be no paracrine effect between glandular and neuroendocrine cells since histologically different cells actively grow in separate sites. It is noteworthy that genetic homogeneity was preferentially observed in neuroendocrine carcinomas. Neuroendocrine components harbor secondary alterations including LOHs, MSI, and *p53* mutations in addition to LOH events occurring in a heterogeneous adenocarcinoma. It is likely that additional alterations in cancer-related chromosomes or genes, particularly the increased LOH dose, haphazardly occur in one of the resting neuroendocrine cells dispersed in the glandular component. This subse-

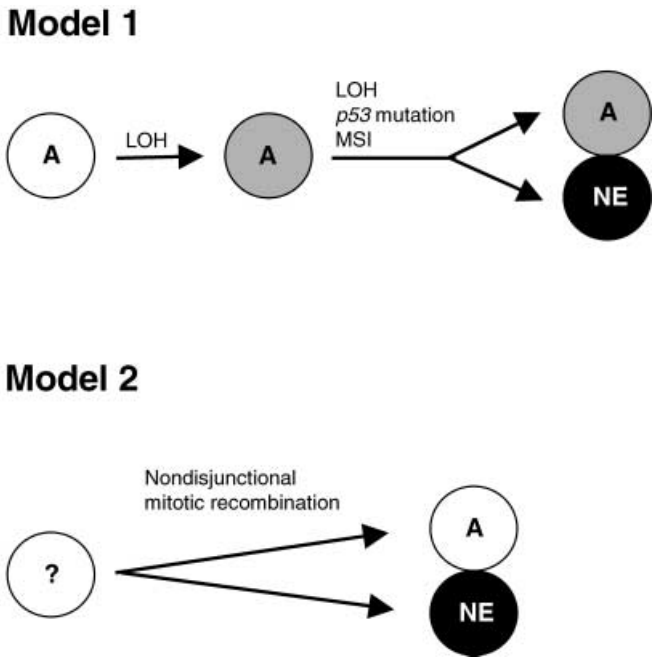

Fig. 5 Models of multi-step progression proposed for the mixed glandular–neuroendocrine gastric carcinoma. The *open* and *closed circles* correspond to the homogeneous clonal expansion of the adenocarcinoma (*A*) and neuroendocrine (*NE*) carcinoma population, respectively. The *gray circles* indicate genetically heterogeneous clonal expansion. *LOH* loss of heterozygosity, *MSI* microsatellite instability. Model 1 is a common genetic pathway through three sequential tumors: initial homogeneous adenocarcinoma, genetically heterogeneous adenocarcinoma, and neuroendocrine carcinoma. Model 2 is an uncommon genetic pathway resulting from a nondisjunctional mitosis in which dual differentiation initially and concurrently arises from a single precursor

quently acquires a selective growth advantage that gives rise to the clonal expansion of a neuroendocrine cell. Such a linear correlation between a heterogeneous adenocarcinoma and a homogeneous neuroendocrine component suggests that mixed tumors evolve through the sequential expansion of three genetic clones: initial homogeneous and secondary heterogeneous adenocarcinomas and neuroendocrine carcinoma (model 1 in Fig. 5).

Of the eight mixed tumors examined, two true composite types had the two components in a balanced proportion, showing a side-by-side pattern [5, 35]. With respect to the linear progression of mixed tumors, composite tumor case 1 is thought to represent a late-forming mixed tumor in which a neuroendocrine carcinoma develops after the formation of a large adenocarcinoma lesion. In contrast, another composite carcinoma (case 8) showing widespread reciprocal LOHs indicates that dual differentiation occurred in parallel after the initial mitosis of a precursor cell (model 2 in Fig. 5). The balanced potential for an outgrowth is likely to have been conferred by similar LOH doses in the two components. The remaining six cases with a neuroendocrine-dominant carcinoma in a one-upon-another pattern appear to reflect early-forming mixed tumors where all adenocarcinomatous components in the six cases were found in the luminal surface of gastric mucosa. The previous investigation of 21 mixed gastric tumors also reported that all cases were composed of adenocarcinomas covering the surface margin and neuroendocrine tumors invading the lymphatic and vascular lumen [17]. These findings suggest that a neuroendocrine carcinoma in a neuroendocrine-dominant carcinoma develops from an early-stage adenocarcinoma. Thus, the proportion and topography of the glandular and neuroendocrine components within a mixed tumor is likely to be influenced by both the temporal relationship and the growth potential of dual differentiation.

No neuroendocrine carcinoma-specific chromosome loss was identified when compared with an adenocarcinoma [6, 7]. This genome-wide LOH study provides evidence that most (six of eight cases) mixed glandular–neuroendocrine gastric carcinomas sequentially evolve from a glandular precursor to neuroendocrine differentiation and, occasionally (one of eight cases), dual differentiation concurrently arises from a single precursor. A relatively large proportion of neuroendocrine differentiation is likely to be associated with the predominant oncogenic potential, which is provided by the increased LOH dose, over the pre-existing adenocarcinoma.

Acknowledgements This study was supported by Ministry of Health and Welfare grant ‘HMP-99-M-03-0001’, Ministry of Education grant ‘1998-021-F00177 and 1998-001-F00031’, and Korea Science and Engineering Foundation (KOSEF) grant ‘971-0710-090-2’.

References

1. Brown NK, Smith MP (1973) Neoplastic diathesis of patients with carcinoid. Report of a case with four other neoplasms. Cancer 32:216–222
2. Caruso ML, Pilato FP, D’Adda T, Baggi MT, Fucci L, Valentini AM, Lacatena M, Bordi C (1989) Composite carcinoid-adenocarcinoma of the stomach associated with multiple gastric carcinoids and nonantral gastric atrophy. Cancer 64:1534–1539
3. Chejfec G, Gould VE (1977) Malignant gastric neuroendocrinomas. Ultrastructural and biochemical characterization of their secretory activity. Hum Pathol 8:433–440
4. Choi SW, Park SW, Lee KY, Kim KM, Chung YJ, Rhyu MG (1998) Fractional allelic loss in gastric carcinoma correlates with growth patterns. Oncogene 17:2655–2659
5. Corsi A, Bosman C (1995) Adenocarcinoma and atypical carcinoid: morphological study of a gastric collision-type tumour in the carcinoma-carcinoid spectrum. Ital J Gastroenterol 27:303-308
6. D’Adda T, Candidus S, Denk H, Bordi C, Höfler H (1999) Gastric neuroendocrine neoplasms: tumour clonality and malignancy-associated large X-chromosomal deletions. J Pathol 189:394–401
7. D’Adda T, Keller G, Bordi C, Höfler H (1999) Loss of heterozygosity in 11q13–14 regions in gastric neuroendocrine tumors not associated with multiple endocrine neoplasia type 1 syndrome. Lab Invest 79:671–677
8. Hermanek P, Altendorf-Hofmann A, Mansmann U, Dworak O, Wittekind C, Hohenberger W (1998) Improvements in staging of gastric carcinoma from using the new edition of TNM classification. Eur J Surg Oncol 24:536-541
9. Kaizaki Y, Fujii K, Kawai T, Saito K, Kurihara K, Fukayama M (1997) Gastric neuroendocrine carcinoma associated with chronic atrophic gastritis type A. J Gastrenterol 32:643–649

10. Klappenbach RS, Kurman RJ, Sinclair CF, James LP (1985) Composite carcinoma-carcinoid tumors of the gastrointestinal tract. A morphologic, histochemical, and immunocytochemical study. Am J Clin Pathol 84:137–143
11. Koo SH, Kwon KC, Shin SY, Jeon YM, Park JW, Kim SH, Noh SM (2000) Genetic alterations of gastric cancer: comparative genomic hybridization and fluorescence in situ hybridization studies. Cancer Genet Cytogenet 117:97–103
12. Kubo T, Watanabe H (1971) Neoplastic argentaffin cells in gastric and intestinal carcinomas. Cancer 27:447–454
13. Lasko D, Cavenee W, Nordenskjöld M (1991) Loss of constitutional heterozygosity in human cancer. Annu Rev Genet 25:281–314
14. Levendoglu H, Cox CA, Nadimpalli V (1990) Composite (adenocarcinoid) tumors of the gastrointestinal tract. Dig Dis Sci 35:519–525
15. Lewin K (1987) Carcinoid tumors and the mixed (composite) glandular-endocrine cell carcinomas. Am J Surg Pathol 11: 71–86
16. Lo Re G, Canzonieri V, Veronesi A, Dal Bo V, Barzan L, Zancanaro C, Trovò M (1994) Extrapulmonary small cell carcinoma: a single-institution experience and review of the literature. Ann Oncol 5:909–913
17. Matsui K, Jin XM, Kitagawa M, Miwa A (1998) Clinicopathologic features of neuroendocrine carcinomas of the stomach. Arch Pathol Lab Med 122:1010–1017
18. Morishita Y, Tanaka T, Kato K, Kawamori T, Amano K, Funato T, Tarao M, Mori H (1991) Gastric collision tumor (carcinoid and adenocarcinoma) with gastritis cystica profunda. Arch Pathol Lab Med 115:1006-1010
19. Moyana TN, Qizilbash AH, Murphy F (1988) Composite glandular-carcinoid tumors of the colon and rectum. Report of two cases. Am J Surg Pathol 12:607–611
20. Nilsson O, Wängberg B, McRae A, Dahlström A, Ahlman H (1993) Growth factors and carcinoid tumours. Acta Oncol 32:115–124
21. Nilsson O, Wängberg B, Kölby L, Schultz GS, Ahlman H (1995) Expression of transforming growth factor alpha and its receptor in human neuroendocrine tumours. Int J Cancer 60:645–651
22. Ooi A, Mai M, Ogino T, Ueda H, Kitamura T, Takahashi Y, Kawahara E, Nakanishi I (1988) Endocrine differentiation of gastric adenocarcinoma. The prevalence as evaluated by immunoreactive chromogranin A and its biologic significance. Cancer 62:1096–1104
23. Peison B, Benisch B (1983) Simultaneous occurrence of malignant carcinoid and adenocarcinoma of stomach. Arch Pathol Lab Med 107:99–100
24. Petersen I, Langreck H, Wolf G, Schwendel A, Psille R, Vogt P, Reichel MB, Ried T, Dietel M (1997) Small-cell lung cancer is characterized by a high incidence of deletions on chromosomes 3p, 4q, 5q, 10q, 13q and 17p. Br J Cancer 75:79–86
25. Rindi G, Azzoni C, Rosa SL, Klersy C, Paolotti D, Rappel S, Stolte M, Capella C, Bordi C, Solcia E (1999) ECL cell line tumor and poorly differentiated endocrine carcinoma of the stomach: prognostic evaluation by pathological analysis. Gastroenterology 116:532-542
26. Sakakura C, Mori T, Sakabe T, Ariyama Y, Shinomiya T, Date K, Hagiwara A, Yamaguchi T, Takahashi T, Nakamura Y, Abe T, Inazawa J (1999) Gains, losses, and amplifications of genomic materials in primary gastric cancers analyzed by comparative genomic hybridization. Genes Chromosomes Cancer 24:299–305
27. Tahara E, Ito H, Nakagami K, Shimamoto F, Yamamoto M, Sumii K (1982) Scirrhous argyrophil cell carcinoma of the stomach with multiple production of polypeptide hormones, amine, CEA, lysozyme, and HCG. Cancer 49:1904–1915
28. Ulich TR, Liao S, Layfield L, Romansky S, Cheng L, Lewin KJ (1986) Endocrine and tumor differentiation markers in poorly differentiated small cell carcinoid of the cervix and vagina. Arch Pathol Lab Med 110:1054–1056
29. Vortmeyer AO, Lubensky IA, Merino MJ, Wang CY, Pham T, Furth EE, Zhuang Z (1997) Concordance of genetic alterations in poorly differentiated colorectal neuroendocrine carcinomas and associated adenocarcinomas. J Natl Cancer Inst 89:1448–1453
30. Waldum HL, Aase S, Kvetnoi I, Brenna E, Sandvik AK, Syversen U, Johnsen G, Vatten L, Polak JM (1998) Neuroendocrine differentiation in human gastric carcinoma. Cancer 83:435–444
31. Watanabe H, Jass JR, Sabin LH (1989) Histological typing of eosophageal and gastric tumors. In: World Health Organization (ed) International histological classification of tumors. Springer, Berlin, pp 20–26
32. Weinberg RA (1991) Tumor suppressor genes. Science 254: 1138-1146
33. Wick MR, Weatherby RP, Weiland LH (1987) Small cell neuroendocrine carcinoma of the colon and rectum: clinical, histologic, and ultrastructural study and immunohistochemical comparison with cloacogenic carcinoma. Hum Pathol 18:9–21
34. Wu MS, Chang MC, Huang SP, Tseng CC, Sheu JC, Lin YW, Shun CT, Lin MT, Lin JT (2001) Correlation of histologic subtypes and replication error phenotype with comparative genomic hybridization in gastric cancer. Genes Chromosomes Cancer 30:80–86
35. Yamashina M, Flinner RA (1985) Concurrent occurrence of adenocarcinoma and carcinoid tumor in the stomach: a composite tumor or collision tumors? Am J Clin Pathol 83:233–236

Virchows Arch (2002) 440:94–101
DOI 10.1007/s004280100485

ORIGINAL ARTICLE

Ruth Østerby · Anders Hartmann
Jens R. Nyengaard · Hans-Jacob Bangstad

Development of renal structural lesions in type-1 diabetic patients with microalbuminuria

Observations by light microscopy in 8-year follow-up biopsies

Received: 7 May 2001 / Accepted: 7 May 2001 / Published online: 13 July 2001
© Springer-Verlag 2001

Abstract Kidney biopsies were obtained in 18 type-1 diabetic patients with microalbuminuria and again 8 years later. Over the first 30 months, a treatment protocol (conventional versus intensified treatment) was followed. The biopsies were embedded into plastic and sectioned serially. The volume of individual glomeruli and the vascular pole area was determined. The number of glomeruli showing capsular drops, fibrinoid lesions, adhesions, extra efferent arterioles and corpuscles totally occluded were counted and expressed as a percentage of the total number of corpuscles. Cortical interstitium and degenerated tubules were estimated by point counting. From baseline to the 8-year biopsy, the group of patients showed significant increase in interstitial volume fraction, mean glomerular volume and vascular pole area. The frequency of glomerular occlusion, fibrinoid lesions, adherences and extra efferent arterioles increased, whereas the frequency of capsular drops did not change, and degenerated tubular profiles showed a non-significant increase. No correlation was seen between these light microscopic observations and the concomitant development of diabetic glomerulopathy. Increase in albumin excretion rate was associated with increase in glomerular volume and vascular pole area. No correlation was seen with the glomerular filtration rate, blood pressure or metabolic control. The increase in structural parameters illustrates the slowly ongoing alteration of renal structures in type-1 diabetic patients with microalbuminuria.

Keywords Diabetic kidney · Glomerular occlusion · Glomerular volume · Microalbuminuria · Renal interstitium

R. Østerby (✉) · J.R. Nyengaard
Electron Microscopy Laboratory, Building 3,
Aarhus Kommunehospital, 8000 Aarhus C, Denmark
e-mail: ruth.osterby@dadlnet.dk
Tel.: +45-8622-0128, Fax: +45-8949-2150

A. Hartmann
Medical Department B, Rikshospitalet, Oslo, Norway

H.-J. Bangstad
Aker Diabetes Research Center, Oslo, Norway

Introduction

Only sparse information is available on the course of renal structural changes in incipient diabetic nephropathy. Thus, our knowledge of the mode of development of the diabetic renal lesions has been obtained from cross-sectional studies of patients in clinically defined stages, representing advancing stages [4, 9, 11].

From the cross-sectional studies, we know that all compartments in the kidney are affected in diabetes. The most characteristic lesions pertain to the glomeruli in terms of the diabetic glomerulopathy. The exact description of the glomerulopathy is based on quantitative electron microscopy. Accompanying the fundamental changes of glomerulopathy, i.e. increase in the extracellular material in the peripheral basement membrane and the mesangial regions, various other structural changes may be observed: the capsular drops, the fibrinoid lesions and adhesions of the tuft to Bowman's capsule [10, 18]. New vessel formation in terms of extra efferent arterioles at the vascular pole has previously been described in type-1 diabetic patients with elevated albumin excretion [15]. Furthermore, in the advanced stages, the total occlusion of some of the corpuscles is an important phenomenon.

Along with the development of glomerulopathy and its various companions [17], structural changes occur in extra-glomerular renal compartments in the arterioles [7, 13, 18] as well as the renal interstitium [1, 5, 8, 19].

In the present paper, we report observations noted primarily using light microscopy of a number of structural changes in baseline biopsies and those obtained 8 years later in type-1 diabetic patients who had microalbuminuria at the time of the baseline biopsy.

Materials and methods

The patients

All patients in the present series originally entered a clinical follow-up study focusing on the effect of intensive insulin treatment [2]. Two patients in the original cohort, which consisted of 20 pa-

Table 1 Clinical data in the series at entry into the study, at the time of the 8-year biopsies or during follow-up. Data are expressed as mean±SD; for albumin excretion rate (AER) the values are median (range)

	Baseline	Follow-up
Age	20±3.6	28.3±3.4
Duration of diabetes (years)	11±2.9	19.4±2.9
AER (µg/min)	32.5 (15–194)	17.5 (2–744)
Glomerular filtration rate (ml/min/1.73m^2)	140±27.2	125±20.3
Systolic blood pressure (mmHg)	128±11.5	[a]126±9.4
Diastolic blood pressure (mmHg)	80±8.5	[a]77.6±6.6
HbA_{1C}	10±1.4	[a]9.3±1.3

[a] Mean during 8-year follow-up

tients, are not included in the present results due to intervening pregnancies.

At entry, all patients had microalbuminuria defined as albumin excretion rate (AER) between 15 µg/min and 200 µg/min in at least two of three consecutive overnight urine samples. Clinical data for the patients at entry are shown in Table 1.

After the baseline biopsies had been taken, patients were allocated to one of two groups, conventional diabetes treatment (multiple insulin injections) or intensified treatment with insulin pumps for an average of 30 months (range 24–33 months). A second biopsy was then taken and the adherence to strict treatment groups was not preserved thereafter, but all patients were followed regularly with determination of blood pressure, AER and HbA_{1C} every fourth month, and glomerular filtration rate (GFR) three times in connection with the biopsies. A third biopsy was performed after a total of 99 months (84–104 months). Two patients did not follow the treatment protocol in the prospective study, but had biopsies taken at 30 months and 99 months and are thus included in the present study. Clinical data concerning the follow-up period are shown in Table 1.

Structural studies

The biopsy tissue was embedded into plastic blocks. For the baseline biopsies vestopal was used, whereas the 8-year biopsies were embedded into epon. Each block of tissue was serially sectioned at 1-µm thickness. The serial sections down through the blocks enabled us to obtain estimates of the following parameters in 17 baseline and all 18 follow-up biopsies.

Glomerular volume

Glomerular volume was estimated by applying Cavalieri's method [6].

Vascular pole area

The area of the glomerular surface where the arterioles enter and exit the glomerular tuft was measured as previously described [14]. The straight line connecting the two reflections of Bowman's capsule was measured in serial sections with 10-µm intervals. The sum of chords multiplied by the distance between levels provides the estimate of the vascular pole area.

Glomerular occlusion

An unbiased estimate of the fraction of glomeruli being totally occluded is obtainable from serial sections counting new appearing open and occluded glomeruli.

The total number of corpuscles counted per biopsy for this estimate as well as those described in the following was on average 37 (range 24–47) in baseline biopsies and 27 (range 15–45) in the follow-up biopsies. One baseline biopsy had to be excluded, since it contained only two glomeruli. All countings were done by one observer (RØ), and baseline and follow-up biopsies were done in parallel after the 8-year biopsies had been obtained.

Capsular drops

The capsular drop is rather specific for diabetes [18]. It is located in Bowman's capsule and protrudes towards the urinary space (Fig. 1). While some capsular drops are huge, others are so small that it necessitates counting in sections with 5-µm intervals.

Fibrinoid lesions

The classical fibrinoid lesions have been described as accompanying the more advanced stages of diabetic glomerulopathy. Typically, they are located in the periphery of the tuft. However, in this study of serial sections, it was noted that a lesion corresponding to the appearance of fibrinoid lesions was sometimes observed just inside the vascular pole (Fig. 2), sometimes in direct continuity with the hyalin in the afferent arteriole. When this structural change extended into the tuft itself, it was counted as a fibrinoid lesion.

Adhesions

The presence of adhesions between the glomerular tuft and Bowman's capsule distant from the vascular pole (Fig. 3) is also an abnormality associated with more advanced stages. The frequency of glomeruli demonstrating this abnormality was estimated from the serial sections, using sections with 5-µm intervals.

Extra efferent arterioles

At the vascular pole region, the occurrence of more than one efferent arteriole was noted and termed "extra efferent arterioles" (Fig. 4, Fig. 5, Fig. 6). The frequency of this phenomenon was expressed as a percentage of the total number of vascular pole regions cut exhaustively in each biopsy.

Interstitial volume fraction

The extent of interstitial tissue within the "tubular cortex" (total cortex minus glomeruli minus larger blood vessels) was estimated with point counting on the section 10 µm into the block from the baseline section [16]. An integral grid with nine fine points for hits on interstitium to each coarse point for hits on tubular cortex was used at a magnification of 727×. A total of eight different blocks were counted in each biopsy.

The composition of the interstitial space was further determined at low-magnification (5000×) electron microscopy in the 8-year biopsies. Visual fields were recorded from three different blocks of tissue in each biopsy using systematic, uniformly random sampling, covering ~85% of the area of the large thin sections. The total block phase was used for the thin section without further trimming. The size of these thin sections was approximately 1200×600 µm^2. The digitised images (SIS – Soft Imaging System, GmbH) were measured on the computer screen using a programme (Dimac, Digital Image Company, CHAMP) in which the appropriate grid could be made. A grid with several sets of points (1:2:6) was used, coarse points with distance of 15 µm for hits on total interstitium, half point distance for hits on capillaries and tubular basement membranes, and "finest" points (1:6) for hits on interstitial cells.

Marked tubular degeneration

Markedly degenerated tubular profiles with extremely thickened and layered basement membrane material (Fig. 7) were observed

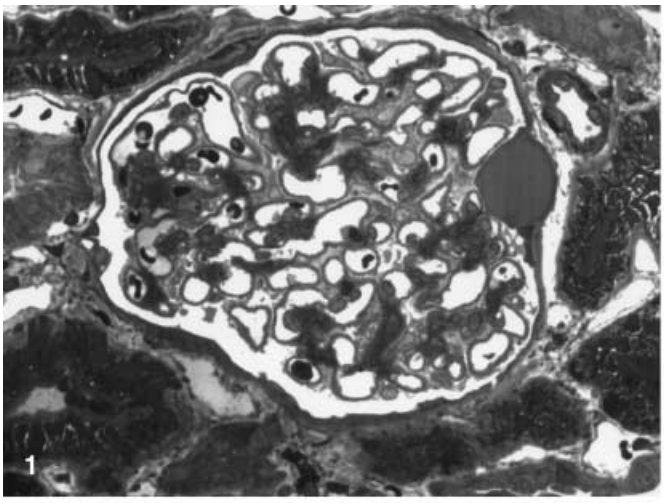

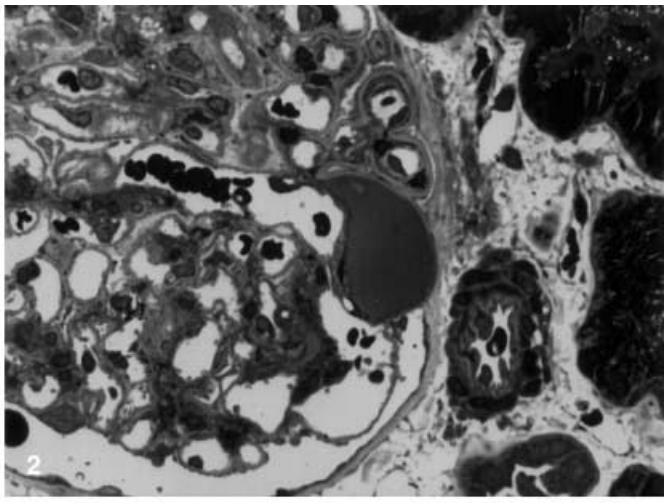

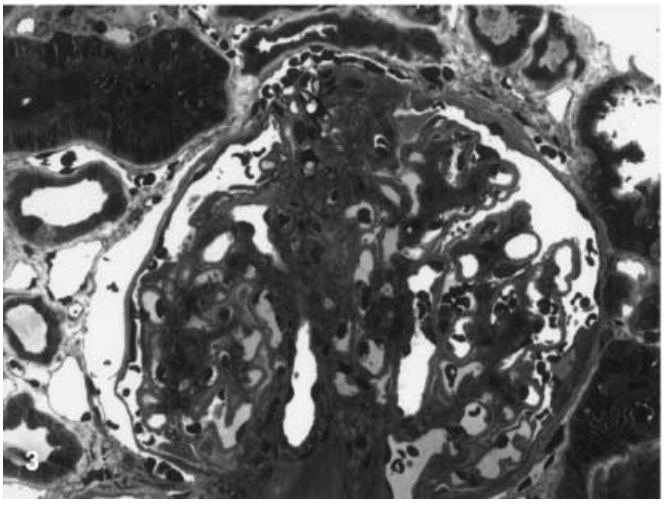

Fig. 1 Profile illustrating a capsular drop localised in the extracellular material of Bowman's capsule and protruding towards the urinary space. Magnification 340×; 1-µm-thick toluidine blue stained section

Fig. 2 An example of a fibrinoid lesion that is localised immediately inside the vascular pole area. It appears more intensively stained than the remainder of the extracellular material. Magnification 430×; 1-µm-thick toluidine blue stained section

Fig. 3 A glomerular profile with an adhesion between the tuft and Bowman's capsule, localised opposite the vascular pole. Magnification 270×; 1-µm-thick toluidine blue stained section

in some biopsies. It is presumed that their occurrence is an expression of a focal fibrosis rather than the diffuse fibrosis estimated with the point counting of the tubular interstitium. The extent of this abnormality was estimated with point counting: at low magnification (73×), the total area of tubular cortex in all of the blocks was estimated in sections 50-µm apart. The total cortical area measured was 18 mm^2 on average (range 4.6–45 mm^2). The area covered by markedly degenerated tubules was estimated by point counting at higher magnification (1140×), using points with a distance of 19 µm (when only a few were present) or 26 µm (in biopsies with more widespread degenerated tubules). Their volume fraction could then be estimated by the ratio of degenerated tubules area to total tubular cortex area.

Statistics

In comparisons between observations at baseline and at follow-up, a Students' paired, two-sided *t*-test was used. The proportional data, X, on extra efferent arterioles was transformed into a normal distribution before statistical testing by:

$$X\left[\frac{\left(\frac{1}{1281}\right)}{1-X\left(\frac{1}{1281}\right)}\right]$$

Correlations among different variables were estimated using the least-square methods.

Table 2 Mean glomerular volume, size of the vascular pole area (VPA) and VPA as a percentage of calculated glomerular surface. Means and CV% (=SD/mean %)

	Baseline biopsies	8-Year biopsies	Students' paired *t*-test
V(G) ($10^6 µm^3$)	2.67 (28)	3.35 (29)	0.0002
VPA ($µm^2$)	2721 (22)	3776 (35)	0.001
VPA/GS (%)	2.99 (10)	3.48 (25)	0.02

Results

Glomerular dimensions

Data on glomerular dimensions are presented in Table 2. Over the 8-year period, a significant increase in glomerular volume and the size of the vascular pole area was observed. Furthermore, vascular pole area increased more than expected from the increase in glomerular size, since its area relative to the calculated glomerular surface [14] was also significantly increased.

Glomerular occlusion

Figure 8 shows the frequency in baseline (mean 1.3%) and the follow-up biopsies (mean 3.8%). The difference between baseline and 8-year biopsy is significant ($2P$=0.03). In these microalbuminuric patients with rather mild structural changes, the frequency was low in all

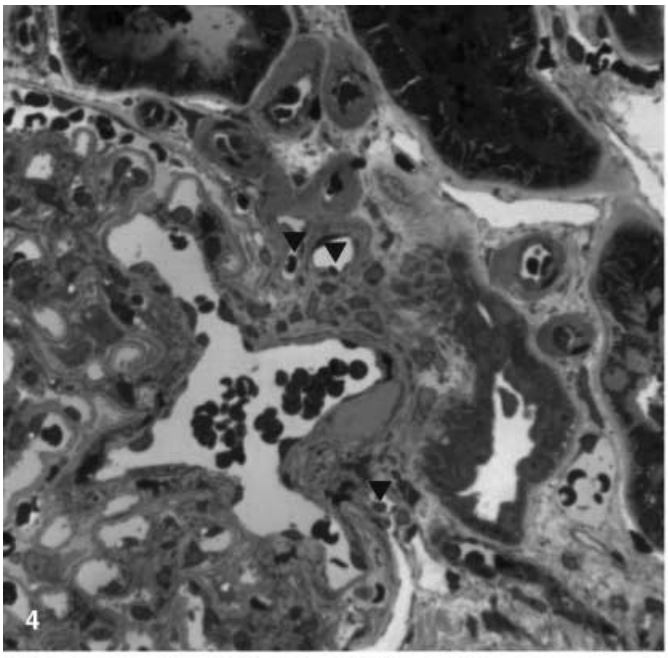

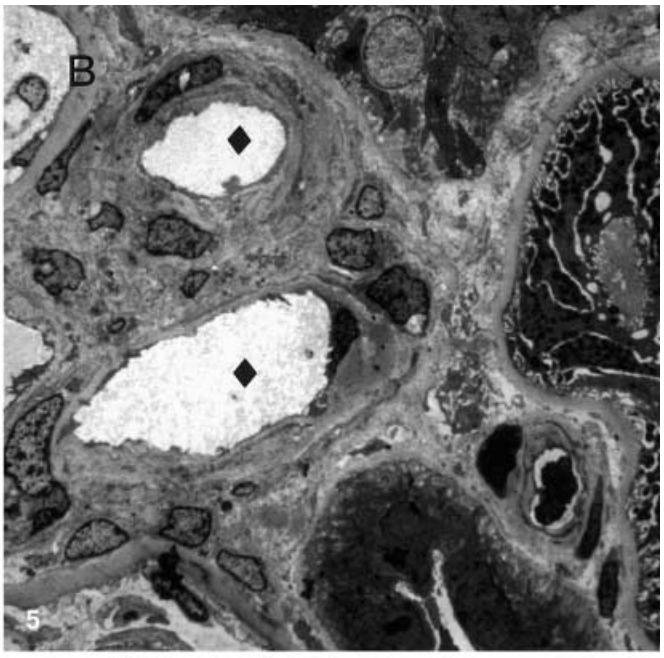

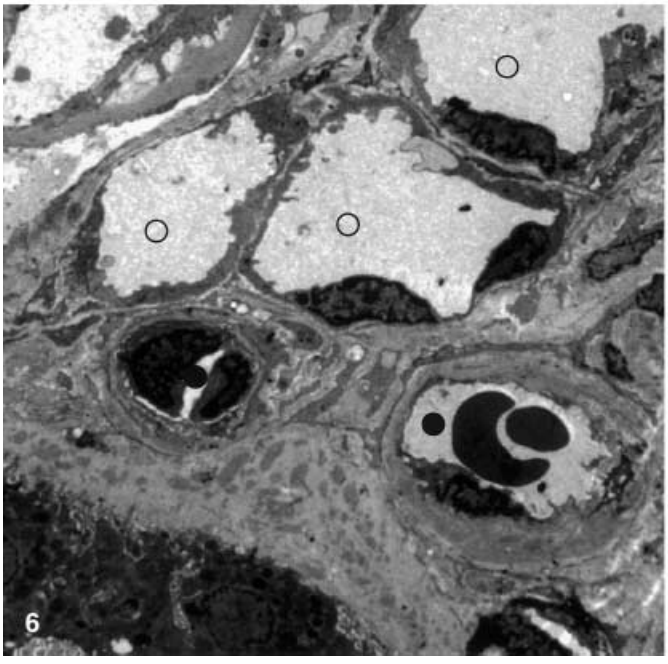

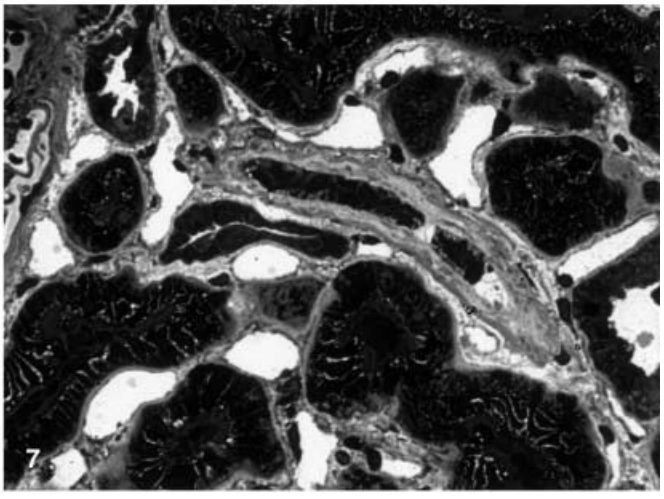

Fig. 4 The vascular pole region shows the profile of the afferent arteriole, with two small efferent arterioles on one side (▼) and another one to the other side (▼). Several profiles of efferent vessels demonstrating marked hyalinisation in the wall are present in the neighbourhood. Light microscopy of 1-µm-thick section. Magnification: 380×

Fig. 5 Electron micrograph showing the side-by-side exit of two efferent arterioles of about equal size (✦). *B* Bowmann's capsule. Magnification 1750×

Fig. 6 In the proximity of a vascular pole region, several vascular profiles are seen: two of them resembling ordinary efferent arterioles with pericytes in the wall (●); other profiles having very thin walls, corresponding to capillary structure (o). Magnification 2550×

Fig. 7 Markedly degenerated tubuli may appear as one single profile amidst tubular profiles of a more normal appearance. Magnification 340×

cases and a maximum of four occluded glomeruli was counted in one biopsy.

Capsular drops

Only one patient in this study did not present capsular drops in either baseline or follow-up biopsy. Thus, this abnormality was quite frequent and there was no significant increase in the frequency from baseline (mean 8.5%) to follow-up (mean 15.8) (2*P*=0.09).

Fibrinoid lesions

These lesions showed a significant increase from baseline to 8-year biopsies (2*P*=0.04). Altogether the frequency was low, being present in 2.4% of the glomeruli

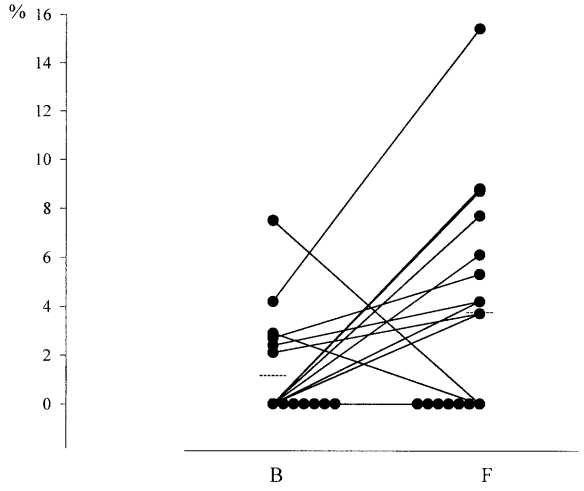

Fig. 8 The number of occluded glomeruli counted in the set of serial sections is expressed as a percentage of the total number of corpuscles. The increase from baseline to follow-up biopsy is statistically significant ($2P$=0.03)

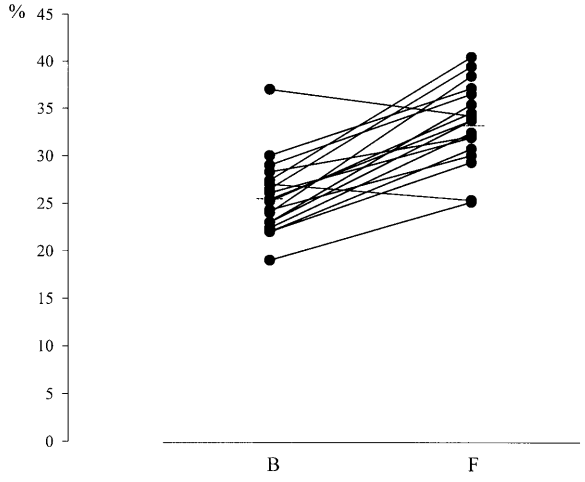

Fig. 10 The interstitial space includes tubular basement membranes, capillaries and any interstitial cells. It is expressed as a fraction of total cortex minus glomeruli minus large blood vessels ($2P<10^{-4}$)

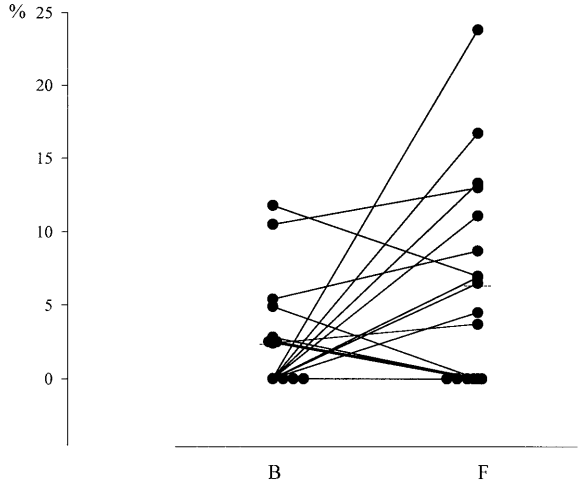

Fig. 9 The frequency of fibrinoid lesions is calculated for each biopsy in the baseline and the 8-year biopsy. Paired *t*-test $2P$=0.04

on average in baseline and in 6.8% in follow-up biopsies (Fig. 9). Included in these counts are localised accumulations of more intensively stained material located immediately inside the vascular pole (Fig. 2). This location was found in 13 of 15 glomeruli in baseline biopsies and in 11 of 31 glomeruli in follow-up biopsies.

Adhesions

Adhesions were extremely rare at baseline, being present in only one biopsy which showed this abnormality in 2 of 42 glomeruli. In the follow-up biopsies, seven patients demonstrated adhesions (group mean 5.2%), and the paired comparison between baseline and follow-up indicated a significant increase ($2P$=0.04). Adhesions were sometimes associated with fibrinoid lesions.

Extra efferent arterioles

Some of the extra blood vessels penetrating the vascular pole were quite thin-walled resembling capillary structure (Fig. 6), whereas others showed a wall composition similar to "normal" efferent arterioles (Fig. 5). In the baseline biopsies, 6 of the 17 cases did not present extra efferent arterioles in the serial sections. The median frequency in the group was 0.10 (range 0–0.30). In the last biopsy, only 3 of the 18 cases did not present extra efferent arterioles. The median value for the group was 0.20 (range 0–0.88). The difference between baseline and 8-year biopsies was statistically significant ($2P$=0.037).

Interstitium

Increase in interstitial volume expressed as fraction of the tubular cortex was very marked ($2P<10^{-4}$) and is illustrated in Fig. 10. Overall, the expansion of the interstitium appeared as a diffuse fibrosis with increased distance between the tubular structures. The compartment analysis performed at low-magnification electron microscopy showed that the total interstitium was composed of 61.2±3.9% (mean±SD) extracellular material, 17.8±2.7% capillary space, 16.4±2.7% tubular basement membrane, and 4.6±1.0% cells. Compared with data obtained in the same way in non-diabetic kidney donors, the inter-tubular capillaries occupied a larger fraction, and the extracellular material a smaller fraction of the total interstitium. Thus, the dominant part of the space is the extracellular material, and cellular accumulations are not a significant part of the picture. However, in a few cases, a more focal fibrosis was also seen. This phenomenon was estimated by quantifying the markedly degenerated tubules.

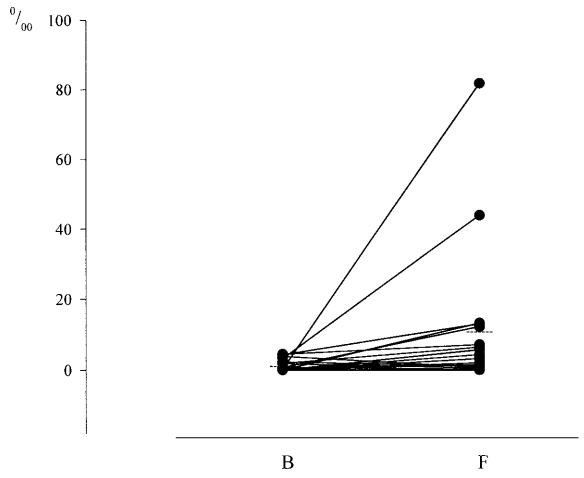

Fig. 11 Degenerated tubular profiles expressed as per thousand (‰) of the tubular cortex defined as explained in Fig. 8 (2*P*=0.06)

Tubular degeneration

Tubular degeneration most likely is a continuous process appearing in the (presumably) earliest phases as tubular segments with a markedly thickened basement membrane. It is obviously impossible to make a clear distinction between this stage and the overall diffuse increase in tubular basement membrane thickness [3]. However, in the (presumably) more advanced stages (Fig. 7), this structural lesion is remarkable and easily identifiable.

The area covered by these structures is estimated as per thousand (‰) of the tubular cortex. Thus, it appears that in the group as a whole, it is not a prominent feature. The increase from baseline (1.3‰) to the 8-year biopsies (10.99‰) falls short of statistical significance (2*P*=0.06). However, it is clear that some individual patients have developed this lesion to a significant degree over the 8-year period (Fig. 11).

Correlations among structural changes

The glomerular volume in the follow-up biopsies did not show any correlation with the expressions of diabetic glomerulopathy (unpublished observations, Bangstad et al.), neither was there any association between the change in glomerular volume and the change in diabetic glomerulopathy from baseline to 8-year biopsies. Among the various structural abnormalities counted, only the frequency of capsular drops correlated with expressions of glomerulopathy in the follow-up biopsies and fibrinoid lesions tended to do so (percentage glomeruli with capsular drop versus BMT, r=0.52, 2*P*=0.03, versus glomerulopathy index, r=0.47, 2*P*=0.05. Fibrinoid lesions versus BMT, r=0.43, 2*P*=0.07, versus mesangial volume fraction, r=0.43, 2*P*=0.07.)

The frequency of extra efferent arterioles tended to correlate with the expressions of glomerulopathy in the 8-year biopsies but did not reach statistical significance. However, a significant correlation was seen between frequency of extra efferent arterioles and glomerular volume (r=0.49, 2*P*=0.04) as well as the size of the vascular pole (r=0.56, 2*P*=0.01).

The frequency of occluded glomeruli did not correlate with glomerulopathy or interstitial volume fraction, but showed a positive correlation with the volume fraction of degenerated tubules (r=0.48, 2*P*=0.046).

Correlations with clinical data

In relationships among the structural variables and GFR, blood pressure and HbA_{1C}, no clear associations were observed. The percentage of occluded glomeruli showed an insignificant (2*P*=0.13) inverse correlation with glomerular filtration rate at the third biopsy. The change in AER from baseline to 8 years did not show any correlation with the various structural data at baseline, but showed a significant correlation with the estimate of mean glomerular volume (r=0.58, 2*P*=0.01), and the size of the vascular pole area (r=0.64, 2*P*=0.004) in the follow-up biopsy. There was no tendency to correlation with the estimate of interstitial volume fraction.

From baseline to last follow-up, four patients had reverted from micro- to normoalbuminuria, the other patients remained microalbuminuric or progressed to proteinuria (*n*=2). The frequency of extra efferent arterioles in the last biopsy was significantly lower in the normoalbuminuric cases than the remainder of the group (2*P*=0.02).

Comparisons between the two groups of patients who were initially allocated to either intensive treatment with insulin pumps or conventional treatment did not show any differences in the estimates described here in the 8-year biopsies, and neither with the changes from baseline to follow-up. The patient group initially intensively treated had an average HbA_{1C} of 8.7% over the 8 years, but this was not statistically significant from the mean value in the conventionally treated group of 9.7%.

Discussion

The serial sectioning of all of the blocks provided a unique possibility to obtain unbiased estimates of frequency within glomeruli of the various structural abnormalities described here. This estimated frequency, however, is not a very precise measure being based on a count of 20–50 glomeruli, and the exact figures should therefore be taken with some caution and may explain the seemingly decreasing frequency in some individual cases.

The capsular drop was described in the diabetic kidney a long time ago, and it may indeed be a very remarkable structure (Fig. 1). The notion in previous descriptive papers that it is seen in early stages of diabetic glomerulopathy are documented with the present countings, since this abnormality was almost as frequent in the baseline

biopsies representing very early stages of diabetic glomerulopathy as in the follow-up biopsies.

Also, the statement that the fibrinoid lesions and adhesions are associated with more advanced glomerulopathy conforms to our observations. Even in the 8-year biopsies, the glomerulopathy was rather modest.

Although the estimates of frequency of extra efferent arterioles are likewise hampered by the rather large imprecision, the present results indicate that this type of new-vessel formation takes place over the years in the stage of incipient nephropathy, and it parallels concomitant changes in glomerular ultrastructure and increasing AER. Furthermore, a significant correlation was found with the size of glomeruli and vascular pole area. It may be speculated that the developing glomerulopathy in concert with the occurrence of occluded glomeruli triggers a compensatory glomerular hypertrophy, and the new-vessel formation may be just one aspect in a complicated series of events. In a recent study of this phenomenon in type-2 diabetic patients with more advanced glomerulopathy (unpublished results), we found a very high frequency, which tended to correlate with the severity of retinopathy. In the type-2 diabetic patients, the associations were compatible with mechanisms as suggested here.

The total obsolescence of some glomeruli is of utmost importance in terms of renal function. Obviously, such glomeruli have completely ceased to function, and their frequency in the kidney is therefore a determinant factor for renal function [17]. In fact, the glomerular occlusion may be one of the most important aspects of renal structural lesions leading to the late decline in GFR in advanced diabetic glomerulopathy. However, our cases dealt with earlier stages and still we could see an increase in frequency over the 8-year period, indicating that the phenomenon starts to present itself at this early stage when the glomerulopathy is still of a quite moderate degree. The mechanisms leading to glomerular occlusion are far from totally clarified. It seems that, in these cases, definitely a very advanced glomerulopathy is not the change occluding the glomerular tuft. Therefore, it is assumed that extra-glomerular changes play a major role. The suspicion as to which changes may be involved focuses on the renal blood vessel system – either the larger blood vessels or the juxta-glomerular arterioles.

We have previously reported that, in the baseline biopsies, the volume fraction of interstitial tissue in the tubular cortex was increased compared with that in non-diabetic control cases [1]. This shows that the interstitial expansion is an early abnormality in the diabetic kidney, and it is not entirely dependent on glomerular occlusion or marked vascular insufficiency. Alternative mechanisms implied in the interstitial expansion have been discussed in a recent comprehensive review [5]. In the present series with a low occurrence of glomerular occlusion, there was no significant correlation between occlusion and the extent of interstitial space. Comparison between baseline and follow-up biopsies indicated that this process is continuing and progressing over the years of diabetes in these patients being identified by their elevated albumin excretion at the entry into the study. We suggest that the occurrence of the markedly degenerated tubular profiles is an expression of alternative interstitial lesions, i.e. the more focal fibrosis, this again being dependent on macroangiopathy or glomerular occlusion. A “focal fibrosis” cannot be identified unambiguously in sections, in particular the small plastic-embedded blocks of tissue are not well suited for this purpose. We suggest that the estimate of frequency of markedly degenerated tubules reflects the phenomenon of focal fibrosis.

Whether the change in AER might have anything to do with any of the structural abnormalities described in this paper is unknown. It could be speculated that the association between increase in albumin excretion versus increase in glomerular volume and, in particular, the vascular pole area is a reflection of one of the mechanisms underlying the increase in AER: with advancing abnormalities in the juxta-glomerular arterioles it seems likely that the glomerulus is not protected by the normal autoregulation, i.e. contraction of the afferent arteriole in response to increase in systemic blood pressure. Thus, any transitory or more permanent increases in systemic blood pressure might be projected into the glomerular tuft which might then contribute to increased albumin leakage over the glomerular filter.

Acknowledgements Expert technical assistance from Ms Birthe Iversen, Ms Lone Lysgaard and Ms Birtha Saugbjerg is gratefully acknowledged, as is the typing of the manuscript by Ms Karin Ø. Kristensen, M.A. This study was supported by grants from Aarhus University Foundation, the Danish Diabetes Association, The Danish Medical Research Council, The Juvenile Diabetes Foundation International no. 190592 and Novo Nordic Foundation, the Norwegian Diabetes Association.

References

1. Bangstad H-J, Østerby R, Dahl JK, Berg KJ, Hartmann A, Nyberg G, Frahm BS, Hanssen KF (1993) Early glomerulopathy is present in young, type 1 (insulin-dependent) diabetic patients with microalbuminuria. Diabetologia 36:523–529
2. Bangstad H-J, Østerby R, Dahl JK, Berg KJ, Hartmann A, Hanssen KF (1994) Improvement of blood glucose control in IDDM patients retards the progression of morphological changes in early diabetic nephropathy. Diabetologia 37:483–490
3. Brito PL, Fioretto P, Drummond K, Kim Y, Steffes MW, Basgen JM, Sisson RS, Mauer M (1998) Proximal tubular basement membrane width in insulin-dependent diabetes mellitus. Kidney Int 53:754–761
4. Fioretto P, Steffes MW, Mauer M (1994) Glomerular structure in nonproteinuric IDDM patients with various levels of albuminuria. Diabetes 43:1358–1364
5. Gilbert RE, Cooper ME (1999) The tubulointerstitium in progressive diabetic kidney disease: more than an aftermath of glomerular injury? Kidney Int 56:1627–1637
6. Gundersen HJ, Bendtsen TF, Korbo L, Marcussen N, Møller A, Nielsen K, Nyengaard JR, Pakkenberg B, Sørensen FB, Vesterby A et al (1988) Some new, simple and efficient stereological methods and their use in pathological research and diagnosis. APMIS 96:379–394
7. Harris RD, Steffes MW, Bilous RW, Sutherland DE, Mauer SM (1991) Global glomerular sclerosis and glomerular arteriolar hyalinosis in insulin dependent diabetes. Kidney Int 40: 107–114

8. Lane PH, Steffes MW, Fioretto P, Mauer SM (1993) Renal interstitial expansion in insulin-dependent diabetes mellitus. Kidney Int 43:661–667
9. Mauer SM, Steffes MW, Ellis EN, Sutherland DE, Brown DM, Goetz FC (1984) Structural-functional relationships in diabetic nephropathy. J Clin Invest 74:1143–1155
10. Olsen S (2000) Light microscopy of diabetic glomerulopathy: the classic lesions. In: Mogensen CE (ed) The kidney and hypertension in diabetes mellitus. Kluwer Academic Publishers, Boston, pp 201–210
11. Østerby R (1992) Glomerular structural changes in type 1 (insulin-dependent) diabetes mellitus: causes, consequences, and prevention. Diabetologia 35:803–812
12. Østerby R, Parving HH, Nyberg G, Hommel E, Jørgensen HE, Løkkegaard H, Svalander C (1988) A strong correlation between glomerular filtration rate and filtration surface in diabetic nephropathy. Diabetologia 31:265–270
13. Østerby R, Bangstad H-J, Nyberg G, Walker JD, Viberti G (1995) A quantitative ultrastructural study of juxtaglomerular arterioles in IDDM patients with micro- and normoalbuminuria. Diabetologia 38:1320–1327
14. Østerby R, Asplund J, Bangstad H-J, Nyberg G, Rudberg S, Viberti G, Walker JD (1997) Glomerular volume and the glomerular vascular pole area in patients with insulin-dependent diabetes mellitus. Virchows Arch 431:351–357
15. Østerby R, Asplund J, Bangstad H-J, Nyberg G, Rudberg S, Viberti GC, Walker JD (1999) Neovascularization at the vascular pole region in diabetic glomerulopathy. Nephrol Dial Transplant 14:348–352
16. Østerby R, Bangstad H-J, Rudberg S (2000) Follow-up study of glomerular dimensions and cortical interstitium in microalbuminuric type 1 diabetic patients with or without antihypertensive treatment. Nephrol Dial Transplant 15:1609–1616
17. Østerby R, Bangstad H-J, Nyberg G, Rudberg S (2001) On glomerular structural alterations in type 1 diabetes – companions of early diabetic glomerulopathy. Virchows Arch 438:129–135
18. Thomsen AC (1965) The kidney in diabetes mellitus. Munksgaard, Copenhagen
19. Ziyadeh FN (1996) Significance of tubulointerstitial changes in diabetic renal disease. Kidney Int Suppl 54:S10–S13

Virchows Arch (2002) 440:102–104
DOI 10.1007/s00428-001-0553-1

CASE REPORT

Magali Colombat · Liliane Boccon-Gibod
Sophie Carton

An unusual renal angiomyolipoma with morphological lymphangioleiomyomatosis features and coexpression of oestrogen and progesterone receptors

Received: 7 May 2001 / Accepted: 31 August 2001 / Published online: 7 November 2001
© Springer-Verlag 2001

Abstract Angiomyolipoma is the most common mesenchymal renal tumour, the clonal origin of which has recently been demonstrated. It is composed of varying amounts of blood vessels, smooth muscle and fat. In this report, we describe a renal angiomyolipoma, which is unusual owing to the presence of a lymphangioleiomyomatosis-like component, occurring in a 41-year-old woman suffering from sporadic lymphangioleiomyomatosis. The diagnosis was based on histopathological and immunohistochemical findings. The tumour consisted of an intimate admixture of two components: one was typical of a classical angiomyolipoma and the other was reminiscent of lymphangioleiomyomatosis. HMB45 positivity was found on 5% of the cells of the angiomyolipoma component. Ten percent of the nuclei of the lymphangioleiomyomatosis and angiomyolipoma components expressed oestrogen receptors and 5% progesterone receptors. This case illustrates a very unusual pattern of a renal angiomyolipoma containing a lymphangioleiomyomatosis-like component. The oestrogen and progesterone immunoreactivity suggests that angiomyolipoma could be hormonally dependent. Therefore, we have emphasised the morphological and immunohistochemical similarities between angiomyolipoma and lymphangioleiomyomatosis.

Keywords Kidney · Angiomyolipoma · Lymphangioleiomyomatosis

M. Colombat · S. Carton (✉)
Service d'anatomie pathologique, Centre Hospitalier Général,
1, Avenue Michel de l'Hospital, 02321 Saint-Quentin, France
e-mail: s.carton@ch-stquentin.fr
Tel.: +23-03-23067411

L. Boccon-Gibod
Service d'anatomie pathologique,
Hopital d'enfants Armand Trousseau, 29,
avenue du docteur Arnold Netter, 75571 Paris Cedex 12, France

Introduction

Angiomyolipoma (AML) is a mesenchymal renal tumour, the clonal origin of which has been reported recently [11]. AML is composed of blood vessels, smooth muscle and mature fat cells. We report a case of renal AML that is unusual in that the tumour, occurring in a 41-year-old woman suffering from sporadic lymphangioleiomyomatosis (LAM), contains a LAM-like component. In this report, we discuss the relationship between AML and LAM.

Case report

A 41-year-old woman was referred to hospital because of recent dyspnoea. She had no particular previous medical history. The chest radiograph showed a left pleural effusion and bilateral reticular opacities. The computed tomography (CT) scan of the thorax revealed multiple thin-walled cysts evenly distributed throughout the lung fields. At thoracocentesis the pleural fluid was chylous. The patient was treated by pleurectomy. The open-lung biopsy obtained at that time showed changes characterised by a haphazard proliferation of smooth muscle cells around bronchioles, in alveolar septa, around arteries, veins, lymphatic spaces and in the pleura. There was no interstitial fibrosis. The diagnosis of LAM was thereby confirmed. No anomaly was detected at the clinical cutaneous and neurological examination. A cerebral CT scan was normal. The abdominal CT scan detected a right renal tumour without fat density located on the posterior side of the kidney. The patient underwent a complete nephrectomy.

Materials and methods

The surgical specimen was fixed with 10% formaldehyde and embedded in paraffin. Sections (3-µm thick) were stained with haematoxylin and eosin. Immunohistochemical analysis was performed using an indirect immunoperoxidase technique with diaminobenzidine (DAB) revelation and the following primary antibodies: anti-smooth muscle actin (Dako, 1A4, 1/200), anti-desmin (Dako, D33, 1/100), anti-HMB 45 (Biogenex, HMB 45, 1/100), anti-oestrogen receptors (Tebu, CC4–5, 1/20) and anti-progesterone receptors (Tebu, 1A6, 1/20).

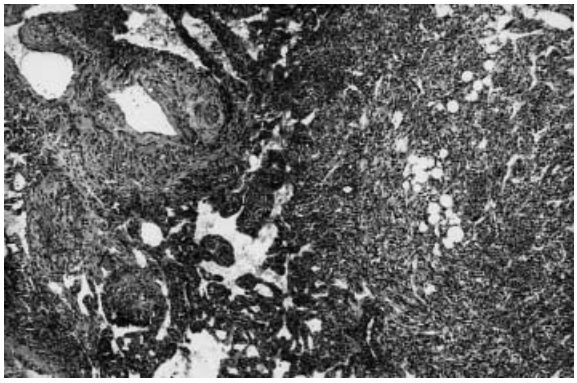

Fig. 1 The tumour is composed of smooth muscle cells, thick-walled blood vessels, areas indistinguishable from lymphangioleiomyomatosis and fat cells (haematoxylin and eosin, original magnification ×10)

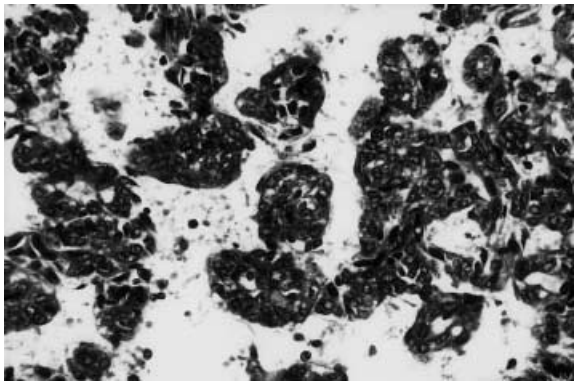

Fig. 2 Morphological pattern indistinguishable from lymphangioleiomyomatosis (haematoxylin and eosin, original magnification ×20)

Pathological findings

The tumour measured 3×2×2 cm. The sectioned surface was whitish with areas of haemorrhage. No lymph node was found. Microscopically, it was not sharply delimited, and it extended into the perirenal fat. It was composed of spindle and epithelioid smooth muscle cells arranged in interlacing bundles and sheets (Fig. 1). The tumour contained, in some areas (20% of the tumour), thin-walled branching vessels surrounded by a thick layer of smooth muscle that had an architecture similar to that of the pulmonary lesions (Fig. 1, Fig. 2). A few cells had enlarged irregular nuclei with prominent nucleoli. Numerous fibrous thick-walled vessels were present (Fig. 1). There were a few isolated mature fat cells (Fig. 1).

The immunohistochemical study indicated diffuse smooth-muscle actin and desmin positivity and smooth-muscle HMB45 positivity on 5% of the cells of the AML component (Fig. 3). Ten percent of the nuclei of the LAM and AML component expressed oestrogen receptors and 5% progesterone receptors.

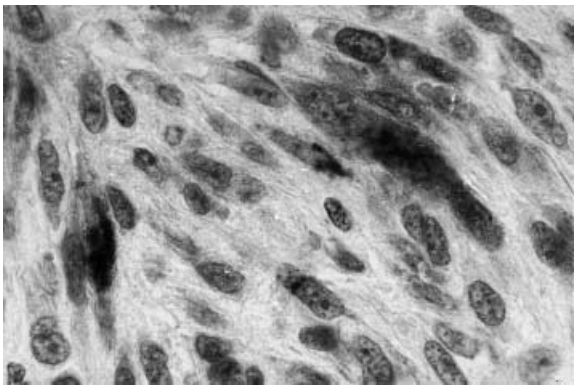

Fig. 3 Focal HMB 45 positivity on the smooth-muscle component (original magnification ×100)

Despite progesterone administration (as intramuscular depot of medroxyprogesterone 500 mg/month), the patient had been developing severe respiratory failure for 9 years. At present pulmonary transplantation is planned, and there has been no recurrence of the renal tumour.

Discussion

LAM is a rare pulmonary disease that affects primarily women. Microscopically, LAM is characterised by a proliferation of benign-appearing smooth muscle cells in the interstitium, around bronchioles, arteries, veins and lymphatic spaces, in alveolar septa and in the pleura. The clinical course is marked by progressive respiratory failure leading to death [7].

In about 50% of cases, LAM is associated with renal AML [2], which is primarily unilateral, small and asymptomatic [7, 11]. There do not appear to be any histological differences between AML that is or is not associated with LAM. The tumours are composed of varying amounts of abnormal thick-walled blood vessels, smooth muscle and mature adipose tissue [4]. A confident radiological diagnosis can be made in almost all cases on the detection of fat in the tumour [4]. Our case is unusual because of the LAM-like component and the low proportion of fat that did not allow its preoperative distinction from a renal cell carcinoma.

Cases in which renal tumours are morphologically indistinguishable from LAM are uncommon. We have found only three cases, which were differently named by the authors in the literature: a renal lymphangiomyoma replacing the kidney of a 79-year-old man (Jacobs et al.) [6], a LAM with pulmonary, retroperitoneal and left renal lesions in a 58-year-old woman (Saegusa et al.) [12] and a renal AML in a 45-year-old woman (L'Hostis et al.) [8]. It is difficult to establish whether these tumours are true lymphangiomyomas (localised lesion) or whether renal involvement occurs by LAM (extensive lesions) or simply AML, because clinical and radiologi-

cal information is generally incomplete. Furthermore, inadequate sampling of the tumour may cause the presence of adipose tissue being missed. Ansari et al. [1] described areas reminiscent of LAM in regional lymph nodes of a 46-year-old woman with renal AML extending into the lymph nodes, and McIntosh et al. [10] reported a case of multiple renal AML occurring with LAM of the regional lymph nodes in a 55-year-old woman. The presence of LAM-like foci in renal AML was also documented by Chan et al. [3].

In LAM and AML, the smooth muscle cells are smooth-muscle actin, desmin (less reliable) and, in variable proportions, HMB45 positive [3, 4, 7, 11]. The nuclei express oestrogen and progesterone receptors in about 50% of cases of LAM and apparently in more than 25% of cases of AML with coexpression in 10% of cases [8, 11]. Tawfik et al. [14] and Uzzo et al. [15] studied the hormonal receptors in two cases in which renal AML was associated with LAM: hormonal receptors were negative in the renal tumours. Recently Logginidou et al. [9] examined 12 specimens of AML from women with sporadic LAM; in 83% of the AML there was oestrogen receptor immunoreactivity with progesterone receptor immunoreactivity in 100%. LAM and AML are thought to be hormonally dependent because of their occurrence primarily in women during their reproductive years and the risk of deterioration during pregnancy [4, 7, 11]. The hypothesis that smooth muscle cells of LAM and AML are closely related is supported by all these data. In our case, the peculiar histological pattern with morphological features of both entities in the same tumour reinforces this concept.

AML and LAM occur in association with tuberous sclerosis complex (TSC) or sporadically [4, 7, 11]. TSC is an autosomal dominant disorder. The diagnosis is made using the criteria described by Gomez [5] and the National Tuberous Sclerosis Association. The diagnosis of TSC requires at least two "presumptive or secondary features among others" [14, 15]. Although AML and LAM are both presumptive criteria, it seems that the association of AML and LAM does not permit a diagnosis of TSC because none of the women with LAM (with or without renal AML) has borne a child with TSC [11]. Two genes are implicated in TSC: these are *TSC 1* on chromosome 9 and *TSC 2* on chromosome 16. A germline mutation of one of these two genes requires a second somatic mutation (loss of heterozygosity). Smoralek et al. [13] found loss of heterozygosity of the *TSC 2* gene in 54% of AML from patients with LAM and in lymph nodes from a woman with retroperitoneal LAM. Although loss of heterozygosity has been found in sporadic AML, the relatively high frequency of *TSC 2* abnormalities suggests that these findings are linked to LAM. Loss of heterozygosity of TSC genes in lung tissue has yet to be evaluated.

References

1. Ansari SJ, Stephenson RA, Mackay B (1991)Angiomyolipoma of the kidney with lymph node involvement. Ultrastruct Pathol 15:531–538
2. Bernstein SM, Newell JD, Adamczyk D (1995) How common are angiomyolipomas in patients with lymphangioleiomyomatosis? Am J Respir Crit Care Med 152:2138–2143
3. Chan JCK, Tsang WYW, Pan MY (1993) Lymphangioleiomyomatosis and angiomyolipoma: closely related entities characterized by hamartomatous proliferation of HMB 45-positive smooth muscle. Histopathology 22:445–455
4. Eble JN (1998) Angiomyolipoma of the kidney. Semin Diagn Pathol 15:21–40
5. Gomez MR (1991) Phenotypes of tuberous sclerosis complex with a revision of diagnostic criteria. Ann N Y Acad Sci 615:1–7
6. Jacobs JE, Sussman SK, Glickstein MF (1989) Renal lymphangiomyoma. A rare cause of a multiloculated renal mass. Am J Roentgenol AJR 152:307–308
7. Johnson S (1999) Lymphangioleiomyomatosis: clinical features, management and basic mechanisms. Thorax 54:254–264
8. L'Hostis H, Deminiere C, Ferriere JM (1999) Renal angiomyolipoma. A clinicopathologic, immunohistochemical, and follow-up study of 46 cases. Am J Surg Pathol 23:1011–1020
9. Logginidou H, Xiang A, Russo I (2000) Frequent estrogen and progesterone receptor immunoreactivity in renal angiomyolipomas from women with pulmonary lymphangioleiomyomatosis. Chest 117:25–30
10. McIntosh GS, Hamilton Dutoit S, Chronos NV (1989) Multiple unilateral angiomyolipomas with regional lymphangioleiomyomatosis. J Urol 142:1305–1307
11. Paradis V, Laurendea I, Viellefond A (1998) Clonal analysis of renal sporadic angiomyolipomas. Hum Pathol 29:1063–1067
12. Saegusa M, Sakuramoto K, Hashimoto H (1993) Lymphangiomyomatosis involving the kidney: a case report. Acta Urol Jpn 39:249–252
13. Smoralek TA, Wessner LL, McCormak FX (1998) Evidence that lymphangiomyomatosis is caused by TCS2 mutations: chromosome 16p13 loss of heterozygosity in angiomyolipomas and lymph nodes from women with lymphangiomyomatosis. Am J Hum Genet 62:810–815
14. Tawfik O, Austenfeld M, Persons D (1996) Multicentric renal angiomyolipoma associated with pulmonary lymphangioleiomyomatosis: case report, with histologic, immunohistochemical, and DNA content analyses. Urology 48:476–480
15. Uzzo RG, Libby DM, Darrocott VE (1994) Coexisting lymphangioleiomyomatosis and bilateral angiomyolipomas in a patient with tuberous sclerosis. J Urol 151:1612–1615

Virchows Arch (2002) 440:111–122
DOI 10.1007/s00428-001-0582-9

REVIEW ARTICLE

Christoph Röcken · Ann Shakespeare

Pathology, diagnosis and pathogenesis of AA amyloidosis

Received: 3 September 2001 / Accepted: 1 November 2001 / Published online: 4 January 2002
© Springer-Verlag 2002

Abstract Amyloid is defined as a proteinaceous tissue deposit that shows a typical green birefringence in polarised light after staining with Congo red, the presence of non-branching linear fibrils of indefinite length with an approximate diameter of 10–12 nm and a distinct X-ray diffraction pattern consistent with Pauling's model of a cross-β fibril. Approximately 45% of generalised amyloidoses are secondary or reactive (AA) amyloidosis. Among the causes of AA amyloidosis are rheumatic diseases, idiopathic diseases, inherited diseases, infectious diseases and malignant tumours. Recent decades have provided significant advances in our understanding of the pathology and pathogenesis of AA amyloidosis. Its pathogenesis is multifactorial involving many variables such as primary structure of the precursor protein, acute phase response, the presence of non-fibril proteins (e.g. amyloid P component, apolipoprotein E, glycosaminoglycans, proteoglycans and basement membrane proteins), receptors, lipid metabolism and proteases. Study of the pathogenesis of AA amyloidosis has provided many insights into the nature of conformational diseases, which may help in the understanding of other members of this particularly heterogeneous group of diseases, such as Alzheimer's disease and transmissible spongiform encephalopathies.

Keywords Amyloid · Serum amyloid A

Conformational diseases

Carrell and Lomas [7] introduced the term "conformational diseases" to include Alzheimer's disease, Creutzfeld-Jacob disease, transmissible spongiform encephalopathies and amyloidoses. According to Carrell and Lomas a conformational disease "...arises when a constituent protein undergoes a change in size or fluctuation in shape, with resultant self-association and tissue deposition." At least part of the protein is correctly folded when it is released in its physiological form, and the conformational disease arises from post-translational modification. This is influenced by genetic variables and the primary structure of the protein. Much of our knowledge and understanding of conformational diseases stems from research on amyloidosis.

C. Röcken (✉) · A. Shakespeare
Department of Pathology,
Otto-von-Guericke-University of Magdeburg,
Leipziger Strasse 44, 39120 Magdeburg, Germany
e-mail: christoph.roecken@medizin.uni-magdeburg.de
Tel.: +49-391-6713179, Fax: +49-391-67190188

Amyloid

Amyloid is defined as a proteinaceous tissue deposit showing: (1) a typical green birefringence in polarised light after staining with Congo red (Fig. 1), (2) the presence of non-branching linear fibrils of indefinite length with an approximate diameter of 10–12 nm (Fig. 1) [66] and (3) a distinct X-ray diffraction pattern consistent with Pauling's model of a cross-β fibril. High resolution electronmicroscopic studies provided evidence that the amyloid fibril contains a core composed of pentosomal particles that have the characteristics of amyloid P component (AP, Fig. 1).Wound around this is a "double-tracked" ribbon-like structure identified as chondroitin sulphate proteoglycan (CSPG) [22]. Covering the surface of this structure is a further ribbon-like double-tracked structure, characterised as heparan sulphate proteoglycan (HSPG, Fig. 1). The fibril protein forms the outermost surface. The basic architecture of amyloid fibrils is similar to that of microfibrils of elastic tissue [22]. The origin of amyloid is diverse, and over 20 different fibril proteins have been described. The precursors of most fibril proteins differ from each other with respect to primary structure and function; fibril proteins are derived from apolipoproteins (apolipoprotein AI, apolipoprotein AII and serum amyloid A), proteohormones (atrial natriuretic peptide, calcitonin, insulin, islet amyloid polypeptide and prolactin), immunoglobulins (λ- and κ-light chain, heavy chain), proteases (lysozyme),

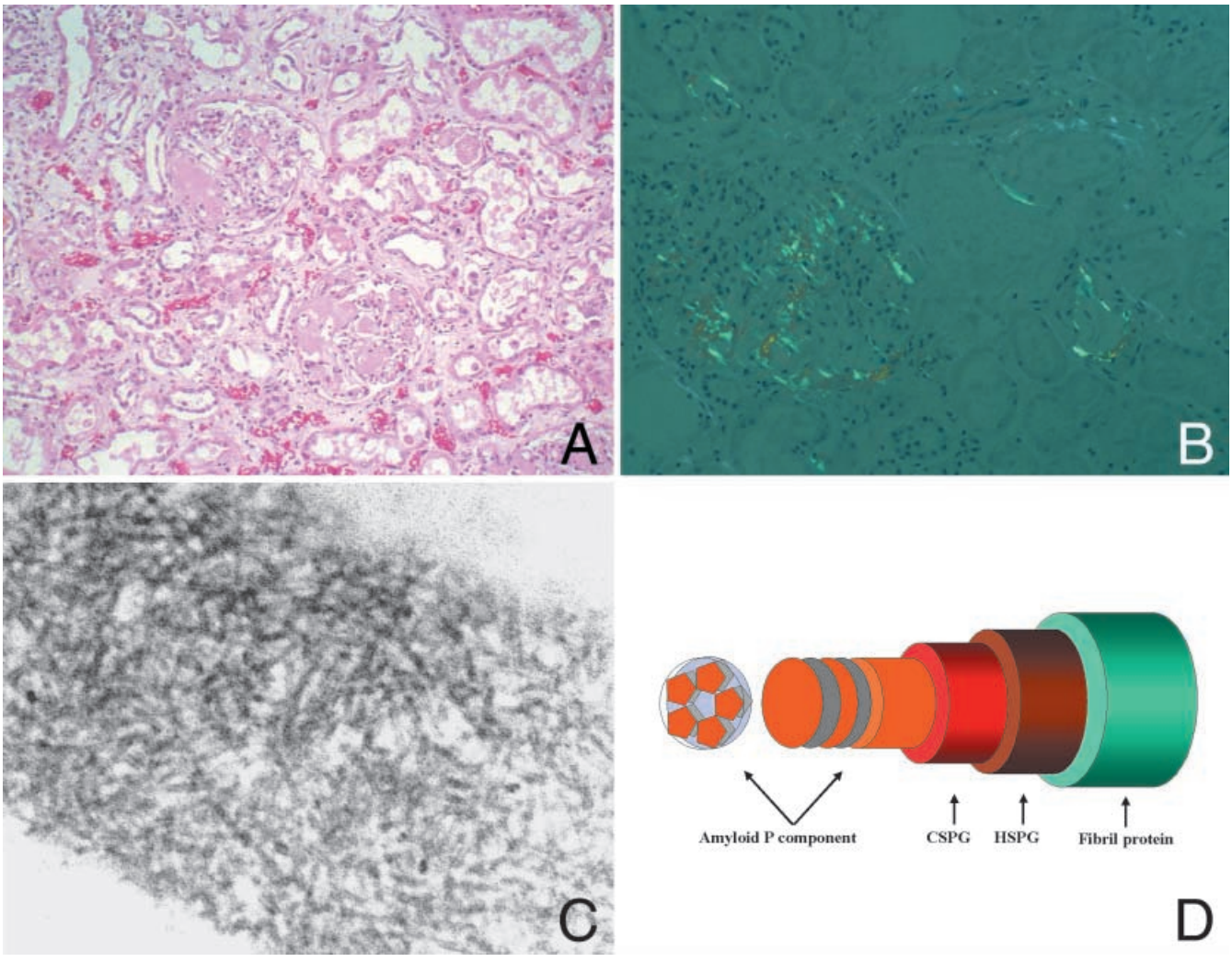

Fig. 1 Amyloid deposits are homogeneous eosinophilic deposits in conventional haematoxylin and eosin-stained sections (**a**) showing a characteristic apple-green birefringence following staining with Congo red (**b**). Using electron microscopy, amyloid is shown to consist of rigid fibrils with a diameter of 10–12 nm and indefinite length (**c**). High-resolution electron microscopic studies provide evidence that amyloid fibrils are a complex three-dimensional structure composed of different components, including amyloid P component, chondroitin sulphate glycosaminoglycans (CSPG), heparan sulphate glycosaminoglycans (HSPG) and filaments of fibril protein aggregates (**d**). Haematoxylin and eosin (**a**), Congo red stain (**b**), electron micoscopy (**c**). Original magnifications: ×20 (**a**), ×40 (**b**), ×80,000 (**c**)

protease inhibitors (cystatin), transmembrane proteins (amyloid precursor protein), transport proteins (transthyretin) and others (gelsolin, fibrinogen, lactadherin, lactoferrin, β2-microglobulin). The only feature common to all these proteins is their ability to form aggregates under specific circumstances, which leads to the formation and deposition of amyloid. Deposits may be local, organ-limited or generalised, and they can affect any organ or tissue type. However, the distribution pattern of amyloid depends on the origin and type of fibril protein deposited.

Amyloidosis

Amyloidosis denotes the disease state that results from the deposition of amyloid. Symptoms depend on the distribution pattern and quantity of the deposits. Although a particular combination of clinical symptoms may be highly indicative of amyloidosis in a given patient, the clinical pictures of different amyloid diseases can be variable. Moreover, a single patient may suffer from different amyloid diseases simultaneously. This review will only focus on the reactive or secondary type of amyloidosis (AA amyloidosis).

AA amyloidosis

Epidemiology

Approximately 45% of all generalised amyloidoses are AA amyloidosis. The onset is usually explosive and among its causes are rheumatic diseases (ankylosing spondylitis and rheumatoid and juvenile arthritis), idiopathic diseases (sarcoidosis, Crohn's disease, ulcerative colitis and Rosai-Dorfman disease), inherited diseases

(familial Mediterranean fever, tumour necrosis factor receptor associated periodic fever syndrome), infectious diseases (tuberculosis and leprosy) and malignant tumours (mesothelioma and Hodgkin's disease) [50, 61]. The absolute and relative prevalences of the individual diseases associated with AA amyloidosis show significant geographical and temporal differences. Until the mid-twentieth century, tuberculosis was one of the most common causes in the West. As its incidence fell as a result of successful antibiotic treatment, chronic rheumatic and idiopathic inflammatory diseases became the leading causes of AA amyloidosis [59, 73]. However, in the Third World and on the Indian subcontinent, chronic infectious diseases such as tuberculosis and leprosy remain the major causes. In approximately 5% of cases of AA amyloidosis no underlying disease can be found.

Pathology

AA amyloid is initially deposited in the spleen followed by the liver and kidney before it finally presents with generalised vascular and interstitial deposits. The reason for this temporal order of amyloid deposition is unknown. Since the precursor protein of AA amyloid (see below) is an apolipoprotein, one may speculate that amyloid occurs initially in the spleen, liver and kidney because these are major sites of lipid and cholesterol metabolism (see below). However, experimental verification of this hypothesis is required.

Clinical features

Proteinuria is often the first clinical presentation of generalised AA amyloidosis, and the severity of albuminuria correlates with patient's prognosis [25]. Extensive involvement of the heart leads to cardiac failure. Adrenocortical insufficiency due to amyloid deposition in the adrenal glands has been described and is usually associated with extensive renal amyloidosis.

Diagnosis

The diagnosis and classification of amyloid requires histological evidence. No clinical or laboratory test has yet superseded histology. Sensitivity and specificity of the histological diagnosis depend on the choice and adequacy of the tissue site sampled, the quantity of deposits in the sample, the quality of the equipment (a good polarisation facility is mandatory) and the awareness of the pathologist. Since AA amyloidosis is a generalised disease it may be diagnosed in any amyloid-containing tissue, but the most common biopsy sites are subcutaneous fat, kidney, rectum and liver. When amyloid is present in small amounts it can be easily overlooked. If present in large amounts, it may be misinterpreted as elastosis in skin and breast tissue specimens or collagenous colitis in intestinal biopsies. Precise classification of the amyloid type is essential, as correct treatment may delay progression of the disease. When amyloid is suspected, Congo red staining must be applied and the specimen viewed in polarised light in a darkened room. Following diagnosis, amyloid is classified either immunohistochemically using specific antibodies directed against defined fibril proteins [59] or biochemically by extracting the fibril proteins from native or formalin-fixed amyloidotic tissue and submitting the protein to amino acid sequencing. Finally, the histopathological diagnosis and classification of amyloid should be correlated with the clinical information, since the clinical information provided may be misleading. For instance, a patient with plasmacytoma (which may be associated with AL amyloidosis) may also suffer from rheumatoid arthritis (which may also be associated with AA amyloidosis), of which the pathologist is unaware.

Pathogenesis of AA amyloidosis

The pathogenesis of AA amyloidosis has been studied in the following ways:

1. The morphology and biochemical composition of human amyloid has been investigated.
2. AA amyloidosis has been studied in various animal species. The disease has been found to occur in dogs, cats, cheetahs, tigers, hares, stone martens, mink, cattle, horses, sheep, mountain gazelles, rabbits, hamsters, guinea pigs, bats, chickens and ducks [24, 57, 90]. As in humans the disease is commonly associated with chronic inflammatory conditions. AA amyloidosis also affects mice; for many years these have been used as an animal model to investigate amyloidogenesis, and they have provided many insights into the disease.
3. In vitro studies have included cell culture experiments as well as protein and structural biochemical determinations.

These investigations have demonstrated that the pathogenesis of AA amyloidosis depends on several different factors (Fig. 2).

The precursor protein

The serum amyloid A (SAA) protein is the precursor of the AA fibril protein deposited in AA amyloidosis. The SAA genes are localised on chromosome 11p15.1 [19, 43]. SAA proteins are a family of homologous proteins that are divided into two groups. The first group comprises type-I acute phase proteins synthesised by the liver, SAA1 and SAA2 (SAA1+2). During an acute phase response, the serum concentration of SAA1+2 increases by as much as 1000-fold to reach concentrations of 1–2 mg/ml [19, 43]; 80% are bound to lipoproteins, and of these 90% become associated with high-density

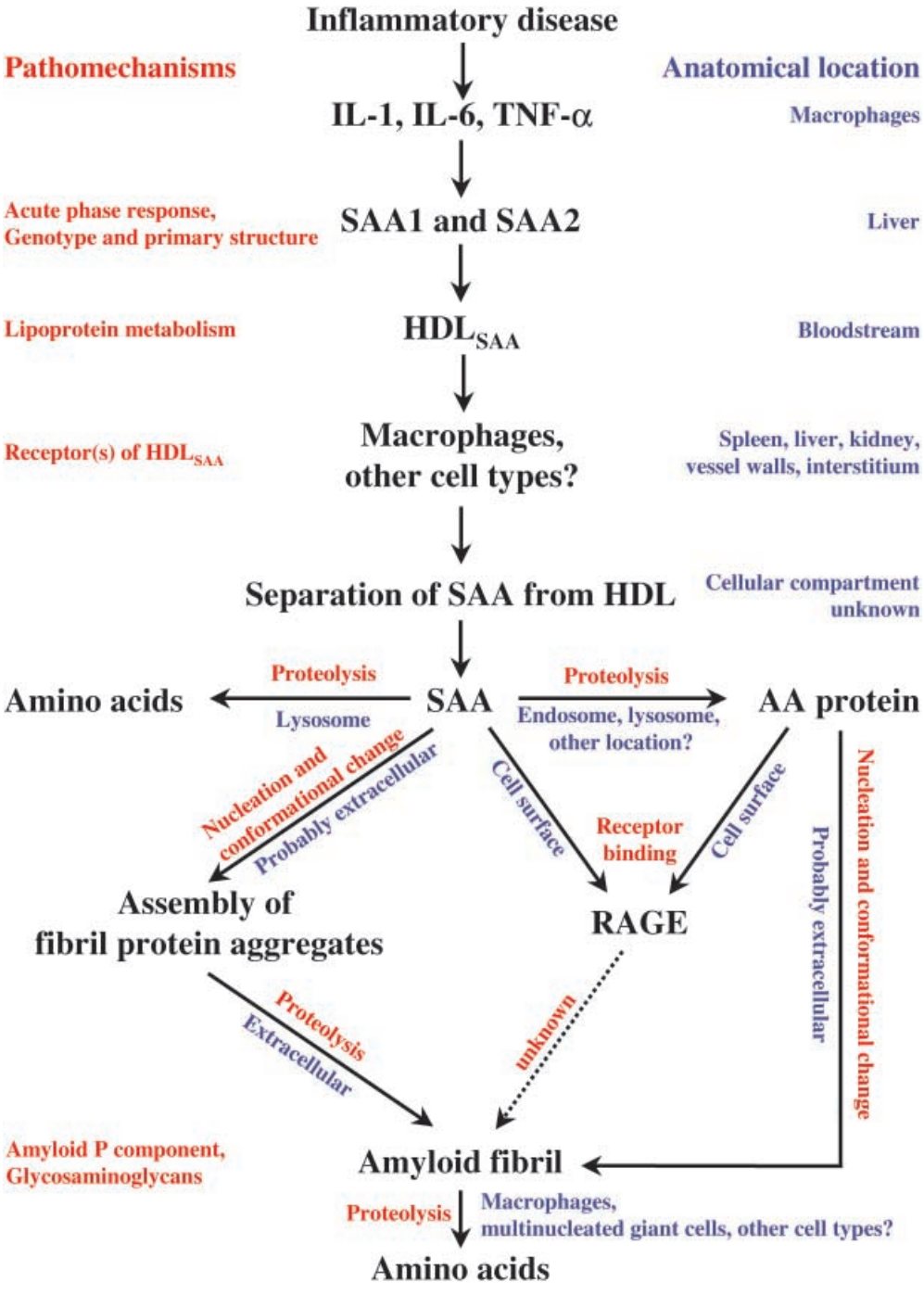

Fig. 2 Summary of the putative pathogenetic pathway(s) leading to the formation and deposition of AA amyloid

lipoproteins (HDL)[19, 43]. The second group of SAA proteins (SAA4 in humans and SAA3 in mice) is expressed constitutively at plasma concentrations of approximately 55 µg/ml; human SAA4 is synthesised by different organs and tissues and is not an acute phase protein [19]. The physiological functions of SAA were recently reviewed by Uhlar and Whitehead [35, 77]; it is not yet known exactly how these functions are associated with the pathogenesis of AA amyloidosis.

The acute phase response

It has been known for a long time that AA amyloidosis occurs after a lengthy period of ongoing inflammatory and/or infectious diseases. Therefore, amyloidosis may not be suspected during the early course of a potential chronic or recurrent inflammatory disease. However, in rare cases it may occur within a year of a clinically apparent inflammatory disease [60]. AA amyloidosis does not occur in the absence of an acute phase response or without elevated serum SAA levels. Synthesis and secre-

tion of acute phase SAA is mediated by cytokines [mainly interleukin (IL)-1, IL-6 and tumour necrosis factor (TNF)-α] [12, 19, 43]. AA amyloid occurring in malignant diseases, such as mesothelioma or Hodgkin's disease, or idiopathic diseases, such as sarcoidosis, may be triggered by cytokines synthesised and secreted by tumour cells or histiocytic cells. These cytokines generate a systemic acute phase response, thereby inducing synthesis of SAA and facilitating the development of AA amyloidosis. The progressive nature of AA amyloidosis largely reflects the persistent nature of the underlying conditions and, due to fluctuations of disease activity, not all patients show evidence of an acute phase response at the very time of diagnosis.

The genotype and primary structure

The primary structure of SAA influences its propensity to form fibril proteins. In amyloid-susceptible mice, SAA1.1 is the only precursor of AA fibril proteins; it differs from SAA2.1 by nine amino acids. Compared with other mouse models, inbred Ce/J mice are resistant to AA amyloidosis because of the unique primary structure of their acute phase SAA, which is a mixture of SAA1.1 and SAA2.1 termed $SAA_{CE/J}$ or SAA2.2. SAA2.2 differs from SAA1.1 by five amino acids and from SAA2.1 by six amino acids [67]. In humans, a specific SAA sequence has not yet been linked to AA amyloidosis, but genotype does appear to influence the incidence of the disease; the SAA1.3 genotype is significantly more common in patients with AA amyloidosis than in those suffering from rheumatoid arthritis without amyloidosis [6, 48, 49]. Studies using synthetic peptides have shown that the first 10–15 amino acids of the molecule are the most important in the formation of amyloid fibrils [81]. All AA fibril proteins analysed to date have an intact N-terminus spanning this region (see below).

Lipoprotein metabolism

SAA attached to HDL (HDL_{SAA}) appears to be the source of the tissue AA fibril protein [20, 74]. There is evidence to support the hypothesis of a link between metabolism of apolipoproteins and lipoproteins and the pathogenesis of amyloid; amyloid deposition occurs initially in organs and tissue sites that are major sites of lipid and cholesterol metabolism, such as the spleen and liver. Furthermore, immunohistochemical studies and sequence analyses have demonstrated the presence of other apolipoproteins in the HDL fraction, such as apolipoprotein A-I (apo A-I) and apolipoprotein E (apo E) in AA deposits [28]. Apo E and HDL are thought to play major roles in reverse cholesterol metabolism, which is the transport of cholesterol from peripheral cells to the liver for re-utilisation or intestinal excretion in bile. Macrophages (m∅) laden with lipid and cholesterol serve as an in vitro model for the study of cholesterol efflux and, therefore, as a source of excess plasma lipids. The amount of cholesterol effluxed from m∅ to HDL is significantly enhanced by the synthesis and presence of apo E. Moreover, a change in the lipid composition of a lipoprotein particle can cause a change in its protein composition. Although, apo A-I and apo A-II can displace SAA from HDL [21], the effect of a varying lipid composition on the binding of SAA is as yet unknown. HDL_{SAA} binds to m∅ and is internalised [37, 58], and m∅ are able to generate amyloid fibrils from SAA in vitro [36].

Receptors

It was shown recently that murine acute phase SAA and murine AA fibril proteins bind to a cell surface receptor of advanced glycation end products (RAGE), which is a signal transduction receptor and does not lead to the internalisation of SAA/AA fibril proteins [89]. However, following binding to RAGE, signal transduction is mediated by $p21^{ras}$, mitogen-activated kinases, ERK1 and ERK2 [75, 89]. The onset of AA amyloidosis is delayed if the binding of acute phase SAA or AA fibril protein to RAGE is blocked [89], but as yet the mechanism for this is unknown. Moreover, it has been demonstrated that HDL_{SAA} is bound and endocytosed by m∅ [30, 37, 58], which suggests a receptor-mediated internalisation pathway for HDL_{SAA} comparable to that for other lipoproteins. Internalisation of HDL_{SAA} may be mediated via binding of SAA to a specific receptor other than RAGE [30], and this interaction is influenced by cell surface glycosaminoglycans [58]. Thus, there is evidence of at least two receptors that bind SAA and AA fibril proteins. Their putative role in the pathogenesis of AA amyloidosis requires further investigation.

Nucleation and conformational change

Since AA amyloidosis is a conformational disease, any change in the secondary structure of SAA may affect the assembly of protein aggregates and amyloid fibrils. Amyloid-enhancing factor (AEF) [33], glycosaminoglycans [42] and basement membrane proteins [31, 42] may facilitate conformational changes by acting as scaffolds (i.e. nucleus). Binding of SAA to any of these components may induce a conformational change towards a β-pleated structure and hence formation of amyloid [31, 33, 42]. Silk, which has a β-pleated secondary structure, may also serve as a scaffold; intravenous injection of silk accelerates the formation and deposition of AA amyloid in the murine model [34].

AP component

AP has been found in the deposits of all amyloid diseases studied to date. AP is identical to serum amyloid P component (SAP), an *N*-glycosylated serum protein that

belongs to the pentraxin group and is homologous with C-reactive protein [54]. SAP is present in plasma as a pentamer where it is able to activate the classical complement system [54]. It is synthesised and metabolised in the liver [54] and binds amyloid fibrils, fibril proteins and sulphated glycosaminoglycans [54]. SAP is a physiological component of the glomerular basement membrane of kidneys, the basement membrane of skin, lung, liver and blood vessels as well as a component of the microfibrils that coat elastic membranes [54]. These microfibrils are structurally similar to amyloid fibrils [22].

SAP may influence the pathogenesis of AA amyloid in the following ways: it may promote fibrillogenesis by binding the fibril protein, it may protect the amyloid fibril from proteolysis and it may be a structural component [22, 54]. However, investigations on SAP-deficient mice have shown that SAP enhances the formation of AA amyloid, whilst not appearing to influence degradation [76, 78]. Aside from its putative pathophysiological role, studies using radiolabelled SAP have demonstrated its use in diagnostics [14]. The amount of SAP in AA amyloid correlates with the extent of amyloid disease [14, 15]. The plasma clearance of SAP also correlates with the severity of the disease and is enhanced in advanced AA amyloidosis. Radiolabelled SAP is rapidly enriched in AA amyloid deposits and stays there for several months [14]. This enrichment of radiolabelled SAP in amyloid deposits can be used for diagnostic purposes to evaluate the extent of amyloidosis, and the procedure has been applied to disease staging in several hundred patients with amyloidosis [14].

Apo E

Apo E has been found in the deposits of various amyloid diseases. It has gained specific attention because the incidence and morbidity of sporadic, non-familial Alzheimer's disease is influenced by the constellation of the apo E alleles [63]. Statistical studies have shown that the clinical course of Alzheimer's disease is influenced by the apo E alleles; carriers of the ε4 allele have a higher incidence and earlier onset of the disease than carriers of the remaining alleles, but the ε4 allele has no influence on the duration or mortality of Alzheimer's disease [63]. Apo E binds to HDL and is thought to direct cholesterol from the periphery back to the liver, a pathway known as reverse cholesterol metabolism (see above). Apo E has also been found in AA amyloid deposits, and it co-purifies with the fibril proteins [11, 28]. Therefore it is possible that apo E also plays a part in the pathogenesis of AA amyloidosis, but this has not been demonstrated as yet [27, 41, 52]. Nevertheless, apo E has been shown to influence AA amyloidogenesis in experiments with knockout mice; apo E accelerates the formation and deposition of AA amyloid but has no effect on the deposition pattern, and lack of apo E does not prevent the formation of AA amyloid [17, 26]. It is not known how apo E mediates this effect.

Glycosaminoglycans and basement membrane proteins

AA amyloidosis, like most other amyloid diseases, is characterised by the temporal and spatial co-deposition of basement membrane proteins and glycosaminoglycans (GAGs) [42]. Laminin, collagen type IV and fibronectin are found in AA amyloid deposits [31, 42]. The transcription of these proteins is upregulated during or immediately before amyloid formation, and it has been speculated that they may influence fibrillogenesis following disruption of the integrity of the interstitial matrix [1, 82]. Laminin binds SAA with high affinity [2]. Biochemical studies support the results of morphological investigations; chondroitin sulphate, dermatan sulphate, heparan sulphate, hyaluronan, CSPG and HSPG have all been found in amyloid deposits [31, 42]. The significance of the galactosaminoglycan and GAG composition for the structure or pathogenesis of AA amyloid and the structure of the amyloid fibril is not fully understood. However, GAGs and proteoglycans bind fibril proteins and AP [31, 42, 54]. Human and murine SAA contains binding sites specific for heparin/heparan sulphate [3]. In vitro experiments using different GAGs showed that only heparan sulphate increased the β-sheet content of murine amyloidogenic SAA [8, 45]. Laminin was also shown to bind murine SAA with high affinity [2], and it may be postulated that binding of SAA to components of the interstitial matrix, such as laminin and GAGs, may facilitate nucleation events leading to fibrillogenesis [2, 3]. This hypothesis remains to be confirmed in vivo. Cell surfaces are coated with GAGs, and interaction of SAA with GAGs may also take place here rather than in the interstitium [58].

Proteases

In patients with AA amyloidosis, the fibril protein is a cleavage product of the precursor protein generated by proteolysis [19]. The AA fibril protein consists of an intact N-terminus, but lacks between 18 and 83 amino acids at the C-terminus (Fig. 3). Thus the N-terminus of SAA is crucial in fibril formation, and the way SAA is cleaved is important in the pathogenesis of AA amyloidosis. Several experimental and clinical studies have also shown that amyloid is protease-sensitive and that amyloidosis is reversible. Use of antibodies directed against fibril proteins may lead to degradation of the deposits [18]; this also requires the activity of proteases. Thus proteases and proteolysis of SAA, the AA fibril protein, and the amyloid deposits may contribute to the pathogenesis and clinical course of AA amyloidosis in the following ways (Fig. 4):

a. Proteolysis of a non-amyloidotic precursor protein may liberate the fibril protein and facilitate amyloidogenesis. This mechanism occurs in Aβ amyloidosis, which is commonly associated with Alzheimer's disease [63], but as yet there is no evidence to suggest

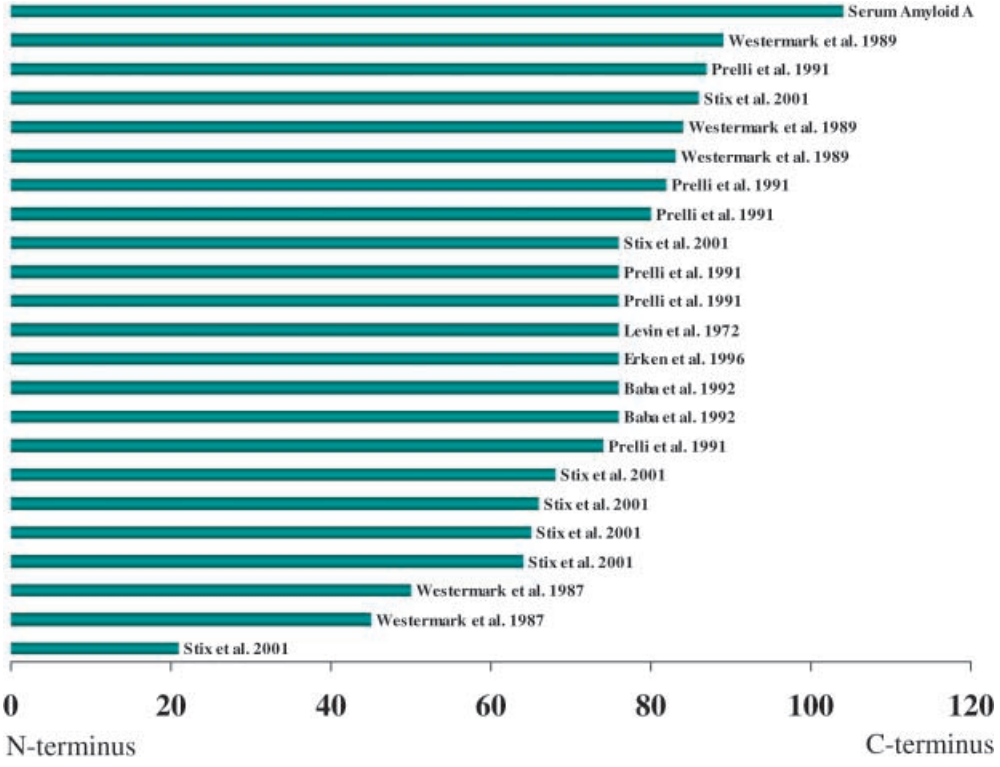

Fig. 3 A list of AA fibril proteins that have been characterised to date. The fibril protein consists of an intact N-terminus and lacks between 18 and 83 amino acids at the C-terminus

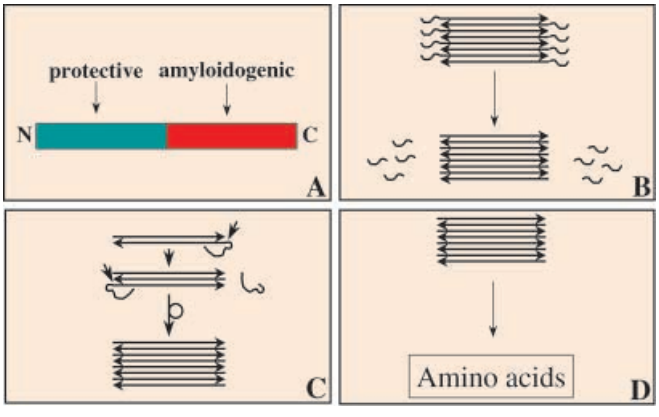

Fig. 4 Potential ways in which proteases and proteolysis of SAA, the AA fibril protein, and the amyloid deposits may contribute to the pathogenesis and clinical course of AA amyloidosis (for details see first paragraph of Proteases section)

that it accounts for AA amyloidosis since the precursor protein has been shown to be potentially amyloidogenic [84, 85].

b. Proteolysis of an amyloidogenic precursor protein may occur before, during or after fibrillogenesis. Proteolysis prior to amyloid formation may have different effects depending on the cleavage site, it may enhance fibrillogenesis by generating fibril proteins that are more prone to self-assembly than the precursor protein or it may prevent fibrillogenesis by degrading the precursor protein in a region that is important for self-assembly such as the N-terminal end of SAA [81] (Fig. 4a). Previous studies [86, 88] have shown that cleavage at the N-terminal end of SAA prevents the formation of amyloid [5, 10, 40, 55, 56, 71, 79, 80]. Proteolysis at the C-terminal end may occur after amyloid has been formed and may remove a redundant peptide [4, 32, 84] (Fig. 4b). Proteolysis during fibrillogenesis may influence fibril assembly. Hypothetically, lateral growth of a scaffold may be blocked sterically by a C-terminal end. Following cleavage of this fragment, lateral fibril growth can proceed (Fig. 4c).

c. Proteolysis following amyloid formation may have no effect or it may lead to the degradation of amyloid (Fig. 4d).

Assuming that proteolysis of SAA and AA fibril proteins affects the pathology of AA amyloidosis, then further investigations are required to determine (1) the proteases involved, (2) the origin of the proteases, (3) the cellular and extracellular compartments involved in proteolysis and (4) the nature of the process, i.e. physiological or pathological. Despite our lack of knowledge in this area, the following evidence indicates that different proteases, and probably different compartments, are involved in the formation and degradation of SAA and AA fibril proteins: (1) the existence of different substrates (“substrate diversity”), i.e. the precursor protein, monomeric fibril protein, oligomeric fibril protein and the “mature” amyloid fibril and (2) the existence of different proteases (“protease diversity”) that cleave either SAA or the fibril proteins.

The contribution of proteases and proteolysis to the pathogenesis of AA amyloidosis has been studied using

either human tissues and cell lines or animal models such as rabbits and mice. Most studies have demonstrated the presence and activity of proteases qualitatively using either tissue homogenates, serum, purified prote-ases, polymorphonucleocytes, neutrophils, lymphocytes or m∅. Two studies were performed in vivo while the majority were in vitro using a variety of substrates: delipidated SAA, recombinant SAA and HDL_{SAA}. In summary, these studies demonstrated cleavage of SAA by the following: serum proteases [68], proteases secreted into culture supernatant by polymorphonucleocytes and m∅ [9, 65, 69], membrane-bound proteases of lymphocytes, neutrophils and m∅ [38, 39, 64] and tissue homogenates from spleen [88], liver [88] and kidney [88]. Protease families that are capable of or responsible for degrading SAA include metalloproteinases, serine proteases and aspartate proteases. Protease inhibitors have been found to be particularly useful in defining enzymes; proteolysis is inhibited by serine protease inhibitors (diisopropylfluorophosphate) [38], α1-antitrypsin [39, 65], phenylmethyl sulphonyl fluoride [9, 65, 69], aspartate protease inhibitors (pepstatin) [65], an elastase inhibitor (Ac-Ala-Ala-Pro-Val-CH_2Cl peptide) [39, 65] and a trypsin inhibitor (soybean trypsin inhibitor) [65]. Specific proteases that cleave SAA are cathepsin G [72], neutral serine esterase [65], cathepsin D [86, 88], elastase [39, 65, 72, 87], cathepsin B [87], collagenase [72, 47] and stromelysin [47] (see below).

Several studies have shown that SAA is degraded stepwise and by different proteases. It may be degraded completely without the occurrence of fragments [13, 38, 64] or incompletely with the generation of fragments resembling the AA fibril proteins in size, antigenicity and/or amino acid sequence [38, 39, 69, 86, 87, 88], depending on the technique used to analyse proteolysis. Complete degradation of SAA without fragments was observed following degradation by m∅ [13, 38] and neutrophils [64] and was assigned to the activity of serine proteases [38, 64]. Incomplete degradation by m∅ has also been attributed to serine proteases and elastase [38, 39, 69]. The site of degradation is still unknown; two studies have excluded intracellular or lysosomal proteolysis of SAA [38, 64], but overall the number of detailed qualitative and quantitative studies aimed at defining cleavage sites is limited.

Serine proteases

Activity of the serine proteases elastase [39, 65, 72, 87] and cathepsin G [72] has been found in amyloidotic tissue, thus both may be involved in the pathogenesis of AA amyloidosis. Elastase cleaves SAA within the N-terminal half of the precursor protein, between Ala27 and Asn28, Ile58 and Ser59 and Ile65 and Gln66, preventing generation of a fibril protein; therefore elastases may be protective. As yet the activity of cathepsin G remains to be elucidated.

Aspartate proteases

Cathepsin D, a lysosomal aspartate protease with an optimum pH in acidic conditions, degrades SAA completely at a concentration of 0.2 U/ml and incompletely at a concentration of 0.02 U/ml [86]. Cleavage occurs between Phe6 and Leu7, Glu9 and Ala10, Asp12 and Gly13, Arg15 and Asp16 and Ala20 and Tyr21. Cathepsin D also cleaves SAA within the N-terminal half of the precursor protein preventing the generation of fibril proteins [86]. Pepstatin, an aspartate protease inhibitor, shortens the lag time for amyloid formation in the murine model of secondary amyloidosis [88]. Aspartate proteases potentially protect the formation of amyloid. Degradation by the lysosomal protease cathepsin D requires internalisation of SAA.

Cysteine proteases

Cathepsin B, a lysosomal cysteine protease, cleaved SAA in vitro between positions 76 and 77 to generate a peptide identical to an AA fibril protein (Arg1 to Ser76) [87]. Therefore, cathepsin B, an endo- and exopeptidase, has the potential to be amyloidogenic. Cathepsin K belongs to the papain family of cysteine proteases and is the most potent mammalian elastase yet described. We demonstrated that cathepsin K is expressed and probably secreted by multinucleated giant cells (MGCs) adjacent to AA amyloid deposits. Furthermore, recombinant cathepsin K completely degraded SAA and AA fibril proteins in vitro at pH 5.5, while less effective degradation took place at pH 7.4. Thus in vitro cathepsin K appears to be protective [62]; in vivo studies are needed to demonstrate the biological significance of these observations. MGCs are considered to be a specific phenotype of m∅, and they are also, though less commonly, found in amyloid deposits to which they often show an intimate spatial relationship [62]. Earlier animal studies suggested that MGCs may be involved in the resorption of amyloid deposits [83]. In contrast to cathepsin D, the proteolytic activity of cathepsin K is not restricted to cellular compartments. The significance of other cysteine proteases, i.e. cathepsins L and X, in the pathogenesis of AA amyloidosis has yet to be determined.

Matrix metalloproteinases

This group of proteases degrades basement membranes and connective tissue and plays an essential role in the homeostasis of the extracellular matrix. An imbalance in the expression and/or activity of matrix metalloproteinases (MMPs) can have important consequences in the development of diseases such as cancer and Alzheimer's disease. Patients suffering from rheumatoid arthritis exhibit significantly increased serum levels of MMP-1, -2, -3 and -9 compared with healthy controls, and the serum level of MMP-3 correlates with the C-reactive protein

level and the erythrocyte sedimentation rate [23], and thus with systemic inflammation [70]. Inflammatory cytokines such as IL-1, IL-6 and TNF-α are potent inducers of some MMPs, including MMP-1, -3 and -9, and they may increase transcription by as much as 100-fold [53]. The production and secretion of MMP-2 and -3 can be stimulated by the acute phase protein SAA [46]. Thus, AA amyloidosis occurs under conditions known to generate significantly increased serum and tissue levels of MMPs, as compared with healthy control individuals. In an immunohistochemical investigation we found MMP-1, -2 and -3 in AA amyloid deposits independent of the organs involved (liver, kidney or spleen) [51]. These findings suggest that MMPs may participate in amyloidogenesis either by processing the precursor protein SAA, by degrading the amyloid deposits or by remodelling the interstitial matrix following amyloid deposition. Our in vitro studies showed that MMP-1, -2 and -3 are able to cleave SAA and AA fibril proteins (AFP) within the region-spanning residues 51 to 57. The following cleavage sites were identified: 57 to 58 for MMP-1, 7 to 8 and 51 to 52 for MMP-2, 7 to 8, 16 to 17, 23 to 24, 51 to 52, 55 to 56, 56 to 57 and 57 to 58 for MMP-3 [71]. Cell culture experiments showed that THP-1 cells (a human monocyte/macrophage cell line) were able to degrade AFP, but this was significantly delayed after the addition of a general metalloproteinase inhibitor (*o*-phenanthroline) to dextran sulphate-stimulated cells. Thus SAA and AFP are susceptible to proteolytic cleavage by MMPs [71]. MMPs are endoproteases that cleave at a physiological pH and may function in the interstitium. Their putative significance in amyloidogenesis was further highlighted by in vivo experiments performed by Hernandez-Pando et al. [16]; following infection of mice with tuberculosis, amyloidosis occurred in the lung when batimastat, a metalloprotease inhibitor, was administered simultaneously. However, this effect was not necessarily related to MMPs. Other metalloproteases may also be involved in the pathogenesis of AA amyloidosis.

Is AA amyloidosis transmissible?

Although it has not yet been demonstrated, one must finally address the transmissibility of AA amyloidosis since some other conformational diseases, such as bovine spongiform encephalopathy (BSE), are known to be transmissible. It is known that development of AA amyloidosis requires either a background of persistent/chronic recurrent inflammatory reaction or increased endogenous synthesis of the precursor protein; the latter is also necessary in the development of BSE, which requires endogenous synthesis of the prion protein. However, in the case of AA amyloidosis, the onset and course of the disease can be influenced by intravenous injection of substances that decrease the lag time for amyloid formation. These include a so-called AEF, silk, AA amyloid fibrils and transthyretin amyloid fragments [33, 34, 44]. The biochemical nature of AEF is not fully known; it probably represents AA amyloid fibrils and is defined by its biological activity. Injection of AEF alone does not cause amyloid formation in mice, and an additional inflammatory stimulus is required, such as silver nitrate or daily casein injections. However, AEF and the inflammatory stimulus do not have to be administered at the same time, and the interval between injections can be as long as 6 months. Thus, although the development of the disease bears some similarity to BSE, at present and based on these observations, AA amyloidosis can be considered only to be potentially transmissible.

Reversibility of amyloid

The deposition of amyloid is not irreversible. Progression of generalised amyloidosis can be delayed or stopped by treatment of the underlying disease; deposits may also regress [18, 83]. Identification of factors that are involved in the formation and degradation of AA amyloid and elucidation of their modes of interaction may help in the development of new treatments.

Conclusion

In recent decades significant advances have been made in our understanding of the pathology and pathogenesis of AA amyloidosis. It is now clear that its pathogenesis is multifactorial and influenced by many variables. These include the primary structure of the precursor protein, an acute phase response, the presence of non-fibril proteins (e.g. AP, apo E, GAGs and proteoglycans), receptors, lipid metabolism and proteases. The process of amyloid deposition in living beings is likely to be much more complicated and subtle than so far imagined [29]. As yet we do not really know which of these variables is an indispensable prerequisite for amyloidogenesis and which is simply a catalyst. Ultimately, the study of the pathogenesis of AA amyloidosis has provided many insights into the nature of conformational diseases and these may help in understanding other diseases belonging to this particularly heterogeneous group.

Acknowledgements This work was supported by grants from the Deutsche Forschungsgemeinschaft (Grant No. RO 1173/3), Bonn Bad-Godesberg, Germany, and the Wilhelm Vaillant-Stiftung, München, Germany.

References

1. Ailles L, Kisilevsky R, Young ID (1993) Induction of perlecan gene expression precedes amyloid formation during experimental murine AA amyloidogenesis. Lab Invest 69:443–448
2. Ancsin JB, Kisilevsky R (1997) Characterization of high affinity binding between laminin and the acute-phase protein, serum amyloid A. J Biol Chem 272:406–413
3. Ancsin JB, Kisilevsky R (1999) The heparin/heparan sulfate-binding site on apo serum amyloid A – implications for the therapeutic intervention of amyloidosis. J Biol Chem 274: 7172–7181

4. Arai K, Miura K, Baba S, Shirasawa H (1994) Transformation from SAA2-fibrils to AA-fibrils in amyloid fibrillogenesis: in vivo observations in murine spleen using anti-SAA and anti-AA antibodies. J Pathol 173:127–134
5. Baba S, Takahashi T, Kasama T, Shirasawa H (1992) Identification of two novel amyloid A protein subsets coexisting in an individual patient of AA-amyloidosis. Biochim Biophys Acta 1180:195–200
6. Baba S, Masago SA, Takahashi T, Kasama T, Sugimura H, Tsugane S, Tsutsui Y, Shirasawa H (1995) A novel allelic variant of serum amyloid A, SAA1 gamma: genomic evidence, evolution, frequency, and implication as a risk factor for reactive systemic AA-amyloidosis. Hum Mol Genet 4:1083–1087
7. Carrell RW, Lomas DA (1997) Conformational disease. Lancet 350:134–138
8. de Beer MC, de Beer FC, McCubbin WD, Kay CM, Kindy MS (1993) Structural prerequisites for serum amyloid A fibril formation. J Biol Chem 268:20606–20612
9. Elliott-Bryant R, Liang JS, Sipe JD, Cathcart ES (1996) Degradation of serum amyloid A in amyloid-susceptible and amyloid-resistant mouse strains. Scand J Immunol 44:223–228
10. Erken E, Gray M, Cohen AS, Skinner M (1996) Sequence analysis of amyloid protein AA from a Turkish patient with familial Mediterranean fever – documentation of its $SAA_{1\alpha}$ derivation. Amyloid 3:173–176
11. Gallo G, Wisniewski T, Choi-Miura NH, Ghiso J, Frangione B (1994) Potential role of apolipoprotein-E in fibrillogenesis. Am J Pathol 145:526–530
12. Gillmore JD, Lovat LB, Persey MR, Pepys MB, Hawkins PN (2001) Amyloid load and clinical outcome in AA amyloidosis in relation to circulating concentration of serum amyloid A protein. Lancet 358:24–29
13. Ham D, Caouras V, Radzioch D, Gervais F (1997) Degradation of amyloid A precursor protein SAA by macrophage cell lines obtained from amyloid resistant and susceptible strains of mice. Scand J Immunol 45:354–360
14. Hawkins PN (1994) Studies with radiolabelled serum amyloid P component provide evidence for turnover and regression of amyloid deposits in vivo. Clin Sci 87:289–295
15. Hawkins PN, Wootton R, Pepys MB (1990) Metabolic studies of radioiodinated serum amyloid P component in normal subjects and patients with systemic amyloidosis. J Clin Invest 86:1862–1869
16. Hernandez-Pando R, Orozco H, Arriaga K, Pavon L, Rook G (2000) Treatment with BB-94, a broad spectrum inhibitor of zinc-dependent metalloproteinases, causes deviation of the cytokine profile towards type-2 in experimental pulmonary tuberculosis in Balb/c mice. Int J Exp Pathol 81:199–209
17. Hoshii Y, Kawano H, Cui D, Takeda T, Gondo T, Takahashi M, Kogishi K, Higuchi K, Ishihara T (1997) Amyloid A protein amyloidosis induced in apolipoprotein-E-deficient mice. Am J Pathol 151:911–917
18. Hrncic R, Wall J, Wolfenbarger DA, Murphy CL, Schell M, Weiss DT, Solomon A (2000) Antibody-mediated resolution of light chain-associated amyloid deposits. Am J Pathol 157:1239–1246
19. Husby G, Marhaug G, Dowton B, Sletten K, Sipe JD (1994) Serum amyloid A (SAA): biochemistry, genetics and the pathogenesis of AA amyloidosis. Amyloid 1:119–137
20. Husebekk A, Skogen B, Husby G, Marhaug G (1985) Transformation of amyloid precursor SAA to protein AA and incorporation in amyloid fibrils in vivo. Scand J Immunol 21:283–287
21. Husebekk A, Skogen B, Husby G (1987) Characterization of amyloid proteins AA and SAA as apolipoproteins of high density lipoprotein (HDL). Displacement of SAA from the HDL-SAA complex by apo AI and apo AII. Scand J Immunol 25:375–381
22. Inoue S, Kisilevsky R (1999) In situ electron microscopy of amyloid deposits in tissues. Methods Enzymol 309:496–509
23. Ishiguro N, Ito T, Obata KI, Fujimoto N, Iwata H (1996) Determination of stromelysin-1, 72 and 92 kDa type IV collagenase, tissue inhibitor of metalloproteinase-1 (TIMP-1) and TIMP-2 in synovial fluid and serum from patients with rheumatoid arthritis. J Rheumatol 23:1599–1604
24. Johnson KH, Westermark P, Sletten K, O'Brien TD (1996) Amyloid proteins and amyloidosis in domestic animals. Amyloid 3:270–289
25. Joss N, McLaughlin K, Simpson K, Boulton-Jones JM (2000) Presentation, survival and prognostic markers in AA amyloidosis. Q J Med 93:535–542
26. Kindy MS, Rader DJ (1998) Reduction in amyloid A amyloid formation in apolipoprotein-E-deficient mice. Am J Pathol 152:1387–1395
27. Kindy MS, de Beer FC, Markesbery WR, Pras M, Aksentijevich I, Kastner D, Kyle R, Solomon A, Woo P (1995) Apolipoprotein E genotypes in AA and AL amyloidoses. Amyloid 2:159–162
28. Kindy MS, King AR, Perry G, de Beer MC, de Beer FC (1995) Association of apolipoprotein E with murine amyloid A protein amyloid. Lab Invest 73:469–475
29. Kisilevsky R (2000) Amyloidogenesis-unquestioned answers and unanswered questions. J Struct Biol 130:99–108
30. Kisilevsky R, Subrahmanyan L (1992) Serum amyloid A changes high density lipoprotein's cellular affinity. A clue to serum amyloid A's principal function. Lab Invest 66:778–785
31. Kisilevsky R, Fraser P (1996) Proteoglycans and amyloid fibrillogenesis. In: Brock GR, Goode JA The nature and origin of amyloid fibrils. John Wiley & Sons Ltd. Chichester, pp 58–72
32. Kisilevsky R, Narindrasorasak S, Tape C, Tan R, Boudreau L (1994) During AA amyloidogenesis is proteolytic attack on serum amyloid A a pre- or post-fibrillogenic event? Amyloid 1:174–183
33. Kisilevsky R, Gruys E, Shirahama TS (1995) Does amyloid enhancing factor (AEF) exist? Is AEF a single biological entity? Amyloid 2:128–133
34. Kisilevsky R, Lemieux L, Boudreau L, Dun-Sheng Y, Fraser P (1999) New clothes for amyloid enhancing factor (AEF): silk as AEF. Amyloid 6:98–106
35. Kluve-Beckerman B, Malle E, Vitt H, Pfeiffer C, Benson M, Steinmetz A (1991) Characterization of an isoelectric focusing variant of SAA1 (ASP-72) in a family of Turkish origin. Biochem Biophys Res Commun 181:1097–1102
36. Kluve-Beckerman B, Liepnieks JJ, Wang LS, Benson MD (1999) A cell culture system for the study of amyloid pathogenesis – amyloid formation by peritoneal macrophages cultured with recombinant serum amyloid A. Am J Pathol 155:123–133
37. Kluve-Beckerman B, Manaloor J, Leipnieks JJ (2001) Binding, trafficking and accumulation of serum amyloid A in peritoneal macrophages. Scand J Immunol 53:393–400
38. Lavie G, Zucker-Franklin D, Franklin EC (1978) Degradation of serum amyloid A protein by surface-associated enzymes of human blood monocytes. J Exp Med 148:1020–1031
39. Lavie G, Zucker-Franklin D, Franklin EC (1980) Elastase-type proteases on the surface of human blood monocytes: possible role in amyloid formation. J Immunol 125:175–180
40. Levin M, Franklin EC, Frangione B, Pras M (1972) The amino acid sequence of a major nonimmunoglobulin component of some amyloid fibrils. J Clin Invest 51:2773–2776
41. Lovat LB, Booth SE, Booth DR, Madhoo S, Holmgren G, Hawkins PN, Soutar AK, Pepys MB (1995) Apolipoprotein E4 genotype is not a risk factor for systemic AA amyloidosis or familial amyloid polyneuropathy. Amyloid 2:163–166
42. Magnus JH, Stenstad T (1997) Proteoglycans and the extracellular matrix in amyloidosis. Amyloid 4:121–134
43. Malle E, Steinmetz A, Raynes JG (1993) Serum amyloid A (SAA): an acute phase protein and apolipoprotein. Atherosclerosis 102:131–146

44. Mambule C, Ando Y, Anan I, Holmgren G, Sandgren O, Stigbrandt T, Tashima K, Suhr OB (2000) Enhancement of AA-amyloid formation in mice by transthyretin amyloid fragments and polyethylene glycol. Biochim Biophys Acta 1474:331–336
45. McCubbin WD, Kay CM, Narindrasorasak S, Kisilevsky R (1988) Circular-dichroism studies on two murine serum amyloid A proteins. Biochem J 256:775–783
46. Migita K, Kawabe Y, Tominaga M, Origuchi T, Aoyagi T, Eguchi K (1998) Serum amyloid A protein induces production of matrix metalloproteinases by human synovial fibroblasts. Lab Invest 78:535–539
47. Mitchell TI, Jeffrey JJ, Palmiter RD, Brinckerhoff CE (1993) The acute phase reactant serum amyloid A (SAA3) is a novel substrate for degradation by the metalloproteinases collagenase and stromelysin. Biochim Biophys Acta 1156:245–254
48. Moriguchi M, Terai C, Koseki Y, Uesato M, Nakajima A, Inada S, Nishinarita M, Uchida S, Nakajima A, Kim SY, Chen CL, Kamatani N (1999) Influence of genotypes at SAA1 and SAA2 loci on the development and the length of latent period of secondary AA-amyloidosis in patients with rheumatoid arthritis. Hum Genet 105:360–366
49. Moriguchi M, Terai C, Koseki Y, Kaneko H, Uesato M, Nishikawa T, Kamatani N (2001) Genotypes at SAA1 locus correlate with the clinical severity of AA-amyloidosis. Amyloid 8:115–120
50. Motoyama T, Honma T, Watanabe H, Honma S, Kumanishi T, Abe S (1993) Interleukin 6-producing malignant mesothelioma. Virchows Arch [B] 64:367–372
51. Müller D, Roessner A, Röcken C (2000) Distribution pattern of matrix metalloproteinases (MMP-1, -2, -3, and -9), tissue inhibitors of matrix metalloproteinases (TIMP-1 and -2), and α2-macroglobulin in cases of generalized AA- and AL amyloidosis. Virchows Arch 437:521–527
52. Okuda Y, Yamada T, Takasugi K, Takeda M, Nanba S, Onishi M, Miyamoto T, Inoue Y (1999) Serum amyloid A (SAA) 1, SAA 2 and apolipoprotein E isotype frequencies in rheumatoid arthritis patients with AA amyloidosis. Ryumachi 39:3–10
53. Parks WC, Mecham RP (1998) Matrix metalloproteinases. Academic Press, San Diego
54. Pepys MB, Booth DR, Hutchinson WL, Gallimore JR, Collins PM, Hohenester E (1997) Amyloid P component. A critical review. Amyloid 4:274–295
55. Prelli F, Pras M, Frangione B (1987) Degradation and deposition of amyloid AA fibrils are tissue specific. Biochemistry 26:8251–8256
56. Prelli F, Pras M, Shtrasburg S, Frangione B (1991) Characterization of high molecular weight amyloid A proteins. Scand J Immunol 33:783–786
57. Roertgen KE, Johnson KH (1996) Amyloidosis. In: Fairbrother A, Locke L, Hoff GL (eds) Noninfectious diseases of wildlife. Iowa State Press, Ames
58. Röcken C, Kisilevsky R (1997) Binding and endocytosis of murine high density lipoprotein from healthy (HDL) and inflamed donors (HDL_{SAA}) by murine macrophages in vitro. A light- and electronmicroscopic investigation. Amyloid 4:259–273
59. Röcken C, Schwotzer E, Linke RP, Saeger W (1996) The classification of amyloid deposits in clinicopathological practice. Histopathology 29:325–335
60. Röcken C, Radun D, Glasbrenner B, Malfertheiner P, Roessner A (1999) Generalized AA-amyloidosis in a 58-year-old Caucasian woman with an 18-month history of gastrointestinal tuberculosis. Virchows Arch 434:95–100
61. Röcken C, Wieker K, Grote HJ, Müller G, Franke A, Roessner A (2000) Rosai-Dorfman disease and generalized AA amyloidosis. A case report. Hum Pathol 31:621–624
62. Röcken C, Stix B, Brömme D, Ansorge S, Roessner A, Bühling F (2001) A putative role for cathepsin K in degradation of AA and AL amyloidosis. Am J Pathol 158:1029–1038
63. Selkoe DJ (2001) Alzheimer's disease: genes, proteins, and therapy. Physiol Rev 81:741–766
64. Shephard EG, de Beer FC, de Beer MC, Jeenah MS, Coetzee GA, van der Westhuyzen DR (1987) Neutrophil association and degradation of normal and acute-phase high-density lipoprotein 3. Biochem J 248:919–926
65. Silverman SL, Cathcart ES, Skinner M, Cohen AS (1982) The degradation of serum amyloid A protein by activated polymorphonuclear leucocytes: participation of granulocytic elastase. Immunol 46:737–744
66. Sipe JD, Cohen AS (2000) History of the amyloid fibril. J Struct Biol 130:88–98
67. Sipe JD, Carreras I, Gonnerman WA, Cathcart ES, de Beer MC, de Beer FC (1993) Characterization of the inbred CE/J mouse strain as amyloid resistant. Am J Pathol 143:1480–1485
68. Skogen B, Natvig JB, Borresen AL, Berg K (1980) Degradation of amyloid-related serum protein SAA by a component present in rabbit and human serum. Scand J Immunol 11:643–648
69. Skogen B, Thorsteinsson L, Natvig JB (1980) Degradation of protein SAA to an AA-like fragment by enzymes of monocytic origin. Scand J Immunol 11:533–540
70. So A, Chamot AM, Péclat V, Gerster J-C (1999) Serum MMP-3 in rheumatoid arthritis: correlation with systemic inflammation but not with erosive status. Rheumatology 38:407–410
71. Stix B, Kähne T, Sletten K, Raynes J, Roessner A, Röcken C (2001) Proteolysis of AA amyloid fibril proteins by matrix metalloproteinases-1, -2, and -3. Am J Pathol 159:561–570
72. Stone PJ, Campistol JM, Abraham CR, Rodgers O, Shirahama TS, Skinner M (1993) Neutrophil proteases associated with amyloid fibrils. Biochem Biophys Res Commun 197:130–136
73. Strege RJ, Saeger W, Linke RP (1998) Diagnosis and immunohistochemical classification of systemic amyloidoses. Report of 43 cases in an unselected autopsy series. Virchows Arch 433:19–27
74. Tape C, Tan R, Nesheim M, Kisilevsky R (1988) Direct evidence for circulating apoSAA as the precursor of tissue AA amyloid deposits. Scand J Immunol 28:317–324
75. Thornalley PJ (1998) Cell activation by glycated proteins. AGE receptors, receptor recognition factors and functional classification of AGEs. Cell Mol Biol 44:1013–1023
76. Togashi S, Lim SK, Kawano H, Ito S, Ishihara T, Okada Y, Nakano S, Kinoshita T, Horie K, Episkopou V, Gottesman ME, Costantini F, Shimada K, Maeda S (1997) Serum amyloid P component enhances induction of murine amyloidosis. Lab Invest 77:525–531
77. Uhlar CM, Whitehead AS (1999) Serum amyloid A, the major vertebrate acute-phase reactant. Eur J Biochem 265:501–523
78. Usui I, Kawano H, Ito S, Hamada Y, Ishihara T, Maeda S (2001) Homozygous serum amyloid P component-deficiency does not enhance regression of AA amyloid deposits. Amyloid 8:101–104
79. Westermark GT, Westermark P, Sletten K (1987) Amyloid fibril protein AA. Characterization of uncommon subspecies from a patient with rheumatoid arthritis. Lab Invest 57:57–64
80. Westermark GT, Sletten K, Westermark P (1989) Massive vascular AA-amyloidosis: a histologically and biochemically distinctive subtype of reactive systemic amyloidosis. Scand J Immunol 30:605–613
81. Westermark GT, Engström U, Westermark P (1992) The N-terminal segment of protein AA determines its fibrillogenic property. Biochem Biophys Res Commun 182:27–33
82. Woodrow SI, Stewart RJ, Kisilevsky R, Gore J, Young ID (1999) Experimental AA amyloidogenesis is associated with differential expression of extracellular matrix genes. Amyloid 6:22–30
83. Wright JR, Ozdemir AI, Matsuzaki M, Binette P, Calkins E (1972) Amyloid resorption: possible role of multinucleated giant cells. The apparent failure of penicillamine treatment. Johns Hopkins Med J 130:278–288
84. Yakar S, Kaplan B, Livneh A, Martin B, Miura K, Ali-Khan Z, Shtrasburg S, Pras M (1994) Direct evidence for SAA deposition in tissues during murine amyloidogenesis. Scand J Immunol 40:653–658

85. Yamada T, Kluve-Beckerman B, Liepnieks JJ, Benson MD (1994) Fibril formation from recombinant human serum amyloid A. Biochim Biophys Acta 1226:323–329
86. Yamada T, Kluve-Beckerman B, Liepnieks JJ, Benson MD (1995) In vitro degradation of serum amyloid A by cathepsin D and other acid proteases: possible protection against amyloid fibril formation. Scand J Immunol 41:570–574
87. Yamada T, Liepnieks JJ, Kluve-Beckerman B, Benson MD (1995) Cathepsin B generates the most common form of amyloid A (76 residues) as a degradation product from serum amyloid A. Scand J Immunol 41:94–97
88. Yamada T, Liepnieks J, Benson MD, Kluve-Beckerman B (1996) Accelerated amyloid deposition in mice treated with the aspartic protease inhibitor, pepstatin. J Immunol 157:901–907
89. Yan SD, Zhu HJ, Zhu AP, Golabek A, Du H, Roher A, Yu J, Soto C, Schmidt AM, Stern D, Kindy M (2000) Receptor-dependent cell stress and amyloid accumulation in systemic amyloidosis. Nat Med 6:643–651
90. Zschiesche W, Jakob W (1989) Pathology of animal amyloidoses. Pharmacol Ther 41:49–83

Virchows Arch (2002) 440:123–127
DOI 10.1007/s004280100525

ORIGINAL ARTICLE

Kanji Mori · Tokuhiro Chano · Ryoji Kushima
Sinsuke Hukuda · Hidetoshi Okabe

Expression of E-cadherin in chordomas: diagnostic marker and possible role of tumor cell affinity

Received: 31 January 2001 / Accepted: 26 July 2001 / Published online: 21 September 2001
© Springer-Verlag 2001

Abstract Chordoma is a relatively rare malignant bone tumor thought to arise from the remnants of the fetal notochord. Chordomas express epithelial cell markers such as cytokeratin and epithelial membrane antigen (EMA), which strongly suggests that the tumor cells grow via the mechanism of epithelial characterized cell–cell interactions. However, there are no known reports that have studied epithelial characterized cell-adhesion molecules such as E-cadherin or epithelial cell adhesion molecule (Ep-CAM) in chordomas. An immunohistochemical investigation was performed in seven cases of chordoma to determine the expression of pan-cytokeratin, Ep-CAM, and E-cadherin. Histological specimens showed the typical appearance of conventional chordoma but for two cases of chondroid chordoma. Cytokeratin was constantly expressed in conventional chordomas, but it was detected among a few cells with physaliphorous appearance in chondroid chordoma cases. Although no Ep-CAM expression was noted, E-cadherin was detected in most chordoma cells irrespective of histological subtypes. The expression of E-cadherin was negative among chondrosarcoma cells in this study as previously reported, and thus constant E-cadherin expression of chordoma cells suggests a role as a useful diagnostic marker to distinguish chondroid chordoma from chondrosarcoma. Furthermore, we speculate that E-cadherin may play a role in tumor cell adhesion and is also involved with histological and clinical features in chordomas.

Keywords Chordoma · E-cadherin · Immunohistochemical study · Diagnostic marker

K. Mori (✉) · S. Hukuda
Department of Orthopedic Surgery,
Shiga University of Medical Science,
Tsukinowa-cho, Seta, Otsu, Shiga, 520-2192, Japan
e-mail: kanchi@belle.shiga-med.ac.jp
Tel.: +81-77-5482252, Fax: +81-77-5482254

T. Chano · R. Kushima · H. Okabe
Department of Clinical Laboratory Medicine,
Shiga University of Medical Science,
Tsukinowa-cho, Seta, Otsu, Shiga, 520-2192, Japan

Introduction

Chordoma is a non-epithelial neoplasm with characteristic histological appearance resembling the fetal notochord. Except for the chondroid variant, the tumor cells tend to have tight cohesion without intervening collagen matrix and form cord- or sheet-like nests. Ultrastructurally, the manner of cellular cohesion resembles that of epithelial tumors, and desmosomes are found at these cellular junctions, occasionally in abundance [13]. Since chordoma is known to have several epithelial markers, such as epithelial membrane antigen (EMA) and cytokeratin, it seems possible that epithelial adhesion molecule is involved in the cellular cohesion. However, epithelial adhesion molecules have not been examined in the chordoma, and their significance in the differential diagnosis has not yet been established.

There are two major adhesion molecules specifically involved in the epithelial adhesion. E-cadherin is a Ca^{2+}-dependent transmembrane glycoprotein that belongs to the cadherin superfamily of cell-adhesion molecules. Epithelial cell adhesion molecule (Ep-CAM) mediates Ca^{2+}-independent homotypic cell–cell adhesions. Previous studies have shown that these molecules are involved in the phenotype and morphogenesis of various tissues [4, 5, 8, 9].

In this study, we have analyzed the role of these two epithelial adhesion molecules in seven cases of chordomas, including two of chondroid type, to evaluate the usefulness of these adhesion molecules as immunohistochemical markers for differential diagnosis.

Materials and methods

Seven cases of chordomas, in patients who received surgery at Shiga University of Medical Science from 1988 to 2000, were employed in this study. The mean age at time of operation was 51.4 years old (range 21–75 years). Four patients were male and three were female. Two chordomas were localized in the sacrum, one was in the cervical spine, and four were intracranial. Two

(cases 6 and 7) of the intracranial lesions were chondroid chordomas, and the others were conventional chordomas. The clinicopathological features of these cases are summarized in Table 1. A total of 11 lesions were surgically resected from these seven cases and investigated histologically. The lesions were fixed in 10% buffered formalin and embedded in paraffin, routinely processed for histopathological examination, and stained with hematoxylin and eosin. Immunohistochemical staining was also performed on the paraffin-embedded tissue specimens. Monoclonal antibodies specific for pan-cytokeratin (AE1/AE3, 1:50 dilution; Dako, Carpinteria, Calif.), Ep-CAM (Ber-EP4, 1:200 dilution; Dako), and E-cadherin (10 µg/ml, Takara Biomedicals, Shiga, Japan) were employed. Sections 5-µm thick were deparaffinized, and endogenous peroxidase activity was blocked using 0.3% hydrogen peroxidase in methanol. The sections were then incubated with the primary monoclonal antibodies at 4°C overnight, followed by incubation with a biotin-labeled secondary antibody. Finally, they were subjected to peroxidase conjugated with streptavidin using a commercially available kit (Universal quick stain kit, Dako). Peroxidase activity was detected using chromogen diaminobenzidine (Dako). A high temperature antigen unmasking pre-treatment using autoclave was utilized for the immunostaining of E-cadherin, and enzymatic pre-digestion with trypsin was performed for the others.

In addition, E-cadherin expression was analyzed in six cases of chondroid tumors (one chondrosarcoma, three enchondromas, and two osteochondromas) to compare the difference between chondroid chordomas and the other chondroid lesions.

Results

In five of the seven cases, the tumors had histologically formed lobular architectures and extracellular mucoid stroma. The tumor cells were connected in a column- or sheet-like arrangement and had vacuolated (physaliphorous) cytoplasms with mild nuclear pleomorphism (Fig. 1a). S-100 was revealed in the majority of the tumor cells in these cases. EMA and cytokeratin were expressed strongly in the majority of the tumor cells in five conventional chordomas (Fig. 1b). Thus, all the lesions of these five cases were revealed to be conventional chordomas. The specimens of cases 6 and 7 showed a prominent chondroid matrix, resembling chondrosarcoma, with cells situated in small lacunae within a stroma more cartilaginous than mucoid (Fig. 2a). S-100 and cytokeratin were expressed in physaliphorous tumor cells of these cases, but these molecules were revealed in few of the tumor cells in the areas of abortive physaliphorous appearance (Fig. 2b). These tumors were confined to the cranial cavity and the tumor did not have direct connection with upper respiratory mucosa or minor salivary gland. Accordingly, sarcomatoid change of the epithelial tumor such as mixed tumor was ruled out and the tumors were diagnosed as chondroid chordomas. As a result of metastasis (case 7), the tumors changed the histological appearance into conventional chordoma. E-cadherin was constantly expressed in chordoma cells, especially at the intercellular adhesion sites (Fig. 1c) in the conventional type. This adhesion molecule was revealed in the majority of the tumor cells (Fig. 2c) in the chondroid variant and even in the areas where keratin-positive cells were quite few. Ep-CAM was not demonstrated in all cases.

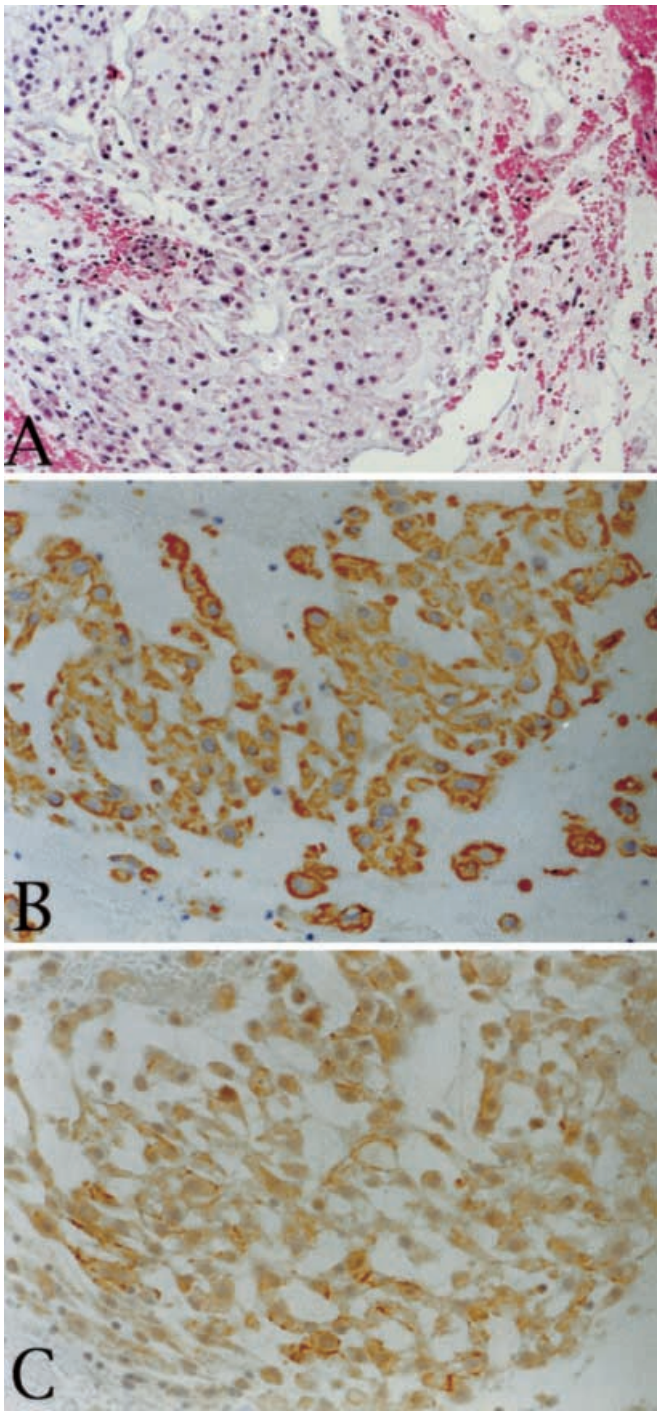

Fig. 1 **a** Typical characteristic findings of a conventional chordoma. A lobular architecture, mucoid matrix, and physaliphorous cytoplasm were confirmed (hematoxylin and eosin, original magnification, ×50). **b** Immunohistochemical study of cytokeratin in conventional chordoma. Positive strong staining was found in the tumor cells (original magnification, ×100). **c** Immunohistochemical study of E-cadherin in conventional chordoma. Expression was found in the tumor cells, especially at the inter-cellular adhesion sites (original magnification, ×100)

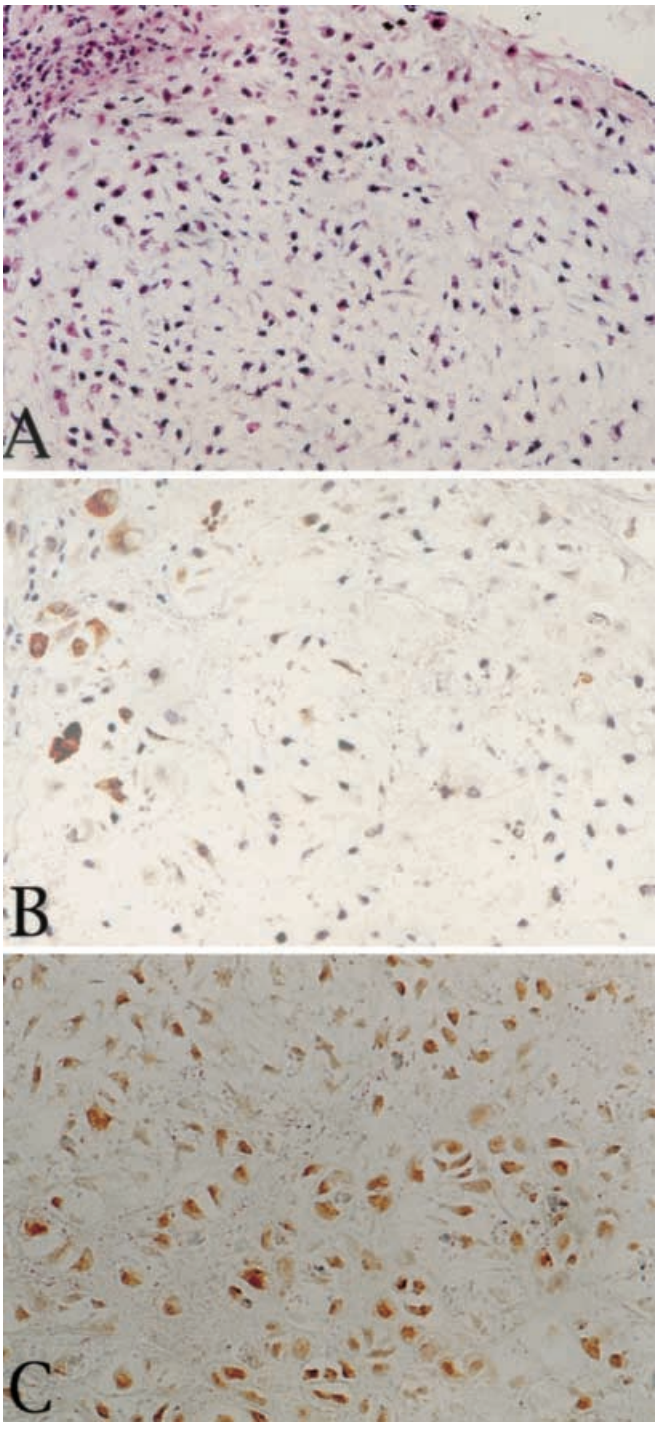

Fig. 2 **a** Histological findings of a chondroid chordoma. The tumor showed a prominent chondroid matrix, resembling chondrosarcoma, with cells situated in small lacunae within a stroma more cartilaginous than mucoid (hematoxylin and eosin, original magnification, ×50). **b** Immunohistochemical study of cytokeratin in chondroid chordoma. Cytokeratin was only detected in several physaliphorous cells (hematoxylin and eosin, original magnification, ×75). **c** Immunohistochemical study of E-cadherin in chondroid chordoma. Almost all tumor cells expressed E-cadherin with or without a physaliphorous appearance (original magnification, ×100)

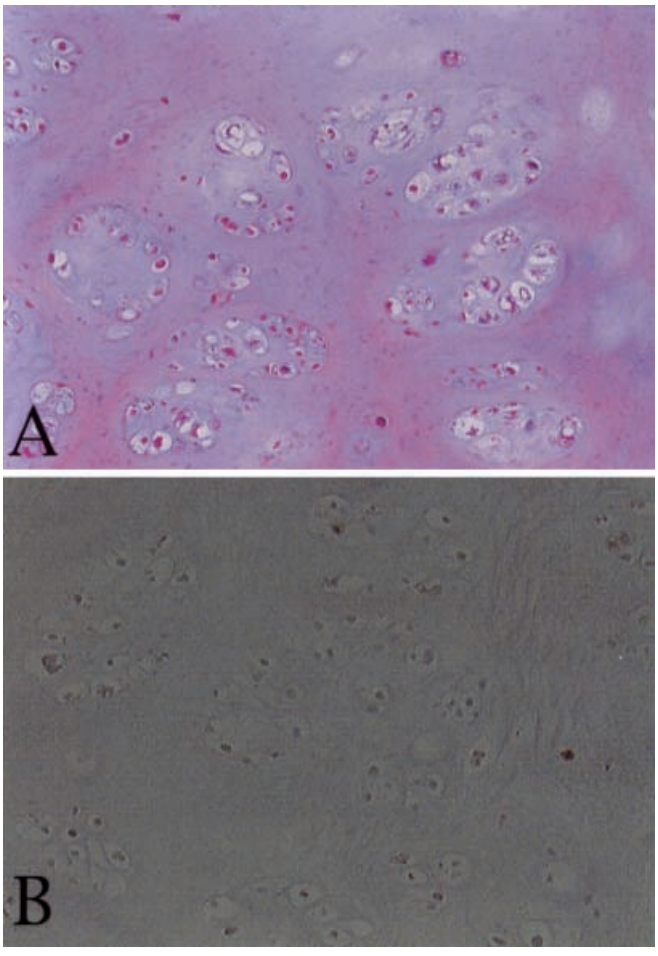

Fig. 3 **a** Histological findings of a chondrosarcoma. The tumor showed a prominent chondroid matrix and cartilaginous cells with mildly nuclear atypia (hematoxylin and eosin, original magnification, ×50). **b** Immunohistochemical study of E-cadherin in chondrosarcoma. No E-cadherin expression is observed (original magnification, ×75)

Regarding E-cadherin expression in the other six cases of chondroid lesions, this type of adhesion molecule was never observed (Fig. 3).

Discussion

Chordomas occasionally occur in children and young adults, although they are uncommon before the age of 30 years, and most patients are in their fifth to seventh decades of life. There is an approximate 2 to 1 male to female ratio. Distant metastasis is rare in this tumor, but it frequently recurs locally after the excision [2, 7, 15]. The cases in the present study had clinical features consistent with these known characteristics. Some patients die as a result of their locally aggressive nature. Certain diagnostic markers have been established to differentiate chordoma from other tumors, and several immunohistochemical analyses have been conducted to support the epithelial characteristics. Although chordomas arise in

the carniospinal axis, some in the spheno-occipital region, particularly those exhibiting a chondroid matrix, resemble chondrosarcoma. Differential diagnosis such chondroid chordoma from chondrosarcoma is difficult because immunoreactivity of EMA and/or cytokeratin in the individual tumor cells is not as constant as in the conventional type [3]. Epithelial tumor cells frequently express either one or both of two major epithelial adhesion molecules – Ep-CAM and E-cadherin. These markers were occasionally revealed in the epithelial neoplasms with difficult to detect EMA or cytokeratin. Accordingly, it is worthwhile to examine the diagnostic value of these two epithelial adhesion molecules in chordomas, and this study examined them in seven cases of chordomas including the chondroid variant.

E-cadherin is the best-characterized cell adhesion molecule of the cadherin superfamily and is a Ca^{2+}-dependent transmembrane glycoprotein [10]. Through their homophilic binding interactions, cadherins play an important role in cell-sorting mechanisms, offering adhesion specificities that govern tissue integrity [14]. Previous studies have shown that this molecule may regulate the invasive phenotype of neoplastic cells [1, 5, 9]. Ep-CAM mediates Ca^{2+}-independent homotypic cell–cell adhesions, and formation of Ep-CAM-mediated adhesions has a negative regulatory effect on adhesions mediated by classic cadherins, which may have strong effects on the differentiation and growth of epithelial cells. Indeed, in vivo expression of Ep-CAM is related to increased epithelial proliferation and negatively correlates with cell differentiation. A regulatory function of Ep-CAM in the morphogenesis of epithelial tissue has been demonstrated for a number of tissues [4, 8].

Our analysis revealed a constant expression of E-cadherin in all of the lesions despite its histological variations, although Ep-CAM expression was absent. These results suggest that the cellular adhesion of chordomas is dominantly mediated by a Ca^{2+}-dependent mechanism, and this character may organize the morphological constructs, such as intra-tumorous calcification, noted occasionally in chordomas. Previous immunohistochemical analysis of human embryos revealed expression of E-cadherin in the embryos younger than 9 weeks, although it disappeared in notochords from specimens older than 10–11 weeks [6]. Since chordoma is speculated to originate from the remnants of the embryonic notochord, expression of E-cadherin in chordoma cells seems to simulate that of early to middle embryonic notochordal cells.

This is the first report that demonstrates the expression of E-cadherin in chordomas and suggests its possible involvement with the cellular interactions in chordoma cells. Furthermore, most interestingly, constant E-cadherin expression was observed in chordoma cells of all cases, even in the cases of chondroid chordoma. E-cadherin expression is demonstrated with a diffusely cytoplasmic staining pattern in chondroid chordomas. For an explanation of this result, it is deduced that the molecule is not able to play a role of cell-adhesion molecule in this subtype, although E-cadherin is produced enough to be detected immunohistochemically. Thus, in this subtype, chondroid change could probably be obtained because of the result of insufficient role of E-cadherin. Indeed, Sormunen et al. demonstrated that E-cadherin was lost from the membranes and stained with only occasional weak intracellular staining in the case of high-grade ductal carcinoma of the breast [12]. In this study, we also confirmed the negative expression of E-cadherin in chondroid tumors such as chondrosarcoma, osteochondromas, and enchondromas, but not for chondroid chordoma. The result is consistent with a previous report that demonstrated completely negative expression of E-cadherin in chondrosarcomas [11], which are difficult to distinguish from chondroid chordoma. Thus, our findings suggest that E-cadherin is a practically useful diagnostic marker to differentiate chondroid chordoma from chondrosarcoma.

Accumulating knowledge regarding these molecular events is crucial to improving our understanding of the biological characteristics of chordomas. Further investigation is required because of the small numbers studied here. Understanding E-cadherin expression in chordoma cells will give further insight into the mechanism of cell adhesion and growth. Thus, such studies may suggest involvement with histological variations and may elucidate the possible roles of the clinical features, i.e. recurrence and/or metastasis, of chordomas.

References

1. Behrens J, Mareel MM, Van Roy FM, Birchmeier W (1989) Dissecting tumor cell invasion: epithelial cells acquire invasive properties after the loss of uvomorulin-mediated cell–cell adhesion. J Cell Biol 108:2435–2347
2. Bjornsson J, Wold LE, Ebersold MJ, Laws ER (1993) Chordoma of the mobile spine. A clinicopathologic analysis of 40 patients. Cancer 71:735–740
3. Burger PC, Scheithauer BW (1994) Tumor of the central nerve system. In: Atlas of tumor pathology, 3rd series. Armed Forces Institute of Pathology, Washington DC, pp 303–306
4. de Boer CJ, van Krieken JH, Janssen-van Rhijn CM, Litvinov SV (1999) Expression of Ep-CAM in normal, regenerating, metaplastic, and neoplastic liver. J Pathol 188:201–206
5. Fahraeus R, Chen W, Trivedi P, Klein G, Obrink B (1992) Decreased expression of E-cadherin and increased invasive capacity in EBV-LMP-transfected human epithelial and murine adenocartinoma cells. Int J Cancer 52:834–838
6. Gotz W, Kasper M, Fischer G, Herken R (1995) Intermediate filament typing of the human embryonic and fetal notochord. Cell Tissue Res 280:455–462
7. Huvos AG (1991) Bone tumors: diagnosis, treatment, and prognosis, 2nd edn. Saunders, Philadelphia, pp 599–624
8. Litvinov SV, van Driel W, van Rhijn CM, Bakker HA, van Krieken JH, Fleuren GJ, Warnaar SO (1996) Expression of Ep-CAM in cervical squamous epithelia correlates with an increased proliferation and the disappearance of markers for terminal differentiation. Am J Pathol 148:865–875
9. Mareel MM, Behrens J, Birchmeier W, De Bruyne GK, Vleminckx K, Hoogewus A, Fiers WC, Van Roy F (1991) Down-regulation of E-cadherin expression in Madin Darby canine (MDCK) cell inside tumors of nude mice. Int J Cancer 47:922–928

10. Ohsugi M, Larue L, Schwartz H, Kemler R (1997) Cell-junctional and cytoskeletal organization in mouse blastocysts lacking E-cadherin. Dev Biol 185:261–271
11. Sato H, Hasegawa T, Abe Y, Sakai H, Hirohashi S (1999) Expression of E-cadherin in bone and soft tissue sarcomas: a possible role in epitherial differentiation. Hum Pathol 30:1344–1349
12. Sormunen RT, Leong AS, Vaaraniemi JP, Fernardo SS, Eskelinen SM (1999) Immunolocalization of the fodrin, E-cadherin, and beta-catenin adhesion complex in infiltrating ductal carcinoma of the breast-comparison with an in vitro model. J Pathol 187:416–423
13. Spjut HJ, Luse SA (1964) Chordoma: an electron microscopic study. Cancer 17:643–656
14. Takeichi M (1991) Cadherin cell adhesion receptor as a morphogenic regulator. Science 251:1451–1455
15. Unni KK (1986) Bone tumors: general aspects and data on 8,542 cases. C. Thomas, Springfield, III, pp 379–393

Virchows Arch (2002) 440:128–133
DOI 10.1007/s00428-001-0551-3

ORIGINAL ARTICLE

Peter J. Barth · Schokufe Ebrahimsade
Achim Hellinger · Roland Moll
Annette Ramaswamy

CD34+ fibrocytes in neoplastic and inflammatory pancreatic lesions

Received: 29 June 2001 / Accepted: 5 September 2001 / Published online: 24 October 2001
© Springer-Verlag 2001

Abstract Besides its function as a matrix-producing cell, the CD34+ fibrocyte has been reported to be an antigen-presenting cell capable of priming naive T cells in situ. Therefore, it has been claimed that the CD34+ fibrocyte may play an important role in host response to tissue damage. The objective of the present study was to analyze the presence and distribution of CD34+ fibrocytes and smooth muscle actin (SMA) reactive myofibroblasts in relation to the underlying pancreatic disease. We investigated a total of 12 pancreatic adenocarcinomas, 7 endocrine tumors of the pancreas, and 8 cases of chronic pancreatitis; in 11 cases, normal pancreatic tissue was available. The stroma of normal pancreatic tissue harbored diffusely scattered CD34+ fibrocytes. Chronic pancreatitis was characterized by an increased number of stromal CD34+ fibrocytes paralleled by a gain of SMA reactive myofibroblasts which were not observed in the normal pancreatic stroma. The stroma of pancreatic ductal adenocarcinomas and endocrine tumors was devoid of CD34+ fibrocytes or showed at least a focal loss of this cell type, whereas SMA reactive myofibroblasts were detected in both endocrine tumors and adenocarcinomas. We conclude that detection of CD34+ fibrocytes may constitute an adjunctive tool in distinguishing chronic pancreatitis from ductal adenocarcinoma since the absence of this cell population strongly favors a neoplastic process. Moreover, CD34+ fibrocytes and myofibroblasts appear to be involved in stromal remodeling associated with chronic pancreatitis and ductal adenocarcinoma.

Keywords Fibrocytes · Myofibroblast · Pancreas · Pancreatitis · Adenocarcinoma · Endocrine tumor

P.J. Barth (✉) · S. Ebrahimsade · R. Moll · A. Ramaswamy
Institute of Pathology, Philipps University Marburg,
Baldingerstraße, 35033 Marburg, Germany
e-mail: barthp@post.med.uni-marburg.de
Tel.: +49-64212862465, Fax: +49-64212865640

A. Hellinger
Department of Surgery, Philipps University Marburg,
Marburg, Germany

Introduction

CD34+ fibrocytes have been detected in normal skin [16], normal breast tissue [4, 20, 24], and in various cutaneous [5, 6, 9, 10, 23] and mesenchymal tumors [13, 17, 19, 20, 21, 22]. To date, the origin of this cell population remains enigmatic, but experimental studies support the assumption that CD34+ fibrocytes derive from myeloid precursors [2]. They can be found in the peripheral blood and invade sites of tissue damage and are capable of connective tissue matrix synthesis [2]. Besides its function as a matrix-producing cell, the CD34+ fibrocyte is a potent antigen-presenting cell capable of priming naive T cells in situ [3]. Therefore, it has been claimed that the CD34+ fibrocyte may play an important role in host response to tissue damage of whatever cause and in specific immune-mediated host defense against invading tumor cells [8].

The occurrence of CD34+ fibrocytes in the peritumoral stroma of skin tumors has been considered to be of diagnostic significance in distinguishing basal cell carcinoma from benign skin appendage tumors, such as trichoepithelioma and its variants [5, 6, 9, 10, 23]. In these studies, the absence of CD34+ fibrocytes in the tumor-associated stroma favors the diagnosis of basal cell carcinoma and vice versa. Similar results have been reported in colon cancer: normal colonic stroma harbors CD34+ fibrocytes, whereas this cell population is absent from the stroma of invasive colon cancer. However, the tumor-associated desmoplastic stroma is characterized by the presence of smooth muscle actin (SMA) reactive myofibroblasts [15]. Recently, a solitary fibrous tumor of the pancreas with CD34+ fibrocytes was described [13], but the pertinent literature yields no information concerning the occurrence and distribution of CD34+ fibrocytes in the pancreas and benign and malignant lesions of the pancreatic parenchyma.

The present study was undertaken to investigate this topic with special reference to pancreatitis and ductal pancreatic carcinoma since the differential diagnosis of these lesions is of clinical significance and may cause significant problems to the surgical pathologist.

Table 1 Epidemiological data of patients with chronic pancreatitis

Case no.	Age (years)	Sex	Presumed cause of pancreatitis
CP1	47	Male	Alcoholism
CP2	58	Female	Unknown
CP3	59	Male	Obstructive, pancreatic acinar cell carcinoma
CP4	61	Male	Obstructive, main pancreatic duct stenosis*
CP5	77	Male	Obstructive
CP6	76	Male	Obstructive, carcinoma of the ampulla of Vater
CP7	74	Female	Obstructive, main pancreatic duct stenosis*
CP8	76	Male	Obstructive, choledocholithiasis

* Main pancreatic duct stenosis proven by means of endoscopic retrograde pancreatography

Table 2 Data of patients with ductal adenocarcinoma

Case no.	Age (years)	Sex	Grading	TNM classification*
DA1	45	Male	G1	pT3 pN0 M0
DA2	56	Female	G2	pT3 pN0 M0
DA3	85	Female	G2	pT3 pN0 M0
DA4	68	Male	G2	pT3 pN0 M0
DA5	70	Male	G2	pT3 pN0 M0
DA6	62	Male	G2	pT3 pN0 M0
DA7	33	Male	G3	pT3 pN0 M0
DA8	69	Male	G2	pT3 pN0 M0
DA9	62	Male	G2	pT4 pN1b M0
DA10	54	Female	G2	pT3 pN1a M0
DA11	67	Male	G2	pT3 pN1a M0
DA12	76	Female	G2	pT2 pN1b M0

* UICC, 4th edn, 1997

Table 3 Data of patients with pancreatic endocrine tumors. *d.n.a.* data not available

Case no.	Age (years)	Sex	Functional type	Size (cm)	Metastasis	Follow-up (years)
ET1	48	Male	Insulinoma	4.0	–	7
ET2	86	Female	Insulinoma	1.2	–	6
ET3	68	Female	Insulinoma	3.5	–	6
ET4	57	Male	Gastrinoma	4.0	–	6
ET5	50	Male	Insulinoma	1.6	–	4
ET6	40	Male	Insulinoma	d.n.a	–	4
ET7	50	Female	Glucagonoma	4.5	+ (Liver)	0.5

Materials and methods

The present study comprises 20 patients who underwent classic Whipple resection or a modified pylorus sparing Whipple procedure. In 12 cases, a ductal adenocarcinoma of the pancreas was diagnosed; in 8 cases the diagnosis of chronic pancreatitis was rendered. The epidemiological data of patients with chronic pancreatitis and ductal adenocarcinoma are summarized in Table 1 and Table 2, respectively. Histologically, the cases of chronic pancreatitis, mostly obstructive in origin, were characterized by stromal fibrosis associated with a mild to moderately interstitial lymphocytic infiltration. Abscess formation or diffuse polymorphonuclear infiltration were not observed; in one case small necroses were found. The presumed cause of chronic pancreatitis is listed in Table 1. Cases of hereditary or auto-immune pancreatitis were not included in the present study.

In 11 of 12 cases with ductal adenocarcinoma, tumor-free pancreatic tissue remotely located from infiltrating carcinoma and devoid of features characteristic of chronic pancreatitis was available and served as normal control.

We additionally investigated a total of seven functionally active differentiated pancreatic endocrine tumors, six of which were treated by enucleation (Table 3). In the remaining case (ET7), a resection of the pancreatic tail was performed. One of the seven patients with an endocrine tumor (ET1) suffered from multiple endocrine neoplasia (MEN) I syndrome, whereas the remaining cases were sporadic endocrine tumors.

After resection or enucleation, the tissues were fixed in a 4% formaldehyde solution and representative tissue blocks were selected. Tissues were embedded in paraffin, cut, and stained with hematoxylin and eosin and Periodic acid–Schiff base for routine purposes.

Immunohistochemistry

Immunohistochemistry was performed using a standard avidin–biotin complex (ABC)-peroxidase method using 3,3'-diaminobenzidine (DAB) as chromogen. CD34 antigen was detected using a monoclonal antibody (QBEND10, Immunotech, Marseille, France) without any tissue pretreatment or dilution of the antibody. SMA was detected using a monoclonal antibody (ASM-1, Progen, Heidelberg, Germany; dilution 1:200) after tissue pretreatment with 0.1% trypsin for 15 min at 37°C.

The number and distribution of stromal $CD34^+$ fibrocytes and SMA reactive myofibroblasts was assessed semi-quantitatively strictly considering that endothelia are also positive for CD34, and SMA reactive cells occur in vessel walls and in periductal myofibroblasts of the pancreas [7].

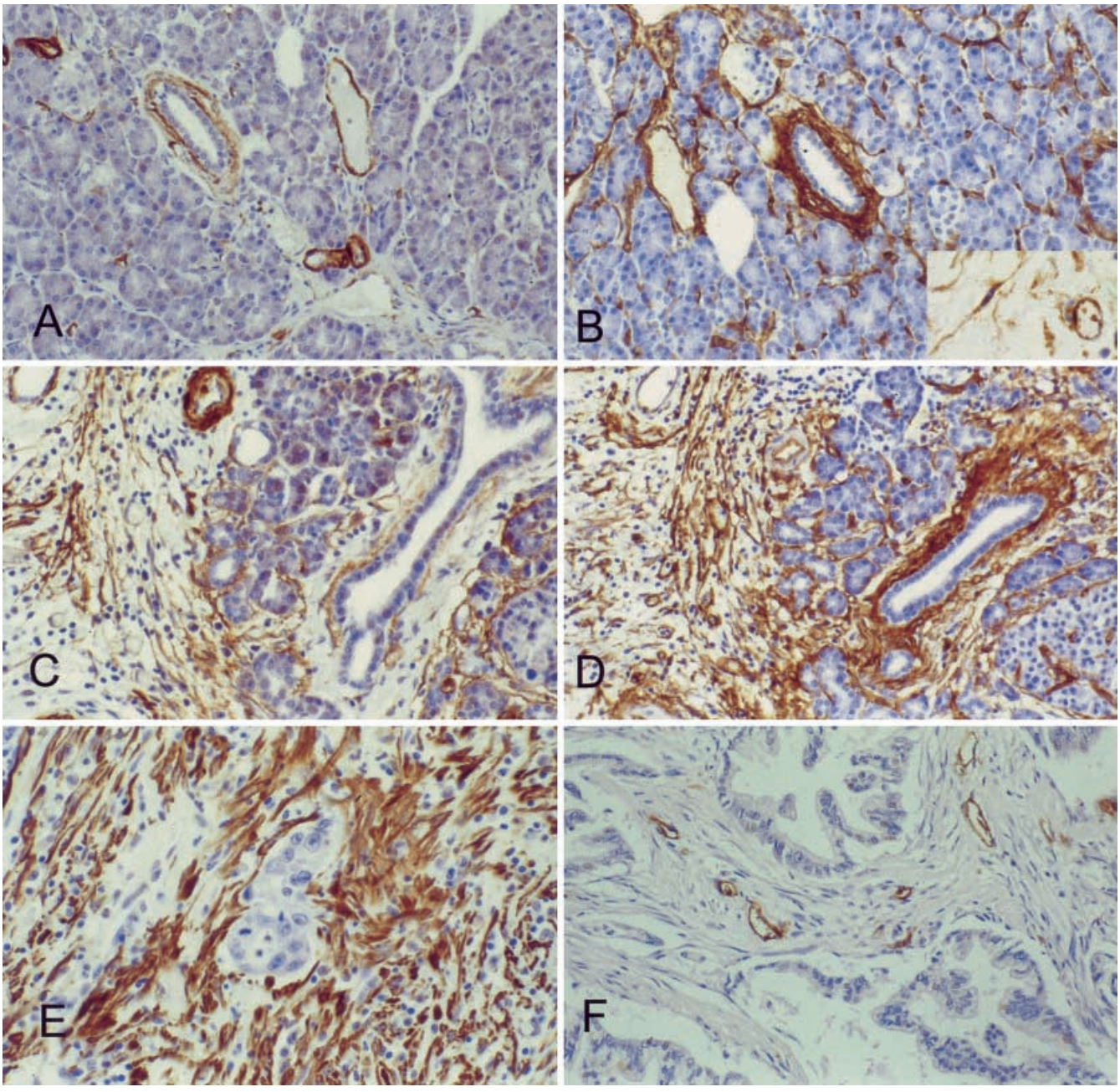

Fig. 1 Normal pancreatic parenchyma harbors few smooth muscle actin (SMA) reactive myofibroblasts surrounding intralobular ducts. SMA is also seen in the walls of arterioles and venules (**a**). $CD34^+$ fibrocytes are characterized by long dendrite-like projections (**b**, *inset*) and encircle acinar, ductal, and vascular structures of the normal pancreas (**b**). In chronic pancreatitis, the numbers of SMA reactive myofibroblasts (**c**) and $CD34^+$ fibrocytes (**d**) appear to be increased. The stroma of ductal adenocarcinoma shows densely packed SMA reactive myofibroblasts (**e**) whereas $CD34^+$ fibrocytes (**f**) are lacking

Results

Normal pancreas

The intra- and extralobular lobular stroma of normal pancreatic tissue was devoid of SMA reactive myofibroblasts except for a few myofibroblasts concentrically surrounding the intralobular ducts (Table 4). SMA staining was also observed in the smooth musculature of muscularized vessels (Fig. 1a). CD34 immunostaining of normal pancreatic tissue disclosed evenly scattered $CD34^+$ fibrocytes encircling the intralobular ducts and acini (Fig. 1b). The $CD34^+$ fibrocytes showed small elongated centrally located nuclei and long slender dendrite-like cytoplasmatic projections intervening with those of neighboring $CD34^+$ fibrocytes forming a loose reticular meshwork. Morphologically $CD34^+$ fibrocytes were clearly distinguishable from CD34-positive endothelial cells (Fig. 1b, inset). The distribution of $CD34^+$ fibrocytes and SMA reactive myofibroblasts showed no significant variation within the examined population (Table 5).

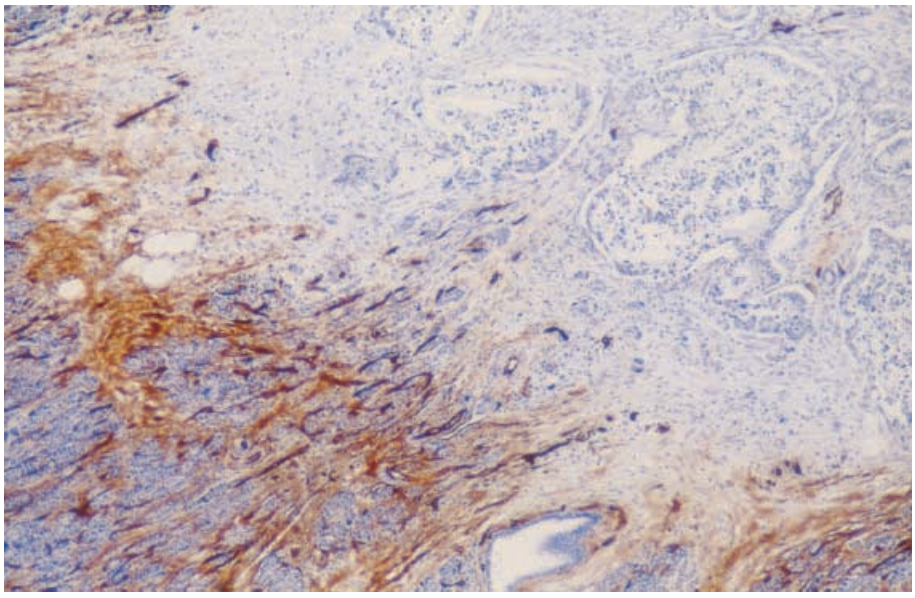

Fig. 2 The interface between tumor-free pancreatic parenchyma (*left* and *lower side*) and ductal adenocarcinoma (*upper right*) is characterized by an abrupt loss of $CD34^+$ fibrocytes. Note positive CD34 staining in intratumoral capillaries which can be well distinguished from the stromal staining due to densely packed $CD34^+$ fibrocytes even at low magnification

Table 4 Distribution of smooth muscle actin (SMA) reactive myofibroblasts in the pancreatic stroma. *0* no SMA reactive myofibroblasts detectable, *0*–+ focal accumulations of SMA reactive myofibroblasts, + diffusely scattered SMA reactive myofibroblasts

Staining score	Normal (*n*=11)	Chronic pancreatitis (*n*=8)	Endocrine tumor (*n*=7)	Adenocarcinoma (*n*=12)
0	11	0	1	0
0–+	0	4	6	0
+	0	4	0	12

Table 5 Distribution of $CD34^+$ fibrocytes in the pancreatic stroma. *0* no $CD34^+$ fibrocytes detectable, *0*–+ focal accumulations of $CD34^+$ fibrocytes, + diffusely scattered $CD34^+$ fibrocytes, ++ diffusely scattered and focally crowded $CD34^+$ fibrocytes

Staining score	Normal (*n*=11)	Chronic pancreatitis (*n*=8)	Endocrine tumor (*n*=7)	Adenocarcinoma (*n*=12)
0	0	0	7	8
0–+	0	0	0	4
+	11	2	0	0
++	0	6	0	0

Chronic pancreatitis

In all cases of chronic pancreatitis, SMA reactive myofibroblasts occurred in the intra- and extralobular parenchyma which, under normal conditions, was devoid of this cell type (Fig. 1c). The distribution of SMA reactive myofibroblasts showed slight variations ranging from focal accumulations to diffusely scattered cells which virtually occupied the whole pancreatic stroma (Table 4). The occurrence of SMA reactive myofibroblasts in chronic pancreatitis was accompanied by an increased number of $CD34^+$ fibrocytes. In most cases investigated (6 of 8), chronic pancreatitis was characterized by an increased number of $CD34^+$ fibrocytes which were predominantly located in areas of diffuse or nodular stromal fibrosis around intralobular ducts and acini (Fig. 1d). Additionally, $CD34^+$ fibrocytes appeared to be increased in number in areas infiltrated by lymphocytes. In areas with predominant stromal edema, $CD34^+$ fibrocytes were less densely arranged, but no areas with complete loss of $CD34^+$ fibrocytes were seen in chronic pancreatitis. In two cases, the distribution of $CD34^+$ fibrocytes was similar to that observed in normal pancreatic parenchyma (Table 5).

Ductal adenocarcinomas

In all cases of ductal adenocarcinoma investigated, SMA reactive myofibroblasts formed thick sheets surrounding the infiltrating tumor cells (Fig. 1e, Table 4). The stroma associated with invasive ductal adenocarcinoma was free of $CD34^+$ fibrocytes in eight cases (Fig. 1f). In the tumor-free pancreatic parenchyma located at the infiltrating border of carcinoma, the $CD34^+$ fibrocytes were increased in number and more densely packed; the transition from tumor-free tissue to invasive

carcinoma was characterized by an abrupt loss of the stromal CD34+ fibrocytes (Fig. 2). Four cases disclosed a subtotal loss of CD34+ fibrocytes with small foci of preserved mophologically normal appearing CD34+ fibrocytes (Table 5).

Pancreatic endocrine tumors

In six of seven endocrine tumors examined, few scattered stromal cells exhibiting a weak immunohistochemical expression of SMA were found (Table 4). CD34+ fibrocytes were completely absent from the stroma of all endocrine tumors investigated, whereas the endothelium of intratumoral vessels showed a normal endothelial expression of CD34 (Table 5).

Discussion

The present study was undertaken in order to analyze the presence and distribution of CD34+ fibrocytes and SMA reactive myofibroblasts in relation to the underlying pancreatic disease. We found that stromal remodeling associated with chronic pancreatitis was characterized by an increased number of stromal CD34+ fibrocytes paralleled by a gain of SMA reactive myofibroblasts which were absent from the normal pancreatic stroma. In contrast, the stroma associated with pancreatic ductal adenocarcinoma and endocrine tumors was devoid of CD34+ fibrocytes in most cases investigated, whereas SMA reactive myofibroblasts were detected in a quantity comparable to that found in chronic pancreatitis.

It has been shown that CD34+ fibrocytes invade areas of tissue damage and take part in matrix repair via collagen synthesis [2]. In the present study, the presumed role of CD34+ fibrocytes in tissue repair was underlined by the fact that the number of stromal CD34+ fibrocytes was found to be increased together with that of SMA reactive myofibroblasts in chronic pancreatitis. Intra- and interlobular proliferation of myofibroblasts mediate fibrogenesis in chronic pancreatitis irrespective of the initiating event. In focal pancreatitis, myofibroblast proliferation plays an important role in the development of duct stenosis and, thus, in further aggravation of the disease process [7]. It remains to be clarified whether SMA reactive myofibroblasts and CD34+ fibrocytes are related in origin. SMA reactive myofibroblasts were also detected in adenocarcinomas and in endocrine tumors, whereas CD34+ fibrocytes disappeared at least focally from the stroma of adenocarcinomas and endocrine tumors. The phenomenon of CD34+ fibrocyte loss is not site specific and has meanwhile been described in the stroma of various invasive carcinomas such as colon cancer [15], basal cell carcinoma of the skin [5, 6, 9, 10, 23], and invasive ductal breast cancer [4]. It is widely accepted that stromal matrix degradation and subsequent stromal invasion are crucial steps in the process of local tumor growth and systemic tumor spread [1, 11, 12, 14, 18].

With the CD34+ fibrocytes being capable of collagen I and III synthesis and therefore taking part in tissue repair, these cells play an important role in maintaining stromal integrity and inhibition of tumor cell migration [2]. Besides its function as a matrix-producing cell, the CD34+ fibrocytes have been shown to express HLA class-II molecules and to act as an antigen-presenting cell [3] indicating that CD34+ fibrocytes might be involved in specific host immune responses to tumor antigens. Therefore, it is of special interest to elucidate what causes CD34+ fibrocytes to disappear from the stroma of pancreatic adenocarcinomas and endocrine tumors. Cells of human endocrine pulmonary tumors are capable of inducing apoptosis in dendritic cells and blocking the differentiation of CD34+ myeloid precursors into mature dendritic cells [8]. This mechanism might explain our finding that the stroma of pancreatic endocrine tumors lacks CD34+ fibrocytes. However, this remains to be clarified in further studies together with the question whether the same is true for adenocarcinomas.

While the diagnosis of pancreatic endocrine tumors is straightforward and can be well substantiated using immunohistochemistry, problems occur when chronic pancreatitis has to be distinguished from pancreatic ductal adenocarcinoma. According to the data of the present study, detection of CD34+ fibrocytes in pancreatic lesions with suspected adenocarcinoma renders this differential diagnosis less probable and favors a benign lesion such as chronic pancreatitis. However, the absence of CD34+ fibrocytes from the stroma of a questionable pancreatic lesion renders the diagnosis of ductal adenocarcinoma much more likely than that of chronic pancreatitis. Generally, negative immunostaining is regarded to be less valuable, but small vessels and capillaries provide an internal control of high reliability when CD34 immunostains are performed. However, due to the relatively low number of cases investigated, the diagnostic impact of CD34+ fibrocytes in distinguishing chronic pancreatitis from adenocarcinoma could not be assessed precisely. Nevertheless, regarding the experiences of the present study, this approach appears to be promising and therefore merits further investigation.

References

1. Brummer O, Athar S, Riethdorf L, Loning T, Herbst H (1999) Matrix-metalloproteinases 1, 2 and 3 and their tissue inhibitors 1 and 2 in benign and malignant breast lesions: an in situ hybridization study. Virchows Arch 435:566–573
2. Bucala R, Spiegel LA, Chesney J, Hogan M, Cerami A (1994) Circulating fibrocytes define a new leukocyte subpopulation that mediates tissue repair. Mol Med 1:71–81
3. Chesney J, Bacher M, Bender A, Bucala R (1997) The peripheral blood fibrocyte is a potent antigen-presenting cell capable of priming naive T cells in situ. Proc Natl Acad Sci USA 94:6307–6312
4. Ebrahimsade S, Barth PJ, Ramaswamy A, Moll R (2001) CD34+ fibroblasts in benign and malignant breast lesions. Cancer Res Clin Oncol 127[Suppl 1]:S41
5. Humphreys TR, Monteiro MR, Murphy GF (2000) Mast cells and dendritic cells in basal cell carcinoma stroma. Dermatol Surg 26:200–203

6. Illueca C, Monteagudo C, Revert A, Llombart-Bosch A (1998) Diagnostic value of CD34 immunostaining in desmoplastic trichilemmoma. J Cutan Pathol 25:435–439
7. Izumi M, Suda K, Torii A, Inamada E (2001) Pancreatic ductal myofibroblasts. Proliferative patterns in various pathologic situations. Virchows Arch 438:442–450
8. Katsenelson NS, Shurin GV, Bykosvkaia SN, Shogan J, Shurin MR (2001) Human small cell lung carcinoma and carcinoid tumor regulate dendritic cell maturation and function. Mod Pathol 14:40–45
9. Kirchmann TT, Prieto VG, Smoller BR (1994) CD34 staining pattern distinguishes basal cell carcinoma from trichoepithelioma. Arch Dermatol 130:589–592
10. Kirchmann TT, Prieto VG, Smoller BR (1995) Use of CD34 in assessing the relationship between stroma and tumor in desmoplastic keratinocytic neoplasms. J Cutan Pathol 22:422–426
11. Koukoulis GK, Howeedy AA, Korhonen M, Virtanen I, Gould VE (1993) Distribution of tenascin, cellular fibronectins and integrins in the normal, hyperplastic and neoplastic breast. J Submicrosc Cytol Pathol 25:285–295
12. Lebeau A, Nerlich AG, Sauer U, Lichtinghagen R, Löhrs U (1999) Tissue distribution of major matrix metalloproteinases and their transcripts in human breast carcinomas. Anticancer Res 19:4257–4264
13. Lüttges J, Mentzel T, Hubner G, Klöppel G (1999) Solitary fibrous tumour of the pancreas: a new member of the small group of mesenchymal pancreatic tumours. Virchows Arch 435:37–42
14. Moch H, Torhorst J, Dürmüller U, Feichter GE, Sauter G, Gudat F (1993) Comparative analysis of the expression of tenascin and established prognostic markers in human breast cancer. Pathol Res Pract 189:510–514
15. Nakayama H, Enzan H, Miyazaki E, Kuroda N, Naruse K, Hiroi M (2000) Differential expression of CD34 in normal colorectal tissue, peritumoral inflammatory tissue, and tumour stroma. J Clin Pathol 53:626–629
16. Narvaez D, Kanitakis J, Faure M, Claudy A (1996) Immunohistochemical study of CD34-positive dendritic cells of human dermis. Am J Dermatopathol 18:283–288
17. Seidal T, Edvardsson H (1999) Expression of c-kit (CD117) and Ki67 provides information about the possible cell of origin and clinical course of gastrointestinal stromal tumours. Histopathology 34:416–424
18. Shoji T, Kamiya T, Tsubura A, Hamada Y, Hatano T, Hioki K, Morii S (1993) Tenascin staining positivity and the survival of patients with invasive breast carcinoma. J Surg Res 55:295–297
19. Silverman JS, Tamsen A (1996) Mammary fibroadenoma and some phyllodes tumour stroma are composed of CD34+ fibroblasts and factor XIIIa+ dendrophages. Histopathology 29:411–419
20. Silverman JS, Tamsen A (1997) Fibrohistiocytic differentiation in subcutaneous fatty tumors. Study of spindle cell, pleomorphic, myxoid, and atypical lipoma and dedifferentiated liposarcoma cases composed in part of CD34+ fibroblasts and FXIIIa+ histiocytes. J Cutan Pathol 24:484–493
21. Sircar K, Hewlett BR, Huizinga JD, Chorneyko K, Berezin I, Riddell RH (1999) Interstitial cells of Cajal as precursors of gastrointestinal stromal tumors. Am J Surg Pathol 23:377–389
22. Suster S, Fisher C (1997) Immunoreactivity for the human hematopoietic progenitor cell antigen (CD34) in lipomatous tumors. Am J Surg Pathol 21:195–200
23. Swanson PE, Fitzpatrick MM, Ritter JH, Glusac EJ, Wick MR (1998) Immunohistologic differential diagnosis of basal cell carcinoma, squamous cell carcinoma, and trichoepithelioma in small cutaneous biopsy specimens. J Cutan Pathol 25:153–159
24. Yamazaki K, Eyden BP (1995) Ultrastructural and immunohistochemical observations on intralobular fibroblasts of human breast, with observations on the CD34 antigen. J Submicrosc Cytol Pathol 27:309–323

Virchows Arch (2002) 440:134–138
DOI 10.1007/s00428-001-0541-5

ORIGINAL ARTICLE

Gary L. Bratthauer · Fattaneh A. Tavassoli

Lobular intraepithelial neoplasia: previously unexplored aspects assessed in 775 cases and their clinical implications

Received: 7 March 2001 / Accepted: 22 July 2001 / Published online: 19 October 2001
© Springer-Verlag 2001

Abstract Lobular intraepithelial neoplasia (LIN) is currently considered a risk factor for the development of invasive breast cancer of varying morphologies (ductal or lobular) and prognoses in either breast. The reason for the high frequency (50%) of subsequent development of invasive ductal cancers remains unclear and the issue unexplored. A total of 775 LIN cases were retrieved from the Armed Forces Institute of Pathology files and separated into three groups using our three-tiered grading system. The presence or absence of simultaneous invasive cancer (ductal or lobular type) and various grades of ductal intraepithelial neoplasia (DIN) were noted for each case and correlated with the grade of LIN. Of the 775 cases, 80% qualified as LIN 2, with the other 20% being relatively evenly split between LIN 1 and LIN 3. Of the 775 cases, 163 cases were pure LIN, while invasive carcinoma was present in 140 cases. The remaining 472 cases were associated with various grades of DIN. The frequency of associated invasive carcinomas (ductal and lobular) increased from 14% in LIN 1 to 23% in LIN 3. Remarkably, while the frequency of invasive lobular carcinoma increased dramatically from 11% in LIN 1 to 86% in LIN 3, the frequency of invasive ductal carcinoma markedly decreased with advancing grade of LIN from 89% in LIN 1 to 14% in LIN 3. Among the cases of LIN unassociated with invasive carcinoma, DIN was present in 75% of LIN 1, 75% of LIN 2, and 66% of LIN 3 cases. The grade of DIN was directly proportional to the grade of LIN. Based on the higher frequency of invasive lobular carcinoma associated with LIN 3, biopsies with LIN 3 should be evaluated diligently for the presence of an associated invasive lobular carcinoma. Furthermore, an excisional biopsy should be performed when LIN 3 is observed in a core biopsy. The high frequency of DIN associated with LIN might suggest that the subsequent invasive ductal carcinomas originate from the associated DIN and that some of this may represent a different phenotype of the same cells that form the LIN lesion. It is also possible that the neoplastic cells may reflect or retain stem cell characteristics with plasticity and the capacity to attain or progress into either a ductal or lobular invasive phenotype.

Keywords Breast · Lobular intraepithelial neoplasia · Invasive lobular carcinoma · Ductal intraepithelial neoplasia · Intraductal hyperplasia · Ductal carcinoma in situ · Invasive ductal carcinoma

Introduction

Lobular intraepithelial neoplasia (LIN) is currently considered a risk factor for the development of invasive breast cancer of varying morphologies and prognoses, in either breast [9]. The disease is characterized by a proliferation of uniform, generally small, loosely cohesive epithelial cells filling and/or distending the lobules. These cells can also spread in a pagetoid fashion into adjacent terminal ducts. Moreover, this condition is multicentric, existing simultaneously in several lobules in multiple quadrants of the breast, and is often bilateral. Although the cells are neoplastic and the lesion is frequently referred to as "carcinoma in situ", only 20–25% of patients develop invasive breast cancer within 15–20 years of diagnosis [4]. The subsequent invasive carcinoma is observed with nearly equal probability in either breast and may be of either lobular or ductal type, again with equal probability. Therefore, the disease of LIN is indicative of a process that may lead to invasive breast cancer of variable histologic appearances and prognoses.

LIN continues to be subdivided into atypical lobular hyperplasia (ALH) and lobular carcinoma in situ (LCIS).

The opinions or assertions contained herein are the private views of the authors and are not to be construed as official or as reflecting the views of the Department of the Army or Department of Defense.

G.L. Bratthauer (✉) · F.A. Tavassoli
Department of Gynecologic and Breast Pathology,
Armed Forces Institute of Pathology,
14th Street and Alaska Avenue NW,
Washington DC 20306-6000 USA
e-mail: bratthauer@afip.osd.mil
Tel.: +1-202-7822567, Fax: +1-202-7823939

The risk factors for either one of the two are not sufficiently different and the tendency toward invasive cancer development (or the prediction of such) is not necessarily increased with the LCIS designation, though some may argue otherwise. In 1978, Haagensen proposed to replace the terms ALH and LCIS with the designation of LN [1]. Although it is now generally agreed that "LIN" is a risk factor and not an obligate precursor of invasive carcinoma, many continue to use the ALH/LCIS subdivision. At the Armed Forces Institute of Pathology (AFIP), we started using the LN designation following the appearance of Haagensen's study. Subsequently, we started to grade the severity of LN from 1 to 3 to determine whether these grades have any predictive value and to ascertain whether or not they correlate with progression, prognosis, or any other aspect of associated breast alterations. An I for intraepithelial was added to distinguish intraepithelial from invasive lobular neoplasias.

Two concerns prompted this retrospective analysis of 775 cases reviewed over a 3-year period in the recent AFIP files. First, we hoped that a careful assessment of associated changes might provide an explanation for the diversity of subsequent invasive carcinomas. Second, we anticipated that the information concerning the types of associated pathology could help predict the direction of disease progression and assist in management decisions when various grades of LIN are encountered in excisional and core biopsies.

Materials and methods

All LIN cases from 1997 through 1999 (775) were retrieved from the records file at the AFIP. The cases used in the study were all those with a diagnosis of LIN rendered at the AFIP as a second opinion. When information was available, the reasons for biopsy varied from mammographically detected microcalcifications or irregular densities to a clinically palpable mass. In many cases, interpretation of LIN was an incidental finding as would be anticipated from data available in the literature. These cases had all been categorized to reflect grade. The criteria that were used for grading are as follows.

LIN 1. A loosely cohesive cellular proliferation partially or completely filling the acinar (ductular) spaces without acinar distension and often with residual acinar (ductular) lumen (Fig. 1a)

LIN 2. Cellular proliferation completely filling and distending at least some of the ductules in the terminal duct lobular unit but preserving distinct ductular outlines (Fig. 1b)

LIN 3. Cellular proliferation filling and maximally distending the ductules to the point of virtual confluence or, more rarely, proliferation of cells with significant cytologic atypia characterized by nuclear pleomorphism (intraepithelial version of invasive pleomorphic carcinoma), or a pure classic signet ring cell population (Fig. 1c)

When the LIN cells are pleomorphic or of the signet ring cell type, maximum distension of acini is not required. These LIN 3 lesions, in general, and particularly those interpreted as such based on cytologic features (pleomorphism or signet ring cells) are extremely rare, can be quite extensive, and can exhibit necrosis and microcalcifications mimicking a ductal process at first glance. In these cases, the loose cohesiveness of the cells and the presence of intracytoplasmic lumens and pagetoid growth patterns help accurate interpretation of the process. Microcalcification also occurs, albeit very rarely, in LIN 1 and LIN 2. The intent of our three-tiered classification was to provide a framework that would incorporate all variants of lobular disease including rare variants.

LIN 1, LIN 2, and LIN 3 cases were separated and other concomitant disease was noted for each. Cases were separated based on the presence or absence of simultaneous invasive cancer (ductal or lobular type), and the presence or absence of ductal intraepithelial neoplasia (DIN) [10]. Cases were also stratified on the basis of different grades of DIN and the absence of any evidence of ductal disease.

Results

A total of 775 cases of LIN were accessioned from 1997 through 1999. A concurrent invasive cancer was present in 140 (18%) of these cases. Invasive ductal carcinoma accounted for 49% of the 140 cases. The results are summarized in Table 1.

During this time period, there were a total of 65 cases examined with a diagnosis of LIN 1. Of these 65 cases, 14 (22%) also had either an intraductal (of DIN 1c or higher-grade type) or invasive carcinoma. Of the 14 patients with carcinoma, 9 had an invasive phenotype and 8 (89%) of these were of a ductal morphology. Therefore, invasive cancer was seen in 9 of 65 or just 14% of women with LIN 1 diagnosed from 1997 through 1999, and in only 1 of the 9 (11%) patients was the invasive cancer of a lobular phenotype.

There were no intraductal neoplasias of DIN 2 or DIN 3 grade (ductal carcinoma in situ grade 2 or 3) among the cases of LIN 1. Of the remaining 51 LIN 1 patients without carcinoma, 37 (73%) also had a DIN 1a (intraductal hyperplasia), DIN 1b (flat epithelial atypia), or DIN 1c (atypical intraductal hyperplasia). The remaining 14 cases (22%) were pure LIN 1 without any associated ductal abnormality or carcinoma.

There were a total of 618 cases of LIN 2 accessioned from 1997 through 1999. Diagnoses of carcinoma either invasive or intraductal accounted for 33% (n=201) of the total. Invasive carcinoma was only present in 110 (18%) of the LIN 2 cases. In contrast to the predominance of invasive ductal carcinoma among LIN 1 cases, 47% of invasive cancers associated with LIN 2 were purely lobular or displayed prominent lobular features. Of the patients with intraductal carcinoma, 41% were of DIN 2 or DIN 3 grade. As for the 417 women who did not have a simultaneous carcinoma, 290 (70%) had either DIN 1a, 1b, or DIN 1c (extensive atypical intraductal hyperplasia). The remaining 127 (21%) had pure LIN 2 without any evidence of ductal abnormality or carcinoma.

There were 92 cases with a diagnosis of LIN 3 during this time frame. A total of 38 (41%) of them also had either invasive carcinoma or a DIN of grade 1c or higher (conventional DCIS, grades 1–3). Twenty-one of the 92 women with LIN 3 (23%) had an ipsilateral invasive carcinoma, but only 3 (14%) showed a purely ductal morphology. The majority (86%) of these 21 invasive carcinomas were of the lobular type, with 4 of them possessing both lobular and ductal features. Of the 17 patients with intraductal carcinoma, 9 (53%) had either DIN 2 or

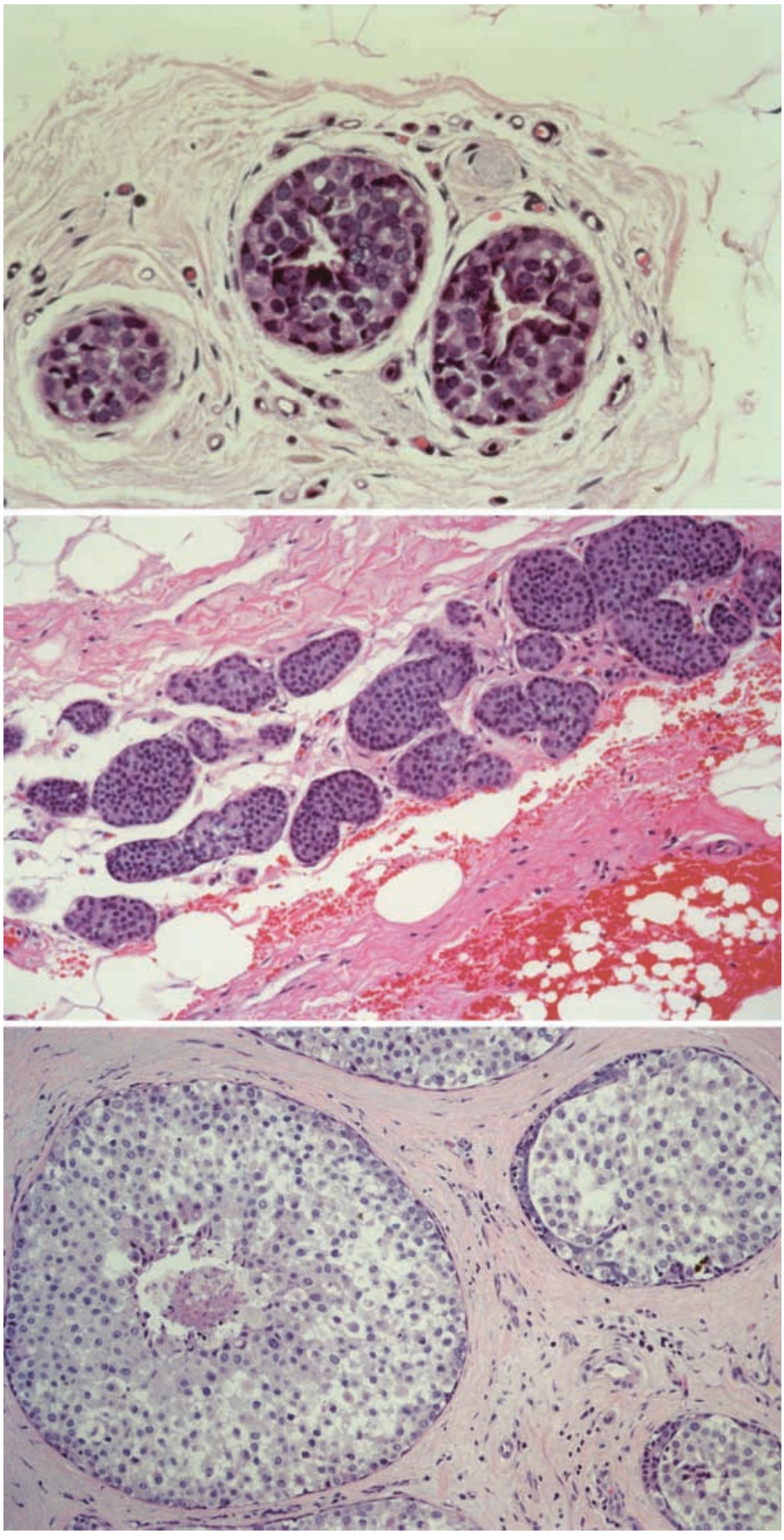

Fig. 1 The typical features of the three grades of lobular intraepithelial neoplasia (LIN). **a** LIN 1: note the increased proliferation without acinar distension or lumen obliteration, crowding the residual ductal epithelium. **b** LIN 2: note the acinar distension with filled lumens but persistence of acinar outlines. **c** LIN 3: note the severe acinar distension by loosely cohesive cells (with residual compressed ductal cells) and overall increased extent of disease with necrosis. Hematoxylin and eosin, **a** ×320, **b**, **c** ×160

Table 1 Concurrent findings in varying grades of lobular intraepithelial neoplasia (LIN). *PLIN* pure lobular intraepithelial neoplasia, *CIVCA* cases with invasive carcinoma, *CIDCA* cases with intraductal carcinoma, *CBIDP* cases with benign intraductal proliferation (intraductal hyperplasia to extensive atypical intraductal hyperplasia), *CNOCA* cases without carcinoma, *DIN* ductal intraepithelial neoplasia, *DCIS* ductal carcinoma in situ

	LIN 1(%)	LIN 2(%)	LIN 3(%)	All (%)
Total number	65	618	92	775
No. PLIN	14 (21)	127 (21)	24 (26)	165 (22)
No. CBIDP	37 (57)	290 (47)	30 (33)	357 (46)
No. CBIDP & PLIN	51 (78)	417 (67)	54 (59)	522 (67)
No. CIVCA	9 (14)	110 (18)	21 (23)	140 (18)
No. CIDCA	5 (8)	91 (15)	17 (18)	113 (15)
No. CIVCA & CIDCA	14 (22)	201 (33)	38 (41)	253 (33)
CIDCA number	5	91	17	113
No. DIN 1c (low-grade DCIS)	1 (20)	43 (47)	8 (47)	52 (46)
No. DIN 2–3 (DCIS grades 2–3)	0	37 (41)	9 (53)	46 (41)
CNOCA number	51	417	54	522
No. DIN 1a-1c (IDH, AIDH, extensive AIDH)	37 (73)	290 (70)	30 (56)	357 (68)

DIN 3. Thirty (56%) of the remaining 54 women without carcinoma also had some DIN 1a, DIN 1b, or DIN 1c (extensive atypical intraductal hyperplasia). There were 24 (26%) cases of pure LIN 3 without any ductal abnormality or carcinoma.

Among a total of 522 LIN unassociated with either in situ or invasive carcinomas, 51 (10%) were LIN 1, 417 (80%) were LIN 2, and 54 (10%) were LIN 3. Of a total of 165 cases of pure LIN, 14 (8%) were LIN 1, 127 (77%) were LIN 2, and 24 (15%) were LIN 3.

Discussion

In analyzing the 775 cases of LIN seen at the AFIP over 3 years, the characteristics of associated invasive cancers almost exactly paralleled data gleaned from over 1100 cases in 18 previously published studies on outcome following a biopsy diagnosis of LCIS/LIN; these data demonstrated roughly a 20% incidence of subsequent invasive cancer that was virtually 50% ductal and 50% lobular in phenotype [9]. This feature, along with the relatively low rate of subsequent invasive cancer development in either breast, has relegated LIN to a marker category portending a higher risk for subsequent development of invasive cancer. On closer scrutiny, assessment of associated pathology in 775 cases of LIN recently reviewed at the AFIP revealed a significant trend toward more prevalent and more aggressive proliferative disease with increasing grade of LIN.

Over the 3-year period of the study, a vast majority of cases (80%) fell into the LIN 2 category. Applying the proposed three-tiered grading criteria, only 8% of the cases qualified as LIN 1. These strict criteria identify a small but uniform group of very early lobular lesions. The LIN 3 cases accounted for 12% of the total and they not only had the most maximally expanded acini or highly atypical, pleomorphic nuclei, but were also among the most extensive of all the LIN lesions. Reflecting 80% of all cases, it makes sense that the features seen in the LIN 2 group were also representative of the entire group of LIN cases as a whole. Given the consultation nature of our practice and the expertise of the pathologists resulting in interpretation of the early lesions (LIN 1), we believe that even a higher proportion of cases in the general practice of pathology fall in the LIN 2 category.

Overall, there was an 18% frequency of associated invasive cancer, and that cancer was within 3% of being split 50:50 between lobular and ductal varieties, whether examining all of the LIN cases or just those designated as LIN 2. However, distinct differences emerged when LIN 2 was compared with the other two groups. The proportion of LIN 1 cases with invasive cancer was 14%, and 89% of these were invasive ductal carcinomas. Among LIN 3 lesions, the frequency of associated invasive carcinoma was 23%, but 86% of these were invasive lobular carcinomas. Advancing from LIN 1 to LIN 3 is associated with a 64% increase in the frequency of invasive carcinoma and more than a 700% increase in the likelihood of these tumors being invasive lobular carcinomas (Table 2). The increasing grade of LIN directly correlates with the frequency of invasive lobular carcinoma; however, there is an almost perfect inverse correlation between the grade of LIN and the frequency of invasive ductal cancer.

At what point then in the progression of lobular disease does the likelihood of developing an invasive lobular cancer exceed the possible occurrence of an invasive ductal cancer? Is the observed increase in the frequency of associated invasive lobular cancer entirely due to increased aggressiveness of the higher-grade LIN? Even

Table 2 Amount of total invasive carcinoma, invasive lobular, and invasive ductal types in different grades of lobular intraepithelial neoplasia (LIN). *IVCA* invasive carcinoma (ductal and lobular), *IVL* invasive lobular carcinoma, *IVD* invasive ductal carcinoma

	% IVCA (*n*)	% IVL(*n*)	% IVD(*n*)
LIN 1	14 (9)	11 (1)	89 (8)
LIN 2	18 (110)	47 (52)	53 (58)
LIN 3	23 (21)	86 (18)	14 (3)

when DIN 1c–DIN 3 are included among the associated cancers, the frequency of associated carcinoma remained directly proportional to lesion grade: 22% in LIN 1, 33% in LIN 2, and 41% in LIN 3. The grade of the DIN lesions also increased with advancing grades of LIN. Higher grade DIN (2 or 3) accounted for 53% of the DIN in the LIN 3 group, 41% of those in the LIN 2 group, and none of those in the LIN 1 group. It is interesting to note that even though the frequency and grade of DIN were highest among LIN 3 patients, invasive ductal carcinoma had the lowest association with LIN 3. This could imply that LIN 3 is far less stable as an intraepithelial process than DIN 2 or DIN 3.

Another interesting finding in comparing these various cases emerged from examination of LIN unassociated with any carcinomas. Fifty-nine percent of LIN 3, 67% of LIN 2, and 78% of LIN 1 cases had no accompanying cancer, invasive or in situ. Among the 54 LIN 3 lesions unassociated with either intraepithelial or invasive cancer, 30(56%) had a low-grade DIN 1a, 1b, or 1c (intraductal hyperplasia to extensive atypical intraductal hyperplasia). Among the 417 LIN 2 and the 51 LIN 1 cases unassociated with in situ or invasive carcinoma, 290 (70%) and 37 (73%) patients had similar lower grade DIN, respectively. There seemed to be a tendency for lower grade DIN to be present in association with lower grade LIN. In a previous study of all types of breast carcinoma, an association with LIN was observed in only a small subset [2].

With the increasing use of needle core biopsy, it is important to have some clues to the nature of lesions that may be present in the remaining breast tissue when LIN is the sole neoplastic proliferation identified in the core biopsy. Therefore, correlation of the type of lesion associated with varying grades of LIN in a large number of cases would be most useful in guiding therapeutic recommendation and could provide valuable information in deciding the optimal management approach. Since a vast majority of core biopsies are due to mammographically detected suspicious microcalcification, and microcalcification is rare in LIN, correlation of the mammographic and pathologic findings is crucial to ascertain accurate sampling of the lesion of mammographic concern if the core biopsy shows only LIN or no calcification. LIN is generally an incidental finding. Therefore, if the core biopsy contains LIN 3, the possibility of an associated invasive lobular carcinoma as well as higher grade DIN must be considered, and, in our opinion, an excisional biopsy is mandatory. A similar conclusion was reached in a recent radiologic study [5]. It should also be noted that microcalcification, detectable mammographically, may occur in LIN 3 [7]. If there is LIN 2, particularly when multiple terminal duct-lobular units are involved, re-excision may be prudent if there is not absolute confirmation that the mammographically detected area of suspicion has been sampled in the core. Core samples with LIN 1 should be examined for the presence of DIN elsewhere. If the basis (most often microcalcification) for the mammographic findings is accounted for in the core sample, further excision is not an absolute necessity.

The reason why a ductal phenotype develops in 50% of the cancers that subsequently occur in LIN patients is unknown and curiously not addressed in the literature. This feature, observed in multiple previous studies that have assessed outcome following a biopsy diagnosis of LIN, was also noted in our study group reflecting concurrent invasive carcinomas, whether assessing the entire group of 775 LIN lesions or the dominant group of 618 LIN 2 cases. Interestingly, not much has been documented regarding reasons or possible mechanisms contributing to this phenomenon. It is conceivable that some of the invasive ductal cancers originate from some of the concurrent DIN. Of the 69 cases with invasive ductal carcinoma, 42 also had a DIN 1c or higher lesion. Another possibility is that, in some cases, an early solid phase of low grade DCIS may be misinterpreted as LIN; assessment of immunoreactive E-cadherin may help to rectify this problem [3, 6, 8]. A more provocative possibility is that one lesion may transform to the other as cellular attributes are gained and lost. Could some of these neoplastic cells manifest a pluripotential stem-cell-like behavior? A further examination of more cases in the LIN 1 and LIN 3 categories as well as investigations at the molecular level may help to better understand this disease.

References

1. Haagensen CD, Lane N, Lattes R, Bodian C (1978) Lobular neoplasia (so-called lobular carcinoma in situ) of the breast. Cancer 42:737–769
2. Haagensen CD, Lane N, Bodian C (1983) Coexisting lobular neoplasia and carcinoma of the breast. Cancer 51:1468–1482
3. Jacobs TW, Pliss N, Kouria G, Schnitt SJ (2001) Carcinomas in situ (CIS) of the breast with indeterminate features. Role of E-cadherin staining in categorization. Am J Surg Pathol 25: 229–236
4. Page DL, Kidd TE, Dupont WD, Simpson JF, Rogers LW (1991) Lobular neoplasia of the breast: higher risk for subsequent invasive cancer predicted by more extensive disease. Hum Pathol 22:1232–1239
5. O'Driscoll D, Britton P, Borrow L, Wishart GC, Sinnatamby R, Warren R (2001) Lobular carcinoma in situ on core biopsy – what is the clinical significance? Clin Radiol 56:216–220
6. Rasbridge SA, Gillett CE, Sampson SA, Walsh FS, Millis RR (1993) Epithelial (E-) and placental (P-) cadherin cell adhesion molecule expression in breast carcinoma. J Pathol 169: 245–250
7. Sapino A, Righi L, Cassoni P, Papotti M, Pietribiasi F, Bussolati G (2000) Mammographically detected in situ lobular carcinomas of the breast. Virchows Arch 436:421–430
8. Siitonen SM, Kononen JT, Helin HJ, Rantala IS, Holli KA, Isola JJ (1996) Reduced E-cadherin expression is associated with invasiveness and unfavorable prognosis in breast cancer. Am J Clin Pathol 105:394–402
9. Tavassoli FA (1999) Pathology of the breast, 2nd edn. Appleton and Lange, Norwalk CT, pp 373–480
10. Tavassoli FA (2001) Ductal intraepithelial neoplasia of the breast. Virchows Arch 438:221–227

Virchows Arch (2002) 440:139–144
DOI 10.1007/s00428-001-0554-0

ORIGINAL ARTICLE

**Ana-Maria Bamberger · Holger Kappes
Carola Methner · Gabriele Rieck · Jens Brümmer
Christoph Wagener · Thomas Löning
Karin Milde-Langosch**

Expression of the adhesion molecule CEACAM1 (CD66a, BGP, C-CAM) in breast cancer is associated with the expression of the tumor-suppressor genes Rb, Rb2, and p27

Received: 29 May 2001 / Accepted: 19 August 2001 / Published online: 8 November 2001
© Springer-Verlag 2001

Abstract The adhesion molecule CEACAM1 (CD66a, BGP, C-CAM) is not only involved in maintaining normal tissue architecture, but also acts as a tumor suppressor in several experimental systems where loss of CEACAM1 expression results in enhanced tumor-cell growth and tumorigenicity. In order to further analyze the role of CEACAM1 in the development of breast cancer, we performed Western-blot analysis and immunohistochemistry with highly specific monoclonal antibodies in a cohort of 68 mammary carcinomas which had also been analyzed for expression of cell-cycle regulatory proteins cyclin D1, cyclin E, p16, p21, p27, Rb, and Rb2, as well as for steroid hormone receptor status, Ki67, and HER2/neu immunoreactivity. High CEACAM1 protein expression as found using both methods correlated significantly with expression of the retinoblastoma proteins Rb (P=0.004 and 0.013) and Rb2/p130 (P=0.003 and 0.007). In addition, we found a weak association of CEACAM1 expression with p27 protein levels (P=0.087 and 0.039), but with none of the other analyzed parameters. These results indicate the possibility of a functional link between cell-adhesion molecules and cell-cycle regulation that might play an important role in the development of mammary carcinomas.

Keywords CEACAM1 · Cell-cycle proteins · Rb · Rb2 · P27 · Breast cancer

A.-M. Bamberger (✉) · H. Kappes · C. Methner · G. Rieck
T. Löning · K. Milde-Langosch
Department of Gynecopathology, Institute of Pathology,
University Hospital Eppendorf, Martinistrasse 52,
20246 Hamburg, Germany
e-mail: abamberger@uke.uni-hamburg.de
Tel.: +49-40-428033162, Fax: +49-40-428034961

J. Brümmer · C. Wagener
Department of Clinical Chemistry, University Hospital Eppendorf,
Martinistr. 52, 20246 Hamburg, Germany

Introduction

Cell adhesion molecules are important mediators of tissue architecture and cellular polarity, which can also modulate proliferation and differentiation processes. CEACAM1 is a member of the carcinoembryonic antigen (CEA) family and the immunoglobulin superfamily [32]. Glycoproteins belonging to this family are expressed in epithelial tissues, such as the colonic mucosa, as well as in cells of the myeloid lineage [32]. CEACAM1 is the human homologue of the adhesion molecule Cell-CAM (C-CAM) of the rat [1, 19], and it has been suggested to function as a ligand for E-selectin [17]. In transfection studies, CEACAM1 mediates homo- and heterophilic binding to other members of the CD66 cluster [28, 33]. In contrast to most of the genes of the CEA family, the CEACAM1 gene predicts a cytoplasmic domain containing sequence motifs involved in signal transduction [7, 13] that has been shown to associate with pp60 c-src [9].

CEACAM1 expression is downregulated in colorectal carcinomas [23], indicating that loss of normal expression of CEACAM1 might play an important role in the pathogenesis of this tumor type. These findings have been recently corroborated by the finding that BGP is one of the 20 genes most frequently downregulated in colonic cancer [35]. Furthermore, immunohistochemical studies have indicated that the CEACAM1 expression pattern is changed in malignant lesions of the human mammary gland [27]. We have recently also described dysregulated CEACAM1 expression in endometrial carcinomas [2] and in placenta-derived tumors [6]. Taken together, these data suggest that CEACAM1 might play an important role as a potential tumor-suppressor gene in several types of tissues. Its exact role and mechanism of function are, however, not yet understood.

In the present study we used Western-blot analysis to determine CEACAM1 expression levels in a cohort of breast tumors that were additionally characterized for the

expression of several other genes, including steroid receptors, HER2/neu, and a broad panel of cell-cycle regulatory proteins (cyclin D1, cyclin E, p21, p27, Rb, Rb2) in order to determine potential associations in expression of CEACAM1 and these factors. CEACAM1 expression was additionally investigated using immunohistochemistry on paraffin-embedded specimens. For both CEACAM1 Western blot and immunohistochemistry, we used the highly specific monoclonal antibody Mab 4D1/C2 [11, 31] which had been previously employed to study expression in several normal human tissues [25], as well as expression in normal and malignant endometrial tissue and placenta [2, 5].

Materials and methods

Cell culture

T47D breast cancer cells, which were used as controls for Western blots, were purchased from American Type Culture Collection (Rockville, Md.) and cultivated as described [3]. Normal granulocytes, used as an additional positive control for Western blot [25], were isolated from buffy coats of normal donors using Ficoll-Paque gradient centrifugation (Pharmacia, Freiburg, Germany).

Tissue collection

All patients were treated at the Hamburg University Hospital, Department of Obstetrics and Gynecology, throughout 1994–1999. We studied 68 breast cancer samples (67 female patients, one male patient, mean age 56.2 years), of which 51 carcinomas were of ductal type, 12 cases were lobular tumors, 4 cases had mucinous differentiation, and 1 case was a medullary carcinoma. Seven tissue samples were from recurrences and 61 from primary tumors. Of the primary tumors, 27 were nodal negative, 33 nodal positive, and one case was of unknown nodal status. The pathological staging of the primary tumors was done as recommended by the Union Internationale Contra la Cancrum (International Union Against Cancer). Twelve tumors were classified as stage 1, 30 tumors as stage 2, 4 tumors as stage 3, and 9 tumors as stage 4. Staging data were unavailable in six cases. According to the histological grading system of Bloom and Richardson [8], 3 specimens were of low malignancy grade (G1), 34 tumors were classified as G2, and 31 cases were high-grade carcinomas (G3).

Western-blot analysis and densitometric evaluation

Extraction of proteins from breast cancer specimens was carried out as described previously [3]. Sodium dodecyl sulfate–polyacrylamide gel electrophoresis was performed using a 6% polyacrylamide gel and a 3% stacking gel, applying 40 µg protein of each sample. Proteins were transferred to a polyvinylidene difluoride membrane (Immobilon P, Millipore, Eschborn, Germany). After overnight incubation at 4°C in blocking solution (0.1 M maleic acid, pH 7.5, 0.15 M NaCl, 0.005% Thimerosal, and 1% blocking reagent, Boehringer Mannheim, Germany), membranes were incubated for 1 h at room temperature with the CD66a-specific monoclonal antibody 4D1/C2 at a final concentration of 1 µg/ml in a mixture of Tris-buffered saline with Tween (TBST) (20 mM Tris HCl, pH 7.6, 0.137 M NaCl, 0.05% Tween 20) and blocking solution (9:1).

Blots were washed 3×10 min in TBST and incubated with the second antibody (peroxidase-conjugated anti-mouse-IgG, 1:2000, Santa Cruz Biotechnology, Heidelberg, Germany) for 1 h at room temperature. After extensive washing, the second antibody was visualized using chemiluminescence reagents (Super Signal West Pico kit, Pierce, Rockfort, Ill.) with Hyperfilm ECL films (Amersham, Braunschweig, Germany). In parallel experiments with the same antibody, 40 µg protein extract from a normal endometrial tissue sample and 40 µg protein from granulocytes were always loaded in the first two wells as controls for comparable exposition of chemiluminescent membranes and for position of the CD66a-specific band.

Western-blot analysis of expression of the steroid receptors ER and PR-A and PR-B, of Rb and Rb2 and actin was performed [3, 4, 21] using the following antibodies at the indicated dilutions in 9:1 TBST/blocking solution: mouse anti-ER (NCL-ER-6F11, Novocastra Laboratories, Ltd., Newcastle upon Tyne, U.K., 1:1000), mouse anti-PR (NCL-PGR, Novocastra, 1:300), mouse anti-Rb (G3–245, BD Pharmingen, Heidelberg, Germany, 1:400), rabbit anti-Rb2 (C-20, Novocastra, 1:300), goat anti-actin (I-19, Santa Cruz, 1:10000). Western-blot analysis of the cell-cycle regulatory proteins cyclin D1, cyclin E, p16, p21, and p27 was performed as described [21]. The cohort of 53 breast cancer patients described in this prior investigation on cell-cycle regulators and AP-1 proteins is included in the present study. The intensities of the specific protein bands were evaluated by means of densitometry (GS-700 Imaging Densitometer, BioRad, München, Germany), calculated as percentage intensity of the control sample and corrected for equal actin loading.

Immunohistochemistry

Serial sections of 4–6 µm were cut from the paraffin blocks and mounted on 3-aminopropyltriethoxysilane-coated slides, deparaffinized in xylene, and rehydrated in graded alcohol to Tris-buffered saline (TBS, 50 mM Tris, 150 mM NaCl, pH 7.4). The slides were microwaved for 5×2 min in 10 mM citrate, pH 6.0. After cooling down for 20 min, the slides were washed in TBS, blocked for 30 min at room temperature with normal goat serum (Dako, Glostrup, Denmark), diluted 1:20 in TBS, and incubated overnight at 4°C with Mab 4D1/C2 at 4 µg/ml in TBS. Non-immune murine serum (Dako) at the same dilution was used as negative control. Alkaline phosphatase anti-alkaline phosphatase detection (Dako) and color development with new-fuchsin were carried out according to standard procedures. The slides were counterstained with hematoxylin and mounted with glycerin/gelatin. ER, PR, Ki67, and erbB2 immunohistochemistry were performed and evaluated as described [4]. Histological and immunohistochemical evaluation were performed independently by two pathologists. In cases of interobserver variability, a third person was consulted.

Results

Expression of the cell adhesion molecule CEACAM1 was investigated using Western-blot analysis in 68 breast cancer samples. As shown in Fig. 1 (upper panel), the tumor samples showed expression of the approximately 140-kDa form of CEACAM1, as had also been described for normal endometrium (which was used as one of two positive controls, marked C2 in the upper panel). Granulocytes, which were employed as the other positive control, expressed the described approximately 180-kDa form (C1 in Fig. 1, upper panel). As can be seen in the representative set of tumors shown in Fig. 1, CEACAM1 expression levels differed in intensity between the individual samples, with 29.4% of the tumors (n=20) showing absent/low expression (0–20% of the densitometric value of the control), 39.7% of the tumors (n=27) showing a medium level of expression (21–100% of the densitometric value of the control), and 30.9% of the tumors

Table 1 Association of CEACAM1 expression as determined using Western-blot analysis and immunohistochemistry (ICH) with expression of Rb, Rb2, and p27

	n	CEACAM1 expression in tumor samples						
		Western-blot results[a]				IHC results[a]		
		0–20% (*n*=20)	21–100% (*n*=27)	101–260% (*n*=21)	*P*	Negative/weak (*n*=39)	Moderate/strong (*n*=29)	*P*
Rb expression[b]								
<1%	20	11	6	3		12	8	
1–10%	18	5	10	3		15	3	
>10%	30	4	11	15	0.004	12	18	0.013
Rb2 expression[b]								
<20%	16	9	7	0		13	3	
20–50%	28	8	12	8		18	10	
>50%	24	3	8	13	0.003	8	16	0.007
p27 expression[c]								
<50%	26	10	12	4		19	7	
>50%	42	10	15	17	0.087	20	22	0.039

[a] Evaluation of CEACAM1 results: see text
[b] Rb expression relative to the MCF7 control cell line
[c] Relative to a control sample

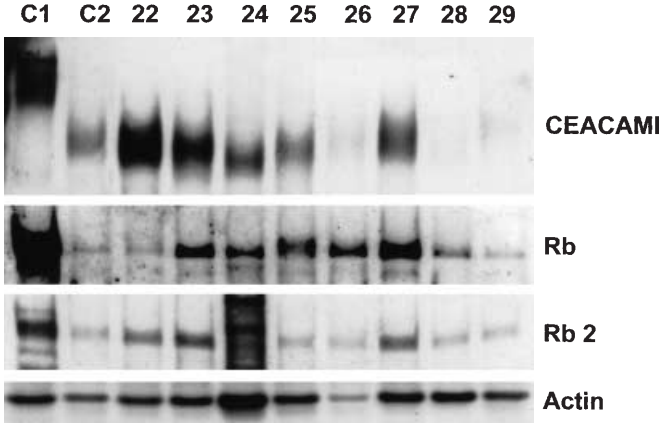

Fig. 1 Western-blot analysis of CEACAM1, Rb, and Rb2 in breast cancer samples. *Upper panel* (CEACAM1): C1=granulocytes, positive control (expressing CEACAM1 with the molecular weight of approximately 180 kDa); C2=normal human endometrium, positive control (expressing CEACAM1 with the molecular weight of approximately 140 kDa); 22–29= breast cancer samples. The positions of the CEACAM1 bands reflect differences in protein glycosylation. *Lower panels* (Rb, Rb2, and actin): C1=T47D breast cancer cells, positive control; C2=normal breast tissue; 22–29= breast cancer samples corresponding to those shown in the *upper panel*

exhibiting high expression levels (101–260% of the densitometric value of the control).

When CEACAM1 expression levels were compared with the hormone receptor status and the clinico-pathological parameters of the tumors, no statistically significant association could be detected (data not shown). By comparing the levels of CEACAM1 expression with the expression levels of cell-cycle regulatory proteins, statistically significant associations could be observed between CEACAM1 expression and the expression of the two retinoblastoma tumor-suppressor genes, Rb (*P*=0.004) and Rb2 (*P*=0.003). In addition, a statistically non-significant association of CEACAM1 and p27 expression was found (*P*=0.087). For a comparison, Western-blot expression of Rb and Rb2 are shown in Fig. 1 for the same samples as shown for CEACAM1 expression.

The data concerning all the analyzed samples are presented in Table 1. For the other investigated cell-cycle proteins (cyclin D1, cyclin E, p16, and p21) and the other analyzed parameters, no statistically significant association could be observed.

In addition to the Western-blot detection method, immunohistochemistry using the same monoclonal antibody was performed on paraffin-embedded sections of the analyzed tumors. Representative samples are shown in Fig. 2. As can be observed, in normal breast epithelium (Fig. 2a) CEACAM1 is localized at the apical (luminal) poles of the cells, as previously described [27]. Panels b–d show typical aspects of CEACAM1 expression as observed in the tumor samples. As shown in Fig. 2b, in better differentiated samples, the apical expression pattern can still be observed, along with areas with reduced/absent CEACAM1 expression (shown also in Fig. 2d). Figure 2c shows another pattern of dysregulated expression, with a change of the apical to a membranous "all-around" pattern, which is in agreement with previous studies in both breast and endometrial tumors [2, 27].

Intensity of the staining was scored from 0 (no expression) to 3 (strong expression). In the analyzed tumors, the score was 0 in 30 cases (44%), 1 in 9 cases (13%), 2 in 21 cases (31%), and 3 in 8 cases (12%). CEACAM1 detection results obtained using immunohistochemistry and Western-blot analysis correlated significantly (*P*=0.001, not shown).

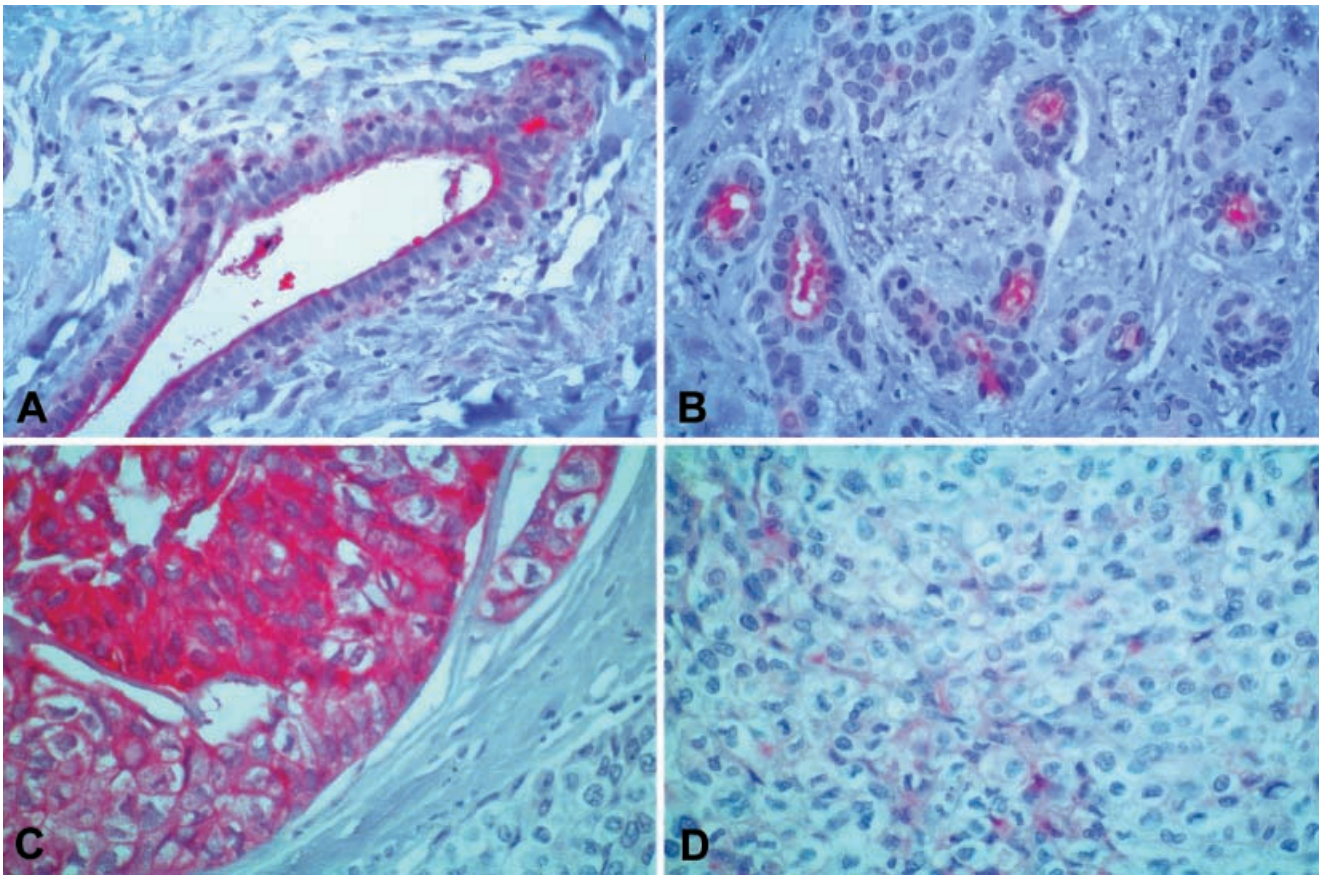

Fig. 2 Immunohistochemical detection of CEACAM1 on paraffin-embedded sections. **a** Normal tissue: apical (luminal) staining for CEACAM1 in normal breast epithelial cells (×400). Tumor samples: **b** apical staining for CEACAM1 along with areas of reduced/lost CEACAM1 expression (×400); **c** membranous "all-around" staining, along with loss of expression (*lower right corner*, ×400); **d** reduced/lost CEACAM1 expression (×400)

For statistical analysis, cases with negative and weak CEACAM1 expression (score 0–1) were combined and compared with those having moderate/strong immunostaining (Table 1), and the intensity of the immunohistochemical staining was correlated with the described clinico-pathological parameters, expression of Ki67, HER2/neu, estrogen and progesterone receptors, and cell-cycle regulatory proteins. Significant correlations were observed again with Rb (0.013) and Rb2 (P=0.007). In addition, CEACAM1 expression correlated significantly with p27 immunoreactivity in the tumor (P=0.039). No significant associations could be observed with any of the other investigated parameters.

Discussion

Normal expression of the adhesion molecule CEACAM1 seems to play an important role in maintaining normal tissue architecture and cellular polarity. CEACAM1 has been implicated as a putative tumor suppressor in several types of tumors. This hypothesis is corroborated by the finding that CEACAM1 is downregulated in colorectal adenomas and carcinomas [23, 24] and has been shown to be one of 20 transcripts displaying the largest decrease in expression in this type of cancer [35]. We have recently shown dysregulated/reduced CEACAM1 expression in endometrial carcinomas [2]. Using immunohistochemistry, unusual CEACAM1 expression patterns were described in benign and malignant breast tissues as well [27]. However, little is known about its exact roles and mechanisms of action.

When CEACAM1 was transfected into a non-expressing colorectal carcinoma cell line [18], tumor growth was strongly reduced. Transfection studies of PC3 prostate tumor cells with CEACAM1 resulted in reduced anchorage-dependent growth and less tumorigenicity in vivo compared with control cells, indicating that CEACAM1 can function as a tumor suppressor in prostate tumorigenesis. In addition, transfection of CEACAM1 antisense vectors into a nontumorigenic prostatic epithelial cell line resulted in tumor formation in nude mice [15]. Since anchorage-independent cell-cycle progress is a feature of the malignant phenotype, in the present study we used Western blot followed by densitometry to investigate the expression levels of CEACAM1 in breast tumor samples and correlated these results with clinico-pathological tumor characteristics and expression levels of several important cell-cycle regulators such as cyclin D1 and cyclin E, the CDK inhibi-

tors p16, p21, and p27, and the retinoblastoma proteins Rb and Rb2. Interestingly, we found statistically significant positive associations of CEACAM1 expression levels as detected using immunohistochemistry or Western blot with the expression levels of both Rb and Rb2, which are key regulators of the cell cycle. In addition, CEACAM1 expression was weakly associated with p27 protein levels.

The members of the retinoblastoma gene family Rb/p105 and Rb2/p130 play a central role in the regulation of cell-cycle progression in mammalian cells [34]. In some experimental systems, both have been shown to have effective tumor-suppressor function [14, 26, 34]. In a recent study by our group in which both breast and endometrial tumors were analyzed, expression of Rb2 was found to correlate with the expression of Rb, ER, and PR-B in breast cancer samples and with PR-A, PR-B, and younger patient age in endometrial carcinomas [22], indicating that loss of Rb2 expression, mostly by transcriptional downregulation, may be involved in dedifferentiation of many endometrial and a subset of mammary carcinomas.

Regarding the observed association of CEACAM1 expression and expression of Rb and Rb2, several potential explanations can be discussed. In contrast to most of the genes of the CEA family, the CEACAM1 gene predicts a cytoplasmic domain-containing a sequence motif involved in signal transduction [7, 13] that has been shown to associate with pp60 c-src [9], a SH2-domain tyrosine kinase with known regulatory function in the cell cycle in several experimental systems [12, 16, 20, 29]. While no direct association of pp60c-src with the Rb protein has been shown so far, expression of v-src in three-dimensional culture in collagen gel was shown to result in sustained Rb phosphorylation [20], and the Rb protein has been shown to interact with another SH2 domain-containing kinase, the Rak nuclear tyrosine kinase, which has growth-suppressing activity [10]. Thus, a regulatory mechanism involving signal transduction pathways activated by CEACAM1 and controlling the cell cycle through Rb is possible. However, the observed correlation between CEACAM1 expression and expression of Rb and Rb2 could also implicate a putative regulatory role of either Rb and Rb2, or transcription factors with which they might interact, in the transcriptional regulation of the CEACAM1 gene, about which very little is known.

In addition to the retinoblastoma proteins, CEACAM1 expression also correlated with expression of the cdk inhibitor p27/kip1. As significant p27 expression is not only found in mammary epithelial and carcinoma cells, but also in stromal cells [21], the differences between the tumors are not as clear-cut as with Rb or Rb2. The fact that the p27 protein detected by our Western-blot method partly derives from the stroma might explain the weaker associations with CEACAM1 expression as compared with the retinoblastoma proteins. An influence of CEACAM1 on p27 expression and cell proliferation was recently described by Singer et al. [30] in experiments with bladder carcinoma cells: perturbation of CEACAM1 function by addition of CEACAM1 antibodies resulted in increased DNA synthesis and decreased p27 protein levels, whereas cyclin E expression did not change. Additional cell-cycle regulatory proteins such as Rb or Rb2 were not analyzed.

While further studies will certainly be necessary to clarify the molecular mechanisms involved, the present study shows for the first time a significant association between the potential tumor-suppressor gene CEACAM1 and the cell-cycle inhibitory proteins Rb, Rb2, and p27, indicating the possibility of a functional link between cell adhesion/tissue architecture and cell-cycle regulation. Loss of this link might lead to dysregulation of the proliferation process of breast cells, especially regarding regulation of proliferation by means of cellular contact and tissue architecture, leading to potentially aggressive proliferation. Early characterization of these parameters might thus prove to be a useful additional prognostic marker of tumor behavior.

Acknowledgement The authors are grateful to Mr. J. Koppelmeyer for excellent photographic work.

References

1. Aurivilius M, Hansen OC, Lazrek MB, Bock E, Öbrink B (1990) The cell adhesion molecule Cell-CAM 105 is an eto-ATPase and a member of the immunoglobulin superfamily. FEBS Lett 264:267–269
2. Bamberger A-M, Riethdorf L, Nollau P, Naumann M, Erdmann I, Götze J, Brümmer J, Schulte HM, Wagener C, Löning T (1998) Dysregulated expression of CD66a (BGP, C-CAM), an adhesion molecule of the CEA family, in endometrial cancer. Am J Pathol 152:1401–1406
3. Bamberger A-M, Methner C, Lisboa BW, Städtler C, Schulte HM, Löning T, Milde-Langosch K (1999) Expression pattern of the AP-1 family in breast cancer: association of fosB expression with a well-differentiated, receptor-positive phenotype. Int J Cancer 84:553–558
4. Bamberger A-M, Milde-Langosch K, Schulte HM, Löning T (2000) Progesterone receptor isoforms PR-B and PR-A in breast cancer: correlations with clinico-pathologic tumor parameters and expression of AP-1 factors. Hormone Res 54:32–37
5. Bamberger A-M, Sudahl S, Löning T, Wagener C, Bamberger CM, Drakakis P, Coutifaris C, Makrigiannakis A (2000) The adhesion molecule CEACAM1 (CD66a, C-CAM, BGP) is specifically expressed by the extravillous intermediate trophoblast. Am J Pathol 156:1165–1170
6. Bamberger A-M, Sudahl S, Wagener C, Löning T (2001) Expression pattern of the adhesion molecule CEACAM1 (C-CAM, CD66a, BGP) in gestational trophoblastic lesions. Int J Gyn Pathol 20:160–165
7. Barnett TR, Kretschmer A, Austen DA, Goebel SJ, Hart JT, Elting JJ, Kamarck ME (1989) Carcinoembryonic antigens: alternative splicing accounts for the multiple mRNAs that code for novel members of the carcinoembryonic antigen family. J Cell Biol 108:267–276
8. Bloom HJG, Richardson WW (1957) Histological grading and prognosis in breast cancer. A study of 1049 cases, of which 359 have been followed 15 years. Br J Cancer 11:359–377
9. Brümmer J, Neumaier M, Göpfert C, Wagener C (1995) Association of pp60c-src with biliary glycoprotein (CD66a), an adhesion molecule of the carcinoembryonic antigen family downregulated in colonic carcinomas. Oncogene 11:1649–1655

10. Craven RJ, Cance WG, Liu ET (1995) The nuclear thyrosine kinase Rak associates with the retinoblastoma protein. Cancer Res 55:3969–3972
11. Drzeniek Z, Lamerz R, Fenger U, Wagener C, Haubeck HD (1991) Identification of membrane antigens in granulocytes and colonic carcinoma cells by a monoclonal antibody specific for biliary glycoprotein, a member of the carcinoembryonic antigen family. Cancer Lett 56:173–179
12. Hall FL, Williams RT, Wu L, Wu F, Carbonaro-Hall DA, Harper JW, Warburton D (1993) Two potentially oncogenic cyclins, cyclin A and cyclin d1, share common properties of subunit configuration, thyrosine phosphorylation and association with the Rb protein. Oncogene 8:1377–1384
13. Hinoda Y, Neumaier M, Hefta SA, Drzeniek Z, Wagener C, Shively C, Hefta LJ, Shively JE, Paxton RJ (1988) Molecular cloning of a cDNA coding biliary glycoprotein I: primary structure of a glycoprotein immunologically cross-reactive with carcinoembryonic antigen. Proc Natl Acad Sci USA 85: 6959–6963
14. Howard CM, Claudio PP, Gallia GL, Gordon J, Giordano GG, Hauck WW, Khalili K, Giordano A (1998) Retinoblastoma-related protein pRb2/p130 and suppression of tumor growth in vivo. J Natl Cancer Inst 90:1451–1460
15. Hsieh J-T, Luo W, Song W, Wang Y, Kleinerman DI, Van NT, Lin S-H (1995) Tumor suppressive role of an androgen-regulated epithelial cell adhesion molecule (C-CAM) in prostate carcinoma cell revealed by sense and antisense approaches. Cancer Res 55:190–197
16. Keach S, Schnierle B, Wyss A, Ballmer-Hofer K (1993) Myristylation and amino-terminal phosphorylation are required for activation of pp60c-src during mitosis. Oncogene 8:575–581
17. Kuijpers TW, Hoogerwerf M, Van der Laan LJ, Nagel G, Van der Schoot CE, Grunert F, Roos D (1992) CD66 nonspecific cross-reacting antigens are involved in neutrophil adherence to cytokine-activated endothelial cells. J Cell Biol 118:457–466
18. Kunath T, Ordonez-Garcia C, Turbide C, Beauchemin N (1995) Inhibition of colonic tumor cell growth by biliary glycoprotein. Oncogene 11:2375–2382
19. Lin SH, Giudotti G (1989) Cloning and expression of a cDNA coding for a rat liver plasma membrane ecto-ATPase. The primary structure of the ecto-ATPase is similar to that of the human biliary glycoprotein I. J Biol Chem 264:14408–14414
20. Marx M, Dorsch O (1997) pp60c-src is required for the induction of a quiescent mesangial phenotype. Kidney Int 51:110–118
21. Milde-Langosch K, Bamberger AM, Methner C, Rieck G, Löning T (2000) Expression of cell cycle regulatory proteins Rb, p16/MTS1, p27/Kip1, p21/Waf1, cyclin D1 and cyclin E in breast cancer: correlations with expression of activating protein-1 family members. Int J Cancer 87:468–472
22. Milde-Langosch K, Goemann C, Methner C, Rieck G, Bamberger AM, Löning T (2001) Expression of Rb2/p130 in breast and endometrial cancer: correlations with steroid hormone receptor status and Rb expression. Br J Cancer 85:546–551
23. Neumaier M, Paululat S, Chan A, Matthes P, Wagener C (1993) Biliary glycoprotein, a potential human cell adhesion molecule, is down-regulated in colorectal carcinomas. Proc Natl Acad Sci U S A 90:10744–10748
24. Nollau P, Scheller H, Kona-Horstmann M, Rohde S, Hagenmüller F, Wagener C, Neumaier M (1997) Expression of CD66a (human C-CAM) and other members of the carcinoembryonic antigen family of adhesion molecules in human colorectal adenomas. Cancer Res 57:2354–2357
25. Prall F, Nollau P, Neumaier M, Haubeck H-D, Drzerniek Z, Helmchen U, Löning T, Wagener C (1996) CD66a (BGP), an adhesion molecule of the carcinoembryonic antigen family, is expressed in epithelium, endothelium, and myeloid cells in a wide range of normal human tissues. J Histochem Cytochem 44:35–41
26. Pupa SM, Howard CM, Invernizzi AM, DeVecchi R, Giani C, Claudio PP, Colnaghi MI, Giordano A, Menard S (1999) Ectopic expression of pRb2/p130 suppresses the tumorigenicity of the c-erbB-2-overexpressing SKOV tumor cell line. Oncogene 18:651–656
27. Riethdorf L, Lisboa BW, Henkel U, Naumann M, Wagener C, Löning T (1997) Differential expression of CD66a (BGP), a cell adhesion molecule of the carcinoembryonic antigen family, in benign, premalignant, and malignant lesions of the human mammary gland. J Histochem Cytochem 45:957–963
28. Rojas M, Fuks A, Stanners CP (1990) Biliary glycoprotein, a member of the immunoglobulin supergene family, functions in vitro as a Ca2+-dependent intercellular adhesion molecule. Cell Growth Differ 1:527–533
29. Shalloway D, Bagrodia S, Chackalaprampil I, Shenoy S, Lin PH, Taylor SJ (1992) c-Src and mitosis. Ciba Found Symp 170:265–275
30. Singer BB, Scheffrahn I, Öbrink B (2000) The tumor growth-inhibiting cell adhesion molecule CEACAM1 (C-CAM) is differentially expressed in proliferating and quiescent cells and regulates cell proliferation. Cancer Res 60:1236–1244
31. Stoffel A, Neumaier M, Gaida F-J, Fenger U, Drzeniek Z, Haubeck H-D, Wagener C (1993) Monoclonal, anti-domain and anti-peptide antibodies assign the molecular weight 160,000 granulocyte membrane antigen of the CD66 cluster to a mRNA species encoded by the biliary glycoprotein gene, a member of the carcinoembryonic antigen gene family. J Immunol 150:4978–4984
32. Thompson J, Grunert F, Zimmermann W (1991) Carcinoembryonic antigen family: molecular biology and clinical perspectives. J Clin Lab Anal 5:344–366
33. Turbide C, Rojas M, Stanners CP, Beauchemin N (1991) A mouse carcinoembryonic antigen gene family member is a calcium dependent adhesion molecule. J Biol Chem 266:309–315
34. Weinberg RA (1995) The retinoblastoma protein and cell cycle control. Cell 81:323–330
35. Zhang L, Zhou W, Velculescu VE, Kern SE, Hruban RH, Hamilton SR, Vogelstein B, Kinzler KW (1997) Gene expression profiles in normal and cancer cells. Science 276:1268–1272

Virchows Arch (2002) 440:145–154
DOI 10.1007/s004280100529

ORIGINAL ARTICLE

**Chiun Chei Li · Bing Xu · Mitsuyoshi Hirokawa
Zhirong Qian · Katsuhiko Yoshimoto
Hidehisa Horiguchi · Takashi Tashiro · Toshiaki Sano**

Alterations of E-cadherin, α-catenin and β-catenin expression in neuroendocrine tumors of the gastrointestinal tract

Received: 22 June 2001 / Accepted: 9 July 2001 / Published online: 7 November 2001
© Springer-Verlag 2001

Abstract Neuroendocrine tumors (NETs) of the gastrointestinal tract comprise a heterogeneous group of neoplasms arising from the diffuse neuroendocrine system. These tumors strongly differ from each other on the basis of different pathogenetic, clinical, functional, histological, and prognostic patterns. Previous studies have shown that abnormal and reduced expression of the E-cadherin/catenin complex in several human cancers is associated with tumor dedifferentiation, advanced clinical stages, and poor survival rate. We assessed correlations between the expression of E-cadherin and catenins, Ki-67, and the following clinicopathological factors: age, embryological site of origin, size, histological growth pattern, the depth of penetration into the intestinal wall, and the presence of metastasis. In this study, reduction of membranous E-cadherin expression to a variable degree was detected in more than two-thirds (42 of 51) of gastrointestinal NETs (19 foregut, 8 midgut, and 24 hindgut) belonging to the complete neuroendocrine neoplastic spectrum [18 well-differentiated NETs, 22 well-differentiated neuroendocrine carcinomas (NECs), and 11 poorly differentiated NECs]. The reduction of E-cadherin expression was concomitant with the reduction of α-catenin (44 of 51) and β-catenin (35 of 51) expression. Our immunohistochemical analysis demonstrated significant differences of percentage of membranous positive cells of E-cadherin, α-catenin, or β-catenin between normal tissues and well-differentiated NETs (P=0.0038, P=0.004, and P=0.0329, respectively), well-differentiated NECs (P<0.001, P<0.001, and P<0.001, respectively) and poorly differentiated NECs (P=0.0002, P<0.0002, and P=0.0002, respectively). Among the gastrointestinal NETs, there were significantly more positive cells of E-cadherin, α-catenin, or β-catenin in well-differentiated NETs than well-differentiated NECs (P=0.0006, P=0.0065, and P=0.0001, respectively) or poorly differentiated NECs (P=0.0053, P=0.0041, and P<0.001, respectively). MIB-1 labeling index generally showed a low proliferative activity in well-differentiated NETs (0.49±0.37) and well-differentiated NECs (0.662± 0.66). A high proliferation rate was observed in poorly differentiated NECs (41.518±16.59). MIB-1 labeling index was significantly higher in poorly differentiated NECs than well-differentiated NETs and well-differentiated NECs (P<0.0001 and P<0.0001, respectively). E-cadherin, α-catenin, and β-catenin expression were correlated significantly with transmural tumor invasion (P<0.0001, P=0.0001, and P<0.0001, respectively) and with size (P=0.0013, P=0.0001, and P<0.0001, respectively). These results indicate that the alteration in the E-cadherin/catenin expression may be involved in the growth and progression of gastrointestinal NETs.

Keywords Gastrointestinal neuroendocrine tumors · E-cadherin · α-Catenin · β-Catenin · Ki-67 · Immunohistochemistry

C.C. Li · B. Xu · M. Hirokawa · Z. Qian · H. Horiguchi
T. Tashiro · T. Sano (✉)
Department of Pathology,
University of Tokushima School of Medicine,
3-18-15 Kuramoto-cho, Tokushima 770-8503, Japan
e-mail: sano@basic.med.tokushima-u.ac.jp
Tel.: +81-88-6337064, Fax: +81-88-6339423

K. Yoshimoto
Otsuka Department of Molecular Nutrition,
University of Tokushima School of Medicine, Tokushima, Japan

Introduction

Neuroendocrine tumors (NETs) of the gastrointestinal tract comprise a heterogeneous group of neoplasms arising from the diffuse neuroendocrine system. These tumors strongly differ from each other on the basis of different pathogenetic, clinical, functional, histological, and prognostic patterns [14, 28]. The histopathological spectrum ranges from classical carcinoids with slow growth and relatively good prognosis to highly malignant neuroendocrine carcinomas (NECs) [5]. Several features of NETs, such as anatomic site, age, primary tumor size, histological growth pattern, or histological depth of supporting tissue invasion, are associated with the patient's

survival [18, 25, 33]. Recent molecular genetic investigations have revealed the involvement of p53 mutations and inactivation of one or several tumor suppressor genes on chromosome 18 in the tumorigenesis of gastrointestinal NETs [15, 22, 32].

Previous reports have demonstrated that E-cadherin and its cytoplasmic binding proteins, the catenins (α-, β-, γ-), are essential for intercellular junctions [11]. E-cadherin is a transmembrane glycoprotein belonging to the family of calcium-dependent cell adhesion molecules. β-Catenin, found along basolateral cell membranes in normal epithelial cells, binds directly to the cytoplasmic domain of E-cadherin; its main role in the E-cadherin/catenin complex is to bind α-catenin to E-cadherin. In addition to its role in cell adhesion, β-catenin has been shown to function as a downstream transcriptional activator of the Wnt/wingless signaling pathway. When translocated to the nucleus, β-catenin acts as a transcription factor forming a complex with the DNA-binding proteins T-cell factor and lymphoid enhancer factor and contributes to acceleration of cell proliferation [2, 4, 30]. In turn, α-catenin is responsible for the binding of the complex to the actin cytoskeleton [12]. To more precisely evaluate intercellular adhesion, it is important to examine not only the expression pattern of E-cadherin in tumoral tissues but also those of α-catenin and β-catenin [9, 11]; abnormal and reduced expression of the E-cadherin/catenin complex in several human cancers is associated with tumor dedifferentiation, advanced clinical stages, and poor survival rate [21, 26, 31]. Ki-67 is a nuclear antigen expressed in proliferating but not resting cells and provides information of the growth fraction in individual tissues and tumors. MIB-1 is a monoclonal antibody that recognizes a fixation resistant epitope of the Ki-67 antigen [3, 8].

In an attempt to elucidate better the tumor biology of NETs and to investigate the role of cellular adhesion molecules in their growth and development, we examined immunohistochemically a series of gastrointestinal NETs for the frequency and pattern of expression of the E-cadherin and catenins. The relationship between their expression and Ki-67 or clinicopathological data was also evaluated.

Materials and methods

Tissue samples

Fifty-seven NETs of the gastrointestinal tract were retrieved from the surgical pathology files of the Department of Pathology, University of Tokushima School of Medicine and affiliated hospitals for the present study. Six tumors, for which depth of invasion could not be definitely confirmed, were excluded. All 51 samples were fixed with formalin and embedded in paraffin immediately after surgical resection. In cases with metastasis, metastatic tissues were obtained and compared with the primary tumors. Paraffin sections were stained using the Grimelius technique, with pan-neuroendocrine markers such as chromogranin A and synaptophysin to confirm the neuroendocrine immunophenotype. The diagnosis of NETs was made on the basis of morphological and immunohistochemical findings and evaluated by two independent pathologists (M.H. and T.S.) for the presence of tumor and to histologically classify the lesions according to the World Health Organization classification [28]. Clinical data for these cases were collected from the medical records.

We assessed correlations between the expression of E-cadherin or catenins and the following clinicopathological factors: age, embryological site of origin, size, histological growth pattern, the depth of penetration into the intestinal wall, and the presence of metastasis. The influence of these factors on prognosis has been previously reported [1, 16, 17, 33].

Immunohistochemistry

E-cadherin, α-catenin, β-catenin, and Ki-67 immunostains based on the labeled streptavidin biotin (LSAB) method were performed on sections from representative blocks of paraffin-embedded tissues used for pathology diagnosis. After deparaffinization and antigen retrieval using a microwave oven technique, the sections were incubated at 4°C overnight with MIB-1 mouse monoclonal antibody (1:50 dilution; Immunotech, Marseilles, France) or with mouse monoclonal antibodies against human E-cadherin, α-catenin, and β-catenin purchased from Transduction Laboratories (1:500 dilution; Lexington, Ky.). Then biotinylated link antibody and peroxidase-labeled streptavidin were applied for 1 h each at room temperature. Sections were washed thoroughly in phosphate-buffered saline between each of the immunostaining procedures. Antigen–antibody complexes were detected using the 3,3′-diaminobenzidine/H_2O_2 reaction. The slides were counterstained lightly with hematoxylin or 1% methyl green and mounted for microscopic examination. Sections incubated in phosphate-buffered saline without the primary antibody served as negative controls.

Evaluation of E-cadherin, α-catenin, and β-catenin expression

Positive control sections were processed from normal gastrointestinal epithelium, previously shown to express high levels of membranous E-cadherin, α-catenin, and β-catenin [6, 9]. In each case, the clear and unequivocally strong membranous staining pattern of the non-dysplastic columnar mucosa served as a positive internal control. All slides were assessed under a light microscope by two independent observers (M. H. and T.S.) without knowledge of the clinical parameters. Normal expression of E-cadherin, α-catenin, and β-catenin was defined as exclusively membranous staining, as seen in the normal gastrointestinal epithelium. A discontinuous or absent membranous staining, with or without cytoplasmic staining, was defined as abnormal. The percentage of tumor cells with normal membranous expression of E-cadherin, α-catenin, and β-catenin in each specimen was graded semi-quantitatively into one of the five-ties scale scoring system (– no staining; + 1–20%; ++ 20–50%; +++ 50–80%; ++++ >80%). In tumor itself, the superficial, mid-, and deep regions were separately analyzed. A global staining for the tumor was calculated as the average of the indices of the superficial, mid-, and deep regions. For β-catenin, tumors were additionally subdivided into either cytoplasmic or nuclear localization. Nuclear expression of β-catenin in tumor cells was considered positive (+) when more than 10% of nuclei were stained and negative (–) when less than 10% were stained. Cytoplasmic staining was considered positive when more than 10% of tumor cells were stained.

MIB-1 labeling index

The proliferating cell index was calculated from each slide according to the intensity of immunopositive nuclei. All definite nuclear immunostaining was considered positive. Vascular components and non-tumorous cells were excluded. To obtain the percentage (labeling index) of MIB-1-immunoreactive nuclei relative to the total neoplastic nuclei in each tumor, five color microphotos at ×200 magnification were taken from the non-overlapping repre-

Table 1 Clinicopathologic characteristics of 51 cases of neuroendocrine tumors (NETs) of the gastrointestinal tract. *f* foregut, *m* midgut, *h* hindgut, *sm* submucosa, *tm* transmural, *ly* lymph nodes

Case no.	Age/sex	Location	Extension	Size (cm)	Metastasis	E-cadherin	α-Catenin	Membranous β-catenin	Nuclear β-catenin	Cytoplasmic β-catenin	MIB-1 (%)
Well-differentiated NETs											
1	62/Male	f	sm	<2	–	++++	+++	+++	–	+	1.09
2	59/Male	f	sm	<2	–	++++	++++	++++	–	–	0.70
3	56/Female	f	sm	<2	–	++	++	++++	–	–	0.65
4	40/Male	f	sm	<2	–	+++	+++	+++	–	–	0.02
5	55/Male	f	sm	<2	–	++++	++++	++++	–	–	0.52
6	64/Male	f	sm	<2	–	+++	+++	+++	–	–	0.30
7	35/Male	f	sm	<2	–	++++	++++	++++	–	–	0.18
8	60/Female	m	sm	<2	–	+++	+++	++++	–	+	0.97
9	64/Male	m	sm	<2	–	+++	+++	+++	–	–	0.80
10	45/Male	m	sm	<2	–	++++	++++	++++	–	–	0.270
11	68/Male	m	sm	<2	–	++++	++++	+++	–	–	0.00
12	45/Male	h	sm	<2	–	+++	+++	+++	–	–	0.46
13	48/Male	h	sm	<2	–	+++	+++	++++	–	–	0.82
14	46/Female	h	sm	<2	–	++	++	++++	–	–	0.27
15	64/Male	h	sm	<2	–	++++	+++	++++	–	–	0.91
16	55/Male	h	sm	<2	–	++	+++	+++	–	–	0.82
17	75/Male	h	sm	<2	–	++	++	++++	–	+	0.99
18	53/Female	h	sm	<2	–	+++	+++	++++	–	–	0.14
Well differentiated NECs											
19	56/Male	f	sm	<2	ly	++++	++	++++	–	+	0.25
20	73/Female	f	tm	<2	–	+++	+++	+++	–	–	1.11
21	54/Male	f	tm	>2	ly	++	++	++	–	+	0.33
22	58/Female	f	tm	<2	–	++	++	++	–	–	0.12
23	72/Male	f	tm	<2	–	++	++	++	+	+	1.20
24	82/Male	m	sm	<2	liver	+++	+++	++++	+	+	1.61
25	63/Female	m	tm	<2	–	++	++	++	–	–	0.33
26	62/Male	h	sm	>2	–	++	++	++++	–	–	0.10
27	62/Male	h	tm	>2	ly	++	+	+++	–	–	2.55
28	57/Male	h	tm	<2	–	+	+	+	–	–	0.13
29	61/Female	h	tm	>2	–	+	+++	++	–	–	0.67
30	73/Female	h	tm	<2	–	+	++	++++	–	–	0.78
31	21/Female	h	tm	<2	–	+++	+++	+++	–	–	0.78
32	81/Male	h	tm	<2	–	+	++	+++	–	–	0.17
33	35/Male	h	tm	<2	–	+++	++++	+++	–	+	1.80
34	68/Female	h	tm	<2	–	+	++	+	–	–	0.21
35	13/Female	h	tm	>2	–	++	++	++	–	–	0.33
36	59/Female	h	tm	<2	–	+++	++	+++	+	+	0.10
37	62/Male	h	tm	<2	–	++	++	++	–	–	0.36
38	34/Male	h	tm	<2	–	+++	+++	+++	–	–	0.00
39	60/Male	h	tm	<2	–	+	+++	++	–	–	0.98
40	46/Male	h	tm	<2	–	++	++	++	–	–	0.00
Poorly differentiated NECs											
41	59/Female	f	sm	<2	–	++++	++++	++++	–	–	36.40
42	72/Male	f	tm	>2	ly	+++	+++	++	+(diffuse)	+	62.20
43	54/Male	f	tm	>2	–	+	+	–	–	–	56.20
44	69/Male	f	tm	>2	liver, pancreas, ly	+	–	+	+	+	19.70
45	84/Female	f	tm	>2	–	+++	++	++	+	–	23.00
46	60/Male	f	tm	>2	–	++	++	++	+	–	41.60
47	70/Male	f	tm	>2	small intestine	++	++	++	–	–	36.40
48	63/Female	m	tm	>2	–	++	++	+	+	–	45.20
49	71/Male	m	tm	>2	–	++	+	+	–	–	69.80
50	68/Male	h	tm	>2	–	–	–	–	–	–	45.00
51	72/Male	h	tm	>2	small intestine, ly	++	++	++	+	+	21.20

Table 2 Comparison of the expression pattern of E-cadherin, α-catenin and β-catenin in paired primary tumor and metastases in neuroendocrine tumors/carcinomas (NECs)

Case no.	E-cadherin		α-Catenin		β-Catenin					
	Primary tumor	Metastases	Primary tumor	Metastases	Membranous		Nuclear		Cytoplasmic	
					Primary tumor	Metastases	Primary tumor	Metastases	Primary tumor	Metastases
Well-differentiated NECs										
19	++++	++++	++	++	++++	++++	–	–	+	+
21	++	++	++	++	++	++	–	–	+	+
24	+++	+++	+++	++	++++	++++	+	+	+	+
27	++	++	+	+	+++	+++	–	–	–	–
Poorly differentiated NECs										
42	+++	+++	+++	+++	++	++	+(diffuse)	+(diffuse)	+	+
44*	+	+	–	–	+	+	+	+	+	+
47*	++	+	++	+	++	+	–	+	–	+
51*	++	+	++	+	++	+	+	+	+	+

*Autopsy was performed

sentative fields, although a greater number of fields were required to fully screen the sectional area, especially in larger specimens. The MIB-1 labeling index was expressed as the percentage of MIB-1-positive cells. Counting was performed without knowledge of the clinical data.

Statistics

Statistical correlation between two independent variables was computed by means of the Spearman rank-correlation coefficient, which does not require normal distribution. The Mann-Whitney U test was used to determine the difference in variability level between the distribution of two independent groups. Probability value $P<0.05$ was considered statistically significant.

Results

Clinicopathologic data

Among 51 cases of NETs, 19 arose in the foregut, 8 in the midgut, and 24 in the hindgut. These cases belonged to the complete neuroendocrine neoplastic spectrum: 18 well-differentiated NETs, 22 well-differentiated NECs, and 11 poorly differentiated NECs. There were 35 males and 16 female patients and the mean age of patients was 57.7 years (range 13–82 years). The tumor size ranged from 0.3 cm to 7 cm with a mean of 2.01 cm. Thirty-six tumors were less than 2.0 cm in average diameter, and 15 measured more than 2.0 cm (Table 1).

Microscopically, tumor cells of well-differentiated NETs and well-differentiated NECs were characterized by granular or clear cytoplasm, round to ovoid nuclei with small inconspicuous nucleoli, granular chromatin, minimal to moderate pleomorphism, and mitotic figures. The cells grew in nests, clusters, or trabeculae, occasionally forming tubular structures. For poorly differentiated NECs, tumor cells were composed of highly atypical, intermediate-sized cells growing in ill-defined aggregates, often with necrosis and prominent vascular invasion. The mitotic index was highly increased. All NETs showed Grimelius argyrophilia and diffuse chromogranin and/ or synaptophysin reactivity.

Twenty-two tumors were confined to the mucosa and submucosa; 29 tumors had infiltrated into the muscularis propria or beyond. Lymph-node metastases were present in six cases, and distant metastasis was seen in four (Table 1). Associated metastases were also examined and compared with primary tumors (Table 2).

Expression of E-cadherin

Membranous E-cadherin staining was localized uniformly at the intercellular borders of histologically normal epithelial cells. No cytoplasmic immunoreactivity was seen in normal epithelia.

All but nine NETs showed a decrease in membranous E-cadherin expression (Fig. 1a); 15 (29.4%) tumors displayed a slightly reduced expression (+++), 18 (35.3%) demonstrated ++ staining, 8 (15.7%) exhibited + staining, and one (1.9%) showed no immunopositive cells (–). The difference in percentage of membranous positive cells between normal tissues and well-differentiated NETs, well-differentiated NECs, or poorly differentiated NECs were statistically significant ($P=0.0038$, $P<0.001$, and $P=0.0002$, respectively, Fig. 2). Among the gastrointestinal NETs, E-cadherin was significantly higher in well-differentiated NETs than well-differentiated NECs or poorly differentiated NECs ($P=0.0006$ and $P=0.0053$, respectively, Fig. 2). There were no significant differences between well-differentiated NECs and poorly differentiated NECs. Furthermore, E-cadherin expression was significantly lower in lesions with transmural invasion and larger than 2.0 cm ($P<0.0001$ and $P=0.0013$, respectively, Fig. 3 and Fig. 4), but it was not correlated

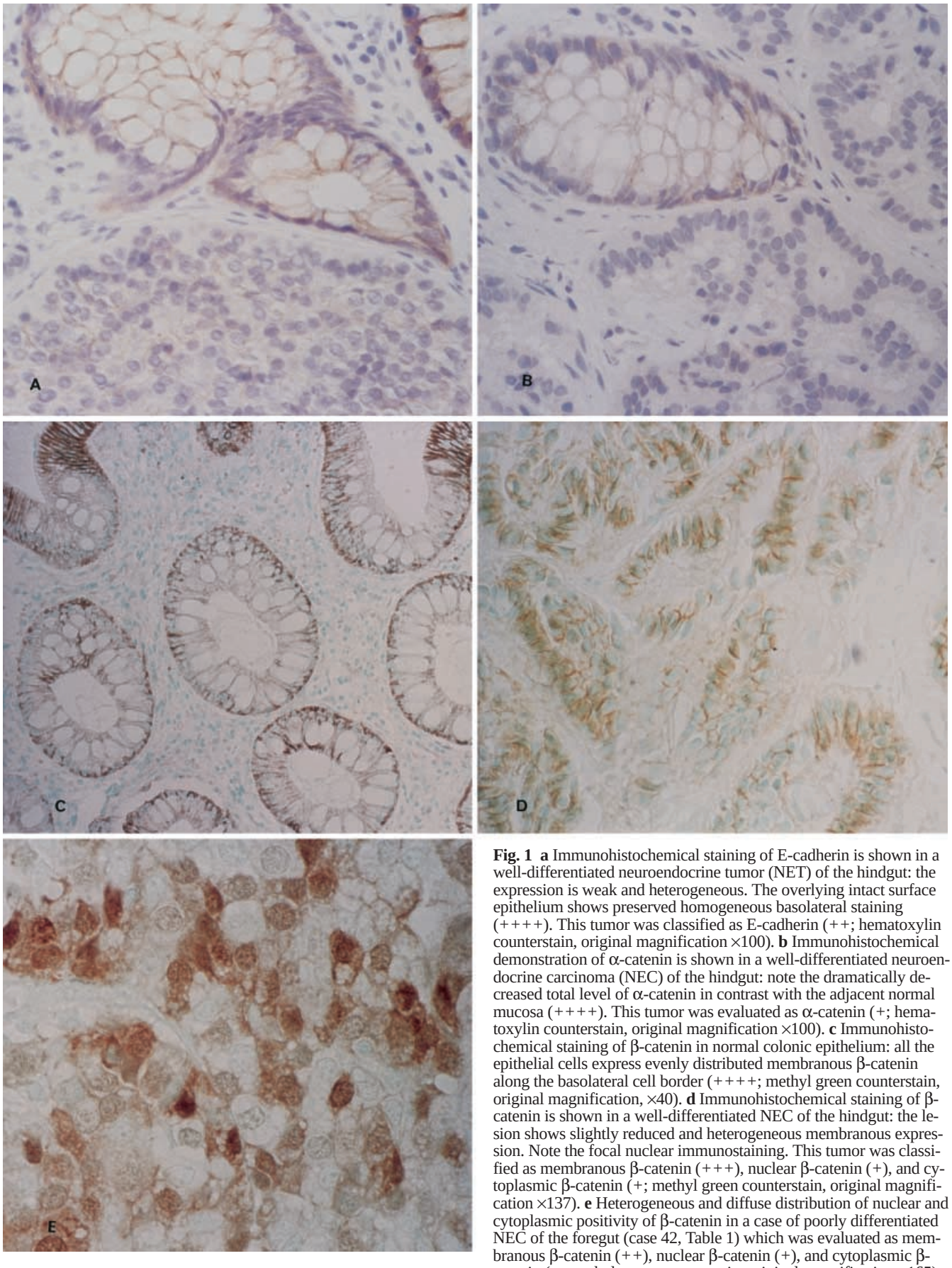

Fig. 1 **a** Immunohistochemical staining of E-cadherin is shown in a well-differentiated neuroendocrine tumor (NET) of the hindgut: the expression is weak and heterogeneous. The overlying intact surface epithelium shows preserved homogeneous basolateral staining (++++). This tumor was classified as E-cadherin (++; hematoxylin counterstain, original magnification ×100). **b** Immunohistochemical demonstration of α-catenin is shown in a well-differentiated neuroendocrine carcinoma (NEC) of the hindgut: note the dramatically decreased total level of α-catenin in contrast with the adjacent normal mucosa (++++). This tumor was evaluated as α-catenin (+; hematoxylin counterstain, original magnification ×100). **c** Immunohistochemical staining of β-catenin in normal colonic epithelium: all the epithelial cells express evenly distributed membranous β-catenin along the basolateral cell border (++++; methyl green counterstain, original magnification, ×40). **d** Immunohistochemical staining of β-catenin is shown in a well-differentiated NEC of the hindgut: the lesion shows slightly reduced and heterogeneous membranous expression. Note the focal nuclear immunostaining. This tumor was classified as membranous β-catenin (+++), nuclear β-catenin (+), and cytoplasmic β-catenin (+; methyl green counterstain, original magnification ×137). **e** Heterogeneous and diffuse distribution of nuclear and cytoplasmic positivity of β-catenin in a case of poorly differentiated NEC of the foregut (case 42, Table 1) which was evaluated as membranous β-catenin (++), nuclear β-catenin (+), and cytoplasmic β-catenin (+; methyl green counterstain, original magnification ×165)

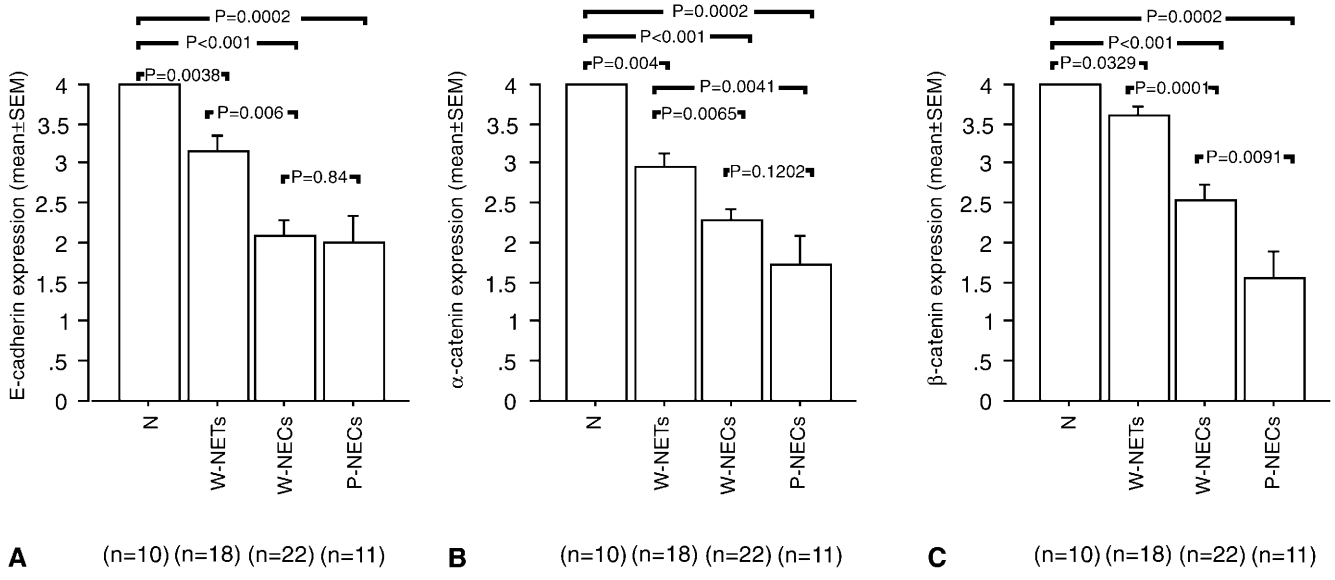

Fig. 2 Comparison of membranous expression of E-cadherin (**a**), α-catenin (**b**), and β-catenin (**c**) among normal gastrointestinal mucosa tissue (*N*) and well-differentiated neuroendocrine tumors (*W-NETs*), well-differentiated neuroendocrine carcinomas (*W-NECs*), and poorly differentiated neuroendocrine carcinomas (*P-NECs*) of the gastrointestinal tract. The percentage of membranous positive cells of W-NETs, W-NECs, P-NECs were significantly lower than N in E-cadherin, α-catenin, and β-catenin

with age, site, histological growth pattern, metastasis, or MIB-1 labeling index.

Expression of α-catenin

All non-tumorous epithelium expressed α-catenin homogeneously at cell–cell boundaries. As shown in Table 1, reduced membranous expression of α-catenin was demonstrated in 44 of the 51 NETs (Fig. 1b). Seventeen (33.3%) tumors showed a slightly reduced expression (+++), 21 (41.1%) displayed ++ staining, 4 (7.8%) exhibited + staining, and the remaining 2 (3.9%) showed complete loss of staining (–). The differences in percentage of the cells with normal expression between normal tissues and well-differentiated NETs, well-differentiated NECs, or poorly differentiated NECs were statistically significant (P=0.004, P<0.001, and P=0.0002, respectively, Fig. 2b). Among the gastrointestinal NETs, α-catenin was significantly higher in well-differentiated NETs than well-differentiated NECs or poorly differentiated NECs (P=0.0065 and P<0.0041, respectively, Fig. 2b). There were no significant differences between well-differentiated NECs and poorly differentiated NECs. Moreover, reduction of α-catenin expression was significantly correlated with transmural invasion and lesions larger than 2.0 cm (P=0.0001 and P=0.0001, respectively, Fig. 3 and Fig. 4), but not with other parameters.

Expression of β-catenin

Uniform, membranous immunoreactivity was localized at the intercellular junctions of normal epithelial cells (Fig. 1c). Table 1 shows the relationship between β-catenin expression and the aforesaid clinicopathologic features of NETs. Sixteen (31.3%) tumors expressed β-catenin homogeneously with the same intensity and pattern of distribution as normal mucosa (++++), 14 (27.4%) exhibited +++ staining, 14 (27.5%) showed ++ staining, 5 (9.8%) displayed + staining, two (3.9%) demonstrated + staining, and the remaining 2 (3.9%) showed complete loss of staining (–). Membranous expression of β-catenin was associated with aberrant cytoplasmic staining in 12 tumors (23.5%). Focal nuclear immunoreactivity was detected in 8 tumors (15.6%) of NETs, but none of the well-differentiated NETs showed nuclear staining for β-catenin (Fig. 1d), and diffuse nuclear accumulation of β-catenin was seen in one poorly differentiated NEC (Fig. 1e).

The differences in percentage of membranous positive cells between normal tissues and well-differentiated NETs, well-differentiated NECs, or poorly differentiated NECs were statistically significant (P=0.0329, P<0.001, and P=0.0002, respectively, Fig. 2c). Among the gastrointestinal NETs, β-catenin was significantly higher in well-differentiated NETs than well-differentiated NECs or poorly differentiated NECs (P=0.0001 and P<0.001, respectively, Fig. 2c). There was also a significant difference between well-differentiated NECs and poorly differentiated NECs (P=0.0091, Fig. 2c). Additionally, reduction of expression was correlated significantly with transmural tumor invasion and lesions larger than 2.0 cm (P<0.0001 and P<0.0001, respectively; Fig. 3 and Fig. 4), but not with age, site, histological growth pattern, metastasis, or MIB-1 labeling index.

No substantial differences were found in E-cadherin, α-catenin, and β-catenin expression between cells located in central region and cells in invasive front level of

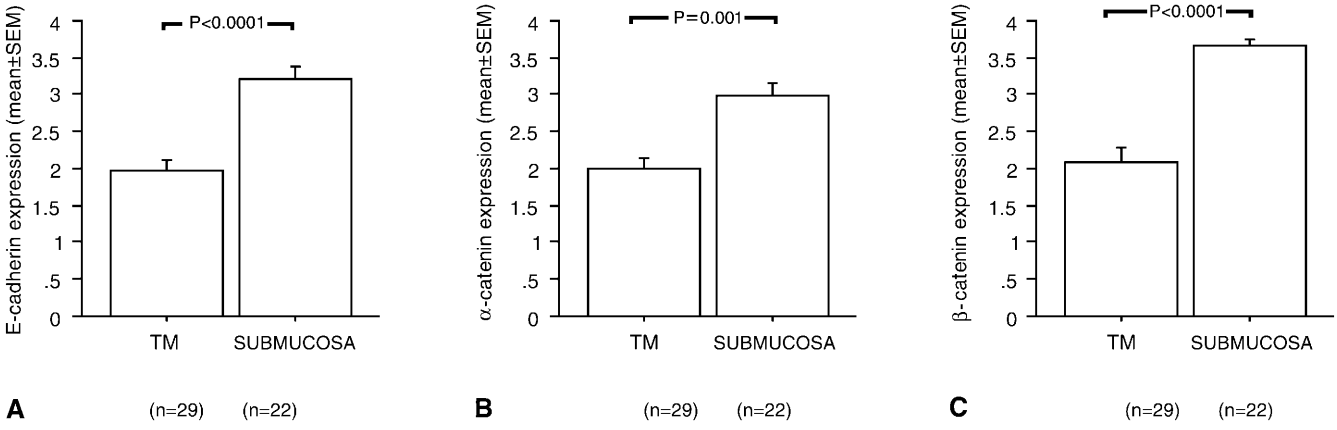

Fig. 3 Membranous expression of E-cadherin (**a**), α-catenin (**b**), and β-catenin (**c**) in tumors with transmural invasion (*TM*) and tumors limited to submucosa. The expression levels of E-cadherin, α-catenin, and β-catenin in TM are significantly lower than these in submucosa ($P<0.0001$, $P=0.001$, and $P<0.0001$, respectively)

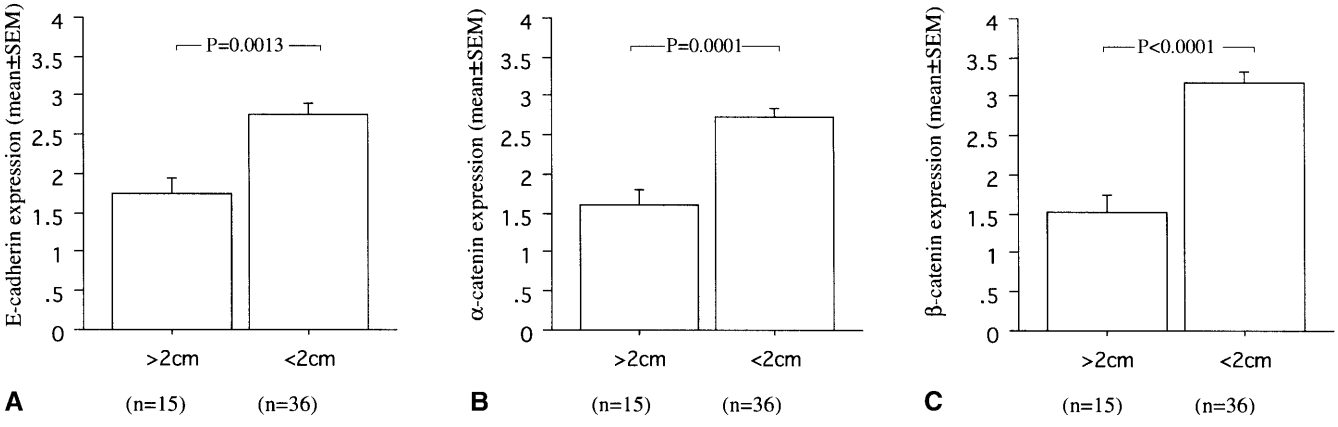

Fig. 4 Comparison of membranous expression of E-cadherin (**a**), α-catenin (**b**), and β-catenin (**c**) between neuroendocrine tumors greater than 2 cm and those smaller than 2 cm. The expression levels of E-cadherin, α-catenin, and β-catenin in tumors greater than 2 cm are significantly lower than in those smaller than 2 cm (P=0.0013, P=0.0001, and P<0.0001, respectively

the same well-differentiated NETs or well-differentiated NECs with transmural extension. However, the pattern of staining in poorly differentiated NECs was heterogeneous in different tumor cell levels, being lowest in the deep region, and 3 (27.2%) of 11 tumors demonstrated a dramatic reduced expression at the invasive front or on isolated invasive tumor cells in comparison with other regions. One of these tumors showed diffuse nuclear β-catenin staining throughout the tumor (case 42, Fig. 1e).

In eight cases, paired primary NECs and their corresponding lymph-node or distant metastases were available for comparison of expression of levels of E-cadherin and catenins. Although the expression of E-cadherin and catenins were coincident with those for primary tumors in six poorly differentiated NECs, the expression of E-cadherin and catenins were reduced in two metastatic tissues compared with their corresponding primary tumors (cases 47 and 51, Table 2).

MIB-1 labeling index

MIB-1 labeling index generally showed a low proliferative activity in well-differentiated NETs (0.49±0.37, mean±SEM) and well-differentiated NECs (0.662±0.66). A high proliferation rate was observed in poorly differentiated NECs (41.518±16.59). The highest rate (69.8%) was seen in one poorly differentiated NET of the midgut (case 49) showing transmural invasion. Although the difference in MIB-1 labeling index between well-differentiated NETs and well-differentiated NECs was not significant, MIB-1 labeling index was significantly higher in poorly differentiated NECs than well-differentiated NETs or well-differentiated NECs ($P<0.0001$ and $P<0.0001$, respectively, Fig. 5). There were no significant differences in MIB-1 labeling index between primary tumor and metastatic tissue. Neither age, site of origin, size, histological growth pattern, invasion, metastasis, E-cadherin, nor α-catenin or β-catenin expression were correlated with MIB-1 labeling index.

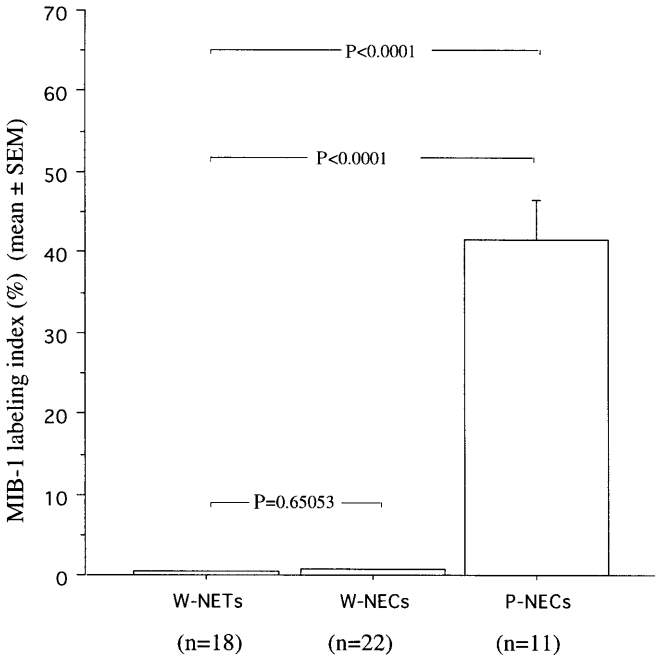

Fig. 5 MIB-1 labeling index in well-differentiated neuroendocrine tumors (*W-NETs*), well-differentiated neuroendocrine carcinomas (*W-NECs*), and poorly differentiated neuroendocrine carcinomas (*P-NECs*) of the gastrointestinal tract. Although the difference in MIB-1 between W-NETs and W-NECs was not significant, MIB-1 labeling index was significantly higher in P-NECs than in W-NETs or W-NECs ($P<0.0001$ and $P<0.0001$, respectively)

Discussion

It has recently been demonstrated in various carcinomas that E-cadherin and catenins are essential for intercellular junctions and that their decreased expression corresponds to poor prognosis associated with the dissemination of tumor cells and the formation of metastases [21, 26, 31]. However, to the best of our knowledge, E-cadherin and α-catenin have never been evaluated in gastrointestinal NETs until now, and only one study of β-catenin has been reported [24]. The focus in this study was on investigating expression of the E-cadherin/catenin complex in an attempt to elucidate better the molecular pathogenesis of gastrointestinal NETs. The relationship between the expression of the E-cadherin/catenin complex and the proliferative activity as measured by MIB-1 labeling index or clinicopathological data was also evaluated to further characterize these tumors.

Our immunohistochemical analysis demonstrated significant differences of percentage of membranous positive cells of E-cadherin, α-catenin, and β-catenin between normal tissues and well-differentiated NETs, well-differentiated NECs, or poorly differentiated NECs. The intensity of E-cadherin and α-catenin immunoreactivity progressively decreased in midgut, foregut, and hindgut tumors. In contrast, β-catenin was more likely to be positive in midgut, followed by hindgut and foregut tumors. No significant differences were observed among these three groups in expression of E-cadherin and catenins. Failure to demonstrate a statistical relationship may, in part, relate to the relatively small number of midgut tumors available for study in our series since the incidence of midgut NETs is very low in the Japanese population [13].

Among the gastrointestinal NETs, expression of E-cadherin, α-catenin, and β-catenin was significantly higher in well-differentiated NETs than well-differentiated NECs or poorly differentiated NECs. Reduced expression of membranous E-cadherin, α-catenin, and β-catenin was observed in tumors with transmural invasion significantly more often than in tumors limited to mucosa or submucosa. Our study also revealed a significant difference in expression of E-cadherin, α-catenin, and β-catenin between NETs greater than 2.0 cm and those smaller than 2.0 cm. This seems to be important since NETs greater than 2.0 cm in dimension are likely to behave in a more aggressive fashion [16, 17, 18, 33]. Moreover, a marked decrease in the expression of E-cadherin and catenins was observed in invasive front levels and isolated invasive tumor cells of three poorly differentiated NECs. In addition, the same findings were absent for well-differentiated NETs and well-differentiated NECs. These results suggest that downregulation of these complex molecules favors invasion and spreading of tumor. From all these findings, we consider that alterations of expression of E-cadherin and catenins may be a frequent event in NETs, especially in tumors larger than 2 cm and with transmural invasion, and poorly differentiated NECs.

It is noteworthy that β-catenin was localized to the nucleus in only 9 (17.6%) of 51 NETs, and 6 of 9 tumors are poorly differentiated NECs (Table 1). Nevertheless, we have to emphasize that nuclear immunoreactivity of β-catenin was not revealed in any of the 18 well-differentiated NETs. In a single study on β-catenin expression in gastrointestinal NETs, the authors reported the abnormal membranous and nuclear β-catenin expression in 8 (36%) of 22 NETs and that it was significantly correlated with the MIB-1 labeling index [24]. Our results were partly congruent with their findings of abnormal membranous and nuclear expression of β-catenin. They, however, did not comment on its correlation, if any, with the depth of penetration of these tumors, nor was the status of E-cadherin or α-catenin expression investigated. Even though the frequency was much lower in our data, it is of interest that the aberrant nuclear β-catenin expression was observed in the gastrointestinal NETs. The processes that result in downregulation of E-cadherin-mediated cell adhesion in human cancers in vivo and in vitro have been dealt with previously, and various mechanisms of alterations were proposed. They include downregulation of E-cadherin expression, its gene mutation, abnormality or deletion of catenins, and biochemical modification of catenins [29]. Nevertheless, neither genetic alterations in the E-cadherin gene nor mutations in exon 3 of the β-catenin gene were detected in NETs [6, 24]. Regarding the third mechanism, stimulation of epidermal growth factor

(EGF) or transforming growth factor-α (TGF-α) on tumor cells through the EGF receptor (EGFR) plays a critical role in malignant progression by increasing the transduction of mitogenic signals and interfering with the E-cadherin/catenin complex [2, 4, 30]. Previous studies have revealed frequent co-expression of TGF-α and EGFR in gastrointestinal NETs, especially in larger lesions [19, 27]. On the basis of our results, it may be speculated that the interactions between TGF-α and EGFR may initiate the cascade of tyrosine phosphorylation resulting in downregulation of the E-cadherin/catenin complex and nuclear β-catenin accumulation, which may play a direct role in the tumor growth and progression in well-differentiated NECs and poorly differentiated NECs. However, other mechanisms are possible. To further clarify this point, other molecular methods might provide important insights into the tumor biology of NETs.

Although the histological architecture of most well-differentiated NETs are almost invariably composed of solid nests, trabecular or sometimes pseudoglandular structures, downregulation of E-cadherin, α-catenin, and β-catenin were observed to a variable degree in more than half of our cases compared with normal gastrointestinal mucosa. Tissue architecture is maintained by cell–cell and cell–extracellular matrix adhesion. The molecules related to cell adhesion include the cadherins, integrins, molecules belonging to the immunoglobulin superfamily, and selectins [23]. As one of the possible explanations, other adhesion-related molecules may compensate for downregulation of the E-cadherin/catenin system to some extent in well-differentiated NETs. Despite the fact that a rather organized cell structure is formed during the growth of NETs, disturbances in cell–cell interaction seem to be present. Although unusual, this event is not surprising since similar results were observed in squamous intraepithelial lesions of the uterine cervix and NETs of the lung [6, 7].

Furthermore, based on our results, the growth rate of well-differentiated NETs and well-differentiated NECs measured by MIB-1 labeling index was very low (0.49±0.37 and 0.66±0.66, respectively) in contrast to poorly differentiated NECs (41.51±16.59); these findings are in general agreement with those in most published reports [1, 20, 27]. In analysis of gastrointestinal NETs, Semba et al. reported a very high MIB-1 labeling index (mean 16.4) compared with our results (mean 9.4) [24]. The sharp difference in the MIB-1 labeling index and the frequency of nuclear β-catenin expression between their results and ours could be explained by the results that the tumors included in their series were overwhelmingly malignant (9 poorly differentiated NECs and 11 well-differentiated NECs of 22 NETs). Our results also demonstrated a significant difference of MIB-1 labeling index between poorly differentiated NECs and well-differentiated NETs or well-differentiated NECs. In our series, the proliferative activities in the majority of well-differentiated NETs and well-differentiated NECs were low and substantially different from poorly differentiated NECs. This view was also supported by the difference of expression of E-cadherin and catenins among these three groups. An previous article reported that poorly differentiated NECs, independent of their sites of origin, have to be regarded as an entity distinct from well-differentiated NETs and well-differentiated NECs, and they may arise from different precursor cell populations [10].

In summary, we showed that decreased or aberrant expression of E-cadherin, α-catenin, and β-catenin was common in NETs of the gastrointestinal tract, and that it was significantly associated with tumor invasion and size. These results indicate that the alteration in the E-cadherin/catenin expression may be involved in the growth and progression of gastrointestinal NETs.

References

1. Al-Khafaji B, Noffsinger AE, Miller MA, DeVoe G, Stemmermann GN, Fenoglio-Preiser C (1998) Immunohistologic analysis of gastrointestinal and pulmonary carcinoid tumors. Hum Pathol 29:992–999
2. Barth AI, Nathke IS, Nelson WJ (1997) Cadherins, catenins and APC protein: interplay between cytoskeletal complexes and signaling pathways. Curr Opin Cell Biol 9:683–690
3. Beer TW, Buchanan R, Matthews AW, Stradling R, Pullinger N, Pethybridge RJ (1998) Prognosis in malignant mesothelioma related to MIB 1 proliferation index and histological subtype. Hum Pathol 29:246–251
4. Behrens J, von Kries JP, Kuhl M, Bruhn L, Wedlich D, Grosschedl R, Birchmeier W (1996) Functional interaction of beta-catenin with the transcription factor LEF-1. Nature 382:638–642
5. Capella C, Heitz PU, Hofler H, Solcia E, Klöppel G (1994) Revised classification of neuroendocrine tumors of the lung, pancreas and gut. Digestion 55[Suppl 3]:11–23
6. Clavel CE, Nollet F, Berx G, Tejpar S, Nawrocki-Raby B, Kaplan HH, van Roy FM, Birembaut PL (2001) Expression of the E-cadherin-catenin complex in lung neuroendocrine tumours. J Pathol 194:20–26
7. de Boer CJ, van Dorst E, van Krieken H, Jansen-van Rhijn CM, Warnaar SO, Fleuren GJ, Litvinov SV (1999) Changing roles of cadherins and catenins during progression of squamous intraepithelial lesions in the uterine cervix. Am J Pathol 155:505–515
8. Gerdes J, Lemke H, Baisch H, Wacker HH, Schwab U, Stein H (1984) Cell cycle analysis of a cell proliferation-associated human nuclear antigen defined by the monoclonal antibody Ki-67. J Immunol 133:1710–1715
9. Gofuku J, Shiozaki H, Tsujinaka T, Inoue M, Tamura S, Doki Y, Matsui S, Tsukita S, Kikkawa N, Monden M (1999) Expression of E-cadherin and alpha-catenin in patients with colorectal carcinoma. Correlation with cancer invasion and metastasis. Am J Clin Pathol 111:29–37
10. Helpap B, Kollermann J (2001) Immunohistochemical analysis of the proliferative activity of neuroendocrine tumors from various organs. Are there indications for a neuroendocrine tumor-carcinoma sequence? Virchows Arch 438:86–91
11. Hirohashi S (1998) Inactivation of the E-cadherin-mediated cell adhesion system in human cancers. Am J Pathol 153:333–339
12. Ilyas M, Tomlinson IP (1997) The interactions of APC, E-cadherin and beta-catenin in tumour development and progression. J Pathol 182:128–137
13. Iwafuchi M, Watanabe H, Noda Y (1989) Gastrointestinal carcinoid tumor of Japanese: incidence and characteristic based on anatomical classification, with special reference to difference between carcinoid tumor and endocrine cell carcinomas. Stomach Intest 24:869–882

14. Klöppel G, Heitz PU, Capella C, Solcia E (1996) Pathology and nomenclature of human gastrointestinal neuroendocrine (carcinoid) tumors and related lesions. World J Surg 20:132–141
15. Lollgen RM, Hessman O, Szabo E, Westin G, Akerstrom G (2001) Chromosome 18 deletions are common events in classical midgut carcinoid tumors. Int J Cancer 92:812–815
16. MacGillivray DC, Synder DA, Drucker W, ReMine SG (1991) Carcinoid tumors: the relationship between clinical presentation and the extent of disease. Surgery 110:68–72
17. McDermott EW, Guduric B, Brennan MF (1994) Prognostic variables in patients with gastrointestinal carcinoid tumours. Br J Surg 81:1007–1009
18. Moertel CG, Sauer WG, Dockerty MB, Baggenstoss AH (1961) Life history of the carcinoid tumor of the small intestine. Cancer 14:901–912
19. Nilsson O, Wangberg B, Kolby L, Schultz GS, Ahlman H (1995) Expression of transforming growth factor alpha and its receptor in human neuroendocrine tumours. Int J Cancer 60:645–651
20. Pelosi G, Fraggetta F, Sonzogni A, Fazio N, Cavallon A, Viale G (2000) CD99 immunoreactivity in gastrointestinal and pulmonary neuroendocrine tumours. Virchows Arch 437:270–274
21. Pignatelli M, Ansari TW, Gunter P, Liu D, Hirano S, Takeichi M, Klöppel G, Lemoine NR (1994) Loss of membranous E-cadherin expression in pancreatic cancer: correlation with lymph node metastasis, high grade, and advanced stage. J Pathol 174:243–248
22. Ramnani DM, Wistuba II, Behrens C, Gazdar AF, Sobin LH, Albores-Saavedra J (1999) K-ras and p53 mutations in the pathogenesis of classical and goblet cell carcinoids of the appendix. Cancer 86:14–21
23. Schweighoffer T, Shaw S (1992) Adhesion cascades: diversity through combinatorial strategies. Curr Opin Cell Biol 4:824–829
24. Semba S, Kusumi R, Moriya T, Sasano H (2000) Nuclear accumulation of α-catenin in human endocrine tumors: association with Ki-67 (MIB-1) proliferative activity. Endocr Pathol 11:243–250
25. Shebani KO, Souba WW, Finkelstein DM, Stark PC, Elgadi KM, Tanabe KK, Ott MJ (1999) Prognosis and survival in patients with gastrointestinal tract carcinoid tumors. Ann Surg 229:815–823
26. Shimazui T, Schalken JA, Giroldi LA, Jansen CF, Akaza H, Koiso K, Debruyne FM, Bringuier PP (1996) Prognostic value of cadherin-associated molecules (alpha-, beta-, and gamma-catenins and p120cas) in bladder tumors. Cancer Res 56:4154–4158
27. Shimizu T, Tanaka S, Haruma K, Kitadai Y, Yoshihara M, Sumii K, Kajiyama G, Shimamoto F (2000) Growth characteristics of rectal carcinoid tumors. Oncology 59:229–237
28. Solcia E, Klöppel G, Sobin LH (2000) Histological typing of neuroendocrine tumors. International histological classification of tumours. World Health Organization. Springer, Berlin Heidelberg New York
29. Takayama T, Shiozaki H, Shibamoto S, Oka H, Kimura Y, Tamura S, Inoue M, Monden T, Ito F, Monden M (1996) Beta-catenin expression in human cancers. Am J Pathol 148:39–46
30. Tao YS, Edwards RA, Tubb B, Wang S, Bryan J, McCrea PD (1996) beta-Catenin associates with the actin-bundling protein fascin in a noncadherin complex. J Cell Biol 134:1271–1281
31. Umbas R, Isaacs WB, Bringuier PP, Schaafsma HE, Karthaus HF, Oosterhof GO, Debruyne FM, Schalken JA (1994) Decreased E-cadherin expression is associated with poor prognosis in patients with prostate cancer. Cancer Res 54:3929–3933
32. Zhao J, de Krijger RR, Meier D, Speel EJ, Saremaslani P, Muletta-Feurer S, Matter C, Roth J, Heitz PU, Komminoth P (2000) Genomic alterations in well-differentiated gastrointestinal and bronchial neuroendocrine tumors (carcinoids): marked differences indicating diversity in molecular pathogenesis. Am J Pathol 157:1431–1438
33. Zeitels J, Naunheim K, Kaplan EL, Straus F 2nd (1982) Carcinoid tumors: a 37-year experience. Arch Surg 117:732–737

Virchows Arch (2002) 440:155–159
DOI 10.1007/s00428-001-0569-6

ORIGINAL ARTICLE

Aldo Scarpa · Simonetta Orlandini
Patrick S. Moore · Nicholas R. Lemoine
Stefania Beghelli · Antonella Baron
Massimo Falconi · Giuseppe Zamboni

Dpc4 is expressed in virtually all primary and metastatic pancreatic endocrine carcinomas

Received: 21 August 2001 / Accepted: 19 September 2001 / Published online: 23 November 2001
© Springer-Verlag 2001

Abstract *DPC4/Smad4* is inactivated in about 50% of pancreatic ductal cancers. It has been recently reported that this gene is also inactivated in neoplasms arising from pancreatic islet cells, a phenomenon suggested to be related to similar progressions of malignancy found in common ductal cancers. To evaluate this possibility, we analysed 20 metastases of pancreatic endocrine carcinomas and their corresponding primary lesion for inactivation of *DPC4* using immunohistochemical staining. In fact, immunohistochemical labelling has been shown to correlate with *DPC4* gene status with high sensitivity and specificity. The cancers included 18 nonfunctioning tumours, one gastrinoma and one VIPoma all with liver, nodal and/or adrenal metastases. Seventeen were well-differentiated and three poorly differentiated endocrine carcinomas. Dpc4 expression was absent in only one primary well-differentiated endocrine cancer and its liver metastasis, while all the remaining 19 primary tumours and their metastases stained positive for the protein. All positively staining cases showed diffuse cytoplasmic and nuclear staining in virtually all neoplastic cells. Our data suggest that *DPC4* is only rarely involved in pancreatic endocrine tumourigenesis and give further weight to the hypothesis that tumours arising from pancreatic exocrine and endocrine epithelia are genetically distinct.

Keywords Pancreas · Carcinoma · Endocrine tumour · *DPC4/Smad4*

A. Scarpa (✉) · S. Orlandini · P.S. Moore · S. Beghelli · A. Baron
G. Zamboni
Dipartimento di Patologia, Sezione di Anatomia Patologica,
Università di Verona, Strada Le Grazie, 37134 Verona, Italy
e-mail: a.scarpa@univr.it
Tel.: +39-045-8074822, Fax: +39-045-8027136

N.R. Lemoine
ICRF Molecular Oncology Unit, Department of Cancer Medicine,
Imperial College School of Medicine, London, UK

M. Falconi
Department of Surgery, University of Verona, Italy

Introduction

Pancreatic tumours arising from islet cells (PETs) are a heterogeneous group of neoplasms clinically classified as functional or nonfunctional according to the presence or absence of symptoms due to hormone hypersecretion by the tumour. These neoplasms are poorly understood from a molecular genetic standpoint, and although they have been analysed for alterations in the four genes most frequently altered in common ductal adenocarcinoma, namely *K-ras*, *p53*, *p16* and *DPC4*, the former two genes are only rarely mutated in PETs [4, 9]. In a study of 12 PETs, the *p16* gene has been reported to be altered in 92% of cases (7 of 8 gastrinomas and 4 of 4 nonfunctional) [10]. However, the recent analysis of larger series of PETs failed to confirm this finding, and mutations have been only observed in a small proportion of insulinomas [3, 9].

The *DPC4/Smad4* gene, a component of the transforming growth factor-β signaling pathway, has been implicated in about half of all pancreatic ductal adenocarcinomas and may be inactivated by mutation of one allele and the loss of the other or alternatively by homozygous deletion [6]. The recent report of alterations in *DPC4* in 5 of 9 malignant but in none of 16 benign PETs would suggest that this gene may be involved in the progression of malignancy in PETs [2]. We have also recently analysed the status of *DPC4* in 41 primary PETs, including 18 malignant cases, by both molecular methods and immunohistochemistry [9], but no alterations were found in any case. Given that loss of expression of Dpc4 has been shown to correlate with the development of infiltrating pancreatic cancer in common adenocarcinomas [13], one might then expect the lack of Dpc4 expression in metastases even in the presence of protein expression in the vast majority of cells in the corresponding primary cancer. If verified, this would also have the more widespread implication that a common molecular pathway is involved in the progression of malignancy of pancreatic exocrine and endocrine epithelia.

Table 1 Clinicopathological data of the pancreatic endocrine carcinomas. *NF* nonfunctioning tumour, *NF20* patient with multiple endocrine neoplasia type 1 syndrome, *F16* gastrinoma, *F17* VIPoma, *WDEC* well-differentiated endocrine carcinoma, *PDEC* poorly differentiated endocrine carcinoma, *AWD* alive with disease, *DOD* died of disease

Case	Sex	Age	Diagnosis	Size (cm)[a]	Metastasis	Dpc-4 immunostain		Follow-up[b]	Postoperative survival
						Primary	Metastasis		
NF 9	Female	47	WDEC	Multiple	Liver	+	+	24	DOD
NF 11	Female	52	WDEC	14	Liver	+	+	37	AWD
NF 13	Female	68	WDEC	5	Liver	+	+	34	AWD
NF 18	Female	56	WDEC	10	Liver	+	+	37	DOD
NF 20	Female	62	WDEC	2	Liver	+	+	77	AWD
NF 22	Female	58	WDEC	1.5	Liver	+	+	50	DOD
NF 24	Female	55	WDEC	6	Liver	+	+	120	AWD
NF 27	Male	48	WDEC	6	Liver	+	+	54	DOD
NF 32	Male	27	PDEC	3	Liver	+	+	11	DOD
NF 37	Male	53	WDEC	4	Liver	+	+	4	AWD
NF 38	Female	61	WDEC	3	Liver, lung	+	+	15	DOD
NF 40	Female	55	WDEC	3.5	Liver	+	+	71	DOD
NF 41	Male	60	PDEC	10	Liver	+	+	2	DOD
NF 42	Female	45	WDEC	2.5	Liver	+	+	24	DOD
NF 43	Female	68	WDEC	6	Liver, lung	+	+	21	DOD
NF 44	Male	40	WDEC	14	Adrenal	+	+	4	DOD
NF 45	Female	75	WDEC	3	Liver	Negative	Negative	12	AWD
NF 46	Male	56	WDEC	6	Liver	+	+	24	AWD
F 16	Female	25	PDEC	4	Liver	+	+	19	DOD
F 17	Male	54	WDEC	2.6	Liver	+	+	66	AWD

[a] Maximum diameter of the primary tumour: NF9 had multiple nodules with the largest measuring 1.5 cm; for cases NF38, NF41, NF43 and NF45 the dimensions are from computed tomography scans as the tumour was not removed and only bioptic material was available

[b] In cases NF39 and NF44, diagnosis preceded surgery by 24 months and 30 months, respectively

To address this possibility specifically, we have analysed 20 metastatic PETs and their corresponding primary cancers for the expression of Dpc4 using immunohistochemical methods. In fact, it has been recently demonstrated that immunohistochemistry is an excellent marker for alteration of *DPC4*, and its negative staining correlates with genetic inactivation in 93% of cases [14]. Thus this high selectivity precludes the need for molecular analyses as *DPC4* status can be assessed by a simple test performed on archival material.

Materials and methods

Primary tumours and metastases

Twenty malignant PETs for which metastatic tissues were available were examined in the present study (Table 1). Tumours were classified according to World Health Organization classification [12]. They included 17 well-differentiated endocrine carcinomas and three poorly differentiated endocrine carcinomas; 18 cancers were nonfunctional and 2 functional (one gastrinoma and one VIPoma). Tumours were characterised using a panel of monoclonal antibodies recognising pan-endocrine markers (chromogranin A, synaptophysin and neuron-specific enolase) and gastrointestinal hormones (insulin, glucagon, somatostatin, pancreatic polypeptide, gastrin, serotonin and vasoactive intestinal peptide). Only those tumours giving rise to an endocrine syndrome were considered as functional. PETs were considered nonfunctional if clinical symptoms were absent, regardless of the immunostaining results. The mean patient age was 53.3±12.4 years and included 7 males and 13 females. All cases were sporadic with the exception of NF20, which came from a multiple endocrine neoplasia type-1 patient. Follow-up data were available for all 20 cases. At a mean follow-up time of 35±30 months, nine patients were still alive with disease, while the remainder had died of their disease.

Cell lines

Four genetically characterised human pancreatic adenocarcinoma cell lines, BI, CFPAC1, PaCa44 and HPAF II [8], were used in this study as controls for Dpc4 immunodetection. All cell lines were cultured in RPMI 1640 medium supplemented with 10% heat-inactivated foetal calf serum (Gibco BRL, Life Technologies, Milan, Italy) and were *Mycoplasma* free.

Immunohistochemistry for Dpc4

Immunohistochemistry was performed on paraffin sections using a monoclonal antibody [Santa Cruz Smad4 (B-8) from Autogen Bioclear, Calne, UK] at a dilution of 1:100 following antigen retrieval by microwaving three times for 10 min each in 10 mM citrate buffer, pH 6. Normal pancreatic structures in the same sections served as positive controls. Immunostaining for cell lines was essentially the same with 2-h incubation for anti-Dpc4 antibody after fixation of cytospin preparations in cold acetone for 5 min.

Immunoblot analysis for Dpc4

Western-blot analysis was performed on one normal pancreas, two samples of primary endocrine tumours (NF9 and NF41) and the four pancreatic adenocarcinoma cell lines. Freshly frozen tissue fragments were minced in dry ice and lysed in 150 mM NaCl, 20 mM HEPES (pH 7.5), 1% Triton X-100, 1% sodium deoxycholate, 0.1% sodium dodecyl sulfate (SDS), 1 mM ethylene diamine tetraacetate, 10 µg/ml chymostatin–leupeptin–aprotinin–pepstatin, 1 mM phenylmethylsulfonyl fluoride and 1 mM dithiothreitol. Cultured cells were directly lysed (2×107 cells/ml). Proteins

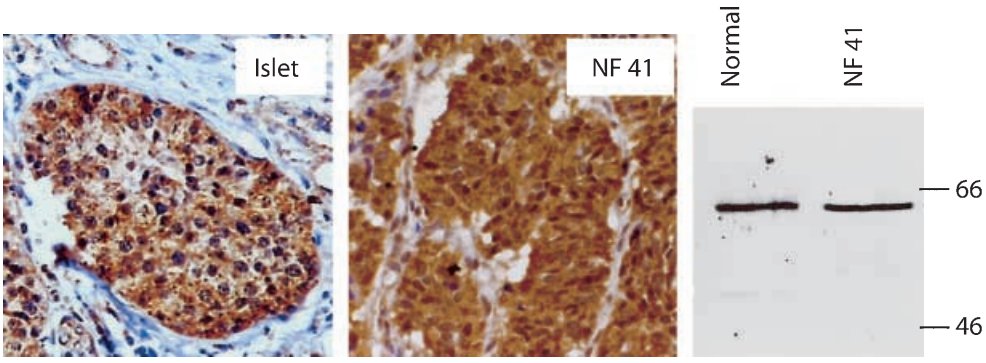

Fig. 1 Example of immunohistochemistry with anti-Dpc4 antibodies of a normal islet of Langerhans and of poorly differentiated pancreatic endocrine cancer NF41. Cytoplasmic and occasional nuclear staining is seen in islet cells while diffuse staining of both cytoplasms and nuclei is evident in cancer cells. On the *right*, the Western-blot analysis of a normal pancreas and cancer NF41 using the same anti-Dpc4 antibody shows the expected band at 64-kDa

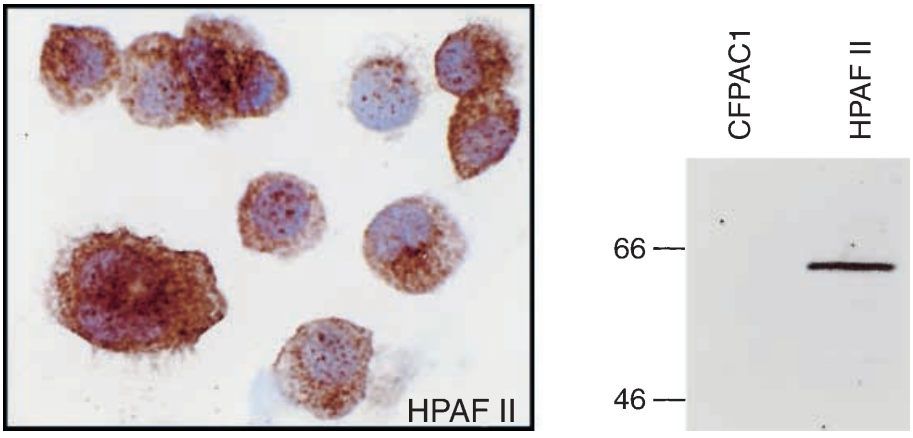

Fig. 2 The pancreatic ductal cancer cell line HPAF II shows positive immunostaining with anti-Dpc4 antibody and the expected 64-kDa band by Western-blot analysis with the same anti-Dpc4 antibody. CFPAC1 ductal carcinoma cell line, which was negative by immunohistochemistry, shows no Dpc4 band at Western-blot analysis

(50 µg) were fractionated by SDS–polyacrylamide gel electrophoresis in a 12% gel, electroblotted onto nitrocellulose membrane (2.5 mA/cm^2 for 30 min) and reacted with the same anti-Dpc4 monoclonal antibody used for immunohistochemistry at a dilution of 1:1000 according to standard procedures. The ECL Western detection system (Amersham, Milan, Italy) was used, and the blot was exposed to X-ray film for 1–60 min.

Results

Specificity of anti-Dpc4 antibody

It has been previously shown by our group and others that immunohistochemistry detects expression of Dpc4 in all normal pancreatic acinar, ductal and islet cells, where strong to intermediate cytoplasmic reactivity with variable nuclear labelling is observed [9, 14]. The cytoplasmic staining of islet cells is usually strong, and the nuclear immunoreactivity is variable from relatively few, as shown in Fig. 1, to virtually all nuclei. Moreover, Dpc4 immunohistochemical staining has been shown to be highly specific and sensitive for inactivation of *DPC4* [14], a finding confirmed in a series of 112 primary pancreatic tumours for which molecular data were available [9]. As further controls for the validity of Dpc4 immunostaining, we studied four human pancreatic cancer cell lines for Dpc4 expression using both Western blot and immunocytochemistry. Two cell lines, BI and CFPAC1, showed no Dpc4 expression by either technique, whereas PaCa44 and HPAF II showed positive immunostaining and the expected band using Western-blot analysis. The results for CFPAC1 and HPAF II are shown in Fig. 2. These data are concordant with the status of the *DPC4* gene in these cell lines. In fact, BI and CFPAC1 have homozygous deletion of the gene, while PaCa44 and HPAF II have no *DPC4* alteration [8]. Thus, ample data exist that validate the use of Dpc4 immunostaining as a marker for *DPC4* inactivation.

Dpc4 expression in primary and metastatic pancreatic endocrine cancers

We thus used immunohistochemistry to study the expression of Dpc4 in 20 metastatic pancreatic endocrine cancers and their corresponding primary lesions. The primary tumours of six of these cases (NF9, NF20, NF22, NF24, NF27 and NF32) have been previously analysed for both Dpc4 immunohistochemical expression and *DPC4* gene status [9]. The immunolabeling for Dpc4 was scored as positive or negative. Tumours scored as positive showed diffuse cytoplasmic and nuclear staining in the vast majority of the tumour cells (>90%, Fig. 1 and Fig. 3). The staining intensity was strong in 16 cases and moderate in three. The proportion of stained nuclei was somewhat variable as it was present in almost all nuclei in 13 cases and in only about 50% of cancer cells in six cases. Tumours scored as negative showed no detect-

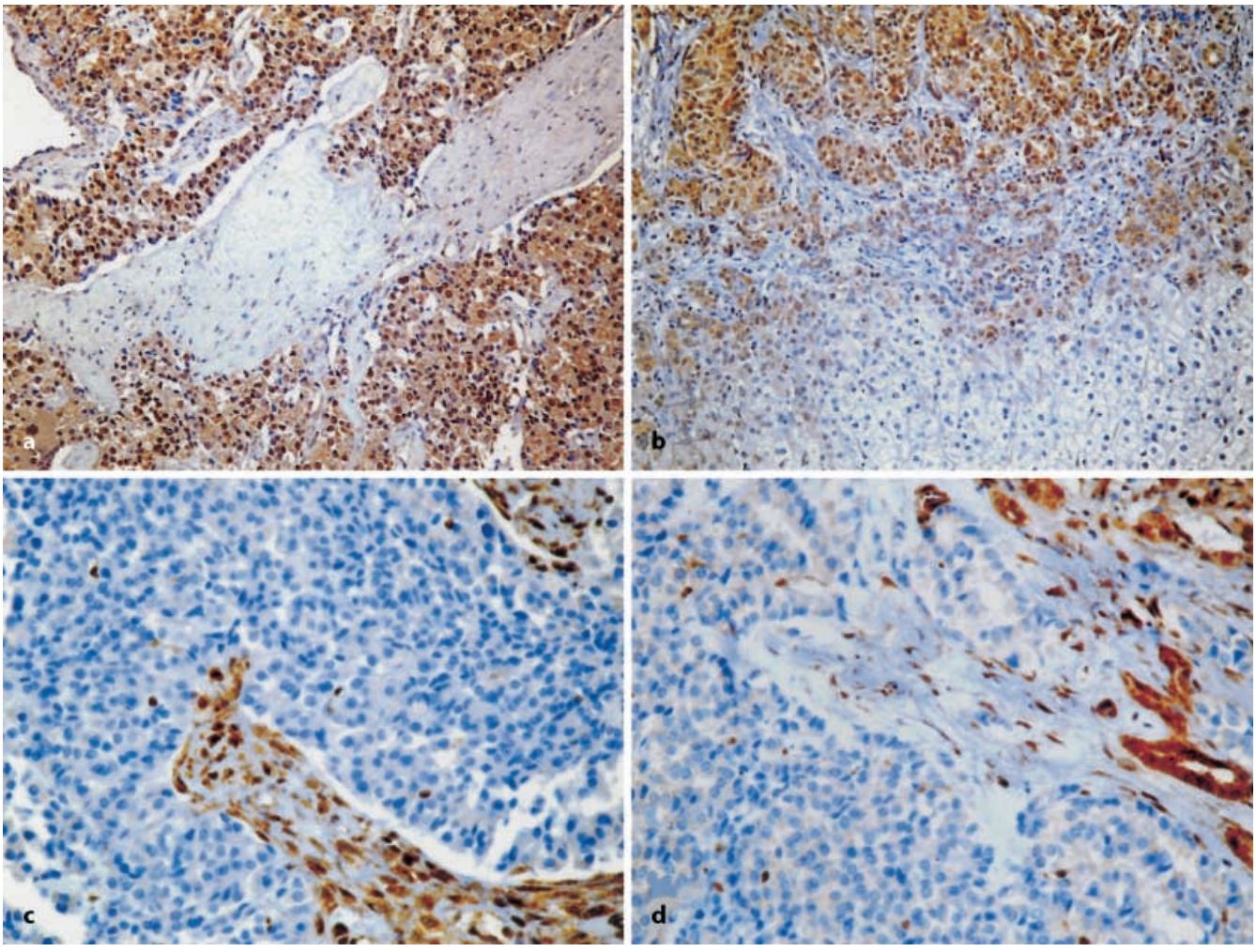

Fig. 3 Representative examples of immunohistochemistry with anti-Dpc4 antibodies. Two primary pancreatic endocrine cancers and their corresponding liver metastasis are shown. Case NF9 shows a clear cytoplasmic staining in all cancer cells of both **a** primary and **b** metastatic lesions, while case NF45 is the only one that lacked Dpc4- expression in both **c** primary and **d** metastatic cancer among the 20 cases studied. Stromal and bile duct cells are a clear internal positive control in **c** and **d**

able cytoplasmic or nuclear Dpc4. Immunohistochemical expression of Dpc4 was detected in all but one of the primary cancers (Fig. 3). Thus 95% (19 of 20) of the tumours in this series showed normal expression of Dpc4, which was confirmed by Western-blot analysis in two cases: well-differentiated cancer NF9 and poorly differentiated cancer NF41 (Fig. 1). The analysis of the metastatic lesions for all 20 PETs for Dpc4 expression showed that only the liver metastasis from the Dpc4-i mmunonegative well-differentiated primary cancer NF45 stained negative. Unfortunately, no molecular or Western-blot analysis could be performed in this case as no frozen material was available. All the other 19 metastases stained positive for the protein.

Discussion

Alterations in the *DPC4* gene have been reported to occur in malignant nonfunctioning PETs [2]. We have recently analysed a series of 41 primary PETs (30 nonfunctioning and 11 functioning), 18 of which were malignant, for alterations in *DPC4* using both molecular and immunohistochemical methods [9]. No molecular alterations were found in any of these cases, and all 36 cases tested using immunohistochemistry showed Dpc4 expression [9]. In this latter study only primary tumours were analysed. Similar findings have also been reported in a series of 41 primary PETs by Allen et al. at a recently held meeting [1]. Therefore, to rule out the possibility that *DPC4* could be involved in the pathogenesis of metastasis through clonal selection for loss or inactivation of the gene product among the primary cancer cells, we performed the present study on 20 metastatic lesions and their corresponding primary cancer. In other words, it might be expected that metastasis could be formed by cancer cells with loss of Dpc4 expression even in the presence of protein expression in the vast majority of cells in the corresponding primary cancer.

Remarkably, expression of Dpc4 was found in all but one of these 20 cancers and their corresponding metas-

tases. The Dpc4 expressing cases included 16 well-differentiated and three poorly differentiated carcinomas, while the only case lacking Dpc4 was a well-differentiated cancer. We conclude that *DPC4* is an infrequent target of inactivation in tumours arising from islet cells, including more aggressive neoplasms and comprising both clinically functioning and nonfunctioning tumours.

A total of 91 primary PETs and 20 metastases have been analysed to date using immunohistochemistry. The 91 primary PETs include: 36 primary tumours in our previous paper [9], which comprised six primary lesions of the present paper; 41 primaries by Allen et al. [1]; 14 additional primaries in the present study. Dpc4 is expressed in 99% (90 of 91) of primary tumours and in 95% (19 of 20) of metastases. It can furthermore be inferred that all the tumours showing positive staining in immunohistochemistry also have at least one intact *DPC4* gene. The status of the *DPC4* gene has been studied in a total of 66 primary PETs, including 27 malignant cases [2, 9]. Gene anomalies were found in only five malignant cases (8%) by Bartsch et al. [2]. Taken together, these data suggest that the previously reported high frequency of *DPC4* gene alteration in malignant PETs may have been biased by serendipity due to the relatively small number of cases studied [2]. In addition, as no detailed histological description of the cases reported by Bartsch et al. is available, the possibility exists that some of those cases could have been of the rare category of mixed exocrine/endocrine tumours. However, the fact that all six cases showing *DPC4* anomalies (five reported by Bartsch et al. and one in the present paper) were malignant suggests that a link, albeit rare, between *DPC4* alteration and malignant transformation of PETs may exist.

In common ductal carcinomas, *DPC4* is frequently altered by either mutation or homozygous deletion [6]. This fact is reflected in the observed frequency of allelic loss in these tumours. In fact, loss of heterozygosity on chromosome 18q is observed in nearly all of these cancers [5]. In contrast however, allelic loss on chromosome 18q is not a highly frequent event in PETs, found in about 20–30% of nonfunctional and 40% of functional tumours [4, 9, 11]. From these data alone, the generally more indolent functioning tumours would also be expected to have inactivation of *DPC4*, although no alterations have been found to date. Thus, chromosome 18q might harbour another tumour-suppressor gene related to PET pathogenesis. At present, mutation of the *MEN1* gene remains the most frequent event found in nonfunctional PETs and in functional tumours other than insulinomas [7]. The present data further strengthen the fact that fundamental genetic differences exist between neoplasms arising from pancreatic exocrine and endocrine epithelia.

Acknowledgements This study was supported by grants from the Associazione Italiana Ricerca Cancro (AIRC) to A.S., Milan, Italy; Consorzio Studi Universitari di Verona, Italy; Ministero Sanitá (Ricerca finalizzata ICS060.2/RF00-57), Rome, Italy; Ministero Università e Ricerca (Cofin 9906218982 and MM06158571), Rome, Italy; Imperial Cancer Research Fund, the Mike Stone Cancer Research Fund and Medical Research Council, UK.

References

1. Allen E, Wilentz R, Yeo C, Argani P, Kern S, Hruban R (2000) DPC-4 expression is intact in neuroendocrine tumors of the pancreas (abstract). Lab Invest 80:70A
2. Bartsch D, Hahn SA, Danichevski KD, Ramaswamy A, Bastian D, Galehdari H, Barth P, Schmiegel W, Simon B, Rothmund M (1999) Mutations of the DPC4/Smad4 gene in neuroendocrine pancreatic tumors. Oncogene 18:2367–2371
3. Bartsch DK, Kersting M, Wild A, Ramaswamy A, Gerdes B, Schuermann M, Simon B, Rothmund M (2000) Low frequency of p16(INK4a) alterations in insulinomas. Digestion 62:171–177
4. Beghelli S, Pelosi G, Zamboni G, Falconi M, Iacono C, Bordi C, Scarpa A (1998) Pancreatic endocrine tumours: evidence for a tumour suppressor pathogenesis and for a tumour suppressor gene on chromosome 17p. J Pathol 186:41–50
5. Hahn SA, Seymour AB, Hoque AT, Schutte M, da Costa LT, Redston MS, Caldas C, Weinstein CL, Fischer A, Yeo CJ, et al (1995) Allelotype of pancreatic adenocarcinoma using xenograft enrichment. Cancer Res 55:4670–4675
6. Hahn SA, Schutte M, Hoque AT, Moskaluk CA, da Costa LT, Rozenblum E, Weinstein CL, Fischer A, Yeo CJ, Hruban RH, Kern SE (1996) DPC4, a candidate tumor suppressor gene at human chromosome 18q21.1. Science 271:350–353
7. Moore P, Missiaglia E, Antonello D, Zamò A, Zamboni G, Corleto V, Falconi M, Scarpa A (2001) The role of disease causing genes in sporadic pancreatic endocrine tumors: MEN1 and VHL. Genes Chromosomes Cancer 32:177–181
8. Moore P, Sipos B, Orlandini S, Sorio C, Real F, Lemoine N, Gress T, Bassi C, Klöppel G, Kalthoff H, Löhr M, Scarpa A (2001) Genetic profile of 22 pancreatic carcinoma cell lines: analysis of K-ras, p53, p16 and DPC4/Smad4. Virchows Arch: Published online 27 June 2001, DOI 10.1007/s004280100474
9. Moore PS, Orlandini S, Zamboni G, Capelli P, Rigaud G, Falconi M, Bassi C, Lemoine NR, Scarpa A (2001) Pancreatic tumors: molecular pathways implicated in ductal cancer are involved in ampullary but not in exocrine nonductal or endocrine tumorigenesis. Br J Cancer 84:253–262
10. Muscarella P, Melvin WS, Fisher WE, Foor J, Ellison EC, Herman JG, Schirmer WJ, Hitchcock CL, DeYoung BR, Weghorst CM (1998) Genetic alterations in gastrinomas and nonfunctioning pancreatic neuroendocrine tumors: an analysis of p16/MTS1 tumor suppressor gene inactivation. Cancer Res 58:237–240
11. Rigaud G, Missiaglia E, Moore P, Zamboni G, Falconi M, Talamini G, Pesci A, Baron A, Lissandrini D, Rindi G, Grigolato P, Pederzoli P, Scarpa A (2001) High resolution allelotype of pancreatic non-functional endocrine tumors: identification of two molecular subgroups with clinical implications. Cancer Res 61:285–292
12. Solcia E, Klöppel G, Sobin LH (2000) Histological typing of endocrine tumours. World Health Organization series. International histological classification of tumours. Springer, Berlin Heidelberg New York
13. Wilentz RE, Iacobuzio-Donahue CA, Argani P, McCarthy DM, Parsons JL, Yeo CJ, Kern SE, Hruban RH (2000) Loss of expression of Dpc4 in pancreatic intraepithelial neoplasia: evidence that DPC4 inactivation occurs late in neoplastic progression. Cancer Res 60:2002–2006
14. Wilentz RE, Su GH, Dai JL, Sparks AB, Argani P, Sohn TA, Yeo CJ, Kern SE, Hruban RH (2000) Immunohistochemical labeling for dpc4 mirrors genetic status in pancreatic adenocarcinomas: a new marker of DPC4 inactivation. Am J Pathol 156:37–43

Virchows Arch (2002) 440:160–165
DOI 10.1007/s004280100499

ORIGINAL ARTICLE

**Kiyoshi Sato · Gen Tamura · Takashi Tsuchiya
Yasushi Endoh · Ken Sakata · Teiichi Motoyama
Osamu Usuba · Wataru Kimura · Masanori Terashima
Satoshi Nishizuka · Tongtong Zou · Stephen J. Meltzer**

Analysis of genetic and epigenetic alterations of the *PTEN* gene in gastric cancer

Received: 20 April 2001 / Accepted: 12 June 2001 / Published online: 7 August 2001
© Springer-Verlag 2001

Abstract The *PTEN* tumor suppressor gene on 10q23.3, responsible for the Cowden and Bannayan-Zonana syndromes, encodes a dual-specificity phosphatase able to dephosphorylate both tyrosine phosphate and serine/threonine phosphate residues. Mutational inactivation of *PTEN* has been reported in various malignancies, including endometrial cancers, ovarian cancers, and glioblastomas. In this study, we investigated *PTEN* gene mutations in 10 gastric cancer cell lines and 58 primary gastric cancers by polymerase chain reaction single strand conformation polymorphism (PCR-SSCP). Hypermethylation of promoter region CpG islands, an alternative mechanism of gene inactivation to coding region mutations, was also evaluated by methylation specific PCR (MSP). Only one (1.7%) of the 58 primary tumors carried a somatic 5-bp deletion in intron 7 of *PTEN*, which did not alter the mRNA sequence, and no mutations were detected in any of the cell lines. Similar levels of *PTEN* mRNA expression were observed in all cell lines and primary tumors studied by RT-PCR, and *PTEN* promoter CpG islands remained unmethylated. Therefore, we conclude that *PTEN* does not participate in gastric carcinogenesis as a tumor suppressor gene.

Keywords *PTEN* · Gastric cancer · Mutation · Hypermethylation

K. Sato · G. Tamura (✉) · T. Tsuchiya · Y. Endoh · K. Sakata
T. Motoyama
Department of Pathology,
Yamagata University School of Medicine, 2–2-2 Iida-nishi,
Yamagata 990–9585, Japan
e-mail: gtamura@med.id.yamagata-u.ac.jp
Fax: +81-23-628-5245

K. Sato · O. Usuba · W. Kimura
Department of Surgery, Yamagata University School of Medicine,
2–2-2 Iida-nishi, Yamagata 990–9585, Japan

M. Terashima
Department of Surgery,
Iwate Medical University School of Medicine, 19–1 Uchimaru,
Morioka 020–8505, Japan

S. Nishizuka
Department of Microbiology and Molecular Genetics,
University of California, Irvine College of Medicine,
Irvine, CA 92697–4025, USA

T. Zou · S. J. Meltzer
Department of Medicine, Gastroenterology Division,
University of Maryland School of Medicine,
Baltimore, MD 21201, USA

Introduction

Recent genetic studies have revealed a consistent set of genetic alterations leading to the development of malignancies in humans, such as activation of proto-oncogenes and inactivation of tumor suppressor genes. However, due to the variety of histologic types and exposure to a range of mutagenic substances, the molecular pathogenesis of gastric cancer is largely unknown, except for the involvement of mutations in the *p53* [35] and *epithelial (E)- cadherin* genes [37], and of microsatellite instability (MSI) due to mismatch repair deficiency [36]. While loss of heterozygosity (LOH) studies have suggested the presence of tumor suppressor genes on several chromosomal arms [38], only a few genes isolated from these regions, such as *APC* and *DPC4 (Smad4)*, exhibited infrequent mutations in gastric cancers [27, 38]. We have previously reported that LOH on 10q was a frequent event in human gastric cancers of the differentiated type [38], suggesting the presence of tumor suppressor gene(s) on this chromosomal arm. Mapping of homozygous deletions on 10q23 followed by representational difference analysis and positional cloning led to the independent isolation of the *PTEN* gene by two groups [21, 33]. *PTEN* was identified as a tumor suppressor gene, encoding a dual-specificity phosphatase that dephosphorylates both tyrosine phosphate and serine/threonine phosphate residues [21, 33]. The in vivo role of *PTEN* appears to be the dephosphorylation of phosphotidylinositol 3,4,5-triphosphate [21, 33].

DNA methylation is an important regulator of gene expression, especially involving CpG-rich areas, known as CpG islands, within the promoter regions of many

genes [3, 4]. While almost all gene-associated CpG islands on autosomal chromosomes are protected from methylation [3], extensive methylation of CpG islands has been associated with transcriptional inactivation of selectively imprinted genes [20, 43] and genes on the inactivated X-chromosome in females [29, 31]. Aberrant methylation of normally unmethylated CpG islands is thought to be a relatively frequent event in cell immortalization or transformation events [1] and has been associated with transcriptional inactivation of defined tumor suppressor genes in human cancers [13, 11, 25]. In this last situation, promoter region hypermethylation appears to be an alternative mechanism to coding region mutation in eliminating tumor suppressor gene function [13, 25]. Therefore, the evaluation of CpG island methylation patterns has become an important tool for understanding regulation of both normal and pathologic gene expression.

In order to examine whether *PTEN* is inactivated genetically and/or epigenetically in gastric cancer, we examined mutation, expression, and promoter hypermethylation of this gene.

Materials and methods

Ten gastric cancer cell lines with variable histologies were studied; a well differentiated adenocarcinoma (MKN7), moderately differentiated adenocarcinomas (MKN28, MKN74), poorly differentiated adenocarcinomas (MKN45, KWS-I), a signet-ring cell carcinoma (KATO-III), endocrine cell carcinomas (ECC10, ECC12), hepatoid carcinoma (TSG-11), and an adenosquamous carcinoma (MKN1). All cell lines were cultured in RPMI containing 10% fetal bovine serum. Fifty-eight pairs of cancerous and non-cancerous gastric mucosa tissue samples were surgically obtained from 58 gastric cancer patients (11 differentiated and four undifferentiated early-stage carcinomas, and 20 differentiated and 23 undifferentiated advanced-stage carcinomas). All these tumor samples were histologically confirmed to contain more than 50% tumor cells, and samples with low tumor cellularity (less than 50%) were excluded from the present study.Tissue samples were immediately frozen and stored at –80 °C until analyzed. DNA was extracted from the 10 cell lines, 58 primary gastric tumor samples and corresponding non-cancerous gastric mucosal samples using SepaGene (Sankojunyaku Co, Tokyo, Japan). Total RNA was extracted from the 10 cell lines and 19 primary gastric tumor samples using TRIZOL reagent (Gibco BRL, Gaithersburg, Md., USA).

Eleven pairs of primers that span the intron-exon boundaries were used to amplify all nine *PTEN* exons described by Sakurada et al. [32]. Polymerase chain reaction (PCR) mixes contained 1×PCR buffer (15 mM Tris-HCl (pH 8.0), 50 mM KCl), 1.5 mM $MgCl_2$, deoxynucleotide triphosphates (200 µM each), 2.5 µ Ci [α-^{32}P] dCTP (Amersham, Buckinghamshire, UK), primers (1 µM each), 0.5 U AmpliTaq Gold DNA polymerase (PE Applied Biosystems, Foster City, Calif., USA) and genomic DNA (100 ng) in a final volume of 10 µl. Amplification was carried out in a GeneAmp PCR System 2400 thermocycler (PE Applied Biosystems) for 35 cycles (15 s at 95°C, 15 s at 55 or 58°C, then 30 s at 72°C), followed by a final 7-min extension at 72°C. PCR products were diluted 1:10 in denaturing loading buffer (95% formamide, 10 mM EDTA (pH 8.0), 0.02% xylene cyanol FF, and 0.02% bromophenol blue), heated at 95°C for 5 min, placed on ice, and 1.5 µl aliquots subjected to electrophoresis. Gels for single strand conformation polymorphism (SSCP) analysis contained 6% polyacrylamide and 5% glycerol. Gels were dried and exposed to Hyperfilm MP autoradiography film (Amersham) for 2–16 h.

Gel fragments containing shifted bands detected by SSCP were excised, immersed in 50 µ l water, heated at 95 °C, and amplified by PCR under the conditions described above for SSCP except for a final volume of 50 µ l. The PCR products were loaded onto nondenaturing 2% agarose gels and bands purified using the QIAquick Gel Extraction Kit (QIAGEN, Tokyo, Japan). The purified PCR products were sequenced with the dRhodamine Terminator Cycle Sequencing Kit (PE Applied Biosystems). Gel electrophoresis, data collection, and analysis were performed using a Genetic Analyzer (model 310, PE Applied Biosystems). LOH was defined as visible changes as previously described [36].

The DNA methylation status of the *PTEN* promoter was assessed using methylation-specific PCR (MSP), as described previously [12]. MSP distinguishes unmethylated from methylated alleles of a given gene based on sequence changes produced after bisulfite treatment of DNA, which converts unmethylated but not methylated cytosines to uracil, and subsequent specific-PCR amplification. Briefly, 1 µg DNA aliquots were denatured by treatment with NaOH and modified by sodium bisulfite. DNA samples were then purified using Wizard DNA purification resin (Promega, Madison, Wis., USA), treated again with NaOH, ethanol precipitated, and resuspended in water. The primers used were 5′-TTTAGCGTTTGTGAGTAGTCGC-3′ (AF143312 nt 1550–1571) and 5′-CCTTCCCTTTCAAAAAAAACCG-3′ (AF143312 nt 1670–1591) (142 bp) for methylated DNA, 5′-GTTTAGGTGAGGGAGATGAGAGAT-3′ (AF143312 nt 1500–1523) and 5′-CACCTTCCCTTTCAAAAAAAACCA-3′ (AF143312 nt 1670–1693) (192 bp) for unmethylated DNA. PCR was performed under the same conditions as described for PCR-SSCP except for a final volume of 20 µl. Sss I Methylase (New England Biolabs, Beverly, MA)-treated DNA and normal peripheral blood DNA served as positive and negative controls, respectively, for bisulfite modification. Finally, 10-µl aliquots of the PCR products were loaded onto nondenaturing 6% polyacrylamide gels, stained with ethidium bromide, and visualized under UV illumination.

RNA samples were reverse-transcribed using AMV RTase XL (Takarasyuzou, Kyoto, Japan) at 42 °C for 30 min. β-actin-specific oligonucleotides were used as a quantitative control. PCR was performed using the primers 5′-AACCCACCACAGCTAGAACT-3′ (U93051 nt 280–299) and 5′-ATACACATAGCGCCTCTGAC-3′ (U93051 nt 509–528) (251 bp) for *PTEN*, 5′-CCAGAGCAAGAGAGGTATCC-3′ and 5′-CTGTGGTGGTGAAGCTGTAG-3′ (436 bp) for β-actin under the same conditions described for PCR-SSCP. Then, 10-µl aliquots of the PCR products were loaded onto nondenaturing 2% agarose gels, stained with ethidium bromide, and visualized under UV illumination.

Statistical analysis was performed using Fisher's exact test.

Results

We investigated all nine *PTEN* gene exons in 10 gastric cancer cell lines and 58 primary gastric cancers by PCR-SSCP (Fig. 1). DNA sequencing analysis of the mobility-shift bands revealed a nucleotide change (C to G) within the 5′-untranslated region (9 bp upstream from the first codon) in two tumors, and a 5-bp deletion in intron 7 in a sample that had shown microsatellite instability (MSI) in a previous study (data not shown) (Fig. 2). For the point mutations, the corresponding normal mucosa DNA samples also exhibited the same mobility-shift bands. Therefore, the nucleotide change is likely to be a polymorphism. For the deletion, the corresponding normal DNA showed the wild-type sequence; therefore, this sequence change may be a somatic mutation due to mismatch repair defects. Sequencing analysis using the primers 5′-TTTGAGTTCCCTCAGCCGTTAC-3′ (U93051 nt 721–742) and 5′-GAAGTTGAACT-

GCTAGCCTCTG-3′ (U93051 nt 1070–1091) (373 bp), revealed that this mutation did not alter the sequence of *PTEN* mRNA (data not shown). Nine of the cell lines and 32 of the primary tumor samples exhibited the polymorphic 5 bp-deletion (ATCTT) in intron 4 previously reported by Kong et al. [16]. Ten out of 24 primary tumor samples informative at this polymorphic site showed apparent LOH (Fig. 3), which was more frequent in advanced cancers (52%; 9/16) than in early cancers (13%; 1/8) (P=0.05) (Table 1). No coding region mutations were found either in cell lines or primary tumors.

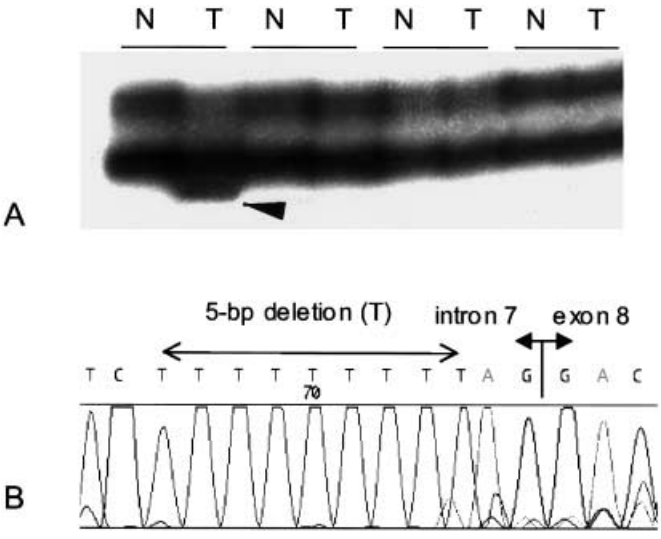

Fig. 2A,B Polymerase chain reaction single strand conformation polymorphism and sequence analyses of *PTEN* exon 8. Mobility shift (**A**) due to a 5-bp (TTTTT) deletion in intron 7 (**B**) is shown. *Arrowhead* mobility shift band, *T* tumor DNA, *N* corresponding normal gastric mucosa DNA

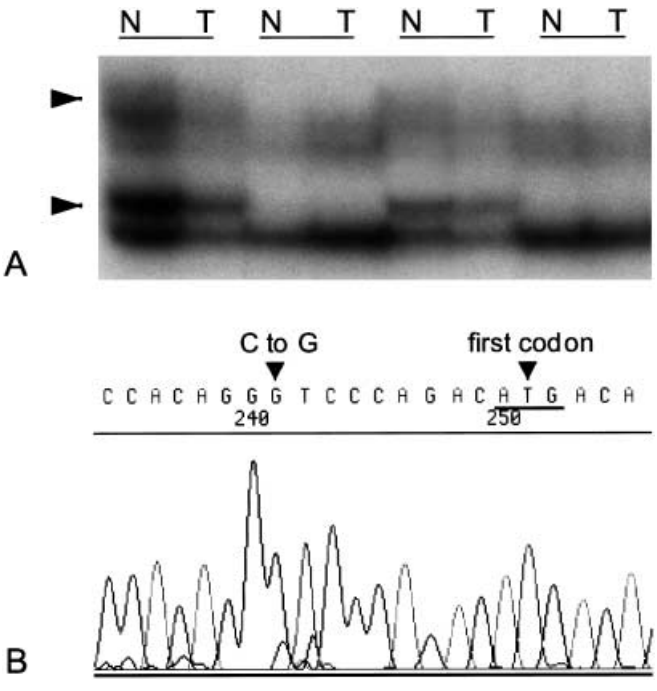

Fig. 1A,B Polymerase chain reaction single strand conformation polymorphism and sequence analyses of *PTEN* exon 1. Mobility shifts (**A**) due to a polymorphism (C to G) within the 5′-untranslated region (**B**) are shown. *Arrowheads* mobility-shift bands, *T* tumor DNA, *N* corresponding normal gastric mucosa DNA

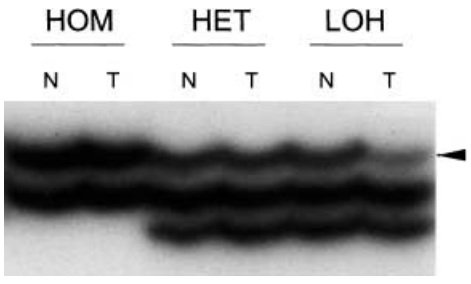

Fig. 3 Polymerase chain reaction single strand conformation polymorphism analysis of *PTEN* exon 4. Mobility shifts due to a polymorphic 5 bp-deletion (ATCTT) in intron 4 are clearly observed. Apparent reduction in intensity of one of the polymorphic bands indicates loss of heterzygosity (*LOH*, *arrowhead*). *T* tumor DNA, *N* corresponding normal gastric mucosa DNA, *HOM* homozygosity, *HET* retained heterozygosity

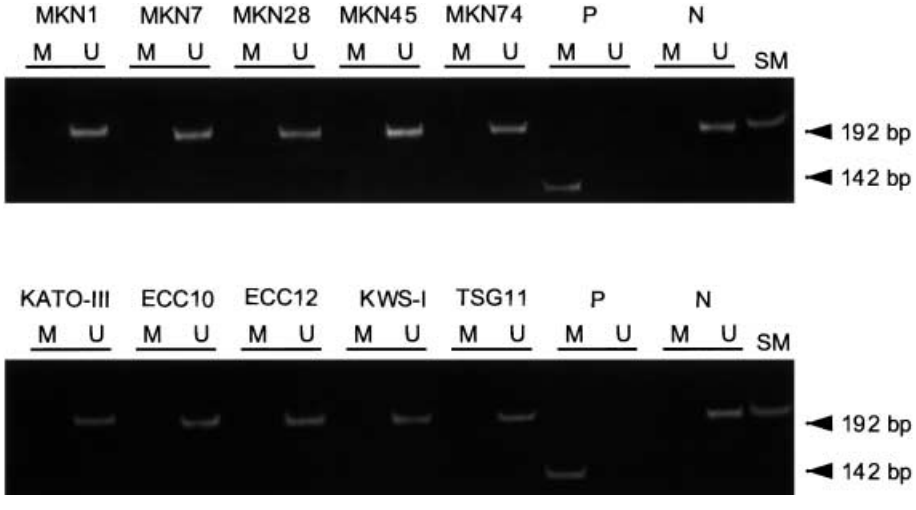

Fig. 4 Methylation-specific polymerase chain reaction analysis of 10 gastric cancer cell lines. All cell lines and a negative control exhibit only unmethylated products. Only a positive control exhibits the methylated product. *M* methylated product, *U* unmethylated product, *P* positive control, *N* negative control, *SM* size marker

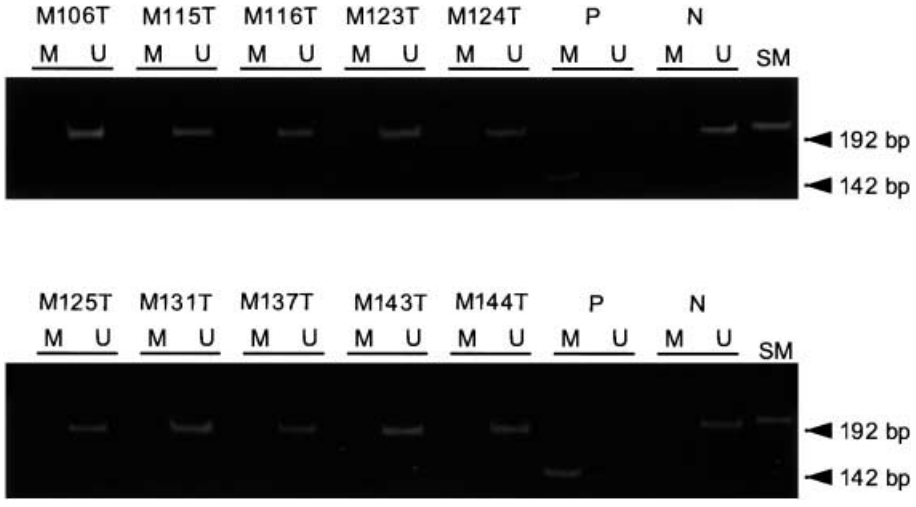

Fig. 5 Methylation-specific polymerase chain reaction analysis of 10 primary gastric cancers. All primary tumors and a negative control exhibit only unmethylated products. Only a positive control exhibits the methylated product. *M* methylated product, *U* unmethylated product, *P* positive control, *N* negative control, *SM* size marker

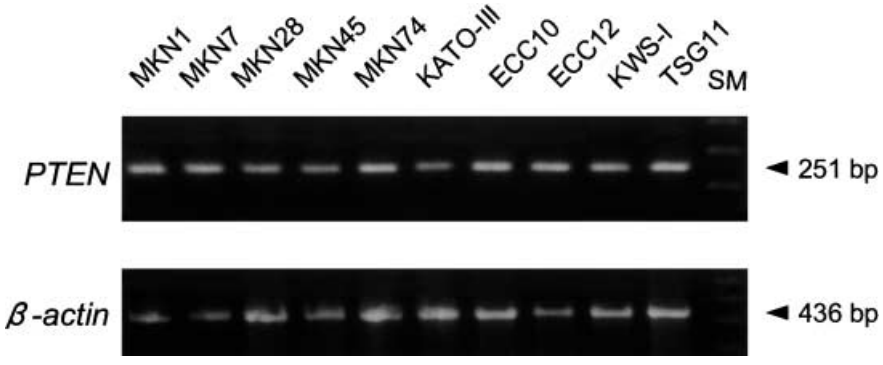

Fig. 6 Reverse transcription polymerase chain reaction of *PTEN* in 10 gastric cancer cell lines. *PTEN* shows similar expression levels in all cell lines. *SM* size marker

Table 1 Association of loss of heterzygosity (*LOH*) involving *PTEN* with clinical stage and histological type. *N** number of informative cases

Clinical stage and histological type	N*	LOH	(%)
Early-differentiated	4	1	(25) [a]
Early-undifferentiated	4	0	(0) [b]
Advanced-differentiated	7	4	(57) [c]
Advanced-undifferentiated	9	5	(56) [d]
Total	24	10	(42)

[a+b] *vs.*[c+d], P=0.05

Only PCR products derived from unmethylated templates were present in the 10 gastric cancer cell lines and 20 primary tumor samples tested by MSP (Figs. 4 and 5), showing retention of unmethylated CpG islands. Sss I-treated DNA revealed only methylated template-derived PCR products, while only unmethylated template-derived PCR products were observed using normal DNA (Figs. 4 and 5). *PTEN* mRNA expression in 10 cell lines and 19 primary tumor samples was assessed by RT-PCR. All samples revealed similar levels of *PTEN* mRNA (Fig. 6).

Discussion

Germline *PTEN* gene mutations have been observed in patients with autosomal dominant hamartomas and are often associated with cancer-predisposing conditions such as the Cowden and Bannayan-Zonana syndromes [22, 24, 23, 26]. Mutations of *PTEN* as well as homozygous deletions have frequently been reported in various malignancies. For instance, mutations of *PTEN* have been reported to occur in 33% to 55% of endometrial carcinomas [16, 18, 40], 25% to 26% of glioblastomas [6, 21,], 21% of ovarian cancers [28] and 13% of prostate cancers [7]. Most of these mutations were reportedly accompanied by loss of the wild-type allele. In breast and thyroid cancers, *PTEN* mutations are thought to be rare (under 5%)[5, 9, 30, 41]. Although the number of tumors analyzed is small, it has been reported that, for gastric cancers, mutations in this gene are absent (0/15)[8] or rare (3.4%; 1/29)[16]. We studied 10 gastric cancer cell lines and 58 primary gastric cancers and confirmed that *PTEN* mutations are rare in gastric cancers. In endometrial cancers, it has been speculated that *PTEN* constitutes a target of MSI, since *PTEN* mutations were more frequently detected in MSI-positive tumors (78%; 14/18 or 86%12/14) than in MSI-negative tumors (35%; 7/20 or 33%; 4/12)[16]. The only mutation detected in

the present study was a 5-bp deletion in a poly (T) tract in intron 7, and a *PTEN* mutation previously observed by Kong et al. [16] in a gastric cancer that was also accompanied by MSI. Therefore, while it is possible that *PTEN* is a target of MSI in a subset of MSI-positive gastric cancers, the frequency is very low.

Aberrant methylation of CpG islands in promoter regions is considered an important mechanism of gene inactivation. Hypermethylation of promoter region CpG islands in tumor suppressor or other tumor-related genes, including retinoblastoma (*RB*), von Hippel-Lindau (*VHL*), *APC*, *p16*, *p15*, *hMLH1*, and *E-cadherin* have been reported in various malignancies [2, 10, 11, 14, 15, 17, 19, 34, 39, 44]. Accumulation of aberrant CpG island methylation has also been hypothesized to be one of the major pathways that contribute to gastric carcinogenesis [42]. We utilized MSP to study the methylation status of the *PTEN* promoter in gastric cancers, and found that all 10 cell lines and 20 primary tumor samples studied consistently expressed *PTEN* mRNA and retained unmethylated promoter CpGs.

Although the PCR-SSCP assay using a polymorphism in intron 4 revealed frequent LOH involving *PTEN*, the rarity of *PTEN* mutations and promoter hypermethylation, and the conserved expression of *PTEN* suggest that *PTEN* is not the target of LOH in gastric cancer. Because LOH at this locus was more frequent in advanced cancers, it is possible that another tumor suppressor gene(s) involved in the progression of gastric cancer may exist within or adjacent to 10q23,3.

References

1. Antequera F, Boyes J, Bird A (1990) High levels of de novo methylation and altered chromatin structure at CpG islands in cell lines. Cell 62:503–514
2. Baur AS, Shaw P, Burri, N, Delacretaz F, Bosman FT, Chaubert P (1999) Frequent methylation silencing of p15(INK4b) (MTS2) and p16(INK4a) (MTS1) in B-cell and T-cell lymphomas. Blood 94:1773–1781
3. Bird AP (1986) CpG-rich islands and the function of DNA methylation. Nature 321: 209–213
4. Bird AP (1992) The essentials of DNA methylation. Cell 70:5–8
5. Bose S, Wang SI, Terry MB, Hibshoosh H, Parsons R (1998) Allelic loss of chromosome 10q23 is associated with tumor progression in breast carcinomas. Oncogene 17:123–127
6. Bostrom J, Cobbers JM, Wolter M, Tabatabai G, Weber RG, Lichter P, Collins VP, Reifenberger G (1998) Mutation of the PTEN (MMAC1) tumor suppressor gene in a subset of glioblastomas but not in meningiomas with loss of chromosome arm 10q. Cancer Res 58:29–33
7. Cairns P, Okami K, Halachmi S, Halachmi N, Esteller M, Herman JG, Jen J, Isaacs WB, Bova GS, Sidransky D (1997) Frequent inactivation of PTEN/MMAC1 in primary prostate cancer. Cancer Res 57:4997–5000
8. Chang JG, Chen YJ, Perng LI, Wang NM, Kao MC, Yang TY, Chang CP, Tsai CH (1999) Mutation analysis of the PTEN/MMAC1 gene in cancers of the digestive tract. Eur J Cancer 35:647–651
9. Dahia PL, Marsh DJ, Zheng Z, Zedenius J, Komminoth P, Frisk T, Wallin G, Parsons R, Longy M, Larsson C, Eng C (1997) Somatic deletions and mutations in the Cowden disease gene, PTEN, in sporadic thyroid tumors. Cancer Res 57: 4710–4713
10. Fleisher AS, Esteller M. Wang S, Tamura G, Suzuki H, Yin J, Zou TT, Abraham JM, Kong D, Smolinski KN, Shi YQ, Rhyu MG, Powell SM, James SP, Wilson KT, Herman JG, Meltzer SJ (1999) Hypermethylation of the hMLH1 gene promoter in human gastric cancers with microsatellite instability. Cancer Res 59:1090–1095
11. Herman JG, Latif F, Weng Y, Lerman MI, Zbar B, Liu S, Samid D, Duan DS, Gnarra JR, Linehan WM, Baylin SB (1994) Silencing of the VHL tumor-suppressor gene by DNA methylation in renal carcinoma. Proc Natl Acad Sci USA 91:9700–9704
12. Herman JG, Graff JR, Myohanen S, Nelkin BD, Baylin SB (1996) Methylation-specific PCR: a novel PCR assay for methylation status of CpG islands. Proc Natl Acad Sci USA 93:9821–9826
13. Herman JG, Jen J, Merlo A, Baylin SB (1996) Hypermethylation-associated inactivation indicates a tumor suppressor role for p15INK4B. Cancer Res 56:722–727
14. Herman JG, Umar A, Polyak K, Graff JR, Ahuja N, Issa JP, Markowitz S, Willson JK, Hamilton SR, Kinzler KW, Kane MF, Kolodner RD, Vogelstein B, Kunkel TA, Baylin SB (1998) Incidence and functional consequences of hMLH1 promoter hypermethylation in colorectal carcinoma. Proc Natl Acad Sci U S A 95:6870–6875
15. Hiltunen MO, Alhonen L, Koistinaho J, Myohanen S, Paakkonen M, Marin S, Kosma VM, Janne J (1997) Hypermethylation of the APC (adenomatous polyposis coli) gene promoter region in human colorectal carcinoma. Int J Cancer 70:644–648
16. Kong D, Suzuki A, Zou TT, Sakurada A, Kemp LW, Wakatsuki S, Yokoyama T, Yamakawa H, Furukawa T, Sato M, Ohuchi N, Sato S, Yin J, Wang S, Abraham JM, Souza RF, Smolinski KN, Meltzer SJ, Horii A (1997) PTEN1 is frequently mutated in primary endometrial carcinomas [letter]. Nat Genet 17:143–144
17. Kuismanen SA, Holmberg MT, Salovaara R, Schweizer P, Aaltonen LA, de La Chapelle A, Nystrom-Lahti M, Peltomaki P (1999) Epigenetic phenotypes distinguish microsatellite-stable and -unstable colorectal cancers. Proc Natl Acad Sci USA 96: 12661–12666
18. Kurose K, Bando K, Fukino K, Sugisaki Y, Araki T, Emi M (1998) Somatic mutations of the PTEN/MMAC1 gene in fifteen Japanese endometrial cancers: evidence for inactivation of both alleles. Jpn J Cancer Res 89:842–848
19. Leung SY, Yuen ST, Chung LP, Chu KM, Chan AS, Ho JC (1999) hMLH1 promoter methylation and lack of hMLH1 expression in sporadic gastric carcinomas with high-frequency microsatellite instability. Cancer Res 59:159–164
20. Li E, Beard C, Jaenisch R (1993) Role for DNA methylation in genomic imprinting. Nature 366:362–365
21. Li J, Yen C, Liaw D, Podsypanina K, Bose S, Wang SI, Puc J, Miliaresis C, Rodgers L, McCombie R, Bigner SH, Giovanella BC, Ittmann M, Tycko B, Hibshoosh H, Wigler MH, Parsons R (1997) PTEN, a putative protein tyrosine phosphatase gene mutated in human brain, breast, and prostate cancer. Science 275:1943–1947
22. Liaw D, Marsh DJ, Li J, Dahia PL, Wang SI, Zheng Z, Bose S, Call KM, Tsou HC, Peacocke M, Eng C, Parsons R (1997) Germline mutations of the PTEN gene in Cowden disease, an inherited breast and thyroid cancer syndrome. Nat Genet 16:64–67
23. Marsh DJ, Dahia PL, Zheng Z, Liaw D, Parsons R, Gorlin RJ, Eng C (1997) Germline mutations in PTEN are present in Bannayan-Zonana syndrome [letter]. Nat Genet 16: 333–334
24. Marsh DJ, Coulon V, Lunetta KL, Rocca-Serra P, Dahia PL, Zheng Z, Liaw D, Caron S, Duboue B, Lin AY, Richardson AL, Bonnetblanc JM, Bressieux JM, Cabarrot-Moreau A, Chompret A, Demange L, Eeles RA, Yahanda AM, Fearon ER, Fricker JP, Gorlin, RJ, Hodgson SV, Huson S, Lacombe D, Eng C (1998) Mutation spectrum and genotype-phenotype

analyses in Cowden disease and Bannayan-Zonana syndrome, two hamartoma syndromes with germline PTEN mutation. Hum Mol Genet 7:507–515
25. Merlo A, Herman JG, Mao L, Lee DJ, Gabrielson E, Burger PC, Baylin SB, Sidransky, D (1995) 5′ CpG island methylation is associated with transcriptional silencing of the tumour suppressor p16/CDKN2/MTS1 in human cancers. Nat Med 1:686–692
26. Nelen MR, van Staveren WC, Peeters EA, Hassel MB, Gorlin RJ, Hamm H, Lindboe CF, Fryns JP, Sijmons RH, Woods DG, Mariman EC, Padberg GW, Kremer H (1997) Germline mutations in the PTEN/MMAC1 gene in patients with Cowden disease. Hum Mol Genet 6:1383–1387
27. Nishizuka S, Tamura G, Maesawa C, Sakata K, Suzuki Y, Iwaya T, Terashima M, Saito K, Satodate R (1997) Analysis of the DPC4 gene in gastric carcinoma. Jpn J Cancer Res 88: 335–339
28. Obata K, Morland SJ, Watson RH, Hitchcock A, Chenevix-Trench G, Thomas EJ, Campbell IG (1998) Frequent PTEN/MMAC mutations in endometrioid but not serous or mucinous epithelial ovarian tumors. Cancer Res 58:2095–2097
29. Pfeifer GP, Steigerwald SD, Mueller PR, Wold B, Riggs AD (1989) Genomic sequencing and methylation analysis by ligation mediated PCR. Science 246:810–813
30. Rhei E, Kang L, Bogomolniy F, Federici MG, Borgen PI, Boyd J (1997) Mutation analysis of the putative tumor suppressor gene PTEN/MMAC1 in primary breast carcinomas. Cancer Res 57:3657–3659
31. Riggs AD, Pfeifer GP (1992) X-chromosome inactivation and cell memory. Trends Genet 8:169–174
32. Sakurada A, Suzuki A, Sato M, Yamakawa H, Orikasa K, Uyeno S, Ono T, Ohuchi N, Fujimura S, Horii A (1997) Infrequent genetic alterations of the PTEN/MMAC1 gene in Japanese patients with primary cancers of the breast, lung, pancreas, kidney, and ovary. Jpn J Cancer Res 88:1025–1028
33. Steck PA, Pershouse MA, Jasser SA, Yung WK, Lin H, Ligon AH, Langford LA, Baumgard ML, Hattier T, Davis T, Frye C, Hu R, Swedlund B, Teng DH, Tavtigian SV.(1997) Identification of a candidate tumour suppressor gene, MMAC1, at chromosome 10q23.3 that is mutated in multiple advanced cancers. Nat Genet 15: 356–362
34. Stirzaker C, Millar DS, Paul CL, Warnecke PM, Harrison J, Vincent PC, Frommer M, Clark SJ (1997) Extensive DNA methylation spanning the Rb promoter in retinoblastoma tumors. Cancer Res 57:2229–2237
35. Tamura G, Kihana T, Nomura K, Terada M, Sugimura T, Hirohashi S (1991) Detection of frequent p53 gene mutations in primary gastric cancer by cell sorting and polymerase chain reaction single-strand conformation polymorphism analysis. Cancer Res 51:3056–3058
36. Tamura G, Sakata K, Maesawa C, Suzuki Y, Terashima M, Saeoh K, Sekiyama S, Suzuki A, Eda Y, Satodate R (1995) Microsatellite alterations in adenoma and differentiated adenocarcinoma of the stomach. Cancer Res 55:1933–1936
37. Tamura G, Sakata K, Nishizuka S, Maesawa C, Suzuki Y, Iwaya T, Terashima M, Saito K, Satodate R (1996) Inactivation of the E-cadherin gene in primary gastric carcinomas and gastric carcinoma cell lines. Jpn J Cancer Res 87:1153–1159
38. Tamura G, Sakata K, Nishizuka S, Maesawa C, Suzuki Y, Terashima M, Eda Y, Satodate R (1996) Allelotype of adenoma and differentiated adenocarcinoma of the stomach. J Pathol 180:371–377
39. Tamura G, Yin J, Wang S, Fleisher AS, Zou TT. Abraham JM, Kong D. Smolinski KN, Wilson KT, James SP, Silverberg SG, Nishizuka S, Terashima M, Motoyama T, Meltzer SJ (2000) E-cadherin gene promoter hypermethylation in primary human gastric carcinomas. J Natl Cancer Inst 92:569–573
40. Tashiro H, Blazes MS, Wu R, Cho KR, Bose S, Wang SI, Li J, Parsons R, Ellenson LH (1997) Mutations in PTEN are frequent in endometrial carcinoma but rare in other common gynecological malignancies. Cancer Res 57:3935–3940
41. Teng DH, Hu R, Lin H, Davis T, Iliev D, Frye C, Swedlund B, Hansen KL, Vinson VL, Gumpper KL, Ellis L, El-Naggar A, Frazier M. Jasser S, Langford LA, Lee J, Mills GB, Pershouse MA, Pollack RE, Tornos C, Troncoso P, Yung WK, Fujii G, Berson A, Steck PA (1997) MMAC1/PTEN mutations in primary tumor specimens and tumor cell lines. Cancer Res 57:5221–5225
42. Toyota M, Ahuja N, Suzuki H, Itoh F, Ohe-Toyota M, Imai K, Baylin SB, Issa JP (1999) Aberrant methylation in gastric cancer associated with the CpG island methylator phenotype. Cancer Res 59:5438–5442
43. Tremblay KD, Saam JR, Ingram RS, Tilghman SM, Bartolomei MS (1995) A paternal-specific methylation imprint marks the alleles of the mouse H19 gene. Nat Genet 9:407–413
44. Yoshiura K, Kanai Y, Ochiai A, Shimoyama Y, Sugimura T, Hirohashi S (1995) Silencing of the E-cadherin invasion-suppressor gene by CpG methylation in human carcinomas. Proc Natl Acad Sci U S A 92:7416–7419.

Virchows Arch (2002) 440:166–171
DOI 10.1007/s004280100497

ORIGINAL ARTICLE

**Teresa Ribalta · A. Julio Martinez · Pedro Jares
Jaume Muntané · Rosa Miquel · Xavier Claramonte
Antonio Cardesa**

Presence of occult cytomegalovirus infection in the brain after orthotopic liver transplantation

An autopsy study of 83 cases

Received: 1 February 2001 / Accepted: 28 May 2001 / Published online: 12 October 2001
© Springer-Verlag 2001

Abstract Cytomegalovirus (CMV) infection remains a highly prevalent systemic complication following orthotopic liver transplantation (LT), accounting for a significant increase in morbidity and affiliated costs. However, unlike other immunosuppressed groups of population, CMV infection of the central nervous system in LT is rarely diagnosed, either clinically or postmortem. Furthermore, in 20% of the LT patients who develop preterminal neurological complications, the etiology remains undetermined. With the hypothesis that at least some of these cases could be related to an occult CMV infection, we examined brain tissue from 83 unselected autopsies of LT patients by morphological, immunohistochemical (IHC), in situ hybridization (ISH), and nested polymerase chain reaction (nested PCR) techniques. Microglial nodules were observed in 17 brains of the LT group (20.4%) but in none of the 36 controls. Isolated positive cells by either IHC, ISH, or both techniques, were identified in 11 LT patients (13.2%) and in 2 controls (5.5%). CMV DNA amplification was obtained from paraffin-embedded tissues in 41 of 81 LT cases (50.6%), and in 5 controls (13.8%) (P=0.00017). Viral inclusion bodies, inflammatory infiltrates, or necrotizing changes were not identified in any case. Our findings indicate an increased susceptibility of the brain of LT patients to occult infection by CMV and suggest that a latent or low-grade infection of the central nervous system could operate as a reservoir of the CMV and play a role in some of the unexplained neurological symptoms that appear in the postoperative period.

Keywords Cytomegalovirus · Liver transplantation · Brain occult infection · Immunohistochemistry · Polymerase chain reaction

T. Ribalta (✉) · P. Jares · J. Muntané · R. Miquel · A. Cardesa
Department of Pathology, Hospital Clinic,
Institut d'Investigacions Biomèdiques August Pi i Sunyer (IDIBAPS),
University of Barcelona Medical School, Villarroel 170,
08036-Barcelona, Spain
e-mail: tribalta@clinic.ub.es
Fax: +34-93-2275717

A.J. Martinez
Department of Neuropathology, Presbyterian Hospital,
University of Pittsburgh Medical School, Pittsburgh, PA, USA

X. Claramonte
Infectious Diseases Service, Hospital Clínic,
Institut d'Investigacions Biomèdiques August Pi i Sunyer
(IDIBAPS), University of Barcelona Medical School,
Barcelona, Spain

Introduction

Cytomegalovirus (CMV) infection remains an important complication in many immunodeficiency settings, including solid organ transplantation [10]. However, the frequency and severity of involvement of the central nervous system (CNS) varies largely in relation to the characteristics of the different immunosuppression states [14]. In contrast to the acquired immunodeficiency syndrome (AIDS), where the infection usually takes the form of ventriculoencephalitis, the most common lesion in patients undergoing organ transplantation is microglial nodule encephalitis [3]. In orthotopic liver transplantation (LT), however, CMV infection often involves the graft and other organs in the postoperative period, and encephalitis rarely develops [12]. When it does, its clinical expression is often non-specific. Likewise, neurologic complications are an important cause of morbidity and mortality in LT patients [14, 16, 17]: over 90% of cases of fatal LT are complicated by a preterminal encephalopathy, whose etiology remains undetermined in 20%.

In organ transplantation, CMV infections commonly result from the reactivation of a latent infection originating from either recipient or donor. It has been demonstrated that, after the resolution of primary infection, CMV can persist in a latent state in various cells throughout the body, including vessel wall cells and bone marrow-derived white blood cells [6, 7]. However, the exact localization of latency is currently unknown, and the pathogenic basis for the reactivation of the infec-

tion is poorly defined. In other transplant settings, such as lung or bone-marrow transplantation, it has been demonstrated that the frequency of morphologically occult CMV infection [as detected by immunohistochemistry (IHC) and/or polymerase chain reaction (PCR)] is higher than the morphologically overt viral infection [1, 4]. Based on that, we developed the hypothesis that at least some of the non-specific neurologic disturbances that may afflict the LT patients may be caused by a latent or low-productivity CMV infection of the CNS. In this paper, we present the results of our search, in the brain tissues of LT patients at autopsy, for the presence of CMV genomic material and gene products, as well as for any histopathological reaction that could be related to a viral infection.

Materials and methods

Autopsy cases

A series of 83 unselected brains obtained by autopsy from LT patients at the Hospital Clinic of Barcelona, Spain (44 cases), and the Presbyterian University Hospital of Pittsburgh, PA, USA (39 cases), between 1983 and 1996 were retrospectively studied. The series includes 45 males and 38 females. The average age at death was 56 years (range 12–76 years). Clinical charts and final autopsy reports were reviewed to obtain serologic, neurologic, and other patient data, as well as any pre- or postmortem evidence of systemic CMV infection. Eighteen cases underwent from two to four LTs. The postoperative survival period from the last LT ranged from 1 day to 4234 days (mean 377 days). All patients received a variety of anti-microbial and immunosuppressive drugs (FK506, steroids, OKT3, cyclosporin A, azathioprine) from immediate postoperative period to the time of their death. Most patients also received prophylactic treatment for CMV after the operation.

Post-transplant neurologic signs and symptoms, including focal or generalized seizures, focal deficits, and altered mental status, which could not be ascribed, pre- or postmortem, to any of the known causes of neurologic complications in LT, were recorded. The cause of death in most of the cases was septicemia, multiorgan failure, or bleeding diathesis, with frequent combination of the three. The neuropathological findings present at autopsy were classified into the following categories: (1) metabolic disorders: hepatic/anoxic encephalopathy, central pontine myelinolysis; (2) cerebrovascular disease, (3) infection, and (4) neoplasms. Thirty-six non-transplanted, immunocompetent age-matched patients (21 males, 15 females), average age 66 years (22–72 years), served as controls. These control cases died from a variety of cardiovascular, neoplastic, degenerative, and infectious diseases. In 31 of them, a neuropathological diagnosis of cerebrovascular, metabolic, infectious, neoplastic, or neurodegenerative disease was rendered.

Methods

The postmortem interval was less than 24 h in all LT and control cases. The brains were fixed by immersion in 15% formalin for 2 weeks and paraffin-embedded. A detailed neuropathological examination was performed at the time of every autopsy diagnosis. Sections studied in all cases included multiple neocortical and limbic areas, basal ganglia, thalamus, hippocampus, ventricle walls, cerebellum and brain stem at different levels. All the original slides, stained using the routine methods, were reviewed to search for microglial nodules, isolated microscopic necrotic foci, viral inclusion bodies, focal perivascular inflammatory cuffings, or any other histopathological change that could be related to a viral encephalitis.

Table 1 Primers for the first conventional polymerase chain reaction (PCR), the nested PCR, and the internal control

Conventional PCR	
Major immediate early gene	5′TGTGTCTGTCAAGTCTG AGC-3′ 5′-TTTCACAGGCGTGACACGTT-3′
Late gene	5′-TGTTCACCTGGCCGCCCTGG-3′ 5′-TTTGGGCGTCGAGGCGATGC-3′
Nested PCR	
Major immediate early gene	5′-CAG TGT CTG AGA TAG AGG AA-3′ 5′-TAT TGA GTA GGA TTA CAG AG-3′
Late gene	5′-CCG CAA CCT GGT GCC CAT GG-3′ 5′-CGTTTGGGTTGCGCAGCGGG-3′
Human β-globin	5′-ACACAACTGTGTTCACTAGC-3′ 5′-CAACTTCATCCACGTTCACC-3′

For the IHC study, paraffin blocks from three different areas of the brain were selected in every case, including frontal cortex and subcortical white matter, caudate nucleus with internal capsule and ventricular wall, and transversal section of medulla oblongata. Sections 5-µm thick were dewaxed in xylene and rehydrated through graded alcohols. Endogenous peroxidase was blocked by a 10-min incubation in 3% hydrogen peroxide in methanol, followed by washing under running tap water. To enhance antigenic recovery, fixed tissue sections were subjected to microwave heating at 100°C for 10 min in Antigen Retrieval Citra solution (BioGenex; dilution 1/10). Normal swine serum (5%, Dako) was then applied for 10 min at room temperature, followed by an anti-CMV monoclonal antibody that reacts with CMV antigens (clone CCH2, DAKO Diagnósticos, Barcelona, Spain) (dilution 1:50), overnight, at 4°C. The bound antibodies were detected using the avidin–biotin–alkaline phosphatase (ABAP) method, with 3-amino 9-ethylcarbazole (AEC) as substrate. In positive cases, additional sections incubated with the same antibody were subsequently studied using a streptavidine–alkaline phosphatase (SAP) technique to confirm the results. Positive control for the CMV antibody consisted of brain tissue samples from an AIDS patient who died with a severe CMV encephalitis (Fig. 4). As negative control, the primary antiserum was replaced by phosphate-buffered saline (PBS).

For the in-situ hybridization (ISH) study, consecutive sections were taken from the same paraffin blocks used for IHC. A biotinylated CMV deoxyribonucleic acid (DNA) probe (Enzo Diagnostics) was applied following the procedure recommendations by the manufacturer. The probe consists of a mixture of two sequences of CMV DNA (17.2-kb and 25.2-kb *Bam*HI fragments) cloned into pBR322. The same case as for the IHC served as positive control of the CMV probe. Sections incubated with the hybridization solution but without the CMV probe were used as negative controls.

DNA for the PCR study was extracted from the same paraffin blocks used for the IHC and ISH studies in 81 LT cases and the control cases. The extraction procedure was performed according to the following protocol: three 10-µm sections from every paraffin block were deparaffinized twice with 800 µl xylene and rinsed in 800 µl absolute ethanol. Each wash was followed by centrifugation for 5 min, and the supernatant was discarded. The final pellets were dried in a spin vacuum, dissolved in 200–300 µl extraction buffer [50 mM Tris, pH 8.5, 1 mM ethylene diamine tetraacetic acid (EDTA), 0.5% Tween 20] containing 100 µg/ml proteinase K (Boehringer-Mannheim) and incubated overnight at 55°C. Proteinase K was inactivated by heating the mix at 96°C for 10 min. After a final centrifugation step, the supernatant was transferred into a new tube and stored at –20°C. A nested PCR strategy was used to detect the presence of CMV. For the first and the nested PCR, specific primers to the major immediate early gene (MIE) and the late gene (LA) were used (Table 1). We used two sets of primers in each PCR to diminish the false-negative cases due to problems in the conservation of the chosen genomic sequences between the various human CMV strains, or DNA degradation because of the postmortem and paraffin block origin of the tissues studied.

Table 2 Summary of clinical, morphologic, immunohistochemical (IHC) and molecular findings in liver transplant and control cases. *N* number of cases, *Ag-CMV* antigenemia for cytomegalovirus positive, *N. S. Neur. Sympt.* non-specific neurologic symptoms, *MN* microglial nodules, *IHC* cases immunopositive, *ISH* cases with labeled cells by in situ hybridization, *nested-PCR* cases with CMV DNA amplification by "nested" polymerase chain reaction, *NE* not evaluated

Cases (*n*)	Ag-CMV[a]	Systemic CMV (pre- or postmortem)	N S Neur. Sympt.[b] (%)	MN (%)	IHC (%)	ISH (%)	Nested-PCR[c] (%)	Total positive cases[d]
LT (83)	34	34	8 (18.2)	17 (20.4)	11 (13)	5 (5.9)	41 (50.6)	43 (51.1)
Controls (36)	NE	0	0	0	2 (5.5)	0	5 (13.8)	5 (13.8)

[a] At least one determination available in 53 LT cases
[b] Information available in 43 cases
[c] Performed in 81 LT cases (P=0.00017, odds ratio 6.36)
[d] P=0.000069, odds ratio 7.02

The first amplification was performed with 2 µl DNA, 2.5 U *Taq* polymerase (Gibco-BRL), 0.4 µM primers, 1.5 mM $MgCl_2$, 100 µM of each dNTP and PCR buffer in a final volume of 50 µl. The PCR conditions were one step at 95°C for 5 min followed by 35 cycles at 95°C for 45 s, 42°C for 45 s, and 72°C for 45 s. The nested PCR was performed as described above, but 2 µl of the first PCR reaction was used as template. The conditions for the nested PCR were: one step at 95°C for 5 min, followed by three cycles of 45 s at 95°C, 45 s at 58°C, and 45 s at 72°C; three cycles with annealing at 56°C, three cycles with annealing at 54°C, and 35 cycles with annealing at 52°C. Amplification of a fragment of the human β-globin gene was used as a control for the presence of amplifiable DNA in the sample. The PCR conditions were the same as described for the nested PCR. All primers used for the first PCR, the nested PCR, and the internal control (human β-globin) are shown in Table 1. The PCR was carried out in a GeneAmp PCR 2400 apparatus or in a 9600 thermal cycler (Perkin-Elmer Cetus, Norwalk, Conn.). PCR amplifications without DNA template were performed at the same time to exclude contamination. Similarly, a case with strong expression of CMV by IHC was used as a positive control for the PCR study. An aliquot of 15 µl of each PCR product was loaded and run in a 2% agarose gel, stained with ethidium bromide, and directly visualized with ultraviolet illumination. PCR was reported as positive if amplification occurred with either the MIE or LA primers.

Statistical analysis

For the statistical analysis, chi-squared (χ^2), odds ratios, and 95% confidence intervals were calculated. Yates-corrected P values were used.

Results

A summary of the main morphologic, IHC, ISH, and PCR results, and the relevant clinical and autopsy data of LT cases and controls is shown in Table 2.

Clinical and autopsy review

Thirty-four of 83 LT patients (40.9%) had clinical or postmortem evidence of relevant CMV disease. CMV antigens were detected in blood at any time during the post-LT period in 34 of the 53 cases (64.1%) in which this information was available. Clinically undetermined neurologic disturbances were documented in the clinical charts in 8 of the 43 patients in which this information was available.

Seventy one of the 83 LT cases (85.5%) showed neuropathological abnormalities. The most significant findings included metabolic disorders: hepatic/anoxic encephalopathy (47 cases: 38 hepatic, 9 anoxic), central pontine myelinolysis (3 cases); cerebrovascular diseases (22 cases: 12 infarcts, 10 hemorrhages); infection (15 cases: 10 fungal, 1 bacterial, 1 toxoplasmic, 3 unknown microbial agent); and neoplasms (3 post-transplant lymphomas). In 21 cases, there was a combination of two or more of these categories. One patient, 76-years old, fulfilled criteria of definite Alzheimer's disease. The neuropathological alterations observed in the control cases were of cerebrovascular type in 17 cases; hepatic encephalopathy in 8 cases; metastatic neoplasms in 2 cases (1 lymphoma, 1 carcinoma); meningoencephalitis in 2 cases (1 bacterial, 1 fungal), and neurodegenerative diseases in 2 cases (1 Alzheimer, 1 Parkinson). No clinical or postmortem evidence of systemic CMV infection was observed in any of the control cases.

Routine, IHC, ISH, and PCR studies

Microglial nodules were found in 17 of the 83 LT cases (20.4%) (Fig. 1) and in none of the control cases. In 8 of the 17 cases, a disseminated CMV infection was evident at autopsy. In the other four cases with microglial nodules, there was a concomitant disseminated fungal (1 aspergillus, 1 candida, 1 candida plus herpes simplex) or bacterial infection (multiple gram-positive cocci). No viral inclusion bodies, necrotic foci or perivascular inflammatory cuffings were identified in any of the 83 LT cases.

Isolated labeled cells were detected either by IHC, ISH, or both techniques, in 11 of the 83 LT cases (13.2%). Most of them were small blood-vessel-related cells, some apparently inside the vessel walls while others were seen laying free within the vessel lumens (Fig. 2, Fig. 3). A possible endothelial nature was suspected for the former because of location of some labeled cells in the inner layer of the vessel wall. The free-floating intraluminal cells could be either detached infected endothelial cells, infected leukocytes, or a combination of both. Very occasionally, other positive cells were seen scattered in the neuropil, and apparently not related to vessels, but their exact nature could not be deduced from morphology. In the control series, only one isolated positive cell in the neuropil was identified in each of two cases (5.5%). Like in the ADIS control case

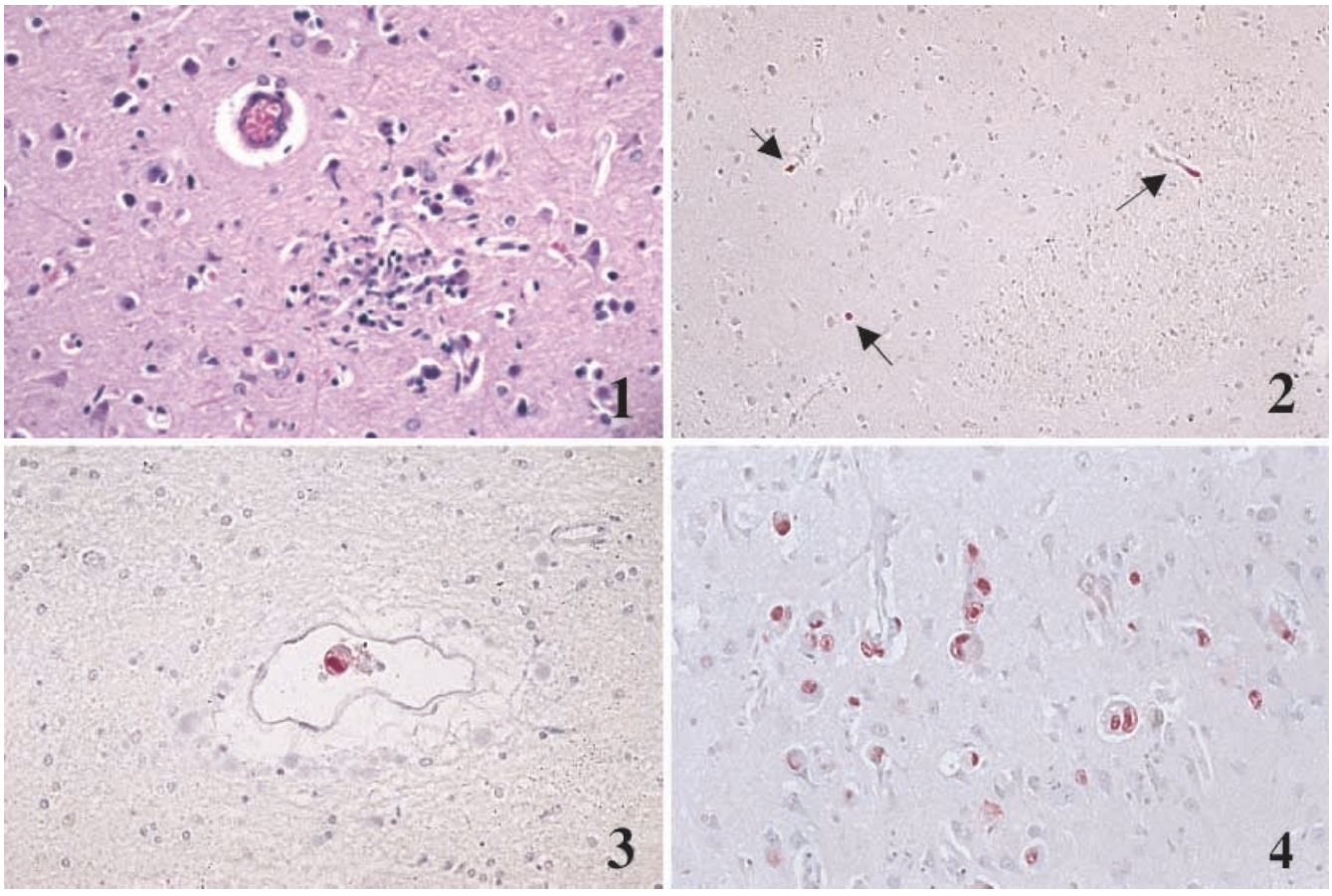

Fig. 1 Microglial nodule in the caudate nucleus of a liver transplant patient (hematoxylin and eosin, original magnification ×100)

Fig. 2 Low-power view of scattered immunoreactive cells (*arrows*), some resembling vascular-related cells, in the brain of a liver transplant patient (anti-cytomegalovirus immunostaining, original magnification ×40)

Fig. 3 An isolated cell lying free in the lumen of an intracerebral vessel showing an intense immunopositive reaction (anti-cytomegalovirus immunostaining, original magnification ×100)

Fig. 4 Control case used for the immunohistochemical study. There are abundant cytomegalovirus (CMV)-infected cells in this full-blown CMV necrotizing encephalitis of an AIDS patient (anti-CMV immunostaining, original magnification ×40)

(Fig. 4), the IHC staining pattern was variable, with cells depicting a nuclear-only or cytoplasmic-only staining, while others showed both nuclear and cytoplasmic positivity. In 22 LT cases and 14 control cases, a focal or diffuse positivity was observed in the cytoplasm of choroid plexus epithelial cells when the ABAP detection system was used. However, these results could not be reproduced when the SAP method was subsequently applied to additional sections in the same areas, suggesting endogen biotin content in these cells as a cause for false positivity with the ABAP detection. The immunoreaction was confirmed using the SAP method in the intraparenchymatous cells, indicating a specific reaction in these cells. Under the conditions used in our study, the ISH technique rendered positive cells in only five LT cases, three of which were also positive for IHC. This low sensitivity of our ISH study might be due to insufficient preservation of DNA of tissues obtained from autopsy.

Specific CMV DNA amplification was obtained by nested PCR in 41 of the 81 LT cases analyzed (50.6%) and in 5 of the 36 cases of the control group (13.9%). This difference was statistically significant [c^2=14.09, *P*=0.00017; odds ratio=6.36 (2.07–20.79); confidence interval=95%]. Twenty-five cases showed amplification for the MIE gene, 16 cases for the LA gene, and 11 cases for both in the LT series (Fig. 5). PCR was positive in all IHC-positive cases except two. The total number of LT cases with either CMV antigenic or genomic material detected in the brain was 43 (51.1%). In the control group, five cases (13.8%) showed a positive result using the PCR technique, two of which were further positive with IHC. This difference is highly statistically significant [c^2=15.82; *P*=0.000069; odds ratio=7.02 (2.29–22.97); confidence interval=95%]. In 20 of the 43 LT cases (46.5%) with antigenic or genomic CMV material in brain, there was clinical or postmortem evidence of CMV infection elsewhere in the body. Of 17 cases in which microglial nodules were identified at routine examination, positive cells by IHC and/or genomic amplification were found in 11, including the above-mentioned 8 cases with CMV disseminated infection at autopsy. In the eight patients with unexplained post-transplant neu-

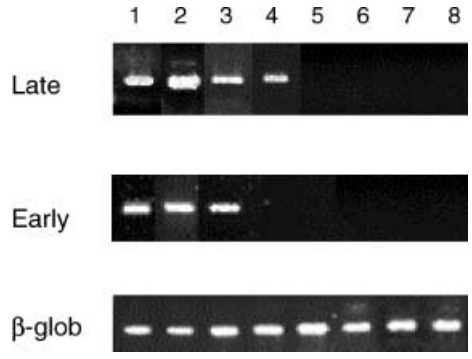

Fig. 5 Electrophoretic analysis of nested polymerase chain reaction products of cytomegalovirus (CMV) DNA from formalin-fixed, paraffin-embedded brain tissue (2% agarose gel). From *left* to *right*: *lane 1* CMV positive control; *lanes 2–3* liver transplantation (LT) cases with amplification of both CMV major immediate early gene (MIE) and late gene (LA); *lane 4* LT case with amplification for CMV LA but not for MIE; *lanes 5–8* LT cases without amplification of CMV DNA

rologic alterations, a post-mortem systemic CMV infection and CMV antigenic and genomic material in brain were observed in four. Although an antigenemic study was not systematically performed in every LT patient, PCR for CMV in the brain was positive in at least seven seronegative patients.

Discussion

In this study, we have shown that genomic material or gene products of CMV are present in postmortem brain tissues of LT patients in a significantly higher proportion than in the control group, including cases without any serologic, clinical, or postmortem evidence of CMV infection. The severe form of necrotizing encephalitis with viral inclusion bodies, frequently found in other immunosuppression states, was not observed in our series. We speculate that, through unknown mechanisms, CMV can remain in the brain of LT patients in a latent or very low level of replication, without causing detectable damage or clinical encephalitis, even in cases of severe systemic infection. The reason for the apparent resistance of the CNS of LT patients to develop a full-blown CMV encephalitis is currently unknown. CMV infection is highly prevalent in the general population [6]. CMV usually remains in the body tissues in a latent status [9] and, after reactivation, it can lead to severe illness especially in immunocompromized and immunosuppressed patients. The exact location of latent CMV in the body and the mechanisms of spread are still a matter of active investigation. In experimental models such as murine CMV, endothelial cells and monocytes of multiple organs have been shown to harbor the virus in a latent status [11], but whether the latent infection stays in vivo, in organ-specific cells, or in ubiquitous elements such as vascular-wall cells, leukocytes, or other cells, has not been determined yet. Murine CMV may also persistently infect neuronal and glial cells in the developing mouse brain [19].

In our study, in addition to microglial nodules, which have been observed in a similar proportion in other large autopsy series of LT patients [15] and extensively related to CMV infection [5], we have identified CMV antigens and genomic material in cells resembling vascular-wall cells and in free-lying intraluminal cells. Although a definite endothelial or leukocytic origin has not been demonstrated in the present study, these findings suggest that vascular-related cells might be one of the possible sites of CMV occult infection in the brain of LT recipients. It has been clearly stated that endothelial infection of the liver graft by CMV is quite common in the post-transplant period [20], this being an important cause of graft rejection. In some LT patients, the infection of the graft spreads out inducing lesions in several organs. CMV could reach the CNS in this phase but, for currently unknown reasons, the virus would not replicate within neural tissue, thus remaining occult in a latent or low-productivity condition, perhaps in vascular-related cells and/or certain nervous tissue cells [8]. Recent reports show that high levels of CMV in cerebrospinal fluid correlate to clinically significant CMV encephalitis in AIDS patients [2]. However, the implications of low levels are still unknown. It cannot be excluded that the presence of the virus in the brain of LT patients, although in a non- or low-productivity form, could generate some kind of neurologic dysfunction, perhaps by inducing secretion of cytokines, infecting vascular endothelium, or producing some malfunction of the neural cells, without the requirement of a cytopathic effect and/or of a cellular immunologic response. Furthermore, pharmacokinetic studies have demonstrated that the upper limit of concentration of ganciclovir in brain is actually only up to 38% of blood concentration [18]. Consequently, systemic CMV infection could be pharmacologically controlled in most peripheral tissues except for the CNS, thus allowing a viral reservoir to be created in this location.

The results of our study provide information on the presence of an occult CMV brain infection in a significant proportion of LT recipients that come to autopsy. Additional studies are required to confirm the nature of the infected cells and to determine the pathogenetic mechanisms of the low-grade CMV infection of brain tissue. It will also be necessary to investigate whether there is a causal relationship to the still unexplained neurologic disturbances that afflict a proportion of LT patients or not. Although in recent years CMV infection has turned into a relatively medically controlled complication in LT recipients, the basic mechanisms of viral spreading and the relationship between latency and reactivation are still poorly understood. This line of research may contribute to advance our knowledge about factors involved in CMV infection of the brain in LT and also in other immunodeficiency settings.

Acknowledgements The authors appreciate the excellent technical assistance of Lucila Fresno, Margarita Mainar, Begoña Alonso, and Elena Gonzalvo. Supported by a grant from the Spanish Ministery of Health (FIS 95-0841). Presented in part at the 74th Annual Meeting of the American Association of Neuropathologists, Minneapolis, MN, 18–21 June 1998.

References

1. Arbustini E, Morbini P, Grasso M, Diegoli M, Fasani R, Porcu E, Banchieri N, Perfetti V, Pederzolli C, Grossi P, Dalla Gasperina D, Martinelli L, Paulli M, Ernst M, Plachter B, Vigano M, Solcia E (1996) Human cytomegalovirus early infection, acute rejection, and major histocompatibility class II expression in transplanted lung. Molecular, immunocytochemical, and histopathologic investigations. Transplantation 61:418–427
2. Arribas JR, Clifford DB, Fichtenbaum CJ, Commins DL, Powderly WG, Storch GA (1995) Levels of cytomegalovirus (CMV) DNA in cerebrospinal fluid of patients with AIDS and CMV infection of the central nervous system. J Infect Dis 172:527–531
3. Arribas JR, Storch GA, Clifford DB, Tselis AC (1996) Cytomegalovirus encephalitis. Ann Intern Med 125:577–587
4. Barberà JA, Martín-Campos JM, Ribalta T, Carreras E, Llopart A, Sierra J, Rozman C, Rodríguez-Roisin R (1996) Undetected viral infection in diffuse alveolar damage associated with bone marrow transplantation. Eur Respir J 9:1195–1200
5. Boos J, Winkler SR, Griffith BP, Kim JH (1989) Viremia and glial nodule encephalitis after experimental systemic cytomegalovirus infection. Lab Invest 61:644–649
6. Bruggeman CA (1993) Cytomegalovirus and latency: an overview. Virchows Arch 64:325–333
7. Fish KN, Soderberg-Naucler C, Mills LK, Stenglein S, Nelson JA (1998) Human cytomegalovirus persistently infects aortic endothelial cells. J Virol 72:5661–5668
8. Grefte A, Van der Giessen M, Van Son W, The TH (1993) Circulating cytomegalovirus (CMV)-infected endothelial cells in patients with an active CMV infection. J Infect Dis 167:270–277
9. Hendrix RMG, Wagenaar M, Slobbe RL, Bruggeman CA (1997) Widespread presence of cytomegalovirus DNA in tissues of healthy trauma victims. J Clin Pathol 50:59–63
10. Kanj SS,Sharara AI, Clavien PA, Hamilton JD (1996) Cytomegalovirus infection following liver transplantation: review of the literature. Clin Infect Dis 22:537–549
11. Koffron AJ, Mueller KH, Kaufman DB, Stuart FP, Patterson B, Abecassis MI (1995) Direct evidence using in situ polymerase chain reaction that the endothelial cell and T-lymphocyte harbor latent murine cytomegalovirus. Scand J Infect Dis Suppl 99:61–62
12. Kusne S, Dummer JS, Singh N, Iwatsuki S, Makowka L, Esquivel C, Tzakis AG, Starzl TE, Ho M (1988) Infections after liver transplantation. An analysis of 101 consecutive cases. Medicine 67:132–143
13. Martínez AJ (1998) The neuropathology of organ transplantation: comparison and contrast in 500 patients. Pathol Res Pract 194:473–486
14. Martínez AJ (1998) The neurology and neuropathology of hepatobiliary and pancreatic transplantation. In: Goetz CG, Aminoff MJ (eds) Handbook of clinical neurology, systemic diseases, vol. 26. Elsevier Science B.V. pp 249–266
15. Martínez AJ, Ahdab-Barmada M (1993) The neuropathology of liver transplantation: comparison of main complications in children and adults. Mod Pathol 6:25–32
16. Martinez AJ, Estol C, Faris AA (1988) Neurologic complications of liver transplantation. Neurol Clin 6:327–348
17. Power C, Poland SD, Kassim KH, Kaufmann JCE, Rice GPA (1990) Encephalopathy in liver transplantation: neuropathology and CMV infection. Can J Neurol Sci 17:378–381
18. Shepp DH, Dandliker PS, de Miranda P, Burnette TC, Cederberg DM, Kirk LE, Meyers JD (1985) Activity of 9-[2-hydroxy-1-(hydroxymethyl)ethoxymethyl]guanine in the treatment of cytomegalovirus pneumonia. Ann Intern Med 103:368–373
19. Shinmura Y, Aiba-Masago S, Kosugi I, Li RY, Baba S, Tsutsui Y (1997) Differential expression of the immediate-early and early antigens in neuronal and glial cells of developing mouse brains infected with murine cytomegalovirus. Am J Pathol 151:1331–1340
20. Waldman WJ, Knight DA (1996) Cytokine-mediated induction of endothelial adhesion molecule and histocompatibility leukocyte antigen expression by cytomegalovirus-activated T cells. Am J Pathol 148:105–119

Virchows Arch (2002) 440:172–180
DOI 10.1007/s004280100507

ORIGINAL ARTICLE

**Helmut H. Popper · Sabine Pailer · Gerd Wurzinger
Herwig Feldner · Christian Hesse · Eva Eber**

Expression of adhesion molecules in allergic lung diseases

Received: 20 February 2001 / Accepted: 19 June 2001 / Published online: 14 September 2001
© Springer-Verlag 2001

Abstract Endothelial adherence and migration of leukocytes into tissue is mediated by different sets of adhesion molecules. The expression of these sets might not only preselect the types of leukocytes that enter the inflammatory sites, but also activate these leukocytes, induce adherence to epithelial cells, and cause the release of cytokines. Atopic asthma, extrinsic allergic alveolitis, and sarcoidosis as examples of immunologic lung diseases were investigated for the expression of adhesion molecules. Bronchial biopsies in chronic obstructive lung disease (COPD) and resected lung tissue of juvenile emphysema were chosen for controls. Immunohistochemistry was done on sections from bronchial and transbronchial biopsies and on smears from bronchoalveolar lavage cells. In all three types of immune disorders, lymphocytes expressed the integrins $\alpha 4/\beta 1$ (VLA4) and ICAM3, whereas lymphocytes in COPD bronchitis and in emphysema controls were unreactive. Eosinophils in atopic asthma bronchitis in contrast to COPD bronchitis also expressed both VLA4 and ICAM3. The expression of VCAM1 on endothelial cells was only seen in atopic asthma and was related to disease activity. The expression of other adhesion molecules was nonspecific. Expression of VCAM1 on endothelial cells and its ligand VLA4 on lymphocytes and eosinophils seems to be a specific event in atopic asthma. Expression of VLA4 and ICAM3 on lymphocytes, however, might be a specific event in all three immune reactions.

Keywords Adhesion molecules · Integrins · Selectins · Atopic asthma · Sarcoidosis · Extrinsic allergic alveolitis · COPD bronchitis

The study was supported by the Austrian Scientific Research Fund project S6709 to HHP, which is gratefully acknowledged.

H.H. Popper (✉) · S. Pailer
Institute of Pathology, Laboratory of Environmental and Respiratory Pathology, University of Graz, Auenbruggerplatz 25, 8036 Graz, Austria
e-mail: popper@uni-graz.at
Tel.: +43-316-380-4405, Fax: +43-316-380-9636

G. Wurzinger · C. Hesse
II Internal and Pulmonary Deptartments, General Hospital, Graz, Austria

E. Eber
Pulmonary Hospital, Enzenbach, Austria

H. Feldner
Hospital of the SVB, Gleichenberg, Austria

Introduction

Different immunologic or allergic lung diseases can be characterized by specific subsets of leukocytes present in bronchoalveolar lavage (BAL) and in tissue sections and by a different morphologic appearance. However, overlapping does occur: Epithelioid cell granulomas are found in sarcoidosis as well as in extrinsic allergic alveolitis (hypersensitivity pneumonia, EAA), although there are differences in the morphology of the granulomas and in the expression of lymphocyte antigens. An eosinophilic bronchitis is seen in various forms of bronchial asthma, in chronic obstructive lung disease (COPD), in bronchiectasis, and in allergic bronchopulmonary aspergillosis (mucoid impaction type). The mechanisms involved in the attraction of different sets of leukocytes may differ considerably.

Leukocyte recruitment to the bronchial mucosa or peripheral lung tissue is regulated by specific, time-dependent, and consecutive steps of expression and activation of adhesion molecules. At first, rolling over of the endothelium is mediated by members of the selectin family. Firm adhesion and transmigration of leukocytes is facilitated by members of the integrin and CAM family of adhesion molecules (for review, see [28]. Integrins and CAMs not only regulate the adherence to endothelial cells and transmigration of leukocytes through blood vessels, but also facilitate the selection of specific types of leukocytes which subsequently can move toward the inflammatory lesion. For example, the influx of eosinophils is mediated via VCAM-1/VLA4 receptor-ligand interaction and the expression of these molecules is upreg-

ulated by interleukins 4 and 5 [38,25] and by the interaction of the c-kit receptor and stem cell factor [37].

The integrin family proteins are composed of two noncovalently associated α and β chains [28]. The integrins composed of the β1 chain are called very late antigens and numbered according to their respective α-chain (VLA1–6). Some are responsible for cell to cell contact (VLA2, VLA3, VLA6) [26], others facilitate adhesion to basement membrane components (VLA1, VLA2, VLA3, VLA5, VLA6) [18, 16, 34], and all facilitate leukocyte movement along matrix proteins, such as collagen, laminin and fibronectin [28, 18]. Three major β2 integrins have been described, combined with CD11a (LFA1), CD11b (MAC1 or complement receptor 3bi), and CD 11c (gp 150/95) [28], respectively. These molecules enable adhesion to different CAMs and to complement receptors [29, 4, 8].

The immunoglobulin superfamily molecules are characterized by immunglobulin domains. Members most often studied are ICAM1 (CD54), ICAM2 (CD102), ICAM3 (CD50), VCAM1 (CD106), and PECAM1 (CD31). These molecules are ligands for the integrins, and are expressed on leukocytes and endothelial cells [28]. The corresponding ligands/receptors for the studied adhesion molecules so far known are given in 1.

The aim of our study was to look for differences in the expression of adhesion molecules in bronchitis associated with either atopic bronchial asthma (ABA) or COPD, and in granulomatous pneumonia in sarcoidosis and EAA. We selected atopic asthma as a type I immune reaction, allergic alveolitis as type III, and sarcoidosis as type IV immune reaction. Chronic bronchitis in COPD was chosen as a non-immune bronchitis, morphologically resembling asthma bronchitis. Biopsies and cells from bronchial washings and BAL were investigated. Differences in the expression of adhesion molecules might provide some new insights into regulatory mechanisms for the transmigration of subsets of granulocytes and lymphocytes in each of these diseases, and thus might also be used as an aid in the differential diagnosis. Understanding the regulatory mechanisms of leukocyte trafficking might be a basis for a new line of therapeutic intervention.

Material and methods

Bronchial biopsies, brush cytology specimens, and cells from bronchial washings were taken from 11 patients with mild atopic bronchial asthma and eight patients with chronic bronchitis combined with COPD. Transbronchial biopsies and cells from BAL were taken from eight patients with EAA and ten patients with sarcoidosis. Bronchial mucosa and peripheral lung tissue from resected specimens from eight cases of juvenile emphysema served as normal control. These tissues are usually devoid of inflammatory infiltrates. We avoided using lung tissues resected from cases of lung carcinoma because inflammation is very often present in these tissues and therefore cannot be regarded as a "normal" control.

Because fixation might dissolve some adhesion molecules, which would erroneously be interpreted as negative, we chose a fixative preserving tissue well and retaining immunoreactivity. Biopsies were fixed in a mixture of 0.5% paraformaldehyde, 0.05 M periodate and 0.037 M lysine-HCl in phosphate-buffered saline (PBS) adjusted to pH 7.4, for 1–4 h. Antigen preservation was tested beforehand; a fixation time of 30 min gave sufficient structural preservation. Diminished antibody reactivity was found to start at 6 h of fixation. After brief rinsing with PBS supplemented with 7% sucrose, the biopsies were frozen in OCT and serial sections of 3- to 4-µm thickness were cryosectioned. The sections

Table 1 Adhesion molecules, their ligands and regulatory system; *?* regulation not identified so far, *AM* adhesion molecule, *IL* interleukin, *IG* immunoglobulin, *PAF* platelet aggregation factor, *MIP* migration inhibitory factor, *MCP* macrophage chemotactic protein, *TNF* tumor necrosis factor, *IFN* interferon, *NAP* platelet-derived neutrophil activating peptide, *GRO* growth regulated oncogene-alpha (chemokine), *RANTES* regulated on activation T cell expressed and secreted

Type of AM	Type, synonyms	Ligands	Source of antibodies and dilution; the β-chain is only given on the first appearance	Regulated
α1 β1	Integrin, VLA1	Laminin, collagen	Chemicon Int. Inc, Temecula, CA, 1:200, Endogen, Boston, MA, 1:50	?
α2 β1	Integrin, VLA2	Laminin, collagen, VLA3?	Chemicon Int. Inc, 1:100	?
α3 β1	Integrin, VLA3	Fibronectin, laminin, collagen, VLA2?	Chemicon Int. Inc, 1:100	?
α4 β1	Integrin, VLA4	VCAM1, fibronectin	Endogen, 1:500	IL-4, IL-5. Stem cell factor
α5 β1	Integrin, VLA5	Fibronectin	Kennebunk, ME, 1:50	?
α6 β1	Integrin, VLA6	Laminin	SA, Marseille, France, 1:30	?
αL β2	LFA1	ICAM1, ICAM2	Monosan, Uden, Netherlands, 1:50	PAF, IL-8
αM β2	MAC1	ICAM1, fibrinogen, C 3bi R	Monosan, 1:50	IL-8, PAF, NAP-2, GROα, MIP-1α, MCP-1, RANTES
αX β2	gp150/95	Fibrinogen, C 3bi R?	Monosan, 1:50, 1:30	MIP-1α, MCP-1, RANTES
ICAM1	IG superfamily	LFA1, MAC1	Bender, Vienna, Austria, 1:100	IL1, IL8, IL 10, IFNγ, TNFα,
ICAM2	IGsuperfamily	LFA1	Bender, Vienna, Austria, 1:100	?
ICAM3	IGsuperfamily	?	Bender, Vienna, Austria, 1:100	?
VCAM1	IG superfamily	VLA4	R&D Systems, Abingdon, UK, 1:100	IL1, IL4, IL8, TNFα

were stained with H&E, Giemsa and Congo red. The latter selectively stained eosinophilic granules. Cell smears and BAL cells were stained as routinely done.

Immunohistochemistry was performed using commercially available antibodies directed against the integrin chains α1–α6, ß1, ß2, CD11a/b/c, the Ig-supergene-family molecules ICAM-1/2/3, and VCAM-1 (see 1. Antibodies were diluted in PBS. Briefly, the tissue sections or cell preparations were incubated with the primary antibodies for 1 h, then rinsed three times with PBS for 10 min each, and incubated with second antibodies (rabbit anti mouse IGG biotinylated, diluted 1:500, Dako, Glostrup, Denmark) for 1 hour. The antibody reaction was visualized using the APAAP system (Dako) as recommended by the manufacturer. Nuclei were counterstained with hematoxylin.

The percentage of positively stained cells was semiquantitated and cases were grouped into 1+=<30%, 2+= 31–70%, and 3+=>70% of positively stained cells. As an example, a positive reaction for VLA4 was declared when a similar amount of lymphocytes on consecutive sections stained positively for α4 as well as for β1, and the distribution pattern of positively stained cells was similar on consecutive sections. Immunotyping of BAL-lymphocytes in lymphocytic alveolitis was done in the routine manner.

Clinical and morphological definition of disease

Patients were included in the study only if they met the criteria for one of the four diseases and after informed consent was obtained. Permission was obtained from the Ethics Committee of the Medical Faculty in Graz.

Atopic asthma was defined by a positive cutaneous Prick test, positive RAST class 3 or 4, and an increased serum level of IgE (>200 U/l). Broncholysis tests were performed in all patients using a ß-sympathicomimetic agent and provocation tests were done using histamine. Symptoms of asthma were present for at least 2 years. Asthma severity was graded according to the criteria of the “International Asthma Report” [24]. Only mild cases of asthma were included. Four to five hours after a specific provocation test bronchial biopsies, bronchial secretions, and brush cytological specimens were taken.

COPD was defined clinically by bronchial obstruction, productive cough with a minimal duration of three months, and more than two recurrences of these symptoms in the last 2 years. Emphysema diagnosis was required and other causes of chronic bronchitis had to be excluded. Grading of COPD was done according to the ATS standards [2]. Bronchial biopsies, brush cytological specimens, and bronchial washings were taken.

Morphologic features of asthma and COPD bronchitis

Chronic bronchitis in asthma was defined by a combination of the following features: lymphocytic and plasmocytic infiltrates, varying numbers of eosinophils, and thickening and hyalinization of the basal lamina. Additional changes, although not a constant feature, were goblet cell hyperplasia (ratio of ciliated to goblet cells <4:1); shedding of reserve and columnar cells, leaving only basal cells attached to the basal lamina; and intraepithelial leukocyte infiltration, consisting mainly of lymphocytes and eosinophils. Edema, subepithelial fibrosis and smooth muscle cell hyperplasia were sometimes present. The features of chronic bronchitis namely, a lympho-plasmocytic infitration of the mucosa, hyperplasia of goblet cells in the surface and glandular epithelium, and an increase in the size of submucosal glands were seen in COPD as in any other chronic bronchitis.

The morphologic differences of asthma and COPD bronchitis in some cases were only marginal, not allowing a differentiation. Eosinophils, a hallmark of ABA, are sometimes also present in similar numbers in COPD bronchitis. Thickening and hyalinization of the basement membranes, characteristic in ABA, is not always seen, especially in ABA of short duration. Such thickening can occasionally be seen in long standing COPD bronchitis. Epithelial shedding of columnar and reserve cells is characteristic in ABA, however, in bronchial biopsies will often be mistaken as an artifact.

EAA was clinically defined as a type III immune reaction against known organic allergens, positive Ouchterlony precipitation test, fever, dyspnea, and a positive exposure history. In all our cases a reaction for either thermolabile fungi or bird proteins were found (farmer's or bird fancier's lung). Morphologically EAA was defined by a suppressor cell dominated lymphocytic alveolitis in BAL and a lymphocytic, partially granulomatous interstitial pneumonia. Epithelioid cell granulomas were present in two cases; infectious organisms were ruled out by special stains. Sarcoidosis was ruled out by a spillover of lymphocytes beyond the boundaries of the granulomas, and by BAL analysis as well as by the clinical features.

Sarcoidosis was defined by clinical criteria, such as raised ACE and immunoglobulins in serum, hypercalcemia, and radiologically by hilar lymphadenopathy and reticulo-nodular interstitial infiltrates on computed tomography (CT) scan. Morphologically, non-necrotizing epithelioid cell granulomas were seen; infectious organisms were excluded by acid fast and silver stains, and *M. tuberculosis* DNA was also excluded by polymerase chain reaction for the insertion sequence 6110 in two of the cases.

Controls

As controls we used lung tissue from patients resected for juvenile emphysema. This is characterized as spontaneous pneumothorax occurring at a young age, sexes affected equally. Emphysema is focally located subplurally in the upper lobes. The etiology is unknown, and no inflammatory changes or fibrosis is seen. In these cases BAL was not available.

All biopsies and cytologic specimens were evaluated by two of the authors (HHP, SP) without knowledge of the clinical diagnosis. Diagnoses in all cases were based on the same sections used for this study.

Results

Bronchitis in atopic asthma (*n*=11)

A 3+ expression of the integrin VLA4 (α4β1) was found on lymphocytes in all cases, and in eight cases a 3+ expression of LFA1 (CD11aβ2). Other integrins were rarely found, and only expressed on single lymphocytes. Eosinophils showed a 3+ expression of VLA4 in all 11 cases and of MAC1 (CD11bβ2) in nine (Figs. 1, 2). Alveolar macrophages in BAL specimens were 3+ positive for LFA1 (CD11aβ2) in eight cases, and 2+ positive for gp150/95 (CD11cβ2) in seven. The bronchial epithelial cells in all cases expressed VLA3 and VLA6 3+ (β1 combined with either α3 or α 6). ICAM1 expression was 2+ on endothelial cells in all cases, and on all bronchial epithelial cells in seven cases. VCAM1 expression was 3+ on endothelial cells of venules and capillaries in five cases. The expression of VCAM1 was only found in biopsies from patients with clinically active disease, which also was correlated with a greater density of infiltrating lymphocytes and eosinophils (Fig. 3). ICAM3 was 3+ expressed on eosinophils and lymphocytes in all cases. Other selectins and addressins were negative, or 1+ on few cells, and only in either one or two cases, respectively.

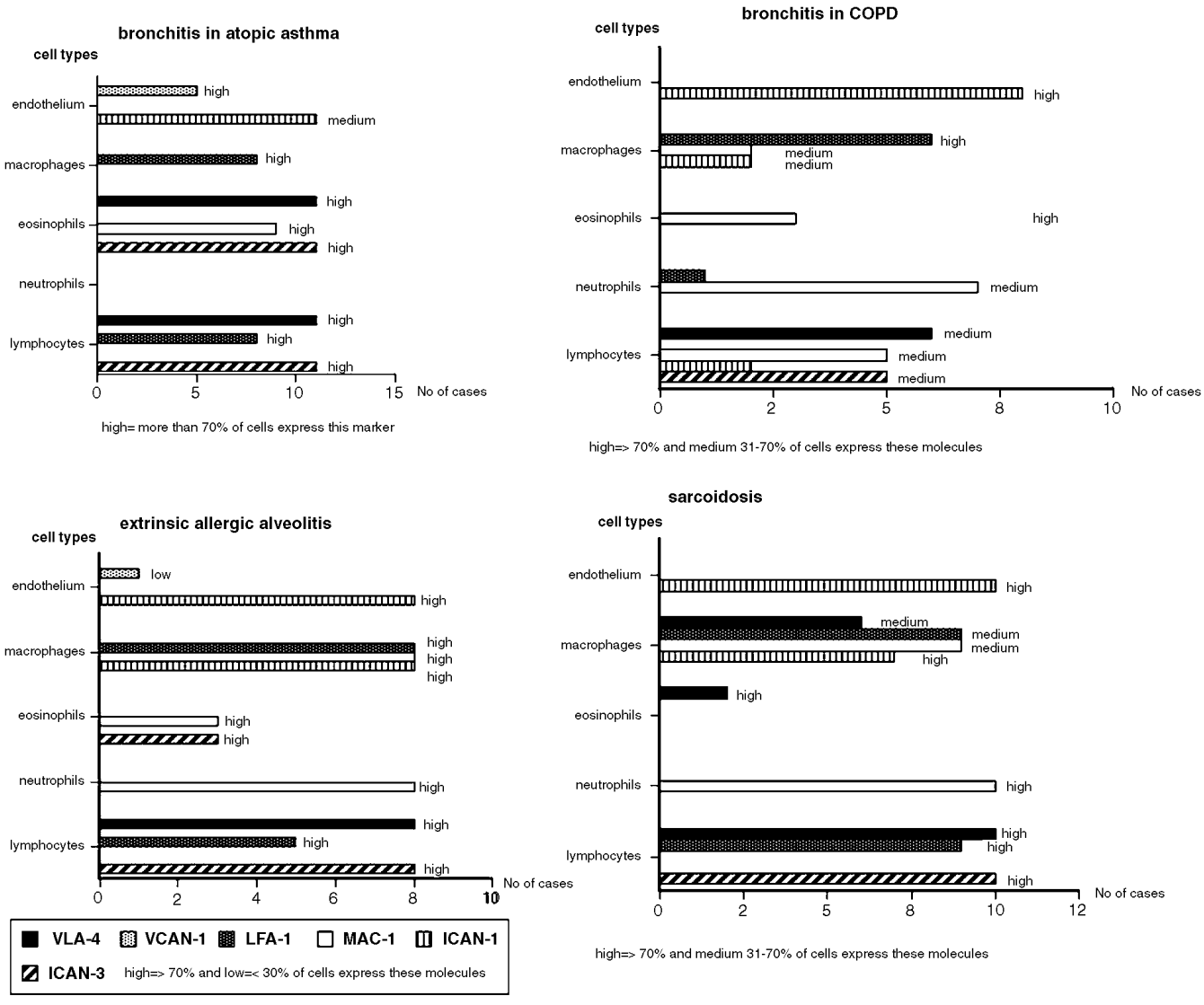

Fig. 1 Expression of different adhesion molecules in atopic asthma bronchitis (*upper left panel*), chronic bronchitis with chronic obstructive lung disease (COPD; *upper right panel*), extrinsic allergic alveolitis (*lower left panel*), and sarcoidosis (*lower right panel*); shown is the expression pattern for the relevant adhesion molecules VLA-4, VCAM-1, LFA-1, MAC-1, ICAM-1, and ICAM-3. As can be seen from the graphs the combined expression of VLA-4 and ICAM-3 on eosinophils and lymphocytes in asthma bronchitis is not paralleled in the other diseases, whereas VLA-4 and ICAM-3 expression on lymphocytes is present on high numbers of lymphocytes in asthma bronchitis, sarcoidosis as well as in extrinsic allergic alveolitis (EAA). Only median expression is seen in COPD bronchitis for these markers. Other markers as ICAM-1 are unspecifically upregulated on many cells in all four diseases

Bronchitis in COPD (*n*=8)

The inflammatory infiltrates in the bronchial mucosa in most cases were composed of lymphocytes and neutrophils, in three cases eosinophils were present. Macrophages were found scattered in seven cases. In two cases there was submucosal fibrosis in addition. In all bronchial biopsies adjacent alveolar tissue was seen, enabling the assessment of the reactivity for adhesion molecules on pneumocytes.

Lymphocytes 2+ expressed VLA1 and VLA4 in five and six cases, respectively. MAC1 and ICAM3 were each found 2+ on lymphocytes in five cases. Expression of VLA6, VLA3, and ICAM1 was seen 1+ on lymphocytes in three, one, and two case, respectively. Neutrophils, similarly to lymphocytes, expressed VLA1, MAC1, and ICAM3 in seven, seven, and six cases, respectively. These cells were 2+ positive for each of the above adhesion molecules. A 2+ expression of VLA3, VLA6, LFA1, and gp150/95 was found on neutrophils in two cases, two cases, one case, and one case, respectively. The eosinophils 3+ expressed VLA1 and MAC1; however, no VLA4 and ICAM3 expression was seen. Alveolar macrophages expressed 3+ VLA1, VLA6, LFA1, and gp150/95 in seven, five, six, and six cases, respectively, whereas a 2+ expression of VLA3, MAC1, and ICAM1 was seen in a minority of cases (Fig. 1).

Epithelial cells of the bronchial mucosa were stained 3+ by antibodies for VLA3 and VLA6. Basal and re-

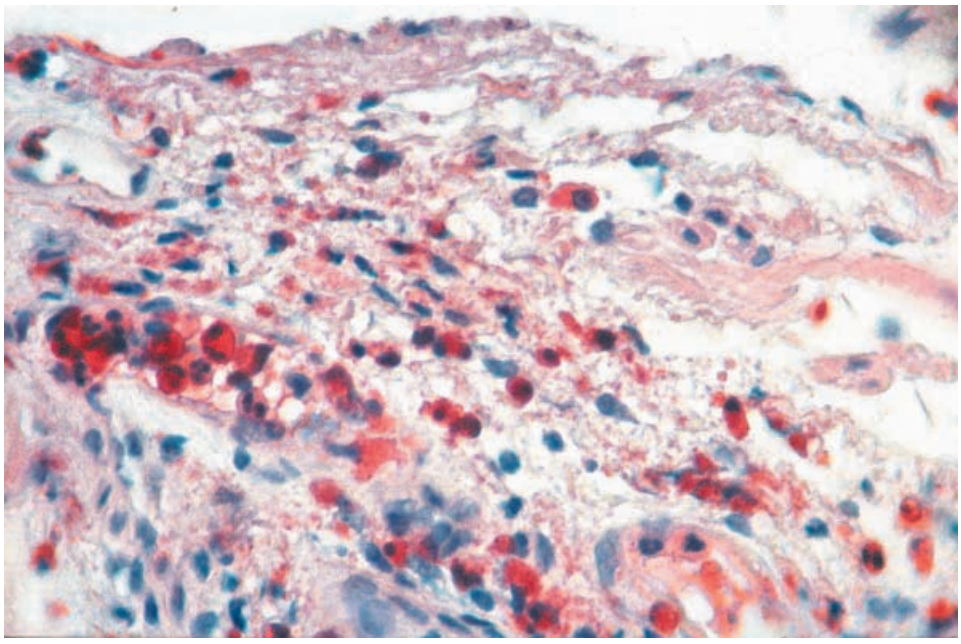

Fig. 2 Eosinophils in asthma bronchitis highlighted by Congo red stain; due to the reaction with acidic (cationic) proteins in eosinophil granules, even the release of granule content could be visualized. Congo red stain, ×250

serve, but not columnar cells were also stained by antibodies for VLA2 and ICAM1 in three cases each. Pneumocytes type I and II were all stained by VLA3-, VLA6-, and ICAM1-antibodies.

Pneumonia and bronchitis in EAA (*n*=8)

The inflammatory cell infiltrate consisted mainly of lymphocytes, macrophages and neutrophils. Lymphocytes were predominantly of the CD^{8+} suppressor cell type. These cells expressed 3+ VLA4 in all, and LFA1 in five cases (Fig. 4). VLA1 and VLA3 were found 2+ on lymphocytes in four and five cases, respectively. Neutrophils expressed MAC1 3+ in all cases. In three cases few eosinophils were present, which all expressed MAC1, but were negative for VLA4. Alveolar macrophages showed a 3+ expression of VLA1, LFA1, MAC1, and gp150/95, whereas VLA3 and VLA5 staining were found 2+ (each in five cases). All pneumocytes and bronchial epithelial cells expressed VLA3 in five cases. ICAM1 was expressed on all endothelial cells of small and medium sized blood vessels, and 3+ on pneumocytes and alveolar macrophages in all cases. ICAM3 was found 3+ on lymphocytes in all cases, and on all eosinophils in the three aforementioned cases (Fig. 1, Fig°5). A 1+ expression of VCAM1 was found on endothelial cells of venules and capillaries, but in only one case, which also had some eosinophils present.

Pneumonia and bronchitis in sarcoidosis (*n*=10)

The inflammatory infiltrate was composed of lymphocytes, predominantly CD^{4+} helper T cells, epithelioid and giant cells, alveolar macrophages, and, focally, neutrophils. Lymphocytes 3+ expressed VLA4 and LFA1 in ten and nine cases, respectively. VLA1 expression was found 2+ on lymphocytes in seven cases. All epithelioid and giant cells expressed MAC1, gp150/95, and VLA1 in six, five, and four cases, respectively. Other integrins (VLA5, LFA1, VLA6) were found only occasionally and on few cells. Alveolar macrophages 2+ expressed VLA1 (eight cases), VLA3 (nine cases), VLA4 (six cases), VLA5 (five cases), and LFA1, MAC1, and gp150/95 each in nine cases. Neutrophils were found and showed a 3+ expression for MAC1 in all cases, and for VLA1 in seven cases (Fig. 1). In two cases single eosinophils, all positive for VLA4, were present. Pneumocytes and bronchial epithelial cells were 3+ positive for VLA3 in all cases, whereas VLA6 expression was rarely seen. ICAM1 was present on all alveolar macrophages in seven cases, and on all endothelial cells of small and medium sized blood vessels, on all pneumocytes, and 3+ on bronchial epithelial cells in all cases (Fig. 6). ICAM3 was expressed 3+ on lymphocytes in all cases, whereas the reactivity for VCAM1 was uniformly negative.

Fig. 3 VCAM1 reactivity in endothelial cells of small venules and capillaries in a case of asthma bronchitis; hematoxylin counterstain, ×500 ▶

Fig. 4 VLA4 selectively stained the majority of lymphocytes in this case of EAA; hematoxylin counterstain, ×220

Fig. 5 ICAM3 on lymphocytes in a case of extrinsic allergic alveolitis; ×220

Fig. 6 ICAM1 in sarcoidosis: pneumocytes, alveolar macrophages, and endothelial cells are stained; in adjacent granulomas some epithelioid cell are also decorated by this antibody; ×220

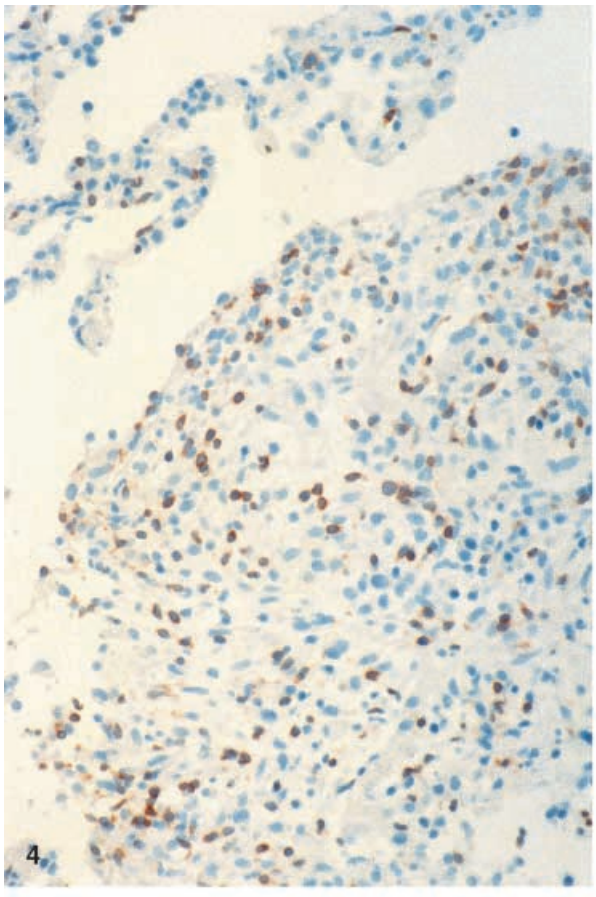
4

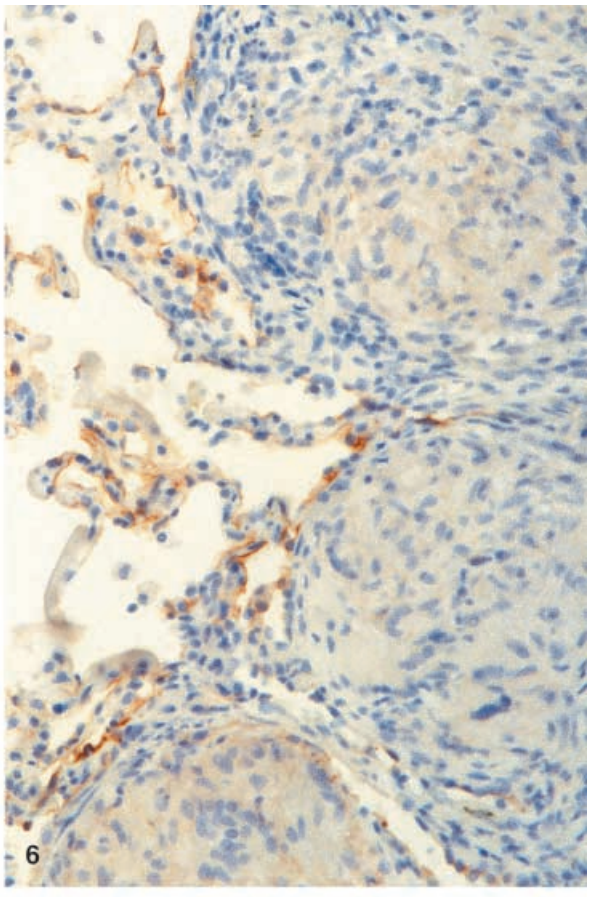
6

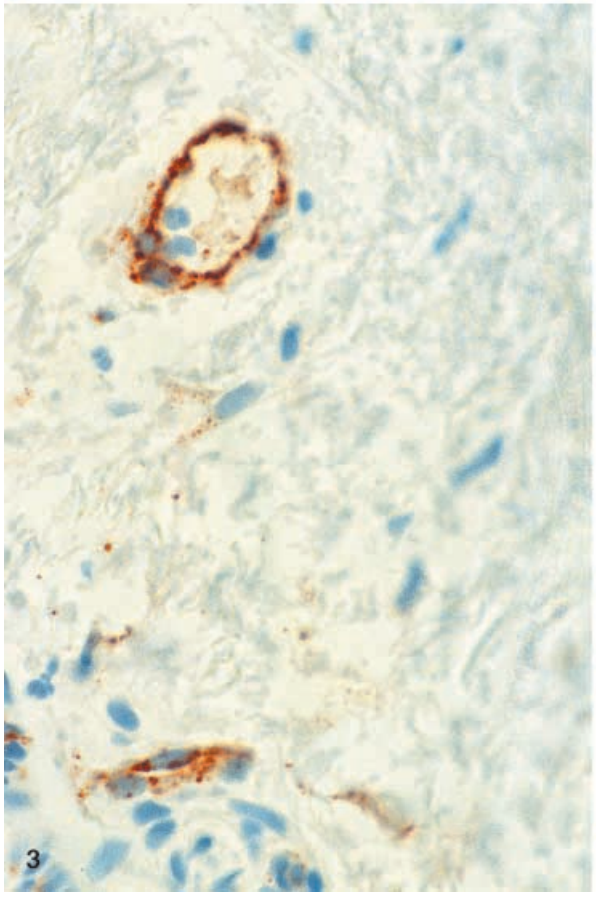
3

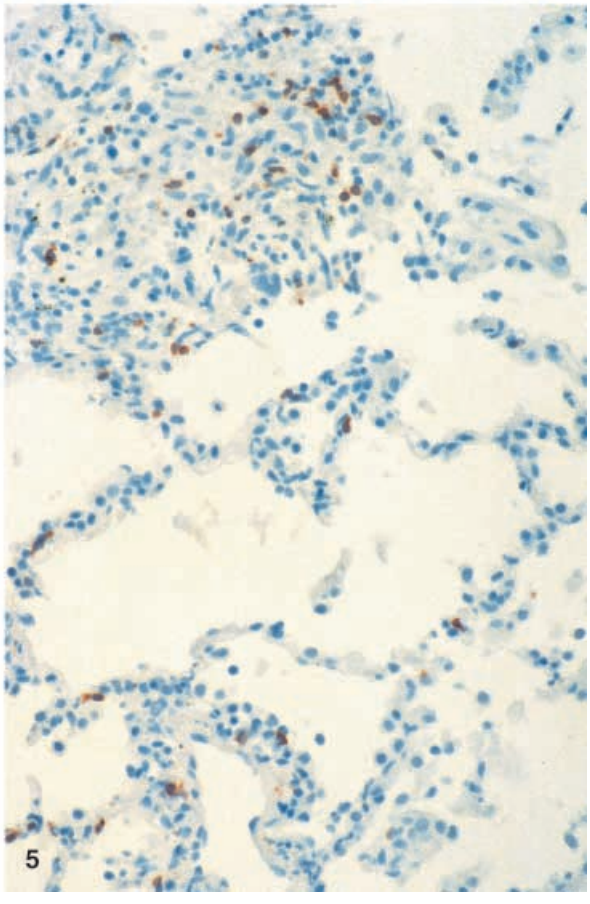
5

Normal control tissue (n=8)

The expression of adhesion molecules in general was 1+ for each cell type. Occasionally encountered lymphocytes and neutrophils were positively stained by VLA4, LFA1, and MAC1 antibodies; eosinophils were not seen. Few alveolar macrophages were present and few of them were positve for VLA1, VLA3, VLA5, and for LFA1, MAC1, and gp150/95. Expression of integrins was present on all bronchial cells. In all cases VLA3 was seen, whereas VLA 1, 2, 5, and 6 were seen in either 2 and 3 cases. The reaction for ICAM1 and 3 was negative in all cases. Pneumocytes in all cases expressed VLA3 2+. Other integrins found were VLA1 and VLA5; however, 1+. Pneumocytes were negative for ICAM1. VCAM1 was not seen in control tissues.

A negative reaction was found for ICAM2 in all five groups. A reaction with antibodies for β3, β4, and β5 was of no importance in our cases; occasionally a 1+ reaction was found (data not shown).

Discussion

Trafficking of lymphocytes and granulocytes from the blood vessels to the site of an immunologic reaction requires adhesion to endothelial cells, transmigration through capillary and venule walls, leukotaxis along matrix proteins, and finally attachment to epithelium and release of enzymes, cytokines, and inflammatory mediators. This all is in part facilitated by the expression of adhesion molecules [4,8]. However, this expression is accomplished in a time- and locus-dependent way, which results in a cascade of activation of sets of adhesion molecules; a distant signaling, is in part facilitated by solubilized, circulating adhesion molecules (i.e., s-ICAM-1) [12, 20, 21].

The expression of some adhesion molecules is associated with general inflammatory conditions and, not surprisingly, can be found in all different kinds of inflammation. Such molecules have been found to include ICAM-1, MAC-1, VLA1, and LFA1 [10, 13, 30, 32, 35]. This is not surprising, since a ligand for LFA1, for example, is complement 3b, which is activated not only in immune reactions, but also in non-immune reactions via the alternative complement pathway [33, 1]. These findings are in contrast to a hypothesis presented in previous studies on the upregulation of ICAM-1. The upregulation was thought to be specifically correlated with the activity and severity of allergic reactions such as asthma [3, 7, 15].

Within the studied sets of adhesion molecules there are distinctive types which are not commonly found, namely, VLA4 and ICAM-3. VLA4 can bind to ICAM-1, or more specifically to VCAM-1, and this interaction has been shown to be associated with the release of cytokines and chemokines from leukocytes [38, 3, 9, 5, 36, 23]. There seems also to be a feedback loop for a release of IL4 and IL5 cytokines which are associated with the leukocytopoiesis and extravasation of eosinophils in and from the bone marrow, probably via sVCAM-1 [25]. In our investigation there was a high percentage of expression of VLA4 on lymphocytes in all three immune diseases and in COPD bronchitis; however, VCAM-1 expression was only seen in ABA and EAA. In sarcoidosis and COPD bronchitis the mechanism of extravasation must be facilitated by the interaction of VLA4 and ICAM-1, which results in a less intense binding [38].

The function of and the ligand for ICAM-3 at present is not known. Interestingly ICAM-3 was present on lymphocytes in ABA, EAA, and sarcoidosis, but not in COPD bronchitis. Another remarkable feature was the expression of VLA4 and ICAM-3 on eosinophils; both molecules were expressed together only in ABA, whereas either the one or the other was independently expressed on eosinophils in EAA and sarcoidosis. In contrast, ICAM-3 was not expressed on eosinophils in COPD bronchitis. This might be interpreted as a selective expression of this adhesion molecule in certain types of allergic diseases.

An interesting, although to date not clearly understandable, expression of adhesion molecules was seen on alveolar macrophages, epithelioid cells, and Langhans giant cells. It is not surprising that epithelioid and Langhans giant cells generally express fewer adhesion molecules than macrophages, because both cell types are immobilized and stay within the granulomas, and therefore might not need adhesion molecule expression for trafficking. Since alveolar macrophages form the cell pool from which epithelioid and Langhans cells differentiate, it is logical that during granuloma formation and differentiation they do not need VLA1, LFA1, VLA3, VLA4, and VLA5 expression, which might be necessary for leukotaxis. However, they still seem to need MAC1 and gp150/95, for which the ligands are C3bR and sialic acid. And indeed, complement activation and interaction with mucopolysaccharides in the matrix do regularly occur in sarcoidosis and EAA [6, 14].

Another interesting feature is the expression of adhesion molecules on epithelial cells. Whereas the expression of VLA3 and VLA6 might reflect the anchoring of the epithelial cells to fibronectin and laminin, the expression of ICAM-1, found in all four disease groups, might be a mechanism by which lymphocytes, neutrophils, and eosinophils attach to these epithelial cells. And this attachment could be the prerequisite for a toxic action of such leukocytes [10, 19, 22].

As in asthma, much emphasis has been placed on ICAM-1 and its soluble form s-ICAM-1 in the regulation of inflammation in sarcoidosis [11, 17] and EAA [27]. Other reports have also focused on LFA1 expression in sarcoidosis or EAA [17, 31]. However, neither LFA1 nor ICAM-1 expression is specifically associated with one of these granulomatous diseases. Their expression might more reasonably be associated with general inflammatory mechanisms. In contrast, VLA4 and ICAM-3 expression on lymphocytes in both diseases and the expression of ICAM-3 on eosinophils in EAA might reflect a more

disease-specific activation pattern. Both molecules seem to be associated with the influx of eosinophils in EAA. Because of the more intense binding of VLA4 expressing lymphocytes to ICAM-1 (compared to VLA1 binding) on endothelial cells in both sarcoidosis and EAA, more lymphocytes are able to enter the site of the allergic/immunologic reaction.

Finally, our results have some practical value. Chronic bronchitis in ABA and COPD might in some cases be morphologically indistinguishable. There are a few cases of EAA in which granulomas are numerous,thereby raising the differential diagnosis of sarcoidosis. In these equivocal cases VLA4 and ICAM-3 antibodies can be used: ICAM-3 expression on eosinophils in a case with sarcoid-like granulomatous pneumonia favors the diagnosis of EAA. Similarly a positive expression of ICAM-3 and VLA4 on eosinophils separates ABA from COPD bronchitis.

In conclusion, the selective expression of ICAM-3, VLA4, and VCAM-1 on lymphocytes and eosinophils in ABA might in part explain the predominant infiltration of eosinophils into the bronchial mucosa. This, together with the liberation of IL-4 and IL-5, facilitating eosinophilia, might be part of the selection process which leads to the characteristic allergic tissue reaction. It is also interesting that in two other immune diseases of the lung, EAA and sarcoidosis, a similar, but not identical, adhesion molecule expression can be seen. Some of the differences in adhesion molecule expression together with other sets of cytokines might be responsible for the different morphologic appearance in these diseases. Our results have shown that the activation/expression of adhesion molecules on leukocytes, endothelial, and epithelial cells seems to follow some common (ICAM-1, VLA1, LFA1) and some more selective (VCAM-1, VLA-4, ICAM-3) pathways. In further investigations this knowledge can be used to study the differences in the cytokine adhesion molecule network in asthma, EAA, and sarcoidosis in more detail.

References

1. Adams DH, Horvath L, Bottaro DP, Interrante R, Catalano G, Tanaka Y, Strain A, Hubscher SG, Shaw S (1994) Hepatocyte growth factor and macrophage inflammatory protein 1 beta: structurally distinct cytokines that induce rapid cytoskeletal changes and subset-preferential migration in T-cells. Proc Natl Acad Sci USA 91: 7144–7148
2. American Thoracic Society (1995) Standards for the diagnosis and care of patients with chronic obstructive pulmonary disease. Am J Respir Crit Care Med 152: S77–S120
3. Bentley AM, Durham SR, Robinson DS, Menz G, Storz C, Cromwell O, Kay AB, Wardlaw AJ (1993) Expression of endothelial and leukocyte adhesion molecules interacellular adhesion molecule-1, E-selectin, and vascular cell adhesion molecule-1 in the bronchial mucosa in steady-state and allergen-induced asthma. J Allergy Clin Immunol 92: 857–868
4. Bevilacqua MP (1993) Endothelial-leukocyte adhesion molecules. Annu Rev Immunol 11: 767–804
5. Bochner BS, Luskinas TW, Gimbrone MA, Newman W, Sterbinsky A, Derse-Anthony CP, Klunk D, Schleimer RP (1991) Adhesion of human basophils, eosinophils, and neutrophils to interleukin-1 activated human vascular endothelial cells: contribution of endothelial adhesion molecules. J Exp Med 173: 1553–1556
6. Chilosi M, Mombello A, Lestani M, Menestrina F, Fiore-Donati L, Cipriani A, Zambello R, Semenzato G (1991) Immunohistochemical characterization of sarcoid granuloma: differentiation antigens and adhesion molecules. Sarcoidosis 8: 171–172
7. De Rose V, Rolla G, Bucca C, Ghio P, Bertoletti M, Baderna P, Pozzi E (1994) Intercellular adhesion molecule-1 is upregulated on peripheral blood T lymphocyte subsets in dual asthmatic responders. J Clin Invest 94: 1840–1845
8. Diamond MS, Springer TA (1994) The dynamic regulation of integrin adhesiveness. Curr Biol 4: 506–517
9. Gosset P, Tillie-Leblond I, Janin A, Marquette CH, Copin MC, Wallaert B, Tonnel AB (1995) Expression of E-selectin, ICAM-1 and VCAM-1 on bronchial biopsies from allergic and non-allergic asthmatic patients. Int Arch Allergy Immunol 106: 69–77
10. Gundel RH, Wegner CD, Torcellini CA, Letts LG (1992) The role of intercellular adhesion molecule-1 in chronic airway inflammation. Clin Exp Allergy 22: 569–575
11. Hamblin AS, Shakoor Z, Kapahi P, Haskard D (1994) Circulating adhesion molecules in sarcoidosis. Clin Exp Immunol 96: 335–338
12. Hashimoto S, Imai K, Kobayashi T, Amemiya E, Takahashi Y, Tomita Y, Iwata T, Suguro H, Yamaguchi M, Yachi A, et al (1993) Elevated levels of soluble ICAM-1 in sera from patients with bronchial asthma. Allergy 48: 370–372
13. Hoogsteden HC, van Hal PT, Wijkhuijs JM, Hop W, Hilvering C (1992) Expression of the CD11/CD18 cell surface adhesion glycoprotein family and MHC class II antigen on blood monocytes and alveolar macrophages in interstitial lung diseases. Lung 170: 221–233
14. Kazatchkine MD, Fearon DT, Silbert JE, Austen KF (1979) Surface-associated heparin inhibits zymosan-induced activation of the human alternative complement pathway by augmenting the regulatory action of the control proteins on particle-bound C3b. J Exp Med 150: 1202–1215
15. Kobayashi T, Hashimoto S, Imai K, Amemiya E, Yamaguchi M, Yachi A, Horie T (1994) Elevation of serum soluble intercellular adhesion molecule-1 (sICAM-1) and sE-selectin levels in bronchial asthma. Clin Exp Immunol 96: 110–115
16. Koukoulis GK, Warren WH, Virtanen I, Gould VE (1997) Immunolocalization of integrins in the normal lung and in pulmonary carcinomas. Hum Pathol 28: 1018–1025
17. Melis M, Gjomarkaj M, Pace E, Malizia G, Spatafora M (1991) M Increased expression of leukocyte function associated antigen-1 (LFA-1) and intercellular adhesion molecule-1 (ICAM-1) by alveolar macrophages of patients with pulmonary sarcoidosis. Chest 100:910–916
18. Mercurio AM (1995) Laminin receptors: Achieving specifically through cooperation. Trends Cell Biol 5: 419–423
19. Montefort S, Gratziou C, Goulding D, Polosa R, Haskard DO, Howarth PH, Holgate ST, Carroll MP (1994) Bronchial biopsy evidence for leukocyte infiltration and upregulation of leukocyte-endothelial cell adhesion molecules 6 hours after local allergen challenge of sensitized asthmatic airways. J Clin Invest 93: 1411–1421
20. Montefort S, Lai CK, Kapahi P, Leung J, Lai KN, Chan HS, Haskard DO, Howarth PH, Holgate ST (1994) Circulating adhesion molecules in asthma. Am J Respir Crit Care Med 149: 1149–1152
21. Mulligan MS, Vaporciyan AA, Warner RL, Jones ML, Foreman KE, Miyasaka M, Todd RF 3rd, Ward PA (1995) Compartmentalized roles for leukocytic adhesion molecules in lung inflammatory injury. J Immunol 154: 1350–1363
22. Nagase T, Fukuchi Y, Matsuse T, Sudo E, Matsui H, Orimo H (1995) Antagonism of ICAM-1 attenuates airway and tissue responses to antigen in sensitized rats. Am J Respir Crit Care Med 151: 1244–1249

23. Nakajima H, Sano H, Nishimura T, Yoshida S, Iwamoto I (1994) Role of vascular cell adhesion molecule-1 / very late activation antigen-4 and intercellular adhesion molecule 1 / lymphocyte function-associated antigen 1 interactions in antigen-induced eosinophil and T cell recruitment into the tissue. J Exp Med 179: 1145–1154
24. National Heart, Lung and Blood Institute (1992) National Institutes of Health. International consensus report on the diagnosis and treatment of asthma. Eur Respir J 5: 601–641
25. Okhawara Y, Lei XF, Stämpfli MR, Marshall JS, Xing Z, Jordana M (1997) Cytokine and eosinophil responses in the lung, peripheral blood, and bone marrow compartments in a murine model of allergen-induced airway inflammation. Am J Respir Cell Mol Biol 16: 510–520
26. Peltonen J, Larjava H, Jaakkola S, Gralnick H, Akiyama SK, Yamada SS, Yamada KM, Uitto J (1989) Localization of integrin receptors for fibronectin, collagen, and laminin in human skin. Variable expression in basal and squamous cell carcinomas. J Clin Invest 84: 1916–1923
27. Pforte A, Schiessler A, Gais P, von Kress S, Beer B, Riethmuller G, Ziegler-Heitbrock HW (1993) Expression of the adhesion molecule ICAM-1 on alveolar macrophages and in serum in extrinsic allergic alveolitis. Respiration 60:221–226
28. Pilewski JM, Albelda SM (1993) Adhesion molecules in the lung. An overview. Am Rev Respir Dis 148: 31–37
29. Sanchez-Madrid F, Nagy J, Robbins E (1983) A human leukocyte differentiation antigen family with distinct a subunits and a common b subunit: the lymphocyte function-associated antigen (LFA-1) C3b/i complement receptor (OKM 1/Mac 1) and the p150/95 molecule. J Exp Med 158: 1785–1795
30. Schaberg T, Rau M, Stephan H, Lode H (1993) Increased number of alveolar macrophages expressing surface molecules of the CD11/CD18 family in sarcoidosis and idiopathic pulmonary fibrosis is related to the production of superoxide anions by these cells. Am Rev Respir Dis 147: 1507–1513
31. Shakoor Z, Hamblin AS (1992) Increased CD11/CD18 expression on peripheral blood leucocytes of patients with sarcoidosis. Clin Exp Immunol 90: 99–105
32. Shijubo N, Imai K, Shigehara K, Honda Y, Koba H, Tsujisaki M, Hinoda Y, Yachi A, Ohmichi M, Hiraga Y, et al (1994) Soluble intercellular adhesion molecule-1 (ICAM-1) in sera and bronchoalveolar lavage fluid of patients with idiopathic pulmonary fibrosis and pulmonary sarcoidosis. Clin Exp Immunol 95: 156–161
33. Sunyer JO, Lambris JD (1998) Evolution and diversity of the complement system of poikilothermic vertebrates. Immunol Rev 166: 39–57
34. Tournier JM, Goldstein GA, Hall DE (1992) Extracellular matrix proteins regulate morphologic and biochemical properties of tracheal glands serous cells through integrins. Am J Respir Cell Mol Biol 6: 461–471
35. van Dinther-Janssen AC, van Maarsseveen TC, Eckert H, Newman W, Meijer CJ (1993) Identical expression of ELAM-1, VCAM-1, and ICAM-1 in sarcoidosis and usual interstitial pneumonia. J Pathol 170: 157–164
36. Weg VB, Williams TJ, Lobb RR, Nourshargh S (1993) A monoclonal antibody recognizing very late activation antigen-4 inhibits eosinophil accumulation in vivo. J Exp Med 177: 561–566
37. Yuan Q, Austin KE, Friend DS, Heidtmann M, Boyce JA (1997) Human peripheral blood eosinophils express a functional c-kit receptor for stem cell factor that stimulates very late antigen 4 (VLA-4) mediated cell adhesion to fibronectin and vascular adhesion molecule 1 (VCAM-1). J Exp Med 186: 313–323
38. Zangrilli JG, Shaver JR, Cirelli RA, Cho SK, Garlisi CG, Falcone A, Cuss FM, Fish JE, Peters SP (1995) sVCAM-1 levels after segmental antigen challenge correlate with eosinophil influx, IL-4 and IL-5 production, and the late phase response. Am J Respir Crit Care Med 151: 1346–1353

Virchows Arch (2002) 440:181–186
DOI 10.1007/s004280100488

ORIGINAL ARTICLE

M. Tsokos · S. Anders · F. Paulsen

Lectin binding patterns of alveolar epithelium and subepithelial seromucous glands of the bronchi in sepsis and controls – an approach to characterize the non-specific immunological response of the human lung to sepsis

Received: 11 April 2001 / Accepted: 21 May 2001 / Published online: 26 July 2001
© Springer-Verlag 2001

Abstract A delayed or deficient immunological protection as well as an overstimulation of the mucosal immune system may act as possible additional promoters of sepsis-induced lung injury in patients suffering from a severe septic condition. Lectin-binding patterns in pulmonary tissue samples obtained at autopsy from septic patients and control individuals were studied using 11 carbohydrate-specific lectins (Con A, UEA, GSA I, GSA II, MPA, PNA, Jac, WGA, MAA, LPA, and SNA). There were no differences in the secretory product of serous parts of bronchial glands detectable in the two study groups, whereas lectin binding patterns of alveolar epithelium and mucous parts of subepithelial seromucous glands were different in sepsis cases when compared to controls. Apart from differences in binding sites for α-mannose, N-acetyl-neuraminic acid and α-(2–6)-galactose (as detected by different expression for Con A, MAA and SNA) in the two study groups, the main finding was that no binding sites for α-N-acetyl-galactosamine (as investigated by MPA immunoreactivity) could be detected on alveolar epithelial cells and mucous parts of subepithelial seromucous glands in sepsis cases in contrast to the presence of such binding sites in the control cases. We hypothesize that the finding of an altered secretory product of alveolar epithelial cells and bronchial glands in sepsis may be a result of specific carbohydrate deprivation or consumption, respectively, possibly due to direct bacterial effects or pathogenetic events in response to bacterial toxins during the complex cascade of the host's systemic inflammatory response in sepsis. The altered type of mucus glycoprotein physiologically secreted by alveolar epithelium and mucous parts of subepithelial seromucous glands of the bronchi with subsequent loss of a considerable proportion of protection of the mucosal barrier in sepsis may play an important additional role in the development of sepsis-induced lung injury.

Keywords Lectins · Mucin · Carbohydrate · Adult respiratory distress syndrome (ARDS) · Sepsis-induced lung injury · Sepsis

M. Tsokos (✉) · S. Anders
Institute of Legal Medicine, University of Hamburg,
Butenfeld 34, 22529 Hamburg, Germany
e-mail: ifrhh@uke.uni-hamburg.de
Tel.: +49-40-42803-2748, Fax: +49-40-42803-3934

S. Anders
Institute of Pathology, University of Hamburg,
Martinistrasse 52, 20246 Hamburg, Germany

F. Paulsen
Department of Anatomy,
Christians-Albrechts-University of Kiel,
Olshausenstrasse 40, 24098 Kiel, Germany

Introduction

Human sepsis is known to be associated with a generalized activation and systemic expression of the host's inflammatory pathways. However, the sequence and detailed mechanisms of the cellular and molecular events involved in the pathogenesis of sepsis are not completely understood yet [2]. Besides a general systemic immunologic imbalance in sepsis, especially in the lungs, local defense mechanisms become insufficient in eliminating the infectious agent and, as a consequence of intense cellular interactions resulting in pulmonary tissue injury, septic conditions often lead to adult respiratory distress syndrome (ARDS), critically impaired lung function, and death [5, 15, 26, 29]. For this reason, delayed or deficient immunological protection and an altered competence of cellular and humoral immunological reactions, as well as an overstimulation of the mucosal immune system, may act as possible additional promoters of sepsis-induced lung injury.

In this context, we hypothesized that non-specific defense mechanisms also are relevant when the type of mucus glycoprotein physiologically secreted by alveolar epithelium and subepithelial seromucous glands of the bronchi is altered and its function is no longer protective.

Accordingly, the aim of this study was to investigate human lung tissue originating from sepsis and control cases with a view to non-specific immunological characteristics of the alveolar epithelium and subepithelial seromucous glands using lectin histochemistry. The binding pattern of eleven different lectins was tested to determine whether they act as indicators for the non-specific immunological response and protection of epithelia in both groups.

Material and methods

Study groups

Lung specimens were obtained from four different lung lobes at autopsy from eight individuals divided in two study groups. The post-mortem intervals were similar in both study groups (range between 1 and 3 days). Information on smoking habits of the individuals included in both study groups was not obtainable. Pneumonic tissue alterations were not detected in any of the selected cases by gross examination of the lungs.

1. Sepsis group: four patients (three males, one female; ages 44–82 years) with a well-documented medical history and diagnosis of sepsis in vivo according to the definition of the American College of Chest Physicians/Society of Critical Care Medicine Consensus Conference [3] who died on the intensive care unit of a large university teaching hospital were included in this study group. The clinical cause of death was ARDS due to sepsis in all cases, and no other cause of death was revealed by autopsy and a thorough histological examination of the relevant internal organs. Table 1 shows the individual clinical and biological characteristics of the patients.
2. Control group: four forensic autopsy cases (three males, one female; ages 23–74) with sudden death due to unnatural causes served as controls. The individuals had no medical history of a septic condition prior to death, and in none of the cases was suspicion aroused by autopsy findings of an underlying infectious disease. No other disease was found at autopsy other than the cause of death (electrocution, *n*=2; hanging, *n*=1; exsanguation (abdominal gun shots), *n*=1). The survival times following the fatal incidents ranged between a few seconds and a few minutes. Cardiopulmonary resuscitation attempts were not performed in any of the cases.

Routine histological examination

Lung specimens were fixed in 4% buffered formalin, embedded in paraffin, cut in 4-to 5-µm sections, and stained with hematoxylin-eosin and periodic acid-Schiff. In each case major bronchi were included in at least one lung specimen.

Lectin histochemistry

For lectin-binding experiments, lung tissue sections deriving from the paraffin blocks used for routine histology were deparaffinized in xylene, rehydrated with a graded series of ethanol, passed into double-distilled water, and finally into TRIS-bufferred saline (0.05 M TRIS, 0.15 M sodium chloride, pH 7.4, TBS), supplemented with 0.02 M $CaCl_2$. The origins and specificities of the lectin conjugates used are listed in Table 2. Incubation of the sections with various fluorescein isothiocyanate (FITC)-conjugated lectin solutions (10 µg/ml) was done in a dark, moist chamber at room temperature for 30 min. After washing the slides three times with TBS, sections were mounted in 10% glycerol in TBS or in Vectashield (Vector Laboratories, Burlingame, Calif., USA). The specificity of the lectin-binding was checked in control experiments by mixing the lectin solution with the corresponding inhibiting sugar at concentrations of 0.2 to 0.5 M prior to incubation for 30 min at room temperature. TBS-mounted sections were used to estimate the autofluorescence of the tissues. All slides were examined using a microscope equipped for epifluorescence (Zeiss-Axiophot, Oberkochen, Germany).

Table 1 Individual clinical and biological characteristics of the patients included in the sepsis group

Case number	Age	Gender	ICU days	Outcome of microbiology (blood cultures in vivo)	Origin of sepsis
1	44	M	5	*Staphylococcus aureus*	Superinfection of varicella infection
2	49	M	23	*Escherichia coli*	Peritonitis (due to perforation of small bowel)
3	43	M	6	*Klebsiella oxytoca*	Peritonitis (due to abdominal gun shots)
4	82	F	15	*Enterobacter cloacae*	Peritonitis (due to ischemic colitis)

Table 2 Origin and carbohydrate specificities of lectin conjugates used in the study (*BSM* bovine submandibular gland mucin, *Fuc* fucose, *Gal* galactose, *GalNAc* N-acetyl-galactosamine, *Glc* glucose, *GlcNAc* N-acetyl-glucosamine, *Man* mannose, *Neu5Ac* N-acetyl-neuraminic acid)

Lectin	Abbreviation	Carbohydrate specificities	Inhibitor
Concanavalin A agglutinin	ConA	α-Man	α-methyl-Man + α-methyl Glc
Ulex europaeus agglutinin	UEA	α-L-Fuc	Fuc
Griffonia simplicifolia I agglutinin	GSA I	α-GalNAc>α-Gal	GalNAc+Gal
Griffonia simplicifolia II agglutinin	GSA II	α(β)-GlcNAc	GlcNAc
Maclura pomifera agglutinin	MPA	α-GalNAc	GalNAc
Arachis hypogaea agglutinin	PNA	D-Gal-β(1–3)GalNAc	Gal
Artocarpus integrifolia	Jac	Gal-β(1–3)GalNAc	Gal
Wheat germ agglutinin	WGA	α-GlcNAc>α-GalNAc>Neu5Ac	GlcNAc, Neu5Ac
Maackia amurensis agglutinin	MAA	Neu5Acα(2–3)Gal	Neu5Ac
Limulus polyphemus agglutinin	LPA	Neu5Acα(2–3)GalNAc>Neu5Acα(2–6)GalNAc	BSM
Sambucus nigra agglutinin	SNA	Neu5Acα(2–6)Gal	Neu5Ac

Grading of lectin staining

The slides were coded and examined without knowledge of their origin from each study group. Ten representative visual fields were randomly selected from the center of the slides and analyzed at ×20 magnification. The staining intensity was determined by a semiquantitative score ranging from (-) to (+++), with (-) representing no staining, (+) weak, (++) moderate and (+++) strong staining intensity.

Results

Routine histological examination

In the sepsis group, different stages of ARDS, including intra-alveolar edema, fibrin deposits covering the alveolar epithelium as hyaline membranes, microthromboses, and intra-alveolar and interstitial fibrosis, were present in all cases. Additionally, vascular engorgement and extensive leukostasis in the pulmonary microvasculature in the absence of interstitial or intra-alveolar inflammatory cell accumulation was found in two cases. In none of the cases included in the sepsis group were pneumonic tissue alterations or any co-existent lung diseases detected. In the control group no pneumonic tissue alterations or preexisting lung diseases were found; in one case (death due to hanging) the pulmonary microvasculature was sporadically engorged showing considerable hyperemia.

Lectin histochemistry

Application of carbohydrate-specific lectins (Con A, UEA, GSA I, GSA II, MPA, PNA, Jac, WGA, MAA, LPA, and SNA) on deparaffinated lung tissue sections from sepsis-associated fatalities and control cases resulted to some extent in different staining patterns of alveolar epithelial cells and subepithelial seromucous glands of the bronchi (Tables 3, 4).

Similarities in the lectin staining pattern of sepsis and controls

We found no marked differences in lectin binding patterns to serous parts of subepithelial seromucous glands in either study group: binding sites for Con A were uniformly distributed throughout serous parts of subepithelial seromucous glands in a strong immunohistochemical staining pattern in both study groups, whereas no immunostaining was seen for the other lectins investigated (results not shown).

In contrast to Con A binding that was detected on alveolar epithelial cells showing a strong immunoreaction in both study groups, no binding sites were found for UEA, GSA I, GSA II, PNA, WGA, and LPA on alveolar epithelium in the two study groups.

Differences in the lectin staining pattern of sepsis and controls

A strong positive staining reaction for SNA was visible in mucous parts of subepithelial seromucous glands in three control cases (Fig. 1), whereas SNA staining was found only in one case of death from septic ARDS (Table 4). Interestingly, this sepsis case showed no SNA staining on alveolar epithelial cells (Table 3) in complete contrast to the remaining three cases, which were strong-

Table 3 Summary of lectin binding to alveolar epithelial cells in sepsis and controls

Study group	Case number	*Con A*	*MAA*	*UEA*	*Jac*	*GSAI*	*GSAII*	*PNA*	*MPA*	*SNA*	*WGA*	*LPA*
Sepsis	1	+++	++	–	–	–	–	–	–	–	–	–
	2	+++	+	–	–	–	–	–	+++	–	–	
	3	+++	+	–	++	–	–	–	+++	–	–	
	4	+++	+	–	+++	–	–	–	+++	–	–	
Control	1	+++	–	–	+++	–	–	–	+	+++	–	–
	2	+++	+	–	–	–	–	++	–	–	–	
	3	+++	++	–	+++	–	–	+	+++	–	–	
	4	+++	–	–	+++	–	–	+	+++	–	–	

Table 4 Summary of lectin binding to mucous parts of subepithelial seromucous glands

Study group	Case number	*Con A*	*MAA*	*UEA*	*Jac*	*GSAI*	*GSAII*	*PNA*	*MPA*	*SNA*	*WGA*	*LPA*
Sepsis	1	–	–	–	+++	–	–	+++	–	+++	++	–
	2	–	–	+++	–	–	–	–	–	++	–	
	3	–	–	–	–	–	–	–	–	+++	–	
	4	–	–	–	–	–	–	–	–	+++	–	
Control	1	++	–	–	–	–	–	–	++	–	+++	–
	2	–	–	+++	–	–	–	+++	+++	++	–	
	3	–	–	–	–	–	–	++	+++	+++	–	
	4	+	–	–	–	–	–	++	+++	++	–	

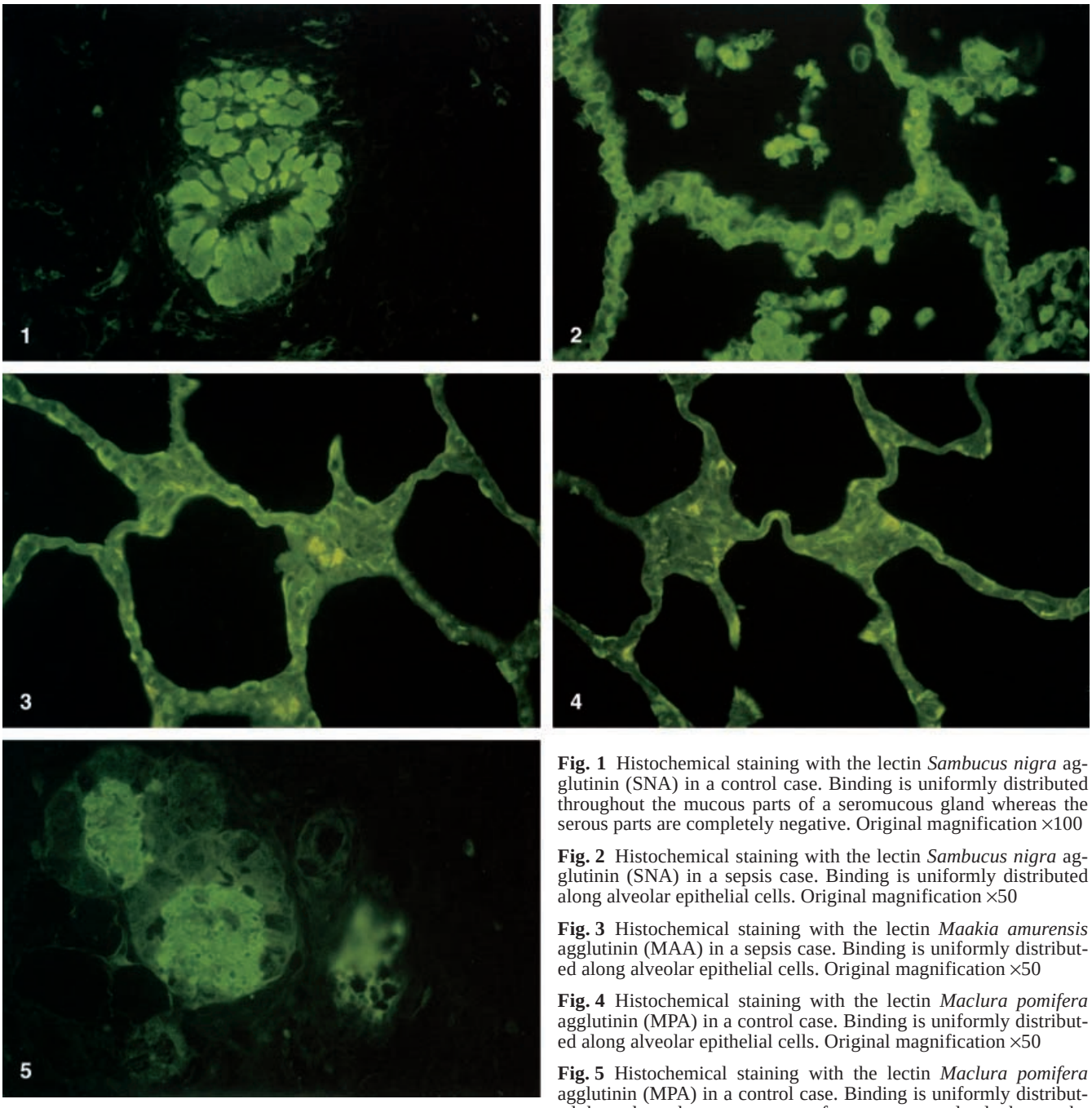

Fig. 1 Histochemical staining with the lectin *Sambucus nigra* agglutinin (SNA) in a control case. Binding is uniformly distributed throughout the mucous parts of a seromucous gland whereas the serous parts are completely negative. Original magnification ×100

Fig. 2 Histochemical staining with the lectin *Sambucus nigra* agglutinin (SNA) in a sepsis case. Binding is uniformly distributed along alveolar epithelial cells. Original magnification ×50

Fig. 3 Histochemical staining with the lectin *Maakia amurensis* agglutinin (MAA) in a sepsis case. Binding is uniformly distributed along alveolar epithelial cells. Original magnification ×50

Fig. 4 Histochemical staining with the lectin *Maclura pomifera* agglutinin (MPA) in a control case. Binding is uniformly distributed along alveolar epithelial cells. Original magnification ×50

Fig. 5 Histochemical staining with the lectin *Maclura pomifera* agglutinin (MPA) in a control case. Binding is uniformly distributed throughout the mucous parts of a seromucous gland whereas the serous parts are completely negative. Original magnification ×100

ly positive for SNA on alveolar epithelium (Fig. 2). While no staining with ConA was seen in any of the sepsis cases, ConA staining was detectable in mucous parts of subepithelial seromucous glands in two of the control cases (Table 4). On comparison of the study groups, slight differences were also apparent for MAA: all sepsis cases showed a positive immunoreaction on alveolar epithelium (Fig. 3), but only two controls expressed MAA binding sites (Table 3). Binding sites for Jac showed an inverse staining reaction when comparing the immunopositivety of mucous parts of subepithelial seromucous glands and alveolar epithelium in the two study groups (Tables 3, 4).

The most striking finding was that in none of the sepsis cases could binding sites for MPA be detected on alveolar epithelial cells or mucous parts of subepithelial seromucous glands, in contrast to a positive staining reaction for MPA in all cases of the control group (Figs. 4, 5, Tables 3, 4).

Discussion

In the present study we used lectin histochemistry to characterize the non-specific immunological response of the alveolar epithelium and subepithelial seromucous glands of the bronchi in sepsis-associated fatalities compared to non-septic controls. We found no differences in the secretory product of serous parts of subepithelial seromucous glands in the two study groups, but there were differences in lectin binding patterns of alveolar epithelial cells and mucous parts of subepithelial seromucous glands of the bronchi between sepsis cases and controls. Our results show that mucin-producing cells not only exist in subepithelial seromucous glands of the bronchi, but are also present in alveolar epithelium: the secretory products of alveolar epithelial cells and mucous parts of subepithelial seromucous glands contain carbohydrates including mannose, N-acetyl-galactosamine, galactose, and N-acetyl-neuraminic acid, whereas with the exception of mannose these carbohydrates are not secreted by serous parts of subepithelial seromucous glands in the bronchi (Tables 3, 4).

Using routine histological staining methods on pulmonary tissue sections we found the typical micromorphological feature of ARDS as described earlier by Bachofen et al. [4] and recently reviewed by Hasleton and Roberts [15]. In addition, recent post-mortem studies have focused on the immunohistochemical expression pattern of different cellular adhesion molecules and other anti-inflammatory proteins to demonstrate the micromorphological correlate of sepsis-induced lung injury [22, 23, 24], whereas little is known about the role of pathological conditions of the local non-specific immunological response of the lungs during sepsis.

The biosynthesis of oligosaccharide chains of glycoproteins is often altered under pathological conditions, and such alterations can be detected with lectins. Lectins are carbohydrate-binding proteins found widely in plant and animal tissues [7, 8, 12, 17]. Their specific carbohydrate-binding properties allow lectins to recognize particular glycoconjugates, suggesting that lectins participate in the regulation of physiological and pathological processes that involve binding of specific glycoconjugates [6, 13, 28]. Histochemical studies of lectin reactivity directly onto tissue sections as performed in the present investigation have proven especially effective in studying lectin binding patterns of human cells in their natural environment [21, 27]. It is very likely that alterations of the mucosal immune system, reflected by differences in lectin binding sites, may act – mainly by a delayed or deficient immunological protection of the mucosal barrier – as possible additional promoters of sepsis-induced lung injury in patients suffering from a severe septic condition.

As is known from the gastrointestinal tract, mucus serves several functions. Besides lubrication and waterproofing of the mucosa to regulate epithelial cell hydration, mucins protect mucosal surfaces against potentially harmful substances such as particles, digestive enzymes, and toxins, as well as bacterial and other infectious agents, and mucus protects mucosal surfaces from infective agents [9, 11, 16, 19, 20, 25]. Intestinal mucus has been observed to carry away bacteria [10]. Moreover, it has been shown that mucus possesses structures that mimic the receptor sites for microorganisms on epithelial cells that facilitate trapping and subsequent disposal of bacteria [1] and viruses [18].

Apart from slight to moderate differences in binding sites for α-mannose, N-acetyl-neuraminic acid, and α-(2–6)-galactose (as detected by different expression for Con A, MAA, and SNA) in alveolar epithelium and bronchial glands in the two study groups, the main finding of our investigation was that no binding sites for α-N-acetyl-galactosamine could be detected in alveolar epithelial cells and mucous parts of subepithelial seromucous glands in sepsis cases, in contrast to the presence of such binding sites in the controls. This reveals the highly specific difference between the sepsis and the control group for the presence/expression of MPA (Tables 3, 4). At present we can only hypothesize that the finding of an altered secretory product of alveolar epithelial cells and mucous parts of subepithelial seromucous glands in our sepsis cases may be a result of specific carbohydrate deprivation or consumption, respectively, possibly due to direct bacterial effects or pathogenetic events in response to bacterial toxins during the complex cascade of excessive pro-inflammatory and anti-inflammatory mediator release involved in the host's systemic inflammatory response and development of sepsis-induced lung injury. Although autopsies were performed in the earlier post-mortem interval and the time elapsed since death (1 to 3 days) were similar in the subjects of the two study groups, one cannot categorically rule out the possibility of post-mortem cellular autolysis affecting lectin expression pattern in individual cases. More cases need to be studied in order to see whether the tendency we observed is reproducible.

We suggest that an alteration of the type of mucus glycoprotein physiologically secreted by alveolar epithelium and mucous parts of subepithelial seromucous glands of the bronchi with subsequent loss of a considerable proportion of protection of the mucosal barrier in sepsis may play an important additional role in the development of sepsis-induced lung injury. Since most intracellular pathogens persist in macrophages and epithelial cells during infection, it is likely that these pathogens contribute to a continual deprivation or consumption of glycoproteins physiologically secreted by alveolar epithelial and glandular cells, respectively, at different time points and stages of infection and may, among other mechanisms, by reducing pathogen clearance amplify the inflammatory response resulting in sepsis-induced lung injury and ARDS.

Indeed, the immunological parameters that influence the progression of sepsis-induced lung injury are likely to be multifactorial, and the precise mechanisms and pathogenetic role of altered lectin binding patterns in septic patients in our study are not clear at present. Since

a more precise identification of the exact mechanisms of the cellular and molecular events involved in the pathogenesis of sepsis-induced lung injury is essential in developing new therapeutic strategies for septic patients, further studies on the subject of different mucosal expression patterns of specific carbohydrates in septic patients are necessary. The results of such forthcoming studies may provide a basis for a clearer understanding of the bacterial factors that influence the host response and course of sepsis-induced lung injury and may indicate whether the observed alterations of lectin binding patterns in the present study simply represent epiphenomena without any causal relationship concerning the clinical course and outcome of septic patients suffering from ARDS, or if the present findings may have future diagnostic or therapeutic implications.

References

1. Abraham SN, Beachey EH (1985) Host defenses against adhesion of bacteria to mucosal surfaces. Host Def Mech 4:63–88
2. Adrie C, Pinsky MR (2000) The inflammatory balance in human sepsis. Intensive Care Med 26:364–375
3. American College of Chest Physicians/Society of Critical Care Medicine Consensus Conference (1992) Definition for sepsis and organ failure and guidelines for the use of innovative therapies in sepsis. Crit Care Med 20:864–874
4. Bachofen H, Schürch S, Weibel ER (1993) Experimental hydrostatic pulmonary edema in rabbit lungs. Am Rev Respir Dis 147:989–996
5. Czermak BJ, Breckwoldt M, Ravage ZB, Huber-Lang M, Schmal H, Bless NM, Friedl HP, Ward PA (1999) Mechanisms of enhanced lung injury during sepsis. Am J Pathol 154:1057–1065
6. Dabelsteen E (1996) Cell surface carbohydrates as prognostic markers in human carcinomas. J Pathol 179:358–369
7. Damjanov I (1987) Lectin cytochemistry and histochemistry. Lab Invest 57:5–20
8. Danguy A, Decaestecker C, Genten F, Salmon I, Kiss R (1998) Applications of lectins and neoglycoconjugates in histology and pathology. Acta Anat (Basel) 161:206–218
9. Failard H, Schauer R (1972) Glycoproteins as lubricants, protective agents, carriers, structural proteins and as participants in other functions. In: Gottschalk A (ed) Glycoproteins. Their composition, structure, and function, part B, 2nd edn. Elsevier, Amsterdam, pp 1246–1267
10. Florey HW (1933) Observations on the functions of mucus and the early stages of bacterial invasion of the intestinal mucosa. J Pathol Bacteriol 37:283–289
11. Forstner JF (1978) Intestinal mucins in health and disease. Digestion 17:234–263
12. Goldstein IJ, Hayes CE (1978) The lectins: carbohydrate-binding proteins of plants and animals. Adv Carbohydr Chem Biochem 35:127–140
13. Hachiya T, Honda T, Kubo K, Sekiguchi M (1999) Expression patterns of type II pneumocyte apical surface glycoconjugates in lung adenocarcinoma cells. Virchows Arch 434:63–69
14. Hasleton PS, Roberts TE (1999) Adult respiratory distress syndrome – an update. Histopathology 34:285–294
15. Hudson LD, Steinberg KP (1999) Epidemiology of acute lung injury and ARDS. Chest 116 [Suppl 1]:74–82
16. Hutch JA (1970) The role of urethral mucus in the bladder defense mechanism. J Urol 103:165–167
17. Kaltner H, Stierstorfer B (1998) Animal lectins as cell adhesion molecules. Acta Anat (Basel) 161:162–179
18. Reuter G, Schauer R, Bumm P (1988) Sialic acids of human nasal mucin, possible targets of influenza C viruses. In: Schauer R, Yamakawa T (eds) Sialic acids. Proceedings of the Japanese German symposium on sialic acids. Berbel-Mendel, Kiel, pp 259–260
19. Reuter G, Struwe R, Feige J, Brede R, Bumm P, Schauer R (1992) Analysis of carbohydrate composition and sialidase activity in oral secretions of patients with tumors in the upper aerodigestive tract. Eur Arch Otorhinolaryngol 249:5–11
20. Schauer R (1992) Sialinsäurereiche Schleime als bioaktive Schmierstoffe. Nachr Chem Tech Lab 40:1227–1231
21. Sivridis E, Giatromanolaki A, Koukourakis M, Agnantis N (2000) Lectin-binding patterns in normal, hyperplastic and neoplastic endometrium: the prognostic value of concanavalin A. Virchows Arch 436:52–58
22. Tsokos M, Fehlauer F (2001) Postmortem markers of sepsis: a quantitative immunohistochemical study using VLA-4 (CD49d/CD29) and ICAM-1 (CD54) for the detection of sepsis-induced lung injury. Int J Legal Med 114:291–294
23. Tsokos M, Fehlauer F, Püschel K (2000) Immunohistochemical expression of E-selectin in sepsis-induced lung injury. Int J Legal Med 113:338–342
24. Tsokos M, Anders S, Paulsen F, Fehlauer F, Püschel K (2001) Comparative evaluation of pulmonary lactoferrin and lysozyme immunoreactivity for the post-mortem diagnosis of death due to sepsis. Virchows Arch 438:376–381
25. Walker WA (1976) Host defense mechanisms in the gastrointestinal tract. Pediatrics 57:901–916
26. Weiland JE, Davis WB, Holter JF, Mohammed JR, Dorinsky PM, Gadek JE (1986) Lung neutrophils in the adult respiratory distress syndrome. Clinical and pathophysiologic significance. Am Rev Respir Dis 133:218–225
27. West KP, Cope JL (1989) The binding of peroxidase-labelled lectins to human endometrium in normal cyclical endometrium and endometrial adenocarcinoma. J Clin Pathol 42:140–147
28. Zhou Q, Cummings RD (1992) Animal lectins: a distinct group of carbohydrate-binding proteins involved in cell adhesion, molecular recognition, and development. In: Fukuda M (ed) Cell surface carbohydrates and cell development. CRC Press, Boca Raton, pp 99–113
29. Zilberberg MD, Epstein SK (1998) Acute lung injury in the medical ICU: comorbid conditions, age, etiology, and hospital outcome. Am J Respir Crit Care Med 157:1159–1164

Virchows Arch (2002) 440:187–194
DOI 10.1007/s004280100493

ORIGINAL ARTICLE

**Thomas Knösel · Simone Petersen · Holger Schwabe
Karsten Schlüns · Ulrike Stein · Peter Michael Schlag
Manfred Dietel · Iver Petersen**

Incidence of chromosomal imbalances in advanced colorectal carcinomas and their metastases

Received: 12 February 2001 / Accepted: 28 May 2001 / Published online: 26 July 2001
© Springer-Verlag 2001

Abstract Comparative genomic hybridization (CGH) was used to screen 54 advanced colon carcinomas, i.e., 24 primary tumors and 30 metastases, for chromosomal alterations. Using a sensitive statistical method for the determination of DNA imbalances and histograms for analysis of the incidence of changes, we identified the DNA over-representation of chromosome 20q as the most common alteration being present in 100% of cases. High incidence deletions were observed on 18q21–18q23 (96%), 4q27–4q28 (96%), 4p14 (87%), 5q21 (81%), 1p21–1p22 (72%), 21q21 (74%), 6q16 (72%), 3p12 (66%), 8p24–8p21 (66%), 9p21 (64%), 11q22 (64%), and 14q13–14q21 (64%). Further frequent over-representation was found on 7q12–7q11.2 (75%), 16p11–16p12 (70%), 19p13 (70%), 9q34 (67%), 19q13 (67%), 13q34 (64%), 13q13 (64%), 17q21 (59%), 22q11 (61%), 8q24 (57%), and 1q21 (57%). Pronounced DNA gains and losses being defined as regions in which the ratio profiles exceeded the values of 1.5 and 0.5, respectively, frequently colocalized with peaks of incidence curve. The use of difference histograms for the comparison of tumor subgroups as well as case-by-case histogram for the analysis of 15 paired tumor samples identified several of the above alterations as relevant for tumor progression and metastasis formation. The study identified additional loci and delineates more precisely those that have been previously reported. For comparative purposes, we have made our primary data (ratio profiles, clinicopathological parameters, histograms) available at the interactive web site http://amba.charite.de/cgh, where the incidence of changes can be determined at individual loci and additional parameters can be applied for the analysis of our CGH results.

T. Knösel · S. Petersen (✉) · K. Schlüns · M. Dietel · I. Petersen
Institute of Pathology, University Hospital Charité,
Schumannstrasse 20-21, 10098 Berlin, Germany
e-mail: iver.petersen@charite.de
Tel.: +49-30-450536050, Fax: +49-30-450536110

H. Schwabe · U. Stein · P.M. Schlag
Department of Surgery and Oncology, RRC,
Charité Campus Buch, 13125 Berlin, Germany

Keywords Colorectal cancer · Metastasis · Comparative genomic hybridization

Introduction

Colorectal cancer is one of the most common forms of human malignancy, especially in industrialized countries, and its incidence is increasing [34]. The majority of colorectal cancers arise from a series of somatic genetic changes [17] that involve activation of ras oncogenes and inactivation of tumor suppressor genes like the APC gene at 5q21, p53 (17p13) as well as Smad2 and Smad4/DPC4 at 18q. In contrast to the large amount of data concerning molecular genetic changes in benign and malignant primary colorectal tumors, the knowledge about such changes associated with the progression of colorectal carcinomas, in particular the metastatic phenotype, is limited. The 5-year survival of Dukes stage D in colorectal cancer patients is less than 5% and has not changed in 50 years [9]. Because cancer therapies often aim at eliminating metastatic cells or preventing their dissemination, understanding the molecular mechanisms of the metastatic progression could help to improve therapy. The purpose of this study was to determine the extent of genetic aberrations in advanced colorectal cancer that might identify genetic events predisposing to metastatic dissemination.

CGH is a powerful molecular cytogenetic method to screen the entire genome for chromosomal imbalances being typical for the vast majority of neoplastic diseases [16]. In colorectal cancer, CGH data are available from several authors [1, 3, 10, 11, 19, 22, 25, 32, 43, 44]. However, only two studies have investigated the chromosomal lesions in advanced colorectal cancers and their corresponding metastases [1, 19].

The aim of this study was to determine the extent of genetic aberrations in advanced colorectal carcinomas and to assess genetic differences between primary and metastatic carcinomas that might serve as genetic markers for tumor dissemination.

Table 1 Tumor collective

Number of specimens	54
Number of patients	34
Primary tumors	24
Metastases	30
Liver	11
Brain	6
Lymph nodes	5
Lung	4
Abdominal wall	4
Stage	
pT2	11
pT3	24
pT4	9
pTx*	10
pN0	17
pN1	6
pN2	21
pNx*	10
pM0	4
pM1	50
Grade	
G1	3
G2	46
G3	5

*Status unknown in metastatic tumors

Materials and methods

Tumor samples

Tumor specimens were mainly obtained during surgical resections at the Department of Surgery of the Charité at Campus Buch. Additionally, tumor specimens of the brain were collected during neurosurgical operations at the Charité Hospital. The tumor collective and TNM categories are summarized in Table 1. The clinicopathological data of the collective and specific information on single cases together with the CGH profile are available at our CGH online tumor database at http://amba.charite.de/cgh. In total, 54 specimens consisting of 24 primary tumors and 30 metastases from 34 patients were investigated using CGH. The metastases were localized in the liver (n=11), brain (n=6), lymph nodes (n=5), lung (n=4), and the abdominal wall (n=4). In 15 cases, paired samples of a primary tumor and a corresponding metastasis were available. The tumor collective presented 50 cases of Dukes stage D, three were Dukes B and one case a Dukes C carcinoma. DNA was extracted from several 30-µm cryostat tissue sections by proteinase K and phenol-chloroform extraction which was verified to consist of a minimum of 70% tumor cells in each case.

CGH analysis

The protocols for CGH preparation have been described previously and are available on our web site at http://amba.charite.de/cgh/. Similarly, image acquisition and digital image analysis were performed as described. At least 15 metaphases/karyograms were analyzed per tumor sample with computation of CGH sum-karyograms and mean ratio profiles with confidence intervals [28, 36].

Determination of chromosomal imbalances

DNA gains and losses were determined using statistical methods, i.e., deviations of the mean FITC:TRITC profiles from the normal ratio of 1.0 were tested for significance using a Student's t-test [27]. In this test, we required at least a significance of 95% to score an alteration as a DNA gain or loss. After the statistical determination of the chromosomal imbalances of each tumor sample, a histogram of all cases was calculated (Fig. 1A). It represents the incidence of DNA gains and losses of this tumor collective along each chromosome, showing gains on the right side of the ideogram and losses on the left of the ideogram, e.g., the maximum value of 100% is reached if all samples of the group carry a change at a specific chromosomal region. The histogram and the ratio profiles of individual tumors are available at our web site at http://amba.charite.de/cgh/.

Pronounced DNA gains and losses were defined as those alterations for which the ratio profiles exceeded the values of 1.5 and 0.5, respectively [30]. They most likely represent high copy number amplifications or multi copy deletions. Numerical aberrations were determined using an algorithm of our custom-made CGH software using the alterations according to a 99% significance threshold.

Comparison of primary tumors and metastases

A difference histogram (Fig. 1B) was generated as described to compare the primary and metastatic carcinomas as tumor subgroups [27]. Only alterations with 99% significance were included into this analysis. The percentage of changes occurring only in the primaries is represented by the green color, whereas the excess of changes in the metastases is shown in red. The white areas beneath the colored part of the histogram represent the percentage of changes that are present in both subgroups. A large colored area thus indicates a pronounced difference between the tumor groups. The differences were tested for significance using a χ^2 test. Areas with 95% significance ($0.01<P<0.05$) are depicted in bright gray, and areas with 99% significance ($P<0.01$) are depicted in dark gray.

Fig. 1 A Summary of all genetic alterations of 54 advanced colorectal carcinomas in a histogram representation. The chromosomal imbalances are shown as incidence curves along each chromosome. Areas on the *left* side of the chromosome ideogram correspond to loss of genetic material; those on the *right* side correspond to DNA gains. The changes were determined using a statistical method: those with 99% significance in the Student t-test are shown in blue, the additional ones with only 95% significance are depicted in green. Pronounced DNA gains and losses being defined as regions where the ratio profile exceeded the fixed thresholds 1.5 and 0.5 are shown in red, most likely corresponding to high-copy amplification and multi-copy deletions, respectively. Heterochromatic areas (centromeric and paracentromeric regions of chromosomes 1, 9, 16, p arms of acrocentric chromosomes) must be excluded from the analysis. **B** Difference histogram of metastasizing primary tumors (n=24) versus metastatic tumors (n=30). The *green areas* represent the percentage of changes that are present only in the primary tumors whereas the *red* indicates the excess of changes of the metastases. The *white areas* beneath the colored part of the histogram represent the percentage of changes that are present in both tumor groups. There is a high concordance with only few significant changes for the metastastic tumor subgroup as indicated by the *gray horizontal lines* (*light gray* regions with 95%, *dark gray* those with 99% significance according to a χ^2 test), e.g., over-representation at 1q22-q23 and deletions at 21q. **C** Case-by-case histogram of 15 paired samples, i.e., primary tumor and corresponding metastasis. Four conditions are represented. *Blue* percentage of chromosomal imbalances that are common in both tumors. *Green* those chromosomal imbalances that are additionally seen in the primary tumor. *Red* those that were extra present in the metastases. *Yellow* proportion with no changes in either group. The *blue areas* dominate again, reflecting the high concordance between primary tumors and metastases. However, the metastases showed additional alterations at several regions, e.g., gains on 1q and losses at 2q, 5q21, 8p, 21q

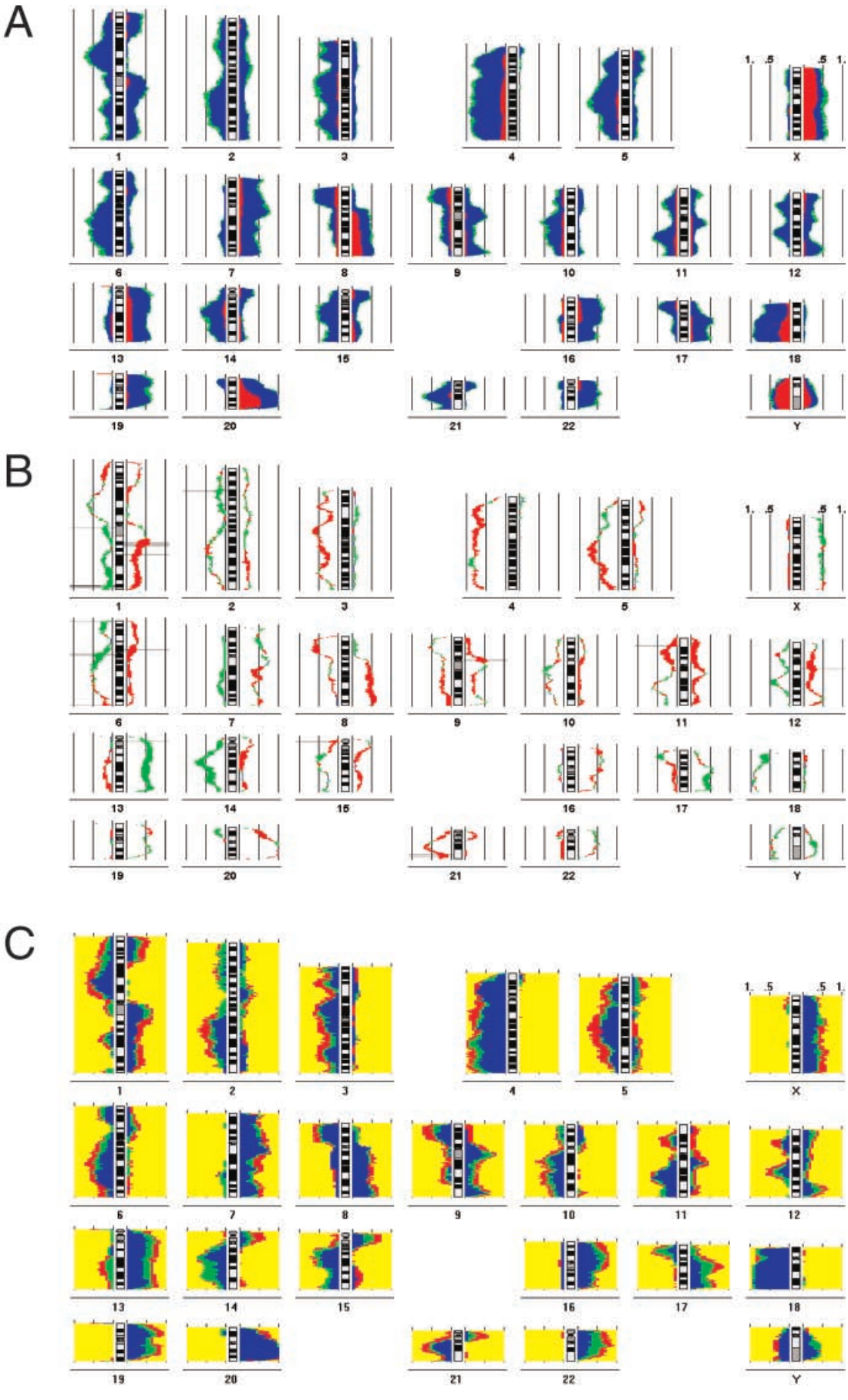
A
1. .5 .5 1.
1
2
3
4
5
X
6
7
8
9
10
11
12
13
14
15
16
17
18
19
20
21
22
Y
B
1. .5 .5 1.
1
2
3
4
5
X
6
7
8
9
10
11
12
13
14
15
16
17
18
19
20
21
22
Y
C
1. .5 .5 1.
1
2
3
4
5
X
6
7
8
9
10
11
12
13
14
15
16
17
18
19
20
21
22
Y

Table 2 Chromosomal imbalances in advanced colorectal carcinomas

	DNA under-representations	DNA over-representations
High incidence changes[a] (≥50%)	18q21–18q23, **4q27–4q28**, **4p14**, **5q21**, 1p21–1p22, **21q21**, **6q16**, **3p12**, **8p21–8p23, 9p21**, 11q22, 14q13–14q21, 3q26, **10q21,** 3p22, 15q15, **10q23,** 2q22–2q24	20q11.2–20q13.2, **7q11.2–7q12**, 16p11.2–16p12, 19p13, 9q34, 19q13.1–19q13.2, 13q34, 13q13, 17q21, 22q11, **8q24**, **1q21,** 7p**, 7q22, 7q36,** 17q24-q25
Pronounced changes[b]	18q12–18q22, 4q21–4q35, 8p22–8p23, 4p15, 9p23–9p24, 10q21, 11q22–11q23, 14q13–14q21	20q13.1–20q13.2, 8q24, 13q13–13q14, 16p11–16p13, 7p
Additional changes in metastases	2q, 3, 5q, 8p, 9p, 10q, 11p, 12p, 21q	1q, 17q12-q21, 17q24-q25, 19p, 19q

[a] The aberrations are listed in the order of the incidence, those probably involved in tumor progression and metastasis formation are indicated in bold type

[b] DNA gain with ratio >1.5; DNA loss with ratio <0.5; only those alterations that occurred at least twice were listed

In addition, we applied a newly developed case-by-case histogram in this study. It visualizes the comparison of paired samples, i.e., the primary tumor and its corresponding metastasis. Within the histogram, the changes are differentiated into four types, i.e., imbalances that are common in both tumors (blue color), those that are present additionally in the primary tumor (green), those that are present additionally in the metastasis (red), as well as no changes at all in both groups (Fig. 1C).

Results

Histogram of 54 advanced colorectal carcinomas

Using statistical analysis to evaluate the chromosomal imbalances, an average of 29.98 aberrations was found per tumor, with gains ranging from 3 to 30 lesions and losses from 8 to 26. The chromosomal imbalances of 54 advanced colorectal carcinomas are summarized in Fig. 1A by a histogram which represents the DNA gains and losses as an incidence curve along each chromosome. The histogram is also available at our CGH online tumor database at http://amba.charite.de/cgh/, where the incidences can be assessed interactively by opening the *Infoscreen* and pointing at specific chromosomal sites using the computer mouse.

In Table 2, the most prevalent changes were listed according to their frequency. The highest incidence of deletions was observed for chromosomes 18q21–18q23 (96%) and 4q27–4q28 (96%), followed by losses at 4p14 (87%), 5q21 (81%), 1p21–1p22 (72%), 21q21 (74%), 6q16 (72%), 3p12 (66%), 8p24–8p21 (66%), 9p21 (64%), 11q22 (64%), and 14q13–14q21 (64%). The most prevalent DNA over-representations were seen on chromosomes 20q11.2–20q13.2 (100%), 7q12–7q11.2 (75%), 6p11–16p12 (70%), 19p13 (70%), 9q34 (67%), 19q13 (67%), 13q34 (64%), 13q13 (64%), 17q21 (59%), 22q11 (61%), 8q24 (57%), and 1q21 (57%). Pronounced DNA copy number changed generally co-localized with peaks of incidence curve, i.e., deletions at 18q12–18q22, 4q21–4q35, 8p22–8p23, 4p15, 9p23–9p24, 10q21, 11q22–11q23, 14q13–14q21, and 21q21, as well as over-representations at 20q13.1–20q13.2, 8q24, 13q13–13q14, 16p11–16p13, and 7p.

Comparison of primary and metastatic carcinomas

The difference histogram of 34 patients comparing the samples of the primaries with the samples of the metastases for statistically significant differences is shown in Fig. 1B. The statistical comparison indicated significant alterations at several regions, e.g., over-representation at 1q22–23 and deletions at 21q.

To visualize those changes that differ most frequently between the primary tumors and their corresponding metastases, we developed a new histogram representation for the comparison of tumor pairs (Fig. 1C). The histogram shows four possible situations. First, both tumors carry the same imbalance at a specific site being visualized by the blue color (status [1,1]). Second, an imbalance is present in the metastasis but not in the primary tumor (status [0,1], red) or vice versa (status [1,0], green). Finally, both tumors have no change at a specific site (status [0,0], yellow) complementing all possibilities to 100%.

In the case-by-case histogram of all 15 tumor pairs, the dominating blue areas reflect the clonal nature of all investigated tumors. The additional changes in the metastatic lesions have a high incidence of gains at 1q, 17q12, 17q24–17q25, 19 and deletions at 2q, 3p, 5q21, 8p, 9p, 10q, 11p, 12p, and 21q.

Discussion

Colorectal cancer is one of the best studied malignant neoplasms at the molecular level. In particular, two different types of genetic instabilities have been established. Microsatellite repeat instability (MIN) is associated with hereditary non-polyposis cancer, but is also present in a subset of sporadic, non-hereditary carcinomas. While MIN may account for up to 15% of cases, the vast majority of colorectal cancers is characterized by chromosomal instability (CIN). Interestingly, colorectal cancer with high-level MIN carry a better prognosis and develop metastases less frequently than microsatellite-stable ones. In addition, there is ample evidence that MIN-positive tumors carry much fewer chromosomal

Table 3 Summary of previously reported comparative genomic hybridization results in colorectal carcinomas

Reference	Number of specimens	DNA gains*	DNA losses*
[32]	16	20q, 13q, 8q, 7p, 1q, 5p	4, 8p, 18q,17p
[43]	5	13q, 20	18q, 5q, 8p
[25]	9	11p, 12q, 16p, 20p, 20q	18q, 22q
[22]	14	13q, 20q, 8q, 7p	18q, 4q, 8p
[1]	26	7p, 8q, 13q, 20q	4, 18, 8p, 22q
[19]	33	20q (85%), 13q (48%), 7p (44%), 8q (44%)	18q (89%), 8p (59%), 1p(56%), 18p (48%)
[44]	14	8q (38%), 20q (38%),	18q (69%), 5q (54%)
[10]	45	20q (67%), 18q (49%), 5p, 6p, 7, 8q, 13q, 17q,19	1p, 3p, 4, 5q, 6q, 8p, 9p, 10, 15q, 17p
[11]	22	20q, 13q, 8q	18q, 8p, 1p
[3]	74	8q (63%), 20q (67%), 13q (44%)	18q (78%), 8p (53%), 17p (57%), 5q (56%)

*The chromosomal imbalances are listed according to their order of frequency

alterations than MIN-negative ones, although neither type of instability seems to be mutually exclusive as initially suggested [11, 20, 38, 42].

In the present study, we used CGH to define the frequency of chromosomal imbalances in a collective of advanced colorectal carcinomas and to search for genetic alterations that are associated with tumor progression and the metastatic phenotype. Although we did not investigate our tumor collective for microsatellite instability, the fact that we observed chromosomal alterations in each tumor suggests that it is present only in a minority of cases and supports the hypothesis that the accumulation of the relevant genetic mutations for tumor progression and metastasis formation is associated with a CIN genotype.

Representation and interpretation of CGH results by histograms

Different types of histograms were generated to determine the frequency of DNA gains and losses. There are several advantages of the histogram approach for the interpretation of CGH results. Most importantly, the chromosomal imbalances are determined by the computer and not manually. We scored the chromosomal imbalances by a statistical test to determine whether the deviation of the ratio profile from the normal value of 1.0 was significant. This is a rather sensitive method which is reflected by the large number of alterations per case and the higher frequency of changes relative to previous studies (Table 3). There is no consensus yet on the best way to score DNA imbalances using CGH. However, our approach offers the possibility to detect deletions with a similar sensitivity as over-representations. Furthermore, statistics have been reported to be the method of choice for the interpretation of CGH results [18, 24]. The application of histograms is independent of the criteria used to determine the imbalances and may similarly be applied to changes scored by fixed-ratio thresholds. To increase the visibility and comparability of our results, we have made our data available at our interactive web site, where the same tumors can be analyzed using all the different evaluation schemes that are popular in CGH analysis. The incidence of changes at specific chromosomal bands can be assessed interactively, thus offering a much better resolution than conventional approaches in which the resolution is usually restricted to chromosomal arms.

Histograms also represent an elegant way to compare tumor collectives. In addition to our previously described difference histogram approach [27], we also used in this study our recently developed case-by-case histogram, which is particularly suited for the analysis of paired tumor samples.

DNA imbalances in advanced colorectal carcinomas – over-representations

Our CGH results show that recurrent chromosomal aberrations in colorectal tumors are manifested as over-representations on several chromosome arms, with the bands showing the highest incidence being listed in Table 2. The data identified additional loci and delineate more precisely those that have been described previously (Table 3).

The highest incidence of gains were found on chromosome 20q, similar to studies by Ried et al. [33] and Korn et al. [19]. In the latter report, also advanced carcinomas, i.e., primary tumors and corresponding liver metastases, were studied. This points to the possibility that the 20q gain is associated with tumor progression. However, it has already been found in the (metastasizing) primary tumors, as shown by the case-by-case histogram suggesting that it represents at least an early change during tumor cell dissemination. Genes that map to 20q include the cellular apoptosis susceptibility (CAS) gene [7], BTAK, a putative severine/threonine kinase gene [39], and AIB1, a steroid receptor coactivator gene [2], which was associated with tumor progression in breast and ovarian carcinomas. Recently, a novel zinc-finger protein-encoding gene mapping to 20q13.2 was found to be amplified in breast cancer [8]. Thus, the amplification at 20q13 is observed in a variety of tumor types and was preferentially associated with an aggressive phenotype.

The DNA gains on 7q had a peak incidence of 75% at the chromosomal band 11q as indicated by the histogram

(Fig. 1A). Since it was also one of the most common changes in our recent study on brain metastases [30], we are convinced that this chromosomal band harbors a gene of importance for metastasis formation.

The gains on chromosome 16p, 19p13 and 19q13 were found frequently in 70% and 67%, respectively. The imbalances at 16p and 19q have been described in previous studies [10, 25]. To our knowledge, no candidate genes have been identified so far.

The gain at 9q34 has not been previously reported in colon carcinomas. However, we have already identified this change in advanced squamous cell carcinomas of the lung [29] and the ABL gene is one candidate gene for this region.

The over-representation on chromosome 13q is a sporadic finding in adenomas, but is much more common in carcinomas. Similar to Ried et al. [32], we also found high-copy number increases being represented by the high proportion of pronounced gains in the histogram of Fig. 1A. Although the entire chromosome is usually affected, the histogram indicated the highest incidence at the telomeric band 13q34, suggesting that it is the most important candidate region. This is in concordance with the fact that small size amplifications of this band were observed in lung carcinomas [27, 30].

Chromosome 17q harbors two subregions with high incidence gains, i.e., 17q12-q21 and 17q24–17q25. The band 17q21 carries the c-erbB2 proto-oncogene (also called HER-2/NEU) which is involved in tumor progression. Its role in colon cancer is controversial [21]. However, we suppose that the amplification of the telomeric regions is at least similarly important for an aggressive phenotype since it was one of the most prevalent gains in our recent study on brain metastases [30]. One putative candidate gene for 17q24-q25 is the Ras-related RAC3 gene, since it belongs to the Rho gene family which has already been implicated in metastasis formation [23].

Although the 1q gain is not a high-incidence change, the difference histogram (Fig. 1B) and the case-by-case histogram (Fig. 1C) clearly indicated that it occurred additionally in the metastases, strengthening the observation in other cancer types that this change is relevant for progression. The gain of 1q21-q25 has been previously reported in metastatic squamous cell carcinomas of the lung [29], in renal clear cell carcinoma [13], and in our brain metastases study indicating the highest incidence for the region 1q21-q23 [30]. Also our difference histogram (Fig. 1B) in this study showed statistically significant gains at 1q22–23.

DNA imbalances in advanced colorectal carcinomas – deletions

Deletions were common on chromosome arms 18q, 4q, 4p, 5q, 1p, 21q, 6q, and 3p. The highest incidence of loss was 96% on chromosome 18q. These findings are in concordance with previous CGH studies (Table 3). At least three candidate tumor suppressor genes have been assigned to this region, DCC, Smad2, and Smad4/DPC 4 [35, 41]. Pronounced DNA deletions were seen most often at 18q22. The DCC gene is one candidate gene in this region. The status of chromosome 18q LOH and loss of DCC protein staining can be used to stratify patients [15, 40]. Loss of activity of one or more genes on 18q does appear to be an important step in tumor development.

We observed deletions of 96% on chromosome 4q and of 87% on 4p. Previous data have already demonstrated a high frequency of these aberrations in colorectal carcinomas. However, only a few authors associate these changes with the metastatic phenotype [1, 19]. Frequent losses involved 18q, 8p, 4q, and 1p in liver metastases [19]. Deletions of chromosome band 4p16 have been observed more frequently in metastases of colorectal carcinomas than in primary tumors [26].

The difference histogram (Fig. 1B) between the primary tumor and the metastases showed additional deletions in metastatic tumors at chromosome 5q. At 5q21 the APC gene is localized, which is linked to adenoma formation constituting a rather early phase in tumor formation. Interestingly, the catenin gene belonging to the signaling pathway of APC was recently associated with progression [6]. Whether or not APC plays a dual role in colon carcinogenesis has still to be investigated. The CGH data at least suggests that 5q21 carries genes that might be involved in metastasis formation.

Deletions on chromosome 1p21–31 seemed to be associated with tumor progression and metastases in a variety of neoplasms [19, 29, 31], supporting the hypothesis that many features of tumor cell dissemination are not specific for one entity but shared between multiple tumor types.

Regarding chromosome 21q, deletions on 21q21 seemed to be correlated with tumor progression in head and neck carcinomas, pancreas, stomach, esophagus, lung, and breast carcinomas [4, 12, 29, 31, 37]. The observed loss indicates that there may be at least one tumor suppressor gene on the long arm of chromosome 21 [14].

Since the long arm of chromosome 6 was also frequently affected in our recent studies on brain metastases and metastases of squamous cell carcinomas of the lung [29, 30], we think that this arm harbors genes that are important in metastases formation. Chromosome arm 3p is also associated with the metastatic phenotype since deletions at 3p12-p14 and 3p22-p25 appeared significantly more frequently in metastatic tumors [30]. Additionally, we found in this study frequent deletions on 3q25 (61%), which has not been described before.

Loss at chromosome 8p has been reported as an independent factor for bad prognosis in head and neck squamous cell carcinoma [5]. Frequent losses on chromosome 9p, 10q, 11p have been also observed in our brain metastases study. To our knowledge the frequent loss at chromosome 12p has not been described before in metastases formation. Interestingly, it shows a relatively narrow peak in the case-by-case diagram.

In summary, our results indicate that distinct chromosomal imbalances are associated with progression and metastasis formation of colorectal carcinomas. It also indicates certain alterations that already occur in the metastasizing primary tumors and may thus play a role in the early phase of tumor cell dissemination (metastasis initializer lesions), whereas others are additionally acquired in the metastases and may therefore be important for the peculiarities of the metastatic phenotype-like organ-specific metastasis formation (metastasis modulator lesions). There is also an overlapping spectrum of alterations with other advanced tumor types. The identification of responsible genes and their role in tumor metastasis formation will be a fascinating task in the forthcoming years, hopefully supplying new markers and targets for the characterization and treatment of the patients.

References

1. Al-Mulla F, Keith WN, Pickford IR, Going JJ, Birnie GD (1999) Comparative genomic hybridization analysis of primary colorectal carcinomas and their synchronous metastases. Genes Chromosomes Cancer 24:306–314
2. Anzick SL, Kononen J, Walker RL, Azorsa DO, Tanner MM, Guan XY, Sauter G, Kallioniemi OP, Trent JM, Meltzer PS (1997) AIB1, a steroid receptor coactivator amplified in breast and ovarian cancer. Science 277:965–968
3. Aust DE, Willenbucher RF, Terdiaman JP, Ferrell LD, Chang CG, Moore DH 2nd, Molinaro-Clark A, Baretton GB, Loehrs U, Waldman FM (2000) Chromosomal alterations in ulcerative colitis-related and sporadic colorectal cancer by comparative genomic hybridization. Hum Pathol 31:109–114
4. Bockmühl U, Wolf G, Schmidt S, Schwendel A, Jahnke V, Dietel M, Petersen I (1998) Genomic alterations associated with malignancy in head and neck cancer. Head Neck 20: 145–151
5. Bockmühl U, Schlüns K, Küchler I, Petersen S, Petersen I (2000) Genetic imbalances with impact on survival in head and neck cancer patients. Am J Pathol 157:369–375
6. Brabletz T, Herrmann K, Jung A, Faller G, Kirchner T (2000) Expression of nuclear beta-catenin and c-myc is correlated with tumor size but not with proliferative activity of colorectal adenomas. Am J Pathol 156:865–870
7. Brinkmann U, Gallo M, Polymeropoulos MH, Pastan I (1996) The human CAS (cellular apoptosis susceptibility) gene mapping on chromosome 20q13 is amplified in BT474 brest cancer cells and part of aberrant chromosomes in breast and colon cancer cell lines. Genome Res 6:187–194
8. Collins C, Rommens JM, Kowbel D, Godfrey T, Tanner M, Hwang SI, Polikoff D, Nonet G, Cochran J, Myambo K, Jay KE, Fruola J, Cloutier T, Kuo WL, Yaswen P, Dairkee S, Giovanola J, Hutchinson GB, Isola J, Kallionemi OP, Palazzolo M, Martin C, Ericsson C, Pinkel D, Albertson D, Li WB, Gray JW (1998) Positional cloning of ZNF217 and NABC1 genes amplified at 20q13.2 and overexpressed in breast carcinoma. Proc Natl Acad Sci U S A 95:8703–8708
9. Dale DC, Federman DD (1996) Scientific American medicine. In: Mayer RJ (ed) Gastrointestinal cancer. Scientific American, Inc., New York, p 14
10. De Angelis PM, Clausen OP Schjolberg A, Stokke T (1999) Chromosomal gains and losses in primary colorectal carcinomas detected by CGH and their associations with tumor DNA ploidy, genotypes and phenotypes. Br J Cancer 80:526–535
11. Georgiades IB, Curtis LJ, Morris RM, Bird CC, Wyllie AH (1999) Heterogeneity studies identify a subset of sporadic colorectal cancers without evidence for chromosomal or microsatellite instability. Oncogene 18:7933–7940
12. Ghadimi M, Schröck E, Walker RL, Wangsa D, Jauho A, Meltzer PS, Ried T (1999) Specific chromosomal aberrations and amplifications of the AIB1 nuclear receptor coactivator gene in pancreatic carcinomas. Am J Pathol 154:525–536
13. Gronwald J, Storkel S, Holtgreve-Grez H, Hadaczek P, Brinkschmidt C, Jauch A, Lubinski J, Cremer T (1997) Comparison of DNA gains and losses in primary renal clear cell carcinomas and metastatic sites: importance of 1q and 3p copy number changes in metastatic events. Cancer Res 57:481–487
14. Hattori M, Fujiyama A, Taylor TD, Watanabe H, Yada T, Park HS, Toyoda A, Ishii K, Totoki Y, Choi DK, Soeda E, Ohki M, Takagi T, Sakaki Y, Taudien S, Blechschmidt K, Polley A, Menzel U, Delabar J, Kumpf K, Lehmann R, Patterson D, Reichwald K, Rump A, Schillhabel M, Schudy A (2000) The DNA sequence of human chromosome. The chromosome 21 mapping and sequencing consortium. Nature 405:311–319
15. Jen J, Kim H, Piantadosi S, Liu Z-F, Levitt RC, Sistonen P, Kinzler KW, Vogelstein B, Hamilton SR (1994) Allelic loss of chromosome 18q and prognosis in colorectal cancer. N Engl J Med 331:213–221
16. Kallionemi A, Kallioniemi OP, Sudar D, Rutovitz D, Gray JW, Waldman F, Pinkel D (1992) Comparative genomic hybridization for molecular cytogenetic analysis of solid tumors. Science 258:818–821
17. Kinzler KW, Vogelstein B (1998) Colorectal tumors. In: Vogelstein B, Kinzler KW (eds) The genetic basis of human cancer, 1st edn. Mc Graw-Hill, New York, pp 565–587
18. Kirchhoff M, Gerdes T, Rose H, Maahr J, Ottesen AM, Lundsteen C (1998) Detection of chromosomal gains and losses in comparative genomic hybridization analysis based on standard reference intervals. Cytometry 31:163–173
19. Korn WM, YasutakeT, Kuo W, Warren RS, Collins C, Tomita M, Gray J, Waldman FM (1999) Chromosomal Arm 20q Gains and other genomic alterations in colorectal cancer metastatic to liver, as analyzed by comparative genomic hybridization and fluorescence in situ hybridization. Genes Chromosomes Cancer 25:82–90
20. Lengauer C, Kinzler KW, Vogelstein B (1998) Genetic instabilities in human cancers. Nature 396:643–649
21. McLeod HL, Murray GI (1999) Tumor markers of prognosis in colorectal cancer. Review. Br J Cancer 79:191–203
22. Meijer GA, Hermsen MA, Baak JP, van Diest PJ, Meuwissen SG, Belien JA, Hoovers JM, Joenje H, Snijders PJ, Walboomers JM (1998) Progression from colorectal adenoma to carcinoma is associated with non-random chromosomal gains as detected by comparative genomic hybridisation. J Clin Pathol 51:901–909
23. Michiels F, Collard JG (1999) Rho-like GTPases: their role in cell adhesion and invasion. Biochem Soc Symp 65:125–146
24. Moore DH 2nd, Pallavicini M, Cher ML, Gray JW (1997) A t-statistic for objective interpretation of comparative genomic hybridization (CGH) profiles. Cytometry 28:183–190
25. Nakao K, Shibusawa M, Tsunoda A, Yoshizawa H, Murakami M, Kusano M, Uesugi N, Sasaki K (1998) Genetic changes in primary colorectal cancer by comparative genomic hybridization. Surg Today 28:567–569
26. Paredes-Zaglul A, Kang JJ, Essig YP, Mao W, Irby R, Wloch M, Yeatman TJ (1998) Analysis of colorectal cancer by comparative genomic hybridization: evidence for induction of the metastatic phenotype by loss of tumor suppressor genes. Clin Cancer Res 4:879–886
27. Petersen I, Bujard M, Petersen S, Wolf G, Goeze A, Schwendel A, Langreck H, Gellert K, Reichel M, Just K, du Manoir S, Cremer T, Dietel M, Ried T (1997) Patterns of chromosomal imbalances in adenocarcinoma and squamous cell carcinoma of the lung. Cancer Res 57:2331–2335
28. Petersen I, Langreck H, Wolf G, Schwendel A, Psille R, Vogt P, Reichel MB, Ried T, Dietel M (1997) Small cell lung cancer is characterized by a high incidence of deletions on chromosomes 3p, 4q, 5q, 10q, 13q and 17p. Br J Cancer 75:79–86
29. Petersen S, Aninat-Meyer M, Schlüns K, Gellert K, Dietel M, Petersen I (2000) Chromosomal alterations in the clonal evolution to the metastatic stage of squamous cell carcinomas of the lung. Br J Cancer 82:65–73

30. Petersen I, Hidalgo A, Petersen S, Schluns K, Schewe C, Pacyna-Gengelbach M, Goeze A, Krebber B, Knosel T, Kaufmann O, Szymas J, von Deimling A (2000) Chromosomal imbalances in brain metastases of solid tumors. Brain Pathol 10:395–401
31. Richard F, Pacyna-Gengelbach M, Schluns K, Fleige B, Winzer KJ, Szymas J, Dietel M, Petersen I, Schwendel A (2000) Patterns of chromosomal imbalances in invasive breast cancer. Int J Cancer 89:305–310
32. Ried T, Knutsen R, Steinbeck R, Blegen H, Schröck E, Heselmeyer K, du Manuoir S, Auer G (1996) Comparative genomic hybridization reveals a specific pattern of chromosomal gains and losses during the genesis of colorectal tumors. Genes Chromosomes Cancer 15:234–245
33. Ried T, Heselmeyer-Haddad K, Blegen H, Schrock E, Auer G (1999) Genomic changes defining the genesis, progression, and malignancy potential in solid human tumors: a phenotype/genotype correlation. Genes Chromosomes Cancer 25: 195–204
34. Ries LAG, Kosary CL, Hankey BF, Miller BA, Edwards BK (1999) SEER Cancer Statistics Review, 1973–1996 Bethesda, MD: National Cancer Institute
35. Riggens GJ, Thiagalingam S, Rosenblum E, Weinstein CL, Kern SE, Hamilton SR, Wilson JK, Markowitz SD, Kinzler KW, Vogelstein B (1996) Mad related genes in human. Nat Genet 13:347–349
36. Roth K, Wolf G, Dietel M, Petersen I (1997) Image analysis for comparative genomic hybridization based on a karyotyping program for Windows. Anal Quant Cytol Histol 19:461–474
37. Sakata K, Tamura G, Nishizuka S, Maesawa C, Suzuki Y, Iwaya T, Terashima M, Saito K, Satodate R (1997) Commonly deleted regions on the long arm of chromosome 21 in differentiated adenocarcinoma of the stomach. Genes Chromosomes Cancer 18:318–321
38. Schlegel J, Stumm G, Scherthan H, Bocker T, Zirngibl H, Rüschoff J, Hofstaedter F (1995) Comparative genomic in situ hybridization of colon carcinomas with replication error. Cancer Res 55:6002–6005
39. Sen S, Zhou H, White RA (1997) A putative serine/threonine kinase encoding gene BTAK on chromosome 20q13 is amplified and overexpressed in human breast cancer cell lines. Oncogene 14:2195–2200
40. Shibata D, Reale MA, Lavin P, Silverman M, Fearon ER, Steele G, Jessup JM, Loda M, Summerhayes IC (1996) The DCC protein and prognosis in colorectal cancer. N Engl J Med 335:1727–1732
41. Thiagalingam S, Lengauer C, Leach FS, Schutte M, Hahn SA, Overhauser J, Willson JK, Markowitz S, Hamilton SR, Kern SE, Kinzler KW, Vogelstein B (1996) Evaluation of candidate tumour supressor genes on chromosome 18 in colorectal cancers. Nat Genet 13:343–346
42. Watanabe T, Wu TT, Catalano PJ, Ueki T, Satriano R, Haller DG, Benson AB 3rd, Hamilton SR (2001) Molecular predictors of survival after adjuvant chemotherapy for colon cancer. N Engl J Med 344:1196–1206
43. Willenbucher RF, Zelman SJ, Ferrell LD, Moore DH 2nd, Waldman FM (1997) Chromosomal alterations in ulcerative colitis-related neoplastic progression. Gastroenterology 113: 791–801
44. Willenbucher RF, Aust DE, Chang CG, Zelman SJ, Ferrell LD, Moore DH, Waldman FM (1999) Genomic instability is an early event during the progression pathway of ulcerative-colitis-related neoplasia. Am J Pathol 154: 1825–1830

Virchows Arch (2002) 440:195–204
DOI 10.1007/s004280100484

ORIGINAL ARTICLE

**Masako Nakanishi · Jyoji Yamate · Shunji Nakatsuji
Mika Ide · Osamu Sawamoto · Mitsuru Kuwamura
Takao Kotani · Sadashige Sakuma**

Establishment of a transplantable tumor line (IP) derived from rat pulmonary carcinoma, developing humoral hypercalcemia of malignancy in IP-bearing rats

Received: 25 September 2000 / Accepted: 10 May 2001 / Published online: 17 July 2001
© Springer-Verlag 2001

Abstract A transplantable tumor line (IP) was established in syngeneic rats from a spontaneous pulmonary carcinoma found in a male F344 rat aged 25 months. A tissue fragment of IP grew into a nodule, 2–3 cm in diameter, 2–3 weeks after implant, and IP has been serially passed through 26 generations. Lined by cuboidal or columnar epithelial cells, the primary tumor consisted of completely alveolar architecture. However, IP tumors developed various growth patterns such as glandular, acinar, trabecular, cord, and solid, and consisting of epithelial cells showing cellular atypia. Ultrastructurally, neoplastic cells had microvilli, basement membranes, and desmosomes, and occasional cells possessed dense cytoplasmic granules. Interestingly, it was shown by the immunohistochemistry, the RT-PCR method, and immunoradiometric assay that IP tumor cells produce parathyroid hormone-related protein (PTHrP). During a 3-week observation period after implant, IP-bearing rats showed severe emaciation, hypercalcemia, and hypophosphatemia, as well as an increase in osteoclastic areas and a decrease in shaft thickness of the femurs. These were considered to be due to a marked elevation of plasma PTHrP levels. Furthermore, IP-bearing rats developed calcification in various organs including the kidneys, lungs, and heart. These findings in IP-bearing rats were similar to those of humoral hypercalcemia of malignancy (HHM) reported in human cancer patients. PTHrP plays a central role in the development of HHM, but the mechanisms of HHM remain poorly understood. IP may become a useful model for studying the pathogenesis of HHM and the pathophysiological role of PTHrP.

Keywords Animal model · Humoral hypercalcemia of malignancy · Parathyroid hormone-related protein · Transplantable rat pulmonary carcinoma

M. Nakanishi · J. Yamate (✉) · M. Ide · M. Kuwamura · T. Kotani
S. Sakuma
Department of Veterinary Pathology,
Graduate School of Agriculture and Biological Sciences,
Osaka Prefecture University, Gakuencho 1–1, Sakai,
Osaka, 599–8531, Japan
e-mail: yamate@vet.osakafu-u.ac.jp
Fax: +81-722-507208

O. Sawamoto
Naruto Research Institute, Otsuka Pharmaceutical Factory,
Inc., Naruto, Tokushima, 772–8601, Japan

S. Nakatsuji
Department of Pathology, Toxicology Research Laboratories,
Fujisawa Pharmaceutical Co., LTD., Kashima 2-chome,
Yodogawa-ku, Osaka, 532–8514, Japan

Introduction

Humoral hypercalcemia of malignancy (HHM) is a well-known paraneoplastic syndrome in human cancer patients. Because the patients undergoing HHM develop systemic calcification leading to dysfunction of the affected organs, the severity of HHM has been regarded as a crucial determinant for prognosis [42]. Human tumors that have been reported hitherto as developing HHM include squamous cell carcinoma, pulmonary adenocarcinoma, renal cell carcinoma, ovarian carcinoma, and breast carcinoma [11, 16, 30, 36, 42]. In veterinary medicine, lymphomas and apocrine gland-derived adenocarcinoma of the anal sac in dogs have been reported to give rise to HHM [32, 41].

Parathyroid hormone-related protein (PTHrP) has been considered to be a major causative factor for the pathogenesis of HHM [5, 25, 35]. Since PTHrP and parathyroid hormone (PTH) share receptors (PTH/PTHrP receptors) in the bone and kidneys, PTHrP is known to have biological functions similar to those of PTH. In human cancer patients it has been speculated that PTHrP produced excessively by neoplastic cells stimulates osteoclastic bone resorption and renal absorption of calcium, resulting in HHM [27, 42]. However, the mechanism of the excessive release of PTHrP by neoplastic cells and the subsequent pathogenesis of the systemic development of HHM have yet to be investigated [22, 26, 30, 40].

We have attempted to establish various transplantable tumor lines from spontaneous tumors found in F344 rats to study biological behavior, morphogenesis, and paraneoplastic manifestations in relation to neoplasia [39, 43, 46, 47]. We have succeeded in our attempt to establish a transplantable tumor line (IP) from a spontaneous pulmonary carcinoma found in an aged F344 rat. It was found to our great interest that IP-bearing rats develop HHM. As experimental rat models of HHM, Rice H-500 (Leydig cell tumor) [12] and Walker carcinosarcoma 256 [19, 29, 33] have been reported so far. To our knowledge, however, there have been no reports on pulmonary carcinoma-derived, HHM-inducible rat tumor lines.

In the present study, biological behavior and morphological characteristics of the primary and IP tumors were examined, and in addition HHM, which developed systemically in IP-bearing rats, was analyzed pathobiologically.

Materials and methods

A primary tumor was found in the caudal lobe of the left lung of a male F344/DuCrj rat aged 25 months. A tissue fragment 2 mm in diameter from the primary tumor was transplanted subcutaneously into the interscapular region of two syngeneic male rats through a trochar under ether anesthesia. Three weeks after the implantation, a subcutaneous tumor developed into a nodule 3 cm in diameter. A portion of the tumor was used for implant in the second generation, and serial transplantations were then made at 2- to 3-week intervals for each generation through the 26th by the implantation manner described above. One to three male F344 rats (6–20 weeks old) were used for the implant in each generation. The transplantable tumor line was designated IP.

Together with the primary tumor, the removed IP tumors and major organs (liver, kidneys, spleen, lungs, and heart) in implanted rats of each generation were examined histologically. The histopathological examinations revealed that calcification had developed in the kidneys, lungs, and heart, suggesting abnormal calcium metabolism indicative of HHM in implanted rats. Therefore, systemic effects of IP transplants were examined in the following experiments (Exs I and II).

Ex I was performed by using 16 male rats at the age of 6 weeks; out of them, 12 rats received a subcutaneous implantation of a tissue fragment of IP at passage 5, and four rats each were examined 1, 2 and 3 weeks after the transplant; the remaining four rats served as sham-operated controls, and were examined 2 weeks after the treatment. Out of 11 20-week-old male rats used in Ex II, eight rats were transplanted subcutaneously with a tissue fragment of IP at passage 15, and four each were examined 2 and 3 weeks after the implant; as sham-operated controls, the remainder were examined 3 weeks after the treatment.

All F344 male rats used in serial transplantations as well as in Exs I and II were purchased from Charles River Japan (Hino, Shiga, Japan) and housed in an animal room controlled at 22±3°C and with a 12-h light/dark cycle. They were given a standard commercial laboratory diet (MF; Oriental Yeast Co. Ltd., Tokyo, Japan) and tap water ad libitum.

In Exs I and II, blood samples were obtained from the abdominal aorta of all rats under anesthesia. Separated serum was assayed for the following substances with an Autoanalyzer 7170 (Hitachi, Tokyo, Japan): calcium, inorganic phosphorus, blood urea nitrogen (BUN), creatinine, aspartate aminotransferase (AST), and alkaline phosphatase (ALP). Plasma separated from blood treated with ethylenediaminetetraacetic acid (EDTA)-2Na was used to determine PTHrP levels. PTHrP levels were measured by immunoradiometric assay (IRMA; Mitsubishi Chemical, Tokyo, Japan) [10, 15]. All rats used were necropsied. The removed tumors were weighed, and tumors and organs (liver, spleen, kidneys, lungs, heart, brain, adrenal glands, skin, salivary glands, harderian glands, thyroids, parathyroids, trachea, tongue, stomach, intestines, pancreas, urinary bladder, aorta, testes, prostate glands, lymph nodes, thymus, skeletal muscle, spinal cord, and eyes) were fixed in 10% neutral buffered formalin. They were embedded in paraffin, sectioned, and stained with hematoxylin-eosin (HE) stain and by the von Kossa method. To detect osteoclasts, both femurs were fixed in 0.1 mol/l cacodylate buffer containing 4% paraformaldehyde and 0.1% glutaraldehyde at 4°C for 1 week. They were then decalcified in EDTA-glycerol solution at 4°C for 3 weeks and embedded in paraffin. Longitudinal sections of the femurs were made and stained with HE and by the tartrate-resistant acid phosphatase (TRAP) method, which is a marker enzyme of osteoclast function [37]. In order to observe the activity of osteoclasts, computer-aided morphometrical analysis was made on the femurs using an Image Analyzer (Mac Scope, Mitani Inc., Tokyo, Japan) with regard to shaft thickness and osteoclastic areas positively reacting to TRAP [45].

Deparaffinized tumor sections were stained immunohistochemically by the Avidin-Biotin Complex method (ABC kit; Dako Corp., Carpinteria, CA, USA). After treatment with microwave for 5 min, the sections were treated with 3% hydrogen peroxide in phosphate-buffered saline (PBS) for 10 min at a room temperature to quench endogenous peroxidase activity. The sections were blocked with 10% goat serum in PBS for 30 min at room temperature and then incubated overnight at 4°C with mouse monoclonal antibodies to cytokeratin (Dako; prediluted) and vimentin (Dako; 1:200 in dilution), and with a rabbit polyclonal antibody to PTHrP (Yanaihara Institute Inc., Shizuoka, Japan; 1:1000). Subsequently, goat anti-mouse or anti-rabbit biotinylated secondary antibody was applied for 1 h at room temperature, followed by streptavidin-peroxidase complex for 40 min at room temperature. After rinsing in PBS, 3,3′-diaminobenzidine tetrahydrochloride (DAB) was used as a substrate for visualization and the sections were counterstained lightly with hematoxylin. Nonimmunized mouse or rabbit sera, used instead of primary antibodies, served as negative controls.

For electron microscopy, small blocks from IP tumors at passages 4, 5, and 6 were fixed in 2.5% buffered glutaraldehyde and postfixed in 1% buffered osmium tetroxide. They were embedded in epoxy resin and sectioned. The ultra-thin sections were stained with uranyl acetate and lead citrate, and examined in an electron microscope (Hitachi, H-600) at 75 kV.

Reverse transcription-polymerase chain reaction (RT-PCR) was performed for PTHrP mRNA detection. Total RNA from IP tumors at passages 23 and 24 was isolated by TRIZOL reagent (Gibco-BRL, Gland Island, NY, USA). The RNA was reverse-transcribed using the Super Script™ Preamplification System (Gibco-BRL, Gaithersburg, MD, USA), and the resulting cDNA was amplified by PCR using Taq DNA polymerase (Takara Shuzou, Otsu, Shiga, Japan) and each of the specific primers for PTHrP or β-actin (control). The following oligonucleotides were used for PCR: the PTHrP sense primer 5′-CAATCCCCTGTGGAGGCTCCA-3′ and the antisense primer 5′-GACCAAGTCGTCACCTCGCAG-3′ [7]: the β-actin sense primer 5′-TAAAGACCTCTATGCCAACAC-3′ and the antisense primer 5′-CTCCTGCTTGCTGATCCACAT-3′ [39]. Samples were subjected to 28 cycles of 1 min of denaturation at 94°C, 1 min of annealing at 61°C and 1 min of synthesis at 72°C.

For examining a possible production of PTHrP by IP tumor cells, tumor tissues removed aseptically from IP at passage 16 were minced with scissors and dispersed with 0.1% trypsin and 0.02% EDTA in PBS for 2 h. The dispersed cells were seeded in plastic tissue culture flasks with RPMI1640 medium (Nissui, Tokyo, Japan) containing 10% fetal bovine serum (FBS; Bioserum, UBC, Japan), 0.03% L-glutamine (Nissui) and penicillin (100 U/ml) and streptomycin (100 µg/ml). The primary cultures were incubated at 37°C in a humidified 5% CO_2 atmosphere. After the 24-h incubation, cells were washed twice with PBS, and RPMI medium without 10% FBS was added to the cultures. After the 24h-incubation, the supernatants were collected for the measurement of PTHrP level using IRMA. Supernatants in the absence of IP cells were used as controls.

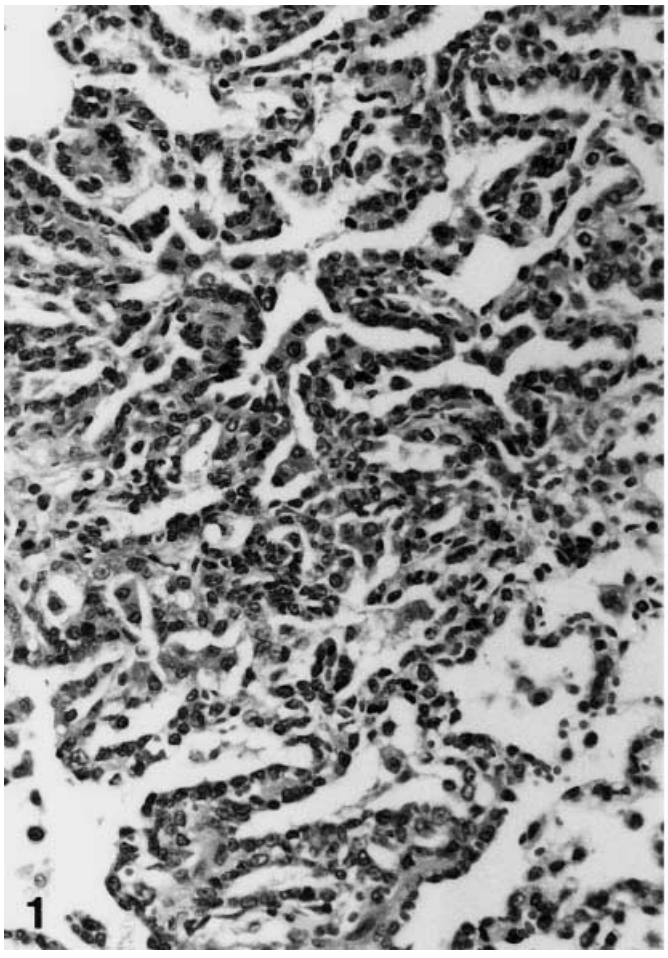

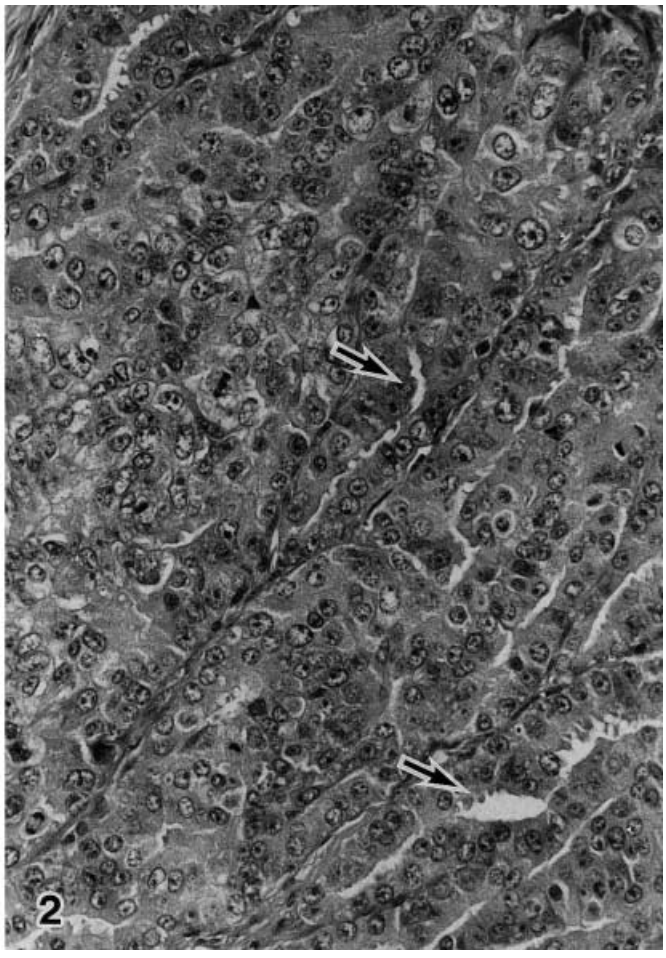

Fig. 1 The primary tumor, showing alveolar architecture consisting of cuboidal or columnar cells with hyperchromatic nuclei. HE, ×300

Fig. 2 Rat pulmonary carcinoma-derived transplantable tumor (IP) at passage 6, showing trabecular and glandular growth patterns. Slit-like lumina formed by mono- and multi-layed neoplastic cells are seen (*arrows*). Mitotic figures are frequently observed. HE, ×400

Data obtained were presented as means±standard error (SE). Paired samples in biochemical items and parameters for bone morphometry were evaluated using Student's *t*-test. Values of $P<0.05$ were considered significant.

Results

A primary tumor found in the caudal lobe of left lung was a grayish nodule, 7 mm in diameter. Histologically, the tumor consisted entirely of alveolar architectures lined by cuboidal or low columnar epithelial cells with hyperchromatic nuclei (Fig. 1). There was no distinct border between tumor and surrounding normal tissues. Mitotic figures were rarely seen, and structural and cellular atypia was not prominent. There were no metastatic lesions or systemic calcium depositions in the rat with the primary tumor. Because all samples of the primary tumor were used for the implantation study and histopathological examination, electron microscopy could not be made.

All of the serial transplantations in syngeneic male rats through the 26th passage were successful. In each generation, transplanted tissue fragments grew into nodules 2–3 cm in diameter within 2–3 weeks after the subcutaneous implantation, and there was no marked difference in tumor growth in different generations. Subcutaneous IP tumors were grayish, well-circumscribed nodules covered by thin fibrous tissues, and neither invasive growth to surrounding tissues nor metastatic lesions in visceral organs were seen in IP-transplanted rats. IP tumors often had necrotic and hemorrhagic areas on their cut surface. Histologically, IP tumors showed trabecular, acinar, glandular, solid, and cord growth patterns, consisting of epithelial cells with abundant cytoplasm and heterochromatic nuclei. Even in high cell density areas, slit-like lumina formed by mono- and multi-layered epithelial cells were seen (Fig. 2). Mitotic figures were frequently seen. Immunohistochemically, neoplastic cells gave a faintly positive reaction for pankeratin, a marker of epithelial cells; the reactions were located mainly in the apex of cells (Fig. 3). Neoplastic cells were negative for vimentin, a mesenchymal marker. Ultrastructurally, microvilli (Fig. 4) and basement membranes were seen

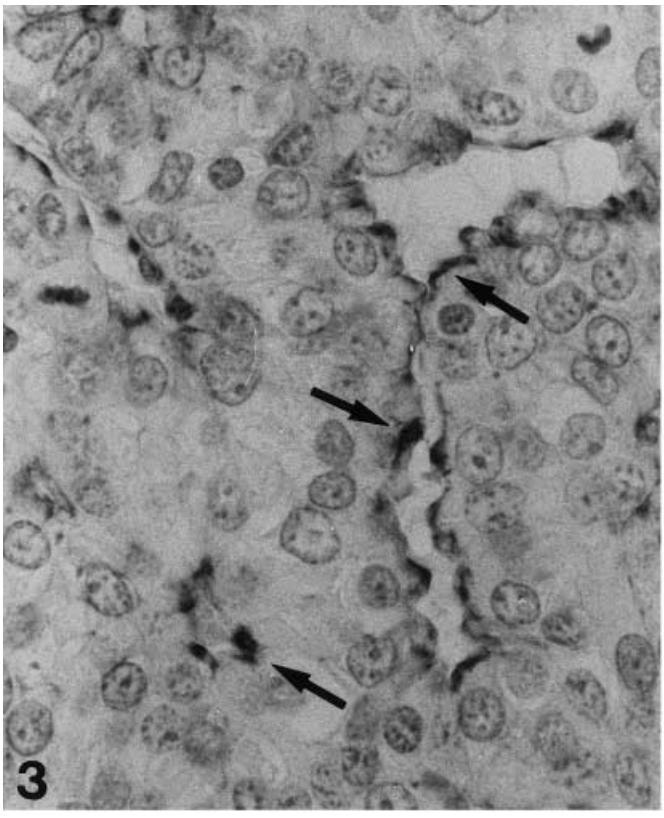

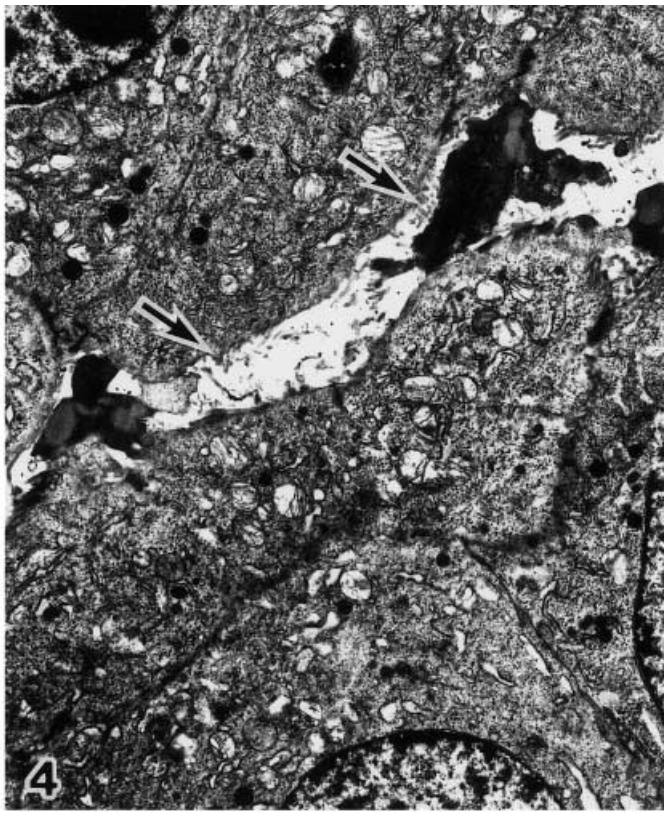

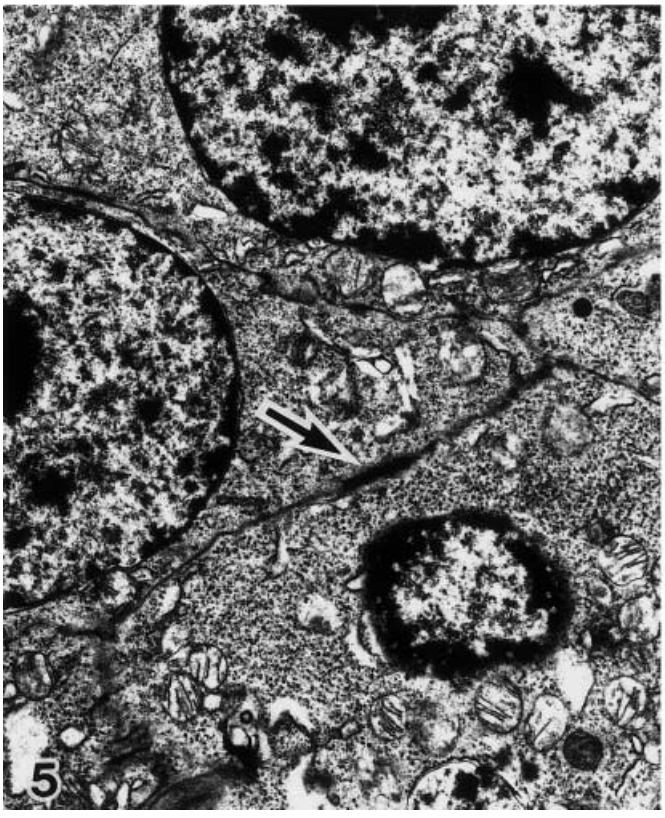

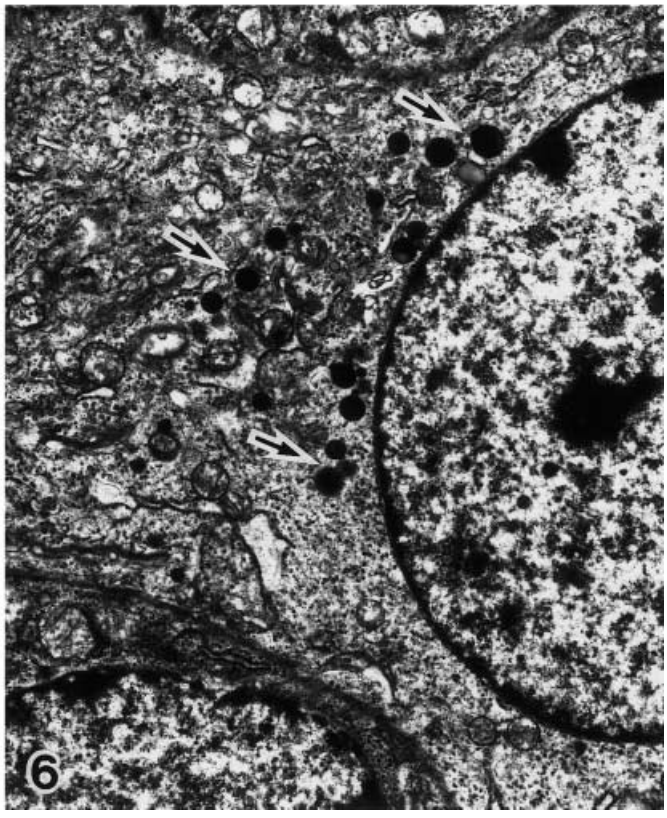

Fig. 3 IP tumor at passage 7. Cytokeratin-positive reactions (*arrows*) are seen in the apex of neoplastic cells. Immunohistochemistry, counterstained with hematoxylin, ×650

Fig. 4 Electron micrograph of neoplastic cells in the IP tumor. Microvilli (*arrows*) are seen. ×3,500

Fig. 5 Electron micrograph of neoplastic cells in the IP tumor. Desmosomes (*arrow*) are present between neoplastic cells. ×5,000

Fig. 6 . Electron micrograph of neoplastic cells in the IP tumor. The cells have many dense granules (200–700 nm in diameter) (*arrows*) in their cytoplasm. ×5,000

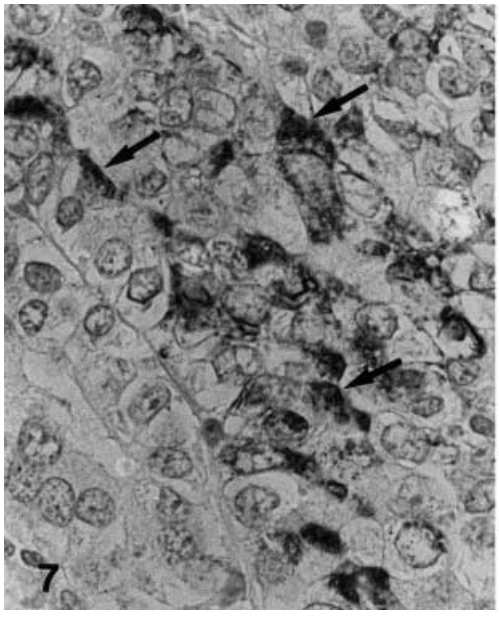

Fig. 7 IP tumor at passage 7. Some neoplastic cells give a positive reaction to parathyroid hormone-related protein (PTHrP) (*arrows*). Immunohistochemistry, counterstained with hematoxylin, ×650

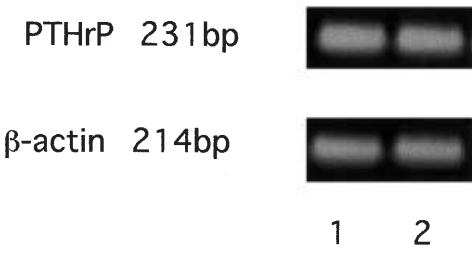

Fig. 8 Expressions of mRNAs of PTHrP and β-actin (control) in IP tumors (*1*, at passage 23; *2*, at passage 24) by the reverse transcription-polymerase chain reaction (RT-PCR). The sizes of amplification bands of PTHrP and β-actin are 231 and 214 bp, respectively

on the free surface and beneath the base of neoplastic cells, respectively. There were desmosomes between neoplastic cells (Fig. 5). Interestingly, some neoplastic cells possessed membrane-bound dense granules 200–700 nm in diameter in their cytoplasm (Fig. 6).

All rats used in serial transplantations developed calcification to varying degrees in the kidneys, lungs, and heart. Thus, we investigated a possible production of PTHrP by neoplastic cells. Immunohistochemically, many but not all neoplastic cells reacted to PTHrP (Fig. 7). There was no difference in the immunoreaction of neoplastic cells between each generation. The RT-PCR method showed the expression of PTHrP mRNA in IP tumor tissues (Fig. 8). Further, PTHrP was detected by IRMA in the supernatants of primarily cultured IP tumor cells (1.9 pM on average), whereas the PTHrP level in cultured medium in the absence of IP cells was below the detection limit of 1.1 pM.

In Exs I and II, systemic influences of IP transplants were investigated pathobiologically. Tumor weights at 1, 2, and 3 weeks in Ex I were 0.7, 7.6, and 13.3 g on average, respectively, and those at 2 and 3 weeks in Ex II were 7.6 and 11.7 g, respectively. Respective mean body weights in control and IP-bearing rats were 186 and 110 g at 2 weeks in Ex I, and 347 and 266 g at 3 weeks in Ex II; IP-bearing rats were severely emaciated, giving an impression of cachexia. As shown in Fig. 9A, a significantly increased calcium level was seen in IP-bearing rats at all examination points in Exs I and II. In Ex I, values of inorganic phosphorus were significantly increased at week 1, but significantly decreased at weeks 2 and 3 (Fig. 9B). BUN and creatinine values both showed a marked elevation at weeks 2 and 3 in Exs I and II (Fig. 9C, D. AST levels at all examination points in Exs I and II were significantly increased in IP-bearing rats (Fig. 9C). ALP also showed significantly increased values in IP-bearing rats in Exs I and II, except at week 2 in Ex I (Fig. 9F). Except for one case at week 3 in Ex I, all IP-bearing rats at weeks 2 and 3 of Exs I and II showed increased plasma PTHrP concentration, levels ranging from 2.2 to 16.5 pM. By contrast, PTHrP concentrations of IP-bearing rats at week 1, and control rats in Exs I and II, were below the detection limit (<1.1 pM) of the IRMA (Fig. 10).

Histologically, the most characteristic finding in IP-bearing rats in Exs I and II was calcification, an abnormality never seen in any organs of control rats. The calcium deposition, demonstrable by von Kossa's stain, was observed mainly in the kidneys, lungs, and heart of IP-bering rats at weeks 2 and 3 in Exs I and II. The grade varied from case to case and from organ to organ, but the severity increased invariably over time. In the affected kidneys, calcification was seen in the renal tubular lumina of the cortex and at the cortico-medullary junction, giving an appearance of intratubular lithogenesis (Fig. 11); in addition, the basement membranes of the renal tubules showed calcification (Fig. 11). In the lungs, calcification was seen along the alveolar septa (Fig. 12). In the heart, calcification had developed in the arteriolar wall and myocardium (Fig. 13), being accompanied by myocardial necrosis and fibrosis. At weeks 2 and 3 of Exs I and II, calcification was also seen in IP-bearing rats in various organs such as gastric glands, epithelial cells and muscle layers of the duodenum, squamous epithelia of the tongue and skin, acinar cells of the pancreas, cortex of the thymus, and tunica media of the aorta.

Computer-aided morphometrical analysis revealed that osteoclastic areas, stained positively by the TRAP method (Figs. 14 and 15), were significantly increased in IP-bearing rats at 2 and 3 weeks in Exs I and II (Fig. 16), as compared with those of control rats. The increased levels were presented as percentage of controls (100%)

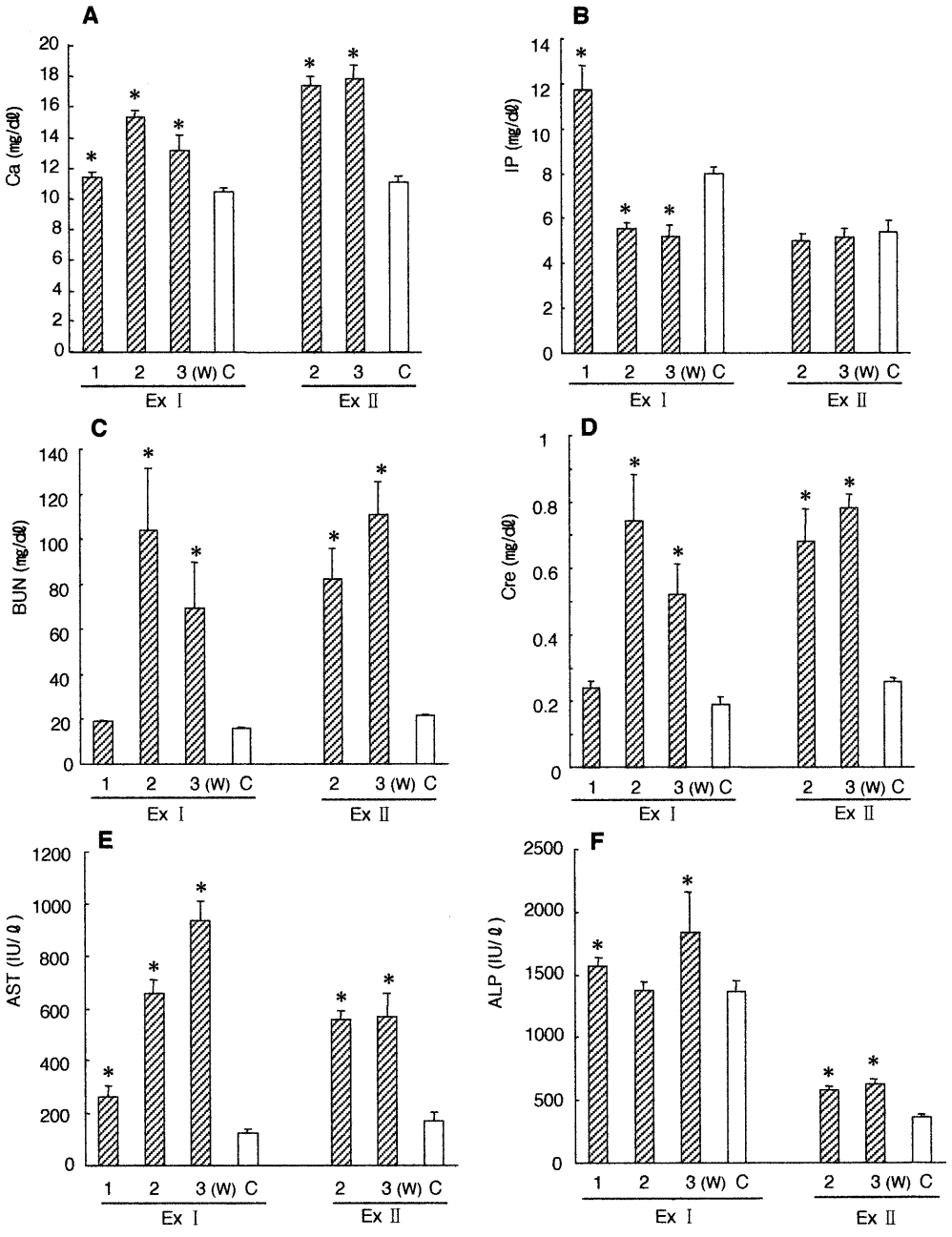

Fig. 9A–F Serum biochemistry. In experiment I (Ex I), 6-week-old rats were transplanted subcutaneously with IP tissue fragments, and examined at 1, 2 and 3 weeks (W) after the implant. Rats aged 20 weeks were used in experiment II(Ex II), and they were examined at 2 and 3 weeks after the subcutaneous implant. *Ca* calcium, *IP* inorganic phosphorus, *BUN* blood urea nitrogen, *Cre* creatinine, *AST* aspartate aminotransferase, *ALP* alkaline phosphatase. *Figures* present means±standard error (SE). * Significantly different from controls (*C*) at $P<0.05$

(Fig. 16); interestingly, the increased levels in IP-bearing rats at weeks 2 and 3 in Ex I were 390 and 380%, on average, repectively, and those on average at weeks 2 and 3 in Ex II showed 1200 and 2000%, respectively. The degree was much greater (threefold at week 2 and fivefold at week 3) in Ex II than in Ex I. Reflecting osteoclastic activity, the shaft thickness of the femurs was signifiantly decreased in IP-bearing rats at weeks 2 and 3 in Exs I and II, in contrast to that of controls (Fig. 17).

Discussion

Spontaneous neoplasms of the lungs occurred at a low incidence (less than 3%) in F344 rats that had been housed for 2 years or more [2]. The pulmonary tumors of epithelial origin in F344 rats are divided mainly into alveolar/bronchiolar adenoma and carcinoma, and squamous cell carcinoma [2]. The present primary tumor showed only alveolar structures, and the epithelia were cuboidal to columnar in shape; no marked cellular atypia or mitotic figures were seen, suggesting a benign nature. However, transplanted IP tumors developed various growth patterns such as trabecular, glandular, acinar, solid, and cord formations. Mitotic figures were often observed in them, and cellular atypia was more prominent, indicating a potential malignancy of the original tumor. The histological differences between the primary tumor and transplanted tumors might, at least in part, be due to the inappropriate nature of subcutaneous tissues as a

transplantation site with regard to the preservation of alveolar structures. Further, undifferentiated neoplastic cells might be selected in the process of transplantation; morphological alterations due to dedifferentiation of neoplastic cells have been reported in long-term serial transplantation of rat nephroblastoma [13] and malignant meningioma [44]. Therefore, with these facts and precedents in mind, we concluded that the present tumors should be regarded as alveolar/bronchiolar carcinoma. In humans, atypical adenomatous hyperplasia of the lungs has been considered to be a precursor of alveolar/bronchiolar carcinoma; the hyperplastic lesions are composed of cuboid or columnar epithelial cells with variable grades of atypia [6]. The present primary tumor might have a nature similar to atypical hyperplasia in humans.

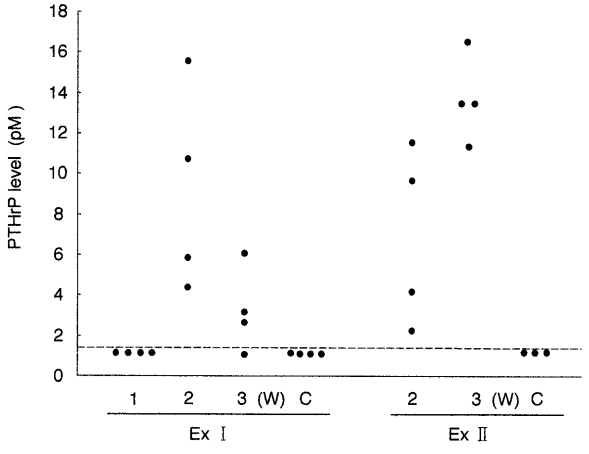

Fig. 10 Plasma PTHrP levels measured by immunoradiometric assay (IRMA) in Exs I and II. *W* weeks after the transplantation, *C* controls. Detectability limit of the IRMA method is <1.1 pM (*dotted line*). Each *circle* shows a PTHrP level of an individual rat

Alveolar/bronchiolar carcinoma in humans consists of an admixture of type 2 alveolar epithelial cells and those showing Clara cell differentiation to varying proportions [17]. Generally, microvilli and lamellar bodies are characteristic of type 2 alveolar epithelial cells, whereas Clara cells are nonciliated and have many membrane-bound dense granules in the cytoplasm [17]. Ultrastructurally, neoplastic cells in IP tumors exhibited an epithelial cell nature in elements such as microvilli, basement membranes, and desmosomes, and there were also cells with cytoplasmic dense granules. It is likely that IP tumors contained both cell types. However, Clara cell differentiation in human alveolar/bronchiolar carcinoma is considered to be due to metaplasia of type 2 alveolar epithelial cells [17]. Thus, the present original tumor might be generated from type 2 alveolar epithelial cells.

PTHrP has been reported to be expressed in normal lung epithelial cells, especially in type 2 alveolar epithe-

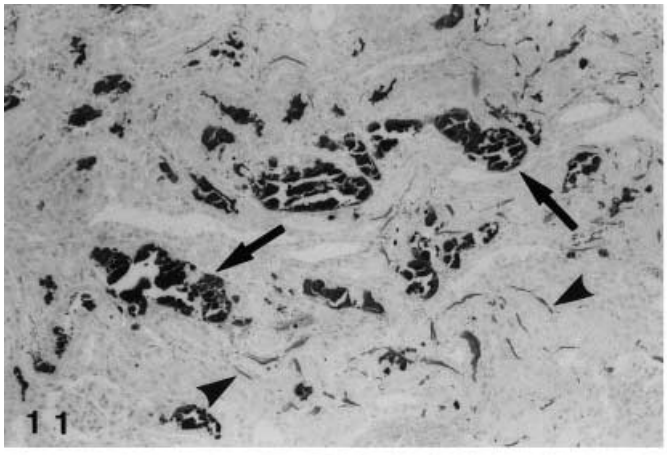

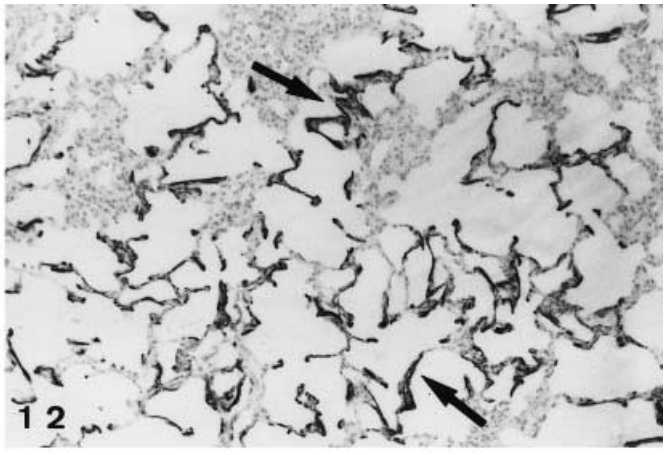

Fig. 11 The kidney of an IP-bearing rat. Calcifications are seen in the lumina (*arrows*) and the basement membranes (*arrowheads*) of the renal tubules. von Kossa's stain, ×100

Fig. 12 The lung of an IP-bearing rat, showing severe calcification (*arrows*) along the alveolar septa. von Kossa's stain, ×100

Fig. 13 The heart of an IP-bearing rat, showing calcification (*arrows*) in an arteriolar wall and the myocardium. von Kossa's stain, ×200

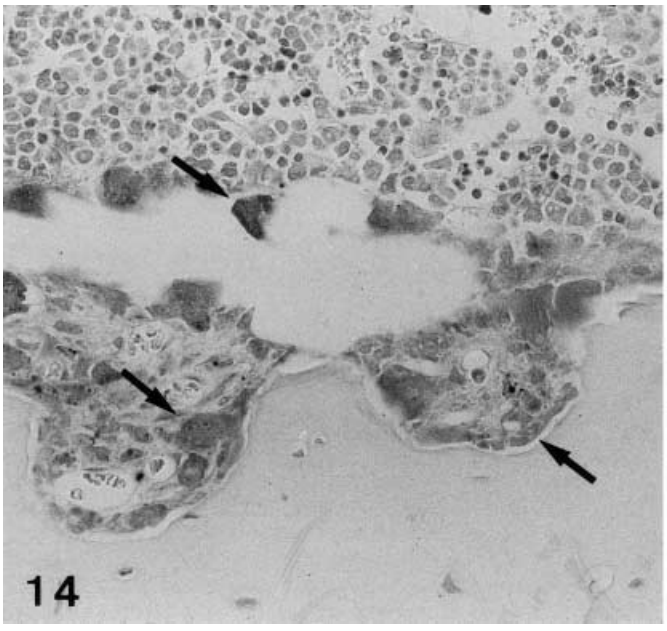

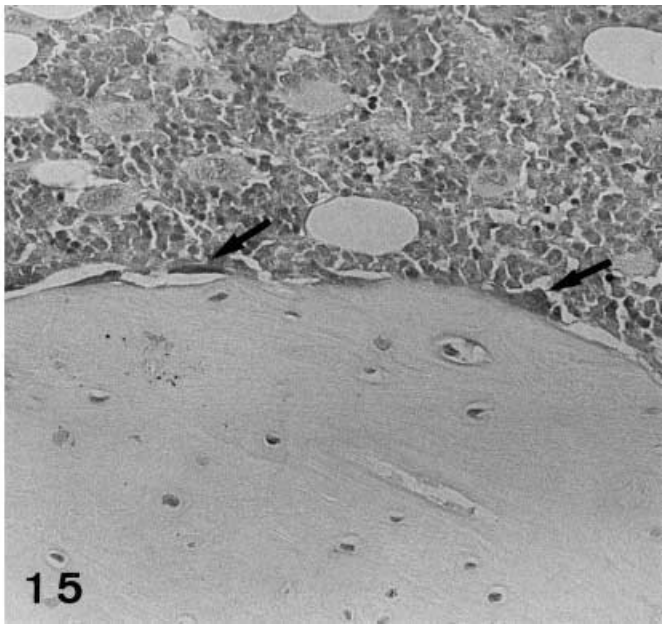

Fig. 14 The femur of an IP-bearing rat. Swelling and increasing of osteoclasts are seen (*arrows*). Tartrate-resistant acid phosphatase (TRAP) method, ×300

Fig. 15 The femur of a control rat. A few osteoclasts are observed (*arrows*). TRAP method, ×300

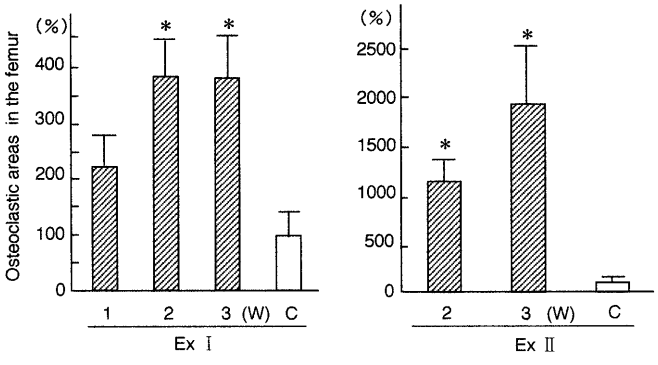

Fig. 16 Osteoclastic areas in the femur in Exs I and II. Figures are represented as means±SE of percentage compared to controls (100%). *Significantly different from controls at $P<0.05$. *W* weeks after the transplantation, *C* controls

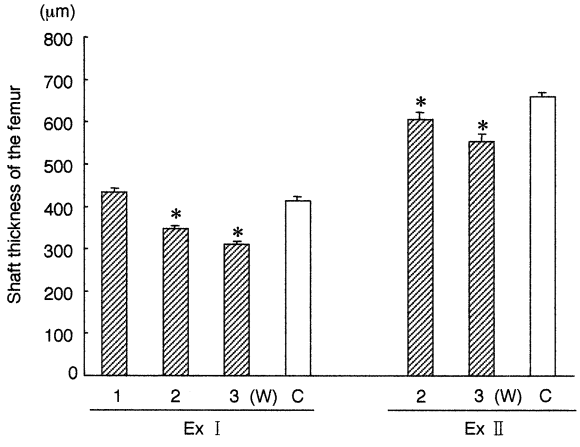

Fig. 17 Shaft thickness of the femur in Exs I and II. *Figures* present means±SE. *Significantly different from controls at $P<0.05$. *W* weeks after the transplantation, *C* controls

lial cells.[3, 9, 14, 18], although the physiological functions in normal lung tissues have yet to be determined. In the present study, it was demonstrated by the immunohistochemistry, the RT-PCR method, and IRMA using culture supernatants that IP tumor cells produce PTHrP. It has recently been shown that the overproduction of PTHrP by human neoplastic cells may be related to an aberration of chromosomes encording PTHrP gene [15], and/or to mutations of *Ras* oncogene [1] or *p*53 [8]. However, mechanisms of PTHrP overproduction remain to be investigated.

In 1987 it was found that PTHrP is the main factor in causing HHM in human cancer patients [5, 25, 35]. HHM is characterized by hypercalcemia and hypophosphatemia [34]. In Exs I and II, IP-bearing rats, particularly at weeks 2 and 3, showed similar changes (Figs. 9A and 9B), although hypophosphatemia was not evident in IP-bearing rats of Ex II. These phenomena were considered to be caused by the PTHrP that was produced excessively by IP tumor cells. Indeed, a marked elevation in plasma PTHrP levels was shown in IP-bearing rats by IRMA (Fig. 10). PTHrP stimulates osteoclastic bone resorption and renal absorption of calcium [31, 40]. The osteoclastic activity and the resultant decrease in shaft thickness were confirmed in IP-bearing rats (Figs. 16 and 17). PTHrP can express its biological functions by binding to PTH/PTHrP receptors [27, 42]. However, since osteoclasts do not have PTH/PTHrP receptors, it has been speculated that the osteoclastic functions might be controlled through various factors produced mainly by osteoblasts with PTH/PTHrP receptors capable of binding to PTHrP

[10]. The mechanisms by which stimulation of osteoblasts by PTHrP promotes the osteoclastic bone resorption remain to be investigated [21, 24, 28, 38].

It is interesting to note that IP-bearing rats at week 1 in Ex I showed a significantly increased level in inorganic phosphorus (Fig. 9B). This suggests that PTHrP first stimulates bone resorption, leading to hyperphosphatemia due to release of minerals, including phosphorus, from the bone; thereafter PTHrP acts on kidneys, resulting in hypercalcemia and hypophosphatemia due to calcium absorption and phosphorus excretion in the kidneys. Furthermore, it is worth noting that osteoclastic areas in IP-bearing rats were remarkably greater (approximately three-fold and five-fold at weeks 2 and 3, respectively) in Ex II than in Ex I (Fig. 16). Young rats (aged 6 weeks in Ex I) have highly active bone formation, whereas bone modeling has been halted in adult rats (aged 20 weeks in Ex II). PTHrP seems to more strongly effect change on completed bone than on developing bone; the influence may depend on an active balance between osteoblasts and osteoclasts.

In cancer patients undergoing HHM, systemic calcification is the most critical condition, having been reported to be most frequently observed in the renal tubules and alveolar walls [15, 20]. Predictably, multiple organ failure caused by systemic calcification has been the direct cause of death [15, 20]. As a result of hypercalcemia, all IP-bearing rats at weeks 2 and 3 in Exs I and II developed systemic calcification, particularly in the kidneys, lungs, and heart; the affected organs were generally similar to those reported in humans. In the present study, affected kidneys showed dysfunction as indicated by significantly increased values of BUN and creatinine (Fig. 9C and 9D). In addition, an abnormal increase in AST values indicated hepatic failure in IP-bearing rats (Fig. 9E). Significantly increased ALP levels might reflect abnormal bone absorption (Fig. 9F). Severe emaciation of IP-bearing rats could be attributable to such conditions. These findings seen in IP-bearing rats are generally in keeping with those of HHM reported in human cancer patients [4, 20].

In conclusion, the present study demonstrated that IP tumor cells overproduced PTHrP, resulting in HHM in IP-bearing rats. We found that IP proved useful in studies on HHM. Two transplantable rat tumors, Leydig cell tumor [12] and Walker mammary carcinosarcoma [19, 29, 33], have been reported as animal models of HHM. IP is a novel rat transplantable tumor line established from a pulmonary carcinoma. Pulmonary carcinoma is the most frequent cause of HHM in humans [15]. Besides PTHrP, various factors produced by neoplasms and/or by tumor-bearing hosts have been implicated as important modulators of the expression of HHM [30]. These factors include interleukins [23, 26], tumor necrosis factors (TNFs) [23, 40], and transforming growth factors (TGFs) [22, 48]. The expressions of mRNAs of TNF-α and TGF-β are being confirmed in IP tumor cells by the RT-PCR method (data not shown). Further studies using the IP model are in progress in our laboratorywith the goal of shedding some light on the pathogenesis of HHM and the pathophysiological roles of PTHrP.

Acknowledgements This work was supported in part by a Grant-in-Aid (No. 09660324 to J. Yamate) for Scientific Research C, the Ministry of Education, Sciences, Sports and Culture, Japan. We wish to thank Dr. H. Okada, Department of Veterinary Pathology, Rakuno Gakuen University, Ebetsu, Hokkaido, Japan, for his kind advice concerning PTHrP antibody; and Dr. S. Tsuchida, Department of Veterinary Surgery, Nippon Veterinary and Animal Science University, Musashino, Tokyo, Japan, for his kindness in providing DNA sequences of rat PTHrP.

References

1. Akilu F, Park M, Goltzman D, Rabbani SA (1997) Induction of parathyroid hormone- related peptide by the *Ras* oncogene: role of Ras farnesylation inhibitors as potential therapeutic agents for hypercalcemia of malignancy. Cancer Res 57:4517–4522
2. Boorman GA, Eustis SL (1990) Lung. In: Boorman GA, Eustis SL, Elwell MR, Montgomery CA Jr, MacKenzie WF (eds) Pathology of the Fischer rat. Academic Press, San Diego New York Boston, pp339–367
3. Brandt DW, Burton DW, Gazdar AF, Oie HE, Deftos LJ (1991) All major lung cancer cell types produce parathyroid hormone-like protein: heterogeneity assessed by high performance liquid chromatography. Endocrinology 129:2466–2470
4. Braude S, Graham A, Mitchell D (1991) Lymphoedema/hypercalcemia syndrome mediated by parathyroid-hormone-related protein. Lancet 337:140–141
5. Burtis WJ, Wu T, Bunch C, Wysolmerski JJ, Insogna KL, Weir EC, Broadus AE, Stewart AF (1987) Identification of a novel 17,000-dalton parathyroid hormone-like adenylate cyclase-stimulating protein from a tumor associated with humoral hypercalcemia of malignancy. J Biol Chem 262:7151–7156
6. Carey FA, Wallace WA, Fergusson RJ, Kerr KM, Lamb D (1992) Alveolar atypical hyperplasia in association with primary pulmonary adenocarcinoma: a clinicopathological study of 10 cases. Thorax 47:1041–1043
7. Falzon M (1996) DNA sequences in the rat parathyroid hormone-related peptide gene responsible for 1,25-dihydroxyvitamin D_3-mediated transcriptional repression. Mol Endocrinol 10:672–681
8. Foley J, Wysolmerski JJ, Broadus AE, Philbrick WM (1996) Parathyroid hormone-related protein gene expression in human squamous carcinoma cells is repressed by mutant isoforms of p53. Cancer Res 56:4056–4062
9. Gröne A, Werkmeister JR, Steinmeyer CL, Capen CC, Rosol TJ (1994) Parathyroid hormone-related protein in normal and neoplastic canine tissues: immunohistochemical localization and biochemical extraction. Vet Pathol 31:308–315
10. Gröne A, McCauley LK, Capen CC, Rosol TJ (1997) Parathyroid hormone/parathyroid hormone-related protein receptor expression in nude mice with a transplantable canine apocrine adenocarcinoma (CAC-8) and humoral hypercalcemia of malignancy. J Endocrinol 153:123–129
11. Guise TA, Yin JJ, Taylor SD, Kumagai Y, Dallas M, Boyce BF, Yoneda T, Mundy GR (1996) Evidence for a causal role of parathyroid hormone-related protein in the pathogenesis of human breast cancer-mediated osteolysis. J Clin Invest 98: 1544–1549
12. Haq M, Kremer R, Goltzman D, Rabbani SA (1993) A vitamin D analogue (EB1089) inhibits parathyroid hormone-related peptide production and prevents the development of malignancy-associated hypercalcemia in vivo. J Clin Invest 91: 2416–2422
13. Hard GC, Nobel RL (1981) Occurrence, transplantation, and histologic characteristics of nephroblastoma in the Nb hooded rat. Invest Urol 18:371–376
14. Hastings RH, Duong H, Burton DW, Deftos LJ (1994) Alveolar epithelial cells express and secrete parathyroid hormone-related protein. Am J Respir Cell Mol Biol 11:701–706
15. Hidaka N, Nishimura M, Nagano K (1998) Establishment of two human small cell lung cancer cell lines: the evidence of

accelerated production of parathyroid hormone-related protein with tumor progression. Cancer Lett 125:149–155
16. Hoekman K, Tjandra YI, Papapoulos SE (1991) The role of 1,25-dihydroxyvitamin D in the maintenance of hypercalcemia in a patient with an ovarian carcinoma producing parathyroid hormone-related protein. Cancer 68:642–647
17. Kitamura H, Kameda Y, Ito T, Hayashi H, Nakamura N, Nakatani Y, Inayama Y, Kanisawa M (1997) Cytodifferentiation of atypical adenomatous hyperplasia and bronchioloalveolar lung carcinoma: immunohistochemical and ultrastrustural studies. Virchows Arch 431:415–424
18. Kitazawa S, Fukase M, Kitazawa R, Takenaka A, Gotoh A, Fujita T, Maeda S (1991) Immunohistologic evaluation of parathyroid hormone-related protein in human lung cancer and normal tissue with newly developed monoclonal antibody. Cancer 67:984–989
19. Kozak S, Rizzoli R, Trechsel U, Fleisch H (1987) Effect of a single injection of two new bisphosphonates on the hypercalcemia and hypercalciuria induced by Walker carcinosarcoma 256/B in thyroparathyroidectomized rats. Cancer Res 47:6193–6197
20. Kumamoto H, Ichinohasama R, Sawai T, Naganuma H, Furukawa Y, Akiu N, Kano M, Ooya K (1998) Multiple organ failure associated with extensive metastatic calcification in a patient with an intermediate state of human T lymphotropic virus type I(HTLV-I) infection: report of an autopsy case. Pathol Int 48:313–318
21. McDonnell GD, Dunstan CR, Evans RA, Carter JN, Hillus E, Wong SY, McNeil DR (1982) Quantitative bone histology in the hypercalcemia of malignant disease. J Clin Endocrinol Metab 55:1066–1072
22. Merryman JI, Dewille JW, Werkmeister JR, Capen CC, Rosol TJ (1994) Effects of transforming growth factor-β on parathyroid hormone-related protein production and ribonucleic acid expression by a squamous carcinoma cell line *in vitro*. Endocrinology 134:2424–2430
23. Mori H, Aoki K, Katayama I, Nishioka K, Umeda T (1996) Humoral hypercalcemia of malignancy with elevated plasma PTHrP, TNFα and IL-6 in cutaneous squamous cell carcinoma. J Derm 23:460–462
24. Morris CA, Mitnick ME, Weir EC, Horowitz M, Kreider BL, Insogna KL (1990) The parathyroid hormone-related protein stimulates human osteoblast-like cells to secrete a 9,000 dalton bone-resorbing protein. Endocrinology 126:1783–1785
25. Moseley JM, Kubota M, Diefenbach-Jagger H, Wettenhall RE, Kemp BE, Suva LJ, Rodda CP, Ebeling PR, Hudson PJ, Zajac JD (1987) Parathyroid hormone-related protein purified from a human lung cancer cell line. Proc Natl Acad Sci USA 84: 5048–5052
26. Nagai Y, Yamato H, Akaogi K, Hirose K, Ueyama Y, Ikeda K, Matsumoto T, Fujita T, Ogata E (1998) Role of interleukin-6 in uncoupling of bone in vivo in a human squamous carcinoma coproducing parathyroid hormone-related peptide and interleukin-6. J Bone Miner Res 13:664–672
27. Orloff JJ, Reddy D, de Papp AE, Yang KH, Soifer NE, Stewart AF (1994) Parathyroid hormone-related protein as a prohormone: posttranslational processing and receptor interactions. Endocr Rev 15:40–60
28. Ralston SH, Boyce BF, Cowan RA, Gardner MD, Fraser WD, Boyle IT (1989) Contrasting mechanisms of hypercalcemia in patients with early and advanced humoral hypercalcemia of malignancy. J Bone Miner Res 4:103–111
29. Rizzoli R, Fleisch H (1987) The Walker 256/B carcinosarcoma in thyroparathyroidectomized rats: a model to evaluate inhibitors of bone resorption. Calcif Tissue Int 41:202–207
30. Rosol TJ, Capen CC (1988) Pathogenesis of humoral hypercalcemia of malignancy. Domest Anim Endocrinol 5:1–21
31. Rosol TJ, Capen CC (1992) Biology of disease: mechanisms of cancer-induced hypercalcemia. Lab Invest 67:680–702
32. Rosol TJ, Capen CC, Weisbrode SE, Horst RL (1986) Humoral hypercalcemia of malignancy in nude mouse model of a canine adenocarcinoma derived from apocrine glands of the anal sac. Lab Invest 54:679–688
33. Schilling T, Blind E, Baier R, Sinn HP, Moallem E, Silver J, Ziegler R, Raue F (1995) Effects of passive immunization against parathyroid hormone-related protein: PTHrP is the responsible factor in mediating hypercalcemia in the Walker carcinosarcoma 256 rat model. J Bone Miner Res 10:7–16
34. Stewart AF, Horst R, Deftos LJ, Cadman EC, Lang R, Broadus AE (1980) Biochemical evaluation of patients with cancer-associated hypercalcemia: evidence for humoral and nonhumoral groups. N Engl J Med 303:1377–1383
35. Strewler GJ, Stern PH, Jacobs JW, Eveloff J, Klein RF, Leung SC, Rosenblatt M, Nissenson RA (1987) Parathyroid hormonelike protein from human renal carcinoma cells: structural and functional homology with parathyroid hormone. J Clin Invest 80:1803–1807
36. Takai E, Yano T, Iguchi H, Fukuyama Y, Yokoyama H, Asoh H, Ichinose Y (1996) Tumor-induced hypercalcemia and parathyroid hormone-related protein in lung carcinoma. Cancer 78:1384–1387
37. Teranishi M, Tani Y, Manabe S (1998) Comparison of age-related bone changes between mini rats and wistar rats. J Toxicol Pathol 11:137–143
38. Teti A, Grano M, Colucci S, Cantatore FP, Loperfido MC, Zallone AZ (1991) Osteoblast-osteoclast relationships in bone resorption: osteoblasts enhance osteoclast activity in a serum-free co-culture system. Biochem Biophys Res Commun 179:634–640
39. Tsujino K, Yamate J, Tsukamoto Y, Kumagai D, Kannan Y, Jippo T, Kuwamura M, Kotani T, Takeya M, Sakuma S (1997) Establishment and characterization of cell lines derived from a transplantable rat malignant meningioma: morphological heterogeneity and production of nerve growth factor. Acta Neuropathol 93:461–470
40. Uy HL, Mundy GR, Boyce BF, Story BM, Dunstan CR, Yin JJ, Roodman GD, Guise TA (1997) Tumor necrosis factor enhances parathyroid hormone-related protein-induced hypercalcemia and bone resorption without inhibiting bone formation *in vivo*. Cancer Res 57:3194–3199
41. Weir EC, Norrdin RW, Matus RE, Brooks MB, Broadus AE, Mitnick M, Johnston SD, Insogna KL (1988) Humoral hypercalcemia of malignancy in canine lymphosarcoma. Endocrinology 122:602–608
42. Wysolmerski JJ, Broadus AE (1994) Hypercalcemia of malignancy: the central role of parathyroid hormone-related protein. Annu Rev Med 45:189–200
43. Yamate J, Tajima M, Toga M, Shibuya K, Ihara M, Kudow S (1991) Heterogeneity of cloned cell lines established from a transplantable rat malignant fibrous histiocytoma. Jpn J Cancer Res 82:298–307
44. Yamate J, Tajima M, Saitoh T, Shibuya K (1994) Biological behaviour and morphological characteristics of a transplantable tumour(MM-KMY) derived from a malignant meningioma in an F344 rat. J Comp Path 111:243–257
45. Yamate J, Ishida A, Tsujino K, Tatsumi M, Nakatsuji S, Kuwamura M, Kotani T, Sakuma S (1996) Immunohistochemical study of rat renal interstitial fibrosis induced by repeated injection of cisplatin, with special reference to the kinetics of macrophages and myofibroblasts. Toxicol Pathol 24:199–206
46. Yamate J, Iwaki M, Kumagai D, Tsukamoto Y, Kuwamura M, Nakatsuji S, Tsunenari I, Kotani T, Sakuma S (1997) Characteristics of a rat fibrosarcoma-derived transplantable tumour line (SS) and cultured cell lines (SS-P and SS-A3–1) showing myofibroblastic and histiocytic phenotypes. Virchows Arch 431:431–440
47. Yamate J, Tsujino K, Kumagai D, Nakatsuji S, Kuwamura M, Kotani T, Sakuma S (1997) Morphological characteristics of a transplantable histiocytic sarcoma (HS-J) in F344 rats and appearance of renal tubular hyaline droplets in HS-J-bearing rats. J Comp Pathol 116:73–86
48. Yin JJ, Selander K, Chirgwin JM, Dallas M, Grubbs BG, Wieser R, Massague J, Mundy GR, Guise TA (1999) TGF-β signaling blockade inhibits PTHrP secretion by breast cancer cells and bone metastases development. J Clin Invest 103:197–206

Virchows Arch (2002) 440:205–208
DOI 10.1007/s004280100535

CASE REPORT

Noriko Kato · Sunao Akiyama · Teiichi Motoyama

Pyloric gland-type tubular adenoma superimposed on intraductal papillary mucinous tumor of the pancreas

Pyloric gland adenoma of the pancreas

Received: 8 May 2001 / Accepted: 7 August 2001 / Published online: 22 November 2001
© Springer-Verlag 2001

Abstract We report a rare case of pyloric gland-type tubular adenoma of the main pancreatic duct. It was a grossly visible polypoid nodule and was composed of closely packed pyloric-type glands. This adenoma was present within an intraductal papillary mucinous adenoma (IPMA). In this IPMA lesion, aggregations of pyloric-type glands were occasionally observed, and most of the cells including ductal lining cells expressed pyloric gland-type mucin. The IPMA of the present case showed more extensive pyloric gland metaplasia or differentiation than commonly noted in IPMAs. We consider this pyloric gland-type tubular adenoma to be derived from a selective growth of IPMA cells showing pyloric gland metaplasia.

Keywords Tubular adenoma · Pancreas · Pyloric gland · Metaplasia · Intraductal papillary mucinous adenoma

Introduction

Metaplastic or hyperplastic pyloric-type glands are sometimes observed in the pancreas [5, 6, 10]. They usually appear as microscopic foci surrounding the main or interlobular ducts. In neoplastic lesions, however, pyloric-type glands are less frequently encountered, and neoplasms purely composed of pyloric-type glands are extremely rare in the pancreas [2].

We report a case of pyloric gland-type tubular adenoma of the main pancreatic duct. Interestingly, it arose within an intraductal papillary mucinous adenoma (IPMA), in which most of the tumor cells expressed pyloric gland-type mucin and occasionally showed pyloric gland metaplasia.

N. Kato (✉) · S. Akiyama · T. Motoyama
Department of Pathology,
Yamagata University School of Medecine,
Yamagata, 990–9585, Japan
e-mail: nkato@med.id.yamagata-u.ac.jp

Clinical history

The patient was a 70-year-old man who complained of epigastric pain and diarrhea for 5 months. Ultrasonography and computed tomography of the abdomen revealed choledocholithiasis and small cystic lesions in the pancreatic body. For choledocholithiasis, endoscopic sphincterotomy was performed. Endoscopic retrograde cholangiography revealed dilatation of the main and branch pancreatic ducts and the presence of a small nodule in the main duct. Laboratory data including CA19–9 were normal. Distal pancreatectomy and splenectomy were performed for the cystic lesions under a working diagnosis of intraductal papillary mucinous tumor.

Materials and methods

The specimen was fixed in formalin and embedded in paraffin. Sections were stained with hematoxylin and eosin and paradoxical concanavalin A. For immunohistochemical studies, sections were incubated with the monoclonal antibody HIK1083 (Kanto Kagaku, Japan), which specifically detects pyloric gland-type mucin [3], and with antibodies against synaptophysin (Dako, Denmark), chromogranin A (Immunotech, France), gastrin (Dako), somatostatin (Dako) and serotonin (Dako), and detected by the streptoavidin-biotin complex system (Nichirei, Japan). For comparative study, we used 3 IPMAs and ten non-neoplastic pancreatic tissues obtained at surgery and autopsy.

DNA was separately extracted from a polypoid lesion, a duct ectatic lesion, and normal pancreatic tissue after their microdissection from the paraffin sections. A nested polymerase chain reaction (PCR) technique combined with *Hpa*II digestion was performed to detect K-ras codon 12 mutations [8]. The primers used were 5′-GACTGAATATAAACTTGTGG-3′ and 5′-TCTATTGTTGGATCATACTT-3′ in the first-round PCR, and 5′-TAAACTTGTGGTAGTTGGAGCC-3′ and 5′-CTATTGTTGGATCATAT TCG-3′ in the second-round PCR. This second set of primers introduces an artificial *Hpa*II digestion site at the 3′ end of the wild-type allele of the K-*ras* gene. Digestion of this allele results in a 77- and a 21-bp fragment. K-*ras* genes with codon 12 mutations do not acquire this *Hpa*II site, and digestion results in a 98-bp fragment. The pattern of digestion was analyzed on a 6% polyacrylamide gel.

Fig. 1 A perpendicular section of a medial resection of the pancreas. A polypoid nodule (*arrow*) was present in the ectatic main pancreatic duct (*arrowhead*). The branch ducts were also ectatic with abundant amounts of mucin

Pathological findings

Gross findings

The main pancreatic duct was dilatated and had a mean diameter of 1 cm. This finding extended to the body of the pancreas, up to 8 cm in length. The main duct contained a grossly visible polypoid lesion about 6 mm in diameter. The cut surface of the lesion was tan and homogenous. Branch ducts were also ectatic with abundant amounts of mucin (Fig. 1), which was observed over approximately 3×8 cm of the head and body.

Histological findings

The polypoid lesion was composed of closely packed pyloric-type tubular glands lined by columnar epithelial cells with abundant clear cytoplasm and crescentic, basally oriented nuclei(Fig. 2a, b). Nuclear atypia was mild and no mitotic figures were observed. Main and branch ducts were ectatic and the lining epithelium focally showed slight papillary projections (Fig. 3 a). The nuclei of the lining cells were oval to short spindle-shaped and closely arranged in some areas (Fig. 3b). Surrounding these ducts, pyloric-type glands aggregated occasionally (Fig. 3d), which was more frequent than observed in three control cases of IPMA (Table 1).

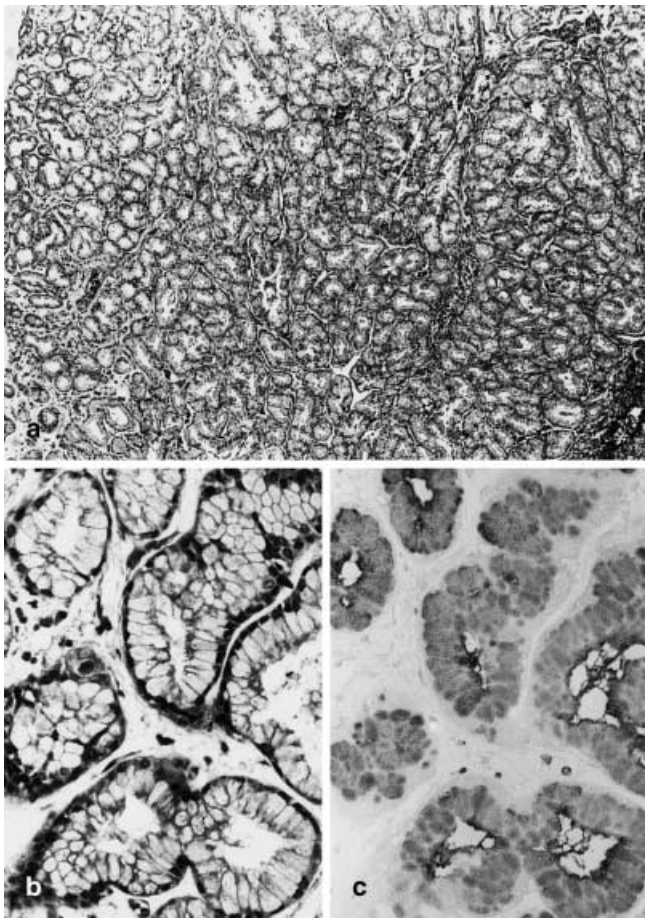

Fig. 2 **a** The polypoid lesion was composed of closely packed tubular glands. **b** They were pyloric-type glands. **c** There was a strong positivity for paradoxical concanavalin A staining in the cytoplasm of pyloric-type glands

Table 1 Pyloric gland metaplasia (PGM) and related histochemical and immunohistochemical findings in normal pancreatic duct, intraductal papillary mucinous adenoma (IPMA) and the present tumor

Tissue	No. of cases showing PGM	Degree of PGM[a]	Positivity for PCS		Reactivity to MoAB HIK1083	
			Ductal lining cells	Metaplastic pyloric glands	Ductal lining cells	Metaplastic pyloric glands
Normal pancreatic duct (n=10)	6	1+	–	+	–	+
Common IPMA (n=3)	3	1+~2+	–	+	–	+
IPMA lesion in the present case		3+	+[b]	+	+[b]	+

PCS paradoxical concanavalin A staining, MoAB monoclonal antibody, – negative, + positive
[a] +, a few; 2+, occasional; 3+, frequent
[b] Diffusely, except with regard to the cells constituting papillary projections

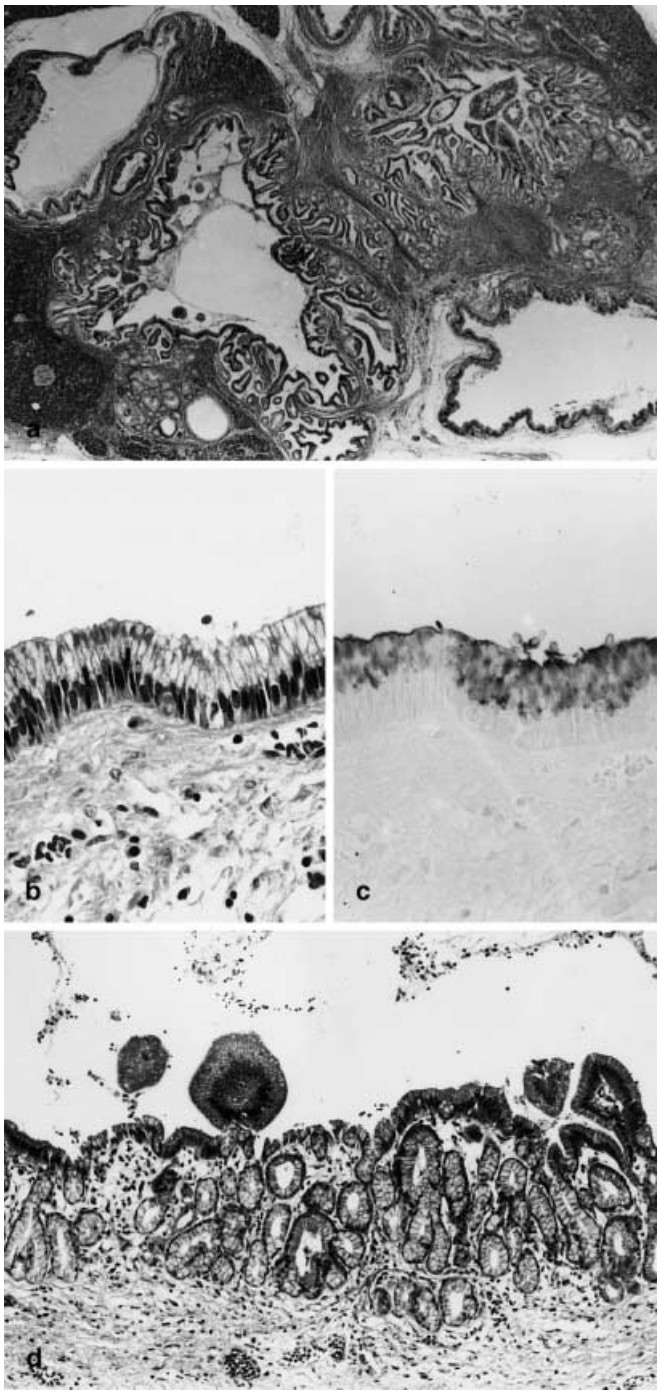

Fig. 3 **a** The main and branch pancreatic ducts were dilated and the lining epithelium focally showed slight papillary projections. **b** The lining epithelium was composed of a single layer of columnar cells, which had oval or short spindle-shaped nuclei. **c** The lining epithelium showed positivity for paradoxical concanavalin A. **d** Surrounding the lining epithelium, pyloric-type glands aggregated

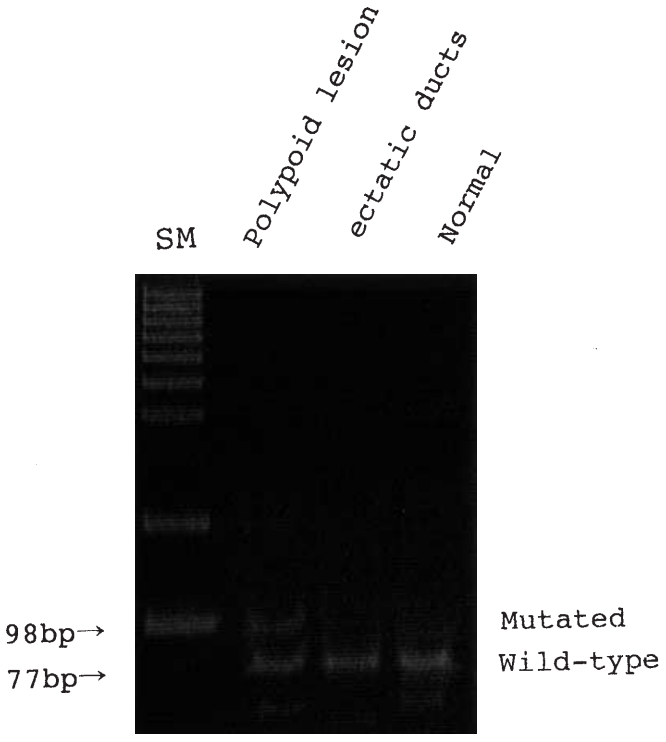

Fig. 4 Mutation analysis of K-*ras*. The persistence of the 98-bp band after *Hpa*II digestion indicated the presence of a K-*ras* codon 12 mutation in the DNA from the polypoid lesion. *SM*, size marker

Histochemical and immunohistochemical findings

Cells composing pyloric-type tubular glands were strongly positive for paradoxical concanavalin A staining (PCS) (Fig. 2 c). Immunohistochemically, these cells were reactive to the monoclonal antibody HIK1083. In contrast to the three control cases of IPMA, most of the epithelial cells lining the ectatic main and branch pancreatic ducts showed a similar staining or reaction pattern (Table 1, Fig. 3c), with the only exception being cells constituting papillary projections. Neither neuroendocrine markers nor hormones were detected in any cells composing pyloric-type glands.

K-*ras* mutation

Alleles with K-*ras* codon 12 mutation were detected in the DNA extracted from the polypoid lesion but not in the DNA from the surrounding ectatic ducts and normal pancreatic tissue (Fig. 4).

Discussion

Pure pyloric gland-type adenoma is a very rare lesion in the pancreas. To our knowledge, only one case has previously been reported [2]. In the present, as well as the previously reported case, a grossly visible polypoid lesion was present in the main pancreatic duct and was composed of closely packed pyloric-type tubular glands. Histochemical and immunohistochemical examinations confirmed that these glands had pyloric gland-type mucin; the glandular cells were strongly positive for paradoxical concanavalin A staining for detecting class III neutral mucin peculiar to gastric pyloric glands and mu-

cous neck cells [4], and they were also stained with monoclonal antibody HIK1083 which specifically recognizes α-linked N-acetylglucosamine residues of class III mucin synthesized in the pyloric glands and mucous neck cells [3]. The presence of alleles with K-*ras* codon 12 mutation supports the neoplastic nature of this lesion. Although this type of adenoma has not been well recognized in the pancreas, it seems to correspond to pyloric gland-type adenoma of the gallbladder [1].

An interesting finding in the present case is that this adenoma arose in the mucin-filled ectatic main duct, part of the lesion of IPMA. Although distinguishing between IPMA and hyperplasia by analysis of K-*ras* mutation alone is difficult [8, 9, 14, 15, 16], this lesion is more likely to be IPMA than hyperplasia based on the finding that nuclei of the columnar epithelial cells were sometimes short, spindle-shaped and closely arranged [7, 11, 12, 13]. This IPMA lesion showed frequent pyloric gland metaplasia or differentiation, i.e., the lining columnar epithelium extended into the surrounding stroma more than it projected toward the ductal lumina, and occasionally it changed into pyloric-type glands. Histochemical and immunohistochemical examinations revealed that cells of the lining epithelium extensively expressed pyloric gland-type mucin. Pyloric gland metaplasia or differentiation was also observed in three control cases of IPMA, but less frequently than in this case. The presence of the IPMA was probably responsible for the occurrence of pyloric gland-type tubular adenoma in this case. Localized proliferation of a deviated clone of IPMA might make an appearance as single tubular adenoma. K-*ras* codon 12 mutation probably occurred in such a clone. In the previously reported case, the adenoma was associated with metaplastic pyloric glands in adjacent tissue [2]. It is postulated that this type of adenoma arises in the background where ductal cells, either non-neoplastic or neoplastic, show a strong tendency to undergo pyloric gland-type metaplasia or differentiation.

Acknowledgements The authors thank Dr. Michio Shimizu, Division of Pathology, Hokkaido University Hospital and Dr. Akio Yanagisawa, Division of Pathology, Cancer Institute, for useful advice.

References

1. Albores-Saavedra J, Vardaman CJ, Vuitch F (1993) Non-neoplastic polypoid lesions and adenomas of the gallbladder. Pathol Annu 28: 145–177
2. Bakotic BW, Robinson MJ, Sturm PDJ, Hruban RH, Offerhaus GJA, Albores-Saavedra J (1999). Pyloric gland adenoma of the main pancreatic duct. Am J Surg Pathol 23: 227–231
3. Ishihara K, Kurihara M, Goso Y, Urata T, Ota H, Katsuyama T, Hotta K (1996) Peripheral α-linked N-acetylglucosamine on the carbohydrate moiety of mucin derived from mammalian gastric gland mucous cells: epitope recognized by a newly characterized monoclonal antibody. Biochem J 318: 409–416
4. Katsuyama T, Ono K, Nakayama J, Kanai M (1985) Recent advances in mucosubstance histochemistry. In: Kawai K (ed) Gastric mucus and mucous secreting cells. Excerpta Medica, Amsterdam, pp 3–18.
5. Klöppel G, Bommer G, Ruckert K, Seifert G (1980) Intraductal proliferation in the pancreas and its relationship to human and experimental carcinogenesis. Virchows Arch A Pathol Anat Histol 387: 221–233
6. Kodama T, Mori W (1983) Morphologic lesions of the pancreatic ducts. Significance of pyloric gland metaplasia in carcinogenesis of the exocrine and endocrine pancreas. Acta Pathol Jpn 33: 645–660
7. Morohoshi T, Kanda M, Asanuma K, Klöppel G (1989) Intraductal papillary neoplasm of the pancreas. A clinicopathologic study of six patients. Cancer 64: 1329–1335
8. Mulligan NJ, Yang S, Andry C, Klein M, O'brien MJ (1999) The role of p21ras in pancreatic neoplasia and chronic pancreatitis. Hum Pathol 30: 602–610
9. Rivera JA, Rall CJN, Graeme-Cook F, del Castillo CF, Shu P, Lakey N, Tepper R, Rattner DW, Warshaw AL, Rustgi AK (1997) Analysis of K-ras oncogene mutations in chronic pancreatitis with ductal hyperplasia. Surgery 121: 42–49
10. Sessa F, Bonato M, Frigerio B, Capella C, Solcia E, Prat M, Bara J, Samloff IM (1990). Ductal cancers of the pancreas frequently express markers of gastrointestinal epithelial cells. Gastroenterol 98: 1655–1665
11. Sessa F, Solcia E, Capella C, Bonato M, Scapa A, Zamboni G, Pellegata NS, Ranzani GN, Rickaert F, Klöppel G (1994) Intraductal papillary-mucinous tumours represent a distinct group of pancreatic neoplasms: an investigation of tumour cell differentiation and K-ras, p53 and c-erbB-2 abnormalities in 26 patients. Virchows Arch 425: 357–367
12. Shimizu M, Itoh H, Okumura S, Hashimoto K, Hanioka K, Ohyanagi H, Yamamoto M, Kuroda Y, Tanaka T, Saitoh Y (1989) Papillary hyperplasia of the pancreas. Hum Pathol 20: 806–807
13. Solcia E, Capella C, Kloppel G (1995) Tumors of the exocrine pancreas. In: Rosai J (ed) Atlas of tumor pathology. Tumors of the pancreas. Armed Forces Institute of Pathology, Washington, DC, pp 53–64
14. Tada M, Ohashi M, Shiratori Y, Okudaira T, Komatsu Y, Kawabe T, Yoshida H, Machinami R, Kishi K, Omata M (1996) Analysis of K-ras mutation in hyperplastic duct cells of the pancreas without pancreatic disease. Gastroenterol 110:227–231
15. Yanagisawa A, Ohtake K, Ohashi M, Hori M, Kitagawa T, Sugano H, Kato Y (1993) Frequent c-Ki-ras oncogene activation in mucous cell hyperplasia of pancreas suffering from chronic inflammation. Cancer Res 53: 953–956
16. Z'graggen K, Rivera JA, Compton CC, Pins M, Werner J, del Castillo CF, Rattner DW, Lewandrowski KB, Rustgi AK, Warshow AL (1997) Prevalence of activating K-ras mutations in the evolutionary stages of neoplasia in intraductal papillary mucinous tumors of the pancreas. Ann Surg 226: 491–500

Virchows Arch (2002) 440:209–214
DOI 10.1007/s004280100504

CASE REPORT

**Antonello Domenico Cabras · Gregor Weirich
Falko Fend · Jörg Nährig · Cesare Bordi
Heinz Höfler · Martin Werner**

Oligoclonality of a "composite" gastric diffuse large B-cell lymphoma with areas of marginal zone B-cell lymphoma of the mucosa-associated lymphoid tissue type

Received: 20 March 2001 / Accepted: 21 June 2001 / Published online: 3 October 2001
© Springer-Verlag 2001

Abstract We analyzed a case of oligoclonal *Helicobacter pylori*-associated, primary gastric diffuse large B-cell lymphoma (DLBCL) with areas of extranodal marginal zone B-cell lymphoma (MZBL) of mucosa-associated lymphoid tissue (MALT) type in a 61-year-old male patient. The patient had two separate tumors, in the corpus and in the antrum, each showing two morphologically distinct components (DLBCL and MZBL of MALT type). To determine the clonal relationship between the large- and small-cell components, we microdissected four samples from morphologically distinct tumor components at both tumor sites. PCR analysis revealed rearranged immunoglobulin heavy chain (IgH) genes of different sizes in three of the four microdissected samples. Cloning and sequencing of the PCR products displayed different IgH gene rearrangements in the two small cell components of the antrum and the corpus. A third genuinely differently rearranged IgH gene was found in the large-cell components of both antrum and corpus. Our results suggest that in primary gastric DLBCL with areas of MZBL of MALT type, the small-cell component may comprise more than one tumor clone. Furthermore, the large-cell component may evolve independently from coexisting MZBL.

Keywords Oligoclonality · IgH gene rearrangement · "Composite" lymphoma

A.D. Cabras (✉) · H. Höfler
Department of Pathology,
GSF-National Research Center for Environment and Health,
Ingolstädter Landstrasse 1, 85764, Neuherberg, Germany
e-mail: ad.cabras@lrz.tum.de
Tel.: +49-89-4140-6102, Fax: +49-89-4140-4915

G. Weirich · F. Fend · J. Nährig · H. Höfler · M. Werner
Institut für Allgemeine Pathologie und Pathologische Anatomie,
Technische Universität, München, Germany

C. Bordi
Dipartimento di Patologia e Medicina di Laboratorio,
Universita' degli Studi di Parma, Italy

Introduction

The new World Health Organization (WHO) classification recommends that primary large-cell lymphoma of the stomach be diagnosed as diffuse large B-cell lymphoma (DLBCL) with or without areas of marginal zone B-cell lymphoma (MZBL), of mucosa-associated lymphoid tissue (MALT) type [11]. In DLBCL with areas of MZBL, MALT type, also called "composite" lymphoma [5], the two tumor components are well delineated, separate, or intermingled areas.

The histogenesis of primary gastric DLBCL has not yet been fully clarified. This situation is mainly due to conflicting results concerning the clonal relationship between MZBL of MALT type and DLBCL areas in the few "composite" lymphomas of the stomach. Identical B-cell clones with corresponding immunglobulin heavy chain (IgH) gene rearrangements in both components [3,21] suggested that the DLBCL had developed as a result of clonal progression from a pre-existing MZBL of MALT type. [13]. In contrast, the lack of corresponding B-cell clones in the small- and large-cell areas of a gastric lymphoma analyzed by Matolcsy et al. [16] supported the idea of a de novo origin for the DLBCL of the stomach [6].

We analyzed a case of primary gastric DLBCL with well separated areas of MZBL of MALT type located in the antrum and in the corpus. In a recently published study, we showed that the "composite" tumor in the antrum had a biclonal IgH gene rearrangement in the small- and large-cell components [1]. We have now analyzed the second "composite" tumour in the corpus which also consisted in well-separated areas of DLBCL. Additionally, the mucosa between the two tumors displaying reactive lymphoid infiltrates was examined. The aim of the present study was to investigate the clonal relationship between the small- and the large-cell components of the two anatomically separated tumors.

Material and methods

Material and clinical data

A 61-year-old white patient had two separate tumors in the gastric corpus and antrum, respectively. Both "composite" lymphomas were circumscribed lesions; the distance between these tumors was 4 cm. Two formalin-fixed, paraffin-embedded tissue blocks, i.e., from the antrum and the corpus, were selected after radical gastrectomy. Each tumor block contained a "composite" DLBCL with areas of MZBL of MALT type. The small- and large-cell components were well separated in both tumor blocks. The histological classification was carried out according to defined criteria [11,5] using 5-µm sections stained with hematoxylin & eosin (HE) and Giemsa. The samples were examined by immunohistochemistry for CD20, CD79a, CD3, CD5, CD10, CD23, IgM, IgA, IgD, kappa and lambda light chains, as well as for *Helicobacter pylori* (HP). Additionally, a tissue block of macroscopically normal mucosa between the two tumors was analyzed. This specimen displayed reactive lymphoid infiltrates histologically. No metastases were present in the ten perigastric lymph nodes. The tumor was stage EI2 according to the Musshoff modification of the Ann Arbor classification [18]. The patient had not received chemotherapy and has been without evidence of disease for 120 months.

Preparation of DNA

The tumor cells were isolated under microscopic control by laser capture microdissection (LCM) from two 10-µm tissue sections previously stained with HE for 15 s. LCM was performed using a PixCell laser capture microscope (Arcturus Engineering, Santa Clara, CA) as described previously [8] (Figure1). The small- and large-cell components of the tumors were isolated from the two different tumor blocks, i.e., corpus and antrum (two samples per block) as well as from two reactive lymphoid infiltrates of the normal mucosa between the tumors. In order to investigate whether the dominant clone(s) found in the microdissected samples were also detectable in the entire tissue sections, DNA was isolated from consecutive sections of both blocks without microdissection. DNA quality was assessed by amplification of the β-actin pseudogene [17,9]. A metal block thermal cycler (PTC-200 MJ Research,Inc., Watertown, Massachusetts, USA). was used for all polymerase chain reaction (PCR) experiments.

IgH gene rearrangements

DNA amplification of the rearranged IgH gene was carried out as a semi-nested hot-start PCR according to a published protocol [25]. A monoclonal positive control (nodal diffuse large B-cell lymphoma) and a negative control (H_2O instead of DNA) were always amplified together with the lymphoma samples. Polyclonal control DNA was isolated from paraffin sections of a case of chronic tonsillitis with and without microdissection as described above. The first amplification (external PCR) was carried out on genomic DNA (50 µg/µl) using an upstream consensus primer, FR3A, specific for the corresponding region within the variable region of IgH (VH) framework III, in combination with a downstream primer, LJH, specific for the joining gene (JH). The second amplification (internal PCR) was performed by substituting the LJH primer with a nested consensus primer VLJH, 5′-labeled with TET (4,7,2′,7′-tetra-chloride-6-carboxifluorescein; MWG-Biotech, Ebersberg). The PCR amplificates were electrophoresed on 3% intermediate melting agarose gels (Metaphor, FMC BioProducts, Rockland, USA) followed by DNA visualization with ethidium bromide. The sequences of the primers used are as follows: FR3A: 5′-ACA CGG CCG TGT ATT ACT GT-3′; LJH: 5′-TGA GGA GAC GGT GAC C-3′; VLJH: 5′-GTG ACC AGG GT(A/C/G/T) CCT TGG CCC CAG-3′. For all tumor and control samples, the PCR analyses from the DNA samples obtained with and without tissue microdissection were performed in three independent experiments.

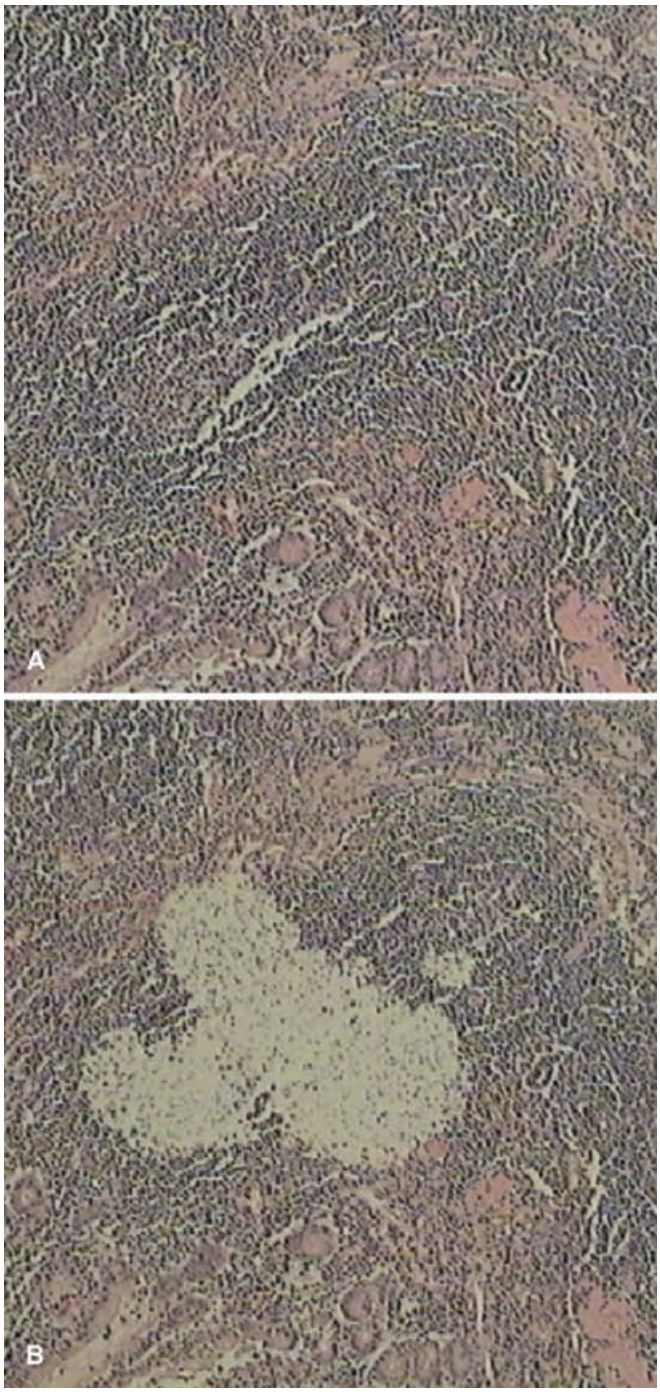

Fig. 1 **a** Marginal zone B-cell lymphoma (MZBL) of mucosa-associated lymphoid tissue (MALT) type component of the corpus before laser capture microdissection. **b** MZBL of MALT type component of the corpus after laser capture microdissection. Original magnification ×40 (**a, b**)

Polyacrylamide gel electrophoresis and fragment analysis

In order to identify the exact length of the clone-specific IgH gene rearrangements, the PCR products were additionally analyzed using an automatic sequencer (ABI PRISM 377, Applied Biosystems, Foster City, CA, USA). For fragment analysis, 1 µl of internal PCR product was mixed with 0.5 µl of loading buffer (25 mM

EDTA, 50 mg/ml of blue dextran), 2.5 µl deionized formamide and 0.5 µl DNA size standard *Genescan*-500 (PE Applied Biosystems, Foster City, CA, USA), labeled with TAMRA (N,N,N′,N′-tetramethyl-6-carboxirodamine) stabilized with 20 mM EDTA (pH 8.0). After denaturing for 5 minutes at 90°C, the samples were separated on denaturing 10% polyacrylamide gels (Long Ranger, FMC BioProducts, Rockland, ME, USA). After electrophoretic separation, the collected data were analyzed using the *Genescan* Analysis Software (Applied Biosystems, Foster City, CA, USA). The length of the PCR amplificates (in basepairs) was calculated using a DNA size standard which co-migrated in every lane. The height of and the area beneath each detected peak were proportional to the concentration of the amplified fragments.

Sequencing of the CDR3 region

The PCR products were purified by agarose gel electrophoresis followed by extraction of the specific DNA band using a QIAquick Gel extraction kit (QIAGEN GmbH, Hilden, Germany). Purified PCR products were polished using *Pfu* DNA polymerase and ligated in pPCR-Script amp SK(+) cloning vector, which was used for transformation of XL10-Gold Kan ultracompetetent cells according to the manufacturer's protocol (PCR-Script amp cloning kit, Stratagene). For each PCR fragment ten clones were selected and sequenced. The DNA of the clones was purified using a QIAprep Miniprep Kit (QIAGEN GmbH, Hilden, Germany) and cycle sequenced using a T3 primer (5′-AAT TAA CCC TCA CTA AAG GG-3′) specific for the plasmid DNA to obtain the sequence of the complete insert. The cycle sequencing was performed using BIG dye deoxy terminators (Applied Biosystems). Sequencing reactions were separated on polyacrylamide gels in an automated sequencer (ABI 377, Applied Biosystems). The sequences of the expressed D and JH segments were compared with those of the published germline D, DIR, and JH segments using the DNASIS v.2.6 program and the IMGT database [12]. The sequences were aligned using the stringent criteria defined by Corbett et al. [4].

Results

Histopathology and immunophenotyping

Histologically, the tissue sections of the tumors from the corpus and antrum each showed a "composite" lymphoma with well-separated areas of DLBCL and MZBL of MALT type infiltrating deeply into the muscularis propria. Pathognomonic lymphoepithelial lesions were present in the MZBL of MALT type components (Fig. 2). The neoplastic cells of both areas (corpus and antrum) were positive for CD20 and CD79a, and negative for IgM, IgD, IgG, IgA CD3, CD5, and CD23 by immunohistochemistry. The MZBL of MALT type of the antrum showed a kappa light-chain restriction and the DLBCL

Fig. 2a–d Composite lymphoma. **a** Marginal zone B-cell lymphoma (MZBL) of mucosa-associated lymphoid tissue (MALT) type component (HE staining), **b** diffuse large B-cell lymphoma (DLBCL) component (HE staining), **c** lymphoepithelial lesion (Cytokeratin immunohistochemistry, antibody: clone AE1/AE3, Novocastra, UK; labeled streptavidin-biotin method), and **d** lymphoepithelial lesion (CD20 immunohistochemistry, AB: clone L26, DAKO, Denmark; LSAB-method). Original magnification ×400 (**a–d**)

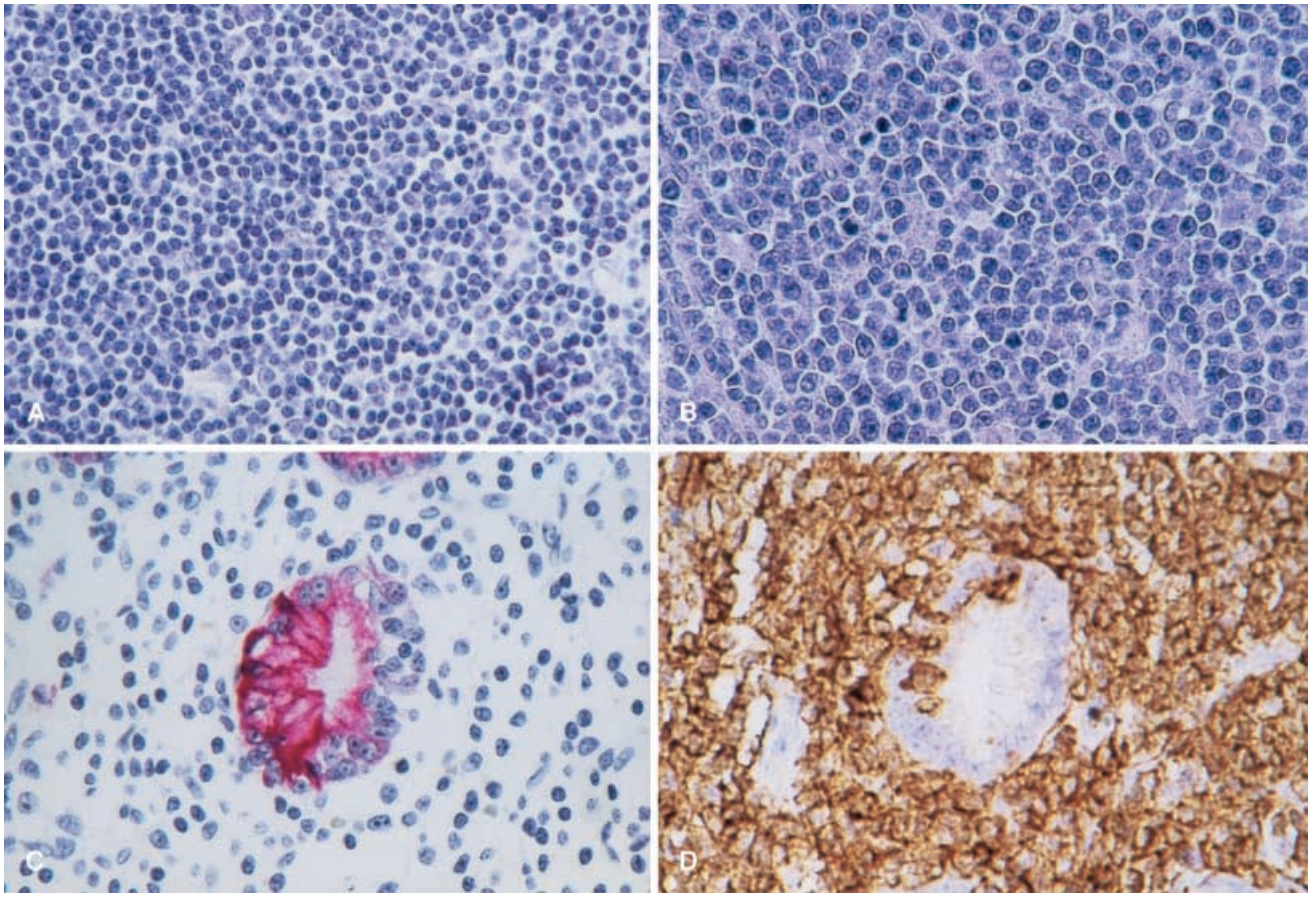

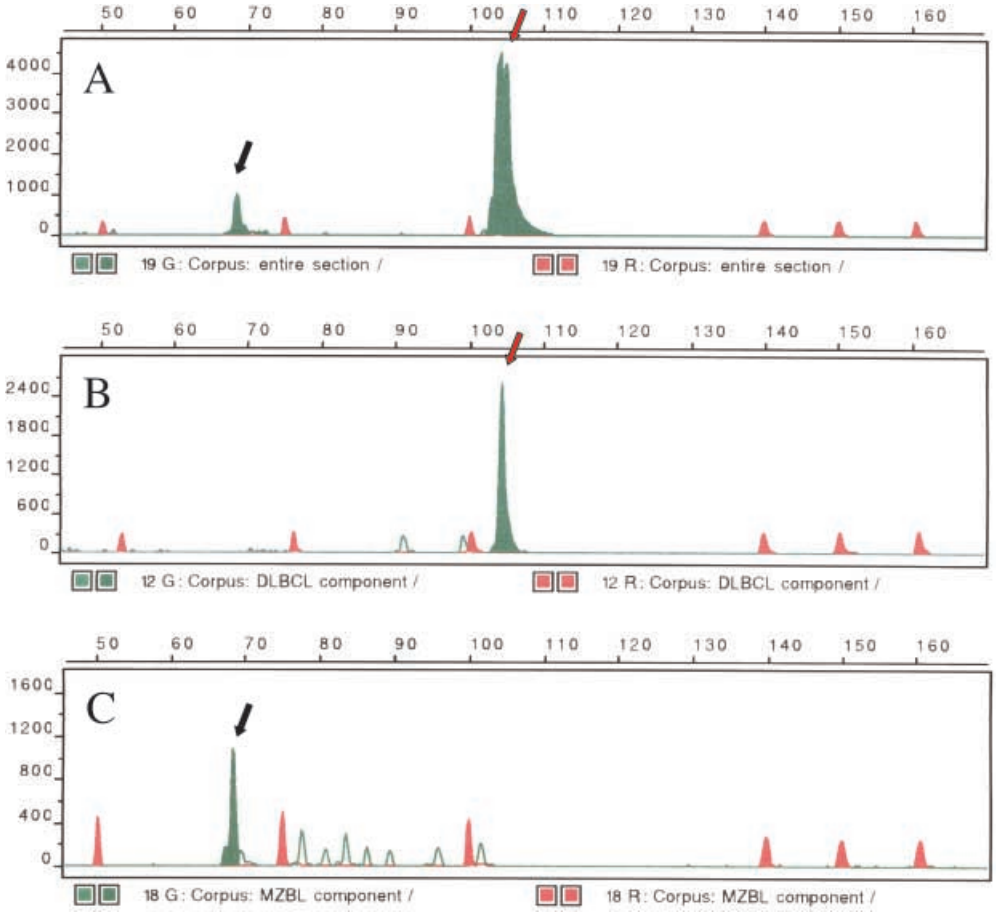

Fig. 3a–c Fragment analysis of frame region 3 polymerase chain reaction products from the corpus. **a** Entire section; **b** microdissected diffuse large B-cell lymphoma (DLBCL) component; **c** microdissected Marginal zone B-cell lymphoma (MZBL) of mucosa-associated lymphoid tissue (MALT)type component. *Red arrows* peaks corresponding to the IgH gene rearrangements of the DLBCL component; *black arrows* peaks corresponding to the IgH gene rearrangements of the MZBL components

components were positive for CD10. HP could be demonstrated by immunohistochemistry (data not shown).

Analysis by agarose gel electrophoresis and *Genescan*

PCR detection of the IgH genes was performed separately from the four morphologically distinct tumor components after LCM, i. e., MZBL, MALT type, and DLBCL components in corpus and antrum, respectively. Metaphor gel analysis of the PCR products showed bands with different sizes in three of four microdissected samples examined. The PCR analyses from whole sections of both tissue blocks without microdissection revealed the two distinct tumor clones in the corpus. In the antrum, however, only the clone of the large-cell component could be detected. *Genescan* fragment analysis confirmed these data. In Fig. 3 are summarized the results of the *Genescan* fragment analysis in the corpus. The reactive lymphoid infiltrates showed a polyclonal pattern (data not shown).

Sequence analysis

Sequence analyses of the cloned PCR products from the four microdissected samples revealed three different rearranged IgH genes. In each of the two MZBL of MALT type components (i.e., the antrum and corpus) the tumor cells had different rearrangements of diversity (D) and JH regions, and contained different VH-(N)-D and D-(N)-JH junctions, thus represented different clones. In contrast, the tumor cells of the DLBCL components present in both tumor blocks had identical rearrangements of diversity (D) and JH regions, and identical VH-(N)-D and D-(N)-JH junctions. They showed no clonal relationship to the two MZBL of MALT type components. The D-regions of these three different sequences showed sequence variations in comparison with the germline sequence. All three sequences were *in-frame*. Figure 4 summarizes these data. The sequence analysis confirmed the polyclonality of the reactive lymphoid infiltrates (data not shown).

Discussion

The coexistence of small- and large-cell components in gastric lymphoma (also called “composite” lymphoma) is a well known phenomenon [6]. The IgH gene rearrangement analysis of our HP-associated, primary gastric “composite” lymphoma revealed that the tumor cells of the corpus and the antrum were only partially genetically related. We found a unique IgH gene rearrangement composed of different D-regions and/or different joining re-

DLBCL component in the antrum and in the corpus

Nucleotide sequences

	VH	N	(D3-22 80%)	N	(D2-8* 81%)	N	(JH3b 90%)
GERMLINE			CTATGATAGT		CATTAGTACAA		CTTTTGATAT
CLONES (1-10)	GCGAGC	GTCTGGGTTTTT	CTATCATACT	GCT	CATTCTTACAA	AGCGTGGGAA	CTCTTGATAT

Amino acid sequence

ASVWVFLSYCSFLQSVGTLD

MZBL component in the antrum

Nucleotide sequences

	VH	N	(D1-26 80%)	N	(JH4 90%)
GERMLINE			TAGTGGGAGCTACTA		TACTTTGACTA
CLONES (1-10)	GCAGCA	TTAA	TGGTGGGACCTCCTA	GA	TCCTTTGACTA

Amino acid sequence

AALMVGPPRSFD

MZBL component in the corpus

Nucleotide sequences

	VH	N	(D3-16 85%)	(JH4 83%)
GERMLINE			GGGGGAG	TGACTA
CLONES (1-10)	ACTGGA	GGGAGCG	GGGGGAC	TGATTA

Amino acid sequence

TGGSGGTD

Fig. 4 Different location of lymphoma infiltrates: tumor-specific sequences of CDR3 gene segments and translated peptides in the four microdissected tumor samples. The sequences are grouped and subdivided into VH, N, D, N, and JH regions. Name of the germline D and JH genes with maximum homology to the segments used in the VDJ joining are shown in the *parentheses* at the appropriate position (overscore). *Underlined*: mismatches with closest germline gene. * D region gene in reverse orientation. For sequence analysis of the antrum see also Cabras et al. [1]

gions in each of the small-cell components. Additionally, these were not clonally related to the large-cell components. Thus, not only were the MZBL of MALT type components of the corpus and of the antrum clonally independent, but even within the same anatomical site each morphologically distinct tumor component (small- and large-cell) appeared to be composed of different coexisting neoplastic clones. In our first analysis [1], where only the small- and the large-cell components of the antrum were analyzed, we classified this "composite" lymphoma as biclonal. The analysis of the small-cell component of the antrum revealed a third malignant clone as a new finding. Indeed, a gastric lymphoma with three different neoplastic clones has never been reported, to the best of our knowledge, and reports of only five biclonal gastric lymphomas have been published so far [1, 16, 27].

Our results are supported by Matolcsy et al. [16] who reported a case of multifocal gastric lymphoma without a clonal link between small- and large-cell components which were characterized by different rearranged IgH genes. Moreover, two distinct neoplastic clones with unique sequences of the rearranged IgH were described in a case of a MZBL of MALT type of the stomach [27]. Apart from primary gastric lymphoma, the coexistence of several genetically distinct neoplastic clones within the same lesion has also been described at nodal or other extranodal sites. Different neoplastic clones with different IgH gene rearrangements in morphologically or immunophenotypically distinct tumor areas has been detected in several nodal "composite" lymphomas [23, 15, 8]. Absence of clonal relationship was also shown in consecutive biopsies of a MZBL of MALT type of the salivary gland [14]. The fact that oligoclonality in the gastric "composite" lymphomas has only rarely been described in the literature may be due to insufficient tissue sampling of the tumor. This is also reflected by our case where only separate analysis of the small- and large-cell components by laser capture microdissection allowed us to detect the two neoplastic clones in the antral tumor.

The association between HP and gastric MZBL of MALT type is well known [26]. HP-associated chronic gastritis may not only show a monoclonal pattern of the IgH gene rearrangement [2, 19], but also microsatellite alterations [20], which indicate that this disease is a prelymphomatous condition. In MZBL of MALT type the presence of somatic hypermutations within the rearranged

IgH have indicated that the neoplastic B-cells originate in a post-germinal center cell [22]. Moreover, the detection of "ongoing mutations" has suggested an important role for antigenic stimulation in the clonal expansion of these tumor cells [7]. The accumulation of further somatic hypermutations, even after eradication of HP, indicates that yet unknown antigens may drive this disease [24]. Clonal selection was already demonstrated in gastric DLBCLs where somatic hypermutations have clearly indicated a previous response of the neoplastic lymphoid cells to an antigenic stimulation [10]. The presence of two separated "composite" tumors in the corpus and in the antrum of our case further suggests that this pathogenic route may have simultaneously triggered B-lymphocytes of the gastric MALT at different anatomical sites, giving rise to two tumors with different neoplastic components. These results challenge the view that, in the gastric "composite" lymphomas, the DLBCL component is always derived from a small-cell precursor [21].

This gastric DLBCL with areas of MZBL of MALT type showed three genuinely different rearranged IgH genes. Thus, phenotypically identical areas may not always be clonally related in these tumors. Moreover, the lack of a clonal relationship between the small and the large cell components suggests that DLBCLs do not necessarily develop always as a clonal progression from a pre-existing low-grade MALT lymphoma, but may have a de novo origin.

References

1. Cabras AD, Candidus S, Fend F, Kremer M, Schulz S, Bordi C, Weirich G, Höfler H, Werner M (2001) Biclonality of gastric lymphomas. Lab Invest (in press)
2. Calvert RJ, Evans PAS, Randerson JA, Jack AS, Morgan GJ, Dixon MF (1996) The significance of B-cell clonality in gastric lymphoid infiltrates. J Pathol 180:26–32
3. Chan JK, Ng CS, Isaacson PG (1990) Relationship between high-grade lymphoma and low-grade B-cell mucosa-associated lymphoid tissue lymphoma (MALToma) of the stomach. Am J Pathol May 136:1153–1164
4. Corbett SJ, Tomlinson IA, Sonnhammer ELL, Buck D, Winter G (1997) Sequence of the immunoglobulin diversity (D) segment locus: a systematic analysis provides no evidence for the use of DIR segments, inverted D segments, "minor" D segments or D-D recombination. J Mol Biol 270:587–597
5. De Wolf-Peeters C, Achten R (1999) The histogenesis of large-cell gastric lymphomas. Histopathology 34:71–75
6. De Wolf-Peeters C, Tierens A (1998) Controversies in MALT lymphoma classification, low and high grade. Histopathology 32:277–278
7. Du M, Diss TC, Xu C, Peng H, Isaacson PG, Pan L (1996) Ongoing mutation in MALT lymphoma immunoglobulin gene suggests that antigen stimulation plays a role in the clonal expansion. Leukemia 10:1190–1197
8. Fend F, Quintanilla-Martinez L, Kumar S, Beaty MW, Blum L, Sorbara L, Jaffe ES, Raffeld M (1999) Composite low grade B-cell lymphomas with two immunophenotypically distinct cell populations are true biclonal lymphomas. A molecular analysis using laser capture microdissection. Am J Pathol 154:1857–1866
9. Ghossein RA, Ross DG, Salomon RN, Rabson AR (1994) A search for mycobacterial DNA in sarcoidosis using the polymerase chain reaction. Am J Clin Path 101:733–737
10. Hallas C, Greiner A, Peters K, Muller-Hermelink HK (1998) Immunoglobulin VH genes of high-grade mucosa-associated lymphoid tissue lymphomas show a high load of somatic mutations and evidence of antigen-dependent affinity maturation. Lab Invest 78:277–287
11. Harris NL, Jaffe ES, Diebold J, Flandrin G, Muller-Hermelink HK, Vardiman J, Lister TA, Bloomfield CD (1999) World Health Organization classification of neoplastic diseases of the hematopoietic and lymphoid tissues: report of the clinical advisory committee meeting, Airlie House, Virginia, November 1997. J Clin Oncol 17:3835–3849
12. Lefranc MP, Giudicelli V, Ginestoux C, Bodmer J, Muller W, Bontrop R, Lemaitre M, Malik A, Barbie V, Chaume D (1999) IMGT, the international ImMunoGeneTics database. Nucleic Acids Res 27:209–212
13. Isaacson PG. (1996) Recent developments in our understanding of gastric lymphomas. Am J Surg Pathol 20 [Suppl 1]: 1–7
14. Lasota J, Miettinen M (1997) Coexistence of different B-cell clones in consecutive lesions of low-grade MALT lymphoma of the salivary gland in Sjögren's disease. Mod Pathol 10: 872–878
15. Matolcsy A, Casali P, Knowles DM (1995) Different clonal origin of B-cell populations of chronic lymphocytic leukemia and large-cell lymphoma in Richter's syndrome. Ann NY Acad Sci 764 496–503
16. Matolcsy A, Nagy M, Kisfaludy N, Kelényi,G (1999) Distinct clonal origin of low-grade MALT-type and high-grade lesions of a multifocal lymphoma. Histopathology 34:6–8
17. Moos M, Gallwitz D (1983) Structure of two human beta-actin related processed genes one of which is located next to a simple repetitive sequence. EMBO J 2:757–761
18. Musshoff, K (1977) Klinische Stadieneinteilung der Nicht-Hodgkin-Lymphome. Strahlentherapie 153:218–221
19. Nakamura S, Aoyagi K, Furuse M, Suekane H, Matsumoto T, Yao T, Sakai Y, Fuchigami T, Yamamoto I, Tsuneyoshi M, Fujishima M (1998) B-cell monoclonality precedes the development of gastric MALT lymphoma in Helicobacter pylori associated chronic gastritis. Am J Pathol 152:1271–1279
20. Peng H, Chen G, Du MQ, Singh N, Isaacson PG, Pan LX (1996) Replication error phenotype and p53 gene mutation in lymphomas of mucosa-associated lymphoid tissue. Am J Pathol 148: 643–648
21. Peng H, Du M, Diss TC, Isaacson PG, Pan L (1997) Genetic evidence for a clonal link between low and high-grade components in gastric MALT B-cell lymphoma. Histopathology 30: 425–429
22. Qin Y, Greiner A, Trunk MJ, Schmausser B, Ott MM, Muller-Hermelink HK (1995) Somatic hypermutation in low-grade mucosa-associated lymphoid tissue-type B-cell lymphoma. Blood 86:3528–3534
23. Sklar J, Cleary ML, Thielemans K, Gralow J, Warnke R, Levy R (1984) Biclonal B-cell lymphoma. N Engl J Med 311: 20–27
24. Thiede C, Alpen B, Morgner A, Schmidt M, Ritter M, Ehninger G, Stolte M, Bayerdorffer E, Neubauer A (1998) Ongoing somatic mutations and clonal expansions after cure of Helicobacter pylori infection in gastric mucosa-associated lymphoid tissue B-cell lymphoma. J Clin Oncol 16:3822–3831
25. Weirich G, Funk A, Hoepner I, Heider U, Noll S, Pütz B, Fellbaum C, Höfler H (1995) PCR-based assays for the detection of monoclonality in non-Hodgkin's lymphoma: application to formalin-fixed, paraffin-embedded tissue and decalcified bone marrow samples. J Mol Med 73:235–241
26. Wotherspoon AC, Ortiz-Hidalgo C, Falzon MR, Isaacson PG (1991) Helicobacter pylori-associated gastritis and primary B-cell gastric lymphoma. Lancet 338:1175–1176
27. Zucca E, Bertoni F, Roggero E, Bosshard G, Cazzaniga G, Pedrinis E, Biondi A, Cavalli F (1998) Molecular analysis of the progression from Helicobacter pylori-associated chronic gastritis to mucosa-associated lymphoid-tissue lymphoma of the stomach New Engl J Med 338:804–833

Virchows Arch (2002) 440:241–248
DOI 10.1007/s00428-001-0583-8

REVIEW ARTICLE

Burkhard Helpap · Günter Klöppel

Neuroendocrine carcinomas of the prostate and urinary bladder: a diagnostic and therapeutic challenge

Received: 27 April 2001 / Accepted: 12 November 2001 / Published online: 29 January 2002
© Springer-Verlag 2002

Abstract This review addresses the various morphological, immunohistochemical and cell kinetic aspects of pure and mixed neuroendocrine carcinomas of the prostate and urinary bladder and of carcinomas with focal neuroendocrine differentiation. It is important that neuroendocrine tumours of the prostate and urinary bladder be clearly distinguished from their nonneuroendocrine counterparts because of differences in treatment and prognosis. In the case of high-grade neuroendocrine carcinomas, early diagnosis and initiation of appropriate chemotherapy may increase survival and potentially induce complete remission in individual cases.

Keywords Prostate carcinoma · Bladder carcinoma · Neuroendocrine tumours · Immunohistochemistry · Therapy

Introduction

Neuroendocrine neoplasms of the prostate and urinary bladder are rare tumours and therefore not well known [20, 63]. Even if diagnosed correctly, they are often not treated appropriately, because the diagnosis does not sufficiently emphasise the term neuroendocrine neoplasm.

Difficulties in the correct categorisation and treatment may also occur with mixed carcinomas showing a neuroendocrine component combined with usual adenocarcinoma structures. This also holds for prostate adenocarcinoma with scattered neuroendocrine cells. A special neuroendocrine tumour is the paraganglioma that occurs particularly in the wall of the urinary bladder. The biologic significance of this tumour is still not well known [11].

B. Helpap (✉)
Department of Pathology,
Academic Hospital of the University of Freiburg, Postfach 720,
78207 Singen, Germany
e-mail: pathologie@hegau-klinikum.de
Tel.: +49-7731-892100, Fax: +49-7731-892105

G. Klöppel
Department of Pathology, University of Kiel, Germany

This review addresses the various morphologic, immunohistochemical and cell kinetic aspects of the neuroendocrine tumours of the prostate and bladder and points out appropriate therapeutic strategies. The designations used for the tumours will follow the recent World Health Organization classification of gastroenteropancreatic neuroendocrine neoplasms. Thus well-differentiated neuroendocrine tumours (NET), corresponding to typical carcinoids, are distinguished from well-differentiated neuroendocrine carcinomas (low-grade NEC) and from poorly differentiated neuroendocrine carcinomas (high-grade NEC), including neuroendocrine small cell carcinomas [9, 57].

Well-differentiated neuroendocrine tumours and carcinomas

Well-differentiated NET or NEC in the prostate, also documented as prostatic carcinoids, are extremely rare tumours that occur isolated or combined with typical adenocarcinomas [4, 8, 16, 23, 40, 65]. Similar tumours in the urinary bladder have not yet been reported. Histologically, prostatic NETs and NECs show carcinoid-like features characterised by solid, acinar and cribriform structures formed by cuboidal or columnar cells. In general, these tumours appear to be less differentiated than their counterparts in the gastrointestinal tract [57]. NECs, in contrast to NETs, show either vascular and/or perineural invasion or metastasis to lymph nodes and distant organs [9]. Immunohistochemically, they express chromogranin A and synaptophysin diffusely and strongly in almost all cells. The proliferation index, measured with MIB-1, is low and can help to differentiate these tumours from small foci of undifferentiated malignant solid or trabecular carcinoma of the prostate, which mimic NET but have a high MIB-1 index.

We have observed two patients with low-grade NEC in the prostate. In both patients, aged 68 years and 86 years, the increased prostate volume had caused symptoms that had led to a urological examination. Se-

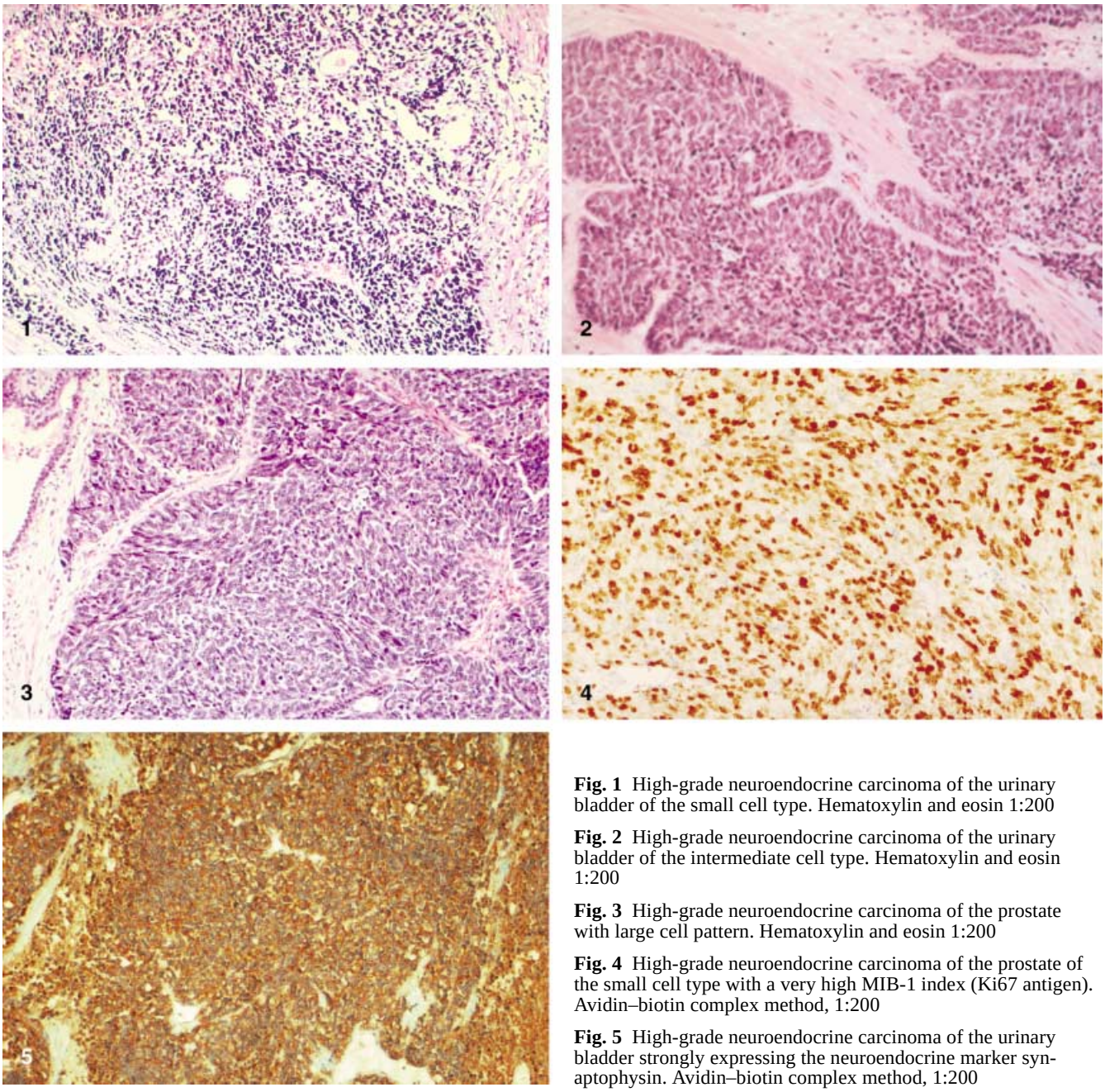

Fig. 1 High-grade neuroendocrine carcinoma of the urinary bladder of the small cell type. Hematoxylin and eosin 1:200

Fig. 2 High-grade neuroendocrine carcinoma of the urinary bladder of the intermediate cell type. Hematoxylin and eosin 1:200

Fig. 3 High-grade neuroendocrine carcinoma of the prostate with large cell pattern. Hematoxylin and eosin 1:200

Fig. 4 High-grade neuroendocrine carcinoma of the prostate of the small cell type with a very high MIB-1 index (Ki67 antigen). Avidin–biotin complex method, 1:200

Fig. 5 High-grade neuroendocrine carcinoma of the urinary bladder strongly expressing the neuroendocrine marker synaptophysin. Avidin–biotin complex method, 1:200

rum prostate-specific antigen (PSA) levels were not elevated. No hormonal symptomatology, such as Cushing's syndrome (reported in one other case with carcinoid-like features [23]) or any expression of endocrine markers in the serum of these patients, was detected. The initial histological analysis yielded the diagnosis of a small cell undifferentiated malignant tumour. This tumour was referred to the consultation service of one of the authors (B.H.) because of the patient's normal PSA level. On the basis of the immunohistological expression of neuroendocrine markers and the moderate proliferative activity, i.e. a moderately increased MIB-1 index, a low-grade NEC was diagnosed. Since the tumour was still limited to the prostate, a radical prostatectomy was performed. A case of a prostatic carcinoid has been reported in a 7-year-old boy who was subsequently diagnosed with multiple endocrine neoplasia type IIb [68].

Poorly differentiated (small cell) neuroendocrine carcinomas

Most NECs of the prostate and almost all NECs of the urinary bladder belong to the poorly differentiated or high-grade category. Compared with all carcinomas of both organs, however, the frequency of high-grade NECs

is very low, ranging from 0.2% to 1.0% [12, 43, 47, 49, 51, 54, 60, 63]. The tumour usually affects patients who are older than 50 years and, in the case of bladder carcinoma, far more men than women. The histological appearance of these tumours resembles that of small cell carcinoma of the lung. The tumour cells are arranged in strands and clusters, are either of oat cell or intermediate type and have hyperchromatic nuclei that lack distinct nucleoli (Fig. 1). Occasionally there is palisading of the peripheral cells of the solid clusters in high-grade NECs of the intermediate type (Fig. 2). A large cell variant may also occur [26] (Fig. 3). The tumours may exhibit a variable degree of necrosis, and the growth pattern is diffusely invasive. An analysis of cell kinetics reveals a MIB-1 proliferation index greater than 80% (Fig. 4). All tumours express synaptophysin, while chromogranin A expression is variable (Fig. 5). High-grade NECs of the prostate are generally negative for PSA and do not express androgen receptors in their nuclei. Occasionally weak PSA expression may be found in isolated groups of cells, a finding that is most likely due to remnants of normal prostatic cells. Rarely, spotty expression of cytokeratin 34βE12 may be seen in high-grade NECs of the urinary bladder. High-grade NECs of the prostate and urinary bladder may be associated with Cushing's syndrome due to the production and secretion of adrenocorticotropic hormone (ACTH), which can be identified immunocytochemically in the tumour cells [20, 23, 46, 67]. Other paraneoplastic syndromes include myasthenic (Eaton-Lambert) syndrome [61], malignant hypercalcemia [38, 48] and a syndrome of inappropriate antidiuretic hormone secretion [24].

The high-grade NECs of the prostate and urinary bladder are still often classified as undifferentiated carcinomas [27, 30, 31]. However, undifferentiated carcinomas have a markedly lower proliferation index and are characterised by PSA expression in the prostate and 34βE12 cytokeratin expression in the urinary bladder. Metastatic high-grade NECs to the prostate or urinary bladder (usually from the lung) are indistinguishable from primary tumours.

Mixed high-grade NECs and adenocarcinomas

Of a series of 27 small cell carcinomas of the prostate, 33% had an additional adenocarcinoma component [43]. Rarely, high-grade NECs may be associated with sarcomatoid and squamous carcinoma components and, in the case of the bladder, with transitional cell carcinomas. In NECs associated with well and poorly differentiated prostatic adenocarcinomas [66], PSA-negative tumour cells of neuroendocrine origin may be seen next to adenocarcinoma components that are positive for PSA. The nuclei of these differentiated prostate carcinoma cells are generally positive for the androgen receptor [27].

Table 1 Outcome of patients treated for neuroendocrine carcinoma of the prostate. *NEC* neuroendocrine carcinoma, *HG* high grade, *LG* low grade, *NEC-AD* with components of glandular adenocarcinoma, *DOD* dead of disease

Author	Patients (*n*)	Diagnosis	Treatment	Survival months	DOD	Outcome
Schron [54]	3	NEC-AD	Chemotherapy	8–25	–	
Oesterling [43]	27	18 NEC 9 NEC-AD	Antiandrogen therapy	17 2–90	22/27	Poor
Moore [41]	50	19 NEC	4 Without therapy, 5 hormone and chemotherapy, 5 hormone, 12 chemotherapy and hormone therapy	2.75	4	Remission
Lo Re [37]	4	NEC-AD	Chemotherapy (cisplatin), radiotherapy		17/19	Remission, partial or complete
Okada [44]	2	NEC-AD	Chemotherapy			
Debras [18]	1	NEC	Chemotherapy (cisplatin, etoposide), radiotherapy	–	–	Complete remission 15 months after diagnosis
Aygum [3]	1	NEC-AD	Chemotherapy, radiotherapy	–	–	Response
Rubenstein [51]	4	1 NEC 3 NEC-AD	Chemo- and hormone therapy	42	4/4	Brief response
Sano [52]	1	NEC	Chemotherapy (cisplatin, etoposide)	3	1/1	–
Buxhofer [7]	1	NEC	High dose chemotherapy, stem cell transplantation	10	1/1	Partial remission
Kanetsuna [32]	1	NEC	Radiotherapy	5	1/1	–
Tsukino [64]	1	NEC HG Meta	Hormone therapy	29	1/1	–
Yu [69]	1	NEC	Chemotherapy	24	1/1	–
Helpap [a]	20 2	NEC HG NEC LG	Hormone therapy 1 Chemotherapy	6.9 2	17/20 –	–

[a] Unpublished data

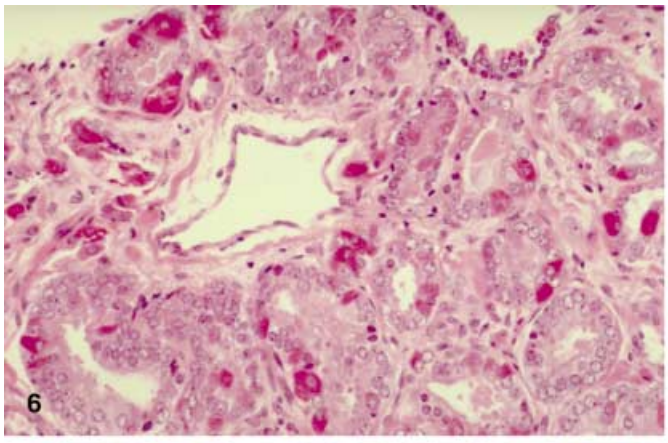

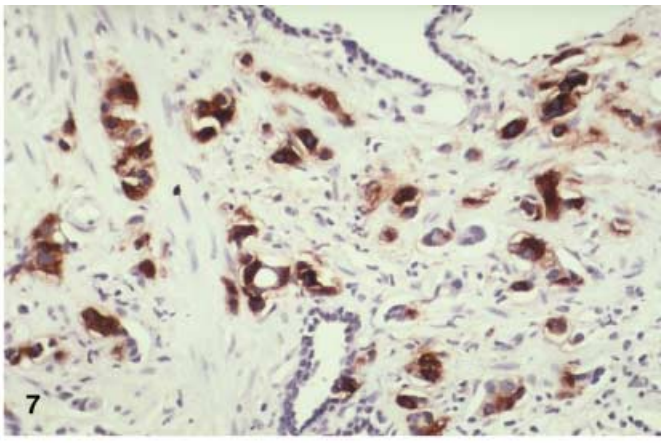

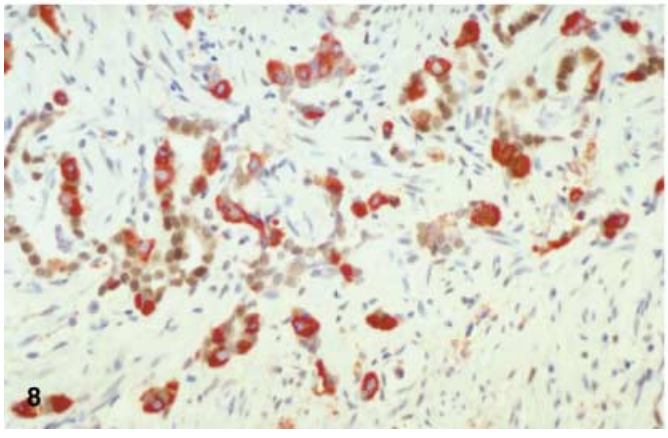

Fig. 6 Adenocarcinoma of the prostate with focal neuroendocrine differentiation ("red cells") within the glands. Hematoxylin and eosin 1:400

Fig. 7 Poorly differentiated adenocarcinoma of the prostate with many chromogranin A-positive neuroendocrine cells. Avidin–biotin complex method, 1:400

Fig. 8 Poorly differentiated adenocarcinoma of the prostate. Double labelling method with chromogranin A (stains the cytoplasm *red*) and nuclear androgen receptor (*brown*). No androgen receptor reaction in chromogranin A positive neuroendocrine cells. Avidin–biotin complex method, 1:400

Table 2 Outcome of patients treated for neuroendocrine carcinoma of the urinary bladder. *NEC* neuroendocrine carcinoma, *HG* high grade, *NEC-AD* with components of glandular adenocarcinoma, *DOD* dead of disease

Author	Patients (*n*)	Diagnosis	Treatment	Survival (months)	DOD	Outcome
Christopher [12]	5	NEC	Chemotherapy	–	3/5	
Yu [69]	1	NEC	Chemotherapy	6	1	
Hailemariam [26]	1	NEC, large cell	Radiotherapy, cysto-prostatectomy	2	1	
Iczkowski [30]	41	21 NEC, 20 NEC-AD	Combination: 20 cystectomy, 14 radiotherapy, 12 chemotherapy	8.8	20/41	11 Patients tumor free
Trias [63]	22	NEC, 20% NEC-AD	Chemotherapy 8/22	6.2	19/22	3 Patients alive with chemotherapy after 6 months
Helpap[a]	16	NEC, HG	1 Cystectomy, 1 chemotherapy	–, 6.9	10/16	

[a] Unpublished data

Prognosis of high-grade NECs

The median survival of patients with high-grade NECs of the prostate is 14 months after diagnosis, with a range of 2–90 months (Table 1). Patients with high-grade NEC of the urinary bladder have a median survival of 6 months after diagnosis (range 1–22 months, Table 2). Since the tumours usually present at an advanced stage, surgical treatment is generally not possible.

Some urologists still choose therapeutic strategies for inoperable high-grade NECs of the prostate that are analogous to those used for typical adenocarcinomas of the prostate, i.e. the patients are treated by blocking androgen receptors. In tumours of the so-called mixed type, this hormone therapy may lower the initially elevated PSA to normal levels, although the prostatic tumour continues to grow because the high-grade portion of the carcinoma fails to respond to hormone therapy. Therefore chemotherapy, perhaps in combination with hormone

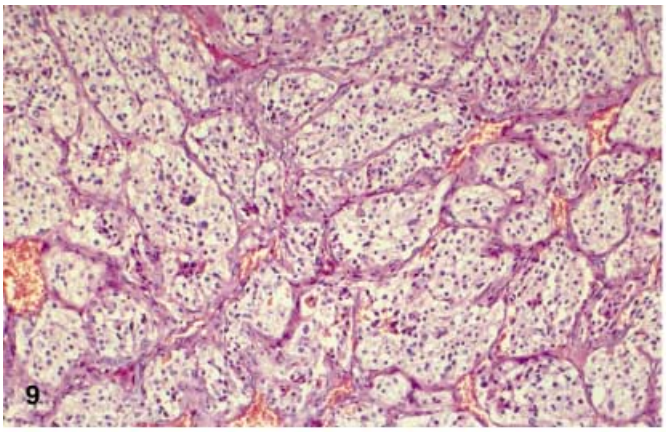

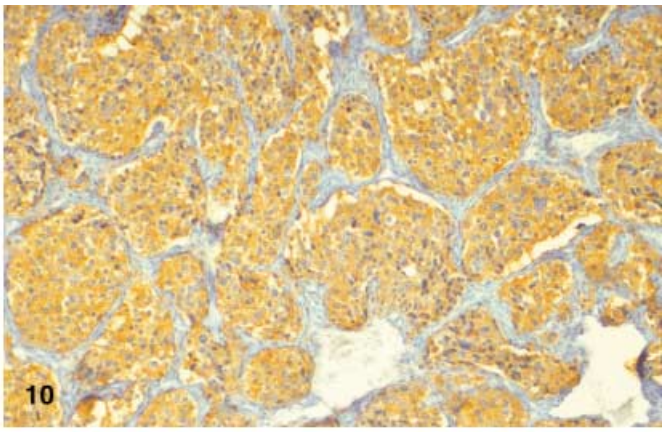

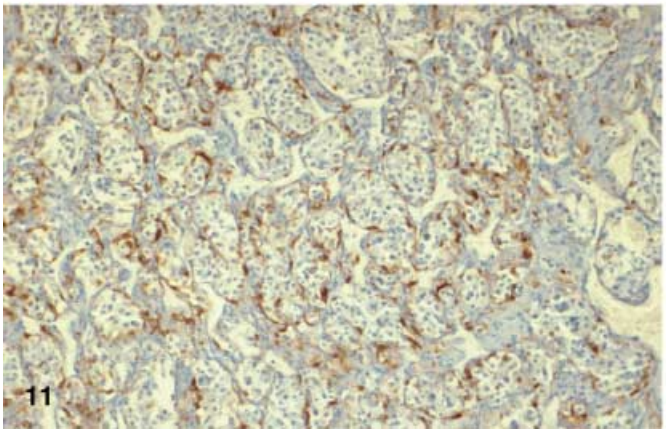

Fig. 9 Extraadrenal paraganglioma of the urinary bladder. Hematoxylin and eosin, 1:200

Fig. 10 Extraadrenal paraganglioma of the urinary bladder with chromogranin A positive chief cells. Avidin–biotin complex method, 1:200

Fig. 11 Extraadrenal paraganglioma of the urinary bladder with S-100 protein-positive sustentacular cells. Avidin–biotin complex method, 1:200

therapy, should be initiated. Table 1 and Table 2 show combined data for some patients treated with chemotherapy combined with hormones or by external radiation. In contrast to untreated patients or those who did not receive appropriate therapy for high-grade NECs, whose mean survival period following diagnosis was 7 months, the appropriately treated patients survived much longer, some up to 90 months (Table 1, Table 2). Partial or even complete remissions have been described in isolated cases [7, 18, 37, 41] (Table 1). These therapeutic successes should prompt the physician to treat high-grade NECs even in advanced stages with chemotherapy despite the dismal prognosis. However, the tumour must be unequivocally classified as a high-grade NEC if the treatment is to be successful.

Adenocarcinoma of the prostate with focal neuroendocrine differentiation

Almost all adenocarcinomas of the prostate contain isolated neuroendocrine cells similar to benign prostate hyperplasia (Fig. 6). Occasionally prostate adenocarcinomas display a great number of neuroendocrine cells (Fig. 7). Carcinomas with scattered neuroendocrine cells, however, which do not exist in the bladder, have nothing in common with low- or high-grade NECs. The neuroendocrine tumour cells in adenocarcinomas seem to develop from atypical secretory tumour cells and are able to express hormones (serotonin, calcitonin, somatostatin) and prostate specific antigen, in contrast to the cells of high-grade NECs [1, 5, 21, 22]. These neuroendocrine cells are negative for the proliferation marker MIB-1 [5], and they do not express the androgen receptor (Fig. 8) [5, 34]. Therefore they appear to be terminally differentiated, unable to proliferate [9, 28, 42] and probably not amenable to hormone or radiation therapy [20]. Their prognostic impact is still unclear. According to some authors, adenocarcinomas of the prostate with many neuroendocrine cells may possibly represent a group of hormone-resistant carcinomas (nonresponders), which progress more rapidly than those with only a few neuroendocrine cells [2, 10, 14, 15, 35]. In these cases it is possible that the density of the neuroendocrine differentiated tumour cells increased during hormone treatment, in comparison with the initial diagnostic biopsy before therapy [10]. Other studies, including our own data, failed to demonstrate an impact on survival [6, 13]. In the most recent study on the prognostic significance of neuroendocrine differentiation, proliferation activity and androgen receptor expression in prostate carcinoma, Segawa and coworkers [55] found that the focal neuroendocrine differentiation of prostate carcinoma is not a prognostic factor.

Paragangliomas

Extraadrenal paragangliomas of the urinary bladder and prostate are, like NETs and NECs of these organs, rare. Groups of paraganglionic cells can be demonstrated in the wall of the urinary bladder and in the outer regions of the prostate [29, 36, 45, 50, 62] and may give rise to paraganglionic tumours. Paragangliomas are characterised by the typical "zellballen" pattern, showing cells that are positive for the neuroendocrine markers chromogranin A and B, neuron-specific enolase and synaptophysin and sustentacular cells which are positive for S-100 protein (Fig. 9, Fig. 10, Fig. 11) [25, 33, 44, 45, 53]. In the urinary bladder these tumours may look like polyps which can be removed by simple excision. Paragangliomas are sometimes accidental findings after radical cystectomy. The paragangliomas of the urinary bladder often present with hematuria and attacks of hypertension during micturition [2, 17, 19, 59]. In almost 20% of cases they are multifocal intramural tumours of the urinary bladder wall. Cheng et al. [11] analysed 16 patients with paragangliomas of the urinary bladder. Only one patient presented in the T1 stage, nine patients were in T2, two patients in T3 and four patients in T4b. One patient had evidence of distant metastases at diagnosis; another was found to have lymph node metastases. One patient died after 1.5 years. The tumour-suppressor gene *p53* was negative, and the MIB-1 index was 1.5% (0.03–7.0%). Paragangliomas of the prostate have only very rarely been described [39, 56] and seem to be predominantly malignant. The significance of these paraganglionic tumours is not related to the high-grade NECs in either organ. The therapy is surgical excision of the tumour. Neither radiation nor chemotherapy are successful because the tumour cells are terminally differentiated.

Conclusion

The low- and high-grade NECs of the prostate and bladder are not a uniform morphologic group and are so rare that no specific therapeutic concept exists. If possible, surgical excision should be performed. High-grade NEC should be treated by chemotherapy, because most tumours are in advanced clinical stages and curative surgery is impossible. Those cases of NEC of the prostate that are treated with hormones do not respond because the tumour cells have no androgen receptor and do not express PSA. Paragangliomas of either organ are also very rare tumours and should be treated by surgical excision. In cases in which there is hormonal activity with production of catecholamines, blood pressure control is essential in the pre- and postoperative phases [58, 59]. The quantity of scattered neuroendocrine cells in prostatic adenocarcinomas seem to be of no prognostic significance [10, 55], although the cells with neuroendocrine differentiation are insensitive to hormonal or radiotherapy. Radical prostatectomy or, in advanced stages, combined hormonal and chemotherapy are the therapeutic strategy in these cases.

References

1. Abrahamsson PA, Wadström LB, Alumets J, Falkmer S, Grimelius L (1987) Peptide-hormone- and serotonin-immunoreactive tumour cells in carcinoma of the prostate. Pathol Res Pract 182:307
2. Abrahamsson PA, Cockett AT, di Sant'Agnese PA (1998) Prognostic significance of neuroendocrine differentiation in clinically localized prostatic carcinoma. Prostate Suppl 8:37–42
3. Aygun C (1997) Small cell carcinoma of the prostate: a case report and review of the literature. Md Med J 46:353–356
4. Azumi N, Shibuya H, Ishikura M (1984) Primary prostatic carcinoid tumor with intracytoplasmic prostatic acid phosphatase and prostate-specific antigen. Am J Surg Pathol 8:545–550
5. Bonkhoff H, Stein U, Remberger K (1995) Endocrine-paracrine cell types in the prostate and prostatic adenocarcinoma are postmitotic cells. Hum Pathol 26:167–170
6. Bubendorf L, Sauter G, Moch H, Schmid HP, Gasser TC, Jordan P, Mihatsch MJ (1996) Ki67 labelling index: an independent predictor of progression in prostate cancer treated by radical prostatectomy. J Pathol 178:437–441
7. Buxhofer V, Ruckser R, Kier P, Habertheuer KH, Zelenka P, Tatzreiter G, Dorner S, Vedovelli H, Sebesta C, Hinterberger W (2000) High dosage therapy with stem cell transplantation in neuroendocrine carcinoma (in German). Acta Med Austriaca 27[Suppl 52]:37–39
8. Capella C, Usellini L, Buffa R, Frigerio B, Solcia E (1981) The endocrine component of prostatic carcinomas, mixed adenocarcinoma-carcinoid tumours and non-tumour prostate. Histochemical and ultrastructural identification of the endocrine cells. Histopathology 5:175–192
9. Capella C, Heitz PU, Höfler H, Solcia E, Klöppel G (1995) Revised classification of neuroendocrine tumours of the lung, pancreas and gut. Virchows Arch 425:547–560
10. Casella R, Bubendorf L, Sauter G, Moch H, Mihatsch MJ, Gasser TC (1998) Focal neuroendocrine differentiation lacks prognostic significance in prostate core needle biopsies. J Urol 160:406–410
11. Cheng L, Leibovich BC, Cheville JC, Ramnani DM, Sebo TJ, Neumann RM, Nascimento AG, Zincke H, Bostwick DG (2000) Paraganglioma of the urinary bladder: can biologic potential be predicted? Cancer 88:844–852
12. Christopher ME, Seftel AD, Sorenson K, Resnick MI (1991) Small cell carcinoma of the genitourinary tract: an immunohistochemical, electron microscopic and clinicopathological study. J Urol 146:382–388
13. Cohen MK, Arber DA, Coffield KS, Keegan GT, McClintock J, Speights VO Jr (1994) Neuroendocrine differentiation in prostatic adenocarcinoma and its relationship to tumor progression. Cancer 74:1899–1903
14. Cohen RJ, Glezerson G, Haffejee Z, Afrika D (1990) Prostatic carcinoma: histological and immunohistological factors affecting prognosis. Br J Urol 66:405–410
15. Cohen RJ, Glezerson G, Haffejee Z (1991) Neuro-endocrine cells – a new prognostic parameter in prostate cancer. Br J Urol 68:258–262
16. Colby TV (1980) Carcinoid tumor of the bladder. A case report. Arch Pathol Lab Med 104:199–200
17. Davaris P, Petraki K, Arvanitis D, Papacharalammpous N, Morakis A, Zorzos S (1986) Urinary bladder paraganglioma (U.B.P.). Pathol Res Pract 181:101–106
18. Debras B, Chautard D, Delva R, Pabot du Chatelard P, Guyetant S, Soret JY (1994) Small cell carcinoma of the prostate. Complete remission after chemoradiotherapy: apropos of a case (in French). Prog Urol 4:569–571

19. Dennis PJ, Lewandowski AE, Rohner TJ Jr, Weidner WA, Mamourian AC, Stern DR (1989) Pheochromocytoma of the prostate: an unusual location. J Urol 141:130–132
20. di Sant'Agnese PA (2000) Divergent neuroendocrine differentiation in prostatic carcinoma. Semin Diagn Pathol 17:149–161
21. di Sant'Agnese PA, de Mesy Jensen KL (1984) Somatostatin and/or somatostatinlike immunoreactive endocrine-paracrine cells in the human prostate gland. Arch Pathol Lab Med 108:693–696
22. Fetissof F, Bruandet P, Arbeille B, Penot J, Marboeuf Y, Le Roux J, Guilloteau D, Beaulieu JL (1986) Calcitonin-secreting carcinomas of the prostate. An immunohistochemical and ultrastructural analysis. Am J Surg Pathol 10:702–710
23. Ghali VS, Garcia RL (1984) Prostatic adenocarcinoma with carcinoidal features producing adrenocorticotropic syndrome. Immunohistochemical study and review of the literature. Cancer 54:1043–1048
24. Ghandur-Mnaymneh L, Satterfield S, Block NL (1986) Small cell carcinoma of the prostate gland with inappropriate antidiuretic hormone secretion: morphological, immunohistochemical and clinical expressions. J Urol 135:1263–1266
25. Grignon DJ, Ro JY, Mackay B, Ordonez NG, el-Naggar A, Molina TJ, Shum DT, Ayala AG (1991) Paraganglioma of the urinary bladder: immunohistochemical, ultrastructural, and DNA flow cytometric studies. Hum Pathol 22:1162–1169
26. Hailemariam S, Gaspert A, Komminoth P, Tamboli P, Amin M (1998) Primary, pure, large-cell neuroendocrine carcinoma of the urinary bladder. Mod Pathol 11:1016–1020
27. Helpap B, Kollermann J (1999) Undifferentiated carcinoma of the prostate with small cell features: immunohistochemical subtyping and reflections on histogenesis. Virchows Arch 434:385–391
28. Helpap B, Kollermann J, Oehler U (1999) Neuroendocrine differentiation in prostatic carcinomas: histogenesis, biology, clinical relevance, and future therapeutical perspectives. Urol Int 62:133–138
29. Hervonen A, Vaalasti A, Partanen M (1978) Paraganglia of the bladder. J Urol 119:335–337
30. Iczkowski KA, Shanks JH, Bostwick DG (1998) Loss of CD44 variant 6 expression differentiates small cell carcinoma of urinary bladder from urothelial (transitional cell) carcinoma. Histopathology 32:322–327
31. Iczkowski KA, Shanks JH, Allsbrook WC, Lopez-Beltran A, Pantazis CG, Collins TR, Wetherington RW, Bostwick DG (1999) Small cell carcinoma of urinary bladder is differentiated from urothelial carcinoma by chromogranin expression, absence of CD44 variant 6 expression, a unique pattern of cytokeratin expression, and more intense gamma-enolase expression. Histopathology 35:150–156
32. Kanetsuna Y (2000) An autopsy case of prostatic neuroendocrine cell carcinoma and adenocarcinoma initially found by brain and abdominal wall metastasis (in Japanese). Nippon Hinyokika Gakkai Zasshi 91:530–533
33. Kliewer KE, Cochran AJ (1989) A review of the histology, ultrastructure, immunohistology, and molecular biology of extra-adrenal paragangliomas. Arch Pathol Lab Med 113:1209–1218
34. Krijnen JL, Janssen PJ, Ruizeveld de Winter JA, van Krimpen H, Schroder FH, van der Kwast TH (1993) Do neuroendocrine cells in human prostate cancer express androgen receptor? Histochemistry 100:393–398
35. Krijnen JL, Bogdanowicz JF, Seldenrijk CA, Mulder PG, van der Kwast TH (1997) The prognostic value of neuroendocrine differentiation in adenocarcinoma of the prostate in relation to progression of disease after endocrine therapy. J Urol 158: 171–174
36. Leestma JE, Price EB Jr (1971) Paraganglioma of the urinary bladder. Cancer 28:1063–1073
37. Lo Re G, Canzonieri V, Veronesi A, Dal Bo V, Barzan L, Zancanaro C, Trovo M (1994) Extrapulmonary small cell carcinoma: a single-institution experience and review of the literature. Ann Oncol 5:909–913
38. Mahadevia PS, Ramaswamy A, Greenwald ES, Wollner DI, Markham D (1983) Hypercalcemia in prostatic carcinoma. Report of eight cases. Arch Intern Med 143:1339–1342
39. Mehta M, Nadel NS, Lonni Y, Ali I (1979) Malignant paraganglioma of the prostate and retroperitoneum. J Urol 121: 376–378
40. Montasser AY, Ong MG, Mehta VT (1979) Carcinoid tumor of the prostate associated with adenocarcinoma. Cancer 44:307–310
41. Moore SR, Reinberg Y, Zhang G (1992) Small cell carcinoma of prostate: effectiveness of hormonal versus chemotherapy. Urology 39:411–416
42. Noordzij MA, van der Kwast TH, van Steenbrugge GJ, Hop WJ, Schroder FH (1995) The prognostic influence of neuroendocrine cells in prostate cancer: results of a long-term follow-up study with patients treated by radical prostatectomy. Int J Cancer 62:252–258
43. Oesterling JE, Hauzeur CG, Farrow GM (1992) Small cell anaplastic carcinoma of the prostate: a clinical, pathological and immunohistological study of 27 patients. J Urol 147:804–807
44. Okada H, Gotoh A, Ogawa T, Arakawa S, Ohbayashi C, Kamidono S (1996) Two cases of small cell carcinoma of the prostate. Scand J Urol Nephrol 30:503–508
45. Ostrowski ML, Wheeler TM (1994) Paraganglia of the prostate. Location, frequency, and differentiation from prostatic adenocarcinoma. Am J Surg Pathol 18:412–420
46. Partanen S, Asikainen U (1985) Oat cell carcinoma of the urinary bladder with ectopic adrenocorticotropic hormone production. Hum Pathol 16:313–315
47. Podesta AH, True LD (1989) Small cell carcinoma of the bladder. Report of five cases with immunohistochemistry and review of the literature with evaluation of prognosis according to stage. Cancer 64:710–714
48. Reyes CV, Soneru I (1985) Small cell carcinoma of the urinary bladder with hypercalcemia. Cancer 56:2530–2533
49. Ro JY, Tetu B, Ayala AG, Ordonez NG (1987) Small cell carcinoma of the prostate. II. Immunohistochemical and electron microscopic studies of 18 cases. Cancer 59:977–982
50. Rode J, Bentley A, Parkinson C (1990) Paraganglial cells of urinary bladder and prostate: potential diagnostic problem. J Clin Pathol 43:13–16
51. Rubenstein JH, Katin MJ, Mangano MM, Dauphin J, Salenius SA, Dosoretz DE, Blitzer PH (1997) Small cell anaplastic carcinoma of the prostate: seven new cases, review of the literature, and discussion of a therapeutic strategy. Am J Clin Oncol 20:376–380
52. Sano K, Miyai K, Yoshida S (1997) Small cell carcinoma of the prostate: a case report. Int J Urol 4:321–323
53. Schmid KW, Schroder S, Dockhorn-Dworniczak B, Kirchmair R, Totsch M, Bocker W, Fischer-Colbrie R (1994) Immunohistochemical demonstration of chromogranin A, chromogranin B, and secretogranin II in extra-adrenal paragangliomas. Mod Pathol 7:347–353
54. Schron DS, Gipson T, Mendelsohn G (1984) The histogenesis of small cell carcinoma of the prostate. An immunohistochemical study. Cancer 53:2478–2480
55. Segawa N, Mori I, Utsunomiya H, Nakamura M, Nakamura Y, Shan L, Kakudo K, Katsuoka Y (2001) Prognostic significance of neuroendocrine differentiation, proliferation activity and androgen receptor expression in prostate cancer. Pathol Int 51:452–459
56. Shapiro B, Gonzalez E, Weissman A, McHugh T, Markel SF (1997) Malignant paraganglioma of the prostate: case report, depiction by meta-iodobenzylguanidine scintigraphy and review of the literature. Q J Nucl Med 41:36–41
57. Solcia E, Klöppel G, Sobin LH (2000) Histological typing of endocrine tumours, 2nd edn. WHO international histological classification of tumours. Springer, Berlin Heidelberg New York
58. Splinter WM, Milne B, Nickel C, Loomis C (1989) Perioperative management for resection of a malignant non-chromaffin paraganglioma of the bladder. Can J Anaesth 36:215–218

59. Sweetser PM, Ohl DA, Thompson NW (1991) Pheochromocytoma of the urinary bladder. Surgery 109:677–681
60. Tetu B, Ro JY, Ayala AG, Johnson DE, Logothetis CJ, Ordonez NG (1987) Small cell carcinoma of the prostate. Part I. A clinicopathologic study of 20 cases. Cancer 59: 1803–1809
61. Tetu B, Ro JY, Ayala AG, Ordonez NG, Logothetis CJ, von Eschenbach AC (1989) Small cell carcinoma of prostate associated with myasthenic (Eaton-Lambert) syndrome. Urology 33:148–152
62. Thrasher JB, Rajan RR, Perez LM, Humphrey PA, Anderson EE (1993) Pheochromocytoma of urinary bladder: contemporary methods of diagnosis and treatment options. Urology 41:435–439
63. Trias I, Algaba F, Condom E, Espanol I, Segui J, Orsola I, Villavicencio H, Garcia Del Muro X (2001) Small cell carcinoma of the urinary bladder. Presentation of 23 cases and review of 134 published cases. Eur Urol 39:85–90
64. Tsukino H, Nagano M, Takehara T, Hamasuna R, Hasui Y, Osada Y (2001) Small cell carcinoma of the prostate: a case report (in Japanese). Hinyokika Kiyo 47:113–116
65. Wasserstein PW, Goldman RL (1979) Primary carcinoid of prostate. Urology 13:318–320
66. Weaver MG, Abdul-Karim FW, Srigley JR (1992) Paneth cell-like change and small cell carcinoma of the prostate. Two divergent forms of prostatic neuroendocrine differentiation. Am J Surg Pathol 16:1013–1016
67. Wenk RE, Bhagavan BS, Levy R, Miller D, Weisburger W (1977) Ectopic ACTH, prostatic oat cell carcinoma, and marked hypernatremia. Cancer 40:773–778
68. Whelan AJ, Bartsch D, Goodfellow PJ (1995) Brief report: a familial syndrome of pancreatic cancer and melanoma with a mutation in the CDKN2 tumor-suppressor gene. N Engl J Med 333:975–977
69. Yu DS, Chang SY, Wang J, Yang TH, Cheng CL, Lee SS, Ma CM (1990) Small cell carcinoma of the urinary tract. Br J Urol 66:590–595

Virchows Arch (2002) 440:249–260
DOI 10.1007/s00428-001-0572-y

ORIGINAL ARTICLE

Gaetano Magro · Michele Bisceglia · Michal Michal
Vincenzo Eusebi

Spindle cell lipoma-like tumor, solitary fibrous tumor and myofibroblastoma of the breast: a clinico-pathological analysis of 13 cases in favor of a unifying histogenetic concept

Received: 11 May 2001 / Accepted: 5 September 2001 / Published online: 4 January 2002
© Springer-Verlag 2002

Abstract We reviewed the clinico-pathological features of a series of 13 cases of benign spindle stromal tumors (BSSTs) of the breast relating to a basic common theme consisting of a well-circumscribed proliferation of vimentin$^+$/CD34$^+$/BCL-2$^+$/CD99$^+$ spindly to oval-epithelioid cells, variably arranged in haphazard to short fascicular growth pattern, with interspersed thick or thin collagen bands. Morphological variations included atypical mono- or multi-nucleated cells in five cases and a mature lipomatous tumor component, varying from focal to prominent, in eight cases. Based on morphological and immunophenotypical features, a distinction was made between two main subtypes of these tumors – fibroblastic and myofibroblastic. The former subtype included two cases respectively represented by a typical solitary fibrous tumor (SFT) and a neoplasm labeled "spindle-cell lipoma (SCL)-like tumor", closely reminiscent of soft tissue SCL. Both tumors had cells with fibroblastic-like appearance, haphazardly arranged and immunoreactive for vimentin, CD34, BCL-2, and CD99. The latter subtype, comprised nine cases exhibiting evidence of myofibroblastic differentiation (desmin and α-smooth muscle actin) which were classified as myofibroblastomas (MFBs). The remaining two cases were defined as "mixed BSSTs", having typical features of diverse neoplasms, respectively represented by a case of MFB with focal SFT and pleomorphic/SCL-like areas, and SFT with focal MFB-like component. The common basic morpho-immunophenotypical features, the possibility that both fibroblastic and myofibroblastic tumors may contain an additional mature lipomatous component, and the existence of hybrid stages (mixed BSSTs) strongly support the view that such tumors belong to the same category of lesions. We postulate that the precursor of all these neoplasms is the vimentin$^+$/CD34$^+$ cells of the mammary stroma, the well-known inherent plasticity of which to differentiate toward several mesenchymal lines, provides the explanation for the phenotypic heterogeneity of these neoplasms. Accordingly, the encompassing term "benign spindle stromal tumors of the breast" is advocated for such tumors.

Keywords Breast · Myofibroblastoma · Solitary fibrous tumor · Spindle cell lipoma · Mesenchymal tumors · Mammary stroma

Introduction

The first report pointing to the breast as a possible location of benign spindle cell tumors, morphologically resembling spindle cell lipoma (SCL) of soft tissues, was that by Toker et al. in 1981 [65]. We consider such tumors as the herald of the postcoming lesions labeled in the literature with different names such as "benign spindle cell tumor" [7, 39], "spindle cell lipoma" [36, 49, 58], fibroma [9], "solitary fibrous tumor" (SFT) [12, 31, 55], "myofibroblastoma" (MFB) [68], "myogenic stromal tumor" [3, 16, 17], and "atypical variant of leiomyoma" [16, 17]. On the whole, this category of neoplasms has received little attention by clinicians and pathologists so that their distinctive features are not yet well delineated. On the contrary, we feel that their awareness and recognition are crucial for the pathologist in daily practice to avoid confusion with other benign and malignant

G. Magro (✉)
Istituto di Anatomia Patologica, Università di Catania,
Via Biblioteca 4, 95124 Catania, Italy
e-mail: gaetano.magro@tiscalinet.it
Tel.: +39-95-310241, Fax: +39-95-316045

M. Michal
Sikl's Department of Pathology, Medical Faculty Hospital,
Alej Svobody 80, 32318 Pilsen, Czech Republic

M. Bisceglia
Servizio di Anatomia Patologica,
IRCCS-Ospedale "Casa Sollievo della Sofferenza",
Viale Cappuccini, 71013 San Giovanni Rotondo (FG), Italy

V. Eusebi
Dipartimento di Oncologia, Sezione di Anatomia,
Istologia e Citologia Patologica "M Malpighi",
Università di Bologna, Ospedale Bellaria, Via Altura 3,
40139 Bologna, Italy

bland-looking monomorphic spindle cell lesions of the breast such as fibromatosis [14, 69], nodular fasciitis [66], inflammatory myofibroblastic tumor (so-called pseudotumor) [6, 52], reactive spindle cell nodule [21], spindle cell metaplastic (sarcomatoid) carcinoma [1, 19, 54, 63, 70], myoepithelioma (myoepithelial carcinoma) [62, 63], and fibrosarcoma/malignant fibrous histiocytoma [29]. Therefore, we reviewed a series of 13 cases of benign spindle cell stromal tumors (BSSTs) of the breast with the aim of defining their distinctive clinical, histological, and immunophenotypical features. Our findings provide evidence that such tumors belong to the same category of lesions, likely arising from the mammary stroma, for which the comprehensive term "benign spindle stromal tumors" seems to be appropriate.

Materials and methods

Thirteen cases of BSSTs of the breast have been collected at the Institute of Anatomical Pathology, University of Catania (Catania, Italy), Servizio Anatomical Pathology Hospital "Casa Sollievo della Sofferenza" (S. Giovanni Rotondo, Italy)'', and Sikl's Department of Pathology, Medical Faculty Hospital, Pilsen (Czech Republic). Some of these cases had been previously reported in literature as small series or single case reports [39, 40, 41, 42, 43]. The clinical data were obtained from the medical records of patients or contributing pathologists.

Hematoxylin and eosin-stained slides of each tumor were reviewed to assess the following parameters: tumor borders, cell types, cytological atypia, mitotic index, hemorrhage, necrosis, additional cellular components, tumor-related matrix, growth patterns, and vascularization. Due to the double cellular component (spindle and oval-epithelioid cells) found in most tumors, each neoplasm was assigned a specific cell type if the predominant cell represented more than 75% of total (Table 1). The present study also included normal female breast samples (five cases) obtained from reduction mammoplasty specimens.

Immunohistochemical studies were performed using the standard labeled streptavidin–biotin technique, with commercially available reagents (LSAB kit, Dako, Glostrup, Denmark). Briefly, sections were dewaxed in xylene for 15 min, rehydrated and treated with 3% H_2O_2 for 10 min to block endogenous peroxidase activity, followed by a rinse in distilled water and a 15-min washing in 0.01 M phosphate-buffered saline (PBS), pH 7.4.

Incubation with primary antibodies to vimentin, α-smooth muscle actin, desmin, CD34, S-100 protein, pancytokeratins, and BCl-2 protein (monoclonal, all from Dako, Glostrup, Denmark), and to estrogen (ER), progesterone (PR) androgen (AR) receptors and CD99 (monoclonal, from Biogenex, San Ramon, Calif.) was performed overnight at 4°C followed by incubation with the linking antibody (biotinylated anti-mouse immunoglobulins) and the peroxidase-conjugated streptavidin for 20 min at room temperature. Tissue sections for sex steroid hormone receptors BCL-2 and CD99 immunostains were pre-treated by microwaving in citrate buffer (pH 6.0) for antigen retrieval. Peroxidase activity was developed in 3,3′-diaminobenzidine (Sigma) substrate with 0.01% H_2O_2 for 5 min. Slides were counterstained with hematoxylin, dehydrated, and mounted. Negative control sections were incubated with PBS in place of the primary antibodies.

Results

Tumors

Clinical findings

Clinical data are summarized in Table 1. There was no history of trauma to the region of the breast in any patient. Physical examination revealed a discrete, solitary nodular mass, usually firm in consistency, which had been slowly growing during the course of 4 months to 2 years. Tumors occurred in both women (five cases) and men (eight cases) aged 41 years up to 87 years. In most cases, ultrasonography (Fig. 1a) and mammography (Fig. 1b) revealed a 1- to 3.5-cm sized, well-circumscribed and dis-homogeneously solid mass devoid of microcalcifications. In one case (case no. 8) a fine-needle aspiration biopsy was performed with a preoperative diagnosis of MFB.

Clinical follow-up was available in nine cases, ranging from to 12 months to 15 years. The clinical behavior

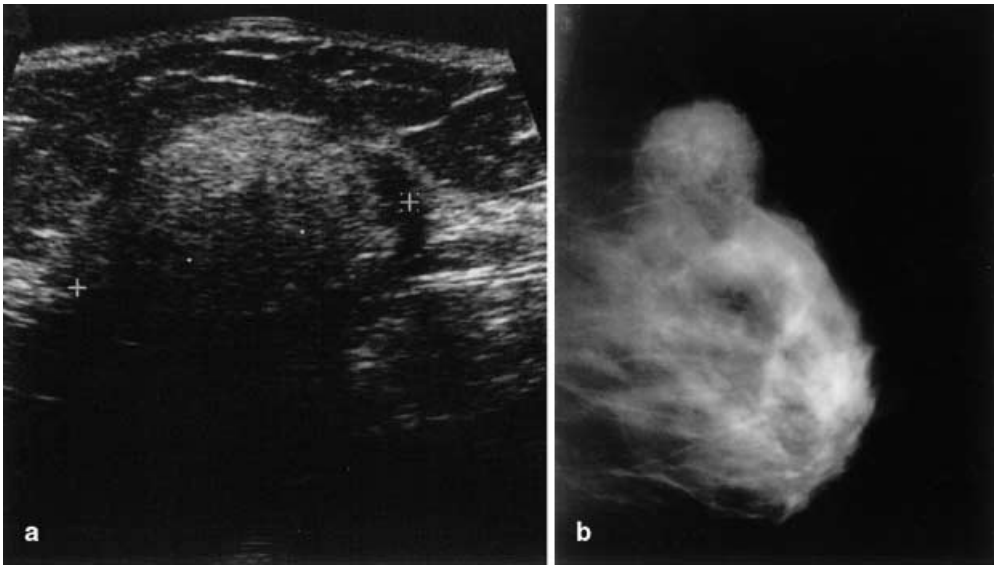

Fig. 1 Case no. 8. Radiological findings of myofibroblastoma (MFB). **a** Ultrasonography revealed a well-circumscribed, dis-homogeneous, 3-cm nodule in the superficial parenchyma of the left breast. **b** Mammographic examination confirmed a nodular and dis-homogeneous mass with circumscribed margins. Hypodense areas within the mass were interpreted as fatty tissue

Table 1 Morphological and immunohistochemical features of the tumors (*Vim* vimentin, *ASMA*?-smooth muscle actin, *ER* estrogen receptor, *PR* progesterone receptors, *AR* androgen receptors, *F* female, *M* male, *SCL* spindle cell lipoma, *SFT* solitary fibrous tumor, *MFB* myofibroblastoma, *PL* pleomorphic lipoma. Immunostaining: +++ diffuse, ++– heterogeneous, +– focal, –– no staining, % percentage of stained cells)

Case	Age (years) and sex	Size (mm)	Tumor borders	Cell types	Atypia	Pattern	Additional components	Matrix	Vim.	CD34	bcl-2	CD99	ASMA	Desmin	ER (%)	PR (%)	AR (%)	Diagnosis
1	60 F	20	Pushing	Spindle	Absent	Haphazard	Predominant fatty component	Fibrous, myxoid	+++	+++	+++	++–	–	–	–	–	–	SCL-like tumor
2	81 M	30	Pushing	Spindle	Absent	Haphazard	Focal fatty component	Fibrous	+++	+++	++–	++–	–	–	–	–	–	SFT
3	49 F	25	Pushing	Epitheliod	Absent	Fascicular, cell clusters	Absent	Fibrous	+++	+++	++–	++–	+++	+++	90	90	60	Epitheliod MFB
4	69 F	20	Pushing	Spindle, epithelioid	Present	Fascicular, cell clusters	Focal fatty component	Fibrous	+++	+–	++–	+++	++-	+++	70	70	–	MFB
5	68 M	25	Pushing	Spindle	Absent	Fascicular	Absent	Fibrous, myxoid	+++	++–	++-	++–	++–	+++	60	80	80	MFB
6	81 M	15	Pushing	Spindle, epithelioid	Present	Fascicular, cell clusters	Focal fatty component	Fibrous	+++	+++	+++	++–	+++	+++	90	90	70	MFB
7	87 M	35	Pushing	Spindle	Absent	Fascicular	Absent	Fibrous	+++	+++	++–	+++	++–	+–	70	80	–	MFB
8	52 F	35	Pushing	Spindle, epithelioid	Absent	Fascicular, cell clusters	Focal fatty component	Fibrous	+++	++–	+–	++–	+++	+++	70	60	60	MFB
9	65 M	25	Pushing	Spindle	Absent	Haphazard	Focal fatty component	Myxoid	+++	++–	+–	+–	+++	+++	30	20	–	Myxoid MFB
10	58 M	36	Pushing	Spindle, epithelioid	Present	Fascicular, haphazard	PL/SCL- and SFT-like areas	Fibrous, myxoid	+++	++–	+–	++–	++–	+–	80	80	–	Mixed tumor: MFB + SFT and PL/SCL components
11	68 M	10	Pushing	Spindle	Present	Haphazard and focally fascicular	Focal fatty component	Fibrous	+++	+++	+++	++–	++–	+–	70	80	–	Mixed tumor: SFT + MFB component
12	45 F	30	Pushing	Spindle, epithelioid	Present	Fascicular	Predominant fatty component	Fibrous	+++	++–	++–	+++	+++	++–	70	70	70	Lipomatous MFB
13	69 M	20	Pushing	Spindle, epithelioid	Present	Fascicular, cell clusters	Predominant fatty component	Fibrous	+++	++–	++–	+++	+++	++–	20	20	10	Lipomatous MFB

was that of a benign tumor in all cases with no recurrence after lumpectomy.

Pathological features

Gross findings

Tumor size ranged from 10 mm to 36 mm in main diameter. Most tumors presented as a single, well-demarcated, firm, unencapsulated or incompletely encapsulated (cases no. 12 and no. 13) mass with an external smooth surface. In most cases the cut surface showed a pale white to grayish mass with a variably whorling appearance; in two cases (no. 12 and no. 13) a lipomatous component was prominent, while myxoid changes predominated in another (no. 9). Calcifications, hemorrhages, and necrosis were not seen.

Histological features

Tumor borders

All tumors had pushing borders and were surrounded by compressed adjacent breast parenchyma. Mammary ducts and lobules were uniformly absent throughout the tumors.

Cell types

Two bland-looking cell types, variably admixed and blending imperceptibly with each other, were identified as spindle and oval-epithelioid cells.

Spindle cells were by far the main basic type, being identified in all but one tumor (case no. 3: epithelioid MFB). Their appearance ranged from fibroblastic-like cells with elongated nuclei and scanty cytoplasm (Fig. 2a, b) to cells with overtly myoid features consisting of moderate to abundant, pale to deep eosinophilic cytoplasm, perinuclear cytoplasmic vacuoles, and nuclei with one or multiple evident small nucleoli (Fig. 2c).

Oval-epithelioid cells were less represented than the spindly ones and variably identified in seven cases, while in one case (no. 3) they were the sole constituent cell type (Table 1). They were oval- to epithelioid-shaped cells with abundant eosinophilic cytoplasm, round to oval and centrally or eccentrically placed nuclei with small evident nucleoli (Fig. 2d and Fig. 3a, b). The cell borders were usually well defined.

Cytological atypia

A variable number of atypical mono- or multi-nucleated spindle and/or epithelioid cells were observed in six cases. Cytological atypia (Fig. 3a, b and Fig. 4b, d) consisted of mild to moderate/severe degree of nuclear pleomorphism. Occasionally multi-nucleated giant cells closely reminiscent of floret-like cells of pleomorphic lipoma of soft tissues were observed (cases no. 3 and no.10) [40].

Mitoses, hemorrhage, and necrosis

Mitoses were absent in all tumors except for two cases (cases no. 10 and no. 11) in which up to two mitoses ×10 HPF were seen. Hemorrhage and necrosis were not identified.

Additional cellular components

Nine cases showed a variable amount of mature lipomatous component, being placed either in the periphery or in the center of tumor. In three cases (no. 1, 12, 13), the fatty component overwhelmed the spindle/epithelioid cellular one, imparting to case no. 1 an aspect closely reminiscent of SCL of soft tissues (Fig. 2a) [39] and to cases no. 12 and no. 13 a distinct nodular or fibromatosis-like growth pattern (cases no. 11, no. 12; Fig. 3c) [43]. In an additional case (no. 10) the lipomatous component was focally pleomorphic, being partly composed of atypical mononucleated and multinucleated cells and floret-like cells similar to those usually observed in pleomorphic lipoma of soft tissues (Fig. 4b).

Tumor-related matrix

Myxoid to hyalinized matrix was detected. The myxoid material which stained with Alcian blue was variably present in amount in four cases, being predominant in case no. 9 (Fig. 3d). The hyalinized component, variably present in all tumors, was represented by either brightly eosinophilic thick or thin collagen bands.

Growth pattern

In most cases (9 of 13), the neoplastic cells displayed myoid appearance and were arranged in short intersect-

Fig. 2 **a** Case no. 1: spindle cell tumor with prominent adipocytic component reminiscent of soft tissue spindle-cell lipoma (SCL). Hematoxylin-eosin; original magnification ×100. **b** Case no. 2: solitary fibrous tumor composed of spindle cells with haphazard to storiform arrangement, singly admixed with collagen fibers. Hematoxylin-eosin; original magnification ×100. **c** Case no. 5: typical myofibroblastoma (MFB) showing cohesive spindle cells without intervening stroma, and with interspersed thick, eosinophilic collagen bands. The cells exhibit overt myoid features such as moderate to abundant eosinophilic cytoplasm and small evident nucleoli. Hematoxylin-eosin; original magnification ×250. **d** Case no. 6: MFB showing desmin$^+$ epithelioid cells arranged in clusters separated by thick collagen bands. Immunohytochemistry; original magnification ×200 ▶

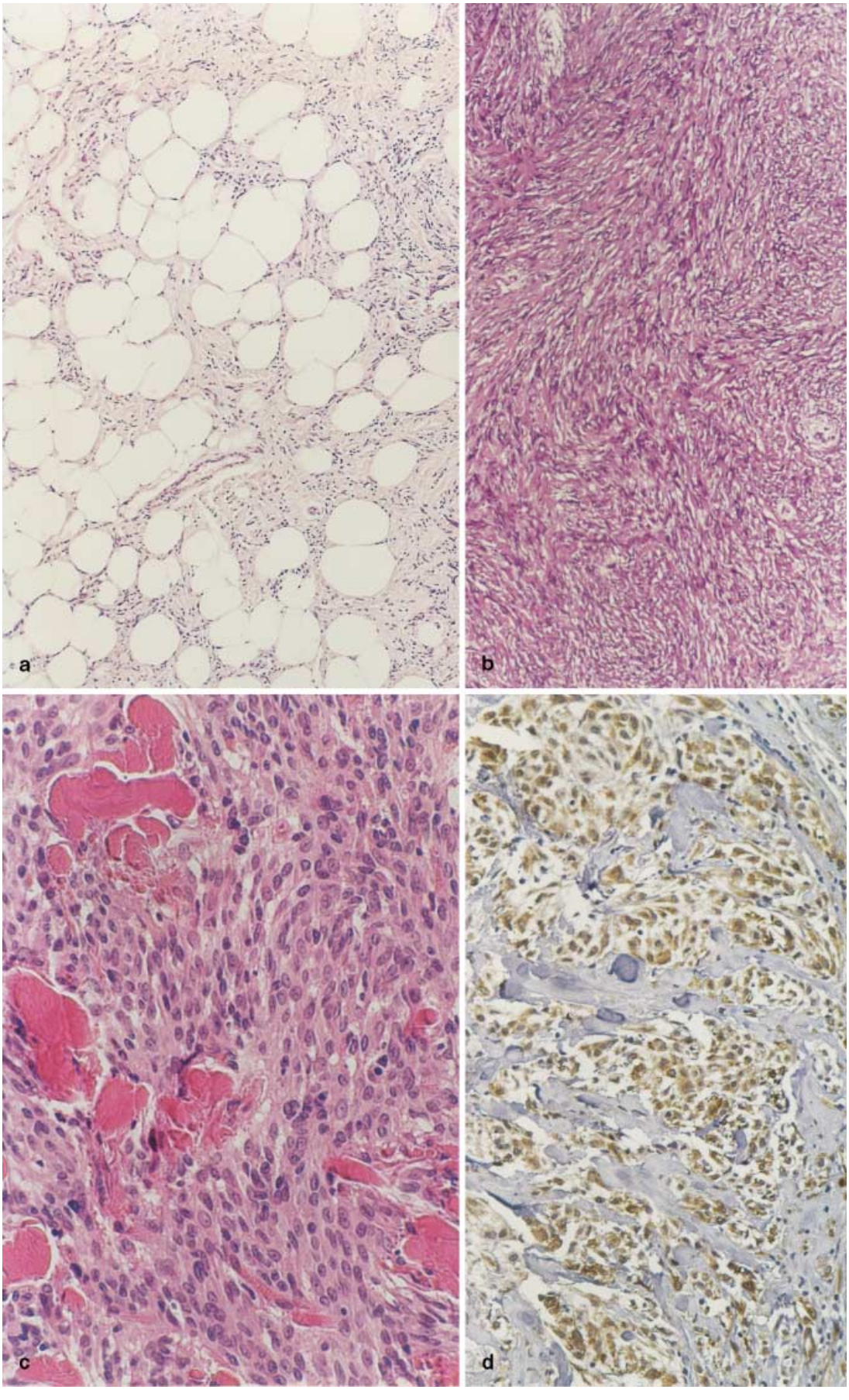
a
b
c
d

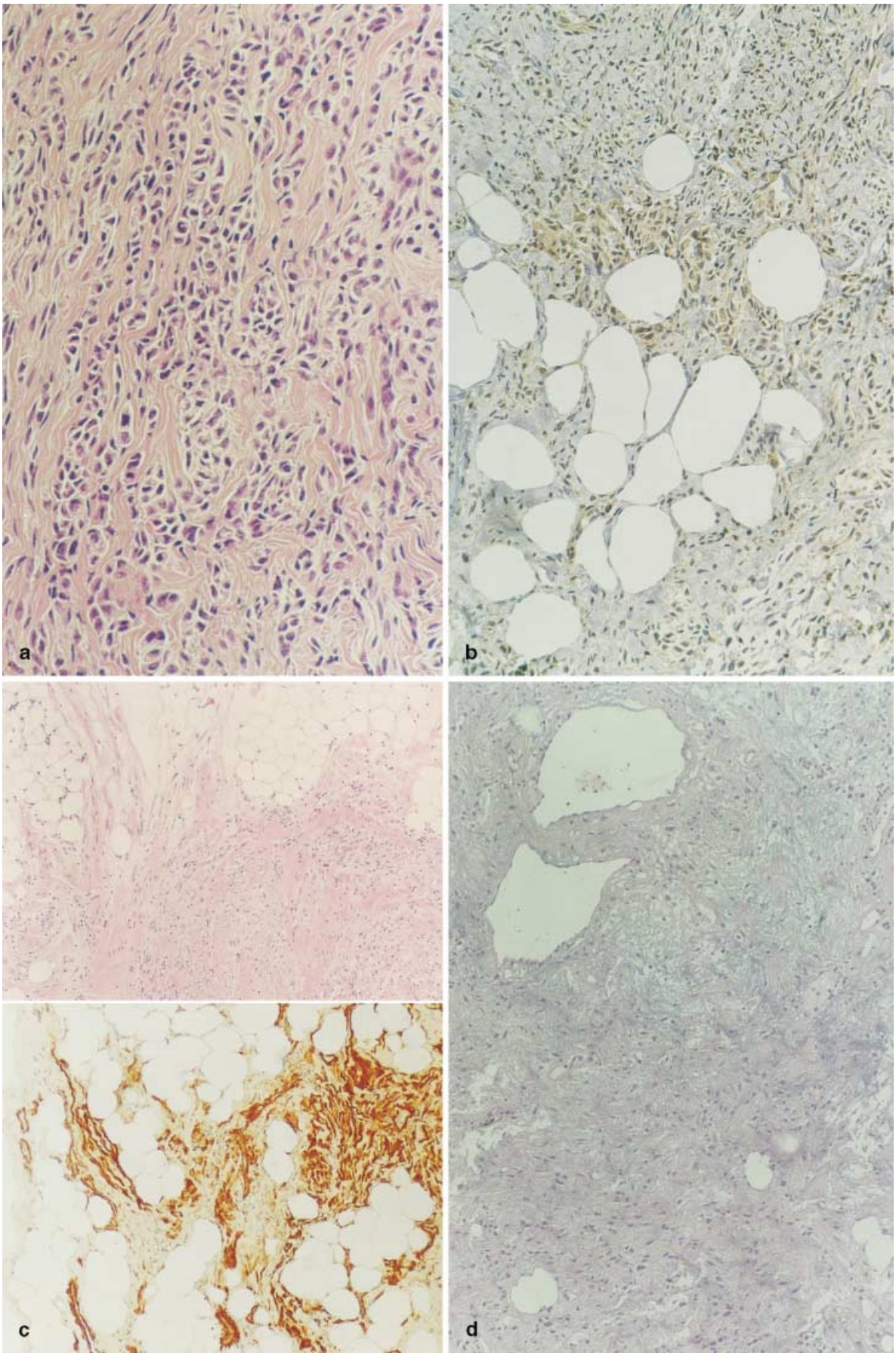

Fig. 3 Legend see page 256

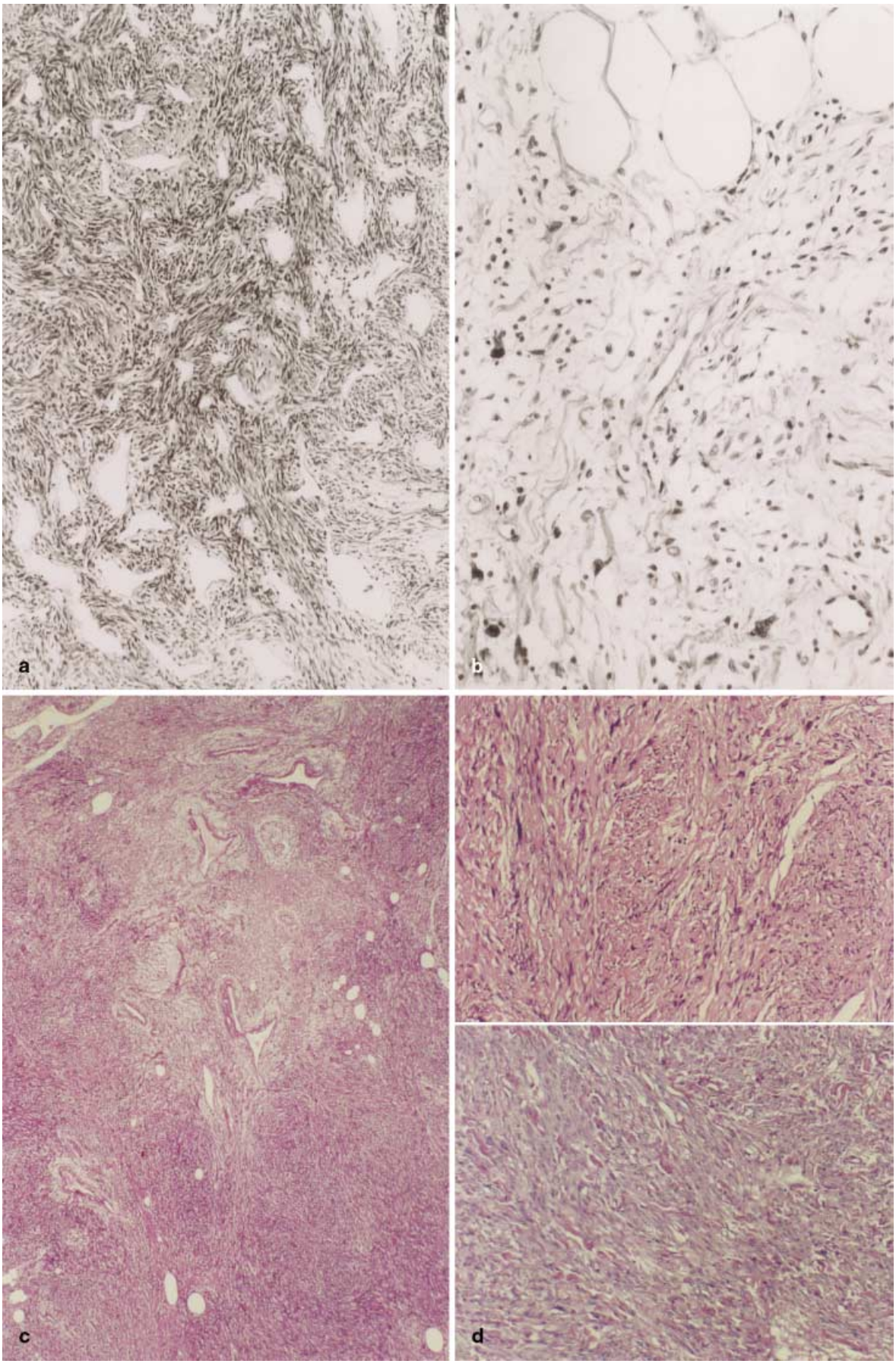

Fig. 4 Legend see page 256

ing fascicles and/or clusters of cohesive cells without intervening stroma, interrupted by thick deeply eosinophilic collagen bands (Fig. 2c). In one case (no. 4), some areas were exclusively composed of atypical epithelioid cells arranged either in single files or as small clusters (Fig. 3a) alternating with islands of adipocytes (Fig. 3b) and resulting in an overall picture resembling that of an infiltrating lobular carcinoma. Only in the remaining four cases, either diffusely (cases no. 1 and no. 2) or focally (cases no. 10 and no. 11), had the cells a solely fibroblastic-like morphology, haphazardly arranged and singly admixed with thin or less frequently thick eosinophilic collagen bands (Fig. 2a, b and Fig. 4a, c, d).

Vascularization

All tumors showed a mild degree of vascular component. Notably, seven cases showed hyalinization and numerous foamy histiocytes in the vascular walls. In one case (no. 10), a vascular hemangiopericytoma-like pattern was seen (Fig. 4a).

Immunohistochemical staining

The results of immunohistochemical stainings are shown in Table 1. Vimentin, CD34, BCL-2 protein, and CD99 (Fig. 3b) were expressed by all tumors, albeit with a variable degree of extension. With the exception of cases no. 1 and no. 2, the other tumors showed additional immunoreactivity for α-smooth muscle actin (Fig. 3c), desmin (Fig. 2d), ER, PR, and AR. Cytokeratins and S-100 protein were consistently negative.

◀ **Fig. 3** **a**, **b** Case no. 4: area composed exclusively of epithelioid cells with moderate to severe degree of nuclear pleomorphism, arranged in Indian files or small clusters separated by eosinophilic collagen bands. Hematoxylin-eosin; original magnification ×200. **b** Atypical epithelioid cells closely admixed with adipocytes are immunoreactive to CD99. Immunohistochemistry; original magnification ×100. **c** Case no. 12: lipomatous myofibroblastoma (MFB). *Top* Spindle cells infiltrate fatty tissue with fibromatosis-like growth pattern. Hematoxylin-eosin; original magnification ×100. *Bottom* Tumor periphery: α-smooth muscle actin$^+$ spindle cells are interspersed among lobules of adipocytes. Immunohistochemistry; original magnification ×100. **d** Case no. 9: myxoid MFB. Spindly cells are embedded within a predominant myxoid matrix. Hematoxylin-eosin; original magnification ×125. This case was positive to myogenic markers

Fig. 4 **a**, **b** Case no. 10. Solitary fibrous tumor (SFT)-like area with typical hemangiopericytoma-like growth pattern (**a** Hematoxylin-eosin; original magnification ×100) and pleomorphic/spindle-cell lipoma (SCL)-like area (**b** Hematoxylin-eosin; original magnification ×200) in an otherwise typical MFB. **c** Case no. 11. Low power of view of SFT. Hematoxylin-eosin; original magnification ×80. **d** Area with the typical features of SFT (*top*) and area with myofibroblastoma (MFB)-like appearance: fascicles of cohesive cells with myoid traits, interrupted by thick collagen bands (*bottom*). Hematoxylin-eosin; original magnification ×125

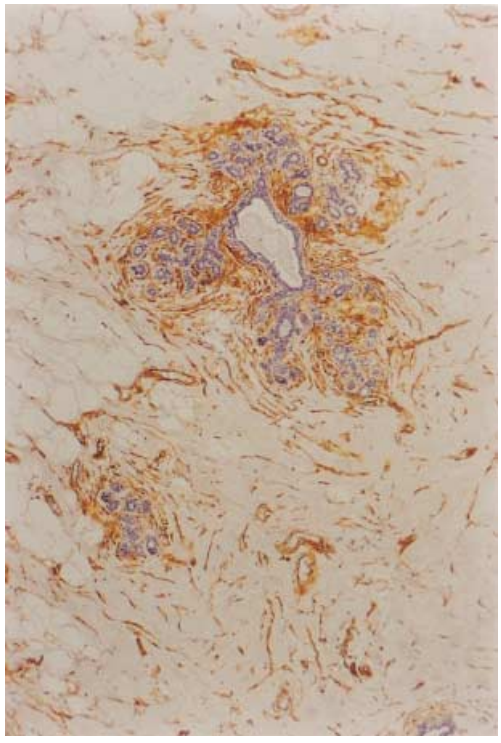

Fig. 5 CD34 stains stromal cells of both intralobular and interlobular mammary stroma. Immunohistochemistry; original magnification ×100

Tumor classification

Most tumors (9 of 13) were classified as MFBs on the basis of their proven myofibroblastic differentiation by means of immunocytochemistry (significant expression of α-smooth muscle actin and desmin) as previously reported [22, 26, 30, 35, 41, 43, 54, 63]. They also exhibited a variable expression of ER, PR, and AR (Table 1).

Two neoplasms (cases no. 1 and no. 2), lacking any evidence of myogenic differentiation, were regarded as fibroblastic in nature and classified as SCL-like tumor and SFT (Table 1), with the former being a bimorphic tumor closely resembling SCL of soft tissues (Fig. 2a) [39]. The latter [42] fulfilled the currently employed morphological and immunoistochemical criteria for pleural and extrapleural SFTs (Fig. 2b) [8, 10, 18, 27, 28, 44, 59].

The remaining two cases were classified as “mixed BSSTs”, having typical features of distinct neoplasms represented within the same lesion. One case (no. 10) was basically a MFB that contained focal SFT-like (Fig. 4a) and pleomorphic/SCL-like areas (Fig. 4b). Notably, SFT-like areas showed a vascular hamangiopericytoma-like pattern, were composed of haphazardly arranged fibroblastic-like cells singly admixed with collagen bands (Fig. 4a), and were lacking any expression of myogenic markers. The other case (no. 11) was basically a SFT with focal MFB-like areas showing the morpho-immunophenotypical features of MFB, such as a myoid

cellular appearances, fascicular arrangement, interspersed broad bands of collagen (4D), and immunoreactivity for myogenic markers.

Normal breast parenchyma

Normal breast parenchyma contained numerous vimentin$^+$/CD34$^+$ fibroblastic-like cells in the lobular and interlobular stroma (Fig. 5) which were occasionally positive for BCL-2.

Discussion

The present series of BSSTs of the breast encompasses a spectrum of lesions sharing several basic common clinical, morphological, and immunophenotypical features that are sufficiently distinctive to warrant their recognition as a distinct family of breast neoplasms. Tumors with similar features had been reported in the literature with different names, frequently used interchangeably, such as "benign spindle cell tumor" [7, 65], "fibroma" [9], "spindle cell lipoma" [49, 58], "solitary fibrous tumor" [12, 31], "myofibroblastoma" [68], "myogenic stromal tumor", or "unusual variant of leiomyoma" [16, 17]. The unifying morphological criterion of all these lesions is a well-circumscribed proliferation of bland-looking spindly to oval-epithelioid cells, haphazardly arranged or forming short fascicles and/or cellular clusters, and variably admixed with thick or less frequently thin collagen bands. Based on the present morphological and immunohistochemical findings, we propose a nosological subdivision into two main subtypes for this category of stromal tumors: the fibroblastic and myofibroblastic BSST of the breast. While both of them have a basic common immunophenotype (vimentin$^+$; CD34$^+$; BCL-2$^+$; CD99$^+$), only the latter type shows additional expression of myogenic markers (α-smooth muscle actin and desmin) and sex steroid hormone receptors (ER, PR, AR).

The fibroblastic tumors in this series were represented by two cases (cases no. 1 and no. 2) classified as SCL-like tumor and SFT, respectively. These tumors were composed exclusively of spindly fibroblastic-like cells haphazardly arranged and alternating with thin collagen fiber bands, and lacking in myogenic markers as well as expression of sex steroid hormone receptors. SFT (case no. 2) exhibited the typical features of pleural and extrapleural SFT and represented the subject of a previous case report [42]. The other fibroblastic tumor (case no. 1), which was also previously separately reported [38], was unusual enough to deserve a specific comment here. It was a bimorphic tumor composed of a mixture of spindly fibroblastic-like cells with a prominent mature lipomatous component, resembling SCL of soft tissues [39]. However, due to the overlapping features between the SCL, mainly the cellular fibrous type, and SFT [10, 37, 54], we prefer the descriptive designation of "SCL-like tumor of the breast" over SCL in that it was not possible to rule out a SFT with fatty component [24, 44, 61].

The myofibroblastic nature of the tumors of the present series was morphologically suspected and immunohistochemically confirmed. Tumors were composed of both spindly and/or oval-epithelioid cells with a morphological myoid appearance and arranged in short fascicles or clusters of cohesive cells without intervening stroma, and interrupted by thick collagen bands, expressing myogenic markers. Notably, the detection of CD99 in MFB is a novel finding which prompted us to include such a tumor in the list of the CD99+ spindle cell tumors, together with SFT, angiofibroma with giant cells, hemangiopericytoma, and synovial sarcoma [53].

Morphological variations on the basic common theme of MFB do exist and could potentially be misinterpreted, particularly in small biopsy specimen or cytology. Potential diagnostic pitfalls are represented by the: (i) detection of atypical cells scattered throughout the tumor or within lipomatous tumor areas [20, 34, 40, 43, 54]; (ii) lipomatous variant that may mimic mainly a primary fibromatosis of the breast [43]; (iii) detection of atypical epithelioid cells arranged in Indian files mimicking an infiltrating lobular carcinoma (case no. 4); and (iv) myxoid variant (case no. 9) that may be potentially confused with other myxoid tumors or tumor-like lesions of the breast.

The differential diagnosis of the BSSTs herein presented includes a wide variety of other benign and malignant bland-looking monomorphic spindle cell lesions of the breast, the morphological and immunohistochemical features of which have been extensively discussed in detail elsewhere [2, 46]. The diagnosis of BSST of the breast is straightforward when the pathologist deals with a circumscribed spindle to epithelioid stromal tumor lacking any epithelial component, with low mitotic activity (<3 mitoses×10 HPF) and devoid of necrosis. The detection of atypical cells is insufficient to warrant a diagnosis of malignancy in this clinicopathological setting, this finding representing likely a degenerative phenomenon similar to what is often observed in other benign spindle cell tumors such as SFT [10], ancient schwannoma, and bizarre leiomyoma. Histology remains pre-eminent in the diagnosis of BSSTs of the breast, and immunocytochemistry may play an important ancillary role in confirming or excluding the presumptive diagnosis.

As far as the histogenesis of the BSSTs of the breast is concerned, we support the view that SCL-like tumor, SFT, and MFB are in the spectrum of a single morpho-biological entity. Arguments in favor of this concept are:

i. All tumors share the same clinical features. They present as a single, painless nodule of the breast, enlarging during the course of a few months or years, usually dis-homogeneously solid and devoid of microcalcifications at ultrasonography and mammography. Their clinical course is invariably benign without evidence of recurrence after lumpectomy.

ii. Grossly, all tumors are well circumscribed and usually unencapsulated nodules, firm in consistency and whitish to gray in color.
iii. Histologically, all tumors have pushing borders and exhibit a common basic theme, i.e., a proliferation of bland-looking vimentin$^+$/CD34$^+$/BCL-2$^+$/CD99$^+$ spindly to oval-epithelioid cells variably admixed with thick or thin collagen bands.
iv. Both fibroblastic tumor (SCL-like tumor and SFT) and MFB may contain variable amounts of mature lipomatous tissue as an integral part of the tumor. In three cases (SCL-like tumor and two MFBs), fatty tissue was predominant over the spindle/epithelioid cell component. Although our SFT had only a few islands of adipocytes, some extrapleural cases with a significant lipomatous component have been described elsewhere [24, 50, 61].
v. Atypical cells, multinucleated floret-like cells, and a predominant myxoid matrix may be encountered in SCL [18], SFT [13, 25, 27, 28], and MFB [34, 40, 43].
vi. SCL-like tumor, SFT, and MFB display a basic common immunophenotype, with neoplastic cells immunoreactive to vimentin, CD34, BCL-2, and CD99 [13, 22, 24, 25, 40, 43], although with a variable degree of expression, especially in MFB.
vii. The existence of ambiguous stages of tumor types (i.e., SCL-like tumor versus SFT with fatty component).
viii. The existence of mixed or hybrid tumors (cases no. 10 and no. 11) composed basically of a MFB with SFT and pleomorphic/spindle cell lipoma-like areas and SFT with MFB-like areas, respectively. These findings confirm previous observations emphasizing the close morphological resemblance among MFB, SFT, and SCL [10, 37, 54, 55] and the possibility that all three tumors may belong to the same category of lesions [10].
ix. Although SFT seems to have a different cytogenetic profile [5, 11], recent studies have demonstrated that MFB of the breast shows the same cytogenetic aberrations of soft tissue SCL [51].

All the above-mentioned observations are strongly in favor of a histogenetic link for the tumors of the present series. As we previously suggested [39, 40, 42, 43], we think that BSSTs arise from a common precursor cell (i.e., the vimentin$^+$/CD34$^+$ cell of the mammary stroma). This is supported by the evidence that the normal intralobular and interlobular mammary stroma contains numerous vimentin$^+$/CD34$^+$ and occasionally BCl-2$^+$ fibroblasts [41, 48, 56, 57, 71], similar to those ubiquitously present in the connective tissues [67]. These cells are considered uncommitted stromal cells and, as such, are endowed with plasticity [42, 48, 60, 67] to undergo multilineage proliferation along different pathways leading to heterogeneous pathological conditions such as SFT and SCL of soft tissues [60], and fibroadenomas, phylloides tumors and pseudoangiomatous hyperplasia in the breast [48]. Another speculative observation suggesting the role of the mammary stroma in tumorigenesis of BSST as a whole is given by the evidence that both fibroblastic and myofibroblastic tumors may contain a variable admixture of two or three lines of differentiation within the same neoplasm such as fibroblastic plus adipocytic in SCL/SCL-like tumor [39, 42, 65], and SFT [24, 44, 50, 61] or fibroblastic plus myofibroblastic (in most cases of MFBs), myofibroblastic plus adipocytic [43] and, as reported elsewhere, myofibroblastic plus smooth muscle [20, 64] or cartilaginous [20, 33, 34, 68] or osseous [33] in rare cases of MFB. This is in accordance with the well-known multidirectional differentiation ability of the mammary stromal cells that may undergo changes in their phenotype in several other breast benign pathological conditions, typical examples of which include fibroadenoma with leiomyomatous component [23, 64], phylloides tumors with fat, bone, cartilage or even skeletal muscle metaplasia [54, 63], hamartomas with adipocytic, smooth muscle, and chondroid stromal components [15, 38, 54], and some breast lesions labeled as "mesenchymoma" in which even three lines of differentiation (e.g., myo-chondro-lipoma) can be documented [4, 32]. Thus, SFT and SCL-like tumors should represent respectively the result of a proliferation of the stromal precursor cell undergoing a fibroblastic-type phenotypic modulation alone or in combination with lipocytic differentitation. However, MFB should reflect the capability of the precursor to acquire an additional myofibroblastic profile along with even other possible cell lines of differentiation. The detection of sex steroid hormone receptors in MFBs but not in the fibroblastic tumors may suggest a hormonal pathogenesis in the former, as previously already reported [41, 47].

Conclusively, the acceptance of a unifying histogene-tic concept for all BSSTs of the breast allows us to regard them as morphological and immunophenotypical variations within a continuous biological spectrum. We believe that the comprehensive term "benign spindle stromal tumor of the breast" is the more appropriate for such category of neoplasms on the basis of their likely origin from mammary stromal cells and in order to distinguish them from other mesenchymal tumors of the breast of different nature, i.e., peripheral nerve sheath tumors. The awareness and recognition of their morphological and immunohistochemical heterogeneity is crucial not only for an accurate nosological classification but mainly for their distinction from other locally aggressive lesions, especially fibromatosis, or other bland looking malignant monomorphic spindle cell tumors.

Acknowledgements We thank Mrs. Antonella Corsaro for expert technical assistance and Mr. Orazio Russo for excellent photographic work.

References

1. Al-Bozom IA, Abrams J (1999) Spindle cell carcinoma of the breast, a mimicker of benign lesions. Case report and review of the literature. Arch Pathol Lab Med 120:1066–1068
2. Al-Nafussi A (1999) Spindle cell tumours of the breast: practical approach to diagnosis. Histopathology 35:1–13
3. Begin LR (1991) Myogenic stromal tumor of the male breast (socalled myofibroblastoma). Ultrastruct Pathol 15:613–622
4. Benisch B, Person B, Sarn J (1976) Benign mesenchymoma of the breast. Mt Sinai J Med 43:530–533
5. Berean KW, Miller RR, Horsman D (1994) Solitary fibrous tumor: cytogenetic analysis (abstract). Mod Pathol 7:149A
6. Bisceglia M, Fusilli S, Zaffarano L, Fiorentino F, Tardio B (1995) Inflammatory pseudotumor of the breast. Case report and literature review. Pathologica 87:59–64
7. Boger A (1984) Benign spindle cell tumor of the male breast. Pathol Res Pract 178:395–398
8. Brunneman RB, Ro JY, Ordonez NG, Mooney J, El-Naggar AK, Ayala AG (1999) Extrapleural solitary fibrous tumor: a clinicopathologic study of 24 cases. Mod Pathol 12:1034–1042
9. Chan KW, Ghadially FN, Alagaratnam TT (1984) Benign spindle cell tumour of breast – a variant of spindle cell lipoma or fibroma of breast? Pathology 16:331–337
10. Chan JKC (1997) Solitary fibrous tumor – everywhere, and a diagnosis in vogue. Histopathology 31:568–576
11. Dal Cin P, Sciot R, Flechter CD (1996) Trisomy 21 in solitary fibrous tumor. Cancer Genet Cytogenet 92:90–91
12. Damiani S, Miettinen M, Peterse JL, Eusebi V (1994) Solitary fibrous tumor (myofibroblastoma) of the breast. Virchows Arch 425:89–92
13. De Saint Aubain Somerhausen N, Rubin BP, Fletcher CD (1999) Myxoid solitary fibrous tumor: a study of seven cases with emphasis on differential diagnosis. Mod Pathol 12:463–471
14. Devouassoux-Shisheboran M, Schammel MDP, Man Y-G, Tavassoli FA (2000) Fibromatosis of the breast. Arch Pathol Lab Med 124:276–280
15. Eusebi V, Cunsolo A, Fedeli F, Severi B, Scarani P (1980) Benign smooth muscle cell metaplasia in breast. Tumori 66:643–653
16. Eyden BP, Ioachim E, Ali HH, Christensen L (1998) Myofibroblastoma of the male breast: a comment on differentiation and terminology. Histopathology 33:576–579
17. Eyden BP, Shanks JH, Ioachim E, Ali HH, Christensen L, Howat AJ (1999) Myofibroblastoma of the breast: evidence favoring smooth-muscle rather than myofibroblastic differentiation. Ultrastruct Pathol 23:249–257
18. Fletcher CDM (ed) (2000) Diagnostic histopathology of tumors, 2nd edn, vol. 2. Churchill Livingstone, London
19. Foschini MP, Dina RE, Eusebi V (1993) Sarcomatoid carcinoma of the breast: proposed definitions for biphasic and monophasic sarcomatoid mammary carcinoma. Semin Diagn Pathol 10:128–136
20. Fukunaga M, Ushigome S (1997) Myofibroblastoma of the breast with diverse differentiations. Arch Pathol Lab Med 121:599–603
21. Gobbi H, TseG, Page DL, Olson SJ, Jensen RA, Simpson JF (2000) Reactive spindle cell nodules of the breast after core biopsy or fine-needle aspiration. Am J Clin Pathol 113: 288–294
22. Gocht A, Bosmuller HC, Bassler R, Tavassoli FA, Moinfar F, Katenkamp D, Schirrmacher K, Luders P, Saeger W (1999) Breast tumors with myofibroblastic differentiation: clinicopathological observations in myofibroblastoma and myofibrosarcoma. Pathol Res Pract 195:1–10
23. Goodman ZD, Taxy JB (1981) Fibroadenomas of the breast with prominent smooth muscle. Am J Surg Pathol 5:99–101
24. Guillou L, Gebhard S, Coindre JM (2000) Lipomatous hemangiopericytoma: a fat-containing variant of solitary fibrous tumor? Clinicopathologic, immunohistochemical, and ultrastructural analysis of a series in favor of a unifying concept. Hum Pathol 31:1108–1115
25. Guillou L, Gebhard S, Coindre JM (2000) Orbital and extraorbital giant cell angiofibroma: a giant cell-rich variant of solitary fibrous tumor? Clinicopathological, immunohistochemical analysis of a series in favor of a unifying concept. Am J Surg Pathol 24:971–979
26. Hamele-Bena D, Cranor HL, Sciotto C, Erlandson R, Rosen PP (1996) Uncommon presentation of mammary myofibroblastoma. Mod Pathol 9:786–790
27. Hasegawa T, Hirose T, Seki K, Yang P, Sano T (1996) Solitary fibrous tumor of the soft tissue. An immunohistochemical and utrastructural study. Am J Clin Pathol 106:325–331
28. Hasegawa T, Matsuno Y, Shimoda T, Hasegawa F, Shimoda T, Sano T, Hirohashi S (1999) Extrathoracic solitary fibrous tumours: their histological variability and potentially aggressive behaviour. Hum Pathol 30:1464–1473
29. Jones MW, Norris HJ, Wargotz ES, Weiss SW (1992) Fibrosarcoma-malignant fibrous histiocytoma of the breast. A clinicopathological study of 32 cases. Am J Surg Pathol 16:667–674
30. Julien M, Trojani M, Coindre JM (1994) Myofibroblastoma of the breast: a study of eight cases. Ann Pathol 14:143–147
31. Khalifa MA, Montgomery EA, Azumi N, Zeman RK, Min KW, Lack EE (1994) Solitary fibrous tumors: a series of lesions, some in unusual sites. South Med J 90:793–799
32. Klouda MJ, Yaremko LM, Howeedy AA, Staren ED (1991) Giant benign mesenchymoma of the breast. Surgery 109:539–542
33. Kobayashi N, Oda K, Yokoi S, Kanda H, Hayakawa S, Tang X, Osamura Y (1996) Myofibroblastoma of the breast: report of a case. Surg Today 26:727–729
34. Lazaro-Santander R, Garcia-Prats MD, Nieto S, Andres-Gozalvo C, Vizcaino V, Vargas-Holguin, Vera-Roman JM (1999) Myofibroblastoma of the breast with diverse histological features. Virchows Arch 434:547–550
35. Lee AHS, Sworn MJ, Theaker JM, Fletcher CDM (1993) Myofibroblastoma of the breast: an immunohistochemical study. Histopathology 22:75–78
36. Lew WYC (1993) Spindle cell lipoma of the breast: a case report and literature review. Diagn Cytopathol 9:434–437
37. Maggio P, Szumigala J, Brooks JJ (1996) CD34 positive spindle cell lipoma: are some cases incipient solitary fibrous tumors (abstract)? Mod Pathol 9:10A
38. Magro G, Bisceglia M (1998) Muscular hamartoma of the breast. Case report and review of the literature. Pathol Res Pract 194:349–355
39. Magro G, Bisceglia M, Pasquinelli G (1998) Benign spindle cell tumor of the breast with prominent adipocytic component. Ann Diagn Pathol 2:306–311
40. Magro G, Fraggetta F, Torrisi A, Emmanuele C, Lanzafame S (1999) Myofibroblastoma of the breast with hemangiopericytoma-like pattern and pleomorphic lipoma-like areas: report of a case with diagnostic and histogenetic considerations. Pathol Res Pract 195:257–262
41. Magro G, Bisceglia M, Michal M (2000) Expression of steroid hormone receptors and their regulated proteins and bcl-2 protein in myofibroblastoma of the breast. Histopathology 36:515–521
42. Magro G, Sidoni A, Bisceglia M (2000) Solitary fibrous tumour of the breast: distinction from myofibroblastoma. Histopathology 37:189–191
43. Magro G, Michal M, Bisceglia M (2000) Lipomatous myofibroblastoma: a potential diagnostic pitfall in the spectrum of the spindle cell lesions of the breast. Virchows Arch 437:540–544
44. Mentzel T, Bainbridge TC, Katenkamp D (1997) Solitary fibrous tumor: clinicopathological, immunohistochemical, and ultrastructural analysis of 12 cases arising in soft tissues, nasal cavity and nasopharynx, urinary bladder and prostate. Virchows Arch 430:445–453

45. Mentzel T, Dry S, Katenkamp D, Fletcher CDM (1998) Low-grade myofibroblastic sarcoma (analysis of 18 cases in the spectrum of myofibroblastic tumors). Am J Surg Pathol 22:1228–1238
46. McMenamin ME, DeSchryver K, Fletcher CDM (2000) Fibrous lesions of the breast. A review. Int J Surg Pathol 8:99–108
47. Morgan MB, Pitha JV (1998) Myofibroblastoma of the breast revisited: an aetiologic association with androgens? Hum Pathol 29:347–351
48. Moore T, Lee AH (2001) Expression of CD34 and bcl-2 in phyllodes tumors, fibroadenomas and spindle cell lesions of the breast. Histopathology 38:62–67
49. Mulvany NJ, Silvester AC, Collins JP (1999) Spindle cell lipoma of the breast. Pathology 31:288–291
50. Nielsen GP, Dickersin GR, Provenzal JM, Rosenberg AE (1995) Lipomatous hemangiopericytoma: a histologic, ultrastructural and immunohistochemical study of a unique variant of hemangiopericytoma. Am J Surg Pathol 31:568–576
51. Pauwels P, Sciot R, Croiset F, Rutten H, Van den Berghe H, Dal Cin P (2000) Myofibroblastoma of the breast: genetic link with spindle cell lipoma. J Pathol 191:282–285
52. Pettinato G, Manivel JC, Insabato L, De Chiara A, Petrella G (1988) Plasma cell granuloma (inflammatory pseudotumor) of the breast. Am J Clin Pathol 90:627–632
53. Renshaw AA (1995) 013 (CD99) in spindle cell tumors. Reactivity with hemangiopericytoma, solitary fibrous tumor, synovial sarcoma, and meningioma but rarely with sarcomatoid mesothelioma. Appl Immunohistochem 3:250–254
54. Rosen PP (ed) (1997) Rosen's breast pathology. Lippincot-Raven, Philadelphia
55. Salomao DR, Crotty TB, Nascimento AG (1997) Myofibroblastoma and solitary fibrous tumors of the breast: histopathological and immunohistochemical comparative study (abstract). Mod Pathol 10:25A
56. Silverman JS, Tamsen A (1996) Mammary fibroadenoma and some phyllodes tumour stroma are composed of CD34+ fibroblasts and factor XIIIa dendrophages. Histopathology 29:411–419
57. Silverman JS, Hamilton J, Tamsen A (1998) Mammary myofibroblastoma: case report and immunohistochemical comparison with stromal hyperplasia showing bimodal CD34+ and Factor XIIIa+ fibrohistiocytic immunophenotype. J Histotechnol 21:335–342
58. Smith DN, Denison CM, Lester SC (1996) Spindle cell lipoma of the breast. A case report. Acta Radiol 37:893–895
59. Suster S, Nascimento AG, Miettinen M, Sickel JZ, Moran C (1995) Solitary fibrous tumors of soft tissue. A clinicopathologic and immunohistochemical study of 12 cases. Am J Surg Pathol 19:1257–126
60. Suster S, Fisher C, Moran CA (1998) Expression of bcl-2 oncoprotein in benign and malignant spindle cell tumors of soft tissue, skin, serosal surfaces, and gastrointestinal tract. Am J Surg Pathol 22:863–872
61. Taccagni G, Sambade C, Nesland J, Terreni MR, Sobrinho-Simoes M (1993) Solitary fibrous tumour of the thyroid: clinicopathological, immunohistochemical and ultrastructural study of three cases. Virchows Arch 422:491–497
62. Tavassoli F (1991) Myoepithelial lesions of the breast. Myoepitheliosis, adenomyoepithelioma and myoepithelial carcinoma. Am J Surg Pathol 15:554–568
63. Tavassoli FA (ed) (1999) Pathology of the breast, 2nd edn. Appleton & Lange, Stamford
64. Thomas TMM, Myint A, Mak CKLM, Chan JK (1997) Mammary myofibroblastoma with leiomyomatous differentiation. Am J Clin Pathol 107:52–55
65. Toker C, Tang CK, Whitely JF, Berkheiser SW, Rachman R (1981) Benign spindle cell breast tumor. Cancer 48:1615–1622
66. Torngren S, Frisell J, Nilsson R, Wiege M (1991) Nodular fasciitis and fibromatosis of the female breast simulating breast cancer. Case report. Eur J Surg 157:155–158
67. Van de Rijn M, Rouse RV (1994) CD34. A review. Appl Immunohistochem 2:71–80
68. Wargotz ES, Weiss, SW, Norris HJ (1987) Myofibroblastoma of the breast. Sixteen cases of a distinctive benign mesenchymal tumor. Am J Surg Pathol 11:493–502
69. Wargotz ES, Norris HJ, Austin RM, Enzinger FM (1987) Fibromatosis of the breast. A clinical and pathological study of 28 cases. Am J Surg Pathol 11:38–44
70. Wargotz WS, Deos PH, Norris HJ (1989) Metaplastic carcinoma of the breast. II. Spindle cell carcinoma. Hum Pathol 20:628–636
71. Ymazaki K, Eyden BP (1995) Ultrastructural and immunohistochemical observations on intralobular fibroblasts of human breast, with observations on the CD34 antigen. J Submicrosc Cytol Pathol 27:309–323

Virchows Arch (2002) 440:261–266
DOI 10.1007/s004280100500

ORIGINAL ARTICLE

**Richard Bachelier · Anne Vincent · Patrice Mathevet
Frédérique Magdinier · Gilbert M. Lenoir
Lucien Frappart**

Retroviral transduction of splice variant *Brca1*-Δ11 or mutant *Brca1*-W1777Stop causes mouse epithelial mammary atypical duct hyperplasia

Received: 6 December 2000 / Accepted: 24 May 2001 / Published online: 22 September 2001
© Springer-Verlag 2001

Abstract We have investigated the effects of the expression of wild-type and mutant *Brca1* alleles on the murine mammary gland morphogenesis and carcinogenesis. Primary cultures of mammary cells from BALB/cByJIco mice were infected with recombinant Babe Puro retroviruses expressing *lac*Z, full-length *Brca1*, splice variant *Brca1*-Δ11, or mutant *Brca1*-W1777Stop alleles. Infected cells were reinjected into the mammary fat pad of a syngeneic virgin mouse whose endogenous epithelium had previously been removed. Four months after reinjection, nulliparous and postlactating mice were checked for the reconstitution of the mammary gland. Stable expression of β-galactosidase was observed in the ducts formed by epithelial mammary cells infected with Babe Puro/*lac*Z retrovirus. Epithelial mammary cells transduced with full-length *Brca1* developed normally, whereas those transduced with *Brca1*-Δ11 or *Brca1*-W1777Stop formed atypical duct hyperplasia associated with reduced branching. These results suggest that ectopically expressed splice variant *Brca1*-Δ11 and mutant *Brca1*-W1777Stop have dominant negative effects.

Keywords Brca1 · Mammary gland morphogenesis · Tumorigenesis

R. Bachelier · A. Vincent (✉) · F. Magdinier · G.M. Lenoir
L. Frappart
Laboratoire de génétique, UMR 5641 CNRS,
Université Claude Bernard Lyon I, Faculté de Médecine,
8 avenue Rockefeller, 69373 Lyon cedex 08, France
e-mail: avincent@rockefeller.univ-lyon1.fr
Tel.: +33-4-78777213, Fax: +33-4-78777220

P. Mathevet
Hôpital Edouard Herriot, Pavillon L,
69437 Lyon cedex 03, France

Present address:
R. Bachelier, National Institutes of Health, Building 10, 9N105,
9000 Rockville Pike, Bethesda, MD 20892, USA

Introduction

Women heterozygous for *BRCA1* germline mutations have a high risk of developing breast or ovarian cancer. Most of the mutations result in premature termination of translation and predicted loss of function of the BRCA1 protein. Moreover, frequent loss of the wild-type allele is observed in the tumors of predisposed patients [15]. These data suggest that *BRCA1* could act as a tumor-suppressor gene. Despite decreased *BRCA1* expression in sporadic breast cancers [11, 19], no *BRCA1* mutation has been detected in these cancers, and few have been found in sporadic ovarian cancers [6].

During murine embryonic development, Brca1 transcripts are mainly expressed in the proliferating tissues of ectodermic and mesodermic origins [9]. Some variations in *BRCA1* expression are associated with the main stages of the mammary gland morphogenesis. In humans, *BRCA1* expression is high in the early stages of prenatal mammary gland development [12]. In the murine mammary gland, the level of *Brca1* messenger RNAs (mRNAs) increases during the puberty and early gestation stages [2, 13]. *Brca1* is required for the murine embryonic development because the germline homozygous invalidation of the murine *Brca1* gene is lethal before gastrulation. Unlike in humans, mice heterozygous for *Brca1* mutation do not develop any cancer [8]. However, a CRE-mediated in-frame excision of exon 11 of the murine *Brca1* gene in epithelial mammary cells results in inhibition of branching and tumor formation, while the introduction of a *p53* +/– background accelerates tumorigenesis [21].

The human and murine *BRCA1* genes encode 220-kDa nuclear proteins of, respectively, 1863 and 1812 amino-acids [9, 14]. Splice variants missing most of exon 11 in humans (*BRCA1*-Δ11b) or the whole exon 11 in mice (*Brca1*-Δ11) encode cytoplasmic proteins of, respectively, 110 kDa [19] and 85 kDa [1]. The full-length BRCA1 protein has been involved in the control

of proliferation of breast epithelial cells [7], maintenance of genomic integrity [17], and transcriptional regulation [4]. In the present studies, we investigated the role of the murine *Brca1* alleles on the mammary gland morphogenesis and carcinogenesis. Recombinant retroviruses expressing full-length *Brca1*, splice variant *Brca1*-Δ11, or mutant *Brca1*-W1777Stop alleles were generated to infect primary cultures of breast epithelial cells. *Brca1*-W1777Stop mimics the human *BRCA1*-R1835Stop mutation, which disrupts the second BRCA1 C-terminal (BRCT) module. Infected cells were reinjected into a cleared fat pad of a syngeneic mouse and examined for morphological alterations.

Materials and methods

Construction of vectors and production of ecotropic viruses

The complementary DNAs (cDNAs) encoding hemagglutinin (HA)-tagged Brca1 and Brca1-Δ11 proteins were cloned as previously described [1]. The murine *Brca1*-W1777Stop mutation (corresponding to human *BRCA1*-R1835Stop) was introduced with the U.S.E. mutagenesis kit (Pharmacia Biotech), using the vector pJ7Ω/*Brca1* as matrix and the following mutagenic primer: 5′-CGTCTTGTGATGTGAGACTGG GTGTTG-3′. The sequence of the mutated *Brca1* cDNA was checked by automatic sequencing.

The *Brca1*-W1777Stop cDNA was amplified with the Expand High-Fidelity PCR System (Roche Diagnostics), with forward primer HA-Brca1: 5′-TTTT**GTCGAC**ATGTATCCTTATGATGT-ACCGGATTATGCGGATTTATCTGCCGTCCAAATTC-3′ and reverse primer 5482R: 5′-GC**GTCGAC**TTAATCATTGGAGTC-TTGTGG-3′.

The HA epitope (YPYDVPDYA) is encoded by underlined nucleotides located at the amino-terminus of Brca1, and bold characters indicate the primers *Sal*I sites. The polymerase chain reaction (PCR) product was subcloned into the retroviral plasmid pBabe Puro after *Sal*I digestion. Replication-defective recombinant retroviruses were obtained by transient calcium phosphate transfection of the retroviral plasmids into the Bosc 23 packaging cell line. Forty-eight hours after transfection, the supernatants were harvested and filtered on 0.45-µm pore-size filters. The titers of the Babe Puro viral stocks were determined by infecting NIH3T3 cells in presence of 8 µg/ml polybrene (Sigma). Retroviral titers were routinely comprised of between 5×10^5 and 1×10^6 colony-forming units (cfu)/ml.

Cell culture and retroviral infections

Cells were grown at 37°C in a 5% CO_2 humidified atmosphere. NIH3T3 and Bosc 23 cell lines were cultured in Dulbecco's modified Eagle's medium (DMEM, Sigma) supplemented with 10% fetal calf serum (FCS, Flobio), penicillin (5 U/ml, Life Technologies), and streptomycin (5 mg/ml, Life Technologies). Primary cultures were prepared by means of collagenase digestion [0.2% collagenase type VIII (Sigma) in DMEM:HAM F-12 1:1] of mammary glands from 10- to 12-week-old female virgin BALB/cByJIco mice for 2 h under gentle shaking. Cells were purified by three sedimentations of 15 min to obtain small segments of ducts (also termed *organoids*) devoid of fat cells and adherent connective tissue. Organoids were plated without further dissociation on 100-mm dishes 24 h before infection and cultured in DMEM:HAM F-12 medium (1:1) containing L-glutamine (200 mM) 10% FCS, gentamycin (50 µg/ml, Sigma), epidermal growth factor (10 ng/ml, Becton Dickinson), cholera toxin (5 ng/ml, Sigma), insulin (5 µg/ml, Becton Dickinson), and hydrocortisone (5 µg/ml, Sigma). Primary cultures were incubated for 8 h in presence of 2×10^6 infectious viral particles in 5 ml complete medium with polybrene (8 µg/ml, Sigma), then covered with fresh medium. The infection step was repeated the following day. Forty-eight hours after the second infection, cells were removed with trypsin, pelleted, and resuspended in 5 µl DMEM:HAM F-12 medium for reinjection. In parallel of each series of infection, we performed control infection with retrovirus expressing the β-galactosidase gene. The efficiency of infection was estimated using X-gal staining.

Mammary gland tissue reconstitution using modified breast epithelial cells

The mammary gland tissue-reconstitution technique was formerly described by Edwards [5]. About 5×10^4 epithelial mammary cells, infected or not, were reinjected using a 25-µl glass microsyringe (Hamilton) into the middle of the fat pad of the fourth right mammary gland of a 3-week-old syngeneic female virgin mouse whose endogenous epithelial tissue had been surgically removed by cauterization. The fourth mammary gland was commonly used for cell reinjection because it is easily individualized. The fourth left mammary gland was used as a control of normal epithelial cell outgrowth. The complete elimination of endogenous epithelial mammary cells was checked in six mice. Thirteen mice were reinjected with noninfected cells as a control of normal morphogenesis of the mammary ductal tree. The infection efficiency and the stability of β-galactosidase expression were estimated on eight mice reinjected with epithelial mammary cells infected with recombinant Babe Puro/*lac*Z retroviruses. The role of the *Brca1* gene on murine mammary gland morphogenesis and carcinogene-

Table 1 Histopathological observations of the fourth right mammary glands 3–12 months after tissular reconstitution

Gene introduced into cells	Number of mice	Observations
None	13	Cells reconstitute an entire epithelium (ducts and alveoli) and normal epithelial tree
β-Galactosidase	8	
Wild-type *Brca1*	7	
Brca1-Δ11	10	All of them with dramatically reduced branching 6 Atypical ductal hyperplasias 2 Intraductal carcinomas 2 Without abnormalities
Brca1-W1777Stop	10	All of them have greatly reduced branching 1 Hyperplastic nodule 3 Atypical ductal hyperplasias 2 Intraductal carcinomas 2 Epithelial hyperplasias 2 Without abnormalities

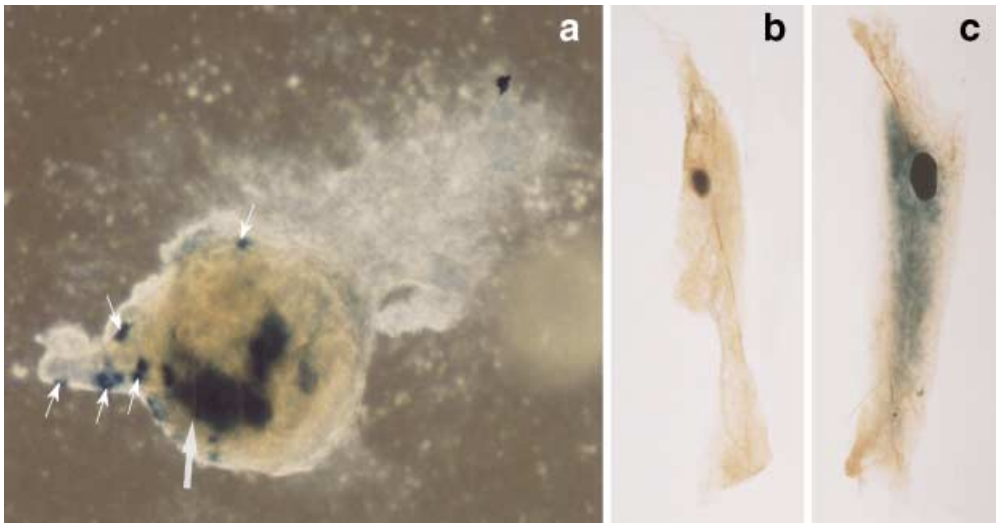

Fig. 1 Stable expression of β-galactosidase after tissular reconstitution using Babe Puro/*lacZ*-infected cells. **a** Organoid infected with recombinant retrovirus Babe Puro/*lac*Z. *Arrows* indicate infected cells expressing β-galactosidase and positive after X-gal staining (*M*: ×20). Whole mounts of the fourth mammary glands from Balb/c ByJiCo mice 2 months after tissular reconstitution using normal breast epithelial cells as a control (**b**) or cells transduced by Babe Puro/*lac*Z (**c**) (*M*: ×3). Glands were removed from mice, fixed in methacarn, stained with Delafield hematoxylin, cleared by immersion in methyl salicylate, and stained with X-gal. A large lymph node is positive by X-gal staining (**b, c**), and staining was observed in the fully recolonized fat pad **c**

sis was investigated by reinjecting in the fourth right mammary gland breast epithelial cells infected with recombinant Babe Puro retroviruses expressing full-length *Brca1* (*n*=7), *Brca1*-Δ11 (*n*=10), or *Brca1*-W1777Stop (*n*=10) (Table 1).

Two to twelve months following the reinjection of epithelial mammary cells, the whole fourth mammary gland of nulliparous or postlactating mice was dissected, fixed in methacarn (chloroform/methanol/acetic acid 3:6:1), stained in Delafield's hematoxylin, and cleared in methyl salicylate. The whole-mount mammary gland was examined using light microscopy then embedded in paraffin. Semi-seriated sections were performed, followed by staining in hemalin:eosin:safran. The sections were examined for the presence of abnormal mammary outgrowths. The efficiency of mammary cell infection with the Babe Puro/*lac*Z retrovirus was estimated by means of X-gal staining of whole-mount mammary glands.

Detection of HA-tagged *Brca1* constructs by PCR assay

Genomic DNAs were extracted from sections of infected mammary glands embedded in paraffin with the Puregene kit (Gentra Systems), according to the manufacturer's instructions. PCR assay was performed by amplification of 200 ng genomic DNA with primers designed to amplify a 202-bp fragment from tag HA to nucleotide +175 of the *Brca1* coding sequence (tag HA: 5′-ATGTATCCTTATGATGTACCGGATT-3′ and m175R: 5′-AAGGCCCTTTCTT CTGGTTAAG-3′).

Results

Efficient infection of mammary cells by retrovirus Babe Puro and stable expression of β-galactosidase

The complete elimination of endogenous epithelial cells of the fourth mammary gland by cauterization was checked in six mice 2 months after surgery. The destruction of the epithelium was effective (Fig. 2b) when compared with normal mammary gland (Fig. 2a) when mice were aged less than 21 days, because persistence of the mammary tissue was observed in two cases of mice operated on after the age of 27 days. When mice were reinjected with noninfected epithelial mammary cells (13 cases), normal development of the epithelium and complete recolonization of the fat pad were observed after 6 months. The infection efficiency of primary cultures of mammary cells was monitored with the recombinant retrovirus Babe Puro/*lac*Z in eight mice. Stable expression of β-galactosidase was observed more than 2 months after the reinjection of infected cells, which developed normally and fully recolonized the fat pad. A large lymph node usually present in the middle of the mammary fat pad was found positive by X-gal staining (Fig. 1, Table 1).

Tissue reconstitution with epithelial mammary cells transduced with full-length *Brca1*

A recombinant Babe Puro retrovirus expressing the HA-tagged full-length *Brca1* allele was generated. Epithelial mammary cells infected with Babe Puro/*Brca1* reconstituted normal ducts in nulliparous (*n*=3) and postlactating (*n*=4) mice, although ectasy (thickened ducts filled with secretions) could be observed in some of the ducts (Table 1).

Retroviral transduction of *Brca1*-Δ11 and *Brca1*-W1777Stop induces mouse epithelial mammary cell hyperplasia

Epithelial mammary cells were infected with retrovirus Babe Puro expressing HA-tagged splice variant *Brca1*-

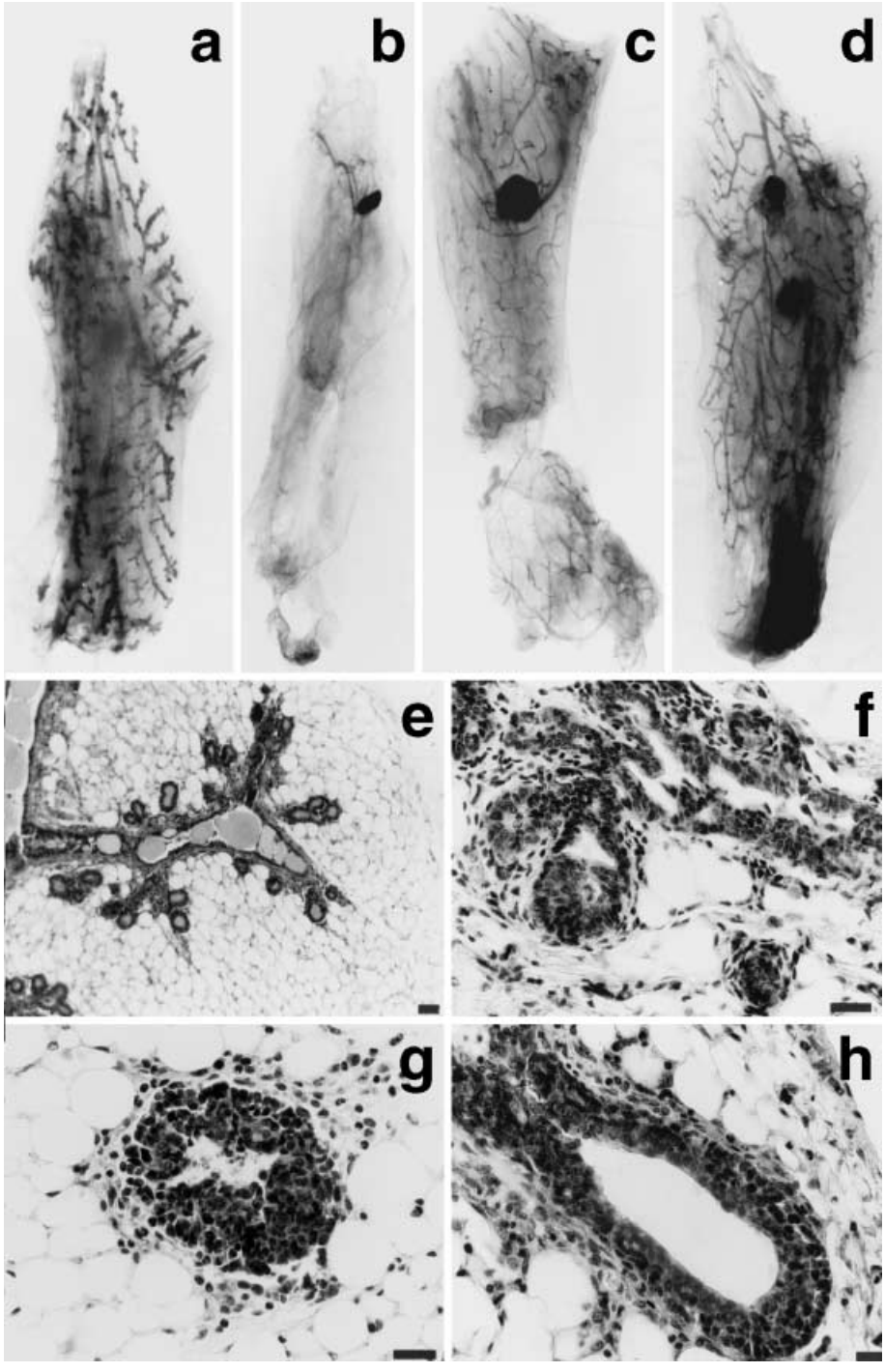

Fig. 2 a–d Whole mounts of the fourth mammary glands from 9-month-old Balb/c ByJiCo mice. Glands were removed from mice, fixed in methacarn, stained with Delafield hematoxylin, and cleared by immersion in methyl salicylate (*M*: ×3). **a** Normal gland with normal branching and lobular differentiation. **b** Fourth left mammary gland whose endogenous epithelial tissue had been surgically removed by cauterization at 3 weeks. The lymph node and the mammary artery are seen. **c** Whole mount of the fourth right mammary gland from a Balb/c ByJICo, 6 months after tissular reconstitution using breast epithelial cells transduced by *Brca1*-Δ11. The branching of the mammary tree is dramatically reduced with few terminal end buds and reduced lobular differentiation. A lymph node is seen in the cross of the mammary artery. **d** Whole mount of the fourth right mammary gland from a Balb/c ByJICo 6 months after tissular reconstitution using breast epithelial cells transduced by *Brca1*-W1777Stop. The branching of the mammary tree is reduced, one lymph node is seen, and the *dark areas* are corresponding to foci of sclerosing adenosis. **e–h** Sections of mice mammary glands stained with hemalin:eosin:safran. **e** Normal mammary gland mainly composed of fat tissues and ducts with alveolar lobuli (*bar* 20 µm). **f–h** Mammary gland 3 months after tissue reconstitution, using breast epithelial cells transduced with HA-tagged Brca1-Δ11 (**f, h**) or Brca1-W1777Stop (**g**). An area of sclerosing adenosis is characterized by proliferation of closely packed ductules exhibiting elongation and distorsion (**f**). Intraductal carcinoma or atypical ductal hyperplasia with a loss of polarity of the cells lining the ducts. These lesions are characterized by proliferation of pleomorphic, atypical cells with little cell debris in the lumen. The ducts are surrounded by inflammatory cells and adipocytes (**g, h**) (*bar* 20 µm)

Δ11 or mutant *Brca1*-W1777Stop alleles and reinjected into the fourth mammary fat pad. In the mammary gland of nulliparous (*Brca1*-Δ11: *n*=5; *Brca1*-W1777Stop: *n*=5) and postlactating (*Brca1*-Δ11: *n*=5; *Brca1*-W1777Stop: *n*=5) mice, the infected cells underwent morphogenesis, with two types of hyperplasia observed for both constructs: atypical intraductal hyperplasia, the duct lumina being completely filled with atypical epithelial cells (Fig. 2g, h; Table 1), or simple terminal duct hyperplasia (Fig. 2f). When compared with a normal mammary gland (Fig. 2a), this phenotype was associated with dramatically reduced branching of the mammary ducts, the presence of few terminal end buds, and reduced lobular differentiation (Fig. 2c, d).

PCR amplification of genomic DNA from paraffin-embedded mouse mammary gland samples infected with *Brca1* constructs

The presence of HA-tagged *Brca1*, *Brca1*-Δ11, and *Brca1*-W1777Stop alleles was checked using PCR amplification of DNA extracted from histological sections of mouse mammary gland. The primers were designed to amplify specifically the transduced constructs with the tag HA sequence at the 5′ end of the cDNA. A 202-bp PCR product was amplified from sections of mammary glands transduced with the different HA-tagged constructs but was not detected in noninfected mammary gland samples (data not shown). These data indicate that the HA-tagged *Brca1* constructs were efficiently integrated into mammary cells after retroviral transduction.

Discussion

The expression level of the human *BRCA1* gene is high during the early stages of prenatal mammary gland development [12]. In the murine mammary gland, *Brca1* expression is increased during puberty and gestation, when epithelial cells proliferate and differentiate [2, 13]. However, the biological functions of the Brca1 protein in this tissue remain elusive. We therefore attempted to further define the role of the *Brca1* gene on the proliferation and differentiation of mammary cells by infecting breast epithelial cells with recombinant retroviruses expressing wild-type and mutant *Brca1* alleles. Epithelial mammary cells transplanted into the fat pad are able to reconstitute a new mammary gland and to differentiate with a pattern characteristic of the transgene [5]. The mammary tissue reconstruction model is therefore highly convenient for the study of genes implicated in the mammary gland morphogenesis and breast carcinogenesis.

Noninfected cells fully recolonized the fat pad of the fourth right mammary gland. Moreover, murine epithelial mammary cells were efficiently infected by the Babe Puro/*lac*Z retrovirus. These modified cells were able to reconstitute a normal mammary ductal tree and stably expressed β-galactosidase more than 2 months after reinjection. Epithelial mammary cells transduced with full-length *Brca1* developed normally, although ectasy could be observed in some of the ducts. Ectasy was probably caused by the accumulation of secretions in the ducts' lumina, which do not come out to the nipple.

The transduction of either splice variant *Brca1*-Δ11 or mutant *Brca1*-W1777Stop alleles in epithelial mammary cells resulted in atypical ductal hyperplasia and simple terminal duct hyperplasia, associated with reduced branching. Intraductal hyperplasias have been infrequently observed in the mouse [18]. These lesions resembled to some extent lesions found in the human breast, especially atypical hyperplasia. Hyperplasia associated with reduced branching of epithelial mammary cells transduced with splice variant *Brca1*-Δ11 or mutant *Brca1*-W1777Stop could result from an impaired differentiation of epithelial mammary cells caused by abnormal Brca1 proteins because no hyperplastic outgrowth has been observed in epithelial mammary cells transduced with full-length *Brca1*. These lesions have been shown to possess some of the molecular changes seen in invasive carcinomas, the term *mammary intraepithelial neoplasia* (MIN) is used for these lesions [3].

Because of paucity of material, we failed in microdissecting paraffin slices and in detecting either exogenous RNA or protein in these samples. Further data should be obtained to directly detect ectopically expressed proteins. Nevertheless, we observed abnormal tissues exclusively in glands recolonized with cells transduced with spliced or mutant *Brca1* alleles and never in control cases transduced with wild-type *Brca1* or in mammary glands injected with noninfected cells. For these same reasons, one can exclude that the histological effects we observed result from alterations of endogenous *Brca1* alleles.

Our results are reminiscent of those obtained by Xu et al. [21], although different methods were used. Indeed, in our study, *Brca1*-Δ11 and *Brca1*-W1777Stop were ectopically expressed in mammary cells containing two endogenous wild-type *Brca1* alleles, whereas a CRE-mediated deletion of *Brca1* exon 11 generates two *Brca1*-Δ11 alleles. Our data suggest that ectopically expressed Brca1-Δ11 and Brca1-W1777Stop proteins could have dominant negative effects, leading to hyperplastic development of epithelial mammary cells. Interestingly, BRCA1-deleted proteins without nuclear localization signals or without carboxy-terminal part are unable to transactivate transcription in vitro [4]. Our results can be explained in different ways: ectopically expressed and endogenous Brca1 proteins could compete for effectors of the Brca1 pathway or the overexpressed proteins could directly inactivate the endogenous Brca1 protein. However, it still has to be investigated whether similar human BRCA1 proteins have such effects in genetically predisposed patients. Such results have been obtained with the Wilm's tumor-suppressor gene (*WT1*). The WT1-mediated transcriptional activation is inhibited by dominant-negative mutant proteins [16] and is regulated by differential splicing [10].

So far, these mechanisms cannot be applied to all the mutations of the human *BRCA1* gene: some mutated BRCA1 transcripts are unstable and some *BRCA1* mutations, such as those located in the first exon, are predicted to result in no protein production [15]. These results provide new insights on Brca1 functional regulation by splicing, on mechanisms leading to tumor formation, and on *BRCA1* genotype/phenotype correlation. Further studies are needed to determine the biological consequences of human *BRCA1* mutations on the protein function, in relationship with the influence of other genetic alterations or of exogenous factors such as hormones.

Acknowledgements We wish to thank Laetitia Boutrand for automatic sequencing and Pascale Peysson for her technical support. R. Bachelier is the recipient of a fellowship from the Comité de la Loire de la Ligue Contre le Cancer. F. Magdinier is the recipient of a fellowship from the Fondation pour la Recherche Médicale. This work was supported by the Comités de l'Ardèche et de la Drome de la Ligue Contre le Cancer and the Association pour la Recherche contre le Cancer.

References

1. Bachelier R, Dalla-Venezia N, Mazoyer S, Frappart L, Lenoir GM, Vincent A (2000) Differential expression and subcellular localization of murine Brca1 and Brca1-Δ11 isoforms in murine and human cell lines. Int J Cancer 88:519–524
2. Blackshear PE, Goldsworthy SM, Foley JF, McAllister KA, Bennett LM, Collins NK, Bunch DO, Brown P, Wiseman RW, Davis BJ (1998) Brca1 and Brca2 expression patterns in mitotic and meiotic cells of mice. Oncogene 16:61–68
3. Cardiff RD, Anver MR, Gusterson BA, Hennighausen L, Jensen RA, Merino MJ, Rehm S, Russo J, Tavassoli FA, Wakefield LM, Ward JM, Green JE (2000) The mammary pathology of genetically engineered mice: the consensus report and recommendations from the Annapolis meeting. Oncogene 19:968–988
4. Chapman MS, Verma IM (1996) Transcriptional activation by BRCA1. Nature 382:678–679
5. Edwards PAW (1993) Tissue reconstitution models of breast Cancer Cancer Surv 16:79–96
6. Futreal PA, Liu Q, Shattuck-Eidens D, Cochran C, Harshman K, Tavtigian S, Bennett LM, Haugen-Strano A, Swensen J, Miki Y, Eddington K, McClure M, Frye C, Weaver-Feldhaus J, Gding W, Gholami Z, Söderkvist P, Terry L, Jhanwar S, Berchuck A, Iglehart JD, Marks J, Ballinger DG, Barrett JC, Skolnick MH, Kamb A, Wiseman R (1994) BRCA1 mutations in primary breast and ovarian carcinomas. Science 266:120–122
7. Holt JT, Thompson ME, Szabo C, Robinson-Benion C, Arteaga CL, King MC, Jensen RA (1996) Growth retardation and tumour inhibition by BRCA1. Nat Genet 12:298–302
8. Hakem R, de la Pompa JL, Sirard C, Mo R, Woo M, Hakem A, Wakeham A, Potter J, Reitmar A, Billia F, Firpo E, Hui CC, Roberts J, Rossant J, Mak TW (1996) The tumor suppressor gene Brca1 is required for embryonic cellular proliferation in the mouse. Cell 85:1009–1023
9. Lane TF, Deng C, Elson A, Lyu MS, Kozak CA, Leder P (1995) Expression of Brca1 is associated with terminal differentiation of ectodermally and mesodermally derived tissues in mice. Genes Dev 9:2712–2722
10. Liu JJ, Wang ZY, Deuel TF, Yong HX (1999) Imbalanced expression of functionally different WT1 isoforms may contribute to sporadic unilateral Wilm's tumor. Biochem Biophys Res Commun 254:197–199
11. Magdinier F, Ribieras S, Lenoir GM, Frappart L, Dante R (1998) Down-regulation of BRCA1 in human sporadic breast cancer; analysis of DNA methylation patterns of the putative promoter region. Oncogene 17:3169–3176
12. Magdinier F, Dalla Venezia N, Lenoir GM, Frappart L, Dante R (1999) BRCA1 expression during prenatal development of the human mammary gland. Oncogene 18:4039–4043
13. Marquis ST, Rajan JV, Wynshaw-Boris A, Xu J, Yin GY, Abel KJ, Weber BL, Chodosh LA (1995) The developmental pattern of Brca1 expression implies a role in differentiation of the breast and other tissues. Nat Genet 11:17–26
14. Miki Y, Swensen J, Shattuck-Eidens D, Futreal PA, Harshman K, Tavtigian S, Liu QY, Cochran C, Bennett LM, Ding W, Bell R, Rosenthal J, Hussey C, Tran T, McClure M, Frye C, Hattier T, Phelps R, Haugenstrano A, Katcher H, Yakumo K, Gholami Z, Shaffer D, Stone S, Bayer S, Wray C, Bogden R, Dayananth P, Ward J, Tonin P, Narod S, Bristow PK, Norris FH, Helvering L, Morrison P, Rosteck P, Lai M, Barrett JC, Lewis C, Neuhausen S, Cannon Albright L, Goldgar D, Wiseman R, Kamb A, Skolnick MH (1994) A strong candidate for the breast and ovarian-cancer susceptibility gene BRCA1. Science 266:66–71
15. Rahman N, Stratton MR (1998) The genetics of breast cancer susceptibility. Annu Rev Genet 32:95–121
16. Reddy J, Morris JC, Wang J, English MA, Haber DA, Shi Y, Licht JD (1995) WT1-mediated transcriptional activation is inhibited by dominant negative mutant proteins. J Biol Chem 270:10878–10884
17. Scully R, Chen J, Ochs RL, Keegan K, Hoekstra M, Feunten J, Livingston DM (1997) Dynamic changes of BRCA1 subnuclear location and phosphorylation state are initiated by DNA damage. Cell 90:425–435
18. Squartini F, Pingitore R (1994) Tumors of the mammary gland. In: Pathology of tumors in laboratory animals – tumors of the mouse, 2nd edn. IARC Scientific Publications, Lyon, pp 47–100
19. Thompson ME, Jensen RA, Obermiller PS, Page DL, Holt JT (1995) Decreased expression of BRCA1 accelerates growth and is often present during sporadic breast progression. Nat Genet 9:444–450
20. Wilson CA, Payton MN, Elliott GS, Buaas FW, Cajulis EE, Grosshans D, Ramos L, Reese DM, Slamon DJ, Calzone FJ (1997) Differential localization, expression and biological toxicity of BRCA1 and the splice variant BRCA1-Δ11b. Oncogene 14:1–16
21. Xu X, Wagner KW, Larson D, Weaver Z, Li C, Ried T, Hennighausen L, Wynshaw-Boris A, Deng CX (1999) Conditional mutation of Brca1 in mammary epithelial cells results in blunted ductal morphogenesis and tumor formation. Nat Genet 22:37–43

Virchows Arch (2002) 440:267–273
DOI 10.1007/s004280100501

ORIGINAL ARTICLE

**Tetsunari Oyama · Takaaki Sano · Toshiaki Hikino
Qi Xue · Kotaro Iijima · Takashi Nakajima
Frederick Koerner**

Microcalcifications of breast cancer and atypical cystic lobules associated with infiltration of foam cells expressing osteopontin

Received: 4 January 2001 / Accepted: 20 May 2001 / Published online: 24 August 2001
© Springer-Verlag 2001

Abstract We studied the pattern of calcification and the expression of osteopontin protein and mRNA by the histiocytes and noninvasive carcinoma cells of 20 breast cancers and the histiocytes and atypical ductal cells of sixteen cases of atypical cystic lobules. Ten breast cancers showed low-grade cribriform carcinoma in situ containing secretory material; the remaining ten cancers displayed high-grade carcinoma in situ with central necrosis characteristic of comedo type carcinoma. Hematoxylin-eosin and Kossa staining revealed calcium hydroxyapatite calcifications in 80% of cribriform type carcinomas, 50% of comedo type carcinomas, and 56% of atypical cystic lobules. Immunohistochemical staining demonstrated osteopontin protein in intraluminal secretory material, necrotic debris, or stroma, and in histiocytes in all the Kossa-positive carcinomas and atypical cystic lobules. In situ hybridization revealed osteopontin mRNA mainly in the histiocytes and especially in those near the calcifications. In two cases, rare carcinoma cells contained osteopontin protein and mRNA. The close relation between hydroxyapatite crystals and osteopontin-producing histiocytes suggests that osteopontin plays a role in the biomineralization that occurs in certain non-invasive breast cancers and atypical cystic lobules. The differences in the morphology of the calcifications and the intraductal contents suggest that the mechanism leading to the osteopontin production might vary depending on the underlying lesion.

Keywords Breast cancer · Atypical cystic lobules · Osteopontin · Microcalcification

This work was partially supported by a grant (C-2) from the Ministry of Education, Science, Sports and Culture of Japan (11670166)

T. Oyama (✉) · T. Sano · T. Hikino · Q. Xue · T. Nakajima
Second Department of Pathology,
Gunma University School of Medicine, Showa-machi 3-39-22,
Maebashi, Gunma 371-8511, Japan
e-mail: oyama@med.gunma-u.ac.jp
Tel.: +81-27-220-7984, Fax: +81-27-220-7981

K. Iijima
Second Department of Surgery,
Gunma University School of Medicine, Maebashi, Gunma, Japan

F. Koerner
James Homer Wright Laboratory of Pathology,
Massachusetts General Hospital, Harvard Medical School,
Boston, MA, USA

Introduction

Microcalcification serves as an important indication of early breast carcinoma. One finds carcinoma in approximately 25% of non-palpable lesions biopsied because the mammogram revealed calcifications [23, 30]. Researchers have described two types of calcifications, type I and type II [9]. Type I microcalcifications appear as colorless, birefringent crystals composed of calcium oxalate (CaC_2CO_4-$2H_2O$). They most often form in apocrine cysts and less commonly in other benign conditions [13]. Type II microcalcifications, which consist of the bone mineral crystal, hydroxyapatite [$Ca_{10}(PO_4)_6(OH)_2$], stain with hematoxylin and the Kossa technique. They occur in both benign and malignant conditions[19, 22], although more commonly in ductal carcinoma in situ (73% of cases) [13] than in benign breast disease (31% of cases) [28]. These hydroxyapatite crystals can take two forms: a “laminar” or “secretory” appearance, or a “granular,” “amorphous,” or “necrotic” appearance [15, 19].

The mechanisms by which calcifications arise have not been clarified fully. Deposition of the crystals in a secreted mucinous or proteinaceous matrix probably creates “secretory” calcifications, whereas precipitation of hydroxyapatite in necrotic cellular debris would seem to give rise to the “granular” type [8]. Recent publications report that bone matrix proteins, which include osteopontin (OP), osteonectin, and bone sialoproteins, play a role in initiating and controlling hydroxyapatite crystallization and in regulating other aspects of mineralization [4, 16, 18]. The studies of Castronovo et al. revealed that the expression of several bone matrix proteins including OP

correlates with the presence of hydroxyapatite microcalcifications [4]. The OP gene encodes highly modified proteins of 55–65 kDa with a preserved integrin binding RGD tripeptide [1]. RGD-mediated cell adhesion and proliferation via OP is proposed to act through the integrin $\alpha_v\beta_3$ [35]. The integrin family of proteins can induce cellular responses such as cell adhesion, changes in intracellular pH, changes and oscillation in intracellular free calcium concentrations, and phosphorylation of tyrosine.

Although OP has been detected in variable but generally high percentages of primary breast cancers [2, 3], the cellular origin of the molecule remains controversial [3, 12, 14, 32, 34, 37]. Brown et al. propose that macrophages serve as the most important source of the protein and that the secreted molecule binds to tumor cells, possibly through the GRGDS cell binding domain in OP [3]. Other authors, using in situ hybridization and matched sections, have concluded that OP originates from tumor cells [12, 32, 34,37]. Sharp et al., for instance, demonstrated that OP transcripts were detected in both invasive and in situ carcinoma components and that the transcripts were not seen in surrounding stromal cells or in peritumoral macrophages [32].

Besides occurring in ductal carcinomas in situ, calcifications of the "secretory" type also form in a lesion that we refer to as "atypical cystic lobule" [25] and others have called "low-grade clinging carcinoma of flat type" [6], "columnar alteration with prominent apical snouts and secretions" [10], "hypersecretory hyperplasia with atypia" [26], and "atypical cystic duct" [21,36]. This alteration represents a proliferation of luminal cells showing low-grade cytological atypia without architectural atypia. The cells often possess apical snouts, and secretory material frequently accumulates in the glandular lumina. This lesion frequently merges with fully established ductal carcinoma in situ of the micropapillary/cribriform type. On the basis of these morphological [10, 25, 26,36], immunohistochemical [21,25], genetic [24], and clinical studies [7], certain authors have suggested that atypical cystic lobules and related lesions represent early stages in the formation of certain types of low-grade ductal carcinoma in situ.

We undertook the following study to correlate the expression of OP with the presence of calcifications in breast cancers and atypical cystic lobules.

Materials and methods

Case selection and classification

Using computer-generated lists of specimens in the departments of pathology of the Massachusetts General Hospital and the Gunma University Hospital, we retrieved cases showing predominantly (nine cases) or exclusively (11 cases) noninvasive ductal carcinoma or atypical cystic lobules. We based the diagnosis of ductal carcinoma in situ on conventional criteria [29] and then subdivided the carcinomas into two groups. Cribriform (Cr) carcinomas show low-grade features, form cribriform or micropapillary architectural patterns, and contain eosinophilic secretions within neoplastic glands. Comedo (Co) carcinomas display intermediate or high grade cytological characteristics and central ("comedo") necrosis of the malignant ductal cells. We used our previously published criteria to make the diagnosis of atypical cystic lobule [25]. The study group comprises ten cases of Cr type carcinoma, ten cases of Co type carcinoma, and 16 cases of ACL.

Sections from 17 of the 20 carcinoma cases contained apparently normal ducts and lobules, which we used for our study of normal tissues and benign changes.

Conventional microscopical examination

Using the original hematoxylin and eosin stained sections, we examined the noninvasive portions of the study cases and recorded the type and location of calcifications, and the presence of foam cells.

Immunohistochemical staining and Kossa staining

Using formalin-fixed and paraffin-embedded sections, immunohistochemical staining for keratin, Kp-1, and OP was performed. Five micrometer paraffin sections were deparaffinized with xylene, soaked through an alcohol series, and washed in phosphate-buffered saline (PBS) (pH 7.4). Following antigen retrieval by means of microwave heating in citrate buffer, the sections were incubated for 1 h with normal goat serum and then reacted with the primary antibodies overnight at 4°C. After the incubation with the secondary antibody for 1 h at room temperature, the conventional avidin-biotin-peroxidase complex method was performed at room temperature using the Vectastain ABC kit (Vector Laboratories Inc., Burlingame, Calif.). Slides were immersed in diaminobenzidine tetrahydrochloride solution, then lightly counterstained with hematoxylin. Immunostaining for Kp1 required pronase predigestion. The antibodies and their dilutions were: monoclonal anti-OP (10A16, IBL, Japan; 1:200), monoclonal anti-keratin (KL-1, Immunotech, France; 1:5), and monoclonal anti-Kp1 (CD68, DAKO, Kyoto, Japan; 1:50). We interpreted brown discoloration of the cytoplasm as a positive result. For negative controls of the OP staining, we stained duplicate sections from each case using OP absorbed primary anti-OP antibody.

Kossa staining was performed according to the usual protocol using formalin fixed and paraffin embedded sections. They were reacted in 5% $AgNO_3$ under sunlight.

In situ hybridization

Sections 4 μm thick were cut from paraffin blocks and mounted on silane coated glass slides. They were then rinsed in ethanol, rehydrated with diethyl pyrocarbinate treatment, and rinsed in 0.1 M PBS. They were treated with 5 μg/ml proteinase K in PBS at 37°C for 30 min to eliminate protein, rinsed in PBS, and refixed in 4% paraformaldehyde in PBS for 5 min. They were rinsed in PBS, and basic protein was removed by incubation in 0.2 M HCl at room temperature for 15 min. After rinsing in PBS, they were rinsed in 0.1 M triethanolamine for 1 min at room temperature then in 0.25% acetic acid in 0.1 M triethanolamine for 10 min. The sections were rinsed in PBS, deparaffinized in xylene, dehydrated in an ethanol series, and air-dried for the hybridization.

The RNA probe for OP was prepared using a digoxigenin (DIG) RNA labeling kit (Boehringer Mannheim, Mannheim, Germany). To produce DIG-labeled RNA, cloned OP DNA was transcribed in vitro with T7 or T3 RNA polymerase in the presence of DIG-UTP. Briefly, DNA in the transcription vector with phage promoter was linearized with restriction enzyme (apa I or xba I). RNA synthesis by in vitro transcription from the phage promoter was performed by incubation of T7 or T3 polymerase with ATP, CTP, GTP, UTP, and DIG-UTP for 2 h at 37°C. After determining the sensitivity of the probe to OP, T7 probes were used with the mixture solution containing 50% deionized formamide, 10 mM

Tris-HCl (pH 7.6), 200 µ/ml tRNA, 10% dextran sulfate (Pharmacia, Uppsala, Sweden), 1× Denhardt's solution, 600 mM NaCl, 0.25% SDS, and 1 mM EDTA (pH 8.0). T3 probes were used at the same dilution as the negative control.

Usually, 15 µl of the probe mixture was applied on a slide and completely sealed with a coverslip. This was followed by the OP probe at 85 °C for 5 min, and the hybridization was carried out overnight at 50°C. After hybridization, the slides were subsequently washed under high stringency conditions with 5× sodium chloride and sodium citrate solution (SSC) at 55°C for 5 min, 50% formamide in 2× SCC at 50 °C for 30 min., 2× SCC at 50°C for 20 min, and 0.2× SCC at 50°C for 40 min (1× SSC contains 0.15 M sodium chloride and 15 mM sodium citrate). After that, the sections were rinsed in buffer 1 solution containing 100 mM Tris HCl (pH 7.6) and 150 mM NaCl at room temperature for 5 min. After the sections were rinsed in 4% block Ace/buffer 1 at room temperature for 60 min and washed 3 times in Tris buffered saline, they were reacted with a peroxidase (PO) conjugated anti-DIG antibody (Dako, Denmark) at 1:500 dilution at room temperature for 60 min. For the ISH signal amplification, the digoxigeninated tyramide was applied to the section at room temperature for 20 min and subsequently reacted by PO conjugated anti-DIG antibody again. After rinsing in PBS-T, the PO was visualized with 0.01 M Tris-HCl buffer (pH 7.4) containing 0.05% 3–3′-diaminobenzidine tetrahydrochloride and 0.015% H_2O_2 for 5 min. Finally, the sections were lightly counterstained with hematoxylin.

Results

Calcifications

Nonneoplastic tissue

The normal breast tissue did not contain calcifications nor did it show a reaction with Kossa staining. Rare microcysts indicating fibrocystic changes harbored type II calcifications of the "secretory" type, which stained with the Kossa technique.

Noninvasive carcinomas

Of 10 cases of Cr type carcinoma, calcifications were observed by hematoxylin and eosin staining in the noninvasive components of 8 cases (80%); black deposits were observed after Kossa staining in all 8 cases (1). All these calcifications displayed the characteristics of "secretory" calcifications. Of 10 cases of Co type carcinoma, calcifications were observed following hematoxylin and eosin staining in the noninvasive components of 5 cases (50%), and black deposits were observed in the central necrotic area of all 5 cases after Kossa staining (2B). These calcifications were of the "granular" or "necrotic" type.

Atypical cystic lobules

Of 16 cases of ACLs, calcifications were observed in 9 (56%), and black deposits were observed following Kossa staining in all 9. All calcifications were of the "secretory" type.

Table 1 Calcification and osteopontin protein expression in noninvasive carcinomas and atypical cystic lobules

Lesions	Cases	Tumor cells	Extracellular material[a]	Histiocytes
Cr carcinoma	10	1 (10%)	8 (80%)	8 (80%)
Kossa + cases	8	1 (12%)	8 (100%)	8 (100%)
Kossa – cases	2	0	0	0
Co carcinoma	10	1 (10%)	8 (80%)	9 (90%)
Kossa + cases	5	1 (20%)	5 (100%)	5 (100%)
Kossa – cases	5	0	3 (60%)	4 (80%)
ACL	16	0	10 (62%)	9 (56%)
Kossa + cases	9	0	9 (100%)	8 (88%)
Kossa – cases	7	0	1 (14%)	1 (14%)

[a] Osteopontin protein was detected by immunohistochemistry in secretory material, necrotic debris, or stroma

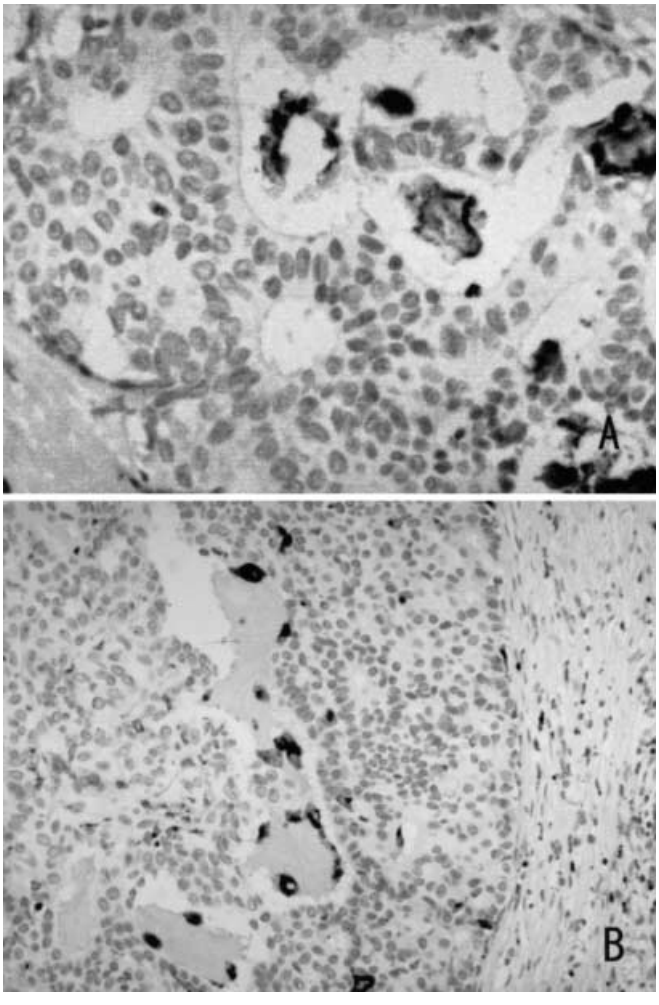

Fig. 1 Cr type carcinoma, immunohistochemical staining for osteopontin (OP, **A** ×320) and Kp-1 (**B** ×160). (OP was observed psammomatous components (**A**) and infiltrating foam cells surrounding the psammoma body were positive for Kp-1 (**B**)

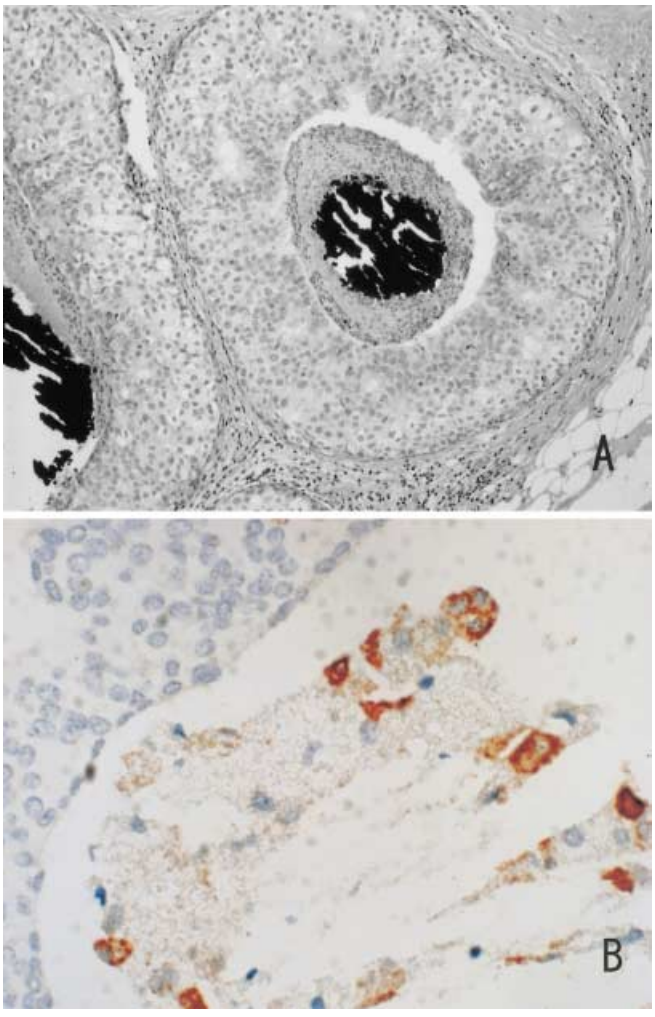

Fig. 2 Co type carcinoma, Kossa staining (**A,** ×80) and in situ hybridization (ISH) for OP mRNA (**B,** ×320). (Black deposits were observed in the center of comedo-necrosis (**A**) and infiltrating histiocytes were positive for OP mRNA by ISH (**B**)

OP expression by immunohistochemistry and in situ hybridization

Nonneoplastic tissue

Normal epithelial cells did not stain for OP protein by immunohistochemistry. We detected very small amounts of the molecule in the extracellular stroma surrounding microcysts containing "secretory" calcifications. Occasional foam cells in foci of adenosis and fibroadenosis also contained the protein. In situ hybridization did not reveal OP mRNA in any epithelial cells, but we detected a signal in a few histiocytes within the lumen of a duct in one case.

Noninvasive carcinomas

Most tumor cells failed to stain for OP protein, but we did detect it in extracellular locations and in histiocytes.

Table 2 Calcification and osteopontin mRNA expression in noninvasive carcinomas and atypical cystic lobules. *nd* not done

Lesions	Cases	Tumor cells	Histiocytes
Cr carcinoma	10	1 (10%)	8 (80%)
Kossa + cases	8	1 (12%)	8 (100%)
Kossa – cases	2	0	0
Co carcinoma	10	1 (20%)	9 (90%)
Kossa + cases	5	1 (20%)	5 (100%)
Kossa – cases	5	0	4 (80%)
ACL			
Kossa + cases[a]	6	0	5 (83%)
Kossa – cases	7	nd	nd

[a] The number of the cases is smaller than numbers in Table 1 because of technical limitations

A few cells in one carcinoma of the Cr and another of the Co type seem to express OP (1), but staining of the stroma surrounding these clusters made it difficult to feel confident that the positive reaction represented genuine staining of the cells. The secretory material within the ducts of eight of ten carcinomas of the Cr type (80%) and the necrotic debris within the ducts of five of ten carcinomas of the Co type (50%) showed a positive reaction for the protein (1). These OP positive cases included all the Kossa-positive carcinomas of both Cr and Co type (eight and five cases, respectively) (1A). Histiocytes (type B foam cells of Damiani [5]), which stained for Kp-1 and failed to stain for keratin, also demonstrated OP protein expression (1B, 2B). These OP-positive histiocytes usually abutted the secretory material in the Cr type of ductal carcinoma in situ or sat within the necrotic cellular debris in the Co type of carcinoma. A thin rim of stroma surrounding ducts harboring ductal carcinoma in situ contained OP.

In situ hybridization identified OP mRNA in histiocytes and rare tumor cells. All the Kossa-positive cases of both the Cr and Co types of carcinoma in situ contained OP mRNA positive histiocytes (2). Rare tumor cells of one carcinoma of the Co type and another carcinoma of the Cr type expressed the mRNA. We could not establish a correspondence between the OP protein positive cells and those showing OP mRNA in the two cases of carcinoma.

Atypical cystic lobules

Of 16 cases of ACL, OP protein was detected in the stroma, histiocytes, or secretory material of 10 (62%). We attempted in situ hybridization in the nine Kossa-positive cases but obtained satisfactory results in only six. Five of them (83%) demonstrated OP mRNA, which we detected only in histiocytes (3A, B; 2).

Negative Controls

All sections stained using the primary anti-OP antibody absorbed with OP failed to show a positive reaction.

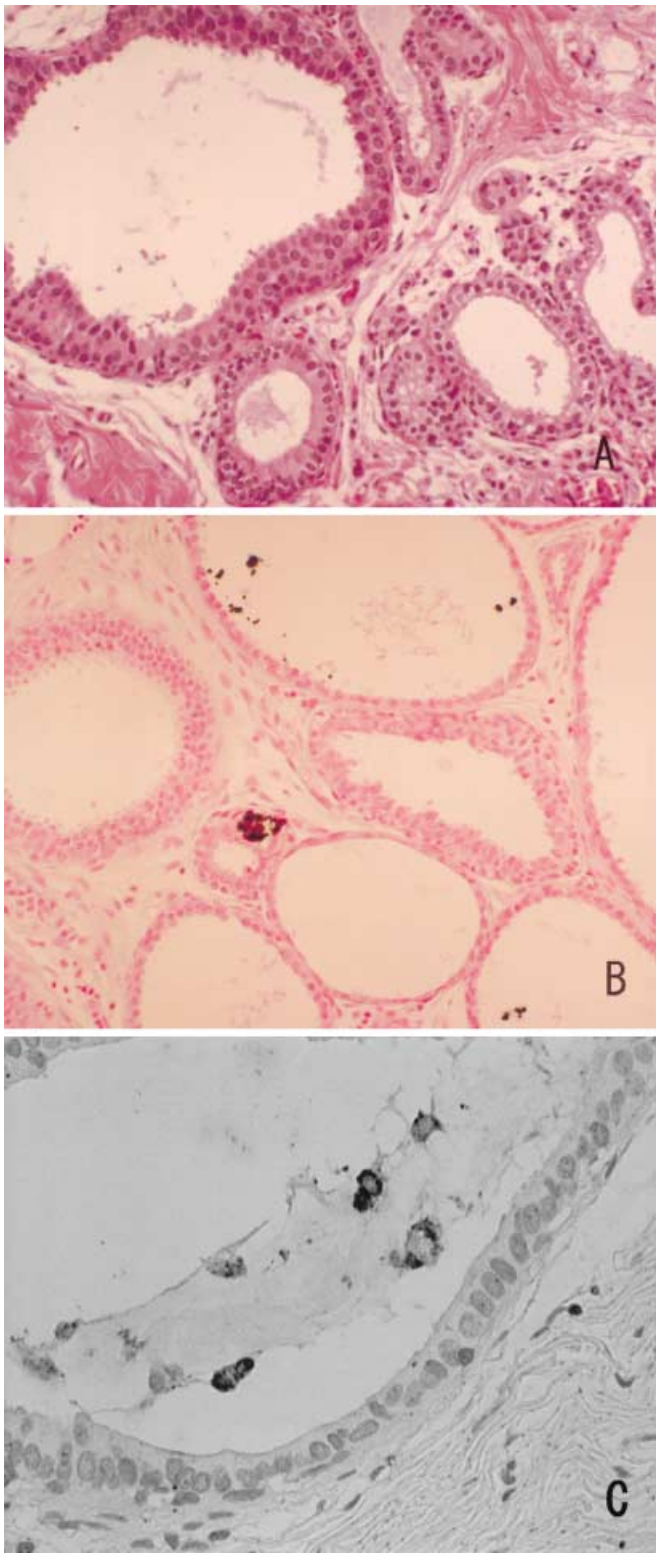

Fig. 3 Atypical cystic lobules, H&E (**A,** ×160) and Kossa stainig (**B,** ×160) and in situ hybridization (ISH) for osteopontin (OP; **C,** ×320). Atypical cystic lobules are composed of atypical luminal cells without architectural atypia (**A**). Black deposits were observed in the center of lumen (**B**). OP was observed in foam cells in the lumen (**C**)

Discussion

The results of our study agree with the general belief that OP plays a role in the biomineralization that occurs in breast cancers. Like Hirota et al. [14] we found that histiocytic foam cells (macrophages) represent the major site of production of OP; we detected it within malignant cells in only a small percentage of the carcinomas. This low frequency of expression of OP protein and mRNA by carcinoma cells conflicts with the results of several groups who report that breast cancer cells contain the protein [2, 3, 32], the mRNA [12], or both [37]. We cannot offer a ready explanation for this discrepancy, but we would point out that the published studies do not present a coherent body of data. For example, the staining protocol used by Bellahcene and Castronovo [2] produced moderate staining in about 20% of samples of normal breast tissue and slight staining in an additional 33%. The failure of Sharp et al. [32] to detect OP protein or mRNA in macrophages likewise raises questions about the authors' techniques, for histiocytes have consistently shown expression of both the protein and its mRNA [3, 14, 37]. By using formalin-fixed tissue, microwave heating, and a monoclonal primary antibody, our methods most closely match those employed by Tuck et al. [37]. Moreover, our demonstration of OP protein and mRNA in histiocytes and our failure to detect either molecule in normal breast tissue agree with their observations [37]. Unlike these authors, who observed OP protein and mRNA in about 25% of invasive breast cancers, we did not detect these molecules in the noninvasive components of most carcinomas. Nine of our cases did contain small amounts of invasive carcinoma, however, and we detected OP protein or mRNA in occasional invasive cells. They number so few that we cannot draw conclusions from these observations, but they suggest to us that this difference in the type of cells studied might explain the difference between our observations and those of Tuck et al. [37].

Whatever the source of the OP, the evidence suggests that the molecule plays a role in the calcium hydroxyapatite deposition that takes place in certain breast cancers. The mechanisms leading to expression of the OP remain undefined, however, and so does its role in the mineralization process. Our observations suggest that different mechanisms account for the OP accumulation seen in different types of ductal carcinomas in situ. For example, the low-grade (Cr) carcinomas in situ that we studied contain eosinophilic secretions and the "secretory" type of hydroxyapatite calcifications. Milk, the physiological secretion of the breast, contains abundant OP [27, 31], so the presence of this protein in these carcinomas might reflect an aberration of the normal process of OP production that occurs during lactation. Researchers have not identified the function of the OP present in milk, but they have shown that the protein inhibits hydroxyapatite crystal growth [18, 17], that the inhibition of calcification requires phosphorylation of the molecule [20], and that milk contains the highly phosphorylated form of OP [33]. One might therefore suggest that OP helps to

prevent the growth and precipitation of hydroxyapatite crystals from this calcium, phosphate, and protein-rich fluid [18] and that the OP present in low-grade ductal carcinomas in situ might have the same effect.

The atypical cystic lobules in our study group show the same "secretory" type of hydroxyapatite calcifications and the same pattern of OP expression as most low-grade (Cr type) ductal carcinomas in situ. The epithelial cells do not contain either the protein or the mRNA; however, extracellular material next to the calcifications stains for the former, and histiocytes contain both molecules. Based on these findings, we conclude that the calcium hydroxyapatite crystals in atypical cystic lobules form through the same mechanism as the calcifications seen in low-grade Cr type of ductal carcinoma in situ.

In the high-grade (Co) carcinoma in situ, on the other hand, the OP expression would seem to represent a component of the inflammatory response to cellular damage. One observes upregulation of the protein in many types of tissue injury and at sites of pathological soft tissue calcifications, such as atherosclerotic plaques, bioprosthetic cardiac valves, and dental plaque [11]. The presence of the molecule in the necrotic material of high-grade ductal carcinoma in situ probably reflects the same phenomenon. Macrophages represent the most important source of OP found in atherosclerotic plaques and calcified valves [38], and our data indicate that these same cells synthesize the majority of the OP seen in the necrotic debris of comedocarcinomas. Studies suggest that OP inhibits matrix mineralization at sites of ectopic calcification [38] and promotes macrophage resorption of dystrophic calcification [11]. Our observation that four of the nine OP containing comedocarcinomas in our study group lack calcifications seems consistent with the belief that OP functions to limit the growth of hydroxyapatite crystals and may thereby protect against dystrophic calcification.

In summary, we detected OP in most cases of both low-grade cribriform and high-grade comedo-type ductal carcinoma in situ; macrophages seem to be the predominant source of the protein. The difference in the type and extent of calcifications in these two types of noninvasive carcinoma suggests that different mechanisms underlie OP expression in the two lesions. Atypical cystic lobules also contain OP expressing histiocytes and calcifications similar to those seen in low-grade ductal carcinomas, and this similarity suggests a link between the two lesions. Our observations also seem consistent with the developing belief that OP functions to inhibit the process of dystrophic calcification.

Acknowledgements We thank to Dr. M Maeda (IBL, Gunma, Japan) for generously supplying the osteopontin probes.

References

1. Bautista DS, Xuan JW, Hota C, Chambers AF, Harris JF (1995) A monoclonal antibody against osteopontin inhibits RGD-mediated cell adhesion to osteopontin. Ann N Y Acad Sci 760:309–311
2. Bellahcene A, Castronovo V (1995) Increased expression of osteonectin and osteopontin, two bone matrix proteins, in human breast cancer. Am J Pathol 146:95–100
3. Brown LF, Papadopoulos-Sergiou A, Berse B, Manseau EJ, Tognazzi K, Perruzzi CA, Dvorak HF, Senger DR (1994) Osteopontin expression and distribution in human carcinomas. Am J Pathol 145:610–623
4. Castronovo V, Bellahcene A (1998) Evidence that breast cancer associated microcalcification are mineralized malignant cells. Int J Oncology 12:305–308
5. Damiani S, Cattani MG, Buonamici L, Eusebi V (1998) Mammary foam cells. Characterization by immunohistochemistry and in situ hybridization. Virchows Arch [A] 432:433–440
6. Eusebi V, Foschini MP, Cook MG, Berrino F, Azzopardi JG (1989) Long-term follow-up of in situ carcinoma of the breast with special emphasis on clinging carcinoma. Semin Diagn Pathol 6:165–173
7. Eusebi V, Feudale E, Foschini MP, Micheli A, Conti A, Riva C, Di Palma S, Rilke F (1994) Long-term follow-up of in situ carcinoma of the breast. Semin Diagn Pathol 11:223–235
8. Foschini MP, Fornelli A, Peterse JL, Mignani S, Eusebi V (1996) Microcalcifications in ductal carcinoma in situ of the breast: histochemical and immunohistochemical study. Hum Pathol 27:178–183
9. Frappart L, Remy I, Lin HC, Bremond A, Raudrant D, Grousson B et al.(1986) Different types of microcalcifications observed in breast pathology. Correlations with histopathological diagnosis and radiological examination of operative specimens. Virchows Arch [A] 410:179–187
10. Fraser JL, Raza S, Chorny K, Connolly JL, Schnitt SJ (1998) Columnar alteration with prominent apical snouts and secretions: a spectrum of changes frequently present in breast biopsies performed for microcalcifications. Am J Surg Pathol 22: 1521–1527
11. Giachelli CM, Steitz S (2000) Osteopontin: a versatile regulator of inflammation and biomineralization. Matrix Biol 19:615–622
12. Gillespie MT, Thomas RJ, Pu ZY, Zhou H, Martin TJ, Findlay DM (1997) Calcitonin receptors, bone sialoprotein and osteopontin are expressed in primary breast cancers. Int J Cancer 73:812–815
13. Gonzalez JE, Caldwell RG, Valaitis J (1991) Calcium oxalate crystals in the breast. Pathology and significance. Am J Surg Pathol 15:586–591
14. Hirota S, Ito A, Nagoshi J, Takeda M, Kurata A, Takatsuka Y, Kohri K, Nomura S, Kitamura Y (1995) Expression of bone matrix protein messenger ribonucleic acids in human breast cancers. Possible involvement of osteopontin in development of calcifying foci. Lab Invest 72:64–69
15. Holland R, Hendriks JHCL (1994) Microcalcifications associated with ductal carcinoma in situ: Mammographic-patholoogic correlation. Semin Diagn Pathol 11:181–192
16. Hunter GK, Goldberg HA (1993) Nucleation of hydroxyapatite by bone sialoprotein. Proc Natl Acad Sci USA 90:8562–8565
17. Hunter GK, Kyle CL, Goldberg HA (1994) Modulation of crystal formation by bone phosphoproteins: structural specificity of the osteopontin-mediated inhibition of hydroxyapatite formation. Biochem J 300:723–728
18. Hunter GK, Hauschka PV, Poole AR, Rosenberg LC, Goldberg HA (1996) Nucleation and inhibition of hydroxyapatite formation by mineralized tissue proteins. Biochem J 317: 59–64
19. Iwase T, Yoshimoto M, Watanabe S, Kasumi, Akiyama F, Sakamoto G (1994). Diagnosis of nonpalpable calcified lesions in the breast. Jpn J Breast Cancer 9:393–402
20. Jono S, Peinado C, Giachelli CM (2000) Phosphorylation of osteopontin is required for inhibition of vascular smooth muscle cell calcification. J Biol Chem 275:20197–20203
21. Kusama R, Fujimori M, Matsuyama I, Fu l, Ishii K, Hama Y, Asanuma K, Shingu K, Kobayashi S, Tsuchiya (2000) Clinico-pathological characteristics of atypical cystic duct (ACD) of the breast: Assessment of ACD as a precancerous lesion. Pathol Int 50:793–800

22. Lanyi M (ed) (1986) Diagnosis and differential diagnosis of breast calcification. Springer, Berlin Heidelberg New York
23. Meyer JE, Eberlein TJ, Stomper PC, Sonnenfeld MR (1990) Biopsy of occult breast lesions. Analysis of 1261 abnormalities. JAMA 263:2341–2343
24. Moinfar F, Man YG, Bratthauer GL, Ratschek M, Tavassoli FA (2000) Genetic abnormalities in mammary ductal intraepithelial neoplasia-flat type ("clinging ductal carcinoma in situ"): a simulator of normal mammary epithelium. Cancer 88:2072–2081
25. Oyama T, Maluf H, Koerner F (1999) Atypical cystic lobules: an early stage in the formation of low-grade ductal carcinoma in situ. Virchows Arch [A] 435:413–421
26. Page DL, Kasami M, Jensen R (1996) Hypersecretory hyperplasia with atypia in breast biopsies, what is the proper level of clinical concern? Pathol Case Rev 1:36–40
27. Rittling SR, Novick KE (1997) Osteopontin expression in mammary gland development and tumorigenesis. Cell Growth Differ 8:1061–1069
28. Rogers LW (1987) Epithelial hyperplasia. In: Page DL, Anderson TJ (eds) Diagnostic histopathology of the breast. Churchill Livingstone, New York
29. Rosen PP (1997) Rosen's breast pathology. Lippincott-Raven, Philadelphia
30. Rosen P, Snyder RE, Urban J, Robbins G (1973) Correlation of suspicious mammograms and x-rays of breast biopsies during surgery. Results in 60 cases. Cancer 31:656–659
31. Senger DR, Perruzzi CA, Papadopoulos A, Tenen DG (1989) Purification of a human milk protein closely similar to tumor-associated secreted phosphoproteins and osteopontin. Biochim Biophys Acta 996:43–48
32. Sharp JA, Sung V, Slavin J, Thompson EW, Henderson MA (1999) Tumor cells are the source of osteopontin and bone sialoprotein expression in human breast cancer. Lab Invest 79: 869–877
33. Sorensen ES, Petersen TE (1994) Identification of two phosphorylation motifs in bovine osteopontin. Biochem Biophys Res Commun 198:200–205
34. Sung V, Gilles C, Murray A, Clarke R, Aaron AD, Azumi N, Thompson EW (1998) The LCC15-MB human breast cancer cell line expresses osteopontin and exhibits an invasive and metastatic phenotype. Exp Cell Res 241:273–284
35. Sung V, Stubbs JT 3, Fisher L, Aaron AD, Thompson EW (1998) Bone sialoprotein supports breast cancer cell adhesion proliferation and migration through differential usage of the alpha(v)beta3 and alpha(v)beta5 integrins. J Cell Physiol 176: 120–156
36. Tsuchiya S (1998) Atypical ductal hyperplasia, atypical lobular hyperplasia, and interpretation of a new borderline lesion. Jpn J Cancer Clin 44:548–555
37. Tuck AB, O'Malley FP, Singhal H, Harris JF, Tonkin KS, Kerkvliet N, Saad Z, Doig CS, Chambers AF (1998) Osteopontin expression in a group of lymph node negative breast cancer patients. Int J Cancer 79:502–508
38. Wada T, McKee MD, Steitz S, Giachelli CM (1999) Calcification of vascular smooth muscle cell cultures: inhibition by osteopontin. Circ Res 84:166–178
39. West D (1986) Structure and function of the phosphorylated residues of casein. J Dairy Res 53:333–352

Virchows Arch (2002) 440:274–279
DOI 10.1007/s004280100526

ORIGINAL ARTICLE

Marika Bogdani · E. Teugels · J. De Grève
C. Bourgain · B. Neyns · M. Pipeleers-Marichal

Loss of nuclear BRCA1 localization in breast carcinoma is age dependent

Received: 18 April 2001 / Accepted: 22 July 2001 / Published online: 4 December 2001
© Springer-Verlag 2001

Abstract Patients carrying a germ line mutation in the BRCA1 gene are predisposed to breast cancer. Somatic BRCA1 mutations were almost never reported in sporadic breast tumors, but several authors have described a decrease in BRCA1 mRNA and protein. In order to further investigate the possible role of BRCA1 in sporadic breast cancer, an improved immunohistochemical protocol was developed and applied on tissue sections obtained from 102 cancer patients belonging to two non-overlapping age groups (less than 40 and more than 60 years). Based on the obtained BRCA1 specific nuclear staining we could distinguish two categories of breast cancer. The staining was present in almost all the nuclei of the normal and the cancer cells in about 50% of young (less than 40 years old) as well as older patients (more than 60 years old). Thus, BRCA1 does not seem to be involved in the genesis of these cancers. In the second category of patients, either a fraction of, or all tumor cells showed no nuclear staining. In this category, no nuclear BRCA1 staining could be observed in the tumor cells of 14 (27%) young and 3 (6%) older patients. Among six young patients bearing a breast tumor showing no BRCA1 nuclear staining at all, one was found to carry a BRCA1 germline mutation. Taken together, our results suggest that the molecular pathway in which the BRCA1 protein participates is disturbed in about 50% of sporadic breast cancer, this effect being more pronounced in tumors of young patients.

Keywords BRCA1 · Immunohistochemistry · Normal breast tissue · Breast cancer

M. Bogdani (✉) · C. Bourgain · M. Pipeleers-Marichal
Department of Pathology, Academic Hospital,
Free University of Brussels (VUB), Laarbeeklaan, 101,
1090, Belgium
e-mail: mbogdani@vub.ac.be
Tel.: +32-2-4774533, Fax: +32-2-4775085

E. Teugels · J. De Grève · B. Neyns
Department of Medical Oncology, Academic Hospital,
Free University of Brussels, Laarbeeklaan, 101, 1090, Belgium

Introduction

The involvement of the BRCA1 gene in familial breast and ovarian cancer is well established. However, whether there is a role for BRCA1 in the development of sporadic breast cancer, which is much more common, is still unclear. Several studies have reported that loss of heterozygosity (LOH) at the 17q21 locus is a common event in sporadic breast cancer [4, 5] and, therefore, it has been postulated that BRCA1 may also play a role in these tumors. However, a somatic mutation of the BRCA1 gene has been reported in only one study [9]. It is therefore not excluded that other mechanisms may lead to alterations in the synthesis of functional BRCA1 protein. One of the proposed mechanisms is the reduction of BRCA1 mRNA expression levels in breast cancer cells [10, 16, 18]. The BRCA1 expression level observed in sporadic breast cancer cells, however, still remains higher than the expression level in breast cancer cells from patients carrying a hereditary BRCA1 mutation [8]. Reduction of BRCA1 protein has been observed in extracts from sporadic breast tumors, with or without LOH at the BRCA1 locus [12, 13]. By immunohistochemistry, loss of nuclear BRCA1 has been observed in part of the sporadic breast tumors [7, 17].

We developed a reliable immunohistochemical method using commercially available antibodies to get more insight in the role of BRCA1 in breast cancer. Using this method, we analyzed the BRCA1 expression in normal and tumor specimens obtained from young and old breast cancer patients.

Materials and methods

Material

Tissue was obtained from patients with breast cancer who underwent breast surgery at the Academic Hospital of the Free University of Brussels (VUB) between 1991 and 1996. This period was chosen because the method for processing of tissue specimens was similar and the more recent the cases, the more likely it was that

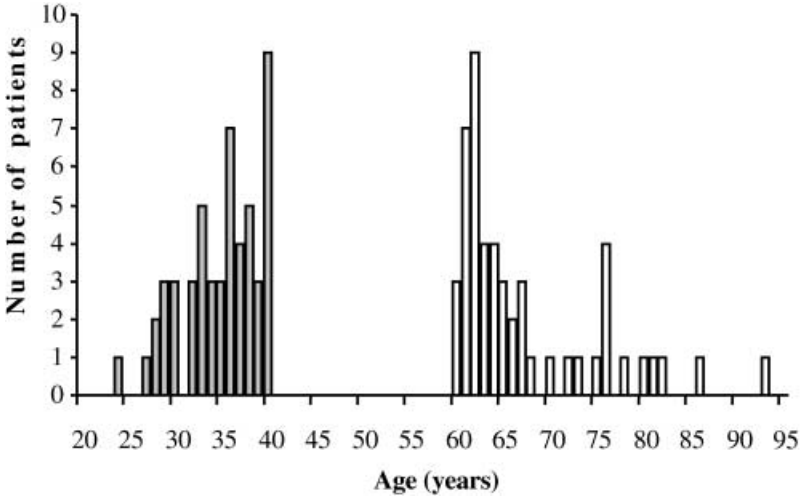

Fig. 1 Age distribution within the two patients groups

the patients were still alive if genetic testing would be required. The tissue specimens were fixed in Bouin's solution for 24 h, and for each patient, one or two representative blocks with normal and tumor tissue were selected.

The specimens were divided in two groups:

- Fifty-two consecutive tumorectomy and mastectomy specimens from patients aged 24–40 years ("young patients"). Microscopically, they were classified as: ductal carcinoma in situ (*n*=5), invasive ductal carcinoma (*n*=37), invasive lobular carcinoma (*n*=4), and medullary carcinoma (*n*=6).
- Fifty consecutive tumorectomy and mastectomy specimens taken from patients aged 60–93 years ("old patients"). Microscopically, they were: ductal carcinoma in situ (*n*=2), invasive ductal carcinoma (*n*=35), invasive lobular carcinoma (*n*=6), medullary carcinoma (*n*=2), tubular carcinoma (*n*=2), and mucinous carcinoma (*n*=3).

The age distribution of the patients is given in Fig. 1. Nine "young" patients and one "old" patient had one relative (mother) with breast cancer. One of these "young" patients had two relatives (mother and sister) with breast or ovarian cancer.

Method

Four affinity-purified rabbit polyclonal antibodies were purchased from Santa Cruz Biotechnology, Inc. (Santa Cruz, CA): D-20 (cat#sc-641) and K-18 (cat#sc-1021) are antibodies raised against a peptide corresponding to amino acids 2–21 and 70–89, respectively, both mapping at the amino terminus of human BRCA1; I-20 (cat#sc-646) recognizes the amino acids 1823–1842, and C-20 (cat#sc-642) reacts with aminoacids 1843–1862, located at the carboxy terminus of human BRCA1.

To find the best working conditions, we tested the four antibodies on testicular and breast tissue sections fixed either in Bouin's or in 4% formalin.

As epitope retrieval method, digestion with trypsin or microwave heating was used. After rehydration, the tissue sections were either treated with 0.1% crude trypsin (Boehringer Mannheim Biochemica, Germany) from bovine pancreas in distilled water containing 0.1% calcium chloride (pH 7.8) at 37° for 5 min or heated in a microwave oven in citrate buffer pH 6 for 9 min at 750 W.

After testing several dilutions, the working dilutions for the primary antibodies were determined. They were for D-20 1:600, for K-18 1:150, for I-20 1:150, and for C-20 1:150. The second antibody (goat anti-rabbit Ig, code RPN 1004, Amersham, England) was used at dilution 1:250.

Several specificity tests for the immunohistochemical staining were performed: the primary antibodies were omitted. substituted with normal rabbit serum or PBS, preabsorbed with an excess of antigenic peptides (D-20 P, cat#sc-641 P; K-18 P, cat#sc-1021 P; I-20 P, cat#sc-646 P; C-20 P, cat#sc-642 P) as recommended by the manufacturer.

With each staining experiment, positive and negative controls for the antibodies were carried out.

The BRCA1 localization pattern was evaluated at the nuclear and cytoplasmic level. The cytoplasmic staining intensity was graded from absent to strong. The immunoreactivity (nuclear and cytoplasmic) was an estimation of the percentage of stained cells.

Blood of six patients whose tumors did not show any BRCA1 nuclear staining was available. Mothers of two of these patients had breast cancer and one of these two patients also had a sister with ovarian cancer. On genomic DNA of these patients a protein truncation test and single strand conformation polymorphism/heteroduplex analysis to search for the presence of mutations in exon 11 and exons 2, 5, and 20, respectively, were performed [6].

The data obtained for each of the two groups of patients as well as the data obtained in normal and tumor tissue were compared using logistic regression analysis and the Wilcoxon signed ranks test. The latter served as an approximate estimation of the difference in nuclear immunoreactivity and cytoplasmic staining intensity between normal and tumor tissue.

All the *P*-values used were two-sided and *P*-values less than 5% were judged to be statistically significant.

Results

Antibody specificity and technique

Since the BRCA1 staining obtained in breast and testicular tissue was absent or weak when applying the basic immunohistochemical procedure, several combinations of fixatives, antibodies, and antigen retrieval methods were tested. The best results with the four antibodies were obtained in Bouin's fixed tissue and trypsinization as epitope retrieval method. The strongest signal was obtained with the D-20 antibody. A summary of the results of these experiments with D-20 and K-18 antibodies is shown in Table 1. Similar results were obtained with I-20 and C-20 antibodies (data not shown).

In epithelial and stromal cells, a common pattern of nuclear and cytoplasmic staining was observed with the four antibodies. In Western blot and immunohistochemical staining controls (preincubation with the corresponding

Table 1 Effect of fixation and antigen retrieval on immunostaining with D-20 and K-18 antibodies. *N* nuclear, *C* cytoplasmic, - absent, +/- doubtful, + weak, ++ moderate, +++ strong staining

Fixative		Formol				Bouin's			
Tissue		Testis		Breast		Testis		Breast	
Localization		N	C	N	C	N	C	N	C
No antigen retrieval:	D-20	–	+/–	–	+/–	+/–	+	+/–	+
	K-18	–	–	–	–	–	–	–	–
Microwave:	D-20	–	+/+++	–	+/+++	–	+/+++	–	+/++++
	K-18	–	–	–	–	–	–	–	–
Trypsin:	D-20	+	+/++	–	+/+++	+/+++	+/+++	+/+++	+/+++
	K-18	–	+/++	–	–	+/+++	+/+++	+/+++	+/+++

Table 2 Immunohistochemistry for BRCA1 protein (D-20 antibody) in normal and tumoral breast. *N* nuclear, *C* cytoplasmic, *No* no staining, +/- doubtful, + weak, ++ moderate, +++ strong straining. Data are expressed as number of cases

Specimen type (number)	Localization		Cytoplasmic staining intensity					% Immunoreactive cells											
	N	C	No	+/–	+	++	+++	Nuclear						Cytoplasmic					
								0	0–5	5–25	25–50	50–75	>75	0	0–5	0–25	25–50	50–75	>75
Normal tissue																			
Young patients (52)	50	52	–	1	8	17	30	2	–	8	1	3	38	–	–	–	–	1	51
Old patients (50)	48	50	–	–	7	16	29	2	–	3	3	–	42	–	–	–	–	1	49
Cancer tissue																			
Young patients (52)	38	52	–	3	18	25	12	14	–	2	6	2	28	–	1	–	1	–	50
Old patients (50)	47	50	–	–	15	21	17	3	2	6	7	6	26	–	1	1	1	1	46

antigenic peptide) the immunopositivity observed with D-20 and K-18 antibodies entirely disappeared, while for I-20 and C-20 antibodies, the signal persisted partially (data not shown). Based on these results, we applied only D-20 and K-18 antibodies for further analysis of the BRCA1 expression.

BRCA1 staining in normal and tumor breast tissue

A detailed summary of BRCA1 localization, immunoreactivity and cytoplasmic staining intensity is given in Table 2. As similar results were obtained with D-20 and K-18 antibodies, only those obtained with D-20 antibody are presented. The staining pattern was similar in the normal tissue from both young and old patients. The cytoplasmic staining intensity varied from weak to strong, while the nuclear staining was present in more than 75% of the cells in the majority of normal tissue samples. The nuclear staining was absent in the normal breast tissue samples of four (two young and two old) patients.

Compared to normal epithelial cells, cancer cells showed variability in BRCA1 staining. In a significant fraction of the breast cancers from young as well as old patients, the BRCA1 immunostaining was comparable in intensity and number of stained cells to that observed in the adjacent normal tissue (Fig. 2 A, B). The tumors and their corresponding adjacent normal tissue obtained an equal score for nuclear immunoreactivity in 24 (46%) young and 25 (50%) old patients; an equal scoring for cytoplasmic staining intensity was observed in 19 (36%) young and 25 (50%) old patients.

The other breast cancers scored less in the neoplastic cells than the adjacent normal tissue for the two parameters (Fig. 2C, D): in the tumors of 10 (19%) young and 21 (42%) old patients the relative amount of the cells with unstained nuclei ranged between 4 and 75%. In 14 (27%) tumors of young and 3 (6%) of old patients, BRCA1 nuclear staining was totally absent. The cells with no nuclear staining were often clustered or mixed with cells with a BRCA1 nuclear staining. The decrease in nuclear immunoreactivity and cytoplasmic staining intensity in the tumor was statistically significant when compared to normal tissue (Wilcoxon signed ranks test, $P<0.01$). In old patients this decrease was seen as a reduction in the nuclear immunoreactivity (Fig. 3 A), while in young patients, this decrease mainly resulted from the occurrence of a high number of cases devoid of any nuclear staining in the cancer cells (Fig. 3B). Nuclear BRCA1 expression was significantly less in the tumors of the young patients (Logistic regression, $P=0.0097$).

Genetic testing

Peripheral white blood cells were obtained from 6 out of 14 young patients with breast cancer that showed no BRCA1 nuclear staining in their tumor. DNA was extracted and analyzed for the presence of a constitutive

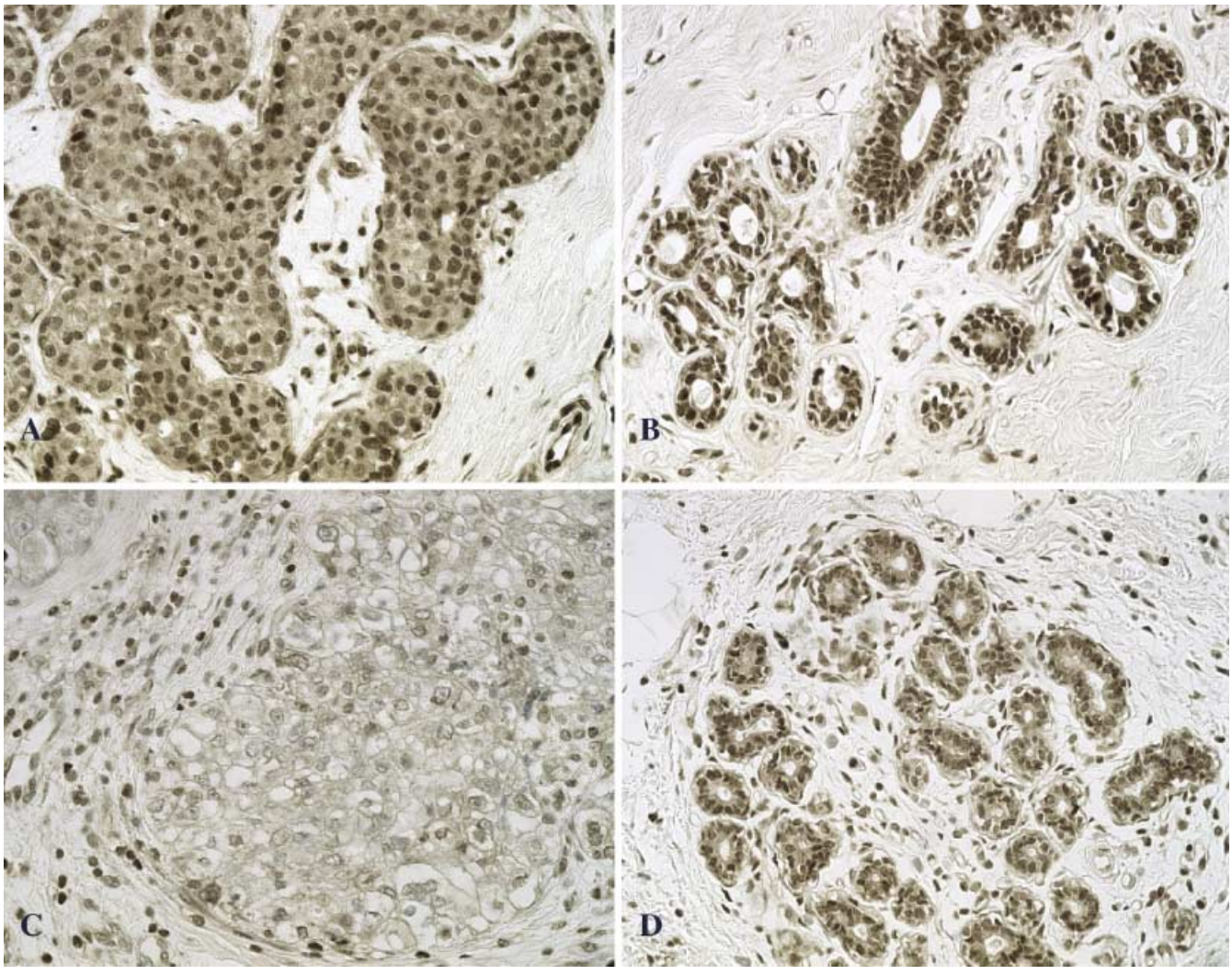

Fig. 2 BRCA1 staining (D-20 antibody) in breast cancer (**A. C**) and adjacent normal tissue (**B, D**). Tumor tissue shows: (1) a BRCA1 staining comparable to that of normal tissue (**A, B**); and (2) a faint to absent BRCA1 staining (**C, D**) (×280)

BRCA1 mutation. In one patient with a family history of breast and ovarian carcinoma, we found a splice site mutation at the exon5/intron 5 boundary (IVS5+3A>G). The RNA study in this patient demonstrated that an alternative splice site located 22 bp within exon 5 was used. In the other five patients we could not detect a mutation.

Discussion

In this study, we aimed to analyze the BRCA1 staining pattern observed in normal and tumoral breast tissue from breast cancer patients. For that reason, we first established a reliable immunohistochemical staining protocol for the BRCA1 protein.

Four commercially available polyclonal antibodies raised against the BRCA1 protein purchased from Santa Cruz Biotechnology (Santa Cruz, CA) were tested. These antibodies have been previously used to stain breast tumor sections [1, 19] but both studies failed to detect a nuclear staining.

In our study, when tissue specimens were fixed in Bouin's fixative or in formalin and embedded in paraffin, only a weak or almost no immunoreactivity was detected with all antibodies. We found that trypsinization was very effective for epitope unmasking in both nuclei and cytoplasm when using Bouin's but not formalin-fixed tissues embedded in paraffin. In both above-mentioned studies [1, 19], only formalin-fixed tissue was used, which could explain the absence of a BRCA1 nuclear staining.

A spotty or diffuse nuclear and a granular cytoplasmic staining seen in our sections was considered to be BRCA1 specific since it was obtained with the four antibodies. But because the carboxy terminal antibodies were found to produce non specific additional staining patterns, the further analysis was performed using the amino terminal antibodies D-20 and K-18.

In order to investigate a possible influence of patient age on the BRCA1 staining pattern, breast tumors from

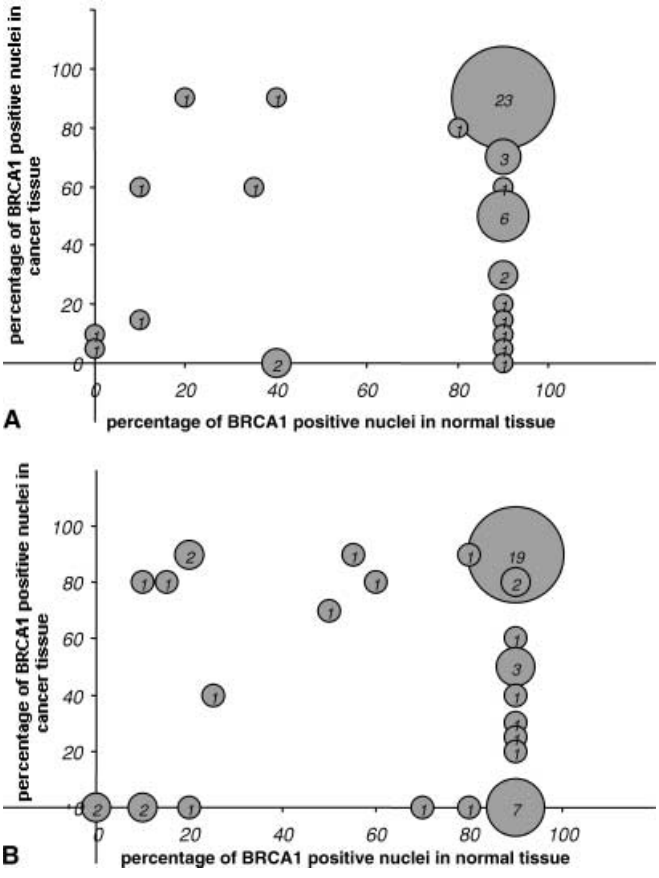

Fig. 3 Nuclear immunoreactivity (D-20 antibody) in normal versus cancer tissue in old (**A**) and young (**B**) patients. Each patient is represented by a *small circle* in the bubble diagram. The size of the bubbles represent the number of patients (as indicated) with identical nuclear immunoreactivity characteristics

two different age groups (younger than 40 or older than 60 years at surgery) were analyzed.

When investigating the normal breast tissue adjacent to a neoplastic lesion, the results were very similar to those seen in breast tissue of nonaffected women: a large majority (80%) of patients showed nuclear immunopositivity in almost all the normal epithelial cells, whereas in the remaining specimens, a nuclear staining was observed in less than 75% of the cells. Since the decrease in the number of immunopositive normal epithelial cells could be observed in young as well as in old patients, we assume that this is not due to age dependent hormonal factors. Other physiological factors must be responsible for the observed differences in BRCA1 expression levels.

Tumor tissue can be easily distinguished morphologically from adjacent normal tissue; therefore, we could estimate the proportion of the nuclear positive cells in both compartments for each patient. In about 50% of specimens, almost all normal and cancer cells showed a nuclear BRCA1 staining. This was observed in both young and old patients. Apparently, in these breast cancers, the molecular pathway leading to the nuclear localization of BRCA1 is not disrupted. In most of the remaining specimens we investigated, however, the percentage of nuclear BRCA1 positive cancer cells was clearly lower. The same proportion of tumors from young and old patients showed a decrease in the percentage of the cells with nuclear BRCA1 staining, but this decrease was more drastic in tumors of young patients. Although the breast tumors differed in nuclear BRCA1 expression, we could not relate this to different biological properties: no significant association was found between nuclear BRCA1 expression and tumor type, grade, size, lymph node involvement, hormone receptor status, or Neu overexpression (data not shown).

A significant fraction of the tumors from young patients showed no nuclear staining at all. It remains an open question whether the total absence of nuclear staining in these tumors results from age specific physiologic parameters (i.e., cyclic endocrine conditions) or is a property of a particular type of breast cancer occurring almost exclusively among young patients. When considering the “mixed” tumors in which cells with stained and unstained nuclei coexist, it is again unclear whether the tumor cells respond differently because they are (epi) genetically different or because an extracellular modulating factor does not reach the optimum concentration throughout the tumor tissue. In these tumors, nuclear negative cells are often clustered, but, while this observation could suggest a clonal proliferation, in some other tumors the BRCA1 nuclear-negative cells were mixed with the positive ones.

A specific BRCA1 granular cytoplasmic staining has been detected in almost all cells of normal and tumor specimens from all patients, indicating that the absence of the nuclear staining does not coincide with a total absence of the BRCA1 protein in the cell. However, a significant decrease in cytoplasmic staining intensity in tumor cells was observed mainly in those tumors showing a decrease in the percentage of cells with nuclear immunoreactivity, and especially in those tumors that showed a decrease in nuclear staining intensity. These observations led us to suggest that the decrease in the BRCA1 mRNA and protein level described by several authors and detected in a significant fraction of breast tissue extracts from sporadic tumors [10, 16, 18] is restricted to those tumors presenting a lower percentage of nuclear positive cells. We therefore believe that, in those cells in which BRCA1 mRNA is expressed at a low level, the total amount of the BRCA1 protein available is insufficient to be efficiently targeted in the nuclear complexes where it is supposed to participate in a DNA repair mechanism [14, 15], giving somatic mutations the possibility of accumulation.

At this moment the mechanism leading to decreased BRCA1 expression in a significant fraction of sporadic cancers is still unknown. It is interesting to note in this respect that BRCA1 promoter hypermethylation was recently reported in a significant fraction of sporadic breast tumors [2,11]. In such tumor samples, nonmethylated promoter sequences were still detected at relatively high levels. Since these nonmethylated sequences are presumably not inactivated, we may assume that the

BRCA1 protein is still partially synthesized in such tumors, which fits well with our immunohistochemical results.

A small fraction of our patients is statistically expected to carry an inherited BRCA1 mutation. The tumors obtained from such patients are supposed to be devoid of nuclear staining [3]. We focused our mutation screening efforts on young patients whose tumors did not show any nuclear staining at all. We identified one patient whose mother and sister died from a breast or ovarian cancer bearing a constitutive / predisposing BRCA1 mutation. In the other five investigated patients, we could not detect a mutation, although, with the mutation screening method used, we covered about 60% of the BRCA1 open reading frame. These results indicate that at least a fraction of the tumors devoid of any nuclear staining are sporadic ones. This also means that the immunohistochemical approach applied on breast cancer tissue sections cannot be used as a prescreening test for isolation of BRCA1 cancer predisposing mutations.

In conclusion, we found that breast cancers can be divided into two main categories according to nuclear BRCA1 immunostaining. In about half of the patients, young and old, the staining is present in almost all the normal and cancer cells. We have no reason to believe that BRCA1 is involved in the genesis of these cancers. In the second category of patients, a variable but significant fraction of the tumor cells shows no nuclear staining. The reason for this difference in BRCA1 expression between the cancer cells is unclear. In a subfraction of these patients no nuclear BRCA1 staining at all could be observed in the tumor cells. These tumors are found almost exclusively among young patients and include those with a hereditary BRCA1 mutation.

Acknowledgements We are grateful to Prof. L. Kaufman, Department of Biostatistics and Medical Informatics, Free University of Brussels, for the statistical analysis of the data.

References

1. Bernard-Gallon DJ, Peffault De Latour M, Rio PG, Penault-LLorca FM, Favy DA, Hizel C, Chassagne J, Bignon YJ (1999) Subcellular localization of BRCA1 protein in sporadic breast carcinoma with or without allelic loss of BRCA1 gene. Int J Oncol 14(4): 653–661
2. Bianco T, Hussey D, Dobrovic A (1999) Methylation-sensitive, single strand conformation analysis (MS-SSCA): A rapid method to screen for and analyze methylation. Hum Mutat 14: 289–293
3. Chen CF, Li S, Chen Y, Chen PL, Lee WH (1996) The nuclear localization sequences of the BRCA1 protein interact with the importin-α subunit of the nuclear transport signal receptor. J Biol Chem 271: 32863–32868
4. Cropp CS, Nevanlinna H, Pyrhönnen S, Stenman UH, Salmikangas P, Albertsen H, White R, Callahan R (1994) Evidence for the involvement of BRCA1 in sporadic breast carcinoma. Cancer Res 54: 2548–2551
5. Futreal A, Soderkvist P, Marks JR, Iglehart JD, Cochran C, Barrett JC, Wiseman RW (1992) Detection of the frequent allelic loss on proximal chromosome 17q in sporadic breast carcinoma using microsatellite length polymorphism. Cancer Res 52(9): 2624–2627
6. Goelen G, Teugels E, Bonduelle M, Neyns B, De Grève J (1999) High frequency of BRCA1 germline mutations in 42 Belgian families with a small number of symptomatic subjects. J Med Genet 36(4): 304–308
7. Jarvis EM, Kirk JA, Clarke CL (1998) Loss of nuclear BRCA1 expression in breast cancers is associated with a highly proliferative tumor phenotype. Cancer Genet Cytogenet 101: 109–115
8. Kainu T, Kononen J, Johannssonn O, Olsson HT, Borg A, Isola J (1996) Detection of germline BRCA1 mutations in breast cancer patients by quantitative messenger RNA in Situ hybridization. Cancer Res 56: 2912–2915
9. Khoo US, Ozçelic H, Cheung ANY, Chow L.WC, Ngan HYS, Done SJ, Liang ACT, Chan VWY, Au GKH, Ng WF, Poon CSP, Leung YF, Loong F, Ip P, Chan GSV, Andrulis IL, Lu J, Ho FCS (1999) Somatic mutations in the BRCA1 in Chinese sporadic breast and ovarian cancer. Oncogene 18: 4643–4646
10. Magdinier F, Ribieras S, Lenuar GM, Frappart L, Dante R (1998) Down-regulation of BRCA1 in human sporadic breast cancer; analysis of DNA methylation patterns of the putative promoter region. Oncogene 17: 3169–3176
11. Mancini DN, Rodenhiser DI, Ainsworth PJ, O'Malley FP, Singh SM, Xing W, Archer TK (1998) CpG methylation within the 5′ regulatory region of the BRCA1 gene is tumor specific and includes a putative CREB binding site. Oncogene 16(9): 1161–1169.
12. Ozçelik H, To MD, Couture J, Bull SB, Andrulis IL (1998) Preferential allele expression can lead to reduced expression of BRCA1 in sporadic breast cancers. Int J Cancer 77:1–6
13. Rio P, Maurizis JC, Peffault De Latour M, Bignon YJ, Bernard-Gallon D (1999) Quantification of BRCA1 protein in sporadic breast carcinoma with or without loss of heterozygosity of the BRCA1 gene. Int J Cancer 80: 823–826
14. Scully R, Anderson S, Chao D, Wei W, Ye L, Young R, Livingston D, Parvin J (1997) Brca1 is a component of the RNA polymerase II holoenzyme. Proc Natl Aca Sci USA 94: 5605–5610
15. Scully R, Chen Y, Plug A, Xiao Y, Weaver D, Feunteun J, Ashley T, Livingston D (1997) Association of BRCA1 with Rad51 in mitotic and meiotic cells. Cell 88: 265–275
16. Sourvinos G, Spandidos DA (1998) Decreased BRCA1 expression levels may arrest the cell cycle through activation of p53 checkpoint in human sporadic breast tumors. Bioch Bioph Res Comm 245: 75–80
17. Taylor J, Lymboura M, Pace PE, Hern RP, Desai AJ, Shousha S (1998) An important role for BRCA1 in breast cancer progression is indicated by its loss in a large proportion of non-familial breast cancers. Int J Cancer 79: 334–342
18. Thompson M, Jensen R, Obermiller P, Page D, Holt J (1995) Decreased expression of BRCA1 accelerates growth and is often present during sporadic breast cancer progression. Nat Genet 9: 444–450
19. Wilson C. et al (1999) Localization of human BRCA1 and its loss in high-grade, non-inherited breast carcinomas. Nat Genet 21: 236–240

Virchows Arch (2002) 440:280–284
DOI 10.1007/s004280100506

ORIGINAL ARTICLE

Josep Lloreta · M. Dolores Ferrer
Josep M. Corominas · Marco Pavesi · Sergi Serrano
Bruce Mackay

Prediction of recurrence and nucleolar features in node-negative breast carcinoma, ductal type, grade II

An ultrastructural study

Received: 6 March 2001 / Accepted: 13 June 2001 / Published online: 18 August 2001
© Springer-Verlag 2001

Abstract One-third of patients with node-negative breast carcinoma develop a local recurrence that will decisively influence their outcome. We conducted this quantitative ultrastructural study to determine the value of nucleolar features in predicting recurrence of node-negative breast carcinomas. Forty-three node-negative infiltrating duct carcinomas were examined by means of electron microscopy. The number of cells with three or more nucleoli (N3), percentage of nucleoli contacting the nuclear membrane (NC), patient age, tumor size, grading, treatment, follow-up time, development of recurrence, and status were recorded. There were no differences in patient age, tumor grade, or modality of surgical treatment. Significant differences were found among patients with and without recurrence for N3 (P=0.02), NC (P=0.01), and tumor size (P=0.01). For N3, the positive predictive value (PPV) was 64.3, and the negative predictive value (NPV) was 72.4 (sensitivity=52.9%; specificity=80.8%; P=0.04). For NC, the PPV was 62.5, and the NPV was 74.1 (sensitivity=58.8%; specificity=76.9%; P=0.02). For tumor size, the PPV was 66.7, and the NPV was 64.9 (sensitivity=23.5%; specificity=92.3%; P not significant). Using logistic regression analysis, independent predictive value was shown for N3, NC, and tumor size. The number of nucleoli per cell and the number of cells with nucleoli in contact with the nuclear membrane have independent predictive value for the development of recurrence in lymph node-negative infiltrating duct carcinoma of the breast. Although electron microscopy is a highly accurate method, improving the precision of light microscopic techniques would allow more universal assessment of these nucleolar features.

Keywords Breast cancer · Electron microscopy · Nucleolus · Prognosis · Recurrence · Ultrastructure

The results of this study were presented in part at the 88th Annual Meeting of the United States and Canadian Academy of Pathology, San Francisco, 1999. For this presentation, M.D. Ferrer was the recipient of the 1999 Pathologist-in-Training Award from the Society for Ultrastructural Pathology

J. Lloreta (✉) · M.D. Ferrer
Department of Pathology, Hospital del Mar-IMAS-IMIM,
Universitat Pompeu Fabra, Passeig Marítim 25–29,
08003 Barcelona, Spain
e-mail: 16975jlt@comb.es
Tel.: +34-93-2483031, Fax: +34-93-2483131

J.M. Corominas · S. Serrano
Hospital del Mar-IMAS-IMIM,
Autonomous University of Barcelona, Passeig Marítim 25,
08003 Barcelona, Spain

M. Pavesi
Department of Medical Statistics,
Institut Municipal d'Investigació Mèdica, Dr. Aiguader 80,
08003 Barcelona, Spain

B. Mackay
Department of Pathology, University of Texas,
MD Anderson Cancer Center, 1515 Holcombe Blvd.,
Houston, TX 77030, USA

Introduction

Approximately one-third of conservatively treated breast carcinomas with uninvolved margins of resection and negative axillary lymph nodes develop a local recurrence that usually determines the outcome of patients [22]. With the continuous improvement in diagnosis and treatment of breast cancer, attention is directed toward prognostic factors that can be used for the prediction of recurrence in the increasingly common node-negative cases. In this regard, much of the current research is aimed at molecular markers [8, 19, 20, 21, 23, 25, 33]. Chromosomal abnormalities, DNA-ploidy, and S-phase fraction [7, 27] have also been investigated, with variable results. Several nuclear grading strategies, including morphometry of cytology or biopsy specimens, have been used to predict recurrence in node-negative breast cancer patients with variable, sometimes paradoxical results [1, 3, 4, 11, 29]. A large body of literature has been devoted to quantifica-

tion of nucleolar organizing regions, chromatin domains related to nucleolar function [6]. Some of these studies contributed promising results [5, 18, 26]. Complex, more accurate nuclear grading methods have recently been published [1], but simple, practical, and reproducible solutions to predicting recurrence of node-negative breast tumors have not been found.

It is well known that margination of nucleoli to the nuclear membrane is more often observed in cells with high metabolic activity [17]. Also, nucleolar size is related to the levels of protein synthesis [9], and increased nucleolar size is used as a cytological criterion for malignant transformation in many settings. When nucleoli are large enough, they can be quantified using light microscopy, particularly in touch imprints that contain whole nuclei instead of nuclear sections [17]. However, it is well known that assembly of portions of nucleolar proteins is often impaired in malignant cells [9], and this results in the presence of multiple small nucleoli that are often below the limit of the light microscope's resolving power. In this size range, low-power electron microscopy (EM) has been shown to be a very accurate method in different settings [10, 12, 13, 16]. Thus, number and margination of nucleoli have been found to be significantly different in two subsets of medullary carcinoma of the breast, i.e., node-positive and node-negative tumors [13]. Nucleoli of infiltrating duct carcinoma cells have not been previously assessed using quantitative EM, and therefore the present ultrastructural study was designed to quantitatively investigate nucleolar features of node-negative breast carcinomas, as well as their specificity, sensitivity, and individual predictive value in the identification of tumors with higher chance of recurrence.

Materials and methods

The present study is based on 43 strictly selected, node-negative infiltrating duct carcinomas processed for EM and separated into two groups: group I, with recurrent tumor (n=17); and group II, with nonrecurrent tumor (n=26). The cases were obtained from the files of the Electron Microscopy Laboratory at the M.D. Anderson Cancer Center. The requirements for inclusion were female sex, pure infiltrating duct pattern, grade-II histology, negative-node status, minimum follow-up of 5 years, and viable tumor tissue adequately preserved for EM, not including necrotic areas. In addition, all patients had been treated according to the same surgical, preoperative, postoperative, and follow-up protocol. Patients with other previous, intercurrent, or subsequent diseases that could influence survival were excluded.

All tumor samples had been randomly taken from fresh, viable tumor tissue, then fixed in 2.5% glutaraldehyde, postfixed in 1% osmium tetroxide, dehydrated in increasing concentrations of ethanol, and embedded in epoxy resin according to the same protocol. Semithin (1 µm) sections were obtained from 5 to 15 plastic blocks in each case, and the block containing the largest amount of viable tumor cells was selected. Thin sections (100 nm) were obtained from two blocks and were stained with uranyl acetate and lead citrate. All cases were examined using a Philips CM100 electron microscope. Random pictures were taken from viable tumor tissue at a constant calibrated magnification of 2700× (original magnification of 900×, plus a steady 3× enlarger factor).

A number of clinico-pathologic and morphologic parameters were recorded in each case: number of cells with one, two, and three or more (N3) nucleoli (Fig. 1, Fig. 2, Fig. 3, Fig. 4); percentage of nucleoli contacting the nuclear membrane (NC) (Fig. 1); age of patient at diagnosis; tumor size; time of follow-up in months; development of recurrence; and status of patient at last follow-up.

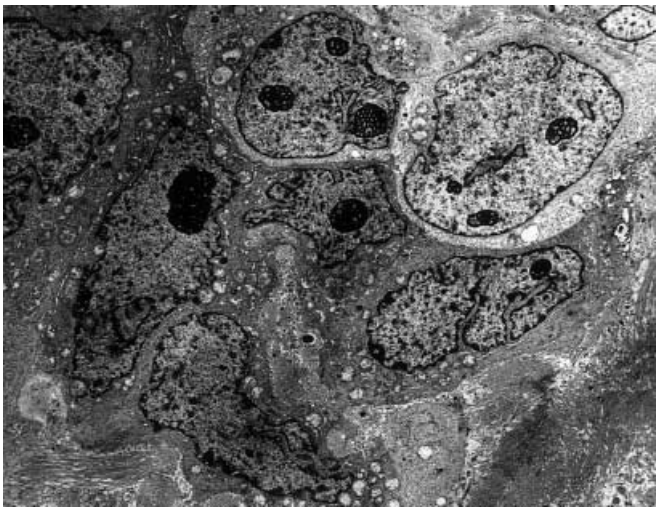

Fig. 1 Recurrent breast carcinoma (group I). Electron microscopy(EM): three or more nucleoli per nuclear section are present in several cells. Delicate invaginations of the nuclear membrane provide sites for close contact with nucleoli. Transmission EM, 900×

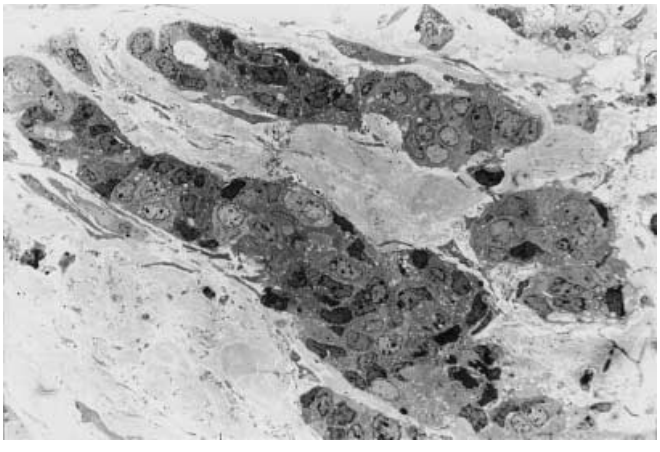

Fig. 2 Light microscopic appearance of the tumor shown in Fig. 1. Toluidine blue, 800×

For quantitative parameters, the minimum number of nuclei that were counted was estimated empirically: it was the minimum value at which the running mean for a given parameter did not change significantly by adding subsequent measurements [14, 15, 28]. All viable tumor cells in which nucleoli could be identified were counted (36–83 cells per case, mean 52 cells).

For statistical analysis, continuous variables were summarized by distribution means and standard deviations (SDs). Distribution median, and minimum and maximum values were shown whenever a variable did not fit normal distribution. Categorical variables were summarized by means of group percentages.

- Univariate analyses: for the recorded parameters, the best cutoff point for establishing the threshold to estimate the probability of recurrence was calculated according to the method reported by Robert et al. [24]. Predictive values, sensibility, and specificity were estimated by the calculating 95% confidence

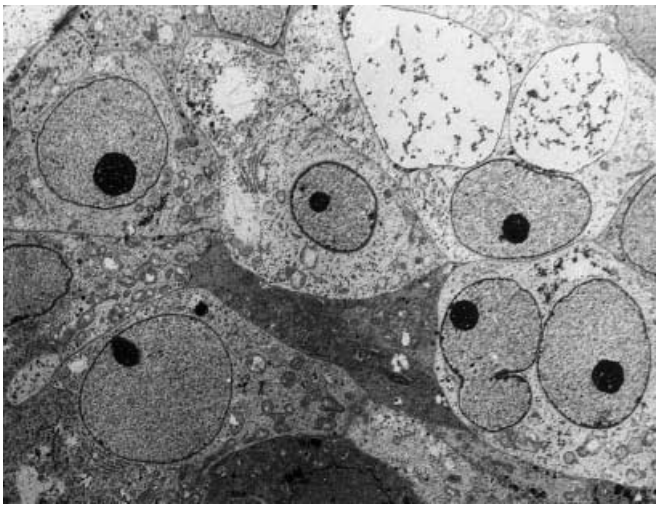

Fig. 3 Nonrecurrent breast carcinoma (group II). Electron microscopy (EM): no more than two nucleoli are present in every plane of nuclear section. In this field, most nucleoli do not contact with the nuclear membrane. Transmission EM, 900×

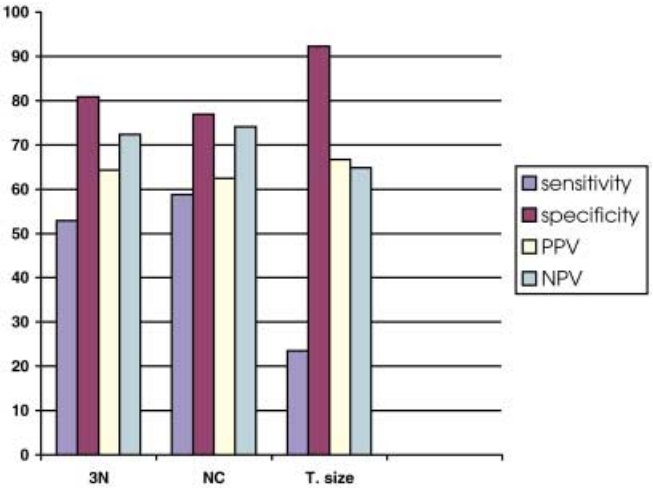

Fig. 5 Comparative sensitivity, specificity, positive predictive value, and negative predictive value for number of cells with three or more nucleoli (N3), number of nucleoli contacting nuclear membrane (NC), and tumor size, in grade-II infiltrating duct carcinomas of the breast

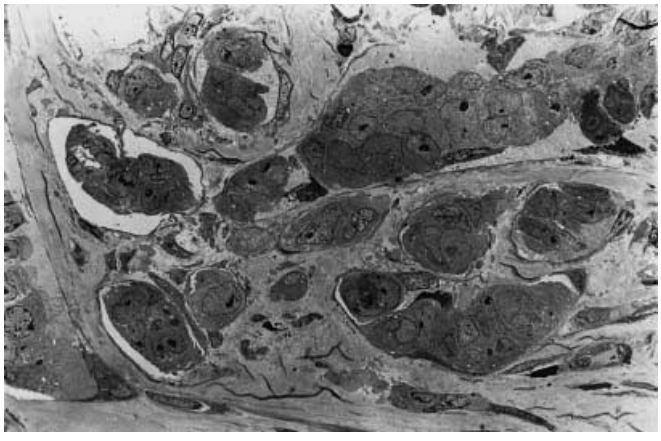

Fig. 4 Light microscopic appearance of the tumor shown in Fig. 3. Toluidine blue, 800×

interval of each proportion. A Chi-square test was used to test the null hypothesis of no difference between group proportions. Whenever any expected value less than 5 was observed in a cell, Fisher's Exact test was used.

- Multivariate analysis: independent predictive values for each study parameter were estimated by adjusting a logistic regression model. Presence of a recurrence was the outcome variable; study parameters were entered into the model as dycotomic factors, according to best cutoff points previously established. Relative risks of presenting the outcome were estimated for each factor by calculating 95% confidence intervals. Statistical analysis was performed using SPSS software (SPSS, Chicago, Ill.).

Results

There were no differences in patient age (group I: range 31–80 years, mean 56 years; group II: range 31–81 years, mean 57 years), tumor grade (all selected cases were grade-II tumors), or modality of surgical treatment (modified radical mastectomy with axillary lymph node dissection in all cases). Tumor size ranged from 1.3 cm to 13 cm in group I (mean±SD 4.5±3.3 cm) and from 0.7 cm to 6 cm in group II (2.8±1.8 cm). In group I, 16 patients were dead after a follow-up of 80.5 months (5–162 months). All group-II patients were alive and free of disease after a follow-up of 155.2 months (60–340 months).

The number of cells with one nucleolus per nuclear section ranged from 9 to 44 in group I (25.4±9.7) and from 2 to 41 in group II (16.5±9). The number of cells with two nucleoli per nuclear section ranged from 0 to 12 in group I (4.4±3.1) and from 0 to 11 in group II (3.4±2.7). The number of cells with three or more nucleoli (N3) per nuclear section (Fig. 1, Fig. 2) ranged from 0 to 6 in group I (1.6±1.6) and from 0 to 5 in group II (0.61±0.98). The number of nucleoli contacting the nuclear membrane (NC) ranged from 30% to 88% in group I (58±17.4%) and from 23% to 80% in group II (44.3±17%). Significant differences between both groups were found for N3 (P=0.02), NC (P=0.01), and tumor size (P=0.01). For N3, PPV was 64.3 and NPV was 72.4, with a sensitivity of 52.9% and a specificity of 80.8% (P=0.04). For NC, PPV was 62.5 and NPV was 74.1, with a sensitivity of 58.8% and a specificity of 76.9% (P=0.02). For tumor size, PPV was 66.7 and NPV was 64.9, with a sensitivity of 23.5% and a specificity of 92.3% (P value not significant). Using logistic regression analysis, independent predictive value was shown for N3 [odds ratio (OR)=5.6; P=0.04], NC (OR=19.3; P=0.01), and tumor size (OR=16.9; P=0.002) (Fig. 5).

Discussion

Grading systems currently used for breast cancer, including the widely accepted Elston and Ellis grading system, take into consideration nuclear features of tumors [30, 31, 32]. In this study, we attempted to minimize the influence of grading in the results by including only cases in a single grade category. Grade-II tumors were chosen because, although this is probably not the most common grade, it is probably the group in which additional information could be most helpful.

The need for an improvement in the prediction of recurrence in node-negative, apparently cured breast cancer is obvious, as this situation is becoming more common with the availability of better methods for early detection, diagnosis, and treatment. Many different studies have addressed this issue using molecular techniques, immunohistochemical markers, light microscopic image analysis, and morphometric and cytometric methods [1, 3, 4, 7, 8, 11, 19, 20, 21, 23, 25, 27, 29, 33]. Thus, *p53* and c-*erb*-B2 have been shown to correlate with survival of patients, but their use in predicting recurrence has not been definitively shown [20]. The content of cathepsin D in stromal cells, but not in tumor cells, has been associated with aggressive behavior, but many conflicting results and methodologic discrepancies among several studies on this subject have not been solved [19]. Ki-67 antigen expression has been shown to be statistically correlated with mitotic counts [33], although the latter are even more subjective than semiquantitative estimates of immunohistochemical results [2, 30, 31, 32].

Previous studies on the correlation between nucleolar features and breast cancer prognosis have been directed mainly to nucleolar organizing regions (AgNOR) [5, 6, 18, 26]. In this regard, it must be emphasized that the features measured using EM in the present series are strictly focused on the nucleolus itself. Although nucleolar organizing regions are located in chromatin domains associated with the nucleolus and, as such, have been related to the metabolic activity of the tumors and to patient outcome, they are different from nucleolar features evaluated in the present series. Some of the reports on AgNOR quantification have shown interesting results [6, 18, 26]. The method, however, is based on a silver-staining technique, which is a relatively time-consuming, sometimes erratic approach that has not been homogeneously reproducible in all hands. These technical difficulties, plus the limitations in objective and precise quantification (the stain is sensitive in detecting AgNOR but, as most silver-based techniques, is not completely specific), have resulted in this method not being included in the protocols of most institutions.

The results of the present ultrastructural study suggest that features of nucleoli in breast cancer cells have a potential role in predicting recurrence of node-negative cases. Compared with tumor size, the two parameters tested (N3 and NC) show lower but still remarkably high specificity and PPV for recurrence. In the present series, both N3 and NC are much more sensitive in predicting recurrence than tumor size, and their NPV is also higher. However, the large size of some tumors in group I could have influenced the value of tumor size in our series. Both ultrastructural parameters show independent predictive value for recurrence using logistic regression analysis. It is important to emphasize that these results were obtained from a very homogeneous set of patients, as we have attempted to minimize potential interference of other variables. In addition to all the selection criteria summarized above (similar histological appearance and grade of tumors, same management protocols, regular and prolonged follow-up, and lack of intercurrent diseases or complications), patients in both groups were treated by means of radical mastectomy, and, therefore, the risk for residual tumor instead of true recurrence being the cause of the relapse was minimized.

The purpose of this study was to investigate the potential value of nucleolar features in predicting recurrence in node-negative patients. The very thin sections used in EM imply that only some of the nucleoli are included, and therefore the resulting figures are relative rather than absolute counts; nevertheless, provided that adequate sampling strategies are used, this approach results in fairly precise and, most importantly, significant counts. Many of the nucleoli that can be identified easily with EM are far beyond the resolving power of the light microscope, even in semi-thin plastic sections, or at least are impossible to identify confidently as such (Fig. 2, Fig. 4). In addition, regarding contact of nucleoli with nuclear membrane, some of the nucleoli that appear separated from the nuclear membrane in cytology or biopsy specimens are actually contacting it through an invagination, and, conversely, some nucleoli that seem to be apposed to the nuclear membrane are in fact separated from it despite being peripherally located in the nucleus.

Most EM laboratories are able to process specimens on a 24-h basis, digital EM cameras have eliminated dark room processing, and a reliable nucleolar count can be available the day after surgery for the cost of one of the antibodies used in breast carcinomas. However, many institutions do not have an EM facility, so further research should be directed toward reproducing the results of this ultrastructural study using high-resolution light microscopy.

In conclusion, ultrastructural assessment of both the number of nucleoli per cell and the number of cells with nucleoli contacting the nuclear membrane has independent predictive value for the development of recurrence in lymph node-negative infiltrating duct carcinoma of the breast. The standardization of simple, quick methods of tissue processing for EM along with the use of digital EM cameras make it a reliable method that can be included in the protocols for pathologic evaluation of breast cancer, but efforts should be directed to reproduce these measurements using the more universally available high-resolution light microscopy. Thus, patients more likely to have tumor recurrence could be identified even preoperatively.

Acknowledgements This work was supported by grant FIS 93/0394 from Fondo de Investigacion Sanitaria, Government of Spain. The authors thank Elsa Ramos, Lydia Shanks, Mannie Steglich, María Andrea García, and Luís Magán for their excellent technical assistance. Dedicated to the memory of Elsa Ramos.

References

1. Albert R, Müller JG, Kristen P, Harms H (1998) Objective nuclear grading for node-negative breast cancer patients: comparison of quasi-3D and 2D image-analysis based on light microscopic images. Lab Invest 78:247–259
2. Baak JPA (1990) Mitosis counting in tumors. Hum Pathol 21:683–685
3. Baak JPA, Laderkarl M, Sorensen FB (1994) Reproducibility of mean nuclear volume and correlation with mean nuclear area in breast cancer: an investigation of various sampling schemes. Hum Pathol 25:80–85
4. Bur M, Andreis C, Garb J, Frank J (1995) The prognostic value of nuclear morphometry in breast cancer (abstract). Lab Invest 72:15
5. Crocker J, Boldy DAR, Egan MJ (1989) How should we count AgNORs? Proposals for a standardized approach. J Pathol 158:185–188
6. Derenzini M, Pession A, Trerè D (1990) Quantity of nucleolar silver-stained proteins is related to proliferating activity in cancer cells. Lab Invest 63:137–140
7. Eliasen CA, Opitz LM, Vamvakas EC, Espiritu EC, Marsh ER, Roses DF, Harris MN, Feiner HD (1991) Flow cytometric analysis of DNA ploidy and S-phase fraction in breast cancer using cells obtained by ex vivo fine-needle aspiration: an optimal method for sample collection. Mod Pathol 4:196–200
8. Fioravanti L, Cappelleti V, Coradini D, Miodini P, Borsani G, Daidone MG, et al (1997) Int-2 oncogene amplification and prognosis in node-negative breast carcinoma. Int J Cancer 74:620–624
9. Ghadially FN (1997) Ultrastructural pathology of the cell and matrix. Butterworth-Heinemann, Boston, pp 58–71
10. Horie A, Ohta M (1981) Ultrastructural features of large cell carcinoma of the lung with reference to prognosis of patients. Hum Pathol 12:423–432
11. Kronqvist P, Kuopio T, Collan Y, Horvath C, Tamm U (1997) The reproducibility of nuclear morphometric measurements in invasive breast carcinoma. Anal Cell Pathol 15:47–59
12. Lloreta-Trull J, Mackay B, Troncoso P, Ribalta-Farrés T, Smith T, Khorana S (1992) Neuroendocrine tumors of the nasal cavity: an ultrastructural and morphometric study of 24 cases. Ultrastruct Pathol 16:165–175
13. Lloreta J, Mariñoso ML, Corominas JM, Cañas MA, Serrano S (1997) Medullary carcinoma of the breast: an ultrastructural and morphometric study of nine cases. Ultrastruct Pathol 21: 499–507
14. Marchevsky AM, Erler BS (1994) Morphometry in Pathology. In: Marchevsky AM, Bartels PH (eds) Image analysis: a primer for pathologists. Raven Press, New York, pp 125–179
15. Mayhew TM, Reith A (1988) Introducing basic principles and methods of stereology and morphometry. In: Reith A, Mayhew TM (eds) Stereology and morphometry in electron microscopy. Hemisphere Publishing, New York, pp 1–12
16. McDonagh D, Vollmer RT, Shelburne JD (1991) Intercellular junctions and tumor behavior in lung cancer. Mod Pathol 4:436–440
17. Montironi R, Braccischi A, Scarpelli M, Matera G, Alberti R (1991) Value of quantitative nucleolar features in the preoperative cytological diagnosis of follicular neoplasias of the thyroid. J Clin Pathol 44:509–514
18. Mourad WA, Erkman-Balis B, Livingston S, Shoukri M, Cox CE, Nicosia SV, Rowlands DT (1992) Argyrophilic nucleolar organizer regions in breast carcinoma. Correlation with DNA flow cytometry, histopathology, and lymph node status. Cancer 69:1739–1744
19. Nadji M, Fresno M, Nassiri M, Conner G, Herrero A, Morales AR (1996) Cathepsin D in host stromal cells, but not in tumor cells, is associated with aggressive behavior in node-negative breast cancer. Hum Pathol 27:890–895
20. O'Malley FP, Saad Z, Kerkvliet N, Doig G, Stitt S, Ainsworth P, Hundal H, Chambers AF, Turnbull DI, Bramwell V (1996) The predictive power of semiquantitative immunohistochemical assessment of p53 and c-erb B-2 in lymph node-negative breast cancer. Hum Pathol 27:955–963
21. Patel DD, Bhatavdekar JM, Chikhlikar PR, Ghosh N, Suthar TP, Shah NG, et al. (1996) Node-negative breast carcinoma: hyperprolactinemia and/or overexpression of p53 as an independent predictor of poor prognosis compared to newer and established prognosticators. J Surg Oncol 62:86–92
22. Quiet CA, Ferguson DJ, Weichselbaum RR, Hellman S (1995) Natural history of node-negative breast cancer. J Clin Oncol 13:1144–1151
23. Reed W, Hannisdal E, Boehler PJ, Gundersen S, Host H, Nesland JM (2000) The prognostic value of p53 and C-erb B-2 immunostaining is overrated for patients with lymph node negative breast carcinoma: a multivariate analysis of prognostic factors in 613 patients with a follow-up of 14–30 years. Cancer 88:804–813
24. Robert C, Vermont J, Bosson JL (1991) Formulas for threshold computations. Comput Biomed Res 24:514–529
25. Siitonen SM, Haapasalo HK, Rantala IS, Helin HJ, Isola JJ (1995) Comparison of different immunohistochemical methods in the assessment of angiogenesis: lack of prognostic value in a group of 77 selected node-negative breast carcinomas. Mod Pathol 8:745–752
26. Smith R, Crocker J (1988) Evaluation of nucleolar organizer region-associated proteins in breast malignancy. Histopathology 12:113–125
27. Troncoso P, Dytch HE, Bibbo M, Wied GL, Dawson PJ (1989) The significance of DNA measurements in a histologically defined subset of infiltrating ductal carcinomas of the breast with long-term follow-up. Anal Quant Cytol Histol 11:166–172
28. True LD (1996) Morphometric applications in anatomic pathology. Hum Pathol 27:450–467
29. Tuczek HV, Fritz P, Schwarzmann P, Wu X, Mähner G (1996) Breast carcinoma: correlations between visual diagnostic criteria for histologic grading and features of image analysis. Anal Quant Cytol Histol 18:481–493
30. Van Diest PJ, Baak JPA (1991) The morphometric prognostic index is the strongest prognosticator in premenopausal lymph node-negative and lymph node-positive breast cancer patients. Hum Pathol 22:326–330
31. Van Diest PJ, Baak JPA, Matze-Cok P, Wisse-Brekelmans ECM, van Galen CM, Kurver PHJ, Bellot SM, Fijnheer J, van Gorp LHM, Kwee WS, Los J, Peterse JL, Ruitenberg HM, Schapers RFM, Schipper MEI, Somsen JG, Willig AWPM, Ariens AT (1992) Reproducibility of mitosis counting in 2,469 breast cancer specimens: results from the Multicenter Morphometric Mammary Carcinoma Project. Hum Pathol 23:603–607
32. Weidner N, Moore DH, Ljung BM, Waldman FM, Goodson WH, Mayall B, Chew K, Smith HS (1993) Correlation of bromodeoxyuridine (BRDU) labeling of breast carcinoma cells with mitotic figure content and tumor grade. Am J Surg Pathol 17:987–994
33. Weidner N, Moore DH, Vartanian R (1994) Correlation of Ki-67 antigen expression with mitotic figure index and tumor grade in breast carcinomas using the novel “paraffin”-reactive MIB1 antibody. Hum Pathol 25:337–342

Virchows Arch (2002) 440:285–290
DOI 10.1007/s004280100495

ORIGINAL ARTICLE

**Koji Hiraoka · Michihisa Zenmyo · Setsuro Komiya
Rikimaru Kawabata · Masahiro Yokouchi
Ritsu Suzuki · Tetsuya Hamada · Seiya Kato
Kensei Nagata**

Relationship of p21 (waf1/cip1) and differentiation n chondrosarcoma cells

Received: 13 March 2001 / Accepted: 28 May 2001 / Published online: 24 August 2001
© Springer-Verlag 2001

Abstract The histological grade of chondrosarcoma correlates well with their clinical behavior and with the patient's survival duration. We have previously demonstrated that p21 was expressed in the hypertrophic chondrocytes of the growth plate. To assess the relationship of p21 (waf1/cip1) to cell differentiation in chondrosarcoma, we examined the p21 expression in 14 cases of chondrosarcoma immunohistochemically and the induction of p21 by insulin-like growth factor-I (IGF-I) during cell differentiation in SW1353 chondrosarcoma cells. p21 immunoreactivity was seen in well-differentiated chondrosarcoma cells and was mutually exclusive with MIB1 reactivity in grade-1 chondrosarcoma. In vitro, the proteoglycan synthesis of SW1353 cells was increased by IGF-I in a dose-dependent manner. However, cell proliferation was not markedly stimulated. Overexpressions of p21 mRNA and *p21 protein* in SW1353 cells were induced by IGF-I 100 ng/ml. Our results suggested that the p21 expression was directly related to tumor differentiation and that the p21 expression was an important mediator for IGF-I in chondrosarcoma cells.

Keywords P21 · Insulin-like growth factor-I (IGF-I) · Chondrosarcoma · Differentiation

K. Hiraoka (✉) · M. Zenmyo · R. Suzuki · T. Hamada · K. Nagata
Department of Orthopedic Surgery,
Kurume University School of Medicine, 67 Asahi-machi,
Kurume, 830-0011, Japan
e-mail: khiraoka@med.kurume-u.ac.jp
Tel.: +81-942-317568, Fax: +81-942-350709

S. Komiya · M. Yokouchi
Department of Orthopedic Surgery,
Kagoshima University Faculty of Medicine,
835-1 Sakuragaoka, Kagoshima, 890-8520, Japan

R. Kawabata · S. Kato
Department of Pathology, Kurume University School of Medicine,
67 Asahi-machi, Kurume, 830-0011, Japan

Introduction

Chondrosarcoma is the second most frequent primary malignant bone tumor. The histological features of conventional chondrosarcoma are subdivided into three grades, I through III, and these have been well correlated with their clinical behavior. The tumor cells of low- to intermediate-grade chondrosarcoma, which have inactive clinical behaviors and low metastatic potentials, often exhibit differentiation to chondrocytes. In chondrocytes including growth cartilage cells, many kinds of hormones, such as parathyroid hormone (PTH) [21] and parathyroid hormone related peptide (PTHrP) [1], and growth factors, such as transforming growth factor-β (TGF-β) [14], insulin-like growth factors (IGFs) [8, 18, 22], fibroblast growth factor (FGF) [15], and bone morphogenetic proteins (BMPs) [16] have been reported to regulate cell proliferation and differentiation.

The cyclin-dependent kinase inhibitor p21 (waf1/cip1) has been reported to play an important role in cell differentiation [2, 12, 27]. p21 immunoreactivity has recently been observed in human tissues, where it seems to be related to cell differentiation [4, 7, 9, 10, 13, 20, 23]. p21 was thought to be regulated by wild-type p53 as a response to DNA damage. However, it has now been shown that p21 can also be induced through p53-independent pathways by growth factors, including TGF-β [3, 5], FGF [11], tumor necrosis factor-α (TNF-α) [24], and platelet-derived growth factor (PDGF) [11]. We previously demonstrated the transcriptional activation of p21 by vitamin D3 or K2 during cell differentiation in p53-deficient osteosarcoma cells [26]. Although IGF-I is also well known as promoting the growth and differentiation of chondrocytes [8, 18, 22], it has not yet been determined whether p21 was induced or not by IGF-I during cell differentiation in chondrocytes or chondrosarcoma cells.

In the present study, we investigated the immunohistochemical p21 expression in chondrosarcoma of histological grades I, II, and III, including various differentiation patterns, and of p21 overexpression by IGF-I in SW1353

chondrosarcoma cells. The aim was to clarify the relationship between p21 expression and differentiation, and to investigate the regulation of the p21 expression by IGF-I in chondrosarcoma.

Materials and methods

Immunohistochemical staining

Fourteen cases of chondrosarcoma were collected after surgical resection in our institute. All tissues were fixed in formalin and embedded in paraffin. The histological grade of these cases was grade I in six cases, grade II in six cases, and grade III in two cases.

Immunohistochemical stainings for *p21* (clone: SX118; BD PharMingen, San Diego, Calif.) and MIB1 (Immunotech, Marseille Cedex, France) for assessing tumor proliferation were performed using an avidin-biotinylated complex (ABC) kit (Vector Laboratories, Burlingame, Calif.). Sections were treated with a microwave antigen retrieval system, then incubated for 1 h at room temperature with a primary antibody (1:200 dilution). The positive controls for p21 immunostaining were sections of lung carcinoma with a known overexpression of p21.

Cell culture

SW-1353 chondrosarcoma cells (ATTC, Rockville, Md.) were cultured in Dulbecco's modified Eagle's medium (DMEM, Nissui Pharmaceutical Company, Tokyo, Japan) supplemented with 10% fetal calf serum (FCS, Bioproducts, Warrenton, Ore.), 100 U/ml penicillin, and 10 mg/ml of streptomycin (Gibco Life Technologies Inc, Gettysburg, Md.).

Cells proliferation assay

MTT (3,(4,5-dimethylthiazol-2-yl)2,5-diphenyltetrazolium bromide; Sigma, St. Louis, Mo.) was dissolved at a concentration of 5 mg/ml in sterile phosphate-buffered saline (PBS) at room temperature, and the solution was further sterilized by filtration and stored at 4°C in a dark bottle with a tight cap. Lysing buffer was prepared as follows: 20% w/v sodium dodecyl sulfate (SDS; Sigma) was dissolved at 37°C in a solution of 50% *N*,*N*-dimethyl formamide (DMF; Wako, Osaka, Japan) and 50% demineralized water using magnetic stirring, and the pH was adjusted to 4.7.

The cells were plated in 96-well dishes and cultured in DMEM supplemented with 10% FCS. After they reached semi-confluence, the cells were washed three times with PBS. Then, following the addition of serum-free medium, incubation was continued for 24 h to arrest cell growth. Medium containing various concentrations of IGF-I (Genzyme/Techne, Cambridge, Mass.) was added to each culture. After incubation for 24 h, the cell growth was determined. A 25-µl aliquot of the 5-mg/ml stock solution of MTT was added to each well and, after 2 h of incubation at 37°C, 100 µl of the extraction buffer was added. After an overnight incubation at 37°C, the optical density at 570 nm was measured using a microplate reader (Bio-Rad Lab, Richmond, Calif.) 96-well multiscanner, employing the extraction buffer as the blank. Unless specified in the text, no mixing was performed, and no medium was removed prior to the addition of any ingredient.

Determination of proteoglycan synthesis

The radioactive [^{35} S]sulfate was purchased from Amersham Japan (Tokyo, Japan). Proteoglycan synthesis by the cells was measured as $^{35}SO_4$ incorporation. The cells were incubated for 24 h in IGF-I-containing medium in 24-well dishes. For the last 18 h of the culture, cells were incubated with [^{35} S]sulfate. The cells were washed with PBS, harvested with 0.5 M NaOH, neutralized with an equal volume of 0.5 M HCl, and placed onto a glass microfiber filter (GF/D Whatman Maidstone, Kent, U.K.). The filter was washed with 10% trichloroacetic acid and placed in vials containing 8 ml scintillation fluid Aquasol-2 (Packard, Meriden, Conn.). The isotope incorporation was measured using a γ scintillation counter LSC-1050 (Aloka, Tokyo, Japan).

Northern-blotting analysis

The cells were plated in 60-mm dishes (1×10^6/dish) and cultured in 5 ml medium. The cells were incubated in serum-free medium for 24 h before the experiment. After the medium was replaced with fresh medium containing 100 ng/ml IGF-I or not, the cells were incubated for a further 24 h. The total RNA was then extracted from the culture using the acid guanidinium isocyanate/phenol/chloroform method. For Northern blotting, total RNA (10 µg) was separated on a 1.0% agarose gel containing 2.4% formaldehyde, then transferred to a positively charged nylon membrane. After fixation under calibrated ultraviolet (UV) irradiation, the membrane was hybridized with a digoxigenin (DIG)-labeled probe for p21 prepared using a DIG-RNA labeling kit (Boehringer, Tokyo, Japan). The blot was visualized using alkaline-phosphatase-labeled anti-DIG antibody and a chemiluminescent substrate, according to the manufacturer's instructions. Quantitative analysis for the blots was performed using NIH imaging software for Macintosh.

Western blotting for p21

The level of p21 expression following stimulation by IGF-I was measured using Western blotting with antihuman rabbit monoclonal p21 antibody (BD Pharmingen). The whole-cell extract was separated on a 10% (30:1, acrylamid:bis) SDS polyacrylamide gel prior to transfer to a nitrocellulose membrane. The membrane was incubated for 2 h at room temperature with a p21 antibody diluted 1:500 in PBS, the immunoreactive proteins were visualized using horseradish-peroxidase-conjugated anti-rabbit immunoglobulin (Dako, Glostrup, Denmark) diluted 1:5000 and the supersignal west pico chemiluminescent substrate (Pierce, Rockford, Ill.). Quantitative analysis for the blots was performed using NIH imaging software for Macintosh.

Statistical analysis

The significance of any difference was analyzed using Student's *t*-tests (two-tailed).

Results

In the 14 cases of chondrosarcoma, the p21 immunoreactivity was mainly observed in the chondrocyte differentiation cells. p21-positive cells showed mild cytologic atypia with lacunae in the cartilagenous matrix or more typically formed small clusters (Fig. 1A). p21-positive staining was restricted to a portion of the cells. MIB1 immunoreactivity was more pronounced in the spindle-shaped tumor cells than in well-differentiated cells (Fig. 2B). p21-positive staining was observed in four of the six grade-I cases, one of the six grade-II cases and was not observed in either of the two grade-III cases. MIB1-positive staining was observed in two of the six grade-I cases, four of the six grade-II cases, and one of the two grade-III cases. The two grade-II and also one

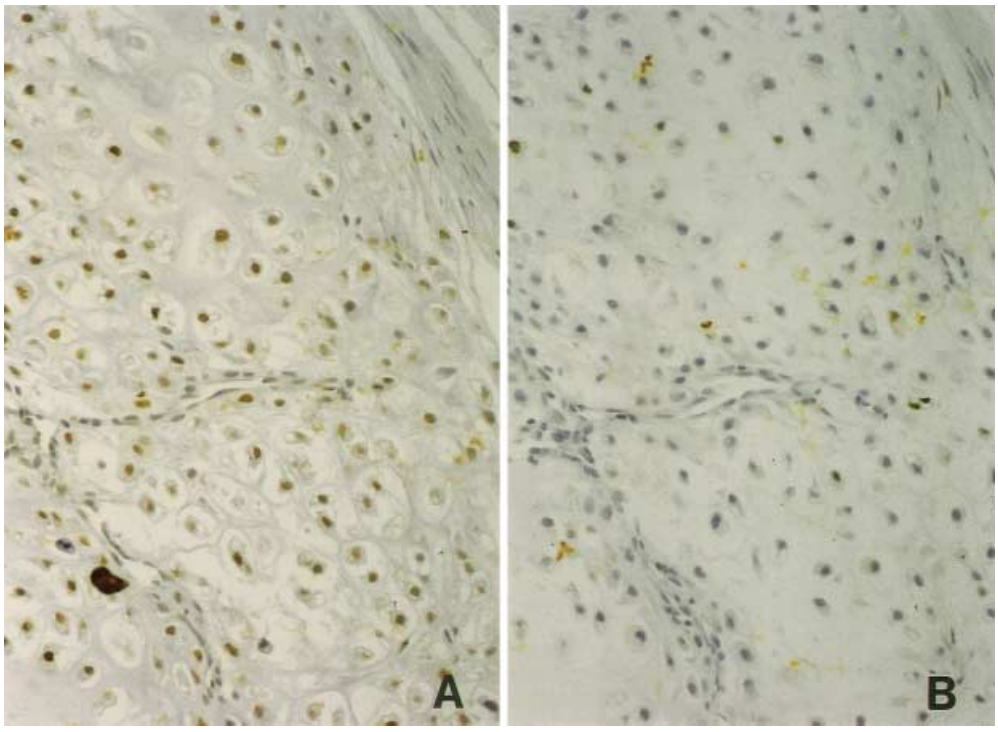

Fig. 1 **A** Immunohistochemical localization of p21 in grade-I chondrosarcoma. p21 immunoreactivity was seen in the cells resembling hypertrophic chondrocytes. **B** A few atypical cells demonstrated weak MIB1-positive staining in this section. Magnification: **A** ×50, **B** ×50

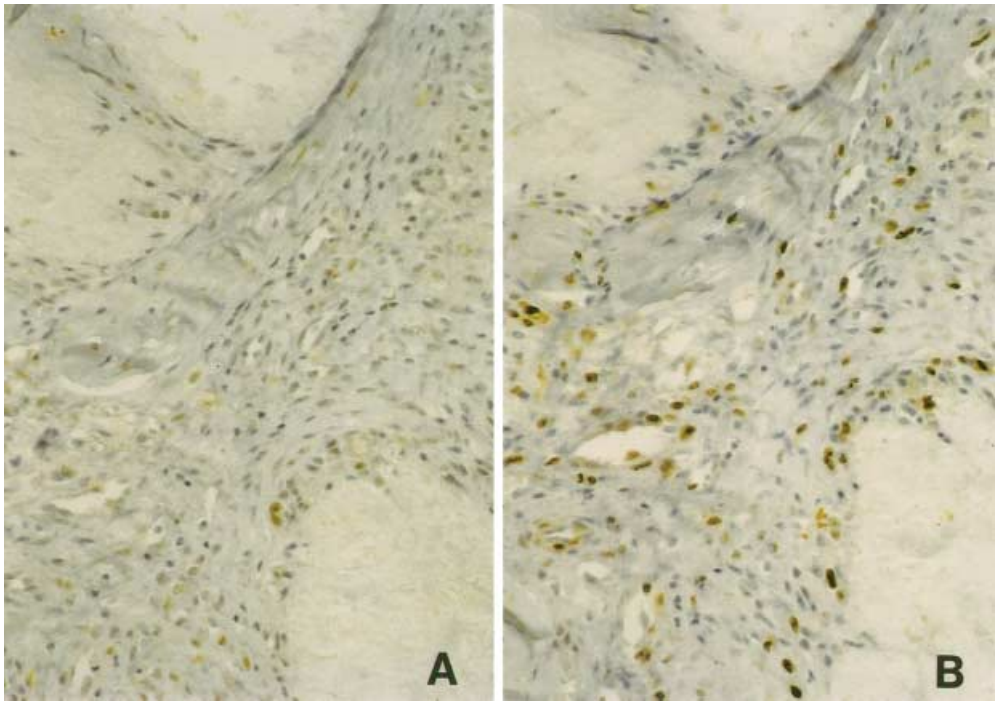

Fig. 2 **A** Grade-III chondrosarcoma cells demonstrated cytologic atypia without lacunae and weak immunoreactivity for p21. **B** MIB1 immunoreactivity was seen in spindle-shaped chondrosarcoma cells. Magnification: **A** ×50, **B** ×50

grade-II tumors expressed both p21 and MIB1. Another grade of chondrosarcoma demonstrated weak p21 expression in the area of strong MIB1-positive staining (Fig. 2A).

The in vitro stimulation effect of IGF-I on SW1353 cell proliferation showed a slight increase in temperature dependence. However, only stimulation by 100 ng/ml IGF-I was significant (P<0.001). This concentration increased the stimulation effect only 1.28-fold compared with controls (Fig. 3).

[^{35} S]sulfate incorporation was measured to estimate proteoglycan synthesis. IGF-I induced a dose-dependent enhancement in [^{35} S]sulfate incorporation by SW1353 cells. Compared with controls, 1, 5, 10, 50, and 100 ng/ml IGF-1 enhanced [^{35} S]sulfate incorporation 1.4-, 1.6-, 1.9-, 1.7-, and 2.1-fold, respectively (each P<0.001; Fig. 4).

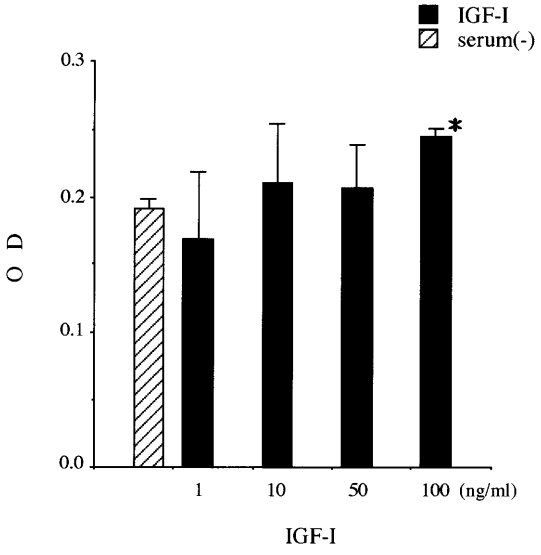

Fig. 3 The effect of insulin-like growth factor (IGF)-I on SW1353 cell proliferation. SW1353 cells were incubated in serum-free medium containing various concentrations of IGF-I (1–100 ng/ml) for 24 h. Cell proliferation was increased by IGF-I 100 ng/ml. *P<0.001

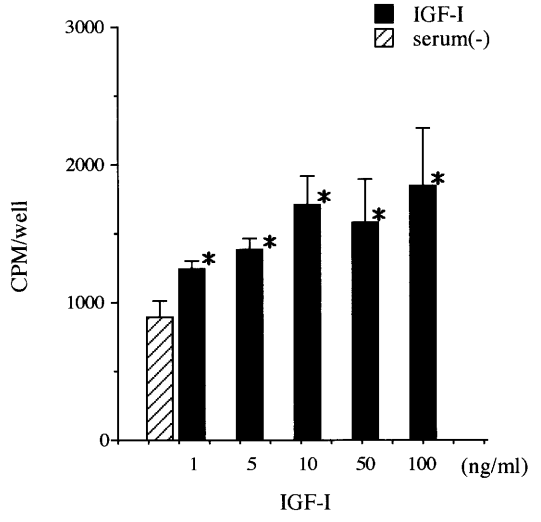

Fig. 4 The effect of insulin-like growth factor (IGF)-I on proteoglycan synthesis of SW1353 cells. Proteoglycan synthesis of the cells was measured as $^{35}SO_4$ incorporation after incubation for 24 h in medium containing IGF-I (1–100 ng/ml). Proteoglycan synthesis was increased in a dose-dependent manner. *P<0.001

We investigated the effect of IGF-I on the p21 mRNA expression in SW1353 cells and found that 100 ng/ml IGF-I enhanced the p21 mRNA expression. Quantitation using NIH imaging showed an approximately twofold enhancement effect (Fig. 5). Similarly, at the protein level, IGF-I caused a dose-dependent enhancement in p21 expression; at a concentration of 10 ng/ml of 2.4-fold and at 100 ng/ml of 3.2-fold (Fig. 6).

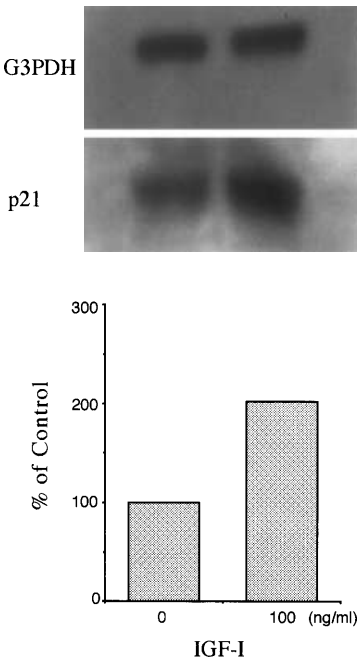

Fig. 5 The effect of insulin-like growth factor (IGF)-I on the p21 gene expression. Northern-blotting analysis showed that the expression of p21 mRNA was increased in the presence of IGF-I 100 ng/ml. The intensity of each band was measured densitometrically, and the amount of p21 mRNA was calculated as a percentage of the control value

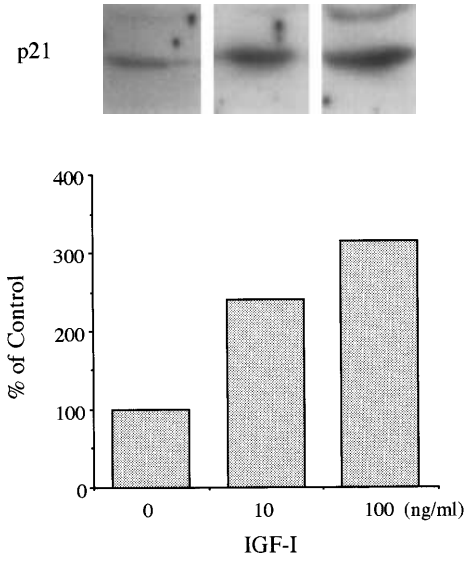

Fig. 6 The effect of insulin-like growth factor (IGF)-I on p21 protein. Western-blotting analysis showed that the production of p21 protein was increased in the presence of IGF-I (10 ng/ml and 100 ng/ml). The intensity of each band was measured densitometrically, and the amount of p21 protein was calculated as a percentage of the control value

Discussion

The mainstay of therapy for chondrosarcoma is surgical resection. Chemotherapy and radiotherapy hold little promise of a cure. The clinical prognosis of chondro-

sarcoma has been correlated relatively well with the grading of the histological malignancy. According to Evans's report, the 5-year survival rate for grades I, II, and III is 90%, 81%, and 43%, respectively, indicating a markedly poor prognosis for poorly differentiated grade III [6]. In the treatment of chondrosarcoma, cell differentiation is an important factor for prognosis, and the elucidation of its regulation is required. However, in various carcinoma cells, such as squamous cell carcinoma [23], thyroid carcinoma [20], adenocarcinoma [4], and leukemic cells [17, 27], it has been reported that the cyclin-dependent kinase inhibitor p21 participated in cell differentiation. It has also been confirmed that p21 accelerated cell differentiation through p53-independent pathways. Beier et al. reported that signaling through the Raf-1/MEK/ERK pathway was necessary for the p21 expression in chondrocytes [2]. In this study, we investigated the expression of p21 in tissues and cultured cells to ascertain the regulation of chondrosarcoma differentiation and discovered the p21 expression in low-grade, well-differentiated chondrosarcoma cells, in which cells resembling hypertrophic chondrocytes were characteristically positive for p21. We previously reported that hypertrophic chondrocytes in growth plates were positive for p21 [25], suggesting that p21 was also involved in the induction of cell differentiation in chondrosarcoma. Although the number of cases included in this study was too small to be correlated with treatment results, previous studies have found a significantly favorable prognosis for p21-positive squamous cell carcinoma of the lung [9] and for p21-positive colorectal carcinoma [13]. However, in laryngeal squamous cell carcinoma [7] and in adenocarcinoma of the lung [9], no correlation has been found between the p21 expression and the prognosis. In chondrosarcoma, the histological grades of differentiation have been clearly correlated with the prognosis; therefore, we speculate that the p21 expression influences the clinical outcome from treatment.

To investigate the regulation of the p21 expression, we stimulated cultured SW1353 chondrosarcoma cells with IGF-I. We found that IGF-I stimulated proteoglycan production in SW1353 cells in a dose-dependent manner, which suggested the induction of differentiation as in normal chondrocytes. However, IGF-I produced little effect on cell proliferation. Therefore, we concluded that IGF-I produced more stimulatory effect on differentiation than on the proliferation of SW1353 cells. The enhancement effect by IGF-I on p21 expression was confirmed at the protein and mRNA levels, suggesting that IGF-I induced the differentiation of chondrosarcoma in conjunction with p21. IGFs have been shown to act on chondrocytes as autocrine factors in their differentiation [22]. However, since not all cells of a chondrosarcoma express p21, we suspect that the mechanism for inhibition in activity exists in the p21 pathways. Numerous studies have recently been carried out regarding the regulatory factors in chondrocyte differentiation, and growth factors – particularly TGF-β [14], IGFs [22], FGF [15], and connective tissue growth factor [19] – have been reported to accelerate the proliferation and differentiation of chondrocytes. Chondrocytes or chondrosarcoma cells may be controlled by these factors in a complex manner, and studies on the interactions of these factors are needed.

Acknowledgements This work was supported in part by a Grant-in-Aid for Scientific Research (C) (10268914) from the Japan Ministry of Education, Science, Sports and Culture. We thank Miss Junko Okubo for technical assistance.

References

1. Amizuka N, Warshawsky H, Henderson JE, Goltzman D, Karaplis AC (1994) Parathyroid hormone-related peptide-depleted mice show abnormal epiphseal cartilage development and altered endochondral bone formation. J Cell Biol 126: 1611–1623
2. Beier F, Taylor AC, LuValle P (1999) The Raf-1/MEK/ERK pathway regulates the expression of the $p21^{Cip1/Waf1}$ gene in chondrocytes. J Biol Chem 274:30273–30279
3. Datto MB, Li Y, Panus JF, Howe DJ, Xiong Y, Wang XF (1995) Transforming growth factor beta induces the cyclin-dependent kinase inhibitor p21 through a p53-independent mechanism. Proc Natl Acad Sci U S A 92:5545–5549
4. Doglioni C, Pelosio P, Laurino L, Macri E, Meggiolaro E, Favretti F, Barbareschi M (1996) p21/waf1/cip1 expression in normal mucosa and in adenomas and adenocarcinomas of the colon: its relationship with differentiation. J Pathol 179: 248–253
5. Elbendary A, Berchuck A, Davis P, Havrilesky L, Bast RC Jr, Iglehart JD, Marks JR (1994) Transforming growth factor β1 can induce CIP1/WAF 1 expression independent of the p53 pathway in ovarian cancer cells. Cell Growth Differ 51: 301–307
6. Evans HL, Ayala AG, Romsdahl MM (1977) Prognostic factors in chondrosarcoma of bone: a clinicopathologic analysis with emphasis on histologic grading. Cancer 40:818–831
7. Hirvikoski P, Kellokoski JK, Kumpulainen EJ, Virtaniemi JA, Johansson RT, Kosma VM (1999) Downregulation of p21/WAF1 is related to advanced and dedifferentiated laryngeal squamous cell carcinoma. J Clin Pathol 52:440–444
8. Hunziker EB, Wagner J, Zapf J (1994) Differential effects of insulin-like growth factor 1 and growth hormone on developmental stages of rat growth plate chondrocytes in vivo. J Clin Invest 93:1078–1086
9. Komiya T, Hosono Y, Hirashima T, Masuda N, Yasumitsu T, Nakagawa K, Kikui M, Ohno A, Fukuoka M, Kawase I (1997) p21 expression as a predictor for favorable prognosis in squamous cell carcinoma of the lung. Clin Cancer Res 3: 1831–1835
10. Marchetti A, Doglioni C, Barbareschi M,Buttitta F, Pellegrini S, Bertacca G, Chella A, Merlo G, Angeletti CA, Palma PD, Bavilacqua G (1996) p21 RNA and protein expression in non-small cell lung carcinomas: evidence of p53-independent expression and association with tumoral differentiation. Oncogene 12:1319–1324
11. Michieli P, Chedid M, Lin D, Pierce JH, Mercer WE, Givol D (1994) Induction of WAF1/CIP1 by a p53-independent pathway. Cancer Res 54:3391–3395
12. Parker SB, Eichele G, Zhang P, Rawls A, Sands AT, Bradley A, Olson EN, Harper JW, Elledge SJ (1995) p53-independent expression of $p21^{Cip\ 1}$ in muscle and other terminally differentiating cells. Science 267:1024–1027
13. Ropponen KM, Kellokoski JK, Lipponen PK, Pietilainen T, Eskelinen MJ, Alhava EM, Kosma VM (1999) p21/WAF1 expression in human colorectal carcinoma: association with p53, transcriptional factor AP-2 and prognosis. Br J Cancer 81:133–140

14. Rosen F, McCabe G, Quach J, Solan J, Terkeltaub R, Seegmiller JE, Lotz M (1997) Differential effects of aging on human chondrocyte responses to transforming growth factor ß. Arthritis Rheum 40:1275–1281
15. Sahni M, Ambrosetti DC, Mansukhani A, Gertner R, Levy D, Basilico C (1999) FGF signaling inhibits chondrocyte proliferation and regulates bone development through the STAT-1 pathway. Genes Dev 13:1361–1366
16. Sailor LZ, Hewick RM, Morris EA (1996) Recombinant human bone morphogenetic protein-2 maintains the articular chondrocyte phenotype in long-term culture. J Orthop Res 14: 937–945
17. Schwaller J, Koeffler HP, Niklaus G, Loetscher P, Nagel S, Fey MF, Tobler A (1995) Posttranscriptional stabilization underlies p53-independent induction of $p21^{WAF1/CIP1/SDI1}$ in differentiating human leukemic cells. J Clin Invest 95:973–979
18. Seong SC, Matsumura T, Lee FY, Whelan MC, Li XQ, Trippel SB (1994) Insulin-like growth factor I regulation of swarm rat chondrosarcoma chondrocytes in culture. Exp Cell Res 211: 238–244
19. Shakunaga T, Ozaki T, Ohara N, Asaumi K, Doi T, Nishida K, Kawai A, Nakanishi T, Takigawa M, Inoue H (2000) Expression of connective tissue growth factor in cartilaginous tumor. Cancer 89:1466–1473
20. Soda G, Antonaci A, Bosco D, Nardoni S, Melis M (1999) Expression of bcl-2, c-erbB-2, p53, and p21 (waf1-cip1) protein in thyroid carcinomas. J Exp Clin Cancer Res 18:363–367
21. Takigawa M, Takano T, Suzuki F (1981) Effects of parathyroid hormone and cyclic AMP analogues on the activity of ornithine decarboxylase and expression of the differentiated phenotype of chondrocytes in culture. J Cell Physiol 106:259–268
22. Takigawa M, Okawa T, Pan HO, Aoki C, Takahashi K, Zue JD, Suzuki F, Kinoshita A (1997) Insulin-like growth factor I and II are autocrine factors in stimulating proteoglycan synthesis, a marker of differentiated chondrocytes, acting through their respective receptors on a clonal human chondrosarcoma-derived chondrocyte cell line, HCS-2/8. Endocrinology 138:4390–4400
23. Tron VA, Tang L, YongWP, Trotter MJ (1996) Differentiation-associated overexpression of the cyclin-dependent kinase inhibitor $p21^{waf-1}$ in human cutaneous squamous cell carcinoma. Am J Pathol 149:1139–1146
24. Yoshida K, Murohashi I, Hirashima K (1996) p53-independent induction of p21(WAF1/CIP1) during differentiation of HL-60 cells by tumor necrosis factor alpha. Int J Hematol 65:41–48
25. Zenmyo M, Komiya S, Hamada T, Hiraoka K, Suzuki R, Inoue A (2000) p21 and parathyroid hormone-related peptide in the growth plate. Calcif Tissue Int 67:378–381
26. Zenmyo M, Komiya S, Hamada T, Hiraoka K, Nagata K, Kato S, Fujii T, Yano H, Irie K (2001) Transcriptional activation of p21 by vitamin D3 or vitamin K2 leads to differentiation of p53-deficient MG-63 osteosarcoma cells. Hum Pathol 32: 410–416
27. Zhang W, Grasso L, McClain CD, Gambel AM, Cha Y, Travali S, Deisseroth AB, Mercer WE (1995) p53-independent induction of WAF1/CIP1 in human leukemia cells is correlated with growth arrest accompanying monocyte/macrophage differentiation. Cancer Res 55:668–674

Virchows Arch (2002) 440:291–297
DOI 10.1007/s004280100496

ORIGINAL ARTICLE

Peter Seifert · Michael Benedic · Peter Effert

Nerve fibers in tumors of the human urinary bladder

Received: 29 March 2001 / Accepted: 25 May 2001 / Published online: 13 July 2001
© Springer-Verlag 2001

Abstract Exophytic tumors of the urinary bladder were examined by means of transmission electron microscopy for the presence of neural tissue because, as yet, there has been hardly any discussion of a neuronal component in the biology of neoplasms. In the stroma and rarely in the epithelium of bladder tumors, fine nerve strands were found to be irregularly distributed. These strands comprised one to a maximum of five axons containing predominantly colocalized clear and dense-core vesicles. Immunohistochemistry revealed some nerve-like structures showing vasoactive intestinal neuropeptide (VIP) reactivity. This response and the combination of vesicle types indicate that parasympathetic cholinergic neurons contribute to the innervation of the tumors. Thus, a morphological basis for neuronal influence on the behavior of such tumors has been demonstrated.

Keywords Innervation · Tumor · Ultrastructure · Urinary bladder · VIP

Introduction

Recently, with a description of two intraocular tumors, it was reported for the first time that neoplastic tissue may be innervated [41]. It appeared therefore of special interest to find out whether these findings might be an organ- or tumor-specific event or whether nerve tissue could also be demonstrated in other neoplasms. The presence of nerve tissue would indicate a neuronal influence on tumor biology and would imply that such tumors are more closely related to the organism as a whole than had previously been thought. Exophytic tumors of the urinary bladder seemed to us a suitable tissue for investigation, because they project into the bladder lumen like little trees, so that there is a clear spatial separation between the exophytic tumor tissue and the wall of the bladder. For the present study, superficial bladder tumors in various degrees of differentiation were examined under the electron microscope.

P. Seifert (✉)
Alfried-Krupp Laboratory for Electron Microscopy,
Department of Ophthalmology, University of Bonn,
Sigmund-Freud-Strasse 25, 53105 Bonn, Germany
e-mail: pseifert@uni-bonn.de
Fax: +49-228-2874817

M. Benedic · P. Effert
Department of Urology, St. Franziskus Hospital, Aachen, Germany

P. Effert
Department of Urology, RWTH, University of Aachen, Germany

Materials and methods

Tissue

Bladder tumor tissue from five male patients was obtained by transurethral resection (Table 1). Immediately after removal, some of the tissue was reserved to be studied and was prepared for transmission electron microscopy (TEM) or for immunohistochemistry. Most of the tissue was fixed in 10% formaldehyde for conventional histopathological processing and hematoxylin and eosin (HE)-staining of paraffin sections. The stage (TNM) and degree of differentiation (G) of the tumors were determined by a pathologist according to the guidelines of the International Union Against Cancer (UICC), taking into account the World Health Organization (WHO)/ISUP consensus classification presented in 1998 [8]. In all cases, they proved to be urothelial bladder carcinomas. As normal control tissue, bladder mucosa biopsies taken from patients with no pathological alterations in this region were used.

Transmission electron microscopy

For conventional TEM, the specimens were fixed with Karnovsky's solution in 0.1 M phosphate buffer (pH 7.3), postfixed in 1% OsO_4, dehydrated in ethanol, and embedded in Durcupan ACM. Ultrathin sections (50 nm) were stained with uranyl acetate and lead citrate, and examined under a Zeiss EM 109 transmission electron microscope.

Immunohistochemistry

The tissue samples were fixed in a mixture of 3% paraformaldehyde and 0.2% glutaraldehyde, dehydrated in ethanol and embedded in paraffin (Paraplast Plus/Merck). For immunohistochemical localization of primary immunoreactions, the avidin–biotin complex method (ABC method) was used. Sections 5- to 7 µm thick

Table 1 List of tumor samples

Tumor no.	1	2	3	4	5
Age of patient (years)	80	60	71	76	69
Degree of differentiation	G1–2	G1	G1	G2	G3
Tumor stage	Ta	Ta	Ta	Ta	pTa
WHO/ISUP classification	2**	1*	1*	2**	3***

1*Papillary neoplasm of low malignant potential
2**Papillary carcinoma, low grade
3***Papillary carcinoma, high grade

were incubated in a moist chamber with primary antibody sera against (i) neuronal marker protein gene product 9.5 (PGP 9.5; Ultra Clone), polyclonal, rabbit, diluted 1:1000; (ii) S 100 protein (catalog no. PU058-UP, BioGenex), polyclonal, rabbit, diluted 1:100; (iii) neuropeptide vasoactive intestinal polypeptide (VIP; catalog no. 64-720, INC Biomedicals), polyclonal, rabbit, diluted 1:1000; (iv) substance P (SP; catalog no. 80509, Serva), monoclonal, rat, diluted 1:150; and (v) smooth muscle actin (code no. M0851, Dako), monoclonal, mouse, diluted 1:100. Immunoreactions were visualized with biotinylated species-specific secondary antibodies (RPN 1004, Amersham) and streptavidin-biotin–peroxidase complexes (RPN 1051 Amersham). To enhance the staining of the horseradish peroxidase reaction product, nickel–ammonium-sulfate was added to the diaminobenzidine-H_2O_2 solution. This technique shows a strong bluish–black reaction product. The specificity of antisera employed was controlled by omission of the primary antisera and substitution by normal phosphate-buffered saline/bovine serum albumin.

Results

General morphology

The neoplasms comprised an outer, epithelial component (lamina epithelialis mucosae) and an inner, connective-tissue component (lamina propria mucosae), which corresponds to the normal layering of the urinary bladder mucosa (Fig. 1, Fig. 2). The subepithelial connective tissue extended into the delicate papillary branches (fronds) of the tumors, forming a thin fibrovascular core (Fig. 3). In one case (sample 2), fine fibrous strands of smooth musculature were discerned in the central connective-tissue core of the papillary tumor, by immunohistochemical tests employing anti-smooth-muscle actin.

Ultrastructural characteristics

The lesions differed from the mucosa of the normal urinary bladder, at least in part and to varying degrees, with respect to the following features of their fine structure.

Often the epithelial cells contained aggregations of small, dark mitochondria, concentrated in one cell compartment (Fig. 3). Individual epithelial cells, mostly near the base of the epithelium, were filled with vesicles of various shapes, sizes and electron densities, so that they looked like endocrine cells (Fig. 4). Cells were also seen to penetrate the basal lamina, producing so-called microinvasions. In some places, the basal lamina was absent and, here, some of the basal epithelial cells had formed microvilli and tight junctions on the stroma side (Fig. 5). These features, normally found in apical positions in the luminal cell layer, indicate a reversal of cell polarity. Except where there were gaps, the epithelial basal lamina was uni- to multilayered (Fig. 6). The subepithelial vascular network was more massively developed than in normal tissue (Fig. 2). Blood vessels had advanced into the epithelium in the connective-tissue papillae, and purely intraepithelial capillaries with an extremely confined pericapillary space [39] were also present (Fig. 7). The basal lamina of the blood vessels was also uni- to multilayered. Some of the fronds contained necrotic blood vessels, largely enclosed in lamellar material. In the stroma, individual cells without a basal lamina were present and often adjacent to the epithelium, as well as epithelium-like cell groups with the morphological characteristics of the tumor's epithelial cells (Fig. 4). There were only a few collagen fibrils in the stroma as a whole and particularly just below the epithelium; smooth muscle cells were observed in one sample (sample 1), in the connective-tissue component of the tumor.

Nerve tissue

The connective-tissue stalks of the tumors were penetrated by a few, very delicate nerve strands (Fig. 8) and, less commonly, the fibrovascular cores in the fronds also contained fine nerve strands (Fig. 3, Fig. 6). These strands were composed of several (maximally five) axons embedded in Schwann cells, or in some cases single axons with or without Schwann cells. In one sample, the

Fig. 1 Structure of an exophytic bladder tumor (schematic). *Arrowhead* frond, *asterisk* urothelium (lamina epithelialis mucosae), *S* stroma (lamina propria mucosae), *L* lumen of the bladder ▶

Fig. 2 Cross section through the "stalk" of an exophytic tumor of the urinary bladder. The central mass of connective tissue is highly vascularized. *U* urothelium (lamina epithelialis mucosae), *S* stroma (lamina propria mucosae), *arrow* blood vessel. *Bar* 0.2 mm

Fig. 3 Delicate fibrovascular core (*arrows*) of a frond. Several axons are visible in section within the connective tissue (*boxed area* enlarged in Fig. 6). *E* epithelial cell, *M* cluster of mitochondria, *V* blood vessel. *Bar* 10 µm

Fig. 4 Epithelium-like group of cells (*stars*) on the stroma side of the basal lamina (*arrows*). One of these cells has the appearance of an endocrine cell (*EC*). *S* stroma. *Bar* 1 µm

Fig. 5 Basal epithelial cells (*E*) of a bladder tumor with reversed polarity, manifest in the loss of the basal lamina (*asterisk*) and the presence of tight junctions (*arrow*) and microvilli (*arrowhead*). *S* stroma, *X* unidentified cell in the stroma. *Bar* 1 µm

Fig. 6 Enlargement of area outlined in Fig. 3, showing single axons (*A*) near the epithelium. *D* dense core vesicles, *arrow* clear vesicles, *arrowhead* basal lamina (here single layered), *E* epithelial cell, *F* fibroblast, *I* intercellular space, *K* collagenous fibrils. *Bar* 1 µm

Fig. 7 Intraepithelial capillary in the urothelium of a bladder tumor. The perivascular space (*arrowhead*) is extremely confined. *Arrow* basal lamina (here multilayered), *E* epithelial cell, *N* nucleus of the endothelial cell. *Bar* 2 µm

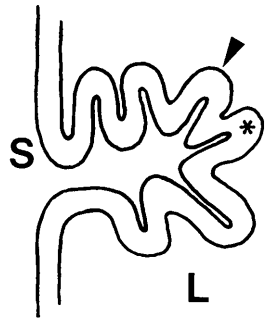

1

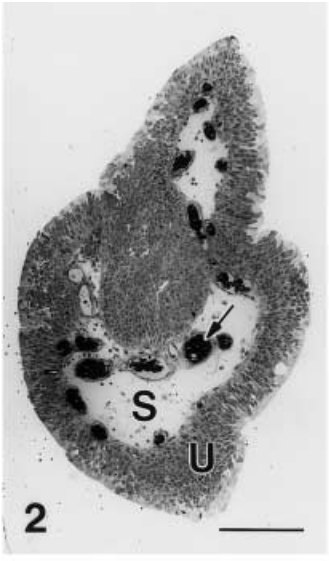

2

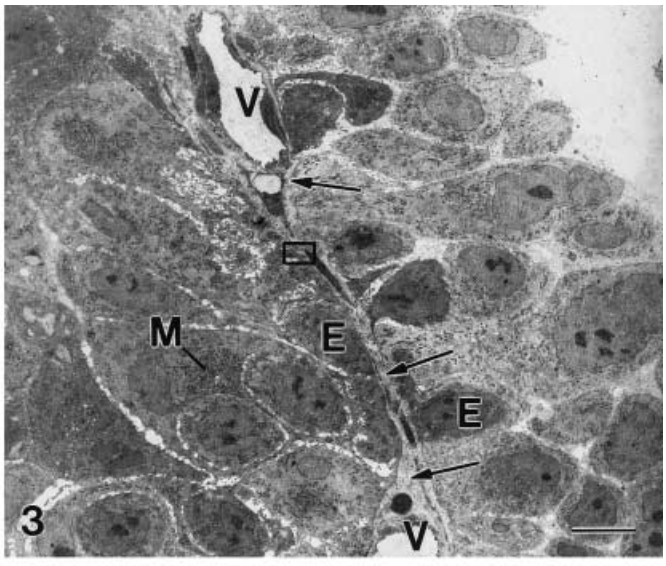

3

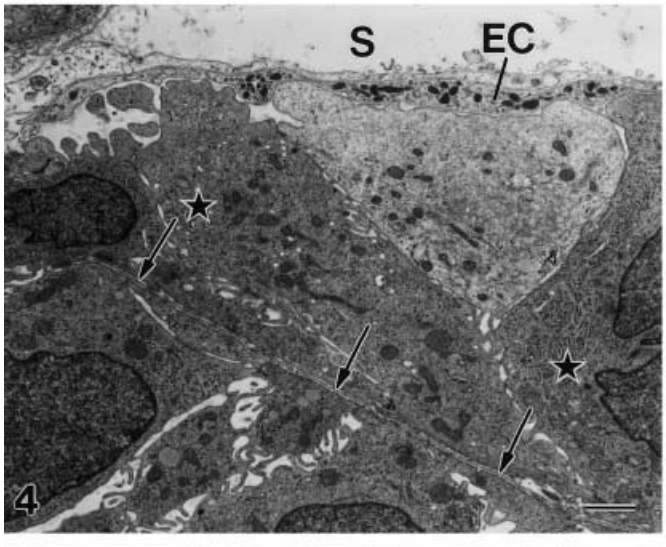

4

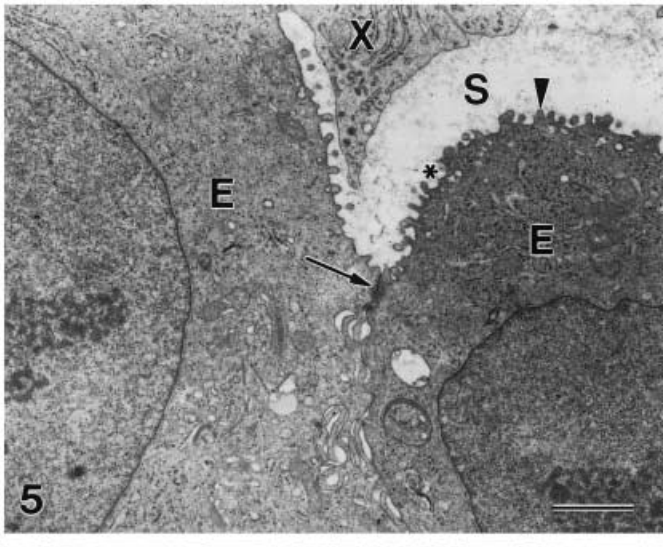

5

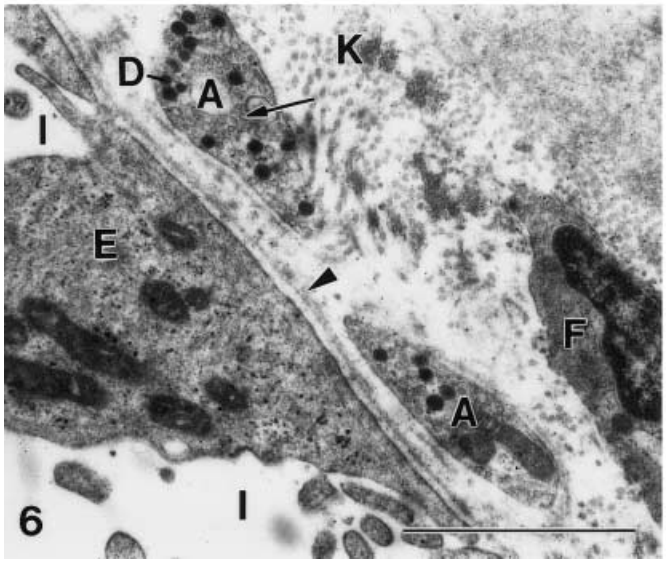

6

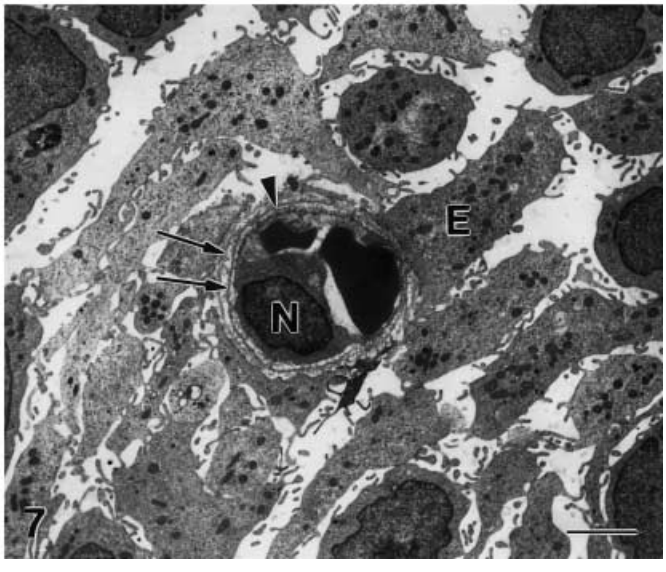

7

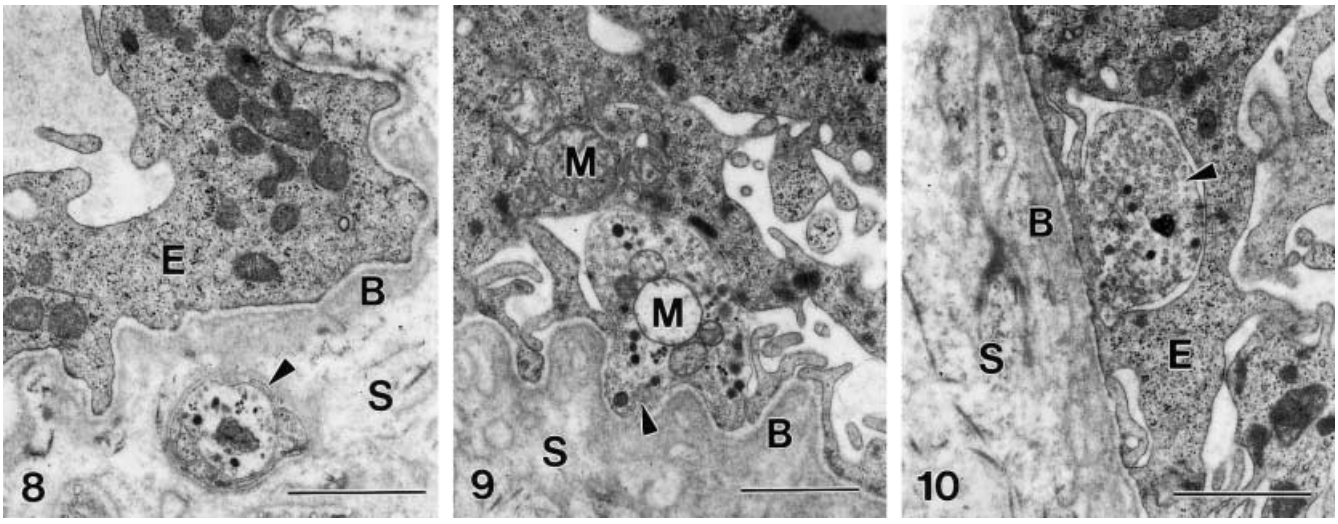

Fig. 8 Delicate nerve strand (*arrowhead*) in the central mass of connective tissue within the stalk of a bladder tumor. *B* basal lamina (here single layered), *E* basal epithelial cell, *S* stroma. *Bar* 1 µm

Fig. 9 Single axon (*arrowhead*) integrated into the base of the epithelium in a bladder tumor. *B* basal lamina, *M* mitochondrion, *S* stroma. *Bar* 1 µm

Fig. 10 Intraepithelial single axon (*arrowhead*) with clear vesicles and dense core vesicles in a bladder tumor. *B* basal lamina, *E* epithelial cell, *S* stroma. *Bar* 1 µm

basal lamina of several such strands was multilayered. The nerve strands were always adjacent to blood vessels, epithelial cells, fibroblasts and migrating cells from the hematopoetic system. Direct morphological contacts with the base of the epithelium (Fig. 9), fibroblasts and unidentified cells in the stroma were also observed. In the intercellular space, a total of four intraepithelial axons were found (Fig. 10). Within the axon profiles, mixed populations of vesicles predominated, consisting of clear vesicles (diameter up to 38 nm) and dense-core vesicles (diameter up to 70 nm; Fig. 6, Fig. 8, Fig. 9, Fig. 10). Their combination characterizes parasympathetic cholinergic neurons [36]. In the controls taken from normal bladder walls, the nerve strands were likewise very sparsely distributed just below the epithelium.

Immunohistochemical tests revealed very few PGP-9.5-immunoreactive nerve-like structures in the stroma of the tumor (Fig. 11). Even less common were VIP reactions (Fig. 12); some of these sites were precisely aligned with PGP-labeled structures in adjacent sections. Similarly, in the normal bladder-wall samples used as a control, the density of PGP-immunoreactive nerve-like structures was very low immediately below the epitheli-

Fig. 11 Tumor of urinary bladder, showing protein gene product (PGP) 9.5-immunoreactive nerve-like structures (*arrows*) in the stroma (*S*) of a frond. *E* epithelium. *Bar* 0.1 mm

Fig. 12 Tumor of urinary bladder, same series of sections as in Fig. 10. Vasoactive intestinal neuropeptide (VIP)-immunoreactive nerve-like structures (*arrows*). *E* epithelium. *Bar* 0.1 mm

Fig. 13 Normal urinary bladder. Protein gene product (PGP) 9.5-immunoreactive nerve-like structures (*arrows*). Thickness and distribution of the fibers decrease distinctly toward the epithelium. *Arrowhead* direction toward the epithelium, *asterisk* subepithelial connective tissue, *V* blood vessel. *Bar* 0.1 mm

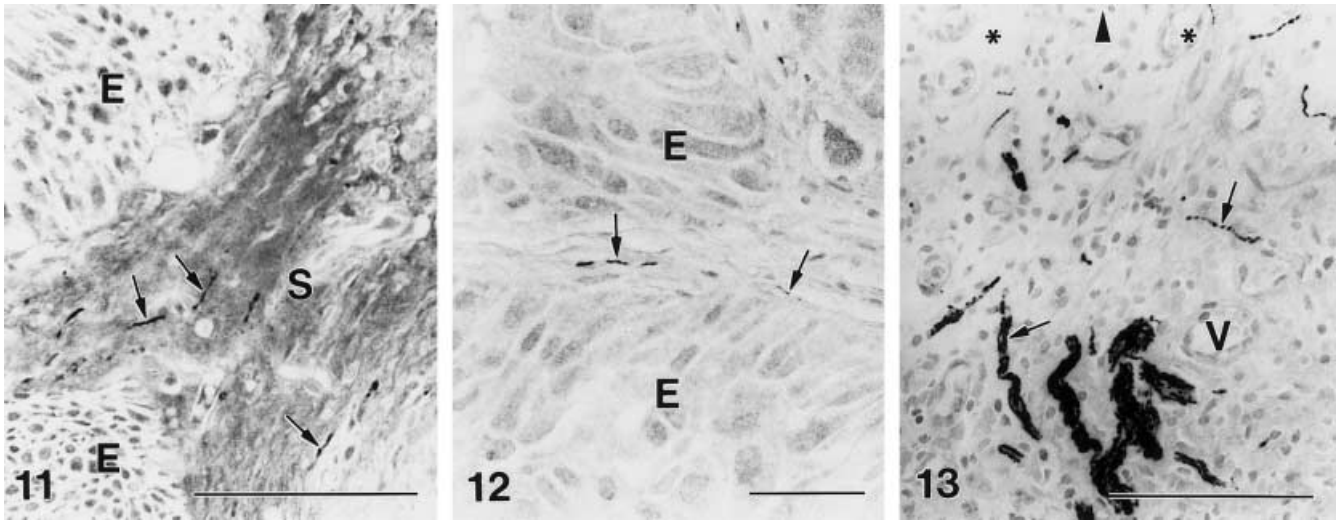

um (Fig. 13), and only a few SP- and VIP-immunoreactive nerve-like structures were detected. At lower levels in the bladder wall, a different picture was obtained: there a massive network of relatively thick nerve-like structures was labeled by PGP and S 100, with a smaller proportion of SP- and VIP immunoreactions.

Discussion

For the question with which the present investigation was concerned, exophytic tumors proved to be a useful model, because the neoplasm is clearly distinguishable from the original tissue. Papillary or solid structures growing out from the bladder wall and into the lumen are new formations, complete with all tissue components.

Ultrastructural differences between tumors and normal tissue in the urinary bladder are quite clear and have been described in previous publications [2, 3, 9, 13, 16, 21, 29, 42]. However, there is some variation in structural detail between the tumors [9, 13], which may also indicate genetic differences [34, 35]. The mitochondrial clusters reflect an enhanced aerobic metabolism [24]. Ultrastructural features have proved very useful for diagnosis of a variety of lesions [see, e.g. 10, 27]. Whether they can also be used as a supplementary diagnostic tool in the case of bladder carcinomas remains to be tested by further comparative ultrastructural investigations with a larger sample size.

All samples from the tumors examined here contained neural tissue. The combination of clear and dense-core vesicles in many axons [36] plus the presence of the neuropeptide VIP is an initial indicator of parasympathetic cholinergic neurons. Hence, we have here another case of innervated neoplastic tissue to accompany the recently described intraocular tumors containing nerve fibers [41]. Prior to that publication, there had been no description in the literature of a newly grown innervation in neoplasmic tissue and, as far as we know, it has not even been mentioned as a theoretical possibility. Nerve fibers in corresponding lesions of the adrenal glands were not regarded as newly formed tissue, because the healthy organ is abundantly innervated and contains considerably more nerve tissue [23].

We did not succeed in revealing the distribution pattern of the nerve fibers by means of the neuronal marker PGP. Evidently, neural structures that are extremely delicate are hard to detect using immunohistochemical labeling. Furthermore, single axons observable in electron micrographs of exocrine glands have been found to be, in principle, not demonstrable with immunohistochemistry [40]. Other authors have also considered negative immunohistochemical findings to be more or less inconclusive [27].

In the normal bladder wall, the tunica/lamina muscularis is richly innervated. Rats have a subepithelial nerve plexus [18] with sensory and effector fibers; our impression is that in humans this plexus is relatively poorly developed. The neurotransmitters involved here, in addition to the classical ones, are said to include certain neuropeptides [see, e.g. 1, 17, 26, 43, 47] and ATP [11, 28], which implies a complex regulatory mechanism. Presumably, the neural elements in the neoplastic tissue are collaterals sent out by such subepithelial nerve fibers. Because nerve fibers cannot in principle exist without a local control by growth factors and hence without function [5], nerve fibers must have a physiological relevance even in tumors, serving as visceral afferents or efferents and influencing the course of the disease. Looking at VIP, various functions have been identified. VIP has been shown to stimulate intracellular accumulation of second messenger cyclic adenosine monophosphate (cAMP) [see, e.g. 6, 22, 46]. cAMP-regulatory effects appear to be influenced by additional factors. In different tumor cell types/cell lines, inductive as well as inhibitory effects have been documented. In various tumor cell lines, VIP has a role in modulation of cell growth, differentiation and specific cell function [see, e.g. 4, 12, 14, 20, 32, 37, 48].

In the tumors we have studied, we do not yet know what spectrum of transmitters is effective and what the effectors are, because it is characteristic of the autonomic nervous system that in large regions there are no direct synaptic contacts between axons and cells. Instead, the transmitters are released from the axons into the extracellular matrix near their effectors and must diffuse across a certain distance in order to reach their targets – or, in the case of visceral afferents (sensory fibers), messenger substances diffuse to the axons. In tumors of the urinary bladder, the neuronal structures are in close proximity to all parts of the tissue, so that any of them might possibly be innervated. They include (i) the well-developed vascular network, which determines growth of the tumor by supplying nutrition, oxygen and various other factors; (ii) cells involved in immune defense, such as lymphocytes, plasma cells and mast cells, which carry receptors for neuropeptides [7, 33, 44, 45] and accordingly are innervated by peptidergic nerve fibers; and (iii) fibroblasts, epithelial cells and endothelial cells, which synthesize matrix components and hence together create the milieu within the tumor, which in turn acts in the opposite direction to influence the behavior of the cells [15, 19, 25, 30, 31, 38].

Whatever components of the tumor tissue may be under neuronal control, in any case the entire tumor will be affected because interactions among all tissues of a tumor are inherent in the system, just as there must be interactions between a tumor and the whole organism by way of the blood and nerve supply. The neurons of the autonomic nervous system do not only optimize cell functions but also regulate them by a feedback system designed to maintain homeostasis. Innervated tumors can thus hardly be regarded as an isolated phenomenon, and it may well be that a neuronal influence on the biology of neoplasms has so far been underestimated.

Acknowledgements The authors thank Ms. Claudine Strack and Ms. Parand Pour Nouroz for their excellent technical assistance and untiring evaluation of tissue sections. The study was funded by the AKDE.

References

1. Alm P, Alumets J, Håkanson R, Owman CH, Sjorberg NO, Stjerqvist M, Sundler F (1981) Enkephalin-immunoreactive nerve fibers in the feline genito-urinary tract. Histochemistry 72:351–355
2. Alroy J (1979) Ultrastructure of canine urinary bladder carcinoma. Vet Pathol 16:693–701
3. Alroy J (1979) Tight junctions adjacent to tumor stromal interface in human invasive transitional cell carcinomas. Virchows Arch 30:289–296
4. Brenneman DE, Nicol T, Warren D, Bowers LM (1990) Vasoactive intestinal peptide: a neurotrophic releasing agent and an astroglial mitogen. J Neurosci Res 25:386–394
5. Campenot RB (1977) Local control of neurite development by nerve growth factor. Proc Natl Acad Sci U S A 74:4516–4519
6. Chen F, O'Dorisio MS, Hermann G, Hayes J, Malarkey WB, O'Dorisio TM (1993) Mechanism of action of long-acting analogs of somatostatin. Regul Pept 44:285–295
7. Depelchin A, Letesson JJ (1981) Adrenaline influence on the immune response: II. Its effects through action on the suppressor T-cells. Immunol Lett 3:207
8. Epstein JI, Amin MB, Reuter VR, Mostofi FK, and the Bladder Consensus Conference Committee (1998) The world health organization/international society of urological pathology consensus classification of urothelial (transitional cell) neoplasms of the urinary bladder. Am J Surg Pathol 22:1435–1448
9. Erlandson RA (1994) Diagnostic transmission electron microscopy of the tumors with clinicopathological, immunohistochemical, and cytogenetic correlations. Raven, NewYork, pp 807–808
10. Erlandson RA, Woodruff JM (1989) Role of electron microscopy in the evaluation of soft tissue neoplasms, with emphasis on spindle cell and pleomorphic tumors. Hum Pathol 29:1372–1381
11. Ferguson DR, Kennedy I, Burton TJ (1997) ATP is released from rabbit urinary bladder epithelial cells by hydrostatic pressure changes – a possible sensory mechanism? J Physiol 505: 503–511
12. Frühwald MC, O'Dorisio MS, Fleitz J, Pietsch T, Reubi JC (1999) Vasoactive intestinal peptide (VIP) and VIP receptors: gene expression and growth modulation in medulloblastoma and other central primitive neuroectodermal tumors of childhood. Int J Cancer 81:165–173
13. Fulker MJ, Cooper EH, Tanaka T (1971) Proliferation and ultrastructure of papillary transitional cell carcinoma of the human bladder. Cancer 27:71–82
14. Gkonos PJ, Guo F, Burnstein KJ (2000) Type I vasoactive intestinal peptide receptor expression in PC3/AR cells is evidence of prostate epithelial differentiation. Prostate 42:137–144
15. Harada T, Shinohara M, Nakamura S, Oka M (1994) An immunohistochemical study of the extracellular matrix in oral squamous cell carcinoma and its association with invasive and metastatic potential. Virchows Arch 424:257–266
16. Hicks RM (1976) Changes in differentiation of the urinary bladder during benign and neoplastic hyperplasia. In: Müller-Bérat N et al. (eds) Progress in differentiation research. North-Holland Publishing Company, Amsterdam, pp 339–353
17. Hökfelt T, Schulzberg M, Elde R, Nilsson G, Terenius L, Said S, Goldstein M (1978) Peptide neurons in peripheral tissues including the urinary tract: immunohistochemical studies. Acta Pharmacol Toxicol 43:79–89
18. Inoué T, Gabella G (1992) The interface between epithelium and lamina propria in the rat urinary bladder. Arch Histol Cytol 55:157–163
19. Iozzo RV (1995) Tumor stroma as a regulator of neoplastic behavior. Lab Invest 73:157–160
20. Jongsma J, Oomen MHA, Noordzij MA, Romijn JC, van der Kwast TH, Schröder FH, van Steenbrugge GJ (2000) Androge-independent growth is induced by neuropeptides in human prostate cancer cell lines. Prostate 42:34–44
21. Koss LG (1977) Some ultrastructural aspects of experimental and human carcinoma of the bladder. Cancer Res 37:2824–2835
22. Kovacs CS, Chik CL, Li B, Karpinski E, Ho AK (1996) Pituitary adenylate cyclase- activating peptide stimulates cyclic AMP accumulation in UMR 106 osteoblast-like cells. J Endocrinol 149:287–295
23. Li Q, Johansson H, Grimelius L (1999) Innervation of human adrenal gland and adrenal cortical lesions. Virchows Arch 435: 580–589
24. Lloreta-Trull J, Serrano S (1998) Biology and pathology of the mitochondrion. Ultrastruct Pathol 22:357–367
25. Madri JA, Williams SK, Wyatt T, Mezzio C (1983) Capillary endothelial cell cultures: phenotypic modulation by matrix components. J Cell Biol 97:153–165
26. Mattiasson A, Ekblade E, Sundler F, Uvelius B (1985) Origins and distribution of neuropeptide Y-, vasoactive intestinal polypeptide and substance P-containing nerve fibers in the urinary bladder of the rat. Cell Tissue Res 239:141–146
27. Mierau GW, Weeks DA, Hicks MJ (1998) Role of electron microscopy and other special techniques in the diagnosis of childhood round cell tumors. Hum Pathol 29:1347–1355
28. Namasivayam S, Eardley I, Morrison JFB (1999) Purinergic sensory neurotransmission in the urinary bladder: an in vitro study in the rat. Br J Urol 84:854–860
29. Pauli BU, Weinstein RS, Alroy J, Aray M (1977) Ultrastructure of cell junctions in FANFT-induced urothelial tumors in urinary bladder of Fischer rats. Lab Invest 37:609–621
30. Pritchett TR, Wang KM, Jones PA (1989) Mesenchymal-epithelial interactions between normal and transformed human bladder cells. Cancer Res 49:2750–2754
31. Ramos DM, Chen BL, Boylen K, Stern M, Kramer RH, Sheppard D, Nishimura SL, Greenspan D, Zardi L, Pytela R (1997) Stromal fibroblasts influence oral squamous- cell carcinoma cell interactions with tenascin-c. Int J Cancer 72:369–376
32. Reubi JC, Waser B, Schmassmann A, Laissue JA (1999) Receptor autoradiographic evaluation of cholecystokinin, neurotensin, somatostatin and vasoactive intestinal peptide receptors in gastro-intestinal adenocarcinoma samples: where are they really located? Int J Cancer 81:376–386
33. Richman DP, Arnason BGW (1979) Nicotinic acetylcholine receptor: evidence for a functionally distinct receptor on human lymphocytes. Proc Natl Acad Sci U S A 76:4632–4635
34. Richter J, Jiang F, Görög J, Sartorius G, Egenter C, Gasser TC, Moch H, Mihatsch MJ, Sauter G (1997) Marked genetic differences between pTa and pT1 papillary bladder cancer detected by comparative genomic hybridization. Cancer Res 57:2860–2864
35. Ruppert J, Tokino T, Sidransky D (1993) Evidence for two bladder cancer suppressor loci on human chromosome 9. Cancer Res 53:5093–5095
36. Ruskell GL (1975) Nerve terminals and epithelial cell variety in the human lacrimal gland. Cell Tissue Res 158:121–136
37. Scholar EM, Paul S (1991) Stimulation of tumor cell growth by vasoactive intestinal peptide. Cancer 67:1561–1564
38. Scott DM, Kumar S, Barnes MJ (1988) The effect of a native collagen gel substratum on the synthesis of collagen by bovine brain capillary endothelial cells. Cell Biochem Funct 6:209–215
39. Seifert P, Sekundo W (1998) Capillaries in the epithelium of pterygium. Br J Ophthalmol 82:77–81
40. Seifert P, Spitznas M (1999) Vasoactive intestinal polypeptide (VIP) innervation of the human eyelid glands. Exp Eye Res 68:685–692
41. Seifert P, Spitznas M (2001) Tumours may be innervated. Virchows Arch 438:228–231
42. Tannenbaum M (1979) Ultrastructural pathology of the human urinary bladder. In: Trump BF, Jones RT (eds) Diagnostic electron microscopy, Vol 2. John Wiley and Sons, New York, pp 221–267
43. Wakabayashi Y, Tomoyoshi T, Fujimiya M, Arai R, Maeda T (1993) Substance P containing axon terminals in the mucosa of the human urinary bladder: pre- embedding immunohisto-

chemistry using cryostat sections for electron microscopy. Histochemistry 100:401–407
44. Walcott B, McLean JR (1985) Catecholamine-containing neurons and lymphoid cells in a lacrimal gland of the pigeon. Brain Res 328:129–137
45. Williams RM, Singh J, Sharkey KA (1994) Innervation and mast cells of the rat lacrimal gland: the effects of age. In: Sullivan DA (ed) Lacrimal gland, tear film, and dry eye syndromes. Plenum Press, New York, pp 67–74
46. Wood CL, O'Dorisio MS, Vassalo LNM, Malarkey WB, O'Dorisio TM (1985) Vasoactive intestinal peptide effects on GH3 pituitary tumor cells: high affinity binding, affinity labeling, and adenylate cyclase stimulation. Comparison with peptide histidine isoleucine and growth hormone-releasing factor. Regul Pept 12:237–248
47. Yokokawa K, Tohyama M, Shiosaka S, Shiotani Y, Sonoda T, Emson PC, Hillyard CV, Girgis S, MacIntyre I (1986) Distribution of calcitonin gene-related peptide- containing fibers in the urinary bladder of the rat and their origin. Cell Tissue Res 244:271–278
48. Zia H, Hida T, Jakowlew S, Birrer M, Gozes Y, Reubi JC, Fridkin M, Gozes I, Moody TW (1996) Breast cancer growth is inhibited by vasoactive intestinal peptide (VIP) hybrid, a synthetic VIP receptor antagonist. Cancer Res 56:3486–3489

Virchows Arch (2002) 440:298–303
DOI 10.1007/s004280100530

ORIGINAL ARTICLE

Peter J. Barth · Schokufe Ebrahimsade
Annette Ramaswamy · Roland Moll

CD34+ fibrocytes in invasive ductal carcinoma, ductal carcinoma in situ, and benign breast lesions

Received: 20 February 2001 / Accepted: 21 June 2001 / Published online: 22 November 2001
© Springer-Verlag 2001

Abstract The present study was undertaken in order to elucidate the question of whether the distribution of stromal CD34+ fibrocytes and smooth muscle actin (SMA)-reactive myofibroblasts differs between benign and malignant lesions of the breast. We investigated a total of 31 ductal carcinomas and 27 specimens with benign lesions of the breast (ductal hyperplasia, sclerosing adenosis, fibroadenoma, phyllodes tumor) and compared the distribution of CD34+ fibrocytes and SMA-reactive myofibroblasts. The stroma of normal breast tissue contained CD34+ fibrocytes, whereas SMA-reactive myofibroblasts were absent. All benign breast lesions exhibited stromal CD34+ fibrocytes and few lesions (fibroadenomas and phyllodes tumor) showed additional SMA-reactive myofibroblasts. In invasive breast cancer the stroma was devoid of CD34+ fibrocytes but a varying number of stromal SMA-reactive myofibroblasts was detectable. In the setting of the present study the loss of CD34+ fibrocytes was specific for invasive breast cancer and ductal carcinoma in situ, whereas SMA-reactive myofibroblasts were observed in different benign and malignant lesions. These findings may be helpful tools in distinguishing benign breast lesions (e.g., sclerosing adenosis) from invasive breast cancer and in characterizing stromal remodeling associated with invasive cancer.

Keywords Fibrocyte · Myofibroplast · Breast · Ductal carcinoma · DCIS

Introduction

Blood-borne CD34+ fibrocytes derive from myeloid precursors and make up about 0.5% of peripheral blood leukocytes [2]. Experimental studies have shown that blood-borne CD34+ fibrocytes invade sites of tissue damage and are capable of connective tissue matrix synthesis [2]. Besides its function as a matrix-producing cell, the CD34+ fibrocyte is a potent antigen-presenting cell capable of priming naive T cells in situ [3]. Therefore, it has been claimed that the CD34+ fibrocyte may play an important role in host response to tissue damage of whatever cause. By means of immunohistochemistry, CD34+ fibrocytes have been detected in the skin [14] – in cutaneous [4, 5, 7, 8, 21] and lipomatous tumors [18,20] – and in a multitude of mesenchymal tumors [11, 15, 18, 19]. However, it remains to be clarified to what extent CD34+ fibrocytes observed in various organs are derived from circulating CD34+ fibrocytes. The occurrence of CD34+ fibrocytes in the peritumoral stroma of skin appendage tumors has been considered to be of diagnostic significance in distinguishing basal cell carcinoma from benign appendage tumors, such as trichoepithelioma and its variants [4, 5, 7, 8, 21]. In these studies, the absence of CD34+ fibrocytes favors the diagnosis of basal cell carcinoma, while the presence of CD34+ fibrocytes tends to rule against such a diagnosis. Similar results have been reported in colorectal adenocarcinoma: normal colonic stroma harbors CD34+ fibrocytes, whereas this cell population is absent from the stroma of invasive adenocarcinoma. On the other hand, the tumor-associated desmoplastic stroma was characterized by the presence of SMA-reactive myofibroblasts [13]. To date, reports investigating the occurrence and distribution pattern of CD34+ fibrocytes in benign and malignant breast lesions have – except for one study analyzing the distribution of CD34+ fibrocytes in fibroadenoma and phyllodes tumors [17] – not yet been published.

We therefore analyzed the occurrence of CD34+ fibrocytes and SMA-reactive myofibroblasts in the mammary gland with special respect to malignancy and other specific types of disease processes.

P.J. Barth (✉) · S. Ebrahimsade · A. Ramaswamy · R. Moll
Institute of Pathology, Philipps-University, 35033 Marburg, Germany
e-mail: barthp@post.med.uni-marburg.de
Tel.: +49-6421-286-2465, Fax: +49-6421-286-5640

Materials and methods

We investigated a total of 24 invasive breast carcinomas and qualitatively compared the distribution of CD34+ fibrocytes and SMA-

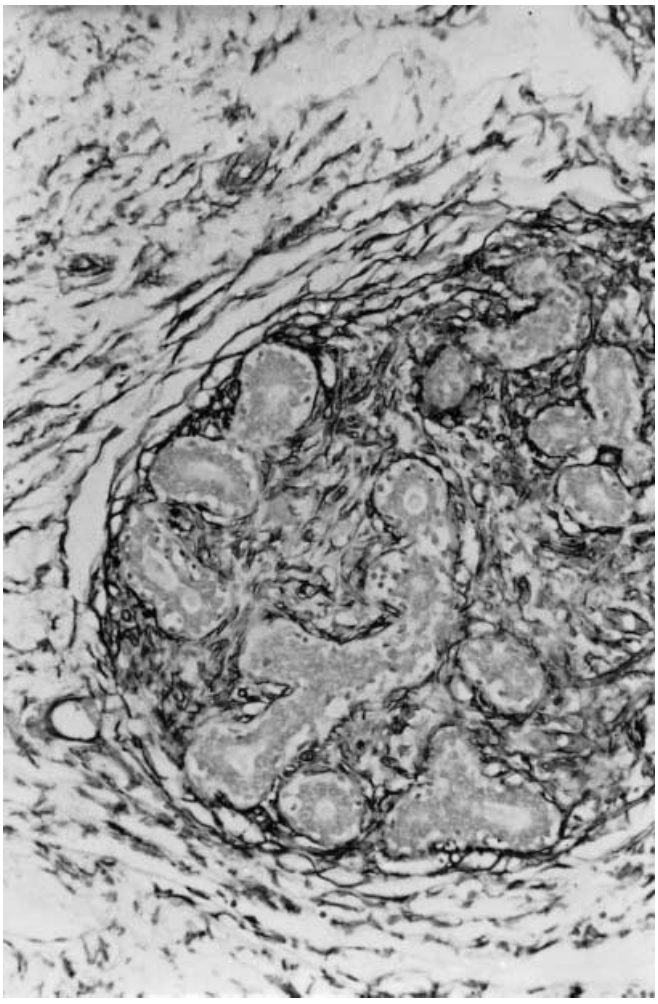

Fig. 1 Normal mammary tissue shows densely packed $CD34^+$ fibrocytes encircling glandular and vascular structures (CD34, ×200 microscopic magnification)

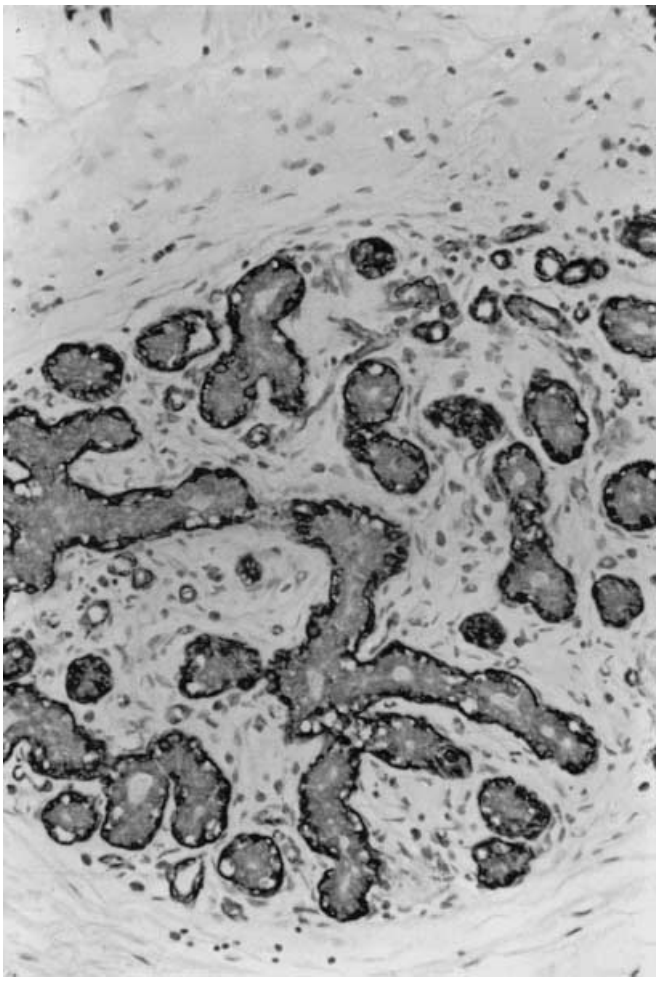

Fig. 2 Smooth muscle actin (SMA) immunohistochemistry decorates acinar myoepithelia whereas the stroma of normal mammary tissue is devoid of SMA-reactive myofibroblasts (SMA, ×200 microscopic magnification)

Table 1 Epidemiologic data and type of benign breast lesions investigated

Number of patients	27
Age range (years)	22–78
Type of lesion	
Sclerosing adenosis	12
Fibroadenoma	7
Phyllodes tumor	1
Microglandular adenosis	1
Ductal hyperplasia	9
Tubular adenoma	1

Table 2 Epidemiologic data of patients with breast carcinoma

Number of patients	31
Age range (years)	34–79
Type of carcinoma	
Invasive ductal	24
Intraductal carcinoma[a]	7
Lesions associated with invasive carcinomas	
Sclerosing adenosis	2
Intraductal carcinoma	14
Ductal hyperplasia	7

[a] Pure intraductal carcinoma not associated with invasive ductal carcinoma

reactive myofibroblasts between stromal areas located within the tumor to areas of tumor free mammary tissue surrounding the carcinoma. Epidemiological data of patients with invasive carcinomas investigated and data concerning tumor properties are summarized in Table 1. In order to be sure that in patients with invasive carcinoma the distribution and number of $CD34^+$ fibrocytes and myofibroblasts in the surrounding tumor-free tissue was unaffected by the fact that an invasive carcinoma was remotely located in the same or contralateral breast, we investigated biopsy specimens of mammary tissue of 27 patients with benign breast lesions. The epidemiological data of these patients are depicted in Table 2. The analysis of stromal alterations associated with intraductal carcinoma (DCIS) was based on specimens of seven patients showing pure DCIS without associated invasive ductal carcinoma (Table 1). In brief, after resection the tissues were fixed in a 4% formaldehyde solution and representative tissue blocks were selected. Tissues were embedded in paraffin, cut, and stained H&E and PAS for routine purposes.

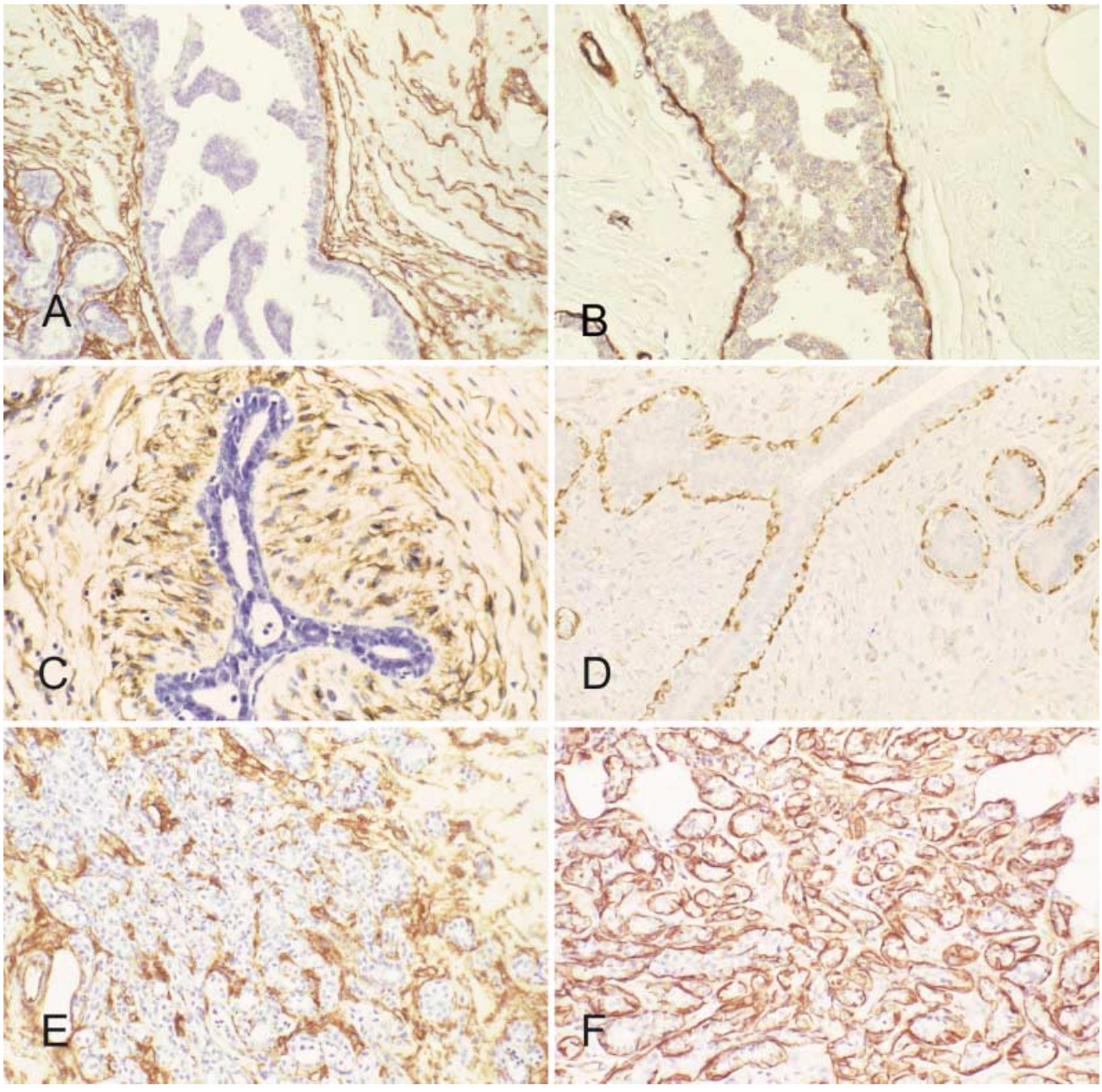

Fig. 3 Ducts with epithelial hyperplasia are surrounded by a normal appearing population of CD34+ fibrocytes (**A**), and smooth muscle actin (SMA) stains myoepithelial cells and smooth muscle of muscularized vessels (**B**). The stroma of fibroadenoma contains numerous CD34+ fibrocytes (**C**), SMA-reactive myofibroblasts are absent. SMA-reactive myoepithelia cover the basement membrane of compressed ducts (**D**). In sclerosing adenosis the stroma contains densely packed CD34+ fibrocytes (**E**), the stroma is free of SMA-reactive myofibroblasts. The small acinar structures are lined by SMA-reactive myoepithelia (**F**). (**A–D**, ×200 microscopic magnification: **E,F** ×100 microscopic magnification)

Immunohistochemistry

Immunohistochemistry was performed using a standard avidin biotin complex (ABC)-peroxidase method using 3,3'-diaminobenzidine (DAB) as chromogen. CD34 antigen was detected by means of a monoclonal antibody (QBEND10, Immunotech, Marseilles, France) without any tissue pretreatment and dilution of the antibody. After tissue pretreatment with 0.1% trypsin for 15 min at 37°C, α-smooth muscle actin was detected using a monoclonal antibody (ASM-1, Progen, Heidelberg, Germany; dilution 1:200).

Results

In normal mammary tissue muscularized blood vessels, glandular ducts, and acini were surrounded by a dense concentric network of CD34+ fibrocytes. These cells showed slender elongated dendrite-like processes featuring a bipolar arrangement; the nuclei were small and inconspicuous. With increasing distance from the aforementioned glandular and vascular structures the density of CD34+ fibrocytes decreased (Fig. 1). SMA was detected in the wall of muscularized vessels and in myoepithelia lining the ductal and acinar basement membranes, whereas SMA-reactive myofibroblasts were not detected

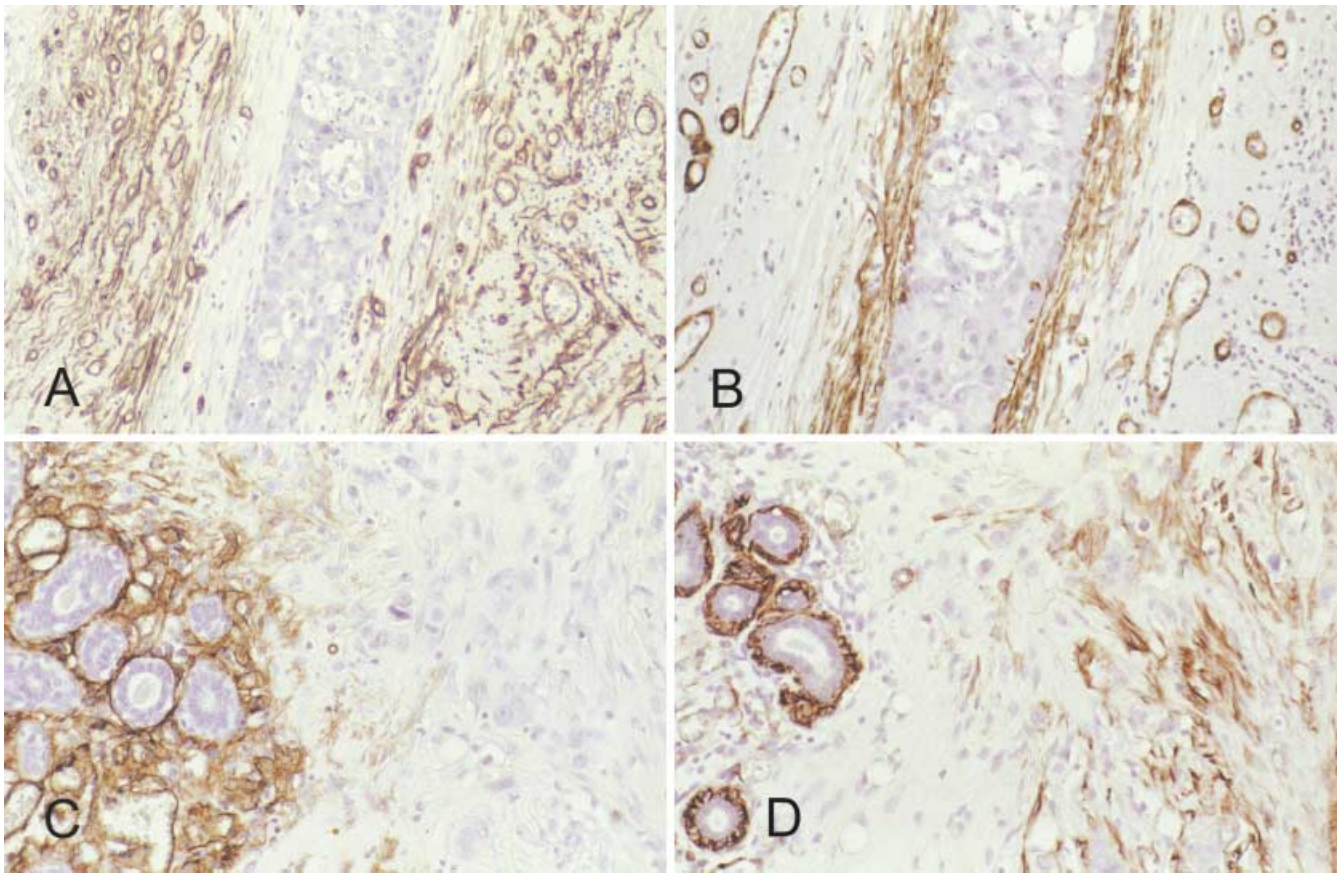

Fig. 4 The stroma surrounding the intraductal carcinoma (DCIS) lacks $CD34^+$ fibrocytes (note CD34 positive endothelial cells in capillaries adjacent to DCIS); areas located more remotely from DCIS show a normal distribution pattern of $CD34^+$ fibrocytes (**A**). DCIS is encircled by a thick layer of smooth muscle actin (SMA)-reactive myofibroblasts (**B**). The stroma of invasive carcinoma is free of $CD34^+$ fibrocytes in the adjacent tumor-free tissue and the CD34+ fibrocytes appear somewhat condensed and closely packed (**C:** *right*, invasive carcinoma; *left*, tumor-free tissue). SMA-reactive myofibroblasts are visible in the stroma of invasive carcinoma (**D:** *right*, invasive carcinoma; *left*, tumor-free mammary tissue). ×200 microscopic magnification

in the stroma of normal breast tissue (Fig. 2). The stroma harboring ducts with epithelial hyperplasia showed a similar distribution of $CD34^+$ fibrocytes (Fig. 3 A) and SMA-reactive myoepithelia (Fig. 3B).

In fibroadenomas $CD34^+$ fibrocytes were scattered uniformly throughout the stroma and did not show the predilection for periglandular and perivascular areas as observed in the normal mammary gland (Fig. 3C). Fibroadenomas with loose, myxoid stroma showed an additional population of SMA-reactive myofibroblasts which were not observed in more sclerotic fibroadenomas (Fig. 3D). In one phyllodes tumor investigated the stroma harbored $CD34^+$ fibrocytes and SMA-reactive myofibroblasts in a fashion similar to that observed in fibroadenomas with loose, myxoid stroma. A similar stromal composition with SMA-reactive myofibroblasts and coexisting $CD34^+$ fibrocytes was observed in the tubular adenoma investigated.

Table 3 $CD34^+$ fibrocytes and smooth muscle actin (*SMA*)-reactive myofibroblasts in the lesions investigated

Type of lesion	$CD34^+$ fibrocytes	SMA-reactive myofibroblasts
Ductal hyperplasia	16/16	0/16
Fibroadenoma	7/7	3/7
Phyllodes tumor	1/1	1/1
Tubular adenoma	1/1	1/1
Sclerosing adenosis	14/14	1/14
Microglandular adenosis	1/1	0/1
DCIS [a]	0/7	5/7
Invasive ductal carcinoma	0/24	20/24

[a] Pure intraductal carcinoma (*DCIS*) not associated with invasive ductal carcinoma

In sclerosing adenosis, the stroma showed abundant densely packed $CD34^+$ fibrocytes (Fig. 3E), and the lobules showed a population of SMA-reactive myoepithelia (Fig. 3F), but SMA-reactive stromal myofibroblasts were not observed except in one case. In this case, an adenosis tumor, stromal SMA-reactive myofibroblasts were detected additionally to the $CD34^+$ fibrocytes (Table 3).

In contrast to normal mammary tissue and ductal hyperplasia, the number of $CD34^+$ fibrocytes was reduced in the stroma surrounding ducts harboring carcinoma in situ, although capillaries with CD34 reactive endothelia were still detectable adjacent to these ducts (Fig. 4 A). On the other hand, ducts with DCIS were encircled by a rim of densely packed SMA-reactive myofibroblasts

which were not detected in the normal breast tissue or in ductal hyperplasia (Fig. 4B).

In all cases investigated, the stroma of invasive carcinomas showed a complete loss of $CD34^+$ fibrocytes, whereas the surrounding mammary tumor-free tissue disclosed a normal distribution of this cell population except for areas which were located at the margin of invasive carcinoma (Fig. 4C). In these regions the $CD34^+$ fibrocytes appeared to be more densely packed than in tumor-free tissue remotely located from the margin of invasive cancer. The endothelium of vessels located in the stroma of invasive carcinoma and those located in tumor-free mammary tissue showed a similar degree and extent of CD34 immunostaining. Twenty of 24 invasive ductal carcinomas disclosed SMA-reactive myofibroblasts forming focal accumulations of various extent (Fig. 4D) (Table 3).

Discussion

$CD34^+$ fibrocytes are a small population of blood-borne dendritic cells capable of antigen-presentation and T-cell priming which have been considered to play a significant role in specific instances of immune response and tissue repair [2, 3]. The distribution of $CD34^+$ fibrocytes has been claimed to be a valuable tool in the differential diagnosis of benign and malignant tumors of the skin appendages [4, 5, 7, 8, 21]. The present study is the first to correlate the presence and distribution of $CD34^+$ fibrocytes with the malignancy of primary breast lesions. The data reported here indicate a strong negative association between the presence of $CD34^+$ fibrocytes and the malignancy of a ductal breast lesion in that invasive ductal carcinomas disclose a complete loss of stromal $CD34^+$ fibrocytes. Moreover, distinct lesions such as sclerosing adenosis that may cause severe differential diagnostic confusion concerning malignancy show a preserved population of $CD34^+$ fibrocytes. Therefore, assessment of $CD34^+$ fibrocytes might play an important role whenever this problem arises. We additionally investigated the occurrence of SMA-reactive stromal myofibroblasts in relation to the type of underlying breast disease. In invasive breast cancer the desmoplastic stroma showed focal accumulations of SMA-reactive myofibroblasts and a complete loss of $CD34^+$ fibrocytes in all cases investigated. Therefore, the data reported in the present study indicate that the loss of $CD34^+$ fibrocytes is a sensitive and specific marker of stromal changes associated with invasive breast cancer. In contrast, the accumulation of SMA-reactive myofibroblasts is less specific and can be observed in benign as well as in malignant lesions of the breast. Moreover, the stroma surrounding ductal carcinoma in situ was also characterized by a loss of $CD34^+$ fibrocytes. Therefore the detection of a loss of $CD34^+$ fibrocytes may be a valuable tool in the detection of DCIS.

The loss of $CD34^+$ fibrocytes is not restricted to invasive breast cancer since similar findings have been reported in basal cell carcinoma of the skin [4, 5, 7, 8, 21] and colorectal adenocarcinoma [13].

Stromal remodeling is an important feature of invasive breast cancer and has predominantly been investigated for tenascin [12, 16] and fibronectins [9]. Breast cancer cells have been shown to be capable of matrix-metalloproteinase synthesis which initiates stromal alterations in invasive cancer [1, 10]. However, this approach might fail to completely explain the periductal loss of $CD34^+$ fibrocytes in DCIS. Neuroendocrine pulmonary tumor cells are capable of inducing apoptosis in dendritic stromal cells which are closely related to the $CD34^+$ fibrocytes by a not yet precisely defined soluble factor [6]. We speculate that in parallel to this finding apoptosis of $CD34^+$ fibrocytes might be initiated by a soluble factor secreted by DCIS cells.

Taking into account that $CD34^+$ fibrocytes are capable of collagen I and collagen III synthesis, it seems to be likely that this cell type may be involved in the process of stromal remodeling in breast cancer [2]. However, it remains unclear whether the phenotypical alterations of the stroma in invasive breast cancer can be explained by alterations of one single type of stromal cell characterized by downregulation of CD34 and upregulation of SMA in this cell type or by a loss of $CD34^+$ fibrocytes and subsequent repopulation of the stroma by SMA-reactive myofibroblasts. The latter process would require an increased proliferation of stromal cells which up to now has not been documented in breast cancer. For explaining the data of the present study, it seems probable that $CD34^+$ fibrocytes are replaced by alternatively differentiated and less immunocompetent mesenchymal cells. This process is probably related to matrix metalloproteinase-induced stromal damage and subsequent stromal remodeling. Interestingly, sites of tissue damage have been shown to be invaded by blood-borne $CD34^+$ fibrocytes [2]. In invasive breast cancer this mechanism seems to fail, leading to a loss of the $CD34^+$ fibrocytes. Bearing in mind that $CD34^+$ fibrocytes may mediate specific immunologic reactions related to antigen-presentation and T-cell priming [3], the loss of this cell population might play an important role in that part of the host response directed against invasive cancer cells that is mediated by infiltrating T-cells [22].

References

1. Brummer O, Athar S, Riethdorf L, Löning T, Herbst H (1999) Matrix-metalloproteinases 1, 2 and 3 and their tissue inhibitors 1 and 2 in benign and malignant breast lesions: an in situ hybridization study. Virchows Arch 435: 566–573
2. Bucala R, Spiegel LA, Chesney J, Hogan M, Cerami A (1994) Circulating fibrocytes define a new leukocyte subpopulation that mediates tissue repair. Mol Med 1: 71–81
3. Chesney J, Bacher M, Bender A, Bucala R (1997) The peripheral blood fibrocyte is a potent antigen-presenting cell capable of priming naive T cells in situ. Proc Natl Acad Sci USA 94: 6307–6312
4. Humphreys TR, Monteiro MR, Murphy GF (2000) Mast cells and dendritic cells in basal cell carcinoma stroma. Dermatol Surg 26: 200–203

5. Illueca C, Monteagudo C, Revert A, Llombart-Bosch A (1998) Diagnostic value of CD34 immunostaining in desmoplastic trichilemmoma. J Cutan Pathol 25: 435–439
6. Katsenelson NS, Shurin GV, Bykosvkaia SN, Shogan J, Shurin MR (2001) Human small cell lung carcinoma and carcinoid tumor regulate dendritic cell maturation and function. Mod Pathol 14: 40–45
7. Kirchmann TT, Prieto VG, Smoller BR (1994) CD34 staining pattern distinguishes basal cell carcinoma from trichoepithelioma. Arch Dermatol 130: 589–592
8. Kirchmann TT, Prieto VG, Smoller BR (1995) Use of CD34 in assessing the relationship between stroma and tumor in desmoplastic keratinocytic neoplasms. J Cutan Pathol 22: 422–426
9. Koukoulis GK, Howeedy AA, Korhonen M, Virtanen I, Gould VE (1993) Distribution of tenascin, cellular fibronectins and integrins in the normal, hyperplastic and neoplastic breast. J Submicrosc Cytol Pathol 25: 285–295
10. Lebeau A, Nerlich AG, Sauer U, Lichtinghagen R, Löhrs U (1999) Tissue distribution of major matrix metalloproteinases and their transcripts in human breast carcinoams. Anticancer Res 19: 4257–4264
11. Lüttges J, Mentzel T, Hubner G, Klöppel G (1999) Solitary fibrous tumour of the pancreas: a new member of the small group of mesenchymal pancreatic tumours. Virchows Arch 435: 37–42
12. Moch H, Torhorst J, Dürmüller U, Feichter GE, Sauter G, Gudat F (1993) Comparative analysis of the expression of tenascin and established prognostic markers in human breast cancer. Pathol Res Pract 189: 510–514
13. Nakayama H, Enzan H, Miyazaki E, Kuroda N, Naruse K, Hiroi M (2000) Differential expression of CD34 in normal colorectal tissue, peritumoral inflammatory tissue, and tumour stroma. J Clin Pathol 53: 626–629
14. Narvaez D, Kanitakis J, Faure M, Claudy A (1996) Immunohistochemical study of CD34-positive dendritic cells of human dermis. Am J Dermatopathol 18: 283–288
15. Seidal T, Edvardsson H (1999) Expression of c-kit (CD117) and Ki67 provides information about the possible cell of origin and clinical course of gastrointestinal stromal tumours. Histopathology 34: 416–424
16. Shoji T, Kamiya T, Tsubura A, Hamada Y, Hatano T, Hioki K, Morii S (1993) Tenascin staining positivity and the survival of patients with invasive breast carcinoma. J Surg Res 55: 295–297
17. Silverman JS, Tamsen A (1996) Mammary fibroadenoma and some phyllodes tumour stroma are composed of CD34+ fibroblasts and factor XIIIa+ dendrophages. Histopathology 29: 411–419
18. Silverman JS, Tamsen A (1997) Fibrohistiocytic differentiation in subcutaneous fatty tumors. Study of spindle cell, pleomorphic, myxoid, and atypical lipoma and dedifferentiated liposarcoma cases composed in part of CD34+ fibroblasts and FXIIIa+ histiocytes. J Cutan Pathol 24: 484–493
19. Sircar K, Hewlett BR, Huizinga JD, Chorneyko K, Berezin I, Riddell RH (1999) Interstitial cells of Cajal as precursors of gastrointestinal stromal tumors. Am J Surg Pathol 23: 377–389
20. Suster S, Fisher C (1997) Immunoreactivity for the human hematopoietic progenitor cell antigen (CD34) in lipomatous tumors. Am J Surg Pathol 21: 195–200
21. Swanson PE, Fitzpatrick MM, Ritter JH, Glusac EJ, Wick MR (1998) Immunohistologic differential diagnosis of basal cell carcinoma, squamous cell carcinoma, and trichoepithelioma in small cutaneous biopsy specimens. J Cutan Pathol 25: 153–159
22. Yakirevich E, Izhak OB, Rennert G, Kovacs ZG, Resnick MB (1999) Cytotoxic phenotype of human infiltrating lymphocytes in medullary carcinoma of the breast. Mod Pathol 12: 1050–1056

Virchows Arch (2002) 440:304–310
DOI 10.1007/s00428-001-0548-y

ORIGINAL ARTICLE

João Pinto-de-Sousa · Leonor David · Celso A. Reis
Raquel Gomes · Liliana Silva · Amadeu Pimenta

Mucins MUC1, MUC2, MUC5AC and MUC6 expression in the evaluation of differentiation and clinico-biological behaviour of gastric carcinoma

Received: 26 July 2001 / Accepted: 5 September 2001 / Published online: 23 October 2001
© Springer-Verlag 2001

Abstract Normal gastric mucosa expresses MUC1 and MUC5AC in foveolar epithelium and MUC6 in mucous neck cells of the body and deep glands of the antrum. Several studies have reported aberrant expression of an under-glycosylated form of MUC1, decreased expression of "gastric" mucins and aberrant expression of "non-gastric" mucins in gastric carcinoma. In this study, we analysed the expression profile of mucins MUC1, MUC2, MUC5AC and MUC6 in 94 gastric carcinomas using immunohistochemistry. Our results showed that: (1) mucin expression is associated with tumour type (MUC5AC with diffuse and infiltrative carcinomas and MUC2 with mucinous carcinomas) but not with the clinico-biological behaviour of the tumours; and (2) mucin expression is associated with tumour location (MUC5AC with antrum carcinomas and MUC2 with cardia carcinomas), indirectly reflecting differences in tumour differentiation according to tumour location.

Keywords Gastric carcinoma · Mucins · MUC1 · MUC2 · MUC5AC

Introduction

Mucins are high molecular weight glycoproteins which constitute the major component of the mucus layer that protects the gastric epithelium from chemical and mechanical aggressions. In humans, at least 14 mucin genes have been identified that code for the mucin proteins. They are designated as MUC1 [17, 26], MUC2 [18], MUC3 [19], MUC4 [32], MUC5AC [1, 20], MUC5B [13], MUC6 [43], MUC7 [5], MUC8 [39], MUC9 [27], MUC11, MUC12, MUC13 [46] and MUC16 [47]. Mucins share a common feature of a tandem-repeat domain rich in serine and threonine residues. These amino acid residues are potential O-glycosylation sites for attachment of the O-glycan chains that constitute up to 80% of the molecular weight of the final mucin glycoprotein [16].

Mucin genes are expressed in a regulated cell- and tissue-specific manner. The stomach provides a good example of such differential expression of mucin genes. MUC1 is detected in mucous cells of the surface epithelium and neck region of the gastric antrum, as well as in pyloric glands and oxynthic glands of the body region [22, 23, 34]. MUC5AC is highly expressed in foveolar epithelium of both body and antrum [2, 11, 23, 33], whereas MUC6 protein expression is limited to mucous neck cells of the body and pyloric glands of the antrum [4, 7, 11, 23, 37].

The mucin expression pattern of gastric carcinoma is heterogeneous. It includes mucins normally expressed in gastric mucosa (MUC1, MUC5AC and MUC6) and de novo expression of the intestinal mucin MUC2 [3, 10, 22, 23, 34, 37, 38, 44]. The heterogeneous pattern of mucin expression, including the expression of the intestinal mucin MUC2, may therefore provide new insights into the differentiation pathways of gastric carcinoma. The pattern of mucin expression may also be used as a clue to bring new insights into the biological behaviour of distinct clinicopathological entities related to the localisation of gastric carcinoma, namely proximal and distal gastric carcinomas.

Here, we report the mucin expression profile in 94 gastric carcinomas using immunohistochemistry with monoclonal antibodies to MUC1, MUC2, MUC5AC and MUC6. We compared the mucin expression profile with the differentiation and clinico-biological behaviour of gastric carcinomas. Particular attention was given to the association between mucin expression profile of the carcinomas and the localisation (cardia, fundus/body, antrum) of the tumours.

J. Pinto-de-Sousa (✉) · A. Pimenta
Serviço de Cirurgia 4 Hospital S. João,
Alameda Prof. Hernâni Monteiro, 4200 Porto, Portugal
e-mail: japs@med.up.pt
Tel.: +351-2-25096908, Fax: +351-2-25096908

J. Pinto-de-Sousa · L. David · A. Pimenta
Medical Faculty of the University of Porto, Porto, Portugal

L. David · C.A. Reis · R. Gomes · L. Silva
Institute of Molecular Pathology and Immunology
of the University of Porto (IPATIMUP), Porto, Portugal

Materials and methods

Tissue samples and histopathological study

Surgical specimens from 94 gastric carcinomas were evaluated retrospectively. These 94 patients represent a subgroup of the total number (*n*=326) of patients submitted to surgical resection of gastric carcinoma in Serviço Cirurgia 4, Hospital S. João, between January 1984 and December 1996. The 94 selected cases were classified in three groups according to the tumour location, following criteria previously described [31]: group 1 – gastric cardia (*n*=22); group 2 – fundus/body (*n*=25); and group 3 – antrum (*n*=47).

Carcinomas were classified according to Laurén [28] and to World Health Organization (WHO) [45] classifications. The growth pattern was classified according to Ming [29]. Size, depth of wall penetration, nodal status and venous invasion were also recorded. The 1997 version of the UICC (Union Internationale Contra la Cancrum) pTNM system was employed to stage the carcinomas [41]. The characteristics of the cases according to the clinicopathological parameters are depicted in Table 1.

Table 1 Summary of the clinical and pathological characteristics of the cases

Parameters	Patients	
	n	%
Tumour site (*n*=94)		
Cardia	22	23.4
Fundus/body	25	26.6
Antrum	47	50.0
Laurén's classification (*n*=91)		
Intestinal	49	53.8
Diffuse	23	25.3
Unclassified	19	20.9
World Health Organization classification (*n*=93)		
Well–moderately differentiated	48	51.6
Poorly differentiated	18	19.4
Signet ring cells	21	22.6
Others	6	6.4
Ming's classification (*n*=90)		
Expansive	30	33.3
Infiltrative	60	66.7
Venous invasion (*n*=94)		
Absent	47	50.0
Present	47	50.0
Lymphatic invasion (*n*=94)		
Absent	11	11.7
Present	83	88.3
Depth of wall penetration (*n*=94)		
T1	13	13.8
T2	46	48.9
T3	31	33.0
T4	4	4.3
Nodal metastases (*n*=94)		
Absent	28	29.8
Present	66	70.2
pTNM stage (*n*=89)		
IA	10	11.2
IB	18	20.2
II	15	16.9
IIIA	21	23.6
IIIB	6	6.7
IV	19	21.4

Antibodies and immunohistochemistry

The expression of MUC1, MUC2, MUC5AC and MUC6 was studied using immunohistochemistry with monoclonal antibodies. The monoclonal antibodies HMFG1 and SM3 were used to detect MUC1 mucin. The HMFG1 antibody is reactive with MUC1 independently of glycosylation [42], whereas SM3 antibody is reactive only with under-glycosylated forms of MUC1 [6]. Monoclonal antibody PMH1 was used to detect MUC2 mucin [35]. Monoclonal antibody CLH2 was used to detect MUC5AC [33], and monoclonal antibody CLH5 was used to detect MUC6 [37].

Sections from the surgical specimens representative of the carcinomas were immunostained using avidin–biotin complex staining as previously described [24, 33]. The paraffin sections were de-waxed and rehydrated. Sections designed for PMH1 (MUC2) were submitted to neuraminidase treatment by incubation with neuraminidase from Clostridium perfringens type VI (Sigma; St Louis, Mo.) diluted in 0.1 M Na-acetate buffer, pH 5.5, to a final concentration of 0.1 U/ml. The incubation was carried out for 2 h at 37°C and was followed by three washings in ice-cold water. Sections were then treated with 0.3% hydrogen peroxide in methanol for 30 min to block endogenous peroxidase, followed by incubation with normal non-immune serum for 20 min. Sections were rinsed with Tris-buffered saline (TBS) and incubated with primary antibodies overnight at 4°C. Sections were rinsed and incubated with a biotin-labelled rabbit anti-mouse secondary antibody, diluted 1:200 in TBS for 30 min, then rinsed and incubated with avidin–biotin peroxidase complex for 1 h. Sections were rinsed and stained for 7 min with 0.05% 3,3 diaminobenzidine tetrahydrochloride (DAB) freshly prepared in 0.05 M Tris/hydroxymethylaminomethane buffer, pH 7.6, containing 0.1% hydrogen peroxide. Sections were counterstained with haematoxylin, dehydrated and mounted. All series included positive controls. Negative controls were performed using conjugate alone.

Classification of immunohistochemistry

Cases were classified according to the immunostaining in two groups: negative (negative or rare/less than 5% of positive cells) or positive (positive in more than 5% of the cells).

Survival analysis

Survival data was obtained from Cancer Registry of Hospital S. João, with a follow-up of 100% of the patients. Fifty-two patients (55.3%) were dead at the end of this study. Cumulative survival was evaluated according to the staining for each mucin and also according to the site of the carcinoma.

Statistical analysis

StatView 5.0 and SPSS 9.0 for Windows computer programs were employed in the statistical analysis of data. Distributions were compared using the chi-squared test or the Fisher's exact test whenever appropriate. Cumulative survival curves were obtained using the Kaplan-Meier limit product [25] and compared using the log rank test. Significance was assumed if *P* values were less than 0.05.

Results

Mucin expression and differentiation profiles of gastric carcinoma

Immunoreactivity for MUC1 glycoforms detected using the HMFG1 antibody was observed in 73 cases (89.0%). Under-glycosylated MUC1 glycoforms detected using the SM3 antibody were observed in 41 cases (50.0%). MUC2 was detected in 21 cases (26.6%), MUC5AC in 44 cases (47.3%) and MUC6 in 18 cases (22.0%). No significant differences were observed between the expression profile of mucins MUC1 (independently of the glycoforms) and MUC6 and the histological classification according to Laurén and Ming.

MUC2 expression was significantly associated with mucinous carcinomas, with all cases (n=4) expressing MUC2 (P=0.01; Fig. 1).

MUC5AC was expressed in 44 carcinomas. The percentage of diffuse carcinomas with positive staining for MUC5AC (65.2%) was significantly higher than that observed in the unclassified carcinomas (33.3%; P=0.04; Table 2; Fig. 1). The percentage of positive cases in intestinal carcinomas (46.9%) lies somewhere in between that of diffuse (65.2%) and unclassified (33.3%) carcinomas. The percentage of MUC5AC immunoreactive cases was significantly higher in infiltrative carcinomas (60.0%) than in expansive carcinomas (27.6%; P=0.01) according to the classification of Ming (Table 2).

Fig. 1 Immunohistochemical staining of gastric carcinoma using monoclonal antibodies. **A** Gastric carcinoma of the diffuse type immunostained with monoclonal antibody CLH2 showing expression of mucin MUC5AC. **B** Gastric carcinoma of the mucinous type immunostained with monoclonal antibody PMH1 showing expression of mucin MUC2

Mucin expression and clinico-biological behaviour of gastric carcinoma

No significant association was found between the immunoreactivity for any of the mucins and the pathological parameters evaluated: size, depth of wall penetration, nodal status, venous invasion and tumour stage. The distribution of the cases according to the immunoreactivity for mucins (MUC1, MUC2, MUC5AC and MUC6) and to the carcinoma location is documented in Table 3. No significant differences were observed between the expression of MUC1 (independently of the glycosylation status) and MUC6 according to the carcinoma location.

Overall differences were observed in the distribution of MUC2 according to tumour location (P=0.04). The comparison of MUC2 expression between each tumour site showed that the percentage of cardia carcinomas expressing MUC2 (50.0%) was significantly higher than that observed in fundus/body carcinomas (17.4%; P=0.03) and in antrum carcinomas (21.1%; P=0.03).

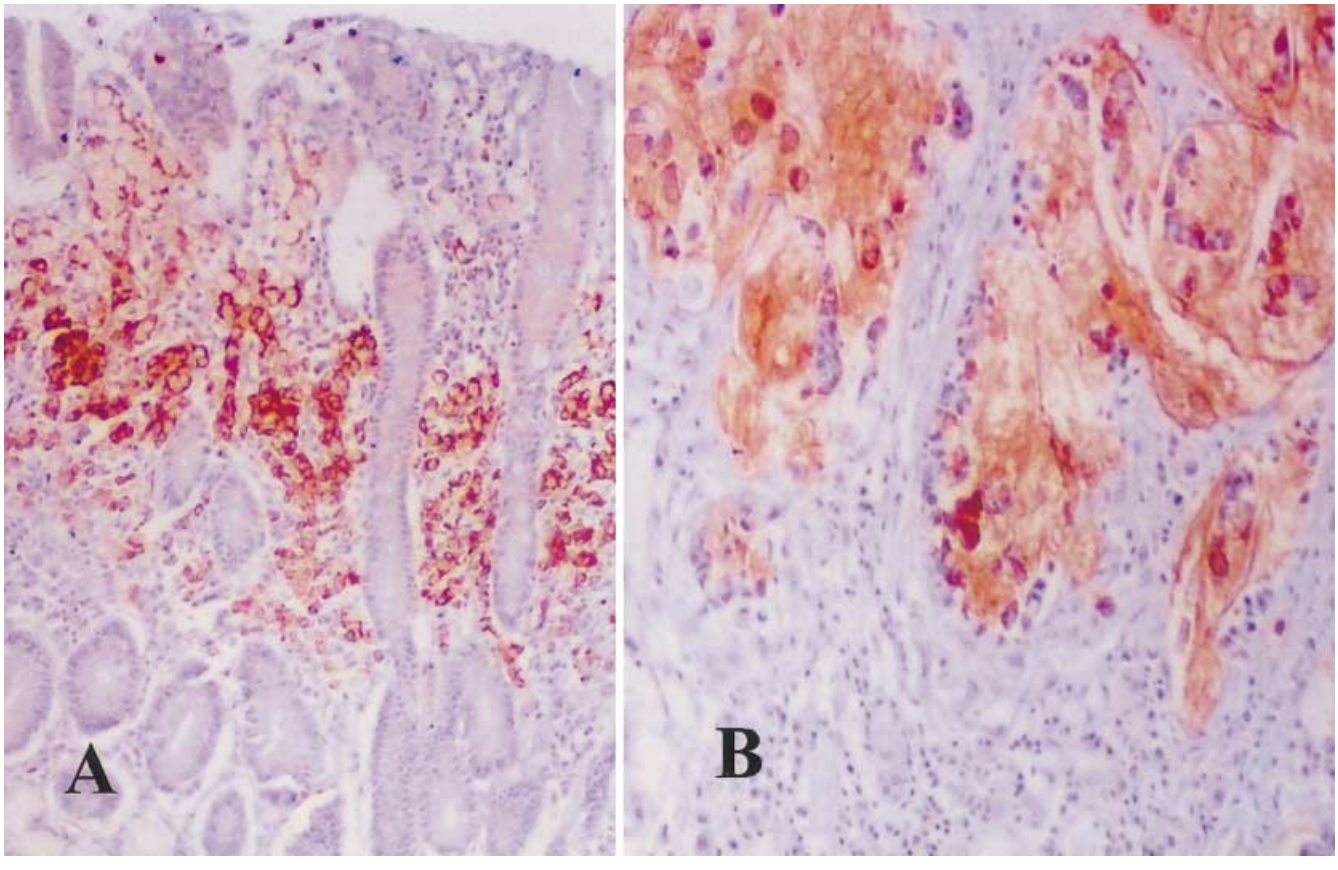

Table 2 MUC5AC immunohistochemical reactivity according to the histological classification of Laurén and Ming. *P* value indicated in the table (*NS* not significant) refers to the global comparison of distribution; in the comparison between diffuse and unclassified carcinomas *P*=0.04

	Negative *n* (%)	Positive *n* (%)	*P* value
Laurén's classification			NS*
Intestinal	26 (53.1)	23 (46.9)	
Diffuse	8 (34.8)	15 (65.2)	
Unclassified	12 (66.7)	6 (33.3)	
Ming's classification			0.01
Expansive	21 (72.4)	8 (27.6)	
Infiltrative	24 (40.0)	36 (60.0)	

The overall distribution of cases immunoreactive for MUC5AC in the different tumour locations was not significantly different. However, the percentage of cases of antrum carcinomas expressing MUC5AC (55.3%) was significantly higher than that of fundus/body carcinomas (29.2%; *P*=0.04).

No significant differences were observed in the overall comparison of cumulative survival according to the expression of MUC1, MUC2, MUC5AC and MUC6 in the gastric tumours. Five-year survival was 25% for patients with MUC1 negative carcinomas and 39% for those with positive carcinomas. Five-year survival was 29.5% for patients without expression of under-glycosylated MUC1 and 43% for those with expression of under-glycosylated MUC1. That of patients without MUC2 expression was 37.6% and those with MUC2 expression had a 31.6% 5-year survival. Regarding the immunoreactivity for MUC5AC, it was observed that the 5-year survival was 39.5% for patients with carcinomas not expressing the mucin and 36.2% for patients with carcinomas expressing the mucin. Five-year survival of patients with carcinomas not expressing MUC6 was 37.7% and that of patients with positive carcinomas was 42.9%. The comparison of survival curves for each tumour site and for each histological type according to stage was not significantly different when positive and negative tumour cases for each mucin were evaluated. No significant differences were observed when positive cases were restricted to those expressing high levels of positive cells (>50%; data not shown).

Discussion

The present study confirmed that the expression of mucins is associated with characteristics of differentiation of gastric carcinomas. We observed that the expression of normal gastric mucins – MUC1, MUC5AC and MUC6 – is modified at different levels in gastric carcinomas. In normal gastric mucosa, MUC5AC mucin is specifically expressed by foveolar and neck cells [33] which are considered as gastric-specific, mucous-producing cells [14]. Our results, showing association of MUC5AC expression and diffuse-type gastric carcinoma (65% of the cases in the present series), are in agreement with previous studies showing that diffuse gastric carcinomas usually keep features of gastric differentiation [8, 14, 33]. In the present study, the expression of MUC5AC was also associated with tumours showing an infiltrative pattern of growth according to the classification of Ming [29]. This association may reflect that most diffuse gastric carcinomas also display an infiltrative growth pattern [9, 28, 29].

MUC6 was expressed in a small percentage (22%) of gastric carcinomas, which is in keeping with previous studies [37]. Expression of MUC6 is associated with mucopeptic differentiation in normal gastric tissues [11, 37]. Our results indicate that mucopeptic differentiation is not a prominent feature in gastric carcinomas and that,

Table 3 Immunohistochemical reactivity for mucins MUC1, MUC2, MUC5AC and MUC6 according to the carcinoma location. *NS* not significant

Mucins	Global *n* (%)	Cardia *n* (%)	Fundus/body *n* (%)	Antrum *n* (%)	*P* value
MUC1					NS
Negative/rare cells	9 (11.0)	0 (0.0)	4 (17.4)	5 (12.8)	
Positive	73 (89.0)	20 (100.0)	19 (82.6)	34 (87.2)	
MUC1 underglycosylated					NS
Negative/rare cells	41 (50.0)	6 (35.3)	13 (56.5)	22 (52.4)	
Positive	41 (50.0)	11 (64.7)	10 (43.5)	20 (47.6)	
MUC2					0.04*
Negative/rare cells	58 (73.4)	9 (50.0)	19 (82.6)	30 (78.9)	
Positive	21 (26.6)	9 (50.0)	4 (17.4)	8 (21.1)	
MUC5AC					NS**
Negative/rare cells	49 (52.7)	11 (50.0)	17 (70.8)	21 (44.7)	
Positive	44 (47.3)	11 (50.0)	7 (29.2)	26 (55.3)	
MUC6					NS
Negative/rare cells	64 (78.0)	15 (78.9)	18 (81.8)	31 (75.6)	
Positive	18 (22.0)	4 (21.1)	4 (18.2)	4 (24.4)	

*This *P* value refers to the global comparison of distribution; in the comparison between cardia and fundus/body cases *P*=0.03 and between cardia and antrum cases *P*=0.03

**This *P* value refers to the global comparison of distribution; in the comparison between antrum and fundus/body cases *P*=0.04

when present, it is not associated with any particular histological type of gastric carcinoma. These observations agree with previous histochemical, immunohistochemical, and ultrastructural observations showing that mucopeptic cells occur only in a few gastric carcinomas, regardless of their histological type [14].

The evaluation of expression of MUC1 in gastric carcinoma was performed using two specific monoclonal antibodies. The HMFG1 monoclonal antibody is reactive with MUC1 independently of the glycosylation [42] and was positive in 89% of the cases. The SM3 monoclonal antibody, which recognises only the under-glycosylated forms of MUC1 mucin [6], was positive in 50% of the cases of the present series. The expression of both fully and under-glycosylated forms of MUC1 was not associated with any particular histological type of gastric carcinoma. In a previous study, we observed a significant association between SM3 immunoreactivity and unclassified gastric carcinomas according to the classification of Laurén [34]. The absence of association with gastric carcinoma differentiation observed in the present work may stem from the smaller number of cases analysed in the present series.

Our results showed that intestinal mucin MUC2 was aberrantly expressed in 26% of gastric carcinomas of the series, which is in accordance with results reported in previous studies [3, 23]. The prominent expression of MUC2 in mucinous gastric carcinomas observed in the present study is also in agreement with previous observations [37]. Expression of MUC2 has also been described in mucinous carcinomas of the colon, pancreas, breast and ovary [21]. Taking into account that in normal cells and in intestinal metaplasia of the stomach MUC2 expression is closely associated with the globet cell phenotype [12, 15, 22, 36], our results suggest that goblet cells are common in mucinous carcinomas, which is in keeping with previous histochemical and ultrastructural observations [14].

In this series we did not observe significant associations between the pattern of mucin expression (MUC1, MUC2, MUC5AC and MUC6) and the clinico-pathological parameters with an influence in the behaviour of gastric carcinoma. We could not confirm, therefore, previous observations showing that in the gastric carcinoma model mucins can have a role in the evaluation of clinico-pathological behaviour. One of the previously described associations was that MUC5AC expression was more frequent in early gastric carcinomas (100%) than advanced carcinomas (58.6%) [33]. This association of MUC5AC with early gastric tumours suggests that all gastric carcinomas retain a “gastric” phenotype during the first steps of neoplastic development [33]. Another previously described finding was the association between MUC1 overexpression and poor outcome of gastric carcinoma patients [3, 34]. In the present series we did not confirm the usefulness of any of the mucins studied, including MUC1 and MUC5AC, in the evaluation of clinical outcome, probably due to the small number of studied cases.

We performed for the first time a comprehensive study of the pattern of mucin expression in gastric carcinomas according to the site of the tumour (cardia, fundus/body and antrum). The pattern of mucin expression may be an important tool for understanding and interpreting the different clinical and pathological entities of gastric carcinoma, i.e. proximal and distal gastric carcinomas [31, 40]. We have found differences in the distribution of MUC2 and MUC5AC in the three locations of gastric carcinoma and found no differences in the distribution of MUC1 (independently of the glycosylation status) and MUC6. The expression of the intestinal mucin MUC2 was more frequent in carcinomas localised in the cardia (50.0%) than in carcinomas in the fundus/body (17.4%) or antrum (21.1%). These results may reflect that cardia carcinomas are resected at more advanced pTNM stages than antrum cases [30, 31, 40] and are in agreement with the hypothesis of a more heterogeneous mucin expression pattern and of de novo expression of non-gastric mucins in advanced gastric carcinomas as described by Ho et al. [23].

In our study, gastric carcinomas located in the antrum had a significantly higher percentage of MUC5AC-expressing cases than those located in the fundus/body. The higher percentage of MUC5AC expression in the antrum may stem from the less advanced tumour stage of antrum carcinoma cases than proximal carcinomas, or from the higher percentage of diffuse carcinomas in the distal stomach [31]. Altogether these two observations reinforce the use of MUC5AC as a differentiation marker with particular relevance in antrum cases.

In summary, we have shown in a comprehensive study of gastric carcinomas evaluated for expression of several mucins (MUC1, MUC2, MUC5AC and MUC6) that: (1) mucin expression is associated with tumour type (MUC5AC with diffuse and infiltrative carcinomas and MUC2 with mucinous carcinomas) but not with the clinico-biological behaviour of the tumours; and (2) mucin expression is associated with tumour location (MUC5AC with antrum carcinomas and MUC2 with cardia carcinomas), indirectly reflecting differences in tumour differentiation according to tumour location.

Acknowledgements The authors thank Prof. Joyce Taylor–Papadimitriou and Dr. Joy Burchell for providing the monoclonal antibodies HMFG1 and SM3. This work was supported by FCT (POCTI/CBO/36376).

References

1. Aubert JP, Porchet N, Crepin M, Duterque-Coquillaud M, Vergnes G, Mazzuca M, Debuire B, Petitprez D, Degand P (1991) Evidence for different human tracheobronchial mucin peptides deduced from nucleotide cDNA sequences. Am J Respir Cell Mol Biol 5:178–185
2. Audie JP, Janin A, Porchet N, Copin MC, Gosselin B, Aubert JP (1993) Expression of human mucin genes in respiratory, digestive, and reproductive tracts ascertained by in situ hybridization. J Histochem Cytochem 41:1479–1485
3. Baldus SE, Zirbes TK, Engel S, Hanisch FG, Moning SP, Lorenzen J, Glossman J, Fromm S, Thiele J, Pichmaier H, Dienes HP (1998) Correlation of the immunohistochemical reactivity of mucin cores MUC1 and MUC2 with histopatological subtype and prognosis of gastric carcinomas. Int J Cancer 79: 133–138

4. Bartman AE, Buisine M-P, Aubert J-P, Niehans GA, Toribara NW, Kim YS, Kelly EJ, Crabtree JE, Ho SB (1998) The MUC6 secretory mucin gene is expressed in a wide variety of epithelial tissues. J Pathol 186:398–405
5. Bobek LA, Tsai H, Biesbrock AR, Levine MJ (1993) Molecular cloning, sequence, and specificity of expression of the gene encoding the lower molecular weight human salivary mucin (MUC7). J Biol Chem 268:20563–20569
6. Burchell J, Taylor-Papadimitriou J, Boschell M, Gendler S, Duhig T (1989) A short sequence, within the amino acid tandem repeat of a cancer-associated mucin, contaions immunodominant epitopes. Int J Cancer 44:691–696
7. Byrd JC, Yan P, Sternberg L, Yunker CK, Scheiman JM, Bresalier RS (1997) Aberrant expression of gland-type gastric mucin in the surface epithelium of Helicobacter pylori-infected patients. Gastroenterology 113:455–464
8. Carneiro F, Moutinho-Ribeiro M, David L, Seixas M, Sansonetty F, Soares P, Serrano A, Sobrinho-Simões M (1992) Signet ring cell carcinoma of the stomach: a morphometric, ultrastructural, and DNA cytometric study. Ultrastruct Pathol 16:603–614
9. Carneiro F, Seixas M, Sobrinho-Simões M (1995) New elements for an updated classification of the carcinomas of the stomach. Pathol Res Pract 191:571–584
10. Carrato C, Balagué C, DeBolos C, Gonzalez E, Gambus G, Planas J, Perini JM, Andreu D, Real FX (1994) Differential apomucin expression in normal and neoplastic gastrointestinal tissues. Gastroenterology 107:160–172
11. DeBolós C, Garrido M, Real FX (1995) MUC6 apomucin shows a distinct normal tissue distribution that correlates with Lewis antigen expression in the human stomach. Gastroenterology 109:723–734
12. Devine PL, McGuckin MA, Birrell GW, Whitehead RH, Sachdev GP, Shield P, Ward BG (1993) Monoclonal antibodies reacting with the MUC2 mucin core protein. Br J Cancer 67:1182–1188
13. Dufosse J, Porchet N, Audie JP, Guyonnet-Dupérat V, Laine A, Van-Seuningen I, Marrakchi S, Degand P, Aubert JP (1993) Degenerate 87-base-pair tandem repeats create hydrophilic/hydrophobic alternating domains in human mucin peptides mapped to 11p15. Biochem J 293:329–337
14. Fiocca R, Villani L, Tenti P, Solcia E, Cornaggia M, Frigerio B, Capella C (1987) Characterization of four main cell types in gastric cancer: foveolar, mucopeptic, intestinal columnar and goblet cells. An histopathologic, histochemical and ultrastructural study of “early” and “advanced” tumours. Pathol Res Pract 182:308–325
15. Gambús G, De Bolós C, Andreu D, Francí C, Egea G, Real FX (1993) Detection of the MUC2 apomucin tandem repeat with a mouse monoclonal antibody. Gastroenterology 104:93–102
16. Gendler SJ, Spicer AP (1995) Epithelial mucin genes. Annu Rev Physiol 57:607–634
17. Gendler SJ, Lancaster CA, Taylor-Papadimitriou J, Duhig J, Peat T, Burchell J (1990) Molecular cloning and expression of human tumor-associated polymorphic epithelial mucin. J Biol Chem 265:15286–15293
18. Gum JR, Byrd JC, Hicks JW, Toribara NW, Lamport DTA, Kim YS (1989) Molecular cloning of human intestinal mucin cDNAs. J Biol Chem 264:6480–6487
19. Gum JR, Hicks JW, Swallow DM, Lagace RE, Byrd JC, Lamport DT, Siddiki B, Kim YS (1990) Molecular cloning of cDNAs derived from a novel human intestinal mucin gene. Biochem Biophys Res Commun 171:407–415
20. Guyonnet Duperat V, Audie JP, Debailleul V, Laine A, Buisine MP, Galiegue-Zouitina S, Pigny P, Degand P, Aubert JP, Porchet N (1995) Characterization of the human mucin gene MUC5AC: a consensus cysteine-rich domain for 11p15 mucin genes? Biochem J 305:211–219
21. Hanski C, Hofmeier M, Schmitt-Graff A, Riede E, Hanski ML, Borchard F, Sieber E, Niedobitek F, Foss HD, Stein H, Riecken EO (1997) Overexpression or ectopic expression of MUC2 is the common property of mucinous carcinomas of the colon, pancreas, breast, and ovary. J Pathol 182:385–391
22. Ho SB, Niehans GA, Lyftogt C, Yan Ps, Cheritz DL, Gumm ET, Dahiya R, Kim YS (1993) Heterogeneity of mucin gene expression in normal, preneoplastic, and neoplastic human gastric epithelium. Cancer Res 53:641–651
23. Ho SB, Shekels LL, Toribara NW, Kim YS, Lyftogt C, Cherwitz DL, Niehans GA (1995) Mucin gene expression in normal, preneoplastic, and neoplastic human gastric epithelium. Cancer Res 55:2681–2690
24. Hsu S, Raine L, Fanger H (1981) A comparative study of the peroxidase-antiperoxidase method and an avidin-biotin complex method for studying polypeptide hormones with radioimmunoassay antibodies. Am J Clin Pathol 75:734–738
25. Kaplan EL, Meier P (1958) Nonparametric estimation from incomplete observations. J Am Stat Assoc 53:457–481
26. Lan MS, Batra SK, Qi W-N, Metzgar RS, Hollingsworth MA (1990) Cloning and sequencing of a human pancreatic tumor mucin cDNA. J Biol Chem 265:15294–15299
27. Lapensee L, Paquette Y, Bleau G (1997) Allelic polymorphism and chromosomal localization of the human oviductin gene (MUC9). Fertil Steril 68:702–708
28. Laurén P (1965) The two histological main types of gastric carcinoma: diffuse and the so-called intestinal-type carcinoma. Acta Pathol Microbiol Scand 64:31–49
29. Ming SC (1977) Gastric carcinoma: a pathobiological classification. Cancer 39:2475–2485
30. Nakane Y, Okamura S, Boku T, Okusa T, Tanaka K, Hioki K (1993) Prognostic differences of adenocarcinoma arising from the cardia and the upper third of the stomach. Am Surg 59: 423–429
31. Pinto de Sousa J, David L, Seixas M, Pimenta A (2001) Clinico-pathological profiles and prognosis of gastric carcinoma from the cardia, fundus/body and antrum. Dig Surg 18: 102–110
32. Porchet N, Van Cong N, Dufosse J, Audie JP, Guyonnet-Duperat V, Gross MS, Denis C, Degand P, Bernheim A, Aubert JP (1991) Molecular cloning and chromosomal localization of a novel human tracheo-bronchial mucin cDNA containing tandemly repeated sequences of 48 base pairs. Biochem Biophys Res Commun 175:414–422
33. Reis CA, David L, Nielsen PA, Clausen H, Mirgorodskaya K, Roepstorff P, Sobrinho-Simões M (1997) Immunohistochemical study of MUC5AC expression in human gastric carcinomas using a novel monoclonal antibody. Int J Cancer 74: 112–121
34. Reis CA, David L, Seixas M, Burchell J, Sobrinho-Simões M (1998) Expression of fully and under-glycosylated forms of MUC1 Mucin in gastric carcinoma. Int J Cancer 79:402–410
35. Reis CA, Sørensen, Mandel U, David L, Mirgorodskaya E, Roepstorff E, Kihlberg J, Hansen JS, Clausen H (1998) Development and characterization of an antibody directed to an á-N-acetyl-D-galactosamine glycosylated MUC2 peptide. Glycoconj J 15:51–62
36. Reis CA, David L, Correa P, Carneiro F, DeBolós C, Garcia E, Mandel U, Clausen H, Sobrinho-Simões M (1999) Intestinal metaplasia of the human stomach displays distinct patterns of mucin (MUC1, MUC2, MUC5AC, MUC6) expression. Cancer Res 59:1003–1007
37. Reis CA, David L, Carvalho F, Mandel U, Bolós C, Mirgorodskaya E, Clausen H, Sobrinho-Simões M (2000) Immunohistochemical study of the expression of MUC6 mucin and co-expression of other secreted mucins (MUC5AC and MUC2) in human gastric carcinomas. J Histochem Cytochem 48:377–388
38. Sakamoto H, Yonezawa S, Utsunomiya T, Tanaka S, Kim YS, Sato E (1997) Mucin antigen expression in gastric carcinomas of young and old adults. Hum Pathol 28:1056–1065
39. Shankar V, Pichan P, Eddy RL Jr, Tonk V, Nowak N, Sait SN, Shows TB, Schultz RE, Gotway G, Elkins RC, Gilmore MS, Sachdev GP (1997) Chromosomal localization of a human mucin gene (MUC8) and cloning of the cDNA corresponding to the carboxy terminus. Am J Respir Cell Mol Biol 16:232–241
40. Siewert JR, Böttcher K, Stein HJ, Roder JD, Busch R (1995) Problem of proximal third gastric carcinoma. World J Surg 19: 523–531

41. Sobin LH, Wittekind CH (eds) (1997) TNM classification of malignant tumours. International Union Against Cancer, 5th edn. John Wiley & Sons, New York
42. Taylor-Papadimitriou J, Peterson JA, Arklie J, Burchell J, Ceriani RL, Bodmer WF (1981) Monoclonal antibodies to epithelium-specific components of the human milk fat globule membrane: production and reaction with cells in culture. Int J Cancer 28:17–21
43. Toribara NW, Roberton AM, Ho SB, Kuo WL, Gum E, Hicks JW, Gum JR, Byrd JC, Siddiki B (1993) Human gastric mucin. Identification of a unique species by expression cloning. J Biol Chem 268:5879–5885
44. Utsunomiya T, Yonezawa S, Sakamoto H, Kitamura H, Hokita S, Aiko T, Tanaka S, Irimura T, Kim YS, Sato E (1998) Expression of MUC1 and MUC2 mucins in gastric carcinomas: its relationship with the prognosis of the patients. Clin Cancer Res 4:2605–2614
45. Watanabe H, Jass JR, Sobin LH (1990) Histological typing of oesophageal and gastric tumors, 2nd edn. WHO international classification of tumors. Springer, Berlin Heidelberg NewYork
46. Williams SJ, McGuckin MA, Gotley DC, Eyre HJ, Sutherland GR, Antalis TM (1999) Two novel mucin genes down-regulated in colorectal cancer identified by differential display. Cancer Res 59:4083–4089
47. Yin BWT, Lloyd KO (2001) Molecular cloning of the CA125 ovarian cancer antigen: identification as a new mucin (MUC16). J Biol Chem (in press)

Virchows Arch (2002) 440:311–317
DOI 10.1007/s004280100531

ORIGINAL ARTICLE

**Elisabete Silva · Ana Teixeira · Leonor David
Fátima Carneiro · Celso A. Reis
Joana Sobrinho-Simões · Jacinta Serpa
Enno Veerman · Jan Bolscher
Manuel Sobrinho-Simões**

Mucins as key molecules for the classification of intestinal metaplasia of the stomach

Received: 14 June 2001 / Accepted: 7 August 2001 / Published online: 15 December 2001
© Springer-Verlag 2001

Abstract Mucins and mucin-associated carbohydrates have a distinct expression pattern that can be modified under pathological conditions. Normal gastric mucosa expresses MUC1 and MUC5AC in foveolar epithelium and MUC6 in the glands. Lewis type-1 chain antigens (Le^a and Le^b) are expressed in foveolar epithelium, whereas Lewis type-2 chain antigens (Le^x and Le^y) are expressed in the glands. In this study we used monoclonal antibodies to evaluate the pattern of mucins and Lewis type-1 carbohydrates in intestinal metaplasia (IM) and compared it with IM types determined using histochemistry. In type-I or complete IM we found expression of MUC2 intestinal mucin and decreased/absent expression of MUC1, MUC5AC and MUC6. In type-II/III or incomplete IM there was co-expression of MUC2 and the mucins expressed in the stomach. No major differences were detected among the three IM types regarding expression of Lewis antigens. Furthermore we observed that sialylated compounds other than sialyl-Le^a are responsible for histochemical detection of sialomucins and that sulpho-$Le^{a/c}$ is expressed in the presence or absence of sulphomucins detected using histochemistry. We conclude that mucin immunohistochemistry may replace classic histochemistry for the classification of IM into complete and incomplete types. The present study challenges the distinction of type-II from type-III IM since we did not observe major differences in the expression profile of mucins and Lewis type-1 carbohydrates. Finally, it seems necessary to evaluate the predictive value of IM according to the presence of specific sulphated carbohydrates (e.g. sulpho-$Le^{a/c}$) rather than histochemically detected sulphomucins.

Keywords Mucins · Lewis type-1 carbohydrates · Intestinal metaplasia · Gastric carcinoma

E. Silva · A. Teixeira · L. David (✉) · F. Carneiro · C.A. Reis
J. Sobrinho-Simões · J. Serpa · M. Sobrinho-Simões
Institute of Molecular Pathology and Immunology
of the University of Porto, IPATIMUP, Porto, Portugal
e-mail: leonor.david@ipatimup.pt

L. David · F. Carneiro · M. Sobrinho-Simões
Medical Faculty of the University of Porto, Porto, Portugal

E. Veerman · J. Bolscher
Department of Dental Basic Sciences, Section Oral Biochemistry,
ACTA, Amsterdam, The Netherlands

L. David
IPATIMUP, Rua Dr. Roberto Frias s/n, 4200 Porto, Portugal

Introduction

Mucins are high molecular weight glycoproteins that constitute the major component of the mucus layer that protects the gastric epithelium from chemical and mechanical aggressions. Twelve mucin genes that code for the protein part of mucins (apomucins) have been identified: *MUC1*, *MUC2*, *MUC3*, *MUC4*, *MUC5AC*, *MUC5B*, *MUC6*, *MUC7* [8], *MUC8* [21], *MUC9* [11], *MUC11* and *MUC12* [27]. *MUC2*, *MUC5AC*, *MUC5B* and *MUC6* genes have been mapped on a cluster on chromosome 11p15.5, and *MUC3*, *MUC11* and *MUC12* have been mapped on another cluster on chromosome 7q22 [27]. The presence of a variable number of tandem repeats that code for amino acid sequences rich in serine and threonine residues is a common characteristic of mucins. These amino acid residues are potential *O*-glycosylation sites for attachment of the glycan side chains that constitute ~80% of the molecular weight of the final mucin glycoproteins.

Normal gastric mucosa produces mainly neutral mucins, except for the mucus-secreting cells of the neck glands that secrete acid mucins [5]. Normal human stomach expresses MUC1, MUC5AC and MUC6. MUC1 and MUC5AC are expressed in the superficial foveolar epithelium, whereas MUC6 is expressed in the mucous neck cells of the body and deeper glands of the antrum. Lewis type-1 chain antigens (Le^a and Le^b) are expressed in the surface foveolar epithelium, whereas Lewis type-2 chain antigens (Le^x and Le^y) are expressed in the glands

[15]. De Bolós et al. [4] demonstrated that the zonal expression of mucins and Lewis antigens is tightly associated and showed that MUC5AC-expressing cells also express Lewis type-1 antigen Le^a, whereas MUC6 expressing cells express Lewis type-2 antigen Le^y.

Mucins and mucin-associated carbohydrate chains have a distinct tissue expression pattern that can be quantitatively and qualitatively modified under pathological conditions [1, 2, 9, 10, 13, 18, 19]. Intestinal metaplasia (IM) was characterised at the histochemical level by the abnormal expression of acid mucins (both sialomucins and sulphomucins) [6]. In IM the expression pattern of both mucins and carbohydrates is modified [10, 16, 18]. Mucin expression in IM can be described under two major profiles: one with decreased expression of MUC1, MUC5AC and MUC6 and de novo expression of the intestinal mucin MUC2 (complete IM); and the other with coexpression of MUC1, MUC5AC, MUC6 and MUC2 (incomplete IM) [18].

Carbohydrate expression in IM also suffers major alterations, including a marked increase in Le^a antigen expression [12, 23, 24, 25] which is thought to reflect the increased activity of FucT III enzyme [29]. López-Ferrer et al. [12] showed that the association between apomucins and Lewis antigens observed in the normal mucosa is lost in IM.

Our aim was to evaluate the mucins and type-1 Lewis antigens distribution pattern in IM and compare it with the "classic" types of IM defined using histochemistry. We used immunohistochemical techniques to detect the expression pattern of mucins (MUC1, MUC2, MUC5AC and MUC6) and carbohydrates (Le^a, Le^b, sialyl-Le^a and sulpho-$Le^{a/c}$) and histochemical techniques to classify IM types according to Filipe and Jass [6].

Materials and methods

Tissue samples and histochemistry

Endoscopic gastric biopsies (n=19) were obtained from asymptomatic volunteers or dyspeptic individuals from northern Portugal working in a shipyard at Viana do Castelo. Tissues were embedded in paraffin, and serial 4-µm sections were obtained for histochemistry and immunohistochemistry.

IM was classified according to Filipe and Jass [6], using alcian blue/periodic acid Schiff and high-iron diamine–alcian blue technique: in type-I (complete) IM the epithelium had mature absorptive non-secretory cells and goblet cells that secreted mainly sialomucins; in type-II (incomplete) IM the epithelium had few or absent absorptive cells, columnar mucous cells that secreted neutral mucins and/or small amounts of sialomucins and goblet cells that secreted sialo and occasionally sulphomucins; and in type-III (incomplete) IM columnar cells secreted predominantly sulphomucins and goblet cells produced sialo and/or sulphomucins.

Antibodies and immunohistochemistry

Monoclonal antibodies were used to detect mucins and type-1 chain carbohydrate antigens (Table 1). Paraffin sections were deparaffinated and rehydrated. Sections to be treated with the antibody against MUC2 (PMH1) were incubated with neuraminidase from type-VI *Clostridium perfringens* (Sigma Chemical Co. St. Louis, Mo.), diluted in 0.2 M sodium acetate buffer (pH 5.4) to a final concentration of 0.1 Units/ml, incubated for 2 h at 37°C and then washed two times in cold water and once in Tris-buffered saline (TBS; pH 7.6). In all sections endogenous peroxidase was blocked using 0.5% hydrogen peroxide (H_2O_2) in methanol for 30 min at room temperature. Sections were washed two times in TBS, incubated with rabbit normal serum, diluted 1:10 in bovine serum albumin (BSA) 10% for 20 min and incubated overnight at 4°C with the primary antibodies (Table 1).

Sections were rinsed, incubated for 30 min with the secondary antibody (biotin-labelled rabbit anti-mouse serum, diluted 1:200 in BSA 5%), rinsed in TBS and incubated with avidin–biotin–peroxidase complex for 1 h. Slides were washed three times in TBS before staining with 1 mg/ml 3.3′-diaminobenzidine tetrahydrochloride prepared in 0.05 M Tris–HCl containing 0.02% H_2O_2. Sections were then stained with haematoxylin, dehydrated and mounted in Entellan.

Table 1 Antibodies, specificity and references

Antibody	Specificity	Reference
HMFG1	MUC1	Taylor-Papadimitriou et al. 1981 [2]
PMH1	MUC2-GalNac	Reis et al. 1998 17]
CLH2	MUC5AC	Reis et al. 1997 [16]
CLH5	MUC6	Reis et al. 2000 [19]
Ca3F4	$Lewis^a$	Young et al. 1981 [28]
BG6	$Lewis^b$	Signet Pathology Systems
HB-80	Sialyl-$Lewis^a$	Magnani et al. 1982 [14]
F2	Sulpho-$Lewis^{a/c}$	Veerman et al. 1997 [26]

Table 2 Patterns of intestinal metaplasia (IM) defined using histochemistry

Number of biopsies	IM		
	Type I	Type II	Type III
8	+	+	–
6	+	–	–
3	–	+	–
2	+	+	+

Results

Characteristics of intestinal metaplasia classified using histochemistry

The results are summarised in Table 2. The 19 biopsies showed 16 foci of type-I IM with mature absorptive non-secretory cells and goblet cells that secreted sialomucins (Fig. 1h), 13 foci of type-II IM with columnar cells that secreted neutral mucins and/or small amounts of sialomucins and goblet cells that secreted sialo and occasionally sulphomucins (Fig. 2a, b) and two foci of type-III IM with columnar cells that secreted predominantly sulphomucins and goblet cells that secreted sialo and/or sulphomucins (Table 2).

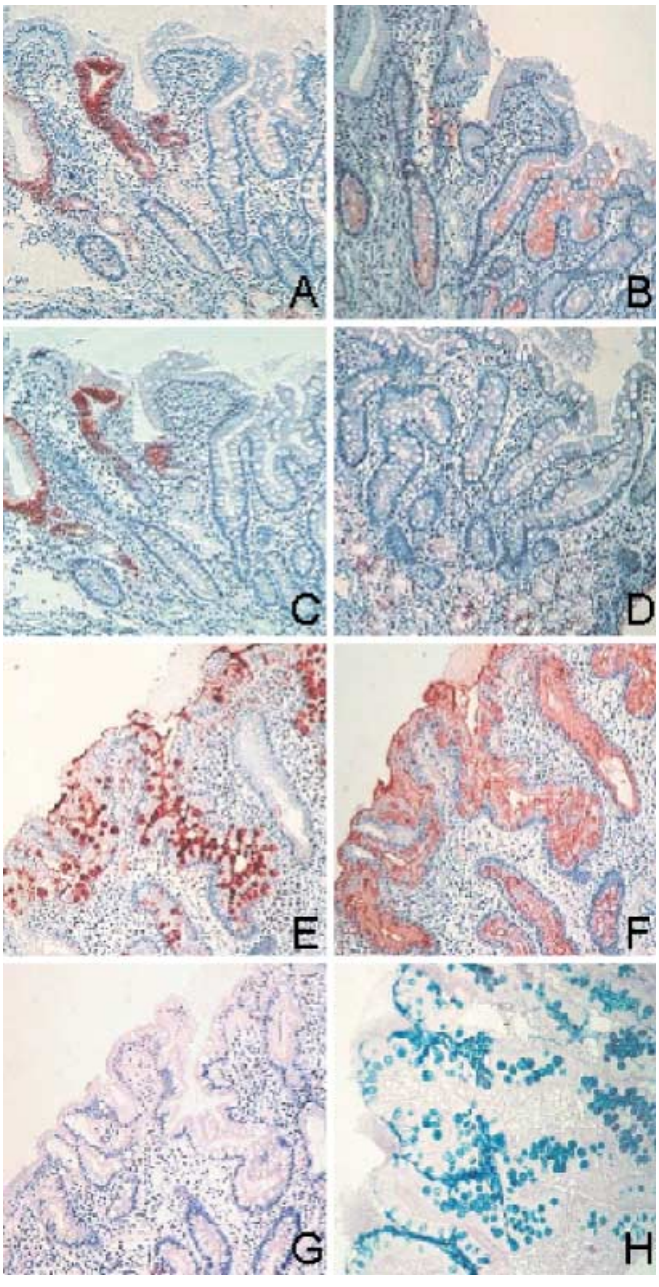

Fig. 1 Histochemical and immunohistochemical staining of serial sections from type-I intestinal metaplasia (IM). **a** IM does not express MUC1. **b** IM shows expression of MUC2 in goblet cells. **c** IM does not express MUC5AC. **d** IM does not express MUC6. **e** IM shows expression of Lewis type-1 chain antigen a (Le^a) in goblet cells. **f** IM shows expression of Lewis type-1 chain antigens b (Le^b) in goblet and columnar cells. **g** IM does not express S-Le^a. **h** Histochemical staining (high-iron diamine–alcian blue) of IM shows goblet cells stained in blue (sialomucins)

Characteristics of intestinal metaplasia classified using immunohistochemistry for MUC1, MUC2, MUC5AC and MUC6

All IM foci (*n*=31) showed MUC2 expression, in most cases (*n*=28) only in goblet cells. Four main patterns of mucin expression were observed in metaplastic tissue (Table 3). In 29.0% of the foci, expression of MUC2 was observed together with MUC1 and MUC5AC (Fig. 2c, d, e). In 25.8% of the foci, MUC2 was expressed together with MUC1. In 19.4% of the foci, only MUC2 was expressed (Fig. 1b). In 19.4% of the foci, the four mucins were expressed. One focus showed expression of MUC2 and MUC6, and one focus showed expression of MUC2 and MUC5AC (Table 3).

Table 3 Patterns of expression of mucins in intestinal metaplasia (IM)

Number of IM foci (%)	MUC1	MUC2	MUC5AC	MUC6
6 (19.4)	–	+	–	–
8 (25.8)	+	+	–	–
1 (3.2)	–	+	–	+
1 (3.2)	–	+	+	–
9 (29.0)	+	+	+	–
6 (19.4)	+	+	+	+

Table 4 Patterns of intestinal metaplasia (IM) defined using immunohistochemistry to type-1 Lewis antigens (Le)

Number of IM foci (%)	Le^a	Le^b	Sialyl-Le^a	Sulpho-$Le^{a/c}$
16 (55.2)	+	+	+	+
2 (6.9)	+	–	+	+
4 (13.8)	+	+	–	+
6 (20.7)	+	+	–	–
1 (3.4)	–	+	–	–

Characteristics of intestinal metaplasia classified using immunohistochemistry for type-1 Lewis antigens, Le^a, Le^b, sialyl-Le^a and sulpho-$Le^{a/c}$

Two cases of the present series were from individuals phenotypically Le^{b-} and were not used for this part of the study. The remaining cases showed 29 IM foci (Table 4). In 16 foci (55.2%) all type-1 Lewis antigens evaluated were expressed (Fig. 2g, h, i, j). Expression of Le^a, Le^b and sulpho-$Le^{a/c}$ was detected in 4 foci (13.8%). Le^a, sialyl-Le^a and sulpho-$Le^{a/c}$ were detected in two IM foci (6.9%). Le^a and Le^b were detected in six foci (20.7%), and there was one focus (3.4%) in which only Le^b was expressed.

Comparison between types of IM classified using histochemistry and patterns of immunohistochemical expression of mucins and type-1 chain carbohydrates

Serial sections were used to compare IM foci with the different histochemical and immunohistochemical stainings. The comparison was performed using as a reference system the classical classification of IM based on histochemistry. The results are summarised in Fig. 3.

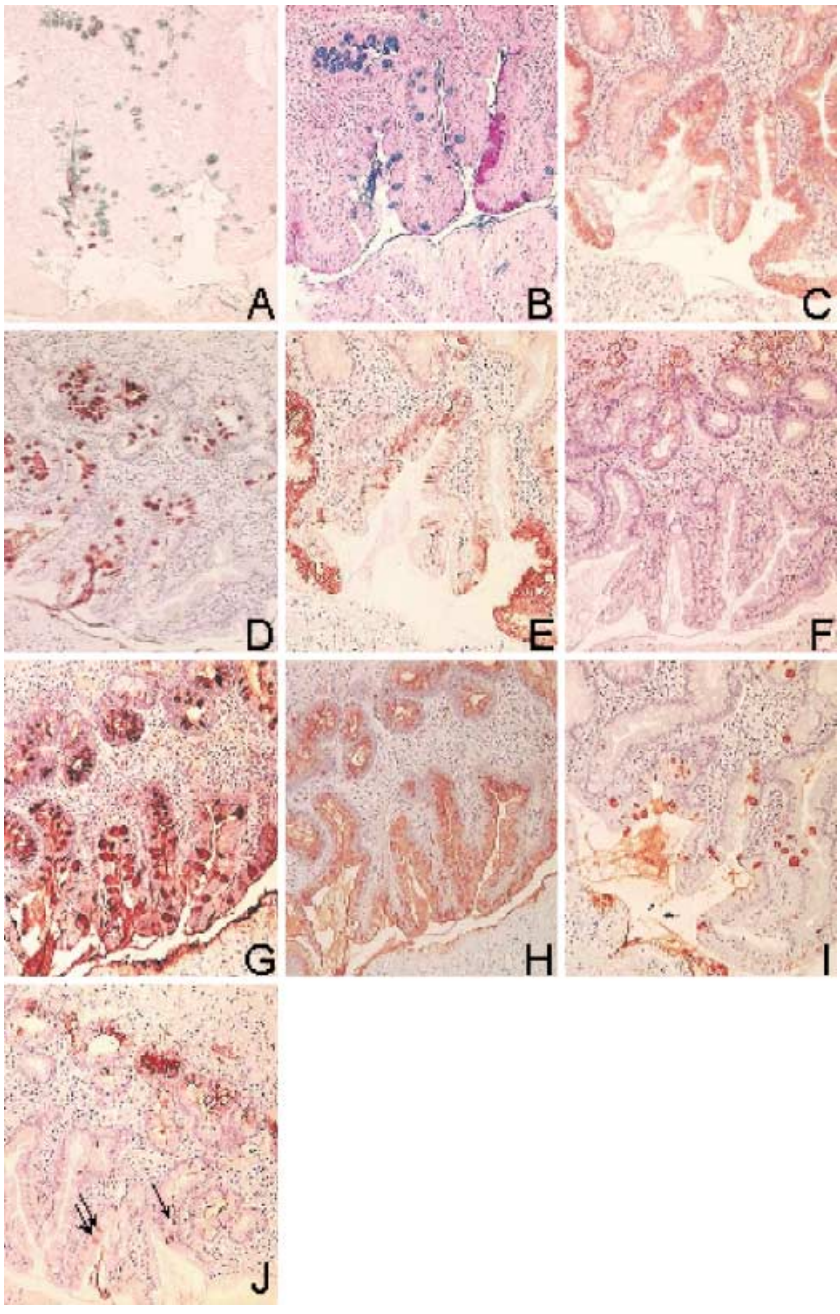

Fig. 2 Histochemical and immunohistochemical staining of serial sections of type-II intestinal metaplasia (IM). **a** Histochemical staining (high-iron diamine–alcian blue) of IM shows goblet cells stained in blue (sialomucins) and in brown (sulphomucins). **b** Histochemical staining (periodic acid Schiff) of IM shows columnar cells with a pink staining (neutral mucins). **c** Expression of MUC1 in goblet and columnar cells. **d** IM shows expression of MUC2 in goblet cells. **e** IM shows expression of MUC5AC in columnar cells. **f** IM does not express MUC6. **g** IM shows expression of Lewis type-1 chain antigen a (Le^a) in both goblet and columnar cells. **h** IM shows expression of Lewis type-1 chain antigen b (Le^b) in both goblet and columnar cells. **i** IM shows expression of Sialyl-Le^a in goblet cells. **j** IM shows expression of sulpho-Le^a in goblet cells (*arrows*)

All foci with type-I IM (*n*=16) expressed MUC2 in goblet cells. MUC1 was expressed in eight foci (50.0%) in columnar cells and in three of those also in goblet cells (Fig. 3). In most foci there was no expression of MUC5AC and MUC6, except in one focus that expressed MUC5AC in goblet cells and one focus that expressed MUC6 in columnar cells. In type-II IM (*n*=16) and type-III IM (*n*=2) there was expression of MUC1, MUC2 and MUC5AC in all foci studied. MUC1 and MUC5AC were expressed both in goblet and columnar cells, whereas MUC2 was predominantly expressed in goblet cells (Fig. 2c, d, e and Fig. 3). MUC6 was expressed in six foci (four in type-II IM and two in type-III IM) always in columnar cells.

As shown in Fig. 3 comparison between IM types regarding the expression of type-1 chain carbohydrates did not show major differences, except for an increased expression of Le^a in columnar cells of types-II and -III IM. In all IM types, sialyl-Le^a and sulpho-$Le^{a/c}$ were mostly expressed in goblet cells, although in some cases they were also present in columnar cells (Fig. 3).

The analysis of serial sections showed that there were nine foci of type-I IM and three foci of type-II IM that did not express sialyl-Le^a despite the presence of sialomucins disclosed using histochemistry. The presence of sulpho-$Le^{a/c}$ in goblet and columnar cells co-existed with the histochemical detection of sulphomucins in type-III IM. Sulpho-$Le^{a/c}$ was also detected in goblet and colum-

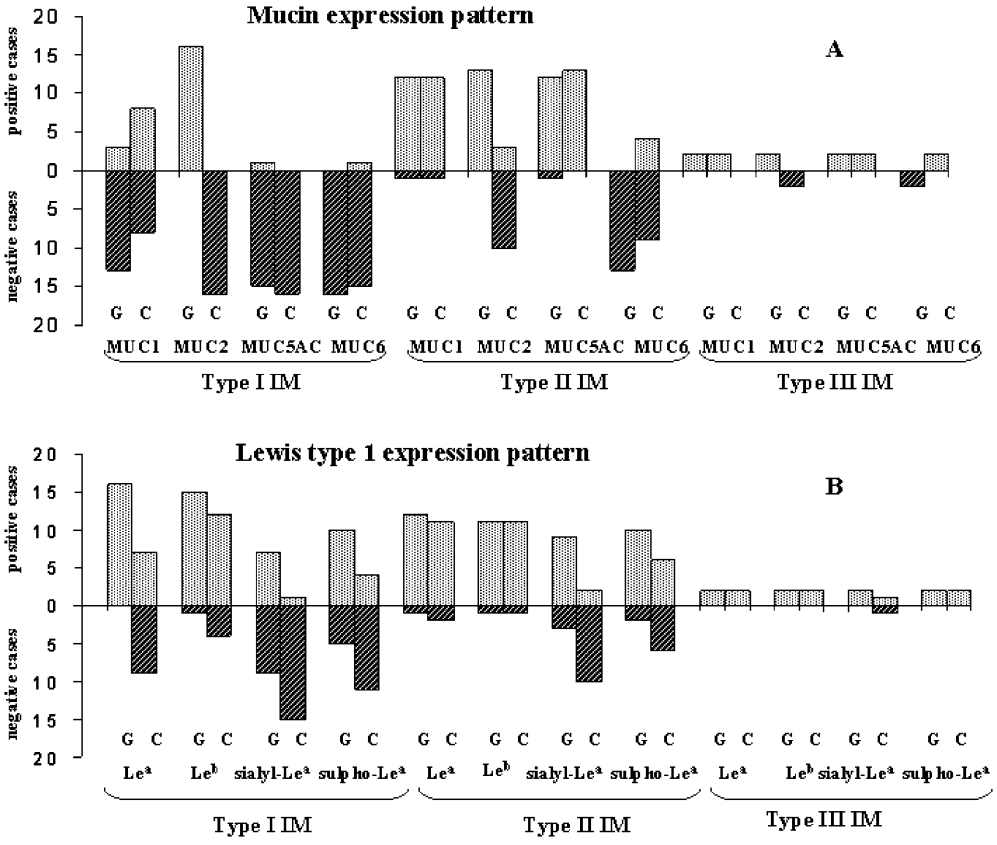

Fig. 3 Diagram representing mucin (**a**) and Lewis type-1 carbohydrate (**b**) expression pattern in intestinal metaplasia (IM). *G* goblet cells, *C* columnar cells. The three types of IM determined using histochemistry (I, II and III) were individualised, and for each type of IM the number of positive and negative cases for G and C cells was plotted according to mucin (**a**) and Lewis type-1 carbohydrate markers (**b**)

nar cells of type-I and type-II IM in the absence of histochemical detection of sulphomucins.

Discussion

We have shown that the mucin expression pattern of IM fits into two well-defined profiles: IM with expression of the intestinal mucin MUC2 and decreased/absent expression of MUC1, MUC5AC and MUC6 (complete IM); and IM with coexpression of the intestinal mucin MUC2 and the mucins usually expressed in the stomach – MUC1, MUC5AC and MUC6 (incomplete IM). These observations confirm previous results from our group both regarding the clear-cut difference between complete and incomplete IM and the similarity of the mucin expression profile in type-II and type-III IM [18]. The relatively higher frequency of type-I IM foci expressing MUC1 in the present series probably stems from a better fixation obtained in the biopsies evaluated in this study.

Lewis type-1 carbohydrate expression was identical in the different types of IM defined using histochemistry, except for the higher frequency of Le^a expression in columnar cells of types-II and -III IM. Anomalous expression of Le^a in IM was previously described by Torrado et al. [24]. In agreement with Torrado et al. [25], we observed that expression of Le^a in type-I IM was predominantly observed in goblet cells, whereas in types-II and -III IM, Le^a was observed both in goblet and in columnar cells. The aberrant expression of Le^a in IM is directly related to an increased expression of FucT III enzyme [29].

Sialyl-Le^a was mainly expressed in goblet cells in type-I IM (Fig. 3), in agreement with the histochemical observations showing sialylated mucin expression in goblet cells. However, in nine foci of type-I IM we did not detect expression of sialyl-Le^a, suggesting that other sialylated structures are expressed in this setting and are detected using histochemistry. One of the sialylated structures frequently expressed in IM is the sialyl-Tn antigen [3] which, in the present series, was expressed in most of the cases that were negative for sialyl-Le^a (data not shown).

In types-II and -III IM, sialyl-Le^a was expressed in goblet cells in most cases and in columnar cells in a smaller number of cases. The sialyl-Le^a expression pattern observed using immunohistochemistry showed partial overlap to the expression pattern of sialomucins determined using histochemistry. In three foci of type-II IM no expression of sialyl-Le^a was observed despite the presence of sialomucins in histochemical studies. Again, the aberrant expression of sialyl-Tn partially explains the observed discrepancies (data not shown).

In type-I IM, sulpho-$Le^{a/c}$ was expressed in goblet and columnar cells, although we did not detect the presence of sulphomucins in columnar cells using the high-iron diamine–alcian blue technique. These findings indicate that histochemistry has lower sensitivity than immunohistochemistry for identification of sulphomucins,

namely sulpho-Le$^{a/c}$. The same applies to the expression of sulpho-Le$^{a/c}$ that we observed in columnar cells of type-II IM foci showing only the presence of sialomucins by histochemistry.

The present study shows that the identification of complete versus incomplete IM is achieved using mucin immunohistochemistry as clearly as using classical histochemical methods using simpler and more reproducible techniques.

Despite the small size of the sample our results challenge the distinction of type-II from type-III IM. In fact, we did not observe any major difference between types-II and -III IM in the expression profile of both mucins and Lewis type-1 carbohydrates. Furthermore, we detected the presence of sulpho-Le$^{a/c}$ in columnar cells of all IM types regardless of the presence or absence of sulphomucins, thus weakening the basis for individualising type-III IM. The results observed in type-III IM in the present study were confirmed in ten cases of type-III IM obtained from gastric mucosa adjacent to gastric carcinomas in surgical specimens (David et al., unpublished observations).

Previous studies have shown the predictive value of identifying type-III IM in the risk assessment for gastric carcinoma development [7, 20]. Since we observed that immunohistochemical detection of sulpho-Le$^{a/c}$ is more "sensitive" than the histochemical detection of sulphomucins, future studies using large series classified using immunohistochemistry should be undertaken in order to evaluate the predictive value of sulpho-Le$^{a/c}$ expression in the context of all types of IM.

The two main conclusions of the present study for clinical and practical purposes are as follows: first, the present IM classification into complete and incomplete types should be performed using the immunohistochemical evaluation of mucin expression rather than histochemistry; second, for the evaluation of risk for gastric carcinoma development in patients with IM, future studies should take into account the expression of specific sulphated carbohydrates (e.g. sulpho-Le$^{a/c}$) rather than histochemical detection of sulphomucins.

Acknowledgements This work was supported by Fundação para a Ciência e a Tecnologia, PRAXIS XXI (Project SAU/14111/1998).

References

1. Biemer-Hüttmann AE, Walsh MD, McGuckin MA, Ajioka Y, Watanabe H, Leggett BA, Jass JR (1999) Immunohistochemical staining patterns of MUC1, MUC2, MUC4, and MUC5AC mucins in hyperplastic polyps, serrated adenomas, and traditional adenomas of the colorectum. J Histochem Cytochem 47:1039–1047
2. Carrato C, Balague C, de Bolós C, Gonzalez E, Gambus G, Planas J, Perini JM, Andreu D, Real FX (1994) Differential apomucin expression in normal and neoplastic human gastrointestinal tissues. Gastroenterology 107:160–172
3. David L, Nesland JM, Clausen H, Carneiro F, Sobrinho-Simões M (1992) Simple mucin-type carbohydrate antigens (Tn, Sialosyl-Tn and T) in gastric mucosa, carcinomas and metastases. Acta Pathol Microbiol Immunol Scand 27:162–172
4. De Bolós C, Garrido M, Real FX, (1995) MUC6 Apomucin shows a distinct normal tissue distribution that correlates with Lewis antigen expression in the human stomach. Gastroenterology 109:723–734
5. Filipe MI (1979) Mucins in the human gastrointestinal epithelium: a review. Invest Cell Pathol 2:195–216
6. Filipe MI, Jass JR (1986) Intestinal metaplasia subtypes and cancer risk. In: Filipe MI, Jass JR (eds) Gastric carcinoma. Churchill Livingstone, London, pp 87–115
7. Filipe MI, Munoz N, Matko I, Kato I, Pompe-Kirn V, Jutersek A, Teuchmann S, Benz M, Prijon T (1994) Intestinal metaplasia types and risk of gastric cancer: a cohort study in Slovenia. Int J Cancer 57:324–329
8. Gendler SJ, Spicer AP (1995) Epithelial mucin genes. Annu Rev Physiol 57:607–634
9. Guillem P, Billeret V, Buisine MP, Flejou JF, Lecomte-Houcke M, Degand P, Aubert JP, Triboulet JP, Porchet N (2000) Mucin gene expression and cell differentiation in human normal, premalignant and malignant esophagus. Int J Cancer 88:856–861
10. Ho SB, Shekels LL, Toribara NW, Kim YS, Lyftogt C, Cherwitz DL, Niehans GA (1995) Mucin gene expression in normal, preneoplastic, and neoplastic human gastric epithelium. Cancer Res 55:2681–2690
11. Lapensee L, Paquette Y, Bleau G (1997) Allelic polymorphism and chromosomal localization of the human oviductin gene (MUC9). Fertil Steril 68:702–708
12. López-Ferrer A, de Bolós C, Barranco C, Garrido M, Isern J, Carlstedt I, Reis CA, Torrado J, Real FX (2000) Role of fucosyltransferases in the association between apomucin and Lewis antigen expression in normal and malignant gastric epithelium. Gut 47:349–356
13. López-Ferrer A, Curull V, Barranco C, Garrido M, Lloreta J, Real FX, de Bolós C (2001) Mucin as differentiation markers in bronchial epithelium – Squamous cell carcinoma and adenocarcinoma display similar expression patterns. Am J Respir Cell Mol Biol 24:22–29
14. Magnani JL, Nilsson B, Brockhaus M, Zopf D, Steplewski Z, Koprowski H, Ginsburg V (1982) A monoclonal antibody-defined antigen associated with gastrointestinal cancer is a ganglioside containing sialylated lacto-N-fucopentose II. J Biol Chem 257:14365–14369
15. Mollicone R, Bara J, Le Pendu J, Oriol R (1985) Immunohistologic pattern of type 1 (Le^a, Le^b) and type 2 (X, Y, H) blood group-related antigens in the human pyloric and duodenal mucosae. Lab Invest 53:219–227
16. Reis CA, David L, Nielsen PA, Clausen H, Mirgorodskaya K, Roepstorff P, Sobrinho-Simões M (1997) Immunohistochemical study of MUC5AC expression in human gastric carcinomas using a novel monoclonal antibody. Int J Cancer 74:112–121
17. Reis CA, Sorensen T, Mandel U, David L, Mirgorodskaya E, Roepstorff P, Kihlberg J, Stig-Hansen JE, Clausen H (1998) Development and characterization of an antibody to an α-*N*-acetil-D-galactosamine glycosylated MUC2 peptide. Glycoconj J 15:51–62
18. Reis CA, David L, Correa P, Carneiro F, de Bolós C, Garcia E, Mandel U, Clausen H, Sobrinho-Simões M (1999) Intestinal metaplasia of human stomach displays distinct patterns of mucin (MUC1, MUC2, MUC5AC, and MUC6) expression. Cancer Res 59:1003–1007
19. Reis CA, David L, Carvalho F, Mandel U, de Bolós C, Mirgorodskaya E, Clausen H, Sobrinho-Simões M (2000) Immunohistochemical study of the expression of MUC6 mucin and coexpression of other secreted mucins (MUC5AC and MUC2) in human gastric carcinomas. J Histochem Cytochem 48:377–388
20. Rokkas T, Filipe MI, Sladen GE (1991) Detection of an increased incidence of early cancer in patients with intestinal metaplasia type III who are closely followed up. Gut 32:1110–1113
21. Shankar V, Pichan P, Eddy RL Jr, Tonk V, Nowak N, Sait SN, Shows TB, Schultz RE, Gotway G, Elkins RC, Gilmore MS, Sachdev GP (1997) Chromosomal localization of a human mucin gene (MUC8) and cloning of the cDNA corresponding to the carboxy terminus. Am J Respir Cell Mol Biol 16:232–241

22. Taylor-Papadimitriou J, Peterson JA, Arklie J, Burchell J, Ceriani RL, Bodmer WF (1981) Monoclonal antibodies to epithelium-specific components of the human milk fat globule membrane: production and reaction with cells in culture. Int J Cancer 28:17–21
23. Torrado J, Blasco E, Cosme A, Gutierrez-Hoyos A, Arenas JI, (1989) Expression of type 1 and type 2 blood group-related antigens in normal and neoplastic gastric mucosa. Am J Clin Pathol 91:249–254
24. Torrado J, Blasco E, Gutierrez-Hoyos A, Cosme A, Lojendio M, Arenas JI (1990) Lewis system alterations in gastric carcinogenesis. Cancer 66:1769–1774
25. Torrado J, Plummer M, Vivas J, Garay J, Lopez G, Peraza S, Carillo E, Oliver W, Muñoz N (2000) Lewis antigen alterations in a population at high risk of stomach cancer. Cancer Epidemiol Biomarkers Prev 9:671–674
26. Veerman ECI, Bolscher JGM, Appelmelk BJ, Bloemena E, van den Berg TK, Nieuw Amerongen AV (1997) A monoclonal antibody directed against high M_r salivary mucins recognizes the SO_3-3Galβ1–3GlcNAc moiety of sulfo-Lewis^a: a histochemical survey of human and rat tissue. Glycobiology 7:37–43
27. Williams SJ, McGuckin MA, Gotley DC, Eyre HJ, Sutherland GR, Antalis TM (1999) Two novel mucin genes down-regulated in colorectal cancer identified by differential display. Cancer Res 59:4083–4089
28. Young WW Jr, Portoukalian J, Hakomori S (1981) Two monoclonal anticarbohydrate antibodies directed to glycosphingolipids with a lacto-N-glycosyl type II chain. J Biol Chem 256:10967–10972
29. Yuzuro I, Nishihara S, Kudo T, Higara T, Morozumi K, Hattori T, Narimatsu H (1998) The aberrant expression of Lewis^a antigen in intestinal metaplastic cells of gastric mucosa is caused by augmentation of Lewis enzyme expression. Glycoconj J 15:799–807

Virchows Arch (2002) 440:318–324
DOI 10.1007/s004280100430

ORIGINAL ARTICLE

**Ken-ichi Suzuki · Yasuo Kokai · Norimasa Sawada
Reiko Takakuwa · Kazuhide Kuwahara
Emiko Isogai · Hiroshi Isogai · Michio Mori**

SS1 *Helicobacter pylori* disrupts the paracellular barrier of the gastric mucosa and leads to neutrophilic gastritis in mice

Received: 15 June 2000 / Accepted: 30 January 2001 / Published online: 28 March 2001
© Springer-Verlag 2001

Abstract *Helicobacter pylori* induces severe neutrophilic infiltration in the lamina propria of the stomach, which leads to gastritis in humans. The possible involvement of a paracellular route for bacterial nutrients and etiologic agents that may play an important role in colonization of the bacteria and cause gastritis has been suggested. To study the functions of the paracellular barrier of gastric surface epithelium, SS1, a strain of *H. pylori* adapted to the murine stomach, was inoculated into the stomachs of C57BL/6 mice. At 4 months after inoculation, SS1 had achieved a high level of colonization (10^6–10^7 colony-forming units/g tissue) associated with neutrophilic infiltration in the lamina propria of the junctional zone. Disruption of the paracellular barrier was observed in the SS1-infected stomachs, as revealed by the invasion of a lanthanum tracer into the paracellular space of the surface epithelium. Only 2% of junctions were permeable in control stomachs, whereas 72% of the paracellular barrier was disrupted in the SS1-infected gastric epithelia. Furthermore, distribution of tight junction-related molecules such as 7H6 antigen, occludin, and cortical actin was affected in the surface epithelium by SS1 infection. The linear expression pattern of occludin was disrupted and became irregular or punctuated. The 7H6 antigen accumulated as aggregates in the apical portion of the surface epithelium and cortical actin became irregular and punctuated. Taken together, these results indicate that infection by SS1 directly or indirectly caused an increase in paracellular permeability and altered the localization of tight junction-related molecules of the gastric surface epithelium. This observation suggests that the paracellular pathway may play a significant role in establishing *H. pylori*-induced gastritis in the clinical setting.

Keywords *Helicobacter pylori* · SS1 · Tight junction · Occludin · 7H6 antigen

K-I. Suzuki · Y. Kokai (✉) · N. Sawada · R. Takakuwa
K. Kuwahara · M. Mori
Department of Pathology,
Sapporo Medical University School of Medicine,
S1W17, Chuo-ku, Sapporo, 060-8556, Japan
e-mail: yasokoki@sapmed.ac.jp
Tel.: +81-11-6112111 ext 2701, Fax: +81-11-6135665

E. Isogai
Department of Preventive Dentistry,
Health Sciences University of Hokkaido, Ishikari-Tobetsu 1757,
Hokkaido, 061-0293, Japan

H. Isogai
Department of Experimental Animal Laboratory,
Sapporo Medical University School of Medicine,
S1W17, Chuo-ku, Sapporo, 060-8556, Japan

Introduction

There is a growing body of evidence that the gram-negative bacterium *Helicobacter pylori* is a pathogen of gastritis and gastric ulcers [5, 11,17]. The inflammatory reaction of host tissues to *H. pylori* is considered to be initiated by a number of soluble factors released from the bacteria [8,9]. *H. pylori* also requires a flow of ions and nutrients from the host mucosa for growth and differentiation [5]. The paracellular pathway of gastric epithelium has been considered an important route for bacterial derivatives in the inflammatory host reaction and the flow of nutrients from the host tissue needed for fully developing pathogenic infection.

The tight junction localizes the most apical of the apposing epithelial cells and acts as a physiological barrier for paracellular transport of water, ions, and nonionic small molecules [1,4]. However, little is known about the involvement of the paracellular pathway of gastric mucosa in this particular infection. Moreover, there is no in vivo study testing the paracellular barrier function using *H. pylori*. This is partly because of the lack of in vivo animal model for *H. pylori* infection [18].

It is agreed that *H. pylori* models are needed for vaccine development and study of the pathogenesis of *H. pylori* in the murine system. However, mouse adaptation of *H. pylori* is a random event and there is extreme variability in colonization [7, 10,15]. Criteria for a mouse

model should be (1) colonization and pathology in the antrum and body, (2) a high level of colonization, and (3) the presence of adhesion to the gastric epithelium [18]. Sydney strain 1 (SS1), is a CagA- and VacA-positive strain of *H. pylori* [16] which achieves a high level of colonization in C57BL/6 mice. Furthermore, the bacteria are reported to be visible at the transitional zone between the antrum and the body of the stomach, with adhesion to the epithelial surface. This culture is available to all, providing a useful murine model for studying the pathogenesis of *H. pylori* infection [16].

In this report, we study changes of tight junctions of gastric mucosa using C57BL/BL6 mice infected with SS1. A high level of colonization was observed, with infiltration of neutrophils into the lamina propria of the transitional zone between the antrum and the body. An apparent increase in paracellular permeability and changes of tight junction-related molecules such as 7H6 antigen, occludin, and actin were observed. These observations indicated that disruption of the paracellular barrier, with altered molecular structures of tight junctions, could be an important event for the type B gastritis caused by *H. pylori*.

Materials and methods

Bacterial growth media, cultures, and reagents

The SS1 was kindly provided by Dr. A Lee [16]. All bacteria were grown on *Campylobacter*-selective agar (CSA) consisting of sterile horse blood (5% vol/vol) in blood agar base no. 2 (Oxoid, Basingstoke, U.K.) containing Skirrow's supplement: 10 mg/l vancomycin (Sigma, St. Louis, Mo., USA), 5 mg/l trimethoprim lactate (Sigma), 2500 IU/l polymyxin B (Sigma), and 5 mg/l amphotericin B (Squibb, Princeton, N.J., USA). The plates were incubated in an incubator set at 10% CO_2 and 95% humidity. For titration of *H. pylori*, a gastric biopsy obtained from the transitional part of each stomach was weighed (about 100 mg) and homogenized with a Dounce homogenizer (Eyela, Tokyo, Japan). These homogenates were serially diluted with brain heart infusion (BHI) broth (Oxoid) and plated on the plates mentioned above. All other reagents were purchased from Sigma unless otherwise stated.

Histologic examination

The stomachs were gently dissected out with a portion of the proximal duodenum and distal esophagus, then placed on a plastic platform and fixed in 10% formalin/PBS. Samples were cut into slices longitudinally, embedded in appropriate orientation in paraffin, and stained with hematoxylin-eosin or Giemsa stain.

Paracellular permeability

Stomach samples were fixed in ice-cold 0.05 M cacodylate buffer (pH 7.4) containing 4% lanthanum nitrate and 2.5% glutaraldehyde for 30 min with gentle agitation and then in ice-cold 0.05% cacodylate buffer (pH 7.4) containing 2.5% glutaraldehyde overnight with several changes of fixatives without lanthanum nitrate [27]. This procedure minimized lateral invasion of lanthanum nitrate between the basement membrane and basolateral space of epithelial cells, which hampers estimation of paracellular permeability by electron microscopy. After fixation, a portion of stomach including the junctional zone between the antrum and body was selected. These samples were cut into pieces and postfixed with 1% osmic acid and 1% potassium ferrocyanide in H_2O for 2 h at 4°C, dehydrated, and embedded in Epon 812 resin (Dupon, Calif., USA). Semi-thin (1 µm) sections were stained with toluidine blue and specimens that included surface epithelium of the junctional zone were selected. Ultra-thin sections were prepared and examined by electron microscopy (JOEL, Tokyo, Japan). The frequency of paracellular invasion of lanthanum nitrate was calculated as the permeability index and expressed in percent: permeability index=(number of paracellular labels beyond the tight junction/number of junctions between apposing surface epithelia)×100. In all samples, at least 100 junctions were examined. Six mice were inoculated with either medium only or bacteria. Three independent experiments were conducted.

Immunohistochemistry

Samples were snap-frozen and 5-µm-thick frozen sections were fixed with methanol/acetone (1:1 vol/vol) at –20°C for 10 min. Fixed samples were washed with PBS several times and incubated with the first antibody as described [25]. Antibodies used were rabbit antioccludin [2,3], rabbit anti-7H6 antigen [23,28], and rabbit anti-ZO-1 (Zymed, San Francisco, Calif., USA) at dilutions of 1:20, 1:20, and 1:100, respectively. Immunostaining was analyzed using an MRC-1024 confocal laser scanning microscope (Bio-Rad, Tokyo, Japan).

Animals

All animals were specific pathogen-free, inbred female C57BL/6 mice 8–10 weeks old (CLEA, Tokyo, Japan). All were housed in the Microbiology Animal House, Health Sciences University of Hokkaido under clean conditions for the duration of the experiments. The animals were fed a commercial diet (CLE-3, CLEA) and given water ad libitum.

Statistical analysis

At least six mice were examined in each experiment and identical protocols were performed three times. The mean response of each experimental group was compared with its simultaneous control using the unpaired Student's *t*-test. Analysis of variance was used to compare the mean responses of experimental and control groups.

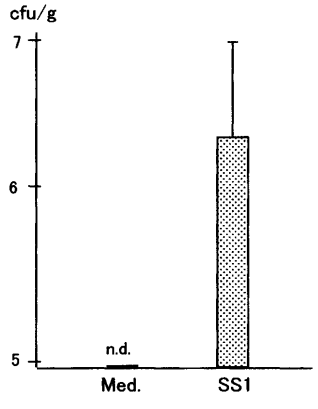

Fig. 1 Colonization of SS1 in the stomach in C57BL/6 mice. 1×10^9 CFU of SS1 in 100 µl of BHI broth was directly inoculated into the stomach. After 4 months, the CFU of each stomach was estimated as described in "Materials and methods". A high level of SS1 colonization (mean 3.8×10^6 CFU/g tissue) was observed. The logarithmic value is shown. The CFU of SS1 was not detectable in control mice (*n.d.*)

Results

Colonization of SS1 in the stomachs of C57BL/6 mice

A total of 1×10^9 colony-forming units (CFU) of SS1 in 100 µl of BHI broth were inoculated into the stomach directly using a blunt-ended 22-gauge needle. For the control, BHI broth only was given. After 4 months, the mice were killed and the CFU of each stomach was calculated. The incubation period was determined by preliminary experiments and the earliest time that gave the most reproducible colonization of SS1 was chosen. As shown in Fig. 1 A, a high level of colonization of SS1 (mean±SD $3.8\pm2.7)\times10^6$ CFU/g of tissue was observed at 4 months after inoculation. Histologic examination with Giemsa staining revealed many characteristic S-shaped bacteria overlying the surface at the junctional zone between the antrum and the body of the stomach (Fig. 2).

Increase of paracellular permeability of the surface epithelium of SS1-colonized mucosa

Paracellular permeability of surface epithelium was assessed by degree of invasion of lanthanum nitrate into the paracellular space of the surface epithelium (Fig. 3). The paracellular space of the surface epithelium of the SS1-colonized stomachs showed labeling of the paracellular space of the apposing epithelial cells by lanthanum nitrate (Fig. 3B), whereas in control mice the invasion of lanthanum nitrate was minimal and stopped at the apical site of the paracellular space (Fig. 3A). The frequency of lateral invasion (beyond tight junctions) was calculated as the permeability index (see Materials and methods section). It was found that this index increased more than 30-fold in SS1-infected mice (72±18%) over control mice (2±2%) (Fig. 4).

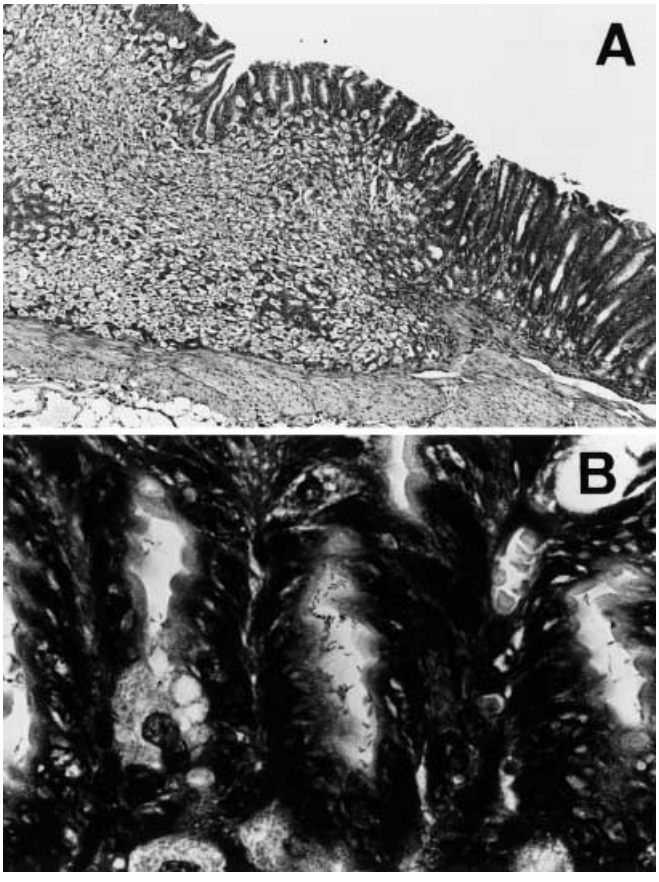

Fig. 2A,B Colonization of SS1 in the transitional zone of the murine stomach. At the junctional zone between the antrum and the body (**A**), histologic examination with Giemsa staining revealed many characteristic S-shaped bacteria overlying the surface (**B**), with neutrophilic infiltration in the lamina propria. Original magnification (**A** ×100, **B** ×400)

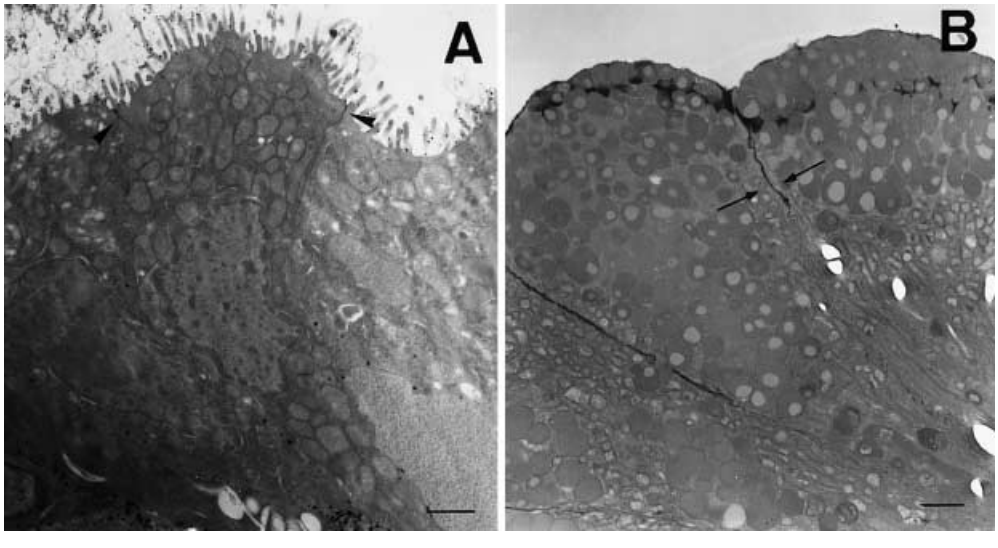

Fig. 3A,B Disruption of the paracellular barrier of the surface epithelium of the SS1-infected murine stomach. Whereas the invasion of lanthanum nitrate was minimal and stopped at the apical site of the paracellular space in control mice (**A,** *arrow*), paracellular spaces of the surface epithelium of the SS1-colonized stomach showed labeling of the paracellular space of apposing epithelial cells by lanthanum nitrate (**B,** *arrows*). *Bar*=1 µm

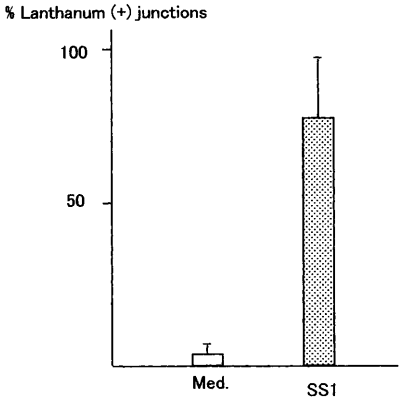

Fig. 4 Increase in paracellular permeability in the SS1-infected murine stomach. The frequency of lateral invasion (beyond tight junctions) shown in Fig. 3 was calculated as the permeability index. This index increased more than 30-fold in the SS1-infected mice (72±18%) over controls (2±2%) ($P<0.01$)

Changes of 7H6 antigen, occludin, and cortical actin in SS1-infected surface epithelium

The distribution of the tight junction-related molecules 7H6 antigen, occludin, and cortical actin was examined by immunohistochemistry. In the control surface epithelial cells, both 7H6 antigen and occludin were concentrated at the most apical of the apposing cells, consistent with the distribution of tight junctions. In clear contrast, both 7H6 antigen and occludin showed clearly distinct distribution patterns in the SS1-infected mice (Fig. 5). Although the immunolocalization of occludin was found still to be at the apex, the staining pattern was irregular and punctuated. The 7H6 antigen showed more evident changes. It failed to localize at the most apical apposing cells and accumulated in the cytoplasm. Cortical actin in the SS1-infected mice was also shown to be changed. It became fainter and a punctuated pattern was observed. Of interest, immunostaining of these molecules on the epithelium rather than the transitional zone of SS1-infected stomach showed little change compared to those of control mice (data not shown).

Transitional zone-specific gastritis in the SS1 infected mice

Histologic examination revealed that infiltration of neutrophils was concentrated in the lamina propria of the SS1-infected stomach with a lower amount of mononuclear cells, indicating transitional zone-specific infiltration of neutrophils (Fig. 6 D). In the control mice, almost no cellular infiltration was observed (Fig. 6B).

Discussion

Using biopsy specimens from human gastric mucosa, structural alterations of tight junctions were observed to occur in close correlation to *H. pylori* infection [13, 19,20]. The inflammatory reaction of host tissues to *H. pylori* is thought to be initiated by soluble factors released from the bacteria [5]. *H. pylori* also require a flow of ions and nutrients from the host mucosa for their growth and differentiation [5]. Because *H. pylori* never invaded the lamina propria, a paracellular pathway in gastric epithelium as a route for the bacterial derivatives might be important for the inflammatory host reaction and flow of nutrients from the host tissue in the development of a fully pathogenic infection. However, human biopsy specimens are not appropriate for the study of paracellular barrier function. With them, very small, basolateral surfaces of specimens are exposed to tracers for the study of barrier functions. This results in nonspecific invasion of the electron-dense tracer and hampers estimation of the paracellular barrier. The murine-adapted *H. pylori* strain SS1 provided the important model for studying the possible involvement of the paracellular barrier in this important infectious disease. A high level of SS1 colonization resulted in impairment of the paracellular barrier function of surface gastric epithelium with changes in tight junction-associated molecules. Disruption of the paracellular barrier was quite evident, as shown by the more than 30-fold increase in lateral invasion of the tracer compared to control mice. The data required careful interpretation, since the present study does not directly specify bacterial factors, which down-regulates paracellular barrier function in the present model. However, massive infiltration of neutrophils in the lamina propria of the transitional zone correlated with the dysfunction of the paracellular barrier, indicating a close relation of the paracellular barrier and neutrophilic gastritis. This is the first demonstration that the paracellular pathway is actually affected in stomachs infected by *H. pylori*.

Although disruption of the paracellular barrier was evident, accompanying alterations of tight junction-associated molecules, the molecular mechanism of the impairment of the paracellular barrier by *H. pylori* is still largely unknown. The present in vivo model may provide several useful experimental systems for understanding the mechanism inhibiting the barrier function of gastric mucosa. It has been reported that *H. pylori* sonicates disrupt the epithelial barrier of T84, a human colon cancer cell line, in a process inhibited by protein kinase C activator [26]. Furthermore, a recent report using heterologous epithelial cell lines suggested that VacA toxin indeed down-regulated the paracellular barrier function of this model epithelium [21]. It should be examined with an in vivo model whether this activity of VacA is actually involved in the development of neutrophilic gastritis. Using a mutant strain derived from SS1, many of these questions could be addressed.

H. pylori infection is highly disseminated in human beings and is strongly linked to gastritis and gastric ulcers. Prolonged infection by *H. pylori* is associated with increased risks of developing gastric adenocarcinoma [6] and mucosa-associated lymphoid tissue (MALT)

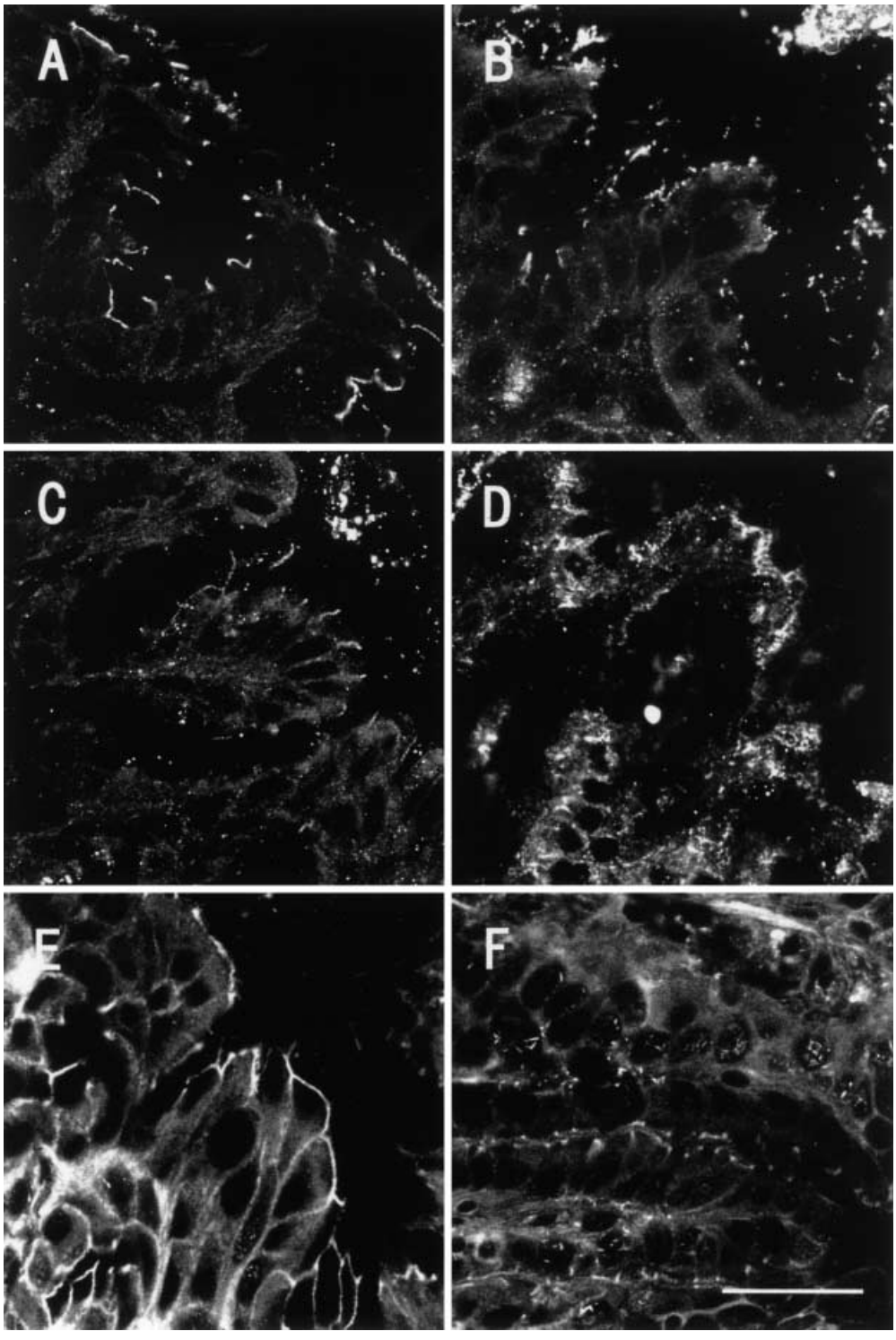

Fig. 5A–F Changes of tight junction-related molecules in the SS1-infected murine stomach. The distribution of the tight junction-related molecules occludin (**A, B**), 7H6 antigen (**C, D**), and cortical actin (**E, F**) was examined in the surface epithelium of control (**A, C, D**) and SS1-infected mice (**B, D, F**). In the control surface epithelial cells, both 7H6 antigen and occludin were concentrated at the most apical of the apposing cells. In the SS1-infected mice, in contrast to the control, the immunolocalization of occludin was found to be irregular and punctuated (**B, A**). The 7H6 antigen (barmotin) failed to localize at the most apical of the apposing cells and accumulated in the cytoplasm (**D, C**). Cortical actin in SS1-infected mice was also shown to become fainter and punctuated (**F, E**). *Bar*=32 μm

lymphomas [22]. As described in the present study, the paracellular barrier was impaired by *H. pylori* infection. This observation suggests the possibility of drug design with the aim of rebuilding the paracellular barrier of gastric mucosa. Since *H. pylori* requires ions and nutrients from the host mucosa, shutting off the route should prevent further colonization by this particular microorganism.

A possible role of paracellular barriers has been suggested in a number of gastrointestinal diseases[14]. Furthermore, adherens and tight junctions have been reported to be altered in several malabsorption diseases. In celiac disease, malabsorption is secondary to the impaired transport of nutrients though the damaged enterocytes. A close link to some type of histocompatibility antigens suggests that a certain antigen evokes antibodies to glu-

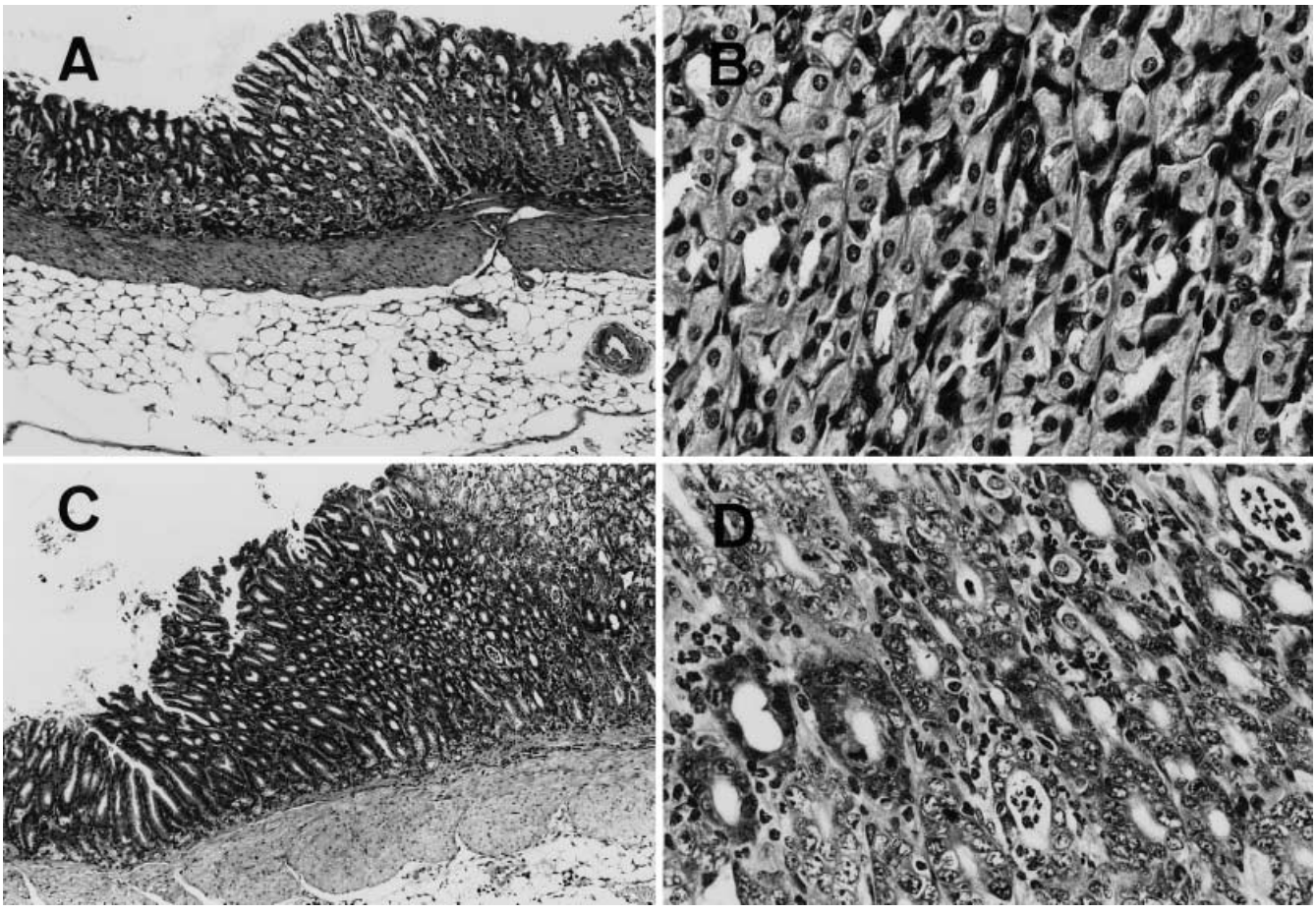

Fig. 6A–D SS1-induced transitional zone-specific neutrophilic gastritis. Histologic examination of the transitional zone of control (**A**, **B**) and SS1-infected mice (**C**, **D**) revealed neutrophilic gastritis in SS1-infected mice but not in controls. Original magnification (**A** and **C** ×100, **B** and **D** ×400)

ten, which results in the binding of gluten to the enterocyte, with subsequent mucosal damage. In ulcerative colitis and Crohn's disease, genetic factors and enterobacterial antigens provoke mucosal injury. Collectively, host immune responses induced by bacterial antigens have been suggested to be central in these inflammatory conditions, which in turn increase paracellular permeability of gastrointestinal epithelium. Indeed, it was shown recently that interleukin-10 is effective for treatment of inflammatory bowel disease in murine models [24]. Interleukin-8, a cytokine secreted by *H. pylori*-infected gastric mucosa, stimulated an impairment of the gastric epithelial barrier and led to leukocyte migration across gastric epithelial cells [12]. Subsequent events of SS1 colonization, such as cytokine secretion, should play an important role for the regulation of paracellular permeability. Considering these host reactions is critical for interpretation of the current result.

In summary, colonization by the *H. pylori* strain SS1 resulted in disruption of the tight paracellular barrier of gastric surface epithelium closely correlated with transitional zone-neutrophilic gastritis. This model system that demonstrates the molecular aspects of the paracellular barrier in relation to the development of neutrophilic gastritis may help us develop ways to cure and prevent *H. pylori* infection and its successive disorders.

Acknowledgements This work was partly supported by grants from the Ministry of Education, Science, Culture, and Sports and Ministry of Health and Welfare of Japan and the Hokkaido Geriatrics Research Institute.

References

1. Anderson JM, Van Itallie CM (1999) Tight junctions: closing in on the seal. Curr Biol 9:R922–924
2. Ando-Akatsuka Y, Saitou M, Hirase T, Kishi M, Sakakibara A, Itoh M, Yonemura S, Furuse M, Tsukita S (1996) Interspecies diversity of the occludin sequence: cDNA cloning of human, mouse, dog and rat-kangaroo homologues. J Cell Biol 133:43–47
3. Atsumi S-I, Kokai Y, Tobioka H, Kuwahara K, Kuwabara H, Takakuwa Y, Sasaki K-I, Sawada N, Mikata T, Mochizuki Y, Imai K, Mori M (1999) Occludin modulates organization of perijunctional circumferential actin in rat endothelial cells. Med Electron Microsc 32:11–19
4. Balda MS, Matter K (1998) Tight junctions. J Cell Sci 111:541–547
5. Blaser MJ (1993) Helicobacter pylori: microbiology of a 'slow' bacterial infection. Trends Microbiol 1:255–260
6. Blaser MJ (2000) Linking *Helicobacter pylori* to gastric cancer. Nat Med 6:376–377

7. Cantorna MT, Balish E (1990) Inability of human clinical strains of *Helicobacter pylori* to colonize the alimentary tract of germfree rodents. Can J Microbiol 36:237–241
8 Cover TL, Puryear W, Perez-Perez GI, Blaser MJ (1991) Effect of urease on HeLa cell vacuolation induced by *Helicobacter pylori* cytotoxin. Infect Immun 59:1264–1270
9. Cover TL (1996) The vacuolating cytotoxin of Helicobacter pylori. Mol Microbiol 20:241–246
10. Ehlers S, Warrelmann M, Hahn H (1988) In search of an animal model for experimental *Campylobacter pylori* infection: administration of *Campylobacter pylori* in rodents. Zentralbl Bakteriol [A] 268:341–346
11. The EUROGAST Study Group (1993) An international association between *Helicobacter pylori* infection and gastric cancer. Lancet 341:1359–1362
12. Fujiwara Y, Arakawa T, Rukuda T, Sasaki E, Nakagawa K, Fujiwara K, Higuchi K, Kobayashi K, Tarnawski A (1997) Interleukin-8 stimulated leukocyte migration across a monolayer of cultured rabbit gastric epithelial cells. Effect associated with the impairment of gastric epithelial barrier function Dig Dis Sci 42:1210–1215
13. Kazi JI, Sinniah R, Jaffrey NA, Alam SM, Zaman V, Zuberi SJ, Kazi AM (1990) Ultrastructural study of *Helicobacter pylori*-associated gastritis. J Pathol 161:65–70
14Kirsner JB, Shorter RG (1982) Recent developments in "nonspecific" inflammatory bowel disease (first of two parts). N Engl J Med 306:775–785
15. Karita M, Kouchiyama T, Okita K, Nakazawa T (1991) New small animal model for human gastric *Helicobacter pylori* infection: success in both nude and euthymic mice. Am J Gastroenterol 86:1596–1603
16. Lee A, O'Rourke J, De Ungria MC, Robertson B, Daskalopoulos G, Dixon MF (1997) A standardized mouse model of *Helicobacter pylori* infection: introducing the Sydney Strain. Gastroenterology 112:1386–1397
17. Marshall BJ, Warren JR (1984) Unidentified curved bacilli in the stomach of patients with gastritis and peptic ulceration. Lancet 1:1311–1315
18. Michetti P, Wadstrom T, Kraehenbuhl JP, Lee A, Kreiss C, Blum AL (1996) Frontiers in *Helicobacter pylori* research: pathogenesis, host response, vaccine development and new therapeutic approaches. Eur J Gastroenterol Hepatol 8:717–722
19. Neri M, Susi D, Bovani I, Laterza F, Mezzetti A, Cuccurullo F (1994) Bacterial mucosal infiltration in *Helicobacter pylori*-associated gastritis: histological and clinical consequences. Am J Gastroenterol 89:1801–1805
20. Noach LA, Rolf TM, Tytgat GN (1994) Electron microscopic study of association between *Helicobacter pylori* and gastric and duodenal mucosa. J Clin Pathol 47:699–704
21. Papini E, Satin B, Norais N, de Bernard M, Telford JL, Rappuoli R, Montecucco C (1998) Selective increase of the permeability of polarized epithelial cell monolayers by *Helicobacter pylori* vacuolating toxin. J Clin Invest 102:813–820
22. Parsonnet J, Hansen S, Rodriguez L, Gelb AB, Warnke RA, Jellum E, Orentreich N, Vogelman JH, Friedman GD (1994) *Helicobacter pylori* infection and gastric lymphoma. N Engl J Med 330:1267–1271
23. Sasaki K-I, Kokai Y, Atsumi S-I, Tobioka H, Sawada N, Hirata K, Mori M (1998) Difference in the expression of three tight junction proteins, barmotin, occludin, and ZO-1, in phenotypically different human colon cancer cell lines. Med Electron Microsc 31:61–67
24. Steidler L, Hans W, Schotte L, Neirynck S, Obermeier F, Falk W, Fiers W, Remaut E (2000) Treatment of murine colitis by lactococcus lactis secreting interleukin-10. Science 289:1352–1355
25. Takakuwa R, Kokai Y, Kojima T, Akatsuka T, Tobioka H, Sawada N, Mori M (2000) Uncoupling of gate and fence functions of MDCK cells by the actin-depolymerizing reagent mycalolide B. Exp Cell Res 257 238–244
26. Terres AM, Pajares JM, Hopkins AM, Murphy A, Moran A, Baird AW, Kelleher D (1998) *Helicobacter pylori* disrupts epithelial barrier function in a process inhibited by protein kinase C activators. Infect Immun 66:2943–2950
27. Zhong Y, Enomoto K, Isomura H, Sawada N, Minase T, Oyamada M, Konishi Y, Mori M (1994) Localization of the 7H6 antigen at tight junctions correlates with the paracellular barrier function of MDCK cells. Exp Cell Res 214:614–620
28. Zhong Y, Saitoh T, Minase T, Sawada N, Enomoto K, Mori M (1993) Monoclonal antibody 7H6 reacts with a novel tight junction-associated protein distinct from ZO-1, cingulin and ZO-2. J Cell Biol 120:477–483

Virchows Arch (2002) 440:325–329
DOI 10.1007/s004280100539

SHORT COMMUNICATION

Uwe Karsten · Peter Stosiek

Fast and sensitive immunodetection of carcinoma cells in sentinel nodes

Received: 3 August 2001 / Accepted: 9 August 2001 / Published online: 28 September 2001
© Springer-Verlag 2001

Abstract In a number of clinical situations, especially in the context of the recent sentinel node concept, lymph-node involvement has to be determined intraoperatively. Since serious and dependable decisions are to be made according to the result of this examination, the most reliable method for the detection of tumour cells should be applied. We and others have shown previously that routine histological examination underestimates lymph-node metastases, and that immunohistochemistry (IHC) significantly improves the accuracy of staging. However, IHC has so far been difficult to apply to the intraoperative examination of cryosections since it has required too much time. We have developed a novel modification of IHC for the rapid detection of metastases of carcinomas in cryosections from lymph nodes. It is based on a unique directly labelled cytokeratin antibody, immunofluorescence, and a specially devised staining solution. This one-step staining procedure can be performed within 10 min. At the same time, its sensitivity is very high. Single tumour cells can easily be detected, and background staining is very low. The high sensitivity could result in a markedly improved reliability of sentinel node-based decisions.

Keywords Lymph node staging · Quick section · Immunohistochemistry · Cytokeratin · Intraoperative diagnosis · One-step staining

Introduction

The histological examination of lymph nodes is an essential part of the TNM classification of carcinomas. We demonstrated more than 10 years ago that the application of immunohistochemistry (IHC) leads to the detection of about 10% additional cases with lymph-node involvement relative to conventional staining [25, 26]. This was confirmed in numerous studies of different types of cancer. Most of the additionally detected metastases consist of small groups of tumour cells. Data available so far are consistent with the assumption that they are of clinical relevance [5, 17].

In a number of clinical cases, e.g. in testicular cancer, lymph nodes have to be examined during surgery, and the result determines how to proceed with the operation [27]. A dramatic increase in intraoperative node examinations can be expected with the emerging sentinel node concept in breast and other cancers [1, 2, 3, 5, 8, 9, 15, 16, 17, 18, 27, 28]. In these cases, in which the result is crucial for the decision making of the surgeon, both the experience of the pathologist and the most reliable detection technique are of utmost importance. So far, however, IHC was not readily applicable to the intraoperative examination of cryosections because it required too much time. A first attempt to apply IHC to quick section diagnosis was undertaken by us in 1992 [24, 27]. Recently, several procedures were published with the same aim [10, 20, 22]. We now propose a novel immunostaining protocol specially devised for this purpose which is highly reliable and can be performed in about 10 min. Its main features are the application of direct labelling, the employment of the immunofluorescence technique, an extremely well-suited monoclonal anti-cytokeratin (CK) antibody, and a specially devised staining solution. This protocol is given in Table 1. In this communication, we outline the rationale of choices made and the results of experiments aimed at optimising the procedure. Finally, we briefly discuss the advantages, limitations and possible fields of application of the method. We have not dealt with topics such as the number and position of sections to be selected or the minimal size of tumour cell clusters considered clinically relevant.

U. Karsten (✉)
Max Delbrück Centre for Molecular Medicine,
Robert-Rössle-Str.10, 13125 Berlin-Buch, Germany
e-mail: ukarste@mdc-berlin.de
Tel.: +49-30-94062863, Fax: +49-30-94062101

P. Stosiek
Institute of Pathology, Karl-Thiem-Klinikum,
03048 Cottbus, Germany

Table 1 Staining protocol. *PBS* phosphate-buffered saline, *TRITC* tetramethylrhodamine B isothiocyanate, *UV* ultraviolet

Working steps

1 Prepare cryostat sections (4-µm thick) on microscope slides
2 Add staining solution to the dry, unfixed sections for 7 min at room temperature
3 Wash three times with PBS
4 Mount with PBS or another suited mounting medium
5 Examine under an epifluorescence microscope at an excitation wavelength of around 550 nm (TRITC filter set). For visualising the counterstained nuclei, switch to UV excitation (around 350 nm)

Staining solution

Monoclonal antibody A45-B/B3-Cy3, 20 µg/ml in PBS, with 0.2% Triton X-100 and 0.5 µg/ml DAPI

Notes

The staining solution should be freshly prepared on the day of use from the following stock solutions. A45-B/B3-Cy3 (50×): 1 mg/ml A45-B/B3-Cy3 in water, with 0.1% Na-azide; stored at +4°C in the dark, stable for at least 1 year. DAPI (1000×): 500 µg/ml 4′,6-diamidino-2-phenylindole in water; can be kept at +4°C in the dark. The addition of DAPI, which selectively stains nuclei, is optional but highly recommended for a better recognition of the nodal tissue structure. Fixation of the cryosections with acetone (10 min at room temperature) is possible but not necessary. PBS as mounting medium is only intended for immediate examination; otherwise, mounting media with 50% glycerol are recommended. Sustainable mounting is possible with Mowiol [21]

Choice of antigen

CKs are still the most reliable marker for the detection of metastases of carcinomas in non-epithelial tissues such as lymph nodes or bone marrow, despite the presence of very small amounts of CK 8 and CK 18 in reticular cells [7]. It is, however, essential not to rely on an antibody specific for a particular CK, since the expression of a single member of the CK family may be downregulated in certain tumours.

Choice of antibody

The monoclonal antibody (mAb) A45-B/B3 (mouse IgG1,κ) is a unique pan-epithelial CK antibody [12, 19, 23]. Although it was classified as a CK 18 antibody during the TD5 Workshop [23], own data show that it does also bind to other CKs. This mAb has been employed in extensive immunohistological studies, in which it was found to react with all CK-containing cells (independently of the presence of CK 18) and was instrumental in the detection of CK in unusual locations [13, 14]. It was found to bind faster than three other commercial pan-CK antibodies to sections ([24] and unpublished results) and proved very powerful in the detection of micrometastases of carcinomas in lymph nodes [25] and in bone marrow [4]. This antibody was provided as a Cy3-labelled conjugate (lot PH1750; 1.16 moles dye per mole antibody) by Micromet (Martinsried/Munich, Germany).

Choice of dye

Epifluorescence is highly sensitive and well suited for the detection of rare positive sites in histological sections provided that background fluorescence is low. From the increasing number of available fluorescent dyes, Cy3 (indocarbocyanine 3.18, M_r 949, excitation maximum 553 nm; emission maximum 575 nm) [6] was chosen for a number of reasons. First, its fluorescence intensity is very high [about 100 times that of fluorescein isothiocyanate (FITC)]. Second, fading is minimal. Third, it is a hydrophilic dye which shows almost no unspecific tissue binding. Finally, at its excitation wavelength (around 550 nm), autofluorescence of lymph-node tissue is negligible in contrast to the situation in the FITC excitation range (around 490 nm). Filter sets devised for TRITC (tetramethylrhodamine B isothiocyanate) are well suited. Texas-red filter sets are not recommended. We employ an Axiophot fluorescence microscope (Zeiss, Jena, Germany) equipped with a digital camera (CF20DXC, Kappa Meßtechnik, Gleichen, Germany), but any other fluorescence microscope with a TRITC filter set would be suited. Observations were made with a 40× lens without oil immersion. The following parameters were varied in order to optimise the staining protocol.

Fixation

Unfixed and acetone-fixed lymph-node sections (10 min at room temperature) were treated with staining solutions containing or lacking Triton X-100. In the presence of 0.2% Triton (Sigma, Deisenhofen, Germany), staining was only marginally different (slightly more intensive after fixation). Without Triton, unfixed sections showed intolerable unspecific binding. We concluded that in the presence of Triton fixation can be omitted.

Dye concentration and time of staining

It is obvious that in short-term incubations both parameters are interdependent. This was extensively examined with unfixed lymph-node sections. The following data

were obtained. First, a minimal penetration time of 5 min is required for 4-µm sections. Second, for 10 min staining, a concentration of 5 µg/ml antibody A45-B/B3 is sufficient. Third, by enhancing the antibody concentration to 10 µg/ml, incubation time can be shortened to 7 min. Fourth, the staining intensity can be further enhanced without unspecific binding by increasing the antibody concentration to 20 µg/ml. For the sake of maximum sensitivity, we recommend this antibody concentration for the standard protocol, although 10 µg/ml may suffice.

Counterstaining

Due to the low background staining of A45-B/B3-Cy3 and the lack of autofluorescence at the excitation wavelength of 550 nm, the structure of the uninvolved lymph-node tissue is barely visible except for a faint CK staining of reticular cells (Fig. 1c). Therefore, it is desirable to counterstain the nodal tissue. This is done by staining the nuclei with 4′-6-diamidino-2-phenylindole (DAPI; Sigma; 0.5 µg/ml added to the staining solution; Fig. 1b). We consider it of advantage that the fluorescence of the nuclei can be switched on and off by changing the filter blocks between TRITC and ultraviolet. For a demonstration of the counterstaining with DAPI, Fig. 1b was produced with a special triple filter (AF Analysentechnik, Tübingen, Germany), which allows the concomitant visualisation of DAPI, FITC, and Texas-red staining. Alternatively, due to the fact that there is always some autofluorescence at FITC excitation, the tissue structure can be made visible without counterstaining by switching to FITC excitation.

As an example, lymph-node cryosections from breast cancer patients stained according to the staining protocol as outlined in Table 1 are shown in Fig. 1. CK-positive carcinoma cells (Fig. 1a) are clearly recognisable against an almost zero background fluorescence of mesenchymal lymph node cells, which are either CK negative or (in case of reticular cells) weakly positive (Fig. 1c). Moreover, the morphological appearance of reticular cells and their CK filaments is strikingly different from that of carcinoma cells, as is clearly visualised in immunofluorescence. The use of fluorescence microscopy may appear unusual for routine histology, but its advantage in detecting small objects is so evident for the intended purpose that it outweighs by far any inconvenience connected with the change of the technique. Compared with indirect IHC, it is much easier to perform and less costly with respect to the staining reagents. Direct immunofluorescence with an antibody to glial fibrillary acidic protein (GFAP) has been successfully employed for the intraoperative diagnosis of neurosurgical tumours [10]. Apart from the diagnostic goal and the use of target antigen, our staining protocol differs from that of these authors by omission of fixation and blocking steps, and addition of Triton X-100 to the staining solution.

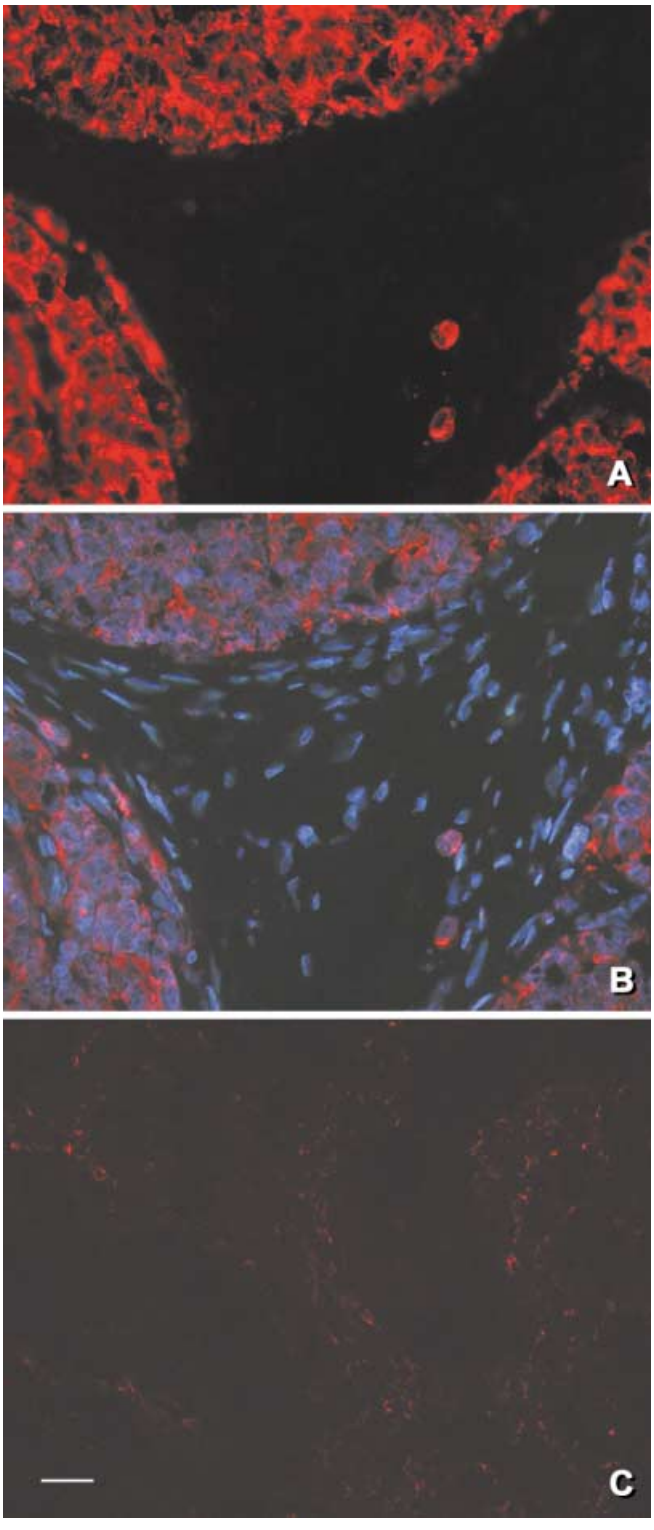

Fig. 1 Cryosections of lymph nodes from breast cancer patients stained according to the staining protocol outlined in Table 1. **a**, **b** Heavily involved node with cytokeratin-positive metastases and two single tumour cells (*red*); **b** counterstaining of the nuclei with 4′-6-diamidino-2-phenylindole (DAPI) is shown (in this case a special triple-filter set DAPI/fluorescein isothiocyanate/Texas red was used, which is not optimal for Cy3). **c** Metastasis-free node showing weak cytokeratin staining of reticular cells. Magnification ×375 (bar 20 µm)

Staining protocols for intraoperative IHC that are not based on immunofluorescence [20, 22, 27] require more time in any case, even with the elegant EPOS (enhanced polymer one-step staining system) procedure, which, in fact, is a two-step procedure since it requires the addition of the substrate. We also consider the fact that the Cy3 label is much smaller than peroxidase an advantage of our procedure.

The sentinel node concept relies on fast and dependable examinations of the primary draining lymph node of a given tumour during surgery. With the described method, the highest possible sensitivity (one tumour cell per section) is easily achieved. As a consequence, depending on the number of sections per node examined, the diagnosis can be given with unsurpassed reliability. Since there is at present some controversy about sentinel node-based decisions in surgery [11, 16], we would argue that a better methodology of nodal examinations, and especially more dependable NO diagnoses could lead to better results with the application of this surgical concept. From the technical point of view, the proposed procedure proved to be simple, fast, sensitive and very satisfying. It is presently being evaluated in three laboratories.

The antibody employed in the present modification is already in use in the immunohistochemical detection of tumour cells in bone marrow [4]. There is every reason to assume that the Cy3-labelled antibody in combination with fluorescence detection will also be applicable to advantage for this purpose. Since non-epithelial tumour cells do not contain CK, the present procedure is only applicable to carcinomas. In case of non-epithelial tumours [3], an analogous procedure with a directly labelled antibody to another relevant tumour marker could be tried.

Acknowledgements The technical assistance of Ms. A. Koberling is gratefully acknowledged. Cy3-labelled antibody A45-B/B3 was kindly provided by Micromet (Martinsried/Munich, Germany). We are also thankful to Prof. P.M. Schlag (Robert Rössle Clinic, Charité, Campus Buch, Humboldt University, Berlin), for his continuing interest and for a series of cryosections of lymph nodes from breast cancer patients.

References

1. Albertini JJ, Lyman GH, Cox C, Yeatman T, Balducci L, Ku N, Shivers S, Berman C, Wells K, Rapaport D, Shons A, Horton J, Greenberg H, Nicosia S, Clark R, Cantor A, Reintgen DS (1996) Lymphatic mapping and sentinel node biopsy in the patient with breast cancer. JAMA 276:1818–1822
2. Bembenek A, Reuhl T, Markwardt J, Schneider U, Schlag PM (1999) Sentinel lymph node dissection in breast cancer. Swiss Surg 5:217–221
3. Bieligk SC, Klimstra DS, Rosai J, Coit DG (1997) The detection of micrometastases in melanoma sentinel nodes by step-sectioning and immunohistochemical staining. Melanoma Res 7[Suppl 1]:S125
4. Braun S, Pantel K, Müller P, Janni W, Hepp F, Kentenich CR, Gastroph S, Wischnik A, Dimpfl T, Kindermann G, Riethmüller G, Schlimok G (2000) Cytokeratin-positive cells in the bone marrow and survival of patients with stage I, II, or III breast cancer. N Engl J Med 342:525–533
5. Dowlatshahi K, Fan M, Bloom KJ, Spitz DJ, Patel S, Snider HC (1999) Occult metastases in the sentinel lymph nodes of patients with early stage breast carcinoma: a preliminary study. Cancer 86:990–996
6. Ernst LA, Gupta RK, Mujumdar RB, Waggoner AS (1989) Cyanine dye labeling reagents for sulfhydryl groups. Cytometry 10:3–10
7. Franke WW, Moll R (1987) Cytoskeletal components of lymphoid organs. I. Synthesis of cytokeratins 8 and 18 and desmin in subpopulations of extrafollicular reticulum cells of human lymph nodes, tonsils, and spleen. Differentiation 36:145–163
8. Giuliano AE, Kirgan DM, Guenther JM, Morton DL (1994) Lymphatic mapping and sentinel lymphadenectomy for breast cancer. Ann Surg 220:391–401
9. Giuliano AE, Dale PS, Turner RR, Morton DL, Evans SW, Krasne DL (1995) Improved axillary staging of breast cancer with sentinel lymphadenectomy. Ann Surg 222:394–401
10. Iwamoto S, Burrows RC, Born DE, Piepkorn M, Bothwell M (2000) The application of direct immunofluorescence to intraoperative neurosurgical diagnosis. Biomol Eng 17:17–22
11. Jones P, Jones S, Humphreys S, Schofield J, Pickering D (2000) Sentinel-node biopsy sampling in breast cancer. Lancet 356:682
12. Karsten U, Widmaier R, Kunde D (1983) Monoclonal antibodies against antigens of the human mammary carcinoma cell line MCF-7. Arch Geschwulstforsch 53:529–536
13. Kasper M, Karsten U (1988) Coexpression of cytokeratin and vimentin in Rathke's cysts of the human pituitary gland. Cell Tissue Res 253:419–424
14. Kasper M, Moll R, Stosiek P, Karsten U (1988) Patterns of cytokeratin and vimentin expression in the human eye. Histochemistry 89:369–377
15. Krag DN, Weaver DL, Alex JC, Fairbank JT (1993) Surgical resection and radiolocalization of the sentinel lymph node in breast cancer using a gamma probe. Surg Oncol 2:335–340
16. Lee AH, Ellis IO, Pinder SE, Barbera D, Elston CW (2000) Pathological assessment of sentinel lymph-node biopsies in patients with breast cancer. Virchows Arch 436:97–101
17. Leong AS (2000) The prognostic dilemma of nodal micrometastases in breast carcinoma. Gan To Kagaku Ryoho [Jap J Cancer Chemother] 27[Suppl 2]:315–320
18. Morgan A, Howisey RL, Aldape HC, Patton RG, Rowbotham RK, Schmidt EK, Simrell CR (1999) Initial experience in acommunity hospital with sentinel lymph node mapping and biopsy for evaluation of axillary lymph node status in palpable invasive breast cancer. J Surg Oncol 72:24–31
19. Nap M, van Wel T, Andrés C, Bellanger L, Bodenmüller H, Bonfrer H, Brundell J, Einarsson R, Erlandsson A, Johansson A, Leca JF, Meier T, Seguin P, Sjödin A, Stigbrand T, Sundström BE, van Dalen A, Wiebelhaus E, Wiklund B, Hilgers J (2001) Immunohistochemical profiles of 30 monoclonal antibodies against cytokeratins 8, 18 and 19. Second report of the TD5 Workshop. Tumor Biol 22:4–10
20. Nomoto S, Nakao A, Ichihara T, Takagi H (1995) Intraoperative quick immunoperoxidase staining: a useful adjunct to routine pathological diagnosis in pancreatic carcinoma. Hepatogastroenterology 42:717–723
21. Osborn M (1994) Immunofluorescence microscopy of cultured cells. In: Celis JE (ed) Cell biology, a laboratory handbook, vol. 2. Academic Press, San Diego, pp 347–354
22. Richter T, Nährig J, Komminoth P, Kowolik J, Werner M (1999) Protocol for ultrarapid immunostaining of frozen sections. J Clin Pathol 52:461–463
23. Stigbrand T, Andrés C, Bellanger L, Bishr-Omari M, Bodenmüller H, Bonfrer H, Brundell J, Einarsson R, Erlandsson A, Johansson A, Leca JF, Levi M, Meier T, Nap M, Nustad K, Seguin P, Sjodin A, Sundstrom B, van Dalen A, Wiebelhaus E, Wiklund B, Arlestig L, Hilgers J (1998) Epitope specificity of 30 monoclonal antibodies against cytokeratin antigens: the ISOBM TD5-1 Workshop. Tumor Biol 19:132–152
24. Stosiek P, Kasper M (1992) Immunhistochemie als Schnellschnitt-Methode. Verh Dtsch Ges Pathol 76:537

25. Stosiek P, Kasper M, Goertchen R, Karsten U (1986) Metastasennachweis beim Mammakarzinom. Vergleichende histologische und immunhistochemische Untersuchungen mittels monoklonaler anti-Zytokeratin-Antikörper an axillären Lymphknoten. Pathologe 7:324–326
26. Stosiek P, Kasper M, Karsten U, Goertchen R (1991) Detection of cancer metastases in regional lymph nodes: comparative histological and immunohistological investigations with the broad-range anticytokeratin monoclonal antibody A45-B/B3. Neoplasma 38:43–47
27. Stosiek P, Wodke A, Kasper M (1993) Immunohistological detection of lymph node metastases in the testicular center as quick section diagnosis during retroperitoneal lymphadenectomy. Pathol Res Pract 189:1010–1014
28. Veronesi U, Paganelli G, Galimberti V, Viale G, Zurrida S, Bedoni M, Costa A, de Cicco C, Geraghty JG, Luini A, Sacchini V, Veronesi P (1997) Sentinel-node biopsy to avoid axillary dissection in breast cancer with clinically negative lymph nodes. Lancet 349:1864–1867

Virchows Arch (2002) 440:330–333
DOI 10.1007/s004280100522

CASE REPORT

**J. Lloreta · O. Bielsa · A. Munné · D. Domínguez
U. Keysers · A. Gelabert · S. Serrano**

Renal cell carcinoma with syncytial giant cell component

Received: 23 January 2001 / Accepted: 26 July 2001 / Published online: 18 September 2001
© Springer-Verlag 2001

Abstract We report a case of clear cell renal cell carcinoma in which a prominent multinucleated giant cell component was intermingled with clear, granular, and spindle cells. Histological, ultrastructural, cytometric, and cytogenetic features of giant cells were similar to those of mononucleated cells in the tumor, and therefore they were not from stromal or osteoclast derivation. These giant cells had homogeneous, finely granular, abundant cytoplasm, often with scalloped cell borders, and contained from 5 to more than 50 nuclei, all of them very similar in size and shape, with prominent central nucleoli. Occasionally, surrounding inflammatory cells were also engulfed in the cytoplasm. This syncytial appearance was more similar to that of some giant cell carcinomas from the lung than to the pleomorphic giant cells often encountered in high grade renal cell tumors. Although the patient is alive and free of disease 6 years after diagnosis, a longer follow-up will be required to assess the potential prognostic influence of this peculiar histological appearance.

Keywords Kidney · Carcinoma · Sarcomatoid · Giant cell

Introduction

The presence of giant cells is well documented in carcinomas of various sites. In most instances, the giant cell component has an osteoclast-like appearance and is related to stromal hemorrhage. This situation has been reported in thyroid gland [6], pancreas [7], liver [12], gall bladder [8], salivary glands [5], colon [4], ovary [17], kidney [3], renal pelvis [11], urinary bladder [10], breast [19], and larynx [16]. In other cases, often from lung origin [1, 2, 9, 15] but also occurring in pancreas [13], urinary bladder [10], and other sites, the giant cells are neoplastic and are associated with poor differentiation and dismal prognosis.

Renal cell carcinomas with osteoclast-like giant cells have been well documented [3]. It is more common to find a variable proportion of neoplastic giant cells in high-grade clear cell renal cell carcinoma, but they are usually a minor component of the tumor, and they are more often found in tumors with sarcomatoid phenotype [18]. Although sarcomatoid renal cell carcinomas are usually high-grade renal cell carcinomas and, as such, have poor prognosis, low-grade spindle cell carcinomas of kidney have also been documented [14]. We report a case of clear cell renal cell carcinoma with abundant syncytial giant cells which were neither of the osteoclastic nor of the more common multinucleated pleomorphic variety. This syncytial giant cell component is probably the result of incomplete cell division or mononucleated cell fusion, and its biological meaning is currently unknown. It is important to recognize the different giant cell varieties that can be observed in renal cell carcinoma because of their potentially different prognostic implications.

Clinical history

The patient was a 50-year-old man who presented with pain in the right lumbar fossa. On ultrasonography, a 10-cm mass was found in the lower half of the right kidney. In an extensive work-up, the tumor was found to be organ confined (stage T2 N0 M0). A subcostal transperitoneal radical nephrectomy was performed. The postoperative course was uneventful. The patient is alive without any evidence of residual disease 6 years after diagnosis.

J. Lloreta (✉) · D. Domínguez
Department of Pathology, Hospital del Mar-I.M.A.S.-I.M.I.M., Universitat Pompeu Fabra, Passeig Marítim 25–29, 08003-Barcelona, Spain
e-mail: 35903@imas.imim.es
Tel.: +34-93-2483031, Fax: +34-93-2483131

A. Munné · U. Keysers · S. Serrano
Department of Pathology, Hospital del Mar – I.M.A.S. – I.M.I.M., Autonomous University of Barcelona, Barcelona, Spain

O. Bielsa · A. Gelabert
Department of Urology, Hospital del Mar – I.M.A.S. – I.M.I.M., Autonomous University of Barcelona, Barcelona, Spain

Materials and methods

The surgical specimen was fixed in 4% buffered formalin solution, after sampling the tumor for cytogenetic studies, taking touch imprints for DNA cytometry, and obtaining small pieces of tumor tissue that were fixed in 2.5% glutaraldehyde for electron microscopy. Standard samples of tumor and kidney were embedded in paraffin and stained with hematoxylin and eosin (HE). Tumor tissue sections were also stained using the periodic acid–Schiff base (PAS) method with and without diastase digestion. Immunohistochemical studies were performed on representative tumor sections using a standard avidin–biotin complex method and diaminobenzidine as chromogen. Antibodies against cytokeratins (Cam 5.2 and AE1/AE3), vimentin, muscle-specific actin, desmin, S-100 protein, HMB-45, and β-HCG were used. Tissue for EM was postfixed in osmium tetroxide, embedded in epoxy resin, thin-sectioned and examined under a CM100 Philips transmission electron microscope. Imprints were stained with the Feulgen method and DNA content of nuclei was measured by means of static cytometry using the SAMBA 2005 software package (Alcatel-TITN, Grenoble, France). Metaphase chromosomes were obtained from cultured tumor cells and investigated using conventional cytogenetic methods.

Pathologic findings

The kidney weighed 542 g. A large tumor with poorly defined margins, measuring 108×79×64 mm, replaced most of the renal parenchyma, extending to the hilar and capsular connective tissue and fat, without involvement of renal vein (Fig. 1). Grossly, the tumor was lobulated, with an irregular, heterogeneous cut surface showing soft, yellow necrotic areas, hemorrhagic areas, and white areas containing viable tumor tissue. Microscopically, the tumor had a striking, extensive component of giant cells, containing from 5 to more than 50 peripherally located nuclei, most of them with large, central nucleoli, and with a homogeneous, finely granular, and eosinophylic cytoplasm (Fig. 2 and Fig. 3). These cells were intermingled with polygonal or spindle mononucleated cells having identical nuclear and cytoplasmic features, although some of them had also clear cell appearance. All tumor cells, including giant cells, were positive with antibodies to cytokeratin Cam 5.2, keratin cocktail AE1/AE3, and vimentin (Fig. 4a–c), although this last antibody was not strongly positive. Antibodies for mus-

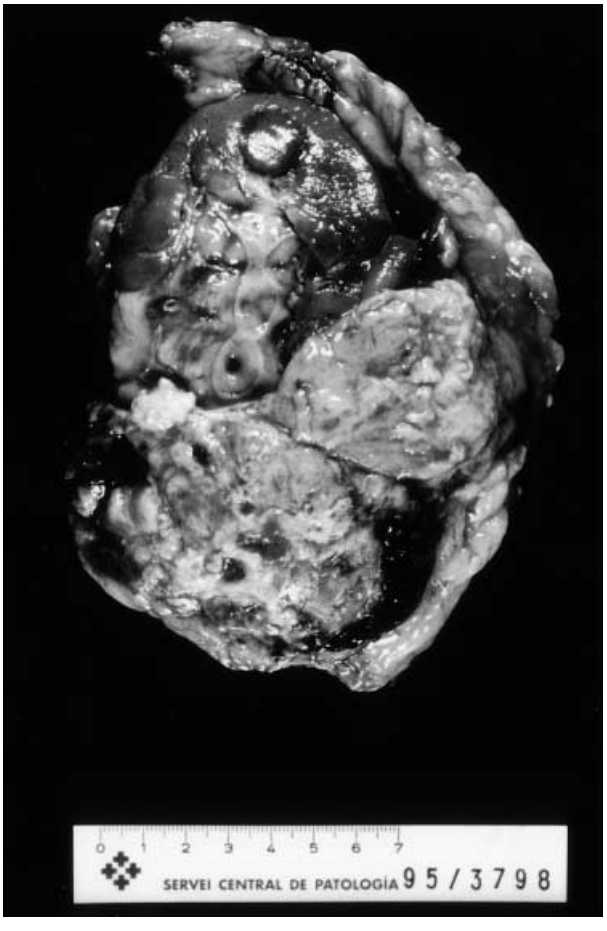

Fig. 1 Macroscopic appearance of the right kidney mass replacing most of the renal parenchyma and extending to the capsular and hilar fat

Fig. 2 Overall histological appearance of the tumor, with huge giant cells interspersed with mononucleated cells

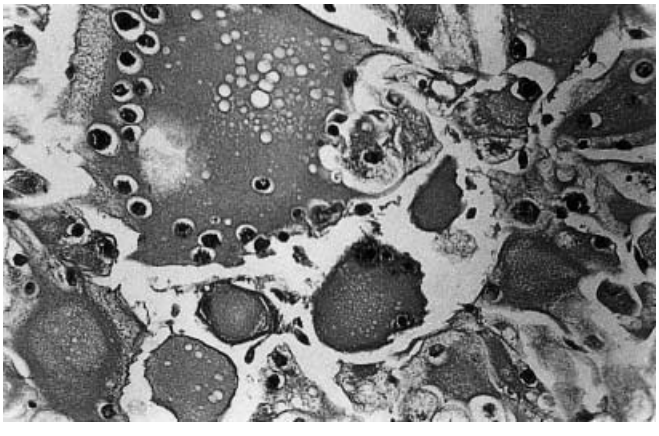

Fig. 3 Both giant multinucleated and mononucleated cells show a similar degree of nuclear atypicality

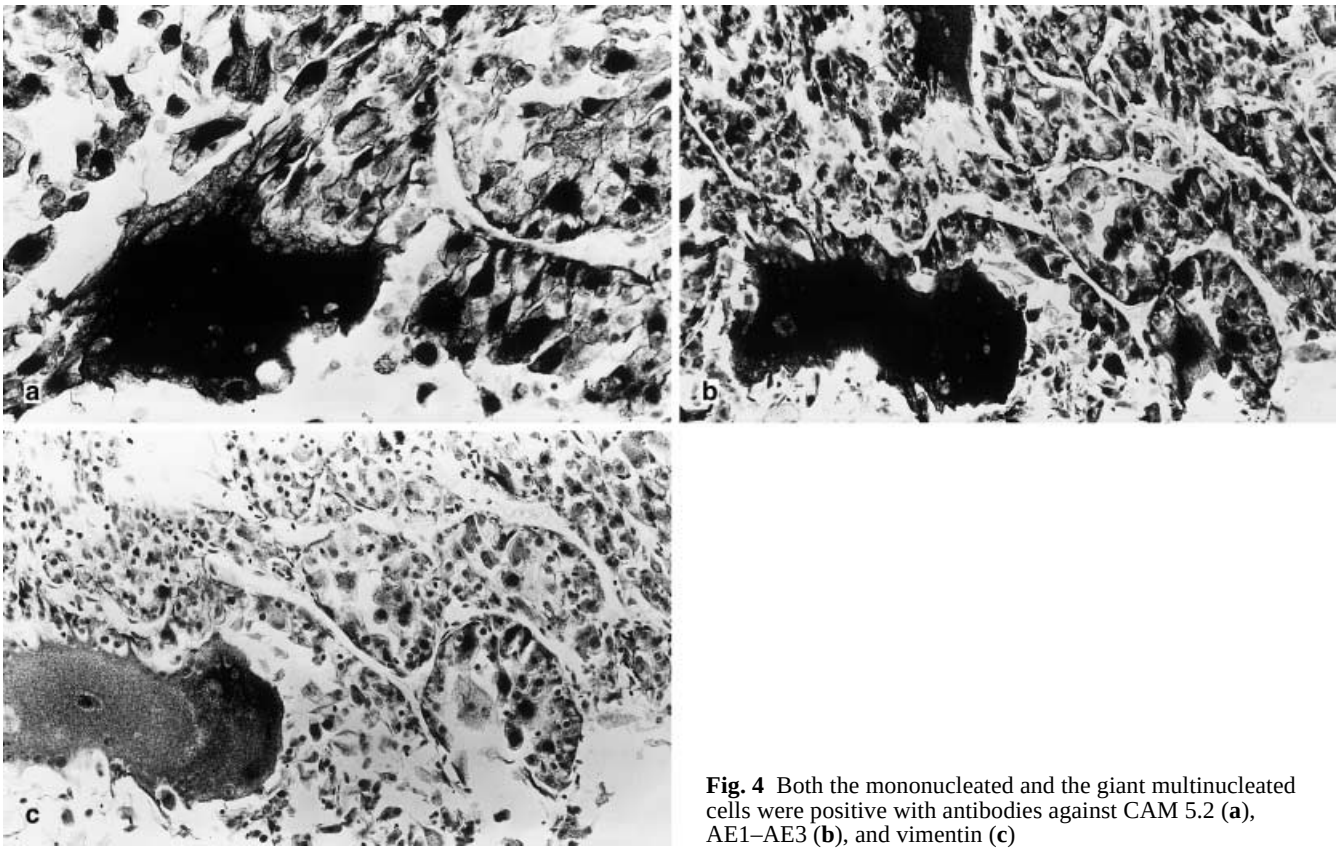

Fig. 4 Both the mononucleated and the giant multinucleated cells were positive with antibodies against CAM 5.2 (**a**), AE1–AE3 (**b**), and vimentin (**c**)

cle-specific actin, desmin, S-100 protein, HMB-45, and β-HCG were negative. Thus, most tumors entering the differential diagnosis of this case, particularly epithelioid angiomyolipoma, or an urothelial tumor with trophoblastic giant cells, can be excluded. The PAS stain was positive in the clear cell areas and was extracted by diastase digestion. On ultrastructural examination, the giant cells had a syncytial appearance, with round, homogeneous peripheral nuclei and wide cytoplasmic areas packed with organelles, mainly rough endoplasmic reticulum, mitochondria, lysosomes, and abundant poliribosomes. Static cytometry performed in tumor imprints revealed 40.5% of aneuploid cells, with 11% of hyperploid cells, and a proliferation index of 8%. According to these results, two cell populations seem to be present: one of them would be composed of conventional clear cells and the other one, probably the hyperploid component, would reflect the presence of the syncytial component; however, there were no cytoplasmic remnants allowing one to distinguish between nuclei of giant and mononucleated cells in Feulgen-stained imprints. The classical (3p–, 5q+) cytogenetic pattern of clear cell renal cell carcinoma was the only chromosomal abnormality found.

Discussion

Hemorrhage-associated osteoclast-like giant cells have been reported in carcinomas from different organs [4, 5, 6, 7, 8, 9, 11, 12, 15, 16, 17, 19] and this feature does not bear any relationship with outcome. Conversely, giant cells of epithelial origin found in carcinomas, particularly from lung, pancreas or urinary bladder [1, 2, 10, 13], are indicative of a high degree of anaplasia and poor prognosis. Although they are rarely mentioned, pleomorphic epithelial giant cells are known to occur in high-grade clear cell renal cell carcinomas, usually with similar prognostic implications. Although prognosis of renal cell carcinoma is more dependent on stage than on histological grade, grade-IV tumors tend to behave aggressively. The features of the giant cells found in the present case are peculiar because of their orderly array of regular nuclei with homogeneously large nucleoli, and thus they are different from conventional bizarre giant cells. Although the fact that the patient is still alive and free of residual disease 6 years after diagnosis seems to support the contention that the presence of syncytial giant cells does not indicate per se a poorer outcome, a longer follow-up will be required to confirm this speculation. Such a situation has been reported in sarcomatoid renal cell carcinoma; although these are usually highly aggressive tumors, Ro et al. subclassified them according to their nuclear features and recognized that not all spindle cell carcinomas of kidney are high-grade tumors [14, 18]. The present tumor is a conventional (clear cell) carcinoma with a syncytial giant cell component. It fulfills the criterion of 30–50% of the tumor being made up of giant cells, conventionally applied to giant cell carcinomas

from other locations, particularly lung [9]. However, we believe that the term “syncytial” would more adequately apply to the giant cells in the present case, and that three instead of two giant cell varieties should be recognized in renal cell carcinoma: osteoclast-like (without influence on prognosis), bizarre giant cells (usually found in high grade, aggressive tumors), and syncytial giant cells probably resulting of defects in cell division or from fusion of mononucleated cells but not necessarily having an adverse meaning. This notion should be tested in large series of renal cell carcinomas containing giant cells from all three varieties.

In conclusion, we report a case of clear cell renal cell carcinoma with a very prominent, neoplastic, syncytial giant cell component. The patient is alive and free of residual disease 6 years after diagnosis. However, a longer follow-up will be required to assess the impact of this peculiar histological appearance in the outcome of the patient.

Acknowledgements This work has been supported by grant FIS 93/0394 (Fondo de Investigación Sanitaria, Spanish Government).

References

1. Bégin P, Sahai S, Wang NS (1983) Giant cell formation in small cell carcinoma of the lung. Cancer 52:1875–1879
2. Chejfec G, Candel A, Jansson DS (1991) Immunohistochemical features of giant cell carcinoma of the lung: patterns of expression of cytokeratins, vimentin, and the mucinous glycoprotein recognized by monoclonal antibody A-80. Ultrastruct Pathol 15:131–138
3. El-Naggar AK, Gaber K, Ordóñez NG (1993) Renal cell carcinoma with osteoclast-like giant cells. Virchows Arch 422:427–431
4. Eshun-Wilson K (1973) Malignant giant-cell tumor of the colon Acta Pathol Microbiol Scand 81:137–144
5. Eusebi V, Martin SA, Govoni E, Rosai J (1984) Giant cell tumor of major salivary glands: report of three cases, one occurring in association with a malignant mixed tumor. Am J Clin Pathol 81:666–675
6. Gaffey MJ, Lack EE, Christ ML, Weiss LM (1991) Anaplastic thyroid carcinoma with osteoclast-like giant cells: a clinicopathologic, immunohistochemical, and ultrastructural study. Am J Surg Pathol 15:160–168
7. Goldberg RD, Michelassi F, Montag AG (1991) Osteoclast-like giant cell tumor of the pancreas: immunophenotypic similarity to giant cell tumor of bone. Hum Pathol 22:618–622
8. Grosso LE, Gonzalez JG (1992) Stromal osteoclast-like giant cells in adenosquamous carcinoma of the gallbladder. Hum Pathol 23:703–706
9. Hammar S (1987) Adenocarcinoma and large cell undifferentiated carcinoma of the lung. Ultrastruct Pathol 11:263–291
10. Holz F, Fox JE, Abell MR (1972) Carcinosarcoma of the urinary bladder. Cancer 29:294–304
11. Kimura K, Ohnishi Y, Morishita H, Amezaki M, Irikura H (1983) Giant cell tumor of the kidney. Virchows Arch 398: 357–365
12. Kuwano H, Sonoda T, Hashimoto H, Enjoji M (1984) Hepatocellular carcinoma with osteoclast-like giant cells. Cancer 54: 837–842
13. Lewandrowski KB, Weston L, Dickersin GR, Rattner DW, Compton CC (1990). Giant cell tumor of pancreas of mixed osteoclastic and pleomorphic cell type: evidence for a histogenetic relationship and mesenchymal differentiation. Hum Pathol 21:1184–1187
14. Lloreta J, Corominas JM, Munné A, Dominguez D, Bielsa O, Gelabert A, Serrano S (1998) Low-grade spindle cell carcinoma of the kidney. Ultrastruct Pathol 22:83–90
15. Mackay B (1989) Advances in the diagnosis of lung tumors. In Hansen HH (ed) Basic and clinical concepts of lung cancer. Kluwer Academic Publishers, Boston, pp 35–51
16. Murrell GL, Lantz HJ (1993) Giant cell tumor of the larynx. Ear Nose Throat J 72:360–361
17. Prat J, Scully RE (1979) Ovarian mucinous tumors with sarcoma-like mural nodules. A report of seven cases. Cancer 44: 1332–1344
18. Ro JY, Ayala AG, Sella A, Samuels ML, Swanson DA (1987) Sarcomatoid renal cell carcinoma: a clinicopathologic study of 42 cases. Cancer 59:516–526
19. Wargotz ES, Norris HJ (1990) Metaplastic carcinomas of the breast: V. Metaplastic carcinoma with osteoclastic giant cells. Hum Pathol 21:1142–1150

Virchows Arch (2002) 440:342
DOI 10.1007/s00428-001-0578-5

ERRATUM

Burkhard Helpap

Nonepithelial neoplasms of the urinary bladder

Published online: 26 January 2002
© Springer-Verlag 2002

Virchows Arch (2001) 439:497–503

The credit line under Table 2 was omitted, so Table 2 is reprinted here in its entirety.

Table 2 Five-year survival rates in sarcomas of the bladder

Tumor type	Grade 1	Grade 2	Grade 3	Total
Malignant fibrous histiocytoma	89.8% (33)	76.5% (160)	48.1% (156)	349
Leiomyosarcoma	92.9% (16)	66.6% (65)	44.7% (67)	148
Malignant schwannoma	77.8% (5)	56.1% (26)	52.1% (41)	72
Rhabdomyosarcoma	0% (0)	74.9% (15)	42.1% (45)	60
Undifferentiated sarcomas	0% (0)	66.9% (43)	40.3% (97)	140

Reprinted with permission from J.M. Coindre, Verh Dtsch Ges Pathol 82:59–63 (1998) (modified)

The online version of the original article can be found at http://dx.doi.org/10.1007/s004280100479

B. Helpap (✉)
Department of Pathology, Hegau-Klinikum Singen,
University of Freiburg, Germany
e-mail: pathologie@hegau-klinikum.de
Tel.: +49-7731-892100, Fax: +49-7731-892105

Virchows Arch (2002) 440:345–352
DOI 10.1007/s00428-002-0617-x

REVIEW ARTICLE

Andrea Tannapfel · Christian Wittekind

Genes involved in hepatocellular carcinoma: deregulation in cell cycling and apoptosis

Received: 9 November 2001 / Accepted: 9 January 2002 / Published online: 6 March 2002
© Springer-Verlag 2002

Abstract Hepatocellular carcinoma (HCC) accounts for 80–90% of liver cancers and is one of the most frequent carcinomas throughout the world. The disease is more prevalent in parts of Africa and Asia than in North and South America and Europe, with a strong etiological association with viral hepatitis, hemochromatosis, known liver (hepatic) carcinogens, and toxins (mycotoxins). Clinical and molecular medical analyses have yielded a considerable amount of information about liver carcinogenesis. Many genes undergo somatic aberrations, with a tendency to cluster at genes involved in cell cycle regulation, in the p53 and Wnt/catenin pathways of signal transduction and cellular adhesion, and in the TGF-β/IGF axis. Since HCC may arise both in liver cirrhosis and in noncirrhotic liver, one may speculate that different hepatocarcinogenetic pathways exist. Recent results of high-output gene analysis using cDNA microarrays support the idea of different genetic alterations in HCC with or without cirrhosis.

Keywords Hepatocellular carcinoma · Genetic alterations · p53 · p16 · p14 · Rb · Cyclin · Catenin

Introduction

Hepatocellular carcinoma (HCC) is the fifth most common cancer worldwide, with estimated 467,000 new cases per year [9, 28]. In developing countries the incidence rates are two- to threefold higher than in developed countries. In low-incidence areas, such as northern Europe and North America, the incidence in men (age-adjusted) is below 5.0 per 100,000 [9]. The variability in HCC incidence rates strongly suggests differences in exposure to risk factors such as infection by hepatitis B and C viruses, cirrhosis of any cause, primary hemochromatosis, and prolonged exposure to aflatoxin B1 [32]. However, the mechanisms of carcinogenesis are poorly understood and seem to differ according to the risk factor involved [54]. As with other kinds of cancer, the etiology and carcinogenesis of HCC are multifactorial and multistage [10]. The multistep process of HCC may be divided into: chronic liver injury, which produces inflammation, cell death, cirrhosis and regeneration, DNA damage, dysplasia, and finally HCC (Fig. 1).

Until now true specific genetic (or epigenetic) changes have not been identified for these stages of carcinogenesis. The genetic changes identified so far include gene amplification (leading to activation of proto-oncogenes), gene deletion or mutation (leading to inactivation of tumor-suppressor genes), and reactivation of telomerase activity. Finally, at a late stage of carcinogenesis genetic changes expressed as chromosomal aberrations are observed [33, 34]. To date more than a dozen genes have been shown to be altered in HCC, with the list probably growing in the coming years due to high output genetic methods. The high number of genes involved in HCC may indicate that different causal factors affect different sets of genes in hepatocytes. In other words, distinct but related genetic pathways are altered during hepatocarcinogenesis, possibly due to different causal factors [52, 63]. Since more than 60–80% of HCC cases arise in liver cirrhosis, and the risk of development of HCC increases to 1–5% per year in patients with cirrhosis, cirrhotic nodules are apparently premalignant lesions of HCC and may already contain genetic aberrations [9]. Since a magnitude of somatic gene and protein changes have been investigated in HCC, we discuss the main regulatory pathways which are altered in HCC. It should be emphasized that these pathways are related to each other, and that the genetic events should not be considered as independent and separate pathways. Furthermore, due to the etiological heterogeneity, we describe differences in the genetic alterations of HCC arising in cirrhosis and those without cirrhosis. It has recently been proposed that six essential alterations in cell physiology dictate malignant transformation, including independence towards growth, anti-

A. Tannapfel (✉) · C. Wittekind
Institute of Pathology, University of Leipzig, Liebigstrasse 26, 04103 Leipzig, Germany
e-mail: tana@medizin.uni-leipzig.de
Tel.: +49-341-9715036, Fax: +49-341-9715069

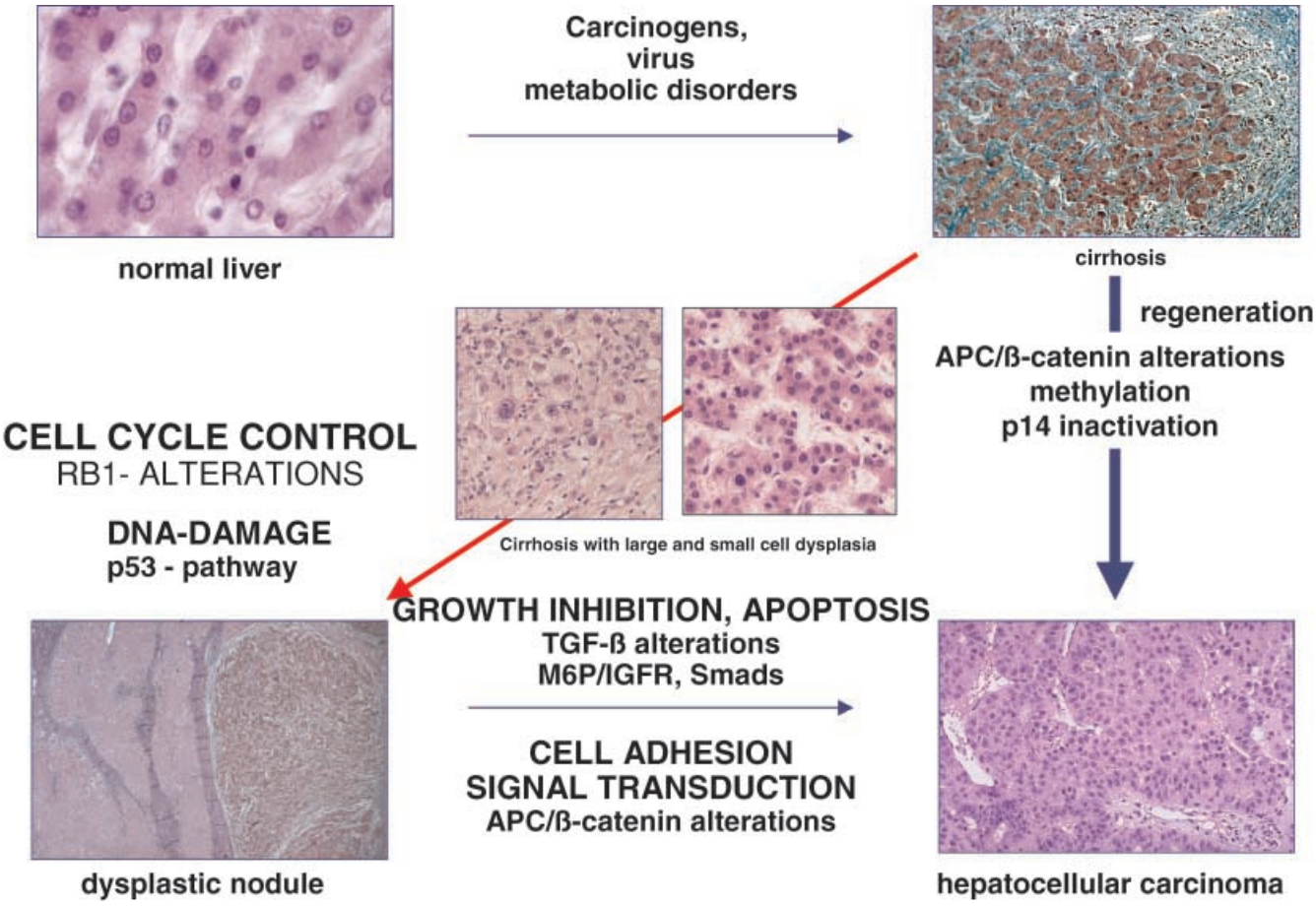

Fig. 1 Multistage process of carcinogenesis

Table 1 Genetic alterations in hepatocellular carcinoma

Gene	Alterations (%)	Type of alteration	References
p53	30 (worldwide)	Mutation	13, 30, 53
p73	32	Overexpression of wild-type protein	39, 45
p63	–	Not expressed in HCC	39, 45
Rb	15	Mutation, LOH	12, 14
Cyclins	–20	Overexpression	4, 47, 50
p16	–59	LOH, promotor methylation	11, 24, 26, 49
p14	–15	LOH, promotor methylation	49
M6P/IGF2R	18–33	LOH, controversial results	5, 20, 55, 61
TGF-βRII	<5	LOH, mutation	6, 20
IGFBP	20	Downregulated	55
IGF2	<5	LOH	20, 55, 61
Smad 2/4	2–6	Mutation	5
PTEN	10	LOH, mutation	18, 42, 62
APC	–	LOH in FAP patients	43
β-Catenin	–26	Mutation	3, 27, 29, 38, 59
E-Cadherin	30	Promotor methylation	41
Axin-1	10	Mutation	38
K-/N-/H-ras	–10	Amplification, mutation	57
c-myc	50	Amplification	9

growth and apoptotic signals, unlimited division, and angiogenetic and metastatic capacities [52]. Mutations in critical genes may range from subtle sequence changes at a few nucleotides to gross chromosomal abnormalities including deletions, amplifications, and translocations of large DNA fragments. This review focuses on the recognized genetic alterations in HCC dividing them into the above-mentioned main regulatory pathways affecting cell cycle regulation and apoptosis (Table 1).

Allelic imbalance and microsatellite instability

Chromosomal instability is characterized by allelic losses and aneuploidy. Most of the genes mutated in HCC are tumor-suppressor genes, and frequent allelic losses (loss of heterozygosity, LOH) leading to the biallelic inactivation have been described. Two systemic approaches, namely comparative genomic hybridization [17, 22, 36] and genome-wide allelotyping [7, 58], have been used to search for gross genetic aberrations commonly exhibited in HCC. By comparative genomic hybridization, chromosomes 1q, 8q, and 17q show gene dose increase while chromosomes 1p, 4q, 8p, 9p, 13q, 16p, 16q, and 17p show gene dose loss [33, 34, 62, 66]. Frequent LOH, or more comprehensive, allelic imbalance (AI), is consistently observed on chromosomes 1p, 4q, 6p, 8p, 13q, 16q, and 17p by whole-genome allelotyping [66]. The chromosome regions with gene dose increase may contain critical oncogenes while those with gene dose loss may contain tumor-suppressor genes. For chromosomes 17p, 13q, 9p, 6q, and 16p, LOH could be related to p53, RB1, p16, IGF2R inactivation [33, 34]. In dysplastic nodules LOH has been observed in low- and high-grade lesions with a prevalence of about 50% and 80%, respectively [58] (own unpublished data).

Identification of the presumed tumor-suppressor genes on chromosomes 1p, 4q, 8p, and 16q remains an open area of research. Positional cloning of the putative genes in these chromosome regions is worthwhile because few of them have yet been identified [66]. Because most of the genetic alterations have been studied individually, and because HCC forms a group of heterogeneous tumors, a comprehensive characterization of the genetic alterations in HCC remains a problem.

Although the genes causing chromosomal instability or allelic imbalance remain unknown, microsatellite instability is caused by inactivation of a DNA mismatch repair gene (predominantly hMLH1 or hMSH2) [25, 37]. It has been shown that most tumors in patients with hereditary nonpolyposis colorectal cancer harbor microsatellite instability (MIN). This phenotype was linked to defects in the DNA mismatch repair genes MSH2 and MLH1 located on chromosomes 2 and 3. In HCC these chromosomal regions are not frequently affected by allelic losses. Furthermore, no mutation in the repeated sequences in *Bax*, *IGF-IIR*, or *MLH* genes (a hallmark of MIN) have been detected so far in HCC. Performing immunohistochemistry for hMLH1 and hMSH2 protein in our patients, we have detected specific positive staining for both hMLH1 and hMSH2 in all HCC examined (unpublished observations). These data strongly suggest an absence of either inactivating mutations of hMLH1 and hMSH2 or promoter hypermethylation of hMLH1 in HCC. Taken together, these findings indicate that – in contrast to allelic imbalance – defective DNA mismatch repair (MMR) does not contribute significantly to hepatocellular carcinogenesis [18, 25, 37].

Cell cycle regulation

The most important pathways that are affected in HCC are the retinoblastoma (Rb) gene, the INK4a-ARF (p14-p16) pathway, and cyclins. pRb, p16, and cyclin D_1 are involved in the regulation of the G_1-S phase transition of the cell cycle [46]. In the cellular program leading to DNA synthesis signals that drive cells into S phase converge at the level of cyclin-dependent kinase (CDK) activity. Rb phosphorylation is mediated by CDKs, whose activity is enhanced by cyclins and inhibited by CDK inhibitors. p16 (INK4A) is further required for p53-independent G_1 arrest in response to DNA-damaging agents. As a result there is an overlap between p53-DNA damage mediating genes and cell cycle [10, 11, 65].

In nonproliferating hepatocytes pRb forms complexes with the E2F transcription factors, which in the complexed form are transcriptionally inactive. Upon phosphorylation by CDK4 pRb is released from its complexes, and "free" E2Fs can promote DNA synthesis. According to this, loss of Rb or its aberrant phosphorylation leads to a loss of growth control at the G_1 phase [12, 14]. The ARF tumor suppressor, encoded by an alternative reading frame of the INK4a-ARF locus, senses "mitogenic current" flowing through the Rb pathway and is induced by abnormal growth promoting signals. By antagonizing Mdm2, a negative regulator of the p53 tumor suppressor, ARF triggers a p53-dependent transcriptional response that diverts incipient cancer cells to undergo growth arrest or apoptosis. Although ARF is not directly activated by signals that damage DNA, its loss not only dampens the p53 response to abnormal mitogenic signals but also renders tumor cells resistant to treatment by cytotoxic drugs and irradiation. Taken together, disturbances in the p16-cyclin D-CDK4-Rb and ARF-Mdm2-p53 pathways could be a main axis of genetic events in HCC because all "players" in these pathway seem to be altered in HCC [4, 24, 26].

The RB gene is one of the best studied tumor-suppressor genes in HCC. Mutations of RB are observed in about 15% of HCC. LOH at chromosome 13q where RB is located is frequently observed in HCC, with a prevalence of 25–48% [12, 14]. An overexpression of cyclins has been observed in about 10–13% of HCC cases [47]. Cyclin D_1, for example, is a known oncogene and a key regulator of cell cycle progression. Amplification of the cyclin D_1 gene and its overexpression have been associated with aggressive forms of human HCC [50]. It has recently been shown in a transgene mouse model that overexpression of cyclin D_1 is sufficient to initiate hepatocellular carcinogenesis [4]. The transduction of antisense cyclin D_1 inhibits tumor growth in a xenograft hepatoma model. Correcting alterations that have occurred in the G_1 phase regulatory machinery may therefore provide a novel weapon to treat and prevent HCC [4].

p16 inactivation, due either to LOH at chromosome 9p or to de-novo methylation of the promoter, is detected

Table 2 Frequency of p53 mutations in hepatocellular carcinoma in relation to geographical area (*AFB1* aflatoxin B_1, *HBV* hepatitis B virus *HCV* hepatitis C virus)

Region	Mutation rate (%)	Affected codon	Correlation
Mozambique	50	249	AFB1
Senegal	67	249	AFB1
China	52	Mostly 249	HBV, AFB1
Taiwan	31	exon 5–8, codon 249: 13%	HBV, AFB1
Japan	28	Exon 5–8, codon 249: 2%	HCV, tumor stage
Europe	25	Exon 5–8, codon 249: 0%	HBV, cirrhosis
United States	20	Exon 5–8, codon 249: <5%	HCV

in up to 60% of HCC cases [11, 24, 26, 48, 49, 57]. p14 alterations are found in about 15% [49]. Our own observations demonstrate that the INK4a-ARF-/p53-pathway is disrupted in 86% of HCC cases, either by p53 mutations or by INK4a-ARF inactivation. Interestingly, an inverse relationship between p53 and p14 exists in our patients: inactivation of p14 was restricted essentially to tumors with wild-type p53. Thus the loss of p14 and mutations of p53 could be mutually exclusive events, suggesting that they may be functionally equivalent in hepatocarcinogenesis [49]. The overall frequency of 9p21 alterations, including deletion and methylation, was 78%. Silencing of INK4a-ARF gene products – coding for critical regulators of cell cycle progression – is therefore one of the most frequent genetic defects in HCC.

p53 and homologues

The p53 tumor-suppressor gene is frequently mutated in human cancers. Additionally, in many cancers p53 function is altered through binding to viral oncoproteins or abrogation of p53 degradation by mdm-2/hdm-2 in concert with p14, as described above. Human p53 protein has been extensively characterized both structurally and functionally. The NH_2 terminus of p53 harbors the transactivation region (amino acids 1–42) that interacts with basal transcriptional machinery in inducing various gene expression but also contains binding sites for negative regulators of p53 transcriptional activity (Mdm2, E1B). The core domain of p53 (amino acids 113–290) is critical to the p53 function as a transcription factor and encompasses residues involved in sequence-specific DNA binding. The DNA-binding domain is the single most frequent site of missense mutations in the p53 gene that contribute to the process of malignant transformation in the cell. The carboxyl terminus of the p53 protein contains the oligomerization domain (amino acids 319–364), which is essential for tetramer formation and for regulatory sequences in the extreme COOH-terminal end (amino acids 364–393) [32].

The identification of two homologues, p63 and p73, revealed that p53 is a member of a family of related transcription factors [39, 45]. Since they share amino acid sequence identity reaching 63% in the DNA-binding domain, p53, p63, and p73 should have redundant functions in the regulation of gene expression. Indeed, p73 can activate p53-regulated genes and suppress growth or induce apoptosis. Moreover, p53 and p73 are both induced by DNA damage – albeit through distinct mechanisms. Other evidence, however, suggests that p63 and p73 are important for regulation of normal development. An extended C-terminal region, not found in p53, is alternatively spliced in p63 and p73. In contrast to p53, p63 and p73 genes are rarely mutated in human cancer. p53, p63, and p73 appear to have overlapping and distinct functions: p53 regulates the stress response to suppress tumors, p63 is essential for ectoderm development, and p73 might regulate both the stress response and development. Because p53 and p73 are linked to different upstream pathways, this family of transcription factors may regulate a common set of genes in response to different extracellular signals [39].

p53 mutations are found in about 30% of HCC cases worldwide. The frequency of all p53 mutations varies between 20% in North America and 67% in Africa (Table 2). Until now all reported mutations (mostly missense, leading to stabilization of protein) have been somatic, indicating that germline p53 mutations do no appear to predispose for HCC. Both the frequency and the type of mutations differ depending on the geographic location and cause of the tumors. Tumor-specific p53 mutations have been identified in several studies, linking the mutation pattern to suspected etiological factors. A selective guanine-to-thymine transversion mutation in codon 249 [AG*G* to AG*T* (transversion italicized) leading to an arginine-to-serine substitution] of the p53 gene has been identified as a "hotspot" mutation for HCC. Epidemiological and experimental evidence suggests that in HCC this mutation is strongly associated with exposure to aflatoxin B_1 in combination with a high level of chronic hepatitis B virus infection in the population [13, 15, 30, 32, 53, 62]. The presence of this "hotspot" mutation in patients with HCC who are from Europe, the United States, Japan, and Australia is extremely low; only three mutations (one in Europe and two in Japan) have been identified among 664 patients with HCC analyzed [1, 45, 53]. Generally, patients who have not been exposed to aflatoxin B_1 or hepatitis virus have a lower prevalence of p53 gene mutations, indicating that other genes involved in the process of hepatocarcinogenesis [56].

In hepatitis B virus infection a functional inactivation of p53 has been shown: The X protein of the virus (HBx) can interact with p53 and may also affect a variety of

signal transduction pathways within the cell. In most instances this small viral protein favors cell survival and probably initiates hepatocarcinogenesis. HBx upregulates the activity of a number of transcription factors including nuclear factor κB, activator protein 1, cAMP-response element binding protein, and thyroxine-binding protein [9, 60].

No specific mutations or interactions have yet been described for p73 and p63 [39, 45]. However, an overexpression of p73 (wild type) has been described in a subset a HCC, indicating a poor prognosis of these patients. Our own data show that p53 mutations in a given tumor are related neither to the absence or presence of p73 nor p63 [45].

Wnt pathway: APC, β-catenin, axin 1, and E-cadherin

Adenomatous polyposis coli (APC) protein has been thought to function as a tumor suppressor through its involvement in the Wnt/β-catenin signaling pathway. The APC/β-catenin pathway is highly regulated and includes actors such as GSK3, CBP, groucho, axin, conductin, and TCF [27, 29, 35]. Furthermore, c-MYC and cyclin D_1 were recently identified as key transcriptional targets of this pathway, indicating a broad overlap between several tumor-permissive pathways. Wnt proteins are involved in a large number of events during tumor development, not only in HCC but also in other types of cancer. Activation of the Wnt pathway can be caused by β-catenin mutation or by an inactivating mutation of the *axin* gene [29, 50]. Somatic mutations of β-catenin have been observed in 19–26% of HCC cases, mostly missense mutations and interstitial deletions of exon 3. These mutations that occur at the N-terminal region of β-catenin lead to a nuclear accumulation of aberrant β-catenin proteins that stimulate the activity of other transcription factors [51, 59]. In dysplastic nodules a cytoplasmic expression of β-catenin has been observed [51]. Axin, an important regulator of β-catenin, is mutated in about 10% of HCC cases, leading to an activation of the Wnt pathway. However, mutations in the *axin* gene have until now been identified only in HCC that lack mutations in the β-catenin gene [3, 27, 29, 38]

It has recently been shown that transduction of the wild-type axin gene (AXIN1) induces apoptosis in HCC cells, indicating that axin 1 may an effective growth suppressor of hepatocytes [38].

Somatic APC mutations are rare events in HCC, but it was recently reported that biallelic inactivation of the APC gene contributed to the development of HCC in a patient with familial adenomatous polyposis and a known germline mutation of the APC gene at codon 208 [43]. E-cadherin, the cytoplasmic anchor protein of β-catenin, is rarely mutated in HCC. However, loss of function due to LOH or de novo methylation occurs in about 30% of HCC cases [41].

Alterations of the TGF-β/IGF-axis

Transforming growth factor (TGF) β induces both growth inhibition and apoptosis in hepatoctyes. TGF-β initiates signaling through heteromeric complexes of transmembrane type I and type II serine/threonine kinase receptors [5]. Activated TGF-β type I receptor phosphorylates receptor-regulated Smads [2, 4]. However, genetic alterations of the TGF-β pathway are mediated by mutations of the Smad2 and Smad4 gene, which occur in about 10% of HCC cases. Mutations of the TGF-β receptor (TGF-β1RII) gene itself is detected in patients with HCC and may also abrogate TGF-β signaling [7, 20].

A potent activator of TGF-β is the mannose-6-phosphate/insulin-like growth factor 2 receptor (M6P/IGF2R). M6P/IGF2R suppresses cell growth through binding to the insulin-like growth factor (IGF) 2 and latent complex of TGF-β. The deregulation of the IGF axis, including the autocrine production of IGFs, IGF binding proteins (IGFBPs), IGFBP proteases, and the expression of the IGF receptors, has also been identified in the development of HCC [6, 20]. Both LOH and mutations of the M6P/IGF2R have been reported in about 30% HCC patients [5]. However, a recently published study from Japan failed to identify relevant alterations the M6P/IGF2R gene [55]. Increased expression of IGF-II, IGF-I receptor, alterations of IGFBP production and the proteolytic degradation of IGFBPs result in an excess of bioactive IGFs. The above-mentioned defective function of the IGF degrading M6P/IGF2R may further potentiate the mitogenic effects of IGFs in the development of HCC [20, 55, 61].

PTEN/MMAC1/TEP1 (PTEN) is a tumor-suppressor gene which is located on chromosome band 10q23.3. Alterations, mainly mutations but also LOH, of PTEN have been reported in about 10% of HCC cases. Recently it was demonstrated that PTEN significantly lowers IGF secretion and also expression of secretory and cellular vascular endothelial growth factor proteins in HCC cell lines and could therefore inhibit tumorigenicity [19, 42, 62].

Taken together, these findings demonstrate that several genes of the complex growth regulatory TGF-β/IGF pathway could be altered during hepatocellular carcinogenesis. The situation is further complicated due to the observation that activation of TGF-β and IGF signaling is observed even in liver cirrhosis, and that complex interactions may exist between hepatitis virus particles at a preneoplastic stage [6].

Distinct hepatocarcinogenic pathways in HCC with or without cirrhosis?

A number of genetic alterations have been described in HCC, and more than 20 genes within at least four carcinogenesis pathways have been shown to be altered in HCC. One of the most frequently affected genes in HCC is p53, and the INK4a-ARF pathway is the most frequently altered in HCC [49]. However, the prevalence of

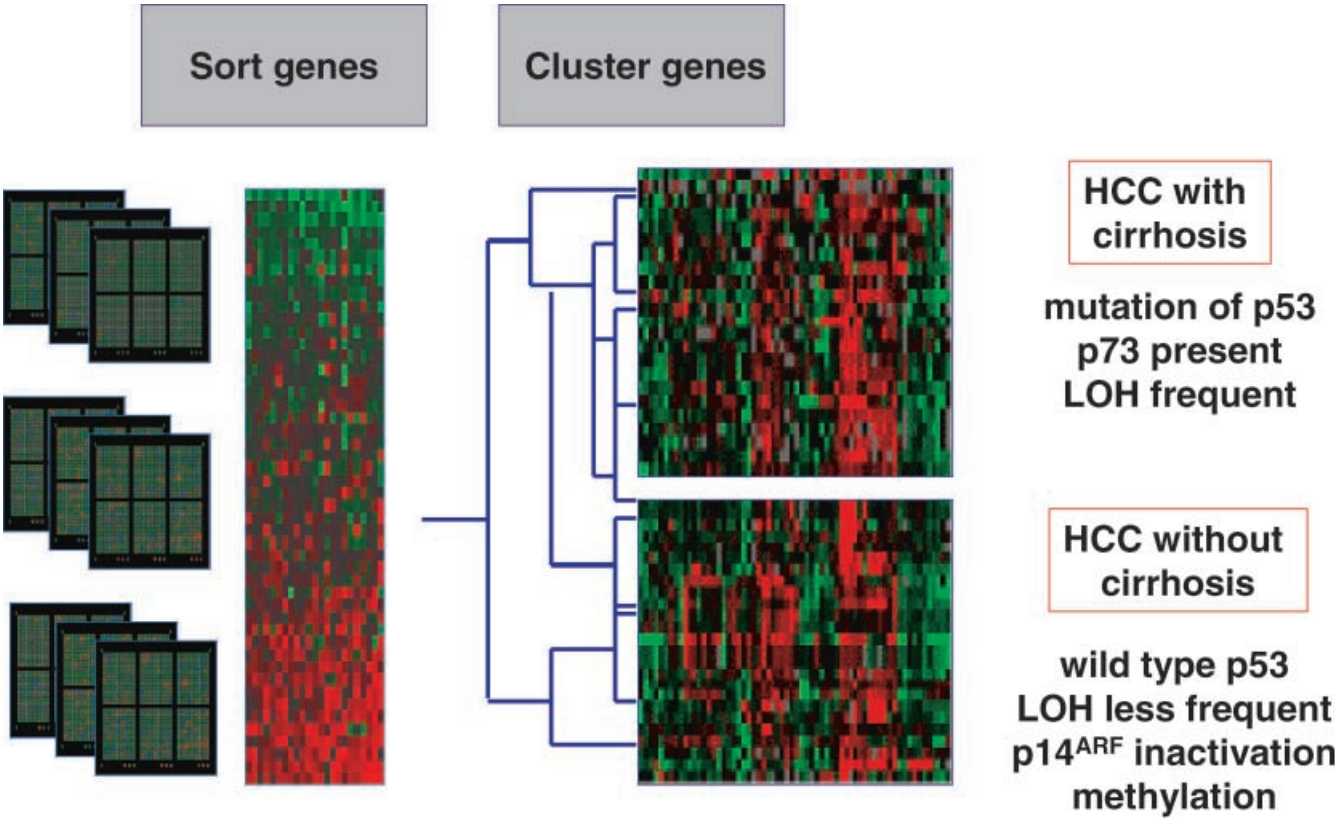

Fig. 2 Microarray analysis of hepatocellular carcinoma defining at least two different pathway of carcinogenesis

genetic alterations described in the literature showed a considerable variance. This may be explained by different causal factors (hepatitis B virus, hepatitis C virus, aflatoxin intake) leading to liver cirrhosis, which is present in up to 90% of HCC cases in high-incidence areas. In contrast, in low incidence areas (e.g., western Europe), the incidence of HCC in a cirrhotic liver is much lower (about 60%).

These differences are not discussed in detail in the current literature, perhaps due to the lack of patients having HCC without cirrhosis [2, 16, 23, 44]. Recent advances in DNA sequencing technology and the development of gene expression arrays have provided more powerful tools to study the expression of thousands of genes in HCC in a single experiment [9, 21, 31]. Gene expression arrays are created by depositing unique complementary DNA (cDNA) fragments on a nylon filter or on glass slides. The filter is then hybridized with labeled cDNA from HCC tissue of interest. The readout is performed by high throughput (phospho-)imagers. Using this new technique in combination with bioinformatics, initial results indicate two different "genetic make-ups" for HCC, depending on whether they arise in cirrhosis or in noncirrhotic liver [40, 61] (Fig. 2). Despite our small number of patients (n=210) a trend towards a lower rate of p53 mutations (and p73 expression), higher prevalence of β-catenin mutations, p14 inactivation, and global gene methylation is observed in HCC without cirrhosis. Further studies on a larger number of patients are obviously necessary to define distinct pathways of hepatocarcinogenesis more precisely in the future. However, until now there are only limited data either in favor or against this new fascinating hypothesis.

References

1. Boix-Ferrero J, Pellin A, Blesa R, Adrados M, Llombart-Bosch A (1999) Absence of p53 gene mutations in hepatocarcinomas from a Mediterranean area of Spain. A study of 129 archival tumour samples. Virchows Arch 434:497–501
2. Chen TC, Chou TB, Ng KF, Hsieh LL, Chou YH (2001) Hepatocellular carcinoma associated with focal nodular hyperplasia. Report of a case with clonal analysis. Virchows Arch 438:408–411
3. Coste A de La, Romagnolo B, Billuart P, Renard CA, Buendia MA, Soubrane O, Fabre M, Chelly J, Beldjord C, Kahn A, Perret C (1998) Somatic mutations of the beta-catenin gene are frequent in mouse and human hepatocellular carcinomas. Proc Natl Acad Sci USA 95:8847–8851
4. Deane NG, Parker MA, Aramandla R, Diehl L, Lee WJ, Washington MK, Nanney LB, Shyr Y, Beauchamp RD (2001) Hepatocellular carcinoma results from chronic cyclin D1 overexpression in transgenic mice. Cancer Res 61:5389–5395
5. De Souza AT, Hankins GR, Washington MK, Orton TC, Jirtle RL (1995) M6P/IGF2R gene is mutated in human hepatocellular carcinomas with loss of heterozygosity. Nat Genet 11:447–449
6. Enomoto A, Esumi M, Yamashita K, Takagi K, Takano S, Iwai S (2001) Abnormal nucleotide repeat sequence in the TGF-betaRII gene in hepatocellular carcinoma and in uninvolved liver tissue. J Pathol 195:349–354

7. Gozuacik D, Murakami Y, Saigo K, Chami M, Mugnier C, Lagorce D, Okanoue T, Urashima T, Brechot C, Paterlini-Brechot P (2001) Identification of human cancer-related genes by naturally occurring Hepatitis B Virus DNA tagging. Oncogene 20:6233–6240
8. Graveel CR, Jatkoe T, Madore SJ, Holt AL, Farnham PJ (2001) Expression profiling and identification of novel genes in hepatocellular carcinomas. Oncogene 20:2704–2712
9. Hamilton SR, Aaltonen LA (eds) (2000) Pathology & genetics: tumours of the digestive system. IARC, Lyon
10. Hanahan D, Weinberg RA (2000) The hallmarks of cancer. Cell 100:57–70
11. Herman JG (1999) Hypermethylation of tumor suppressor genes in cancer. Semin Cancer Biol 9:359–367
12. Higashitsuji H, Itoh K, Nagao T, Dawson S, Nonoguchi K, Kido T, Mayer RJ, Arii S, Fujita J (2000) Reduced stability of retinoblastoma protein by gankyrin, an oncogenic ankyrin-repeat protein overexpressed in hepatomas. Nat Med 6:96–99
13. Hosono S, Chou MJ, Lee CS, Shih C (1993) Infrequent mutation of p53 gene in hepatitis B virus positive primary hepatocellular carcinomas. Oncogene 8:491–496
14. Hsia CC, Di Bisceglie AM, Kleiner DE, Farshid M, Tabor E (1994) RB tumor suppressor gene expression in hepatocellular carcinoma from patients infected with the hepatitis B virus. J Med Virol 44:67–73
15. Hsu IC, Metcalf RA, Sun T, Welsh JA, Wang NJ, Harris CC (1991) Mutational hotspot in the p53 gene in human hepatocellular carcinomas. Nature 350:427–428
16. Ishizaki M, Ashida K, Higashi T, Nakatsukasa H, Kaneyoshi T, Fujiwara K, Nouso K, Kobayashi Y, Uemura M, Nakamura S, Tsuji T (2001) The formation of capsule and septum in human hepatocellular carcinoma. Virchows Arch 438:574–580
17. Kallioniemi A, Kallioniemi OP, Sudar D, Rutovitz D, Gray JW, Waldman F, Pinkel D (1992) Comparative genomic hybridization for molecular cytogenetic analysis of solid tumors. Science 258:818–821
18. Kanzler S, Meyer E, Lohse AW, Schirmacher P, Henninger J, Galle PR, Blessing M (2001) Hepatocellular expression of a dominant-negative mutant TGF-beta type II receptor accelerates chemically induced hepatocarcinogenesis. Oncogene 20:5015–5024
19. Kawamura N, Nagai H, Bando K, Koyama M, Matsumoto S, Tajiri T, Onda M, Fujimoto J, Ueki T, Konishi N, Shiba T, Emi M (1999) PTEN/MMAC1 mutations in hepatocellular carcinomas: somatic inactivation of both alleles in tumors. Jpn J Cancer Res 90:413–418
20. Kawate S, Takenoshita S, Ohwada S, Mogi A, Fukusato T, Makita F, Kuwano H, Morishita Y (1999) Mutation analysis of transforming growth factor beta type II receptor, Smad2, and Smad4 in hepatocellular carcinoma. Int J Oncol 14:127–131
21. Kim MY, Park E, Park JH, Park DH, Moon WS, Cho BH, Shin HS, Kim DG (2001) Expression profile of nine novel genes differentially expressed in hepatitis B virus-associated hepatocellular carcinomas. Oncogene 20:4568–4575
22. Kusano N, Shiraishi K, Kubo K, Oga A, Okita K, Sasaki K (1999) Genetic aberrations detected by comparative genomic hybridization in hepatocellular carcinomas: their relationship to clinicopathological features. Hepatology 29:1858–1862
23. Laurent-Puig P, Legoix P, Bluteau O, Belghiti J, Franco D, Binot F, Monges G, Thomas G, Bioulac-Sage P, Zucman-Rossi J (2001) Genetic alterations associated with hepatocellular carcinomas define distinct pathways of hepatocarcinogenesis. Gastroenterology 120:1763–1773
24. Liew CT, Li HM, Lo KW, Leow CK, Chan JY, Hin LY, Lau WY, Lai PB, Lim BK, Huang J, Leung WT, Wu S, Lee JC (1999) High frequency of p16INK4A gene alterations in hepatocellular carcinoma. Oncogene 18:789–795
25. Macdonald GA, Greenson JK, Saito K, Cherian SP, Appelman HD, Boland CR (1998) Microsatellite instability and loss of heterozygosity at DNA mismatch repair gene loci occurs during hepatic carcinogenesis. Hepatology 28:90–97
26. Matsuda Y, Ichida T, Matsuzawa J, Sugimura K, Asakura H (1999) p16 (INK4) is inactivated by extensive CpG methylation in human hepatocellular carcinoma. Gastroenterology 116:394–400
27. Morin PJ, Sparks AB, Korinek V, Barker N, Clevers H, Vogelstein B, Kinzler KW (1997) Activation of beta-catenin-Tcf signaling in colon cancer by mutations in beta-catenin or APC. Science 275:1787–1790
28. Murray C JL, Lopez AD (1997) Mortality by cause for eight regions of the world: global burden of disease study. Lancet 349:1269–1276
29. Nakamura T, Hamada F, Ishidate T, Anai K, Kawahara K, Toyoshima K, Akiyama T (1998) Axin, an inhibitor of the Wnt signalling pathway, interacts with beta-catenin, GSK-3beta and APC and reduces the beta-catenin level. Genes Cells 3:395–403
30. Oda T, Tsuda H, Scarpa A, Sakamoto M, Hirohashi S (1992) p53 gene mutation spectrum in hepatocellular carcinoma. Cancer Res 52:6358–6364
31. Okabe H, Satoh S, Kato T, Kitahara O, Yanagawa R, Yamaoka Y, Tsunoda T, Furukawa Y, Nakamura Y (2001) Genome-wide analysis of gene expression in human hepatocellular carcinomas using cDNA microarray: identification of genes involved in viral carcinogenesis and tumor progression. Cancer Res 61:2129–2137
32. Ozturk M (1991) p53 mutation in hepatocellular carcinoma after aflatoxin exposure. Lancet 338:1356–1359
33. Pineau P, Nagai H, Prigent S, Wei Y, Gyapay G, Weissenbach J, Tiollais P, Buendia MA, Dejean A (1999) Identification of three distinct regions of allelic deletions on the short arm of chromosome 8 in hepatocellular carcinoma. Oncogene 18:3127–3134
34. Qin LX, Tang ZY, Sham JS, Ma ZC, Ye SL, Zhou XD, Wu ZQ, Trent JM, Guan XY (1999) The association of chromosome 8p deletion and tumor metastasis in human hepatocellular carcinoma. Cancer Res 59:5662–5665
35. Rubinfeld B, Souza B, Albert I, Müller O, Chamberlain SH, Masiarz FR, Munemitsu S, Polakis P (1993) Association of the APC gene product with β-catenin. Science 262:1731–1734
36. Sakakura C, Hagiwara A, Taniguchi H, Yamaguchi T, Yamagishi H, Takahashi T, Koyama K, Nakamura Y, Abe T, Inazawa J (1999) Chromosomal aberrations in human hepatocellular carcinomas associated with hepatitis C virus infection detected by comparative genomic hybridization. Br J Cancer 80:2034–2039
37. Salvucci M, Lemoine A, Saffroy R, Azoulay D, Lepere B, Gaillard S, Bismuth H, Reynes M, Debuire B (1999) Microsatellite instability in European hepatocellular carcinoma. Oncogene 18:181–187
38. Satoh S, Daigo Y, Furukawa Y, Kato T, Miwa N, Nishiwaki T, Kawasoe T, Ishiguro H, Fujita M, Tokino T, Sasaki Y, Imaoka S, Murata M, Shimano T, Yamaoka Y, Nakamura Y (2000) AXIN1 mutations in hepatocellular carcinomas, and growth suppression in cancer cells by virus-mediated transfer of AXIN1. Nat Genet 24:245–250
39. Sayan AE, Sayan BS, Findikli N, Ozturk M (2001) Acquired expression of transcriptionally active p73 in hepatocellular carcinoma cells. Oncogene 20:5111–5117
40. Shirota Y, Kaneko S, Honda M, Kawai HF, Kobayashi K (2001) Identification of differentially expressed genes in hepatocellular carcinoma with cDNA microarrays. Hepatology 33:832–840
41. Slagle BL, Zhou YZ, Birchmeier W, Scorsone KA (1993) Deletion of the E-cadherin gene in hepatitis B virus-positive Chinese hepatocellular carcinomas. Hepatology 18:757–762
42. Stambolic V, Suzuki A, de la Pompa JL, Brothers GM, Mirtsos C, Sasaki T, Ruland J, Penninger JM, Siderovski DP, Mak TW (1998) Negative regulation of PKB/Akt-dependent cell survival by the tumor suppressor PTEN. Cell 95:29–39

43. Su LK, Abdalla EK, Law CH, Kohlmann W, Rashid A, Vauthey JN (2001) Biallelic inactivation of the APC gene is associated with hepatocellular carcinoma in familial adenomatous polyposis coli. Cancer 92:332–339
44. Su Q, Benner A, Hofmann WJ, Otto G, Pichlmayr R, Bannasch P (1997) Human hepatic preneoplasia: phenotypes and proliferation kinetics of foci and nodules of altered hepatocytes and their relationship to liver cell dysplasia. Virchows Arch 431:391–406
45. Tannapfel A, Wasner M, Krause K, Geissler F, Katalinic A, Hauss J, Mössner J, Engeland K, Wittekind C (1999) Expression of p73 and its relation to histopathology and prognosis in hepatocellular carcinoma. J Natl Cancer Inst 91:1154–1158
46. Tannapfel A, Geissler F, Köckerling F, Katalinic A, Hauss J, Wittekind C (1999) Apoptosis and proliferation in relation to histopathological variables and prognosis in hepatocellular carcinoma. J Pathol 187:439–445
47. Tannapfel A, Grund D, Katalinic A, Uhlmann D, Köckerling F, Haugwitz U, Wasner M, Hauss J, Engeland K, Wittekind C (2000) Decreased expression of p27 protein is associated with advanced tumor stage in hepatocellular carcinoma. Int J Cancer 89:350–355
48. Tannapfel A, Benicke M, Katalinic A, Uhlmann D, Köckerling F, Hauss J, Wittekind C (2000) Frequency of p16 (INK4A) alterations and K-ras mutations in intrahepatic cholangiocarcinoma of the liver. Gut 47:721–727
49. Tannapfel A, Benicke M, Weinans L, Katalinic A, Uhlmann D, Hauss J, Wittekind C (2001) INK4a-ARF alterations and p53 mutations in hepatocellular carcinomas. Oncogene 20:7104–7109
50. Tetsu O, McCormick F (1999) Beta-catenin regulates expression of cyclin D1 in colon carcinoma cells. Nature 398:422–426
51. Tran van Nhieu J, Renard CA, Wei Y, Cherqui D, Zafrani ES, Buendia MA (1999) Nuclear accumulation of mutated beta-catenin in hepatocellular carcinoma is associated with increased cell proliferation. Am J Pathol 155:703–710
52. Unsal H, Yakicier C, Marcais C, Kew M, Volkmann M, Zentgraf H, Isselbacher KJ, Ozturk M (1994) Genetic heterogeneity of hepatocellular carcinoma. Proc Natl Acad Sci USA 91:822–826
53. Vautier G, Bomford AB, Portmann BC, Metivier E, Williams R, Ryder SD (1999) p53 mutations in British patients with hepatocellular carcinoma: clustering in genetic hemochromatosis. Gastroenterology 117:154–160
54. Vogel A, Kneip S, Barut A, Ehmer U, Tukey RH, Manns MP, Strassburg CP (2001) Genetic link of hepatocellular carcinoma with polymorphisms of the UDP-glucuronosyltransferase UGT1A7 gene. Gastroenterology 121:1136–1144
55. Wada I, Kanada H, Nomura K, Kato Y, Machinami R, Kitagawa T (1999) Failure to detect genetic alteration of the mannose-6-phosphate/insulin-like growth factor 2 receptor (M6P/IGF2R) gene in hepatocellular carcinomas in Japan. Hepatology 29:1718–1721
56. Weihrauch M, Lehnert G, Köckerling F, Wittekind C, Tannapfel A (2000) p53 mutation pattern in hepatocellular carcinoma in workers exposed to vinyl chloride. Cancer 88:1030–1036
57. Weihrauch M, Benicke M, Lehnert G, Wittekind C, Wrbitzky R, Tannapfel A (2001) Frequent k-ras-2 mutations and p16 (INK4A) methylation in hepatocellular carcinomas in workers exposed to vinyl chloride. Br J Cancer 84:982–989
58. Wong N, Lai P, Lee SW, Fan S, Pang E, Liew CT, Sheng Z, Lau JW, Johnson PJ (1999) Assessment of genetic changes in hepatocellular carcinoma by comparative genomic hybridization analysis: relationship to disease stage, tumor size, and cirrhosis Am J Pathol 154 37–43
59. Wong CM, Fan ST, Ng IO (2001) Beta-catenin mutation and overexpression in hepatocellular carcinoma: clinicopathologic and prognostic significance. Cancer 92:136–145
60. Wu CG, Salvay DM, Forgues M, Valerie K, Farnsworth J, Markin RS, Wang XW (2001) Distinctive gene expression profiles associated with Hepatitis B virus x protein. Oncogene 20:3674–3682
61. Yakicier MC, Irmak MB, Romano A, Kew M, Ozturk M (1999) Smad2 and Smad4 gene mutations in hepatocellular carcinoma. Oncogene 18:4879–4883
62. Yakicier MC, Legoix P, Vaury C, Gressin L, Tubacher E, Capron F, Bayer J, Degott C, Balabaud C, Zucman-Rossi J (2001) Identification of homozygous deletions at chromosome 16q23 in aflatoxin B1 exposed hepatocellular carcinoma. Oncogene 20:5232–5238
63. Yang S, Lin HZ, Hwang J, Chacko VP, Diehl AM (2001) Hepatic hyperplasia in noncirrhotic fatty livers: is obesity-related hepatic steatosis a premalignant condition? Cancer Res 61:5016–5023
64. Yao YJ, Ping XL, Zhang H, Chen FF, Lee PK, Ahsan H, Chen CJ, Lee PH, Peacocke M, Santella RM, Tsou HC (1999) PTEN/MMAC1 mutations in hepatocellular carcinomas. Oncogene 18:3181–3185
65. Yoshikawa H, Matsubara K, Qian GS, Jackson P, Groopman JD, Manning JE, Harris CC, Herman JG (2001) SOCS-1, a negative regulator of the JAK/STAT pathway, is silenced by methylation in human hepatocellular carcinoma and shows growth-suppression activity. Nat Genet 28:29–35
66. Zhao X, Li J, He Y, Lan F, Fu L, Guo J, Zhao R, Ye Y, He M, Chong W, Chen J, Zhang L, Yang N, Xu B, Wu M, Wan D, Gu J (2001) A novel growth suppressor gene on chromosome 17p13.3 with a high frequency of mutation in human hepatocellular carcinoma. Cancer Res 61:7383–7387

Virchows Arch (2002) 440:353–361
DOI 10.1007/s00428-001-0552-2

ORIGINAL ARTICLE

Josef Zamecnik · Roman Kodet

Value of thyroid transcription factor-1 and surfactant apoprotein A in the differential diagnosis of pulmonary carcinomas: a study of 109 cases

Received: 8 May 2001 / Accepted: 31 August 2001 / Published online: 19 October 2001
© Springer-Verlag 2001

Abstract Thyroid transcription factor-1 (TTF-1) and surfactant apoprotein A (SP-A) belong to tissue-specific markers expressed in the normal respiratory epithelium. Both proteins are expressed in some lung carcinomas, and they have potential diagnostic use. We performed an immunohistochemical study on 109 tumors to determine the usefulness of monoclonal SP-A (PE-10) and TTF-1 (8G7G3/1) antibodies in distinguishing primary and metastatic lung carcinomas (*n*=54) from a broad spectrum of nonpulmonary tumors (*n*=55). An immunoperoxidase method using a streptavidin–biotin kit was applied on paraffin sections. We found positive results for TTF-1 and SP-A in 75% and 46% of pulmonary adenocarcinomas and in 50% and 25% of pulmonary non-neuroendocrine large cell carcinomas (LCCs), respectively. Small cell lung carcinomas were TTF-1 positive in 89% of cases and completely negative for SP-A. Squamous cell carcinomas and carcinoid tumors were negative for both proteins. In the group of nonpulmonary tumors, TTF-1 was detected in 8 of 11 thyroid carcinomas and SP-A in 1 of 6 colorectal carcinomas. Other tumors, including seven cases of pleural mesothelioma, were negative for both TTF-1 and SP-A. The expression of both antibodies was independent of primary and metastatic sites of the tumor. We observed a significant decrease of SP-A immunoreactivity in poorly differentiated lung adenocarcinomas. The combination of anti-TTF-1 with anti-SP-A does not increase the diagnostic usefulness of TTF-1 alone. Because of its diagnostic utility TTF-1 should be added to a panel of antibodies used for assessing tumors of unknown origin.

Keywords Lung neoplasms · Adenocarcinoma · Transcription factors · Nuclear proteins · Pulmonary surfactant

J. Zamecnik (✉) · R. Kodet
Department of Pathology, Charles University,
2nd Medical School, V uvalu 84, 150 06 Prague, Czech Republic
e-mail: josef.zamecnik@lfmotol.cuni.cz
Tel.: +420-2-24435635, Fax: +420-2-24435620

Introduction

Lung cancer continues to represent a leading cause of cancer-related deaths in humans with adenocarcinoma as the most frequent histological subtype. Due to overlapping morphological features, it may be difficult to distinguish pulmonary carcinomas from metastatic tumors of other primary sites [1, 22]. Thyroid transcription factor-1 (TTF-1) and surfactant apoprotein A (SP-A) belong to recently recognized tissue-specific molecular markers. Their specific expression in the normal airway epithelium suggests that SP-A and TTF-1 may be useful in identifying neoplasms of pulmonary origin [2, 21, 32].

TTF-1 is a tissue-specific homeodomain-containing transcription factor of the Nkx2 gene family that is expressed in the thyroid gland, lungs, and in some restricted areas of the diencephalon during development [15, 21, 36]. Strong conservation of the TTF-1 gene among mammalian species and a temporal–spatial distribution of its polypeptide product in the developing lungs and thyroid gland confirm the important role of this transcription factor in early differentiation and morphogenesis [15, 27].

TTF-1 mRNA and the protein remain detectable in the postnatal period in human thyroid and respiratory epithelium, particularly in type-II pneumocytes and Clara cells [9, 13, 36]. In follicular thyroid cells, TTF-1 was found to bind to DNA promoters of thyreoglobulin and thyreoperoxidase genes activating their expression. In lung epithelial cells TTF-1 activates the transcription of surfactant apoproteins (A, B, C) and Clara cell secretory protein [4]. The ability of TTF-1 to activate transcription of different sets of genes in the thyroid gland and in the lungs as well as its function in the developing brain remain unclear.

SP-A together with other surfactant apoproteins and Clara cell secretory protein play an important role in the function and homeostasis of the pulmonary surfactant [37] reducing the surface tension of the alveolar interface [19, 20]. Alveolar type-II cells are the primary site of synthesis of surfactant apoproteins, but SP-A mRNA and the protein are also present in nonciliated bronchi-

olar (Clara) cells and in some cells of the tracheobronchial epithelium and glands [17].

Previous studies indicated that pulmonary adenocarcinomas including bronchioloalveolar carcinomas contain SP-A mRNA [5] as well as immunoreactive SP-A protein detectable with monoclonal antibody PE-10 [23, 25, 26, 35]. Furthermore, TTF-1 has been demonstrated in pulmonary adenocarcinomas [3, 7, 9, 14, 16], in pulmonary small cell carcinomas (SCLC) [9, 11, 28], and in thyroid carcinomas [14].

In the current study we performed immunohistochemical examination of a number of various tumors to determine the potential usefulness of monoclonal anti-SP-A and anti-TTF-1 antibodies in distinguishing primary and metastatic lung carcinomas from a broad spectrum of nonpulmonary tumors. The study of the reactivity of these markers in different lung tumors could be of benefit in our understanding the molecular events of their neoplastic transformation.

Table 1 Results of immunohistochemical staining with thyroid transcription factor-1 (TTF-1) antibody in pulmonary tumors. Parentheses indicate metastatic tumors

	Cases studied	Percentage of positive cells				Positive cases	%
		0%	1–10%	11–50%	51–100%		
Adenocarcinoma	24 (6)	5 (1)	1 (0)	5 (2)	13 (3)	18 (5)	75
Acinar/papillary/solid	19 (6)	5 (1)	1 (0)	4 (2)	9 (3)	13 (5)	68
Bronchioloalveolar	5 (0)	0 (0)	0 (0)	1 (0)	4 (0)	5 (0)	100
Squamous cell carcinoma	7 (3)	7 (3)	0 (0)	0 (0)	0 (0)	0 (0)	0
Large cell carcinoma	8 (3)	3 (0)	1 (0)	2 (2)	2 (1)	4 (3)	50
Small cell lung carcinoma	9 (5)	1 (1)	0 (0)	1 (0)	6 (3)	8 (4)	89
Typical carcinoid	6 (0)	6 (0)	0 (0)	0 (0)	0 (0)	0 (0)	0

Table 2 Results of immunohistochemical staining with surfactant apoprotein A (SP-A, PE-10) antibody in pulmonary tumors. Parentheses indicate metastatic tumors

	Cases studied	Percentage of positive cells				Positive cases	%
		0%	1–10%	11–50%	51–100%		
Adenocarcinoma	24 (6)	10 (3)	3 (0)	7 (2)	4 (1)	11 (3)	46
Acinar/papillary/solid	19 (6)	8 (3)	3 (0)	5 (2)	3 (1)	8 (3)	42
Bronchioloalveolar	5 (0)	2 (0)	0 (0)	2 (0)	1 (0)	3 (0)	60
Squamous cell carcinoma	7 (3)	7 (3)	0 (0)	0 (0)	0 (0)	0 (0)	0
Large cell carcinoma	8 (3)	5 (1)	1 (1)	1 (1)	1 (0)	2 (1)	25
Small cell lung carcinoma	9 (5)	9 (5)	0 (0)	0 (0)	0 (0)	0 (0)	0
Typical carcinoid	6 (0)	5 (0)	0 (0)	0 (0)	0 (0)	0 (0)	0

Table 3 Results of immunohistochemical staining in extrapulmonary tumors. *M* metastatic tumors, *TTF*-1 thyroid transcription factor-1, *SP-A* surfactant apoprotein A

	Cases studied (M)	TTF-1 positive (%)	SP-A positive (%)
Thyroid carcinoma	11 (6)	8 (73)	0 (0)
Papillary	3 (2)	3 (100)	0 (0)
Follicular	5 (4)	5 (100)	0 (0)
Medullary	2 (0)	0 (0)	0 (0)
Anaplastic	1 (0)	0 (0)	0 (0)
Epitheloid mesothelioma	7 (2)	0 (0)	0 (0)
Biliary tract carcinoma	5 (1)	0 (0)	0 (0)
Colon carcinoma	6 (5)	0 (0)	1 (17)
Pancreatic carcinoma	6 (2)	0 (0)	0 (0)
Gallbladder carcinoma	1 (0)	0 (0)	0 (0)
Breast carcinoma	4 (3)	0 (0)	0 (0)
Prostate carcinoma	5 (1)	0 (0)	0 (0)
Malignant thymoma	2 (0)	0 (0)	0 (0)
Squamous cell carcinoma of head/neck	2 (2)	0 (0)	0 (0)
Renal cell carcinoma	2 (0)	0 (0)	0 (0)
Malignant melanoma	1 (1)	0 (0)	0 (0)

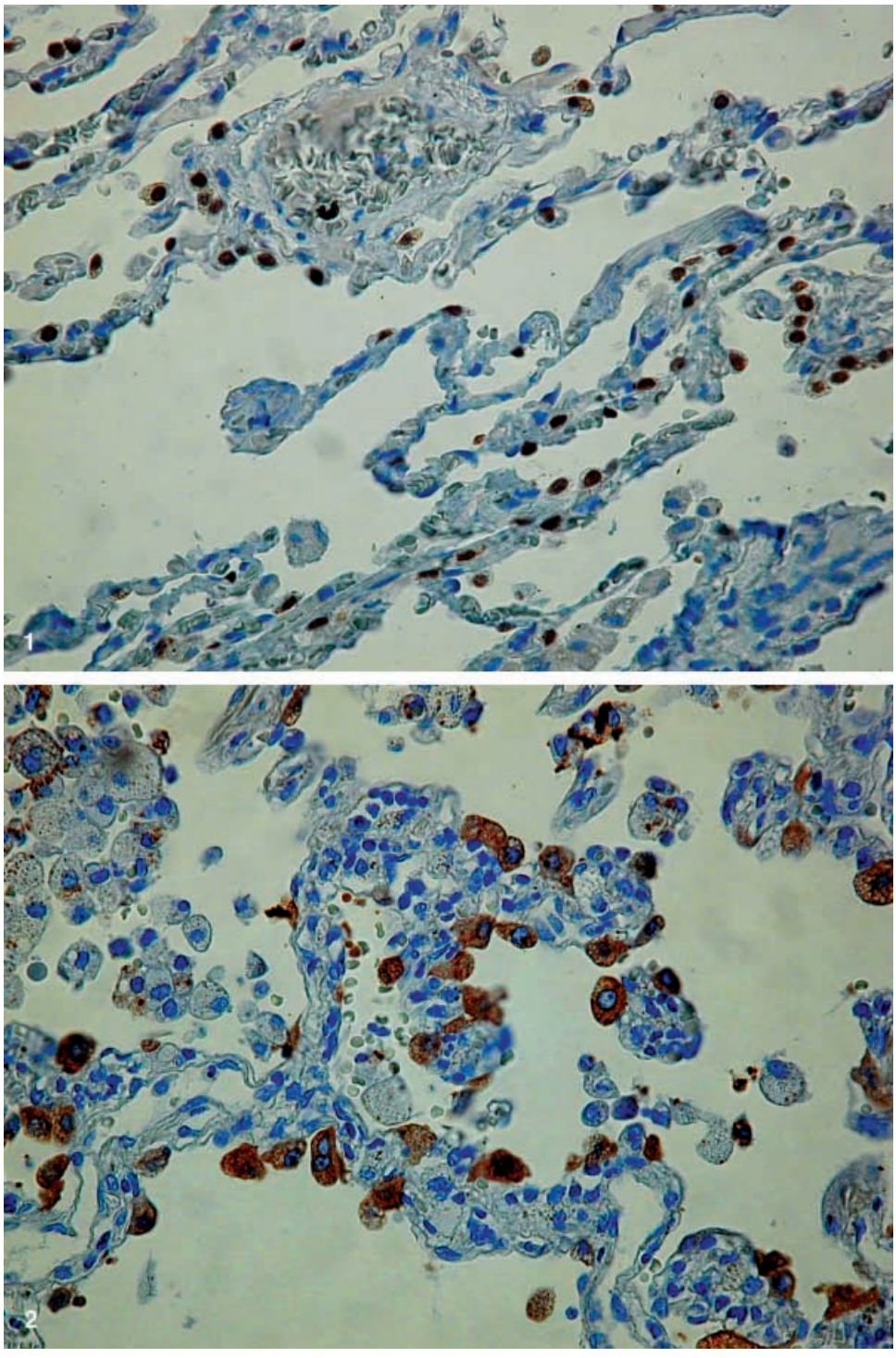

Fig. 1 Nuclear immunoreactivity for thyroid transcription factor-1 (TTF-1) in normal type-II pneumonocytes (counterstained lightly with hematoxylin, original magnification ×400)

Fig. 2 Normal type-II pneumonocytes are positively stained for surfactant apoprotein A in the cytoplasm (counterstained lightly with hematoxylin, original magnification ×400)

Materials and methods

Study material

The incidence and distribution of SP-A and TTF-1 immunoreactivity were analyzed in 109 tumors retrieved from the surgical pathology archives. The tumors included in this series were all resection specimens, small and needle biopsies were excluded. Resected tissues were routinely fixed in 10% formalin, and they were embedded in paraffin.

The tumors under study comprise 54 pulmonary carcinomas and 55 nonpulmonary carcinomas. Of lung carcinomas, the tumor tissue was obtained from the primary sites in 37 cases; in 17 patients the tissue was analyzed from the metastatic sites (Table 1 and Table 2). Lung carcinomas were classified according to criteria outlined by the World Health Organization [40]. For adenocarcinomas, the level of differentiation was established on the basis of investigation of the whole resected tumor considering the degree of glandular formation, the degree of cell atypia, the presence of solid areas, the mitotic activity, and the extent of necrosis as described previously [24]. LCCs included in the study did not show

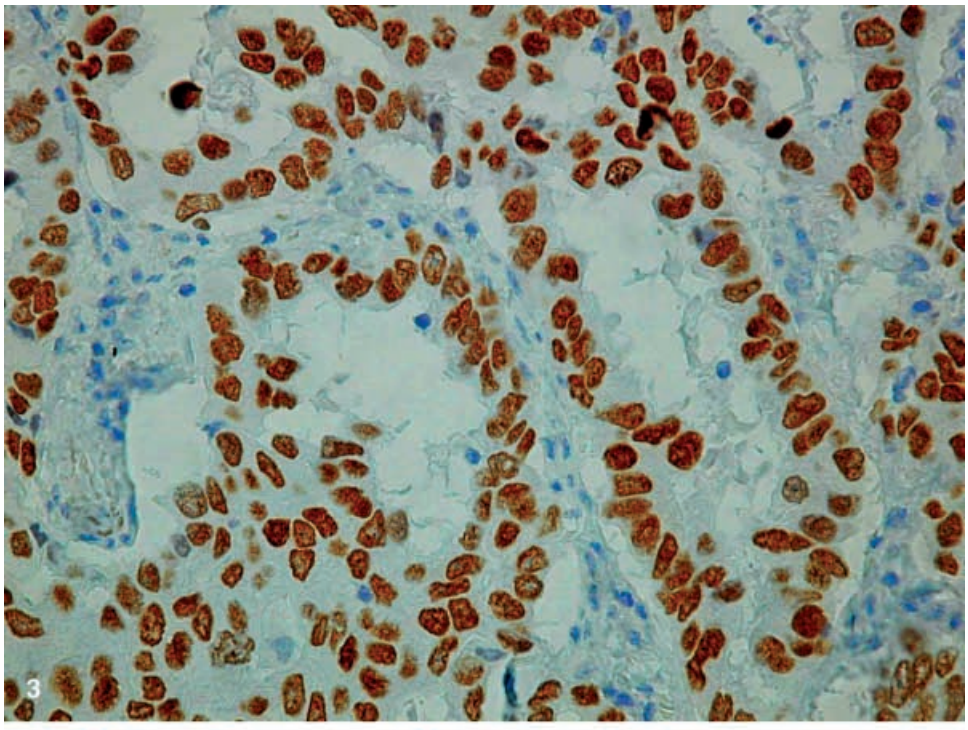

Fig. 3 Immunohistochemical demonstration of thyroid transcription factor-1 (TTF-1) in well-differentiated pulmonary adenocarcinoma (counterstained lightly with hematoxylin, original magnification ×400)

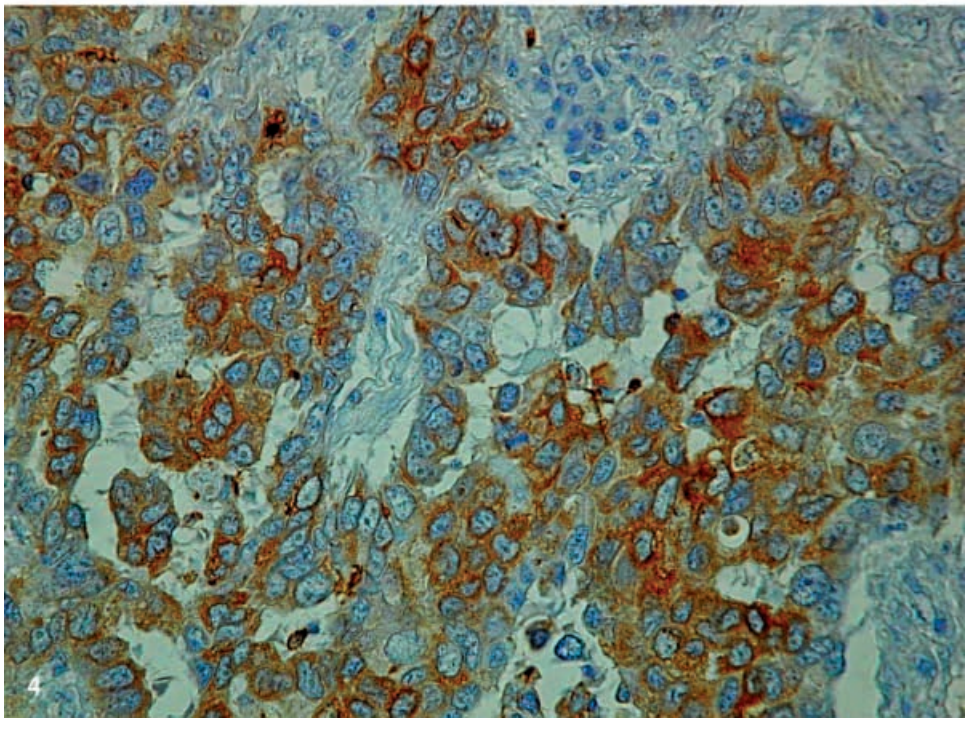

Fig. 4 Immunohistochemical demonstration of surfactant apoprotein A in well-differentiated pulmonary adenocarcinoma (counterstained lightly with hematoxylin, original magnification ×400)

neuroendocrine differentiation according to criteria defined by Colby et al. [6]. The group of 55 nonpulmonary carcinomas consists of 35 tumors from the primary sites and of 23 metastatic carcinomas (Table 3). The origin of the investigated metastatic tumors was verified by comparing their histological features with primary tumors resected simultaneously or at an earlier period. Cases with more than one known primary tumor were excluded.

Immunohistochemical examination

Tissue sections were deparaffinized in xylene and rehydrated through decreasing concentrations of ethanol to water. In sections to be incubated with TTF-1 antibody, heat-induced epitope retrieval (HIER) was performed in sodium citrate buffer solution (pH 6.0) warming to 96°C in a water bath for 40 min. After subsequent cooling for 20 min and inhibition of endogenous peroxidase, the sections were incubated with TTF-1 antibody (overnight at 4°C). Mouse monoclonal antibody (clone 8G7G3/1, Neomarkers Co., Fremont, Calif., USA) was used and diluted 1:100. The antigen–antibody

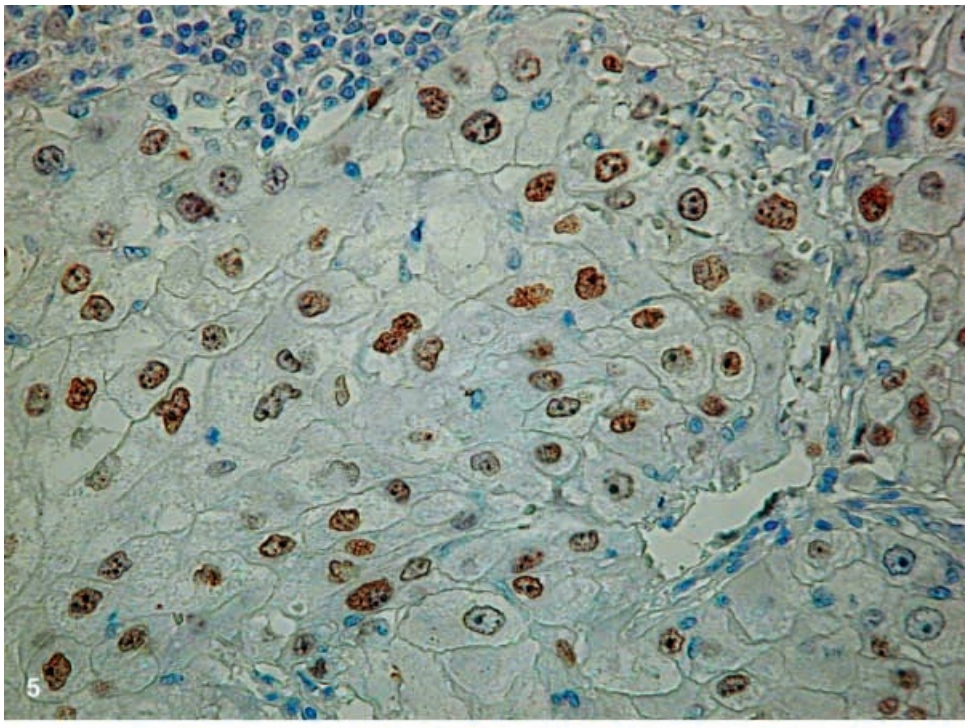

Fig. 5 Pulmonary large cell carcinoma showing nuclear thyroid transcription factor-1 (TTF-1) positivity (counterstained lightly with hematoxylin, original magnification ×400)

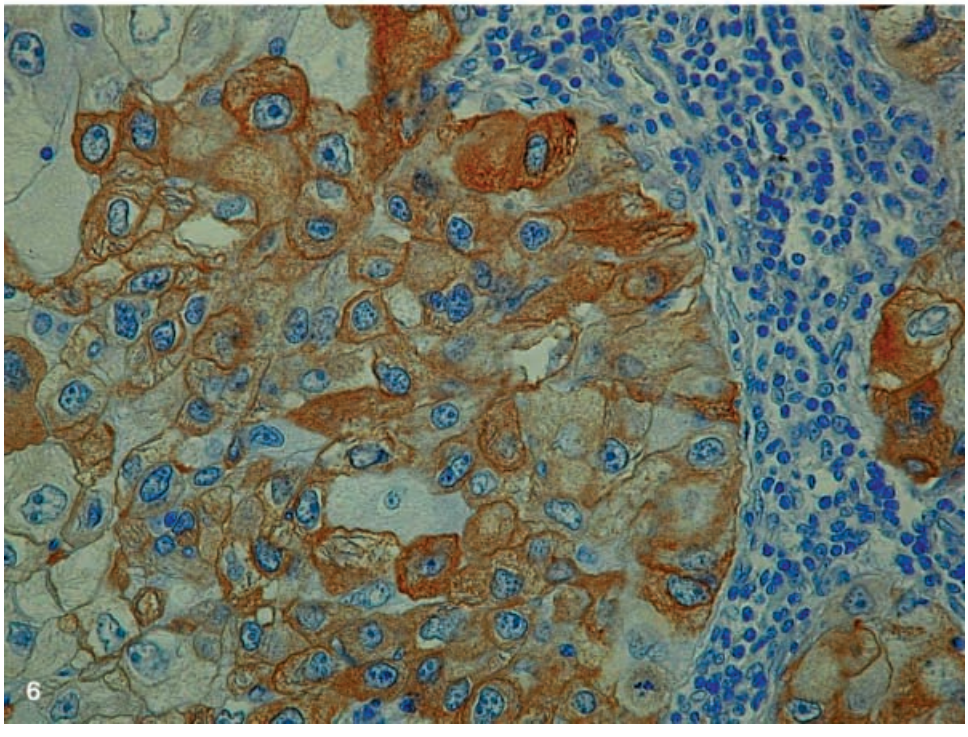

Fig. 6 Diffuse cytoplasmic immunoreactivity for surfactant apoprotein A (SP-A) in a pulmonary large cell carcinoma (counterstained lightly with hematoxylin, original magnification ×400)

complexes were visualized using a biotin-streptavidin detection system (Dako ChemMate Detection kit, Denmark) with 3,3′-diaminobenzidine (DAB, Fluka Chemie GmbH., Germany) as chromogen.

After predigestion with 0.1% trypsin (Dako Co.) in phosphate-buffered saline and inhibition of endogenous peroxidase, tissue sections to be incubated with SP-A antibody were subjected to HIER in a saturated solution of lead thiocyanate (Aldrich Chem. Co., Switzerland) using a microwave oven, as previously described [12]. The sections were incubated overnight at 4°C with SP-A antibody (mouse monoclonal antibody, clone PE-10, Dako Co., dilution 1:75). Streptavidin–biotin kit (LSAB2 System HRP, Dako Co.) was applied for immunolocalization of the antigen. Chromogenic visualization development was obtained using DAB. All sections were counterstained with Harris' hematoxylin, dehydrated, cleared, and mounted. Positive and negative controls were provided with each assay.

Immunostaining was evaluated semiquantitatively according to the percentage of positive tumor cells, i.e. 0%, less than 10%, 10–50%, greater than 50%. Nuclear staining only was considered for a positive result with anti-TTF-1, whereas for SP-A the intracytoplasmic staining was typical. To exclude evaluation of equivocal reactions, staining was considered positive if more than 10% of the neoplastic cells were stained.

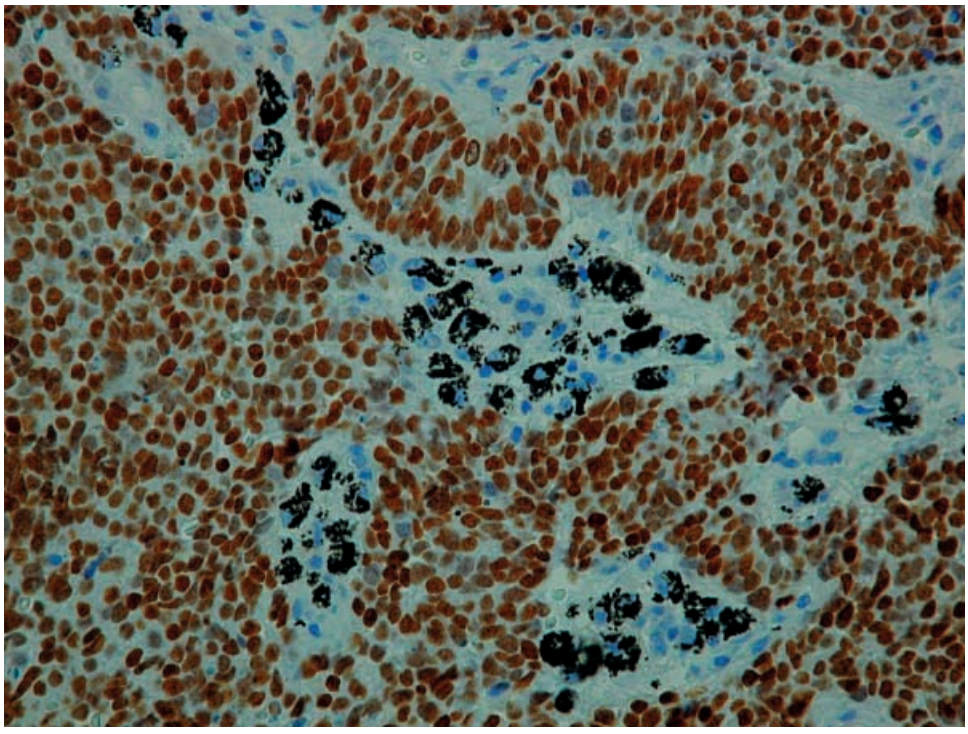

Fig. 7 Intense nuclear immunoreactivity for thyroid transcription factor-1 (TTF-1) in a lymph node metastasis of a small cell lung carcinoma (counterstained lightly with hematoxylin, original magnification ×400)

Results

In non-neoplastic lung, an intense nuclear TTF-1 staining and the intracytoplasmic finely granular immunoreaction product of SP-A (PE-10) were observed in type-II pneumocytes and in nonciliated bronchiolar cells (Fig. 1 and Fig. 2). Alveolar macrophages were also stained positively by PE-10 in some cases; however, the immunoproduct was significantly coarser than that of the normal type-II pneumocytes. Only rarely positive SP-A staining in glandular lumina or alveoli was observed. Care was taken to distinguish non-neoplastic cells entrapped within the tumor. No significant differences between non-neoplastic and malignant cells were observed in the staining pattern with TTF-1 antibody. With anti-SP-A, the cytoplasm of malignant cells was stained in a more diffuse pattern than the finely granular foam-like appearance in type-II pneumocytes. The results of immunoreactivity of the investigated tumors for both TTF-1 and SP-A are summarized in Table 1, Table 2, and Table 3.

In the group of pulmonary carcinomas, immunoreactive TTF-1 and SP-A were detected in 75% and 46% of pulmonary adenocarcinomas (Fig. 3 and Fig. 4) and in 50% and 25% of pulmonary non-neuroendocrine LCCs (Fig. 5 and Fig. 6), respectively. Small cell carcinomas were TTF-1 positive in 89% of cases (Fig. 7). They were negative for SP-A. Squamous cell carcinomas and carcinoid tumors were negative with both antibodies. None of the pulmonary carcinomas was simultaneously negative for TTF-1 and positive for SP-A. The expression of both TTF-1 and SP-A had essentially the same features in primary and metastatic sites of the investigated pulmonary tumors.

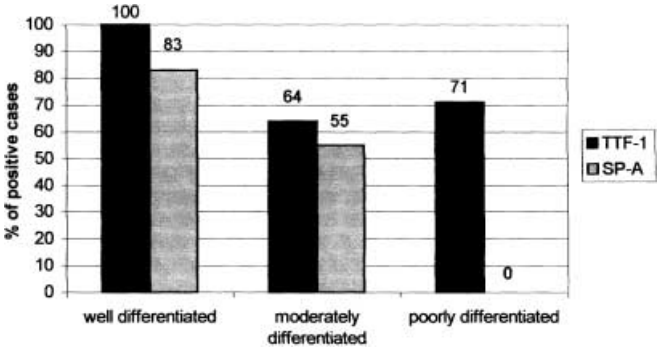

Fig. 8 Pulmonary adenocarcinomas – a comparison of the differentiation grade with the percentage of positive cases for thyroid transcription factor-1 (TTF-1) and surfactant apoprotein A (SP-A)

No correlation between the distribution of TTF-1 expression in pulmonary adenocarcinomas and histological differentiation was seen. However, a significant decrease of SP-A immunoreactivity was observed in association with a loss of differentiation of these tumors (Fig. 8, Table 4).

All investigated nonpulmonary carcinomas except for carcinomas of the thyroid gland were negative for TTF-1 in the current study. TTF-1 was diffusely positive in both primary sites and metastases of papillary and follicular thyroid carcinomas; no positive TTF-1 signal was seen in medullary and anaplastic thyroid carcinoma. A variable nonspecific intracytoplasmic granular TTF-1 positivity in normal hepatocytes, pancreatic acinar cells, and in the glandular epithelium of the gastric body was detected. Anti SP-A gave a focal positive staining in one of six co-

Table 4 Distribution of surfactant apoprotein A (SP-A) positivity among pulmonary adenocarcinomas of various degree of differentiation

	0%	1–10%	11–50%	51–100%	Positive cases (%)
Well differentiated	1	0	3	2	5/6 (83)
Moderately differentiated	4	1	4	2	6/11 (55)
Poorly differentiated	5	2	0	0	0/7 (0)

lon carcinomas, but it was completely negative in all other extrapulmonary neoplasms investigated in this study. All positive and negative controls stained appropriately.

Discussion

Immunohistochemistry using anti-SP-A and anti-TTF-1 antibodies was performed in an attempt to compare the sensitivity and specificity of the two antibodies and to assess their use in distinguishing pulmonary carcinomas from non-pulmonary malignant tumors. The positive immunoreactivity of SP-A and TTF-1 in non-neoplastic type-II pneumocytes and Clara cells observed in our study is in agreement with previous observations [17, 36].

Eighteen of 24 investigated pulmonary adenocarcinomas were stained by TTF-1, which corresponds to a sensitivity of 75%. This finding is in agreement with previous studies with the same monoclonal anti-TTF-1 antibody (clone 8G7G3/1), which indicated sensitivities of 75% [29] and 76% [18]. Our results are also consistent with the sensitivity of 76% reported by Bejarano et al. [3], who used a polyclonal antibody against TTF-1, and are slightly higher than those reported by Kaufmann et al. (68%) [16]. The cause of the discrepancy may be due to a high proportion of pulmonary adenocarcinomas of mucinous subtype investigated in the latter study. Only one of ten cases of mucinous adenocarcinomas was positively stained with anti-TTF-1 in that study.

In concordance with other authors [8, 16, 18, 29], we observed TTF-1 positivity in all thyroid carcinomas of the follicular cell origin, but not in any other of a wide range of extrapulmonary tumors. Due to discrimination of thyroid carcinomas from other tumors by the morphology and by the highly specific and sensitive immunohistochemical detection of thyroglobulin, their TTF-1 expression should not be misleading in making the diagnosis of pulmonary carcinoma. Among non-small cell carcinomas, only one TTF-1 positive gastric carcinoma and one endometrial carcinoma were reported so far [3]. However, the latter group used rat polyclonal antibody against TTF-1, which could produce the different result [3].

The presence of immunoreactive SP-A was detected in 46% of the pulmonary adenocarcinomas only, which confirms the findings of a previous study carried out by Kaufmann et al. [16] who reported 45% of 98 investigated adenocarcinomas stained with the antibody PE-10. A large number of pulmonary adenocarcinomas would be, therefore, underestimated relying on this stain only. SP-A is not expressed in nonpulmonary tissues as was confirmed by in situ hybridization and by immunohistochemical examinations [10, 31]. However, immunoreactivity for SP-A was present in one of the six colorectal carcinomas investigated in the present study. The unexpected positivity was reported by other authors in various tumors – in 3 of 7 thyroid carcinomas, in 6 of 15 prostatic carcinomas [16], and in 6 of 13 pulmonary metastases of breast carcinomas [3]. The exact reason of this cross-reactivity is unclear, but it is possible that it results from a relationship of the structure of SP-A with a number of cellular proteins. SP-A shares homology with a number of calcium-dependent lectins, as well as with type-IV collagen [10, 32]. Moreover, an uptake of the surfactant apoproteins has been demonstrated in several types of cells, including fibroblasts [33].

In contrast to the study published by Bejarano et al. [3], we observed a significant decrease in SP-A expression in relation to the degree of dedifferentiation of pulmonary adenocarcinoma.

The monoclonal antibody against TTF-1 had a considerably higher sensitivity for pulmonary adenocarcinoma than anti-SP-A (PE-10). None of the pulmonary carcinomas was negative for TTF-1 and positive for SP-A. This is obviously due to the fact that the transcription of TTF-1 controls the production of surfactant apoproteins [38]. In summary, the combination of TTF-1 with antibody against SP-A did not increase the sensitivity of our investigations over the use of TTF-1 alone.

Regarding non-neuroendocrine LCCs of the lung, TTF-1 was also more often detectable than SP-A. Kaufmann et al. [16] showed TTF-1 and SP-A immunoreactivity in 40% and 10% of non-neuroendocrine LCCs, respectively. Based on these findings they speculated that within a heterogeneous group of pulmonary LCCs TTF-1-positive cases belong to those with a glandular differentiation observed at the ultrastructural level.

TTF-1 expression in 89% SCLCs was another interesting finding in this study, but none of the investigated tumors displaying clear neuroendocrine features, such as carcinoid tumors and thyroid medullary carcinoma, was positive. A similar observation made by Fabbro et al. [9] led to a hypothesis that pulmonary carcinoids could be derived from a different stem cell line than SCLCs. In contrast, pulmonary squamous cell carcinomas, which have an evident epithelial origin, do not express TTF-1. Moreover, Folpe et al. [11] demonstrated the expression of TTF-1 in 35% of 51 carcinoid tumors. In spite of 98% sensitivity of TTF-1 for SCLCs, Ordonez [28] has recently demonstrated that TTF-1 is not a specific marker for SCLCs. He observed TTF-1 positivity in nonpulmonary small cell carcinomas of the gastrointestinal tract, of the urinary bladder, and of the uterine cervix. None-

theless, TTF-1 with its high sensitivity to SCLC might be a good immunohistochemical marker for distinguishing SCLCs from small cell carcinomas of other primary sites, especially if used in combination with cytokeratin 20 [28].

Because of the worldwide progressive increase in the incidence of pleural mesotheliomas [30], surgical pathologists are more frequently faced with the diagnostic challenge to distinguish the epitheloid variant of mesothelioma from peripheral adenocarcinomas of the lung with pleural involvement. The immunohistochemical diagnosis is based on the use of a panel of adenocarcinoma- and mesothelioma-associated antibodies which differ in their sensitivity and specificity in reacting with either adenocarcinomas or mesotheliomas [29, 34, 39]. The 100% specificity of TTF-1 for pulmonary adenocarcinoma versus mesothelioma observed in the current study is in agreement with others [18, 29], and it indicates that the introduction of TTF-1 into the battery of antibodies to assess pleural-based malignancies may be especially useful.

Even though the number of cases investigated in this series is limited, we can conclude that antibodies to SP-A and TTF-1 are not entirely sensitive and specific for pulmonary carcinomas to be solely relied on in establishing the diagnosis. However, with TTF-1 we possess a tool to resolve this issue in a substantial number of cases, and this is of important practical value.

Acknowledgements The study was supported by the research programs VZ no. 111300003 and VZ FNM 000 00064 203.

References

1. Askin FB (1993) Something old? Something new? Second primary or pulmonary metastasis in the patient with known extrathoracic carcinoma. Am J Clin Pathol 100:4–5
2. Auten RL, Watkins RH, Shapiro DL, Horowitz S (1990) Surfactant apoprotein A (SP-A) is synthesized in airway cells. Am J Respir Cell Mol Biol 3:491–496
3. Bejarano PA, Baughman RP, Biddinger PW, Miller MA, Fenoglio Preiser C, al Kafaji B, Di Lauro R, Whitsett JA (1996) Surfactant proteins and thyroid transcription factor-1 in pulmonary and breast carcinomas. Mod Pathol 9:445–452
4. Bohinski RJ, Di Lauro R, Whitsett JA (1994) The lung-specific surfactant protein B gene promoter is a target for thyroid transcription factor 1 and hepatocyte nuclear factor 3, indicating common factors for organ-specific gene expression along the foregut axis. Mol Cell Biol 14:5671–5681
5. Broers JL, Jensen SM, Travis WD, Pass H, Whitsett JA, Singh G, Katyal SL, Gazdar AF, Minna JD, Linnoila RI (1992) Expression of surfactant associated protein-A and Clara cell 10 kilodalton mRNA in neoplastic and non-neoplastic human lung tissue as detected by in situ hybridization. Lab Invest 66: 337–346
6. Colby TV, Koss MN, Travis WD (1994) Small cell carcinoma and large cell neuroendocrine carcinoma. In: Colby TV, Koss MN, Travis WD (eds) Tumors of the lower respiratory tract. AFIP atlas of tumor pathology, 3rd series, fascicle 13. Armed Forces Institute of Pathology, Washington, pp 235–237
7. Di Loreto C, Di Lauro V, Puglisi F, Damante G, Fabbro D, Beltrami CA (1997) Immunocytochemical expression of tissue specific transcription factor-1 in lung carcinoma. J Clin Pathol 50:30–32
8. Di Loreto C, Puglisi F, Di Lauro V, Damante G, Beltrami CA (1998) TTF-1 protein expression in pleural malignant mesotheliomas and adenocarcinomas of the lung. Cancer Lett 124: 73–78
9. Fabbro D, Di Loreto C, Stamerra O, Beltrami CA, Lonigro R, Damante G (1996) TTF-1 gene expression in human lung tumours. Eur J Cancer 32A:512–517
10. Floros J, Phelps DS, Kourembanas S, Taeusch HW (1986) Primary translation products, biosynthesis, and tissue specificity of the major surfactant protein in rat. J Biol Chem 261:828–831
11. Folpe AL, Gown AM, Lamps LW, Garcia R, Dail DH, Zarbo RJ, Schmidt RA (1999) Thyroid transcription factor-1: immunohistochemical evaluation in pulmonary neuroendocrine tumors. Mod Pathol 12:5–8
12. Gown AM, de Wever N, Battifora H (1993) Microwave based antigenic unmasking: a revolutionary new technique for routine immunohistochemistry. Appl Immunohistochem 1:256–266
13. Guazzi S, Price M, De Felice M, Damante G, Mattei MG, Di Lauro R (1990) Thyroid nuclear factor 1 (TTF-1) contains a homeodomain and displays a novel DNA binding specificity. EMBO J 9:3631–3639
14. Holzinger A, Dingle S, Bejarano PA, Miller MA, Weaver TE, DiLauro R, Whitsett JA (1996) Monoclonal antibody to thyroid transcription factor-1: production, characterization, and usefulness in tumor diagnosis. Hybridoma 15:49–53
15. Ikeda K, Clark JC, Shaw White JR, Stahlman MT, Boutell CJ, Whitsett JA (1995) Gene structure and expression of human thyroid transcription factor-1 in respiratory epithelial cells. J Biol Chem 270:8108–8114
16. Kaufmann O, Dietel M (2000) Expression of thyroid transcription factor-1 in pulmonary and extrapulmonary small cell carcinomas and other neuroendocrine carcinomas of various primary sites. Histopathology 36:415–420
17. Khoor A, Gray ME, Hull WM, Whitsett JA, Stahlman MT (1993) Developmental expression of SP-A and SP-A mRNA in the proximal and distal respiratory epithelium in the human fetus and newborn. J Histochem Cytochem 41:1311–1319
18. Khoor A, Whitsett JA, Stahlman MT, Olson SJ, Cagle PT (1999) Utility of surfactant protein B precursor and thyroid transcription factor 1 in differentiating adenocarcinoma of the lung from malignant mesothelioma. Hum Pathol 30:695–700
19. King RJ (1982) Pulmonary surfactant. J Appl Physiol 53:1–8
20. King RJ, Klass DJ, Gikas EG, Clements JA (1973) Isolation of apoproteins from canine surface active material. Am J Physiol 224:788–795
21. Lazzaro D, Price M, de Felice M, Di Lauro R (1991) The transcription factor TTF-1 is expressed at the onset of thyroid and lung morphogenesis and in restricted regions of the foetal brain. Development 113:1093–1104
22. Leonard RJ, Nystrom JS (1993) Diagnostic evaluation of patients with carcinoma of unknown primary tumor site. Semin Oncol 20:244–250
23. Linnoila RI, Jensen SM, Steinberg SM, Mulshine JL, Eggleston JC, Gazdar AF (1992) Peripheral airway cell marker expression in non-small cell lung carcinoma. Association with distinct clinicopathologic features. Am J Clin Pathol 97:233–243
24. Mackay B, Lukeman JM, Ordonez NG (1991) Tumors of the lung. Saunders, Philadelphia, p 100
25. Mizutani Y, Nakajima T, Morinaga S, Gotoh M, Shimosato Y, Akino T, Suzuki A (1988) Immunohistochemical localization of pulmonary surfactant apoproteins in various lung tumors. Special reference to nonmucus producing lung adenocarcinomas. Cancer 61:532–537
26. Nicholson AG, McCormick CJ, Shimosato Y, Butcher DN, Sheppard MN (1995) The value of PE-10, a monoclonal antibody against pulmonary surfactant, in distinguishing primary and metastatic lung tumours. Histopathology 27:57–60
27. Oguchi H, Pan YT, Kimura S (1995) The complete nucleotide sequence of the mouse thyroid-specific enhancer-binding protein (T/EBP) gene: extensive identity of the deduced amino acid sequence with the human protein. Biochim Biophys Acta 1261:304–306

28. Ordonez NG (2000) Value of thyroid transcription factor-1 immunostaining in distinguishing small cell lung carcinomas from other small cell carcinomas. Am J Surg Pathol 24: 1217–1223
29. Ordonez NG (2000) Value of thyroid transcription factor-1, E-cadherin, BG8, WT1, and CD44S immunostaining in distinguishing epithelial pleural mesothelioma from pulmonary and nonpulmonary adenocarcinoma. Am J Surg Pathol 24: 598–606
30. Peto J, Decarli A, La Vecchia C, Levi F, Negri E (1999) The European mesothelioma epidemic. Br J Cancer 79:666–672
31. Phelps DS, Floros J (1988) Localization of surfactant protein synthesis in human lung by in situ hybridization. Am Rev Respir Dis 137:939–942
32. Phelps DS, Harding HP (1987) Immunohistochemical localization of a low molecular weight surfactant-associated protein in human lung. J Histochem Cytochem 35:1339–1342
33. Rice WR, Sarin VK, Fox JL, Baatz J, Wert S, Whitsett JA (1989) Surfactant peptides stimulate uptake of phosphatidylcholine by isolated cells. Biochim Biophys Acta 1006: 237–245
34. Riera JR, Astengo-Osuna C, Longmate JA, Battifora H (1997) The immunohistochemical diagnostic panel for epithelial mesothelioma: a reevaluation after heat-induced epitope retrieval. Am J Surg Pathol 21:1409–1419
35. Singh G, Scheithauer BW, Katyal SL (1986) The pathobiologic features of carcinomas of type II pneumocytes. An immunocytologic study. Cancer 57:994–999
36. Stahlman MT, Gray ME, Whitsett JA (1996) Expression of thyroid transcription factor-1 (TTF-1) in fetal and neonatal human lung. J Histochem Cytochem 44:673–678
37. Weaver TE, Whitsett JA (1991) Function and regulation of expression of pulmonary surfactant-associated proteins. Biochem J 273:249–264
38. Whitsett JA, Glasser SW (1998) Regulation of surfactant protein gene transcription. Biochim Biophys Acta 1408:303–311
39. Wick MR, Loy T, Mills SE, Legier JF, Manivel JC (1990) Malignant epithelioid pleural mesothelioma versus peripheral pulmonary adenocarcinoma: a histochemical, ultrastructural, and immunohistologic study of 103 cases. Hum Pathol 21:759–766
40. WHO (1982) The World Health Organization histological typing of lung tumours. Second edition. Am J Clin Pathol 77:123–136

Virchows Arch (2002) 440:362–366
DOI 10.1007/s00428-001-0570-0

ORIGINAL ARTICLE

Xingpei Hao · Ian M. Frayling · Teresa C. Willcocks
Wei Han · Ian P.M. Tomlinson · Massimo N. Pignatelli
Theresa P. Pretlow · Ian C. Talbot

β-Catenin expression and allelic loss at *APC* in sporadic colorectal carcinogenesis

Received: 18 September 2001 / Accepted: 18 October 2001 / Published online: 25 January 2002
© Springer-Verlag 2002

Abstract β-catenin is involved in E-cadherin-mediated cell adhesion, intracellular signal transduction, and also interacts with adenomatous polyposis coli (APC) protein. We previously found that 31% of colorectal adenomas and 84% of carcinomas showed reduced membranous staining of β-catenin, while 46% of adenomas and 79% of carcinomas displayed β-catenin nuclear expression. Importantly, a reciprocal relationship between reduced membranous and increased nuclear β-catenin expression was demonstrated in the development from adenoma to carcinoma. To clarify whether this relates to an abnormality of the APC gene (*APC*), we have now studied allele loss in microdissected tissues from 74 adenomas and 21 carcinomas (sporadic cases, previously immunostained for β-catenin) by analysis of the microsatellites *D5S346*, *D5S82* and *D5S299*. Fifty-five tumors (57.8%) showed allele loss at *APC* (no difference between adenomas and carcinomas). Thirty-one of these 55 (31/55, 56.4%) displayed both increased nuclear localization and reduced membranous staining of β-catenin, and thirteen tumors (13/55, 23.6%) manifested either nuclear expression without changes in membranous expression or reduced membranous staining without nuclear expression (9 and 4 cases, respectively), while 11 (11/55, 20.0%) preserved normal membranous expression. Adenomas and carcinomas showing both nuclear and reduced membranous expression of β-catenin, compared with those with normal membranous expression, tended to show allele loss ($P<0.01$). In addition, 24 (24/95, 25.6%) tumors showed a change in the pattern of β-catenin expression, but did not exhibit allele loss. These results suggest that although there may be a number of mechanisms responsible for changes in β-catenin expression in colorectal tumors, dysfunction of *APC* may be the major cause of this phenomenon.

Keywords *APC* · Allele loss · β-catenin · Colorectum · Adenoma · Carcinoma

This work was supported by the Imperial Cancer Research Fund.

X. Hao (✉) · I.C. Talbot
Academic Department of Pathology
and Imperial Cancer Research Fund Colorectal Cancer Unit,
St Mark's Hospital, Harrow, UK
e-mail: xhao@biogenex.com
Tel.: +1-925-543-1332, Fax: +1-925-543-1339

X. Hao
Biogenex, 4600 Norris Canyon Road, San Ramon, CA 94583, USA

I.M. Frayling
Imperial Cancer Research Fund Colorectal Cancer Unit,
St Mark's Hospital, Harrow, UK

T.C. Willcocks
School of Biosciences, University of Westminster, London, UK

X. Hao · W. Han · T.P. Pretlow
Institute of Pathology, Case Western Reserve University,
Cleveland, USA

I.P.M. Tomlinson
Molecular and Population Genetics Laboratory,
Imperial Cancer Research Fund, 44 Lincoln's Inn Fields,
London WC2A 3PX, UK

M.N. Pignatelli
Department of Histopathology,
Imperial College School of Medicine, Hammersmith Hospital,
London, UK

I.M. Frayling
Cambridge University Department of Medical Genetics,
Molecular Genetics Laboratory, Addenbrooke's Hospital,
Cambridge, UK

Introduction

β-Catenin, a cytoplasmic protein, links E-cadherin to α-catenin, together forming the E-cadherin/catenin complex [28], which plays a crucial role in the organization and maintenance of epithelial integrity and in suppression of tumor invasion and metastasis [34]. In addition, β-catenin is involved in intracellular signaling, which is mediated through its interaction with the T cell factor (TCF) family of transcription factors, leading to the nuclear translocation of β-catenin [16] and activation of targeted genes, such as *c-myc* [11] and *cyclin D1* [35].

Furthermore, increased expression of β-catenin in the early embryogenesis of *Xenopus* leads to reduplication of the dorsal axis [9], suggesting that β-catenin may govern cell fate choices.

The *APC* tumor suppressor gene is located on chromosome 5q21 [8, 24]. Germ-line mutations in *APC* are responsible for familial adenomatous polyposis (FAP), and somatic mutations [both point mutations and loss of heterozygosity (LOH)] are frequently found in both FAP-associated and sporadic colorectal adenomas and carcinomas [8, 15, 20, 29]. *APC* mutations are probably initiating events in tumorigenesis. APC protein is involved in β-catenin regulation [30, 33] and increased nuclear and cytoplasmic β-catenin expression may be one of the main effects of *APC* mutation [23]. Through its effects on β-catenin expression, APC may further affect cadherin-mediated cell adhesion.

By means of immunohistochemistry, we have previously shown that β-catenin membranous expression decreased progressively as the lesions proceeded from mild to moderate to severe dysplasia in adenomas and further reduced from adenomas to carcinomas, whereas β-catenin nuclear expression increased progressively in that process [10]. However, the changes appeared to occur throughout tumorigenesis, rather than as an early event, as might be expected if these changes were simply a result of *APC* (or β-*catenin*) mutation. To clarify whether or not this phenomenon is related to *APC* dysfunction, we have used loss of heterozygosity (LOH) at *APC* as a marker of *APC* mutation, antibodies for APC being unreliable in fixed, archival material. The relationship between *APC* LOH and β-catenin expression has been examined in tissues previously immunostained for the latter protein.

Materials and methods

Tissue samples

Paraffin-embedded blocks of 74 adenomas (23 with mild, 33 with moderate, and 18 with severe dysplasia) and 21 carcinomas which had previously been immunostained for β-catenin were retrieved from the archives of the Academic Department of Pathology, St Mark's Hospital [10]. Serial 4–5 μm sections were cut. One section was stained with hematoxylin and eosin (H&E) for histological classification and others were lightly stained with hematoxylin for microdissection. To ensure consistency in the grading of dysplasia, the H&E-stained sections were first read by one observer (XPH), and the results were compared with those in the original histopathological reports. Any cases in which there was doubt about the grading of dysplasia were read again by another histopathologist (ICT), and an agreement was reached.

Immunohistochemistry

Immunohistochemistry and scoring methods were as previously described [10].

Microdissection and DNA preparation

Samples for DNA extraction were specifically microdissected from the briefly hematoxylin stained sections according to the defined structure and the paired histologically normal epithelial or stromal cells. For most of the tumors the microdissected material comprised at least 75% tumor tissues, even though a few samples, especially small adenomas, may contain a little more stroma or other normal tissues. The microdissected cell populations were digested with 200 mg/l proteinase K in a 100 to 200 μl solution containing 10 mmol/l Tris-Cl (pH 8.3), 50 mmol/l KCl, at 55°C for 24–48 h. Proteinase K was inactivated at 96°C for 10 min. Cell debris was pelleted by centrifugation and the supernatant was used for the subsequent microsatellite analysis.

Determination of allelic loss at *APC*

Allelic loss at *APC* was determined by polymerase chain reaction (PCR)-based testing for LOH at three flanking microsatellites *D5S346*(GDB:181171) [32], *D5S82*(GDB:185754) [4], and *D5S299* (GDB:180445) [39]. Tumor and paired normal tissues were simultaneously amplified using fluorescent-labeled forward primers. PCR products were then electrophoresed on an ABI Prism 377XL Semi-Automated Fluorescent DNA Analyzer (Perkin-Elmer Applied Biosystems, Foster City, Cal., USA), and the results were analyzed using GeneScan Software (version 2.0.2, Perkin-Elmer) as previously described [7]. Briefly, any loci displaying only a single peak (homozygous) or extra band that differed by multiples of 2 bp from their normal counterpart (i.e., loci exhibiting microsatellite instability) were excluded from the analysis and classified as "not informative." In informative cases, allelic loss in any one of the three markers was considered to have occurred when one allele peak in tumor tissue was reduced to less than 50% of its value in the normal DNA (relative to the other allele), after taking account of baseline fluorescence levels and "stutter" bands. Allelic loss at *APC* was itself considered to have occurred if at least one of the three markers tested showed LOH.

Statistical Analysis

The χ^2 test was used to determine the statistical significance of any associations within and between the molecular and clinical data.

Results

Allelic loss at *APC* in adenomas and carcinomas

The results of analysis for LOH at *APC* in the adenomas and carcinomas, in relation to clinicopathological variables, are summarized in Tables 1 and 2. Forty-two adenomas (42/74, 56.8%) and 13 carcinomas (13/21, 61.9%) showed LOH (Fig. 1). The frequency of LOH was not related overall to either differentiation, Dukes' stage, or metastasis of carcinomas (Table 2, $P>0.35$, $P>0.25$, $P>0.25$, respectively), or to either the degree of dysplasia or size of adenomas (Table 1, both $P>0.10$), although there was a borderline lower frequency of LOH in small and mildly dysplastic tumors (perhaps resulting from technical problems in removing all stromal and normal tissue when studying these lesions). There was also no difference between the frequency of LOH in adenomas and carcinomas (Table 3, $P>0.50$).

β-catenin expression in adenomas and carcinomas

As reported before [10], 31% of adenomas and 84% of carcinomas displayed reduced membranous expression

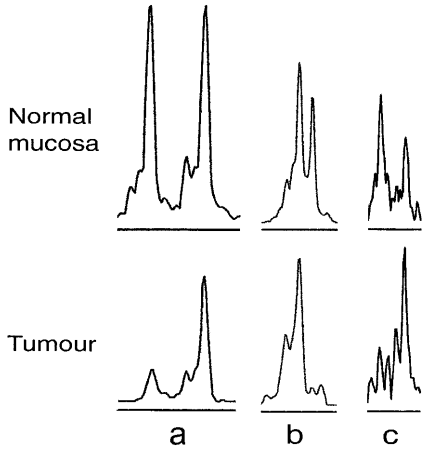

Fig. 1 LOH at *APC* in an adenoma with mild dysplasia (Marker *D5S346*) (**a**), an adenoma with moderate dysplasia (Marker *D5S82*) (**b**), and a carcinoma (Marker *D5S299*) (**c**)

Table 1 LOH at *APC* in colorectal adenomas in relation to size and dysplasia

	LOH at *APC*		
	+	–	*P*
Dysplasia			
Mild	9	14	>0.10, <0.20
Moderate	22	11	
Severe	11	7	
Size (cm)			
<1	9	13	>0.10, <0.25
1–2	23	13	
>2	10	6	

χ^2 test, Mild *vs* Moderate *vs* Severe, <1 cm *vs* 1–2 cm *vs* >2 cm. Note that χ^2 test for Mild *vs* Others = 4.11, $P<0.05$ and χ^2 test for <1 cm *vs* Others=3.23, $P<0.10$

Table 2 LOH at *APC* in colorectal carcinomas in relation to differentiation and staging

	LOH at *APC*		
	+	–	*P*
Differentiation			
Well	3	1	>0.35, <0.50
Moderate	9	7	
Poorly	1	0	
Dukes' Stage			
A	7	6	>0.25, <0.50
B	2	1	
C	4	1	
Metastasis			
Yes	4	1	>0.05, <0.10
No	9	7	

χ^2 test, Well Differentiated *vs* Moderately + Poorly Differentiated; Stage A *vs* Stage B+C

Table 3 LOH at *APC* in adenomas and carcinomas

	LOH at *APC*	
	+	–
Adenomas	42	32
Carcinomas	13	8

χ^2 =0.17, $P>0.50$

Table 4 LOH at *APC* and β-catenin expression in colorectal tumors

	LOH at *APC*	
	+	–
Normal membranous staining *, **, ***	11	16
Reduced membranous + nuclear staining	31	12
Preserved membranous + nuclear staining	9	7
Reduced membranous + no nuclear staining	4	5

*χ^2=7.5, $P>0.05$ (Normal membranous staining) *vs* (Reduced membranous + nuclear staining) *vs* (Preserved membranous + nuclear staining) *vs* (Reduced membranous + no nuclear staining)
**χ^2=6.79, $P<0.01$ (Normal membranous staining) *vs* (Reduced membranous + nuclear staining)
***χ^2=4.50, $P<0.05$ (Normal membranous staining) *vs* (Other)

of β-catenin, while 46% of adenomas and 79% of carcinomas exhibited nuclear expression. Both decreased membranous and increased nuclear β-catenin expressions were correlated with increasing degrees of dysplasia in adenomas. Carcinomas showed further, significantly decreased membranous but increased nuclear expression compared with adenomas. There were associations between reduced membranous and enhanced nuclear expression of β-catenin in both adenomas and carcinomas. In the present study with 95 tumors (74 adenomas and 21 carcinomas) (Table 4), 43 showed both reduced membranous and increased nuclear staining whereas 27 had preserved normal membranous staining. Sixteen tumors displayed nuclear expression but with preserved membranous staining, while nine tumors exhibited reduced membranous staining but without nuclear localization.

LOH at *APC* and β-catenin expression

The relationship between LOH at *APC* and β-catenin expression is shown in Table 4. Fifty-five adenomas and carcinomas exhibited LOH. Among them 31 (31/55, 56.4%) displayed both increased nuclear and reduced membranous staining of β-catenin, while 11 (11/55, 20.0%) kept normal membranous staining. In nine tumors membranous staining was preserved in the presence of nuclear expression, whereas four cases displayed reduced membranous staining but no nuclear expression. Although there was no association between LOH at *APC* and β-catenin expression overall ($P>0.05$), adenomas and carcinomas exhibiting both nuclear and reduced membranous expression of β-catenin showed a signifi-

cantly higher frequency of LOH compared with those with normal membranous staining ($P<0.01$). Moreover, tumors with alterations of β-catenin expression as regards either nuclear localization or reduced membranous expression – that is, tumors with both nuclear localization and reduced membranous expression plus tumors with only nuclear expression plus tumors with only reduced membranous expression – displayed a higher frequency of LOH at *APC* compared with those with normal membranous staining ($P<0.05$). However, in 24 tumors (24/95, 25.3%) no LOH was detected despite abnormal β-catenin expression in either nuclear localization or reduced membranous expression.

Discussion

In this study, we have demonstrated that more than half of colorectal adenomas and carcinomas show LOH at *APC*, which we have used as a convenient marker of *APC* mutation. The frequency of LOH was not associated either with the degree of dysplasia or size in adenomas, or with differentiation, Dukes' stage, or metastasis in carcinomas. This is in line with other findings [3], and further confirms that inactivation of *APC* is an early event in colorectal carcinogenesis. There is no evidence that subsequent events in carcinomas, such as chromosomal instability (CIN), affect the frequency of 5q LOH. Importantly, we have found loss of *APC* to be correlated with redistribution of β-catenin expression in colorectal tumors. Tumors with LOH tend to show reduced membranous and increased nuclear β-catenin expression.

T cell transcription factor (Tcf) and lymphoid enhancer-binding factor (Lef) are the products of a small subfamily of vertebrate high mobility group box transcription factor genes [5, 26, 37]. This family includes Lef-1, Tcf-1, -3, and -4 [6, 38, 40], which are functionally different [26, 37]. Tcf-4 is expressed in normal colonic epithelium and in colorectal tumors[16]. β-Catenin has been shown to interact with the Tcf/Lef family of DNA binding proteins [2, 21], forming β-catenin-Tcf/Lef complexes, which result in the nuclear translocation of β-catenin. A stable β-catenin-hTcf-4 complex which was constitutively active was observed in nuclei of $APC^{-/-}$ colon cancer cells; reintroduction of APC removed β-catenin from hTcf-4 and abrogated the transcriptional transactivation [16], implying that normal APC protein suppresses formation of β-catenin-Tcf/Lef complexes. Nuclear localization of β-catenin was also demonstrated in FAP patients, where β-catenin could not associate with mutant APC proteins with a lost central region, including a β-catenin binding domain, but could associate with glutathione-S-transferase-fused APC protein containing a β-catenin binding domain [12]. In addition, APC protein is known to localize to plasma membrane sites which are actively involved in cell migration [19, 25], implying that APC may play a role in regulating cell adhesiveness. These results are in accord with our demonstration that allelic loss of, and by implication mutation at, *APC* is significantly associated with reduced membranous and increased nuclear expression of β-catenin in colorectal neoplasms.

Some tumors showing both nuclear and reduced membranous expression, or showing either nuclear or reduced membranous expression, do not display LOH at *APC*. Although it must be borne in mind that a proportion of tumors may have APC abnormality caused by point mutations in both *APC* alleles, mutations in *APC* may not be the sole cause of changes in β-catenin expression. This is evidenced by the facts that mutation in β-*catenin* in the human gastric cancer cell line HSC-39 abolishes cell–cell adhesion, despite the high expression of E-cadherin [27], and that cell–cell adhesiveness is recovered after transfecting vectors of β-*catenin* into HSC-39 cells [13]. Mutations in β-*catenin* may also activate β-catenin-Tcf signaling in colon cancer [22]; β-*catenin* mutations were found in nearly half of colorectal tumors lacking *APC* mutations, even in adenomas less than 6 mm [31]. Taken together, these data suggest that β-*catenin* mutation can be at least partly responsible for deranged regulation of β-catenin-Tcf signaling. In addition, phosphorylated β-catenin has been shown to be able to modulate the E-cadherin/catenin complex [1, 14, 17]. Other factors such as wingless-type (*Wnt*) frizzled proteins and earlier members of the *Wnt* signaling pathway could also control β-catenin expression and may be involved in human colon tumorigenesis [36]. Moreover, nitric oxide has been demonstrated to enhance the level of cytoplasmic and nuclear β-catenin in mouse colonic epithelial cells in culture [18] and may be responsible for some of the regulation of β-catenin expression which we observed.

In conclusion, we have demonstrated that allelic loss at, and, by implication, mutation in *APC* are significantly associated with reduced membranous expression and nuclear accumulation of β-catenin, suggesting that inactivation of *APC* has a major role in the shift of β-catenin expression from membrane to nucleus. Other abnormalities such as β-*catenin* mutation, perhaps in combination with changes in other molecules interacting with β-catenin, may also play a role in modulating β-catenin expression.

Acknowledgements We wish to thank Graham Clark and Andrew Davies of the ICRF Equipment Park for their assistance with the LOH analysis.

References

1. Balsamo J, Leung TC, Ernst H, Zanin MKB, Hoffman S (1996) Regulated binding of a PTP1B-like phosphatase to N-cadherin: control of cadherin-mediated adhesion by dephosphorylation of β-catenin. J Cell Biol 134:801–813
2. Behrens J, von Kries JP, Kühl M, Bruhn L, Wedlich D, Grosschedl R, Birchmeier W (1996) Functional interaction of β-catenin with the transcriptional factor LEF-1. Nature 382:638–642
3. Boland CR, Sato J, Appelman HD, Bresalier RS, Feinberg AP (1995) Microallelotyping defines the sequence and tempo of allelic losses at tumour suppressor gene loci during colorectal cancer progression. Nature Medicine 1:902–909

4. Breukel C, Tops C, van Leeuwen C, van der Klift H, Nakamura Y, Fodde R, Khan PM (1991) CA repeat polymorphism at the *D5S82* locus, proximal to adenomatous polyposis coli (*APC*). Nucleic Acids Res 19:5804
5. Castrop J, Hoevenagel R, Young JR, Clevers H (1992) A common ancestor of the mammalian transcription factors TCF-1 and TCF-1α/LEF-1 expressed in chicken T cells. Eur J Immunol 22:1327–1330
6. Castrop J, van Norren K, Clevers H (1992) A gene family of HMG box factors with homology to TCF-1. Nucl Acids Res 20:611
7. Frayling IM, Bodmer WF, Tomlinson IP (1997) Allele loss in colorectal cancer at the Cowden Disease/Juvenile polyposis locus on 10q. Cancer Genet Cytogenet 97:64–69
8. Groden J, Thliveris A, Samowitz W, Carlson M, Gelbert L, Albertsen H, Joslyn G, Stevens J, Spirio L, Robertson M, Sargeant L, Krapcho K, Wolff E, Burt R, Hughes JP, Warrington J, McPherson J, Wasmuch J, Le Paslier DL, Abderrahim H, Cohen D, Leppert M, White R (1991) Identification and characterization of the familial adenomatous polyposis gene. Cell 66:589–600
9. Gumbiner BM (1995) Signal transduction of β-catenin. Curr Opin Cell Biol 7:634–640
10. Hao XP, Tomlinson IP, Ilyas M, Palazzo JP, Talbot IC (1997) Reciprocity between membranous and nuclear expression of β-catenin in colorectal tumours. Virchows Arch 431:167–172
11. He TC, Sparks AB, Rago C, Hermeking H, Zawel L, da Costa LT, Morin PJ, Vogelstein B, Kinzler KW (1998) Identification of c-MYC as a target of the APC pathway. Science 281:1509–1512
12. Inomata M, Ochiai A, Akimoto S, Kitano S, Hirohashi S (1996) Alteration of β-catenin expression in colonic epithelial cells of familial adenomatous polyposis patients. Cancer Res 56:2213–2217
13. Kawanishi J, Kato J, Sasaki K, Fujii S, Watanabe N, Niitsu Y (1995) Loss of E-cadherin-dependent cell-cell adhesion due to mutation of the β-*catenin* gene in a human cancer cell line, HSC-39. Mol Cell Biol 15:1175–1181
14. Kinch MS, Clark GJ, Der CJ, Burridge K (1995) Tyrosine phosphorylation regulates the adhesions of *Ras*-transformed breast epithelia. J Cell Biol 130:461–471
15. Kinzler KW, Nilbert MC, Su LK, Vogelstein B, Bryan TM, Levy DB, Smith KJ, Preisinger AC, Hedge P, MeKechnie D, Finniear R, Markham A, Groffen J, Boguski MS, Altschul SF, Horii A, Ando H, Miyoshi Y, Miki Y, Nishisho I, Nakamura Y (1991) Identification of *FAP* locus genes from chromosome 5q21. Science 253:661–664
16. Korinek V, Barker N, Morin PJ, van Wichen D, de Weger R, Kinzler KW, Vogelstein B, Clevers H (1997) Constitutive transcriptional activation by a β-catenin-TCF complex in *APC*$^{-/-}$ colon carcinoma. Science 275:1784–1787
17. Kypta RM, Su H, Reichardt LF (1996) Association between a transmembrane protein tyrosine phosphatase and the cadherin-catenin complex. J Cell Biol 134:1519–1529
18. Mei JM, Hord NG, Winterstein DF, Donald SP, Phang JM (2000) Differential formation of beta-catenin/lymphoid enhancer factor-1 DNA binding complex induced by nitric oxide in mouse colonic epithelial cells differing in adenomatous polyposis coli (Apc) genotype. Cancer Res 60:3379–3383
19. Midgley CA, White S, Howitt R, Save V, Dunlop MG, Hall PA, Lane DP, Wyllie AH, Bubb VJ (1997) APC expression in normal human tissues. J Pathol 181:426–433
20. Miyoshi Y, Ando H, Nagase H, Nishisho I, Horii A, Miki Y, Mori T, Utsunomiya j, Baba S, Petersen G, Hamilton SR, Kinzler KW, Vogelstein B, Nakamura Y (1992) Germline-mutations of the *APC* gene in 53 familial adenomatous polyposis patients. Proc Natl Acad Sci USA 89:4452–4456
21. Molenaar M, van de Wetering M, Oosterwegel M, Peterson-Maduro J, Godsave S, Korinek V, Roose J, Destrée O, Clevers H (1996) XTcf-3 transcription factor mediates β-catenin-induced axis formation in *Xenopus* embryos. Cell 86:391–399
22. Morin PJ, Sparks AB, Korinek V, Barker N, Clevers H, Vogelstein B, Kinzler KW (1997) Activation of β-catenin-Tcf signaling in colon cancer by mutations in β-*catenin* or *APC*. Science 275:1787–1790
23. Munemitsu S, Albert I, Souza B, Rubinfeld B, Polakis P (1995) Regulation of intracellular β-catenin levels by the adenomatous polyposis coli (APC) tumor-suppressor protein. Proc Natl Acad Sci USA 92:3046–3050
24. Nakamura Y (1993) The role of the adenomatous polyposis coli (*APC*) gene in human cancers. Adv Cancer Res 62:65–68
25. Näthke IS, Adams CL, Polakis P, Sellin JH, Nelson WJ (1996) The adenomatous polyposis coli tumour suppressor protein localizes to plasma membrane sites involved in active cell migration. J Cell Biol 134:165–179
26. Oosterwegel M, van de Wetering M, Timmerman J, Kruisbeek A Destrée O, Meijlink F, Clevers H (1993) Differential expression of the HMG box factors TCF-1 and LEF-1. Development 118:439–448
27. Oyama T, Kanai Y, Ochiai A, Akimoto S, Oda T, Yanagihara K, Nagafuchi A, Tsukita S, Shibamoto S, Ito F, Takeichi M, Matsuda H, Hirohashi S (1994) A truncated β-catenin disrupts the interaction between E-cadherin and α-catenin: a cause of loss intercellular adhesiveness in human cancer cell lines. Cancer Res 54:6282–6287
28. Ozawa M, Baribault H, Kemler R (1989) The cytoplasmic domain of the cell adhesion molecule uvomorulin associates with three independent proteins structurally related in different species. EMBO 8:1711–1717
29. Powell SM, Zilz N, Beazer-Barclay Y, Bryan TM, Hamilton SR, Thibodeau SN, Vogelstein B, Kinzler KW (1992) APC mutations occur early during colorectal tumorigenesis. Nature 359:235–237
30. Rubinfeld B, Souza B, Albert I, Müller O, Chamberlain SH, Masiarz FR, Munemitsu S, Polakis P (1993) Association of the APC gene product with β-catenin. Science 262:1731–1734
31. Sparks AB, Morin PJ, Vogelstein B, Kinzler KW (1998) Mutational analysis of the APC/β-catenin/Tcf pathway in colorectal cancer. Cancer Res 58:1130–1134
32. Spirio L, Nelson L, Ward K, Burt R, White R, Leppert M (1993) A CA-repeat polymorphism close to the adenomatous polyposis coli (*APC*) gene offers improved diagnostic testing for familial APC. Am J Hum Genet 52:286–296
33. Su LK, Vogelstein B, Kinzler KW (1993) Association of the APC tumor suppressor protein with catenins. Science 262:1734–1737
34. Takeichi M (1991) Cadherin cell adhesion receptors as a morphogenetic regulator. Science 251:1451–1455
35. Tetsu O, McCormick F (1999) Beta-catenin regulates expression of cyclin D1 in colon carcinoma cells. Nature 398:422–426
36. Uthoff SM, Eichenberger MR, McAuliffe TL, Hamilton CJ, Galandiuk S (2001) Wingless-type frizzled protein receptor signaling and its putative role in human colon cancer. Mol Carcinog 31:56–62
37. van de Wetering M, Castrop J, Korinek V, Clevers H (1996) Extensive alternative splicing and dual promoter usage generates TCF-1 protein isoforms with differential transcription control properties. Mol Cell Biol 16:745–752
38. van Genderen C, Okamura RM, Farinas I, Quo RG, Parslow TG, Bruhn L, Grosschedl R (1994) Development of several organs that require inductive epithelial-mesenchymal interactions is impaired in LEF-1 deficient mice. Genes Dev 8:2691–2704
39. van Leeuwen C, Tops C, Breukel C, van der Klift H, Fodde R, Khan PM (1991) CA repeat polymorphism at the *D5S299* locus linked to adenomatous polyposis coli (*APC*). Nucleic Acids Res 19:5805
40. Verbeek S, Izon D, Hofhuis F, Robanus-Maandag E, te Riele H, van de Wetering M, Oosterwegel M, Wilson A, MacDonald R, Clevers H (1995) An HMG-box-containing T-cell factor required for thymocyte differentiation. Nature 374:70–74

Virchows Arch (2002) 440:367–375
DOI 10.1007/s00428-001-0566-9

ORIGINAL ARTICLE

Suzuko Moritani · Hiroyuki Sugihara
Ryoji Kushima · Takanori Hattori

Different roles of p53 between Epstein-Barr virus-positive and -negative gastric carcinomas of matched histology

Received: 2 April 2001 / Accepted: 27 September 2001 / Published online: 23 November 2001
© Springer-Verlag 2001

Abstract To clarify the role of p53 in the development of Epstein-Barr virus (EBV)-associated gastric carcinoma, we examined DNA-ploidy pattern, the immunoreactivity of p53, p21^{WAF1} and Ki-67 and the incidence of mitosis and apoptosis in EBV-positive and -negative gastric carcinomas of similar histology: a lace pattern and/or gastric carcinoma with lymphoid stroma. There was no significant difference in DNA-ploidy pattern, Ki-67 index or frequencies of mitosis and apoptosis between the two groups. In deeply invasive tumours (involving the muscularis propria or deeper), p53-positive ones were rare in the EBV-encoded small RNA (EBER)-positive group and very common in the EBER-negative group, while in superficial tumours, around one-half of them were p53-positive in both groups. In p53-positive superficial tumours, p21^{WAF1}-positive ones accounted for 80% in the EBER-positive group and were scarce in the EBER-negative group. It is thus possible that p53 immunoreactivity reflects the overexpression of wild-type p53 and the stabilization of mutant p53 in the EBER-positive and -negative groups, respectively. The role of p53 in tumour development seems to be smaller in EBER-positive than in -negative gastric carcinomas.

Keywords Epstein-Barr virus · Gastric carcinoma · p53 · p21^{WAF1} · DNA ploidy pattern

Introduction

Epstein-Barr virus (EBV)-associated gastric carcinomas show characteristic histological patterns such as "gastric carcinoma with lymphoid stroma (GCLS)" and a "lace pattern". They are well known to take the better clinical course than that of conventional gastric carcinomas [23, 31, 33]. This favourable prognosis has been ascribed to markedly intense immune reaction characterised by infiltration of cytotoxic T-lymphocytes around tumour cell nests [27]. In this study, we examined this issue of outcome by disclosing the biological characteristics inherent in EBV-positive tumour cells.

DNA-ploidy pattern reflects the degree of chromosomal instability and offers a key to understanding the biological characteristics of neoplasms. The DNA-ploidy pattern of EBV-associated gastric carcinomas, however, has not been studied so far. The abundant lymphoid stroma in this type of tumour makes it difficult to isolate neoplastic cells in high concentration enough for conventional flow cytometric DNA-ploidy analysis. To circumvent this difficulty, we adopted static cytofluorometry instead of flow cytometry.

Since the DNA-ploidy pattern of gastric carcinomas is known to be different between differentiated and undifferentiated types [9, 16], we considered that it was necessary to match the histology when the DNA-ploidy pattern was compared between the EBV-positive and -negative groups. However little attention has been paid to the EBV-negative gastric carcinomas, which show similar histology to the EBV-positive carcinomas [22]: a lace pattern and/or GCLS. Using this type of tumour as the control, we could evaluate the DNA-ploidy pattern of EBV-positive gastric carcinomas without any bias caused by their unique histology.

Structural and numerical chromosomal changes are caused by DNA strand breaks and nondisjunction/genome duplication, respectively. They are detected at the G_2/M checkpoint. Wild-type p53 protein is known to play a role in the maintenance of the normal ploidy at the G_2/M checkpoint [4, 5], as well as in giving G_1 arrest and apoptosis after DNA damage [20]. Abnormal function of the G_2/M checkpoint through various mechanisms allows the proliferation of cells with abnormal chromosomal numbers, leading to the emergence of DNA aneuploidy. Such an alteration of DNA ploidy was reported to be correlated with p53 abnormality [2]. When all the checkpoint functions are lost, cell cycling may be accelerated, giving an enhanced mitotic index (MI).

S. Moritani (✉) · H. Sugihara · R. Kushima · T. Hattori
Department of Pathology, Shiga University of Medical Science, Seta-Tsukinowa-cho, Ohtsu, Shiga, 520-2192, Japan
e-mail: mori@belle.shiga-med.ac.jp
Tel.: +81-77-5482168, Fax: +81-77-5439880

Table 1 Epstein-Barr virus-positive gastric carcinomas. p53 positivity and p21 expression when immunoreactivity of the mucosa and submucosa or deeper were different, each result was shown divided by "/". *AI* apoptotic index, *MI* mitotic index, *C* cardiac region, *Mid* middle region, *A* antral region, *m* lamina propria, *sm* submucosa, *mp* muscularis propria, *ss* subserosa, *se* serosal exposure, *tub1* well differentiated tubular adenocarcinoma, *tub2* moderately differentiated tubular adnocarcinoma including "lace pattern", *por1* poorly differentiated adenocarcinoma of solid type. [gastric carcinoma with lymphoid stroma (GCLS) belongs to this category], *por2* poorly differentiated adenocarinoma of non-solid type, *sig* signet-ring cell carcinoma, *D* DNA diploidy, *AD* DNA diploiy with polyploidy, *AA* DNA aneuploidy, *no* no lesion, *nt* not tested, *ni* not informative

No.	Age	Sex	Site	Depth	Histology (m deeper than sm)	DNA-ploidy pattern	p53 positivity	p21 expression	MI (/1000 cells)	Ki-67 (%)	AI (/1000 cells)
1	47	Male	Mid	M	Tub2>sig	AA	+	+	16.3	52.9	8.4
2	50	Male	C	M	Tub3=por1	AD	–	–	6.8	59.2	21.3
3	72	Male	C	Sm	Tub1+tub2+por/tub1+tub2+por	D	–	–	3.1	66.4	16.1[a]
4	64	Male	C	Sm	Tub2>por1/por1>tub2	D	–	+/–	8.4	71	13.2[a]
5	57	Male	C	Sm	Tub2=por1/por1>tub2	AA	–	–	9.1	63.2	22.7
6	42	Male	C	Sm	Tub2/por1>tub2	AD	–	–	13.5	65	13.5
7	51	Male	Mid	Sm	Tub2=por1/por1	AA	+	+/–	18.3	63.4	18.7
8	48	Male	C	Sm	Tub2>por1/por1	AD	+	+	22.7	83.2	22.7
9	48	Male	C	Sm	Sig>por1/por1	AD	–	–	7.7	60.9	18.9
10	68	Male	Mid	Sm	Tub2/por1	AA	+	–	20.5	56	9.6
11	50	Male	C	Sm	Por1/por1	D	–	–	11.2	59.7	16
12	68	Male	C	Sm	Por1>tub2/por1	AD	–	–	13.8	63.2	8.7
13	65	Male	C	Sm	Tub2>por1/por1>tub2	AD	+	– / –	11.2	53.7	10.7
14	50	Male	C	Mp	Tub2>por1	AD	–	–	11.9	77.7	7.6
15	61	Male	C	Mp	Por>tub2>sig/por2/por1	AD	–	–	10.3	68.1	14.5
16	74	Male	C	Mp	No/por1	AD	–	– / –	5	52	8.5
17	62	Female	A	Ss	Tub2/por1>tub2	D	–	–	9.7	53.7	11.7
18	69	Male	C	Ss	Tub1>por1/por1>tub1	AA	+	–	15.1	63.1	7.9
19	47	Male	C	Ss	Tub2>sig/por2	AA	–	–	13.9	56.7	13
20	62	Male	C	Ss	Tub2=por1/por1	AD	–	–	15.2	52.3	4.1
21	64	Male	A	Se	Por1/por1	AA	–	ni	17.8	63.3	11.5
22	62	Male	C	Se	Por1/por1	AD	–	+ / –	11.5	63.5	15.5
23	56	Male	Mid	Se	No/por1>tub2	AA	–	–	17.1	69.3	22.8

[a] Double stainings of DAPI and EBER were available

Most common abnormalities of the p53 gene are missense mutations in exons 5–8 [18]. The mutant protein is known to be often resistant to degradation, and such stabilised protein can be detected immunohistochemically [18]. True overexpression of wild-type p53 is observed transiently after ionizing or UV radiation [18] and persistently in some virus-related tumours [19].

P53 abnormalities and DNA-ploidy alterations were considered to occur as relatively late events in tumourigenesis of conventional gastric carcinomas [15, 30], while p53 abnormalities were recently reported to be infrequent in EBV-positive gastric carcinomas even in an advanced stage [10, 17, 19, 24]. In the present study, we thus compared p53 immunoreactivity and its relationship to DNA-ploidy pattern and the depth of tumour invasion between EBV-positive and -negative gastric carcinomas of matched histological pattern. Additionally, downstream events of p53, such as incidence of apoptosis, mitosis and p21^{WAF1} protein expression [6] as well as DNA-ploidy pattern, were also examined to evaluate the function of p53 in each tumour.

Materials and methods

We used 23 EBV-positive and 19 EBV-negative gastric carcinomas, which were selected from the files of the First Department of Pathology, Shiga University of Medical Science. EBV infection was examined using in situ hybridization (ISH) for EBV-encoded small RNA (EBER). The 19 EBER-negative carcinomas were selected by the histological appearance common to EBV-associated gastric carcinomas (Fig. 1): (1) moderately differentiated tubular adenocarcinomas in the mucosa showing branching/anastomosing tubular pattern (lace pattern) with varying degrees of lymphoid infiltration in the stroma [31] and (2) poorly differentiated adenocarcinomas with heavy lymphoid infiltration, which were recognizable as GCLS, in the submucosa or deeper. None of these 19 EBER-negative carcinomas had a history of pre-operative chemotherapy or radiation therapy. Age, sex and histological findings in each case are shown in Table 1 and Table 2. All the materials were surgically resected, fixed in 10% buffered formalin for no longer than 5 days and embedded in paraffin, from which 4-µm serial sections were made. We described the location, histological type and the depth of invasion following the general rules of the Japanese Research Society for Gastric Cancer [12]. The tumours that were confined to the mucosa (m) or the submucosa (sm) were called "superficial" carcinomas, and those that invaded the muscularis propria (mp) or deeper were called "deeply invasive" carcinomas.

To detect EBER, we used Epstein-Barr virus-EBER kit (Kreatech Diagnostics, Amsterdam) following the manufacturer's instructions. In brief, 4-µm sections were digested with 2.5 µg/ml pepsin (pH 2.0) for 30 min at 37°C. After washing with Tris-buffered saline (TBS), the sections were hybridized with digoxigenin-labeled oligonucleotide probe for EBER (Kreatech Diagnostics) for 2 h at 37°C. After washing with TBS, the signals of EBER were detected using an alkaline phosphatase/anti-alkaline phosphatase system. Nuclear fast red was used for counterstaining. As a positive control for ISH, we used an epipharyngeal carcinoma in which EBV infection had already been demonstrated.

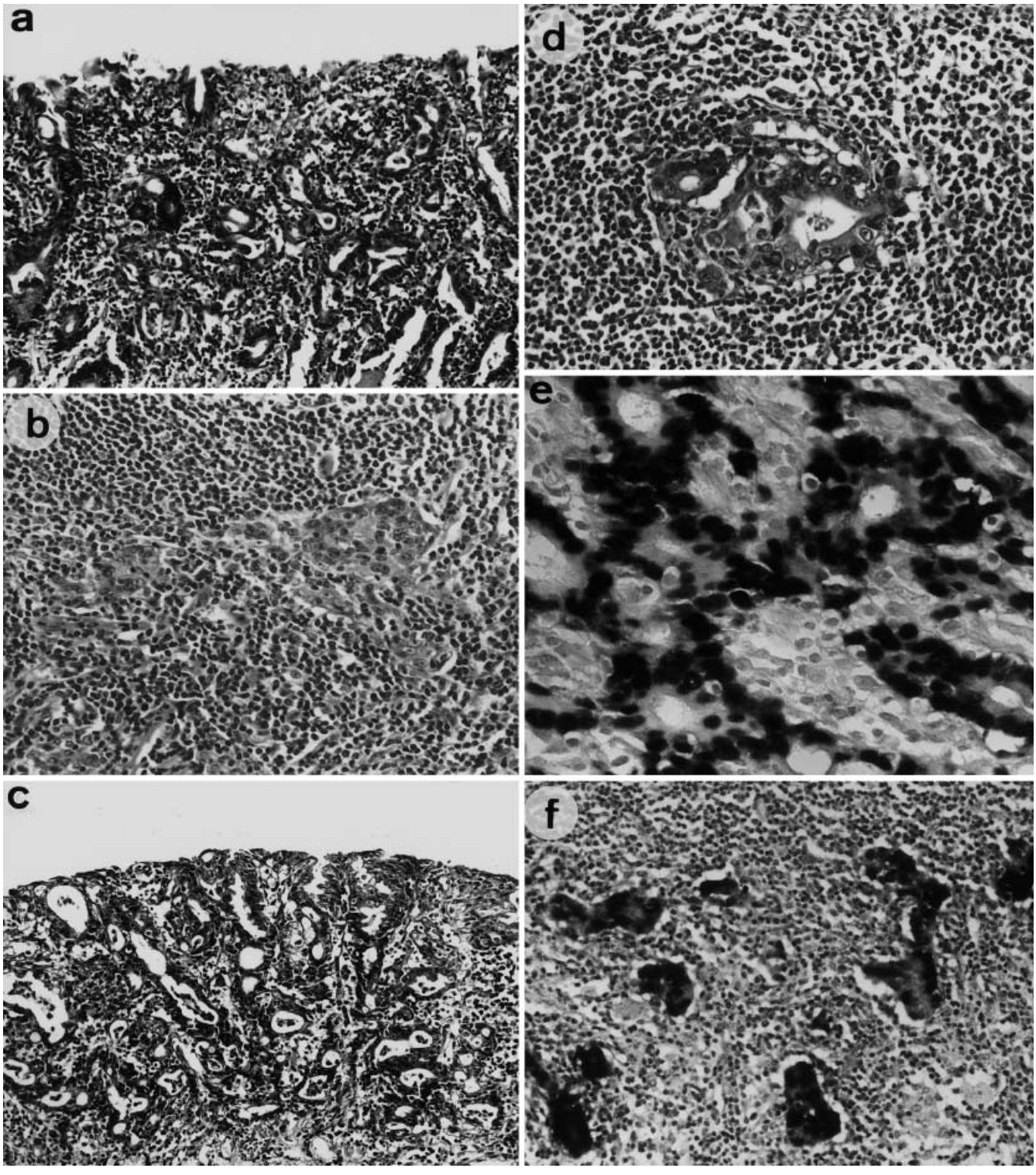

Fig. 1 Histological patterns of Epstein-Barr virus-encoded small RNA (EBER)-positive and -negative gastric carcinomas. **a** Intramucosal lesion of EBER-positive gastric carcinoma showing a lace pattern. Haematoxylin and eosin, ×75. **b** Extramucosal lesion of EBER-positive gastric carcinoma, demonstrating a gastric carcinoma with lymphoid stroma (GCLS). Haematoxylin and eosin, ×120. **c** EBER-negative gastric carcinoma showing lace pattern. Haematoxylin and eosin, ×75. **d** EBER-negative gastric carcinoma showing GCLS. Haematoxylin and eosin, ×120. **e**, **f** in situ hybridisation for EBER. Strong signals are in virtually all the nuclei of cancer cells and not in the non-neoplastic stromal cells. ×400 (**e**), ×120 (**f**)

Table 2 Epstein-Barr virus (EBV)-encoded small RNA (EBER)-negative gastric carcinomas showing similar histological patterns to the EBV-positive gastric carcinomas. *AI* apoptotic index, *MI* mitotic index, *C* cardiac region, *Mid* middle region, *A* antral region, *m* lamina propria, *sm* submucosa, *mp* muscularis propria, *ss* subserosa, *se* serosal exposure, *tub1* well differentiated tubular adenocarcinoma, *tub2* moderately differentiated tubular adnocarcinoma including "lace pattern", *por1* poorly differentiated adenocarcinoma of solid type. [gastric carcinoma with lymphoid stroma (GCLS) belongs to this category], *por2* poorly differentiated adenocarinoma of non-solid type, *sig* signet-ring cell carcinoma, *D* DNA diploidy, *AD* DNA diploiy with polyploidy, *AA* DNA aneuploidy, *no* no lesion, *nt* not tested, *ni* not informative

No.	Age	Sex	Site	Depth	Histology (m/deeper than sm)	DNA-ploidy pattern	p53 positivity	p21 expression	MI (/1000 cells)	Ki-67 (%)	AI (/1000 cells)
1	61	Male	A	M	Tub2 / no	AA	–	–	19.5	97	14.3
2	63	Female	A	M	Tub2/no	AD	–	–	5.2	45.8	4.63
3	61	Male	Mid	M	Tub2/no	AD	–	Ni	8.42	49.3	20.7
4	52	Male	Mid	M	Tub2/no	AA	+	–	13.3	70.7	11
5	67	Female	A	Sm	Tub2/tub2>por1	AD	–/+	–/–	20.5	61.1	19.4
6	54	Male	C	Sm	Tub2/tub2	AA	+	–	9.5	71.8	14
7	62	Male	Mid	Sm	Por1>tub2/por1	AA	–	–	22.8	57.4	20.4
8	54	Male	Mid	Sm	Tub2/por1	AD	+	–	12	64.9	14.4
9	71	Male	Mid	Sm	Tub1+tub2+por1/por1	AA	–	–	9.8	76.3	26.5
10	47	Female	CMid	Sm	Tub2/por2	AD	+	–	6.4	56.9	6
11	65	Female	Mid	Mp	Por1/por1	D	–	–	7.1	49.5	6
12	57	Male	A	Mp	No/por1	AA	+	–	14.8	86.5	12.5
13	77	Female	Mid	Mp	No/por1	AD	+	–	15.5	72.4	12.1
14	50	Male	Mid	Mp	Tub2/tub2	AA	–	+/–	19.8	55.1	19.8
15	68	Male	C	Ss	Por1+tub1/por1	AD	+	Ni	9.3	68.1	10.6
16	67	Male	Mid	Ss	No/por1	AA	+	–	17.4	53.3	23.2
17	55	Female	A	Ss	No/por1	D	+	–	11.8	53.2	14.9
18	81	Male	C	Se	Tub2/por1>por2	AA	+	Ni	29.7	52.5	21
19	41	Male	A	Se	No/por1	AD	+	Ni	22	70.7	12.8

To prepare nuclear suspension for DNA cytometry, we made two 50-µm thick sections in each case from which, after dewaxing and light hematoxylin staining, intramucosal and extramucosal tumour tissues were taken separately (if possible) under a stereoscopic microscope (Leica, MZ12, Bensheim). The tissue fragments were minced mechanically and treated with 2% Na–ethylene diamine tetraacetate in 0.1 M phosphate buffer for 60 min and then 200 µg/ml proteinase K (Merck, Darmstadt, Germany) for 30 min at 37°C and fixed in Carnoy's solution. Drop smears of isolated nuclei were made and stained with 50 ng/ml 4′,6-diamino-2-phenylindole (DAPI, Wako Pure Chemical, Osaka, Japan) [7]. For each sample, we measured nuclear DNA contents of at least 300 tumour cells and 50 lymphocytes (as an internal diploid control) with a fluorescence cytophotometer (P100, Nikon, Tokyo, Japan). In the DNA histograms, the stemline with the G_0/G_1 peak ranging from 1.8 C to 2.2 C and that with the same peak greater than 2.2 C were tentatively defined as DNA-diploidy and DNA-aneuploidy, respectively. Polyploidy was defined as the minor population of which the nuclear DNA contents exceeded three times as much as the G_0/G_1 peak DNA content of its stemline. We classified DNA-aneuploidy and DNA-diploidy with polyploid population as the "abnormal ploidy" and DNA-diploidy without polyploid population as the "normal ploidy".

To test the accuracy with which we identified the tumour cells, we also tried dual-colour analysis of EBER and DNA. To visualise the ISH signals of EBER on the nuclei during DNA cytofluorometry, we used tyramide signal-amplification system (TSA-Direct kit, NEN Life Science Products, Boston, Mass.) following the manufacturer's instructions. In brief, after digestion with 10 µg/ml proteinase K, the same probe as tissue sections were hybridised for 2 h at 37°C, washed and then treated with peroxidase-conjugated anti-digoxigenin antibody (Boehringer, Mannheim) for 2 h at 37°C. After washing, they were incubated with Fluorophore Tyramide in the kit at room temperature in a dark humid box for 10 min, followed by DAPI staining as described above. Specificity of signals was checked by the disappearance of rhodamine signals after RNase treatment for 1 h at 37°C. DNA contents of EBER-positive tumour cells and lymphocytes as the internal control were measured using two single-band filter blocks alternately: G-2E/C and UV-2B (Nikon) for rhodamine and DAPI, respectively. The DNA histograms were analysed as described above.

Immunohistochemical staining for p53, $p21^{WAF1}$ and Ki-67 was performed using monoclonal antibodies against p53 (DO-7, 1:100, Dako, Copenhagen, Denmark), $p21^{WAF1}$ (WAF1(Ab-1), 1:100, Calbiochem, Cambridge, Mass.), and Ki-67 (MIB-1, 1:100, Novocastra, Newcastle upon Tyne, U.K.) and a streptavidin–biotin detection system (Histofine, Nichirei Corporation, Tokyo, Japan) within 48 h after cutting to avoid the antigen deterioration. We did antigen retrieval at 121°C for 5 min in distilled water for p53 and microwave treatment (500 W) for 10 min and 30 min in citrate buffer at pH 6.0 for Ki-67 and $p21^{WAF1}$, respectively. As positive controls for p53 and $p21^{WAF1}$, we used a gastric carcinoma and a squamous cell carcinoma of the uterine cervix, respectively, in which immunoreactivity of p53 and $p21^{WAF1}$ had already been demonstrated. Non-neoplastic gastric surface epithelium was also used for the internal control of $p21^{WAF1}$ [3]. The staining was judged as negative after confirming the reproducibility of the negative results. If internal control for $p21^{WAF1}$ was not stained, such cases were regarded as "not informative". The germinal centres of normal lymphoid follicles in the same slides were used for the internal positive control of Ki-67.

As to p53 and $p21^{WAF1}$, we defined a tumour to be positive when 30% or more of the tumour cells stained positively. Ki-67-positive nuclei were counted in a total of at least 1000 cells, and the Ki-67 index was expressed as the number of positive tumour cells/1000 tumour cells. We counted the numbers of mitosis and apoptosis in at least 10 randomly selected fields in each tumour. The MIs and apoptotic indices (AIs) were expressed as the numbers of mitosis and apoptosis in 1000 tumour cells, respectively. Apoptotic cells were identified on haematoxylin–eosin slides by markedly condensed homogeneous nuclei with or without nuclear fragmentations [13].

The results were statistically analysed using the Chi-square test and Fisher's exact test. The differences with the *P* values smaller than 0.05 were considered to be significant.

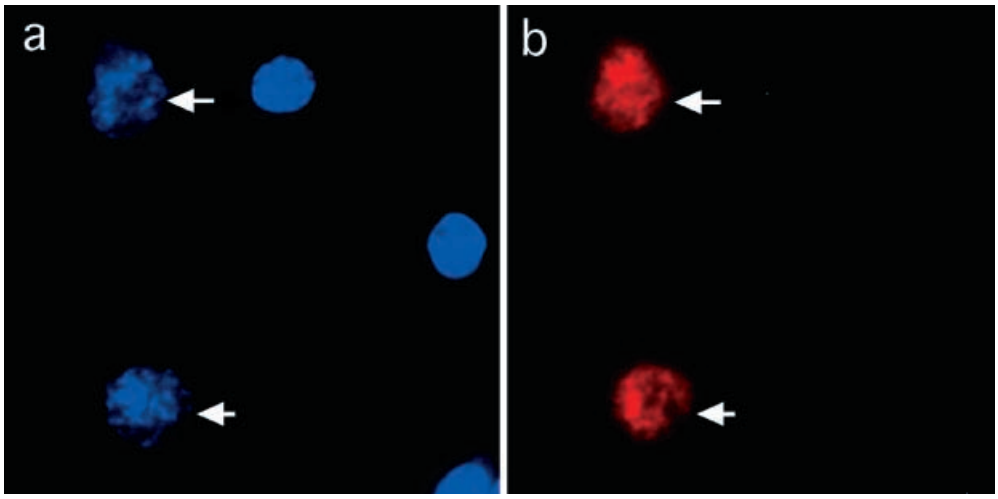

Fig. 2 Double staining of 4′,6-diamino-2-phenylindole (DAPI) and Epstein-Barr virus-encoded small RNA (EBER) on the smear preparation of the nuclei isolated from an EBER-positive gastric carcinoma. Of the DAPI-stained nuclei (**a**) larger ones of cancer cells (*arrows*) have positive rhodamine signals of EBER and (**b**) smaller ones of normal lymphocytes do not, ×600

Table 3 Distribution of DNA-ploidy pattern in Epstein-Barr virus-encoded small RNA (EBER)-positive and -negative gastric carcinomas. *AA* aneuploidy, *AD* diploidy with polyploidy, *D* diploidy

		Total	AA (%)	AD (%)	D (%)
EBER-positive	Total	23	8 (34.8)	11 (47.8)	4 (17.4)
	Superficial	13	4 (30.8)	6 (46.2)	3 (23)
	Deeply invasive	10	4 (40)	5 (50)	1 (10)
EBER-negative4	Total	19	9 (47.4)	8 (42.1)	2 (10.5)
	Superficial	10	5 (50)	5 (50)	0
	Deeply invasive	9	4 (44.4)	3 (33)	2 (22.3)

Results

Clinicopathological data of EBER-positive and -negative tumours are shown in Table 1 and Table 2, respectively. The average age of the patients made little difference between the EBER-positive and -negative groups: 58 years and 55 years, respectively. Both groups showed male predominance; the male to female ratios were 22:1 and 13:6 in EBER-positive and negative groups, respectively. The EBER-positive tumours were preferentially located in the cardiac (C) region; 17 (74%) of the 23 EBER-positive tumours and 4 (21%) of the 19 EBER-negative tumours were located in the C region (P=0.0029). Most of the EBER-positive tumours displayed characteristic histologies as described in the materials and methods section (Fig. 1). The histological patterns unusual for EBV-associated gastric carcinomas were encountered in cases 3, 9, 15 and 19. However, the lace pattern and/or GCLS were partly detected in these cases (Table 1). Signals of EBER were confined to the nuclei of tumour cells and diffusely distributed in the tumour areas (Fig. 1e, f). Rhodamine signals of EBER were also confined to the tumour cells on the smear slides with double staining for EBER and DAPI (Fig. 2).

DNA-ploidy patterns of the tumours examined are shown in Table 1, Table 2 and Table 3. In the seven cases asterisked in Table 1, we succeeded in double stainings DNA and EBER, which enabled us to measure the DNA contents exclusively of EBER-positive tumour cells. In these seven cases, the DNA-ploidy patterns of EBER-positive nuclei were very similar to those of the nuclei that were morphologically selected by their atypia with simple DAPI staining (Fig. 3). The incidences of aneuploidy/abnormal ploidy in EBER-positive and -negative tumours were 35%/83% and 47%/90%, respectively (Table 3). There was no statistically significant difference in the incidence of aneuploidy or abnormal ploidy between the two groups and between the superficial and the deeply invasive tumours in each group.

Ki-67 index, MI and AI are shown in Table 1 and Table 2. There was little difference in these indices between the EBER-positive and -negative groups. The MI correlated with aneuploidy. It was statistically significant in the EBER-positive group (P=0.0115) and not statistically significant in the EBER-negative group (P=0.0644). There were few correlations among p53 immunoreactivity, Ki-67 index, MI and AI in either group.

The results on p53 immunoreactivity are shown in Table 4. Six (26%) of the 23 EBER-positive tumours and 12 (63%) of the 19 EBER-negative ones were p53-positive. The incidence of p53-positive tumours was significantly lower in the EBER-positive group than in the EBER negative one (P=0.0277). This tendency became clearer when it was compared within deeply invasive tumours. Ten percent of the EBER-positive and 78% of the EBER-negative ones were p53-positive (P=0.0109), while in superficial tumours the incidence of p53-positive tumours made little difference between the EBER-positive and -negative groups (P=0.6850). These tendencies remained unchanged when the tumours were limited to those of the abnormal ploidy pattern (Table 4). p53-positive tumours in the EBER-negative group tended to

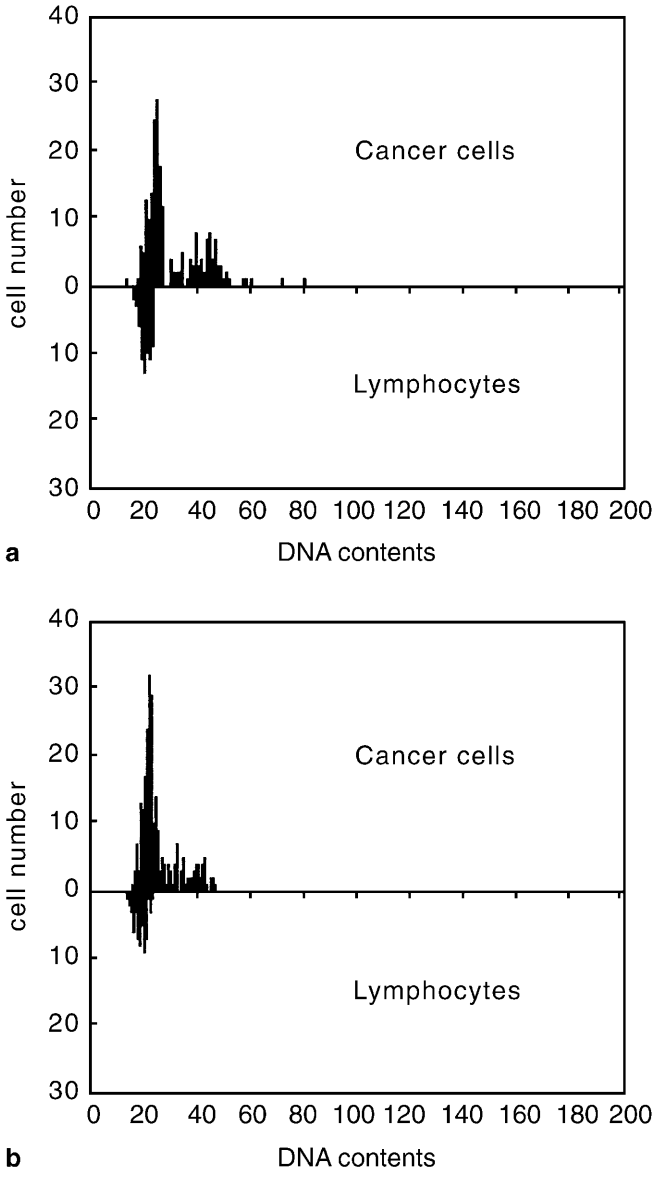

Fig. 3 DNA-ploidy pattern of the extramucosal part of an Epstein-Barr virus-encoded small RNA (EBER)-positive tumour (case 18 in Table 1). The DNA-ploidy patterns were very similar between the EBER-positive nuclei (**a**) and the nuclei morphologically selected by their atypia (**b**). They commonly show small shifts of G_0/G_1 peak from the 2 C standard

show homogeneous and strong immunoreactivity (Fig. 4a), while those in the EBER-positive tumours tended to show sporadic and relatively weak staining (Fig. 4b).

Immunoreactivity of p21*WAF1* is shown in Table 1, Table 2 and Table 5. Four (80%) of the five p53-positive, EBER-positive, superficial tumours were p21*WAF1* positive (Fig. 4c), while none of the five p53-positive, EBER-negative superficial tumours were p21*WAF1* positive (P=0.0476). p21*WAF1*-positive cells were mostly distributed in the superficial part of the intramucosal lesions, and the positive nuclei were quite sparse or absent

Table 4 P53-immimoreactivity in Epstein-Barr virus-encoded small RNA (EBER)-positive and -negative tumours. Numbers in parentheses indicate p53 immunoreactivity in the tumours of abnormal ploidy pattern

		EBER+	EBER–	*P* value
Superficial	p53(+)	5 (5)	5 (5)	
	p53(–)	8 (5)	5 (5)	
	Total	13 (10)	10 (10)	0.685
Deeply invasive	p53(+)	1 (1)	7 (6)	
	p53(–)	9 (8)	2 (1)	
	Total	10 (9)	9 (7)	0.0109 (0.0087)

Table 5 Relationship of p21*WAF1* expression to p53 immunoreactivity in superficial tumours. *EBER* Epstein-Barr virus-encoded small RNA

	EBER(+)		EBER(–)	
	(a) p53(+)*, **	(b) p53(–)	(c) p53(+)	(d) p53(–)
p21(+)	4	1	0	0
p21(–)	1	7	5	5
Total	5	8	5	5

*P=0.0319 for a–b
**P=0.0476 for a–c

in the submucosa or deeper in all the p21*WAF1*-positive tumours except in case 8 of Table 1, which were diffusely positive in the entire lesion.

Discussion

This is the first report on the DNA-ploidy pattern of EBV-positive gastric carcinomas. Because of the abundance of lymphoid stroma, we used static cytofluorometry that enabled us to measure the DNA contents of individual cells, simultaneously differentiating tumour cells from lymphocytes by their nuclear morphology. We further tried a dual-colour analysis of EBER and DNA on the smear slides to confirm the accuracy of morphological identification of tumour cells. But ISH signals detected as fluorescence were too dim for this purpose without enzyme–histochemical signal amplification. We hence applied the tyramide signal-amplification system [1, 14] to the dual-colour analysis to measure the DNA contents exclusively of EBER-positive tumour cells. Another merit of static cytofluorometry is an ability to detect small polyploid populations that cannot be detected by the usual flow-cytometric analysis. It is important to distinguish DNA diploidy with polyploidy from that without polyploidy because the presence of polyploidy is also considered to reflect chromosomal instability, possibly reflecting near-diploid aneuploidy at the chromosome level [29].

We found that the DNA-ploidy pattern was similar between EBER-positive and –negative groups of histo-

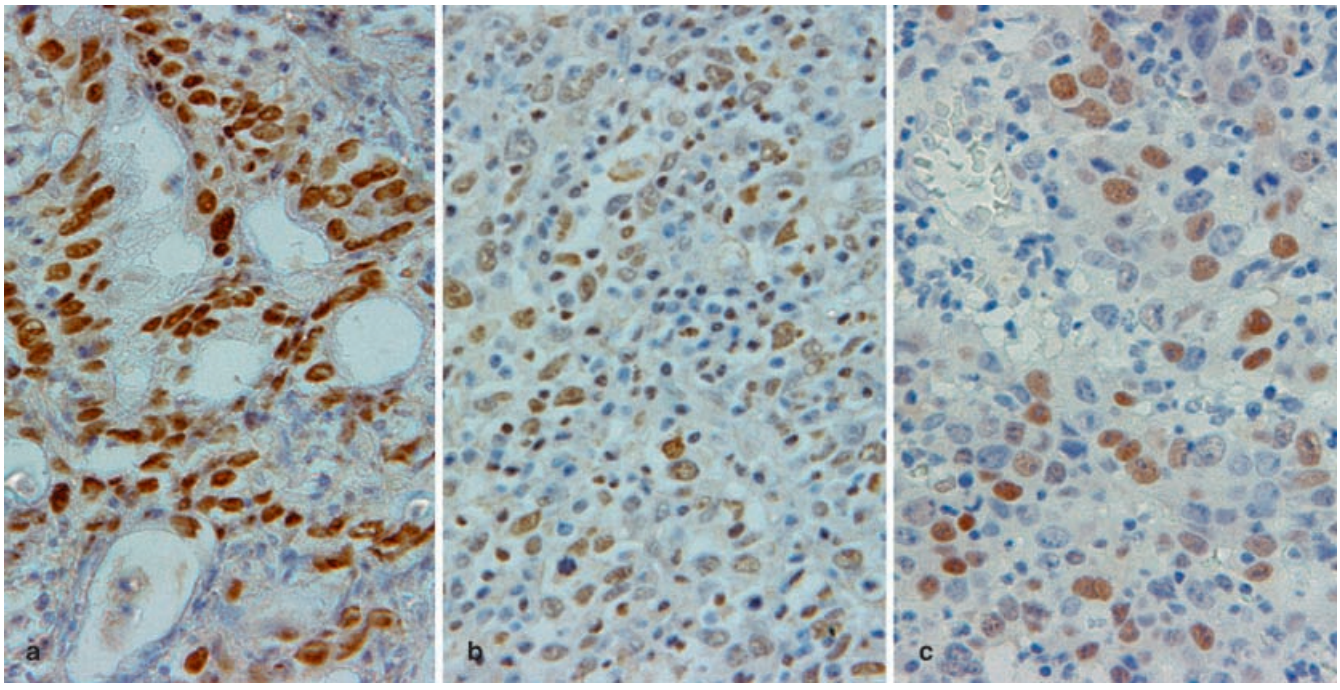

Fig. 4 Immunohistochemistry for p53 and p21^{WAF1}. **a** A p53-positive, EBER-negative superficial carcinoma (case 8 of Table 2). **b** A p53-positive, EBER-positive superficial carcinoma (case 7 of Table 1). This tumour was also positive for p21^{WAF1} (**c**). Its p53 immunoreactivity is less homogeneous and weaker than that of the EBER-negative tumour

logically matched gastric carcinomas and that the incidence of DNA aneuploidy was lower in both EBER-positive and –negative groups than that of conventional gastric carcinomas, which was reported to be around 70% [8, 21, 34]. This lower incidence of DNA aneuploidy seems to be a common characteristic of tumours showing the lace pattern and/or GCLS regardless of EBV infection in the tumour.

It was reported that enhanced cell proliferation and the emergence of polyploidy and aneuploidy were closely related to p53 abnormalities, which may elicit the disturbance of checkpoint function [2, 4]. We thus compared the relationship of p53 immunoreactivity with DNA-ploidy pattern and cell proliferative activity between the EBER-positive and –negative groups. We confirmed thereby that the incidence of p53-positive tumours was significantly lower in EBER-positive than in EBER-negative tumours as already noted [10, 17, 19, 24], although the previous reports did not match the depth of tumour invasion and histological type between the EBER-positive tumours and their control groups. We found that this difference was mostly ascribed to the deeply invasive tumours and was not observed in the superficial ones (Table 4). Because there was little difference in the immunoreactivity of p53 between the intramucosal and the extramucosal parts in most of the individual tumours examined (Table 1 and Table 2), it is unlikely that p53 immunoreactivity had disappeared during tumour progression. Rather, in EBER-positive tumours, the p53-negative tumours may have invaded the deeper part more readily than the p53-positive ones.

In this study, we regarded not only DNA aneuploidy but also DNA diploidy with polyploidy as abnormal ploidy patterns. This abnormal ploidy pattern accounted for more than 80% of the tumours, whether they were EBER-positive or -negative. Most of the p53-positive tumours we examined showed the abnormal ploidy pattern in both EBER-positive and -negative groups, being consistent with the previous reports [11, 15, 30]. In the deeply invasive tumours of the abnormal ploidy pattern, however, p53-positive tumours were much less frequent in the EBER-positive group than in the EBER-negative one (Table 5), although the incidence of the abnormal ploidy pattern made little difference between these groups as mentioned above. These findings of the EBER-positive group may be explained by abnormalities of the G_2/M checkpoint function that are independent of p53, such as direct suppression of the G_2/M checkpoint function by a subset of EBV latent gene products [25, 32].

In superficial tumours of the abnormal ploidy pattern, there was no difference in the incidence of p53-positive tumours between the EBER-positive and -negative groups (Table 5). Interestingly, however, some effects of p53 were different between them; in EBER-positive superficial tumours, most of the p53-positive tumours were p21^{WAF1}-positive, whereas, in EBER-negative ones, none of the p53-positive tumours examined were p21^{WAF1}-positive. The former pattern can be explained by the overexpression of wild-type p53, while the latter pattern is consistent with the presence of mutant p53, though it was reported that p21^{WAF1} expression was not always linked to p53 expression [3]. This explanation is supported by the

pattern of p53 immunoreactivity; it was weaker and heterogeneous in the EBER-positive group and strong and homogeneous in the EBER-negative group (Fig. 4). The former and the latter patterns were observed in tumours with the absence and the presence of the p53 gene mutation, respectively [19, 24]. The $p21^{WAF1}$ possibly induced by overexpression of wild-type p53 [6], however, did not appear to cause G_1 arrest [28] or suppression of cell proliferation [26] because there was no significant difference in Ki-67 index, MI or AI between the EBER-positive and -negative tumours. Thus, the possible overexpression of p53 may be secondary to the DNA damage elicited by viral gene products. Such normal responses of p53 seemed to be retained in about one-third of the superficial tumours and mostly lost in the deeply invasive tumours, reflecting tumour progression. This progression may be a reason why the p53-negative tumours selectively invaded the deeper part of gastric wall in the EBER-positive group.

Our results imply that the role of p53 in tumourigenesis is different between EBER-positive and -negative groups, reflecting at least two alternative transforming pathways. P53 mutation possibly plays a minor and a crucial role in the development of EBV-positive and -negative gastric carcinomas, respectively. This may be related to the favourable outcome of EBV-positive gastric carcinomas. To prove this hypothesis, we must examine p53 gene mutation in the tumours used in the present study.

References

1. Bobrow MN, Harris TD, Shaughnessy KJ, Litt GJ (1989) Catalyzed reporter deposition, a novel method of signal amplification. Application to immunoassays. J Immunol Methods 125:279–285
2. Carder P, Wyllie AH, Purdie CA, Morris RG, White S, Piris J, Bird CC (1993) Stabilized p53 facilitates aneuploid clonal divergence in colorectal cancer. Oncogene 8:1397–1401
3. Craanen ME, Blok P, Offerhaus GJA, Meijer GA, Dekker W, Kuipers EJ, Meuwissen SGM (1999) $p21^{Waf1/Cip1}$ expression and the p53/MDM2 feedback loop in gastric carcinogenesis. J Pathol 189:481–486
4. Cross SM, Sanchez CA, Morgan CA, Schimke MK, Ramel S, Idzerda RL, Raskind WH, Reid BJ (1995) A p53-dependent mouse spindle checkpoint. Science 267:1353–1356
5. Dasika GK, Lin SC, Zhao S, Sung P, Tomkinson A, Lee EY (1999) DNA damage-induced cell cycle checkpoints and DNA strand break repair in development and tumorigenesis. Oncogene 18:7883–7899
6. El-Deiry WS, Tokino T, Velculescu VE, Levy DB, Parsons R, Trent JM, Lin D, Mercer WE, Kinzler KW, Vogelstein B (1993) WAF1, a potential mediator of p53 tumor suppression. Cell 75:817–825
7. Hamada S, Fujita S (1983) DAPI staining improved for quantitative cytofluorometry. Histochemistry 79:219–226
8. Hattori T (1993) DNA ploidy pattern and cell kinetics. In: Nishi M, Ichikawa H, Nakajima T, Maruyama K, Tahara E (eds) Gastric cancer. Springer, Berlin Heidelberg New York, pp 184–195
9. Hattori T, Hosokawa Y, Fukuda M, Sugihara H, Hamada S, Takamatsu T, Nakanishi K, Tsuchihashi Y, Kitamura T, Fujita S (1984) Analysis of DNA ploidy patterns of gastric carcinomas of Japanese. Cancer 54:1591–1597
10. Hsieh LL, Lin PL, Chen TC, Ou JT (1998) Frequency of Epstein-Barr virus-associated gastric adenocarcinoma in Taiwan. Cancer Lett 129:125–129
11. Ichiyoshi Y, Oiwa H, Tomisaki S, Sakaguchi Y, Ohno S, Maehara Y, Sugimachi K (1997) Overexpression of p53 is associated with growth pattern and prognosis in advanced gastric cancer. Hepatogastroenterology 44:546–553
12. Japanese Research Society of Gastric Cancer (ed) (1993) The general rules for the gastric cancer study, 1st edn. Kanehara Press, Tokyo
13. Kerr JFR, Wyllie AH, Currie AR (1972) Apoptosis: a basic biological phenomenon with wide-ranging implications in tissue kinetics. Br J Cancer 26:239–257
14. Kerstens HMJ, Poddighe PJ, Hanselaar AGJM (1995) A novel in situ hybridization signal amplification method based on the deposition of biotinylated tyramide. J Histochem Cytochem 43:347–352
15. Kitayama Y, Sugimura H, Tanaka M, Nakamura S, Kino I (1995) Expression of p53 and flow cytometric DNA analysis of isolated neoplastic glands of the stomach: an application of the gland isolation method. Virchows Arch 426:557–562
16. Korenaga D, Haraguchi M, Okamura T, Baba H, Saito A, Sugimachi K (1989) DNA ploidy and tumor invasion in human gastric cancer. Arch Surg 124:314–318
17. Kume T, Oshima K, Shinohara T, Takeo H, Yamashita Y, Shirakusa T, Kikuchi M (1999) Low rate of apoptosis and overexpression of bcl-2 in Epstein-Barr virus-associated gastric carcinoma. Histopathology 34:502–509
18. Lane DP (1994) p53 and human cancers. Br Med Bull 50:582–599
19. Leung SY, Chau KY, Yuen ST, Chu KM, Branicki FJ, Chung LP (1998) P53 overexpression is different in Epstein-Barr virus-associated and Epstein-Barr virus-negative carcinoma. Histopathology 33:311–317
20. Lin D, Shields MT, Ullrich SJ, Appella E, Mercer WE (1992) Growth arrest induced by wild-type p53 protein blocks cells prior to or near the restriction point in late G_1 phase. Proc Natl Acad Sci U S A 89:9210–9214
21. Macartney JC, Camplejohn RS, Powell G (1986) DNA flow cytometry of histological material from human gastric cancer. J Pathol 148:273–277
22. Moritani S, Kushima R, Sugihara H, Hattori T (1996) Phenotypic characteristics of Epstein-Barr virus-associated gastric carcinomas. J Cancer Res Clin Pathol 122:750–756
23. Oda K, Tamaru J, Takenouchi T, Mikata A, Nunomura M, Saitoh N, Sarashina H, Nakajima N (1993) Association of Epstein-Barr virus with gastric carcinoma with lymphoid stroma. Am J Pathol 143:1063–1071
24. Ojima H, Fukuda T, Nakajima T, Nagamachi Y (1997) Infrequent overexpression of p53 protein in Epstein-Barr virus-associated gastric carcinomas. Jpn J Cancer Res 88:262–266
25. Parker GA, Touitou R, Allday MJ (2000) Epstein-Barr vitus EBNA3C can disrupt multiple cell cycle checkpoints and induce nuclear division divorced from cytokinesis. Oncogene 19:700–709
26. Rousseau D, Cannella D, Boulaire J, Fitzgerald P, Fotedar A, Fotedar R (1999) Growth inhibition by CDK-cyclin and PCNA binding domains of p21 occurs by distinct mechanisms and is regulated by ubiquitin–proteasome pathway. Oncogene 18:4313–4325
27. Saiki Y, Ohtani H, Naito Y, Miyazawa M, Nagura H (1996) Immunophenotypic characterization of Epstein-Barr virus-associated gastric carcinoma: massive infiltration by proliferating $CD8^+$ T-lymphocytes. Lab Invest 75:67–76
28. Sherr CJ, Roberts JM (1999) CDK inhibitors: positive and negative regulators of G1-phase progression. Genes Dev 13:1501–1512
29. Sugihara H, Hattori T, Fukuda M, Katsura K, Fujita S (1993) Progression of signet ring cell carcinomas in the human stomach. Cancer 71:1938–1947

30. Tamura G, Kihana T, Nomura K, Terada M, Sugimura T, Hirohashi S (1991) Detection of frequent p53 gene mutations in primary gastric cancer by cell sorting and polymerase chain reaction single-strand conformation polymorphism analysis. Cancer Res 51:3056–3058
31. Uemura Y, Tokunaga M, Arikawa J, Yamamoto N, Hamasaki Y, Tanaka S, Sato E, Land CE (1994) A unique morphology of Epstein-Barr virus-related early gastric carcinoma. Cancer Epidemiol Biomarkers Prev 3:607–611
32. Wade M, Allday MJ (2000) Epstein-Barr virus suppresses a G2/M checkpoint activated by genotoxins. Mol Cell Biol 20:1344–1360
33. Watanabe H, Enjoji M, Imai T (1976) Gastric carcinoma with lymphoid stroma. Cancer 38:232–243
34. Yonemura Y, Sugiyama K, Fujimura T, Aretxabala X, Kamata T, Kosaka T, Yamaguchi A, Miwa K, Miyazaki I (1988) Correlation of DNA ploidy and proliferative activity in human gastric cancer. Cancer 62:1497–1502

Virchows Arch (2002) 440:376–380
DOI 10.1007/s00428-001-0575-8

ORIGINAL ARTICLE

**Masaki Miyamoto · Ken Haruma · Toru Hiyama
Tomoari Kamada · Hiroshi Masuda · Fumio Shimamoto
Kazuhiko Inoue · Kazuaki Chayama**

High incidence of B-cell monoclonality in follicular gastritis: a possible association between follicular gastritis and MALT lymphoma

Received: 23 May 2001 / Accepted: 23 October 2001 / Published online: 26 January 2002
© Springer-Verlag 2002

Abstract Many studies have indicated a close association between gastric mucosa-associated lymphoid tissue (MALT) lymphoma and *Helicobacter pylori* (*Hp*) infection. Follicular gastritis (FG), a rare type of gastritis, is also closely associated with *Hp* infection and histologically similar to MALT lymphoma. However, there are few studies investigating the relationship between FG and MALT lymphoma. To clarify the issue, we examined the B-cell monoclonality in FG by immunoglobulin heavy chain (IgH) gene rearrangement. Seventy FG patients (all *Hp*-positive, 23 males and 47 females, median age 33 yr) were investigated; 70 age-and gender-matched non-FG *Hp*-positive controls and 24 non-FG *Hp*-negative controls were also examined. Two gastric biopsies, one from the antrum and one from the corpus, were obtained from each patient. DNA was extracted from formalin-fixed, paraffin-embedded biopsy specimens. IgH gene rearrangement was examined by semi-nested polymerase chain reaction (PCR). In the antral mucosa, monoclonal B-cell populations were detected in 19 (32%) of 60 FG, in 6 (10%) of 60 *Hp*-positive controls, and in none of 20 *Hp*-negative controls. In the corporal mucosa, monoclonal B-cell populations were detected in 14 (30%) of 47 FG, in 6 (11%) of 54 *Hp*-positive controls, and in none of 20 *Hp*-negative controls. The incidence of monoclonal B-cell populations in the FG patients was higher than in both *Hp*-positive and *Hp*-negative controls ($P<0.05$). The monoclonal B-cell populations disappeared after successful *Hp* eradication in 8 of 8 FG patients examined. These data suggest that FG may be strongly associated with MALT lymphoma, and that *Hp* eradication therapy may be indicated in FG.

Keywords Follicular gastritis · Immunoglobulin heavy chain · B-cell monoclonality · PCR

M. Miyamoto · T. Hiyama · T. Kamada · H. Masuda · K. Chayama
First Department of Internal Medicine,
Hiroshima University School of Medicine, Hiroshima, Japan

K. Haruma (✉)
Division of Gastroenterology, Department of Internal Medicine,
Kawasaki Medical School, 577 Matsushima,
Kurashiki 701-0192, Japan
e-mail: kharuma@med.kawasaki-m.ac.jp
Tel.: +81-86-4621111, Fax: +81-86-4621199

F. Shimamoto
Department of Anatomical Pathology,
Hiroshima University Hospital, Hiroshima, Japan

K. Inoue
Department of Internal Medicine, Matsue Red Cross Hospital,
Matsue, Japan

Introduction

Recent reports have described an increasing incidence of malignant lymphoma in Western countries [2, 7, 28]. However, the pathogenesis and prevention of this disease remain unclear. Gastric mucosa-associated lymphoid tissue (MALT) lymphoma is notable for its strong association with *Helicobacter pylori* (*Hp*) infection and as a premalignant lesion of malignant lymphoma [16, 17].

Isaacson first proposed the entity "malignant B-cell lymphoma of mucosa-associated lymphoid tissue" [16]. This tumor has a characteristic morphology corresponding to a low-grade lymphoma and includes lesions that were once referred to as "reactive lymphoreticular hyperplasia" of the stomach. Gastric MALT lymphoma arises from mucosal lymphoid tissue that is acquired as a result of chronic inflammation, chiefly caused by *Hp* infection [17]. B-cell monoclonality is detected in 80 to 90% of MALT lymphomas by immunoglobulin heavy chain (IgH) gene rearrangements [27].

Follicular gastritis (FG) is defined as a chronic gastritis in which there are large numbers of prominent lymphoid follicles in addition to a mononuclear infiltrate [9]. It shows no lymphoepithelial lesions and no abnormal composition of the lymphoid infiltrate. Although FG is strongly associated with *Hp* infection [1, 4] and is histologically similar to MALT lymphoma, there are few studies investigating the relationship between FG and MALT lymphoma. [3, 11, 26] Therefore, we addressed this issue by examining the IgH gene rearrangements to clarify whether FG is a precursor of MALT lymphoma.

Patients and methods

Patients

Seventy FG patients were selected from Hiroshima University Hospital and its affiliated hospitals between January 1990 and December 2000 (23 males and 47 females with a median age of 33 years; range, 13–59). Seventy age-and gender-matched non-FG *Hp*-positive patients and 24 non-FG *Hp*-negative patients were chosen at random from the medical records as controls. All subjects underwent upper gastrointestinal endoscopy and were evaluated *Hp* infection by histologic and serologic studies. No patient had any localized lesions, such as peptic ulcers or malignancies. Informed consent was obtained from all patients prior entry into the study. Out of 70 FG patients, 18 received *Hp* eradication therapy.

DNA extraction

Sections (4 µm thick) were prepared from formalin-fixed and paraffin-embedded gastric biopsy specimens. The DNA was extracted from the tissues with 20 µl of extraction buffer (100 mM Tris-HCl, 2 mM ethylene diamine tetraacetic acid, pH 8.0, 400 µg/ml of proteinase K) and incubated at 55°C overnight. The tubes were boiled for 7 min to inactivate the proteinase K, and then 2 µl of these extracts was used for the polymerase chain reaction (PCR) amplifications.

IgH gene rearrangements

Analysis of IgH gene rearrangements was performed using semi-nested PCR according to the method of Ono et al. with some modification [22]. Briefly, each 25-µl reaction mixture contained 1 X PCR buffer II [8.0 mM Tris-HCl (pH 8.3), 40 mM KCl] (Perkin-Elmer, Branchburg, N.J., USA), 4 mM $MgCl_2$, 0.3 mM of each deoxynucleotide triphosphate, 100 pmol of each primer, 2 µl of genomic DNA, and 1.25 units of Taq Gold DNA polymerase (Perkin-Elmer). Each PCR cycle consisted of 2 min of denaturation at 95°C, 1 min of annealing at 55°C, and 2 min of extension at 72°C. The sequences of the primers were: for the V region, 5′-ACA′CGG′C(C/T)(G/C)′TGT′ATT′ACT′GT-3′ (termed FR3A); for the J region, 5′-TGA′GGA′GAC′GGT′GAC′C-3′ (termed LJH); and 5′-GTG′ACC′AGG′GTN′CCT′TGG′CCC′CAG-3′ (termed VLJH). The first PCR stage consisted of 30 cycles with primers LJH and FR3A. Two microliters of the first-stage PCR product was used as the template for the second-stage PCR, and 30 cycles were performed using primers VLJH and FR3A. The products of the second PCR stages were electrophoresed on 16% acrylamide gel and stained with ethidium bromide. The gel was photographed using Eagle Eye II (Stratagene, Cal., USA). In this assay, a monoclonal B-cell population is present if there is a single rearranged IgH gene, as indicated by a single 100-200 bp band. A polyclonal B-cell population is present if there are polyclonal rearrangements of IgH gene, which appears as a broadly smeared set of bands.

We analyzed the relationship between IgH gene rearrangements and the pathologic features. The pathologic features, which includes the grade of inflammation, activity, atrophy, and lymphoid follicles, were scored according to the updated Sydney System [9]. Activity (neutrophils), inflammation (mononuclear cells), and atrophy were graded on a scale of 0 to 3 (0: none, 1: mild, 2: moderate, 3: severe). The specimens were also examined for the prevalence of lymphoid follicles (0: absent, 1: present). We also analyzed the effects of *Hp* eradication on the IgH gene rearrangements in 18 FG patients after 1 year.

Statistical analysis

Statistical differences were evaluated using the chi-square test and Mann-Whitney U test. A value of $P<0.05$ was regarded as statistically significant. Data are expressed as the mean ±SE.

Table 1 Incidence of B cell monoclonality in follicular gastritis (*FG*) and non-FG patients

	Antrum	Corpus	Total
FG	19/60 (32%)[a,b]	14/47 (30%)[b, c]	26/60 (43%)[b, c]
non-FG (*HP*+)	6/60 (10%)	6/54 (11%)	10/60 (17%)
non-FG (*HP*–)	0/20 (0%)	0/20 (0%)	0/20 (0%)

[a] $P<0.01$ compared with non-FG (*Hp*+) patients
[b] $P<0.01$ compared with non-FG (*Hp*–) patients
[c] $P<0.05$ compared with non-FG (*Hp*+) patients

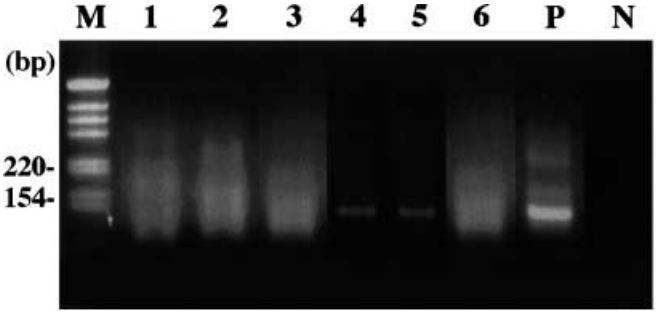

Fig. 1 Analysis of the immunoglobin heavy chain (IgH) gene rearrangement in samples from the follicular gastritis patients. The patient numbers are shown above the *lanes*. *P lane* contains a known gastric diffuse B-cell lymphoma sample, *N lane* contains PCR without template DNA, and *M lane* contains size markers. The DNA from patients 4 and 5 display a single band, indicating monoclonal B-cell populations, whereas the DNA from 1, 2, 3, and 6 display B-cell polyclonal patterns

Results

In the antral mucosa, 60 (87%) of 70 FG, 60 (87%) of 70 *Hp*-positive controls, and 20 (83%) of 24 *Hp*-negative controls were informative for the analysis of IgH gene rearrangements. In the antral mucosa, monoclonal B-cell populations were detected in 19 (32%) of 60 informative FG and in 6 (10%) of 60 informative *Hp*-positive controls, but in none of 20 informative *Hp*-negative controls. In the corporal mucosa, 47 (87%) of 54 FG, 54 (87%) of 62 *Hp*-positive controls, and 20 (83%) of 24 *Hp*-negative controls were informative for the analysis of IgH gene rearrangements. In the corporal mucosa, monoclonal B-cell populations were detected in 14 (30%) of 47 informative FG and in 6 (11%) of 54 informative *Hp*-positive controls, but in none of 20 informative *Hp*-negative controls. The incidence of monoclonal B-cell populations in the informative FG patients were significantly higher than in the informative *Hp*-positive controls and *Hp*-negative controls ($P<0.05$, for each). (Table 1; Fig. 1).

The pathologic features (according to the updated Sydney System) of FG were as follows: in the antrum, inflammation (B-cell monoclonal) (n=19) vs. B-cell polyclonal (n=41) 2.6±0.1 vs. 2.7±0.1, activity, 0.8±0.1 vs. 0.8±0.1, atrophy, 0.5±0.1 vs. 0.2±0.1, lymphoid follicles, 0.7±0.1 vs. 0.6±0.1; and in the corpus, inflammation (B-cell monoclonal (n=14) vs. B-cell polyclonal (n=33) 1.7±0.2 vs.1.7±0.1), activity, 0.5±0.1 vs. 0.6±0.1,

Table 2 Effect of *Hp* eradication on IgH rearrangements. *Hp* was successfully eradicated from all 18 FG patients. *M* monoclonal, *P* polyclonal

Before	After	Patients (*n*)
M	P	8
P	P	10

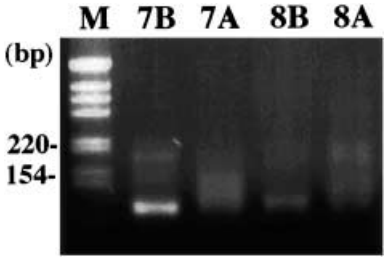

Fig. 2 Analysis of IgH gene rearrangement in follicular gastritis patients before and after *Helicobacter pylori* (*Hp*) eradication therapy. The patient numbers are shown above the *lane*. *B* before *Hp* eradication, *A* after *Hp* eradication, *M* size markers. The monoclonal B-cell populations disappeared after successful *Hp* eradication (*case 7. 8*)

atrophy, 0.1±0.1 vs. 01±0.0, lymphoid follicles, 0.4±0.1 vs. 0.2±0.1. The pathologic features of FG did not significantly differ between the cases with and without B-cell monoclonality.

The FG patients with B cell monoclonality were significantly older than those without B cell monoclonality (36.9±2.3 year vs. 29.2±2.1 year). On the other hand the gender ratio and the presence of other lesions were not significantly different in those with and without B cell monoclonality.

Eight FG patients with B-cell monoclonality received *Hp* eradication therapy. The monoclonal B-cell populations disappeared after successful *Hp* eradication in all eight FG patients (Table 2; Fig. 2). The histologic features improved with successful *Hp* eradication (Fig. 3). Ten FG patients who had a polyclonal B-cell infiltration also received *Hp* eradication therapy. The polyclonal B-cell populations remained after successful *Hp* eradication in all ten FG patients.

Discussion

This is a report describing the relationship between FG and MALT lymphoma including the significance of *Hp* eradication therapy for FG from the standpoint of IgH gene rearrangements. The incidence of identifying monoclonal B-cell populations in the gastric mucosa was higher in FG than in the *Hp*-positive controls and the *Hp*-negative controls. Successful *Hp* eradication therapy improved the B-cell monoclonality. Therefore, our data suggest that FG may be strongly associated with MALT lymphoma and that *Hp* eradication therapy may decrease the risk for MALT lymphoma.

Hp infects nearly one half of the world's population [17]. It is currently accepted that *Hp* plays a causative role not only in chronic gastritis, peptic ulcer disease, and gastric carcinoma, but also in gastric lymphoma, especially the MALT type [1, 14, 15, 17, 18, 29]. *Hp* infection is also considered to be the underlying cause of FG [10].

The analysis of IgH gene rearrangements in biopsy specimens by PCR can identify monoclonal B-cell populations [33]. Wan et al. reported that false-positive monoclonal bands were detected when the number of PCR

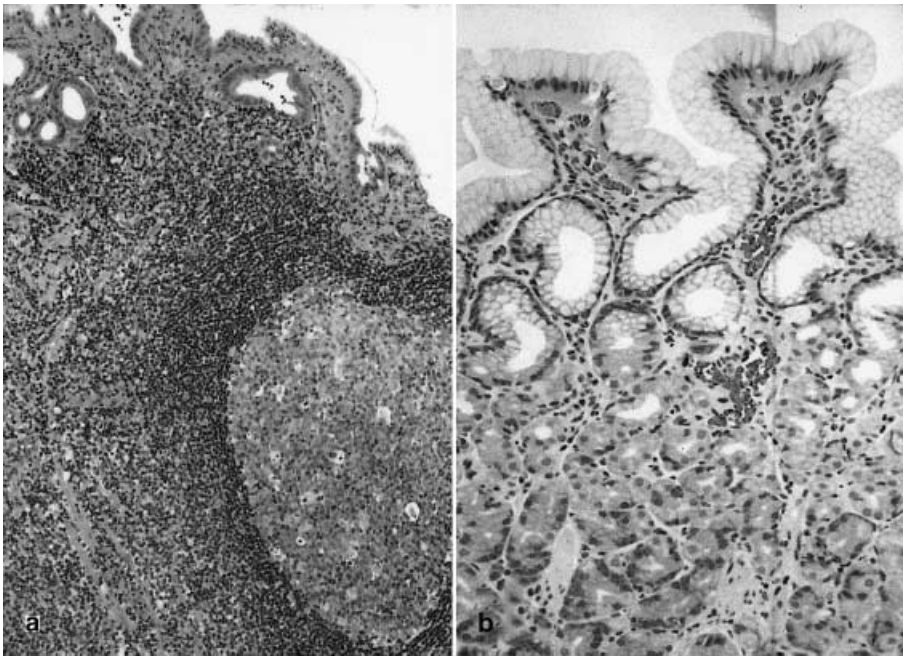

Fig. 3 Antral biopsy specimen showed lymphoid follicle formation and marked lymphoid aggregates before *Hp* eradication therapy (*case 7B*). The lymphoid follicle formation and marked lymphoid aggregates disappeared after the successful *Hp* eradication (*case 7A*)

"targets" (cell equivalents) was reduced to an average of six per sample [32]. Our group has reported that we could rule out this possibility since the DNA pattern did not change from a polyclonal-type to a monoclonal-type when relatively few lymphoid cells were analyzed [15]. During B-cell differentiation, the genes coding for the IgH and light chains rearrange to determine the structure of the Ig produced by the cell. This occurs through processes of deletion and splicing of DNA segments from the variable (V), diversity (D), joining (J), and constant regions of the gene to form unique coding sequences [6, 13]. The rearranged Ig gene has been shown to contain three hypervariable regions surrounded by framework regions which are well conserved [30]. These regions are called complementarity determining regions (CDR) I, II, and III [30]. The DNA sequence of CDR-III is unique to each IgH and characterizes the clonality of B-cell lineage cells. Detection of IgH gene rearrangements is thought to be helpful for distinguishing gastric lymphoma from reactive diseases [20]. Ono et al. also reported that B-cell monoclonality was detected in 88% of primary gastric lymphomas, whereas monoclonarity was not observed in reactive lymphoreticular hyperplasia, chronic gastritis (CG), or gastric ulcers [22].

Several authors have reported investigations into the incidence of B-cell monoclonality in *Hp*-associated gastritis [3, 11, 15, 26]. Calvert reported that B-cell monoclonality was detected in 11% (3/28) of *Hp*-associated gastritis [3]. El-Zimaity reported that the correct interpretation of clonality by PCR remains unclear, because B-cell monoclonality is observed not only in MALT lymphoma but also in *Hp*- associated gastritis. (MALT lymphoma: 88% (22/39), *Hp*-associated gastritis: 38% (15/39) [11]. Saxona et al. reported that B-cell monoclonality was common in *Hp* gastritis with lymphoid hyperplasia. (50%, 10/20) [26]. They also reported none of these patients had developed lymphoma (follow-up 21–44 months) and that B-cell monoclonality was a useful feature in favoring a reactive process.

In this study, the incidences of monoclonal B-cell populations both in the antrum and the corpus were significantly higher in the FG patients than in the *Hp*-positive controls and the *Hp*-negative controls. Nakamura et al. reported that IgH gene rearrangements were detected in 79% of *Hp*-associated gastritis patients who developed MALT lymphoma, but only in 21% of *Hp*-associated gastritis patients who did not [20]. The detection of B-cell monoclonality facilitates not only making the diagnosis, but also may be a predictive marker for the histologic genesis of gastric lymphoma. We could not confirm that FG was really a precursor of MALT lymphoma. However, our data suggest that FG may be strongly associated with MALT lymphoma among *Hp*-associated gastritis. In addition, *Hp* eradication therapy may be beneficial for FG patients, since the regression of FG has been observed after eradication [33]. Indeed, the monoclonal B-cell populations disappeared after successful eradication in our study.

There is accumulating evidence indicating that chronic inflammation can induce gene mutations, gene amplification, DNA strand breaks, deletions, or translocations in the affected cells [25]. In MALT lymphomas, various genetic alterations have been reported, such as mutations in the *p53* [10], c-*myc* [28], and *p16* genes [21], plus microsatellite instability [23] and chromosome translocations [8]. Further studies on such genetic changes in FG may clarify the relationship between FG and MALT lymphoma.

Atrophic gastritis and intestinal metaplasia are known as precursors of gastric cancer [18]. Recently, chemoprevention by *Hp* eradication therapy has been tried for gastric cancer. Uemura reported that *Hp* eradication inhibited the development of new gastric cancer after endoscopic resection of early gastric cancer [31]. Correa also reported that *Hp* eradication contributed to the chemoprevention of gastric dysplasia (gastric atrophy and / or intestinal metaplasia) [5]. In conclusion, our data suggest that FG may be strongly associated with MALT lymphoma and that the *Hp* eradication therapy may decrease the risk of developing MALT lymphoma. *Hp* eradication therapy for FG may be advisable, and long-term follow-up may be necessary to evaluate the results of therapy.

Acknowledgments We thank Dr. Masaaki Sumioka, Dr. Chiyuki Watanabe, Dr. Masaru Nakamura, Dr. Hiroyasu Yamada, Dr. Masaru Imagawa, Dr. Soichiro Kido, and Dr. Mitsuhiro Mihara for providing FG samples. We thank Dr. Takashi Nashisaka and Dr. Toshiyuki Fukuhara for their help in reviewing the pathology. This research project was supported in part by a grant from the Tsuchiya Memorial Medical Foundation, Hiroshima, Japan.

References

1. Blaser MJ (1990) *Helicobacter pylori* and the pathogenesis of gastroduodenal inflammation. J Infect Dis 161: 626–633
2. Broccia G, Cocco P, Casula P (2001) Incidence of non-Hodgkin's lymphoma and Hodgkin's disease in Sardinia, Italy: 1974–1993. Hematologica 86: 58–63
3. Calvert RJ, Evans PA, Randerson JA, Jack AS, Morgan GJ, Dixon MF (1996) The significance of B-cell clonality in gastric lymphoid infiltrates. J Pathol 180: 26–32
4. Correa P (1988) Chronic gastritis: a clinicopathological classification. Am J Gastroenterol 83: 504–509
5. Correa P, Fontham ET, Bravo JC, Bravo LE, Ruiz B, Zarama G, Realpe JL, Malcom GT, Li D, Johnson WD, Mera R (2000) Chemoprevention of gastric dysplasia: randomized trial of antioxidant supplements and anti-*Helicobacter pylori* therapy. J Natl Cancer 92: 1881–1888
6. Cossman J, Uppenkamp M, Sundeen J, Coupland R, Raffeld Ml (1988) Molecular genetics and the diagnosis of lymphoma. Ann Pathol Lab Med 112: 117–127
7. Davis DL, Blair A, Hoel DG (1993) Agricultural exposures and cancer trends in developed countries. Environ Health Perspect 100: 39–44
8. Dielamm J, Baens M, Wlodarska I, Stefanova-Ouzounova M, Hernandes JM, Hossfeld DK, Wolf-Peeters CD, Hagemeijer A, Berghe HV, Marynen P (1999) The apoptosis inhibitor gene *API2* and a novel 18q gene, *MLT*, are recurrently rearranged in the t (11; 18)(q21; q21) associated with mucosa-associated lymphoid tissue lymphomas. Blood 93: 3601–3609
9. Dixon MF, Genta RM, Yardley JH, Correa P, and the participants in the international workshop on the histopathology of gastritis (1996) Classification and grading of gastritis: the Updated Sydney System. Am J Surg Pathol 20: 1161–1181

10. Du M, Peng H, Singh N, Isaacson PG, Pan L (1995) The accumulation of *p53* abnormalities is associated with progression of mucosa-associated lymphoid tissue lymphoma. Blood 86: 4587–4593
11. El-Zimaity HM, El-Zaatari FA, Dore MP, Oweiss S, Gutierrez O, Yukusul M, Ramchntesingh J, Graham DY (1999) The differential diagnosis of early gastric mucosa-associated lymphoma: polymerase chain reaction and paraffin section immunophenotyping. Mod Pathol 12: 885–894
12. Genta RM, Lew GM, Graham DY (1993) Changes in the gastric mucosa following eradication of *Helicobacter pylori*. Mod Pathol 6: 281–289
13. Gulley ML, Ross DW (1991) Progress in molecular diagnosis of lymphoma and leukemia. Clin Biotechnol 3: 95–99
14. Hansson LE, Engstrand L, Nyren O, Evans DJ, Lindgren A, Bergstrom R, Andersson B, Athlin L, Bendtsen O, Tracz P (1993) *Helicobacter pylori* infection: independent risk indicator of gastric carcinoma. Gastroenterology 105: 1098–1103
15. Hiyama T, Haruma K, Kitadai Y, Miyamoto M, Tanaka S, Yoshihara M, Sumii K, Shimamoto F, Kajiyama G (2001) B-cell monoclonarity in *Helicobacter pylori*-associated chronic atrophic gastritis. Virchows Archiv 438: 232–237
16. Isaacson PG (1990) Lymphomas of mucosa-associated lymphoid tissue (MALT). Histopathology 16: 617–619
17. Isaacson PG (1995) The MALT lymphoma concept updated. Ann Oncol 6: 319–320
18. Kawaguchi H, Haruma K, Komoto K, Yoshihara M, Sumii K, Kajiyama G (1996) *Helicobacter pylori* infection is the major risk factor for atrophic gastritis. Am J Gastroenterol 91: 959–962
19. Marshall BJ (1993) *Helicobacter pylori:* a primer for 1994. Gastroenterology 105: 241–247
20. Nakamura S, Aoyagi K, Furuse M, Suekane H, Matsumoto T, Yao T, Sakai Y, Fuchigami T, Yamamoto I, Tsuneyoshi M, Fujishima M (1998) B-cell monoclonality precedes the development of gastric MALT lymphoma in *Helicobacter pylori*-associated chronic gastritis. Am J Pathol 152: 1271–1279
21. Neumeister P, Hoefler G, Beham-Schmid C, Schmidt H, Apfelbeck U, Schaider H, Linkesch W, Sill H (1997) Deletion analysis of the *p16* tumor suppressor gene in gastrointestinal mucosa-associated lymphoid tissue lymphomas. Gastroenterology 112: 1871–1875
22. Ono H, Kondo H, Saito D, Yoshida S, Shirai K, Yamaguchi H, Yokota T, Hosokawa K, Fukuda H, Hayashi S, Ochiai A, Ogura Y (1993) Rapid diagnosis of gastric malignant lymphoma from biopsy specimens: detection of immunoglobulin heavy chain rearrangement by polymerase chain reaction. Jpn J Cancer Res 84: 813–817
23. Peng H, Chen G, Du M, Singh N, Isaacson G, Pan L (1996) Replication error phenotype and *p53* gene mutation in lymphomas of mucosa-associated lymphoid tissue. Am J Pathol 148: 643–648
24. Peng H, Diss T, Isaacson PG, Pan L (1997) C-*myc* gene abnormalities in mucosa-associated lymphoid tissue (MALT) lymphomas. J Pathol 181: 381–386
25. Rosin MP, Anwar WA, Ward AJ (1994) Inflammation, chromosomal instability, and cancer: the schistosomiasis model. Cancer Res 54: 1929–1933
26. Saxena A, Moshynska O, Kanthan R, Bhutani M, Maksymiuk AW, Lukie BE (2000) Distinct B-cell clonal bands in *Helicobacter pylori* gastritis with lymphoid hyperplasia. J Pathol 190: 47–54
27. Sorrentino D, Ferraccioli GF, Avellini C, Vita SD, Avellini C, Beltrami CA, Labombarda A, Bernardis V, Biase FD, Trevisi A, Pivetta B, Boiocchi M, Bartoli E (1996) B-cell clonality and infection with *Helicobacter pylori:* implications for development of gastric lymphoma. Gut 38: 837–840
28. Swerdlow AJ, dos Santos Silva I, Reid A, Qiao Z, Brewster DH, Arrundale J (1998) Trends in cancer incidence and mortality in Scotland: description and possible explanations. Br J Cancer 77 Suppl 3: 1–55
29. The Eurogast study group (1993) An international association between *Helicobacter pylori* and gastric cancer. Lancet 34: 1359–1362
30. Tonegawa S (1983) Somatic generation of antibody diversity. Nature 302: 575–581
31. Uemura N, Mukai T, Okamoto S, Yamaguchi S, Mashiba H, Taniyama K, Sasaki N, Haruma K, Sumii K, Kajiyama G (1997) Effect of *Helicobacter pylori* eradication on subsequent development of cancer after endoscopic resection of early gastric. Cancer Epidemiol Biomarkers Prev 6: 639–642
32. Wan JH, Sykes PJ, Orell SR, Morley AA (1992) Rapid method for detecting monoclonality in B-cell lymphoma in lymph node aspirates using the polymerase chain reaction. J Clin Pathol 45: 420–423
33. Wotherspoon AC, Doglioni C, Diss TC, Pan L, Moschini A, Boni M, Isaacson PG (1993) Regression of primary low-grade B-cell gastric lymphoma of mucosa-associated lymphoid tissue type after eradication of *Helicobacter pylori*. Lancet 342: 575–577
34. Yamada M, Hudson S, Tounay O, Bittenbender S, Shane SS, Lange B, Tsujimoto Y, Caton A, Rovera G (1989) Detection of minimal disease in hematopoietic malignancies in the B-cell lineage by third complementarity determining region (CDR-3) specific probes. Proc Natl Acad Sci USA 86: 5123–5127

Virchows Arch (2002) 440:381–386
DOI 10.1007/s004280100527

ORIGINAL ARTICLE

Shigeki Sekine · Tatsuhiro Shibata · Yuko Yamauchi
Yukihiro Nakanishi · Tadakazu Shimoda
Michiie Sakamoto · Setsuo Hirohashi

β-Catenin mutations in sporadic fundic gland polyps

Received: 23 May 2001 / Accepted: 3 August 2001 / Published online: 19 September 2001
© Springer-Verlag 2001

Abstract Fundic gland polyp (FGP) is the most common gastric polyp. It occurs sporadically or in association with familial adenomatous polyposis (FAP). FAP patients carry germline mutations of the adenomatous polyposis coli (APC) gene, and previous studies have revealed frequent somatic mutations of the APC gene in FGPs associated with FAP. Although inactivation of the APC gene contributes to histogenesis of FGPs associated with FAP, this rarely happens in sporadic cases. Loss of the APC gene promotes abnormal accumulation of β-catenin, and mutation of GSK-3β phosphorylation sites in the β-catenin gene can have a similar effect. To elucidate the contribution of β-catenin gene mutation to the histogenesis of sporadic FGP, we analyzed β-catenin gene mutation in exon 3 in 45 FGP lesions obtained from 35 patients. Somatic mutations were found in 29 lesions: 28 were missense mutations and one was an in-frame deletion. All of the missense mutations were confined to the former two serine residues of the GSK-3β phosphorylation sites and their flanking residues (codons 32, 33, 34, 37). Analysis in cases with multiple FGPs revealed a different mutation in each lesion, indicating their multicentric origin. Therefore, a significant proportion of sporadic FGPs have genetic alterations involving β-catenin stabilization, as did FAP-associated FGPs.

Keywords Fundic gland polyp · β-catenin

Introduction

Fundic gland polyp (FGP) is the most common gastric polyp. It is found in 0.8–1.9% of all endoscopic examinations and accounts for up to 47% of gastric polyps [9, 12, 21]. FGPs occur sporadically or in association with familial adenomatous polyposis (FAP). While FGPs associated with FAP tend to be more numerous than sporadic FGPs, both lesions are histologically identical [16]. FGPs have long been regarded as non-neoplastic because, in most cases, the lesions show no cellular atypia and their polypoid appearance seems to be caused by cystic dilatation of the fundic glands, not by apparent epithelial proliferation (Fig. 1). Recently, somatic mutation and allelic loss of the adenomatous polyposis coli (APC) gene was reported in FGPs of FAP patients [1, 24]. It has also been reported that FGPs associated with FAP frequently show dysplasia of the overlying foveolar epithelium [25]. These reports suggest that FGPs associated with FAP are neoplastic lesions. In contrast, APC gene alteration and epithelial dysplasia are rarely found in sporadic FGPs [1, 25].

Desmoid and hepatoblastoma are also known as complications of FAP. These tumors associated with FAP frequently harbor somatic APC gene alterations [6, 14]. However, in sporadic cases, APC gene alterations are less common than in FAP-associated cases, and β-catenin gene mutation is frequent [10, 22]. APC forms a complex with β-catenin, axin, and GSK-3β, and formation of the complex induces degradation of β-catenin by phosphorylation on the serine/threonine residues encoded in exon 3 of the β-catenin gene [17]. Both mutations in the GSK-3β phosphorylation sites of β-catenin and inactivation of APC similarly cause stabilization of β-catenin, leading to upregulation of Tcf/Lef-dependent transcriptional activity. Therefore, both genetic alterations might play a similar role in the genesis of these tumors. These observations prompted us to investigate whether alteration of the β-catenin gene could be a histogenetic cause of sporadic FGPs.

Materials and methods

We studied 45 biopsy samples of sporadic FGPs obtained from 35 patients who had undergone endoscopic examination at the

S. Sekine · T. Shibata · Y. Yamauchi · Y. Nakanishi · M. Sakamoto
S. Hirohashi (✉)
Pathology Division, National Cancer Center Research Institute and Hospital, 5-1-1 Tsukiji, Chuo-ku, Tokyo 104-0045, Japan
e-mail: shirohas@ncc.go.jp
Tel.: +81-3-35422511, Fax: +81-3-32482463

T. Shimoda
Clinical laboratory Division, National Cancer Center Hospital, Tokyo, Japan

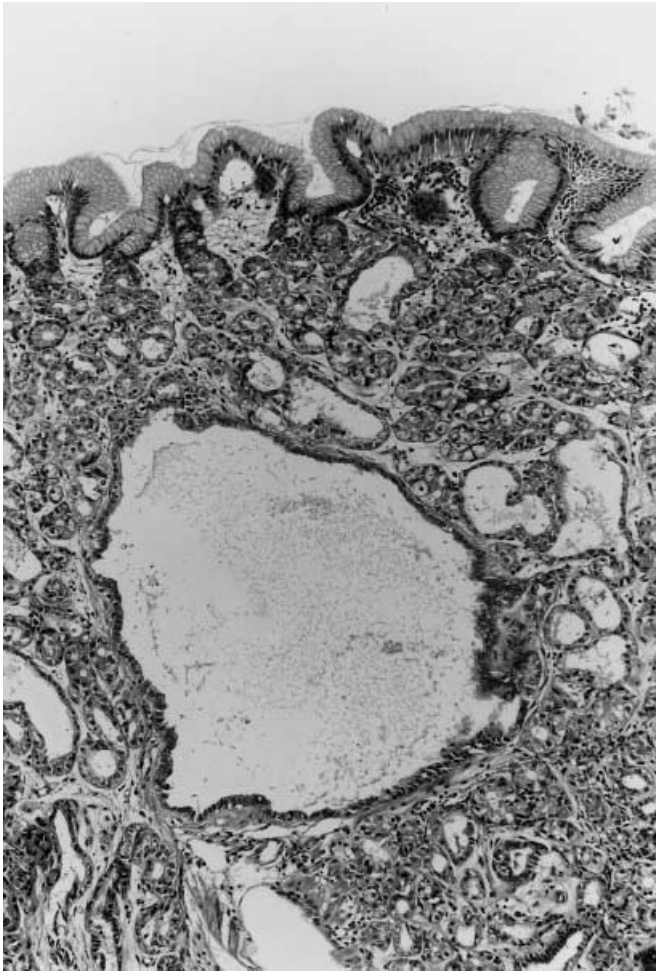

Fig. 1 Typical histology of a fundic gland polyp. Note the dilated glands lined by oxyntic epithelium. Both the foveolar epithelium and the oxyntic epithelium show no cellular atypia

Table 1 Somatic β-catenin gene alterations in sporadic fundic gland polyps

Case	Age/sex	Affected codon	Mutation
1	56/Female	37	TCT(Ser)→TTT(Phe)
2	41/Female	33	TCT(Ser)→TTT(Phe)
3	66/Female	–	
4	42/Male	–	
5	39/Male	–	
6	50/Female	33	TCT(Ser)→TGT(Cys)
7	63/Female	37	TCT(Ser)→GCT(Ala)
8	52/Male	33	TCT(Ser)→GCT(Ala)
9	50/Female	–	
10	69/Male	37	TCT(Ser)→TTT(Phe)
11	45/Female	37	TCT(Ser)→TGT(Cys)
12	56/Female	37	TCT(Ser)→TTT(Phe)
13	62/Female	32	GAC(Asp)→TAC(Tyr)
14	42/Female	–	
15	62/Male	37	TCT(Ser)→CCT(Pro)
16	62/Female	21–80	180 bp deletion
17	58/Female	32	GAC(Asp)→TAC(Tyr)
18	67/Female	–	
19	36/Male	–	
20	63/Female	37	TCT(Ser)→GCT(Ala)
21	70/Female	–	
22	59/Female	–	
23	47/Female	32	GAC(Asp)→TAC(Tyr)
24	50/Male	32	GAC(Asp)→TAC(Tyr)
25	52/Male	–	
26	46/Female	32	GAC(Asp)→TAC(Tyr)
27–1	37/Male	32	GAC(Asp)→GGC(Gly)
27–2		37	TCT(Ser)→TAT(Tyr)
28–1	64/Female	–	
28–2		–	
29–1	62/Female	32	GAC(Asp)→TAC(Tyr)
29–2		33	TCT(Ser)→TAT(Tyr)
29–3		33	TCT(Ser)→TTT(Phe)
29–4		37	TCT(Ser)→TTT(Phe)
30–1	50/Male	32	GAC(Asp)→TAC(Tyr)
30–2		33	TCT(Ser)→TGT(Cys)
31–1	47/Female	33	TCT(Ser)→TTT(Phe)
31–2		–	
32–1	63/Female	32	GAC(Asp)→AAC(Asn)
32–2		32	GA C(Asp)→TAC(Tyr)
34–1	50/Female	34	GGA(Gly)→CGA(Arg)
34–2		–	
34–3		–	
35–1	42/Female	37	TCT(Ser)→TTT(Phe)
35–2		–	

National Cancer Center Hospital, Tokyo. No patients had undertaken any long-term omeprazole treatment. These biopsy samples were fixed with 10% formalin and embedded in paraffin. No lesions were associated with foveolar dysplasia. Several 5-μm-thick sections of each specimen were stained by hematoxyin and eosin and subjected to microdissection. The epithelial components of the FGPs, including the foveolar epithelium and oxyntic epithelium of cystically dilated glands, were microdissected using a laser capture microdissection system, LM200 (Olympus, Tokyo, Japan). Biopsy specimens from non-neoplastic gastric or duodenal mucosa or microdissected stromal components served as normal controls.

The microdissected samples were incubated in 20 μl DNA extraction buffer [50 mM Tris-HCl, pH 8.0, 1 mM ethylene diamine tetraacetic acid (EDTA), 0.5% Tween 20, 200 μg/ml proteinase K] at 37°C overnight. Proteinase K was inactivated by heating at 100°C for 10 min. Of the DNA sample, 5 μl was subjected to polymerase chain reaction (PCR) with a previously described pair of intronic primers encompassing exon 3 of the β-catenin gene, G-F (5′-CCAATCTACTAATGCTAATACTG-3′) and G-R (5′-CTGCATTCTGACTTTCAGTAAGG-3′) [15]. PCR was performed under the following conditions: 3 min at 95°C for initial denaturing, followed by 40 or 45 cycles of 94°C for 15 s, 58°C for 30 s, and 72°C for 60 s, and final extension at 72°C for 5 min. The PCR products were electrophoresed in a 2% agarose gel, visualized under ultraviolet light with ethidium bromide staining and recovered using a QIAquick Gel Extraction Kit (Qiagen, Hilden, Germany). Isolated PCR products were sequenced using a Bigdye Terminator Cycle Sequencing Ready Reaction Kit (Perkin Elmer, Foster City, Calif.) and analyzed on an Applied Biosystems 310 Genetic Analyzer (Perkin Elmer). Sequencing was performed in both directions using primers G-F and G-R.

To determine which epithelial component of the FGPs harbored the β-catenin mutation, five mutation-positive samples were subjected to further analysis. The foveolar epithelium and cystically dilated glands were separately microdissected and analyzed using PCR and direct sequencing, as described above.

All samples for mutational analysis were also subjected to immunohistochemical staining of β-catenin on formalin-fixed, paraffin-embedded sections using the avidin–biotin complex method, as described previously [11]. The primary antibody used was monoclonal anti-β-catenin antibody (Transduction Laboratories, Lexington, Ky.; C19220, 1:250 dilution). 3.3'-Diaminobenzidine tetrahydrochloride was used as a chromogen. For comparison, 6 samples of unremarkable fundic gland mucosa and 11 FGP samples obtained from 9 FAP patients were also stained.

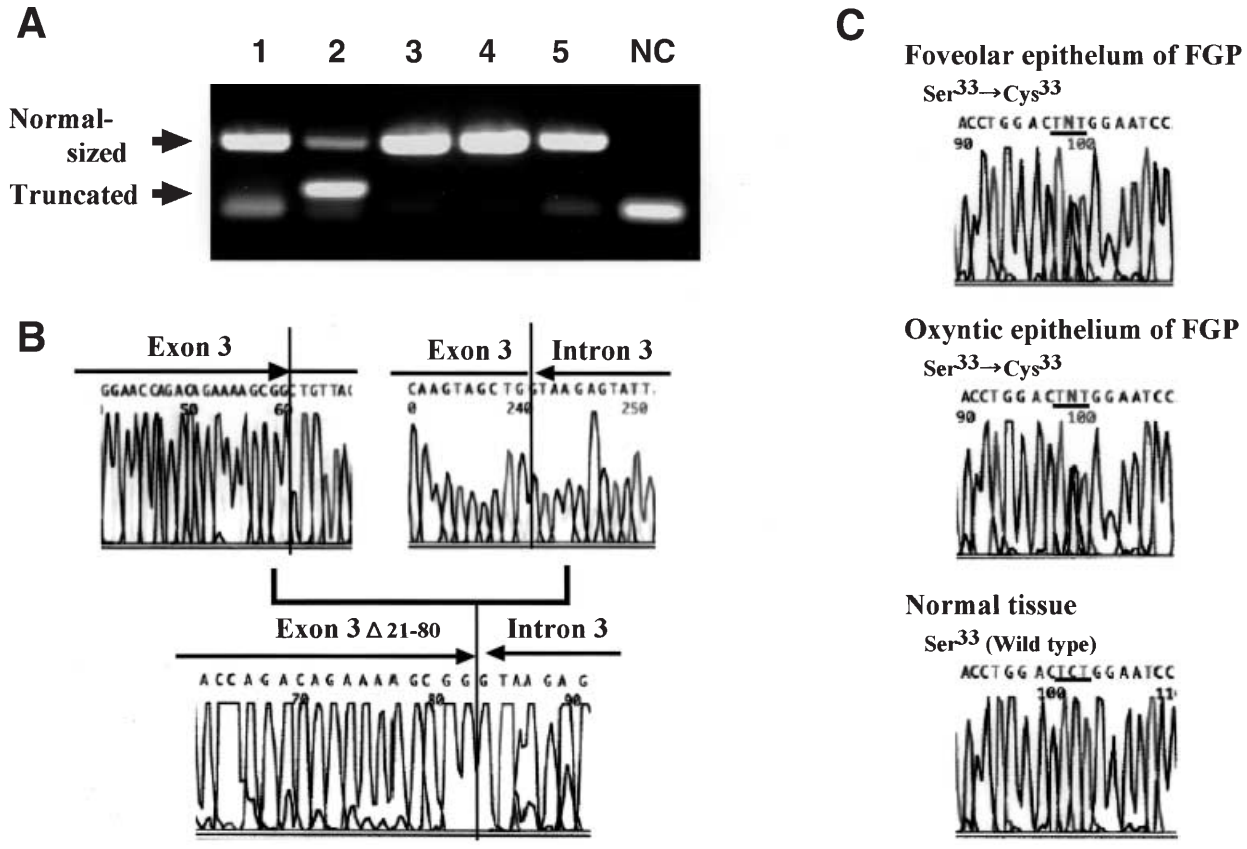

Fig. 2 a In one lesion, a truncated polymerase chain reaction product is present, together with a normal-sized product (*lane 2*; case 16). The faint band below the truncated band is the primer dimer (*NC* negative control). b Direct sequencing of the truncated product reveals an in-frame 180-bp deletion of exon 3. **c** Direct sequencing of the β-catenin gene using microdissected samples. Point mutation is detected in samples obtained from foveolar epithelium and oxyntic epithelium (case 6)

Results

Microdissection and direct sequencing analysis revealed somatic β-catenin gene alterations in 29 of the 45 sporadic FGP lesions analyzed (Table 1). Twenty-eight were missense mutations of the former two serine residues at GSK-3β phosphorylation sites or of amino acids flanking the first serine residues. In one case, a smaller PCR product was detected, together with the normal-sized product (Fig. 2A). Each product was separately recovered and sequenced. The shorter product showed a 180-bp deletion of the 3′ end of the exon 3, which resulted in an in-frame deletion of codons 21–80 (Fig. 2B). The normal-sized product showed no mutation. No mutations were detected in the non-neoplastic epithelium or the stromal component in any of the cases. In three patients with multiple polyps (cases 27, 29, 30), different lesions taken from the same patient had different mutations.

We next determined whether the two different epithelial components (overlying foveolar epithelium and cystically dilated fundic gland) in FGP have the same genetic alteration of β-catenin. We separately microdissected these two components from five FGPs harboring mutations (cases 1, 2, 6, 20, 24) and analyzed them using direct sequencing (Fig. 2C). The same mutations were found in samples obtained from both components in all lesions examined.

Immunohistochemical study for β-catenin protein showed membranous staining similar to normal fundic gland mucosa in sporadic cases (Fig. 3A, B). Neither cytoplasmic nor nuclear accumulation was observed. Most of the FGPs associated with FAP showed membranous staining similar to that found in the sporadic cases (Fig. 3C). However, in three lesions from FAP cases, focal nuclear accumulation of β-catenin was observed in the foveolar epithelium (Fig. 3D).

Discussion

Alterations of the β-catenin gene are found in various neoplasms, such as colorectal carcinoma, hepatocellular carcinoma, endometrial adenocarcinoma and pilomatricoma [3, 5, 15, 20, 24]. Most of the alterations affected the GSK-3β phosphorylation sites and are considered to inhibit proteosomal degradation and cause cytoplasmic and nuclear accumulation of β-catenin. This leads to the activation of Tcf/Lef-dependent transcription and upregulation of target genes, including c-myc and cyclin D1, which play an important role in tumorigenesis [7, 23]. We detected β-catenin mutations in 29 of the 45 sporadic FGPs. These included 28 missense mutations and 1 inframe deletion. All the missense mutations found in

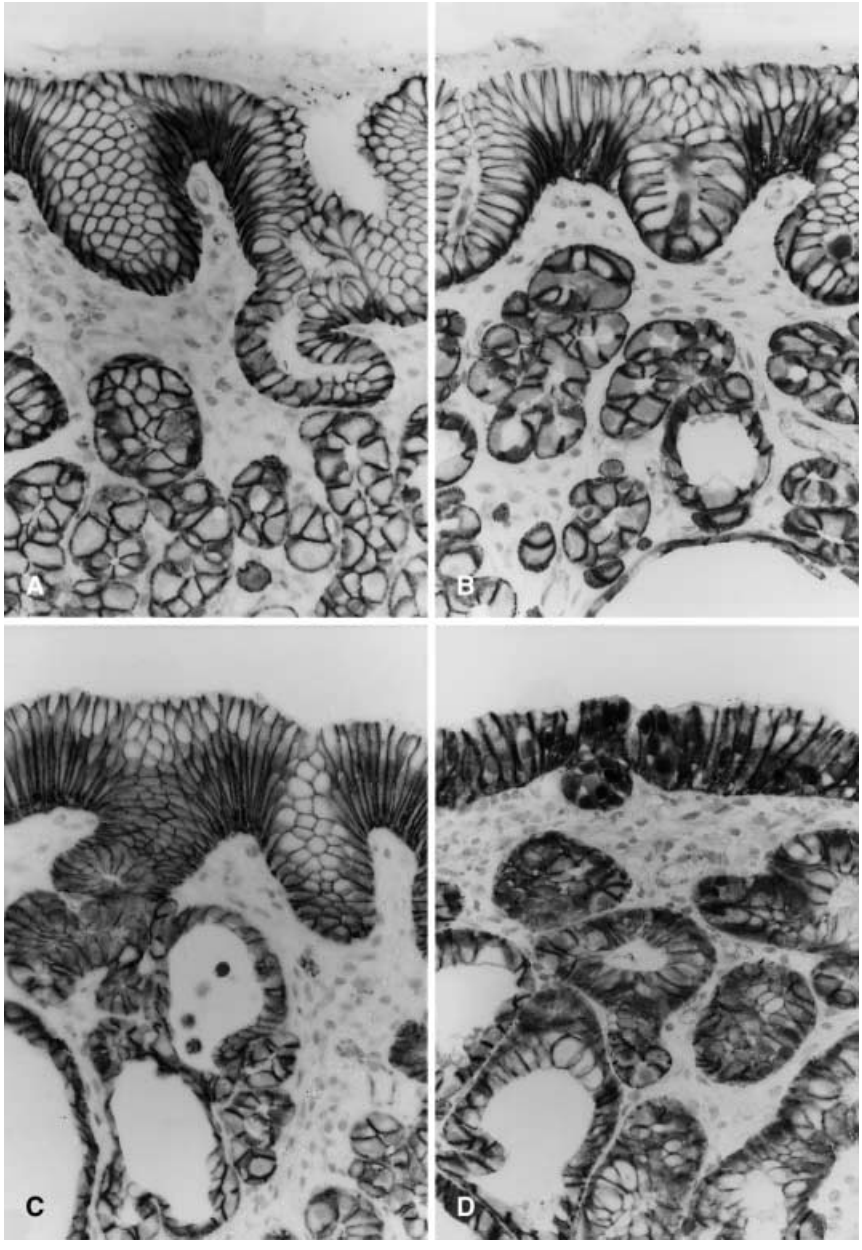

Fig. 3 Immunohistochemistry of β-catenin in normal fundic gland mucosa (**a**), sporadic fundic gland polyp (FGP; **b**) and familial adenomatous polyposis (FAP)-associated FGP (**c** and **d**). Most lesions show membranous staining and neither cytoplasmic nor nuclear accumulation (**a**–**c**). Focal nuclear staining alone is observed in the foveolar epithelium of FAP-associated FGPs (**d**)

the present study caused amino acid substitution of GSK-3β phosphorylation sites or of residues flanking one of these phospohorylation sites. These are similar to the mutations that have been reported in other tumors. As somatic mutation and loss of heterozygosity of the APC gene are reported in FGPs associated with FAP [1, 24], genetic alteration leading to β-catenin stabilization plays an important role in histogenesis of FGPs.

It has been reported that FGPs are multiple in about 60% of sporadic cases [13, 21]. In one study, an average of four polyps (range 1–11) was described [13]. In our analysis of patients with multiple lesions, four patients had a different mutation in each lesion, indicating that the lesions were multicentric.

Initially, we thought that β-catenin mutation would be limited to the foveolar epithelium, because dysplasia associated with FGPs is observed exclusively in the foveolar epithelium and not in the dilated cystic glands [25]. To clarify this issue, we separately analyzed the mutational state of β-catenin in these two components in mutation-positive cases. The mutational states in the two components corresponded in all the lesions studied. The presence of aberrant proliferative activity in the epithelial cells of the dilated glands has been demonstrated using MIB-1 immunohistochemistry [16]. This might also support the idea that the dilated oxyntic glands in FGPs also harbor genetic alterations. β-Catenin mutations might occur in the progenitor cells which can differentiate into either foveolar epithelium or oxyntic epithelium.

In various tumors containing β-catenin or APC gene mutations, cytoplasmic and/or nuclear β-catenin accumulation has been demonstrated immunohistochemically

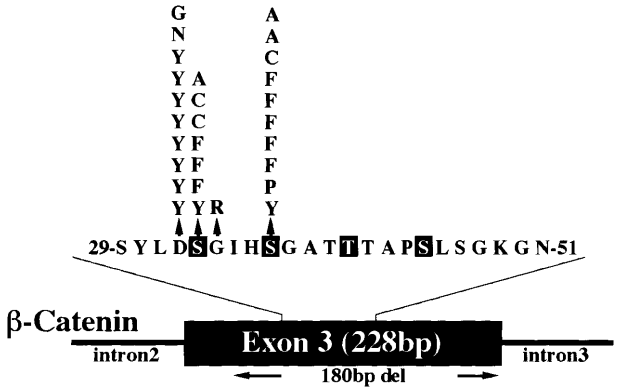

Fig. 4 β-Catenin gene alterations in fundic gland polyps (FGPs). All of the missense mutations were restricted to the former two serine residues and flanking residues of the first serine residue. One case showed a 180-bp deletion in exon 3

[3, 5, 11, 15]. Although β-catenin gene mutations would also be expected to upregulate β-catenin protein levels in FGPs, no significant accumulation of β-catenin was observed in sporadic cases, regardless of their mutational status. It is possible that even increases in β-catenin protein levels too subtle to be detected by immunohistochemistry can still trigger the formation of FGPs.

Most of the previous studies have shown that there is no histological or immunohistochemical difference between FGPs in FAP patients and sporadic FGPs [12, 16]. The only reported difference is the frequent association of foveolar dysplasia in FGPs of FAP patients. Wu et al. reported that 25% of cases of FAP-associated FGPs had epithelial dysplasia, compared with only 1% of sporadic cases [25]. FAP-associated FGPs frequently harbor truncating APC gene mutations, in contrast to frequent β-catenin gene mutations in sporadic FGPs. Recently, a positive effect of truncated APC on nuclear accumulation of β-catenin and upregulation of Tcf/Lef-dependent transcription have been reported [8, 18]. This could explain the nuclear accumulation of β-catenin found exclusively in FAP-associated FGPs and frequent development of dysplasia in FAP-associated cases. In one mutation survey of the β-catenin gene in colorectal adenomas and carcinomas, the percentage of β-catenin mutation was lower in larger adenomas and invasive carcinomas than in smaller adenomas [19]. β-Catenin mutation and inactivation of APC might not be equivalent, and inactivation of APC should be similarly advantageous in colorectal tumorigenesis and dysplasia formation in FGPs.

Recently, Abraham et al. reported β-catenin gene mutations in 91% of sporadic FGPs [2]. Although the frequency of mutations reported here is even higher than in our results, their results are mostly in agreement with ours including multicentricity of the lesions, presence of identical mutations in two different components, and absence of immunohistochemically apparent β-catenin accumulation in sporadic cases [2] (Fig. 4). Interestingly, in both studies, the missense mutations were restricted to the former two serine residues and their flanking residues (codons 32, 33, 34, 37). In other tumors, such accumulation of mutation sites of the β-catenin gene mutations has not been described. This preference for mutational sites might indicate a distinctive effect of phosphorylation of the each serine/threonine residue on β-catenin turnover.

FGPs are not considered to be precancerous lesions, and they never progress to carcinoma. The only exception has been one reported case of gastric adenocarcinoma accompanied by FGP in a patient with attenuated FAP [26], although an increased risk of gastric carcinoma has been reported in FAP patients. In colorectal tumorigenesis, activation of the β-catenin-Tcf/Lef pathway by inactivation of APC or by β-catenin gene mutation is thought to be the critical and earliest step [4]. It is interesting that the same genetic alterations cause no further malignant progression in FGPs even though both FGPs and colorectal adenomas are glandular epithelial lesions of the alimentary tract. Considering the frequency and multiplicity of FGPs, somatic "oncogenic" mutation seems to occur more frequently than we previously thought, and only specific genetic alterations might trigger a carcinogenesis in certain somatic cells.

Acknowledgements This research was supported in part by a Grant-in-Aid for Second Term Comprehensive 10-year Strategy for Cancer Control from the Ministry of Health, Labour and Welfare, Japan.

References

1. Abraham SC, Nobukawa B, Giardiello FM, Hamilton SR, Wu TT (2000) Fundic gland polyps in familial adenomatous polyposis: neoplasms with frequent somatic adenomatous polyposis coli gene alterations. Am J Pathol 157:747–754
2. Abraham SC, Nobukawa B, Giardiello FM, Hamilton SR, Wu TT (2001) Sporadic fundic gland polyps: common gastric polyps arising through activating mutations in the beta-catenin gene. Am J Pathol 158:1005–1010
3. Chan EF, Gat U, McNiff JM, Fuchs E (1999) A common human skin tumour is caused by activating mutations in beta-catenin. Nat Genet 21:410–413
4. Chung DC (2000) The genetic basis of colorectal cancer: insights into critical pathways of tumorigenesis. Gastroenterology 119:854–865
5. Fukuchi T, Sakamoto M, Tsuda H, Maruyama K, Nozawa S, Hirohashi S (1998) Beta-catenin mutation in carcinoma of the uterine endometrium. Cancer Res 58:3526–3528
6. Giardiello FM, Petersen GM, Brensinger JD, Luce MC, Cayouette MC, Bacon J, Booker SV, Hamilton SR (1996) Hepatoblastoma and APC gene mutation in familial adenomatous polyposis. Gut 39:867–869
7. He TC, Sparks AB, Rago C, Hermeking H, Zawel L, da Costa LT, Morin PJ, Vogelstein B, Kinzler KW (1998) Identification of c-MYC as a target of the APC pathway. Science 281:1509–1512
8. Henderson BR (2000) Nuclear-cytoplasmic shuttling of APC regulates beta-catenin subcellular localization and turnover. Nat Cell Biol 2:653–660
9. Kinoshita Y, Tojo M, Yano T, Kitajima N, Itoh T, Nishiyama K, Inatome T, Fukuzaki H, Watanabe M, Chiba T (1993) Incidence of fundic gland polyps in patients without familial adenomatous polyposis. Gastrointest Endosc 39:161–163
10. Koch A, Denkhaus D, Albrecht S, Leuschner I, von Schweinitz D, Pietsch T (1999) Childhood hepatoblastomas frequently carry a mutated degradation targeting box of the beta-catenin gene. Cancer Res 59:269–273

11. Kondo Y, Kanai Y, Sakamoto M, Genda T, Mizokami M, Ueda R, Hirohashi S (1999) Beta-catenin accumulation and mutation of exon 3 of the beta-catenin gene in hepatocellular carcinoma. Jpn J Cancer Res 90:1301–1309
12. Lee RG, Burt RW (1986) The histopathology of fundic gland polyps of the stomach. Am J Clin Pathol 86:498–503
13. Marcial MA, Villafana M, Hernandez-Denton J, Colon-Pagan JR (1993) Fundic gland polyps: prevalence and clinicopathologic features. Am J Gastroenterol 88:1711–1713
14. Miyaki M, Konishi M, Kikuchi-Yanoshita R, Enomoto M, Tanaka K, Takahashi H, Muraoka M, Mori T, Konishi F, Iwama T (1993) Coexistence of somatic and germ-line mutations of APC gene in desmoid tumors from patients with familial adenomatous polyposis. Cancer Res 53:5079–5082
15. Miyoshi Y, Iwao K, Nagasawa Y, Aihara T, Sasaki Y, Imaoka S, Murata M, Shimano T, Nakamura Y (1998) Activation of the beta-catenin gene in primary hepatocellular carcinomas by somatic alterations involving exon 3. Cancer Res 58:2524–2527
16. Odze RD, Marcial MA, Antonioli D (1996) Gastric fundic gland polyps: a morphological study including mucin histochemistry, stereometry, and MIB-1 immunohistochemistry. Hum Pathol 27:896–903
17. Polakis P (2000) Wnt signaling and cancer. Genes Dev 14:1837–1851
18. Rosin-Arbesfeld R, Townsley F, Bienz M (2000) The APC tumour suppressor has a nuclear export function. Nature 406: 1009–1012
19. Samowitz WS, Powers MD, Spirio LN, Nollet F, van Roy F, Slattery ML (1999) Beta-catenin mutations are more frequent in small colorectal adenomas than in larger adenomas and invasive carcinomas. Cancer Res 59:1442-1444
20. Sparks AB, Morin PJ, Vogelstein B, Kinzler KW (1998) Mutational analysis of the APC/beta-catenin/Tcf pathway in colorectal cancer. Cancer Res 58:1130–1134
21. Stolte M, Sticht T, Eidt S, Ebert D, Finkenzeller G (1994) Frequency, location, and age and sex distribution of various types of gastric polyp. Endoscopy 26:659–665
22. Tejpar S, Nollet F, Li C, Wunder JS, Michils G, dal Cin P, Van Cutsem E, Bapat B, van Roy F, Cassiman JJ, Alman BA (1999) Predominance of beta-catenin mutations and beta-catenin dysregulation in sporadic aggressive fibromatosis (desmoid tumor). Oncogene 18:6615–6620
23. Tetsu O, McCormick F (1999) Beta-catenin regulates expression of cyclin D1 in colon carcinoma cells. Nature 398:422–426
24. Toyooka M, Konishi M, Kikuchi-Yanoshita R, Iwama T, Miyaki M (1995) Somatic mutations of the adenomatous polyposis coli gene in gastroduodenal tumors from patients with familial adenomatous polyposis. Cancer Res 55:3165–3170
25. Wu TT, Kornacki S, Rashid A, Yardley JH, Hamilton SR (1998) Dysplasia and dysregulation of proliferation in foveolar and surface epithelia of fundic gland polyps from patients with familial adenomatous polyposis. Am J Surg Pathol 22: 293–298
26. Zwick A, Munir M, Ryan CK, Gian J, Burt RW, Leppert M, Spirio L, Chey WY (1997) Gastric adenocarcinoma and dysplasia in fundic gland polyps of a patient with attenuated adenomatous polyposis coli. Gastroenterology 113: 659–663

Virchows Arch (2002) 440:387–391
DOI 10.1007/s004280100528

ORIGINAL ARTICLE

**Beatriz Lifschitz-Mercer · David J. Elliott
Josephine Issakov · Leonor Leider-Trejo
Letizia Schreiber · Faina Misonzhnik · Avi Eisenthal
Batia Bar-Shira Maymon**

Localization of a specific germ cell marker, *DAZL1*, in testicular germ cell neoplasias

Received: 1 March 2001 / Accepted: 2 July 2001 / Published online: 23 November 2001
© Springer-Verlag 2001

Abstract *DAZ-like 1* (*DAZL1*) is a germ cell-specific protein expressed in both male and female gonads. The *DAZL1* gene, which maps to chromosome 3 in humans, is an autosomal homologue to the *Deleted in AZoospermia* (*DAZ*) gene(s) located on the Y chromosome. We studied the expression of *DAZL1* by means of immunohistochemistry in order to determine its distribution among testicular germ cell neoplasias and among the intratubular lesions in their vicinity. Our results demonstrated that expression of *DAZL1* protein was consistently observed in scattered cells in all intratubular germ cell neoplasias (IGCN) of the unclassified type, as well as in some of the intratubular seminomas. Foci of *DAZL1* immunopositive cells were detected in pure seminomas, while single immunopositive cells were dispersed in the seminomatous component of mixed germ cell neoplasias. All the nonseminomatous components were negative for *DAZL1* expression. These findings demonstrate an antigenic heterogeneity of seminoma cells. The localization of a specific germ cell protein, *DAZL1*, in the putative ontogenic progenitor, IGCN, and in their putative derivative, seminoma, provides further support for the hypothesis that IGCN is the precursor of germ cell neoplasias.

Keywords *DAZL1* · Germ cell marker · Human testicular neoplasias · Immunohistochemistry

B. Lifschitz-Mercer · J. Issakov · L. Leider-Trejo · L. Schreiber
F. Misonzhnik · A. Eisenthal · B.B. Maymon (✉)
Institute of Pathology, Tel-Aviv Sourasky Medical Center,
Sackler Faculty of Medicine, Tel-Aviv University,
6 Weizman Street, Tel-Aviv 64239, Israel
e-mail: maymonrb@bezeqint.net
Tel.: +972-3-6973530, Fax: +972-3-6973610

D.J. Elliott
Institute of Human Genetics, University of Newcastle,
Newcastle, UK

Introduction

One of the most well-known regions responsible for germ cell differentiation is the *azoospermia factor* (*AZF*) region located on the Y chromosome. Men with deletions in this region are azoospermic or severely oligozoospermic [26]. A gene family, *Deleted in AZoospermia* (*DAZ*), was mapped to this region [15] and has been found to be deleted in 3–13% of men with severe spermatogenic defects [3, 15, 22, 29). The protein encoded by the *DAZ* gene(s) is expressed exclusively in the male germ line [8].

Although the *DAZ* gene cluster is on the Y chromosome of humans, the autosomal homologous gene was mapped to chromosome 3 and termed *Deleted in AZoospermia-like* (*DAZL*)1 [19, 20, 21, 31]. This autosomal gene, *DAZL1*, is specifically expressed in the testis and ovary [19, 20, 21, 31], both in prenatal and postnatal germ cells [2, 4, 18, 27]. By means of immunohistochemistry, the *DAZL1* protein was recently localized in the gonocytes in the testis of human fetuses [18], but only in the spermatocytes of adult testis [18].

The role of *DAZL1* gene expression has not yet been fully elucidated, and most of the information concerning its function has come from animal studies of the homologous gene. Interestingly, loss of function of the mouse homologous gene, *Dazl*, leads to both male and female infertility characterized by prenatal loss of germ cell populations [17].

The *DAZL1* protein profile in germ cell-derived malignancies has not been evaluated. We reasoned that a specific germ cell marker might contribute to the study of the origin and progression of germ cell neoplasias. We examined the most commonly occurring germ cell-derived malignancy in humans, testicular germ cell tumors, by using an immunohistochemical method to assess *DAZL1* protein distribution in individual histologic types of germ cell neoplasias and in the intratubular germ cell neoplasias (IGCN) in their vicinity. Special attention was given to unclassified IGCN, which consist of basilar

germ cells with an undifferentiated phenotype and a yet unoccupied tubule lumen, because cell proliferation is still uncommitted to a specific germ cell tumor type at this stage [16, 28].

Materials and methods

Twenty-three specimens of seminomatous and non-seminomatous germ cell tumors were obtained from the archives of the Institute of Pathology, Tel-Aviv Sourasky Medical Center, from the years 1995–2000 (Table 1). The tissues were fixed in 4% buffered formalin for approximately 24 h and embedded in Paraplast (Oxford Labware, St. Louis, Mo., USA). The blocks which incorporated tumor and adjacent seminiferous tubules were selected for the study. Histopathological evaluations were performed on the main tumoral mass and both on the distal tubules exhibiting spermatogenesis and on adjacent areas containing IGCN. Intratubular lesions of both the unclassified type and those with a seminomatous phenotype were present in the vicinity of the tumors in all 23 study cases.

Immunohistochemistry

Immunohistochemical staining was performed with an antibody (rabbit in origin) generated against the mouse *Dazl* protein [17] at the MRC Human Genetics Unit, Western General Hospital, Edinburgh, Scotland. The antibody was found to recognize the human homologue, *DAZL1* [18]. The methodology for the generation of the antibody was previously described elsewhere [17].

Three-micrometer sections mounted on Super Frost/Plus glass (Menzel, Glaser, Braunschweig, Germany) were processed by a labeled-(strept) avidin–biotin (LAB-SA) method using a HISTOSTAIN plus kit (Zymed, San Francisco, Calif., USA). Heat-induced antigen retrieval was performed by temperature-controlled microwave treatment using an H2800 model processor (Energy Bean Sciences, Inc., Agawan, Mass., USA) in 10 mM citrate buffer, pH 6.0, for 12 min at 97ºC. The sections were treated with 3% H_2O_2 for 5 min, followed by a 10-min incubation with the universal blocker, CAS-BLOCK (Zymed). The sections were incubated for 1 h with 1:20 diluted purified IgG anti-*DAZL1* antibody. A biotinylated second antibody was applied for 10 min, followed by incubation with horseradish peroxidase-conjugated streptavidin (HRP-SA) for 10 min. The slides were washed thoroughly with Optimax wash buffer (Biogenix, San Romon, Calif., USA) following each incubation. The immunoreaction was visualized by an HRP-based chromogen/substrate system, including diaminobenzidine (DAB)-brown chromogen (Liquid DAB substrate kit; Zymed). The sections were then counterstained with Mayer's hematoxylin (which stains the nuclei a blue color), dehydrated in ascending ethanol concentration, cleared in xylene and mounted for microscopic examination.

Negative controls were performed by substituting pre-immune serum for the primary antibody. Tubules representing spermatogenesis located distal to the tumor served as "built-in" controls for the antibody immunoreactivity.

Results

Spermatocytes of seminiferous tubules distal to the main tumoral mass were positively stained by the anti-*DAZL1* antibody. The immunopositive reactivity was demonstrated in the cytoplasm of spermatocytes (Fig. 1 A). Other cells of the germinal line (spermatogonia and round spermatids) were negatively stained (Fig. 1A). Neither the somatic cells in the tubules (Sertoli and myoid cells) nor the interstitial Leydig cells reacted with the *DAZL1* antibody (Fig. 1A).

Immunoreactivity for the *DAZL1* protein was consistently observed in all the IGCN lesions of the unclassified type (Fig. 1B) as well as in some of the intratubular seminomas (Fig. 1C). The immunoreactive intratubular lesions showed scattered *DAZL1*-positive cells (Fig 1B-C). This pattern of *DAZL1* immunoreactivity was observed in intratubular lesions located in the vicinity of both seminomatous and nonseminomatous neoplasias.

Analysis of invasive germ cell neoplasias revealed the presence of foci of immunopositive-stained cells to be confined to pure seminoma cells (Fig. 1D), whereas the branching fibrous septa containing an inflammatory infiltrate were entirely negative for *DAZL1* expression (Fig. 1D). Single immunoreactive cells were present in the seminomatous component of mixed germ cell tumors (Fig. 1E). The immunostaining of the marker was exhibited in the atypical cells' cytoplasm in all cases (Fig. 1B–E).

All the nonseminomatous germ cell neoplasias were negative for *DAZL1* expression.

Discussion

In the current study, the germ cell marker, *DAZL1*, was applied for the first time to the study of testicular germ cell neoplasias. *DAZL1* was found to be expressed in IGCN and in seminomas. The localization of the specific

Table 1 Classification of the germ cell tumors

Subjects (23 male adults aged 22–46 years)	Tumor type	
	Pure	Mixed
13	Classical seminoma	
2	Embryonal carcinoma	
4		Seminoma and embryonal carcinoma
1		Embryonal carcinoma, yolk sac tumor, immature teratoma, choriocarcinoma
1		Seminoma, embryonal carcinoma and yolk sac tumor
1		Yolk sac tumor, choriocarcinoma, and teratoma
1		Seminoma, embryonal carcinoma, and immature teratoma

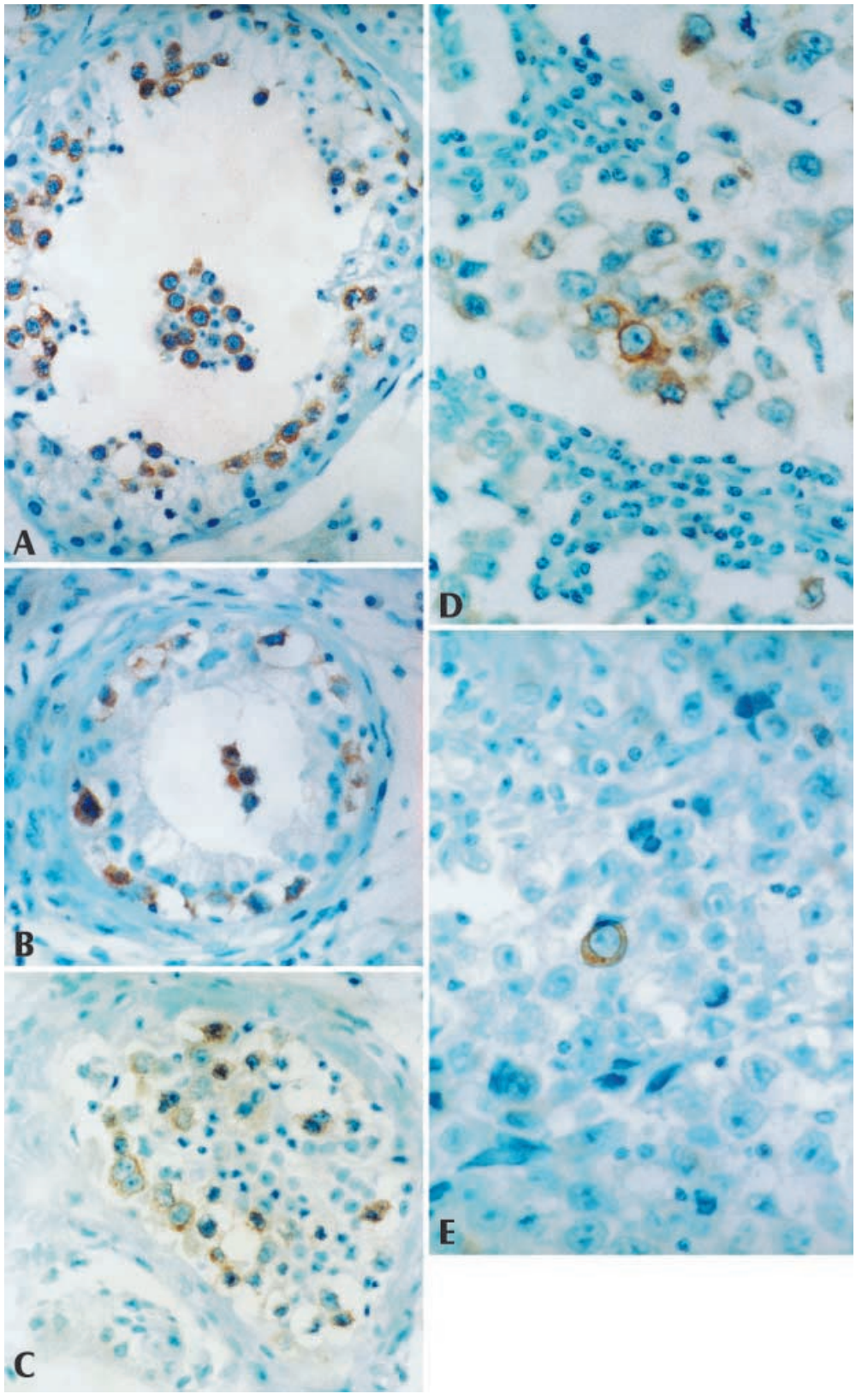

Fig. 1A–E Immunohistochemical staining for the *DAZL1* protein. **A** Seminiferous tubule representing spermatogenesis. Spermatocytes are immunoreactive. **B** An intratubular germ cell neoplasia (IGCN) of the unclassified type. Immunoreactivity is demonstrated in atypical cells. **C** Intratubular seminoma: the immunoreactivity is noted in atypical cells. **D** Focal expression of the marker in a pure seminoma. **E** The seminomatous component of a mixed germ cell tumor. A single cell is positively stained. *DAZL1* immunostaining is seen to be confined to the cells' cytoplasm in all cases (**A–E**). **A–E**, original magnification ×400. Antibody binding was visualized using DAB as a substrate to generate a brown color. Sections were counterstained with Mayer's hematoxylin which stains the nuclei blue in color

germ cell marker, *DAZL1*, in the putative ontogenic progenitor, IGCN, and in the putative derivative, seminoma, provides further support for the hypothesis that IGCN is the precursor of germ cell neoplasia.

Much effort has been expended in studying the origin and differentiation patterns of germ cell neoplasias using morphological, immunohistochemical; and genetic criteria [1, 5, 10, 11, 30]. Based on the model of a germ cell tumor's histogenesis [25], it is widely accepted that all forms of testicular germ cell tumors – with the notable exception of spermatocytic seminoma – are derived from a common precursor, originally recognized and described as IGCN and also designated as carcinoma in situ of the testis [23].

None of the commonly used immunohistochemical IGCN markers, i.e., placental alkaline phosphatase (PLAP), TRA-1–60, 43–9F, M2A, D2–40, and C-kit, have any particular "germ-cell specificity" but rather are known to have a wide distribution in different tissues [6, 7, 9, 12, 13, 24]. For example, anti-PLAP antiserum is raised against a placental protein, anti-TRA-1-60 antiserum is directed against embryonal carcinoma, and anti-43-9F antiserum is directed against ovarian carcinoma [6, 7]. In contrast, *DAZL1* protein is unique in its exclusive expression in the gonads [2, 4, 18, 19, 21, 27, 31].

These common immunohistochemical markers of IGCN are known to be expressed in early primordial germ cells and gonocytes but not in normal differentiated ones [6, 7, 9, 12, 13, 24]. *DAZL1* protein is unique in its consistent expression in gonocytes and in differentiated germ cells in adults [4, 18]. This pattern of expression suggests that it plays a crucial role in germ cell differentiation and development.

Findings on the dynamic subcellular distribution of the *DAZL1* protein in human germ cells were recently reported [18]. In that study, intense *DAZL1* immunostaining was found in the nuclei of fetal gonocytes, with weaker staining in their cytoplasm, while *DAZL1* immunostaining was present only within the cytoplasm of pachytene spermatocytes in adult testes [18]. The immunohistochemical similarity of gonocytes and IGCN cells is widely documented [6, 7, 9, 12, 13, 24]. Interestingly, only a cytoplasmic and not a nuclear distribution of the *DAZL1* protein was demonstrated in the immunopositive cells of the IGCN lesions assessed in our current study.

The scattered expression of *DAZL1* protein in both intratubular and invasive seminomas is indicative of the antigenic heterogeneity of seminomas cells, despite their morphological uniformity and their close spatial localization. Seminoma cells were previously found to differ in their expression of intermediate filaments [5] and other markers, such as M2A and TRA-60 [14]. This antigenic heterogeneity indicates that seminoma cells may be in different stages of progression and suggests a heterogeneous differentiation potential to be inherent in this neoplasia.

The current study's observations contribute to our understanding of the histogenesis of testicular germ cell neoplasia. Further investigation on the expression of *DAZL1* in ovarian malignancies are underway in order to gain an understanding of the distribution of this newly discovered germ cell-specific marker in female germ cell neoplasias.

Acknowledgments The authors express their gratitude to Prof. H. J. Cooke and Dr. M. Ruggiu for the generous gift of the *Dazl* antibody. Dr. R. Maymon is thanked for designing the presentation of the findings. Prof. B. Czernobilsky is thanked for revising the histopathologic description. Mr. M. Zion is thanked for the excellent preparation of the histological slides. Ms. Esther Eshkol is thanked for editorial assistance.

References

1. Atkin NB, Fox MF, Baker MC, Jackson Z (1993) Chromosome 12-containing markers, including two dicentrics, in three I(12p)-negative testicular germ cell tumors. Genes Chromosomes Cancer 6: 218–221
2. Brekhman V, Itskovitz-Eldor J, Yodko E, Deutsch M, Seligman J (2000) The *DAZL1* gene is expressed in human male and female embryonic gonads before meiosis. Mol Hum Reprod 6: 465–468
3. Chang SY, Tsai MY (1999) Deletion of azoospermic factor genes in Chinese azoospermic and severe oligozoospermic patients. J Assist Reprod Genet 16: 237–240
4. Dorfman DM, Genest DR, Reijo R (1999) Human *DAZL1* encodes a candidate fertility factor in women that localizes to the prenatal and postnatal germ cells. Hum Reprod 14: 2531–2536
5. Fogel M, Lifschitz-Mercer B, Moll R, Kushnir I, Jacob N, Waldherr R, Livoff A, Franke WW, Czernobilsky B (1990) Heterogeneity of intermediate filament expression in human testicular seminomas. Differentiation 45: 242–249
6. Giwercman A, Cantell L, Marks A (1991) Placental-like alkaline phosphatase as a marker of carcinoma-in-situ of the testis. Comparison with monoclonal antibodies M2A and 43–9F. APMIS 99: 586–594
7. Giwercman A, Andrews PW, Jørgensen N, Müller J, Grame N, Skakkebaek NE (1993) Immunohistochemical expression of embryonal marker TRA-1–60 in carcinoma in-situ and germ cell tumors of the testis. Cancer 72: 1308–1314
8. Haberman B, Mi H-F, Edelmann A, Bohring C, Bäckert I-T, Kiesewetter F, Aumüller G, Vogt PH (1998) *DAZ* (*Deleted in Azoospermia*) genes encode proteins located in human late spermatids and in sperm tails. Hum Reprod 13: 363–369
9. Hustin J, Collette J, Franchimont P (1987) Immunohistochemical demonstration of placental alkaline phosphatase in various states of testicular development and in germ cell tumors. Int J Androl 10: 29–35
10. Lifschitz-Mercer B, Fogel M, Moll R, Jacob N, Kushnir I, Livoff A, Waldherr R, Franke WW, Czernobilsky B (1991) Intermediate filament protein profiles of human testicular nonseminomatous germ cell tumors: correlations of cytokeratin synthesis to cell differentiation. Differentiation 48: 191–198
11. Lifschitz-Mercer B, Elliott DJ, Leider-Trejo L, Schreiber-Bramante L, Hassner A, Eisenthal A, Bar-Shira Maymon B (2000) Absence of *RBM* expression as a marker of intratubular (in situ) *g*erm cell neoplasia of the testis. Hum Pathol 31: 1116–1120
12. Marks A, Sutherland DR, Bailey D, Iglesias J, Law J, Lei M, Yeger H, Banerjee D, Baumal R (1999) Characterization and distribution of an oncofetal antigen (M2A antigen) expressed on testicular germ cell tumours. Br J Cancer 80: 569–578
13. Meyts ER, Jørgensen N, Müller J, Skakkebaek NE (1996) Prolonged expression of the c-kit receptor in germ cells of intersex fetal testes. J Pathol 178: 166–169
14. Meyts ER, Kvist M, Skakkebaek NE (1996) Heterogeneity of expression of immunohistochemical tumour markers in testicular carcinoma in situ: pathogenetic relevance. Virchows Arch 428: 133–139

15. Reijo R, Lee TY, Salo P, Alagappan R, Brown I, Rosenberg M, Rozen S, Jaffe T, Straus D, Hovatta O (1995) Diverse spermatogenic defects in humans caused by Y chromosome deletions encompassing a novel RNA binding protein gene. Nat Genet 10: 383–393
16. Rosai J (1996) Male reproductive system: testis. In: Ackerman's surgical pathology, 8th edn. Mosby, St. Louis
17. Ruggiu M, Speed R, Taggart M, Mckay SJ, Kilanowski F, Saunders P, Dorin J, Cooke HJ (1997) The mouse *Dazla* gene encodes a cytoplasmic protein essential for gametogenesis. Nature 389: 73–77
18. Ruggiu M, Saunders P, Cooke HJ (2000) Dynamic subcellular distribution of the *DAZL* protein is confined to primate male germ cells. J Androl 21: 470–477
19. Saxena R, Brown LG, Hawkins T, Alagappan RK, Skaletsky H, Reeve MP, Rejio R, Rozen S, Dinulos M, Disteche CM, Page DC (1996) The *DAZ* gene cluster on the human Y chromosome arose from an autosomal gene that was transposed, repeatedly amplified and pruned. Nature Genet 14: 292–298
20. Seboun E, Barbaux S, Bourgeron T, Nishi S, Algonik A, Egashira M, Nikkawa N, Bishop C, Fellous M, Mcelreavey K, Kasahara M (1997) Gene sequence, localization, and evolutionary conservation of *DAZLA*, a candidate male sterility gene. Genomics 41: 227–235
21. Shan Z, Hirschmann P, Seebacher T, Edelmann A, Jauch A, Morell J, Urbitsch P, Vogt PH (1996) A SPGY copy homologous to the mouse gene *Dazla* and the Drosophila gene *boule* is autosomal and expressed only in the human male gonad. Hum Molec Genet 5: 2005–2011
22. Simoni M, Gromoll J, Dworniczak B, Rolf C, Abshagen K, Kamischke A, Carani C, Meschede D, Behre HM, Horst J, Nieschlag E (1997) Screening for deletions of the Y chromosome involving the *DAZ* (*Deleted in AZoospermia*) gene in azoospermia and oligozoospermia. Fertil Steril 67: 542–547
23. Skakkebaek NE (1972) Possible carcinoma-in-situ of the testis. Lancet ii: 516–517
24. Soosay GN, Bobrow L, Happerfield L, Parkinson MC (1991) Morphology and immunohistochemistry of carcinoma *in situ* adjacent to testicular germ cell tumours in adults and children: implications for histogenesis. Histopathology 19: 537–544
25. Srigley JR, Mackay B, Toth P, Ayala A (1988) The ultrastructure and histogenesis of male germ neoplasia with emphasis on seminoma with early carcinomatous features. Ultrastruct Pathol 12: 67–86
26. Tiepolo L, Zuffardi O (1976) Localization of factors controlling spermatogenesis in the nonfluorescent portion of the human Y chromosome long arm. Hum Genet 34: 119–124
27. Tsai M-Y, Chang S-Y, Lo H-Y, Chen I-H, Huang F-J, Kung F-T, Lu Y-J (2000) The expression of *DAZL1* in the ovary of the human female fetus. Fertil Steril 73: 627–630
28. Ulbright TM (1997) Neoplasms of the testis. In: Bostwick DG, Eble JN (eds) Urologic surgical pathology, 1st edn. Mosby, St. Louis
29. Vogt PH, Edelmann A, Kirsch S, Henegariu O, Hirschmann P, Kiesewetter F, Kohn FM, Schill WB, Farah S, Ramos C, Hartmann M, Hartschuh W, Meschede D, Behre HM, Castel A, Nieschlag E, Weidner W, Grone H-J, Jung A, Engel W, Haidl G (1996) Human Y-chromosome *azoospermia factors (AZF*) mapped to different subregions in Yq11. Hum Mol Genet 5: 933–943
30. Vos A, Oosterhuis JW, de Jong B, Buist J, Schraffordt-Koops H (1990) Cytogenetics of carcinoma in situ of the testis. Cancer Genet Cytogenet 46: 75–81
31. Yen PH, Chai NN, Salido EC (1996) The human autosomal gene *DAZLA* – testis specificity and a candidate for male-infertility. Hum Molec Genet 5: 2013–2017

Virchows Arch (2002) 440:392–396
DOI 10.1007/s004280100505

ORIGINAL ARTICLE

A. W. Bates · S. I. Baithun

Secondary solid neoplasms of the prostate: a clinico-pathological series of 51 cases

Received: 12 April 2001 / Accepted: 26 June 2001 / Published online: 31 July 2001
© Springer-Verlag 2001

Abstract The incidence, presentation, and macroscopic and histological features of secondary solid neoplasms of the prostate gland are described with reference to their differential diagnoses. A continuous series of autopsy and surgical cases from the Royal London Hospital from 1907 to the present yielded a total of 51 secondary neoplasms involving the prostate: 24 at post-mortem examination and 27 surgical specimens. The histology of these specimens was re-examined. In 34 cases, tumour reached the prostate by direct spread: 29 from the bladder and 5 from the rectum. The most common primary sites of metastases to the prostate were lung (eight cases) and pancreas (two cases). There were isolated examples of metastases from the bladder, rectum, skin (malignant melanoma), breast, eye (malignant melanoma), adrenal cortex and gallbladder. Secondary neoplasms represented 2.1% of all neoplasms in surgical specimens, a similar proportion of the total number of malignant solid neoplasms as secondary tumours at other sites in the genitourinary tract. The patients were usually symptomatic, presenting with prostatism, haematuria or pelvic pain, almost always in those with widely disseminated disease.

Keywords Prostate · Metastasis · Secondary tumour

Introduction

Secondary neoplasms of the urinary tract and male genital tract account for some 1.6–3% of all genitourinary neoplasia [5, 8, 9]. The diagnostic implications vary from site to site: secondary neoplasms of the bladder can mimic a variety of primary neoplasms [4], whereas secondary testicular neoplasms in adults tend to be histologically distinctive [9]. Secondary neoplasms of the prostate are usually incidental findings at autopsy; in one series, 5.6% of patients who had died from neoplasia showed evidence of metastatic spread to the prostate at autopsy [22]. Secondary prostatic neoplasia is less often reported in surgical specimens and, in another series of more than 30,000 patients undergoing treatment for malignant disease, a clinical diagnosis of prostatic secondaries was made in only three patients (0.01%) [15]. Clinically, secondary prostatic tumours have been reported with symptoms mimicking those of primary prostate cancer [13]. Here, we review 51 cases of secondary solid neoplasms of the prostate, with emphasis on their histological appearance and differential diagnoses.

A.W. Bates (✉) · S.I. Baithun
Department of Histopathology and Morbid Anatomy,
Institute of Pathology, The Royal London Hospital,
London E1 1BB, UK
e-mail: A.Bates@bartsandthelondon.nhs.uk
Tel.: +44-207-3777347, Fax: +44-207-3777030

Materials and methods

A review of a complete series of consecutive autopsy and surgical cases from the Royal London Hospital group from 1907 to the present, including a total of some 14,500 male post-mortem examinations and 11,945 prostatic resections and biopsies, was undertaken. Histological sections of all secondary neoplasms of the prostate were reviewed, with additional immunohistochemical staining if indicated. Histology of one case was recorded in the original report but was unavailable for review. Tumours were accepted as secondary if (a) there was evidence of infiltration by invasive tumour from an adjacent structure (direct spread); (b) if the histological appearance of a tumour was comparable with that of a known primary tumour from another site; or (c) in the absence of a tissue diagnosis of primary tumour, if the histological appearances were not compatible with a primary neoplasm (e.g., tumour cells confined to vascular channels). Transitional-cell carcinoma was accepted as secondary if there was prostatic invasion and a documented primary tumour arising in the bladder. Invasive transitional-cell carcinoma in the presence of dysplastic urothelium in situ within prostatic ducts was considered to be primary. Because of variable reporting of diffuse disease such as leukaemia in organs not routinely examined histologically and the likely under-representation in biopsy material collected before the recognition of mucosa-associated lymphoid tissue (MALT)-type lymphomas, it was not possible to retrieve these cases adequately from the diagnostic indices available. Therefore, leukaemias and lymphomas were not included in the review.

Immunohistochemistry was performed on paraffin sections cut from archived blocks. Polyclonal antibodies to prostate-specific antigen (PSA, Dako A0562) and prostatic acid phosphatase (PAP, Vector Novocastra NCL-PAP) were used, and sections were incu-

Table 1 Secondary tumours of the prostate: autopsy and surgical cases

Age	Primary site	Direct spread (D) / metastasis (M)	History	Histology
Surgical cases				
64	Bladder	D	Previous cystectomy for transitional-cell carcinoma	Poorly differentiated transitional-cell carcinoma
76	Bladder	D	Lower abdominal pain; prostatism	Poorly differentiated transitional-cell carcinoma of bladder invading prostate
70	Bladder	D	Previous bladder cancer; prostatism	Invasive transitional-cell carcinoma
70	Bladder	D	Prostatism	Transitional-cell carcinoma of bladder invading prostate
68	Bladder	D	Acute retention of urine; haematuria	Transitional-cell carcinoma of bladder invading prostate
70	Rectum	D	Antero-posterior resection 3 years previously	Adenocarcinoma of colonic type
63	Lung	M	Dysuria; carcinomatosis	Free lymphatic embolus of small cell carcinoma; no evidence of prostatic primary
61	Bladder	D	1-Year history of pain in right buttock	Prostatic and ischial biopsies: poorly differentiated transitional-cell carcinoma
77	Bladder	M	Carcinoma of bladder	Transitional-cell carcinoma present in a vessel
68	Bladder	D	1-Year history of pain in left buttock; prostatism	Poorly differentiated invasive transitional-cell carcinoma with squamous areas
70	Bladder	D	Haematuria; retention; bladder tumour, G3 pT2a	Invasive poorly differentiated transitional-cell carcinoma
52	Rectum	D	Prostatism; anterior resection of rectal adenocarcinoma	Poorly differentiated mucinous adenocarcinoma
82	Bladder	D	Transitional-cell carcinoma, G3 pTa	Moderately differentiated transitional-cell carcinoma within lymphatics
69	Rectum	D	Anterior resection of Dukes' C adenocarcinoma; haematuria	Moderately differentiated adenocarcinoma consistent with previous rectal primary
83	Bladder	D	Recurrent bladder tumours	Moderately differentiated invasive transitional-cell carcinoma
60	Bladder	D	Cystectomy	Prostatic invasion by transitional-cell carcinoma
63	Bladder	D	Cystectomy	Poorly differentiated transitional-cell carcinoma
64	Bladder	D	Cystectomy	Poorly differentiated transitional-cell carcinoma
68	Bladder	D	G3 pT4 transitional-cell carcinoma	Prostatic lymphatic invasion by poorly transitional-cell carcinoma
74	Bladder	D	G3 pT4a transitional-cell carcinoma	Poorly differentiated transitional-cell carcinoma
76	Bladder	D	G3pT4a at least transitional-cell carcinoma	Poorly differentiated transitional-cell carcinoma
58	Bladder	D	Transitional-cell carcinoma arising from bladder neck	Poorly differentiated transitional-cell carcinoma
74	Bladder	D	G3 pT4 transitional-cell carcinoma	Moderately differentiated transitional-cell carcinoma
71	Bladder	D	Transitional-cell carcinoma of bladder	Poorly differentiated transitional-cell carcinoma
70	Bladder	D	Previous G3 pT4a transitional-cell carcinoma	Poorly differentiated transitional-cell carcinoma
81	Bladder	D	Prostatism; bladder neck involved by tumour	Poorly differentiated transitional-cell carcinoma with squamous foci
70	Bladder	D	Transitional-cell carcinoma; G2 pT2 at least	Moderately differentiated transitional-cell carcinoma
Autopsy cases				
63	Bladder	D	Carcinomatosis	Direct spread to prostate
55	Lung	M	Solitary prostatic secondary	Small cell carcinoma; intravascular spread
60	Lung	M	Carcinomatosis; solitary nodule in prostate	Small cell carcinoma
39	Bladder	D	Previous partial cystectomy; one nodule in prostate	Invasive transitional-cell carcinoma
70	Rectum	M	Previous antero-posterior resection; one nodule in right lobe of prostate	Adenocarcinoma of colonic type
70	Skin	M	Melanomatosis; multiple nodules in prostate	Malignant melanoma
65	Bladder	D	Carcinomatosis	Transitional-cell carcinoma
65	Rectum	D	Colostomy; carcinomatosis; invasion of posterior prostate	Moderately differentiated adenocarcinoma
68	Breast	M	Carcinomatosis; small prostate (multiple nodules)	Adenocarcinoma
59	Pancreas	M	Carcinomatosis; two 0.8-cm nodules in prostate	Poorly differentiated infiltrative adenocarcinoma
64	Pancreas	M	Carcinomatosis; multiple nodules in right lobe of prostate	Moderately differentiated adenocarcinoma

Table 1 (continued)

Age	Primary site	Direct spread (D) / metastasis (M)	History	Histology
59	Lung	M	Carcinomatosis; one metastasis in middle lobe of prostate	Poorly differentiated large cell carcinoma
67	Eye	M	Enucleation; melanomatosis; 3.8-cm metastasis in anterior prostate	Malignant melanoma
56	Bladder	D	Carcinomatosis; infiltration of posterior left lobe of prostate	Poorly differentiated transitional-cell carcinoma
52	Bladder	D	Previous cystectomy; carcinomatosis; infiltration of upper prostate	Poorly differentiated transitional-cell carcinoma
61	Lung	M	Carcinomatosis; solitary prostatic secondary	Poorly differentiated large cell carcinoma; intravascular spread
52	Adrenal	M	Carcinomatosis; two metastases in lateral lobes of prostate	Adrenal cortical carcinoma; intravascular spread
60	Rectum	D	Previous colectomy; three 3-cm prostatic secondaries	Moderately differentiated adenocarcinoma
57	Gallbladder	M	Carcinomatosis; multiple prostatic secondaries	Poorly differentiated adenosquamous carcinoma
44	Bladder	D	Carcinomatosis	Transitional-cell carcinoma
63	Lung	M	Carcinomatosis; one 2-cm mass left lobe of prostate	Poorly differentiated adenocarcinoma; intravascular spread
71	Bladder	D	Carcinomatosis	Transitional-cell carcinoma
66	Lung	M	Carcinomatosis; multiple prostatic secondaries	No histology available
83	Lung	M	Carcinomatosis; two metastases to prostate	Small cell carcinoma

bated with a commercially available detection kit (Vectastain Universal Elite ABC PK-6200, Novocastra Laboratories, Newcastle-upon-Tyne, UK). Peroxidase activity was developed with 3–3′-diaminobenzidine (Biogenex, Wokingham, UK).

Results

A total of 51 secondary solid tumours of the prostate were identified (Table 1). Patient age ranged from 39 years to 83 years, with a median age of 66 years. There were 24 post-mortem cases, representing 0.2% of all male autopsies (including both neoplastic and non-neoplastic causes of death); these were incidental findings not recorded as having been symptomatic during life. Metastases to the prostate at autopsy were accompanied by carcinomatosis or melanomatosis in all except one case, a solitary metastasis from a rectal primary. The 27 surgical specimens comprised 23 trans-urethral resections, 3 cystectomies and one needle core biopsy. In trans-urethral resections, the weight of material recovered ranged from 1 g to 10 g. Serum acid phosphatase was reported to be slightly increased in two cases. Presenting symptoms included prostatism, haematuria, acute urinary retention and pelvic pain. In only one case did a metastasis to the prostate provide the initial histological diagnosis of malignancy – a small cell carcinoma of the lung.

Most secondary tumours reached the prostate by direct spread, either from the bladder (29 cases) or rectum (5 cases). Of 17 metastases, lung and pancreas were the only primary sites represented more than once, with eight and two cases, respectively (Fig. 1). Histology was available from 16 of these cases and showed five adenocarcinomas, four small cell carcinomas, four poorly differentiated carcinomas, two malignant melanomas and an adrenal cortical carcinoma. Tumour was noted in vascular channels within the prostate in six of these cases (Fig. 2). Immunohistochemical staining properties did not seem to be affected by the age of the material. One additional case, initially interpreted as a small cell carcinoma metastatic to prostate with a concomitant prostatic adenocarcinoma, was rediagnosed on review as a primary small cell carcinoma of the prostate; the small cell component was negative for PSA and neuroendocrine markers. Histological features of metastatic tumours included a well-circumscribed appearance, infiltration of tumour between non-neoplastic prostate glands (Fig. 3), absence of prostatic intraepithelial neoplasia in adjacent glands and intravascular tumour cells.

During the same period, there were 19 primary transitional-cell carcinomas of the prostate, amounting to 0.8% of all malignant neoplasms of the prostate. These carcinomas typically caused symptoms of prostatism or urinary retention in patients aged 43–91 years (median, 67 years).

Discussion

Reviews of archival material at a single institution have shown that secondary neoplasms account for a similar proportion of the total in surgical material from the prostate (2.1%), testis (1.6%) [9], bladder (2.3%) [5] and kidney (3%) [8]. The post-mortem incidence of secondary solid tumours of the prostate in the present series (0.2%) is probably an under-representation, because histological

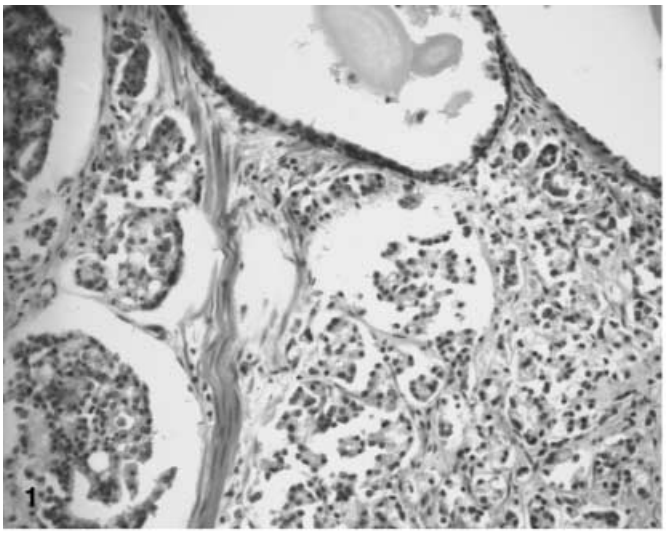

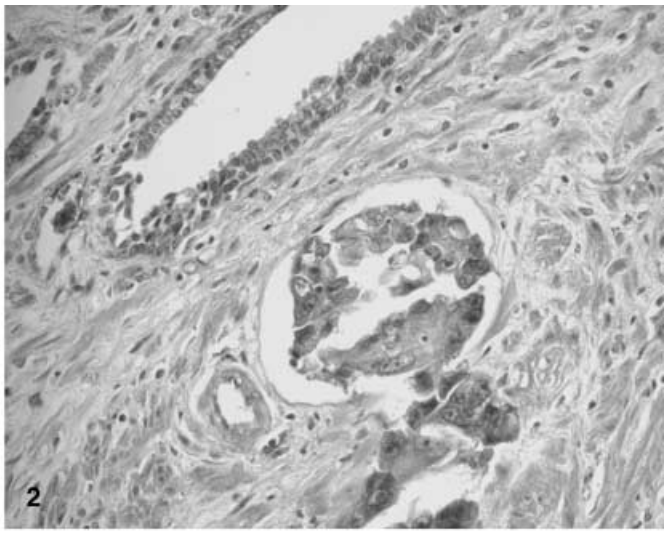

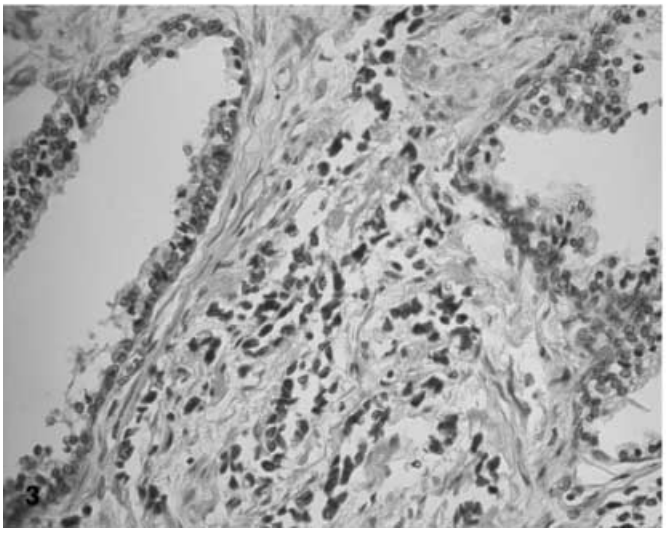

Fig. 1 Cribriform adenocarcinoma metastatic to the prostate from a pancreatic primary. Prostatic glands containing corpora amylacea are seen at *top*. The tumour is prostate-specific antigen negative, and the patient had carcinomatosis. ×125

Fig. 2 Prostatic tissue showing tumour emboli within vascular spaces: adenocarcinoma from a lung primary. ×240

Fig. 3 Small cell carcinoma of the lung metastatic to the prostate. Note the pattern of infiltration of small groups of cells between prostatic glands. ×240

examination was usually performed at autopsy only if warranted by the macroscopic findings. Previous studies demonstrated metastatic solid tumours in the prostate in 0.5% of 3663 male autopsies [15] and in 1% of 5962 autopsies of patients who died of malignancy [22]. As at other sites in the genitourinary tract, prostatic involvement in metastatic disease appears to be a late phenomenon; such patients almost invariably have carcinomatosis [22], and symptomatic secondary prostatic tumour carries a very poor prognosis [2].

Direct spread of transitional-cell carcinoma of the bladder represents the most common secondary prostatic neoplasm. Previous series have shown primary transitional-cell carcinoma of the prostate to comprise some 1–5% of all prostatic malignancies [10]. Our series yielded a somewhat lower range, perhaps because of stricter criteria to exclude tumours originating from the bladder; however, primary transitional-cell carcinoma of the prostate cannot be entirely excluded by a history of transitional-cell carcinoma of the bladder, because separate primary tumours can arise in the bladder and prostate as a consequence of the multicentricity of tumour growth [14]. This distinction is not crucial, because the presence or absence of prostatic stromal invasion, rather than the site of origin of the lesion, determines the prognosis [7]. If detailed mapping of the prostate is performed in cases of primary bladder cancer, Pagetoid spread of tumour along prostatic duct urothelium is quite a frequent finding (9 of 20 cases in one series) [17]. Distinction between poorly differentiated prostatic adenocarcinoma and transitional-cell carcinoma can be problematic in needle core biopsies; PAP and PSA immunostaining is usually but not invariably positive in the former diagnosis, whereas positivity for cytokeratins 7 and 20 favours the latter [3].

Most metastatic solid prostate tumours did not resemble primary prostatic neoplasms histologically. An exception was small cell carcinoma (the most common histological type of metastasis) that shows no morphological difference with primary small cell carcinoma, as was reported in a patient as young as 23 years [16]. Though rare (0.5–2% of all prostatic carcinomas), primary small cell carcinoma is one of the most aggressive prostatic tumours, believed to derive from a putative stem cell [12]. The presence of areas of histologically typical prostatic adenocarcinoma, as in our case, suggests the tumour's primary origin; however, the distinction may be difficult in a small sample because small cell carcinoma of the prostate is typically PSA and PAP negative [12]. Thyroid transcription factor-1 (TTF-1) immunostaining, normally positive in small cell lung carcinoma, has been suggested as a means of differentiating small cell lung carcinomas

from other small cell carcinomas [19], though TTF-1 is expressed by at least some small cell prostatic carcinomas [1]. Rare histological subtypes of primary prostatic adenocarcinoma have been described that can mimic adenocarcinoma metastatic from other sites, e.g., mucinous, signet-ring cell and ductal endometrioid types, but these usually show PSA and PAP positivity, which distinguishes them from metastatic disease, though occasionally a primary prostatic tumour may prove PSA and PAP negative [20].

Metastatic solid tumours are thought to reach the prostate principally by intravascular spread, and the frequent finding of metastatic cells within vascular channels in the present series supports this observation. Surprisingly, considering the prevalence of prostatic adenocarcinoma in older age groups, there are only two reported cases of prostatic adenocarcinoma as the recipient of tumour-to-tumour metastasis [11]. Prostatic metastases are almost invariably associated with widely disseminated malignancy, but initial histological diagnosis of malignancy by prostatic metastasis is very rare [21], and we found only one such case in the present series. Leukaemias and lymphomas, excluded from the present series, represent the most common type of non-primary prostatic malignancy [22], sometimes producing obstructive symptoms [6]; prostatic biopsy has been recommended in these circumstances [18]. As at other sites in the genitourinary tract, correct histological identification of secondary tumours is important because hormonal or surgical treatment is usually not indicated.

References

1. Agoff SN, Lamps LW, Philip AT, Amin MB, Schmidt RA, True LD, Folpe AL (2000) Thyroid transcription factor-1 is expressed in extrapulmonary small cell carcinomas but not in other extrapulmonary neuroendocrine tumours. Mod Pathol 13:238–242
2. Bamberger MH, Romas NA (1990) Clinically significant metastatic melanoma to prostate. Urology 35:445–447
3. Bassily NH, Vallorosi CJ, Akdas G, Montie JE, Rubin MA (2000) Coordinate expression of cytokeratins 7 and 20 in prostate adenocarcinoma and bladder urothelial carcinoma. Am J Clin Pathol 113:383–388
4. Bates AW, Baithun SI (1998) The differential diagnosis of secondary and unusual primary tumours of the bladder. Curr Diagn Pathol 5:188–197
5. Bates AW, Baithun SI (2000) Secondary neoplasms of the bladder are histological mimics of nontransitional cell primary tumours: clinicopathological and histological features of 282 cases. Histopathology 36:32–40
6. Butler MR, O'Flynn JD (1973) Prostatic disease in the leukaemic patient, with particular reference to leukaemic infiltration of the prostate – a retrospective clinical study. Br J Urol 45:179–183
7. Cheville JC, Dundore PA, Bostwick DG, Lieber MM, Batts KP, Sebo TJ, Farrow GM (1998) Transitional cell carcinoma of the prostate: clinicopathologic study of 50 cases. Cancer 82:703–707
8. Chin Aleong J, Bates AW, Baithun SI (2000) Secondary neoplasms of the kidney: a clinico-pathological review of 443 cases (abstract). J Pathol 190[Suppl 1]:42
9. Dutt N, Bates AW, Baithun SI (2000) Secondary neoplasms of the male genital tract with different patterns of involvement in adults and children. Histopathology 37:323–331
10. Goebbels R, Amberger L, Wernert N, Dhom G (1985) Urothelial carcinoma of the prostate. Appl Pathol 3:242–254
11. Grignon DJ, Ro JY, Ayala AG (1989) Malignant melanoma with metastasis to adenocarcinoma of the prostate. Cancer 63:196–198
12. Helpap B, Köllermann J (2001) Immunohistochemical analysis of the proliferative activity of neuroendocrine tumors from various organs. Are there indications for a neuroendocrine tumor – carcinoma sequence? Virchows Arch 438:86–91
13. Hodge GB, Carson CC (1985) Oat cell carcinoma of lung masquerading as prostatic carcinoma. Urology 25:69–70
14. Ito T, Wada T, Furusato M, Aizawa S (1997) Prostatic involvement of bladder carcinoma. Nippon Hinyokika Gakkai Zasshi 88:677–683
15. Johnson DE, Chalbaud R, Ayala AG (1974) Secondary tumours of the prostate. J Urol 112:507–508
16. Madersbacher S, Schatzl G, Susani M, Maier U (1994) Prostatic metastasis of a small cell lung cancer in a young male. Eur Urol 26:267–269
17. Mahadevia PS, Koss LG, Tar IJ (1986) Prostatic involvement in bladder cancer. Prostate mapping in 20 cystoprostatectomy specimens. Cancer 58:2096–2102
18. Merimsky E, Baratz M, Kahn Y (1981) Leukaemic infiltration of the prostate. Br J Urol 53:150–151
19. Ordónez NG (2000) Value of thyroid transcription factor-1 immunostaining in distinguishing small cell lung carcinomas from other small cell carcinomas. Am J Surg Pathol 24:1217–1223
20. Segawa T, Kakehi Y (1993) Primary signet ring cell adenocarcinoma of the prostate: a case report and literature review. Hinyokika Kiyo 39:565–568
21. Smedley HM, Brown C, Turner A (1983) Ectopic ACTH-producing lung cancer presenting with prostatic metastasis. Postgrad Med J 59:371–372
22. Zein TA, Huben R, Lane W, Pontes JE, Englander LS (1955) Secondary tumours of the prostate. J Urol 133:615–616

Virchows Arch (2002) 440:397–403
DOI 10.1007/s004280100532

ORIGINAL ARTICLE

Petra C. Stangl · Friedrich Herbst · Peter Birner
Georg Oberhuber

Crohn's disease of the appendix

Received: 23 May 2001 / Accepted: 6 August 2001 / Published online: 23 November 2001
© Springer-Verlag 2001

Abstract Although appendectomy is often the first surgical procedure in patients with Crohn's disease (CD), only few data exist on appendiceal CD. The aim of this study was to analyze appendices of CD patients undergoing surgery. We analyzed 149 specimens from consecutive patients with CD who underwent primary right ileocolonic or (sub)total colonic resection. The appendix was present in 90 resection specimens. Histologic findings were compared with those of 180 age and sex matched controls. Thirty-six appendices showed histologic signs of CD (40%): A transmural inflammation was found in 24 cases (67%), and a mucosal inflammation in 12 cases (33%). Histologic hallmarks of mucosal involvement were focal or discontinuous inflammation with crypt distortion and a histiocytic and lymphocytic predominant inflammation. Furthermore, epitheloid granulomas and erosions or ulcers with abundant histiocytes at the lesions base were observed. In comparison to controls luminal obliteration was significantly overrepresented in CD whereas acute phlegmonous appendicitis was underrepresented ($P<0.01$). Patients with CD of the appendix showed a more widespread colonic involvement than those without ($P<0.01$). This study shows that CD of the appendix exhibits specific histologic features that allow a differentiation from non-CD-associated appendicitis. CD-associated appendicitis is a frequent event, probably signifying a more widespread colonic involvement.

Keywords Crohn's disease · Appendix · Histology · Gastrointestinal inflammation

Introduction

Crohn's disease (CD) is an inflammatory disorder that may affect any part of the gastrointestinal (GI) tract between the mouth and the anus. With respect to the percentage of involvement of the appendix there are only few and inconsistent data available on the type and frequency of inflammation in CD [2, 7, 9, 10, 11, 13, 14, 19, 26]. Probably owing to differing histologic criteria the percentage has been reported to range from 0 to 54% (Table 1).

Although the appendix appears to be of minor interest in the study of CD, this is not entirely true. First, it is well known that surgeons frequently encounter CD patients with lower right-sided abdominal pain simulating signs and symptoms of acute appendicitis. In these patients appendectomy is often performed as a first surgical procedure [5, 10, 18, 27] with the appendix being inflamed either as part of the disease itself or unrelated to

P.C. Stangl
Departments of Clinical Pathology and Surgery,
University of Vienna, Medical School, Währinger Gürtel 18-20,
1090 Vienna, Austria

F. Herbst
Department of Surgery, University of Vienna,
Medical School, Währinger Gürtel 18-20, 1090 Vienna, Austria

P. Birner · G. Oberhuber (✉)
Department of Clinical Pathology, University of Vienna,
Medical School, Währinger Gürtel 18–20, 1090 Vienna, Austria
e-mail: Pathologie@t-online.de
Tel.: +49-7551-5083, Fax: +49-7551-67077

G. Oberhuber
Pathologie Überlingen, Alte Nussdorferstr. 36, 88662 Überlingen,
Germany

Table 1 Reading on Crohn's disease (*CD*) of the appendix (*nm* not mentioned)

Author	Patients (*n*)	CD of the appendix (%)
Crohn 1932 [2]	14	0.0
Warren 1948 [26]	83	24.0
Rappaport 1951 [19]	35	49.0
Lockhart-Mummery 1964 [14]	32	16.0
Lennard-J. 1969 [13]	nm	25.0
Larsen 1970 [11]	26	54.0
Kovalcik 1977 [10]	15	7.0
Hamano 1985 [7]	22	4.5
Kahn 1992 [9]	24	50.0

CD, or appearing normal. In particular in these patients, clear histologic criteria of CD of the appendix must be developed to allow an early diagnosis of this disease. Second, several studies support the contention that the appendix may play an important role in chronic inflammatory bowel disease (IBD) as it may somehow be related to the development of ulcerative colitis [21, 20]. This supports the contention that more data on the appendix are needed to appreciate its function in IBD. For example, it is not known whether involvement of the appendix in CD heralds a particular type of CD with a particular pattern of involvement of the colon.

The present study was undertaken to answer the following questions: Are there histologic criteria that allow a definite diagnosis of CD based on appendectomy specimens? What is the percentage of involvement of the appendix in patients with CD undergoing surgery due to the development of complications? Which parts of the colon are involved in patients with CD of the appendix, and is there a difference when compared to CD patients with a normal appendix? Is there any clinical parameter in CD that is associated with a higher rate of appendiceal involvement?

Patients and methods

In order to detect the percentage of appendiceal involvement in CD, records of all CD patients undergoing intestinal resection at the Department of Surgery of the University Hospital in Vienna in between January 1993 and October 1999 were retrieved from our medical files. A total of 149 patients were found to have undergone primary ileocoecal resection, primary right hemicolectomy, or primary (sub)total colectomy due to the occurrence of complications of CD. An appendix was found in 90 cases while in 59 cases the appendices were not present. According to the medical files 52 patients underwent appendectomy before intestinal resection while in the remaining seven cases the fate of the organ was unknown. These seven patients may either have undergone appendectomy, or the appendix was not found in pathological gross examination.

Patients who underwent appendectomy before intestinal resection were contacted by phone. In 14 of these cases histologic slides of the appendices were traced and sent to us for evaluation. In the remainder of cases the histologic slides could not be analyzed, either because the pathological files were not found or the patients were lost to follow-up.

As a minimum, two circumferential cross sections and the tip of the appendix were subjected to histologic examination. In cases with grossly altered appendices up to six circumferential cross sections were examined. All cases were histologically reevaluated by one pathologist (GO). Because the aim of this study was to define the morphology of the lesions to be encountered in CD, and to rule out that they were also part of the morphological spectrum of non-CD-associated appendicitis, the pathologist was not blinded to patient history.

All surgical specimens were fixed in buffered formalin (8%) and embedded in paraffin. Two sections 2–4 µm in thickness were taken from each block and stained with hematoxylin-eosin for histologic examination.

The diagnosis of CD was based on the histology of resection specimens, clinical symptoms, blood tests, microbiological findings, gastrointestinal endoscopy with biopsy, and radiological findings [ultrasound (enteroclysma), computed tomography, irrigoscopy, or bowel run through].

The histologic diagnosis of CD in small and large bowel resection specimens was based on standard criteria [14, 16, 22, 23, 8, 25, 15, 12, 24]. Histologic features suggesting mucosal CD of the appendix included elongation and distortion of the crypts either focally or diffusely and discontinuous or focal inflammatory infiltration (by lymphocytes, neutrophils, and histiocytes) of the lamina propria with or without epitheloid granulomas. Submucosal involvement was recognized through submucosal granulomas and lymphoid follicles. Transmural CD was characterized by the occurrence of either granulomas or well-developed lymphoid aggregates or both at the border of the muscularis propria and subserosa, with or without an infiltration of the muscular layer by mononuclear leukocytes. Fissural lesions or small bizarre-configured ulcers were considered as part of the spectrum of CD when our criteria were met.

Controls

To compare histologic findings in CD with those of patients undergoing appendectomy for suspected appendicitis, 180 age- and sex-matched controls known to be free of CD were retrieved from our files. The histology of all specimens was reevaluated. Diagnostic categories included obliteration of the lumen (by fibrous tissue and proliferated nerve fibers); the presence of appendicoliths; acute mucosal appendicitis (mucosal inflammation with neutrophilic granulocytes); erosive, ulcerative, and acute phlegmonous (transmural neutrophilic infiltration in combination with erosions or ulcers) appendicitis; gangrene; and perforation.

Statistics

All statistical analyses were performed using SPSS Version 7.0 (SPSS, Chicago, Ill). Unless otherwise specified data are given as median (range). Probability values ≤0.05 were considered significant. Chi-square test, ANOVA, Wilcoxon's test, and Pearson's correlation coefficient were used, as appropriate.

Results

Among the 90 patients (Table 2) with an available appendix in the resected specimens, there were 42 men (47%) and 48 women (53%) with a median age of 29.5 years (range 15–74 years). Ileocoecal resection was performed in 68 cases (76%), right hemicolectomy in 12 (13%), and (sub)total colonic resection in 10 (11%). Preoperative medication included steroids (n=15, 17%), 5-aminosalicylate (n=17, 19%), or both (n=17, 19%). Azathioprine was added in seven cases to steroids and 5-aminosalicylate, and one patient was administered azathioprine alone (9%). Thirty-three patients (36%) received no medication. There was no statistically significant difference in clinical data between patients with an appendix in the resection specimen and those without one. For more data see Table 2.

Histology in appendices of CD patients

All patients had active CD in at least one site of the resected specimens, and in 36 cases (40%) the appendix was considered to be involved (Table 3).

Lesions considered to be CD-associated were either confined to the mucosa or a so-called transmural inflammation was observed: In 12 appendices (33%) only mucosal lesions were found. The appearance of these le-

Table 2 Findings in Crohn's disease (*CD*) patients with and without involvement of the appendix

	Appendix CD positive (*n*=36)	Appendix CD negative (*n*=54)
Male	15 (42%)	27 (50%)
Female	21 (58%)	27 (50%)
Age at surgery (in years)	29.3 (15–50)	32.9 (16–74)
Surgical procedure (number of patients)		
Ileocoecal resection	24 (67%)	44 (82%)
Right hemicolectomy	5 (14%)	7 (13%)
(Sub)total colectomy	7 (19%)	3 (6%)
Gross findings in resection specimens (number of patients)		
Fistulas only	5 (14%)	10 (18%)
Stenoses only	8 (22%)	15 (28%)
Stenoses and fistulas	15 (42%)	22 (41%)
None	8 (22%)	7 (13%)
Clinical findings (number of patients)		
Pain	17 (47%)	26 (48%)
Diarrhea	1 (3%)	2 (4%)
Pain and diarrhea	8 (22%)	6 (11%)
(Sub)ileus	10 (28%)	20 (37%)
Preoperative medication (number of patients)		
Steroids	5 (14%)	10 (19%)
Salazopyrine	5 (14%)	12 (22%)
Steroids and salazopyrine	8 (22%)	9 (16%)
Azathioprine	7 (19%)	1 (2%)
None	11 (31%)	22 (41%)
Laboratory investigations [median (range)]		
Iron (μg/dl)	29 (4–77)	39 (4–121)
Orosomucoid (mg/dl)	195 (88–339)	134 (38–268)
Albumine (g/l)	39 (10–64)	40 (22–61)
C-reactive peptide (mg/dl)	5.8 (0.5–24)	5.7 (0–19.8)
Erythrocytes (T/l)	4.4 (3.5–5.5)	4.4 (2.4–5.5)
Hemoglobine (g/dl)	11.8 (7.8–15.7)	11.7 (5.2–15.3)
Leucocytes (G/l)	10.9 (4.5–18.2)	9.6 (3.2–20.5)
Platelets (G/l)	408 (120–872)	380 (135–675)

The comparison of findings in patients with CD-positive and CD-negative appendices revealed that only the number of patients receiving azathioprine was significantly different ($P<0.01$)

Table 3 Histologic criteria of CD-associated appendicitis

Focal inflammation with crypt destruction, histio-and lymphocyte-predominant inflammation
Discontinuous inflammation with significant crypt distortion
Giant cells of Langerhans type and noncaseating granulomas
Erosions with histiocyte predominant inflammation at the edge of the lesion
Subserosal lymphoid aggregates

sions was reminiscent of CD of the colon with focal inflammation of small groups of glands with crypt destruction being found in ten cases (Fig. 1). The inflammatory infiltrate was composed of histiocytes and lymphocytes and only few or no neutrophilic granulocytes. Two specimens also displayed erosions which were lined by mononuclear cells (Fig. 2) with an epitheloid appearance. Giant cells of the Langerhans type were found in three cases and well-developed epitheloid granulomas in three further cases (Fig. 1).

Transmural inflammation was found in 24 specimens (67%). The development of lymphoid follicles at the border of the muscularis propria and the subserosal fatty tissue was considered the hallmark of transmural inflammation. In contrast to the findings in the terminal ileum and of the colon, the number of the lymphoid follicles found in the subserosa was low. However, their characteristic appearance (Figs. 3 and 4) allowed them to be distinguished from lymphoid aggregates in cases with acute phlegmonous non-CD-associated appendicitis. Lymphoid aggregates in acute phlegmonous appendicitis are composed of mononuclear leukocytes that are scattered in the subserosa and focally form loose aggregates that show an ill-defined border. In contrast, lymphoid follicles of CD show a clear-cut border and an organized structure.

The mucosa of cases with transmural inflammation showed discontinuous inflammation with crypt distortion

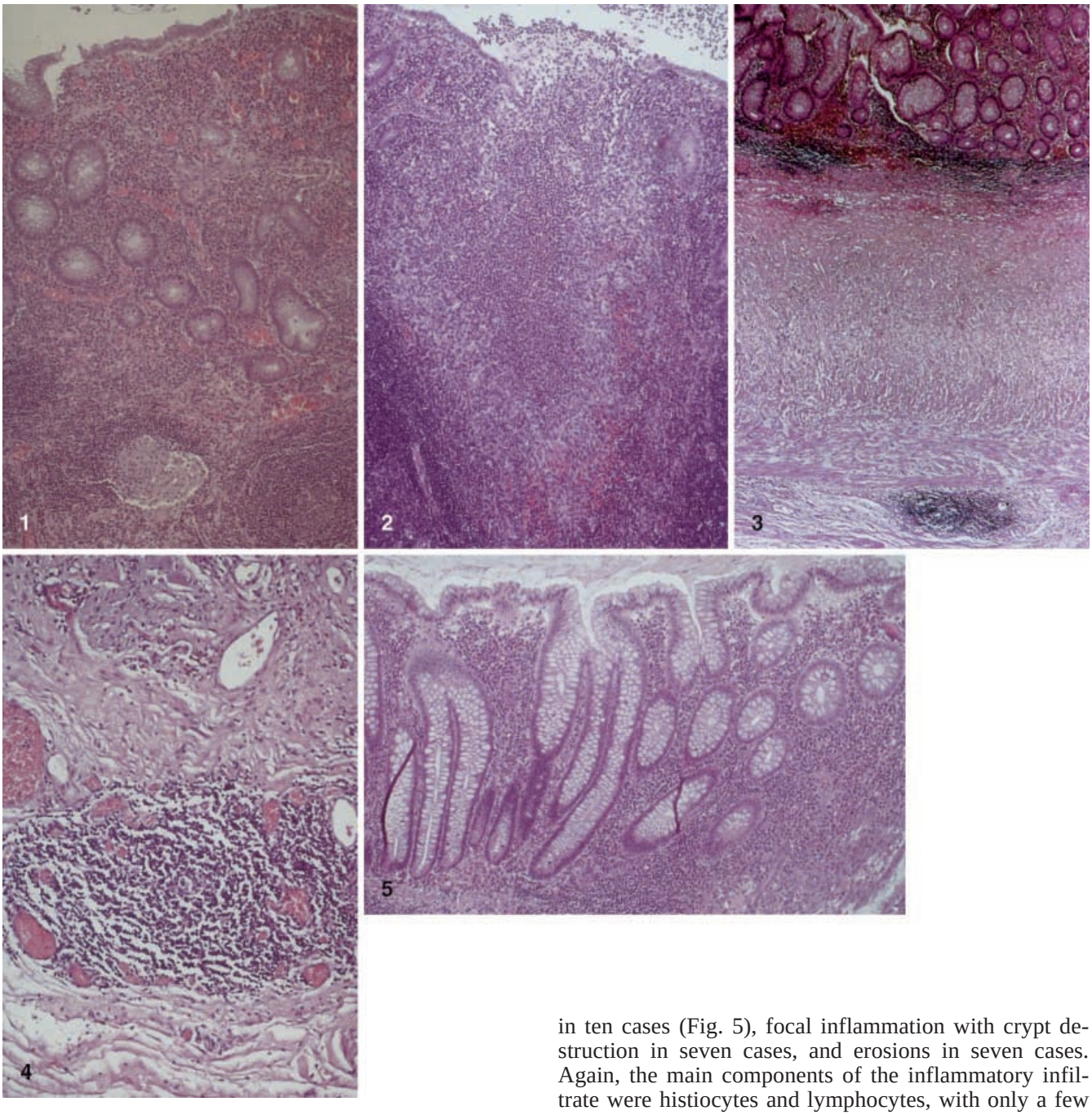

Fig. 1 Focal inflammation of the mucosa with crypt destruction. Please note that the inflammatory infiltrate is composed of aggregated epitheloid cells. Hematoxylin and eosin, original magnification, ×300

Fig. 2 Erosion of the appendix in a patient with CD. The base of the lesion is typically lined by epitheloid histiocytes. Hematoxylin and eosin, original magnification, ×300

Fig. 3 CD of the appendix with the features of a so-called transmural inflammation represented by the lymphoid follicle at the border of the muscularis propria and the subserosa. Hematoxylin and eosin, original magnification, ×100

Fig. 4 Lymphoid follicles at the border of the muscularis propria and the subserosa. They signify the so-called transmural inflammation in CD. Hematoxylin and eosin, original magnification, ×400

Fig. 5 CD of the appendix with crypt distortion. Please note the elongation and branching of the crypts. Hematoxylin and eosin, original magnification, ×300

in ten cases (Fig. 5), focal inflammation with crypt destruction in seven cases, and erosions in seven cases. Again, the main components of the inflammatory infiltrate were histiocytes and lymphocytes, with only a few neutrophilic granulocytes. Ulcerations were found in seven cases, fibrous obliteration of the tip in five cases. Epitheloid granulomas were observed in six of these specimens.

CD patients without involvement of the appendix

Fifty-four specimens (60%) were considered to be free of CD lesions. Fibrous luminal obliteration of the tip or of the entire appendix was found in 23 cases (43% versus 14% in specimens with CD lesions; $P<0.01$), whereas 25 (46%) cases showed normal appendix. In the remainder either mucosal inflammation or erosions were

Table 4 Histologic findings in CD patients and controls (*CD* Crohn's disease, *pos* positive, *neg* negative, *vs* versus, *app* appendix, *ns* not significant)

	Controls *n*=180	CD-pos. app. *n*=36 (40%)	CD-neg. app. *n*=54 (60%)	CD vs controls	CD-pos. vs CD-neg. app.
Luminal obliteration	22 [a] (12%)	5 [d] (14%)	23 (43%)	*P*<0.01	*P*<0.01
Ulcers	5 [a] (3%)	13 [e] (36%)	2 (4%)	*P*<0.01	*P*<0.01
Ulcerophlegmonous appendicitis	107 [a] (59%)	0	0	*P*<0.01	ns
Acute appendicitis with mucosal neutrophilic inflammation	20 [a] (11%)	0	4 [b] (7%)	ns	ns
Perforation	19 [a] (11%)	0	0	*P*<0.01	ns
Fecaliths	15 [a] (8%)	0	2 [c] (4%)	ns	ns
Normal appendix	37 (21%)	0	25 (46%)	ns	*P*<0.01

[a] Some cases are mentioned in several groups
[b] In one case an obliteration was also found
[c] In one case an otherwise normal appendix was observed
[d] All were combined with transmural inflammation
[e] Nine cases were associated with transmural inflammation, in four cases discontinuous mucosal inflammation (histiocytic and lymphocytic predominant) was present

observed, with a histology comparable to that found in inflamed control specimens.

Comparison of histologic findings in CD patients and controls

In comparison to the 180 age- and sex-matched control, patients with CD developed luminal obliteration (31% versus 12%; $P<0.01$) and erosions or ulcers (18% versus 3%; $P<0.01$) at a significantly higher rate (Table 4). Acute phlegmonous appendicitis or perforations were completely absent in the CD group ($P<0.01$). The following features, considered typical of CD, were not found in controls: lymphoid aggregates in the subserosa, significant crypt distortion, and erosions and ulcers with histiocytes as the predominant cell type lining the border. Also, focal inflammation, which occurred in both groups, showed a different histology: In controls with focal inflammation with or without crypt destruction, neutrophils were the predominant cell type infiltrating the crypts. In contrast, in CD the inflammatory infiltrate in cases with focal inflammation was composed of histiocytes and lymphocytes, whereas neutrophilic granulocytes were a minor population (Fig. 1).

Findings in CD patients undergoing appendectomy before ileocolonic resection

From the 52 patients in whom appendectomy was previously performed, sections of 14 appendices were received from outside hospitals and histologically reevaluated. These specimens were from six men and eight women with a median age of 26.5 years (range 20–50 years). Duration between appendectomy and primary intestinal resection ranged from 0.4 to 20 years (median 4 years). In two appendices, active CD with transmural inflammation was found. The other appendices were considered free of active CD. In 12 specimens the histology appeared normal. An obliteration of the lumen was found in two cases, and acute non-CD-associated appendicitis was observed in the remainder, with two specimens showing neutrophilic mucosal infiltration, one showing ulcers, and one showing acute phlegmonous appendicitis.

Gastrointestinal sites involved in CD patients with or without CD of the appendix

Overall, CD of the terminal ileum was the most frequent finding (n=84, 93%), followed by colonic involvement (n=59, 66%). In cases with CD of the appendix, inflammation consistent with CD was observed in the colon in 89% (n=32), whereas in patients with CD-negative appendices, colonic involvement was observed in only 50% (n=27, $P<0.01$). Furthermore, involvement of both the right and left colon was found significantly more often in patients with appendiceal involvement (53% versus 26%, $P<0.01$). In cases with CD of the right colon, the cecum was most often affected (n=17, 71%).

Upper endoscopy was performed in 36 out of 90 patients. Subjects with CD of the appendix showed a higher percentage of involvement of the upper-GI tract (41% versus 16%), but the difference did not reach statistical significance, most likely due to the small number of cases.

A comparable number of patients with or without CD of the appendix were on either steroids, 5-aminosalicylate, or both. In contrast, significantly more patients with appendiceal involvement had received azathioprine compared to those without appendiceal involvement (19% versus 2%, $P<0.01$) (Table 2).

Discussion

Data published so far on the involvement of the appendix in CD published show a percentage ranging from 0 to 54% (Table 1) [2, 7, 9, 10, 11, 13, 14, 19, 26]. In this study the appendix was involved in 40% of patients with CD who had undergone primary right ileocolonic or (sub)total colonic resection due to CD-related complications.

Histologically, several types of lesions were demonstrated to be typical for CD of the appendix after comparison with the histology in control specimens. Similar to findings in the remainder of the GI tract, focal or discontinuous inflammation of the mucosa with or without lengthening and distortion of the crypts are hallmarks of this disease. In contrast to control appendectomy specimens, where the inflammatory infiltrate was composed mainly of neutrophilic granulocytes, in CD-associated inflammation histiocytes and lymphocytes predominated.

Considering crypt distortion the appendix may pose more problems to the pathologist when compared to the colon. This is because the appendix harbors numerous, often hyperplastic, lymphoid follicles that are known to induce distortion of the crypts. Therefore, only a significant elongation and distortion of crypts in combination with an increased inflammatory (lymphoplasmocytic) infiltration of the mucosa is consistent with CD.

In patients with ulcerative colitis with involvement of the appendix the histologic hallmark is a diffuse inflammatory infiltration of the mucosa of the entire appendix in combination with diffuse architectural abnormalities. Although this pattern of involvement may also occur in CD, it was not found in our collective.

Another important histologic sign of CD of the appendix is the presence of abundant histiocytes at the border of ulcers or erosions. Clearly, epitheloid granulomas are another important diagnostic feature; however, they are found only in a percentage of patients (in our study, 25%). Furthermore, other diseases such as tuberculosis or infection with *Yersinia pseudotuberculari*s, or a foreign body reaction, may also produce granulomas and should be carefully ruled out [25]. Granulomas are particularly useful when interpreted in context with other histologic findings [3] such as discontinuous inflammation – comparable to the interpretation of granulomas in the stomach [4]. In our opinion one of the most important histologic features of CD in the appendix is the presence of lymphoid aggregates at the border of the muscularis propria and subserosa. In most cases it is associated with an infiltration of the muscular layer by mononuclear leukocytes. In comparison, in patients with acute non-CD-associated phlegmonous appendicitis, lymphoid aggregates are smaller and lack a clear border. Furthermore, the muscular layer shows a predominant neutrophilic infiltration, which is not the case in CD.

Obliteration of the appendiceal lumen was significantly overrepresented in patients with CD (31% versus 12% in CD-negative controls, $P<0.01$). In the majority of cases obliteration was not found in combination with active CD appendicitis but in appendices that otherwise appeared normal ($P<0.01$). The obliteration might be explained by a recurrent inflammation in the course of CD leading to subsequent scarring. Less likely is the possibility that CD patients may be more prone to non-CD-related inflammation of the appendix resulting in obliteration [1, 17].

In contrast to control patients acute phlegmonous appendicitis was completely absent in patients with CD, whereas erosions and ulcers were found frequently (18%). Neither did Larsen and coworkers find any case of acute phlegmonous appendicitis in patients with CD [11]. In comparison, more than half of the appendices (59%) of control patients showed an acute phlegmonous appendicitis, mirroring data in the literature [6]. The absence of acute phlegmonous appendicitis in CD patients is best explained by a selection bias and not by a resistance to non-CD-associated appendicitis. This notion is supported by the fact that CD patients analyzed in this study underwent surgery because of CD-associated complications and not because of a disease of the appendix. Indeed, in the group of CD patients who underwent appendectomy before ileocolonic resection, one case of phlegmonous appendicitis was found.

In subjects with CD of the appendix a colonic involvement was observed more often when compared to the remaining CD cases (89%). Right-sided colonic involvement alone was not observed significantly more often in this group – only involvement of the right and left colon. This could be because the appendix is developmentally and anatomically a part of the colon and therefore shows a comparable susceptibility to involvement, which is particularly obvious in cases with widespread colonic CD. Although there was a trend toward a more frequent involvement of the upper-GI tract, the low number of cases undergoing upper endoscopy did not allow a definite conclusion. Significantly more patients with CD of the appendix were treated with azathioprine, suggesting that involvement of the appendix is found in patients with a more severe course of the disease.

In conclusion, we show that appendiceal involvement is frequent in patients with CD who undergo ileocolonic resection. In most cases CD of the appendix was associated with widespread involvement of the colon. Histologic criteria heralding involvement of the appendix are similar to those applied in the colon and allow differentiation of non-CD-associated appendicitis.

Acknowledgements We would like thank to the following pathologists from Austrian outside clinics for providing histologic slides of appendices (in alphabetical order): O. Braun (Horn), H.P. Dinges (Klagenfurt), H. Hanak (Vienna), M. Klimpfinger (Vienna), D. Kosak (Vienna), G. Kronik (Krems), S. Naude (Mödling), O. Pendl (Vienna), W. Pescosta (Vienna), W. Pflanzl and G. Bayer (Oberwart), W. Stiglbauer (Wr. Neustadt), and G. Widhalm (Vienna). The authors thank G. Granditsch (Vienna) for helpful discussion.

References

1. Arnbjornsson E, Bengmark S (1983) Obstruction of the appendix lumen in relation to pathogenesis of acute appendicitis. Acta Chir Scand 149:789–891
2. Crohn B, Ginzburg L, Oppenheimer G (1932) Regional ileitis: a pathological and clinical entity. JAMA 99:1323–1329
3. Dudley TH Jr, Dean PJ (1993) Idiopathic granulomatous appendicitis, or Crohn's disease of the appendix revisited. Hum Pathol 24:595–601
4. Ectors NL, Dixon MF, Geboes KJ, Rutgeerts PJ, Desmet VJ, Vantrappen GR (1993) Granulomatous gastritis: a morphological and diagnostic approach. Histopathology 23:55–61

5. Fonkalsrud EW, Ament ME, Fleisher D (1982) Management of the appendix in young patients with Crohn's disease. Arch Surg 117:11–14
6. Fujita W, Shigemoto H, Nishimoto T, Tsukiyama K, Ugaji Y (1985) Acute appendicitis: a study on 118 patients [in Japanese]. Nippon Geka Gakkai Zasshi 86:464–469
7. Hamano K (1985) Surgical treatment of Crohn's disease – recurrence and prognosis in operated cases [in Japanese]. Nippon Geka Gakkai Zasshi 86:1324–1327
8. Jenkins D, Balsitis M, Gallivan S, Dixon MF, Gilmour HM, Shepherd NA, et al (1997) Guidelines for the initial biopsy diagnosis of suspected chronic idiopathic inflammatory bowel disease. The British Society of Gastroenterology Initiative. J Clin Pathol 50:93–105
9. Kahn E, Markowitz J, Daum F (1992) The appendix in inflammatory bowel disease in children. Mod Pathol 5:380–383
10. Kovalcik P, Simstein L, Weiss M, Mullen J (1977) The dilemma of Crohn's disease: Crohn's disease and appendectomy. Dis Colon Rectum 20:377–380
11. Larsen E, Axelsson C, Johansen A (1970) The pathology of the appendix in morbus Crohn and ulcerative colitis. Acta Pathol Microbiol Scand Suppl 212:161–165
12. Le Berre N, Heresbach D, Kerbaol M, Caulet S, Bretagne JF, Chaperon J, et al (1995) Histological discrimination of idiopathic inflammatory bowel disease from other types of colitis. J Clin Pathol 48:749–753
13. Lennard-Jones JE, Morson BC (1969) Changing concepts in Crohn's disease. Dis Mon:1–37
14. Lockhart-Mummery HE, Morson BC (1964) Crohn´s disease of the large intestine. Gut 5:493–509
15. Nostrant TT, Kumar NB, Appelman HD (1987) Histopathology differentiates acute self-limited colitis from ulcerative colitis. Gastroenterology 92:318–328
16. Oberhuber G (1998) Histology of chronic inflammatory bowel diseases: Implications for clinical diagnosis. Chir Gastroenterol Interdiszip Gespr 14:90–96
17. Olsen BS, Holck S (1987) Neurogenous hyperplasia leading to appendiceal obliteration: an immunohistochemical study of 237 cases. Histopathology 11:843–849
18. Oren R, Rachmilewitz D (1992) Preoperative clues to Crohn's disease in suspected, acute appendicitis. Report of 12 cases and review of the literature. J Clin Gastroenterol 15:306–310
19. Rappaport H, Burgoyne FH, Smetana HF (1951) The pathology of regional enteritis. Mil Surg 109:463–502
20. Russel MG, Stockbrugger RW (1998) Is appendectomy a causative factor in ulcerative colitis? Eur J Gastroenterol Hepatol 10:455–457
21. Rutgeerts P, D'Haens G, Hiele M, Geboes K, Vantrappen G (1994) Appendectomy protects against ulcerative colitis. Gastroenterology 106:1251–1253
22. Schmitz-Moormann P, Schag M (1990) Histology of the lower intestinal tract in Crohn's disease of children and adolescents. Multicentric Paediatric Crohn's Disease Study. Pathol Res Pract 186:479–484
23. Schmitz-Moormann P, Himmelmann GW, Brandes HJ (1983) [Chronic inflammatory bowel diseases. Diagnosis based on biopsy sections]. Z Gastroenterol 18:21–26
24. Shivananda S, Hordijk ML, Ten Kate FJ, Probert CS, Mayberry JF (1991) Differential diagnosis of inflammatory bowel disease. A comparison of various diagnostic classifications. Scand J Gastroenterol 26:167–173
25. Tanaka M, Riddell RH (1990) The pathological diagnosis and differential diagnosis of Crohn's disease. Hepatogastroenterology 37:18–31
26. Warren S, Sommers SC (1948) Cicatrizing enteritis (regional enteritis) as a pathologic entity: analysis of one hundred and twenty cases. Am J Pathol 24:474–501
27. Wettergren A, Munkholm P, Larsen LG, Meinecke B, Langholz E, Jess P, et al (1991) Granulomas of the appendix: is it Crohn's disease? Scand J Gastroenterol 26:961–964

Virchows Arch (2002) 440:404–409
DOI 10.1007/s004280100521

ORIGINAL ARTICLE

A. Sakamoto · Y. Oda · H. Yamamoto · Y. Oshiro
K. Miyajima · E. Itakura · S. Tamiya · Y. Honda
A. Ishihara · Y. Iwamoto · M Tsuneyoshi

Calponin and h-caldesmon expression in atypical fibroxanthoma and superficial leiomyosarcoma

Received: 5 April 2001 / Accepted: 30 July 2001 / Published online: 7 November 2001
© Springer-Verlag 2001

Abstract To evaluate smooth muscle differentiation, myogenic markers [desmin, alpha-smooth muscle actin (SMA), and muscle-specific actin (HHF35)] have been widely used. Calponin and h-caldesmon, which are cytoskeleton-associated actin-binding proteins, have been reported to be more specific myogenic markers, especially since myofibroblasts express a small amount of h-caldesmon. Atypical fibroxanthoma (AFX) occurs in the sun-exposed skin of the elderly and follows a benign clinical course. Histologically, AFX, which is a pleomorphic spindle cell tumor and considered to be a superficial variant of malignant fibrous histiocytoma, also mimics leiomyosarcoma. AFX has been thought to differentiate along pathways with fibrohistiocytic and myofibroblastic phenotypes. AFX (*n*=10), superficial leiomyosarcoma (S-LMS) (*n*=17) and benign fibrous histiocytoma (BFH) (*n*=17) were analyzed for myofibroblastic and smooth muscle differentiation immunohistochemically from the viewpoint of comparison. AFX and BFH showed immunoreactivities respectively for calponin (3/10, 11/17), desmin (3/10, 1/17), SMA (3/10, 13/17), and HHF35 (1/10, 5/17), but failed to express h-caldesmon (0/10, 0/17). S-LMS had a high immunoreactive rate of calponin (17/17), desmin (13/17), SMA (16/17), and HHF35 (16/17), while also expressing caldesmon (11/17). The results reveal that AFX and BFH have immunoreactivities for several myogenic markers, with myofibroblastic differentiation (calponin: ±, h-caldesmon: –), but without the smooth muscle differentiation seen in S-LMS (calponin:+, h-caldesmon: ±). In addition, calponin and h-caldesmon are considered to be useful markers for distinguishing AFX from S-LMS.

Keywords Atypical fibroxanthoma · Superficial leiomyosarcoma · Benign fibrous histiocytoma · Calponin · H-caldesmon

Grant sponsor: Grant-in-Aid for Cancer Research from the Fukuoka Cancer Society, Fukuoka, Japan and Grant-in-Aid for General Scientific Research from the Ministry of Education, Science and Culture (12670167) Tokyo, Japan.

A. Sakamoto · Y. Oda · H. Yamamoto · K. Miyajima · E. Itakura
S. Tamiya · M. Tsuneyoshi (✉)
Department of Anatomic Pathology, Pathological Sciences,
Graduate School of Medical Sciences, Kyushu University,
3-1-1 Maidashi, Higashi-ku, Fukuoka, 812-8582, Japan
e-mail: masazumi@surgpath.med.kyushu-u.ac.jp
Tel.: +81-92-6426061, Fax: +81-92-6425968

Y. Iwamoto
Department of Orthopaedic Surgery,
Graduate School of Medical Sciences, Kyushu University,
Fukuoka, Japan

Y. Oshiro
Department of Pathology, Matsuyama Red Cross Hospital,
Matsuyama, Japan

Y. Honda
First Department of Pathology, Faculty of Medicine,
Kumamoto University, Kumamoto, Japan

A. Ishihara
Department of Pathology, Nobeoka Hospital, Miyazaki, Japan

Introduction

Calponin and h-caldesmon are cytoskeleton-associated proteins and both are expressed in smooth muscle and myoepithelial cells. Calponin is a calmodulin-, F-actin-, and tropomyosin-binding protein and is considered important in the regulation of smooth muscle contraction [7, 8, 24, 25]. Caldesmon has two isoforms, high-molecular-weight (h-caldesmon) and low-molecular-weight (l-caldesmon) [23, 26], and h-caldesmon has been reported to be specific for smooth muscle cells [14, 26]. It combines with calmodulin, tropomyosin, and actin and is thought to regulate cellular contraction [23]. In addition to smooth muscle cells, calponin, but not h-caldesmon, has been reported to be expressed in myofibroblastic lesions, such as desmoid and nodular fasciitis [17, 27]. Therefore, h-caldesmon is considered to be a useful marker for distinguishing smooth muscle tumors from myofibroblastic tumors [6, 17].

Helwig [11] initially designated the term “atypical fibroxanthoma” (AFX) in 1961. AFX is typically a nodu-

lar ulcerative lesion arising from the sun-exposed skin of the head and neck in the elderly. In its less common forms, the tumor occurs on the extremities and trunk [3, 5]. A report demonstrated UV-induced p53 mutations occurring at dipyrimidine sites in AFX, suggesting a central role for UV radiation in the pathogenesis of AFX [4].

AFX, which is a pleomorphic spindle cell tumor, is widely recognized as being a variant of malignant fibrous histiocytoma (MFH) occurring in the dermis [5, 28]. When AFX is less pleomorphic, it becomes indistinguishable from leiomyosarcoma [2]. Furthermore, AFX is known to express the myogenic markers mentioned above as well as histiocytic markers. Accordingly, it has been thought that AFX differentiates along multiple pathways with a bimodal pattern of fibrohistiocytic and myofibroblastic phenotypes [15].

To evaluate smooth muscle differentiation when making a diagnosis, alpha-smooth muscle actin (SMA) and muscle-specific actin are usually used immunohistochemically [21, 22]. However, these markers are not specific, since they have been identified not only in leiomyosarcoma, but also in AFX [15, 16, 19].

In order to evaluate myogenic differentiation in AFX in comparison with that in superficial leiomyosarcoma and benign fibrous histiocytoma, we examined calponin, h-caldesmon, and other myogenic markers [desmin, alpha-SMA, and muscle-specific actin (HHF35)] in these tumors. Ki-67 expression (cell-proliferation marker, MIB-1-LI) and some clinicopathological features were also compared.

Materials and methods

Specimens

Ten cases of AFX, 17 cases of superficial leiomyosarcoma (S-LMS), and 17 cases of benign fibrous histiocytoma (BFH) were collected from the histopathological files at our institute. In this study, we use the term “superficial” for leiomyosarcoma centered within the cutis or subcutis, in line with previous reports [9, 10]. In addition, the cases of benign fibrous histiocytoma were selected at random. Histopathological features were investigated and compared between AFX, S-LMS, and BFH using hematoxylin-eosin (H&E)-stained microscopic specimens. Formalin-fixed paraffin-embedded tissue blocks of these cases were used for immunohistochemical analysis.

We evaluated the frequency of mitotic figures, the presence of xanthoma cells, the degree of inflammatory elements, the involvement of appendages, and presence of giant cells in each case. The degree of inflammatory elements was assessed (absent, slight, mild, moderate, and dense).

Immunohistochemistry

Four-micron-thick histological sections of 10% formalin-fixed, paraffin-embedded materials were cut, mounted on glass slides coated by 3-aminopropyltriethoxysilane, and air dried overnight at room temperature. The sections were deparaffinized in xylene and rehydrated in ethanol. After dehydration, endogenous peroxidase was blocked by methanol containing 0.3% H_2O_2 for 30 min in the case of all of the above-mentioned antibodies. The sections were incubated with the primary antibody at 4°C overnight, followed by reaction with the streptavidin-biotin complex method using an SAB-PO kit (Nichirei, Tokyo, Japan). The sections were then finally reacted in a 3,3′ diaminobenzidine, peroxytrichloride substrate solution, counterstained with hematoxylin, and then mounted.

As for the antibodies for h-caldesmon and Ki-67, specimens were pretreated by heating in a microwave oven, while in the case of anti-calponin, specimens were preincubated in Trypsin (Sigma Chemical, St. Louis, MO, USA) in phosphate-buffered saline (PBS) for 30 min at 37°C. The antibodies used in this study were all mouse monoclonal antibodies and their dilutions were 1:200 for anti-calponin (CALP, Dako, Carpinteria, CA., USA), 1:400 for anti-h-caldesmon (h-CD, Dako, Carpinteria, CA, USA), 1:100 for anti-desmin (D33, Dako A/S, Glostrup, Denmark), 1:5,000 for anti-alpha-SMA (1A4, Sigma BioSciences, St. Louis, MO, USA), 1:200 for anti-muscle-specific actin (HHF35, Biomedia Corp, Foster City, CA, USA), and 1:100 for anti-Ki-67 (MIB-1, Immunotech, Marseilles, France).

Assessment of immunoreactivity

We evaluated the immunoreactivities of calponin, h-caldesmon, desmin, SMA, and HHF35 in the cytoplasm of tumor cells. The extent of staining in tumor cells was classed using a scoring system: 0 when <5% of tumor cells were stained; 1+ when ≥5% but <30% of the tumor cells were stained; 2+ when ≥30% but <80% of the tumor cells were stained; and 3+ when ≥80% of the tumor cells were stained. All scores greater than 1+ were interpreted as positive results, the others as negative results. Regarding Ki-67, in the selected areas containing the largest number of MIB-1-positive nuclei cells, the MIB-1-labeling index (MIB-1-LI) was estimated as the percentage of positive cells, counting at least 1,000 tumor cells.

Statistical analysis

The data regarding immunohistochemistry, clinicopathological features, and MIB-1-LI were evaluated using the Mann-Whitney *U*-test. A P value of <0.05 was considered to indicate statistical significance.

Results

Clinical features

The average ages (in years) of patients with these lesions were as follows; AFX (71.3; range, 46–92), S-LMS (55.9; 21–88), and BFH (27.0, 18–39) in descending order, with a significant difference between AFX or S-LMS and BFH (P<0.01). There was no significant difference between the average age of patients with AFX and S-LMS.

AFX showed a male-female predominance of 7 to 3 (M/F: 2.3/1), while S-LMS showed an 11 to 6 female predominance (M/F: 1/1.8). BFH showed no gender bias, occurring in 8 males and 9 females (M/F: 1/1.1). AFX occurred on the sun-exposed skin of the head, neck, and finger (9/10; 90%), except for one case on the leg (10%). AFX is known to occur in two clinical settings, on the head and neck of older people and on the extremities or trunk of younger people [3]. In this study, seven cases occurred on the head and neck (82, 84, 65, 71, 73, 92 and 86 years old). The other three AFX cases occurred

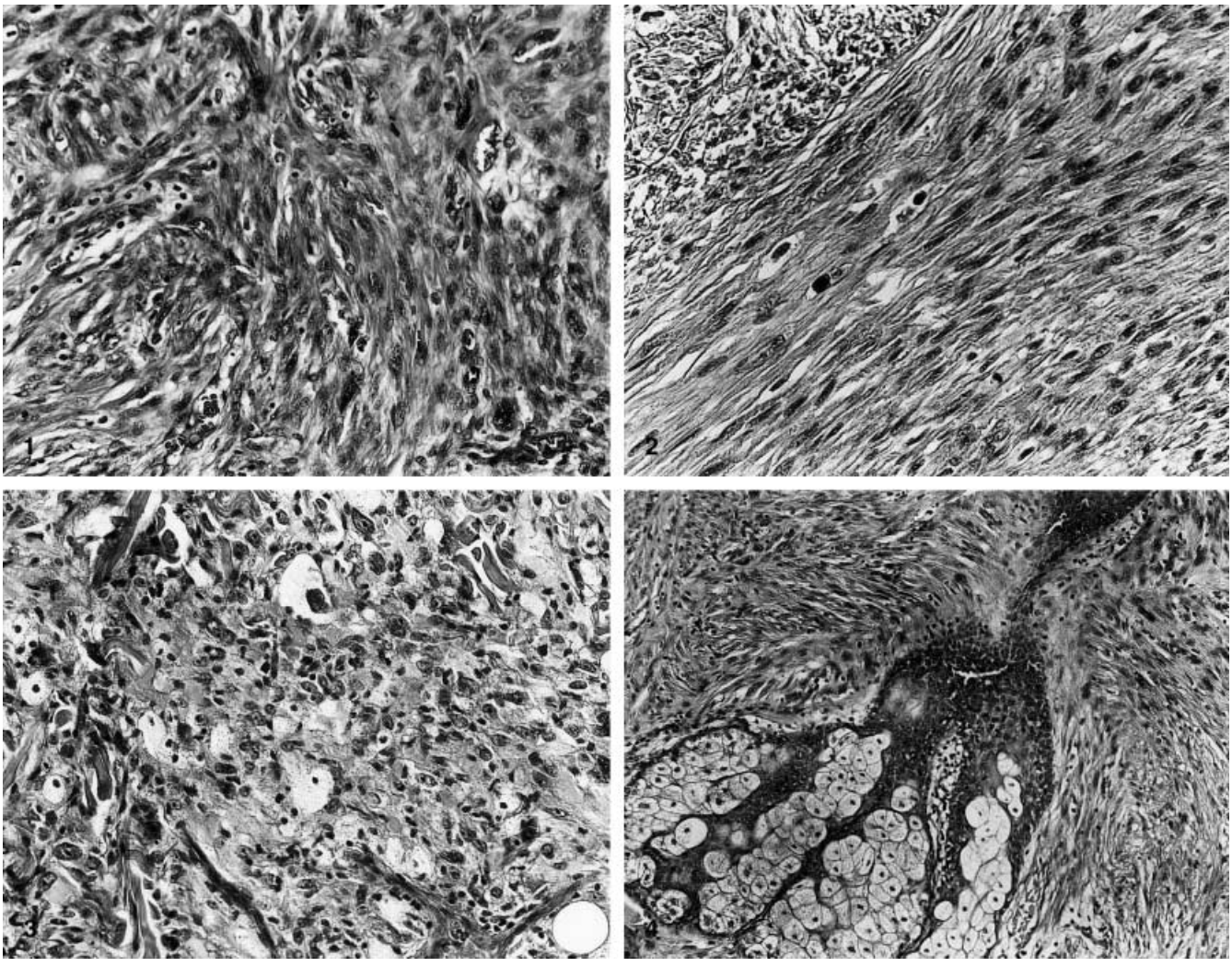

Fig. 1 Atypical fibroxanthoma, demonstrating proliferation of atypical spindle or epithelioid cells arranged in a haphazard or disorderly pattern, ×200

Fig. 2 Superficial leiomyosarcoma, which is composed of spindle cells with blunt-ended nuclei arranged in interlacing fascicles, ×250

Fig. 3 Atypical fibroxanthoma. Xanthoma cells can be frequently observed, some of which have enlarged nuclei suggesting neoplastic cells, ×200

Fig. 4 Atypical fibroxanthoma. Appendage involvement within the lesion can be observed, ×100

on the extremities. these in the three youngest patients in our series of AFX (50, 46, and 64 years old). Fifteen out of the 17 cases of S-LMS (89%) occurred on the trunk, lower extremities, or proximal upper extremities, all of which sites can be assumed to have been mostly shielded from sun exposure. In the other two cases of S-LMS, the lesions occurred on the wrists (12%). In contrast, BFH occurred at various sites without showing any special tendency. Furthermore, in our series, recurrence was recognized in six out of the 17 cases of S-LMS (35%), but not in any of the 10 AFX or 17 BFH) cases. The average size (in centimeters) of these lesions was as follows: S-LMS (4.7; range, 1.3–15.0), AFX (1.4; 1.0–3.0), and BFH (0.8; 0.5–1.3) in descending order, with a significant difference between S-LMS and AFX ($P<0.01$), between S-LMS and BFH ($P<0.01$), and between AFX and BFF ($P<0.01$).

Histological features

AFX is a nodular ulcerative lesion composed of various proportions of a mixture of spindle, pleomorphic, and epithelioid cells, arranged in a haphazard or disorderly pattern (Fig. 1). In this study, seven cases occurred on the head and neck and these were all of the pleomorphic type. Among the three AFX cases that occurred on the extremities, two were pleomorphic (one on the finger and one on the leg), while the other case was spindle cell/non-pleomorphic in type (on the finger). In a previous report, some of the AFX cases which occurred on the extremities were assumed to be examples of atypical benign fibrous histiocytoma [1]. However, the two AFX cases which occurred on the fingers in our series had UV-induced p53 mutations of C-T transitions at dipyri-

Table 1 Summary of immunohistochemical features of AFX and superficial leiomyosarcoma. *AFX* atypical fibroxanthoma, *S-LMS* superficial leiomyosarcoma, *BFH* benign fibrous histiocytoma, *SMA* smooth muscle actin, *HHF35* muscle-specific actin

Lesions	Calponin	h-Caldesmon	Desmin	SMA	HHF35
AFX	3/10 (30%)	0/10 (0%)	3/10 (30%)	3/10 (30%)	1/10 (10%)
S-LMS	17/17 (100%)	11/17 (65%)	13/17 (76%)	16/17 (94%)	16/17 (94%)
BFH[a]	11/17 (65%)	0/17 (0%)	1/17 (6%)	13/17 (76%)	5/17 (29%)

[a] BFHs were selected at random from our histological files

midine sites [20]. The BFH cases were located in the dermis or the superficial subcutis. BFH consisted of fibroblastic cells and histiocytic cells arranged in short interlacing fascicles or a vague storiform pattern. The tumor cells of BFH demonstrated no pleomorphism. Leiomyosarcoma was composed primarily of spindle cells with blunt-ended nuclei arranged in an interweaving and fascicular fashion (Fig. 2).

Mitotic figures were often seen (1–8/10 high-power fields, HPFs) in all (10/10) of the AFX cases as well as in 15 of 17 (88%) S-LMS cases, again commonly (1–10/10 HPFs). Atypical mitotic figures were also seen both in the AFX (5/10; 50%) and the S-LMS (6/17; 35%) cases. On the other hand, obvious mitotic figures including atypical types could not be recognized in our BFH cases (0/17). Xanthoma cells were seen in the AFX (3/10; 30%) (Fig. 3) and S-LMS (1/17; 6%) cases, but not in the BFH cases (0/17). Inflammatory elements (lymphocytes, plasma cells, and neutrophils) were present in all the AFX cases, being denser in the tumor borders and the ulceration sites than in the center of the lesions. AFX cases seemed to have a larger amount of inflammatory elements (moderate to dense) than BFH (mainly slight to mild) or S-LMS (mainly slight) cases.

Appendage involvement within the lesions, suggesting undestroyed adnexal structures, was frequently seen in the AFX cases (5/10; 50%) (Fig. 4) in contrast to the S-LMS (0/17) and BFH (0/17) cases; however. we cannot deny the influence of the superficial location of AFX. Osteoclast-type multinucleated giant cells were seen in AFX (3/10; 30%) and S-LMS (2/17; 12%) cases, while Touton-type giant cells were only seen in BHF cases (3/17; 18%).

Immunohistochemical findings

The immunohistochemical results are summarized in Table 1. AFX was immunoexpressed in calponin (3/10; 30%), desmin (3/10; 30%), alpha-SMA (3/10; 30%) and muscle-specific actin (1/10; 10%), while the expression of h-caldesmon was absent (0/10). Similar to AFX, BHF showed no h-caldesmon expression (0/17), although it showed expression of calponin (11/17; 65%), desmin (1/17; 6%), alpha-SMA (13/17; 76%), and muscle-specific actin (5/17; 29%). S-LMS showed a high positive immunoexpression rate for calponin (17/17; 100%), desmin (13/17; 76%), alpha-SMA (16/17; 94%), and muscle-specific actin (16/17; 94%), in addition to the expression of h-caldesmon (11/17; 65%) (Figs. 5 and 6).

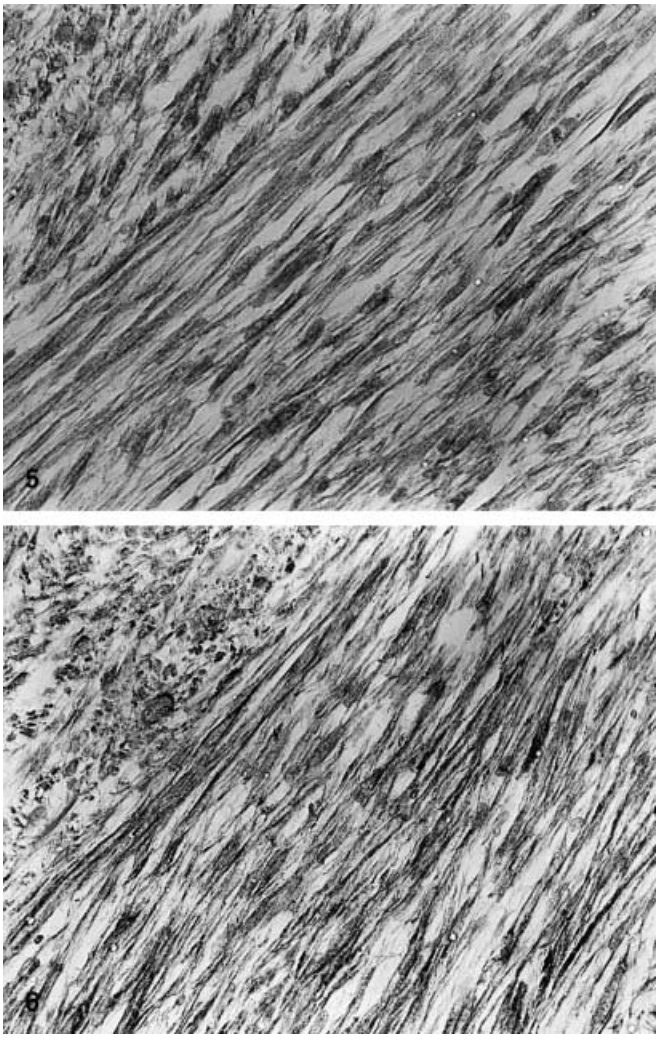

Fig. 5 Leiomyosarcoma, showing positive cytoplasmic immunoreaction for calponin, ×300

Fig. 6 Leiomyosarcoma, showing positive cytoplasmic immunoreaction for h-caldesmon, ×300

These features of positive/negative calponin and negative h-caldesmon immunoexpressions seen in both AFX and BFH seem to confirm that these tumors have myofibroblastic differentiation, in contrast to the reversed features of positive calponin and positive/negative h-caldesmon expressions suggesting smooth muscle differentiation, which were seen in S-LMS.

The average MIB-1-LIs in descending order are as follows: S-LMS, 18.8±3.5; AFX, 16.7±2.2; and BFH,

2.8±0.8; with a significant difference between both AFX and S-LMS and BFH ($P<0.01$). The difference in the MIB-1-LI between AFX and S-LMS was not significant.

Discussion

In this study, we evaluated the immunohistochemical reactivity of two actin-binding, cytoskeleton-associated proteins of calponin and h-caldesmon, as well as other myogenic markers of desmin, alpha-SMA, and muscle-specific actin (HHF35). In normal tissue, both calponin and h-caldesmon are consistently present in smooth muscle tissue and absent in skeletal muscle and other mesenchymal cell types [7]. In previous studies, the expressions of calponin and h-caldesmon in benign smooth muscle tumors have been consistent [17, 27]. In addition to being expressed in smooth muscle cells, calponin was also expressed in myofibroblastic lesions, such as desmoid and nodular fasciitis. On the other hand, h-caldesmon was only expressed to a very small degree in myofibroblastic lesions. Therefore, calponin and h-caldesmon are thought suitable for use as markers of myogenic differentiation in the evaluation of soft-tissue tumors, especially when attempting to distinguish smooth muscle differentiation from myofibroblastic differentiation [17, 27].

AFX is a pleomorphic spindle cell tumor. Since it remains difficult to distinguish AFX from MFH due to their close histological resemblance, AFX is widely recognized as being a variant of MFH that arises in the dermis [5, 28]. A less atypical variant of AFX has been reported, and in those cases leiomyosarcoma is also taken into consideration as a differential diagnosis [2]. AFX demonstrates multidirectional differentiation and morphologically heterogeneous features with a bimodal pattern of fibrohistiocytic and myofibroblastic phenotypes, on the basis that the expression of alpha-SMA has been described in 41% [15], while that of muscle-specific actin has also been described in 27–67% of AFX cases [15, 16, 19]. These actin-positive cells in AFX may reflect either the presence of reactive myofibroblasts or the differentiation of tumor cells into myofibroblasts. However, spindle, epithelioid, and bizarre atypical cells in AFX have been reported to express the above actins, although the cell type and the content of these positive cells varied from case to case [15]. In our study, three out of the ten cases of AFX (30%) showed staining for alpha-SMA, while one of them (10%) expressed muscle-specific actin. In addition, three of the ten cases of AFX (30%) showed staining for calponin, whereas none of them showed any reaction for h-caldesmon. On the other hand, all the cases of S-LMS expressed calponin (17/17; 100%) and approximately half of them expressed h-caldesmon (11/17; 65%). These results seemed to confirm that tumor cells of AFX, unlike S-LMS, have myofibroblastic differentiation but not smooth muscle differentiation. Furthermore, the immunoexpressions of calponin and h-caldesmon could possibly be useful markers in distinguishing AFX from S-LMS.

In a previous report, some uterine leiomyosarcomas showed h-caldesmon reactivity in the well-differentiated but not in the poorly differentiated areas. This led to the suggestion that there is a loss of h-caldesmon during tumor progression [13]. Accordingly, the reduced expression of h-caldesmon in our series of S-LMS might suggest a malignant character in leiomyosarcoma; however, there was no significant difference in the MIB-1-LI between the cases of S-LMS with h-caldesmon expression and those without.

Moreover, there was no significant difference between AFX and S-LMS with regard to the MIB-1-LI, as is also true for AFX and MFH [18]. However, despite rare reports of aggressive behavior, AFX almost always follows a benign clinical course [6]. Indeed, in this study, recurrence was recognized in S-LMS (6/17; 35%), but not in AFX cases (0/10). In addition to differences between their recurrent rates and tumor sites, AFX or S-LMS also differed in size (average size: AFX, 1.4 cm; S-LMS, 4.6 cm). Histologically, appendage involvement, suggesting an undestroyed appendage, was seen only in AFX (5/10; 50%), and not in S-LMS (0/17). A superficial location might contribute to the favorable clinical behavior [12] and the pathological differences noted between AFX and S-LMS; however, it is also possible that all these differences may simply be due to the peculiar pathogenesis of AFX.

In summary, we have evaluated, in addition to some clinicopathologic data in AFX, S-LMS, and BFH, the expression of calponin, h-caldesmon, and other myogenic markers. AFX shows myofibroblastic differentiation, on the basis of positive/negative calponin and negative h-caldesmon immunoexpressions. In contrast, S-LMS shows smooth muscle differentiation with positive calponin and positive/negative h-caldesmon. In addition, calponin and h-caldesmon are thought to be useful markers for distinguishing AFX from S-LMS.

Acknowledgements The English used in this manuscript was revised by Miss K. Miller (Royal English Language Centre, Fukuoka, Japan).

References

1. Beham A, Fletcher CD (1990) Atypical ‘pseudosarcomatous’ variant of cutaneous benign fibrous histiocytoma: report of eight cases. Histopathology 17:167–169
2. Calonje E, Wadden C, Wilson-Jones E, Fletcher CD (1993) Spindle-cell non-pleomorphic atypical fibroxanthoma: analysis of a series and delineation of a distinctive variant. Histopathology 22: 247–254
3. Dahl I (1976) Atypical fibroxanthoma of the skin. A clinicopathological study of 57 cases. Acta Pathol Microbiol Immunol Scand [A] 84:183–197
4. Dei Tos AP, Maestro R, Doglioni C, Gasparotto D, Boiocchi M, Laurino L, Fletcher CD (1994) Ultraviolet-induced p53 mutations in atypical fibroxanthoma. Am J Pathol 145: 11–17
5. Enzinger FM, Weiss SW (1995) Soft tissue tumors, 3rd edn. Mosby, St Louis
6. Fretzin DF, Helwig EB (1973) Atypical fibroxanthoma of the skin. A clinicopathologic study of 140 cases. Cancer 31: 1541–1552

7. Frid MG, Shekhonin BV, Koteliansky VE, Glukhova MA (1992) Phenotypic changes of human smooth muscle cells during development: late expression of heavy caldesmon and calponin. Dev Biol 153: 185–193
8. Gimona M, Herzog M, Vandekerckhove J, Small JV (1990) Smooth muscle specific expression of calponin. FEBS Lett 274: 159–162
9. Gustafson P, Willen H, Baldetorp B, Ferno M, Akerman M, Rydholm A (1992) Soft tissue leiomyosarcoma. A population-based epidemiologic and prognostic study of 48 patients, including cellular DNA content. Cancer 70: 114–119
10. Hashimoto H, Daimaru Y, Tsuneyoshi M, Enjoji M (1986) Leiomyosarcoma of the external soft tissues. A clinicopathologic, immunohistochemical, and electron microscopic study. Cancer 57: 2077–2088
11. Helwig EB (1963) Atypical fibroxanthoma. Proceedings of 18th Annual Tumor Seminar of San Antonio Society of Pathologists. Tex State J Med 59: 664–667
12. Helwig EB, May D (1986) Atypical fibroxanthoma of the skin with metastasis. Cancer 57: 368–376
13. Horiuchi A, Nikaido T, Ito K, Zhai Y, Orii A, Taniguchi S, Toki T, Fujii S (1998) Reduced expression of calponin h1 in leiomyosarcoma of the uterus. Lab Invest 78: 839–846
14. Lazard D, Sastre X, Frid MG, Glukhova MA, Thiery JP, Koteliansky VE (1993) Expression of smooth muscle-specific proteins in myoepithelium and stromal myofibroblasts of normal and malignant human breast tissue. Proc Natl Acad Sci USA 90: 999–1003
15. Longacre TA, Smoller BR, Rouse RV (1993) Atypical fibroxanthoma. Multiple immunohistologic profiles. Am J Pathol 17: 1199–1209
16. Ma CK, Zarbo RJ, Gown AM (1992) Immunohistochemical characterization of atypical fibroxanthoma and dermatofibrosarcoma protuberans. Am J Clin Pathol 97: 478–483
17. Miettinen MM, Sarlomo-Rikala M, Kovatich AJ, Lasota J. (1999) Calponin and h-caldesmon in soft tissue tumors: consistent h-caldesmon immunoreactivity in gastrointestinal stromal tumors indicates traits of smooth muscle differentiation. Mod Pathol 12: 756–762
18. Oshiro Y, Fukuda T, Tsuneyoshi M (1995) Atypical fibroxanthoma versus benign and malignant fibrous histiocytoma. A comparative study of their proliferative activity using MIB-1, DNA flow cytometry, and p53 immunostaining. Cancer 75: 1128–1134
19. Ricci A, Cartun RW, Zakowski MF (1988) Atypical fibroxanthoma. A study of 14 cases emphasizing the presence of Langerhans' histiocytes with implications for differential diagnosis by antibody panels. Am J Surg Pathol 12: 591–598
20. Sakamoto A, Oda Y, Itakura E, Oshiro Y, Nikaido O, Iwamoto Y, Tsuneyoshi M (2001) Immunoexpression of ultraviolet photoproducts and p53 mutation analysis in atypical fibroxanthoma and superficial malignant fibrous histiocytoma. Mod Pathol 14: 581–588
21. Skalli O, Ropraz P, Trzeciak A, Benzonana G, Gillessen D, Gabbiani G (1986) A monoclonal antibody against alpha-smooth muscle actin: a new probe for smooth muscle differentiation. J Cell Biol 103: 2787–2796
22. Skalli O, Schurch W, Seemayer T, Lagace R, Montandon D, Pittet B, Gabbiani G (1989) Myofibroblasts from diverse pathologic settings are heterogeneous in their content of actin isoforms and intermediate filament proteins. Lab Invest 60: 275–285
23. Sobue K, Tanaka T, Kanda K, Ashino N, Kakiuchi S (1985) Purification and characterization of caldesmon77: a calmodulin-binding protein that interacts with actin filaments from bovine adrenal medulla. Proc Natl Acad Sci USA 82: 5025–5029
24. Takahashi K, Hiwada K, Kokubu T (1986) Isolation and characterization of a 34,000-dalton calmodulin- and F-actin-binding protein from chicken gizzard smooth muscle. Biochem Biophys Res Commun 141: 20–26
25. Takahashi K, Hiwada K, Kokubu T (1987) Occurrence of anti-gizzard P34 K antibody cross-reactive components in bovine smooth muscles and non-smooth muscle tissues. Life Sci 41: 291–296
26. Ueki N, Sobue K, Kanda K, Hada T, Higashino K (1987) Expression of high and low molecular weight caldesmons during phenotypic modulation of smooth muscle cells. Proc Natl Acad Sci USA 84: 9049–9053
27. Watanabe K, Kusakabe T, Hoshi N, Saito A, Suzuki T (1999) h-Caldesmon in leiomyosarcoma and tumors with smooth muscle cell-like differentiation: its specific expression in the smooth muscle cell tumor. Hum Pathol 30: 392–396
28. Wick MR, Fitzgibbon J, Swanson PE (1993) Cutaneous sarcomas and sarcomatoid neoplasms of the skin. Semin Diagn Pathol 10: 148–158

Virchows Arch (2002) 440:410–417
DOI 10.1007/s004280100533

ORIGINAL ARTICLE

Toshimi Satoh · Osamu Tokunaga

Intracellular oxidative modification of low density lipoprotein by endothelial cells

Received: 1 November 2000 / Accepted: 23 July 2001 / Published online: 22 November 2001
© Springer-Verlag 2001

Abstract We investigated intracellular oxidative modification of low density lipoprotein (IOM-LDL) by endothelial cells (ECs) and the role of ferritin in this process. IOM-LDL was examined by immunocytochemistry with an anti-oxidized phosphatidylcholine antibody and by lipid peroxidation assay. Incubation of LDL-treated ECs (human umbilical vein endothelial cells, passage 3) with ferritin produced cytoplasmic immunostain with the antibody, especially in large or giant ECs, and the formation of thiobarbituric acid-reactive substance (TBARS) in these cells. These observations suggest that ECs can perform IOM-LDL. Incubation with the iron chelator deferoxamine or pretreatment of LDL-treated ECs with deferoxamine suppressed ferritin-induced IOM-LDL by greater than 60%. Antioxidants dimethylsulphoxide and butylated hydroxytoluene markedly inhibited IOM-LDL, but mannitol did so only mildly. Catalase and superoxide dismutase had little or no effect on IOM-LDL. Apoferritin substituted for ferritin did not induce IOM-LDL. Our data suggest that IOM-LDL is mediated by intracellular hydroxyl radical formation, which is catalyzed mainly by free iron released from ferritin, and that ECs contribute to the development of atherosclerosis via IOM-LDL.

Keywords Endothelial cell · LDL · Intracellular oxidation · Ferritin

Introduction

Recent studies suggest that oxidative modification of low density lipoprotein (LDL) plays an important role in atherogenesis [33, 45]. Oxidatively modified LDL is recognized by a scavenger receptor, or acetylated LDL receptor, and can induce the transformation of monocytes/macrophages into lipid-laden foam cells [10]. Our institute previously reported development of fatty streak-like lesions when human umbilical vein endothelial cell (EC)-modified LDL and human blood mononuclear cells were subjected to a three-dimensional culture system [46].

EC-induced oxidation of LDL is presumed to be an extracellular event, and cellular oxidative stress appears to be essential for oxidative modification of LDL [25, 34]. Intracellular iron has been shown to be critical for the induction of oxidative stress in ECs. Recently, using iron-chelator fungistat 8-hydroxyquinoline, which transports iron into ECs, Van Lentan et al. [40] showed that free iron in cultured arterial wall cells is critical for oxidative modification of LDL in medium. It is widely accepted that hydroxyl radicals, which contribute to lipid peroxidation [26, 32], are generated intracellularly by the iron-catalyzed Haber-Weiss reaction [17]. Considering these findings and the fact that ECs have been shown to take up LDL in vitro [42] and in vivo [41], the question is raised as to whether LDL taken up by ECs is oxidatively modified under intracellular oxidative stress.

Ferritin is a major storage site for iron in biological systems. Epidemiologic studies of human subjects have shown serum ferritin concentrations to be positively correlated with coronary heart disease and with carotid atherosclerosis [11, 15, 31]. Hypercholesterolemia in conjunction with increased serum ferritin increases the risk of such diseases [15, 31]. In a rabbit model of hypercholesterolemia, serum ferritin levels were shown to be elevated in animals that were iron-loaded, and those animals developed more atherosclerotic lesions than did control animals [2]. However, some reports have disputed the contribution of ferritin to the risk of atherosclerosis or coronary artery disease [1, 21].

In the present study, we investigated intracellular oxidative modification of LDL (IOM-LDL) and the role of ferritin in lipid peroxidation in a cell-culture system. To avoid uptake of oxidized LDL from the cell culture me-

Supported in part by a Grant-in-Aid from the Ministry of Education, Science and Culture, Japan (10670210)

T. Satoh (✉) · O. Tokunaga
Department of Pathology, Saga Medical School,
5–1–1 Nabeshima, Saga 849–8501, Japan
e-mail: satoht2@post.saga-med.ac.jp
Tel.: +81-952-343264, Fax: +81-952-34-2055

dium, we incubated LDL-pretreated ECs with ferritin in medium supplemented with lipoprotein-deficient serum. We then evaluated IOM-LDL immunocytochemically and biochemically.

Materials and methods

Isolation and culture of endothelial cells

Human umbilical vein endothelial cells (HUVECs) were harvested from human umbilical veins and cultured according to a previously described method [37, 46] but with some modifications. The cells were grown in medium RPMI 1640 without phenol red (Nissui Pharmaceutical Co., Tokyo, Japan), 0.294 g/l L-glutamine (GIBCO-BRL, Grand Island, NY), 15 µg/ml endothelial-cell growth supplement (Collaborative Research, Lexington, MA), 100 µg/ml heparin (Sigma Chemical Co., St. Louis, MO), 600 IU/ml penicillin + 600 µg/ml streptomycin (Pen-Strep, Sigma), and 1.25 µg/ml amphotericin B (Sigma) (Medium A) supplemented with 15% fetal bovine serum (FBS, Microbiological Associates, Logan, Utah) in a humidified incubator at 37°C in 5% CO_2 and 95% O_2. The cells were grown first in 60-mm dishes (Iwaki Glass, Tokyo, Japan). The medium was replaced every 2 days until the cells reached confluence. When the cells reached confluence, cells were passaged at a 1:3 split ratio with 0.05% trypsin-EDTA (Sigma) and seeded in 60-mm dishes. At passage 3, the cells were grown in 35-mm culture dishes (Iwaki Glass). HUVECs were grown on glass coverslips placed in 35-mm dishes. All culture dishes and glass coverslips were coated with 1% gelatin. Confluent cells at passage 3 were used for all experiments. Under phase-contrast microscopy, confluent cells displayed a cobblestone morphology. Identity of HUVECs was confirmed further by indirect immunofluorescence microscopy for the presence of von Willebrand factor.

Preparation of human LDL

Human LDL (density, 1.019 to 1.063 g/ml) was isolated from the plasma of healthy, normolipidemic male volunteers by sequential floating ultracentrifugation. Lipoprotein-deficient fetal bovine serum (LPDS, density >1.215 g/ml) was also prepared by ultracentrifugation. LDL was used for experiments immediately after preparation. Before use, the isolated fractions were dialyzed against physiological saline for 24 h at 4°C to remove EDTA. The initial thiobarbituric acid-reactive substance (TBARS) level of native LDL isolated in this manner was <0.5 ±0.07 nmol/mg cholesterol.

Oil Red O staining of cultured cells

LDL uptake by ECs was determined by lipid staining as described by Vlodavsky et al. [42] but with slight modifications. Cells were washed with phosphate-buffered saline (PBS) three times, rinsed in 70% ethanol for 2–3 s to block the interaction between PBS and Oil Red O, and then stained with Oil Red O Cells were then washed with 70% ethanol three times, fixed in 10% formalin for 20 min, and coverslipped for image analysis.

Antibodies and immunocytochemistry

Indirect immunocytochemistry of cultured HUVECs was performed to detect ferritin and oxidized LDL with the following primary antibodies: anti-horse spleen ferritin (rabbit polyclonal antibody, diluted 1:500; Sigma) and anti-oxidized phosphatidylcholine antibody (FOH1a/DLH3, mouse IgM monoclonal antibody, a gift from Dr. Itabe, Teikyo University, Tokyo, Japan) [12]. Cells were washed with PBS three times, fixed in 10% formalin for 20 min, and permeabilized with 0.01% saponin in PBS for 30 min at room temperature. Cells were incubated with 3% H_2O_2 in methanol for 30 min and then washed with PBS. After incubation in PBS containing 10% normal rabbit or mouse serum for 30 min at room temperature, the cells were incubated with primary antibody overnight at room temperature and then washed three times with PBS. The reaction was visualized with streptavidin-biotin-peroxidase complex (Histofine kit, Nichirei Co., Tokyo, Japan) using 3,3′-diaminobenzidine tetrahydrochloride (DAB, Sigma) as a chromogen substrate. The cells were counterstained with hematoxylin and coverslipped for image analysis. For each experiment, negative controls were established by substituting normal rabbit serum or isotype-matched mouse immunoglobulin for the primary antibody.

Image analysis

Color images of Oil Red O staining or immunostaining of HUVECs were obtained with a 3 CCD color camera (HC-2500 3 CCD, Fuji Film, Tokyo, Japan) mounted on a standard microscope (BHS-F; Olympus, Tokyo, Japan) and digitized with a two-dimensional analysis system (Mac SCOPE, Mitani Corporation, Fukui, Japan) connected to a Macintosh computer system (Power Macintosh 7100/80AV). We analyzed three sites from each specimen in all experiments. Three fields of 2.25 mm^2 were selected at random from the confluent monolayer of cells. Integrated density values for Oil Red O staining and immunostaining were determined after setting an appropriate threshold and were expressed as values/mm^2. The mean integrated density obtained from three independent experiments was used as a representative value for each specimen and in the statistical analysis.

Thiobarbituric acid-reactive substances assay

Formation of thiobarbituric acid-reactive substances (TBARS) was used as another indicator of lipid oxidation. Confluent cells were scraped off the plate with a rubber spatula, washed twice with 0.9% NaCl, and suspended in 1 ml 0.9% NaCl. An aliquot (0.1 ml) of this suspension was analyzed for protein content, and a 0.5 ml aliquot was analyzed fluorometrically for TBARS as described by Ohkawa et al. [23] with a spectrophotofluorometer (Model RF-540; Shimazu, Tokyo, Japan) at excitation 515 nm and emission 553 nm. TBARS content in postculture medium was determined by the method of Yagi [22]. TBARS values were expressed as nanomoles malondialdehyde (nM MDA) per milligram protein by extrapolation from external standard curves based on MDA formed from 1, 1, 3, 3-tetramethoxypropane.

Other assays

Protein levels were assayed by the method of Lowry [18] with bovine serum albumin as the standard. Cholesterol levels were determined with a cholesterol oxidase kit (Sigma). LDL concentrations in the present study are given in milligrams of cholesterol.

Statistical analysis

All data are expressed as mean±SEM. Statistical differences between means were determined by Student's *t*-test for unpaired data or by one-way ANOVA and Bonferonni correction. $P<0.05$ was considered statistically significant.

Experimental protocols

To assess the uptake of LDL by HUVECs, confluent cells were incubated for 6, 12, and 24 h with LDL (80, 160, and 240 mg/dl) in heparin-free Medium A supplemented with 15% FBS. At the designated time point, aliquots were removed and HUVECs washed

with PBS three times and then incubated with fresh Medium A supplemented with 15% lipoprotein-deficient fetal borine serum (LPDS) for 30 min to stimulate internalization of LDL. Aliquots were then removed, and the cells were stained with Oil Red O. LDL-treated cells in the following experiments were prepared by incubation with different concentrations of LDL for a given time; then internalization of LDL, removal of aliquots, and three washes with PBS were performed as described above.

To investigate the uptake of ferritin by HUVECs, confluent cells were incubated for 6, 12, and 24 hours with ferritin (1, 10, and 100 µg/ml) in Medium A supplemented with 15% LPDS. At the designated time, aliquots were removed, and the cells were processed for immunocytochemistry with anti-ferritin antibody.

To determine whether IOM-LDL occurred and to examine whether IOM-LDL was time- or LDL dose-dependent, as well as to ascertain the effect of ferritin, LDL-treated ECs (80, 160, and 240 mg/dl, 24 h) were incubated for 6, 12, and 24 h with ferritin (100 µg/ml) in Medium A supplemented with 15% LPDS. At the designated time, aliquots were removed for determination of TBARS, and the cells were subjected to immunocytochemical analysis with FOH1a/DLH3 (DLH3) followed by image analysis. To further confirm IOM-LDL, one coverslip of non-LDL-treated cells and three coverslips of LDL-treated cells (240 mg/dl, 24 h) were incubated in the same 60 mm-dish for 24 h with ferritin (100 µg/ml) in Medium A supplemented with 15% LPDS. Cells were processed similarly for immunocytochemical analysis with DLH3 followed by image analysis.

Iron chelators, free radical scavengers, catalase, superoxide dismutase (SOD), and apoferritin were used to determine whether free iron from ferritin and hydroxyl radicals is involved in IOM-LDL by HUVECs. Briefly, LDL-treated cells (240 mg/dl, 24 h) were incubated for 24 h with ferritin (100 µg/ml) in Medium A supplemented with 15% LPDS in the presence of an iron chelator (0.5 mM deferoxamine), hydroxyl radical scavengers [(10 mM dimethylsulfoxide (Sigma) or 50 mM mannitol (Sigma)], a general chain-breaking antioxidant [(50 M butylated hydroxytoluene (Sigma)], 25 U/ml catalase (Sigma), or 1000 U/ml superoxide dismutase (Sigma). In separate experiments, LDL-treated cells (240 mg/dl, 24 h) were first pretreated for 30 min with 0.5 mM deferoxamine and then incubated for 24 h with ferritin (100 µg/ml) in medium A supplemented with 15% LPDS. In some experiments, LDL-treated cells (240 mg/dl, 24 h) were incubated for 24 h with 100 µg/ml apoferritin alone in Medium A supplemented with 15% LPDS. After these incubations, aliquots were removed, and the cells were subjected to immunocytochemical analysis with DLH3 and image analysis.

Results

Uptake of LDL and ferritin by HUVECs: time and dose dependencies

Uptake of LDL occurred in a time- and dose-dependent manner up to 24 hours, as shown in Fig. 1. Granular perinuclear Oil Red O staining of the cytoplasm was observed, indicating uptake of LDL (Fig. 2). Large (>100 µm in diameter) and giant (>250 µm in diameter) HUVECs, having one large nucleus or multiple nuclei, showed an increased uptake of LDL when compared to small HUVECs (≤100 µm in diameter) (P<0.05). Uptake of ferritin increased dose-dependently, peaked at 12 hours, and declined thereafter, as shown in Fig. 3. Ferritin was also detected in the cytoplasm in a pattern similar to that of LDL (Fig. 4).

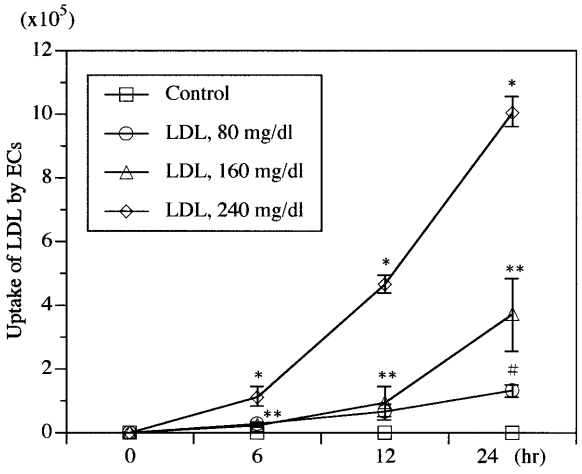

Fig. 1 Uptake of *LDL* by HUVECs. Confluent HUVECs were incubated for 6, 12, and 24 h with LDL (80, 160, 240 mg/dl) in heparin-free Medium A supplemented with 15% FBS followed by internalization of LDL. At each time point, the cells were subjected to Oil Red O staining and evaluated quantitatively by image analysis as described in "Materials and methods." Control cells were treated similarly in the absence of LDL. Values are expressed as mean ± SEM of three independent experiments. *Significant difference (P<0.05) between cells treated with 240 mg/ml and 160, 80, or 0 mg/ml LDL (control). **Significant difference (P<0.05) between cells treated with 160 mg/ml and 80 or 0 mg/ml LDL (control). # Significant difference (P<0.05) between cells treated with 80 mg/ml and 0 mg/ml LDL (control)

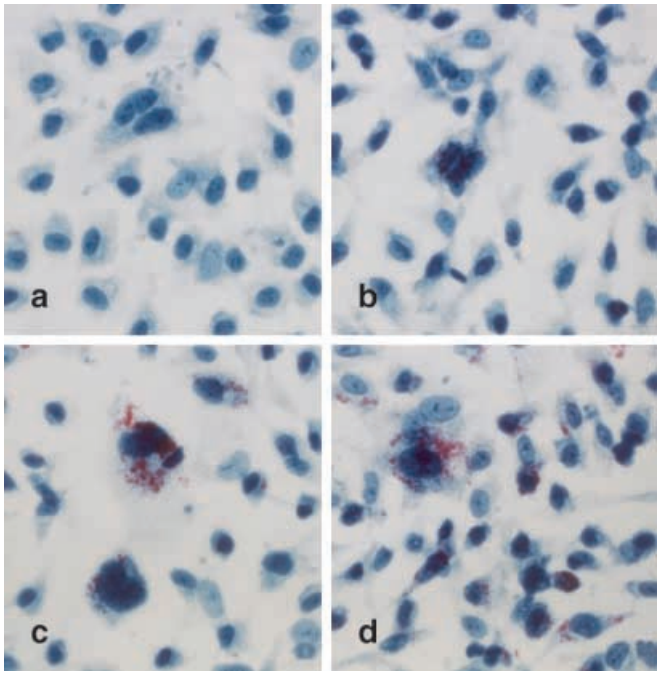

Fig. 2 Oil Red O staining of confluent HUVECs. Confluent HUVECs were incubated for 6, 12, and 24 h with LDL (240 mg/dl) in heparin-free Medium A supplemented with 15% FBS followed by internalization of LDL. At each time point, the cells were subjected to Oil Red O staining as described in "Materials and methods." Control cells were treated similarly in the absence of LDL. Granular and perinuclear cytoplasmic staining were present in large and giant cells with mononucleation or multinucleation compared to small mononucleated cells (**b–d**); **b** (6 h); **c** (12 h); and **d** (24 h). No positive staining was observed in control cells (**a**, 24 h). Original magnification 200×

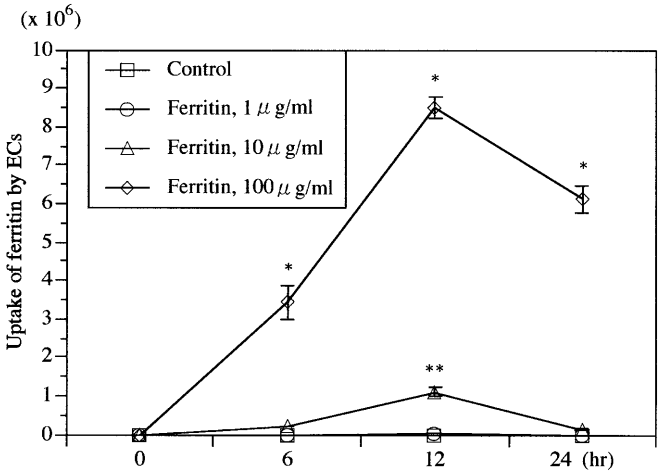

Fig. 3 Uptake of ferritin by HUVECs. Confluent HUVECs were incubated for 6, 12, and 24 h with ferritin (1, 10, and, 100 µg/ml) in Medium A supplemented with 15% LPDS. At each time point, aliquots were removed, the cells were processed for immunocytochemistry using anti-ferritin antibody, and the cells were evaluated quantitatively by image analysis as described in "Materials and methods." Control cells were treated similarly in the absence of ferritin. Values are expressed as mean±SEM of three independent experiments. *Significant difference (P<0.05) between cells treated with 100 µg/ml and 10, 1, or 0 µg/ml ferritin (control). **Significant difference (P<0.05) between cells treated with 10 mg/ml and 1 or 0 µg/ml ferritin (control)

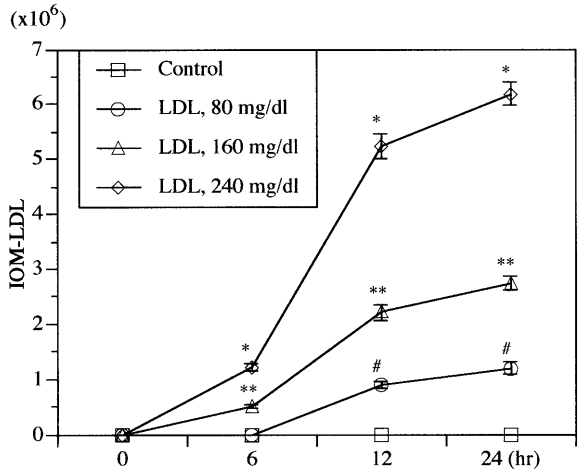

Fig. 5 IOM-LDL by HUVECs. LDL-treated HUVECs (80, 160, and 240 mg/dl, 24 h) were incubated for 6, 12, and 24 h with ferritin (100 µg/ml) in Medium A supplemented with 15% LPDS. At each time point, aliquots were removed, and the cells were processed for immunocytochemistry with DLH3 followed by image analysis as described in "Materials and methods." Control cells were treated similarly in the absence of LDL. Values are expressed as mean±SEM of three independent experiments. *Significant difference (P<0.05) between cells treated with 240 mg/ml and 160, 80, or 0 mg/ml LDL (control). **Significant difference (P<0.05) between cells treated with 180 mg/ml and 80 or 0 mg/ml LDL (control). # Significant difference (P<0.05) between cells treated with 80 mg/ml and 0 mg/ml LDL (control)

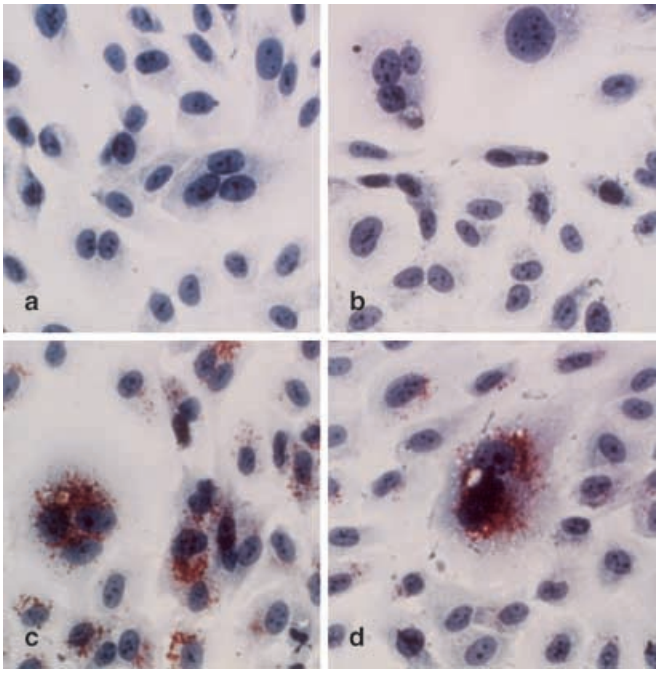

Fig. 4 Immunostaining of confluent HUVECs with anti-ferritin antibody. Confluent HUVECs were incubated for 6, 12, and 24 h with ferritin (100 µg/ml) in Medium A supplemented with 15% LPDS. At each time point, aliquots were removed, and the cells were processed for immunocytochemistry using anti-ferritin antibody as described in the Materials and methods. Control cells were treated similarly in the absence of ferritin. Granular and perinuclear cytoplasmic staining of large and giant cells with mononucleation or multinucleation compared to small mononucleated small cells (**b–d**); **b** (6 h), **c** (12 h), and **d** (24 h). No positive staining was observed in control cells (**a**, 24 h). Original magnification 200×

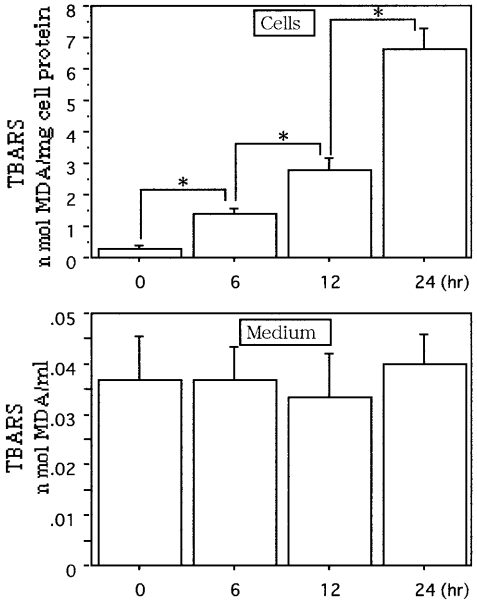

Fig. 6 Lipid peroxidation in HUVECs and postculture medium LDL-treated HUVECs (240 mg/dl, 24 h) were incubated for 6, 12, and 24 h with ferritin (100 µg/ml) in Medium A supplemented with 15% LPDS. At each time point, aliquots and cells were processed for determination of thiobarbituric acid-reactive substance (*TBARS*) as described in "Materials and methods." Values are expressed as mean ± SEM of three independent experiments. * P<0.05

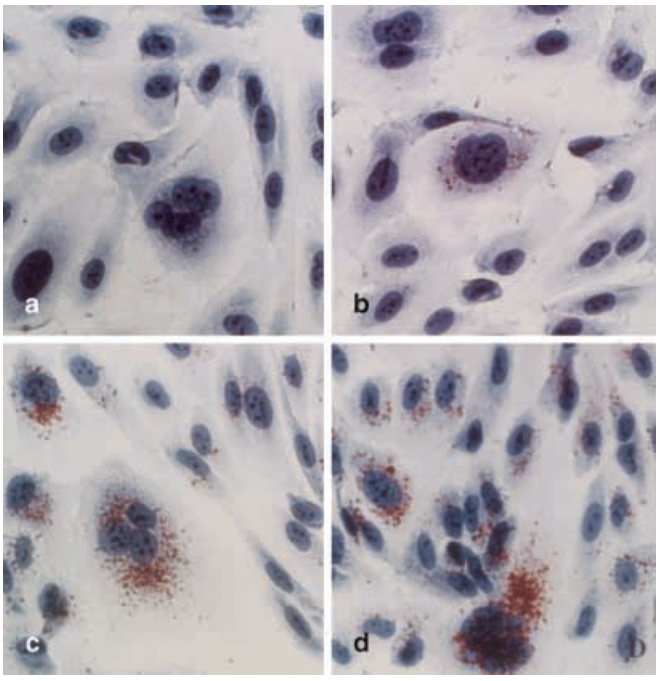

Fig. 7 Immunostaining of confluent HUVECs with DLH3. LDL-treated HUVECs (240 mg/dl, 24 h) were incubated for 6, 12, and 24 h with ferritin (100 μg/ml) in Medium A supplemented with 15% LPDS. At each time point, aliquots were removed, and the cells were processed for immunocytochemistry with DLH3/FOH1a as described in "Materials and methods." Control cells were treated similarly in the absence of LDL. Granular and perinuclear cytoplasmic staining was present in large and giant cells with mononucleation or multinucleation compared to small mononucleated cells (**b–d**); **b** (6 h), **c** (12 h), and **d** (24 h). No positive staining was observed in control cells (**a**, 24 h). Original magnification 200×

IOM-LDL by HUVECs: time and dose dependencies

DLH3 immunostaining also varied in a time- and LDL concentration-dependent manner up to 24 h, as shown in Fig. 5. TBARS levels were significantly increased in a time-dependent manner, whereas levels in postculture media were not significantly altered (Fig. 6). DLH3 immunostaining of cells showed a pattern similar to that of LDL and ferritin (Fig. 7). LDL-treated ECs (240 mg/dl, 24 h) grown on glass coverslips and incubated in a 60-mm dish with ferritin in Medium A supplemented with 15% LPDS displayed DLH3 immunostaining, whereas non-LDL-treated cells did not (data not shown). DLH3 immunostaining appeared in a ferritin concentration-dependent manner (Fig. 8) as well as in an LDL concentration-dependent manner (Fig. 9). These observations confirm that LDL-treated HUVECs perform IOM-LDL, mediated presumably by ferritin.

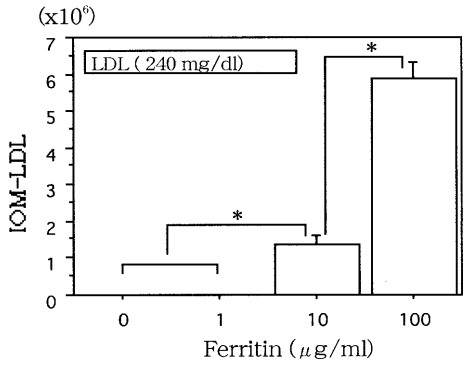

Fig. 8 Effect of ferritin concentration on *IOM-LDL*. LDL-treated HUVECs (240 mg/dl, 24 h) were incubated for 24 h with ferritin (1, 10, 100 μg/ml) in Medium A supplemented with 15% LPDS. At each time point, aliquots were removed, and the cells were processed for immunocytochemistry with DLH3 followed by image analysis as described in "Materials and methods." Values are expressed as mean±SEM of three independent experiments. * $P<0.05$

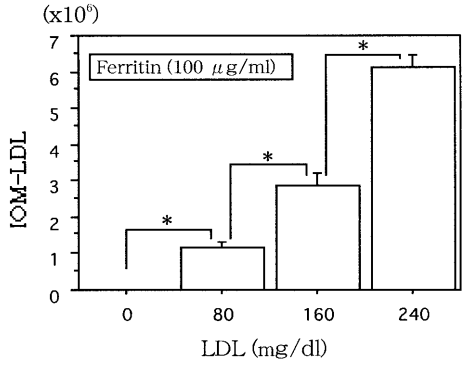

Fig. 9 Effect of LDL concentration on *IOM-LDL*. LDL-treated HUVECs (80, 160, 240 mg/dl, 24 h) were incubated for 24 h with ferritin (100 μg/ml) in Medium A supplemented with 15% LPDS. At each time point, aliquots were removed, and the cells were processed for immunocytochemistry with DLH3 followed by image analysis as described in "Materials and methods." Values are expressed as mean±SEM of three independent experiments. * $P<0.05$

Effect of iron chelators and free radical scavengers on IOM-LDL

Suppression of IOM-LDL by iron chelators, free radical scavengers, catalase, superoxide dismutase (SOD), and apoferritin is shown in Fig. 10. IOM-LDL induced by ferritin was inhibited more than 60% by preincubation of LDL-treated cells with deferoxamine (DFX) or the simultaneous addition of DFX to ferritin. Lipophilic, cell membrane-permeant antioxidants, such as dimethylsulphoxide (DMSO) and butylated hydroxytoluene (BHT), inhibited ferritin-induced IOM-LDL by 79.9% and 99.8%, respectively, in comparison to control values. Mild suppression by mannitol was likely due to the scavenging of aqueous hydroxyl radicals but not lipid-phase hydroxyl radicals, and because mannitol hardly passes

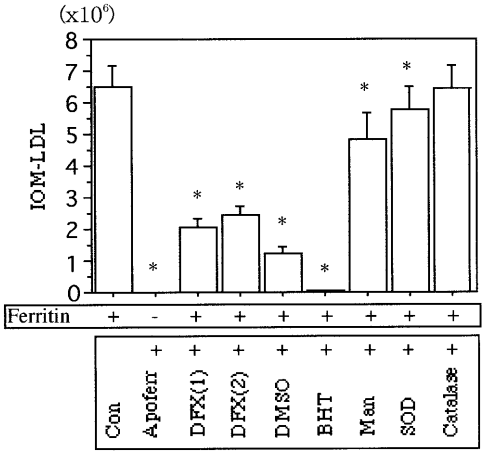

Fig. 10 Suppression of *IOM-LDL*. LDL-treated HUVECs (240 mg/dl, 24 h) were incubated for 24 h with ferritin (100 µg/ml) in Medium A supplemented with 15% LPDS in the presence of 0.5 mM deferoxamine [*DFX(1)*], 10 mM dimethyl sulphoxide (*DMSO*), 50 mM mannitol, 50 M butylated hydroxytoluene (*BHT*), 25 U/ml catalase, or 1000 units/ml superoxide dismutase (*SOD*). In some experiments, LDL-treated cells (240 mg/dl, 24 h) were first pretreated for 30 min with 0.5 mM deferoxamine [*DFX(2)*] in Medium A supplemented with 15% LPDS and, after washing with PBS three times, subsequently incubated for 24 h with ferritin (100 µg/ml) in Medium A supplemented with 15% LPDS. In some experiments, LDL-treated cells (240 mg/dl, 24 h) were incubated for 24 h with 100 µg/ml apoferritin in Medium A supplemented with 15% LPDS. After these incubations, aliquots were removed, and the cells were processed for immunocytochemical analysis using with DLH3 followed by image analysis as described in "Materials and methods." As a control, LDL-treated cells (240 mg/dl, 24 h) were incubated for 24 h with ferritin (100 µg/ml) alone in Medium A supplemented with 15% LPDS. Values are expressed as mean ±SEM of three independent experiments. * $P<0.05$ vs. control

through the cell membrane to reach the intracellular site of hydroxyl radical formation. Catalase, which inhibits hydroxyl radical production from extracellular sources, and SOD, which inhibits superoxide formation from extracellular sources, had little or no effect on IOM-LDL induced by ferritin in comparison to control values. Apoferritin substituted for ferritin did not induce IOM-LDL. These observations suggest that IOM-LDL is mediated by free radical production that is catalyzed mainly by free iron released from ferritin.

Discussion

The present study provides evidence that IOM-LDL occurs in HUVECs. Because the liver rapidly clears oxidatively modified LDL, we suggest that IOM-LDL within HUVECs is important as an early event in atherosclerosis. This notion is supported in part by the findings of Clara et al. [5] who showed that apolipoprotein B and an epitope present on oxidatively modified LDL are colocalized in arterial ECs and media of experimental rats after intravenous or intraperitoneal injection of native LDL. However, neither apoprotein B nor oxidatively modified LDL could be detected in the ECs or media after intraperitoneal injection of oxidized LDL.

Antibody FOH1a/DLH3 (DLH3) recognizes oxidized phosphatidylcholine (PC) but not native or chemically-modified LDL such as acetylated LDL or MDA-treated LDL [12, 13]. The epitope detected by DLH3 is a lyso-PC backbone, hydrophilic function of the sn-2 acyl chain, and a short or straight sn-2-chain [13] and is produced in the LDL oxidation system with ferrous iron [12]. There is growing evidence that oxidized PC products play an important role in atherogenesis. Watson et al. [43] have shown that oxidized PC induces endothelial expression of adhesion molecules as well as monocyte migration. Oxidized PC has also been shown to be susceptible to decomposition to lyso-PC [35], which has been shown to induce endothelial expression of adhesion molecules [16]. Although the exact products of oxidized PC were not investigated in the present study, our data suggest that ECs may an important role in atherogenesis via intracellular production of oxidized PC.

Studies have provided conflicting evidence concerning the role of ferritin in atherosclerosis [2, 3, 4, 11, 14, 15, 21, 24, 31]. Non-iron-bound apoferritin may sequester free iron and protect against cellular damage [4, 14]. In the present study, apoferritin did not induce IOM-LDL. Ferritin mRNA has been detected in the arterial wall including ECs in early and advanced atherosclerotic lesions in humans [24]. However, in vitro studies have demonstrated that ferritin can catalyze lipid peroxidation under conditions in which iron is released from ferritin [26]. Catalytically active free iron that can stimulate lipid peroxidation has been detected in gruel samples from advanced atherosclerotic lesions in humans [32]. These findings suggest that even if newly synthesized apoferritin or non-iron-bound apoferritin sequesters free iron, the consequent iron-bound ferritin can be a potential source of catalytically active free iron. In the present study, approximately 60% of the observed IOM-LDL depended on catalytically active free iron and was inhibited by deferoxamine. Because no free iron has been detected in human peripheral blood [8], our data suggest that the relation between elevated serum ferritin and atherosclerosis may be, at least in part, explained by the release of catalytically active iron from ferritin in ECs. However, the fact that IOM-LDL was partially inhibited by deferoxamine compared to the complete inhibition by butylated hydroxytoluene suggest sthat free iron-independent oxidative mechanisms may be also active in HUVECs.

Although specific mechanisms were not examined in the present study, iron mobilized from ferritin appears to be essential for the formation of free iron-catalyzed IOM-LDL. Two mechanisms of iron mobilization from ferritin iron are proposed. First, release of iron from ferritin occurs by a process that involves reduction of ferric iron to ferrous iron [9, 44]. In vitro studies have shown that endogenous physiological reductants such as superoxides [44], nitric oxide [27], reduced flavins [7], and glutathione [20] mediate the reductive release of iron from ferritin. Cultured ECs have been shown to generate

these reductants [19, 30, 34]. A second mechanism may be that iron is liberated from ferritin as a consequence of intracellular degradation of this protein within acidic autophagolysosomes. Once formed, free iron can catalyze the formation of hydroxyl radicals by the Haber-Weiss reaction.

In the present study, large and giant HUVECs showed increased uptake of LDL and ferritin and increased oxidative modification of LDL when compared to small HUVECs. Some laboratories, including ours, have reported that morphological heterogeneity of ECs in human and animal atherosclerosis is characterized by the occurrence of multinucleated large or giant ECs [28, 36, 37]. The number of multinucleated large ECs is correlated with the severity of atherosclerosis in humans [36] and with the duration of cholesterol feeding in rabbits [36]. Some authors have shown that multinucleated giant ECs accumulate in areas of repeated endothelial injury or in areas of high cell turnover such as atherosclerotic lesions in humans [1, 6, 28, 29, 37]. In addition, multinucleated giant ECs do not incorporate H^3-thymidine or BrdU [29, 36, 37]. Taken together, these findings indicate a probability that multinucleated giant ECs are senescent cells. However, endothelial senescence does not necessarily imply a decrease in all functions [38, 39]. The question remains whether endothelial heterogeneity plays a role in atherogenesis. We have provided evidence that endothelial heterogeneity may, at least in part, directly affect atherogenesis through IOM-LDL by large and giant, including multinucleated, ECs.

Two study limitations should be addressed. First, the lowest concentration of ferritin to induce IOM-LDL was 10 μg/ml. This is 4.4–to 7.2-fold greater than the maximum serum ferritin concentration observed in previous population studies of human coronary heart disease (0.01–2.27 μg/ml) [31] and of human carotid atherosclerosis (0.01–1.39 μg/ml) [15]. Second, arterial ECs may differ from HUVECs in their properties. Because development of atherosclerosis is a long-standing process, long-term studies with arterial ECs and ferritin concentrations close to those in human subjects are needed to evaluate the possible role of IOM-LDL in atherogenesis.

In conclusion, the results of the present study indicate that ECs may perform IOM-LDL under certain conditions. Although our findings cannot be applied directly to human atherosclerosis, our results are consistent with the notion that ECs play an important role in the initiation and progression of atherosclerosis via IOM-LDL.

References

1. Antonov AS, Nikolaeva MA, Kuueva TS, Romanov YA, Babaev VR, Bystrevskaya VB, Perov NA, Repin VS, Smirnov VN (1986) Primary culture of endothelial cells from atherosclerotic human aorta. 1. Identification, morphological and ultrastructural characteristics of two endothelial cell subpopulations. Atherosclerosis 59:1–19
2. Araujo JA, Romano EL, Brito BE, Parth_ V, Romano L, Bracho M, Montanó RF, Cardier J (1995) Iron overload augments the development of atherosclerotic lesions in rabbits. Arterioscler Thromb Vas Biol 15:1172–1180
3. Aronow WS (1993) Serum ferritin is not a risk factor for coronary artery disease in men and women aged ≥ 62 years. Am J Cardiol 72:347–348
4. Balla G, Jacob HS, Balla J, Rosenberg M, Nath K, Apple F, Eaton JW, Vercellotti GM (1992) Ferritin: a cytoprotective antioxidant stratagem of endothelium. J Biol Chem 267:18148–18153
5. Calara F, DimayugaP, Niemann A, Thyberg J, Diczfalusy U, Witztum JL, Palinski W, Shah PK, Cercek B, Nilsson J, Regnsrom J (1998) An animal model to study local oxidation of LDL and its biological effects in the arterial wall. Arterioscler Thromb Vasc Biol 18:884–893
6. Cotton R, Wartman WB (1961) Endothelial patterns in human arteries. Arch Pathol 71: 3–12
7. Dognin J, Crichton RR (1975) Mobilization of iron from ferritin fractions of defined iron content by biological reductants. FEBES Lett 54:234–236
8. Gutterridge JM, Rowley DA, Halliwell B (1981) Superoxide-dependent formation of hydroxyl radicals in the presence of iron salts. Detection of "free" iron in biological system by using bleomycin-dependent degradation of DNA. Biochem J 199:263–265
9. Halliwell B (1978) Superoxide-dependent formation of hydroxyl radicals in the presence of iron chelaters. FEBS Lett 92:321–326
10. Henriksen T, Mahoney EM, Steiberg D (1981) Enhanced macrophage degradation of low density lipoprotein previously incubated with cultured endothelial cells: recognition by receptors for acetylated low density lipoproteins. Proc Natl Acad Sci USA 78:6499–6503
11. Hughes K, Choo M, Kuperan P, Ong CN, Aw TC (1998) Cardiovascular risk factors in non-insulin-dependent diabetes compared to non-diabetic controls: a population-based survey among Asians in Singapore. Atherosclerosis 136:24–31
12. Itabe H, Takeshita E, Iwasaki H, Kimura J, Yoshisa Y, Imanaka T, Takano T (1994) A monoclonal antibody against oxidized lipoprotein recognizes foam cells in atherosclerotic lesions. Complex formation of oxidized phophatidylcholines and polypeptides. J Biol Chem 269:15274–15279
13. Itabe H, Yamamoto H, Suzuki M, Kawai Y, Nakagawa Y, Suzuki A, Imanaka T, Takano T (1996) Oxidized phophatidylcholines that modify proteins. J Biol Chem 271:33208–33217
14. Juckett MB, Balla J, Balla G, Jessrun J, Jacob HS, Vercelloti GM (1995) Ferritin protects endothelial cells from oxidized low density lipoprotein in vitro. Am J Pathol 147:782–789
15. Kiechl S, Aichner F, Gerstenbrand F, Egger G, Mair A, Rungger G, Spogler F, Jarosch E, Oberhollenzer F, Willeit J (1994) Body iron stores and presence of carotid atherosclerosis. Arterioscler Thromb 14:1625–1630
16. Kume N, Cybulsky M, Gimbrone M (1992) Lysophosphatidylcholine, a component of atherogenic lipoproteins, includes mononuclear leukocytes adhesion molecules in cultured human, and rabbit arterial endothelial cells. J Clin Invest 90: 1138–1144
17. Kvietys PR, Inauen W, Bacon BR, Grisham MB (19989) Xanthine oxidase-induced injury to endothelium: role of intracellular iron and hydroxyl radical. Am J Physiol 257:1640–1646
18. Lowry OH, Rosebrough NJ, Farr AL, Randall RJ (1951) Protein measurement with the Folin phenol reagent. J Biol Chem 193:265–275
19. Matsubara T, Ziff M (1986) Increased superoxide anion release from human endothelial cells in response to cytokines. J Immunol 137:3295–3298
20. Mazur A, Baez S, Shorr E (1955) The mechanism of iron release from ferritin as related to its biological properties. J Biol Chem 213:147–160
21. Moore M, Folom AR, Barnes RW, Eckfeldt JH (1995) No association between serum ferritin and asymptomatic carotid atherosclerosis. The Atherosclerosis Risk in Communities (ARIC) study. Am J Epidermol 141:719–723

22. Nishizaki I, Hagihara M, Tsunekawa H, Maseki M, Yagi K (1981) Lipid peroxide levels of serum lipoprotein fractions of diabetic patients. Biol Med 25:373–378
23. Ohkawa H, Ohishi N, Yagi K (1979) Assay for lipid peroxides in animal tissue by thiobarbituric acid reaction. Anal Biochem 95:351–358
24. Pang JHS, Jiang MJ, Chen YL, Wang FW, Wang DL, Chu SH, Chau LY (1996) Increased ferritin gene expression in atherosclerotic lesion. J Clin Invest 97:2204–2212
25. Parthasarathy S, Wieland E, Steinberg D (1989) A role of endothelial lipoxygenase in the oxidative modification of low density lipoprotein. Proc Natl Acad Sci USA 86:1046–1050
26 Reif DW (1992) Ferritin as a source of iron for oxidative damage. Free Radical Biol Med 270:417–427.
27. Reif DW, Simmons RD (1990) Nitric oxide mediates iron release from ferritin. Arch Biochem Biophys 283:537–541
28. Repin VS, Dolgov VV, Zaikina OE, Novikov ID, Antonov AS, Nokolaeva MA, Smirnov VN (1984) Heterogeneity of endothelium in human aorta-A quantitative analysis of scanning electron microscopy. Atherosclerosis 50:35–52
29. Romanov YA, Balyasnikova IV, Bystrevskaya VB, Byzova TV, Ilyinskaya OP, Krushinsky AV, Lastis RV, Soboleva EL, Tararak EM, Smirnov VN (1995) Endothelial heterogeneity and intimal blood-borne cells. Relation to human atherosclerosis. Recent advances in atherosclerosis research. Atherosclerosis III. Numano F, Wissler RW (eds). Ann NY Acad Sci 748:12–39
30. Rosen GM, Freeman BA (1984) Detection of superoxide generated by endothelial cells. Proc Natl Acad Sci USA 81:7269–7273
31. Salonen JT, Nyysönen K, Korpela H, Tuomilehto J, Seppanen R, Salonen R (1992) High stored iron levels are associated with excess risk of myocardial infarction in eastern Finnish men. Circulation 86:803–811
32. Smith C, Mitchinson MJ, Arouma OI, Halliwell B (1992) Stimulation of lipid peroxidation and hydroxyl-radical generation by the contents of human atherosclerotic lesions. Biochem J 286:901–905
33. Steinberg D, Parthasarathy S, Carew TE, Khoo JC, Witztum JL (1989) Beyond cholesterol: modifications of low density lipoprotein that increase its atherogenecity. N Eng J Med 320: 915–924
34. Steinbrecher UP (1988) Role of superoxide in endothelial-cell modification of low density lipoproteins. Biochim Biophys Acta 959:20–30
35. Steinbrecher UP, Pritcherd PH (1989) Hydrolysis of phospahtidylcholine during LDL oxidation is mediated by platelet-activating factor acetylhydrolase. J Lipid Res 30:305–315
36. Tashiro K, Shimoyama T, Haraoka S, Tokunaga O, Watanabe T (1994) Endothelial heterogeneity in experimentally-induced rabbit atherosclerosis. Demonstration of multinucleated giant cells by scanning electron microscopy and cell culture. Virchows Archiv 435:521–529.
37. Tokunaga O, Fan J, Watanabe T (1989) Atherosclerosis and age-related multinucleated variant cells in primary culture from human aorta. Am J Pathol 135:967–976
38. Tokunaga O, Yamada T, Fan J, Watanabe T (1991) Age-related decline in prostacyclin synthesis by human cultured endothelial cell. Am J Pathol 138:941–949
39. Tokunaga O, Fan J, Watanabe T, Kobayashi M, Kumazaki T, Mitsui Y (1992) Immunohistoligic localization in aorta and biosynthesis of endothelin-1 by cultured human aortic endothelial cells. Lab Invest 67:210–217
40. Van Lentan BJ, Prieve J, Navab M, Hama S, Lusis AJ, Fogelman AM (1995) Lipid-induced changes in intracellular iron homeostasis in vitro and in vivo. J Clin Invest 95:2104–2110
41. Vasile E, Simionescu M, Simionescu N (1983) Visualization of the binding, endocytosis, and transcytosis of low-density lipoprotein in the arterial endothelium in situ. J Cell Biol 96:1677–1689
42. Vlodavsky I, Fielding PE, Fielding CJ, Gospodarovitz D (1978) Role of contact inhibition in the regulation of receptor-mediated uptake of low density lipoprotein in cultured vascular endothelial cell. Proc Natl Acad Sci USA 75:356–360
43. Watson AD, Navab M, Hama SY, Prescott SM, Stafforini DM, McIntyre TM, Ladu BN, Fogelman AM, Berliner JA (1995) Effects of platelet-activating factor acetylhydrolase on the formation and action of minimally oxidized low density protein. J Clin Invest 95:774–782
44. Williams DM, Lee GR, Cartwright GE (1974) The role of superoxide anion radical in the reduction of ferritin iron by xanthine oxidase. J Clin Invest 53:665–667
45. Witztum JL, Steinberg D (1991) Role of oxidized low density lipoprotein in atherogenesis. J Clin Invest 88:1785–1792
46. Yamada T, Fan J, Shimokama T, Tokunaga O, Watanabe T (1992) Induction of fatty streak-like lesions in vitro using a culture model system simulating arterial intima. Am J Pathol 141:1435–1444

Virchows Arch (2002) 440:418–424
DOI 10.1007/s00428-001-0543-3

ORIGINAL ARTICLE

Radina Ivanova · Paula Soares · Patrícia Castro
Manuel Sobrinho-Simões

Diffuse (or multinodular) follicular variant of papillary thyroid carcinoma: a clinicopathologic and immunohistochemical analysis of ten cases of an aggressive form of differentiated thyroid carcinoma

Received: 20 April 2001 / Accepted: 23 August 2001 / Published online: 12 December 2001
© Springer-Verlag 2001

Abstract In an attempt to advance and improve the characterization of the so-called diffuse follicular variant of papillary thyroid carcinoma (diffuse FVPTC) we studied a series of 59 thyroid carcinomas consecutively treated in a specialized center. The clinicopathologic and some of the immunohistochemical characteristics (uPA-R, Lewis X, Sialyl Lewis X, and MIB-1) of ten cases of FVPTC displaying a multinodular or diffuse pattern of growth, and histologic features similar to those previously described in diffuse FVPTC, were compared with those of common papillary thyroid carcinoma (PTC, 25 cases) and common FVPTC (8 cases). Cases of diffuse FVPTC differed significantly from common PTC and FVPTC in targeting younger patients and in exhibiting a prevalence of multicentricity, extrathyroid extension, nodal metastasis, and vascular invasion. Immunohistochemically, diffuse FVPTC cases were characterized by the overexpression of uPAR and sialyl Lewis X. No differences were observed regarding MIB 1 immunoreactivity. Regardless of the term used to designate the multicentric, invasive form of FVPTC (diffuse or multinodular FVPTC) it is crucial to acknowledge the existence of cases of FVPTC with a guarded prognosis that should be distinguished from the classic, uninodular form of FVPTC.

Keywords Papillary thyroid carcinoma · Diffuse follicular variant · uPA-R · Lewis X · Sialyl Lewis X · MIB-1

R. Ivanova
Laboratory of Pathomorphology,
Clinical Center of Endocrinology, Medical University, Sofia, Bulgaria

P. Soares · P. Castro · M. Sobrinho-Simões (✉)
Institute of Molecular Pathology and Immunology
of the University of Porto (IPATIMUP), Rua Dr. Roberto Frias s/n, 4200 Porto, Portugal
e-mail: sobrinho.simoes@ipatimup.pt
Tel.: +351-2-5570700, Fax: +351-2-5570799

P. Soares · M. Sobrinho-Simões
Department of Pathology, Medical Faculty of Porto, Porto, Portugal

Introduction

Papillary carcinoma is the most common malignant tumor of the thyroid gland and exhibits an extremely broad morphologic spectrum. Numerous clinicopathologic studies have documented the usually indolent clinical course and good overall prognosis carried by most papillary thyroid carcinomas (PTCs) [5]. Despite this, there is also evidence that some morphologic features of PTC are associated with a guarded prognosis [5, 8, 9].

The follicular variant of papillary thyroid carcinoma (FVPTC) is the most common subtype of PTC, after conventional (common) PTC. It was described by Lindsay in 1960 [13] and further characterized by Chen and Rosai [7]. FVPTC is composed of follicles with or without solid areas, has characteristic "clear" or papillary type nuclei, and resembles common PTC in biologic and clinical behavior [7]. Later on, two other types of FVPTC were described – one following a less aggressive and the other a more aggressive course than common FVPTC [1, 19]. The former is the macrofollicular variant of PTC described by Albores-Saavedra et al. [1]; the authors reported 17 cases of encapsulated thyroid carcinoma, displaying a predominance of macrofollicles (>50% of the tumor area) and an extremely low incidence of metastases. The latter is the diffuse follicular variant of PTC (diffuse FVPTC) described by Sobrinho-Simões et al. [19]; this variant occurs predominantly in young females and is characterized by an extensive involvement of one or both lobes of the thyroid gland and by an aggressive clinical behavior: the eight patients of the series developed metastases in the lungs and/or bones with or without concurrent regional lymph node metastases [19].

In 1995, Mizukami et al. [14] reported a case of diffuse FVPTC in a 13-year-old boy with lung metastases and regional node recurrence early after thyroid surgery; these authors [14] suggested that the diffuse FVPTC lies somewhere between follicular and papillary carcinoma regarding both biologic behavior and nuclear morphology, despite acknowledging that it should be included in the large group of PTCs.

Recently, Guo et al. [11] reported a series of cases of FVPTC displaying signs of biologic and clinical aggressiveness. These they designated "aggressive follicular variant of PTC". At variance with the cases of diffuse FVPTC on record [14, 19], those described by Guo et al. [11] were characterized by single, very large tumors.

The putative relationship between the clinical aggressiveness of PTC and some immunohistochemical features of the neoplastic cells remains controversial [3, 8, 9]. There is, however, enough evidence to suggest that E-cadherin [20], some native and some sialylated Lewis antigens [3, 10], urokinase-type plasminogen activator-receptor (uPA-R)[21], and MIB-1 [11] may provide meaningful prognostic information in PTC.

The clinicopathologic features of FVPTC remain to be better defined and further studies specifically addressing the analysis of cases of FVPTC carrying a guarded clinical course are necessary if progress is to be made in understanding this variant of PTC.

The aim of this paper was to describe the clinicopathologic and some immunohistochemical characteristics of ten cases of FVPTC displaying a multinodular or, less frequentely, a diffuse pattern of growth and histologic features similar to those previously described in the so-called diffuse variety of FVPTC [19] in order to achieve a better classification of the tumors and a more adequate treatment of the patients.

Materials and methods

Tumor specimens

The histologic slides of all the cases diagnosed as thyroid adenoma or thyroid carcinoma, consecutively diagnosed at the Clinical Centre of Endocrinology and Gerontology, Medical University, Sofia, Bulgaria, for a period of 2 years (1997–1998) were reviewed by two pathologists (RI and MSS). The diagnosis of thyroid carcinoma was confirmed in 59 patients (Table 1). The histologic classification of the carcinomas was made according to the criteria of Hedinger et al. [12] and Rosai et al. [16].

Morphologic features

Of the 59 cases, 10 were classified as diffuse FVPTC according to the following criteria: (a) involvement of the whole thyroid gland or of an entire lobe; (b) exclusively or predominantly follicular growth pattern; (c) no (or rare) psamomma bodies; (d) no fibrosis; and (e) discrete or no lymphocytic infiltration. Eight tumors were classified as common FVPTCs (Table 1). The criteria used in the diagnosis of both types of FVPTC are summarized in Table 2.

Clinicopathologic evaluation

Each case was evaluated regarding the following clinicopathologic parameters: age at diagnosis, gender, tumor size (diameter of the largest nodule), predominant histologic pattern of growth, multicentricity (considered as synonym for intrathyroid dissemination), extrathyroid extension, lymph-node metastasis, and venous invasion.

Immunohistochemistry

The expression of urokinase-type plasminogen activactor-receptor (uPA-R), Lewis type-2 histo-blood group antigens (Lewis X, sialyl Lewis X) and MIB-1, were analyzed by immunohistochemistry in every case of diffuse FVPTC (n=10) and FVPTC (n=8) and in a randomly selected sample of common PTC (n=8). Immunohistochemical analysis was performed using the avidin-biotin-peroxidase procedure. Briefly, sequential histologic sections (4-µm thickness) from paraffin-embedded material of each case were mounted in gelatin-coated slides. The avidin-biotin-peroxidase complex staining method was applied. Sections designed for neuraminidase treatment (Sialyl Lewis X) were washed three times in phosphate-buffered saline (PBS) and incubated with neuraminidase from *Clostridium perfringens* type VI (Sigma, Mo.) diluted in a 0.1-M sodium acetate buffer, pH 5.5, to the final concentration of 0.1 U/ml. The incubation, carried out for 2 h at 37°C was followed by three washings in ice-cold water. All the sections were treated with 0.3% v/v H_2O_2 in methanol for 30 min to block endogenous peroxidase activity. The sections were incubated for 20 min with normal immune serum with 1:5 dilution on Tris-buffered saline (TBS) containing 25% of bovine serum albumin (BSA) to eliminate non-specific staining. Excess normal serum was removed and replaced by the specific monoclonal antibodies. After overnight incubation at 4°C, slides were incubated with a 1:200 dilution of biotin-labeled secondary antibody for 30 min. Sections were incubated with avidin-biotin-peroxidase complex (10 mg/ml of biotin-labeled peroxidase) for 30 min, followed by staining with 0.05% diaminobenzidine, freshly prepared in 0.05% Tris buffer, pH 7.6, containing 0.01% hydrogen peroxide. Finally, sections were counterstained with hematoxylin, dehydrated, and mounted. Dilution of primary antibodies, biotin-labeled secondary antibodies, and avidin-biotin-peroxidase complex was made with TBS containing 12.5% BSA.

Negative controls of the immunostaining were carried out by omission of the primary antibody. As a positive control, sections from previously studied cases of other tissues, known to be positive for each of the primary antibodies were used.

Immunostained sections were classified in all but the MIB-1 study as positive or negative; the percentage of positive cells was semi-quantitatively evaluated into the following categories: 0–0 as 5%; 1–5 as 25%; 2–25 as 50%; 3–50 as 75% and 4+ as more than 75% of positive cells. The intensity of the staining was classified as absent (0), weak (1), medium (2), or strong (3). For each case and each marker, we calculated a staining score by multiplying the value attributed to the percentage of stained cells by that of the staining intensity. Evaluation of the percentage of immunoreactive cells for MIB-1 was made counting 1000 tumor cells in random fields.

Statistical analysis

Results are expressed as percentage or mean (±SEM). The Chi-square test with the Yates correction and a non-parametric test procedure (Mann-Whitney test) were used in the statistical analysis of the results. Two values were considered significantly different when $P<0.05$.

Table 1 Classification of the 59 thyroid carcinomas

Diagnosis	*n* (%)	
Papillary carcinoma		53 (89.8)
– Common type	25 (42.4)	
– Microcarcinoma	7 (11.7)	
– Follicular variant	8 (13.6)	
– Diffuse follicular variant	10 (16.9)	
– Tall cell	2 (3.4)	
– Diffuse sclerosing variant	1 (1.7)	
Follicular carcinoma		3 (5.1)
– Minimally invasive	2 (3.4)	
– Widely invasive	1(1.7)	
Poorly differentiated carcinoma		1 (1.7)
Undifferentiated carcinoma		1 (1.7)
Medullary carcinoma		1 (1.7)

Table 2 Summary of the morphologic features of common and diffuse (or multinodular) follicular variant of papillary thyroid carcinoma (FVPTC)

	Common FVPTC	Diffuse (or multinodular) FVPTC
Thyroid involvement	Focal	Whole thyroid or an entire lobe
Growth pattern	Uninodular[a]	Multinodular or diffuse
Tumor borders	Well-defined fibrous capsule	Unencapsulated pushing borders or absence of a clear cut delineation between the tumor and the adjacent parenchyma
Histologic features	Variable with a predominance of medium-sized follicles	Variable with a predominance of microfollicles and/or trabeculae[b]
Nuclear features	Similar to those of classic papillary thyroid carcinoma	Similar to those of classic papillary thyroid carcinoma
Other morphologic features	No necrosis; no fibrosis; no lymphocytic infiltration; no or rare psammoma bodies; no or rare mitotic figures; rare signs of vascular invasiveness	No necrosis; no fibrosis; no lymphocytic infiltration; no or rare psammoma bodies; no or rare mitotic figures; frequent signs of vascular invasiveness[b]

[a] Occasionally two independent encapsulated nodules may be found
[b] These features reflect the experience obtained in the present study

Table 3 Summary of the clinicopathologic data and comparison between diffuse follicular variant of papillary thyroid carcinoma (FVPTC), common PTC, and (common) FVPTC

	Common PTC (*n*=25)	*P* value[a]	Diffuse FVPTC (*n*=10)	*P* value[b]	Common FVPTC (*n*=8)	*P* value[c]
Gender (male;female)	8; 17	NS	1; 9	NS	0; 8	NS
Mean age (years±SEM)[e]	42.5±3.3	0.008	26.8±3.3	0.008	40.3±2.3	NS
Tumor size (cm±SEM)[e]	2.0±0.2	NS	2.5±0.3	NS	2.3±0.4	NS
Multicentricity (%)	24.0	0.002	80.0[d]	0.0007	0	NS
Extrathyroid extension (pT; %)	12.0	0.0006	70.0	0.003	0	NS
Lymph-node metastasis (%)	36	0.019	80.0	0.004	12.5	NS
Venous invasion (%)	20	0.0009	80.0	0.0007	0	NS

[a] Comparison of diffuse FVPTC and common PTC
[b] Comparison of diffuse FVPTC and CFVPTC
[c] Comparison of common PTC and CFVPTC
[d] In two cases of diffuse FVPTC the tumoral tissue involved the whole thyroid lobe
[e] All other comparisons where done using χ^2- test with Yates' correction except here where we used the Mann-Whitney test

Results

The classification of the 59 carcinomas is summarized in Table 1.

Every case of diffuse FVPTC displayed a predominant microfollicular/trabecular growth pattern (Fig. 1a). In most cases there were also foci composed of medium- or large-sized follicles (Fig. 1b). Papillae, psamomma bodies, fibrosis, and lymphocytic infiltration were not observed at all or were rare and inconspicuous in every case of diffuse FVPTC (Table 2).

Clinicopathologic data

The clinicopathologic data and the comparison between diffuse FVPTC and common PTC and FVPTC are summarized in Table 3.

Age and gender

The age of patients with diffuse FVPTC (26.8±3.3 years) was significantly lower than those of patients with common PTC (42.5±3.3 years) and FVPTC (40.3±2.3 years). The predominance of females was higher, though not significantly, in the group of patients with diffuse FVPTC and FVPTC than in those with common PTC (Table 3).

Tumor size

The mean size of the largest nodules of the cases of diffuse FVPTC was not significantly larger than the mean sizes of the tumors classified as common PTC or FVPTC (Table 2).

Multicentricity, extrathyroid invasion, lymph-node metastasis, and venous invasion

The presence of all these features was significantly more frequent in diffuse FVPTC than in common PTC and FVPTC (Table 3).

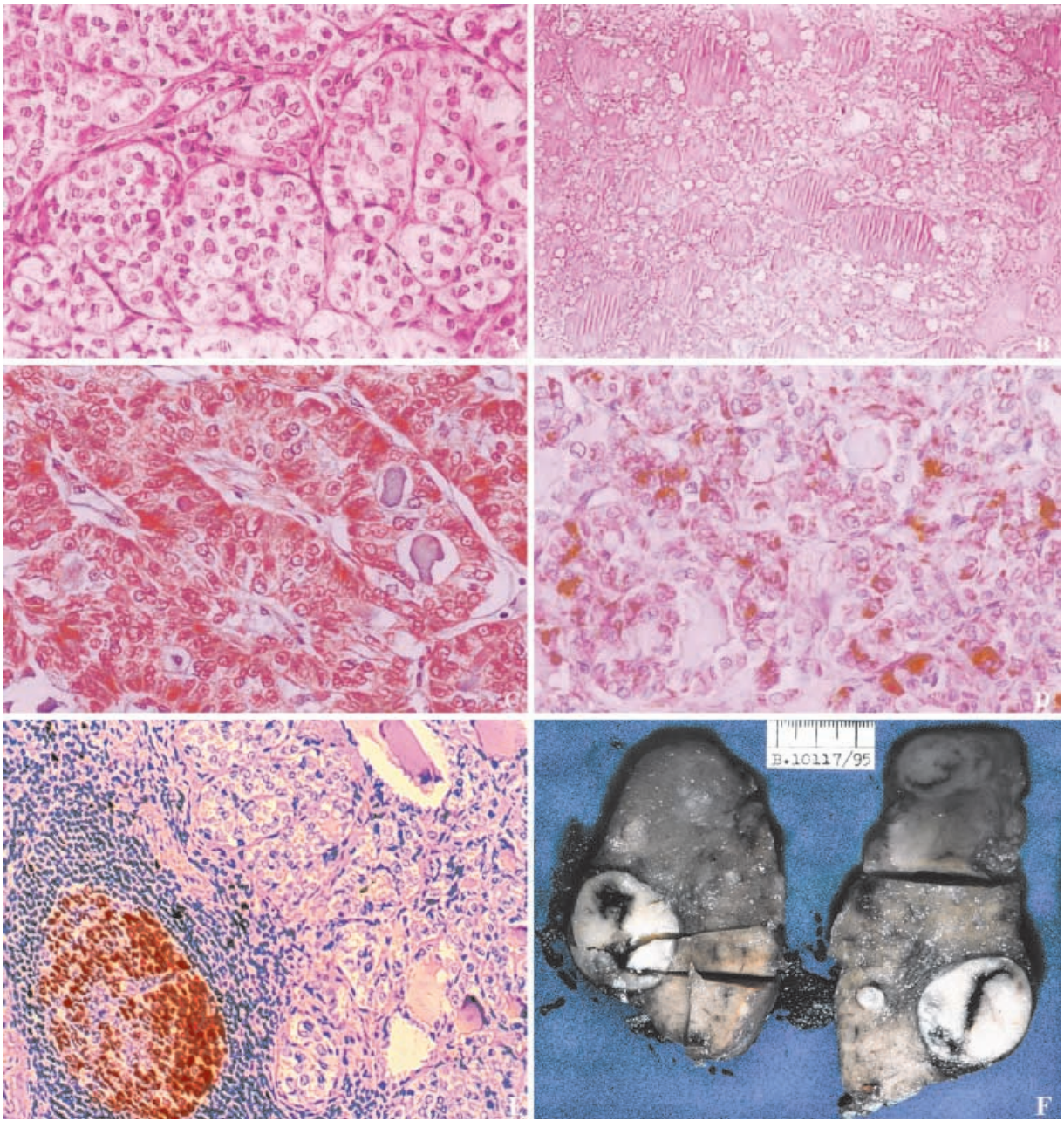

Fig. 1 **a**, **b** Hematoxylin and eosin (H&E) staining of representative sections of two cases of diffuse follicular variant of papillary thyroid carcinoma (DFVPTC). The case depicted in **a** displays a trabecular pattern of growth, and the case depicted in **b** shows medium- or large-sized follicles (H&E ×400 and ×100, respectively). **c**, **d**, **e** Immunohistochemical staining of representative sections of DFVPTC. Strong uPAR staining in **c** (×400) and dispersed Sialyl Lewis X immunoreactivity in **d** (×400). **e** Note the absence of MIB-1 immunoreactivity in the tumor cells in contrast to the nuclear staining observed in the internal positive control (lymphocytes of lymphoid follicle; ×100). **f** Macroscopic appearance of a diffuse FVPTC with a multinodular growth pattern

Immunohistochemical data

Immunohistochemistry and histologic classification

The results obtained in the comparison of the three groups of thyroid carcinoma (diffuse FVPTC, common PTC and FVPTC) are summarized in Table 4.

uPA-R

The score for uPA-R expression was significantly higher in diffuse FVPTC (Fig. 1c) than in common PTC. The same holds true regarding the percentage of positive cells (P=0.01). The score for uPA-R was higher, though not significantly, in diffuse FVPTC than in FVPTC (Table 4).

Table 4 Summary of the immunohistochemical data and comparison between diffuse follicular variant of papillary thyroid carcinoma (FVPTC), common PTC, and (common) FVPTC

	Common PTC (*n*=8)	*P* value[a]	Diffuse FVPTC (*n*=10)	*P* value[b]	Common FVPTC (*n*=8)	*P* value[c]
Score uPA-R (mean±SEM)	5.0±1.3	0.016	9.9±1.1	NS	8.0±0.5	NS
Score LewX (mean±SEM)	4.4±1.4	0.014	0.4±0.3	NS	0.9±0.4	0.050
Score SLewX (mean±SEM)	2.9±1.2	NS	3.2±0.6	0.005	0.7±0.4	NS
MIB-1 (mean±SEM)	0.9±0.2	NS	1.3±0.2	NS	1.4±0.3	NS

[a] Comparison of diffuse FVPTC and common PTC (Mann-Whitney test)

[b] Comparison of diffuse FVPTC and FVPTC (Mann-Whitney test)

[c] Comparison of common PTC and FVPTC (Mann-Whitney test)

Lewis X and Sialyl Lewis X

The immunostaining score for Lewis X antigen was significantly higher in common PTC than in diffuse FVPTC and in FVPTC (Table 4). The same holds true regarding the intensity of the staining for Lewis X (*P*=0.03).

The immunostaining score for Sialyl Lewis X (Fig. 1d) was significantly higher in diffuse FVPTC than in FVPTC. The same holds true regarding the intensity of the staining (*P*=0.020). The score for Sialyl Lewis X was higher, though not significantly, in diffuse FVPTC than in common PTC (Table 4). The ratio between the scores for Sialyl Lewis X and Lewis X was significantly higher in diffuse FVPTC than in common PTC (*P*=0.0004) and FVPTC (*P*=0.018).

MIB-1

The evaluation of MIB-1 did not reveal significant differences between the three groups of thyroid carcinoma. The percentage of neoplastic cells expressing MIB 1 was usually very low and similar in diffuse FVPTC (1.3± 0.2), common PTC (0.9±0.2), and FVPTC (1.4±0.3) (Table 4). The low percentage of cells expressing MIB1 was also observed when the analysis was focused in areas of extrathyroid extension or venous invasion of diffuse FVPTC (Fig. 1e).

Immunohistochemical data versus clinicopathologic parameters

The uPA-R score was higher, though not significantly, in cases presenting extrathyroid invasion than in cases without extrathyroid invasion. There was also a significant association between higher MIB 1 index and higher uPA-R score (*P*=0.04). Sialyl Lewis X expression was significantly associated with the presence of multicentricity (intrathyroid dissemination; *P*=0.006) and extrathyroid invasion (*P*=0.016). No significant association was found between Lewis X immunostaining and any of the clinicopathologic parameters.

Discussion

The results obtained in the present study raise interesting issues at three different levels: epidemiology, nomenclature, and pathobiology. Regarding epidemiology, this series is noteworthy for the high frequency of papillary carcinomas with an exclusively or predominantly follicular growth pattern and, among such tumors, for the very high prevalence of the so-called diffuse FVPTC. The absence of Hürthle cell carcinomas is further of note.

In most series on record the prevalence of the FVPTC does not exceed 5% of clinically evident papillary carcinomas, and whenever the diffuse FVPTC has been individualized it scored at 1–2% [18, 19]. It is difficult to explain the high percentage of cases of the FVPTC in the present series – namely the 17% diffuse FVPTC cases – since the series is not only very small but composed of patients in a specialized Clinic for Endocrinological Disorders. We think there is no reason to start assuming that one may be facing a real increase in the incidence of the aforementioned clinically aggressive variant of PTC, as it was seen in areas affected by the Chernobyl accident [15]. It is likely that the present series, apart from being restricted to a 2-year period of cases, may be biased toward the selection of cases of PTC displaying signs of clinical aggressiveness (multinodularity, nodal metastization).

The second issue concerns nomenclature. The designation “Diffuse FVPTC” was advanced in 1990 [19] in order to identify a subset of PTC with a widely invasive follicular growth pattern, usually in a diffuse or multinodular fashion and involving one or both lobes of the thyroid, in contrast to the uninodular, well circumscribed, and frequently encapsulated appearance of common FVPTC [19].

In most cases of diffuse FVPTC the tumor grossly resembles a multinodular goiter, not a neoplasm with satellite nodules [19]. Whenever the nodules are composed of medium or large-sized follicles, the differential diagnosis with multinodular, “adenomatous”, goiter can be extremely difficult in frozen sections, as was also stressed by Chan and Tsang [6].

In our experience the diagnostic problem has diminished since the neoplasia in most cases of diffuse FVPTC we have seen in recent years occurs as fairly distinct whitish nodules dispersed throughout the thyroid paren-

chyma (Fig. 1f), the nodules of which usually display a microfollicular or trabecular growth pattern. Provided one is able to identify the typical nuclei of PTC these tumors do not raise difficult diagnostic problems in paraffin sections. The same does not hold true for frozen sections, and diagnosis goes on being a problem in many cases of diffuse FVPTC that resemble a multinodular goiter.

In some cases of diffuse FVPTC predominantly composed of trabeculae (as seen in Fig. 1a), it may be difficult to make the differential diagnosis with poorly differentiated insular thyroid carcinoma. However, the presence of nuclei resembling those of classic PTC, the coexistence of areas composed of neoplastic follicles with dense or peripheral scalloped colloid, the absence of necrotic foci, and the extremely low mitotic index will in most instances indicate the diagnosis of diffuse FVPTC.

We do not know the reason for the apparent change in the predominant growth pattern of the nodules of the diffuse FVPTC – in our first series, only two of the nine cases were composed of nodules displaying a predominantly microfollicular growth pattern [19] – but we realize that such change contributes to a turn from the perhaps less appropriate term "diffuse" as the qualifier for this "subvariant" of FVPTC. The same holds true regarding the gross appearance of the lesions, which tend to be "multinodular" rather than "diffuse" (in the present series only two of ten cases of diffuse FVPTC involved diffusely a whole thyroid lobe).

Since we have not been able to come out with a better designation – "Follicular variant of PTC with an invasive, multinodular growth pattern" seems descriptive but too long – we decided to keep, at least for the time being, the "old" designation, although we feel it would be better to also include the designation "multinodular" ("diffuse/multimodular"). The alternative advanced by Guo et al. [11] – "Aggressive follicular variant of PTC" – does not seem adequate for two reasons: (1) it introduces clinical parameters into an entity we consider as a morphologic variant, albeit with clinical relevance (see below); and (2) it represents an umbrella designation that will put together cases of diffuse FVPTC with cases of common FVPTC displaying large size and extrathyroid extension and/or vascular invasiveness. Finally, with regard to pathobiology, we think we have obtained evidence that reinforces the clinicopathologic individualization of diffuse FVPTC and allows some progress in the understanding of its pathogenesis.

The present series confirms that diffuse FVPTC occurs almost exclusively in young females and displays a multinodular or diffuse growth pattern. The neoplastic nodules have pushing borders but usually lack a well-defined capsule. Most of the nodules are composed of microfollicles or trabeculae. Psammoma bodies, lymphocytic infiltration, and desmoplasia are rarely, if ever, seen.

As previously stressed [19] most cases of diffuse FVPTC display signs of clinical aggressiveness. In the present series – from which no data on distant metastases were available – the most striking features of the tumors were their local, nodal, and vascular invasiveness. Curiously, the tumors were not significantly larger than those of common PTC and FVPTC.

At variance with Guo et al. [11], we did not find a higher MIB-1 index nor a higher p53 immunoexpression (data not shown) in the cases of diffuse FVPTC relative to cases classified as common PTC or FVPTC. We also did not find major differences between diffuse FVPTC and FVPTC regarding the expression of E-cadherin and simple mucin antigens (data not shown). The expression of Sialyl Lewis X antigen was significantly higher in diffuse FVPTC than in FVPTC; such expression was also associated with multicentricity and extrathyroid extension, thus confirming the putative role of Sialyl Lewis X in the invasiveness of the neoplastic cells [4, 18].

The comparison of diffuse FVPTC with common PTC disclosed a less intense expression of native histo-blood group antigen Lewis X in diffuse FVPTC than in the latter. This finding fits with the previously reported association between the expression of some carbohydrate antigens and a predominantly papillary pattern of growth of PTC [3, 10].

The major differences between diffuse FVPTC and common PTC concerned the immunoexpression of uPAR and the ratio between Sialyl Lewis X and Lewis X, which were significantly higher in the former than in the latter. The percentage of uPA-R positive cells was also higher in diffuse FVPTC than in common PTC. Since the immunoexpression of both uPA-R and Sialyl Lewis X were found to be associated with extrathyroid invasion, it is tempting to suggest that these molecules play a pathogenic role in this setting.

Summing up, we think it is important to distinguish the classic, uninodular FVPTC, which closely resembles the so-called "Lindsay tumor" [13] from the multicentric, invasive form of FVPTC. The latter is probably responsible, together with some large-sized, vascularly invasive cases of FVPTC [11], for the higher incidence of lung metastases in FVPTC than in common PTC [5]. Regardless of the term used to designate the multicentric, invasive form of FVPTC (diffuse or multinodular FVPTC), it is crucial to acknowledge the existence of certain cases of FVPTC that carry a guarded prognosis and that should be correctly diagnosed and appropriately treated.

Acknowledgements The authors wish to thank Professor Mário Seixas for his help in the photo editing and Mrs. Fátima Magalhães for her excellent secretarial assistance. We thank also Doctor Patrícia Sabino de Matos for providing the macro picture of a case of diffuse FVPTC. This study was in part supported by Fundação Calouste Gulbenkian and project PRAXIS/P/SAU/13/167/98.

References

1. Albores-Saavedra J, Gould E, Vardaman C, Vuitch F (1991) The macrofollicular variant of papillary thyroid carcinoma: a study of 17 cases. Hum Pathol 22: 1195–1205
2. Alves P, Soares P, Fonseca E, Sobrinho-Simões M (1999) Papillary thyroid carcinoma overexpressed fully and underglycosylated mucins together with native and sialylated simple mucin antigens and histo-blood group antigens. Endoc Pathol 10: 305–313

3. Alves P, Soares P, Rossi S, Fonseca E, Sobrinho-Simões M (1999) Clinicopathologic and prognostic significance of the expression of mucins, simple mucin antigens and histo-blood group antigens in papillary thyroid carcinomas. Endoc Pathol 10: 315–324
4. Amado M, Carneiro F, Seixas M, Clausen H, Sobrinho-Simoes M (1998) Dimeric sialyl-Le(x) expression in gastric carcinoma correlates with venous invasion and poor outcome. Gastroenterology 114: 462–470
5. Carcangiu ML, Zampi G, Pupi A, Castagnoli A, Rosai J (1985) Papillary carcinoma of the thyroid. a clinicopathologic study of 241 cases treated at the University of Florence, Italy. Cancer 55: 805–828
6. Chan JKC, Tsang WYW (1995) Endocrine malignancies that may mimic benign lesions. Semin Diagn Pathol 12: 45–63
7. Chen KT, Rosai J (1977) Follicular variant of thyroid papillary carcinoma: a clinicopathologic study of six cases. Am J Surg Pathol 1: 123–130
8. Fonseca E, Soares P, Rossi S, Sobrinho-Simoes M (1997) Prognostic factors in thyroid carcinomas. Verh Dtsch Ges Pathol 81: 82–96
9. Fonseca E, Sobrinho-Simoes M (1995) Diagnostic problems in differentiated carcinomas of the thyroid. Pathol Res Pract 191: 318–331
10. Fonseca E, Sobrinho-Simoes M (1998). Expression of Lewis antigens in papillary carcinoma of the thyroid gland. Virchows Arch 432: 483
11. Guo X, Kleiner D, Fischette M, Merino MJ (1999) Aggressive follicular variant of papillary carcinoma (abstract). Lab Invest 79: 67A
12. Hedinger C, Williams ED, Sobin LH (1988) Histologic typing of thyroid tumours. World Health Organization – Histological Classification of Tumours. Springer Verlag Berlin Heidelberg New York
13. Lindsay S (1960) Carcinoma of the thyroid gland: a clinical and pathologic study of 239 patients at the University of California Hospital. Charles C Thomas Springfield, Ill.
14. Mizukami Y, Nonomura A, Michigishi T, Ohmura K, Noguchi M, Ishizaki T (1995) Diffuse follicular variant of papillary carcinoma of the thyroid. Histopathology 27: 575–577
15. Nikiforov YE, Heffess CS, Korzenko AV, Fagin JA, Gnepp DR (1995) Characteristics of follicular tumors and nonneoplastic thyroid lesions in children and adolescents exposed to radiation as a result of the Chernobyl disaster. Cancer 76: 900–909
16. Rosai J, Carcangiu ML, DeLellis RA (1992) Tumors of the thyroid gland. 3rd ser. Armed Forces Institute of Pathology. Washington
17. Satoh H, Ishikawa H, Kamma H, Yamashita YT, Takahashi H, Ohtsuka M, Hasegawa S (1997) Serum Sialyl Lewis X-i antigen levels in non-small cell lung cancer: correlation with distant metastasis and survival. Clin Cancer Res 3: 495–499
18. Sobrinho Simões M (1995) Tumors of the thyroid: a brief overview with emphasis on the most controversial issues. Curr Diagn Pathol 2: 15–22
19. Sobrinho-Simões M, Soares J, Carneiro F, Limbert E (1990). Diffuse follicular variant of papillary carcinoma of the thyroid: report of eight cases of a distinct aggressive type of hyroid tumor. Surg Pathol 3: 189–203
20. von Wasielewski R, Rhein A, Werner M, Scheumann GF, Dralle H, Potter E, Brabant G, Georgii A (1997) Immunohistochemical detection of E-cadherin in differentiated thyroid carcinomas correlates with clinical outcome. Cancer Res 57: 2501–2507
21. Zanetti A, Stoppacciaro A, Marzullo A, Ciabatta M, Fazioli F, Prat M, Comoglio PM, Baroni CD, Ruco LP (1998) Expression of Met protein and urokinase-type plasminogen activator receptor (uPA-R) in papillary carcinoma of the thyroid. J Pathol 18: 287–291

Virchows Arch (2002) 440:425–435
DOI 10.1007/s00428-001-0545-1

ORIGINAL ARTICLE

Koichi Ohshima · Qiang Liu · Tetsuya Koga
Junji Suzumiya · Masahiro Kikuchi

Classification of cell lineage and anatomical site, and prognosis of extranodal T-cell lymphoma – natural killer cell, cytotoxic T lymphocyte, and non-NK/CTL types

Received: 3 May 2001 / Accepted: 27 August 2001 / Published online: 6 December 2001
© Springer-Verlag 2001

Abstract Due to their minority among the non-Hodgkin lymphomas, classification of extranodal T-cell lymphomas, including those of the natural killer (NK) cell type, has long been controversial and unclear, and the clinical outcome is not well clarified. Recently, new well-defined disease entities have been described based on tumor cell biology combined with anatomical site, clinical features, Epstein-Barr virus (EBV) status, and cell lineage as determined by immunophenotype and genotype. Cytological features are usually not specific, and there are no morphologic correlates with the classification of extranodal T/NK-cell lymphomas. From a human T-cell lymphotropic virus type 1 (HTLV-1) endemic area in Japan, we report here the analysis of 144 cases of extranodal T-cell lymphoma, from which fresh tissues were available. As the clinicopathological features were known, we simply reclassified the cases according to cell lineage and anatomical site. The extranodal T-cell lymphomas were classified into three types on the basis of cell lineage: (1) natural killer cell (NK) type [sCD3–, CD56+, T-cell receptor gene (TCR) germline], (2) cytotoxic T lymphocyte (CTL) type [sCD3+, TIA-1+, TCR rearranged, CD8+/–, CD4–/+], and (3) non-NK/CTL type [sCD3+, TIA–1–, TCR rearranged, CD4+/–, CD8–/+]. In addition to cell lineage, the anatomical site and clinical features were added for subclassification. NK type tumors (35 cases) included the lymphoblastic type, nasal/nasal-type NK lymphoma, and NK leukemia. The CTL type (46 cases) included anaplastic large cell lymphoma (ALCL), cutaneous type, intestinal, γδ T-cell type, and an unspecified type. The non-NK/CTL type (63 cases) included adult T-cell leukemia/lymphoma (ATLL), mycosis fungoides (MF), and an unspecified type. With the exception of ATLL and MF, most extranodal T-cell lymphomas had a cytotoxic phenotype of NK type or CTL type and were often associated with EBV infection. MF and the unspecified type within the non-NK/CTL tumors, with the exception of ATLL, had a favorable prognosis. However, NK and CTL types, with the exception of ALCL, were associated with a poor prognosis. Our results indicate that anatomical site and cell lineage are useful predictors of clinical outcomes of extranodal T-cell lymphomas.

Keywords Extranodal T-cell lymphoma · Cell lineage · NK cell · CTL · Cytotoxic marker

K. Ohshima (✉) · Q. Liu · J. Suzumiya · M. Kikuchi
Department of Pathology, School of Medicine,
Fukuoka University, Nanakuma 7-45-1, Jonanku,
Fukuoka 814-01, Japan
e-mail: ohshima@fukuoka-u.ac.jp
Fax: +81-92-8617300

T. Koga
Department of Dermatology, School of Medicine,
Kyushu University, Fukuoka, Japan

Introduction

New insights into the pathogenesis of lymphoid malignancies have recently been acquired using novel genetic, molecular, and immunological techniques. Based on new information from both clinical and histological findings, the "Revised European-American Lymphoma" (REAL) classification was recently proposed [14]. A new WHO classification is still in progress [15]. According to both of these classifications, lymphomas with a T-cell phenotype represent a heterogeneous group of diseases with different histopathological features, tumor sites, and cells of origin. They include peripheral T-cell lymphomas (PTCLs) derived from αβ cells, as well as some recently recognized entities such as γδ hepatosplenic lymphomas and natural killer (NK) cell lymphomas [17]. Cytological features are usually not specific, and there are no morphological correlates. PTCLs appear to relate to clinical syndromes, and location (nodal versus extranodal and specific extranodal sites) is particularly important in determining the biological behavior of the disease [15]. In addition, the clinical behavior of this group of tumors is not well recognized since, among non-Hodgkin lymphomas, PTCLs are in the minority compared to B-cell lymphomas [15].

Most extranodal T-cell/NK-cell lymphomas have a cytotoxic phenotype. In contrast, nodal lymphomas, with the exception of anaplastic large cell lymphoma, rarely exhibit a cytotoxic phenotype [18, 25, 27]. Cytotoxic cells include NK-cells and cytotoxic αβ and γδ T lymphocytes (CTLs). These cells play a major role in defense against neoplastic processes and viral infections [18]. Expression of T-cell-restricted intracellular antigen (TIA-1) is characteristic of cytotoxic cells irrespective of their activation status [1, 36].

Epstein-Barr virus (EBV) sequences have been detected by in situ hybridization (ISH) in nasal NK-cell lymphomas and in non-hepatosplenic γδ T-cell lymphomas [2, 3]. EBV infection has not been detected in hepatosplenic γδ lymphomas thus far [12, 13].

Adult T-cell leukemia/lymphoma (ATLL) is a peripheral T-cell neoplasm associated with infection with human T-cell lymphotropic virus type 1 (HTLV-1) [34]. Our region of Kyushu is an endemic area for HTLV-1 infection [33]. ATLL often causes lymphadenopathy but primary extranodal presentations, in particular cutaneous, have also been detected [31].

Under the new WHO classification, extranodal NK/T-cell lymphoma, nasal-type, enteropathy-type T-cell lymphoma, hepatosplenic T-cell lymphoma, subcutaneous panniculitis-like T-cell lymphoma, and blastic NK-cell lymphoma are proposed to comprise the extranodal T-cell and NK-cell neoplasms. Their incidence is very rare. Clinically, some of these tumors overlap, and are not well characterized as distinct disease entities. I n this study, we retrospectively reviewed 144 cases of extranodal T-cell lymphomas from which fresh tissues were available. For convenience, the extranodal T-cell lymphomas were phenotypically and genotypically reclassified simply into three types: NK, CTL, and non-NK/CTL types. We also analyzed their clinicopathological behaviors, including anatomical sites and EBV or HTLV-1 status.

Materials and methods

Case selection

All cases came from the files of the Department of Pathology at Fukuoka University, Japan. Cases were defined as extranodal lymphoma when the patient presented with primary extranodal disease without obvious lymphadenopathy at diagnosis. Cases were excluded if a second biopsy within 3 months revealed nodal involvement. A diagnosis of T-cell lymphoma was made when tumor cells were positive for one or more pan T markers without pan B marker reactivity. To facilitate extensive immunohistochemical investigation, only cases with fresh tissues available were selected for analysis. Paraffin sections were stained with hematoxylin-eosin (H-E), Giemsa, periodic acid-Schiff (PAS), and Gomori's silver impregnation. Information regarding HTLV-1 antibody status was obtained from clinicians and medical records. A diagnosis of ATLL was established when HTLV-1 antibody (ATLA) was positive and monoclonal proviral HTLV-1 DNA was identified in the tissue by Southern blot analysis (Fig. 1). Lymphoblastic lymphoma arising from extranodal sites was excluded from this study because T-cell acute lymphoblastic leukemia (T-ALL) could not be differentiated from T-lymphoblastic lymphoma/leukemia in the extranodal sites.

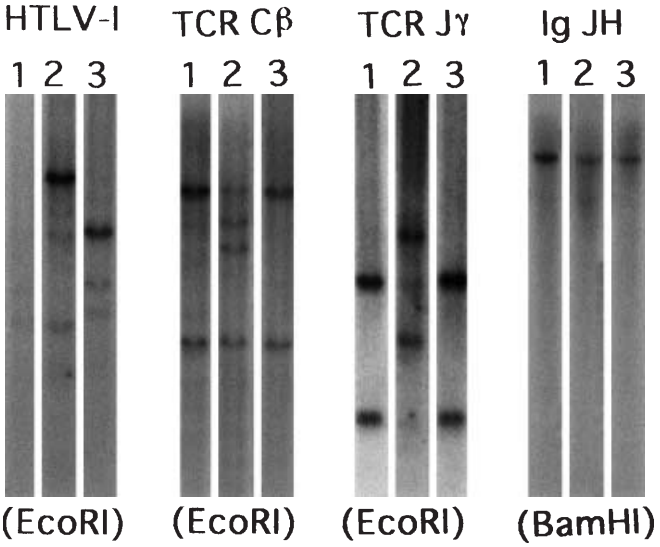

Fig. 1 Representative results of Southern blotting. **a** HTLV-1 analysis: *lane 1* placental DNA (negative control), *lane 2* positive control, *lane 3* ATLL. **b** TCR Cβ, Jγ, and Ig JH: *lane 1* placental germline DNA, *lane 2* a T-cell lymphoma exhibiting clonal rearrangement of Cβ and Jγ, *lane 3* a NK-cell lymphoma showing germline of TCR Cβ, Jγ, and Ig JH

Immunohistochemistry

Immunostaining was performed using both paraffin sections and frozen sections. The antibodies used were CD1 (OKT6; Ortho, Raritan, N.J.), CD2 (T11; Coulter, Hialeah, Fla.), sCD3 (surface CD3, Leu 4; Becton Dickinson [BD], San Jose, Calif.), cCD3 (cytoplasmic CD3, CD3; Dako, Glostrup, Denmark), CD4 (OKT4; Ortho), CD5 (Leu-1; BD), CD7 (Leu9; BD), CD8 (OKT8; Ortho), CD10 (CALLA; BD), CD15 (Leu M1; BD), CD19 (B4; Coulter), CD20 (B1; Coulter), CD20 (L26; Dako), CD25 (IL-2R; BD), CD30 (Ki-1; Dako), CD30 (Ber H2; Dako), CD45RO (UCHL-1; Dako), CD56 (Leu 19; BD), CD57 (Leu7; BD), CD103 (HML1; Dako), TCRβ (βF1; T-cell Diagnostic, Cambridge, Mass.), TCRδ (δ1; T-cell Diag.), Ki-67 (MIB1; Immunotech, Cedex, France), TIA-1 (Coulter), Perforin (T-cell Diag.), Granzyme B (Pharmacell, Paris, France), Fas L (N-20; Santa Cruz Biotechnology, Santa Cruz, Calif.), and p80 (Nichirei, Tokyo, Japan).

Southern blot analysis

A proportion of the frozen tissue was used for DNA isolation and gene analysis. Details of the examination methods have been reported previously [21, 23]. In this study, we examined the T-cell receptor genes Cβ and Jγ, the immunoglobulin heavy chain (JH) gene and the proviral DNA of HTLV-1 (Fig. 1).

In situ hybridization

To investigate the presence of EBV in tumors, we performed ISH for EBV RNA (EBER-1). The method has been described in detail elsewhere [24]. Southern blot analysis for the EBV internal repeat W-region (EBV-W) was also performed.

Statistical analysis

Survival curves were calculated according to the Kaplan and Meier method (SAS system, SAS Institute Inc., N.C.) as described in our previous papers [25, 26]. Survival analysis was performed using the generalized Wilcoxon test. Differences were considered significant if the *P* value was less than 0.05.

Results

A total of 144 cases of extranodal T-cell lymphoma were included in this study. Their distribution according to anatomic sites was as follows: skin, 78; nasopharynx, 23; gastrointestinal tract, 21; oral cavity, 7; liver, 9; others, 5. Thus, in this series the skin was the most frequently involved site in extranodal T-cell lymphoma.

Our 144 cases were classified into three types on the basis of cell lineage as determined by phenotypes and cytotoxic markers (Table 1): (1) NK type [sCD3–, CD56+, T-cell receptor gene (TCR) germline] (35 cases); (2) cytotoxic T lymphocyte (CTL) type [sCD3+, TIA-1+, TCR rearranged] (46 cases); and (3) non-NK/CTL type [sCD3+, TIA-1–, TCR rearranged] (63 cases) (Table 1 and Table 2). In addition to cell lineages, anatomic site, morphology, and clinical features were added to the subclassifications (Table 2 and Table 3).

Classification

NK type

Nasal and nasal-type NK-cell lymphoma. Eighteen cases presented as nasal lymphomas and one as an oral lymphoma. Cutaneous presentation was noted in nine cases. Histologically, pleomorphic cytology, angiocentricity, and necrosis were observed (Fig. 2). The immunophenotype was CD56+CD2+cCD3+/–sCD3–CD4–CD8–/+CD19–CD20–CD25–CD30–TCR βF1–TCR δ1–. TCR genes were expressed in the germline indicating true NK-cell origin. The cytotoxic markers TIA-1 and granzyme B were positive in all cases examined. EBV was detected in all 18 nasal NK-cell lymphomas by ISH and Southern blot analysis (Fig. 2). However, EBV was detected in only six of nine cutaneous NK lymphomas. Subcutaneous involvement was observed in all cases of cutaneous NK-cell lymphomas, but epidermotropism was detected in only half of the cases (Fig. 4).

Aggressive NK-cell leukemia. Liver biopsy was performed in all five cases of aggressive NK leukemia. The portal area and sinusoids exhibited diffuse infiltration with pleomorphic lymphoma cells (Fig. 3). The immunophenotype, genotype, and cytotoxic markers were the same as those of NK lymphoma. EBV was detected in all cases.

NK lymphoblastic lymphoma. These tumors consisted of lymphoblastic cells with a NK phenotype. In the present study, two cases presented as nasal lymphoma. Immunologically, nuclei were positive for TdT. The immunophenotype was CD56+CD2+cCD3+/–sCD3–CD4–CD8–

Table 1 Criteria for defining the three cell lineages. – negative, + positive, +/– positive cases were common rather than negative cases, –/+ negative cases were common rather than positive cases

Type	sCD3	CD56	TIA1	TCR	CD8	CD4
Natural killer cell (NK) type	–	+	+	Germ line	–/+	–
Cytotoxic T lymphocyte (CTL) type	+	–/+	+	Rearranged	+/–	–/+
Non-NK/CTL type	+	–	–	Rearranged	–/+	+/–

Table 2 Definition of extranodal T/NK cell lymphoma according to disease entities

Cell lineage	Disease entity	Virus		Immunohistochemistry										
		EBV	HTLV-I	CD2	CD3	CD5	CD7	CD19	CD20	CD25	CD30	TdT	TCRαβ	TCRγδ
NK type	lymphoblastic type	–	–	+	+/–	–	+/–	–	–	–	–	+	–	–
	lymphoma type	+	–	+	+	–	+/–	–	–	–	–	–	–	–
	leukemia type	+	–	+	+	–	+/–	–	–	–	–	–	–	–
CTL type	Cutaneous[a]	–/+	–	+	+	+	+	–	–	–/+	–	–	+	–
	Gastrointestinal T	+/–	–	+	+	+	+	–	–	–/+	–	–	+	–
	γδ T cell lymphoma	+/–	–	+	+	+	+/–	–	–	–	–	–	–	+
	Anaplastic large cell lymphoma Cutaneous, p80– Systemic, p80+	–	–	+	+	+	+/–	–	–	+	+	–	+	–
	unspecified CTL	+/–	–	+	+	+	+	–	–	–/+	–	–	+	–
Non-NK/CTL type	Adult T cell leukemia/lymphoma	–	+	+	+	+	–	–	–	+/–	–/+	–	+	–
	Mycosis Fungoides	–	–	+	+	+	+	–	–	–/+	–	–	+	–
	unspecified non-NK/T	–	–	+	+	+	+	–	–	–/+	–	–	+	–

[a] Cutaneous CTL included two cases with subcutaneous-paniculitis-like T cell lymphoma (one CD56+ case and one CD56– cases)

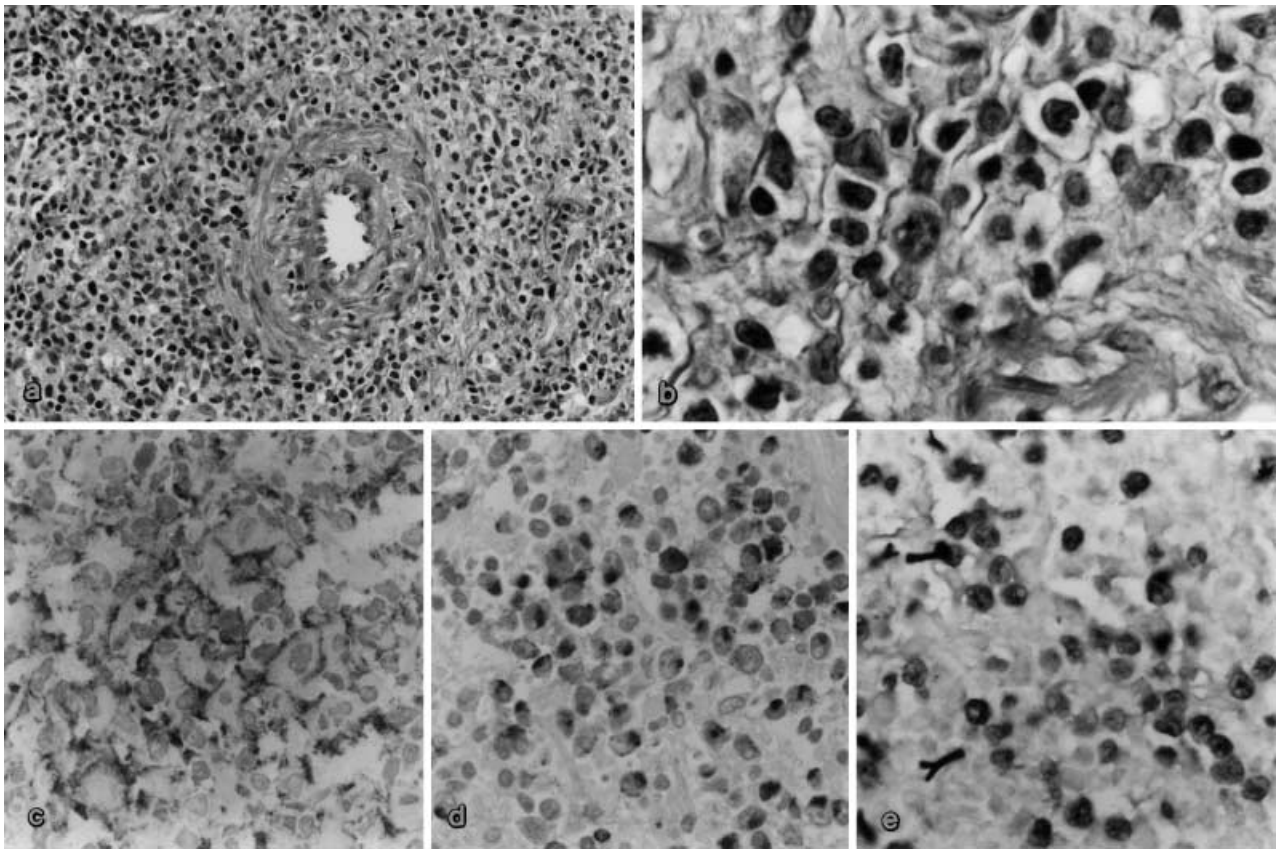

Fig. 2 Characteristics of nasal NK-cell lymphoma. **a** Infiltrates are pleomorphic and angiocentrism is evident. Magnification ×100. **b** Neoplastic cells show pleomorphic histology. Magnification ×400. **c** Neoplastic cells are positive for CD56. Magnification ×200. **d** Neoplastic cells show cytoplasmic positivity for cytotoxic marker TIA-1. Magnification ×200. **e** All neoplastic cells are EBV positive by EBER-1 in situ hybridization. Magnification ×200

Table 3 Distribution of extranodal T/NK cell lymphoma according to disease entities

Cell lineage	Disease entities	*N*	*n*		*n*
NK		35			
	Lymphoblastic type		2		
	Lymphoma type		28		
				Nasal	18
				Cutaneous	9
				Other site	1
	Leukemia type		5		
CTL		46			
	Cutaneous[a]		13		
				CD56+ (CD8 +/–)	8
				CD56– (CD8+)	5
	Gastrointestinal T[b]		13		
	γδ T cell lymphoma		5		
				Hepatosplenic	4
				Other site	1
	Anaplastic large cell lymphoma		8		
				Cutaneous	2
				Systemic	6
	Unspecified CTL		7		
Non-NK/CTL		63			
	Adult T cell leukemia/lymphoma		44		
	Mycosis Fungoides		16		
	Unspecified non-NK/CTL		3		
Total		144			

[a] Cutaneous CTL included two cases with subcutaneous-panniculitis-like T cell lymphoma (one CD56+ case and one CD56– cases)

[b] Enteropathy was detected in four cases

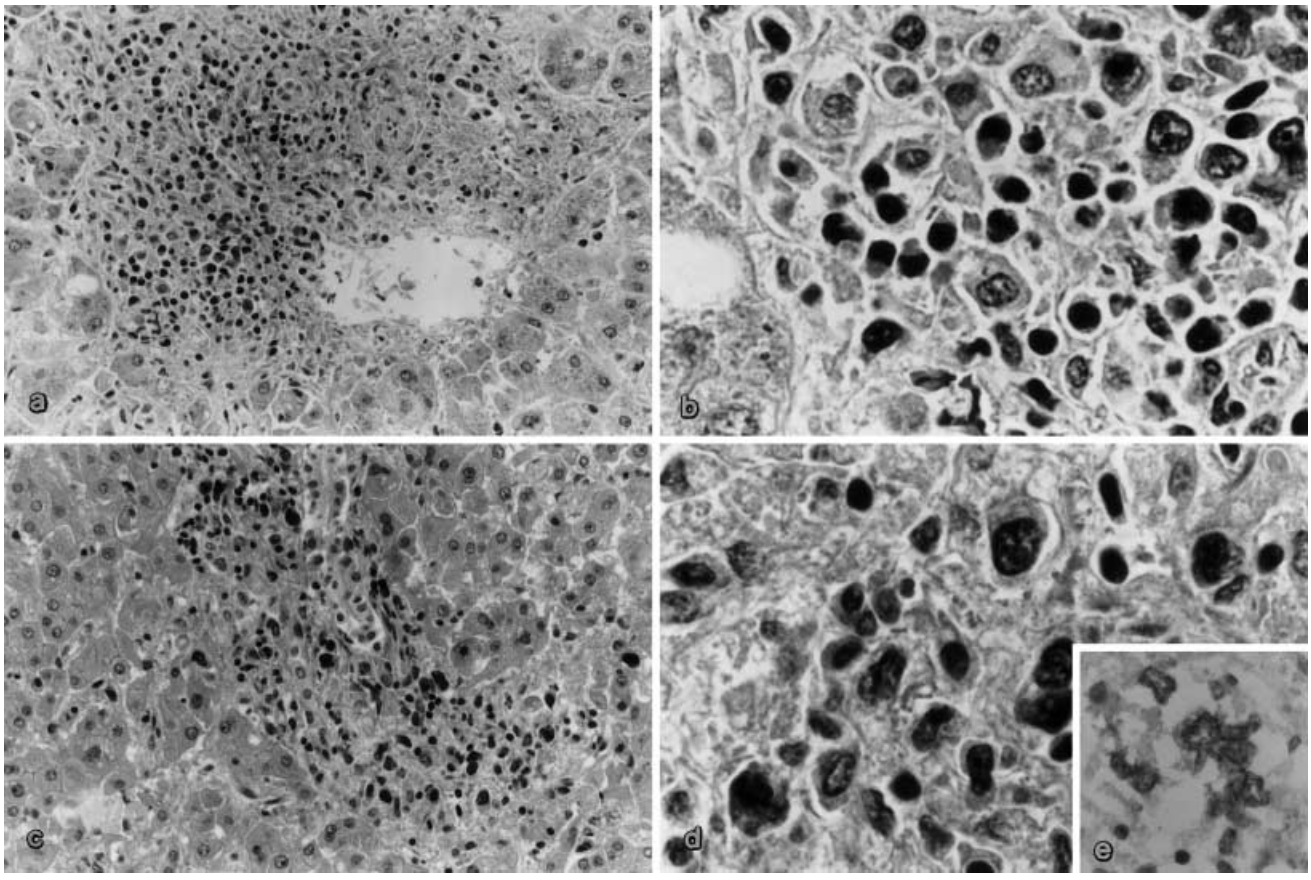

Fig. 3 Characteristics of NK-cell leukemia and hepatosplenic γδ T-cell lymphoma. **a** NK-cell leukemia. The portal area exhibits infiltrates of pleomorphic neoplastic cells. Magnification ×100. **b** Magnification ×400. **c** Hepatosplenic γδ T-cell lymphoma. Portal area shows infiltrates of pleomorphic neoplastic cells. Magnification ×100. **d** Magnification ×400. **e** Neoplastic cells showing positive cytoplasmic staining for TCR δ1. Magnification ×200

CD25–CD30–. TCR genes were germline and EBV was not detected.

CTL type

Cutaneous lymphoma. Subcutaneous and cutaneous involvement was observed; however, epidermotropism was noted in only 4 of 13 cases. Histologically, pleomorphic cytology, angiocentricity, and zonal necrosis were frequently present, as in nasal NK lymphoma. In two cases, involvement was limited to the subcutaneous region (Fig. 4). The diagnosis of subcutaneous panniculitis-like T-cell lymphoma was thus made. The immunophenotype of cutaneous lymphoma was CD2+cCD3+sCD3+CD4–CD8+/–CD19–CD20–CD25–/+CD30–TCR βF1+TCR δ1–. CD56 was positive in 8 of the 13 cases. In all 13, TCR genes exhibited rearrangement, and cytotoxic markers were positive. EBV was detected in four cases.

Gastrointestinal T-cell lymphoma. Five of thirteen cases presented with gastric involvement, and seven cases involved the small intestine. Enteropathy was detected in only four cases. The immunophenotypic profile was CD3+CD4+/–CD8+/–CD56–/+CD103–/+TCR βF1+TCR δ1–. TCR gene analysis revealed rearrangement of Cβ and/or Jγ. In ten cases, CD56 was studied and was positive in three. In eight cases, CD103 was studied and was positive in two. TIA-1 was positive in all 13 cases; however perforin was positive in seven cases, Fas L was positive in eight, granzyme B was positive in seven, and EBV was positive in five.

γδ T-cell lymphoma. Four patients presented with hepatosplenic and bone marrow involvement. One patient had a tumor in the small intestine plus multi-organ involvement. Histopathological examination of the four cases revealed diffuse infiltration into the splenic red pulp and hepatic sinusoids (Fig. 3). The immunophenotype was TCR δ1+TCR βF1–CD1–CD2+cCD3+sCD3+CD4–CD7+CD8–/+CD25–CD30–CD56+/–CD57–. TCR Jγ rearrangement was evident. The cytotoxic markers TIA-1 and granzyme B were positive and EBV was detected in four of the five cases.

Anaplastic large cell lymphoma (ALCL) of T-cell origin. Eight patients exhibited diffuse proliferation of anaplastic large cells (Fig. 4). Two cases were of the cutaneous type and the remainder were systemic. The immunophe-

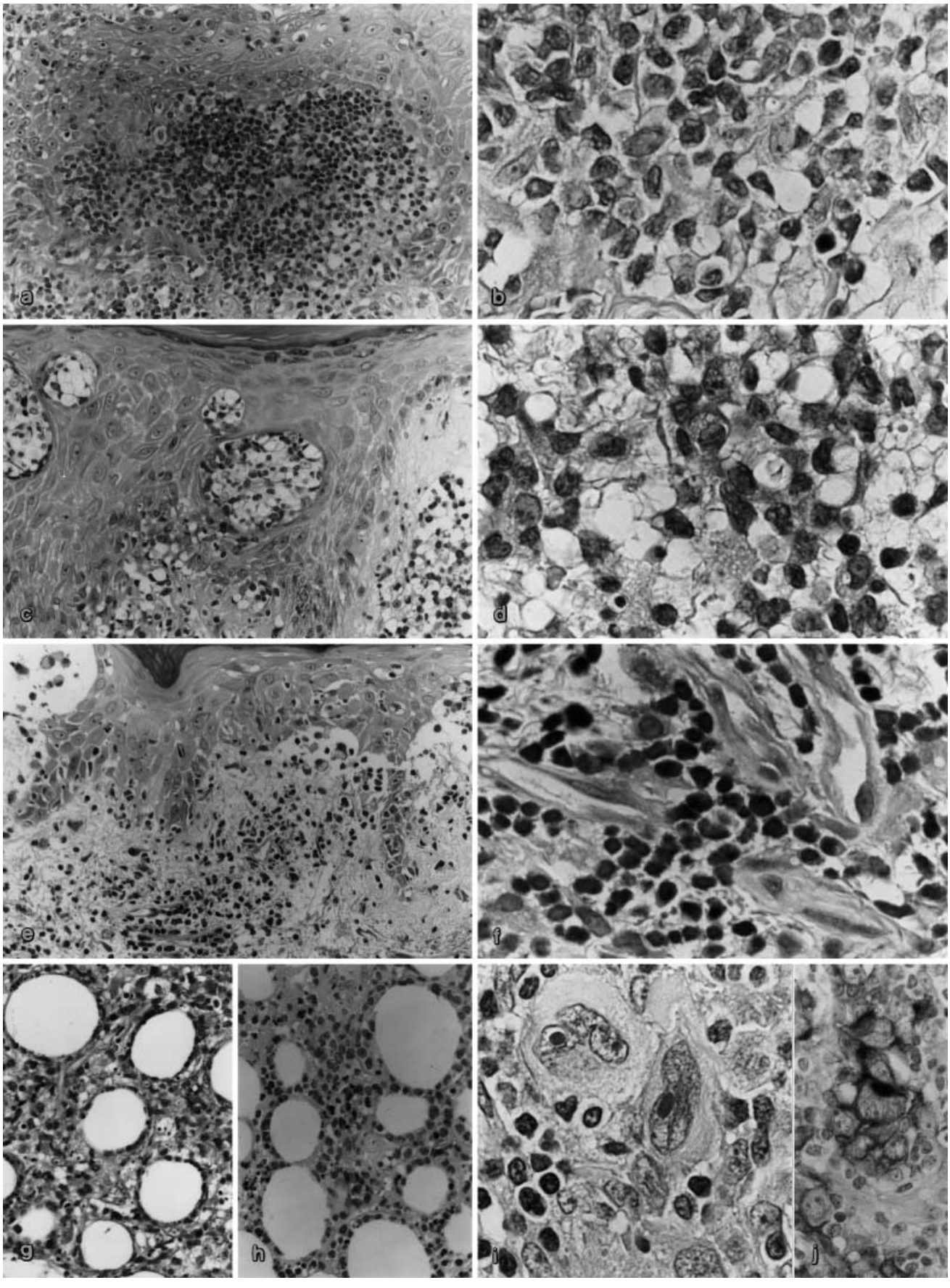
a
b
c
d
e
f
g
h
i
j

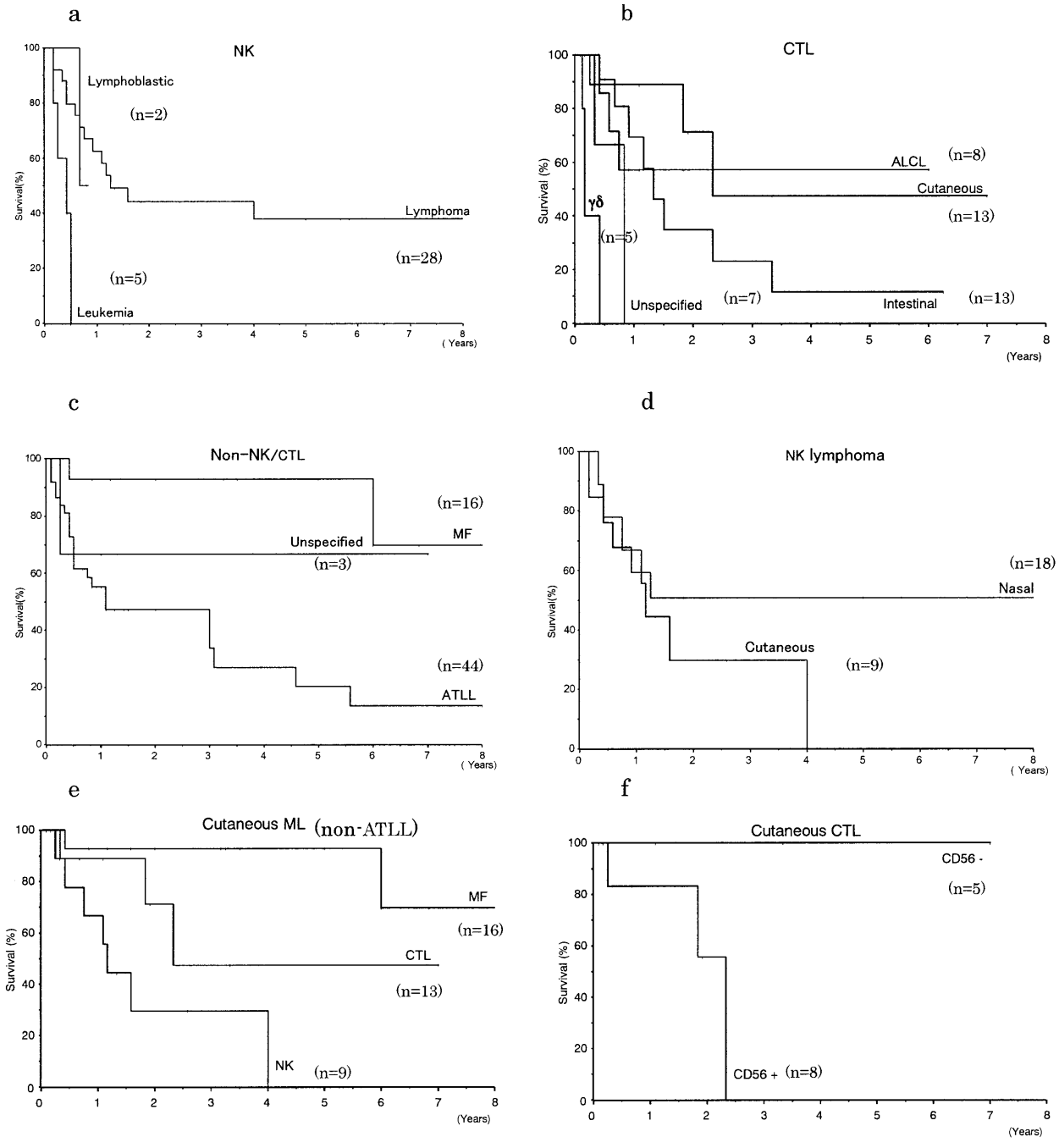

◀ **Fig. 4** Histopathological spectrum of cutaneous lymphoma. **a** MF. Neoplastic cells proliferate in the upper dermis with effacement of Grenz zone and exocytosis. **b** A higher magnification of **a**. **c** ATLL. Neoplastic cells infiltrate into the epidermis forming Pautrier's microabscesses. **d** A higher magnification of **c**. **e** Cutaneous CTL lymphoma. Epidermotropism and necrosis were observed. **f** A higher magnification of **e**. **g** Cutaneous NK-cell lymphoma. Subcutaneous involvement was observed. **h** Subcutaneous panniculitis-like T-cell lymphoma. Subcutaneous involvement was observed. **i** ALCL. The proliferation of neoplastic cells exhibits morphology of anaplastic large cells. **j** Anaplastic cells are CD30-positive. Magnification **a**, **c**, **e**, **g**, and **h** ×100; **j** ×200; **b**, **d**, **f**, **i** ×400

Fig. 5 Survival curves for extranodal T-cell lymphoma. **a** NK type. NK leukemia and NK blastic lymphoma carried a poor prognosis. NK-cell lymphoma had an intermediate prognosis. **b** CTL type. ALCL carried a relatively favorable prognosis; however, other CTL type tumors had a poor prognosis, in particular the aggressive γδ T-cell and unspecified CTL lymphomas. **c** Non-NK/CTL type. MF and unspecified tumors had a good prognosis, but ATLL was associated with a poor prognosis. **d** Of the NK-cell lymphomas, nasal NK-cell lymphoma carried a better prognosis than cutaneous NK-cell lymphoma. **e** Of the cutaneous lymphomas, with the exception of cutaneous ATLL, MF had a good prognosis, and CTL type carried a better prognosis than NK type tumors. In cutaneous lymphoma, non-NK/CTL was MF. **f** CD56-positive cutaneous CTL lymphomas had a poor prognosis, whereas the prognosis was better for CD56-negative tumors

notype of these tumors was CD30+CD2+cCD3+sCD3+/–CD4+/–CD8–/+CD19–CD20-CD25+/–. TCR βF1 and TIA-1 were positive and EBV was negative. Three of five cases with systemic disease exhibited p80 positivity, but the two cutaneous cases were p80 negative.

Unspecified CTL lymphoma. Our series included seven cases that could not be categorized into one of the above CTL subtypes. Tumor sites were the lung, soft tissues, and nasal cavity including the tonsil, pharynx, maxillary sinus, and soft palate. Immunohistochemistry revealed an immunophenotype of CD1–CD2+cCD3+sCD3+CD4–/+CD8+/–TCRβF1+δ1–. Cytotoxic markers were positive in all seven cases and EBV was detected in three cases.

Non-NK/CTL type

Adult T-cell leukemia/lymphoma (ATLL). Of 44 cases, 36 patients presented with cutaneous lesions. Cases with primary presentation involving the intestine, stomach, tonsils, liver, and even soft tissue were also identified. In cutaneous lesions, epidermotropism was frequently observed, with Pautrier's microabscess evident (Fig. 4). Monoclonal proviral HTLV-1 was detected in all cases on Southern blot analysis. The TCR gene was rearranged. The immunophenotypic profile was CD1–CD2+cCD3+sCD3+CD4+CD5+CD7–CD8–/+CD10–CD15–CD19–CD20–CD25+/–CD30–/+TCRβF1+δ1–Ki–67 (>20%). TIA-1 was negative. Histological analysis confirmed ALCL in five CD30-positive cases (four from skin). EBV was not detected and p80 was negative.

Mycosis fungoides (MF). Upper dermis infiltrates and epidermotropism were observed in all 16 cases of MF (Fig. 4). No monoclonal proviral HTLV-1 or EBV was detected. The immunophenotype was CD1–CD2+cCD3+sCD3+CD4+CD7+CD8–/+CD15–CD19–CD20–CD25–/+CD30–TCRβF1+δ1–Ki–67 (<20%). TIA-1 was negative. The phenotype of MF was similar to that of ATLL, except for expression of CD7, CD25 and Ki-67: CD7 was positive in MF but negative in ATLL. CD25, an IL-2 receptor, was positive in most cases of ATLL (88%) but negative in most cases of MF (23%), and Ki-67 positivity in over 20% of lymphoma cells was observed in most cases of ATLL (80%) but not MF (14%).

Unspecified non-NK/CTL lymphoma. Our series included three cases that could not be categorized into one of the above non-NK/CTL subtypes. Tumor sites were tonsils and soft tissues. The immunophenotype was almost the same as that of MF. EBV was not detected.

Survival time

Among the non-NK/CTL type tumors, MF and unspecified non-NK/CTL lymphoma exhibited a favorable prognosis, whereas ATLL exhibited a poor prognosis. NK type tumors also carried a poor prognosis, in particular NK-cell leukemia, which had an aggressive course to death within 6 months. Of the NK-cell lymphomas, nasal tumors had a better prognosis than cutaneous disease. This was probably because half of the nasal NK-cell lymphomas were clinically limited to nasal spaces (Fig. 5).

Of the CTL type lymphomas, ALCL and cutaneous CTL carried a relatively favorable prognosis, but the prognosis for the other types was poor. In particular, γδ T-cell lymphoma and unspecified CTL lymphoma had an aggressive course resulting in death within 6 months (Fig. 5).

Of the cutaneous lymphomas, MF had a good prognosis, and the CTL type had a relatively better prognosis than NK type tumors. CD56-positive cutaneous CTL lymphomas carried a poor prognosis; the prognosis was better for CD56-negative tumors. The reason for this difference, however, remains unclear (Fig. 5).

In summary, the favorable prognosis groups were MF and the unspecified group within the non-NK/CTL type, and ALCL within the CTL type tumors. The poor prognosis groups included NK type, CTL type (except ALCL), and ATLL within the non-NK/CTL type.

Discussion

In the present study, extranodal T-cell lymphomas were classified into three types on the basis of cell lineage: (1) NK type [sCD3–, CD56+, T-cell receptor gene (TCR) germline]; (2) cytotoxic T lymphocyte (CTL) type [sCD3+, TIA-1+, TCR rearranged, CD8+/–, CD4–/+]; and (3) non-NK/CTL type [sCD3+, TIA–1–, TCR rearranged, CD4+/–, CD8–/+]. The NK type included lymphoblastic lymphoma, nasal/nasal-type lymphoma, and aggressive NK leukemia. The CTL type included anaplastic large cell lymphoma (ALCL), cutaneous lymphoma, intestinal lymphoma, γδ T-cell lymphoma and unspecified CTL lymphoma. The non-NK/CTL type included adult T-cell leukemia/lymphoma (ATLL), mycosis fungoides (MF) and unspecified non-NK/CTL lymphoma.

With the exception of MF, almost one-third of T-cell lymphomas arise as primary tumors in extranodal sites, and these lymphomas are biologically different from their nodal counterparts [19]. The REAL and new WHO classifications [15] have emphasized the importance of site and included such new categories as hepatosplenic γδ T-cell lymphoma, subcutaneous panniculitis-like T-cell lymphoma, nasal and nasal-type T-cell lymphoma, enteropathy-type intestinal T-cell lymphoma, and primary cutaneous anaplastic large cell lymphoma. However, cytological features are not distinctive, with most having pleomorphic small, medium, or large cell or anaplastic cytological features. The definition of extranodal T-cell and NK-cell tumors is especially difficult due to the combination of anatomical site, cell lineage, and clinical features [19].

ATLL is a peripheral T-cell lymphoma associated with HTLV-1 infection [33]. Lymphadenopathy or leukemia is the usual presentation, but extranodal presentation is not uncommon [24]. Of the 144 cases of extranodal peripheral T-cell lymphoma we studied here, 44 patients (30.6%) had ATLL, a slightly lower prevalence than observed in our previous series of nodal tumors [25] in which 247 (43.2%) of 572 cases of nodal T-cell lymphoma were confirmed as ATLL. Taken together, our results indicate that ATLL forms a major subset of both nodal and extranodal T-cell lymphomas in our HTLV-1 endemic area.

Skin is the most common extranodal site involved in ATLL [10, 26]. Cutaneous ATLL exhibits a wide spectrum of clinical and histological manifestations, and the differentiation from MF is very difficult [10]. Both diseases are of mature CD4+ T-cell origin. Immunohistochemically, ATLL is often CD25+CD7– and Ki-67 (>20%), whereas, in contrast, MF is CD25–CD7+ and Ki-67 (<20%). ATLL is associated with HTLV-1, whereas MF is not [4]. However, since MF has been documented in occasional HTLV-1 carriers, the definitive diagnosis of HTLV-1-associated ATLL can be made only when monoclonal proviral DNA is confirmed in tumor cells by Southern blot or inverse polymerase chain reaction (PCR) [25, 35].

Most extranodal T-cell lymphomas, except MF and ATLL, are of cytotoxic cell origin (T-cell or NK-cell). The cytotoxic T-cell lymphomas contain a mixture of cell types αβ and γδ. Cytotoxic protein TIA-1 is expressed in cytotoxic T- and NK-cells, independent of their activation status, whereas perforin and granzyme B are increased after activation [9, 29]. CD56 expression is observed in at least a subset of extranodal T-cell lymphomas and most NK-cell neoplasms. Most nasal peripheral T/NK-cell lymphomas are of NK-cell origin [17]. However, recently, Chiang et al. [7] classified nasal NK/T-cell lymphomas into four phenotypic groups: TCRγ–sCD3–CD56+, TCRγ–sCD3+CD56+, TCRγ+sCD3+CD56+, and TCRγ+sCD3+CD56–. The first group was considered to represent NK-cell lymphoma while the others represented T-cell lymphoma. We included 18 cases of nasal NK-cell lymphoma in this study. Four cases of nasal lymphoma with an immunophenotype of CD56+sCD3+ TCR R were classified as unspecified CTL type in this study. In our study, nasal lymphomas of NK and CTL type were EBV-positive and cytotoxic antigen TIA-1-positive. Difference between NK and CTL types could not be confirmed clinically.

Several blastic neoplasms with NK antigen expression have been reported. Usually cytotoxic granules are absent, EBV is negative, and TdT is positive as in T lymphoblastic lymphoma [11]. In the present study, TdT was also positive and EBV was negative in blastic tumors. The NK blastic lymphoma appeared to carry a poorer clinical prognosis than the nodal T-lymphoblastic lymphoma [25].

Tumors arising in other extranodal sites, with features similar to nasal NK-cell lymphomas, are now defined as nasal-type NK-cell lymphomas [6, 16, 20]. However, the cell of origin and EBV status of this tumor type remain controversial. Of the 11 cases reported by Natkunam et al. [22], EBV was present in 5 (45%), whereas all 13 cases reported by Chan et al. [6] were EBV positive. In this study, we have presented 10 cases of nasal-type NK-cell lymphomas: nine cases from skin, and one from gingiva. Our results confirm the finding of previous reports that skin is the most common site of nasal-type NK-cell lymphoma, and six of nine cases (67%) in our study were EBV positive.

The present study included 13 cases of cutaneous CTL cell lymphoma, all of which were of cytotoxic αβ T-cell origin and almost all were CD8-positive. Three entities of cytotoxic T-cell lymphoma with cutaneous presentation have been described up to now: cytotoxic CD8-positive cutaneous T-cell lymphoma, subcutaneous panniculitis-like T-cell lymphoma, and cutaneous NK-cell lymphoma [5, 30]. However, the relationship between and differentiation of these lymphomas is not well understood. EBV was more likely to be associated with CD56-positive than CD56-negative CTL cases. CD56-positive cutaneous CTL lymphomas carried a poor prognosis, whereas the prognosis was better for CD56-negative cases; however, the reason for this remains unclear [5, 30]. In our study, two cases were diagnosed as subcutaneous panniculitis-like T-cell lymphoma. Clearly, further studies are necessary to investigate cutaneous CTL lymphomas.

ALCL is clinically and pathologically heterogeneous. p80 expression is associated with a cytogenetic abnormality, t(2:5)(p23;q35), and systemic ALCLs are p80-positive while primary cutaneous ALCLs are p80-negative. Previous reports have suggested a favorable outcome for p80-positive cases [21, 32]. In the present study, eight cases of ALCL from different anatomic sites were examined. All eight were positive for TIA-1 and negative for EBV. Three of five systemic cases were p80 positive, but one cutaneous case was p80 negative. Due to the small numbers, detailed analysis could not be performed with respect to p80-positive versus p80-negative ALCLs. However, all extranodal ALCLs carried a favorable prognosis.

In this study, 21 cases presented with primary gastrointestinal manifestations, of which five were ATLL and three were ALCL. It is not clear whether the remaining 13 cases could be classified as enteropathy-type intestinal T-cell lymphoma: enteropathy was observed only in four cases. Geographic variation of association with EBV has been observed. One study from Mexico documented 100% EBV positivity, while a series from Western Europe demonstrated EBV in only 10% of cases [8, 28]. In our present study, EBV was detected in about half of the cases. Celiac disease is very rare in Japan in comparison with Western countries. This geographic difference may be associated with the difference between intestinal T-cell lymphoma and the typical enteropathy-type T-cell lymphoma.

Most peripheral T-cell lymphomas are of αβ T-cell origin and only a small proportion are of γδ T-cell deri-

vation. Of the latter group, patients with hepatosplenomegaly comprise a distinct disease entity designated hepatosplenic γδ T-cell lymphoma [9]. Previous papers reported that hepatosplenic γδ T-cell lymphomas expressed activated cytotoxic markers and were EBV negative [2, 9, 29]. Our cases of the hepatosplenic variant were positive for activated cytotoxic markers such as granzyme B, perforin, and Fas L. Four of five cases of γδ T-cell lymphoma were EBV-positive by ISH. Geographic divergence could also underlie these differences.

In summary, we have presented here an analysis of 144 cases of extranodal T-cell lymphoma from an HTLV-1 endemic area, and described the clinical, pathological, immunohistochemical, and genotypic findings and EBV status of these tumors. The extranodal T-cell lymphomas comprised a heterogeneous group: numerous pathological and clinical disease entities were represented. However, the cell lineage and anatomical site were useful in defining extranodal T/NK-cell lymphoma and determining the prognosis. It is apparent that further study is required to better characterize these diseases and their pathogenesis, particularly at the molecular level.

Acknowledgement This study was supported in part by a Grant-in-aid for the Encouragement of Young Scientists from the Ministry of Education, Science and Culture, Japan.

References

1. Anderson P (1995) TIA-1: structural and functional studies on a new class of cytolytic effector molecule. Curr Top Microbiol Immunol 198: 131–143
2. Arnulf B, Copie Bergman C, Delfau Larue MH, Lavergne Slove A, Bosq J, Wechsler J, Wassef M, Matuchansky C, Epardeau B, Stern M, Bagot M, Reyes F, Gaulard P (1998) Nonhepatosplenic gammadelta T-cell lymphoma: a subset of cytotoxic lymphomas with mucosal or skin localization. Blood 91: 1723–1731
3. Avinoach I, Halevy S, Argov S, Sacks M (1994) γ/δ T-cell lymphoma involving the subcutaneous tissue and associated with a hemophagocytic syndrome. Am J Dermatopathol 16: 426–433
4. Bazarbachi A, Soriano V, Pawson R, Vallejo A, Moudgil T, Mattutes E, Peries J, Molina A, de The H, Schulz TF, Catovsky D, Gill PS (1997) Mycosis fungoides and Sezary syndrome are not associated with HTLV-I infection: an international study. Br J Haematol 98: 927–933
5. Berti E, Tomasini D, Vermeer MH, Meijer CJLM, Alessi E, Willemze R (1999) Primary cutaneous CD8-positive epidermotropic cytotoxic T cell lymphomas: a distinct clinicopatholgic entity with an aggressive clinical behavior. Am J Pathol 155: 483–492
6. Chan JKC, Sin VC, Wong KF, Ng CS, Tsang WYW, Chan CH, Cheung MMC, Lau WH (1997) Non-nasal lymphoma expressing the natural killer cell marker CD56: a clinicopathologic study of 49 cases of an uncommon neoplasm. Blood 89: 4501–4513
7. Chiang AKS, Chan ACL, Srivastava G, Ho FCS (1997) Nasal T/natural killer (NK)-cell lymphomas are derived from Epstein-Barr virus-infected cytotoxic lymphocytes of both NK- and T-cell lineage. Int J Cancer 73: 332–338
8. Chott A, Haedicke W, Mosberger I, Fodinger M, Winkler K, Mannhalter C, Muller-Hermelink HK (1998) Most CD56+ intestinal lymphomas are CD8+CD5- T-cell lymphomas of monomorphic small to medium size histology. Am J Pathol 153: 1483–1490
9. Cooke CB, Krenacs L, Stetler-Stevenson M, Greiner TC, Raffeld M, Kingma DW, Abruzzo L, Frantz C, Kaviani M, Jaffe ES (1996) Hepatosplenic T-cell lymphoma: a distinct clinicopathologic entity of cytotoxic γδ T-cell origin. Blood 88: 4265–4274
10. DiCaudo DJ, Perniciaro C, Worrell JT, White JW, Cockerell CJ (1996) Clinical and histologic spectrum of human T-cell lymphotropic virus type I-associated lymphoma involving the skin. J Am Acad Dermatol 34: 69–76
11. DiGiuseppe JA, Louie DC, Williams JE, Miller DT, Griffin CA, Mann RB, and Borowitz MJ (1997) Blastic natural killer cell leukemia/lymphoma: a clinicopathologic study. Am J Surg Pathol 21:1223–1230
12. Farcet JP, Gualard P, Marolleau JP, Le Couedic JP, Henni T, Gourdin M, Divine M, Haioun C, Zafrani ES, Goossens M, Hercend T, Reyes F (1990) Hepatosplenic T-cell lymphoma: Sinonasal/sinusoidal localization of malignant cells expressing the T-cell receptor γδ. Blood 75: 2213–2229
13. Gualard P, Bourquelot P, Kanavaros P, Haioun C, Le Couedic JP, Divine M, Goossens M, Zarfrani ES, Farcet JP, Reyes F (1990) Expression of the alpha/beta and gamma/delta T-cell receptors in 57 cases of peripheral T-cell lymphomas. Am J Pathol 137: 617–628
14. Harris NL, Jaffe ES, Stein H, Banks PM, Chan JKC, Cleary ML, Delsol G, de Wolf-Peeters C, Flini B, Gatter KC, Grogan TM, Isaacson PG, Knowles DM, Mason DY, Muller-Hermelink HK, Pileri SA, Pilis MA, Ralfkiaer E, Warnke RA (1994) A revised European-American classification of lymphoid neoplasms: a proposal from the international lymphoma study group. Blood 84: 1361–1392
15. Harris NL, Jaffe ES, Diebold J, Flandrin G, Muller-Hermelink HK, Vardiman J, Lister TA, Bloomfield CD (2000) The World Health Organization classification of neoplastic diseases of the haematopoietic and lymphoid tissues: report of the clinical advisory committee meeting, Airlie House, Virginia, November, 1997. Histopathology 36: 69–87
16. Jaffe ES, Chan JKC, Su IJ, Frizzera G, Mori S, Feller AC, Ho FCS (1996) Report of the workshop on nasal and related extranodal angiocentric T/Natural killer cell lymphoma: definition, differential diagnosis, and epidemiology. Am J Surg Pathol 20: 103–111
17. Jaffe ES, Krenacs L, Raffeld M (1997) Classification of T-cell and NK-cell neoplasms based on the REAL classification. Ann Oncol 8: S17–S24
18. Kägi D, Ledermann B, Bürki K, Zinkernagel RM, Hengartner H (1995) Lymphocyte-mediated cytotoxicity in vitro and in vivo: mechanisms and significance. Immunol Rev 146: 95–115
19. Kinney MC (1999) The role of morphologic features, phenotype, genotype, and anatomic site in defining extranodal T-cell or NK-cell neoplasms. Am J Clin Pathol 111: s104–s118
20. Nakamura S, Suchi T, Koshikawa T, Kitoh K, Koike K, Komatsu H, Iida S, Kagami Y, Ogura M, Katoh E, Kurita S, Suguki H, Kobashi Y, Yamabe H, Hirabayashi N, Ueda R, Takahashi T (1995) Clinicopathologic study of CD56 (NCAM)-positive angiocentric lymphoma occurring in sites other than the upper and lower respiratory tract. Am J Surg Pathol 19: 284–296
21. Nakamura S, Shiota M, Nakagawa A, Yatabe Y, Kojima M, Motoori T, Suzuki R, Kagami Y, Ogura M, Morishima Y, Mizoguchi Y, Okamoto M, Seto M, Koshikawa T, Mori S, Suchi T (1997) Anaplastic large cell lymphoma: a distinct molecular pathologic entity: a reappraisal with special reference to p80NPM/ALK expression. Am J Surg Pathol 21: 1420–1432
22. Natkunam Y, Smoller BR, Zehnder JL, Dorfman RF, Warnke RA (1999) Aggressive cutaneous NK and NK-like T-cell lymphomas: clinicopathologic, immunohistochemical, and molecular analyses of 12 cases. Am J Surg Pathol 23: 571–581
23. Ohshima K, Kikuchi M, Masuda Y, Kobari S, Sumiyoshi Y, Eguchi F, Mohtai H, Yoshida T, Takeshita M, Kimura N (1991) Defective provirus form from human T-cell leukemia virus type I in adult T-cell leukemia/lymphoma: clinicopathological features. Cancer Res 51: 4639–4642

24. Ohshima K, Takeo H, Kikuchi M, Kozuru M, Uike N, Masuda Y, Yoneda S, Takeshita M, Shibata T, Akamatsu M (1994) Heterogeneity of Epstein-Barr virus infection in angioimmunoblastic lymphadenopathy type T-cell lymphoma. Histopathology 25: 569–579
25. Ohshima K, Suzumiya J, Sato K, Kanda M, Sugihara M, Haraoka S, Takeshita M, Kikuchi M (1998) Nodal T-cell lymphoma in an HTLV-1 endemic area: proviral HTLV-1 DNA, histological classification and clinical evaluation. Br J Haematol 101: 703–711
26. Ohshima K, Suzumiya J, Sato K, Kanda M, Haraoka S, Kikuchi M (1999) B-cell lymphoma of 708 cases in Japan: incidence rates and clinical prognosis according to the REAL classification. Cancer Lett 135: 73–81
27. Ohshima K, Suzumiya J, Sugihara M, Kanda M, Shimazaki K, Haraoka S, Kikuchi M (1999) Clinical, immunohistochemical and phenotypic features of aggressive nodal cytotoxic lymphomas, including α/β, γ/δ T-cell and natural killer cell types. Virchows Arch 435: 92–100
28. Qaintanilla-Martinez L, Lome-Maldonado C, Ott G, Gschwendtner A, Gredler E, Reyes E, Angeles-Angeles A, Fend F (1997) Primary non-Hodgkin's lymphoma of the intestine: high prevalence of Epstein-Barr virus in Mexican lymphomas as compared with European cases. Blood 89: 644–651
29. Salhany KE, Feldman M, Kahn M, Peritt D, Schretzenmair RD, Wilson DM, Dipaola RS, Glick AD, Kant JA, Nowell PC, Kamoun M (1997) Hepatosplenic γδ T-cell lymphoma: ultrastructural, immunophenotypic, and functional evidence for cytotoxic T lymphocyte differentiation. Hum Pathol 28: 674–685
30. Savoia P, Fierro MT, Novelli M, Quaglino P, Verrone A, Geuna M, Bernengo MG (1997) CD56-positive cutaneous lymphoma: a poorly recognized entity in the spectrum of primary cutaneous disease. Br J Dermatol 137: 966–971
31. Shimoyama M (1991) Diagnostic criteria and classification of clinical subtypes of adult T-cell leukemia/lymphoma: a report from the Lymphoma Study Group (1984–87). Br J Haematol 79: 428–437
32. Shiota M, Nakamura S, Ichinohasama R, Abe M, Akagi T, Takeshita M, Mori N, Fujimoto J, Miyauchi J, Mikata A, Nanba K, Takami T, Yamabe H, Takano Y, Izumo T, Nagatami T, Mohri N, Nasu K, Satoh H, Katono H, Fujimoto J, Yamamoto T, Mori S (1995) Anaplastic large cell lymphomas expressing the novel chimeric protein p80NPM/ALK: a distinct clinicopathologic entity. Blood 86: 1954–1960
33. Tajima K, Tominaga S (1985) Epidemiology of adult T-cell leukemia/lymphoma in Japan. Curr Top Microbiol Immunol 111: 53–66
34. Takatsuki K (1985) Overview of adult T-cell leukemia/lymphoma. Jpn Soc Res 25: 97–103
35. Takemoto S, Matsuoka M, Yamaguchi K, Takatsuki K (1994) A novel diagnostic method of adult T-cell leukemia: monoclonal integration of human T-cell lymphotropic virus type I provirus DNA detected by inverse polymerase chain reaction. Blood 84: 3080–3085
36. Tian Q, Streuli M, Saito H, Schlossman SF, Anderson P (1991) A polyadenylate binding protein localized to the granules of cytolytic lymphocytes induces DNA fragmentation in target cells. Cell 67: 629–639

Virchows Arch (2002) 440:436–440
DOI 10.1007/s00428-001-0598-1

CASE REPORT

**Silke Gronau · Christiane K. Menz · Ingo Melzner
Richard Hautmann · Peter Möller
Thomas F.E. Barth**

Immunohistomorphologic and molecular cytogenetic analysis of a carcinosarcoma of the urinary bladder

Received: 21 September 2001 / Accepted: 22 November 2001 / Published online: 8 February 2002
© Springer-Verlag 2002

Abstract Carcinosarcomas of the urinary bladder are malignant biphasic tumors with an epithelial and a spindle cell component. For the histogenesis of the two components, a biclonal and a monoclonal origin are discussed. We present the immunomorphology and molecular cytogenetics of such a case. The immunohistology of biopsies of the urinary bladder revealed a poorly differentiated urothelial carcinoma (GIII) and a co-existing pleomorphic, spindle cell leiomyosarcoma (GIII). The two components were microdissected and further analyzed for gains and losses of chromosomal material using comparative genomic hybridization. In addition, loss of heterozygosity analyses were included. The tumor components revealed as overlapping core aberrations losses on the short arm of chromosome 9 and on the long arm of chromosome 11. However, both components showed additional aberrations exclusively detected in one of the components. The occurrence of overlapping aberrations strongly argues for a monoclonal origin of this tumor with a common ancestor. The additional aberrations of the components point to an independent and divergent course of tumor progression in both components.

Keywords Carcinosarcoma · Molecular cytogenetics · Clonality analysis

Introduction

Carcinosarcomas are rare biphasic malignant tumors with an epithelial and a spindle cell component in which the mesenchymal component does not express any epithelial markers [16]. For the histogenesis of these tumors, two hypotheses have been put forward:

i. The multiclonal hypothesis, proposing that the tumor originates from different stem cells, resulting in a composite tumor
ii. The monoclonal hypothesis, proposing that the tumor originates from a single pluripotential stem cell with an extremely divergent differentiation during tumor progression [4]

Cytogenetic studies may help to evaluate both hypotheses. In a single experiment, comparative genomic hybridization (CGH) can provide an overview regarding gains and losses of chromosomal material in a tumor cell population. The comparison of the results may help to elucidate the histogenesis of the components: different aberrations in the two components make a strong case for the origin being in different stem cells with individual tumor progression and independent accumulation of genetic changes; in contrast, overlapping genetic aberrations in both compartments favor the origin as being from one pluripotential stem cell and an (at least partly) common pathway during tumor progression. The aim of this study was to test both hypotheses on a typical case of carcinosarcoma of the urinary bladder.

Clinical history

A 77-year-old woman was admitted with macrohematuria and pain projected to the urinary bladder. Cytoscopy showed a tumor with a diameter of 4 cm on the base of the urinary bladder. Due to advanced stage and with a palliative intention, the tumor was only partly resected by transurethral resection. The patient died 3 months later due to heart failure. No autopsy was performed.

Materials and methods

The resected tissue was fixed in buffered formaldehyde and embedded in paraffin. In addition to conventional staining (hematox-

S. Gronau
Department of Otorhinolaryngology and Head and Neck Surgery, University of Ulm, Germany

C.K. Menz · I. Melzner · P. Möller · T.F.E. Barth (✉)
Institute of Pathology, Ulm University, Albert-Einstein-Allee 11, 89081 Ulm, Germany
e-mail: thomas.barth@medizin.uni-ulm.de
Tel.: +49-731-5023300, Fax: +49-731-5023884

R. Hautmann
Department of Urology, University of Ulm, Germany

ylin and eosin, periodic acid-Schiff) immunohistochemistry was performed using an indirect streptavidin–biotin method [2]. The following primary antibodies were used in the indicated dilutions: anti-vimentin (clone VIM3B4, 1:10) from Camon (Wiesbaden, Germany), anti-actin (clone HHF35, 1:100) from BioGenex Laboratories (San Ramon, Calif.), anti-desmin (clone D33, 1:10) from Camon, anti-carcinoma-embryonic antigen (CEA, clone II-7, 1:10) from Dako (Hamburg, Germany), anti-basal cell keratin (clone 34ß E12, 1:200) from Enzo (Farmingdale, N.Y.), anti-human leukocyte antigen (HLA)-DR (clone TAL 1B5, 1:1000) from Dako and anti-Ki-67 (clone MIB1, 1:200) from Dianova (Hamburg, Germany).

CGH

Serial sections were prepared from formalin-fixed, paraffin-embedded tissue. After staining with hematoxylin and eosin, the spindle cell and the epithelial component as well as nontumorous tissue were marked and dissected with a microblade under microscopic control and further processed. The tissue was digested with proteinase K (10 mg/ml) overnight in sodium ethylene diamine tetraacetate (EDTA) buffer (75 mM NaCl, 25 mM EDTA, pH 8), and the DNA extracted using a commercial extraction kit (Qiagen, Hilden, Germany). After DNA extraction the small amounts of DNA gained were amplified using a standard protocol with degenerated oligoprimers [14]. CGH was performed as previously described [9]. Briefly, universally amplified genomic DNA was labeled with biotin by nick translation after the degenerated oligonucleotide primers had been removed using suitable columns. As the control probe DNA isolated from normal tonsils of healthy individuals was differentially labeled with digoxigenin. One microgram biotin-labeled tumor DNA, 1 µg digoxigenin-labeled control DNA, and 70 µg human Cot-1-DNA (BRL Life Sciences, Gaithersburg, Md.) were cohybridized to slides with metaphase cells from the blood of a healthy donor. After hybridization, control and test DNAs were detected via rhodamine and fluorescein isothiocyanate (FITC), respectively. Images of more than 15 metaphase cells were recorded, and the ratio of FITC/rhodamine fluorescence intensities were calculated along each individual chromosome and averaged using dedicated software (ISIS, MetaSystems, Version 1.80, Altlussheim, Germany). Ratio values of 1.25 and 0.8, which have been proven to provide robust criteria for diagnosing over- and underrepresentation, were used as upper and lower thresholds for the identification of chromosomal imbalances [1]. Of the chromosomal regions recognized to be critical in CGH analyses, the centromeric regions, the Y chromosome, 1p32-p36 and chromosome 19 were not scored in the results for reasons specified elsewhere [11]. Furthermore, the experiments were performed twice, confirming the results in each case. In contrast, in a hybridization experiment with DNA extracted from morphologically tumor-free areas of the tissue, no gains or losses were detected by CGH. The ISIS system was used for image analysis.

Loss of heterozygosity (LOH) analysis was performed using microsatellite analysis with published protocols and markers [12]. The following microsatellite markers synthesized at MWG Biotech (Munich, Germany) were used (the corresponding chromosomal location is given in brackets): D6S310 (6q23.3-q25); D9S2136 (9p21), D11S987 (11q13.3); D11S1345 (11q23–24).

Pathologic findings

Histopathology and immunohistology

In the multiple biopsies, microscopy revealed a malignant tumor with a distinct spindle cell and a distinct epithelial component (Fig. 1a, b). The epithelial component consisted of plump cells with partly vesicular nuclei and prominent nucleoli. The spindle cell compartment was characterized by elongated cells with pleomorphic, condensed nuclei, and scattered atypical mitoses (Fig. 1a, b).

Table 1 Immunohistochemical analysis of the spindle cell and epithelial component of the carcinosarcoma (+ positive; – negative). *CEA* carcinoma-embryonic antigen, *HLA* human leukocyte antigen

Antigen	Epithelial cell component	Spindle cell component
Vimentin	–	+
Actin	–	+
Basal cell keratin	+	–
Desmin	–	–
CEA	+	–
HLA-DR	+	+
Ki-67	10–20%	60–70%

Immunohistochemically, the epithelial component was positive for CEA, HLA-DR, and basal cell keratin and negative for desmin, vimentin, and actin. The Ki-67 proliferation index was estimated by counting 100 cells in two tumor areas and was approximately 10–20%. The pleomorphic spindle cell component was strongly positive for vimentin, HLA-DR, and actin, and negative for CEA, desmin, and basal cell keratin (Fig. 1c, d). The immunohistological data are summarized in Table 1. The Ki-67 proliferation rate was about 60–70%. The morphology and immunohistochemistry led to the diagnosis of a carcinosarcoma composed of a transitional cell carcinoma (GIII) and a leiomyosarcoma (GIII).

CGH

The epithelial compartment revealed losses on the short arm of chromosome 9 and the long arm of chromosome 11. In addition, a loss on chromosome 6 and a gain on chromosome 11 were detected. The CGH karyotype of the epithelial component according to international system for human cytogenetic nomenclature was: reverse in situ hybridization (rev ish) diminished (dim) 6q14-q27, 9p21-p24, 11q24-q25, enhanced (enh) 11q14-q22. Like the epithelial component, the spindle cell component showed losses on the short arm of chromosome 9 and on the long arm of chromosome 11. In addition, losses were detected on the short arms of chromosomes 8 and 10 (CGH karyotype of the spindle cell component: rev ish dim 8p22-p23, 9p21-p24, 10p14-p15, 11q22-q25). Partial CGH karyotypes of the two components are shown in Fig. 1e, f.

LOH

To confirm the CGH results four markers were selected according to the losses detected by CGH. Of these four markers, three revealed a homozygous state in the normal tissue. Therefore, these loci could not be further analyzed by LOH. Only the marker 11S1345 clearly showed a heterozygous state in the DNA from the normal tissue.

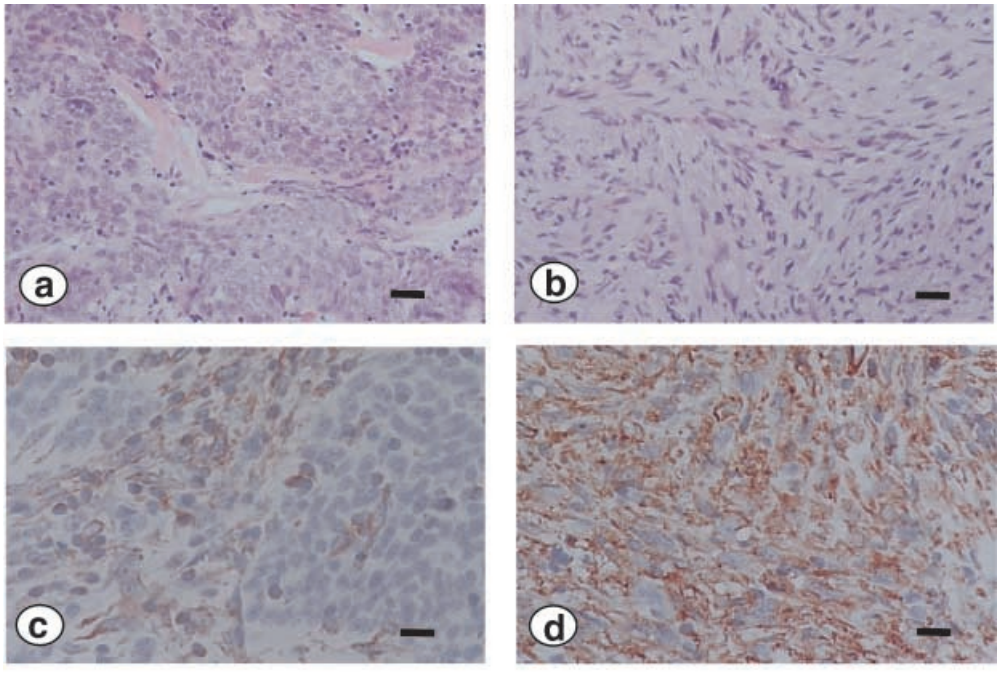
a
b
c
d

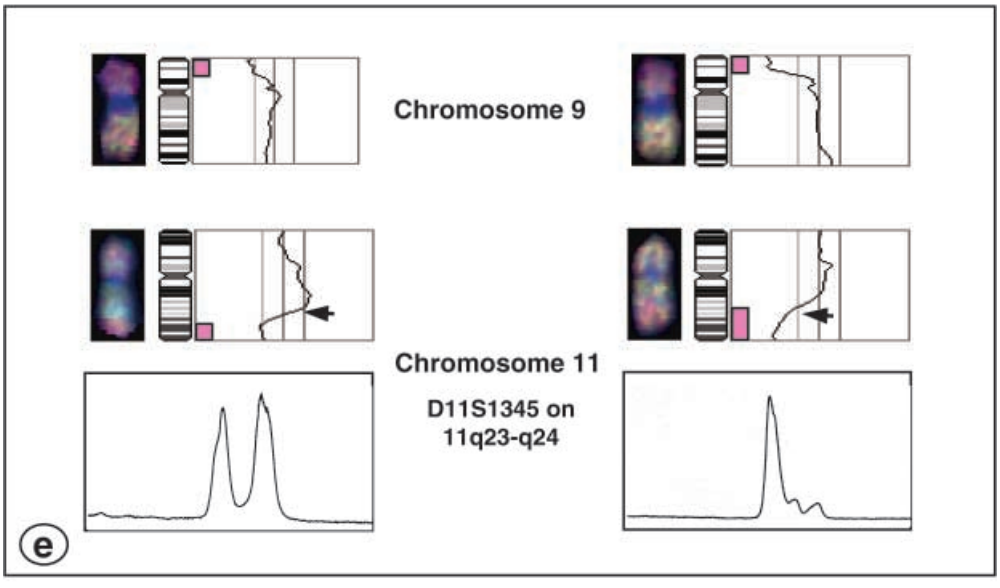
Chromosome 9
Chromosome 11
D11S1345 on
11q23-q24
e

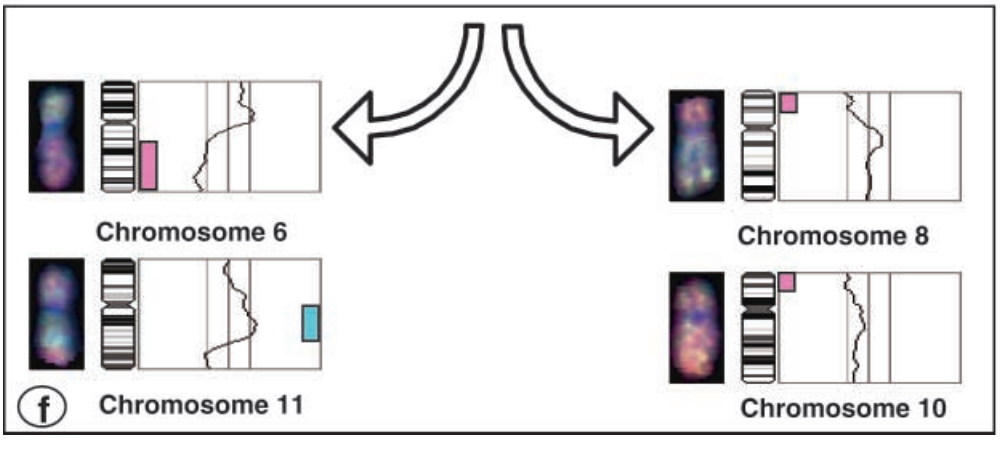
Chromosome 6
Chromosome 11
Chromosome 8
Chromosome 10
f

For this marker a loss of heterozygosity was detected in the spindle cell component, therefore confirming the loss of chromosomal material in this region. In contrast, the epithelial component showed a heterozygous state as did the normal control tissue (Fig. 1e).

Discussion

Carcinosarcomas are rare biphasic malignant tumors with an epithelial and a spindle cell component. We have used microdissection of the two components of such a carcinosarcoma with subsequent CGH analysis. Using this approach, losses on the short arm of chromosome 9 and on the long arm of chromosome 11 were found in both components. The commonly deleted region in both components included chromosomal region 9p21. This is the chromosomal localization of the tumor-suppressor gene *TP*16. Losses on the short arm of chromosome 9, including deletion of *TP*16, have been previously reported in both components of carcinosarcomas of different localizations and are an early finding in superficial urothelial carcinomas [6, 8]. These overlapping losses on chromosome 9 and on chromosome 11 are evidence of a clonal origin of the case studied and confirm various cytogenetic studies of carcinosarcomas of the urinary bladder, the breast, and the female genital tract [6, 7, 13, 15]. In addition to the overlapping aberrations, our study revealed gains and losses exclusively detected in the epithelial and in the spindle component. In the epithelial component these losses were located on the long arm of chromosome 6 and a gain was located on the long arm of chromosome 11, whereas the spindle cell component showed further losses on the short arms of chromosomes 8 and 10. These findings support the view of a clonal origin of the components with diverging pathways originating from a certain point of tumor progression (Fig. 1). Whether this point of divergence coincides with the emergence of the two morphological phenotypes or whether the secondary genetic aberrations detected are only epiphenomena of complex biologic events remains elusive. Recently, several factors such as the zinc finger transcription factor SNAIL and transforming growth factor beta1 have been individualized as mediators in the process of transdifferentiation from an epithelial cell to a mesenchymal cell [5, 10]. The respective genes are localized on chromosomes 20 and 19. In our case, CGH failed to show gains or losses of chromosomal material in these regions. However, this does not exclude subtle structural alterations in these loci since the resolution of CGH lies in between 10 Mb [3].

In order to confirm the CGH results LOH analysis was performed. Only the marker located on 11q23-q24 was useful to confirm the CGH results since the other three markers tested revealed a homozygous state in the normal tissue. However, the marker D11S1345 on 11q23-q24 confirmed the loss of chromosomal material in the spindle cell component as detected by CGH.

In conclusion, the data presented herein suggest that the two components of the carcinosarcoma have a common genetic background. Furthermore, the additional genetic changes detected in the two components may be regarded as a reflection of the biphenotypic appearance of this tumor and are thought to suggest the divergent pathways during independent tumor progression.

◀ **Fig. 1** **a**, **b** Histomorphology of the carcinosarcoma. **a** The epithelial component is characterized by plump cells with large, vesicular nuclei and prominent nucleoli. **b** The spindle cell component shows elongated, partly twisted cells with pleomorphic and hyperchromatic nuclei. (Hematoxylin and eosin, ×92; *scale bar* 50 µm). **c**, **d** Immunohistology. **c** The epithelial component is negative for vimentin. Scattered stromal cells are strongly vimentin-positive. **d** Vimentin is strongly positive in the tumor cells of the spindle cell component (×184; *scale bar* 100 µm). **e**, **f** Partial comparative genomic hybridization (CGH) ideograms and average ratio profiles of the epithelial and spindle cell component. The tumor DNA is detected in green via fluorescein isothiocyanate (FITC), the control DNA in red via rhodamine. The chromosomes are counterstained in blue with 4,6-diamidino-2-phenylindole (DAPI). On the *right side* of the ideogram the average ratio profiles of the FITC/rhodamine fluorescence are plotted. The *central line* indicates a ratio value of 1.0; the *line to the left* indicates a value of 0.8, the *line to the right* a value of 1.25. An average of 20 chromosomes were evaluated for the ratio profile. **e** Average profiles of chromosomes 9 and 11 of the epithelial and spindle cell component: in both components, overlapping losses on the short arms of chromosomes 9 and 11 are seen as indicated by the shift to the left of the average ratio profile beyond the diagnostic threshold of 0.8 (for the detailed CGH karyotype see "Results"). The *red bars* indicate the chromosomal region on the ideogram corresponding to losses of chromosomal material in the given region (see also reddish hybridization signals on the overlay hybridization of chromosome 9 and 11 indicating losses of chromosomal material). The profile of loss of heterozygosity (LOH) analysis in the lower part with the marker D11S1356 on 11q23-q24 reveals a clear LOH for the spindle cell component while the epithelial component shows a normal status therefore confirming the CGH profile of the epithelial component in this region. *Arrows* mark the respective chromosomal position of the marker D11S1356. **f** Additional gains and losses of chromosomal material in the epithelial and spindle cell component (*left and right arrow*, respectively). The ratio profiles reveal losses of chromosomal material of the epithelial component on the long arm of chromosome 6 and a gain of chromosomal material on the long arm of chromosome 11 [regions of loss and gain are marked by a *red bar* (loss) and a *green bar* (gain) in analogy to the reddish and greenish hybridization signals on the chromosomes]. In contrast, the spindle cell component shows additional losses on the short arms of chromosomes 8 and 10 (chromosomal region marked by *red bars*)

Acknowledgements The skilful technical assistance of Ms. Sabine Gantner, Ms. Iwona Nerbas, and Ms. Karola Dorsch is gratefully acknowledged. This work was supported by grants from the Deutsche Krebshilfe (70-2310-Ba) and from the Medical Faculty of the University of Ulm (P.640).

References

1. Barth TFE, Benner A, Bentz M, Döhner H, Möller P, Lichter P (2000) Risk of false positive results in comparative genomic hybridization. Genes Chromosomes Cancer 28:353–357
2. Barth TFE, Leithäuser F, Döhner H, Bentz M, Pawlita M, Schmid U, Möller P (2000) Primary gastric apoptosis-rich T-cell lymphoma co-expressing CD4, CD8, and cytotoxic molecules. Virchows Arch 436:357–364

3. Bentz M, Plesch A, Stilgenbauer S, Döhner H, Lichter P (1998) Minimal sizes of deletions detected by comparative genomic hybridization. Genes Chromosomes Cancer 21:172–175
4. Bloxham CA, Bennett MK, Robinson MC (1990) Bladder carcinosarcomas: three cases with diverse histogenesis. Histopathology 16:63–67
5. Cano A, Perez-Moreno MA, Rodrigo I, Locascio A, Blanco MJ, del Barrio MG, Portillo F, Nieto MA (2000) The transcription factor snail controls epithelial-mesenchymal transition by repressing E-cadherin expression. Nat Cell Biol 2:76–83
6. Fujii H, Yoshida M, Gong ZX, Matsumoto T, Hamano Y, Fukunaga M, Hruban RH, Gabrielson E, Shiarai T (2000) Frequent genetic heterogeneity in the clonal evolution of gynecological carcinosarcoma and its influence on phenotypic diversity. Cancer Res 60:114–120
7. Halachmi S, DeMarzo AM, Chow NH, Halachmi N, Smith AE, Linn JF, Nativ O, Epstein JI, Schoenberg MP, Sidransky D (2000) Genetic alteration in urinary bladder carcinosarcoma: evidence of a common clonal origin. Eur Urol 37:350–357
8. Hartman A, Rosner U, Schalke G, Dietmaier W, Zaak D, Hofstaedter F, Knuechel R (2000) Clonality and genetic divergence in multifocal low-grade superficial urothelial carcinoma as determined by chromosome 9 and p53 deletion analysis. Lab Invest 80:709–718
9. Lichter P, Bentz M, Joos S (1995) Detection of chromosomal aberrations by means of molecular cytogenetics: painting of chromosomes and chromosomal subregions and comparative genomic hybridization. Methods Enzymol 254:334–391
10. Piek E, Moustakas A, Kurisaki A, Heldin CH, ten Dijke P (1999) TGF-beta I receptor/ALK-5 and Smad proteins mediate epithelial to mesenchymal transdifferentiation in NmuMG breast epithelial cells. J Cell Sci 112:4557–4568
11. Solinas-Toldo S, Wallrapp C, Müller-Pillasch F, Bentz M, Gress T, Lichter P (1996) Mapping of chromosomal imbalances in pancreatic carcinoma by comparative genomic hybridization. Cancer Res 56:3803–3807
12. Starosik P, Greiner A, Schwarz S, Patzner J, Schultz A, Müller-Hermelink HK (2000) The role of microsatellite instability in gastric low- and high-grade lymphoma development. Am J Pathol 157:1129–1136
13. Teixeira MR, Qvist H, Bohler PJ, Pandis N, Heim S (1998) Cytogenetic analysis shows that carcinosarcomas of the breast are of monoclonal origin. Genes Chromosomes Cancer 22:145–151
14. Telenius H, Carter NP, Bebb CE, Nordenskjold M, Ponder BA, Tunnadiffe A (1992) Degenerate oligonucleotide-primed PCR: general amplification of target DNA by a single degenerate primer. Genomics 13:718–725
15. Torenbeeck R, Blomjous CEM, Van der Valk P, Meijer CJLM (1997) Sarcomatoid carcinoma vs. carcinosarcoma of the urinary bladder. J Urol Pathol 6:27–41
16. Torenbeeck R, Hermsen MAJA, Meijer GA, Baak JPA, Meijer CJLM (1999) Analysis by comparative genomic hybridization of epithelial and spindle cell components in sarcomaid carcinoma and carcinosarcoma: histogenetic aspects. J Pathol 189:338–343

Virchows Arch (2002) 440:449–450
DOI 10.1007/s00428-001-0574-9

ERRATUM

A. Ubiali · A. Benetti · M. Papotti · V. Villanacci
G. Rindi

Genetic alterations in poorly differentiated endocrine colon carcinomas developing in tubulo-villous adenomas: a report of two cases

Published online: 1 February 2002
© Springer-Verlag 2002

Virchows Arch (2001) 439:776–781

In the original publication there were some errors in Fig. 1D and in the legends to Fig. 1 and Fig. 2. Figure 1 has been corrected and is reprinted here. The microsatellites defined originally as D11S69, D11S61, D11S58 and D11S55 should be: D18S69, D18S61, D18S58 and D18S55.

In the legend to Fig. 2, "...**e** Representative examples of the allelic status for microsatellite markers on 11q (D11S913), 3p (BAT26)..." should have been "...**e** Representative examples of the allelic status for microsatellite markers on 11q (D11S913), 2p (BAT26)...."

The online version of the original article can be found at http://dx.doi.org/10.1007/s004280100475

A. Ubiali · A. Benetti · V. Villanacci · G. Rindi (✉)
Pathology Service 2, University of Brescia and Spedali Civili,
Piazza Spedali Civili, 1, 25124 Brescia, Italy
e-mail: guido.rindi@unipr.it
Tel.: +39-0521-991636, Fax: +39-0521-292710

M. Papotti
Surgical Pathology III, University of Turin, Turin, Italy

G. Rindi
Department of Pathology and Laboratory Medicine,
University of Parma, via A. Gramsci, 14, 43100 Parma, Italy

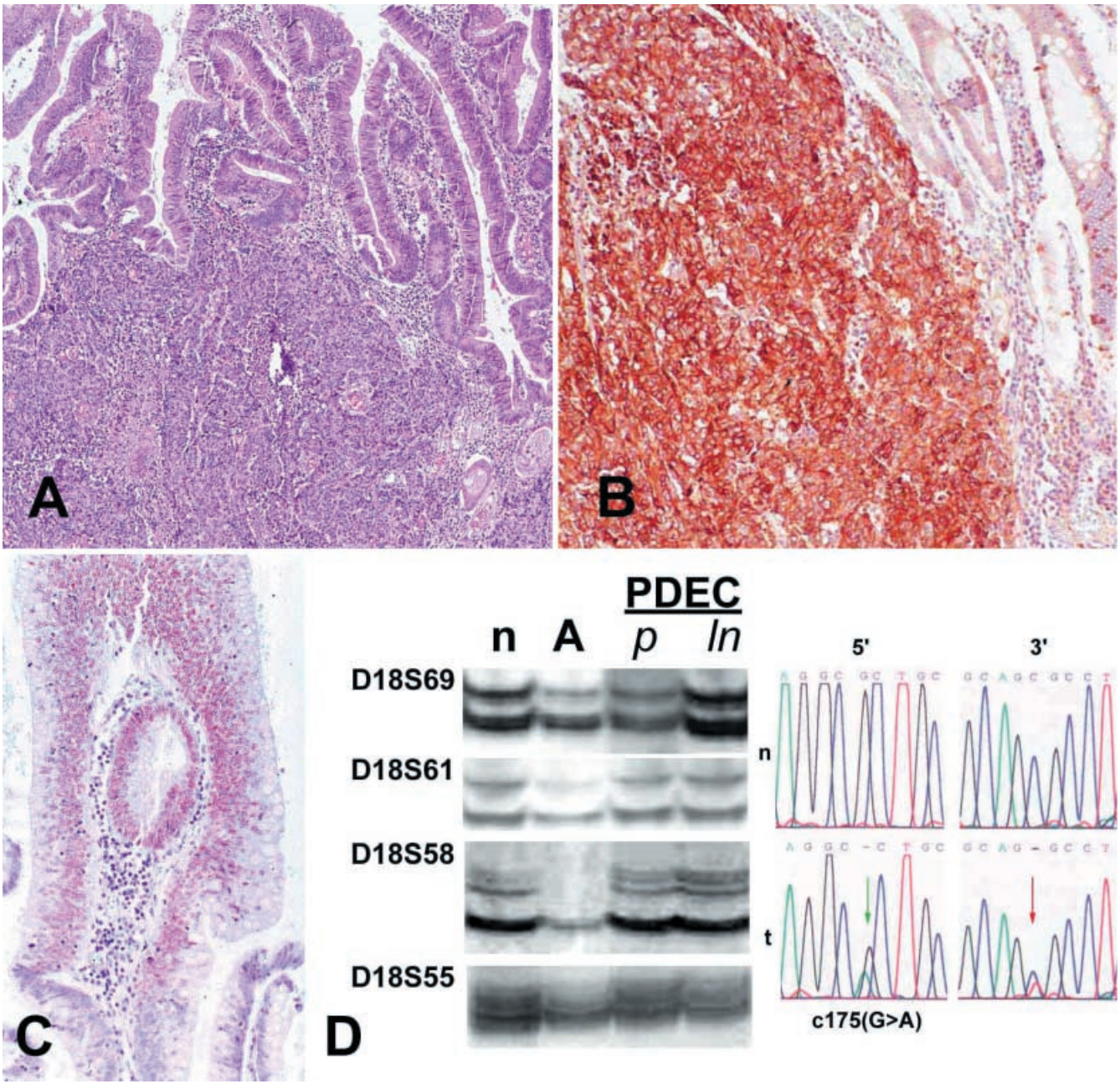

Fig. 1a–d Patient A: histopathological findings. **a** The typical solid structure with focal necrosis of the poorly differentiated endocrine carcinoma (PDEC, *lower part* of the micrograph) growing within the tubulo-villous adenoma (*upper part* of the micrograph). **b** The intense and diffuse immunoreactivity for synaptophysin of the PDEC cells: note the absence of significant immunoreactivity in the adenoma cells. **c** *p53* overexpression/accumulation in the nuclei of the adenoma cells: note that some cells at the base of the villous growth are negative. **a** H&E; **b**, **c** immunoperoxidase, SABC method. Molecular genetic findings. **d** (*left part*) Allelic status of four microsatellite markers on 18q in DNA from normal tissue (*n*), adenoma (*A*), PDEC primary (*p*) and lymph-node metastasis (*ln*). In **a** samples all the four microsatellite markers show signal reduction indicative for allelic loss; this is evident for D18S61 and D18S58, but also appreciable for D18S69 and D18S55, as demonstrated after quantification (not shown). **d** (*right part*) Sequence analysis of *p53* exon 5 in normal tissue (*n*) and in PDEC cells (*t*) showing the G>A substitution at codon 175, (c175(G>A), *arrows*); note that the electropherogram shows also a normal signal for both strands (5′ and 3′), indicative of mixed amplified DNA, possibly due either to double tumor cell population or to normal cell contamination

Virchows Arch (2002) 440:453–460
DOI 10.1007/s00428-002-0623-z

REVIEW ARTICLE

James D. Mueller · Birgit Bethke · Manfred Stolte

Colorectal de novo carcinoma: a review of its diagnosis, histopathology, molecular biology, and clinical relevance

Received: 15 November 2001 / Accepted: 17 January 2002 / Published online: 21 March 2002
© Springer-Verlag 2002

Abstract The effort to reduce colorectal adenocarcinoma mortality increasingly depends on detection and removal of precancerous adenomas by colonoscopy. Sporadic reports have described small, aggressive carcinomas that do not appear to develop from adenomas and have been called "de novo" carcinomas. These lesions seem to challenge the basis of colorectal surveillance and are therefore a controversial topic. This review presents the history of the de novo concept, the problems concerned with the histopathologic diagnosis of these lesions and what is presently known about their clinical and molecular biologic features in comparison with the more common ex adenoma type of colorectal carcinomas. This information will show that, despite their rarity, it is important for both pathologists and gastroenterologists to be aware of these lesions.

Keywords Colorectal carcinoma · De novo · Histopathology · Molecular biology

Introduction

Colorectal carcinogenesis: the de novo concept

The term "de novo" colorectal carcinoma dates from several decades ago, before the widespread acceptance of the adenoma-carcinoma concept. It defined a carcinogenetic pathway, in which normal colonic mucosa could directly give rise to carcinoma "de novo" without the intervening steps of an adenoma [15]. This idea was supported by the fact that most colon carcinomas at that time were usually detected as large tumor masses causing bowel obstruction or bleeding and only rarely had adenoma remnants in their vicinity [10].

As colonoscopy developed and increasingly smaller carcinomas and large numbers of adenomas could be obtained for pathologic study, the concept of adenomas as localized areas of "dysplasia" from which most, if not all, colorectal carcinomas develop was established [16, 30]. This concept was solidified by Vogelstein et al. [48], who showed that a stepwise accumulation of genetic errors occurs parallel to the path of progression along the adenoma-carcinoma pathway. The colorectal adenoma-carcinoma sequence became a classic paradigm for tumor development to the point that the "de novo" concept of colorectal carcinogenesis was effectively abandoned.

Revival of the de novo concept in Japan

Beginning in the mid 1980s, several Japanese authors began to report that they could detect very small colorectal carcinomas, many of which were less than 1.0 cm in diameter [19, 22, 23, 41]. Endoscopic techniques had made particular progress in Japan due to the high incidence of gastric carcinoma there and the development of systematic screening to detect it at an early stage. Applying the same techniques to the colorectum, Japanese endoscopists also found that similar small carcinomas could be detected there. Since these tumors were so small without adenomatous elements in their vicinity, it seemed that these tumors had not originated from any precursor lesion and so they were given the name "de novo" carcinoma by several authors [23, 41].

Controversy in the West

As these reports of de novo carcinoma reached the western world, both pathologists and endoscopists received the idea of this new entity with skepticism. One problem was the fact that there are significant differences between Japanese and western pathologists' criteria for the diag-

J.D. Mueller (✉)
Department of Pathology, Brigham and Women's Hospital,
75 Francis Street, Boston, MA 02115, USA
e-mail: jmueller@rics.bwh.harvard.edu
Tel.: +1-617-7325984, Fax: +1-617-7326177

B. Bethke · M. Stolte
Institut für Pathologie, Klinikum Bayreuth,
Preuschwitzer Straße 101, 95445 Bayreuth, Germany

nosis of colorectal carcinoma [40], so that many of the de novo carcinoma cases reported in Japan that lacked submucosal invasion were not carcinomas according to European or North American criteria [46]. Western endoscopists were not convinced since they had also been performing careful endoscopies but had found these lesions much less frequently than the Japanese [36]. Some speculated that epidemiological differences related to the overall lower rate of colorectal carcinoma in Japan could explain the rarity of de novo type carcinoma in the West [7].

Recently, however, several reports from the western world have found that small colorectal carcinomas can be detected at a similar frequency when endoscopic techniques such as those used in Japan are employed [5, 18, 37, 42, 43, 44]. In 1995, our group published a series in Germany describing 155 de novo carcinomas collected between 1988 and 1994 that were no more than 1.0 cm in diameter [45]. Although it is still very difficult to estimate their incidence, these reports have demonstrated conclusively that de novo colorectal carcinomas are not only a Japanese phenomenon. The question still remains, however, whether the name "de novo" is really appropriate, since it seems highly unlikely that carcinoma can arise directly from normal colonic mucosa considering the weight of the available molecular pathologic data.

Definition of de novo carcinoma

A continuing problem with de novo carcinoma as an entity is that it has no universally accepted definition. By definition, its only essential feature is that it lacks any histologically identifiable adenomatous elements in its vicinity. In fact, for this reason, some authors have stated that most colon carcinomas arise by the de novo pathway, since adenomas can only be identified in a minority of advanced carcinomas [24], although this ignores the fact that a preexistent adenoma is likely to be destroyed by a large tumor. Our own studies [5, 31, 34], as well as those of other groups [13], have defined de novo carcinoma as being 1.0 cm or less in diameter, since the chance of a carcinoma having arisen in an adenoma and then the adenomatous elements being destroyed is much less at this small size.

However, not all small colon carcinomas are de novo carcinomas since even small tumors may have remaining adenoma elements. The distinction between de novo carcinoma and a carcinoma arising from an adenoma ("ex adenoma carcinoma") may actually be quite difficult since it rests on deciding between high-grade and low-grade dysplasia (or high- and low-grade intraepithelial neoplasia according to the new Vienna classification [39, 52]) in the epithelium above or adjacent to the invasive carcinoma. Studies in the western world, including our own, have required that invasion of the submucosa be present, but some examples of de novo carcinoma cited in the Japanese literature do not correspond to western definitions of carcinoma, since no submucosal invasion is present.

For these reasons, studies that describe de novo, de novo type, flat, or small-superficial colorectal carcinomas may or may not be examining similar lesions and are, therefore, very difficult to compare with one another. This is another factor that has hampered the acceptance and awareness of these lesions by pathologists.

Clinicopathologic, endoscopic features

Estimates of the frequency of de novo colorectal carcinoma vary according to how they are defined, but, if the 1.0-cm diameter is used as a criterion, they appear to account for approximately 5% or less of colorectal carcinomas [11, 36]. This figure can only be a rough estimate since there is no systematic screening that would detect such small asymptomatic lesions, and since once a carcinoma has become advanced it is no longer possible to make any reliable statement about whether it originated as an ex adenoma or a de novo type. However, the fact that the National Polyp Study showed that adenoma clearance leads to a marked reduction in the rate of colorectal cancer incidence [49] is evidence that the contribution of de novo carcinoma to colorectal carcinoma incidence must be quite small. There are no clinical characteristics that distinguish de novo from ex adenoma colorectal carcinoma in terms of distribution within the colorectum (they are both predominantly left-sided lesions), age of the patients (similar in both type), and association with other lesions (de novo carcinomas have been found in association with adenomas and even ex adenoma carcinomas elsewhere in the colon) [4]. An association of de novo carcinoma with a familial carcinoma syndrome such as FAP or HNPCC has not been described.

The endoscopic appearance of small colorectal carcinoma has been classified in Japan in a manner similar to early gastric carcinoma. The types include type I (polypoid), type IIa (slightly raised), type IIb (flat), type IIc (slightly depressed), and type III (depressed), along with combinations of these (i.e., IIc + IIa) [28, 41]. The term "superficial colorectal carcinoma" is often used and comprises types IIa through III, or anything that is not polypoid (more than twice the height of the surrounding mucosa). Small superficial colorectal carcinomas may be of the de-novo type histologically; however, this term is not synonymous with de novo carcinoma, since de novo carcinoma may be polypoid (type I) and small superficial colorectal carcinomas may still contain adenoma elements in their vicinity.

Among small superficial colorectal tumors, most Japanese sources have found that de novo type carcinomas are most often flat or depressed lesions [2, 25] and that the depressed lesions in particular appear to be more aggressive since they apparently invade through the muscularis mucosa more rapidly [20, 21]. In contrast, a western series that has classified de novo carcinomas according to their endoscopic appearance have found that the majority are slightly raised IIa or polypoid (I) lesions I [5].

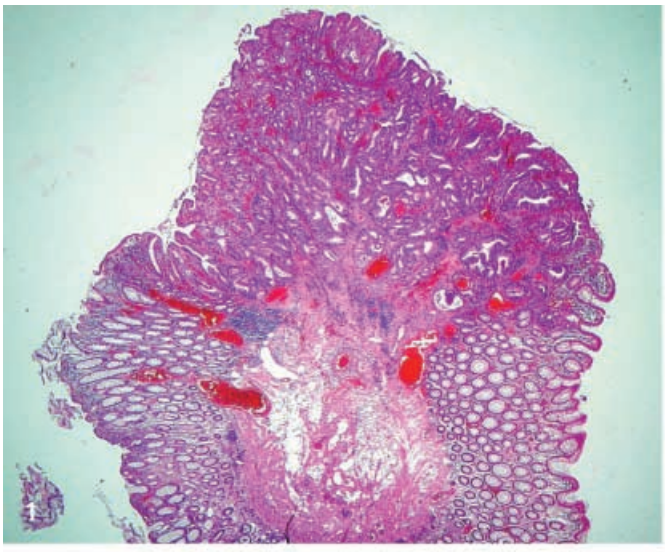

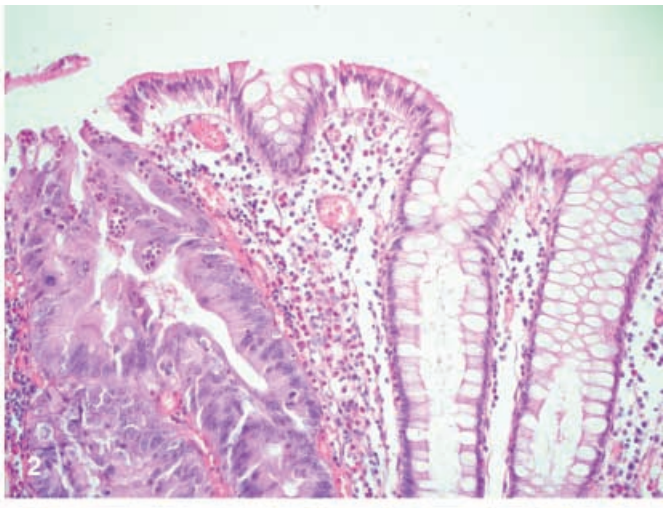

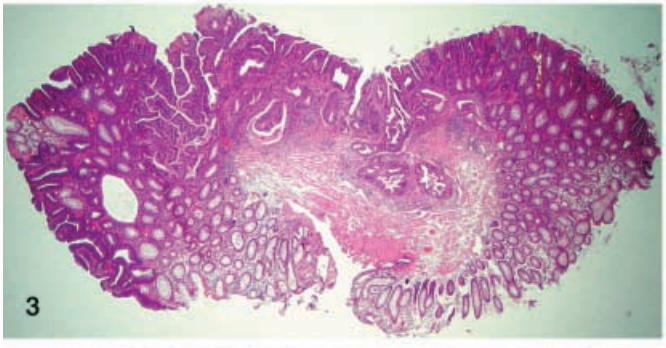

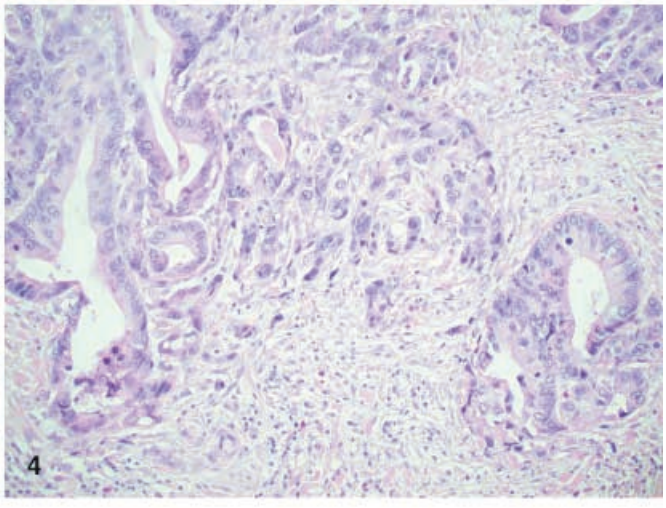

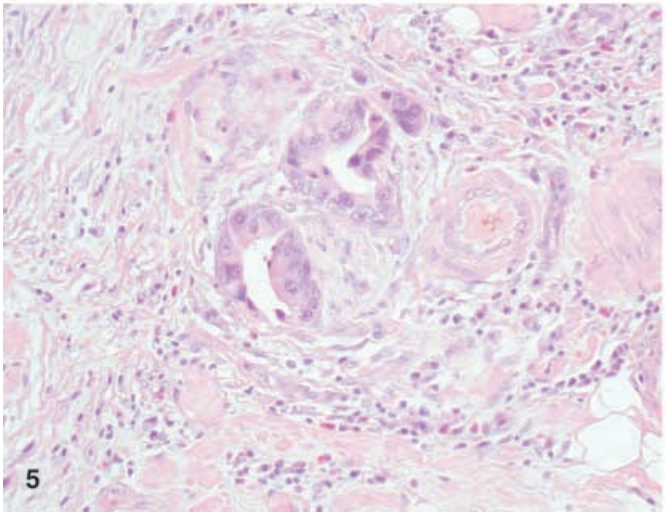

Fig. 1 An example of a de novo carcinoma. This lesion was only 0.7 cm in diameter and was seen as a slightly raised, reddish area by means of colonoscopy. The carcinoma invades the submucosa and has no evidence of any adenomatous components in its vicinity. (Hematoxylin and eosin stain, original magnification 25×)

Fig. 2 A higher magnification of the lesion in Fig. 1 shows a very sharp transition from normal colonic mucosa to carcinoma. No evidence of adenoma is seen. (Hematoxylin and eosin stain, original magnification 200×)

Fig. 3 Another de novo carcinoma. This lesion was 1.0 cm in diameter and was seen by colonoscopy to be a slightly sunken reddish area in the sigmoid colon. (Hematoxylin and eosin stain, original magnification 25×)

Fig. 4 Tumor cell dissociation at the invasion front of a de novo carcinoma (Hematoxylin and eosin stain, original magnification 200×)

Fig. 5 Perineural invasion in the submucosal layer in a case of de novo carcinoma (Hematoxylin and eosin stain, original magnification 200×)

Histopathology and clinical behavior

De novo colorectal carcinoma is usually tubular adenocarcinomas that by definition show a sharp transition from normal appearing colonic mucosa to highly dysplastic epithelium at the edges of the lesions (Fig. 1, Fig. 2, and Fig. 3). It has been found that de novo carcinomas of the pT1 category are more likely to be poorly differentiated than pT1 ex adenoma carcinomas, to have a higher rate of tumor cell dissociation at the invasion front (Fig. 4) and to more often show lymphatic and blood vessel invasion (Fig. 5) [5]. The combination of these features means that de novo carcinomas are more likely than ex adenoma carcinomas to fall into the high-risk category for a subsequent resection following poly-

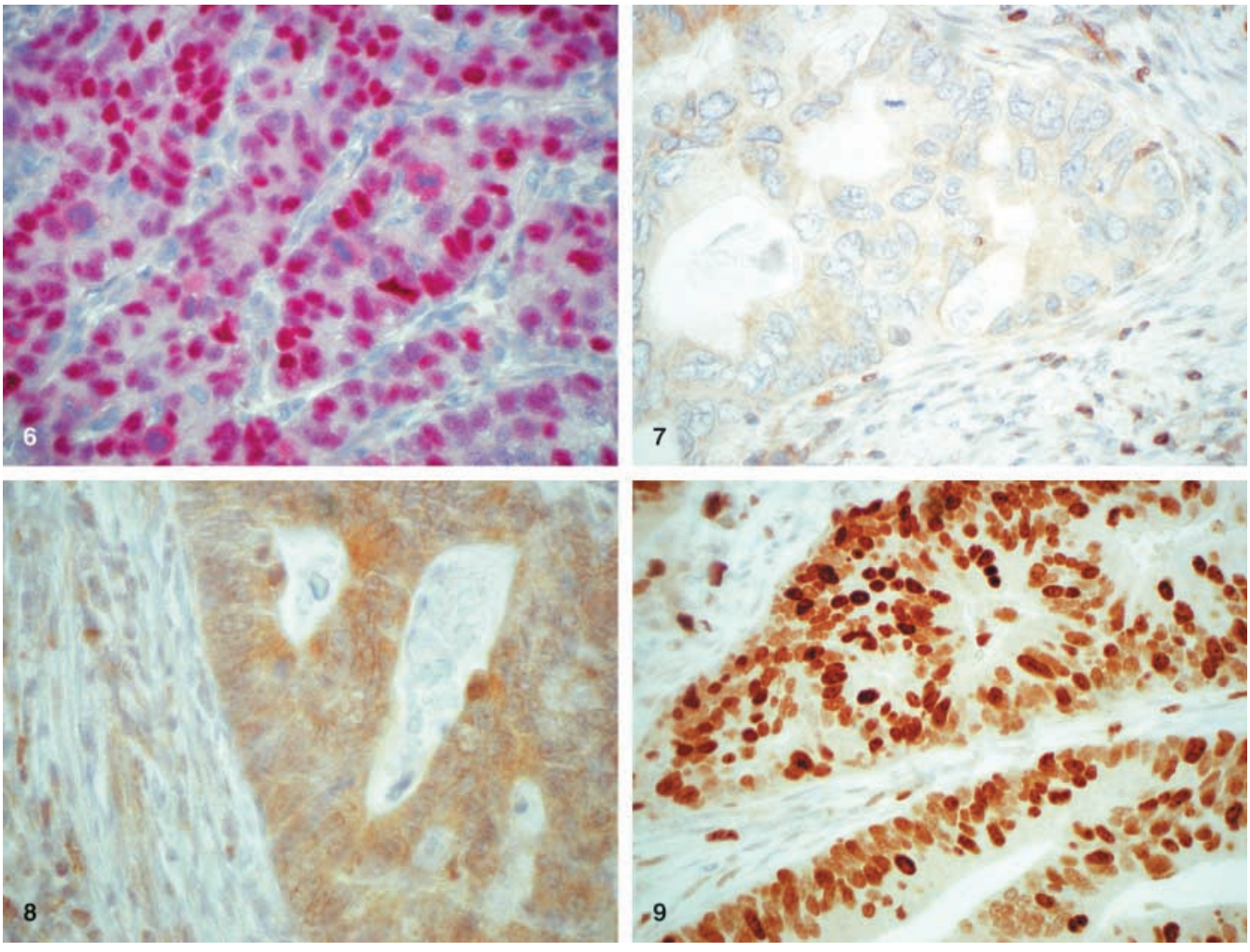

Fig. 6 P53 protein overexpression in a case of de novo carcinoma. Nearly every nucleus in the tumor shows strong staining for p53 (APAAP stain, DO1 monoclonal antibody for p53, Oncogene Science, Cambridge Mass.; original magnification 400×)

Fig. 7 Bcl-2 protein expression in a case of de novo carcinoma. Only weak expression that is much less than surrounding lymphocytes in the tumor stroma is seen (DAB stain, Dako antibody for bcl-2; original magnification 400×)

Fig. 8 Bcl-2 protein expression in a case of ex adenoma carcinoma. In contrast to Fig. 7, strong expression that is nearly as strong as lymphocytes in the tumor stroma is seen (DAB stain, Dako antibody for bcl-2; original magnification 400×)

Fig. 9 Ki-67 antigen expression in a case of de novo carcinoma. This Mib-1 antibody for Ki-67 shows staining in approximately 80% of the tumor cells (DAB stain, Dako antibody for Mib-1; original magnification 400×)

pectomy, although the de novo type is not inherently a high-risk lesion. As expected from their histopathology, de novo carcinomas appear to be more clinically aggressive than the usual ex adenoma carcinomas. There are few studies that have specifically examined this question, but single case reports have described carcinomas less than 1 cm in size that have deeply invaded the bowel wall and have had nodal metastases [17, 47].

Molecular biologic studies

One of the most intriguing questions in connection with the de novo type of colorectal carcinoma is concerned with the mechanism of origin of these tumors. A few studies have been preformed that have sought to compare these lesions with known molecular events in the ex adenoma pathway, the results of which are summarized below.

p53

In a study published in 1996, we have found that p53 protein overexpression occurred at a just significantly higher rate in de novo type carcinomas than in carcinomas arising ex adenoma (Fig. 6) [31]. Of 50 de novo carcinomas in our study, thirty-one (62%) overexpressed p53 protein compared with 23 (42%), of 50 ex adenoma cases (P=0.045). At the genomic level in a similar comparative study of groups of 50 carcinomas, we found that the rate of loss of heterozygosity (LOH) at a locus on 17p near the *p53* gene was significantly higher in de novo than in ex adenoma carcinomas (73% vs 37%, P=0.004) [32]. Comparing p53 protein overexpression

with LOH on 17p, we found the expected significant correlation only in the ex adenoma group. For the group of de novo carcinomas, there was no significant correlation between LOH at 17p and p53 overexpression, although we were unable to perform p53 gene sequence analysis on these cases, this finding suggests that p53 is nearly always abnormal in the de novo type carcinomas, either by a point mutation resulting in protein overexpression but not LOH, or by loss of a significant portion of 17p.

There have been other studies of *p53* in de novo carcinoma, most of which have not found the significantly higher rate of p53 abnormalities that we have. Using PCR-SSCP, Hasegawa screened groups of de novo and "polyp-forming" carcinomas for *p53* mutations and found similar rates of 40% for the de novo and 36.7% for the polyp-forming carcinomas [14]. These lower rates for de novo carcinoma may be explained by the inclusion of so-called "intramucosal" cancers in his study. In 1991, Hanski et al. [13] found that p53 was overexpressed in 72% of 29 ex adenoma carcinomas, and 76% of 25 de novo carcinomas, but these groups did not include tumors with significant mucin production that were more often of the ex adenoma type and had a lower rate of p53 overexpression.

bcl-2, Mib-1 (Ki-67 antigen) expression

Along with the study of p53 protein overexpression, we also found that de novo carcinomas had an overall trend toward weaker expression of bcl-2 protein (Fig. 7 and Fig. 8) [31]. Since bcl-2 expression functions in the inhibition of apoptosis and has been found to be increased in colorectal adenomas [27], a relative decrease in bcl-2 expression can be taken as a sign of disordered cellular proliferation. We have also found a slight trend in the de novo carcinoma cases toward higher percentages of Mib-1 nuclear staining (Fig. 9), although the differences were not significant.

Cell adhesion: E-cadherin and CD44 expression

In a recent publication comparing de novo and ex adenoma carcinomas, we found that E-cadherin was significantly more often less strongly expressed than in a comparable group of ex adenoma carcinomas [50]. Of 42 ex adenoma pT1 carcinomas, 79% retained a normal level of E-cadherin expression compared with just over half of the de novo group (Fig. 10). This finding appears to be closely related to the higher proportion of de novo cases with tumor cell dissociation on the invasion front.

In a study published in 1998, we stained groups of de novo and ex adenoma carcinomas with a panel of antibodies for pan-CD44 and several variants including CD44v6 [33]. We found that the variants 3, 7, 8, and 10 were expressed in only a few cases, while the pan-CD44 antibody and variants 5 and 6 were expressed in a majority of the cases but tended to be quite heterogeneous within the tumor in both groups. No significant difference in CD44 expression was found between the types of lesions for any of the variants. However, a surprising result was seen when comparing the expression of pan-CD44, CD44v5 and CD44v6 in the different areas of the de novo and ex adenoma cases. The bases of the crypts far from the tumor in the normal-appearing mucosa usually showed staining for these three variants and became a full-thickness stain in "transitional" mucosa within 3–4 crypts of the carcinoma or adenoma (Fig. 11 and Fig. 12) and then became heterogeneous in the adenoma and carcinoma elements. This represented a marked similarity between the adenomatous elements of the ex adenoma and the transitional mucosa of the de novo cases. This may be evidence of an adenoma that was previously present in this area that was completely destroyed by the growth of the de novo carcinoma. In support of this idea, one Japanese author has also found that transitional mucosa is often seen in the vicinity of de novo carcinoma [29].

Stromelysin-3 (ST-3) expression

ST-3 is a metalloproteinase first described in 1990 [3] which is expressed in early tumor invasion [12, 51] and is associated with the degree of invasiveness in some tumors [35]. We have found that a significantly higher proportion of de novo cases had extensive staining for ST-3 (P=0.014) than in a comparable group of ex adenoma cases (Fig. 13) [50]. ST-3 expression was also significantly associated with more poorly differentiated lesions and showed strong statistical correlation with tumor cell dissociation on the tumor front and, particularly, with the likelihood of vascular invasion. We have consistently found that carcinoma cases with extensive ST-3 expression (greater than 67% of the tumor stromal interface with expression) have both tumor cell dissociation and vascular invasion.

MSI and LOH

Aside from the 17p chromosomal arm, we have compared microsatellite instability and LOH at loci on the 1p, 2p, 8p, and 5q near the *APC* gene and 18q near the DCC gene [32]. The overall rate of microsatellite instability was very low in both groups, and the rates of LOH showed no significant differences at these five chromosomal arms between the two types. The rates of LOH at the *DCC* and *APC* loci were relatively frequent in both groups, an indication that the de novo group arose by a similar pathway as the ex adenoma cases, and that the *APC* gene, which is known to play a key role in the development of adenomas [40], is also involved in their development, which would not be expected if no adenoma precursor form was present. In a study of a small number (6) of cases of flat colon carcinomas, Aoki found that two had mutations of the *APC* gene by se-

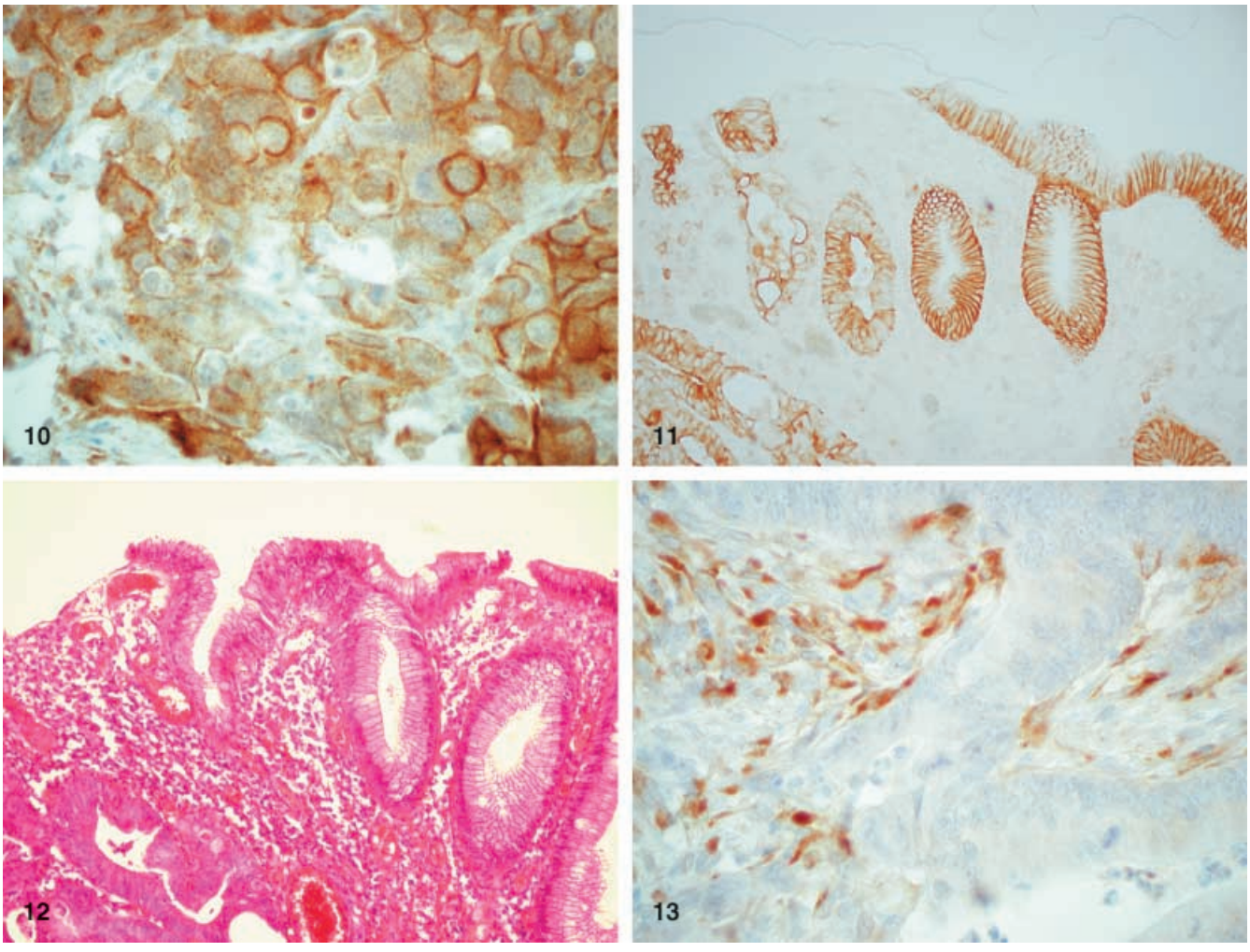

Fig. 10 E-cadherin expression in a case of de novo carcinoma. E-cadherin is normally seen as a uniform stain on the cell membrane, but at the tumor invasion front of this de novo carcinoma, staining is markedly heterogeneous (DAB stain, Dako AEC antibody for E-cadherin; original magnification 400×)

Fig. 11 CD44v6 expression in a case of de novo carcinoma, showing that the normal appearing colonic mucosa adjacent to the tumor shows strong expression. This pattern of expression was also seen in a adenomatous areas of ex adenoma carcinomas. (DAB stain, VVF18 antibody for CD44v6, Bender Corporation, Vienna, Austria; original magnification 400×)

Fig. 12 The same area as Fig. 11, showing the transitional mucosa next to the tumor. (Hematoxylin and eosin stain; original magnification 400×)

Fig. 13 Stromelysin-3 expression in a case of de novo carcinoma showing the characteristic strong expression in fibroblasts adjacent to tumor cells nests. The tumor cells themselves are negative for ST-3. (DAB stain, 5ST-4A9 antibody for ST-3 (Prof. P. Chambon, Pasteur Institute, Strasbourg, France; original magnification 400×)

quence analysis [1] and four of six had *p53* mutations when sequenced at exons 5 though 9. However, only one of these six lesions had invasion of the submucosa and would have been considered to be a carcinoma by our criteria.

K-ras

A few studies of small colorectal carcinomas including de novo carcinoma have focused on the aspect of flat versus polypoid growth. The results of several studies have shown that mutations of K-ras are much less common in flat than in polypoid lesions. Aoki found that none of the six flat lesions he studied had a mutation of *K-ras* in codons 12 or 13 [1], and Minamoto found *K-ras* mutations in only 17% and 16% of 12 “superficial (flat)” colorectal carcinomas and 31 flat adenomas, respectively, a much lower figure than would be expected in polypoid lesions in which approximately 50% show *K-ras* mutations. Similarly, Laurent-Puig found that 27% of a group of de novo, versus 48% of non-mucinous, carcinomas had mutations of *K-ras* [26].

MUC2

A study performed in Germany, using the same definition of de novo carcinoma that we used [6], studied the expression of MUC2, the protein core of intestinal mucin, which has been reported to be lower in normal mucosa than in non-mucinous colorectal carcinomas. In

this study, MUC2 expression was found in 6 of 29 ex adenoma carcinomas and in none of 28 de novo lesions.

Summary

Taken together, these studies indicate that de novo type carcinomas have most, if not all, of the same molecular pathologic defects that can be found in colorectal carcinomas in general. There is even some indirect evidence that an adenoma phase is a part of the development of these tumors. The differences that stand out are quantitative and all point to a carcinoma that is more "advanced" than one would expect for such a small lesion and is in keeping with the features of their histopathology that also point in this direction.

An interesting parallel to the de novo pathway is the situation in which carcinoma arises in the setting of inflammatory bowel disease. These tumors can be macroscopically inconspicuous and arise as flat lesions that can extensively invade the bowel wall. As with de novo carcinoma, early mutations of p53 are thought to play a key role in the development of IBD-associated dysplasia and carcinoma [8, 9] and may be responsible in some way for the development of both the de novo and IBD-related carcinoma phenotype.

Conclusion

Although it probably accounts for only a small percentage of colorectal carcinoma, de novo lesions are important for two reasons. First, from a clinical point of view, with the recognition that de novo type carcinomas can also be found in the western world, endoscopists must appreciate that not all carcinomas arise in a predictable fashion from adenomas that are large and easily detectable. Attention should also be paid to small, inconspicuous lesions since there is a chance that these may also harbor a carcinoma. Second, from the academic perspective, the initial studies of the entity of de novo carcinoma indicate that, in a minority of lesions, an acceleration of the molecular events leading to carcinoma may occur, resulting in a lesion that appears to have arisen de novo from normal mucosa. In other words, there is no clear evidence for a separate de novo pathway; instead it seems certain that preexisting adenomatous structures are destroyed by the accelerated growth of the de novo carcinoma. Future studies will have to be directed at the question of which mechanisms are responsible for this acceleration.

References

1. Aoki T, Takeda S, Yanagisawa A, Kato Y, Ajioka Y, Watanabe H, Kudo S, Nakamura Y (1994) APC and p53 mutations in de novo colorectal adenocarcinomas. Hum Mutat 3:342–346
2. Ajioka Y, Watanabe H, Kazama S, Hashidate H, Yokoyama J, Yamada S, Takaku H, Nishikura K (2001) Early colorectal cancer with special reference to the superficial nonpolypoid type from a histopathologic point of view. World J Surg 24:1075–180
3. Basset P, Bellocq JP, Wolf C, Stoll I, Hutin P, Limacher JM, Podhajcer OL, Chenard MP, Rio MC, Chambon P (1990) A novel metalloproteinase gene specifically expressed in stromal cells of breast carcinomas. Nature 348:699–704
4. Bedenne L, Faivre J, Boutron MC, Piard F, Cauvin JM, Hillon P (1992) Adenoma–carcinoma sequence or "de novo" carcinogenesis? A study of adenomatous remnants in a population-based series of large bowel cancers. Cancer 69:883–888
5. Bethke B, Walter T, Stolte M (1995) Endoskopische Polypektomie: vergleich der Häufigkeit kolorektaler Ex-Adenoma- und De-novo-Frühkarzinome. Coloproctology 17:176–183
6. Blank M, Klussman E, Krüger-Krasagakes S, Schmitt-Gräff A, Stolte M, Bornhoeft G, Stein S, Xing P, McKenzie I, Verstinijen C, Rieken P, Otto E, Hanski C (1992) Expression of MUC2-mucin in colorectal adenomas and carcinomas of different histological types. Int J Cancer 59:301–306
7. Bond JH (1995) Small flat adenomas appear to have little clinical importance in western countries. Gastrointest Endosc 42:184–187
8. Brentnall TA, Crispin DA, Rabinovitch PS, Haggitt RC, Rubin CE, Stevens AC, Burmer GC (1994) Mutations in the p53 gene: an early marker of neoplastic progression in ulcerative colitis. Gastroenterology 107:369–378
9. Burmer GC, Crispin DA, Kolli VR, Haggitt RC, Kulander BG, Rubin CE, Rabinovitch PS (1991) Frequent loss of a p53 allele in carcinomas and their precursors in ulcerative colitis. Cancer Commun 3:167–172
10. Crawford BE, Stromeyer FW (1983) Small nonpolypoid carcinomas of the large intestine. Cancer 51:1760–1763
11. Driman DR (1994) Flat adenomas and flat carcinomas: do you see what I see? Gastrointest Endosc 40:106–109
12. Hahnel E, Harvey JM, Joyce R, Robbins PD, Sterrett GF, Hahnel R (1993) Stromelysin-3 expression in breast cancer biopsies: clinico-pathological correlations. Int J Cancer 55:771–74
13. Hansky C, Bornhoeft G, Shimoda T, Hanski M, Lane D, Stein H, Rieken E (1992) Expression of p53 protein in invasive colorectal carcinomas of different histologic types. Cancer 70:2772–2777
14. Hasegawa H, Ueda M, Furukawa K, Watananbe M, Teramoto T, Mukai M (1995) p53 gene mutations in early colorectal carcinoma. de novo vs. adenoma-carcinoma sequence. Int J Cancer 64:47–51
15. Helwig EB (1947) The evolution of adenomas of the large intestine and their relation to carcinoma. Surg Gynecol Obstet 84:36–49
16. Hermanek P (1992) Dysplasie-Karzinom-Sequenz im Kolorektum. Zentralbl Chir 117:476–482
17. Herrera L, Hanna S, Castillo N, Petrelli NJ (1991) Primary de novo adenocarcinoma of the colon measuring 8 mm in diameter with lymph node metastases. Report of a case. Dis Colon Rectum 34:275–279
18. Hunt D (1990) Endoscopic diagnosis of small flat carcinoma of the colon. Report of three cases. Dis Colon Rectum 33:814–815
19. Kudo S (1993) Endoscopic mucosal resection of flat and depressed types of early colorectal cancer. Endoscopy 25:455–461
20. Kudo S, Tamura S, Nakajima T, Hirota S, Asano O, Kusaka H (1995) Depressed type of colorectal cancer. Endoscopy 27:54–57
21. Kudo S, Kashida H, Tamura T (2001) Early colorectal cancer: flat or depressed type. J Gastroenterol Hepatol 15[Suppl]: D66–D70
22. Kuramoto S (1989) Flat early cancers of the large intestine. Cancer 64:950–955
23. Kuramoto S, Oohara T (1987) Minute cancers arising de novo in the human large intestine. Cancer 61:829–834
24. Kuramoto S, Oohara T (1995) How do colorectal cancers develop? Cancer 75:1534–1538
25. Kurisu Y, Shimoda T, Ochiai A, Nakanishi Y, Hirata I, Katsu KI (1999) Histologic and immunohistochemical analysis of early submucosal invasive carcinoma of the colon and rectum. Pathol Int 49:608–616

26. Laurent-Puig P, Olschwang S, Delattre O, Validire P, Melot T, Mosseri V, Salmon RJ, Thomas G (1991) Association of K-ras with differentiation and tumor formation pathways in colorectal carcinoma. Int J Cancer 49:220–223
27. Mateo MS, Sanchez-Beato M, Martinez JC, Orfao A, Orradre JL, Piris MA (1995) p53, Rb and bcl-2 expression during the cell cycle: a study in phytohaemagglutinin stimulated lymphocytes and microwave irradiated lymphoid tissue sections. J Clin Pathol 48:151–159
28. Moreira LF, Iwagaki H, Hizuta A, Sakagami K, Orita K (1992) Outcome in patients with early colorectal carcinoma. Br J Surg 79:436–438
29. Mori M, Mimori K, Adachi Y, Akiyoshi T (1996) Cell proliferation kinetics are abnormal in transitional mucosa adjacent to colorectal carcinoma (letter). Br J Surg 83:870–871
30. Morson BC (1974) Evolution of cancer of the colon and rectum. Cancer 34[Suppl]:845–849
31. Mueller JD, Mueller E, Hoepner I, Jutting J, Bethke B, Stolte M, Hofler H (1996) Expression of bcl-2 and p53 in de novo and ex-adenoma colon carcinoma: a comparative immunohistochemical study. J Pathol 180:259–265
32. Mueller JD, Haegele N, Keller G, Mueller E, Saretzky G, Bethke B, Stolte M, Höfler H (1998) Loss of heterozygosity and microsatellite instability in de-novo versus ex-adenoma carcinomas of the colorectum. Am J Pathol 153:1977–1984
33. Mueller JD, Heider KH, Oberhuber G, Mueller E, Bethke B, Stolte M, Höfler H (1998) Comparison of CD44 expression in early colorectal carcinomas of the de novo and ex-adenoma types. Virchows Archiv 433:407–414
34. Mueller JD, Mueller E, Keller G, Bethke B, Stolte M, Hofler H (1999) Gibt es Unterschiede zwischen ex Adenoma- und de novo-Kolonkarzinomen? Verh Dtsch Ges Pathol 83:139–147
35. Muller D, Wolf C, Abecassis J, Millon R, Engelmann A, Bronner G, Rouyer N, Rio MC, Eber M, Methlin G (1993) Increased stromelysin 3 gene expression is associated with increased local invasiveness in head and neck squamous cell carcinomas. Cancer Res 53:165–169
36. Owen DA (1996) Flat adenoma, flat carcinoma, and de novo carcinoma of the colon. Cancer 77:3–6
37. Rembacken BJ, Fujii T, Cairns A, Dixon MF, Yoshida S, Chalmers DM, Axon AT (2001) Flat and depressed colonic neoplasms: a prospective study of 1000 colonoscopies in the UK. Lancet 355:1211–1124
38. Schlemper RJ, Itabashi M, Kato Y, Lewin KJ, Riddell RH, Shimoda T, Sipponen P, Stolte M, Watanabe H (1998) Differences in the diagnostic criteria used by Japanese and western pathologists to diagnose colorectal carcinoma. Cancer 82:60–69
39. Schlemper RJ, Riddell RH, Kato Y, Borchard F, Cooper HS, Dawsey SM, Dixon MF, Fenoglio-Preiser CM, Flejou JF, Geboes K, Hattori T, Hirota T, Itabashi M, Iwafuchi M, Iwashita A, Kim YI, Kirchner T, Klimpfinger M, Koike M, Lauwers GY, Lewin KJ, Oberhuber G, Offner F, Price AB, Rubio CA, Shimizu M, Shimoda T, Sipponen P, Solcia E, Stolte M, Watanabe H, Yamabe H (2001) The Vienna classification of gastrointestinal epithelial neoplasia. Gut 47:251–225
40. Shibata H, Toyama K, Shioya H, Ito M, Hirota M, Hasegawa S, Matsumoto H, Takano H, Akiyama T, Toyoshima K, Kanamaru R, Kanegae Y, Saito I, Nakamura Y, Shiba K, Noda T (1997) Rapid colorectal adenoma formation initiated by conditional targeting of the Apc gene. Science 278:120–123
41. Shimoda T, Ikegami M, Fusisaki J, Matsui T, Aizawa S, Ishikawa E (1989) Early colorectal carcinoma with special reference to its development de novo. Cancer 64:1138–1146
42. Smith GA, Oien KA, O'Dwyer PJ (1999) Frequency of early colorectal cancer in patients undergoing colonoscopy. Br J Surg 86:1328–1331
43. Smyrk TC, Lanspa SJ, Lynch HT (1990) Small, nonpolypoid colonic neoplasms. Dis Colon Rectum 33:814–815
44. Snover DG (1982) Minute adenocarcinoma of the colon arising in flat mucosa: five cases asking the question: does de novo carcinoma exist? Lab Invest 46:78A–79A
45. Stolte M (1995) Colorectal mini-de novo carcinoma; a reality in Germany too. Endoscopy 27:286–290
46. Tada T, Iida M, Matsumoto T, Yao T, Aoyagi K, Koga H, Tanoue Y, Fujishima M (1995) Small flat cancer of the rectum: clinicopathologic and endoscopic features. Gastrointest Endosc 42:109–113
47. Trecca A, Fujii T, Kato S, Hasebe T, Tajiri H, Yoshida S (1998) Small advanced colorectal adenocarcinomas: report on three cases. Endoscopy 30:493–445
48. Vogelstein B, Fearon ER, Hamilton SR, Kern SE, Preisinger AC, Leppert M, Nakamura Y, White R, Smits AM, Bos JL (1988) Genetic alterations during colorectal-tumor development. N Engl J Med 319:525–532
49. Winawer SJ, Zauber AG, Ho MN, O'Brien MJ, Gottlieb LS, Sternberg SS, Waye JD, Schapiro M, Bond JH, Panish JF, et al (1993) Prevention of colorectal cancer by colonoscopic polypectomy. The National Polyp Study Workgroup. N Engl J Med 329:1977–1981
50. Wlodarczyk J, Bethke B, Mueller E, Stolte M, Mueller JD (2001) A comparative study of E-cadherin and stromelysin-3 expression in de novo and ex adenoma carcinoma of the colorectum. Virchows Archiv (in press)
51. Wolf C, Rouyer N, Lutz Y, Adida C, Loriot M, Bellocq JP, Chambon P, Basset P (1993) Stromelysin 3 belongs to a subgroup of proteinases expressed in breast carcinoma fibroblastic cells and possibly implicated in tumor progression. Proc Natl Acad Sci U S A 90:1843–1847
52. World Health Organization Classification of Tumours: Pathology and Genetics of Tumours of the Digestive System (2000) IARC Press, Lyon, France

Virchows Arch (2002) 440:461–475
DOI 10.1007/s00428-002-0609-x

ORIGINAL ARTICLE

M. Papotti · M. Bongiovanni · M. Volante · E. Allìa
S. Landolfi · L. Helboe · M. Schindler · S.L. Cole
G. Bussolati

Expression of somatostatin receptor types 1–5 in 81 cases of gastrointestinal and pancreatic endocrine tumors

A correlative immunohistochemical and reverse-transcriptase polymerase chain reaction analysis

Received: 2 August 2001 / Accepted: 21 December 2001 / Published online: 23 March 2002
© Springer-Verlag 2002

Abstract Somatostatin receptors (SSTRs) have been extensively mapped in human tumors by means of autoradiography, reverse-transcriptase polymerase chain reaction (RT-PCR), in situ hybridization (ISH) and immunohistochemistry (IHC). We analyzed the SSTR type 1–5 expression by means of RT-PCR and/or IHC in a series of 81 functioning and non-functioning gastroenteropancreatic (GEP) endocrine tumors and related normal tissues. Moreover, we compared the results with clinical, pathological and hormonal features. Forty-six cases (13 intestinal and 33 pancreatic) were studied for SSTR 1–5 expression using RT-PCR, IHC with antibodies to SSTR types 2, 3, 5 and ISH for SSTR2 mRNA. The vast majority of tumors expressed SSTR types 1, 2, 3 and 5, while SSTR4 was detected in a small minority. Due to the good correlation between RT-PCR and IHC data on SSTR types 2, 3, and 5, thirty-five additional GEP endocrine tumors were studied with IHC alone. Pancreatic insulinomas had an heterogeneous SSTR expression, while 100% of somatostatinomas expressed SSTR5 and 100% gastrinomas and glucagonomas expressed SSTR2. Pre-operative biopsy material showed an overlapping immunoreactivity with that of surgical specimens, suggesting that the SSTR status can be detected in the diagnostic workup. It is concluded that SSTRs 1–5 are heterogeneously expressed in GEP endocrine tumors and that IHC is a reliable tool to detect SSTR types 2, 3 and 5 in surgical and biopsy specimens.

Keywords GEP · Somatostatin receptors · Pancreatic islets · Neuroendocrine tumor · Immunohistochemistry · RT-PCR

M. Papotti (✉) · M. Bongiovanni · M. Volante · E. Allìa
S. Landolfi · G. Bussolati
Department of Biomedical Sciences and Oncology,
University of Turin, Via Santena 7, 10126 Torino, Italy
e-mail: mauro.papotti@unito.it
Tel.: +39-011-6706514, Fax: +39-011-6635267

L. Helboe
Lundbeck, Copenhagen, Denmark

M. Schindler · S.L. Cole
Glaxo Institute of Applied Pharmacology,
University of Cambridge, UK

M. Schindler
Boehringer Ingelheim Pharma KG, Cardiovascular research,
Biberach, Germany

Introduction

The role of somatostatin analogues in the clinical setting is well established: long-acting analogues have been used for more than 10 years to treat endocrine tumors, and octreotide scintigraphy is widely used for tumor localization and even for radio-guided surgery [5, 9, 15, 16, 19, 22, 45]. The rationale behind these clinical applications is based on the widespread occurrence of somatostatin receptors (here abbreviated SSTR – according to the GenBank nomenclature) in human tumors, with special reference to endocrine tumors [42]. To date, five SSTR subtypes have been identified (types 1–5) [23, 27, 50, 51] with different affinities for the natural ligand somatostatin as well as for synthetic analogues. SSTRs have been extensively mapped in human endocrine and non-endocrine tumors by means of autoradiography, Northern blot, reverse-transcriptase polymerase chain reaction (RT-PCR) and in situ hybridization (ISH) [4, 10, 14, 20, 24, 29, 30, 31, 32, 33, 34, 39, 44]. Irrespective of the original location of the tumor, most studies demonstrated a high incidence of SSTR1 and SSTR2 (and to a minor degree of the other types).

In recent years, several authors have developed antibodies for immunohistochemical demonstration of SSTR subtypes [8, 13, 17, 35, 40, 41, 43]. Such polyclonal antibodies, raised against peptide fragments of all five known SSTR subtypes, were mostly used for the immu-

nohistochemical demonstration of SSTR in brain regions or in normal human or animal tissues. RT-PCR has the great advantage of a high sensitivity, but does not allow the precise SSTR cellular localization, which can be obtained by parallel ISH or immunohistochemical investigations [17, 25, 32, 33, 43].

In gastro-entero-pancreatic (GEP) endocrine tumors, SSTRs were analyzed using various procedures, including immunohistochemistry (IHC) for SSTR2. Expression of this receptor type in a variable percentage of pancreatic tumors and intestinal carcinoids, and a correlation between presence of SSTRs and scintigraphic localization and/or response to octreotide therapy were reported [13, 19, 22]. However, individual methods to reveal SSTRs were compared and correlated in a limited case series of GEP endocrine tumors, and immunohistochemical detection was restricted to SSTR2A analysis only. An exception was the large studies of the groups of Jais and Wulbrand [12, 49], who investigated all five SSTR subtypes using the highly sensitive RT-PCR technique and found high levels of SSTR1, 2 and 5 mRNA expression and low amounts of SSTR3 and SSTR4 mRNA. However, no parallel data on SSTR cellular localization were presented.

The aim of this study was to analyze the expression of SSTRs 1–5 by means of RT-PCR and/or IHC in a large series of 81 functioning and non-functioning GEP endocrine tumors and to compare the results with clinical, pathological and hormonal features. Specific antibodies to SSTRs 2, 3 and 5 (which are the subtypes with the highest affinity for octreotide) were used in parallel with the analysis of mRNA expression levels. A heterogeneous distribution of SSTR in both pancreatic and intestinal endocrine tumors was observed and the immunohistochemical SSTR detection was found to be a reliable diagnostic tool in both surgical and pre-operative biopsy specimens, relative to mRNA analysis.

Materials and methods

Case selection

Forty-six GEP endocrine tumors, in which fresh frozen material was available for mRNA analysis (13 and 33 tumors of gastrointestinal and pancreatic origin, respectively), were collected from the pathology files of the University of Turin. These tumors were studied for SSTR expression by means of RT-PCR and IHC. Since the results of the two procedures showed a good correlation (see below), the study was expanded to 35 additional GEP neoplasms in which formalin-fixed and paraffin-embedded tissue blocks were available for immunohistochemical staining only. The reason for entering additional cases was to investigate SSTR expression in all types of hormone-producing pancreatic tumors and to analyze a series of aggressive (metastatic) intestinal carcinoids to compare SSTR expression with the tumor stage. Overall, 81 cases were entered in the present study, including 28 gastrointestinal and 53 pancreatic endocrine tumors.

In four cases, the frozen material was represented by liver or lymph-node metastatic tissue, in the absence of frozen tissue from the primary tumor. In seven additional cases, both primary tumors and the corresponding metastatic deposits were analyzed in parallel using IHC. Finally, in four cases, the pre-operative cytological or biopsy material was also retrieved and studied in parallel with the corresponding surgical sample.

Four carcinoids of the gastric body were associated with chronic atrophic gastritis and neuroendocrine cell hyperplasia [2]. In these cases, also peritumoral normal and hyperplastic neuroendocrine cells were investigated for SSTR expression.

All cases were reviewed on conventional hematoxylin and eosin-stained slides and on slides immunostained for endocrine markers, and classified following the recent World Health Organization (WHO) classification of endocrine tumors [46]. Clinicopathological data including sex, age, tumor location and size, hormonal status and lymph-node or distant metastases were obtained for all patients. Follow-up data were available for 54 patients.

Normal pancreas

Although this study was not specifically designed to study SSTR distribution in normal pancreatic islets, peritumoral pancreatic tissue, when present, as well as two control cases of non-neoplastic pancreatic tissue, were also investigated to compare the immunohistochemical reactivity of the currently employed SSTR antibodies with that reported in the literature.

RT-PCR for SSTRs 1–5

Total RNA was extracted from a frozen tumor fragment adjacent to that used for conventional histopathological diagnosis using the Tri Reagent (Molecular Research Center Inc., Cincinnati, Ohio.) extraction kit following manufacturer's recommendations. To avoid contamination with normal peritumoral pancreatic or lymphatic tissue, frozen sections were rapidly stained with conventional hematoxylin and eosin, and the normal tissue possibly present was removed with a surgical blade. The concentration of RNA was estimated by means of spectrophotometry, and RNA degradation assessed using 1% agarose gel electrophoresis. Total RNA (1 µg) was first digested with 10 U RNase-free DNase (Boehringer, Mannheim, Germany) in a 10-µl solution containing 2 mM $MgCl_2$ to avoid DNA contamination. The solution was kept at room temperature (RT) for 10 min, then heated for 5 min at 70°C to inactivate DNase; 40 pM of oligodeoxythymidine primer (oligo dT_{16}) was added and the solution heated at 70°C for 10 min, then chilled on ice to allow primer hybridization. The final solution was reverse transcribed using 100 U superscript reverse transcriptase (Gibco BRL, Gaitersburg, Md.), and complementary DNA (cDNA) was generated in a 50-µl final reaction volume containing 50 mM Tris-HCl pH 8.3, 75 mM KCl, 3 mM $MgCl_2$, 10 mM DTT, 1 mM dNTPs and 20 U RNasin (Promega, Madison, Wis.). The solution was incubated at 37°C for 90 min, then the enzymes inactivated by heating at 70°C for 10 min. Omission of RT enzyme served as a negative control for further PCR amplification reactions. RNA integrity was determined by performing a PCR reaction for β_2-microglobulin [7]. Only cases positive for β_2-microglobulin mRNA amplification were considered informative for SSTR expression analysis.

PCR experiments were carried out in a 10-µl final reaction volume containing 1 µl cDNA template, 1 pM sense and antisense oligonucleotide primers, 10 mM Tris-HCl pH 8.3, 50 mM KCl, 200 nM deoxynucleotide triphosphates (dNTPs), 1 mM $MgCl_2$ and 0.5 U *Taq* polymerase (GeneAmp, Perkin Elmer, Roche, Branchburg, N.J.). The primers used for RT-PCR and the corresponding specific annealing temperatures are reported in Table 1. β_2-microglobulin and SSTR2 PCR reactions were performed under the following conditions: 35 cycles, each cycle consisting of denaturation at 94°C for 1 min, annealing at specific temperatures for 1 min and extension at 72°C for 2 min. PCR conditions for SSTR3 (35 cycles) and SSTR5 (40 cycles) were as follows: denaturation at 94°C for 45 s, annealing at specific temperatures for 1 min and extension at 72°C for 1 min. SSTR1 and SSTR4 PCR reactions were performed under the following conditions: 40 cycles, each cycle consisting of denaturation at 94°C for 1 min, annealing at specific temperatures for 30 s and extension at 72°C for 75 s. PCR products were visualized under UV light in 1% agarose gel containing 0.5 µg/ml ethidium bromide. Omission of cDNA in

Table 1 Sequences of primers used for reverse transcriptase-polymerase chain reaction (PCR)

Primer	Position	GenBank accession no.	Size of PCR product (bp)	Annealing temperature (°C)	References
β2-Microglobulin					
Sense: 5′acccccactgaaaaagatga3′	284–303	XM_007650	114	55	[7]
Antisense: 5′atcttcaaacctccatgatg3′	378–397				
SSTR1					
Sense: 5′gctacgtgctcatcattgcta3′	725–745	NM_001049	401	60	[20]
Antisense: 5′ggactccaggttctcaggttg3′	1105–1125				
SSTR2					
Sense: 5′cagtcatgagcatcgaccga3′	402–421	NM_001050	283	61	[50]
Antisense: 5′gcaaagacagatgatggtga3′	665–684				
SSTR3					
Sense: 5′tcatctgcctctgctacctg3′	662–681	NM_001051	221	57	[20]
Antisense: 5′gagcccaaagaaggcaggct3′	863–882				
SSTR4					
Sense: 5′atcttcgcagacaccagacc3′	547–576	NM_001052	321	60	[20]
Antisense: 5′atcaaggctggtcacgacga3′	848–867				
SSTR5					
Sense: 5′gccggcctctacttcttcgtg3′	847–866	NM_001053	153	60	[20]
Antisense: 5′ccgtggcgtcagcgtccttgg3′	980–999				

the PCR mixture served as negative control. The RNA extracted from an H716 neuroendocrine colon carcinoma cell line known to express SSTR served as a positive control for SSTR amplification. To confirm the specificity of SSTR PCR reactions, PCR products were agarose-gel purified (Concert Gel Extraction Systems, Gibco BRL, Life Technologies, Milan, Italy) and ethanol precipitated, then subjected to nucleic acid direct sequencing using a fluorescence-based sequencing kit (Applied Biosystems, Weiterstadt, Germany); electrophoresis and data analysis were carried out in an automated DNA sequencer ABI PRISM 377 (Applied Biosystems), following manufacturer's recommendations. The RT-PCR was not quantitative. Nevertheless, we used the same controls as those used in a former study on SSTR2 mRNA expression in neuroblastomas using quantitative RT-PCR [44]. Control tissues found in the previous tests to express a number of SSTR2 mRNA molecules lower than 10^5 were negative in the present RT-PCR analysis, while the presence of a strong amplification band corresponded to a number of SSTR2 mRNA molecules larger than 10^7. No undefined bands were found in the present cases, and the tumors were recorded as positive or negative based on the presence or absence of a specific band, irrespective of its intensity.

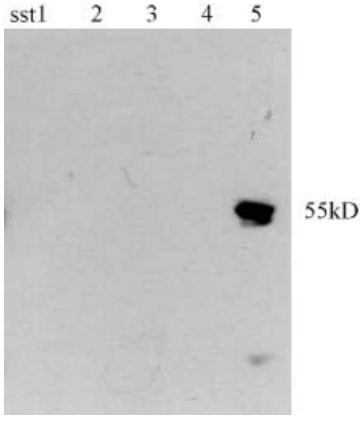

Fig. 1 Western blot of anti-human somatostatin receptor (SSTR)5 antibody (MK86) reactivity in transfected Chinese hamster ovary (CHO) cells expressing SSTR1–5 (*columns* 1–5). A specific band is present in SSTR5-transfected cells only

Antibodies–SSTR2

A polyclonal antibody anti-SSTR2 was produced and characterized by one of us (MS) [40, 41]. This antibody (coded K230) was raised in sheep and was specific for a sequence of 20 amino acids of the C-terminal portion of the SSTR2A (KSRLNETTETQRTLLNEDLQ, positions 347–366). Another antibody to SSTR2A, purchased from Biotrend/Gramsch Laboratories (Schwabhausen, Germany) was also used and found to have an overlapping reactivity pattern with the former SSTR2 antiserum. The antibody to SSTR3 was purchased from Biotrend/Gramsch Laboratories. The characterization of these latter antibodies was reported by Schultz et al [43]. The serum anti-SSTR5 (coded MK86) was produced in the laboratory of one of us (MS) against the human SSTR5 receptors (see below).

Production and characterization of anti-SSTR5 antibodies

The following peptide sequence was synthesized (amino acid single letter code): CGAKDADATEPRPDR (corresponding to a carboxy-terminal fragment of human SSTR5, positions 325–339). The peptide was coupled to keyhole limpet hemocyanin (KLH; Sigma, Poole, UK) and injected into one rabbit (MK86). Test bleeds were taken after each booster injection, and a terminal bleed was carried out. Serum was obtained from this bleed and used in IHC and Western blotting. The specificity of the novel SSTR5 antiserum was confirmed by means of Western-blot experiments on membranes obtained from Chinese hamster ovary (CHO) cells expressing the recombinant human SSTR types 1–5, carried out as described elsewhere [40]. Application of anti-human SSTR5 antiserum yielded a signal in CHO cells expressing the respective SSTR5 only (Fig. 1). In these experiments, a broad band with smeared appearance was observed with a molecular weight centered at approximately 55 kDa. No cross-reactivity was observed to any other cell line expressing recombinant SSTRs different from type 5 (Fig. 1). Pre-adsorption controls were carried out by pre-incubating the antibodies with 100 μM of the antigenic

Table 2 Summary of clinico-pathological features of 81 gastroenteropancreatic endocrine tumors

	Gastrointestinal	Pancreatic
Total no. of cases	28	53
Diagnosis (WHO 2000):		
Well-differentiated endocrine tumor	6	37
Well-differentiated endocrine carcinoma	19	14
Poorly differentiated endocrine carcinoma	3	2
Hormonal status (no. of cases)	Gastrin (3)	Insulin (25), glucagon (5), somatostatin (4), gastrin (5), pancreatic polypeptide (1), vasoactive intestinal peptide (1), non functioning (14)
Sex male/female	14/14	25/28
Age (median, years)	60	56
Tumor size (mean, cm)	2.8	4.0
Location	Stomach (6), ileum (13), appendix(4), colon/rectum (5)	Head (22), Body-tail (31)
Metastases (regional lymph node or liver)	16/28 (57.1%)	17/53 (32%)
Studied using reverse-transcriptase polymerase chain reaction and immunohistochemistry	13	33
Studied using immunohistochemistry only (Table 3)	15	20

peptide for 16–18 h prior to immune reactions and resulted in the abolition of the signal in either Western blotting or immunohistochemical studies, using human pituitary gland formalin-fixed sections as positive controls (data not shown).

Immunohistochemistry

Sections (4- to 5-µm-thick) from buffered formalin-fixed, paraffin-embedded tissue, adjacent to those used for conventional histopathological and immunohistochemical examination, were collected onto poly-L-lysine-coated slides. Primary antibodies to SSTR2A (commercial serum), SSTR3 and SSTR5 were applied to tissue sections with prior antigen retrieval (three 3-min passages in microwave oven at 750 W in 10 mM citrate buffer pH 6.0) for 30 min at RT, at the dilutions of 1/20000, 1/40000 and 1/35000, respectively. The other anti-SSTR2A antiserum (K230) was applied overnight at 4°C at a dilution of 1/2000 with no prior antigen retrieval. The immune reactions were then revealed with the immunoperoxidase technique using the streptavidin–peroxidase kit (Dako, Glostrup, Denmark) and a further amplification with biotinylated-tyramide (GenPoint, Dako, diluted 1/5) with the subsequent washing step performed in hot PBS (at 95°C) to reduce the background and increase the sensitivity, as described by Volante et al. [48]. Diaminobenzidine was used as chromogen, followed by a weak nuclear counterstain (or no counterstain in selected cases). Control stainings for all antibodies included immunoperoxidase reaction on serial sections using pre-absorbed serum or buffer instead of the primary antibody. All pancreatic endocrine tumors were immunostained in parallel sections for insulin (polyclonal, diluted 1/400, Dako) glucagon (polyclonal, diluted 1/5, BioGenex, San Ramon, Calif.) somatostatin (polyclonal, diluted 1/3000, Serotec, Oxford, UK) and gastrin (polyclonal, diluted 1/50, BioGenex).

Double immunostaining for each SSTR subtype and individual pancreatic hormones was performed in the two control pancreatic tissues and in selected tumors with peritumoral islets available for co-localization studies. A sequential immunohistochemical procedure under the same conditions described above was performed, finally revealing the receptor proteins with green fluorescence and the pancreatic hormones of alpha, beta or delta cells with red fluorescence. For the purpose of co-localization analysis of receptor types and single pancreatic hormones, 250 cells (for each cell type) were counted in nearby islets and the relative percentage of cells co-localizing either SSTR type was recorded.

In situ hybridization

Selected tumors (12 cases, including 7 tumors with discrepant RT-PCR and IHC findings) were also analyzed for SSTR2 mRNA expression by means of a non-radioactive, tyramide deposition-based ISH technique. The detailed procedure was described elsewhere [24] and employed a 48-bp oligonucleotide corresponding to positions 91–139 of the SSTR2 gene [50]. Appropriate negative controls in all the cases investigated included hybridization of parallel sections using an unrelated probe specific for Ebstein-Barr virus mRNA. The specificity of the hybridization signal was also confirmed in some cases using a sense probe, omitting the specific probe or pre-treating the sections with RNAse.

Clinico-pathological correlation

The results of SSTR analysis were compared with clinico-pathological data, including age, sex, tumor location and size, recurrence or metastases, tumor grade, and hormonal status. Statistical evaluation was performed by means of the ANOVA and chi-square (Yates corrected) tests. The data were also related to the outcome in those patients in which this information was available. This study was performed in accordance with the ethics standards laid down in the 1964 Declaration of Helsinki.

Results

Clinico-pathological data

The relevant clinico-pathological data of 53 pancreatic and 28 gastrointestinal endocrine tumors are summarized in Table 2. The majority of cases were well-differentiated endocrine tumors (carcinoids) or well-differentiated endocrine carcinomas. Five cases of poorly differentiated endocrine carcinomas (with small or large cell features) were also included. The male to female ratio was approximately 1 in both groups of pancreatic and intestinal tumors, with the patients' median age being 56 years and 60 years in the two groups, respectively. The pancreatic and gastrointestinal tumors measured 0.4–20 cm

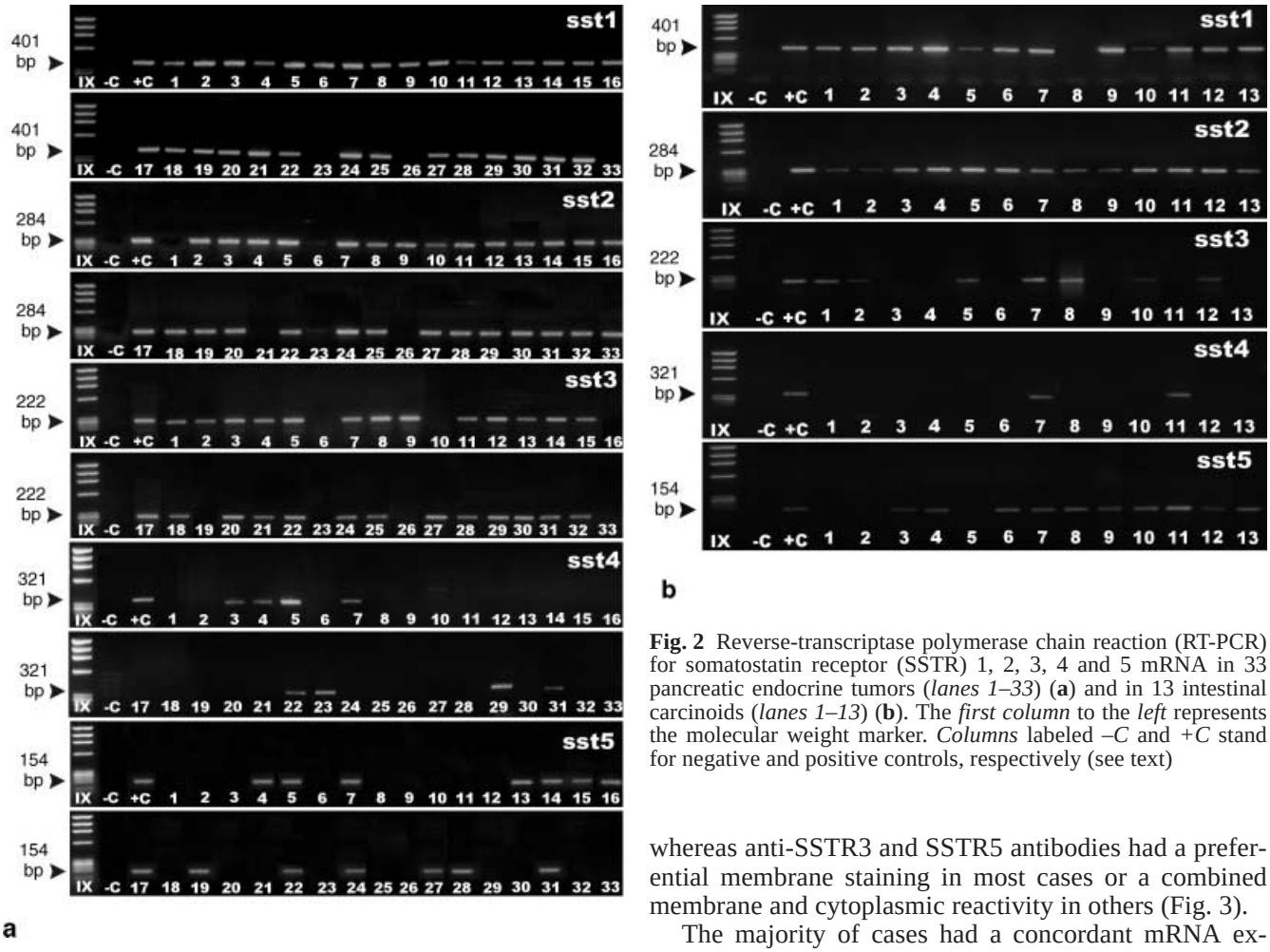

Fig. 2 Reverse-transcriptase polymerase chain reaction (RT-PCR) for somatostatin receptor (SSTR) 1, 2, 3, 4 and 5 mRNA in 33 pancreatic endocrine tumors (*lanes 1–33*) (**a**) and in 13 intestinal carcinoids (*lanes 1–13*) (**b**). The *first column* to the *left* represents the molecular weight marker. *Columns* labeled *–C* and *+C* stand for negative and positive controls, respectively (see text)

(mean 4.0 cm) and 0.3–11 cm (mean 2.8 cm), respectively. Lymph-node and/or liver metastases were observed in 57.1% of intestinal tumors and in one-third (33.9%) of pancreatic tumors.

SSTR in pancreatic endocrine tumors

RT-PCR analysis, performed in 33 cases, showed mRNA amplification of SSTR1 in 30 of 33 (90.1%), of SSTR2 in 28 of 33 (84.8%), of SSTR3 in 26 of 33 (78.8%), of SSTR4 in 8 of 33 (24.2%) and of SSTR5 in 14 of 33 (42.4%) cases (Fig. 2a, Table 3). In all cases, the preservation of total mRNA was ensured by detectable amplification of β2-microglobulin mRNA. IHC was performed using anti-SSTR 2, 3 and 5 antibodies. The immunohistochemical reactivity was markedly heterogeneous, being in some cases focally positive (in less than 25% of tumor cells, scored one plus, +; Table 3) and in others diffusely immunostained in over 50% of tumor cells (score +++). Some cases had an intermediate reactivity with between 25% and 50% of tumor cells positive (score ++). A cell membrane distribution of the immunoreactivity was present with anti-SSTR2 antibodies, whereas anti-SSTR3 and SSTR5 antibodies had a preferential membrane staining in most cases or a combined membrane and cytoplasmic reactivity in others (Fig. 3).

The majority of cases had a concordant mRNA expression, as detected by RT-PCR analysis, and protein expression, as shown by IHC. Discrepant cases included two tumors that failed to stain with anti-SSTR2 antibodies, despite a positive RT-PCR. In addition, a focal immunoreactivity for SSTRs 2, 3 and 5 was observed in one, one and four cases, respectively, in the absence of the corresponding mRNA amplification. This is likely due to tumor heterogeneity, since most cases had a focal SSTR immunoreactivity and, although care was taken to freeze tumor fragments adjacent to those used for conventional histopathological analysis, it cannot be excluded that the tumor cell populations of the two samples had a divergent differentiation pattern.

IHC was performed with anti-SSTR2, 3 and 5 antibodies in 22 additional tumors from 20 patients, in which frozen tissues were not available. Two patients (case nos. 35 and 39 – Table 3) had two separate tumor nodules producing a different hormone. For the purpose of correlative analysis between SSTR expression and hormone production, they were kept separate. SSTR2 immunoreactivity was found in 15 of 22 tumors (68.2%), SSTR3 in 8 of 22 (36.4%) and SSTR5 in 14 of 22 (63.6%).

Taking together all data on SSTR expression, it appeared that the majority of pancreatic endocrine tumors were expressing multiple SSTR subtypes, being at least

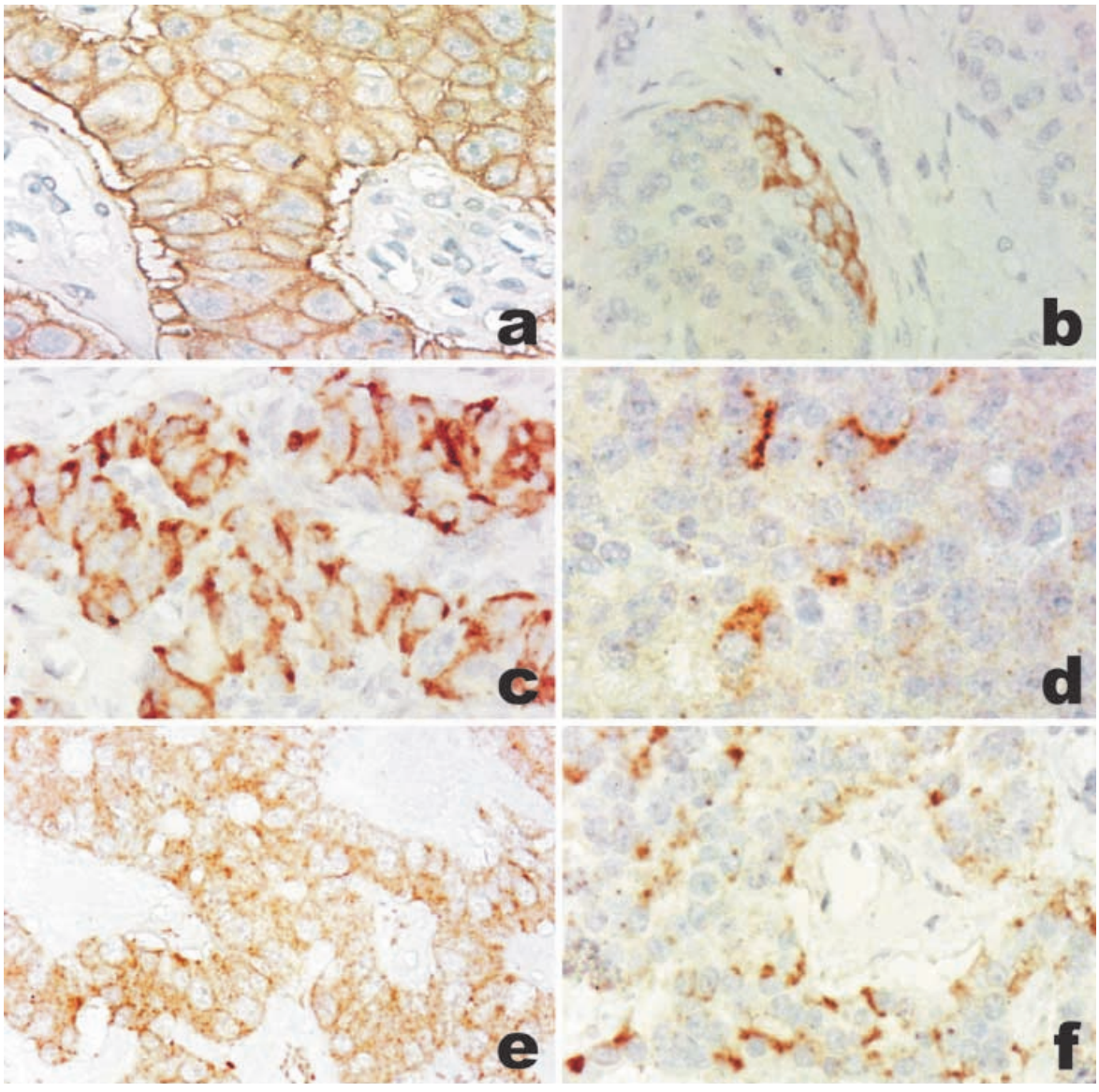

Fig. 3 **a** Case 32. Pancreatic gastrinoma diffusely positive (score +++) for somatostatin receptor (SSTR)2A at the cell membrane level. **b** Case 31. Pancreatic insulinoma showing a focal (score +) positivity for SSTR2A with predominant membraneous pattern. **c** Case 31. Strong membrane staining for SSTR3 in most tumor cells (score +++). **d** Case 3. A weak cytoplasmic staining in single tumor cells with membrane reinforcement is present in a pancreatic insulinoma (score +). **e** Case 37. Diffuse cytoplasmic staining with membrane reinforcement in a pancreatic somatostatinoma using the novel MK86 antibody to SSTR5 (score +++). **f** Case 15. Heterogeneous SSTR5 staining in a non-functioning pancreatic tumor with both cytoplasmic and membranous pattern (score ++). (**a**–**f** ×200). **g**–**i** Case 8. The pre-operative fine needle aspirate of this insulinoma metastatic to the liver shows a tumor cell cluster in the cell block (**g**) positive for chromogranin A (**h**) and for SSTR2A, which is localized at the cell membrane of most tumor cells (**i**) (**g**–**i** ×400). **l**–**n** Case 14. Non-functioning pancreatic tumor. The same tumor area expresses SSTR2 at protein level (positive SSTR2A immunoperoxidase) (**l**) and also at mRNA level (positive ISH reaction) (**m**). No staining is present hybridizing a parallel section with an unrelated probe (**n**) (**l**–**n** ×400). **o** Expression of SSTR in normal pancreatic islets. Relative percentages of SSTR2, SSTR3 and SSTR5 co-localization in normal pancreatic islet cells (*left*). An example of double immunofluorescence staining of somatostatin in delta cells (*red*) and SSTR5 (*green*) is shown to the *right*. All delta cells are positive for SSTR5 (*yellow color*), showing either cell membrane (*arrows*) or cytoplasmic (*arrowheads*) staining (×400)

three SSTR types present in 75% of cases and being only four of 55 tumors completely negative.

The SSTR immunoreactivity pattern was overlapping in lymph-node or liver metastases studied in parallel with the corresponding primary tumor. In addition, the pre-operative biopsy material (fine needle aspirate of a lymph-node or liver metastasis) of three cases gave overlapping results relative to the corresponding surgically resected tumor (Fig. 3).

In six cases, ISH for SSTR2 mRNA was performed and showed a concordant pattern with respect to RT-PCR data. A diffuse cytoplasmic positivity was present in the positive cases (Fig. 3), but not in parallel sections stained with an unrelated or sense probe.

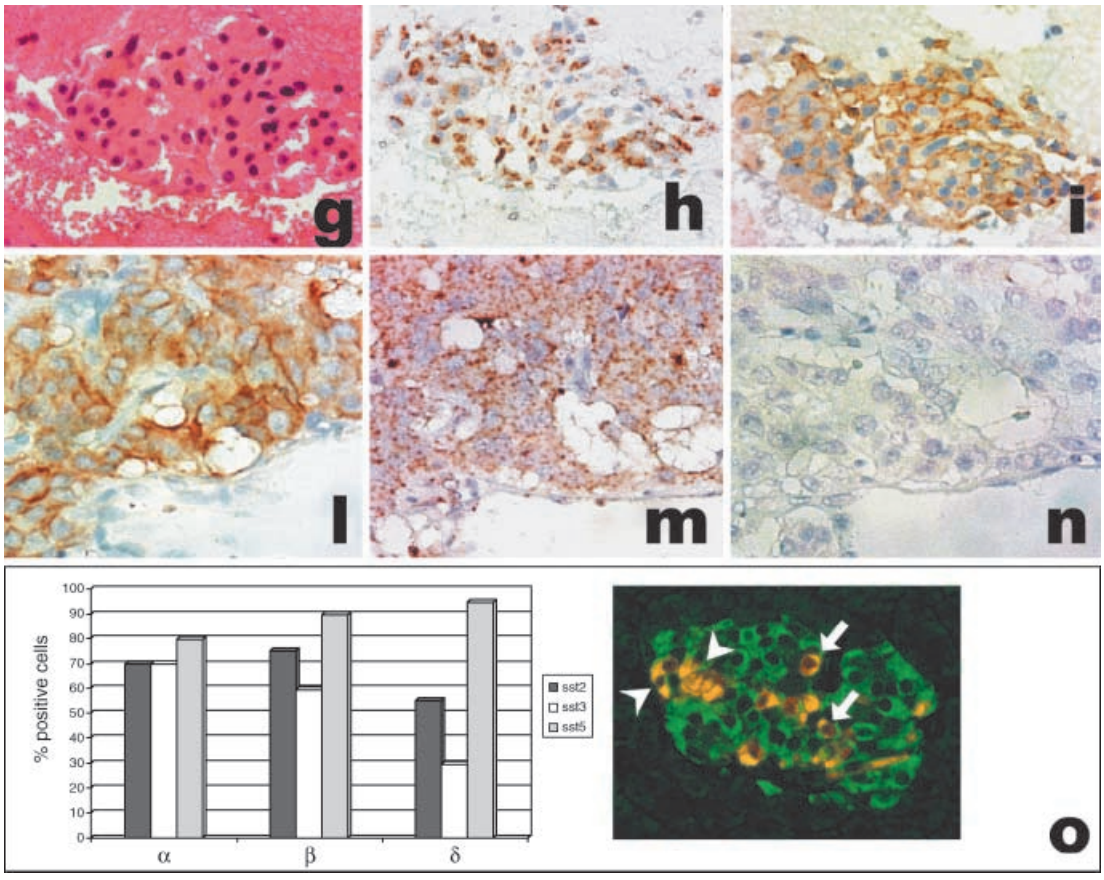

Fig. 3 g–o

When the SSTR expression was evaluated with regard to hormonal activity of the tumors, it turned out that SSTRs were heterogeneously distributed among different functioning or non-functioning endocrine tumors (Fig. 3). Generally, SSTR1 was diffusely expressed in endocrine tumors of the pancreas, as well as SSTR2, which was present in all glucagon (five cases) and gastrin-producing tumors (eight cases, including three located in the duodenum). SSTR3 and SSTR5 were expressed in approximately two-thirds of tumors, with no apparent restriction to a given hormonally active tumor, with the only exception of SSTR5 expressed in all four somatostatin-producing tumors. Finally, SSTR4 was poorly expressed in pancreatic endocrine tumors, being the specific mRNA present in only 8 of 33 tumors (24.2%). Interestingly, all such cases were insulinomas. Non-functioning tumors were not specifically associated with a specific SSTR subtype, irrespective of their size, tumor grade or biological behavior. Two cases, both high grade and metastatic tumors, were negative for all SSTR subtypes.

Normal pancreatic islets

The immunohistochemical expression of SSTRs 2, 3 and 5 was controlled in peritumoral pancreatic islets and in two control cases of normal pancreas, using double stainings with two-color immunofluorescence. SSTR2 was present in all cell types, co-localizing with 70% of alpha cells, 75% of beta cells and 55% of delta cells. SSTR3 co-localized with 70% of alpha cells, 60% of beta cells and less than one-third of delta cells. SSTR5 was present in 80% of alpha cells, 90% of beta cells, and in virtually all delta cells (95%; Fig. 3).

SSTR in gastrointestinal endocrine tumors

RT-PCR analysis, performed in 13 cases, showed mRNA amplification of SSTR1 in 12 of 13 (92.3%), of SSTR2 in 13 of 13 (100%), of SSTR3 in 7 of 13 (53.8%), of SSTR4 in 2 of 13 (15.4%) and of SSTR5 in 10 of 13 (76.9%) cases (Fig. 2b, Table 4). All the cases analyzed had a detectable level of the housekeeping gene β2-microglobulin mRNA, thus confirming the total mRNA quality. IHC was performed with anti-SSTR2, 3 and 5 antibodies. The immunohistochemical reactivity was extremely heterogeneous, as for pancreatic tumors. A cell membrane immunoreactivity was present with anti-SSTR2 antibodies, while in SSTR3 and SSTR5 stained cases, cell membrane and cytoplasmic reactivities were combined in some cases (Fig. 4).

The majority of cases had concordant mRNA and protein expression. Discrepant cases had a focal immunoreactivity for SSTR2, 3 and 5 in one, two and one cases, respectively, despite a negative RT-PCR reaction.

Table 3 Somatostatin receptor (SSTR) expression in endocrine tumors of the pancreas. *M* male, *F* female, *WDET* well-differentiated endocrine tumor, *WDEC* well-differentiated endocrine carcinoma, *PDEC* poorly differentiated endocrine carcinoma, *PP* pancreatic polypeptide, *VIP* vasoactive intestinal peptide, *LN* lymph node, *NED* no evidence of disease, *DOD* dead of disease, *DOC* dead other causes, *AWD* alive with disease, *IHC* immunohistochemistry, *RT-PCR* reverse-transcriptase polymerase chain reaction, – negative, + positive in <25% of tumor cells, ++ positive in 25–50% of tumor cells, +++ positive in >50% of tumor cells, *nd* not done

No.	Sex/ age	Location/ size (cm)	Diagnosis	Hormonal status	Metastases	Follow-up (years)	SSTR1	SSTR2		SSTR3		SSTR4	SSTR5	
							RT-PCR	IHC	RT-PCR	IHC	RT-PCR	RT-PCR	IHC	RT-PCR
1	M/44	Body/1	WDET	Insulin		NED 2	+	–	–	+	+	–	–	–
2	F/56	Head/1.4	WDET	Insulin		NED 6.5	+	+++	+	++	+	–	++	–
3	M/58	Body/2	WDET	Insulin		NED 3.5	+	–	+	+	+	+	–	–
4	F/72	Tail/4	WDET	Insulin		NED 4.5	+	+	+	+++	+	+	+++	+
5	F/39	Body/1.8	WDET	Insulin		NED 4	+	++	+	+	+	+	++	+
6	F/55	Head/0.9	WDET	Insulin		NED 4	+	–	–	–	–	–	–	–
7	M/60	Body/1.2	WDET	Insulin		NED 8.5	+	nd	+	nd	+	+	nd	+
8	M/62	Tail/5	WDEC	Insulin	Liver	DOD 1	+	+++	+	+	+	–	–	–
9	M/50	Tail/4	WDET	PP		NED 6.5	+	+	+	+	+	–	–	–
10	M/54	Tail/11	WDET	Glucagon		NED 4	+	+	+	–	–	–	–	–
11	F/63	Tail/7	WDET	VIP	LN	DOD 2	+	+	+	+	+	–	+	–
12	F/69	Tail/6	WDEC	Insulin		NED 11	+	++	+	+	+	–	–	–
13	M/44	Head/5	WDET	Non-functioning		DOD 0.1	+	+	+	+	+	–	+++	+
14	F/59	Body-tail/4	WDEC	Non-functioning	LN	NED 4	+	+++	+	+	+	–	+	+
15	M/49	Head/6	WDET	Non-functioning	Liver	DOC 4.5	+	+	+	+	+	–	++	+
16	F/54	Head/3.5	WDET	Non-functioning	LN	Lost	+	++	+	–	–	–	+	+
17	F/44	Body/3	WDEC	Non-functioning	LN	DOD 2	+	++	+	+	+	–	+	+
18	F/70	Head/3.5	WDET	Non-functioning		NED 1	+	+	+	+	+	–	–	–
19	F/64	Head/2.3	WDEC	Non-functioning	LN	DOD 1.2	+	+	+	–	–	–	+	+
20	M/55	Head/2	WDEC	Non-functioning	Liver	NED	+	+	+	+	+	–	–	–
21	M/56	Body-tail/3	WDET	Insulin		Lost	+	+	–	+	+	–	+	–
22	F/59	Head/1.5	WDET	Insulin		NED 3	+	+++	+	+++	+	+	+++	+
23	M/52	Body/1	WDET	Insulin		NED 11	–	+	–	–	–	+	–	–
24	F/26	Tail/2	WDET	Insulin		NED 5.5	+	+	+	++	+	–	++	+
25	M/23	Head/1	WDET	Insulin		Lost	+	–	+	+	+	–	–	–
26	F/29	Tail/0.5	WDET	Insulin		NED 0.6	–	–	–	+	–	–	–	–
27	F/56	Body/1	WDET	Insulin		NED 11	+	nd	+	nd	+	–	nd	+
28	F/61	Tail/1	WDET	Insulin		Lost	+	nd	+	nd	+	–	nd	+
29	F/72	Head/1.5	WDET	Insulin		Lost	+	nd	+	nd	+	+	nd	–
30	F/76	Head/2	WDET	Non-functioning		Lost	+	nd	+	nd	+	–	nd	–
31	F/59	Body/2.5	WDET	Insulin		Lost	+	+	+	+++	+	+	+++	+
32	M/28	Body-tail/7.5	WDEC	Gastrin	Liver	AWD 0.5	+	+++	+	+	+	–	+	–
33	M/76	Head/11	PDEC	Non-functioning	LN	DOD 0.5	–	–	+	–	–	–	–	–
34	M/62	Tail/1.2	WDET	Insulin		Lost	nd	+	nd	–	nd	nd	+	nd
35	F/27	Body-tail/2.5	WDET	Insulin/glucagon		Lost	nd	–/++	nd	–/++	nd	nd	–/–	nd
36	F/61	Body/1.5	WDET	Insulin		Lost	nd	–	nd	–	nd	nd	+	nd
37	F/55	Head/2	WDET	Somatostatin		Lost	nd	+++	nd	+	nd	nd	+++	nd
38	M/48	Tail/10	WDET	Somatostatin		Lost	nd	+	nd	–	nd	nd	+	nd
39	M/46	Body-tail/7	WDET	Insulin/somatostatin		DOC 8.5	nd	++/–	nd	–/–	nd	nd	–/++	nd

Table 3 (continued)

No.	Sex/ age	Location/ size (cm)	Diagnosis	Hormonal status	Metastases	Follow-up (years)	SSTR1	SSTR2		SSTR3		SSTR4	SSTR5	
							RT-PCR	IHC	RT-PCR	IHC	RT-PCR	RT-PCR	IHC	RT-PCR
40	F/54	Head/2.5	WDEC	Gastrin	LN	Lost	nd	+	nd	–	nd	nd	+	nd
41	F/59	Head/3.5	WDET	Gastrin		Lost	nd	++	nd	–	nd	nd	++	nd
42	M/58	Head/4	WDEC	Non-functioning	LN	DOD 1	nd	–	nd	–	nd	nd	–	nd
43	M/67	Head/0.6	WDET	Glucagon	LN	DOC 1	nd	+	nd	–	nd	nd	+	nd
44	F/67	Body/0.4	WDET	Glucagon		DOC 0.4	nd	+	nd	+	nd	nd	+	nd
45	M/54	Head/3	WDET	Insulin		NED 9	nd	–	nd	–	nd	nd	–	nd
46	M/55	Head/2.8	WDEC	Gastrin	LN	Lost	nd	+	nd	+	nd	nd	+	nd
47	F/57	Tail/13	WDET	Insulin		NED 7.5	nd	+	nd	–	nd	nd	–	nd
48	F/39	Head/7	WDEC	Gastrin	LN	DOC 14	nd	+++	nd	+	nd	nd	–	nd
49	M/54	Body/6	WDEC	Glucagon	Liver, lung	DOD 1	nd	+	nd	–	nd	nd	++	nd
50	M/46	Tail-spleen/12	WDEC	Somatostatin		NED 2	nd	–	nd	+	nd	nd	+	nd
51	M/20	Body-tail/20	PDEC	Non-functioning	LN	DOD 1	nd	–	nd	–	nd	nd	–	nd
52	F/59	Body-tail/3.5	WDEC	Non-functioning		NED 2	nd	++	nd	+	nd	nd	+	nd
53	M/57	Head/2	WDET	Non-functioning		NED 1	nd	++	nd	++	nd	nd	++	nd

IHC alone was performed with anti-SSTR2, 3 and 5 antibodies in 15 additional tumors, 8 of which had lymph-node and/or liver metastases. SSTR2 immunoreactivity was found in 12 of 15 tumors (80%), SSTR3 in 9 of 15 (60%) and SSTR5 in 12 of 15 (80%). In four cases of gastric body carcinoid associated with chronic atrophic gastritis and hyperplasia of neuroendocrine ECL cells, small hyperplastic nests as well as single endocrine cells scattered in the gastric glands were also positive for SSTR2 immunostaining (Fig. 4).

Taking together all data on SSTR expression, it appeared that the majority of gastrointestinal endocrine tumors were expressing multiple SSTR subtypes, with at least three SSTR types present in 90% of cases (with one tumor expressing all five types and three others having four of five SSTR types expressed) and with only one case completely negative (a poorly differentiated endocrine carcinoma).

As for the pancreatic tumors, the SSTR immunoreactivity pattern was overlapping in lymph-node or liver metastases relative to that of the primary tumor, as well as in pre-operative biopsy material (fine needle aspirate of a liver metastasis; Fig. 4) and in the corresponding surgically resected tumor.

In six cases, ISH for SSTR2 mRNA was performed and showed a concordant pattern with respect to RT-PCR data. A diffuse cytoplasmic staining was present in the positive cases, but not in parallel sections stained with an unrelated or sense probe (Fig. 4).

Clinico-pathological correlation

No statistically significant correlation was observed between SSTR expression (any type) and either sex, age, tumor size, tumor location or biological behavior. With regard to tumor grade, the rare poorly differentiated endocrine carcinomas (five cases) appeared to express SSTR to a lower extent, although the figures are too small to allow a definite conclusion on this point. Comparing the extent of SSTR expression with the clinical outcome in the 54 patients in which this information was

Fig 4 a–c Case 8. Duodenal gastrinoma metastatic to a lymph node. Somatostatin receptor (SSTR)2 is diffusely expressed as detected by positive immunoreaction (**a**, score +++) and positive in situ hybridization (ISH) for SSTR2 mRNA (**b**). No stain is present in a parallel section hybridized with an unrelated probe (**c**). (**a**–**c** ×200). **d** Case 9. Ileal endocrine tumor showing strong membrane SSTR3 immunoreactivity in most tumor cells (score +++) (×400). **e** Case 16. Ileal endocrine tumor with a predominant membranous pattern of staining with the SSTR5 antibody (score +++). A normal intestinal gland (*top*) is negative (×400). **f**–**g** Case 28. A gastric carcinoid associated with chronic atrophic gastritis and neuroendocrine ECL-cell hyperplasia (as shown by chromogranin A immunostaining) (**f**) are both positive for SSTR2 immunoreaction (**g**, *arrows*). (**f**–**g** ×200); **h**–**j** Case 6. The pre-operative fine needle aspirate of an ileal carcinoid metastatic to the liver shows tumor cell clusters in the cell block (**h**) diffusely positive for SSTR2A (**i**) with the staining localized at the cell membrane (**j**) (**h**–**i** ×200, **j** ×400) ▶

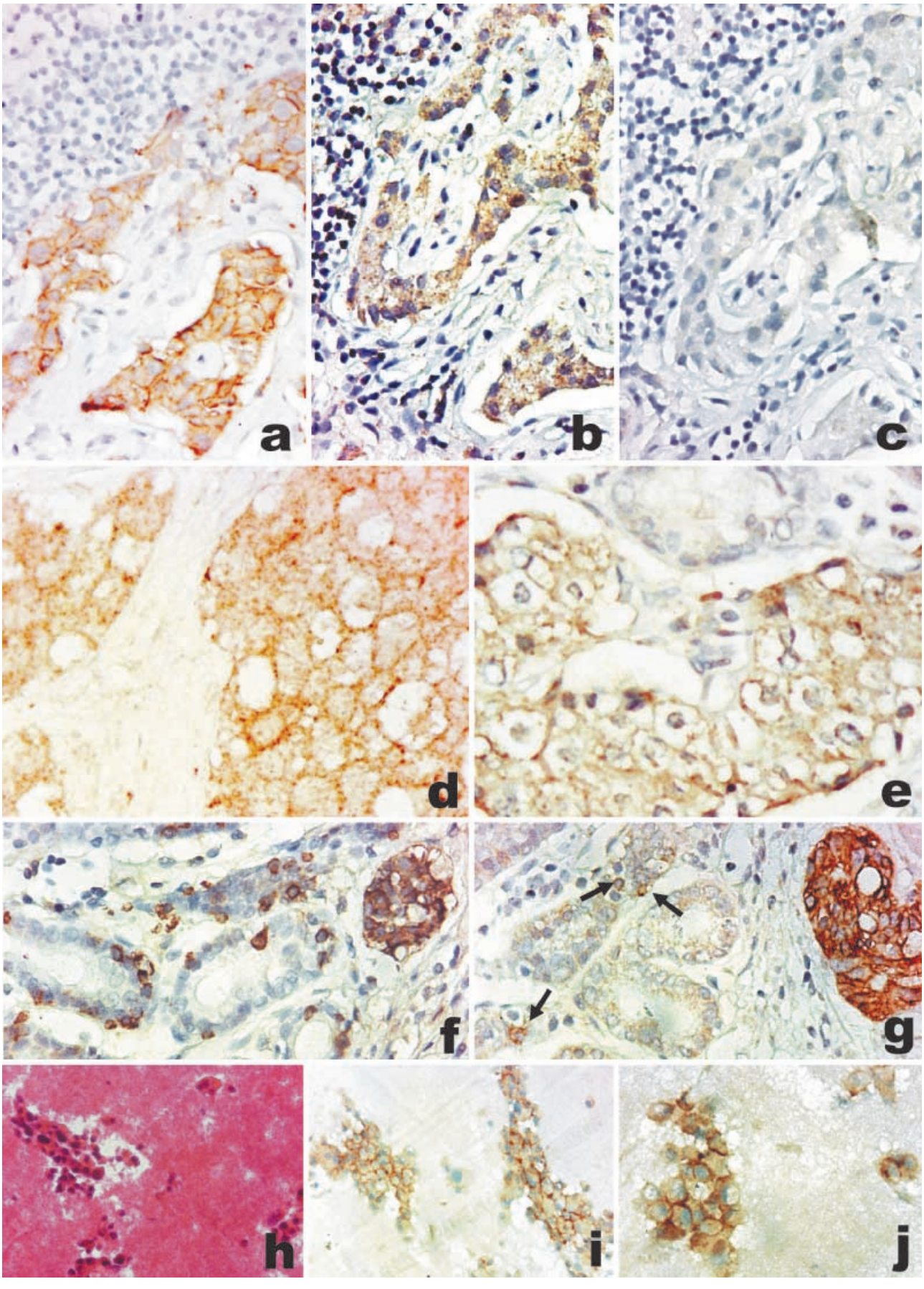

Fig 4 a–c Legend see page 469

Table 4 Somatostatin receptor (SSTR) expression in endocrine tumors of the gastrointestinal tract. *M* male, *F* female, *WDET* well-differentiated endocrine tumor, *WDEC* well-differentiated endocrine carcinoma, *PDEC* poorly differentiated endocrine carcinoma, *LN* lymph node, *NED* no evidence of disease, *DOD* dead of disease, *DOC* dead other causes, *AWD* alive with disease, *IHC* immunohistochemistry, *RT-PCR* reverse-transcriptase polymerase chain reaction, – negative, + positive in <25% of tumor cells, ++ positive in 25–50% of tumor cells, +++ positive in >50% of tumor cells, *nd* not done

No.	Sex/ age	Location/ size (cm)	Diagnosis	Hormonal status	Metastases	Follow-up (years)	SSTR1	SSTR2		SSTR3		SSTR4	SSTR5	
							RT-PCR	IHC	RT-PCR	IHC	RT-PCR	RT-PCR	IHC	RT-PCR
1	F/52	Appendix/1.5	WDEC		Peritoneum	DOC 0.1	+	+++	+	+++	+	–	–	–
2	F/68	Appendix/1.5	PDEC			DOC 6	+	–	+	+	+	–	–	–
3	M/40	Stomach/7	WDEC			NED 7.5	+	+++	+	–	–	–	+++	+
4	M/69	Ileum/2	WDEC		Liver		+	–	+	+	–	–	++	+
5	M/66	Ileum/4	WDEC		Peritoneum	NED 5.5	+	+	+	++	+	–	++	–
6	F/34	Ileum/2	WDEC		Liver	NED 1	+	+	+	–	–	–	+	+
7	M/62	Ileum/1	WDEC			NED 5	+	++	+	+++	+	+	+	+
8	M/50	Duodenum/2	WDEC	gastrin	LN		–	+++	+	++	+	–	+	+
9	M/54	Ileum/1.5	WDEC		Liver, LN	NED 1	+	+++	+	+	–	–	+	+
10	F/69	Ileum/1.5	WDEC			NED 3.5	+	+	+	+++	+	–	+	+
11	F/55	Duodenum/1.5	WDEC	gastrin		NED 6	+	+	+	–	–	+	+	+
12	M/52	Colon/3	WDEC		LN		+	nd	+	nd	+	–	nd	+
13	F/47	Rectum/1	WDEC		Liver		+	nd	+	nd	–	–	nd	+
14	M/31	Duodenum/0.8	WDEC	gastrin	LN	NED 7.5	nd	+	nd	+++	nd	nd	+++	nd
15	F/29	Rectum/11	PDEC		LN		nd	–	nd	–	nd	nd	–	nd
16	F/69	Ileum/5	WDEC		LN	NED 6	nd	+	nd	–	nd	nd	++	nd
17	M/74	Colon/3.5	WDEC		LN		nd	+	nd	–	nd	nd	–	nd
18	M/66	Stomach/0.2	WDET				nd	+	nd	++	nd	nd	++	nd
19	F/21	Appendix/1	WDET				nd	+	nd	+	nd	nd	+	nd
20	F/68	Appendix/0.6	WDET			NED 3	nd	+	nd	+	nd	nd	+	nd
21	M/71	Ileum/2.5	WDEC				nd	+++	nd	+	nd	nd	–	nd
22	M/60	Ileum/0.8	WDEC		Liver		nd	+++	nd	–	nd	nd	+	nd
23	M/60	Duodenum/10	WDEC		LN		nd	–	nd	–	nd	nd	+	nd
24	F/67	Stomach/1.5	WDET			NED 2	nd	+++	nd	+	nd	nd	++	nd
25	F/64	Stomach/3.8	WDEC		LN	NED 0.8	nd	–	nd	+	nd	nd	+	nd
26	M/66	Rectum/7	PDEC		LN	DOD 2	nd	+	nd	+	nd	nd	+	nd
27	F/57	Stomach/0.3	WDET				nd	++	nd	+	nd	nd	+	nd
28	F/50	Stomach/0.5	WDET			NED 5	nd	++	nd	–	nd	nd	+	nd

available, it appeared that no specific association was present between SSTR content and biological behavior. Finally, comparing pancreatic and gastrointestinal endocrine tumors, it can be noticed that the percentage of SSTR subtype expression in the two groups is relatively similar, with SSTRs 1 and 2 present in the vast majority of GEP tumors, SSTRs 3 and 5 expressed by approximately two-thirds of cases and SSTR 4 only occasionally represented in these tumors (mostly insulinomas).

Discussion

IHC using specific antibodies is a reliable tool to reveal SSTR

In 46 GEP endocrine tumors, SSTR 1–5 expression was found in a consistent percentage of cases with the exception of SSTR4, which was poorly represented (20%). These findings are the result of RT-PCR and immunohistochemical analyses. The literature data, mostly obtained from small case series (with few exceptions) [12, 49] are largely heterogeneous both in terms of SSTR expression results and methods employed to demonstrate them. On the contrary, we analyzed SSTR types 1–5 in a relatively large series of tumors and compared two sensitive techniques – RT-PCR and IHC with tyramide amplification. With regard to the former, few studies have detected SSTR types 1–5 mRNA in GEP tumors. While most authors agree on a high (>60%) SSTR1 and 2 and moderate (50%) SSTR5 expression, conflicting results were observed for SSTRs 3 and 4, which were found in nearly half of the cases of endocrine pancreatic tumors by some authors [12, 32], but very poorly represented according to others [49]. IHC, however, is the last entry in the list of techniques used to reveal SSTR, and takes advantage from the possibility of a topographical SSTR localization within tumor cells using highly specific antibodies. So far, only SSTR2A immunoreactivity has been thoroughly characterized in GEP endocrine tumors, with other SSTR types so far having been detected by mRNA analysis alone.

In the current study, SSTRs 2, 3 and 5 were studied by means of IHC with specific antibodies and were found to correlate with RT-PCR data in over 90% of cases, supporting the data already published on SSTR2A immunohistochemical detection [14, 33] and expanding them to SSTR types 3 and 5. The latter were detected using a commercial antibody to SSTR3 and a novel antibody to SSTR5 developed in our laboratory. Both SSTR3 and SSTR5 immunostainings showed a preferential cell membrane subcellular distribution, as typically observed for SSTR2A [24, 33]. In some cases, however, an associated cytoplasmic reactivity was also found, as described for SSTR2A in tumors of other organs, too [38]. A similar pattern of reactivity for SSTRs 2, 3 and 5 was also observed in biopsy or fine needle aspirate cytology specimens obtained pre-operatively from metastatic liver nodules or primary pancreatic tumors, relative to the corresponding surgical samples.

This indicates that the SSTR profile can be investigated using IHC in the course of the diagnostic work-up of a GEP tumor directly on small pre-operative biopsy specimens. A negative result, however, might not definitely exclude the presence of a given SSTR type, since 20–30% of operated cases had a focal immunoreactivity and the biopsy sample may not contain SSTR immunoreacive cells. In any case, a positive immunohistochemical SSTR detection may open new prospects for somatostatin analogue-based radio-imaging and radiotherapy of GEP endocrine tumors.

Interpretation criteria of SSTR expression need to be defined

Cases showing discrepant results between IHC and RT-PCR accounted for up to 10% of cases in each SSTR type (namely, four, three and five cases for SSTRs 2, 3 and 5, respectively). These included two tumors positive by RT-PCR alone that failed to show the corresponding SSTR immunoreactivity, a finding possibly due to poor antigen preservation after fixation or low amount of receptor protein (below the threshold of detectability of immunohistochemical procedure). The remaining cases were negative by RT-PCR and had a focal reactivity (less than 20%) in tumor cells. This unexpected finding is possibly related to tumor heterogeneity, although care had been taken to freeze a fragment adjacent to that used for conventional histopathological examination. Considering weak or focally positive reactions, it remains to be ascertained whether the immunohistochemical evaluation (and probably also SSTR evaluation in general, with any method) may require a semi-quantitative procedure or a cut-off value, to better interpret borderline findings. An answer to this point will stem from clinical studies on large series of GEP tumors treated with somatostatin analogues. The available literature data [10, 13, 19, 22, 26, 36] showed that a relatively good correlation exists between SSTR expression (evaluated by autoradiography or RT-PCR) and in vivo detection of functional receptors by means of octreotide scintigraphy, although discrepant cases were also found [13]. Unfortunately, no cases of the present series underwent clinical evaluation with octreotide.

Correlative SSTR expression in pancreatic islet cells and related endocrine tumors

Although not specifically designed as a study on normal pancreatic islets, we had the opportunity of mapping the individual SSTR types in peritumoral pancreatic islet cells, as well as in two normal pancreatic tissues used as controls. This was of special interest because of discrepant data on the immunohistochemical localization of SSTR in pancreatic endocrine cell types. Kumar et al. [18] found SSTRs 1 and 2 in alpha and beta cells and SSTR5 in beta and delta cells, with SSTRs 3 and 4 poor-

ly represented in the pancreas. The data on SSTR2 are in agreement with the findings of Reubi et al. in human [34] and Mitra et al. [21] and Hunyadi et al. [11] in rat pancreas. Conversely, Portela-Gomes and co-workers [28] observed a wide occurrence of SSTR subtypes in all pancreatic endocrine cells, (range 60–100% of individual cell types). In this study, considering specifically only a predominant cell membrane immunoreactivity, we found SSTR2 expressed in 70%, 75% and 55% of alpha, beta and delta cells, respectively; SSTR3 expressed in two-thirds of alpha and beta cells but in less than 30% of delta cells; and finally SSTR5 co-localized in virtually all delta cells and in 80–90% of alpha and beta cells. These figures are in agreement those of Portela-Gomes et al. [28] and Kumar et al. [18] on SSTR5 in delta cells and Reubi et al. [34] and Strowski et al. [47] on SSTR2 in alpha and beta cells. The results of Kumar et al. [18] on other SSTR types are slightly different, possibly due to the fact that these authors used antibodies to rat SSTRs. In particular, SSTR3 expression was very low in the experience of both Kumar et al. [17] and Kubota et al. [16], while both RT-PCR and IHC were strongly positive in our cases.

With regard to SSTR expression in pancreatic neoplasms, SSTR2 was widely expressed by gastrin- and glucagon-producing tumors (100% of cases), including three duodenal gastrinomas. In addition, all somatostatin-producing tumors were SSTR5 positive, a finding which parallels the profile of normal delta cells, as described above. Incidentally, three of four cases had a combined membrane and cytoplasmic positivity, in agreement with the data of Reubi et al. [38] on SSTR2A immunoreactivity in somatostatinomas. As far as insulin-producing tumors are concerned, SSTR2 was present in 76% of tumors, thus confirming that these tumors are rich in SSTR2, just as normal beta cells are [14, 33, 34, 49]. Irrespective of the hormonal product, most tumors expressed SSTR1 (as demonstrated by RT-PCR data only) and two-thirds of them were rich in SSTR3. This is at variance with Wulbrand's findings [49], who showed that SSTR3 was absent in the pancreatic tumors. This difference is surprising since in Wulbrand's [49] and in the present studies, the same primer sequences were used for RT-PCR. Apart from possible technical details (e.g., tissue preservation and storage), other factors related to individual tumors may account for these discrepancies. Only 20% of cases expressed SSTR4, being all such cases insulinomas. Finally, non-functioning tumors did not appear to be associated with a special SSTR expression profile. The relatively large series of 14 cases here studied showed a heterogeneous pattern of SSTR expression, as also observed in the seven non-functioning pancreatic tumors of Wulbrand's series [49]. Nevertheless, the amount of receptors identified in all but two cases (both aggressive tumors) suggests that somatostatin analogue treatment may be a useful adjunct in these tumors, as also suggested by Bartsch [1].

A separate comment is deserved for the two cases with multiple pancreatic nodules producing different hormones. Interestingly, IHC (and ISH for SSTR2) could demonstrate a selective expression of SSTR subtypes in different nodules, with SSTRs 2 and 5 confined to the insulin and somatostatin-producing nodules, respectively, in one case, and with SSTRs 2 and 3 present in the glucagon-producing tumor, but not in the insulin-positive nodule, of the second case. The clinical implications of this differential SSTR expression in combined endocrine tumors are not fully understood, but such a receptor profile might better address the therapeutic strategy with subtype-selective somatostatin analogues [6, 36, 37], in the case of inoperable disease or recurrent tumors.

The observed correlation between the SSTR subtype(s) expression in normal islet cells and in their related hormone-producing tumors, was also detected in normal/hyperplastic neuroendocrine ECL cells of the oxyntic gastric mucosa and their related carcinoid tumors.

Possible association of reduced SSTR expression and tumor grade

Taking into account clinical and pathological parameters of GEP endocrine tumors, we were unable to disclose any specific association between SSTR subtype expression and either sex, age, tumor location and size, tumor stage or clinical outcome (in the 54 cases in which this information was obtained). In GEP adenocarcinomas, however, an inverse relationship between SSTR2 expression and tumor stage was found [3]. With regard to tumor grade, as observed in tumors of other locations (e.g., lung) [24], poorly differentiated endocrine carcinomas had an apparently reduced SSTR content. Three of five cases (60%) of poorly differentiated carcinomas had no or only one SSTR type focally expressed in their tumor cell population (as opposed to 12% of well-differentiated cases with only one or no SSTR type expressed).

Conclusion

a. SSTR expression in GEP endocrine tumors is heterogeneous; SSTRs 1 and 2 are the types most commonly detected (over 80%), followed by SSTRs 3 and 5 present in two-thirds of cases and by SSTR4 which is poorly represented in GEP tumors.
b. RT-PCR is a highly sensitive technique to reveal SSTRs but needs to be combined with methods that allow confirmation of the receptor protein localization in tumor cells.
c. Immunohistochemical detection of SSTR2, and also of SSTRs 3 and 5, is a reliable procedure for the study of formalin-fixed tissues, including biopsy and cytological pre-operative material.
d. Hormonally active pancreatic tumors have a preferential SSTR5 expression in “somatostinomas” and SSTR2 positivity in “gastrinomas” and “glucagonomas”. “Insulinomas” express all SSTR types (ranging from 40% to 90% of cases). Non-functioning tumors

express all SSTR types (but SSTR4) in 60–90% of cases.

e. A correlation was observed between SSTR subtype expression in normal islet cells and neuroendocrine gastric cells and in the corresponding endocrine tumors.

f. SSTR expression is not related to tumor stage or outcome but is related to tumor grade, with high-grade endocrine carcinomas having a reduced SSTR content.

Acknowledgements Work was supported by grants from the Italian Ministry of University and Research (ex 60% to MP) and Ministry of Health (ICS 030.12/RF99.28) and from the Italian Association for Cancer Research (AIRC, Milan).

References

1. Bartsch DK, Schilling T, Ramaswamy A, Gerdes B, Celik I, Wagner HJ, Simon B, Rothmund M (2000) Management of nonfunctioning islet cell carcinomas. World J Surg 24:1418–1424
2. Bordi C, Annibale B, Azzoni C, Marignani M, Ferraro G, Antonelli G, D'Adda T, D'Ambra G, Delle Fave G (1997) Endocrine cell growths in atrophic body gastritis. Critical evaluation of a histological classification. J Pathol 182:339–346
3. Buscail L, Saint-Laurent N, Chastre E, Vaillant JC, Gespach C, Capella G, Kalthoff H, Lluis F, Vaysse N, Susini C (1996) Loss of sst2 somatostatin receptor gene expression in human pancreatic and colorectal cancer. Cancer Res 56:1823–1827
4. Corleto VD, Scopinaro F, Angeletti S, Materia A, Basso N, Polettini E, Annibale B, Schillaci O, D'Ambra G, Marignani M, Gualdi G, Bordi C, Passaro EJ, Delle Fave G (1996) Somatostatin receptor localization of pancreatic endocrine tumors. World J Surg 20:241–244
5. Eriksson B, Oberg K (1999) Summing up 15 years of somatostatin analog therapy in neuroendocrine tumors: future outlook. Ann Oncol 10:S31–S38
6. Fehmann HC, Wulbrand U, Arnold R (2000) Treatment of endocrine gastroenteropancreatic tumors with somatostatin analogues. Recent Results Cancer Res 153:15–22
7. Gussow D, Rein R, Ginjaar I, Hochstenbach F, Seemann G, Kottman A, Ploegh HL (1987) The human beta 2-microglobulin gene. Primary structure and definition of the transcriptional unit. J Immunol 139:3132–3138
8. Helboe L, Moller M, Norregaard L, Schiodt M, Stidsen CE (1997) Development of selective antibodies against the human somatostatin receptor subtypes sst1-sst5. Brain Res Mol Brain Res 49:82–88
9. Hofland LJ, Breeman WA, Krenning EP, de Jong M, Waaijers M, van Koetsveld PM, Macke HR, Lamberts SW (1999) Internalization of [DOTA degrees,125I-Tyr3] octreotide by somatostatin receptor-positive cells in vitro and in vivo: implications for somatostatin receptor-targeted radio-guided surgery. Proc Assoc Am Physicians 111:63–69
10. Hofland LJ, Liu Q, Van Koetsveld PM, Zuijderwijk J, Van Der Ham F, De Krijger RR, Schonbrunn A, Lamberts SW (1999) Immunohistochemical detection of somatostatin receptor subtypes sst1 and sst2A in human somatostatin receptor positive tumors. J Clin Endocrinol Metab 84:775–780
11. Hunyady B, Hipkin RW, Schonbrunn A, Mezey E (1997) Immunohistochemical localization of somatostatin receptor SST2A in the rat pancreas. Endocrinology 138:2632–2635
12. Jais P, Terris B, Ruszniewski P, LeRomancer M, Reyl-Desmars F, Vissuzaine C, Cadiot G, Mignon M, Lewin MJ (1997) Somatostatin receptor subtype gene expression in human endocrine gastroentero-pancreatic tumours. Eur J Clin Invest 27:639–644
13. Janson ET, Stridsberg M, Gobl A, Westlin JE, Oberg K (1998) Determination of somatostatin receptor subtype 2 in carcinoid tumors by immunohistochemical investigation with somatostatin receptor subtype 2 antibodies. Cancer Res 58:2375–2378
14. Kimura N, Pilichowska M, Date F, Kimura I, Schindler M (1999) Immunohistochemical expression of somatostatin type 2A receptor in neuroendocrine tumors. Clin Cancer Res 5:3483–3487
15. Krenning EP, Bakker WH, Breeman WA, Koper JW, Kooij PP, Ausema L, Lameris JS, Reubi JC, Lamberts SW (1989) Localisation of endocrine-related tumours with radioiodinated analogue of somatostatin. Lancet 1:242–244
16. Kubota A, Yamada Y, Kagimoto S, Shimatsu A, Imamura M, Tsuda K, Imura H, Seino S, Seino Y (1994) Identification of somatostatin receptor subtypes and an implication for the efficacy of somatostatin analogue SMS 201–995 in treatment of human endocrine tumors. J Clin Invest 93:1321–1325
17. Kumar U, Laird D, Srikant CB, Escher E, Patel YC (1997) Expression of the five somatostatin receptor (SSTR1–5) subtypes in rat pituitary somatotrophes: quantitative analysis by double-layer immunofluorescence confocal microscopy. Endocrinology 138:4473–4476
18. Kumar U, Sasi R, Suresh S, Patel A, Thangaraju M, Metrakos P, Patel SC, Patel YC (1999) Subtype-selective expression of the five somatostatin receptors (hSSTR1–5) in human pancreatic islet cells: a quantitative double-label immunohistochemical analysis. Diabetes 48:77–85
19. Lamberts SW, Hofland LJ, van Koetsveld PM, Reubi JC, Bruining HA, Bakker WH, Krenning EP (1990) Parallel in vivo and in vitro detection of functional somatostatin receptors in human endocrine pancreatic tumors: consequences with regard to diagnosis, localization, and therapy. J Clin Endocrinol Metab 71:566–574
20. Mato E, Matias-Guiu X, Chico A, Webb SM, Cabezas R, Berna L, De Leiva A (1998) Somatostatin and somatostatin receptor subtype gene expression in medullary thyroid carcinoma. J Clin Endocrinol Metab 83:2417–2420
21. Mitra SW, Mezey E, Hunyady B, Chamberlain L, Hayes E, Foor F, Wang Y, Schonbrunn A, Schaeffer JM (1999) Colocalization of somatostatin receptor sst5 and insulin in rat pancreatic beta-cells. Endocrinology 140:3790–3796
22. Nilsson O, Kolby L, Wangberg B, Wigander A, Billig H, William-Olsson L, Fjalling M, Forssell-Aronsson E, Ahlman H (1998) Comparative studies on the expression of somatostatin receptor subtypes, outcome of octreotide scintigraphy and response to octreotide treatment in patients with carcinoid tumours. Br J Cancer 77:632–637
23. Panetta R, Greenwood MT, Warszynska A, Demchyshyn LL, Day R, Niznik HB, Srikant CB, Patel YC (1994) Molecular cloning, functional characterization, and chromosomal localization of a human somatostatin receptor (somatostatin receptor type 5) with preferential affinity for somatostatin-28. Mol Pharmacol 45:417–427
24. Papotti M, Croce S, Macri L, Funaro A, Pecchioni C, Schindler M, Bussolati G (2000) Correlative immunohistochemical and reverse transcriptase polymerase chain reaction analysis of somatostatin receptor type 2 in neuroendocrine tumors of the lung. Diagn Mol Pathol 9:47–57
25. Papotti M, Kumar U, Volante M, Pecchioni C, Patel YC (2001) Immunohistochemical detection of somatostatin receptor types 1–5 in medullary carcinoma of the thyroid. Clin Endocrinol (Oxf) 54:641–649
26. Papotti M, Croce S, Bellò M, Bongiovanni M, Allia E, Schindler M, Bussolati G (2001) Expression of somatostatin receptor types 2, 3 and 5 in biopsies and surgical specimens of human lung tumours. Virchows Arch 439:787–793
27. Patel YC (1997) Molecular pharmacology of somatostatin receptor subtypes. J Endocrinol Invest 20:348–367
28. Portela-Gomes GM, Stridsberg M, Grimelius L, Oberg K, Janson ET (2000) Expression of the five different somatostatin receptor subtypes in endocrine cells of the pancreas. Appl Immunohistochem Molecul Morphol 8:126–132

29. Reubi JC, Hacki WH, Lamberts SW (1987) Hormone-producing gastrointestinal tumors contain a high density of somatostatin receptors. J Clin Endocrinol Metab 65:1127–1134
30. Reubi JC, Maurer R, von Werder K, Torhorst J, Klijn JG, Lamberts SW (1987) Somatostatin receptors in human endocrine tumors. Cancer Res 47:551–558
31. Reubi JC, Kvols LK, Waser B, Nagorney DM, Heitz PU, Charboneau JW, Reading CC, Moertel C (1990) Detection of somatostatin receptors in surgical and percutaneous needle biopsy samples of carcinoids and islet cell carcinomas. Cancer Res 50:5969–5977
32. Reubi JC, Schaer JC, Waser B, Mengod G (1994) Expression and localization of somatostatin receptor SSTR1, SSTR2, and SSTR3 messenger RNAs in primary human tumors using in situ hybridization. Cancer Res 54:3455–3459
33. Reubi JC, Kappeler A, Waser B, Laissue J, Hipkin RW, Schonbrunn A (1998) Immunohistochemical localization of somatostatin receptors sst2A in human tumors. Am J Pathol 153:233–245
34. Reubi JC, Kappeler A, Waser B, Schonbrunn A, Laissue J (1998) Immunohistochemical localization of somatostatin receptor sst2A in human pancreatic islets. J Clin Endocrinol Metab 83:3746–3749
35. Reubi JC, Laissue JA, Waser B, Steffen DL, Hipkin RW, Schonbrunn A (1999) Immunohistochemical detection of somatostatin sst2a receptors in the lymphatic, smooth muscular, and peripheral nervous systems of the human gastrointestinal tract: facts and artifacts. J Clin Endocrinol Metab 84:2942–2950
36. Reubi JC, Schar JC, Waser B, Wenger S, Heppeler A, Schmitt JS, Macke HR (2000) Affinity profiles for human somatostatin receptor subtypes SST1-SST5 of somatostatin radiotracers selected for scintigraphic and radiotherapeutic use. Eur J Nucl Med 27:273–282
37. Reubi JC, Schaer JC, Wenger S, Hoeger C, Erchegyi J, Waser B, Rivier J (2000) SST3-selective potent peptidic somatostatin receptor antagonists. Proc Natl Acad Sci USA 97:13973–13978
38. Reubi JC, Waser B, Liu Q, Laissue JA, Schonbrunn A (2000) Subcellular distribution of somatostatin sst2A receptors in human tumors of the nervous and neuroendocrine systems: membranous versus intracellular location. J Clin Endocrinol Metab 85:3882–3891
39. Schaer JC, Waser B, Mengod G, Reubi JC (1997) Somatostatin receptor subtypes sst1, sst2, sst3 and sst5 expression in human pituitary, gastroentero-pancreatic and mammary tumors: comparison of mRNA analysis with receptor autoradiography. Int J Cancer 70:530–537
40. Schindler M, Sellers LA, Humphrey PP, Emson PC (1997) Immunohistochemical localization of the somatostatin SST2(A) receptor in the rat brain and spinal cord. Neuroscience 76:225–240
41. Schindler M, Holloway S, Humphrey PP, Waldvogel H, Faull RL, Berger W, Emson PC (1998) Localization of the somatostatin sst2(a) receptor in human cerebral cortex, hippocampus and cerebellum. Neuroreport 9:521–525
42. Schonbrunn A (1999) Somatostatin receptors present knowledge and future directions. Ann Oncol 10:S17–S21
43. Schulz S, Schulz S, Schmitt J, Wiborny D, Schmidt H, Olbricht S, Weise W, Roessner A, Gramsch C, Hollt V (1998) Immunocytochemical detection of somatostatin receptors sst1, sst2A, sst2B, and sst3 in paraffin-embedded breast cancer tissue using subtype- specific antibodies. Clin Cancer Res 4:2047–2052
44. Sestini R, Orlando C, Peri A, Tricarico C, Pazzagli M, Serio M, Pagani A, Bussolati G, Granchi S, Maggi M (1996) Quantitation of somatostatin receptor type 2 gene expression in neuroblastoma cell lines and primary tumors using competitive reverse transcription-polymerase chain reaction. Clin Cancer Res 2:1757–1765
45. Slooter GD, Mearadji A, Breeman WA, Marquet RL, de Jong M, Krenning EP, van Eijck CH (2001) Somatostatin receptor imaging, therapy and new strategies in patients with neuroendocrine tumours. Br J Surg 88:31–40
46. Solcia E, Kloppel G, Sobin LH (2000) Histological typing of endocrine tumours. Springer, Berlin Heidelberg New York
47. Strowski MZ, Parmar RM, Blake AD, Schaeffer JM (2000) Somatostatin inhibits insulin and glucagon secretion via two receptors subtypes: an in vitro study of pancreatic islets from somatostatin receptor 2 knockout mice. Endocrinology 141:111–117
48. Volante M, Pecchioni C, Bussolati G (2000) Post-incubation heating significantly improves tyramide signal amplification. J Histochem Cytochem 48:1583–1585
49. Wulbrand U, Wied M, Zofel P, Goke B, Arnold R, Fehmann H (1998) Growth factor receptor expression in human gastroenteropancreatic neuroendocrine tumours. Eur J Clin Invest 28:1038–1049
50. Yamada Y, Post SR, Wang K, Tager HS, Bell GI, Seino S (1992) Cloning and functional characterization of a family of human and mouse somatostatin receptors expressed in brain, gastrointestinal tract, and kidney. Proc Natl Acad Sci USA 89:251–255
51. Yamada Y, Reisine T, Law SF, Ihara Y, Kubota A, Kagimoto S, Seino M, Seino Y, Bell GI, Seino S (1992) Somatostatin receptors, an expanding gene family: cloning and functional characterization of human SSTR3, a protein coupled to adenylyl cyclase. Mol Endocrinol 6:2136–2142

Virchows Arch (2002) 440:476–484
DOI 10.1007/s00428-001-0558-9

ORIGINAL ARTICLE

Karl-Ludwig Schaefer · Daniel H. Wai
Christopher Poremba · Eberhard Korsching
Frans van Valen · Toshifumi Ozaki
Werner Boecker · Barbara Dockhorn-Dworniczak

Characterization of the malignant melanoma of soft-parts cell line GG-62 by expression analysis using DNA microarrays

Received: 6 August 2001 / Accepted: 18 September 2001 / Published online: 4 December 2001
© Springer-Verlag 2001

Abstract GG-62 is a cell line previously thought to be derived from an atypical Ewing tumor (ET). Reverse-transcriptase polymerase chain reaction revealed an in-frame fusion between the Ewing sarcoma gene (*EWS*) codon 325 and the activating transcription factor 1 gene (*ATF1*) codon 65 which permits the production of chimeric EWS-ATF1 oncoproteins. We also identified the genomic breakpoint resulting from a reciprocal t(12;22)(q13;q12), which is the hallmark of malignant melanoma of soft parts (MMSP). We applied Affymetrix human cancer G110 arrays to compare the gene expression patterns of GG-62 and other cell lines derived from small blue round cell tumors of childhood. Hierarchical clustering of 463 differentially expressed genes distinguished GG-62 from the ETs, as well as the neuroblastomas, and revealed a cluster of 36 upregulated genes. Several of these genes are involved in signal transduction pathways that may be critical for maintaining cell transformation; some examples are avian erythroblastic leukemia viral oncogene homolog 3 (*ERBB3*), neuregulin 1 (*NRG1*), fibroblast growth factor 9 (*FGF9*), and fibroblast growth factor receptor-1 (*FGFR1*). Furthermore, genes near the chromosome-12q13 breakpoint exhibited increased expression of GG-62 including *ERBB3*, *NR4A1* (nuclear receptor subfamily 4, group A, member 1), cyclin-dependent kinase 2 (*CDK2*), and alpha 5 integrin (*ITGA5*). Altogether our findings demonstrate the MMSP derivation of GG-62 and may shed light on the mechanisms of tumorigenesis in this rare disease.

Keywords Malignant melanoma of soft parts · Expression microarray

Karl-Ludwig Schaefer and Daniel H. Wai contributed equally to this work.

K.-L. Schaefer · D.H. Wai · C. Poremba · E. Korsching
W. Boecker · B. Dockhorn-Dworniczak (✉)
Gerhard-Domagk-Institute of Pathology, University of Münster, Domagkstrasse 17, 48149 Münster, Germany
e-mail: dwornib@uni-muenster.de
Tel.: +49-251-8355449, Fax: +49-251-8355460

F. van Valen · T. Ozaki
Laboratory for Experimental Orthopaedic Research, University of Münster, Domagkstrasse 3, 48149 Münster, Germany

Introduction

Malignant melanoma of soft parts (MMSP), also called clear cell sarcoma of the tendons, is a rare lesion which may exhibit melanocytic differentiation and accounts for only 0.8–1.0% of all malignancies of the musculoskeletal system [6, 14, 22]. This entity, which usually affects adolescents and young adults, is commonly associated with tendons and aponeuroses and is believed to be derived from neuroectodermal tissues [3]. MMSP is typified by the presence of a balanced t(12;22)(q13;q12) rearrangement: the result is a fusion between the Ewing sarcoma gene (*EWS*) and activating transcription factor 1 gene (*ATF1*) which permits the expression of EWS-ATF1 oncoproteins [42]. ATF, along with cAMP response element binding protein (CREB) and cAMP response element modulator (CREM), comprise a bZIP sub-family of transcription factors that regulate gene expression via homo- or heterodimeric binding to cyclic AMP response elements (CREs; [23]). EWS-ATF1 is able to bind CREs independently of cAMP induction due to a partial deletion of the ATF1 kinase-inducible domain [24]; moreover, the fusion protein has been shown to act as a potent activator of several cAMP-inducible promoters [1, 11]. Therefore, EWS-ATF1 may exert its oncogenic properties via the induction or deregulation of genes that govern transcription, cell division, and signal transduction.

MMSP is a member of the group of small blue round cell tumors (SBRCTs) of childhood, which also includes Ewing tumor (ET), neuroblastoma (NB), rhabdomyosarcoma, lymphoma, and desmoplastic small round cell tumor [5]. In 85% of ETs, the characteristic t(11;22)(q24;q12) rearrangement generates a *EWS-FLI1* fusion transcript encoded by the derivative 22 [7, 9]. In the remaining 15% of the cases, variant chromosome-22 translocations result in in-frame gene fusions with *ERG* [12, 32, 41], *ETV1* [17], *E1AF* [18], and *FEV* [27].

In the past, the differential diagnosis of SBRCTs has presented considerable challenge to pathologists. Even though the identification of tumor-specific chromosomal rearrangements within these entities led to the application of rapid and more accurate diagnostic methods [8], these were restricted to analyzing the expression levels of individual genes [31]. Recent developments have included the introduction of oligonucleotide microarray technology to facilitate tumor class prediction [13, 15]. These powerful tools permit the generation of genome-wide expression profiles and, when coupled with data analysis protocols, reveal entire clusters of differentially expressed genes. For example, Khan et al. [19] have demonstrated that the PAX3-FKHR chimeric protein, found in alveolar rhabdomyosarcomas, stimulates a myogenic transcription program that is not activated by normal PAX3.

GG-62 is a cell line previously thought to have originated from an atypical ET [36, 38]. Here, we present evidence that indicates the true identity of GG-62 as being a MMSP line. We demonstrate that GG-62 cells, in fact, express *EWS-ATF1* transcripts and, furthermore, characterize the genomic breakpoints. In order to identify differentially expressed genes in this MMSP cell line, which allows the discovery of specifically activated signaling pathways, we used expression microarrays to compare transcription profiles between GG-62 and ten other pediatric solid-tumor cell lines.

Materials and methods

Reverse-transcription polymerase chain reaction

Total RNA was prepared and reverse-transcribed using the First-Strand cDNA Synthesis Kit (Amersham Pharmacia Biotech). Reverse-transcription polymerase chain reaction (RT-PCR) for *EWS-FLI1* or *EWS-ERG* fusions was carried out as previously described [9, 29]. For detecting *EWS-ATF1* fusion transcripts using RT-PCR, first-strand cDNA obtained with a dT_{18} primer was used, and PCR employed primers A1 5′-CATGAGTGGCCCTGATAACC-3′ (*EWS*) and A2 5′-AGATGGGAGTTGGAACAGACA-3′ (*ATF1*) under the following conditions: 94°C for 4 min, followed by 35 cycles of 94°C for 30 s, 55°C for 30 s, and 72°C for 45 s. DNA products were purified (QIAquick PCR Purification Kit, Qiagen) and sequenced using the SequiTherm EXCEL II Long-Read DNA Sequencing Kit-ALF (automated laser fluorescence; Epicenter Technologies) according to the manufacturer's cycle sequencing protocol using Cy5-labeled primers A1 and A2, respectively. Gel electrophoresis, data collection, and analysis were performed on an ALFexpress sequencer (Amersham Pharmacia Biotech).

Southern-blot analysis of genomic DNA

Genomic DNAs were prepared according to the Puregene protocol (Biozym, Hess. Oldendorf, Germany). Five micrograms of DNA was digested (*Hin*d III or *Sac* I, Eurogentec; *Pst* I, Advanced Biotechnologies), electrophoresed on a 0.8% agarose gel, and transferred onto positively charged nylon membranes (Roche Diagnostics) using the VacuGene XL vacuum blotting system (Amersham Pharmacia Biotech) according to the manufacturer's hydrochloric acid depurination protocol. The membranes were hybridized overnight at 42°C with 20 µg/ml of an internal DIG-dUTP-labeled *EWS* probe spanning intron 9 generated by primers B1 5′-GCTTCAATAAGCCTGGTGGT-3′ and B2 5′-GTCCTTCATCCATGGGTCCT-3′. Chemiluminescent detection was carried out with anti-DIG-alkaline phosphatase (1:10000; Roche Diagnostics, Mannheim) and CSPD (1:100; Roche Diagnostics) according to the supplier's instructions. Signals were obtained by exposing X-ray film to the membranes for 3 h.

Cloning and sequencing the GG-62 EWS breakpoint

GG-62 genomic DNA was digested with *Pst* I (Advanced Biotechnologies). The fragments were self-ligated and subjected to nested inverse PCR using the Expand High Fidelity PCR System (Roche Diagnostics). First- and second-round PCR using primer pairs 5′-TGATCTGGCAGACTTCTTTAAGC-3′/ 5′-ATCTACAGGTGGGCCTTTCA-3′ and 5′-GCAGTGTGGGGTTGTTAAGG-3′/ 5′-TAGAGCTCGGGCCTTTCAGAGACAACAA-3′ (which introduces an additional GAGCTC-*Sac* I recognition sequence), respectively, were both performed as follows: (1) 94°C for 2 min, (2) 10 cycles of 94°C for 15 s, 58°C for 30 s, and 68°C for 4 min, (3) 25 cycles of 94°C for 15 s, 58°C for 30 s, and 68°C for 4 min adding 5 s per cycle, and (4) 68°C for 7 min. The 3.7-kb product was purified (QIAquick, Qiagen), and a 2.5-kb *Pst* I/*Sac* I fragment was cloned into pPCR-Script Amp SK(+) (Stratagene, La Jolla, Calif.). Subsequent sequencing of this clone using primer B2 was performed at Eurogentec (Belgium) on an ABI 377 Prism sequencer.

Cell culture

Besides the MMSP cell line (GG-62), six ET lines (CADO-ES-1, RD-ES, RM-82, SK-N-MC, VH-64, and WE-68) [36] and four NB lines (Kelly, NGP, SH-EP, and SH-SY5Y) [28, 30, 35] were included in our study. All cell lines were maintained under standard procedures as previously described [39].

Complementary RNA preparation and microarray hybridization

The preparation and processing of labeled and fragmented cRNA targets is detailed by Affymetrix (Santa Clara, Calif.). Total RNAs were prepared from cells using TRIzol reagent (Life Technologies). A T7-$(dT)_{24}$ primer (Eurogentec) was used to synthesize double-stranded T7-tailed cDNAs directly from 20 µg of each total RNA, as previously described [25] (SuperScript Choice System for cDNA Synthesis, Life Technologies). Biotinylated (BIO) cRNAs were in vitro transcribed from 0.5 µg of each cDNA (BIO-11-CTP and BIO-16-UTP; BioArray HighYield RNA Transcript Labeling Kit, Enzo Diagnostics) and fragmented. cRNA (10 µg) cocktails were hybridized to Affymetrix human cancer G110 arrays. The microarrays were washed as required (Affymetrix) and stained on a GeneChip Fluidics Station 400 using 10 µg/ml streptavidin-phycoerythrin (Molecular Probes, Ore.). Microarray images were obtained with a GeneArray Scanner (Hewlett Packard).

Microarray data analysis

GeneChip Analysis Suite 3.3 (Affymetrix) translated the scanned images into expression analysis files. The average fluorescence intensity of each array was scaled to that of SK-N-MC to permit direct comparisons. An average difference intensity value (AD, a numerical value corresponding to the expression level based on the hybridization fluorescence intensities) of 20 was assigned to all values below 20. Cluster analysis using Cluster 2.11 and TreeView 1.50 ([10]; http://rana.lbl.gov/) permitted visualization of these results. Gene probe sets were selected for cluster analysis based on two criteria: (1) an AD ratio (maximum AD/minimum AD) of at least 6.0 across the 11 samples and (2) at least one sample demonstrating a positive fraction value greater than 0.5.

Each sample hybridization was performed twice, and data analysis was based on the average value for the corresponding probe set.

Quantitative real-time PCR

For a selected set of genes, the microarray derived expression data were evaluated using quantitative PCR with the LightCycler system (Roche Diagnostics, Mannheim, Germany). cDNA was prepared using the first strand cDNA synthesis kit (Amersham Pharmacia, Freiburg, Germany) according to the manufactures protocol, and 2 µl was amplified in a 20-µl reaction containing 2 mM $MgCl_2$, 0.5 µM each primer, and LightCycler-DNA Master SYBR Green I mix. Neuregulin 1 (*NRG1*) cDNA was amplified using primers NRG1–1 (5′-AGATGTCCGAGCGCAAAG-3′) and NRG1–2 (5′-AACTGGTTTCACACCGAAGG-3′), the fibroblast growth factor 9 (*FGF9*) cDNA using primers FGF9–1 and FGF9–2 (5′-AGCCCGGTTTTGTTAAGTGA-3′ and 5′-GCTGTGGTCTTTCCTGGTTC-3′, respectively), and primers FGFR1–1 (5′-CTCTGAGTATGAGCTTCCCGA-3′) and FGFR1–2 (5′-CCACTTTGGTCACACGGTT-3′) were employed for quantifying the fibroblast growth factor receptor 1 (*FGFR1*). An initial denaturation at 95°C for 2 min was followed by 35 cycles of denaturation at 94°C for 1 s, annealing at 60°C for 10 s, and extension at 72°C for 10 s.

All examinations were performed in duplicate, and data analysis was done using the LightCycler Software. We employed a relative quantification method in which the gene-expression levels from the cell lines were compared with data from a dilution series (1:1, 1:2, 1:4, 1:8, 1:16, 1:32, 1:64) of the GG-62 sample. The specificity of the PCR products was confirmed with the LightCycler Software's melting-curve analysis feature.

Results

The cell line GG-62 was originally derived from a fibula-destructing tumor of a 25-year-old woman. Histological examination showed a PAS-positive round cell sarcoma with moderate mitotic activity. The tumor cells positively stained for S100 and vimentin (Fig. 1) but not for cytokeratin. Due to its unusual large-cell feature, the tumor was diagnosed as an atypical EWS [37].

Fig. 1 Histological characterization of tumor cells giving rise to GG-62. Tumor cells from fibula-destructing tumor in a 25-year-old female stained with haematoxylin and eosin (**a**), and positively for vimentin (**b**), and S100 (**c**)

We performed RT-PCR on total RNA isolated from GG-62 cells but failed to detect either *EWS-FLI1* or *EWS-ERG* fusions. Nevertheless, Southern-blot analysis revealed the presence of a *EWS* gene rearrangement. This was most prominent with *Hin*d III-digested DNA using a *EWS* intron 9 probe which liberated a 9-kb fragment that was not present in the normal control DNA (Fig. 2a). In ETs and even some rare SBRCTs of childhood, fusions between *EWS* and genes encoding DNA-binding proteins other than *FLI1* or *ERG* are known [21]. Therefore, we proceeded to determine whether or not the GG-62 cell line harbors one of these reciprocal *EWS* rearrangements. RT-PCR demonstrated that an *EWS-ATF1* mRNA was indeed present in this cell line. Moreover, sequencing of the PCR product demonstrated an in-frame fusion between *EWS* gene codon 325 and *ATF1* gene codon 65 (Fig. 2b) permitting the production of chimeric EWS-ATF1 oncoproteins. Together with the histological findings, these results led to the re-classification of GG-62 as a MMSP instead of a ET.

To support these results we sought to identify one of the genomic breakpoints corresponding to this gene rearrangement. First, we performed nested inverse PCR on *Pst* I-digested and self-ligated GG-62 genomic DNA. This resulted in a 3.7-kb product which was subsequently digested with *Pst* I and *Sac* I to generate a 2.5-kb fragment that was directionally cloned into pPCR-Script Amp SK(+). DNA sequencing of this clone revealed intronic sequences of *ATF1* joined to the *EWS* gene in intron 9 (Fig. 2c).

We investigated differential gene expression of GG-62 in comparison with six ETs and four NBs using Affymetrix human cancer G110 arrays carrying 1992 human cDNAs. These cDNAs represent over 1700 genes that have been associated with cancer. (Databases that contain complete expression data are available upon request.) Clustering of 463 differentially expressed genes is shown in Fig. 3a. The cell lines were readily grouped into two subclusters, and GG-62 was identified as being

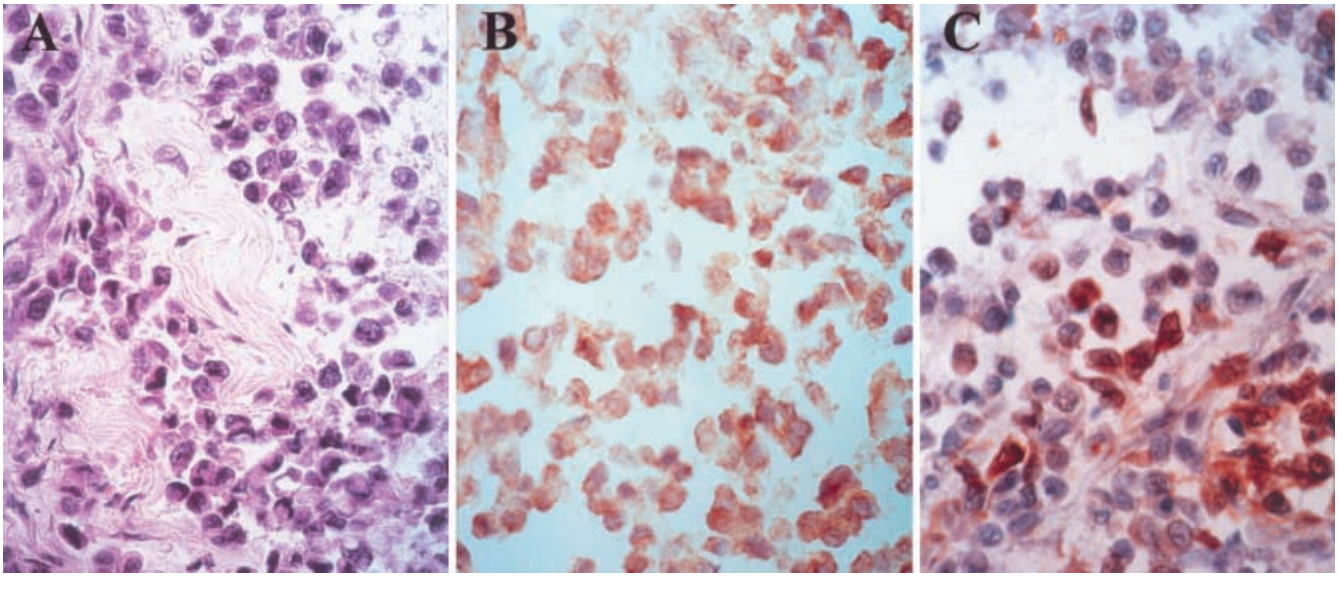

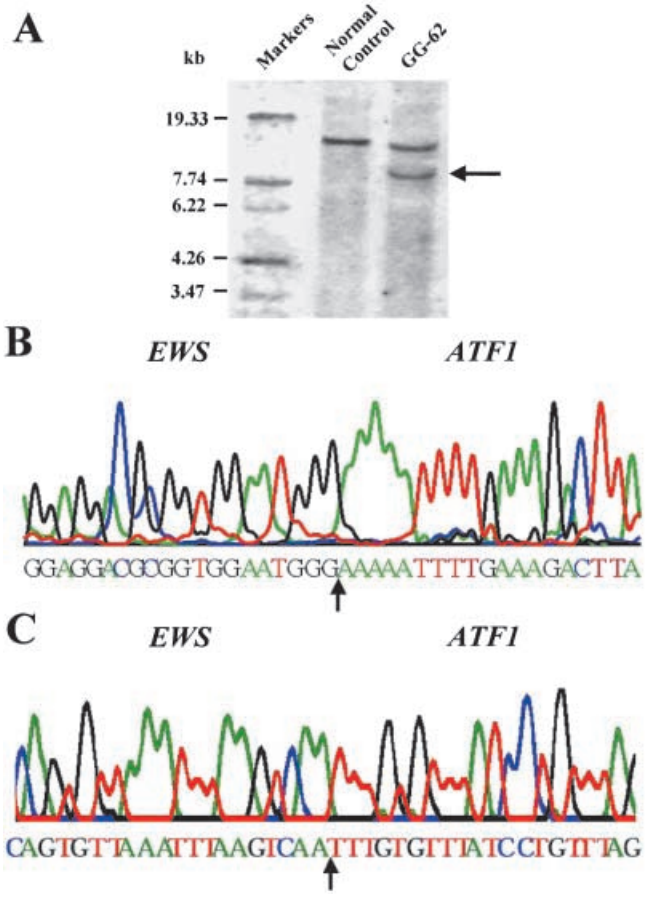

Fig. 2 Identification of Ewing sarcoma (*EWS*)-activating transcription factor 1 (*ATF1*) gene fusion in GG-62. **a** Southern-blot analysis of GG-62 DNA. *Hin*d III-digested genomic DNA (5 µg per lane) was loaded on a 0.8% agarose gel and transferred onto a nylon membrane. A 573-bp DIG-dUTP-labeled *EWS* intron 9 probe was hybridized to the filter. Both GG-62 and normal control DNA exhibited a 13-kb wild-type *EWS* band. An additional 9-kb fragment was observed in GG-62 (*arrow*) which indicates a rearrangement of the second *EWS* allele. **b** Cycle-sequencing analysis of reverse-transcription polymerase chain reaction (RT-PCR) products. RT-PCR was performed on GG-62 total RNA to detect *EWS-ATF1* chimeric transcripts. The products were analyzed using an automated laser-fluorescence sequencer. Sequence analysis revealed an in-frame fusion between *EWS* and *ATF1* sequences with the fusion junction indicated by an *arrow*. **c** Sequencing of genomic DNA. A DNA fragment containing the rearranged 3′-part of the *EWS* gene was cloned by reverse PCR amplification of the GG-62 genomic DNA using *EWS* exon 9 specific primers. Sequence analysis (Eurogentec, Belgium) revealed that this fragment spans to the breakpoint of the t(12;22)(q13;q12) translocation derived from the der(12). The gene fusion between *ATF1* and *EWS* is indicated by an *arrow*

more similar to the NB cell lines than ETs. However, a cluster of 36 probe sets exhibited markedly increased expression in GG-62 and separated the MMSP cell line clearly from the NBs and the ETs (Fig. 3b). These genes can be organized into distinct groups based on function and cellular localization (Table 1). For example, several genes encode cell surface receptors or ligands including avian erythroblastic leukemia viral oncogene homolog 3 (*ERBB3*), neuregulin 1 (*NRG1*), fibroblast growth factor 9 (*FGF9*), and fibroblast growth factor receptor-1 (*FGFR1*). Other genes are critical for cell cycle control including cyclin D2 (*CCND2*), thymidine kinase 1 (*TK1*), and yeast mitotic arrest deficient homolog-like 1 (*MAD1L1*).

Real-time PCR using the LightCycler system was used as an independent method for validation of microarray experiments and assessing relative gene expression for a subset of genes. *NRG1*-, *FGF9*-, and *FGFR1*-expression levels, determined using quantitative RT-PCR for GG-62, six ES cell lines and three NB samples were highly comparable to expression-microarray data (Fig. 4). For all the three genes, we could confirm that they are obviously upregulated in GG-62 relative to the ES and NB samples.

Apart from the clustering results, we also revealed increased levels of expression in GG-62 of several genes located at chromosome 12q13, telomeric to the 3′-end of the *ATF1* gene, which is activated by the t(12;22) rearrangement (Fig. 5). Expression data for five different genes located in this region were supplied by the GeneChip analyses. Within the set of eleven tumor cell lines analyzed, the four genes adjacent to the breakpoint clearly show the highest expression level in GG-62. These genes include *ERBB3*, nuclear receptor subfamily 4, group A, member 1 (*NR4A1)*, cyclin-dependent kinase 2 (*CDK2*), and alpha 5 integrin (*ITGA5*). Only the most distal (approximately seven megabases apart) gene, signal transducer and activator of transcription 6 (*STAT6*), shows no elevated mRNA level.

Discussion

Recurring chromosomal translocations are closely associated with the etiology of pediatric solid tumors. These rearrangements may either deregulate one partner gene

Fig. 3 a Hierarchical clustering of expression microarray data. Normalized expression data for the 11 cell lines was generated by GeneChip Analysis Suite 3.3. An average intensity difference (AD) of 20 was assigned to all values below 20. All 1992 gene probe sets were subjected to two criteria prior to cluster analysis: (1) an AD ratio (max AD/min AD) of at least 6.0 across the 11 samples and (2) at least one sample demonstrating a positive fraction greater than 0.5. Cluster 2.11 and TreeView 1.50 were used to analyze and visualize the remaining 463 filtered probe sets. In this cluster diagram, columns represent cell lines, while rows determine individual genes. Cluster analysis divided the 11 cell lines into two major groups, with GG-62 (*purple*) being grouped with the neuroblastoma cell lines (*green*) as opposed to the Ewing tumor samples (*blue*). Relative gene expression is indicated by color and ranges from highly increased (*intense red*) to highly decreased (*intense green*). A cluster of 36 genes (*purple bar*) was specifically upregulated in GG-62. **b** GG-62 specific gene cluster. This cluster comprises 36 genes which have increased expression predominantly in GG-62 including avian erythroblastic leukemia viral oncogene homologue 3 (*ERBB3*), neuregulin 1 (*NRG1*), fibroblast growth factor 9 (*FGF9*), and fibroblast growth factor receptor-1 (*FGFR1*). Other upregulated genes are *NR4A2* (nuclear receptor subfamily 4, group A, member 2) and *MAD1L1* (yeast mitotic arrest deficient homolog-like 1)

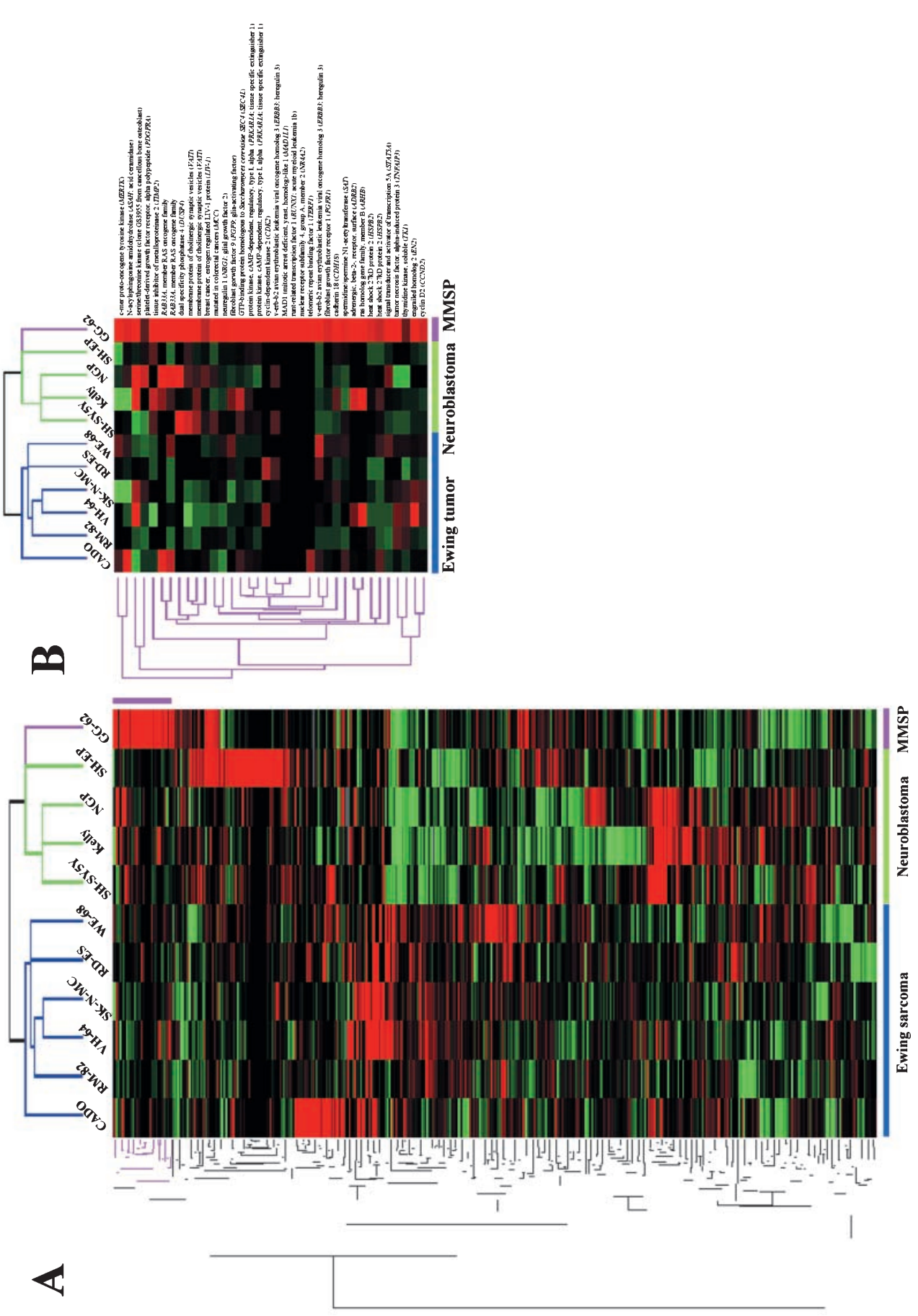

Fig. 3 Legend see page 479

Table 1 Genes differentially upregulated in GG-62 cells

Group	Abbreviation	Name
Secreted products	*FGF9*	Fibroblast growth factor 9 (glia-activating factor)
	NRG1	Neuregulin 1 (glial growth factor 2)
	TIMP2	Tissue inhibitor of metalloproteinase 2
Surface receptors/ Transmembrane proteins	*ADRB2*	Adrenergic, beta-2-, receptor, surface
	CDH18	Cadherin 18
	ERBB3	v-erb-b2 Avian erythroblastic leukemia viral oncogene homolog 3 (heregulin 3)
	FGFR1	Fibroblast growth factor receptor 1
	LIV-1	Breast cancer, estrogen regulated LIV-1 protein
	MERTK	c-mer Proto-oncogene tyrosine kinase
	MCC	Mutated in colorectal cancers
	PDGFRA	Platelet-derived growth factor receptor, alpha polypeptide
	VATI	Membrane protein of cholinergic synaptic vesicles
Cytoplasmic (signaling)	*ARHB*	Ras homolog gene family, member B
	PRKAR1A	Protein kinase, cAMP-dependent, regulatory, type I, alpha (tissue specific extinguisher 1)
	RAB33A	Member RAS oncogene family
Cytoplasmic (others)	*ASAH*	N-acylsphingosine amidohydrolase (acid ceramidase)
	HSPB2	Heat shock 27kD protein 2
	SAT	Spermidine/spermine N1-acetyltransferase
	SEC4L	GTP-binding protein homologous to *Saccharomyces cerevisiae* SEC4
	TK1	Thymidine kinase, soluble
Nuclear (cell cycle)	*CCND2*	Cyclin D2
	CDK2	Cyclin-dependent kinase 2
	MAD1L1	MAD1 (mitotic arrest deficient, yeast, homolog)-like 1
	TERF1	Telomeric repeat binding factor 1
Nuclear (transcription/DNA)	*EN2*	Engrailed homolog 2
	RUNX1	Runt-related transcription factor 1 (acute myeloid leukemia 1b)
	STAT5A	Signal transducer and activator of transcription 5A
	TNFAIP3	Tumor necrosis factor, alpha-induced protein 3
Nuclear (others)	*DUSP4*	Dual specificity phosphatase 4
	NR4A2	Nuclear receptor subfamily 4, group A, member 2
Unknown		Serine/threonine kinase (clone GS3955 from cancellous bone osteoblast)

or, more commonly, permit the expression of oncogenic fusion transcripts. However, these cytogenetic abnormalities have also proved to be useful as diagnostic and prognostic aids to assist the selection of the most appropriate treatment [26, 31]. These translocations frequently disrupt transcription-factor genes; this results in the ectopic, constitutive activation of both normal and novel target genes. Therefore, tumor-type specific functional pathways can be identified by generating and comparing gene expression profiles.

GG-62 is a cell line previously thought to be derived from an atypical ET. However, the identification of *EWS-ATF1* fusion transcripts has led to a new diagnosis of MMSP. This result underscores the value of molecular genetic detection of fusion transcripts in obtaining an accurate diagnosis. The t(12;22) in GG-62 cells results in hybrid transcripts with *EWS* codon 325 juxtaposed to *ATF1* codon 65. The predicted chimeric proteins consist of the N-terminal domain of EWS linked to the bZIP DNA-binding domain of ATF1 [42]. In order to identify characteristic signaling pathways, we performed gene expression analysis of GG-62 in comparison with cell lines derived from six ETs and four NBs. Cluster analysis of 463 differentially expressed genes revealed 36 genes specifically upregulated in GG-62.

We observed the increased expression of both *NR4A2* and *MAD1L1* in GG-62 cells. *NR4A2* expression is regulated by a 5′-flanking region which contains a CRE [34]. Similarly, *MAD1L1* expression is mediated by CREB/ATF-related transcription factors and can also be induced by HTLV-1 Tax oncoprotein [2]. Our results support the hypothesis that EWS-ATF1 may target promoters containing ATF-1 binding sites but which are normally regulated via other ATF-family members or other signals including Tax [1].

The cAMP-dependent transcription factors ATF1, CREB, and CREM, are activated by phosphorylation by protein kinase A (PKA). In the absence of cAMP-induction, the PKA catalytic subunits are sequestered and inactivated by regulatory subunits encoded by *PRKAR1A*. However, because EWS-ATF1 proteins lack a complete ATF1 N-terminal kinase-inducible domain, they function independently of activation by PKA [24]. Nevertheless, our observation of *PRKAR1A* upregulation in GG-62

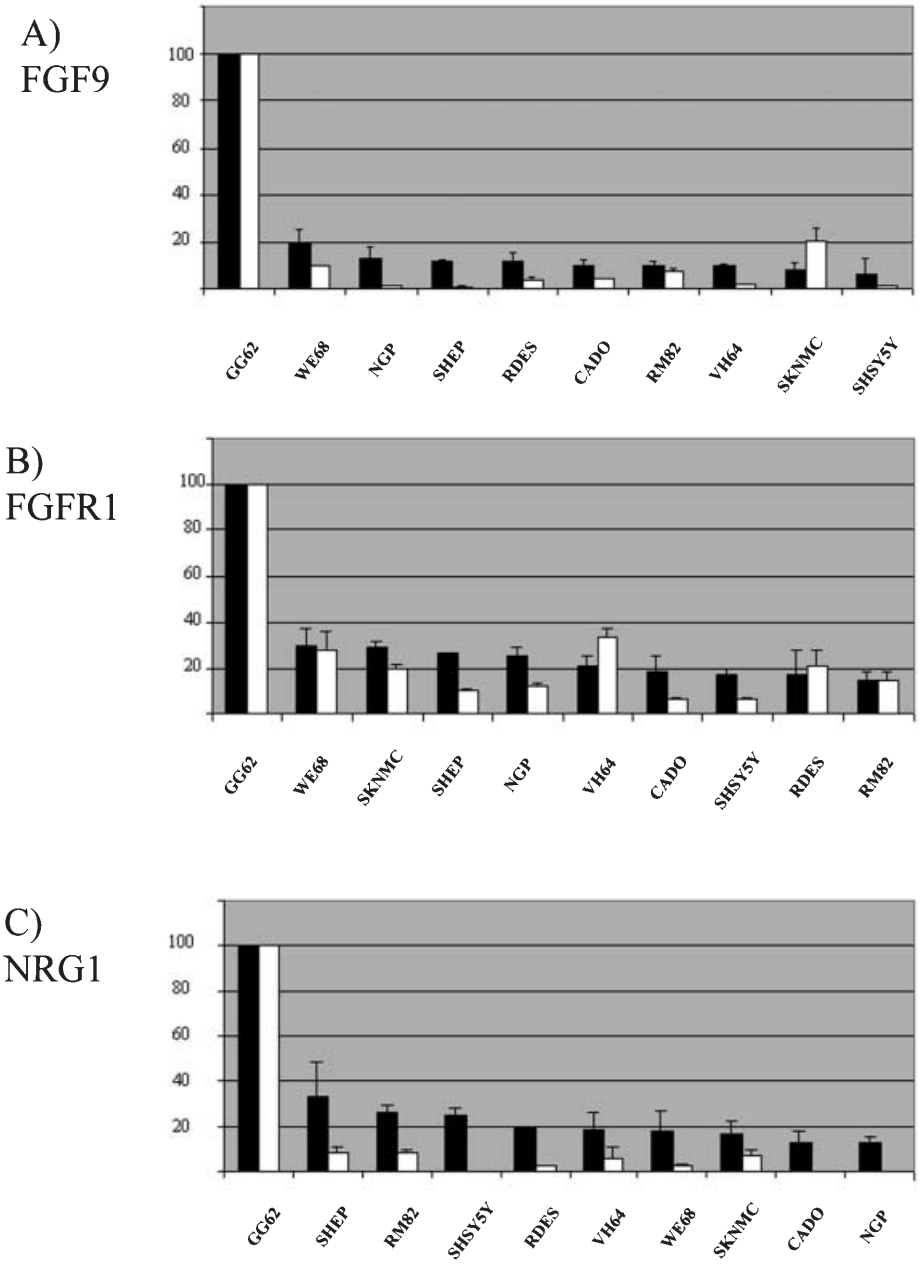

Fig. 4 Relative expression of *FGF9* (**a**), *FGFR1* (**b**), and *NRG1* (**c**) determined by expression microarrays and quantitative polymerase chain reaction. The average difference (*AD*) intensity values from GG-62, six Ewing tumor cell lines (CADO-ES-1, RD-ES, RM-82, SK-N-MC, VH-64, and WE-68) and three neuroblastoma samples (NGP, SH-EP, and SH-SY5Y) were compared with expression as determined by the LightCycler instrument. Both microarray AD values (*black*) and LightCycler concentrations (*white*) are expressed as percentages with respect to GG-62, the highest-expressing cell line. Each sample was analyzed in duplicate using both methods, and the *error bars* indicate one standard deviation. (Note: the relationship between microarray AD values and relative gene expression is not linear)

cells may indicate a futile attempt by the cells to counter the constitutive activity of EWS-ATF1.

Cluster analysis also identified genes that may not be directly upregulated by EWS-ATF1; nevertheless, they can be organized into distinct signaling pathways. We hypothesize that these additional genes are also required for maintaining a transformed or malignant phenotype. For example, *ERBB3* and *NRG1* encode a receptor tyrosine kinase and its ligand, respectively. The co-expression of this pair of genes suggests the presence of a specific autocrine loop which promotes cell growth and transformation. In fact, a NRG1-ERBB3 loop has been observed in differentiating embryonic rat muscle cells [20]. Two other upregulated genes are *FGF9* and *FGFR1*. Although FGF9 was characterized as a ligand mainly for FGFR3 [16], FGF9 has very recently been shown to modulate the expression of several *FGFRs* including *FGFR1* [4]. The maintenance of FGF9 production itself requires stimulation by the secreted Sonic Hedgehog (*SHH*) gene product [33], which is likely to have biological properties similar to those of another Hedgehog family member, Indian hedgehog (*IHH*), as demonstrated in studies of the chicken homologues *Shh* and *Ihh*, respectively [40]. Our microarray results indicate that IHH is, in fact, upregulated 3.5-fold in GG-62 compared with the lowest-expressing cell lines. Therefore, IHH production by GG-62 cells may initiate specific signaling pathways regulating *FGF9* and *FGFR1*. It

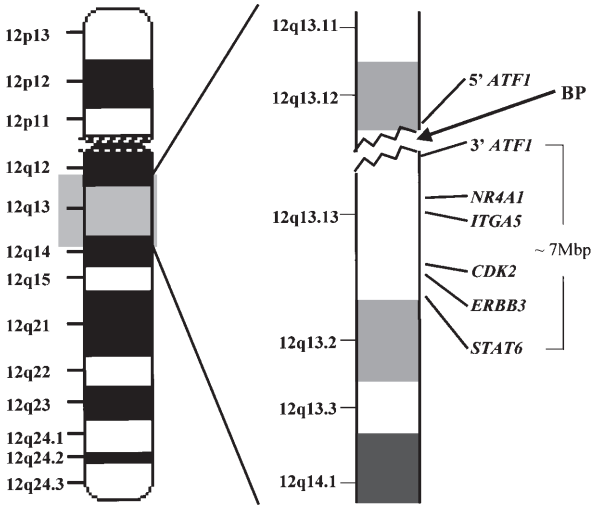

Fig. 5 Genes located on chromosome 12q13. Genes in the vicinity of the chromosome 12 breakpoint (*BP*) exhibited increased expression in GG-62. *ATF1* activating transcription factor 1, *CDK2* cyclin-dependent kinase 2, *ERBB3* avian erythroblastic leukemia viral oncogene homologue 3, *ITGA5* integrin, alpha 5, *NR4A1* nuclear receptor subfamily 4, group A, member 1, and *STAT6* signal transducer and activator of transcription 6, interleukin-4 induced. Localizations of genes and distances in mega-basepairs (*Mbp*) were obtained from the Entrez Map View human genome database build 22 at http://www.ncbi.nih.gov

remains to be determined whether MMSP cells also produce SHH or the Hedgehog signal transducers patched (PTC) and smoothened (SMO) [40] in addition to FGF9's receptor, FGFR3 [16].

For three of the genes mentioned above, quantitative RT-PCR was used to validate expression-microarray data. *NRG1*, *FGF9*, and *FGFR1* indeed could be confirmed to be upregulated particularly in GG-62 emphasizing the relevance of the signaling pathways involved.

A more detailed analysis of the raw expression data identified a group of genes including *CDK2*, *ERBB3*, *ITGA5*, and *NR4A1*, indicating GG-62 as having the highest expression levels among the cell lines analyzed in this study. These four genes are all located at chromosome 12q13 and telomeric to the 3′ end of *ATF1*, which is activated by the t(12;22) translocation. Only a fifth gene that was also differentially expressed across the 11 cell lines and which is the furthest away (seven megabases) from the chromosome-12 breakpoint, the interleukin-4 induced signal transducer and activator of transcription 6 (*STAT6*), was only moderately upregulated in GG-62 relative to the other samples. Our observations suggest that the t(12;22)(q13;q12) rearrangement found in GG-62, which is characteristic of MMSP, may also influence the expression of genes within close proximity to its breakpoints.

Oligonucleotide microarrays permit the simultaneous expression analysis of thousands of genes, and comparing the expression profiles by cluster analysis allows the clear distinction of the different tumor entities. Even if functional experiments are still required to evaluate the biological impact of our in silico data, we were able to show that these tools are particularly suitable to screen for the downstream targets of chimeric transcription factors which function in deregulating gene expression. In addition, our study brings to light signaling pathways that may be indispensable for the growth of the GG-62 tumor cells and may therefore serve as potential targets for novel therapies. While further experiments are required to investigate whether or not the pathways identified in GG-62 are relevant to MMSPs in general, our findings can provide important new clues in the etiology of this rare tumor.

Acknowledgements We sincerely thank Petra Fischer, Lydia Grote, Dagmar Haves, Petra Meier, Ulrike Neubert, Frauke Schmidt, and Anja Sommer for their excellent technical assistance. This study was supported by grants from IZKF Muenster (G2) and the DFG (Po 529/5–1).

References

1. Brown AD, Lopez-Terrada D, Denny C, Lee KA (1995) Promoters containing ATF-binding sites are de-regulated in cells that express the EWS/ATF1 oncogene. Oncogene 10: 1749–1756
2. Chen X, Zachar V, Chang C, Ebbesen P, Liu X (1998) Differential expression of Nur77 family members in human T-lymphotropic virus type 1-infected cells: transactivation of the TR3/nur77 gene by Tax protein. J Virol 72:6902–6906
3. Chung EB, Enzinger FM (1983) Malignant melanoma of soft parts. A reassessment of clear cell sarcoma. Am J Surg Pathol 7:405–413
4. Cohen RI, Chandross KJ (2000) Fibroblast growth factor-9 modulates the expression of myelin related proteins and multiple fibroblast growth factor receptors in developing oligodendrocytes. J Neurosci Res 61:273–287
5. Cohn SL (1999) Diagnosis and classification of the small round-cell tumors of childhood (comment). Am J Pathol 155: 11–15
6. Degryse HR (1997) Lesions of uncertain origin. In: De Schepper AM, Parizel PM, Ramon F, De Beuckeleer L, Vandevenne JE (eds) Imaging of soft tissue tumors, Springer, Berlin Heidelberg New York, pp 325–344
7. Delattre O, Zucman J, Plougastel B, Desmaze C, Melot T, Peter M, Kovar H, Joubert I, De Jong P, Rouleau G (1992) Gene fusion with an ETS DNA-binding domain caused by chromosome translocation in human tumours. Nature 359:162–165
8. Dockhorn-Dworniczak B, Schafer KL, Dantcheva R, Blasius S, Winkelmann W, Strehl S, Burdach S, van Valen F, Jurgens H, Bocker W (1994) Diagnostic value of the molecular genetic detection of the t(11;22) translocation in Ewing's tumours. Virchows Arch 425:107–112
9. Dockhorn-Dworniczak B, Schafer KL, Blasius S, Christiansen H, Koscielniak E, Ritter J, Winkelmann W, Jurgens H, Bocker W (1997) Assessment of molecular genetic detection of chromosome translocations in the differential diagnosis of pediatric sarcomas. Klin Padiatr 209:156–164
10. Eisen MB, Spellman PT, Brown PO, Botstein D (1998) Cluster analysis and display of genome-wide expression patterns. Proc Natl Acad Sci U S A 95:14863–14868
11. Fujimura Y, Ohno T, Siddique H, Lee L, Rao VN, Reddy ES (1996) The EWS-ATF-1 gene involved in malignant melanoma of soft parts with t(12;22) chromosome translocation, encodes a constitutive transcriptional activator. Oncogene 12:159–167
12. Ginsberg JP, de Alava E, Ladanyi M, Wexler LH, Kovar H, Paulussen M, Zoubek A, Dockhorn-Dworniczak B, Juergens H, Wunder JS, Andrulis IL, Malik R, Sorensen PH, Womer RB, Barr FG (1999) EWS-FLI1 and EWS-ERG gene fusions are associated with similar clinical phenotypes in Ewing's sarcoma. J Clin Oncol 17:1809–1814

13. Golub TR, Slonim DK, Tamayo P, Huard C, Gaasenbeek M, Mesirov JP, Coller H, Loh ML, Downing JR, Caligiuri MA, Bloomfield CD, Lander ES (1999) Molecular classification of cancer: class discovery and class prediction by gene expression monitoring. Science 286:531–537
14. Graadt van Roggen JF, Mooi WJ, Hogendoorn PC (1998) Clear cell sarcoma of tendons and aponeuroses (malignant melanoma of soft parts) and cutaneous melanoma: exploring the histogenetic relationship between these two clinicopathological entities. J Pathol 186:3–7
15. Harrington CA, Rosenow C, Retief J (2000) Monitoring gene expression using DNA microarrays. Curr Opin Microbiol 3: 285–291
16. Hecht D, Zimmerman N, Bedford M, Avivi A, Yayon A (1995) Identification of fibroblast growth factor 9 (FGF9) as a high affinity, heparin dependent ligand for FGF receptors 3 and 2 but not for FGF receptors 1 and 4. Growth Factors 12: 223–233
17. Jeon IS, Davis JN, Braun BS, Sublett JE, Roussel MF, Denny CT, Shapiro DN (1995) A variant Ewing's sarcoma translocation (7;22) fuses the EWS gene to the ETS gene ETV1. Oncogene 10:1229–1234
18. Kaneko Y, Yoshida K, Handa M, Toyoda Y, Nishihira H, Tanaka Y, Sasaki Y, Ishida S, Higashino F, Fujinaga K (1996) Fusion of an ETS-family gene, EIAF, to EWS by t(17;22)(q12;q12) chromosome translocation in an undifferentiated sarcoma of infancy. Genes Chromosomes Cancer 15:115–121
19. Khan J, Bittner ML, Saal LH, Teichmann U, Azorsa DO, Gooden GC, Pavan WJ, Trent JM, Meltzer PS (1999) cDNA microarrays detect activation of a myogenic transcription program by the PAX3-FKHR fusion oncogene. Proc Natl Acad Sci U S A 96:13264–13269
20. Kim D, Chi S, Lee KH, Rhee S, Kwon YK, Chung CH, Kwon H, Kang MS (1999) Neuregulin stimulates myogenic differentiation in an autocrine manner. J Biol Chem 274: 15395–15400
21. Kim J, Pelletier J (1999) Molecular genetics of chromosome translocations involving EWS and related family members (in process citation). Physiol Genomics 1:127–138
22. Kransdorf MJ, Murphey MD (1997) Neurogenic tumors. In: Kransdorf MJ, Murphey M (eds) Imaging of soft tissue tumors. Saunders, Philadelphia, pp 255–273
23. Lee KA, Masson N (1993) Transcriptional regulation by CREB and its relatives. Biochim Biophys Acta 1174:221–233
24. Li KK, Lee KA (1998) MMSP tumor cells expressing the EWS/ATF1 oncogene do not support cAMP-inducible transcription. Oncogene 16:1325–1331
25. Mahadevappa M, Warrington JA (1999) A high-density probe array sample preparation method using 10- to 100- fold fewer cells. Nat Biotechnol 17:1134–1136
26. Mitelman F (2000) Recurrent chromosome aberrations in cancer. Mutat Res 462:247–253
27. Peter M, Couturier J, Pacquement H, Michon J, Thomas G, Magdelenat H, Delattre O (1997) A new member of the ETS family fused to EWS in Ewing tumors. Oncogene 14: 1159–1164
28. Preis PN, Saya H, Nadasdi L, Hochhaus G, Levin V, Sadee W (1988) Neuronal cell differentiation of human neuroblastoma cells by retinoic acid plus herbimycin A. Cancer Res 48: 6530–6534
29. Reiner SL, Zheng S, Corry DB, Locksley RM (1993) Constructing polycompetitor cDNAs for quantitative PCR. J Immunol Methods 165:37–46
30. Sadee W, Yu VC, Richards ML, Preis PN, Schwab MR, Brodsky FM, Biedler JL (1987) Expression of neurotransmitter receptors and myc protooncogenes in subclones of a human neuroblastoma cell line. Cancer Res 47:5207–5212
31. Sorensen PH, Triche TJ (1996) Gene fusions encoding chimaeric transcription factors in solid tumours. Semin Cancer Biol 7:3–14
32. Sorensen PH, Lessnick SL, Lopez-Terrada D, Liu XF, Triche TJ, Denny CT (1994) A second Ewing's sarcoma translocation, t(21;22), fuses the EWS gene to another ETS-family transcription factor, ERG. Nat Genet 6:146–151
33. Sun X, Lewandoski M, Meyers EN, Liu YH, Maxson RE Jr, Martin GR (2000) Conditional inactivation of Fgf4 reveals complexity of signalling during limb bud development. Nat Genet 25:83–86
34. Torii T, Kawarai T, Nakamura S, Kawakami H (1999) Organization of the human orphan nuclear receptor Nurr1 gene. Gene 230:225–232
35. Van Roy N, Forus A, Myklebost O, Cheng NC, Versteeg R, Speleman F (1995) Identification of two distinct chromosome 12-derived amplification units in neuroblastoma cell line NGP. Cancer Genet Cytogenet 82:151–154
36. Van Valen F (1999) Ewing's sarcoma family of tumors. In: Masters JRW, Palsson B (eds) Human cell culture. Kluwer, London, pp 55–85
37. Van Valen F, Winkelmann W, Jurgens H (1992) Expression of functional Y1 receptors for neuropeptide Y in human Ewing's sarcoma cell lines. J Cancer Res Clin Oncol 118:529–536
38. Van Valen F, Winkelmann W, Jurgens H (1992) Type I and type II insulin-like growth factor receptors and their function in human Ewing's sarcoma cells. J Cancer Res Clin Oncol 118:269–275
39. Van Valen F, Hanenberg H, Jurgens H (1994) Expression of functional very late antigen-alpha 1, -alpha 2, -alpha 3 and -alpha 6 integrins on Ewing's sarcoma and primitive peripheral neuroectodermal tumour cells and modulation by interferon-gamma and tumour necrosis factor-alpha. Eur J Cancer 30A:2119–2125
40. Vortkamp A, Lee K, Lanske B, Segre GV, Kronenberg HM, Tabin CJ (1996) Regulation of rate of cartilage differentiation by Indian hedgehog and PTH-related protein (see comments). Science 273:613–622
41. Zoubek A, Dockhorn-Dworniczak B, Delattre O, Christiansen H, Niggli F, Gatterer-Menz I, Smith TL, Jurgens H, Gadner H, Kovar H (1996) Does expression of different EWS chimeric transcripts define clinically distinct risk groups of Ewing tumor patients? J Clin Oncol 14:1245–1251
42. Zucman J, Delattre O, Desmaze C, Epstein AL, Stenman G, Speleman F, Fletchers CD, Aurias A, Thomas G (1993) EWS and ATF-1 gene fusion induced by t(12;22) translocation in malignant melanoma of soft parts. Nat Genet 4:341–345

Virchows Arch (2002) 440:485–490
DOI 10.1007/s00428-001-0547-z

ORIGINAL ARTICLE

Jo Van Dorpe · Paola Dal Cin
Stanislawa Weremowicz · Fred Van Leuven
Ivo de Wever · Herman Van den Berghe
Christopher DM Fletcher · Raf Sciot

Translocation of the *HMGI-C* (*HMGA2*) gene in a benign mesenchymoma (chondrolipoangioma)

Received: 25 July 2001 / Accepted: 5 September 2001 / Published online: 7 November 2001
© Springer-Verlag 2001

Abstract Mesenchymomas are neoplasms in which there are at least two types of differentiated cells of mesenchymal derivation other than fibrous tissue. Chondrolipoangioma is a rare type of mesenchymoma composed predominantly of cartilage and adipose tissue with vascular elements and myxoid tissue present in lesser proportions. Cytogenetic analysis was performed on a case of chondrolipoangioma and revealed a t(12;15) (q13;q26) as the sole chromosome abnormality in 40 metaphases analyzed. However, using fluorescence in situ hybridization (FISH) analysis, a complex rearrangement was found involving chromosomes 2, 12, and 15, with a cryptic rearrangement of the gene (*HMGI-C*; *HMGA2*) coding for high-mobility group I protein. This finding suggests a role for the *HMGI-C* gene also in the pathogenesis of this uncommon benign tumor type, in addition to its well-established role in the pathogenesis of common benign tumors such as lipomas, uterine leiomyomas, pulmonary chondroid hamartomas, and endometrial polyps.

Keywords Chondrolipoangioma · Cartilage-containing benign mesenchymoma · Fluorescence in situ hybridization · Conventional cytogenetic analysis · HMGI-C · HMGA2

J. Van Dorpe · R. Sciot (✉)
Department of Pathology, University Hospital St.-Raphaël, Katholieke Universiteit Leuven, Minderbroedersstraat 12, 3000 Leuven, Belgium
Tel.: +32-16-336540, Fax: +32-16-336548

J. Van Dorpe
Department of Pathology, AZ VUB Jette, Laarbeeklaan 101, 1090 Brussels, Belgium

F. Van Leuven · H. Van den Berghe
Center for Human Genetics, Katholieke Universiteit Leuven, Gasthuisberg O & N, Leuven, Belgium

P. Dal Cin · S. Weremowicz · C.D.M. Fletcher
Department of Pathology, Brigham and Women's Hospital, Boston, Massachusetts, USA

I. de Wever
Surgical Oncology, University Hospitals, Katholieke Universiteit Leuven, Leuven, Belgium

Introduction

Mesenchymoma was established as a distinct pathological entity by Stout in 1948 [16]. He defined it as a distinct neoplasm composed of two or more mesenchymal elements not ordinarily found together in a tumor – such as bone and cartilage. "Undifferentiated" and "fibrosarcomatous" or "fibrous" areas are present in a wide range of mesenchymal tumors and therefore must not be counted as one of the components [11]. Stout's original article dealt only with malignant tumors, but he stated that the tumor occurred in both benign and malignant forms. Benign mesenchymoma constitutes a heterogeneous group of tumors. Angiomyolipomas, angiolipomas, and chondrolipomas could be described as benign mesenchymomas, but the term is more often used for rare tumors with a complex mixture of mesenchymal tissues. A subgroup of benign mesenchymomas are composed of cartilage, mature fat, and vascular elements and can be described as chondrolipoangiomas (or cartilage-containing benign mesenchymomas) [3, 9]. To the best of our knowledge, cytogenetic analysis of this type of benign mesenchymoma has not been reported previously. Here, we report a benign mesenchymoma (chondrolipoangioma) exhibiting a t(12;15)(q13;q26) with a cryptic rearrangement of the gene (*HMGI-C*; *HMGA2*) coding for the high-mobility group I protein.

Clinical history

A 50-year-old man presented with a painless mass in the right buttock, which had been present for several months, causing numbness of the right leg when sitting down. Physical examination revealed a mass with a diameter of 8 cm located posterior to the greater trochanter of the right hip. Motor and sensory examination of the right leg were normal. Plain radiographs revealed a partially calcified mass adjacent to the right hip. Magnetic resonance imaging showed a well-circumscribed partially calcified mass deep in the gluteal muscles, posterior to the femoral neck and lateral to the sciatic nerve. Metastatic work-up of the lungs, liver, and bones was negative. An incisional biopsy was performed. The biopsy showed "neoplastic" fat and myxoid tissue with calcifications. A

definitive diagnosis was not possible on this material. The tumor was completely excised with a rim of uninvolved muscle and soft tissue. The patient was without evidence of recurrence 4 years postoperatively.

Materials and methods

The incisional biopsy and the resection specimen were received fresh. Fragments from the incisional biopsy and from the lesion in the resection specimen were used for short-term culturing (4 days) after overnight disaggregation with collagenase, as described previously [8, 12]. Chromosome analysis was performed on G-banded metaphases. The remaining tissue was fixed in neutral buffered formalin (6%). Ossified parts of the resection specimen were decalcified in ethylene diamine tetraacetic acid (EDTA) after fixation. Multiple tissue blocks were embedded in paraffin, cut to 5 µm, and stained with hematoxylin and eosin. Selected paraffin sections were immunohistochemically stained with antibodies against S100 protein (polyclonal, 1:500; Dako, Glostrup, Denmark), alpha smooth muscle actin (monoclonal antibody, 1:200; Sigma, St. Louis, Mo.), desmin (monoclonal antibody, 1:20; Eurodiagnostics, Apeldoorn, the Netherlands), cytokeratin (monoclonal antibody KL1, 1:75; Immunotech, Marseille, France), and epithelial membrane antigen (monoclonal antibody, 1:50; Dako) using a three-step immunoperoxidase procedure.

Fluorescence in situ hybridization (FISH) with biotin- and digoxigenin-labeled cosmids 142H1 and 27E12, which map to the 5′ and 3′ region of the *HMGI-C* gene, respectively, was performed on metaphase spreads from the tumor culture, as previously described [19]. Further FISH investigation was performed on the same tumor metaphase cell spreads with the alpha satellite DNA probes specific for the centromeric region of chromosomes 1, 2, and 3 (A-group chromosomes; Oncor, Gaithersburg, Md.).

Results

The incisional biopsy had a diameter of 1.5 cm and consisted of adipose tissue showing fat cells of varying diameters and myxoid tissue. The resection specimen contained a 10×7×7-cm measuring mass (Fig. 1). The mass was well circumscribed and could be enucleated from the surrounding skeletal muscle. The cut surface had a variegated appearance. Fat, cartilage, and bone could be recognized macroscopically. Rare small cysts were seen in the cartilaginous areas. The tumor was extensively sampled for microscopic analysis. Histologically, mature adipose tissue and cartilage were the two predominant tissues (Fig. 2). Other components of the tumor were myxoid tissue, bone, fibrous tissue, smooth muscle, and aberrant blood vessels. The different components were intermixed in a haphazard fashion. The adipose tissue consisted of irregular lobules separated by incomplete fibrous septa of varying thickness (Fig. 2a). The fat cells showed some variation in size and shape. Lipoblasts, however, were not present. Cell nuclei were eccentrically placed, small, and flattened. Nuclear atypia was not seen. Large areas of the adipose tissue had a prominent myxoid matrix, but a delicate plexiform capillary pattern typical for myxoid liposarcoma was not present. The areas with cartilaginous differentiation were intermingled with the adipose tissue. There were

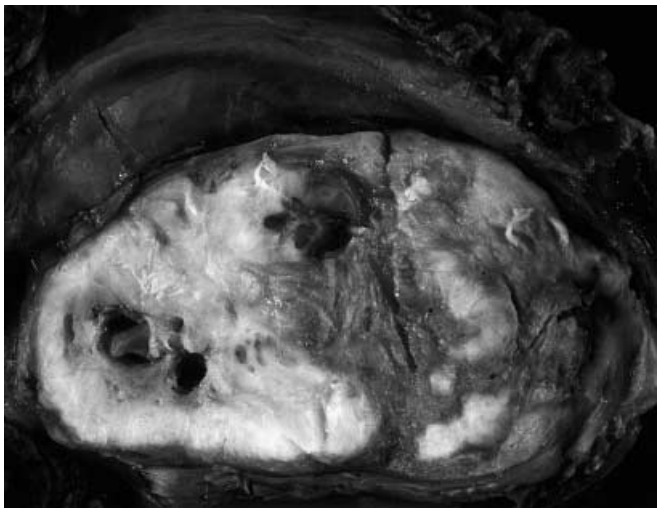

Fig. 1 The tumor is well circumscribed. The cut surface has a variegated appearance. Fat and cartilage are the main components and can be recognized macroscopically

chondromyxoid areas as well as large areas of mature hyaline cartilage (Fig. 2b, c). The hyaline cartilage showed foci with increased cellularity, but there was only minimal pleomorphism, and mitoses were absent. Areas of ossification consisting of mature trabecular bone and intertrabecular mature fat were present in the cartilage (Fig. 2b). The myxoid component was moderately cellular and was composed of delicate spindle or stellate cells and abundant mucoid material. In most areas, there was a gradual transition between myxoid tissue, adipose tissue (adipose tissue with myxoid matrix), and cartilage (chondromyxoid areas). The adipose tissue and the myxoid tissue showed angiomatous areas with dilated thin-walled vessels and abnormally formed, thick-walled vessels; the vascular lumina were sometimes eccentrically placed (Fig. 2d). Irregularly distributed compact bundles of smooth muscle cells and fibrous septa were present in the angiomatous areas. A rim of compressed fibrous tissue was present at the periphery of the tumor. Immunohistochemical staining for alpha smooth muscle actin and desmin confirmed the presence of compact bundles of smooth muscle cells. The chondrocytes and adipocytes stained for S100 protein, but the spindle cells did not show neural differentiation. Staining for cytokeratin and epithelial membrane antigen was negative.

All 40 G-banded metaphases obtained from 3-day-old cultures of both the incisional biopsy and the lesion in the resection specimen showed a t(12;15)(q13;q26) as

Fig. 2 **a** Low-power view showing adipose tissue. The fat lobules are irregular and separated by incomplete fibrous septa. Hematoxylin and eosin (HE), ×26. **b** Low-power view showing hyaline cartilage and mature trabecular bone. HE, ×26. **c** Chondromyxoid tissue and adipose tissue with a myxoid matrix. HE, ×42. **d** Fibrous tissue with numerous abnormally formed, thick-walled vessels (angiomatous tissue). HE, ×42 ▶

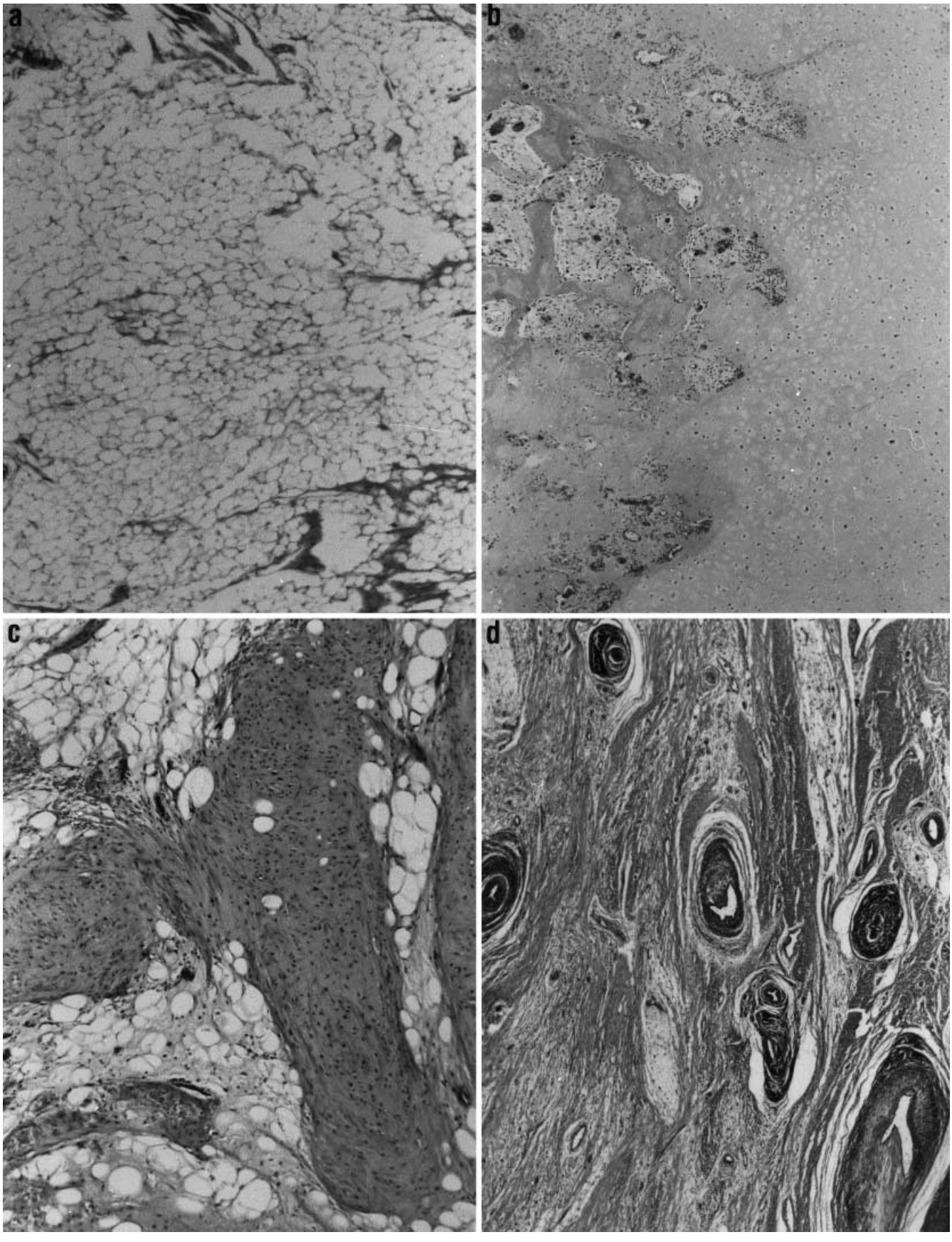
a
b
c
d

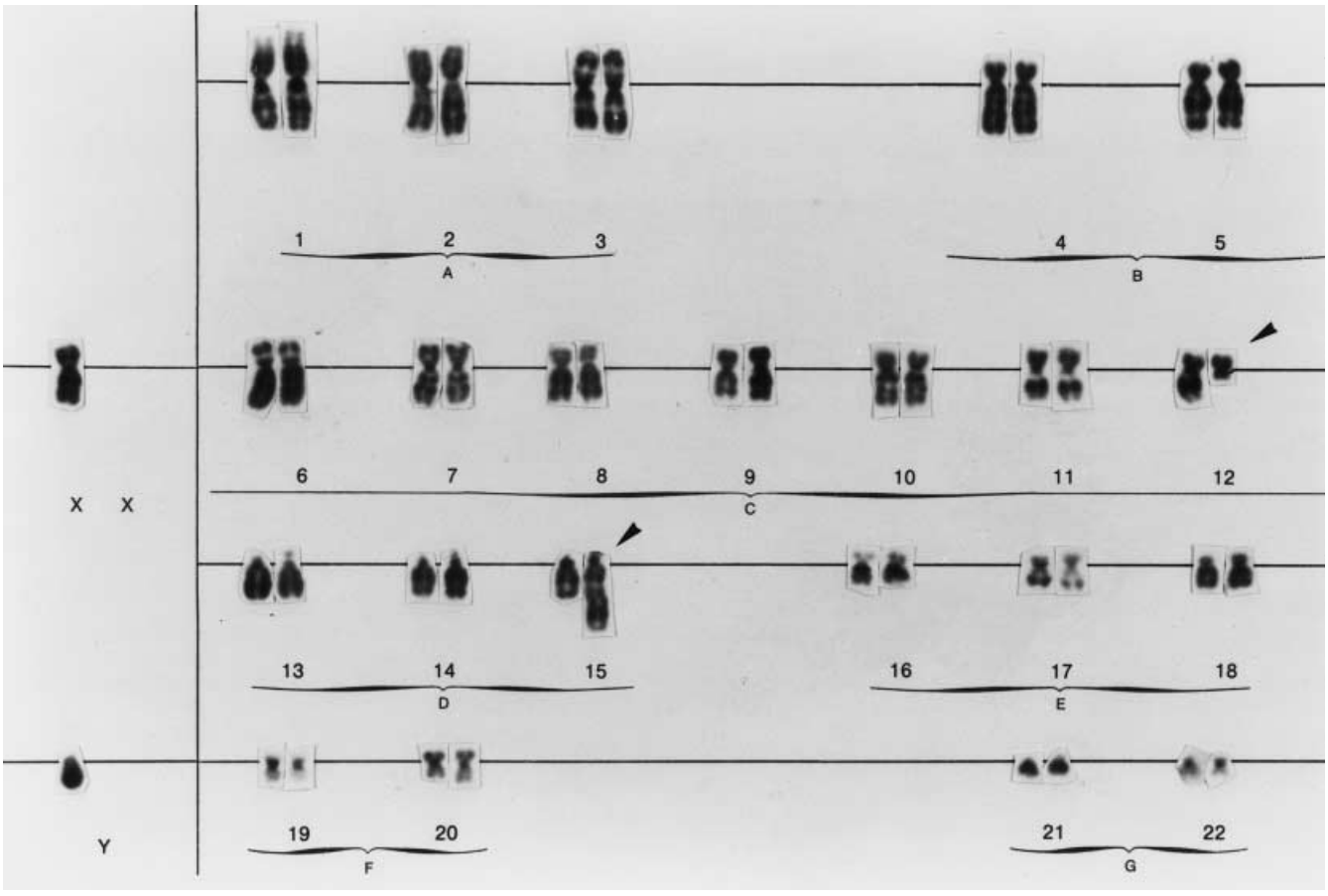

Fig. 3 G-banded metaphase showing t(12;15)(q13;q26)

the sole chromosomal abnormality (Fig. 3). A normal male karyotype was found on phytohemagglutinin (PHA)-stimulated peripheral lymphocytes.

FISH analysis performed with *HMGI-C* specific cosmids 142H1 (5′) and 27E12 (3′) revealed an unexpected (cryptic) complex chromosome rearrangement. Both cosmids hybridized to the normal chromosome 12 and to an unidentified A-group chromosome (data not shown). This chromosome was subsequently identified using FISH as derivative chromosome 2, der(2), using the 27E12 cosmid and the chromosome-specific alpha satellite DNA probe (D2Z; Oncor) (Fig. 4a, b). The breakpoints at chromosome 12 occurred at the 5′ end of the *HMGI-C* proximal to the 142H1 cosmid and at the 3′ end of the *HMGI-C* distal to the 27E12 cosmid, resulting in translocation of the entire *HMGI-C* gene to the telomeric region of the long (q) arm of derivative chromosome 2, der(2). The remaining 12q was subsequently translocated to the 15q26 band, as suspected by conventional cytogenetic analysis.

Discussion

The tumor had the typical features of a lesion reported variably in the literature as chondrolipoangioma [9] or cartilage-containing benign mesenchymoma [3] and fitted the definition of benign mesenchymoma [16]. The chondrolipoangioma contained fat cells with some variation in size and shape and cartilage with foci of increased cellularity, but morphological indicators to support a diagnosis of liposarcoma, such as lipoblasts, significant nuclear pleomorphism, increased mitotic activity, or infiltration, were absent [4]. Foci of hyaline cartilage have been reported in some myxoid liposarcomas, but other patterns of mesenchymal differentiation were not present in these cases [15].

Ten well-documented cases of chondrolipoangioma have been reported in the literature [1, 3, 5, 7, 9, 14, 17]. Patients with a chondrolipoangioma have ranged in age from 7 years to 55 years. Most chondrolipoangiomas are well circumscribed and occur in the soft tissues of the limbs or the trunk. Recurrences or malignant behavior have never been reported. Some authors consider benign mesenchymomas to be hamartomatous malformations [2], but the presence of a clonal chromosomal aberration in the present case supports the neoplastic nature of chondrolipoangiomas. Malignant transformation has never been reported in a benign mesenchymoma [3].

The genes coding for the HMGI proteins, *HMGI-C* (*HMGA2*) on chromosome 12q15 and *HMGI*(*Y*) (*HMGA1b*) on chromosome 6p21, are increasingly implicated in the pathogenesis of a variety of malignant and benign tumors [18]. Specific chromosomal rearrange-

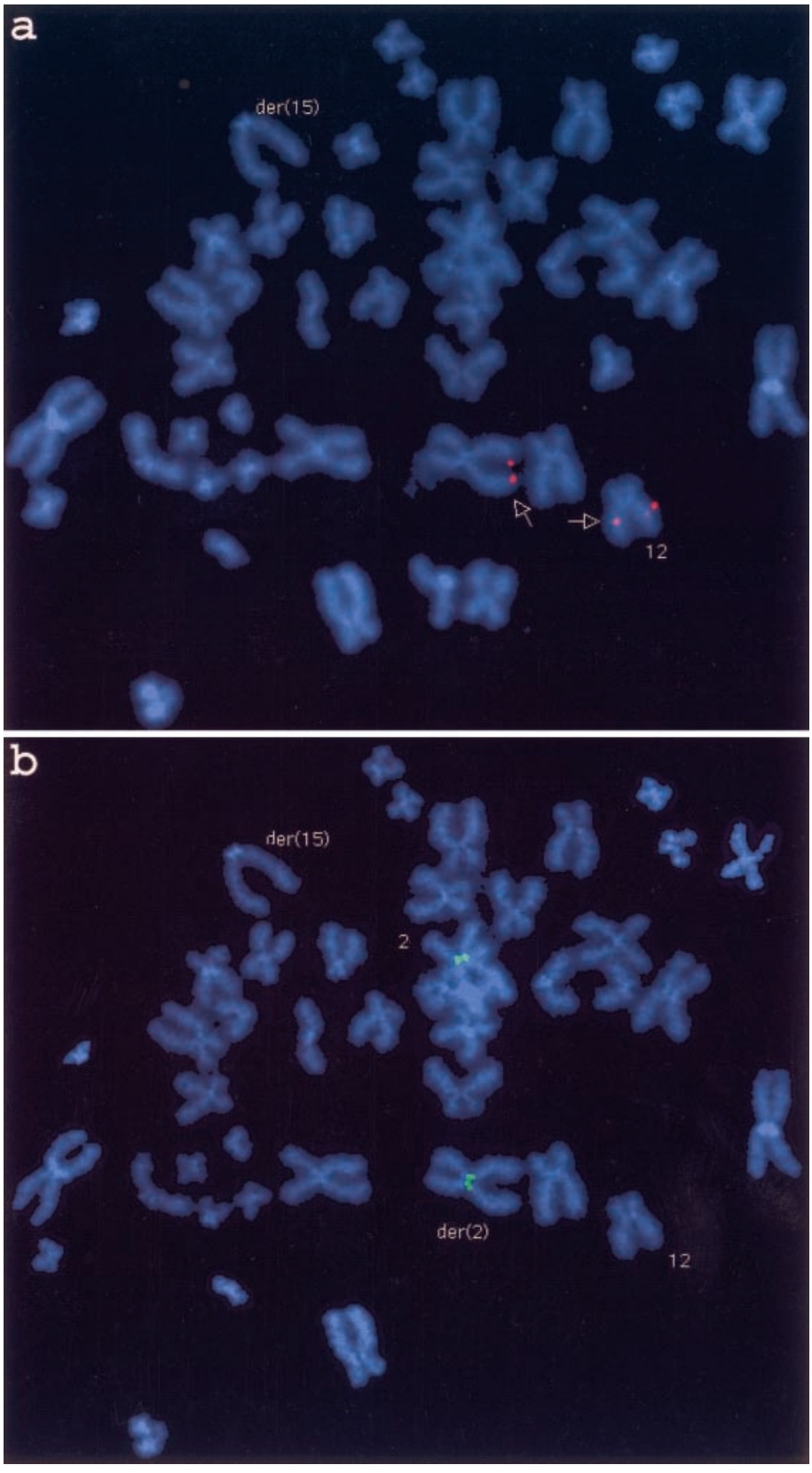

Fig. 4 **a** Representative tumor metaphase cell showing the hybridization signals (*red*) for cosmid 27E12, specific for the 3′ end of the *HMGI-C*, on the normal chromosome 12 and one of the A-group chromosomes (*arrows*). **b** Same metaphase cell hybridized with alpha satellite probe specific for the centromeric region of chromosome 2 (D2Z; Oncor). Hybridization signals are present on a normal chromosome 2 and on the derivative chromosome 2, der(2), carrying the *HMGI-C* gene

ments involving the *HMGI-C* or *HMGI*(*Y*) gene are the most frequent chromosomal alterations in common benign tumors such as lipomas, uterine leiomyomas, hamartomas of the lung and breast, fibroadenomas of the breast, pleomorphic adenomas of salivary gland, and endometrial polyps. In the present case, FISH analysis showed a complex rearrangement involving chromosomes 2, 12, and 15, resulting in translocation of an entire copy of the *HMGI-C* gene. Rearrangements of the *HMGI-C* gene in benign tumors often result in intragenic rearrangements leading to chimeric fusion products, but transfer of the entire coding region of the gene (5′ break of the *HMGI-C* gene), as seen in this chondrolipoangioma, have also been reported in other benign tumors, such as pulmonary chondroid hamartoma [6], but most commonly in uterine leiomyomas [13]. It is thought that translocation of the *HMGI-C* gene results in deletion of silencer promoter elements or in juxtaposition to enhancer elements leading to dysregulation of *HMGI-C* expression.

Although uncommon, complex rearrangements involving the *HMGI-C* gene are sometimes seen in other benign tumors such as uterine leiomyomas and lipomas [10]. Interestingly, in these tumors the complex rearrangements do not seem to correlate with any histopathologic or clinical feature. In conclusion, we report translocation of the *HMGI-C* gene in a rare benign mesenchymoma. The finding of this rearrangement also in uncommon tumors with distinctive morphology underscores the important and widespread role of *HMGI* genes in the pathogenesis of human neoplasia.

Acknowledgements This text presents research results of the Belgian program of Interuniversity Poles of Attraction initiated by the Belgian State, Prime Minister's Office, Science Policy Programming. The authors want to thank Mr. M. Rooseleers for preparing the photographs.

References

1. Batliwalla RK, Deshpande CK (1966) Benign mesenchymoma: a case report. Indian J Cancer 3:131–135
2. Dehner LP (1975) Somatic soft tissues. In: Kissane JM (ed) Pathology of infancy and childhood, 2nd edn. CV Mosby, St Louis, pp 1139–1171
3. Dorfman HD, Levin S, Robbins H (1980) Cartilage-containing benign mesenchymomas of soft tissue: report of two cases. J Bone Joint Surg 62:472–475
4. Enzinger FM, Weis SW (eds) (1995) Soft tissue tumors, 3rd edn. CV Mosby, St Louis, pp 431–466
5. Hudson TM, Bertoni F, Enneking WF (1985) Case report: computed tomography of a benign mesenchymoma of soft tissue. J Comput Assist Tomogr 9:205–208
6. Kazmierczak B, Meyer-Bolte K, Tran KH, Wockel W, Breightman I, Rosigkeit J, Bartnitzke S, Bullerdiek J (1999) A high frequency of tumors with rearrangements of genes of the HMGI(Y) family in a series of 191 pulmonary chondroid hamartomas. Genes Chromosomes Cancer 26:125–133
7. Le Ber MS, Stout AP (1962) Benign mesenchymomas in children. Cancer 15:598–605
8. Limon J, Dal Cin P, Sandberg AA (1986) Application of long-term collagenase disaggregation for the cytogenetic analysis of human solid tumors. Cancer Genet Cytogenet 23:305–313
9. Milchgrub S, McMurry NK, Vuitch F, Dorfman HD (1990) Chondrolipoangioma: a cartilage-containing benign mesenchymoma of soft tissue. Cancer 66:2636–2641
10. Mitelman F (ed) (1998) Catalog of chromosome aberrations in cancer '98, version 1. CD-ROM. John Wiley & Sons, New York
11. Newman PL, Fletcher CDM (1991) Malignant mesenchymoma: clinicopathologic analysis of a series with evidence of low-grade behaviour. Am J Surg Pathol 15:607–614
12. Peakman CD, Moreton MF, Robinson A (1977) Prenatal diagnosis: techniques used to help in ruling out maternal cell contamination. J Med Genet 14:37–39
13. Schoenberg Fejzo M, Ashar HR, Krauter KS, Powell WL, Rein MS, Weremowicz S, Yoon SJ, Kucherlapati RS, Chada K, Morton CC (1996) Translocation breakpoints upstream of the HMGIC gene in uterine leiomyomata suggest dysregulation of this gene by a mechanism different from that in lipomas. Genes Chromosomes Cancer 17:1–6
14. Setoyama M, Miyauchi H, Kanekura T, Tashiro M (1985) A case of benign mesenchymoma containing cartilageous tissue components with enchondral ossification. J Dermatol 12:519–525
15. Siebert JD, Williams RP, Pulitzer DR (1996) Myxoid liposarcoma with cartilaginous differentiation. Mod Pathol 9:249–252
16. Stout AP (1948) Mesenchymoma, the mixed tumor of mesenchymal derivatives. Ann Surg 127:278–290
17. Takato T, Soyano S, Naka Y, Mishina M (1984) Benign mesenchymoma of the sole. Ann Plast Surg 13:150–153
18. Tallini G, Dal Cin P (1999) HMGI(Y) and HMGI-C dysregulation: a common occurrence in human tumors. Adv Anat Pathol 6:237–246
19. Weremowicz S, Morton CC (1999) Is HMGIC rearranged due to cryptic paracentric inversion of 12q in karyotypically normal uterine leiomyomas? Genes Chromosomes Cancer 24:172–173

Virchows Arch (2002) 440:491–497
DOI 10.1007/s00428-001-0544-2

ORIGINAL ARTICLE

Laura Masi · Cecilia Malentacchi
Domenico Campanacci · Alessandro Franchi

Transforming growth factor-β isoform and receptor expression in chondrosarcoma of bone

Received: 25 June 2001 / Accepted: 23 August 2001 / Published online: 20 October 2001
© Springer-Verlag 2001

Abstract It has been shown that transforming growth factor-β (TGF-β) has a potent stimulatory effect on the growth of chondrosarcoma cells in vitro. In order to examine the production of this family of growth factors and their receptors in vivo, we studied the expression of TGF-β isoforms 1, 2, and 3 and of TGF-β receptor types I and II (TGF-βRI and TGF-βRII) in a series of 24 chondrosarcomas of bone using immunohistochemistry and reverse-transcription polymerase chain reaction analysis. For comparison, five enchondromas and five osteochondromas were also analyzed. TGF-β1 was expressed in 3 benign lesions (30%) and 18 chondrosarcomas (75%), with a significantly higher expression in grade-2 and -3 tumors than in grade-1 tumors (P=0.002). TGF-β2 was identified in 8 benign lesions (89%) and 21 chondrosarcomas (87.5%), with increased expression in grade-2 and -3 chondrosarcomas in comparison with grade-1 tumors (P=0.05). TGF-β3 was detected in 6 benign lesions (60%) and 17 chondrosarcomas (70.8%), with no significant differences between chondrosarcomas of different histologic grade (P=0.6). Twenty-three chondrosarcomas (95.8%) expressed both TGF-β receptor types I and II. Reverse-transcription polymerase chain reaction analysis performed on ten chondrosarcomas confirmed the presence of low or absent levels of TGF-β1 and -β2 mRNA in grade-1 chondrosarcomas, while grade-2 chondrosarcomas presented high levels of transcript of both cytokines. High levels of TGF-βRI and RII mRNA were also detected. Chondrosarcomas with TGF-β1 and TGF-β2 overexpression (>20% of tumor cells) had a significantly higher expression of the cell proliferation marker MIB-1 (P=0.006 and P=0.0003, respectively), while no significant correlation was found between TGF-β3 expression and proliferative activity (P=0.5). When TGF-β isoform and receptor expression were examined with respect to disease-free survival, TGF-β1 overexpression was significantly associated with a shorter disease-free survival (P=0.004, log-rank test). Our data indicate that TGF-β isoforms are produced by neoplastic cells of chondrosarcomas and could have a potential role as autocrine growth stimulators in these neoplasms.

Keywords Chondrosarcoma · TGF-β · TGF-β receptors · Immunohistochemistry · mRNA

L. Masi
Endocrine Unit, University of Florence Medical School, Florence, Italy

C. Malentacchi
Section of Human Genetics, Department of Physiopathology, University of Florence Medical School, Florence, Italy

D. Campanacci
Unit of Orthopedic Oncology, Azienda Ospedaliera Careggi, Florence, Italy

A. Franchi (✉)
Department of Human Pathology and Oncology, Viale G.B. Morgagni 85, 50134 Florence, Italy
e-mail: franchi@unifi.it
Tel.: +39-55-416951, Fax: +39-55-4379868

Introduction

Transforming growth factor β (TGF-β) is a potent cell regulatory peptide that variably affects proliferation, differentiation, and extracellular matrix synthesis. At least three TGF-β isotypes with similar biologic activities have been identified in mammals, which exert their autocrine/paracrine functions through the interaction with specific heterodimeric receptor complexes formed by two different transmembrane proteins (TGF-βRI and TGF-βRII) [26]. High contents of TGF-β1 are accumulated in cartilage tissue, where the growth factor is produced by chondrocytes and released in the extracellular matrix in latent forms, consisting of a 100-kDa complex of TGF-β conjugated with a latency-associated peptide (LAP) and of a large latent complex formed by the small 100-kDa complex covalently bound to the latent TGF-β binding protein 1 (LTBP1) [1, 2, 3, 23]. Activation of even small amounts of latent TGF-β may have dramatic effects on cartilage, since chondrocytes exhibit phenotypic responses to the active growth factor at concentrations 10- to 100-fold below plasma levels of TGF-β (1–50 ng/ml) [1].

TGF-β has been implicated in the growth of several neoplasms, and recent studies have suggested that dysregulation of TGF-β autocrine control appears to have a role in the growth of bone tumors, such as Ewing's sarcoma and osteosarcoma [9, 18, 20]. In addition, in vitro studies have demonstrated that TGF-β1 is produced by human chondrosarcoma cells [5], and the cytokine has a potent stimulatory effect on the growth of rat chondrosarcoma [12, 19]. However, no information is currently available concerning the production of this family of growth factors by human chondrosarcomas in vivo. Therefore, we studied the expression of TGFβ-1, β2, β3 and of TGF-βRI and -RII in a series of 24 chondrosarcomas of bone and 10 benign cartilaginous lesions of bone using immunohistochemistry and reverse-transcription polymerase chain reaction (RT-PCR) analysis for mRNA determination. Furthermore, we correlated TGF-β isoform expression in chondrosarcomas with the histologic grade of the tumor and with proliferative activity assessed by means of MIB-1 immunostaining.

Subjects and methods

Subjects

Our study was conducted on 24 consecutive conventional chondrosarcomas of bone from 24 patients. Complete clinical information was available for all patients, and paraffin-embedded tissue blocks not submitted to decalcification procedures were retrieved in each case to perform the immunohistochemical analysis. Fourteen patients were male and ten were female, with ages ranging at the time of diagnosis between 25 years and 71 years (median 52 years). Thirteen tumors were located in the trunk, including the pelvis (8 patients) and the scapula (5 patients), whereas 11 involved the extremities, including the femur (7 patients), the humerus (3 patients), and the tibia (1 patient). One patient who developed a chondrosarcoma of the femur was affected by Ollier's disease. Six patients had stage-IA chondrosarcoma [7], 4 had stage-IB chondrosarcoma, 1 had stage-IIA chondrosarcoma, 12 had stage-IIB chondrosarcoma, and 1 had a stage-IIIA chondrosarcoma. All patients underwent surgical treatment consisting of surgical resection in 22 cases, curettage in 1 case, and amputation in 1 case. Hematoxylin and eosin stained sections were employed by one pathologist (A.F.) to grade each lesion according to the criteria of Evans [8]. Ten patients had grade-1 tumors, 10 had grade-2 tumors, and 4 had grade-3 tumors.

Patients were followed for a minimum of 36 months or until death (median follow-up 62 months). There were four patients who presented with local failures and six who presented with distant failures. Of the four patients who developed local recurrence, three also developed distant metastases. Four patients were alive with disease and three died due to metastasis after 14, 24, and 36 months from diagnosis.

In addition, we studied a group of ten benign cartilaginous lesions, including five enchondromas and five osteochondromas.

Immunohistochemistry

Immunohistochemical staining was done on formalin-fixed, paraffin-embedded tumor tissue fragments using the avidin–biotin complex (ABC) technique (Vector, Burlingame, Calif.). The primary rabbit polyclonal antibodies against TGF-β1, TGF-β2, TGF-β3, TGF-βRI, and TGF-βRII (Santa Cruz Biotechnology, Calif.) were applied at 1:50 dilution. A semi-quantitative system was employed to evaluate the level of antigen expression: immunoreactivity was scored as either absent (–), low (+, less than 20% of positive tumor cells), moderate (++, 21–75% of positive tumor cells), or diffuse (+++, more than 75% of positive tumor cells). Proliferative activity was evaluated using the MIB-1 monoclonal antibody (Immunotech, Marseille, France) after microwave pretreatment of dewaxed and rehydrated sections. Scoring of the immunostaining was performed using a standard light microscope equipped with an eyepiece grid of 10×10 squares and a 40× objective. In each case, at least 500 tumor cells were counted from areas with high and low expression of the antigen and the results were expressed as percentage of positive cells.

Negative controls were obtained by substituting the primary antibody with non-immune rabbit or mouse serum.

Reverse-transcription polymerase chain reaction analysis

RT-PCR was performed using total RNA obtained from fresh tumor tissue fragments. The sequences of sense and antisense primers employed were as previously described [16]. The RT procedure was performed using the 3′ primers under the following conditions: RT at 42°C for 50 min, inactivation of reverse transcriptase at 70°C for 15 min, and RNase H digestion at 37°C for 20 min. One PCR cycle (30 cycles total) consisted of denaturation at 94°C for 1 min, annealing at 56°C for 1 min, and polymerization at 72°C for 1 min. PCR products were electrophoresed on 1–1.5% agarose gel, visualized by ethidium bromide staining, and photographed under ultraviolet light.

Statistical analysis

Statistical analysis was performed using Statistica 5.1 software (Statsoft Inc., Tulsa, Okla.). Two-tailed Fisher's exact test was used to analyze the correlation between TGF-β isoform expression and the histologic features of the lesions. The Mann-Whitney U test and one-way analysis of variance (ANOVA) were used to assess the differences in proliferative activity determined on tumor tissue sections, according to TGF-β isoform expression and histologic features of the lesion. The cumulative probability of disease-free survival was calculated using the Kaplan-Meier method. Logrank analysis was employed to compare curves. *P* values <0.05 were considered significant.

Results

The results of the immunohistochemical studies are summarized in Table 1. Overall, cytoplasmic positivity for TGF-β1 was identified in neoplastic cells of 18 chondrosarcomas (75%) and in 3 benign lesions (30%). TGF-β1

Table 1 Correlation between transforming growth factor (TGF)-β isoform and receptor (RI and RII) expression, proliferative activity and histologic features in 34 cartilaginous lesions of bone

	TGF-β1	TGF-β2	TGF-β3	TGF-βRI	TGF-βRII	MIB-1
Benign lesions (10)	0	1	0	ND	ND	0.3%
G1 chondrosarcomas (10)	0	5	3	8	8	0.6%
G2/G3 chondrosarcomas (14)	9	13	2	12	12	12.6%
P value (G2/3 vs G1)	0.002	0.05	0.6	1	1	<0.001

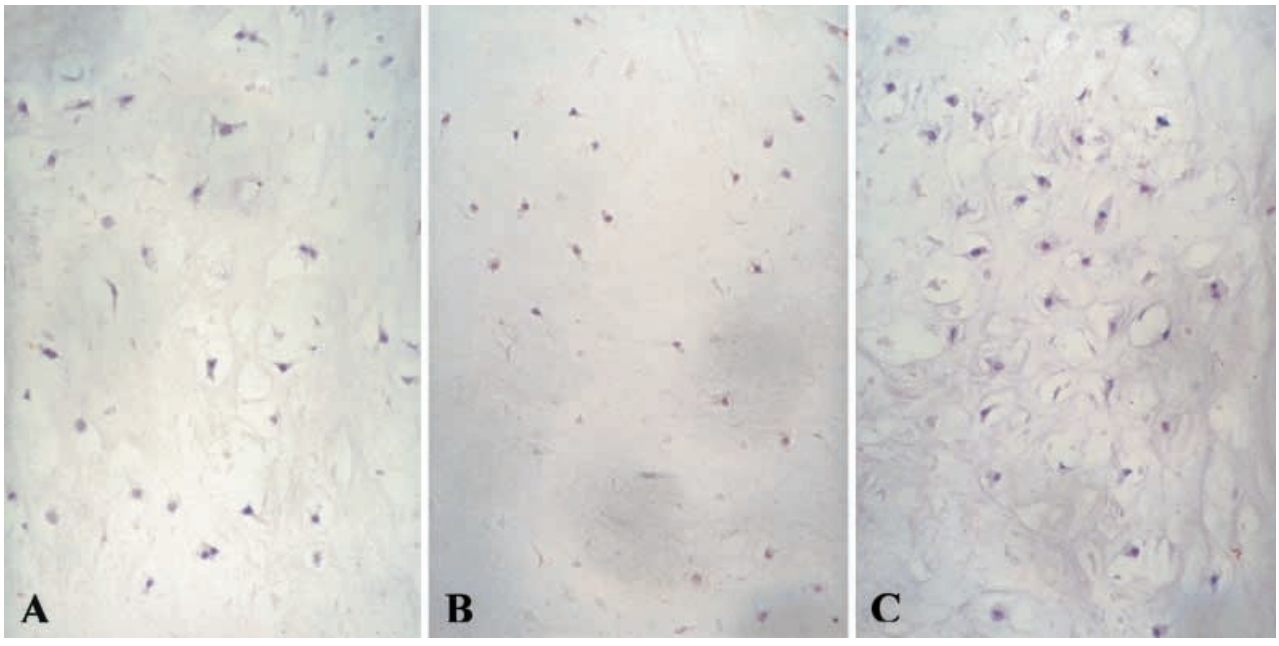

Fig. 1 Absence of transforming growth factor (TGF)-β1 (**a**), -β2 (**b**) and -β3 (**c**) expression in a grade-1 chondrosarcoma

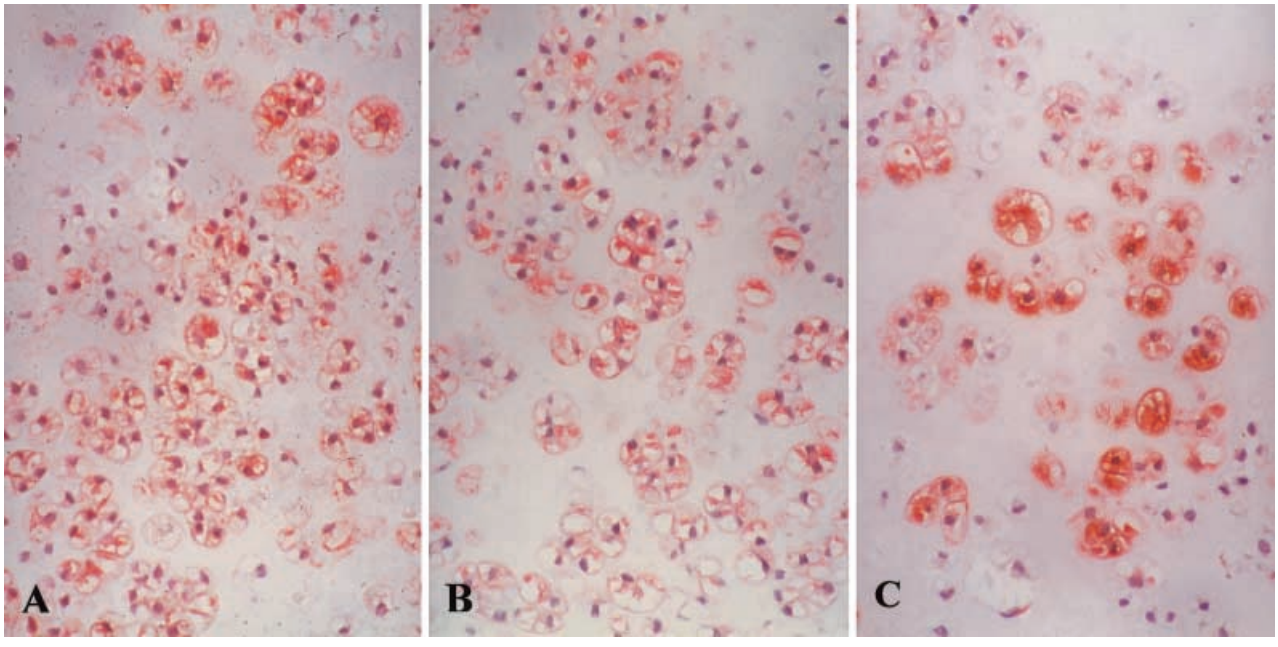

Fig. 2 Grade-2 chondrosarcoma showing diffuse and intense positivity for transforming growth factor (TGF)-β1 (**a**), -β2 (**b**) and -β3 (**c**) in neoplastic cell cytoplasm

expression was significantly higher in the group of chondrosarcomas, where it was scored as moderate or diffuse in nine cases, than among benign lesions, where only focal positivity was observed (P=0.0007). Notably, grade-1 chondrosarcomas were either negative or showed only focal positivity (<20% of neoplastic cells) (Fig. 1a), while the nine tumors showing positivity in more than 20% of tumor cells were either grade-2 or grade-3 chondrosarcomas (P=0.002; Fig. 2a). Therefore, there was no significant difference in the expression of TGF-β1 between grade-1 chondrosarcomas and benign cartilaginous lesions (P=1).

TGF-β2 was detected in 21 chondrosarcomas (87.5%), 18 of which had more than 20% of positive cells, and in 8 benign lesions (89%), with only one case showing more than 20% of positive cells (P=0.001). However, as for TGF-β1, there was no significant difference in the expression of the cytokine between grade-1 chondrosarcomas and benign lesions (P=0.1). The expression of TGF-β2 increased significantly in grade-2

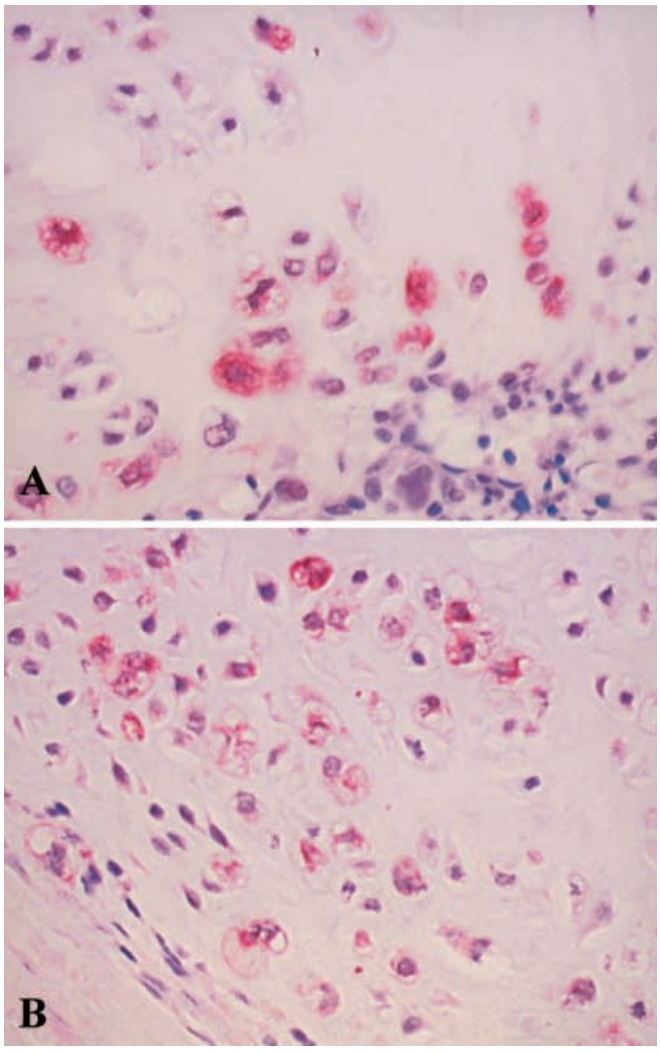

Fig. 3 Transforming growth factor beta receptor 1 (TGF-βRI; **a**) and -RII (**b**) expression in a grade-2 chondrosarcoma

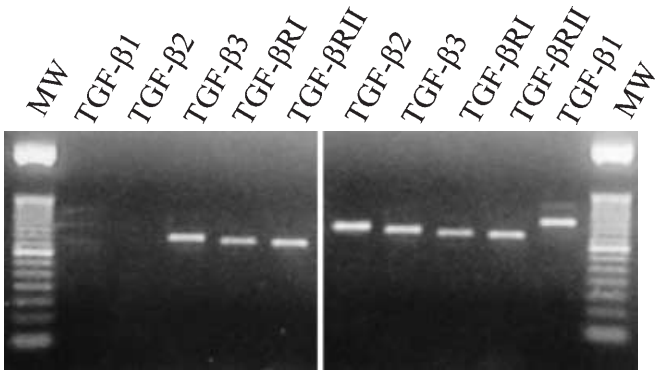

Fig. 4 Reverse-transcription polymerase chain reaction (RT-PCR) analysis of transforming growth factor (TGF) ligand and receptor mRNAs in human chondrosarcomas. Visualization using ethidium bromide staining. The PCR-product sizes are: TGF-β1 448 bp; TGF-β2 439 bp; TGF-β3; 435 bp; TGF-βRI 420 bp; TGF-βRII 410 bp. *Left* Grade-1 chondrosarcoma showing absent levels of TGF-β1 and -β2 and high levels of TGF-β3, TGF-βRI and -RII. *Right* Grade-3 chondrosarcoma showing high levels of TGF-β1, -β2, -β3 and of TGF-βRI and -RII

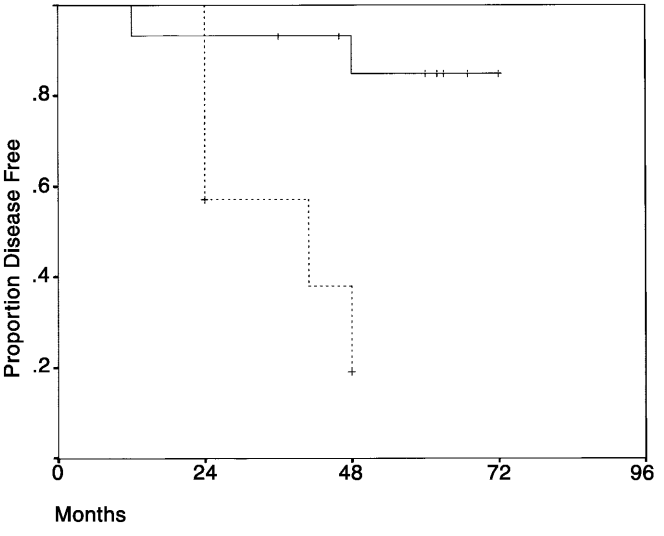

Fig. 5 Disease-free interval of patients with chondrosarcoma according to the expression of transforming growth factor (TGF)-β1. The *solid line* indicates chondrosarcoma with absent or low expression (<20% of tumor cells) of TGF-β1 and the *dotted line* indicates chondrosarcomas with TGF-β1 expression in more than 20% of tumor cells

and grade-3 chondrosarcomas (13 of 14 lesions with >20% of positive neoplastic cells; Fig. 2b) in comparison with grade-1 tumors (5 of 10 lesions with >20% of positive neoplastic cells; Fig. 1b; P=0.05).

Finally, TGF-β3 was detected in 17 chondrosarcomas (70.8%) and 6 benign lesions (60%). Enchondromas and osteochondromas showed only focal expression of the cytokine, while the distribution of the immunostaining was more variable in chondrosarcomas (Fig. 1c and Fig. 2c). However, no significant differences of TGF-β3 expression were observed between benign and malignant cartilaginous lesions (P=0.3) or between chondrosarcomas of different histologic grades (P=0.6).

All chondrosarcomas were also investigated for the presence of TGF-β receptor types I and II, and 23 of 24 specimens (95.8%) demonstrated positive staining for both receptors, that in most cases was scored as moderate to diffuse (20 of 23 cases, Fig. 3).

In a subset of ten chondrosarcomas (seven grade-1 and three grade-2 lesions), we performed RT-PCR analysis on fresh tumor tissue fragments. In each case, the results of mRNA analysis were in agreement with those of the immunohistochemical analysis, confirming the presence of low or absent levels of TGF-β1 and -β2 mRNA in grade-1 chondrosarcomas, while grade-2 chondrosarcomas presented high levels of transcript of both cytokines (Fig. 4); comparable levels of TGF-β3 mRNA were expressed by grade-1 and -2 chondrosarcomas. In accordance with the results of the corresponding immunohistochemical analysis, all the specimens tested also showed high levels of transcript for TGF-β receptor types I and II (Fig. 4).

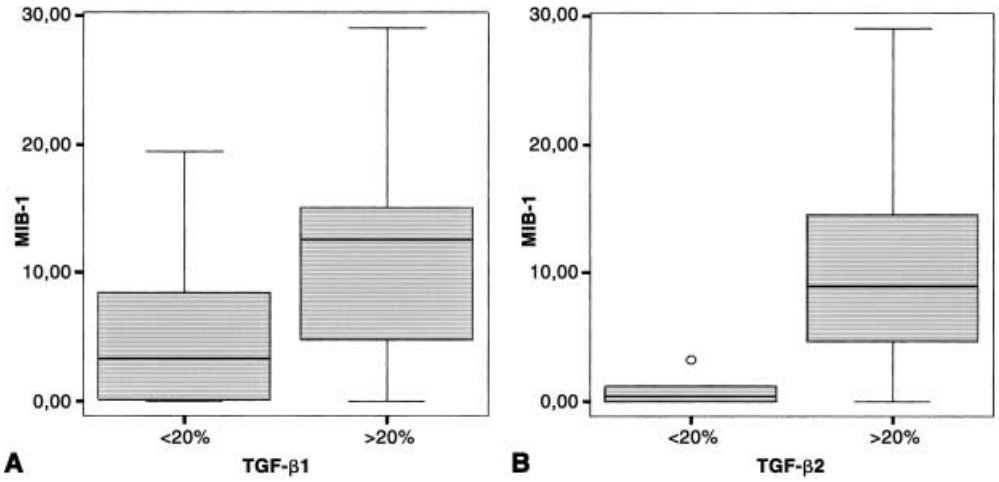

Fig. 6 MIB-1 labeling index in 24 cases of chondrosarcoma of bone, according to transforming growth factor (TGF)-β1 (**a**) and -β2 (**b**) expression. Proliferative activity determined by MIB-1 nuclear immunostaining was significantly higher in chondrosarcomas expressing TGF-β1 and -β2 in more than 20% of neoplastic cells (P=0.006 and P<0.001, respectively; Mann-Whitney U test). Box and whisker plot displaying median and interquartile range and largest and smallest values that are not outliers (*whiskers*). Cases with values that are between 1.5 and 3 box lengths from the upper and lower edge of the box are called outliers and are designated with a circle

We then analyzed the disease-free interval of chondrosarcoma patients according the immunohistochemical expression of TGF-β isoforms and receptors. Patients with tumors showing overexpression of TGF-β1 (>20% of positive neoplastic cells) had a significantly shorter disease-free interval than patients with tumors showing absent or low expression of the cytokine (Fig. 5; P=0.004, log-rank test). Conversely, we found no significant correlation between the immunohistochemical levels of TGF-β2, TGF-β3, TGF-βRI, and TGF-βRII and the disease-free interval in our series of chondrosarcomas of bone (P values=0.4, 0.1, 0.6, and 0.8, respectively; log rank test).

The marker of cell proliferation MIB-1 was detected in 19 cases of chondrosarcoma (range 0–29.1%) and in 4 benign cartilaginous lesions (range 0–1.4%). The percentage of neoplastic cells with nuclear staining was significantly increased in grade-2 and -3 lesions in comparison with grade-1 lesions and benign lesions (P<0.001, ANOVA). Analysis of MIB-1 staining with respect to TGF-β isoform expression revealed that chondrosarcomas with TGF-β1 and TGF-β2 overexpression (>20% of tumor cells) had a significantly higher proliferative activity than chondrosarcomas with only focal or negative immunostaining (P=0.006 and P<0.001, respectively; Mann Whitney U test; Fig. 6), while no significant correlation was found between TGF-β3 expression and cell proliferation (P=0.5, Mann Whitney U test).

Discussion

In vitro studies have shown that proliferative activity of cartilage cells can be stimulated by several factors, including basic fibroblast growth factor (bFGF), insulin-like growth factors (IGFs), epidermal growth factor (EGF), interleukin (IL)-6, and TGF-β [4, 10, 15, 22, 25]. Since normal and neoplastic cartilage cells are immersed in abundant extracellular matrix which may represent a physical barrier for exogenous growth factors to reach the chondrocytes, factors that are produced by chondrocytes themselves are therefore important in modulating proliferation of these cells in an autocrine fashion.

Previous studies have shown that a human chondrosarcoma cell line established from an aggressive chondrosarcoma produces abundant mRNA encoding for TGF-β1 [5], and this cytokine is capable of stimulating proliferative activity of Swarm rat chondrosarcoma cells [12, 19]. In the present study, we demonstrated that human chondrosarcomas expressed the TGF-β isoform in vivo, and the levels of expression of TGF-β1 and -β2 were higher than those present in benign cartilaginous lesions. In addition, according to our analysis, there was a positive correlation between TGF-β1 and -β2 expression and the histologic grade of the tumor.

Histologic grading of chondrosarcomas, which is based on cellularity of the tumor and cytological atypia, is considered a good indicator of clinical aggressiveness for these neoplasms, since several studies have demonstrated that grade-2 and grade-3 tumors have a significantly worse prognosis than grade-1 tumors [8]. The presence of higher levels of TGF-β1 and -β2 mRNA and protein in grade-2 and -3 chondrosarcomas suggests that an elevated expression of these cytokines may contribute substantially to determine an aggressive phenotype in these tumors. In accordance, in the current study, the expression of TGF-β1 was correlated with clinical outcome, since tumors with overexpression of the cytokine demonstrated a significantly shorter event-free survival. Similar results were obtained by our group with regard to osteosarcomas, in which TGF-β1 was

found to be expressed at significantly higher levels in high-grade tumors than in low-grade tumors [9]. However, the immunohistochemical evaluation of TGF-β isoform expression cannot be used, according to our data, to help in the distinction between grade-1 chondrosarcomas and benign cartilaginous lesions because no significant difference was observed in the distribution of TGF-β isoforms in these two groups of cartilaginous lesions.

TGF-β1 has been identified as a potent growth stimulator for Swarm rat chondrosarcoma cells in vitro, and this effect was synergistically increased by IL-6 and IGF-1 [11, 17]. In accordance with previous studies, we observed a significant positive correlation between histologic tumor grade and proliferative activity assessed by MIB-1 proliferation marker expression in human chondrosarcomas [21, 27, 28]. Interestingly, we also found that MIB-1 proliferative index was significantly correlated with TGF-β1 and -β2 expression, while no correlation was evidenced for TGF-β3, suggesting that these factors could be important autocrine growth regulators in human chondrosarcomas.

Chondrocytes produce and store TGF-β in latent form, and the active homodimer can be released from the latent complex by means of several mechanisms, including the action of thrombospondin and the enzymatic activities of plasmin generated from plasminogen by plasminogen activator [6]. These latter enzymatic activities are present in normal and neoplastic chondrocytes [24], and it is therefore possible that active TGF-β is released in the microenvironment by neoplastic chondrocytes themselves, where it may exert its stimulatory effects on the neoplastic growth in an autocrine fashion. Interestingly, chondrosarcomas showing overexpression of proteases, such as urokinase plasminogen activator, are of higher histologic grade and have increased risk of local recurrence and distant metastasis [13], an aggressive clinical behavior that may be, at least in part, due to the release and activation of growth factors, such as TGF-β, stored in the extracellular matrix.

Finally, in order to promote cell proliferation, TGF-β must bind to specific signaling receptors, TGF-βRI and -RII. These receptors are expressed during intramembranous and endochondral ossification, as well as in mature articular cartilage, with a distribution that overlaps that of TGF-β isoforms [11, 14]. In contrast to osteosarcomas, which in most cases exhibit an aberrant TGF-β receptor pattern [17], according to our analysis human chondrosarcomas express high levels of TGF-β receptor types I and II irrespective of the histologic grade, both at the mRNA and protein levels. These receptors could therefore mediate the effects of TGF-β isoforms on cell cycle control in neoplastic chondrocytes.

In conclusion, the present study supports the existence of an autocrine loop of TGF-β in human chondrosarcomas that could be involved in the growth control of these neoplasms. Analysis of TGF-β isoform expression could potentially be a useful adjunct to define tumor aggressiveness in patients with chondrosarcomas.

Acknowledgements This study was supported by a grant from the Italian Association for Cancer Research (Milan).

References

1. Bonewald LF (1996) Transforming growth factor-β. In: Bilezikian JP, Raisz LG, Rodan GA (eds) Principles of bone biology. Academic Press, San Diego, pp 647–659
2. Bonewald LF, Wakefield LM, Oreffo RO, Escobedo A, Twardzik DR, Mundy GR (1991) Latent forms of transforming growth factor β (TGF-β) derived from bone cultures: identification of a naturally occurring 100 kDa complex with similarity to recombinant latent TGFβ. Mol Endocrinol 5:741–751
3. Boyan BD, Schwartz Z, Park-Snyder S, Dean DD, Yang F, Twardzik D, Bonewald LF (1994) Latent transforming growth factor β is produced by chondrocytes and activated by extracellular matrix vescicles upon exposure to 1,25-(OH)2D3. J Biol Chem 269:28374–28381
4. Canalis E, McCarthy TL, Centrella M (1988) Growth factors and bone remodeling. J Clin Invest 81:277–281
5. Chansky H, Robbins JR, Cha S, Raskind WH, Conrad EU, Sandell LJ (1998) Expression of cartilage extracellular matrix and potential regulatory genes in a new human chondrosarcoma cell line. J Orthop Res 16:521–530
6. Crawford SE, Stellmach V, Marphy-Ullrich JE, Ribeiro SMF, Lawler J, Hynes RO, Boivin GP, Bouck N (1998) Thrombospondin-1 is a major activator of TGF-β1 in vivo. Cell 93: 1159–1170
7. Enneking WF (1990). Clinical musculoskeletal pathology. University of Florida Press, Gainesville, Florida
8. Evans HL, Ayala AG, Romsdahl MM (1977) Prognostic factors in chondrosarcoma of bone: a clinicopathologic analysis with emphasis on histologic grading. Cancer 40:818–831
9. Franchi A, Arganini L, Baroni G, Calzolari A, Capanna R, Campanacci D, Caldora P, Masi L, Brandi ML, Zampi G (1998) Expression of transforming growth factor- isoforms in osteosarcoma variants: association of TGF-1 with high grade osteosarcomas. J Pathol 185:284–289
10. Froger-Gaillard B, Charrier AM, Henet S, Ronot X, Adolphe M (1989) Production of insulin-like growth factors and their binding proteins by rabbit articular chondrocytes: relationship with cell multiplication. Endocrinology 124:2365–2372
11. Fukumura K, Matsunaga S, Yamamoto T, Nagamine T, Ishidou Y, Sakou T (1998) Immunolocalization of transforming growth factor-beta s and type I and type II receptors in rat articular cartilage. Anticancer Res 18:4189–4193
12. Guerne PA, Lotz M (1991) Interleukin-6 and transforming growth factor-beta synergistically stimulate chondrosarcoma cell proliferation. J Cell Physiol 149:117–124
13. Hackel CG, Krueger S, Grote HJ, Oshiro Y, Hodges S, Johnston DA, Johnson ME, Roessner A, Ayala AG, Czerniak B (2000) Overexpression of cathepsin B and urokinase plasminogen activator is associated with increased risk of recurrence and metastasis in patients with chondrosarcoma. Cancer 89:995–1003
14. Horner A, Kemp P, Summers C, Bord S, Bishop NJ, Kelsall AW, Coleman N, Compston JE (1998) Expression and distribution of transforming growth factor-beta isoforms and their signaling receptors in growing human bone. Bone 23:95–102
15. Iwamoto M, Sato K, Nakashima K, Fuchihata H, Suzuki F, Kato Y (1989) Regulation of colony formation of differentiated chondrocytes in soft agar by transforming growth factor-beta. Biochem Biophys Res Commun 159:1006–1011
16. Jakowlew SB, Moody TW, Mariano JM (1997) Transforming growth factor-beta receptors in human cancer cell lines: analysis of transcripts, protein and proliferation. Anticancer Res 17: 1849–1860
17. Kloen P, Jenninngs CL, Gebhardt MC, Springfield DS, Mankin HJ (1994) Expression of transforming growth factor-beta (TGF-β) receptors, TGF-β1 and TGF-β2 production and autocrine growth control in osteosarcoma cells. Int J Cancer 58:440–445

18. Kloen P, Gebhardt MC, Perez-Atayde A, Rosemberg AE, Springfield DS, Gold LI, Mankin HJ (1997) Expression of transforming growth factor- (TGF-) isoforms in osteosarcomas. TGF-3 is related to disease progression. Cancer 80:2230–2239
19. Matsumura T, Whelan MC, Li XQ, Trippel SB (2000) Regulation by IGF-I and TGF-beta1 of Swarm-rat chondrosarcoma chondrocytes. J Orthop Res 18:351–355
20. McCune B, Patterson K, Chandra RS, Kapur S, Sporn MB, Tsokos M (1993) Expression of transforming growth factor isoforms in small round cell tumors of childhood. An immunohistochemical study. Am J Pathol 142:49–59
21. Nawa G, Ueda T, Mori S, Yoshikawa H, Fukuda H, Ishiguro S, Funai H, Uchida A (1996) Prognostic significance of Ki67 (MIB1) proliferation index and p53 over-expression in chondrosarcomas. Int J Cancer 69:86–91
22. Osborn K, Trippel SB, Mankin HJ (1989) Growth factor stimulation of adult articular cartilage. J Orthop Res 7:35–42
23. Pedrozo HA, Schwartz Z, Mokeyev T, Ornoy A, Xin-Sheng W, Bonewald LF, Dean DD, Boyan BD (1999) Vitamin D3 metabolites regulate LTBP1 and latent TGF-β1 expression and latent TGF-β1 incorporation in the extracellular matrix of chondrocytes. J Cell Biochem 72:151–165
24. Pedrozo HA, Schwartz Z, Robinson M, Gomes R, Dean DD, Bonewald LF, Boyan BD (1999) Potential mechanisms for the plasmin-mediated release and activation of latent transforming growth factor-beta1 from the extracellular matrix of growth plate chondrocytes. Endocrinology 140:5806–5816
25. Prins PAA, Lipèman JM, Sokoloff L (1982) Effect of purified growth factors on rabbit articular chondrocytes in monolayer culture I. DNA synthesis. Arthrirtis Rheum 25:1217–1227
26. Roberts AB, Sporn MB (1990) Peptide growth factors and their receptors. In: Roberts AB, Sporn MB (eds) Handbook of experimental pharmacology. Springer, Berlin Heidelberg New York, pp 419–472
27. Scotlandi K, Serra M, Manara MC, Maurici D, Benini S, Nini G, Campanacci M, Baldini N (1995) Clinical relevance of Ki67 expression in bone tumors. Cancer 75:806–814
28. Scully SP, Layfield LJ, Harrelson JM (1997) Prognostic markers in chondrosarcoma: evaluation of cell proliferation and of regulator of the cell cycle. Sarcoma 1:79–87

Virchows Arch (2002) 440:498–504
DOI 10.1007/s00428-002-0622-0

ORIGINAL ARTICLE

**Ana S. Rocha · Paula Soares · José Carlos Machado
Valdemar Máximo · Elsa Fonseca · Kaarle Franssila
Manuel Sobrinho-Simões**

Mucoepidermoid carcinoma of the thyroid: a tumour histotype characterised by P-cadherin neoexpression and marked abnormalities of E-cadherin/catenins complex

Received: 21 September 2001 / Accepted: 8 January 2002 / Published online: 21 March 2002
© Springer-Verlag 2002

Abstract The cadherin/catenins complex regulates cell–cell adhesion and motility and is believed to have an invasion suppressor role. Primary mucoepidermoid carcinoma of the thyroid (MECT) is a rare tumour characterised by a distinct morphological appearance and a questionable histogenesis. The coexistence of papillary thyroid carcinoma (PTC) foci in many patients with MECT suggests an association between the two tumour histotypes. In an attempt to clarify the putative relationship between MECT and PTC, we analysed tissue from 11 patients with MECT by immunohistochemistry (E-, P- and N-cadherins and α-, β- and γ-catenins). The E-cadherin gene was also analysed by polymerase chain reaction (PCR)/single-strand conformation polymorphism (SSCP). The results were compared with a control group of normal thyroid, classical PTC and the diffuse sclerosing variant of PTC. Compared with normal thyroid and PTC, MECT displays marked abnormalities of the cadherin/catenin complex. Such abnormalities include the consistent neoexpression of P-cadherin and major alterations in the expression of E-cadherin and the three catenins. Our results point to the close relationship between the de novo expression of P-cadherin and the disruption of the cadherin/catenins complex with the squamoid phenotype of MECT.

A.S. Rocha · P. Soares · J.C. Machado · V. Máximo · E. Fonseca
M. Sobrinho-Simões (✉)
Institute of Molecular Pathology
and Immunology of the University of Porto,
R. Roberto Frias s/n, 4200-465 Porto, Portugal
e-mail: sobrinho.simoes@ipatimup.pt
Tel.: +351-22-5570700, Fax: +351-22-5570799

P. Soares · J.C. Machado · E. Fonseca · M. Sobrinho-Simões
Medical Faculty of Porto, Porto, Portugal

K. Franssila
Department of Radiotherapy and Oncology,
Helsinki University Central Hospital, Finland

E. Fonseca · M. Sobrinho-Simões
Hospital de S. João, Porto, Portugal

Keywords Thyroid · Mucoepidermoid carcinoma of the thyroid · E-Cadherin · P-Cadherin · Catenins

Introduction

Cadherins are single-pass transmembrane proteins that mediate Ca^{2+}-dependent homophilic cell–cell adhesion. In adherens junctions, the cytoplasmic domain of cadherins binds to β- or γ-catenin, which in turn binds to the actin-associated protein α-catenin [24, 39]. Defects in cadherin-mediated adhesion are associated with several characteristics of malignant transformation, such as dedifferentiation, high motility and invasive growth [2, 36].

Loss of or reduction in cell adhesion by abnormalities at the level of expression or function of E-cadherin has often been described in human cancers [6]. In thyroid, a minimal or absent immunoexpression of E-cadherin has been described in poorly differentiated/undifferentiated carcinomas in contrast to a variable degree of immunoreactivity in differentiated carcinomas [5, 33, 37]. In the latter group, a significant association has been described between loss of E-cadherin and unfavourable prognosis [37].

Alterations in β-catenin may also play an important role in the tumourigenesis of several human neoplasias [16, 17, 26]. Cerrato et al. [11] reported the absence of immunoreactivity for β- and γ-catenins in anaplastic carcinomas, whereas papillary thyroid carcinoma (PTC) and follicular carcinoma showed heterogeneously decreased immunoexpression, with a marked down-regulation of γ-catenin. Böhm et al. [4] also reported a decreased expression of α-, β- and γ-catenins in differentiated thyroid carcinomas, with a higher prevalence of γ-catenin down-regulation; moreover, these authors observed that follicular carcinomas showed reduced staining for all the catenins more often than PTC. Mutations in the β-catenin gene, with nuclear localisation of the protein, have been described in poorly differentiated and anaplastic carcinomas by Garcia-Rostan et al. [16, 17].

In recent studies on classical PTC and its diffuse sclerosing variant (DSV), we detected several types of abnormalities in the E-cadherin/catenins complex, such as E-cadherin and β- and γ-catenin down-regulation/aberrant localisation [28]. We have also detected neoexpression of P-cadherin in areas of squamous metaplasia of both PTC and DSV [28].

Despite its rarity, mucoepidermoid carcinoma is one of the most interesting histotypes of thyroid tumours. This peculiar neoplasia was first described by Rathigan et al. [27], who pointed out its (superficial) resemblance to mucoepidermoid carcinoma of the salivary gland because it comprises glandular and solid or squamoid areas, frequently in a cellular, fibrotic stroma. Since then, six similar tumours have consecutively been reported by Fialho et al. [14], Franssila et al. [16], Mizukami et al. [23] and Harach et al. [19] under the name of mucoepidermoid carcinoma of the thyroid (MECT).

Cases of MECT merging with classical PTC and DSV of PTC, squamous carcinoma [12] and anaplastic carcinoma of the thyroid [10, 30] have been reported to date. The histogenesis of MECT remains controversial [9, 10, 30], but the coexistence of PTC foci in many patients with MECT and the squamoid differentiation of MECT support the assumption that MECT is related to PTC [9, 10, 30].

Taking this into consideration, we decided to study the immunoexpression of E-, P- and N-cadherins and α-, β- and γ-catenins in 11 patients with MECT and to evaluate the integrity of the entire coding sequence of the E-cadherin gene in this group of tumours. The main objective of this study was to clarify the role of cell–cell adhesion molecules in the acquisition of the MECT phenotype and to make progress in understanding the putative differences and similarities between MECT and PTC.

Material and methods

Tumour specimens

Representative histological slides and paraffin blocks were retrieved from the files of the Departments of Pathology of the Medical Faculty of Porto, Portugal, the University Central Hospital of Helsinki, Finland and the University Health Centre of Rio de Janeiro, Brazil. Some of the patients had been sent for consultation to the Department of Pathology of the Medical Faculty of Porto. No frozen samples were available from any of the patients.

The 11 tumours were independently diagnosed as MECT by two pathologists (KF and MS-S) according to the criteria presented in the WHO booklet [20] and by Rosai et al. [29]. The specimens were also classified according to the co-existence of PTC foci, presence of necrosis, prominence of desmoplasia and/or lymphocytic infiltration, and histological appearance of the adjacent thyroid parenchyma. In two specimens (patients 1 and 6), the immunohistochemical study was performed in metastatic foci because no material was available from the primary tumours.

A series of specimens from 18 patients with PTC and 8 with DSV previously reported [28, 33] was used for comparative purposes.

Immunohistochemistry

Immunohistochemistry was performed using the avidin–biotin–peroxidase (ABC) complex with an additional step for microwave antigen retrieval as previously described [28]. The following antibodies were used: for E-cadherin, HECD-1 (Zymed, San Francisco, CA), diluted 1:200; P-cadherin, clone 56 (Transduction Laboratories, Lexington, UK), diluted 1:75; N-cadherin, clone 3B9 (Zymed, San Francisco, CA), diluted 1:400; anti α-,β-and γ-catenins, clones 5, 14 and 15 (Transduction Laboratories, Lexington, UK), diluted 1:200, 1:1000 and 1:500, respectively.

Normal thyroid was used as a positive control for all the antibodies except for P- and N-cadherins, for which normal skin and normal heart tissue, respectively, were used.

Scoring of immunostaining

Two observers (ASR and MS-S) independently scored the immunostaining using a semi-quantitative approach; the specimens were classified according to the intensity of the immunoreactivity as follows: -, no expression was detectable; ↓↓, the signal was very low; ↓, positive but still weaker than the positive controls; =, the intensity matched the positive control. The immunoreactivity patterns were also classified according to the signal localisation as membranous, diffuse cytoplasmic or granular with perinuclear distribution.

Tumour microdissection and genomic DNA extraction

Genomic DNA was extracted from 10-μm sections of paraffin-embedded material adjacent to those used for histology and immunohistochemistry. In order to reduce contamination from adjacent non-tumoural tissue, including lymphocytes/stromal cells, and to separate different histotypes of tumours in the same section, we selected the areas to microdissect in continuous haematoxylin-eosin-stained sections. After deparaffinisation and proteinase K digestion, the samples were precipitated with 1 volume of isopropanol for 2 h at –20°C, washed in 70% ethanol and eluted in water.

Mutation screening by PCR/SSCP

The analysis was performed for the 16 exons of the E-cadherin coding sequence, including the intron/exon boundaries.

PCR reactions were based on the conditions reported by Berx et al. [3]. The cycling conditions were 45 cycles of 45 s at 94°C, 45 s at the appropriate annealing temperature and 75 s at 72°C. The sequences of the primers and the annealing temperatures were as previously described [3].

PCR products were diluted 1:1 with a loading buffer (95% formamide, 0.05% bromophenol blue and 0.05% xylene cyanol) and denaturated for 10 min at 95°C. Electrophoresis of 10 μl of these samples was carried out in 40% mutation detection enhancement (MDE) gels, run at 180 V for 16 h, either with glycerol (20°C) or without (8°C). The gels were silver stained and transferred to Whatmann paper and dried on a vacuum gel drier.

Sequencing

Both mobility shifts and the corresponding normal bands were excised from the paper and eluted in water. These templates were used for reamplification PCR under the same conditions as previously described. The PCR products were purified and sequenced using the ABI Prism Big Dye Cycle Sequencing kit (Perkin Elmer, Foster City, CA) and an ABI Prism 377 DNA sequencer (Perkin Elmer, Foster City, CA).

Results

Histology

The clinico-pathological characteristics of the specimens from the 11 patients are summarised in Table 1. The his-

Table 1 Clinico-pathological characteristics of 11 patients with MECT

Patient no.	Sex	Age (years)	Tumour material available for immunohistochemistry	Coexistence of PTC foci	Necrotic foci	Desmoplasia	Prominent lymphocytic infiltrate	Adjacent thyroid parenchyma
1	f	20	Three nodal metastatic foci	Yes	Yes	Intense	Yes	Lymphocytic thyroiditis
2	f	25	Primary tumour	No	Yes	Intense	No	Not evaluated
3	f	67	Primary tumour	No	Yes	Intense	No	Not evaluated
4	m	11	Primary tumour and nodal metastasis	Yes	Yes	Intense	No	Not evaluated
5	m	47	Primary tumour	Yes (DSV)	No	Intense	Yes	Not evaluated
6	f	18	Nodal metastasis	Yes	No	Intense	Yes	Lymphocytic thyroiditis
7	f	46	Primary tumour	No	No	Moderate	Yes	Lymphocytic thyroiditis
8	f	34	Primary tumour	Yes	No	Intense	Yes	Lymphocytic thyroiditis
9	f	18	Primary tumour	Yes	No	Intense	Yes	Lymphocytic thyroiditis
10	f	11	Primary tumour	Yes	No	Intense	Yes	Lymphocytic thyroiditis
11	m	47	Primary tumour	Yes	No	Intense	Yes	Lymphocytic thyroiditis

PTC, papillary thyroid carcinoma; DSV, diffuse sclerosing variant of PTC.

Table 2 Immunohistochemical data on E- and P-cadherins and α-, β- and γ-catenins in 11 patients with MECT

Patient no.	E-Cadherin		P-Cadherin		α-Catenin		β-Catenin		γ-Catenin	
	Localisation	Intensity	Localisation	Intensity	Localisation	Intensity	Localisation	Intensity	Localisation	Intensity
1	Cytoplasmic	↓↓	Cytoplasmic	↓↓	–	–	Membranous	↓	Cytoplasmic	↓
	Cytoplasmic	↓↓	Cytoplasmic	↓↓	Membranous	↓↓	Membranous	↓	–	–
	Cytoplasmic	↓↓	Membranous/Cyt	↓	–	–	–	–	Membranous	↓↓
2	Cyt/granular	↓	Cytoplasmic	↓↓	–	–	Membranous	↓	–	–
3	Cytoplasmic	↓↓	–	–	Cytoplasmic	↓	–	–	Cytoplasmic	↓
4	Cytoplasmic	↓	Membranous	=	Membranous	=	Membranous	=	–	–
	Cytoplasmic	↓↓	Membranous	=	Cytoplasmic	↓↓	–	–	–	–
5	Cytoplasmic	↓↓	Membranous	=	Membranous	=	Membranous	=	Membranous	=
6	Cytoplasmic	↓	Membranous	=	Membranous	=	–	–	–	–
7	Granular	NA	Cytoplasmic	↓↓	Cytoplasmic	↓	Membranous	=	Membranous	=
8	Granular	NA	Cytoplasmic	↓↓	Membranous	=	Membranous	=	Membranous	=
9	–	–	Cytoplasmic	↓↓	Membranous	=	Membranous	=	Membranous	=
10	Granular	NA	Cytoplasmic	↓	–	–	Membranous	=	–	–
11	Cytoplasmic	↓↓	Membranous	=	–	–	Membranous	↓	–	–

The results are expressed in comparison with those obtained in normal follicular cells, and in the case of P-cadherin with normal skin. =, the intensity of the staining matched the positive control; ↓, reduced expression; ↓↓, very reduced expression; –, no expression at all; NA, not applicable.

tological appearance of a typical case of MECT (patient no. 8) is shown in Fig. 1a.

Immunohistochemistry

The results obtained in the 11 MECT patients regarding P-cadherin and membrane immunoreactivity for E-cadherin and the three catenins are summarised in Table 2.

E-Cadherin. Tissue sections from the 11 MECT patients were examined with HECD-1 antibody that recognises the extracellular domain of E-cadherin. The results are summarised in Table 2.

In the "normal" adjacent thyroid parenchyma, strong homogenous staining along the intercellular borders of the epithelial cells was observed; a similar pattern was seen, focally, in the co-existent foci of PTC. In contrast, all the MECT specimens displayed a very abnormal pattern of expression. Six displayed reduced expression restricted to the cytoplasm, and four showed a very strong signal with a granular perinuclear localisation (Fig. 1b–d). The remaining specimen (patient 9) had no E-cadherin expression (Table 2). The granular pattern of immunoreactivity in four patients and the absence of expression in one patient cannot be attributed to technical problems, e.g. poor preservation, because the pattern of immunoexpression was membranous in the co-existent foci of PTC and in the adjacent thyroid parenchyma (Fig. 1e).

P-Cadherin. In contrast to the absence of P-cadherin expression observed in normal thyroid and in the co-existent foci of PTC, positive immunoexpression was detected in ten of the 11 MECT patients (Table 2). A clear cell–cell border pattern was observed in four patients (Fig. 1f), whereas there was weak to moderate staining in the cytoplasm in six patients (Fig. 1f). Patient 3 was negative for P-cadherin expression (Table 2).

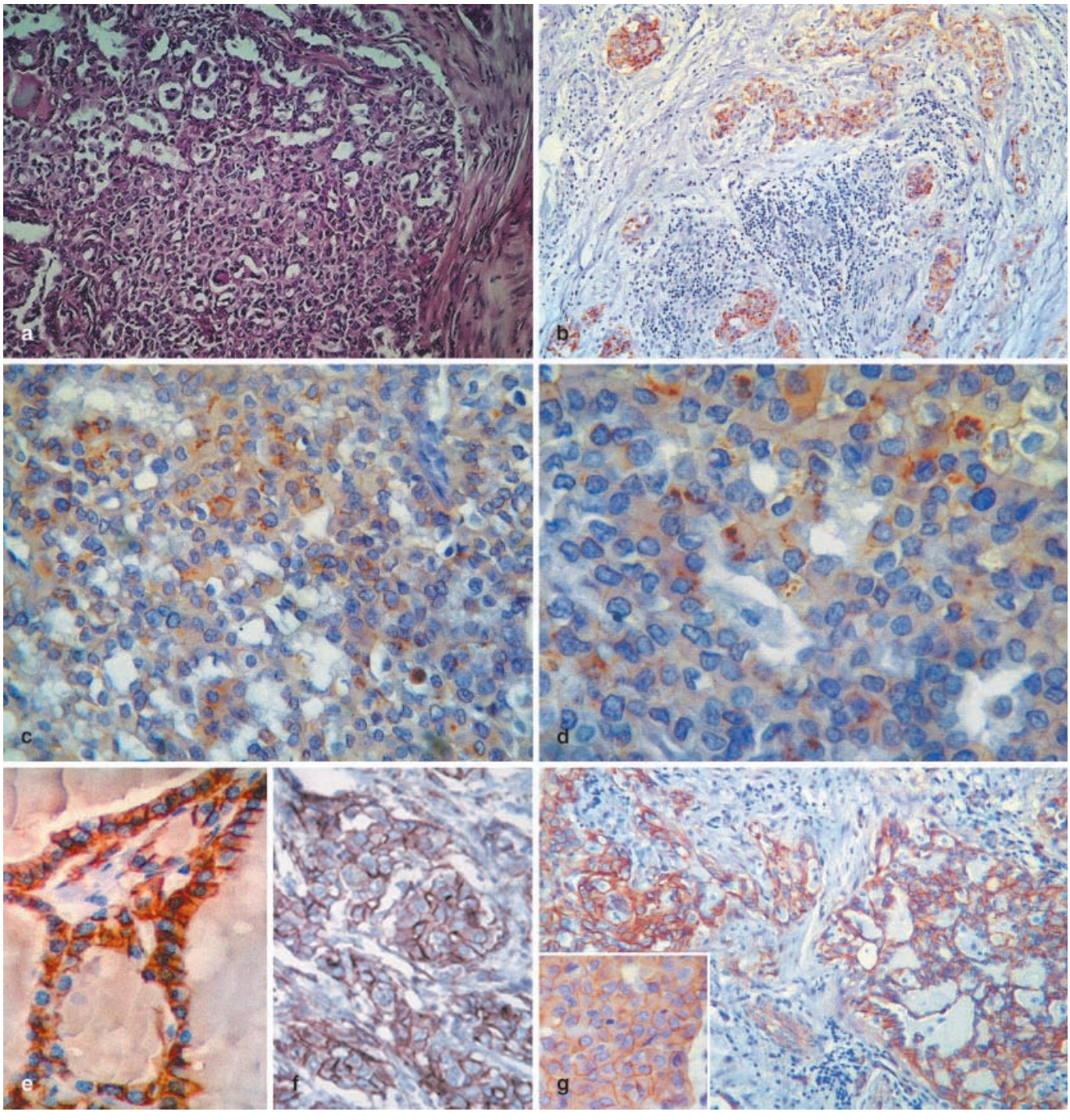

Fig. 1 **a** The histological appearance of tissue from patient no. 8 is characterised by nests of neoplastic cells forming glandular spaces and solid, squamoid areas involved by a fibrotic stroma. H&E, ×100. **b** Low-power magnification of tissue from patient no. 8 showing intense desmoplasia, prominent lymphocytic infiltration and E-cadherin granular perinuclear staining. ×100. **c,d** E-Cadherin granular perinuclear staining in tissue from patient no. 7. ×200 (**c**), ×400 (**d**). **e** The adjacent thyroid parenchyma in patient no. 7 displays a normal membranous E-cadherin staining pattern. ×400. **f** Strong P-cadherin membranous staining in tissue from patient no. 4. ×400. **g** The membranous positivity for β-catenin can be seen in this low-power magnification of a representative sample from patient no. 5. ×150. *Inset*, membranous and cytoplasmic staining for β-catenin in this area of tissue from patient no. 2. ×400

N-Cadherin. The 11 MECT patients displayed no immunoreactivity for N-cadherin, which was not present in the adjacent thyroid parenchyma or in the co-existent foci of PTC.

α-Catenin. MECT displayed a similar pattern of expression regarding both intensity and localisation to that of normal thyroid in four of the 11 patients (Table 2). In two patients (nos. 3 and 7), immunoreactivity was reduced and diffuse in the cytoplasm. The remaining four

specimens were completely negative for α-catenin, except for one of the nodal metastases in patient 1, which displayed weak membrane positivity (Table 2); in these four patients, most of the co-existent foci of PTC exhibited normal α-catenin expression.

The specimens from patient 4 presented different α-catenin expression profiles in the primary tumour and in the metastasis; the former retained normal protein expression, while the latter displayed marked down-regulation accompanied by translocation of the signal to the cytoplasm (Table 2).

β-Catenin. Nine of the 11 MECT patients displayed β-catenin at sites of cell–cell contact (Table 2); the intensity of the signal usually matched that of the positive control or was slightly reduced (Fig. 1g). Staining was usually homogeneously spread throughout the tumour section. Patients 3 and 6 and the metastasis in patients 1 and 4 displayed no immunoreactivity (Table 2), despite the normal pattern of β-catenin expression in the co-existent focus of PTC in patient 6.

γ-Catenin. Four of the 11 MECT patients had a normal pattern of expression in terms of both intensity and localisation (Table 2). Two specimens (patients 1 and 3) displayed strong to moderate cytoplasmic immunoexpression, together, in patient 1, with very weak membranous staining (Table 2). Patients 2, 4, 6, 10 and 11 showed no immunoreactivity at all (Table 2), despite the normal pattern of γ-catenin expression in most of the co-existent foci of PTC.

Molecular analysis of the E-cadherin gene by PCR/SSCP

All the 16 exons, including exon/intron boundaries, of the E-cadherin gene were analysed in the 11 specimens from MECT patients.

Normal SSCP patterns were obtained in MECT for all the amplicons studied.

With the exception of a single case of DSV (which had the missense mutation A592T), we did not detect any E-cadherin mutations in the DSV and PTC patients previously studied [28, 33].

Discussion

It has been suggested that disturbances in cell–cell adhesion, namely in the expression of E-cadherin [5, 28, 33, 37] and α-,β- and γ-catenins [4, 11, 16, 17, 28], may play a pathogenic role in thyroid carcinogenesis.

Primary MECT is a rare thyroid tumour characterised by a distinct morphological appearance and a questionable histogenesis [9, 10, 15, 23, 27, 29, 30].

Despite the ongoing controversy on the putative cell of origin of MECT [9, 10, 30], it is widely accepted that MECT share most of the epidemiological and clinicopathological features of PTC (predominance of young females, nodal metastisation, indolent biological behaviour) and often co-exist with foci of classical PTC [29, 30]. Some of the histological features of MECT (squamoid differentiation, lymphoid infiltration, desmoplastic response, decreased or absent thyroglobulin immunoreactivity) are commonly present in DSV of PTC [29, 30], thus reinforcing the evidence for a relationship between MECT and PTC.

In the present study, we defined the immunoexpression pattern of cadherins/catenins in MECT and evaluated the integrity of the E-cadherin gene. We also compared the results obtained in the study of MECT with those previously obtained in the study of classical PTC and DSV [28, 33].

The first interesting result regarding MECT concerns the neoexpression of P-cadherin, a protein not present in the normal thyroid gland [32]. In the present study, we observed positivity for P-cadherin in ten of the 11 MECT patients. Moreover, this expression was present throughout the tumoural tissues regardless of the prominence of squamoid differentiation in contrast to its absence in the co-existent PTC foci. This observation contrasts with our previous results in PTC and DSV, in which we observed P-cadherin expression but solely in foci of squamous metaplasia [28]. Our results suggest that P-cadherin expression is associated with squamous differentiation of the thyroid gland and that such differentiation is a hallmark of MECT.

Recent publications on the expression of P-cadherin and breast cancer [25, 34] showed an important role for this molecule in breast carcinogenesis. In this model, expression of P-cadherin is associated with poor survival and constitutes an independent prognostic indicator [34]; it is also associated with an infiltrative growth pattern [34]. This may argue in favour of a role for P-cadherin in the acquisition of more aggressive behaviour in breast tumours. Since most MECT follow an indolent clinical course [1, 30], our finding of an almost universal positivity for P-cadherin suggests that in this thyroid tumour histotype, as in PTC and DSV, P-cadherin is a marker of epidermoid differentiation rather than a marker of clinical aggressiveness.

The mechanisms that regulate P-cadherin expression are mostly unknown. The sequencing of the 5'-flanking region of P-cadherin gene has shown an Sp-1 binding site and a CpG island [22]; cytosine methylation of this region has been described in P-cadherin-negative prostate cancer cell lines, thus leading to the conclusion that methylation might play a role in this setting. However, the in vitro results have not been confirmed by in vivo findings, in which a lack of expression in cancer specimens was not associated with methylation of the promoter [22].

Another consistent finding in MECT was the abnormal E-cadherin expression, with the protein being diffusely distributed in the cytoplasm or accumulated in granules with a perinuclear localisation. We also observed absence of E-cadherin in one patient (no. 9). The cytoplasmic localisation of E-cadherin has been associated with alterations of the phosphorylation status of

members of adherens junctions with concomitant loss of connection of E-cadherin with the cytoskeleton [18]. The granular pattern suggests an accumulation of E-cadherin in Golgi vesicles, which might indicate a deficiency in protein transport to the cellular membrane (such a deficiency may be due to a defect in the actin polymerisation process, which is known to be important for the correct localisation of the E-cadherin/catenin complex [35]).

We observed a dissociation between the expression of E-cadherin and that of α-, β- and γ-catenin, with a loss of membrane-associated E-cadherin and occasional retention of the normal localisation of the catenins (e.g. patients 5, 8 and 9). A similar observation was reported by Cerrato et al. [11] and Rocha et al. [28] in some patients with follicular and papillary carcinoma of the thyroid. These findings indicate that β- and γ-catenins can establish connections with membrane-associated molecules other than cadherins; this possibility has already been demonstrated with regard to the association between β-catenin and c-erbB2 [31], MUC-1 [38] and EGF-R [21].

α-Catenin was down-regulated or even absent in seven MECT patients; three of these specimens were totally negative for α-catenin; absence of α-catenin immunoexpression has not been observed in PTC or DSV [28]. In the three specimens negative for α-catenin, there was also absence of expression for γ-catenin (patients 2, 10 and 11). Three of the four specimens with normal immunoreactivity for α-catenin also showed normal expression of both β- and γ-catenin (patients 5, 8 and 9); these three specimens apparently normal for the three catenins had major abnormalities of E-cadherin expression (apart from expressing P-cadherin; Table 2).

β-Catenin expression was absent in two patients and partially absent in two other patients. The remaining seven specimens displayed normal immunoexpression. This finding is similar to those reported in DSV [19, 28]. The normal membranous expression of β-catenin in patients with abnormal E-cadherin might be due to the binding of β-catenin to P-cadherin, although De Boer et al. [13] described a higher affinity of P-cadherin to γ-catenin than to β-catenin. In contrast to Garcia-Rostan et al. [16, 17], we did not find nuclear immunoreactivity for β-catenin in any MECT patients (also absent in PTC and DSV).

γ-Catenin expression was lost in five MECT patients and reduced and abnormally localised in two additional ones. These alterations, which outnumber those detected in PTC and DSV [28], may reflect methylation of the gene promoter resulting in silencing of the gene or a structural alteration like the one detected in a gastric carcinoma cell line [8].

We did not observe major differences in the immunostaining pattern between the primary tumour and the nodal metastasis in the single patient (no. 4) in which both tissues were available. This finding contrasts with the results reported by Bukholm et al. [7] in breast carcinoma, but its validity is obviously limited by the size of the sample.

In summary, like DSV on a smaller scale, MECT displays marked abnormalities of the cadherin/catenins complex compared with normal thyroid and PTC. Such abnormalities may be divided in two groups: (1) consistent neoexpression of P-cadherin and (2) marked abnormality of E-cadherin expression and/or of several of the three catenins. Such alterations apparently do not depend upon mutations, since there are usually a heterogeneous pattern of expression and slight differences when primary tumours are compared with metastases or metastases are compared with one another ([28], present study).

On the basis of the data of the present study together with previously obtained data in classical PTC and DSV [28], it is tempting to suggest that, like MECT, the DSV variant of PTC differs from classical PTC due to major and variable alterations of the cadherins/catenins complex. It remains to be found whether such phenotypic alterations reflect structural genetic hits or, as appears more likely from the available data, whether they merely reflect epigenetic changes. The aetiopathogenic mechanism or mechanisms involved in the acquisition of the phenotypic features of MECT also remain to be clarified.

Acknowledgements We would like to thank Dr. Geert Berx for his excellent advice and for useful discussions. This study was supported by PRAXIS XXI grants (ASR, PS, JCM and VM) and by the PRAXIS project P/SAL/13167/1.

References

1. Baloch ZW, LiVolsi VA (2000) Newly described tumours of the thyroid. Curr Diag Pathol 6:151–164
2. Behrens J, Mareel MM, Van Roy FM, Birchmeier W (1989) Dissecting tumor cell invasion: epithelial cells acquire invasive properties after the loss of uvomorulin-mediated cell-cell adhesion. J Cell Biol 108:2435–2447
3. Berx G, Cleton-Jansen AM, Nollet F, de Leeuw WJ, van de Vijver M, Cornelisse C, van Roy F (1995) E-cadherin is a tumour/invasion suppressor gene mutated in human lobular breast cancers. EMBO J 14:6107–6115
4. Böhm J, Niskanen L, Kiraly K, Kellokoski J, Eskelinen M, Hollmen S, Alhava E, Kosma VM (2000) Expression and prognostic value of alpha-, beta-, and gamma-catenins indifferentiated thyroid carcinoma. J Clin Endocrinol Metab 85:4806–4811
5. Brabant G, Hoang-Vu C, Cetin Y, Dralle H, Scheumann G, Molne J, Hansson G, Jansson S, Ericson LE, Nilsson M (1993) E-cadherin: a differentiation marker in thyroid malignancies. Cancer Res 53:4987–4993
6. Bracke ME, Van Roy FM, Mareel MM (1996) The E-cadherin/catenin complex in invasion and metastasis. Curr Top Microbiol Immunol 213:123–161
7. Bukholm IK, Nesland JM and Borresen-Dale AL (2000) Re-expression of E-cadherin, α-catenin and β-catenin, but not of γ-catenin, in metastatic tissue from breast cancer patients. J Pathol 190:15–19
8. Caca K, Kolligs FT, Ji X, Hayes M, Qian J, Yahanda A, Rimm DL, Costa J and Fearon ER (1999) Beta- and gamma-catenin mutations, but not E-cadherin inactivation, underlie T-cell factor/lymphoid enhancer factor transcriptional deregulation in gastric and pancreatic cancer. Cell Growth Differ 10:369–376
9. Cameselle-Teijeiro J (1996) Mucoepidermoid carcinoma and solid cell nests of the thyroid (letter to the editor). Hum Pathol 27:861

10. Cameselle-Teijeiro J, Febles-Perez C, Sobrinho-Simoes M (1995) Papillary and mucoepidermoid carcinoma of the thyroid with anaplastic transformation: a case report with histologic and immunohistochemical findings that support a provocative histogenetic hypothesis. Pathol Res Pract 91:1214–1221
11. Cerrato A, Fulciniti F, Avallone A, Benincasa G, Palombini L, Grieco M (1998) Beta- and gamma-catenin expression in thyroid carcinomas. J Pathol 185:267–272
12. Chan JK, Albores-Saavedra J, Battifora H, Carcangiu ML, Rosai J (1991) Sclerosing mucoepidermoid thyroid carcinoma with eosinophilia. A distinctive low-grade malignancy arising from the metaplastic follicles of Hashimoto's thyroiditis. Am J Surg Pathol 15:438–448
13. de Boer CJ, van Dorst E, van Krieken H, Jansen-van Rhijn CM, Warnaar SO, Fleuren GJ, Litvinov SV (1999) Changing roles of cadherins and catenins during progression of squamous intraepithelial lesions in the uterine cervix. Am J Pathol 155:505–515
14. Fialho F, Basilio-de-Oliveira CA, Azevedo N et al (1981) Carcinoma mucoepidermoide da tireoide. Folha Médica 82:397–402
15. Franssila KO, Harach HR, Wasenius VM (1984) Mucoepidermoid carcinoma of the thyroid. Histopathology 8:847–860
16. Garcia-Rostan G, Camp RL, Herrero A, Carcangiu ML, Rimm DL, Tallini G (2001) Beta-catenin dysregulation in thyroid neoplasms: down-regulation, aberrant nuclear expression, and CTNNB1 exon 3 mutations are markers for aggressive tumor phenotypes and poor prognosis. Am J Pathol 158:987–996
17. Garcia-Rostan G, Tallini G, Herrero A, D'Aquila TG, Carcangiu ML, Rimm DL (1999) Frequent mutation and nuclear localization of beta-catenin in anaplastic thyroid carcinoma. Cancer Res 59:1811–1815
18. Gumbiner BM (2000) Regulation of cadherin adhesive activity. J Cell Biol 148:399–403
19. Harach HR, Day ES, de Strizic NA (1996) Mucoepidermoid carcinoma of the thyroid. Report of a case with immunohistochemical studies. Medicina (B Aires) 46:213–216
20. Hedinger C, Williams ED, Sobin LH (1998) Histological typing of thyroid tumours. In: World Health Organization (ed) International histologic classification of tumours, 2nd edn. Springer Verlag, Berlin Heidelberg New York, p 9
21. Hoschuetzky H, Aberle H and Kemler R (1994) Beta-catenin mediates the interaction of the cadherin–catenin complex with epidermal growth factor receptor. J Cell Biol 127:1375–1380
22. Jarrard DF, Paul R, van Bokhoven A, Nguyen SH, Bova GS, Wheelock MJ, Johnson KR, Schalken J, Bussemakers M, Isaacs WB (1997) P-Cadherin is a basal cell-specific epithelial marker that is not expressed in prostate cancer. Clin Cancer Res 3:2121–2128
23. Mizukami Y, Matsubara F, Hashimoto T, Haratake J, Terahata S, Noguchi M, Hirose K (1984) Primary mucoepidermoid carcinoma in the thyroid gland. A case report including an ultrastructural and biochemical study. Cancer 53:1741–1745
24. Ozawa M, Baribault H, Kemler R (1989) The cytoplasmic domain of the cell adhesion molecule uvomorulin associates with three independent proteins structurally related in different species. EMBO J 8:1711–1717
25. Palacios J, Benito N, Pizarro A, Suarez A, Espada J, Cano A, Gamallo C (1995) Anomalous expression of P-cadherin in breast carcinoma. Correlation with E-cadherin expression and pathological features. J Pathol 146:605–612
26. Park WS, Oh RR, Park JY, Kim PJ, Shin MS, Lee JH, Kim HS, Lee SH, Kim SY, Park YG, An WG, Kim HS, Jang JJ, Yoo NJ, Lee JY (2001) Nuclear localization of beta-catenin is an important prognostic factor in hepatoblastoma. J Pathol 193:483–490
27. Rathigan RM, Roque JL, Bucher RL (1977) Mucoepidermoid carcinoma of the thyroid gland. Cancer 39:210–249
28. Rocha AS, Soares P, Seruca R, Maximo V, Matias-Guiu X, Cameselle-Teijeiro J, Sobrinho-Simoes M (2001) Abnormalities of the E-cadherin/catenin adhesion complex in classical papillary thyroid carcinoma and in its diffuse sclerosing variant. J Pathol 194:358–366
29. Rosai J, Carcangiu ML, DeLellis RA (1992) Atlas of tumor pathology: tumors of the thyroid gland, 3rd series. AFIP, Washington, p 109
30. Sambade C, Franssila K, Basilio-de-Oliveira CA, Sobrinho-Simões M (1990) Mucoepidermoid carcinoma of the thyroid revisited. Surg Pathol 3:271–280
31. Shibata T, Ochiai A, Kanai Y, Akimoto S, Gotoh M, Yasui N, Machinami R, Hirohashi S (1996) Dominant negative inhibition of the association between β-catenin and c-erbB-2 by N-terminally deleted β-catenin suppresses the invasion and metastasis of cancer cells. Oncogene 13:883–889
32. Shimoyama Y, Hirohashi S, Hirano S, Noguchi M, Shimosato Y, Takeichi M, Abe O (1989) Cadherin cell-adhesion molecules in human epithelial tissues and carcinomas. Cancer Res 49:2128–2133
33. Soares P, Berx G, van Roy F, Sobrinho-Simoes M (1997) E-cadherin gene alterations are rare events in thyroid tumors. Int J Cancer 70:32–38
34. Soler AP, Knudsen KA, Salazar H, Han AC, Keshgegian AA (1999) P-cadherin expression in breast carcinomas indicates poor survival. Cancer 86:1263–1272
35. Vasioukhin V, Bauer C, Yin M, Fuchs E (2000) Directed actin polymerization is the driving force for epithelial cell–cell adhesion. Cell 100:209–219
36. Vleminckx K, Vakaet L Jr, Mareel M, Fiers W, van Roy F (1991) Genetic manipulation of E-cadherin expression by epithelial tumor cells reveals an invasion suppressor role. Cell 66:107–119
37. von Wasielewski R, Rhein A, Werner M, Scheumann GF, Dralle H, Potter E, Brabant G, Georgii A (1997) Immunohistochemical detection of E-cadherin in differentiated thyroid carcinomas correlates with clinical outcome. Cancer Res 57:2501–2507
38. Yamamoto A, Bharti A, Li Y and Kufe D (1997) Interaction of the DF3/MUC1 breast carcinoma-associated antigen and beta-catenin in cell adhesion. J Biol Chem 272:12492–12494
39. Yap AS, Brieher WM, Gumbiner BM (1997) Molecular and functional analysis of cadherin-based adherens junctions. Annu Rev Cell Dev Biol 13:119–146

Virchows Arch (2002) 440:505–511
DOI 10.1007/s00428-002-0620-2

ORIGINAL ARTICLE

Yesim Gürbüz · Volker Kahlke · Günter Klöppel

How do gastric carcinoma classification systems relate to mucin expression patterns? An immunohistochemical analysis in a series of advanced gastric carcinomas

Received: 31 October 2001 / Accepted: 11 January 2002 / Published online: 21 March 2002
© Springer-Verlag 2002

Abstract Gastric carcinoma classifications differ in their value for distinguishing tumors according to their morphological pattern, functional properties, and biological significance. In this study we evaluated which of three established classification systems is best correlated with the expression patterns of certain mucins. A total of 160 gastric carcinomas from Turkey and Germany were screened immunohistochemically for the expression of MUC1, MUC2, MUC5AC, and MUC6, and the results were related to the different tumor categories in Lauren's, Carneiro's, and Goseki's classifications. It was found that in all three classifications carcinomas belonging to the gland-forming category most commonly expressed MUC1: 78% of Goseki's grade I carcinomas, 81.1% of Lauren's intestinal type carcinomas, and 82.8% of Carneiro's glandular type. MUC2 was expressed in all Goseki grade II carcinomas, which comprise the mucinous type, while it was not significantly associated with any of the other classifications. MUC5AC was found in all Goseki grade IV carcinomas, i.e., signet ring cell carcinomas. It was also significantly associated with Carneiro's mixed type and isolated cell type carcinomas, while there was no correlation with any of Lauren's types. MUC6 failed to show a relationship with any of the categories of the various classifications. We conclude that Goseki's classification is best correlated with MUC expression patterns because it distinguishes clearly between MUC1-positive gland-forming carcinomas, MUC2-positive mucinous ones, and MUC5AC-positive signet ring cell carcinomas. It is likely that each of these gastric carcinoma types has its own carcinogenesis.

Y. Gürbüz (✉) · G. Klöppel
Department of Pathology, University of Kiel, Michaelisstrasse 11, 24105 Kiel, Germany
e-mail: gkloeppel@path.uni-kiel.de
Tel.: +49-431-5973400, Fax: +49-431-5973462

V. Kahlke
Department of General and Thoracic Surgery, University of Kiel, Michaelisstrasse 11, 24105 Kiel, Germany

Keywords Gastric carcinoma classifications · Lauren's · Goseki's · Carneiro's · Mucin expression · MUC1 · MUC2 · MUC5AC · MUC6 · Immunohistochemistry

Introduction

Gastric carcinoma is a highly variable malignancy with respect to epidemiology, genetics, morphology, and biological behavior. This heterogeneity may be due to the fact that gastric carcinoma is caused by exogenous factors (i.e., nitrosamines and *Helicobacter pylori*) and endogenous factors (i.e., E-cadherin mutation) [2, 27]. It has therefore been hypothesized that the phenotypic spectrum found in various countries depends on whether intrinsic or extrinsic causal factors are prevailing [7].

To identify these phenotypic differences at the morphological level in a comparable and reproducible manner it is necessary to have a classification system that recognizes all types of gastric carcinoma adequately. The WHO classification has its merits, in that it presents histologically well described tumor categories. However, it is a purely descriptive classification that has very little relationship to prognosis and biological behavior [3, 24]. The most commonly used classification system for gastric carcinomas is that of Lauren [7, 12], and it has proven to be the most useful classification from the epidemiological standpoint [3, 6]. Its disadvantage is that it only roughly stratifies gastric carcinoma into three histopathological types, i.e., diffuse, intestinal, and unclassified, and is of little prognostic relevance. In 1992 and 1997 two other gastric carcinoma classification systems were proposed, one by Goseki et al. [9] and one by Carneiro [3], both of which are supposed to be related to prognosis. The Goseki et al. classification is based on gland formation and mucin production and distinguishes four grades, gland forming, mucinous, isolated cell with mucin production, and isolated cell without mucin production. Carneiro's classification recognizes a glandular type, an isolated cell type and a mixed type.

The mucin gene family consists of at least nine MUC genes whose tissue distribution has mainly been studied

with antibodies recognizing the core protein of the different mucins [4, 8]. In the normal stomach three mucins, MUC1, MUC5AC, and MUC6, show cell type specific expression. MUC1and MUC5AC are expressed in superficial epithelium of antral and oxyntic glands, while MUC6 is found in pyloric glands in the antrum and mucous neck cells of the body. The immunohistochemical expression patterns of these three mucins show interesting relationships between cellular differentiation and prognosis in gastric carcinomas [1, 13, 15, 18, 23].

The purpose of this work was to apply three recognized classification systems, i.e., those of Lauren, Goseki, and Carneiro, to a series of gastric carcinomas and investigate how the mucin expression patterns of the tumors fit the variously defined histological categories. Since the functional and biological properties of gastric carcinomas may be reflected in the tumors' ability to produce and secrete certain types of mucin, it would be of interest to determine which of the three classification systems is best correlated with the mucin immunophenotype.

Material and methods

The study included 20 patients examined between 1996 and 2000 at the Department of Pathology, Kocaeli University Medical Faculty, 60 cases diagnosed between 1993 and 2000 at the Department of Pathology, Antalya Government Hospital, and 80 cases examined between 1993 and 1996 at the Department of Pathology, University of Kiel. The cases were selected randomly, and early gastric carcinomas were excluded. The tumors were staged according to the TNM classification. All available microscopic slides were evaluated, and the tumors were classified histologically according to the Lauren, Carneiro, and Goseki classifications [3, 6, 9]. Because these classification systems use varying differentiation criteria, such as gland formation and mucin production, no further grading was applied to this series of gastric carcinomas. One appropriate tissue block (usually also containing nonneoplastic gastric mucosa) was selected from each patient's tumor for the immunohistochemical evaluation.

From each paraffin-embedded tumor tissue block microscopic slides containing two 4-µm sections on one slide (one for the negative control) were prepared. The sections were deparaffinized at 56°C for 12 h, then treated with xylene, absolute alcohol, and 96% alcohol. The slides were washed with tap water, and the appropriate buffer was added before applying specific antigen retrieval. This was followed by staining with antibodies to MUC1 (Ma695, Novo-Castra, Newcastle, UK), MUC2 (Ccp58, Novo-Castra), MUC5AC (CLH2, Chemicon, Temecula, Calif., USA) and MUC6 (CLH5, Novo-Castra). After incubation with secondary antibody and chromogen the sections were washed with tap water, then distilled water, and counterstained with Mayer's hemalum. They were then treated with 1% ammonia, rinsed in distilled water and mounted in glycerin gel. Negative controls were run with nonimmune serum and positive controls with the appropriate tissue.

The results were evaluated according to the modified scoring scale used by Reis et al. [20]. Briefly, tumors containing less than 25% immunostained cells were scored 1+, tumors with 25% – 50% positive cells 2+, and tumors with more than 50% positive cells 3+. The SPSS χ^2 test was used to evaluate the results. *P* values less than 0.05 were regarded as statistically significant.

Results

The TNM classification of the 160 gastric carcinomas revealed 7 tumors in stage Ib, 33 in stage II, 72 in stage IIIa, 14 in stage IIIb, and 34 in stage IV. When the tumors were classified histologically according to Lauren, serosal invasion was most frequently found in the unclassified type (89%), followed by the diffuse type (68.4%) and the intestinal type (67%). Lymph node metastasis of the N1 or N2 category was found in 89.4% of tumors of the diffuse type, followed by the intestinal type (83.5%) and the unclassified type (66.6%). In Goseki's classification, serosal invasion was most frequent in grade II carcinomas (82%), followed by grade IV (71%), grade I (70%), and grade III carcinomas (66%), while lymph node metastases occurred in all grade II carcinomas (100%), in 87% of grade IV carcinomas, in 83% of grade III carcinomas, and 80.5% of grade I carcinomas. In Carneiro's classification, solid-type carcinomas had the highest rate of serosal invasion (87.5%), followed by the mixed type (70.6%), the glandular type (66.6%), and the isolated type (66.6%). Lymph node metastases were most frequent in the isolated type (90%), followed by the mixed type (86%), the glandular type (79.6%), and the solid type (75%).

Table 1 MUC expression in gastric carcinomas stratified according to Lauren's classification

	Intestinal (*n*=85)		Diffuse (*n*=57)		Unclassified (*n*=18)		*P*
	n	%	*n*	%	*n*	%	
MUC 1	68	82.0	25	43.8	9	50.0	<0.0001
MUC 2	41	48.2	34	59.6	12	66.6	>0.22
MUC 5AC	57	67.0	46	80.7	12	66.6	>0.181
MUC 6	27	31.7	14	24.5	7	38.8	<0.448

Table 2 MUC expression in gastric carcinomas stratified according to Goseki's classification

	Grade I (*n*=77)		Grade II (*n*=11)		Grade III (*n*=41)		Grade IV (*n*=31)		*P*
	n	%	*n*	%	*n*	%	*n*	%	
MUC 1	60	78.0	6	54.5	21	51.2	16	51.6	<0.008
MUC 2	34	44.0	11	100.0	17	41.4	25	80.6	<0.0001
MUC 5AC	53	68.8	9	81.8	22	53.6	31	100.0	<0.0001
MUC 6	25	32.4	3	27.2	9	22.0	11	35.4	>0.578

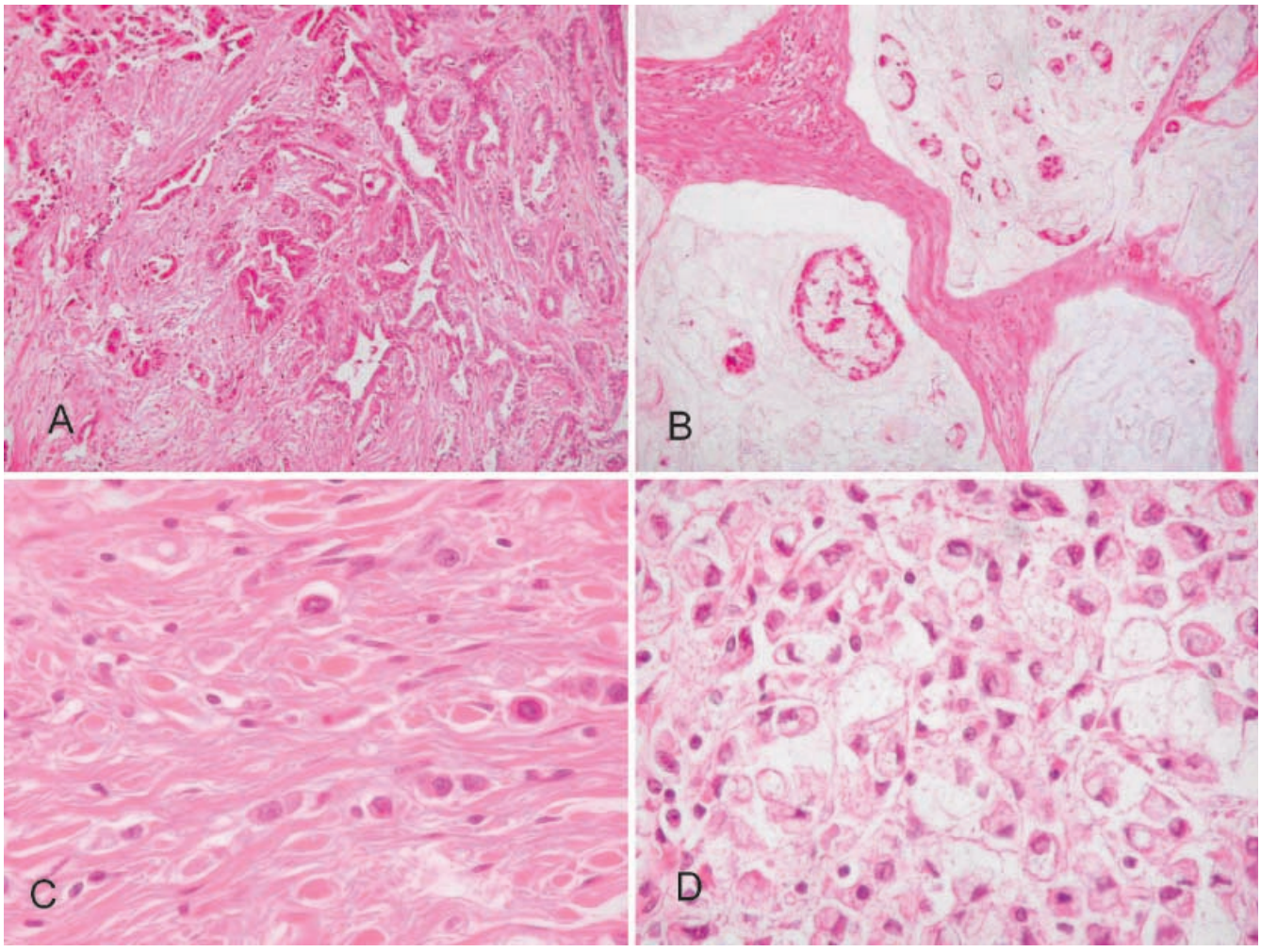

Fig. 1A–D Histological types of gastric carcinoma classified according to Goseki. **A** Gland-forming carcinoma without excessive mucin production (Goseki grade I). Hematoxylin and eosin, ×5. **B** Mucinous adenocarcinoma with excessive extracytoplasmic mucin production (Goseki grade II). Hematoxylin and eosin, ×5. **C** Diffuse infiltrating carcinoma without gland formation and mucin production (Goseki grade III). Hematoxylin and eosin, ×20. **D** Signet ring cell carcinoma without gland formation, but with intracytoplasmic mucin production (Goseki grade IV). Hematoxylin and eosin, ×20

Table 3 MUC expression in gastric carcinomas stratified according to Carneiro's classification

	Mixed (*n*=58)		Glandular (*n*=64)		Isolated cell (*n*=30)		Solid (*n*=8)		*P*
	n	%	*n*	%	*n*	%	*n*	%	
MUC 1	37	63.7	53	82.8	10	33.3	3	37.5	<0.0001
MUC 2	35	60.3	29	45.3	17	56.6	6	75.0	>0.223
MUC 5AC	48	82.7	39	61.0	24	80.0	4	50.0	<0.018
MUC 6	21	36.2	17	26.5	6	20.0	4	50.0	>0.224

Tables 1, 2, 3 show the correlation between the expression of the different MUC glycoproteins and the various categories distinguished in the three gastric carcinoma classification systems. Table 4 summarizes the relative frequency of expression of the various MUC glycoproteins for all cases. Figure 1 shows the main histopathological types of gastric carcinoma observed in this study.

Table 4 Relative frequency of immunoreactivity for MUC1, MUC2, MUC5AC, and MUC6 in 160 gastric carcinomas

	n	%
MUC 1	103	64.4
MUC 2	87	54.4
MUC 5AC	115	72.0
MUC 6	48	30.0

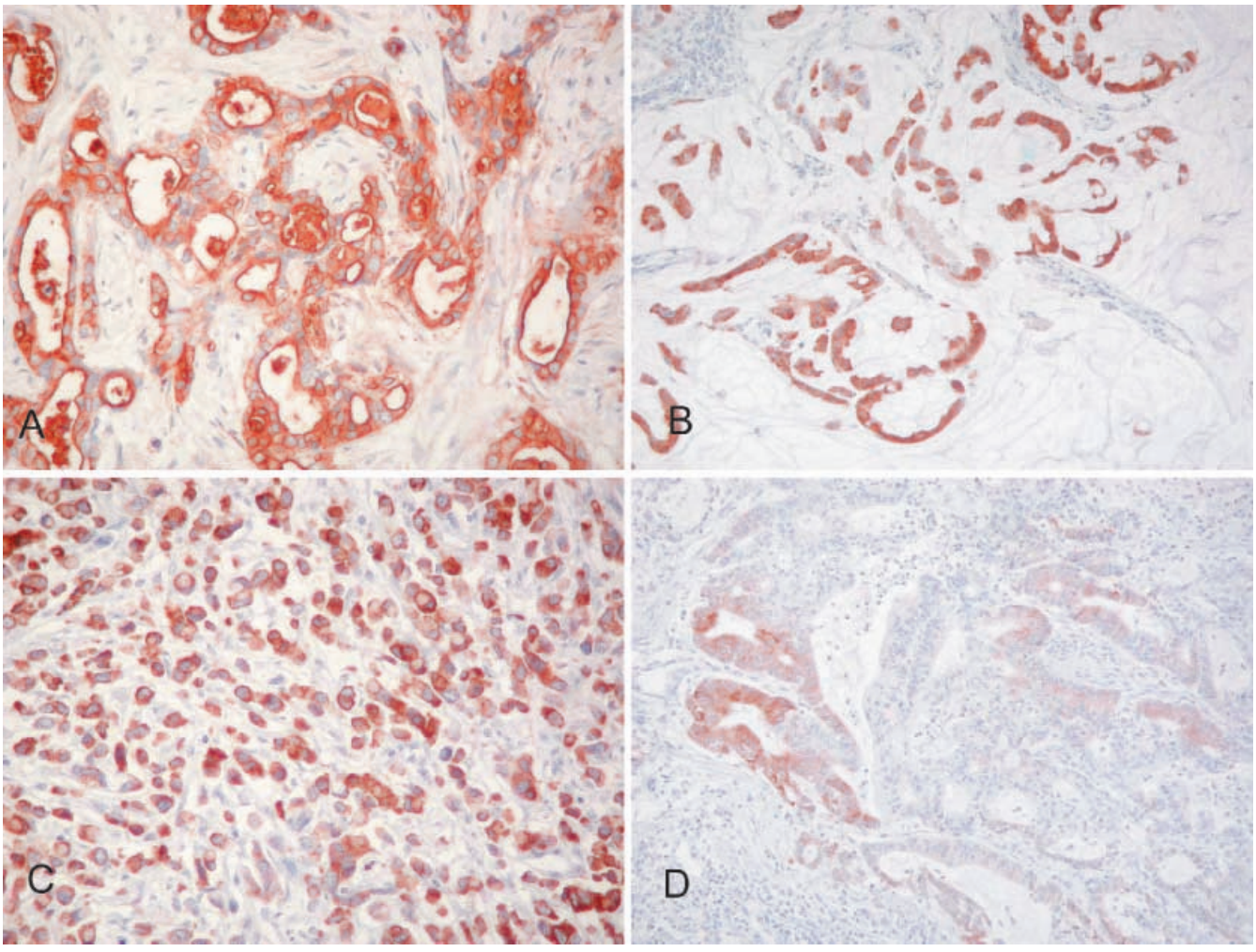

Fig. 2A–D MUC expression in gastric carcinomas classified according to Goseki. **A** Mainly apical and membranous MUC1 immunoreactivity in Goseki grade I gastric carcinoma. MUC1, ×10. **B** Intracytoplasmic MUC2 immunoreactivity in Goseki grade II gastric carcinoma. MUC2, ×10. **C** Intracytoplasmic MUC5AC immunoreactivity in Goseki grade IV gastric carcinoma. MUC5AC, ×10. **D** Focal and faint MUC6 immunoreactivity in Goseki grade I carcinoma. MUC6, ×10

MUC1 expression was observed in most of the cases, generally at apical and intraluminal but occasionally also intracytoplasmic localizations (Fig. 2A). In Lauren's classification MUC1 immunoreactivity was almost twice as common in intestinal type carcinomas (81.1%, >50% scoring 2+) as in diffuse type carcinomas (43.8%, >50% scoring 2+). In Carneiro's classification MUC 1 was most commonly expressed in glandular carcinomas (82.81%, >50% scoring 2+), followed by mixed carcinomas (54.5%, >50% scoring 1+), and in Goseki's classification in grade I carcinomas (77.9%, >50% scoring 2+), followed by grade II carcinomas (54.5%, >50% scoring 2+; Tables 1, 2, 3). There was a statistically significant correlation between MUC1 expression and the gland forming category in all three classifications.

In approx. one-half of the cases MUC2 immunoreactivity was observed in cytoplasmic localizations (Table 4). It was observed in all carcinomas of the mucinous type (Fig. 2B). Since in Goseki's classification this tumor type is considered separately as grade II carcinoma, 100% of these carcinomas were MUC2 positive (>50% scored 3+; Table 2).

MUC5AC expression was observed in intracytoplasmic localizations in 71.9% of cases. It was more common in Lauren's diffuse type (80.7%, >50% scoring 3+) than in the intestinal type (67%, >50% scoring 1+), and in Carneiro's mixed (82.75%, >50% scoring 2+) and isolated cell (80%, >50% scoring 3+) types than in the glandular type (61%, >50% scoring 1+; Fig. 2C). In Goseki's classification 100% of grade IV carcinomas stained for MUC5AC (>50% scoring 3+), while grade III carcinomas showed the lowest expression (53.6%, >50% scoring 1+) (Table 2). Statistically significant differences were observed in Carneiro's (P<0.018) and Goseki's (P<0.0001) classifications (Tables 2, 3).

MUC6 expression was generally focal and weak (>50% scored 1+; Fig. 2D) and was not correlated with any category of any classification (Tables 1, 2, 3).

MUC 5AC was observed in 72% of cases, followed by MUC1, MUC2, and MUC6 (Table 4). Mucin coex-

pression was observed in 119 cases (74.4%). Coexpression of four different mucins was observed in 18 of the cases (11.2%). MUC1 staining tumors showed serosal invasion in 72% of the cases and lymph node metastasis in 83.4%; MUC2 staining tumors revealed serosal invasion in 78% of the cases and lymph node metastasis in 85%; MUC5AC staining tumors showed serosal invasion in 70.4% of the cases and lymph node metastasis in 88%; MUC1 staining tumors showed serosal invasion in 72% of the cases and lymph node metastasis in 83.4% and MUC6 staining tumors revealed serosal invasion in 85% of the cases and lymph node metastasis in 58.3%.

Discussion

Gastric carcinoma is one of the most complex human malignancies, and its morphological spectrum is difficult to relate to epidemiology, etiology, pathogenesis, and biological behavior. As a result, none of the currently employed gastric carcinoma classifications are fully satisfactory to either epidemiologists, pathologists, or surgeons [24]. In this study we examined which of three established classification systems best recognizes the functional properties of the tumors, as reflected by their mucin expression patterns. We found that Goseki's classification is most accurately correlated with the mucin expression profile of MUC1, MUC2, and MUC5AC in gastric carcinomas.

It is well established that in normal gastric mucosa MUC1 and MUC5AC are expressed in superficial gastric epithelium of the body and antrum, while MUC6 is detected in pyloric glands in the antrum and mucous neck cells of the body [8]. MUC2 is an intestinal mucin that is not expressed in normal gastric mucosa but is detected in goblet cells of intestinal metaplasia [23, 26]. Immunohistochemical investigations of MUC expression in gastric carcinomas revealed that the tumors' MUC expression patterns follow in part the mucin expression profile of the normal gastric mucosa, show relations with histopathological tumor subtypes, and may have an impact on prognosis [13, 21, 22].

The most commonly used gastric carcinoma classification is that of Lauren, which recognizes intestinal, diffuse, and unclassified subgroups. From the standpoint of epidemiology the Lauren classification is meaningful. However, it has no prognostic relevance, and, moreover, it puts all gastric carcinomas that have both intestinal and diffuse components in the unclassified subgroup [3, 7]. The Goseki classification system based on gland formation and on mucus production by the tumor cells classifies gastric carcinomas into four grades. Different from other classification systems, isolated cell carcinomas are considered as mucin producing (grade IV) or non-mucin producing (grade III) the classical signet ring cell carcinoma being in the grade IV category [9]. The main basis of this classification system seems logical. However, some gastric carcinomas have such a complex and heterogeneous pattern that it is not easy to decide on a standard pattern in some cases. There is contradictory evidence as to whether the Goseki classification is predictive of patient survival. Some studies have shown it not to be so [17, 25], while others have found it to be directly related to prognosis [16, 24]. One study found Goseki grade III carcinomas to be an indicator of a poor prognosis, while another [16] showed Goseki grades II and IV to be correlated with a poor prognosis.

In 1997 Carneiro [3] developed a new classification system that distinguishes four histological types, glandular, isolated cell, solid, and mixed. This new classification points out the differences in the biological behavior of gland forming and isolated cell gastric carcinomas. The mixed carcinomas, which have the worst prognosis, encompass carcinomas with an isolated cell component associated with another component. However, the diagnosis of mixed carcinoma may cause difficulties because the presence of a second component in the tumor occupying 5% of its volume may change the classification [3].

MUC1 is a membrane-associated mucin expressed widely throughout the body, but relatively sparsely in the gastric epithelium. Immunoreactivity ranging between 24.3% and 100% in gastric carcinoma series have been reported in the literature [1, 13, 15, 21, 28]. Concordant with our findings, MUC1 expression is more common in tumors with a gland-forming pattern than in those without [13, 19, 21, 26]. In each of the three classification systems evaluated we found that MUC1 expression to be correlated significantly with the gland forming category of gastric carcinoma.

MUC2 expression is observed in the small intestine and the right colon but not in normal gastric mucosa [26]. As with Reis et al. [23] and Pinto-de-Sousa et al. [19], we observed 100% MUC2 immunoreactivity in Goseki grade II tumors including all mucinous carcinomas, which therefore differed significantly from all the remaining tumor categories. The two other classification systems failed to showed statistically significant differences between their tumor categories and MUC2 expression. In particular, we did not observe any relationship between MUC2 expression and a gland-forming pattern. This suggests that a gland-forming pattern bears no clear relationship to intestinal differentiation, as postulated by Correa's model of gastric carcinogenesis and Lauren's classification [5, 6]. On the other hand, the selective expression of MUC2 in gastric carcinoma of the mucinous type confirms again that mucinous (colloid) carcinomas are a specific morphological entity, because this phenomenon is shared by all mucinous tumors regardless of whether they originate from the ovary, pancreas, breast, and colon [10, 14, 29]. Common to these neoplasms also seems to be a more favorable prognosis than in the mucin-producing carcinomas of the usual MUC1 positive type [13].

MUC5AC is expressed in superficial foveolar epithelium of the normal gastric mucosa and commonly in gastric carcinomas with a diffuse pattern [19, 20, 23]. As to be expected, we also observed a high percentage of

MUC5AC immunoreactivity in Lauren's diffuse type carcinomas and Carneiro's carcinomas with isolated cell and mixed patterns. A 100% expression, however, was observed only in Goseki grade IV carcinomas, which comprise signet ring cell carcinomas.

MUC6, the mucin that occurs in the mucous cells of the neck zone and in the antral glands, was expressed focally and faintly in almost one-third of gastric carcinomas, but had no relationship to the various histopathological categories of the three classification systems. It therefore seems to play no role in distinguishing certain types of gastric carcinomas [23].

Coexpression of mucin was a frequent finding in all gastric carcinomas and not restricted to any special histological type. Coexpression of different kinds of mucin in the same cell can also be observed in foci of incomplete metaplasia [22].

In summary, our correlation of these three gastric carcinoma classification systems with the mucin expression patterns of the carcinomas reveals that Goseki's classification is best correlated with MUC expression patterns because it distinguishes clearly between MUC1-positive gland-forming carcinomas, MUC2-positive mucinous carcinomas, and MUC5AC-positive signet ring cell carcinomas. It is likely that each of these gastric carcinoma types has its own carcinogenesis. Goseki's is also the only classification that distinguishes between the mucin-producing and non-mucin-producing isolated cell carcinoma type. This distinction may be very important in that MUC5AC-producing isolated cell carcinomas, which probably originate from superficial foveolar cells of the gastric mucosa, may be considered better differentiated tumors than non-mucin-producing isolated carcinomas, which must be regarded as poorly differentiated. This interpretation is in line with data showing that this gastric carcinoma type has the worst prognosis [24]. Since we also observed a high rate of MUC5AC immunoreactivity in Carneiro's mixed pattern tumors, it can be speculated that most of the mixed carcinomas started as signet ring cell tumors and only later showed dedifferentiation during tumor progression. In line with this interpretation is the observation of Reis et al. [20] and Hattori and Kushima [11] that MUC5AC expression is higher in early gastric carcinomas than in advanced carcinomas. Alternatively, mixed carcinomas might arise from two clones with differing differentiation.

Acknowledgements Y.G. was a fellow of the Alexander von Humboldt-Stiftung, Bonn, Germany. We are grateful to Ms. Maike Pacena and Ms. Anja Paulus for their excellent technical assistance and Mrs. Kay Dege for editing the manuscript.

References

1. Baldus SE, Zirbes TK, Engel S, Hanisch FG, Monig SP, Lorenzen J, Glossmann J, Fromm S, Thiele J, Pichlmaier H, Dienes HP (1998) Correlation of the immunohistochemical reactivity of mucin peptide cores MUC1 and MUC2 with the histopathological subtype and prognosis of gastric carcinomas. Int J Cancer 79:133–138
2. Becker KF, Atkinson MJ, Reich U, Becker I, Nekarda H, Siewert JR, Hofler H (1994) E-cadherin gene mutations provide clues to diffuse type gastric carcinomas. Cancer Res 54:3845–3852
3. Carneiro F (1997) Classification of gastric carcinomas. Curr Diagn Pathol 4:51–59
4. Carvalho F, David L, Aubert JP, Lopez-Ferrer A, De Bolos C, Reis CA, Gartner F, Peioxoto A, Alves P, Sobrinho-Simoes M (1999) Mucins and mucin-associated carbohydrate antigens expression in gastric carcinoma cell lines. Virchows Arch 435:479–485
5. Correa P (1988) A human model of gastric carcinogenesis. Cancer Res 48:3554–3560
6. Fenoglio-Preiser CM, Noffsinger AE, Stemmermann GN, Lantz PE, Listrom MB, Rilke FO (1999) The neoplastic stomach. In: Fenoglio-Preiser CM, Noffsinger AE, Stemmermann GN, Lantz PE, Listrom MB, Rilke FO (eds) Gastrointestinal pathology. An atlas and text, 2nd edn. Lippincott-Raven, Philadelphia, pp 237–274
7. Fenoglio-Preiser C, Carneiro F, Correa P, Guilford P, Lambert R, Megraud F, Muñoz N, Powell SM, Rugge M, Sasako M, Stolte M, Watanabe H (2000) Gastric carcinoma. In: Hamilton SR, Aaltonen LA (eds) Pathology and genetics of tumours of the digestive system. WHO classification of tumours. IARC, Lyon, pp 39–52
8. Gendler SJ, Spicer AP (1995) Epithelial mucin genes. Annu Rev Physiol 57:607–634
9. Goseki N, Takizawa T, Koike M (1992) Differences in the mode of the extension of gastric cancer classified by histological type: new histological classification of gastric carcinoma. Gut 33:606–612
10. Hanski C, Hofmeier M, Schmitt-Gräff A, Riede E, Hanski ML, Borchard F, Sieber E, Niedobitek F, Foss HD, Stein H, Riecken EO (1997) Overexpression or ectopic expression of MUC2 is the common property of mucinous carcinomas of the colon, pancreas, breast, and ovary. J Pathol 182:385–391
11. Hattori T, Kushima R (2001) [Gastric differentiated stomach adenocarcinoma]. Pathologe 22:97–104
12. Lauren P (1965) The two histological main types of gastric carcinoma: diffuse and so-called intestinal-type carcinoma. Acta Pathol Microbiol Scand 64:31–49
13. Lee HS, Lee HK, Kim HS, Yang HK, Kim YI, Kim WH (2001) MUC1, MUC2, MUC5AC, and MUC6 expressions in gastric carcinomas. Their roles as prognostic indicators. Cancer 92:1427–1434
14. Lüttges J, Zamboni G, Longnecker D, Klöppel G (2001) The immunohistochemical mucin expression pattern distinguishes different types of intraductal papillary mucinous neoplasms of the pancreas and determines their relationship to mucinous noncystic carcinoma and ductal adenocarcinoma. Am J Surg Pathol 25:942–948
15. Machado JC, Nogueira AM, Carneiro F, Reis CA, Sobrinho-Simoes M (2000) Gastric carcinoma exhibits distinct types of cell differentiation: an immunohistochemical study of trefoil peptides (TFF1 and TFF2) and mucins (MUC1, MUC2, MUC5AC, and MUC6). J Pathol 190:437–443
16. Martin IG, Dixon MF, Sue-Ling H, Axon AT, Johnston D (1994) Goseki histological grading of gastric cancer is an important predictor of outcome. Gut 35:758–763
17. Mönig S, Baldus SE, Collet PH, Zirbes TK, Bollschweiler E, Thiele J, Dienes HP, Hölscher AH (2001) Histological grading in gastric cancer by Goseki classification: correlation with histopathological subtypes and prognosis. Anticancer Res 21:617–620
18. Nakagawa K, Akagi J, Takai E, Tamori Y, Okino T, Kako H, Egami H, Ogawa M (1999) Prognostic values of MUC-1 molecule expressing cytokine receptor-like epitope and DF3 in patients with gastric carcinoma. Int J Oncol 14:425–435
19. Pinto-De Sousa J, David L, Reis CA, Gomes R, Silva L, Pimenta A (2001) Mucins MUC1, MUC2, MUC5AC and MUC6 expression in the evaluation of differentiation and clinico-biological behaviour of gastric carcinoma. Virchows Arch DOI 10.1007/s00428-001-0548-y

20. Reis CA, David L, Nielsen PA, Clausen H, Mirgorodskaya K, Roepstorff P, Sobrinho-Simoes M (1997) Immunohistochemical study of MUC5AC expression in human gastric carcinomas using a novel monoclonal antibody. Int J Cancer 74:112–121
21. Reis CA, David L, Seixas M, Burchell J, Sobrinho-Simoes M (1998) Expression of fully and under-glycosylated forms of MUC1 mucin in gastric carcinoma. Int J Cancer 79:402–410
22. Reis CA, David L, Correa P, Carneiro F, De Bolos C, Garcia E, Mandel U, Clausen H, Sobrinho-Simoes M (1999) Intestinal metaplasia of human stomach displays distinct patterns of mucin (MUC1, MUC2, MUC5AC, and MUC6) expression. Cancer Res 59:1003–1007
23. Reis CA, David L, Carvalho F, Mandel U, De Bolos C, Mirgorodskaya E, Clausen H, Sobrinho-Simoes M (2000) Immunohistochemical study of the expression of MUC6 mucin and co-expression of other secreted mucins (MUC5AC and MUC2) in human gastric carcinomas. J Histochem Cytochem 48:377–388
24. Songun I, van de Velde CJ, Arends JW, Blok P, Grond AJ, Offerhaus GJ, Hermans J, van Krieken JH (1999) Classification of gastric carcinoma using the Goseki system provides prognostic information additional to TNM staging. Cancer 85:2114–2118
25. Stachura J, Popiela T, Kulig J, Urbanczyk K, Heitzman J (1998) Lauren's and Goseki's grade distribution does not change along with the progression from an early to advanced gastric carcinoma. Pol J Pathol 49:151–153
26. Taylor KL, Mall AS, Barnard RA, Ho SB, Cruse JP (1998) Immunohistochemical detection of gastric mucin in normal and disease states. Oncol Res 10:465–473
27. Uemura N, Okamoto S, Yamamoto S, Matsumura N, Yamaguchi S, Yamakido M, Taniyama K, Sasaki N, Schlemper RJ (2001) Helicobacter pylori infection and the development of gastric cancer. N Engl J Med 345:784–789
28. Utsunomiya T, Yonezawa S, Sakamoto H, Kitamura H, Hokita S, Aiko T, Tanaka S, Irimura T, Kim YS, Sato E (1998) Expression of MUC1 and MUC2 mucins in gastric carcinomas: its relationship with the prognosis of the patients. Clin Cancer Res 4:2605–2614
29. Yasuda K, Adachi Y, Shiraishi N, Yamaguchi K, Shiromizu A, Kitano S (2001) Pathology and prognosis of mucinous gastric carcinoma. J Surg Oncol 76:272–277

Virchows Arch (2002) 440:512–518
DOI 10.1007/s004280100534

ORIGINAL ARTICLE

Michael Ebsen · Olaf Anhenn · Christian Roder
Konrad Morgenroth

Morphology of adenovirus type-3 infection of human respiratory epithelial cells in vitro

Received: 20 February 2001 Accepted: 23 July 2001 / Published online: 24 October 2001
© Springer-Verlag 2001

Abstract The adenovirus is a non-enveloped DNA virus which may lead to severe diseases of the respiratory tract. In order to study the influence of virus infection on primary cultured peribronchial submucosal gland cells, we performed in vitro infection with human adenovirus type 3. Peribronchial submucosal glands are the main source of tracheobronchial mucus and, therefore, play a major pathophysiological role in common pulmonary diseases such as bronchial asthma, chronic obstructive pulmonary disease and cystic fibrosis. The success of infection was verified by means of immunofluorescence and transmission electron microscopy. Infection follows a certain timetable with a climax of paracristalline intranuclear virus inclusions after 48 h of infection. Virus particles could be detected in the nucleus as well as in peripheral and perinuclear cytoplasmatic vacuoles. The release of virus capsids from the nucleus could be visualized using transmission electron microscopy and immunofluorescence with antibodies against hexon proteins. Two different kinds of mechanisms of transition of newly synthesized virus capsids from the nucleus into the cytoplasm could be identified. Due to an increasing cytopathic effect, viruses spread from cytoplasm after longer terms of infection. Cytopathic effects and cytoskeleton aspects under this virus infection could be characterized using immunofluorescence with several monoclonal antibodies against different cytokeratins.

Keywords Adenovirus · Confocal scanning microscope · Transmission electron microscope · Hexon protein

M. Ebsen (✉) · O. Anhenn · K. Morgenroth
Department of Pathology, Ruhr-University Bochum,
Universitätstr. 150, 44780 Bochum, Germany
e-mail: Michael.Ebsen@ruhr-uni-bochum.de
Tel.: +49-234-3227299, Fax: +49-234-3214200

C. Roder
Department of Virology, Ruhr-University Bochum, Bochum,
Germany

Introduction

In 1953, Rowe first described a filterable agent that disrupted surgically removed adenoidal tissue of children [21]. These adenoviruses are responsible for a small portion of acute respiratory morbidity in the general population and about 5–10% of respiratory illness in children. Besides respiratory diseases, adenoviruses cause epidemic conjunctivitis, and they have been associated with a variety of additional clinical syndromes, e.g., infantile gastroenteritis [11, 12].

More recently, adenoviral genes and virion components have been dissected and reassembled in different ways for ferrying foreign DNA into cells; the resulting formulations have been tested as vectors for vaccine delivery and gene therapy [14, 20]. In patients with chronic obstructive pulmonary disease (COPD), the integration of adenoviral DNA (E1A-gene) and the expression of the corresponding protein was demonstrated [7, 15].

Adenoviruses grow in a variety of cells, for example primary human kidney cells (HEK), the A549 cell line, HEP-2, or HeLa cells [2, 4]. In the late 1980s, primary cell culture models of human and animal peribronchial submucosal glands cells were established, and the physiological and secretory characteristics of these cells were described in detail [5, 8, 9, 10, 23, 24]. Adenovirus infection of this special cell type has not yet been performed.

Airway secretions originate from at least three secretory cell types: epithelial goblet cells, and serous and mucous tracheobronchial submucosal gland cells [13, 16]. The submucosal glands are considered to be the main source of tracheobronchial mucus [1]. Hypercrinia and dyskrinia are important pathophysiological parameters in several pulmonary diseases, such as bronchial asthma, COPD, and cystic fibrosis.

In order to study the morphological changes and the influence on the mechanisms of secretion in these special cell types caused by adenovirus infection, human peribronchial submucosal glands cells were infected with human adenovirus type 3 for different periods of time

and investigated by means of light microscopy and transmission electron microscopy (TEM). Success of infection was controlled using immunofluorescence (IF), and changes in the cytoskeleton assembly were controlled by examination of cytokeratin (Ck) expression.

Materials and methods

Materials

Main bronchi and lobe bronchi from 25 patients with different pulmonary diseases (nine squamous cell carcinomas, four adenocarcinomas, two adenosquamous carcinomas, one small cell carcinoma, one giant cell carcinoma, one hemagioperizytoma, one carcinoid, one hamartochondroma, one echinococcus cyst, one cicatrization, one bronchiectasis, one interstitial fibrosis, and one pneumonia) were obtained directly after surgical resection. Nine patients were female (average age 53.2 years) and sixteen patients were male (average age 57.1 years). Bronchi were rinsed in phosphate-buffered saline (PBS) and suspended overnight in bronchial epithelial cell medium (PromoCell, serum-free, containing 0.5 ng/ml epidermal growth factor, 5 µg/ml insulin, 0.5 µg/ml hydrocortisone, 0.5 µg/ml epinephrine, 6.5 ng/ml triiodothyronine, 10.0 µg/ml transferrin, 0.1 ng/ml retinoic acid, 2 ml bovine pituitary extract) and 1% antibiotics. The bronchial epithelium was removed by means of sharp dissection and the gland-rich submucosal tissue was dissected from cartilage and adventitia. Tissue fragments were recovered by centrifugation (1000×*g*, 5 min). The pellet was then enzymatically disaggregated with buffered collagenase type I (Sigma) and desoxyribonuclease (Sigma) in two successive cycles each for 1 h. After disaggregation, the cells were resuspended in the above-described medium. Flasks for the first passage were covered with fibronectin (Becton Dickinson). Cells were incubated at 37°C in 5% CO_2/95% air, and medium (PromoCell) was changed every second day. Fiboblasts were coarsely removed by means of trypsinization. Confluency was reached after 3–4 weeks. Cells were then plated on flasks (Saarstedt) for second-passage cultivation. These second-passage cells were used for investigation.

Virus infection

After reaching subconfluency, cells were infected with human adenovirus type 3 (kindly provided by Prof. Dr. Werchau, Department of Virology, Ruhr University, Bochum, Germany). Time intervals of infection varied from 20 min to 40 min and from 8, 12, 16, 24, 36, 48, 54, to 72 h. Infection was done under standard culture conditions. The multiplicity of infection was 0.1 or 1.0.

Light microscopy

Light microscopic investigations were done on semi-thin sections of Epon embedded material for TEM (see below). These semi-thin sections were performed on a Reichert Om U3 Ultramicrotome (Leica). During infection, cells were observed under an inverted phase-contrast microscope (Olympus IMT-2) in order to evaluate cell morphology and cytopathic effects under culture conditions.

Transmission electron microscopy

For TEM examination, cells were detached from flask bottom by means of trypsinization (PromoCell). Cells were fixed for 2 h in 2.5% glutaraldehyde in phosphate buffer (pH 7.2). After postfixation in osmiumtetroxide and block contrastation with uranyl acetate, they were dehydrated in graded series of ethanol and embedded in Epon 812. Semi-thin sections were cut using a Reichert Om U3 Ultramicrotome, stained with methylene blue for 2 min, and evaluated under the light microscope. Ultrathin sections of selected cell areas were stained with lead citrate and examined using TEM (Zeiss EM 900). They were compared with their non-infected counterparts.

Immunofluorescence

For indirect IF investigations, cells from the second passage were grown on Chamber Slides (Nunc). Cultivation was performed until subconfluency. After 10 min of fixation in either an ethanol/acetic acid solution or neutral buffered formalin (3%), cells were washed in PBS three times. Incubation with the primary antibodies (Table 1) was carried out for 2 h. Incubation with the Alexa-labelled (Molecular Probes) secondary antibodies was done for 1 h in a dilution of 1 to 200. As negative controls, non-infected cells from the same passage were used. Examination was carried out using a confocal laser scanning microscope (CLSM, Leica) or an epifluorescence microscope (Leica, Dialux 20).

Table 1 Primary antibodies used

Antigen	Species cross reactivity	Clone	Host	Ig class / subtype	Manufacturer	Order-no.
Ck 4	Human, cat, dog, guinea pig, goat, hamster, rabbit, sheep	6B10	Mouse	IgG_1	Sigma Germany	C5176
Ck 5/6	Human	D5/16B4	Mouse	IgG_1	Boehringer Germany	1 273 396
Ck 7	Human	OV-TL 12/30	Mouse	IgG_1	BioGenex USA	MU255-UC
Ck 8	Human	4.1.18	Mouse	IgG_1	Boehringer Germany	1 238 817
Ck 10	Human	DEK-10	Mouse	IgG_1	BioGenex USA	MU201-UC
Ck 13	Human	KS-1A3	Mouse	IgG_1	Sigma Germany	C0791
Ck 17	Human, rat	Ks 17.E3	Mouse	IgG_{2b}	Progen Germany	61036
Ck 18	Human	CY-90	Mouse	IgG_1	Sigma Germany	C8541
Ck 19	Human	Ks 19.1 (A53-B/A2)	Mouse	IgG_{2a}	Progen Germany	61010
Ck Pan	Human	AE1 & AE3	Mouse	IgG_1	BioGenex USA	MU071-UC
Ck Pan	Human	Polyclonal antiserum	Rabbit	IgG	BioGenex USA	PU071-UC
Hexon	Adenovirus	Polyclonal antiserum	Goat	IgG	Biodesign USA	B65101G
Adenovirus (nuclear mesh)	Adenovirus	H-60	Mouse	IgG_1	Biotrend Germany	0152–0004

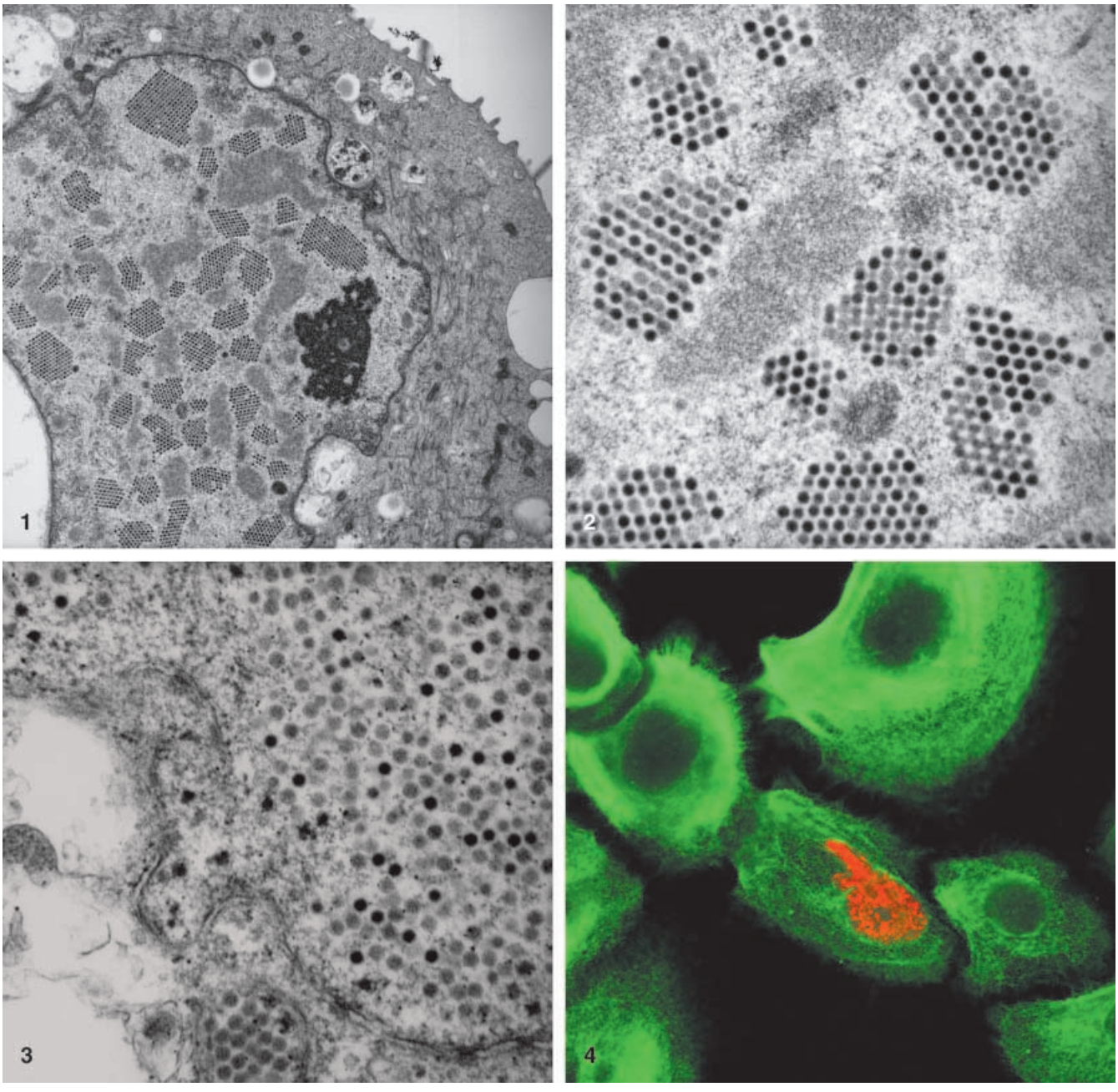

Fig. 1 Typical virus inclusions in the form of paracristalline figures in the nucleus and cytoplasm with perinuclear and peripheral vacuoles (type-2 cell), 48 h after infection; multiplicity of infection 1, transmission electron microscopy ×7000

Fig. 2 Parallel arranged formations of virus capsids within karyoplasm (no areas of cytoplasm in this detail) 48 h after infection; multiplicity of infection 1, transmission electron microscopy ×20,000

Fig. 3 Protrusions of the nuclear membrane filled with virus capsids, scattered virus capsids in the neighboring karyoplasm, next to the nuclear membrane cytoplasm with few vacuoles (type-2 cell, detail), 48 h after infection; multiplicity of infection 1, transmission electron microscopy ×20,000

Fig. 4 Anti-Ck Pan green, anti-adenovirus-MAb red, 24 h after infection. Adenovirus-infected epithelial cell with intranuclear inclusion bodies. Formation of an adenovirus-bearing nuclear protrusion that reaches into the cytoplasm; multiplicity of infection 1, confocal laser scanning microscope ×50

Results

Light microscopy

After 24 h of infection, the first intranuclear inclusions could be observed under the light microscope. They appeared in different geometrical forms and were localized in different compartments of the nucleus. Only about 10% of the cells showed these inclusions. Most of these inclusions were found after 48 h of infection. After 36 h and 48 h of infection, cytopathic effects were rare. After 72 h, there was an increase in cell death and a disaggregation of cytoplasmic structures as shown by light microscopy and inverted phase-contrast microscopy (Figs. 1, 2, 3, 4, 5, 6, 7, 8, 9, 10).

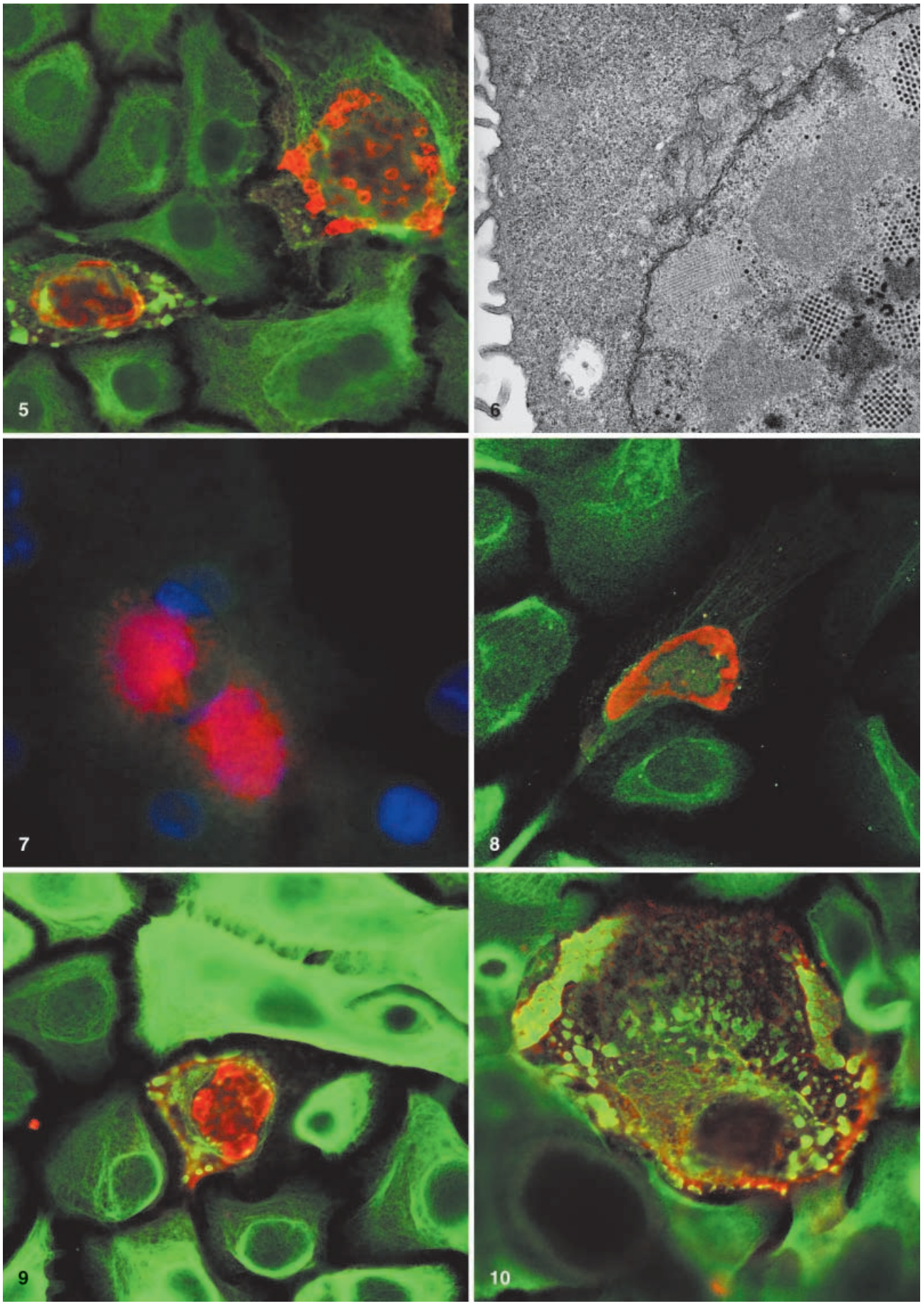

Figs. 5–10 Legends see page 516

Transmission electron microscopy

We were able to discriminate morphologically different types of normal peribronchial submucosal gland cells by their content, volume, and localization of vacuoles. One type is characterized by only very few perinuclear vacuoles (type 1). Another type shows more centrally located vacuoles, which may reach to more peripheral sites of cytoplasm (type 2). The third type is characterized by many focally confluent vacuoles in all parts of the cytoplasm (type 3). A division of cytoplasm in an inner electron dense and an outer electron lucent part is present in all postulated cell types.

During the different times of infections, we were able to find characteristic morphological changes. Beginning 24 h after infection, we could see the first intranuclear inclusions. They were arranged in parallel geometric groups consisting of several virus capsids (Fig. 1). Numbers of capsids included in these paracristalline structures varied from some to more than 100 (Fig. 2). Virus capsids measured 60–90 nm. At highest magnifications (140,000- and 250,000-fold), the capsids showed no connection to each other; they had an almost round appearance.

They were scattered in the nucleus, often arranged in association with electron-dense parts of the chromatin. Precursors of these virus aggregations could be seen in the form of chess field patterns near to the membrane of the nucleus (Fig. 6). Climax of the formation of these inclusions was found after 48 h. Cytopathic effects were low until this stage of infection.

After 48 h of infection, the nuclear membrane showed bulging protrusions at different locations of the nucleus (Fig. 3). In the beginning, most of these formations were not filled with detectable virus material. Later on, the protrusions were occupied with dense aggregates of capsids. In the surrounding karyoplasm, capsids spread from the paracristalline virus formations and were found in loose distribution. Near to these nuclear changes we could find vacuoles in cytoplasm which contained single laying capsids.

After 54 h of infection, cytopathic effects increased and, until 72 h of infection, most of the cells lost their integrity. In the course of cytolysis, virus particles could spread from the cells. Investigations at early times of infections failed to show the adherence of virus. Using light and electron microscopy, we were unable to observe and follow the way of the virus or its particles through cytoplasm. At early times of infection, the number of vacuoles increased. In the course of the infection, the content of vacuoles was stable and, after 48 h of infection, we were able to show capsids in the vacuoles.

Immunofluorescence

The first positive intranuclear reactions for the hexon protein could be found 16 h after infection. The intranuclear inclusions were scattered throughout the karyoplasm. They were found at the highest level after 48 h of infection. Similar to the TEM findings, a perinuclear reaction or a reaction situated at the borderline of nuclear membrane was detectable.

The expression of Cks showed conspicuous changes during the time course of infection. Cks indicating a higher differentiation state of the cells (Ck 8, 18, and 19) lost their filamental organization and built great intracytoplasmic aggregations (Fig. 10). Cks typical of more simple differentiated cells (Ck 5/6, 7, and 17) showed smaller aggregations, sometimes colocalized with the adenoviral hexon protein or complete capsids (Fig. 9). These changes began 24 h after infection and reached their peak 48 h after infection. Ck 10 (a marker for keratinization) and Ck 13 (a marker for cornea-type epithelium) showed a fine granular expression in non-infected cells and up to 16 h after infection, but began 24 h after infection to show a filamental expression type in infected cells as revealed by simultaneously staining for the hexon protein (Fig. 8).

One of the critical events in the time course of infection is the transition of newly synthesized adenoviral capsids from the nucleus into the cytoplasm. We were able to discriminate two distinct mechanisms of this transition. One was characterized by the formation of vacuoles originating from the nuclear envelope. These vacuoles were filled with capsid conglomerates with the same appearance as the intranuclear inclusion bodies (Fig. 5). The second mechanism was characterized by

◀ **Fig. 5** Anti-Ck 5/6 green, anti-adenovirus hexon protein red, 48 h after infection. Intracytoplasmic lying hexon-positive formations exhibit the same morphology as the intranuclear inclusions; multiplicity of infection 1, confocal laser scanning microscope ×50

Fig. 6 Precursor forms of virus aggregates in the form of a chess field pattern near to the nuclear membrane, next to the nucleus in cytoplasm one single vacuole (type-1 cell), 36 h after infection; multiplicity of infection 1, transmission electron microscopy ×12,000

Fig. 7 Anti-adenovirus-MAb red, DNA blue (DAPI), 48 h after infection; formation of anti-adenovirus-positive spikes reaching from the nuclear envelope into the cytoplasm; multiplicity of infection 1, conventional epifluorescence microscopy ×50

Fig. 8 Anti-Ck 10 green, anti-adenovirus-hexon protein red, 40 h after infection. Anti-hexon protein-positive cell showing a filamental expression pattern of Ck 10. Surrounding hexon-negative cells only present a granular expression of Ck 10; multiplicity of infection 1, confocal laser scanning microscope ×50

Fig. 9 Anti-Ck7 green, anti-adenovirus-hexon protein red, 48 h after infection. Anti-hexon protein-positive cell with small cytoplasmic vacuoles that react positive with anti-Ck 7. In the surrounding virus-negative cells that exhibit the typical filamental expression of Ck 7, multiplicity of infection 1, confocal laser scanning microscope ×50

Fig. 10 Anti-Ck 19 green, anti-adenovirus-hexon protein red, 48 h after infection. Anti-hexon protein-positive cell shows greater cytoplasmic vacuoles in which Ck 19 could be seen in a disaggregated pattern. In the cytoplasm, the anti-hexon protein-antiserum decorates filamental structures; multiplicity of infection 1 confocal laser scanning microscope ×50

the formation of spikes that were positively decorated with the monoclonal mouse antibody against adenovirus and extended from the nuclear envelope into the cytoplasm (Fig. 4 and Fig. 7).

Discussion

The adenovirus is a non-enveloped DNA virus with an icosahedral capsid composed of 252 capsomeres composed of 240 nonvertex hexon capsomeres and 12 vertex pentons [17]. Protruding from each of the pentons is an antenna-like structure called the fiber.

Peribronchial submucosal gland cells are the main source of tracheobronchial mucus [1]. Dyskrinia and hypersecretion play a major role in several pulmonary diseases. Mechanisms of dyskrinia and hypersecretion under virus infection are of utmost interest in understanding pathophysiological pathways. Next to cultivation of bronchial epithelial cells, the possibility of cultivating peribronchial submucosal gland cells exists [22, 24].

Adenovirus infection has been established in a series of cell lines. Infection of the mentioned primarily cultured peribronchial gland cells has not been investigated so far. In peribronchial submucosal gland cells, adenovirus infection follows a certain timetable in the manifestation of the morphological changes similar to those changes shown in other cell lines [6]. Infection is mostly characterized by the detection of intranuclear virus inclusions. These inclusions show a pathognomonic pattern of virus formation [3]. As described, we could detect precursor forms of the fully arranged paracristalline inclusions. Furthermore, the disaggregation and release from the nucleus were visible using TEM and IF. It is known from the literature that the E1B 19-kDa adenoviral protein interacts with the cytoplasmic intermediate filaments [4, 25, 28] and with the nuclear lamins [18, 19, 25, 26, 27]. Because of this, it seems likely that the mechanism of capsid transition from the nucleus into the cytoplasm by the formation of spikes bases on the immunological and developmental relationship of intranuclear lamins and intracytoplasmic cytokeratins both inserting in the nuclear membrane from their site of expression and that the adenovirus uses this filamental guide to leave the nucleus. We were able to characterize the capsid formation with its precursor lesions, the release from nucleus, and the cytoplasmic release in the course of cell lysis after long terms of infection. The cytopathic effects could also be shown by the reaction for Cks. These effects were characterized by building certain forms of aggregations in cytoplasm. With the panel of antibodies against Cks, the differentiation of infected cells and changes of cytoskeleton expression patterns under infection could be compared and correlated with the ultrastructural changes and characteristics. The mentioned bulging protrusions of the nuclear membrane have not been described before [17].

Early events of infection, as for example virus adsorption or cytoplasmic transfer of virus particles toward the nucleus, failed to be visualized. The morphological changes, especially for longer periods of infection, could be underlined by the investigation of the Ck expression. The release of capsids from nucleus, the formation of virus-bearing vacuoles, the cytoplasmic transport and, finally, the release of virus from the cell in the course cytopathic effects are also characterized by changes in the formation of the Cks [4].

In the course of infection, cell life is reduced to the production and release of the virus. After a short increase of secretion synthesis, the cell reduces its production of mucus in order to carry out virus formation. A directed formation of vacuoles as seen in uninfected peribronchial gland cells is no longer observed under infection. The amount and the size of vacuoles decreases. Vacuolation and transport of the vacuoles is more or less part of virus release from the cytoplasm, as shown by the TEM results. To confirm this, an overall increase of mucous production under virus infection could not be evaluated.

In conclusion, this in vitro system provides the possibility, on the one hand, to show the morphological alterations of human adenovirus infection in these special cell types and, on the other hand, to demonstrate changes in the mechanisms of the production of secretions and its components.

References

1. Basbaum CB, Finkbeiner WE (1989) Mucus-producing cells. In: Massaro D (ed) Lung cell biology. Marcel Dekker, New York, pp 37–79
2. Beltz GA, Flint SJ (1979) Inhibition of Hela cell protein during adenovirus infection. J Mol Biol 131:353–373
3. Bierwolf D, Schramm T, Bender E, Cunderlik V, Graffi A (1968) Elektronenmikroskopische Untersuchungen zur Vermehrung und Feinstruktur des Adenovirus Typ 3. Arch Geschwulstforsch 32:35–57
4. Chen PH, Ornelles DA, Shenk T (1993) The adenovirus L3 23-kilodalton proteinase cleaves the amino-terminal head domain from cytokeratin 18 and disrupts the cytokeratin network of HeLa cells. J Virol 67:3507–3514
5. Culp DJ, Penny DP, Martin MG (1983) A technique for the isolation of submucosal gland cells from cat trachea. J Appl Physiol 56:1076–1082
6. Ebsen M, Anhenn O, Melkus FW, Roder C, Morgenroth K (2000) Adenovirusinfection of human peribronchial submucosal gland cells in vitro. Eur Respir J 16[Suppl 31]:19A
7. Elliott WM, Hayashi S, Hogg JC (1995) Immunodetection of adenoviral E1A proteins in human lung tissue. Am J Respir Cell Mol Biol 12:642–648
8. Finkbeiner WE, Basbaum CB (1988) Monoclonal antibodies directed against human airway secretions. Localization and characterization of antigens. Am J Pathol 131:290–297
9. Finkbeiner WR, Nadel JA, Basbaum CB (1986) Establishment and characterization of cell line derived from bovine tracheal glands. In Vitro Cell Dev Biol Anim 22:561–567
10. Finkbeiner WE, Carrier SD, Teresi CE (1993) Reverse transcription-polymerase chain reaction (RT-PCR) phenotypic analysis of cell cultures of human tracheal epithelium, tracheobronchial glands and lung carcinoma. Am J Respir Cell Mol Biol 9:547–556
11. Flewett TH, Bryden AS, Davies H, Morris CA (1975) Virus particles in gastroenteritis? Epidemic viral enteritis in a long-stay childrens's ward. Lancet 1:4–5

12. Jawetz E (1959) The story of shipyard eye. BMJ 1:873–879
13. Jeffrey PK, Reid L (1977) The ultrastructure of the airway lining and its development. In: Hodson WA (ed) The development of the lung. Marcel Dekker, New York, pp 87–134
14. Lee SG, Gruber WC (1999) Adenoviruses. In: Dolin R, Wright PF (eds) Viral infections of the respiratory tract, vol. 127. Marcel Dekker, New York, pp 223–251
15. Matsuse T, Hayashi S, Kuwano K, Keunecke H, Jefferies WA, Hogg JC (1992) Latent adenoviral infection in the pathogenesis of chronic airways obstruction. Am Rev Respir Dis 146:177–184
16. Meyrick B, Reid L (1970) Ultrastructure of cells in the human bronchial submucosal glands. J Anat 107:281–299
17. Nermut MV (1987) Adenoviridae. In: Nermut MV, Steven AC (eds) Animal virus structure, perspectives in medical virology, vol. 3. Elsevier, Amsterdam, pp 373–390
18. Rao L, Perez D, White E (1996) Lamin proteolysis facilitates nuclear events during apoptosis. J Cell Biol 135:1441–1455
19. Rao L, Modha D, White E (1997) The E1B 19 K protein associates with lamins in vivo and its proper localization is required for inhibition of apoptosis. Oncogene 15:1587–1597
20. Rosenfeld MA, Siegfried W, Yoshimura K, Yoneyama K, Fukayama M, Stier LE, Paakko PK, Gilardi P, Stratford-Perricaudet L, Perricaudet M, Jallat S, Pavirani A, Lecocq LP, Crystal RG (1991) Adenovirus-mediated transfer of a recombinant á-1-antitrypsin gene to the lung epithelium in vivo. Science 252:431–434
21. Rowe WP, Huebner RJ, Gillmore LK, Parrott RH, Ward TG (1953) Isolation of a cytopathogenic agent from human adenoids undergoing spontaneous degeneration in tissue culture. Proc Soc Exp Biol Med 84:570–573
22. Sommerhoff CP, Finkbeiner WE (1990) Human tracheobronchial submucosal gland cells in culture. Am J Respir Cell Mol Biol 2:41–50
23. Taylor GW, Chopra DP, Mathieu PA (1993) Differences in secretory profiles of epithelial cell cultures derived from human tracheal and bronchial mucosa and submucosal glands. Epith Cell Biol 2:163–169
24. Tournier JM, Merten MD, Meckler Y, Hinrasky J, Fuchey C, Puchelle E (1990) Culture and characterization of human tracheal glands. Am Rev Respir Dis 141:1280–1288
25. White E, Cipriani R (1989) Specific disruption of intermediate filaments and the nuclear lamina by the 19-kDa product of the adenovirus E1B oncogene. Proc Natl Acad Sci USA 86:9886–9890
26. White E, Blose SH, Stillman W (1984) Nuclear envelope localization of an adenovirus tumor antigen maintains the integrity of cellular DNA. Mol Cell Biol 4:2865–2875
27. Zhai ZH, Nickerson JA, Krochmalnic G, Penman S (1987) Alterations in nuclear matrix structure after adenovirus infection. J Virol 61:1007–1018
28. Zhang Y, Schneider RJ (1994) Adenovirus inhibition of cell translation facilitates release of virus particles and enhances degradation of the cytokeratin network. J Virol 68:2544–2555

Virchows Arch (2002) 440:519–526
DOI 10.1007/s004280100537

ORIGINAL ARTICLE

Stephan Ihrler · Christian Zietz
Andrea Sendelhofert · Stephan Lang
Sabine Blasenbreu-Vogt · Udo Löhrs

A morphogenetic concept of salivary duct regeneration and metaplasia

Received: 15 June 2001 / Accepted: 13 August 2001 / Published online: 27 October 2001
© Springer-Verlag 2001

Abstract The exact mechanisms of physiological regeneration and of metaplastic processes of the salivary duct have not been definitely established, although regeneration from a putative uncommited stem cell population has long been favored. In the present study, double immunohistochemical labeling for Ki 67 and α-actin or different cytokeratin subtypes, respectively, made possible an exact localization and quantification of cellular proliferation in the regular salivary duct and in different types of metaplasia. Our data demonstrate a baseline proliferative capacity in all five cell types of the salivary duct. Luminal secretory cells of the acinus and intercalated duct regenerate independently from myoepithelial or basal cells. In contrast, the renewal of oxyphilic cells in the striated and excretory duct is maintained by proliferation and differentiation of basal cells. The great majority of metaplasias develops from uncommitted, Bcl-2 positive basal cells of striated/excretory ducts which possess an enormous capacity for pluridirectional morphogenetic differentiation. Despite this important role of basal cells, our findings demonstrate that all cell types principally have to be considered as potential progenitor cells for salivary gland tumors. The improved insight into regenerative and metaplastic processes of the salivary duct may contribute to a better understanding of the complex formal carcinogenesis.

Keywords Salivary gland · Basal cell · Regeneration · Metaplasia · Cytokeratin filaments

S. Ihrler (✉) · C. Zietz · A. Sendelhofert · S. Blasenbreu-Vogt
U. Löhrs
Institute of Pathology, Ludwig-Maximilians-University,
Thalkirchnerstrasse 36, 80337 Munich, Germany
e-mail: Stephan.Ihrler@lrz.uni-muenchen.de
Tel.: +49-89-51604672, Fax: +49-89-51604043

S. Lang
Department of ENT, Head and Neck Surgery,
Ludwig-Maximilians-University, Munich, Germany

Introduction

Epithelial metaplasia (MP) is defined as a reactive transition of a differentiated epithelium into another type of differentiated epithelium that is characterized by impaired or altered function and is not physiological within this site. Nowadays, a direct transition of differentiated cells into metaplastic cells is no longer postulated, instead the idea that there is a development of MP from proliferating uncommitted reserve cells ("stem cell MP"; [23]). Salivary glands harbor a great variety of metaplastic alterations: oncocytic MP, mucous (goblet) cell MP, sebaceous MP, squamous cell MP and so-called necrotizing sialo-MP [6, 13, 17, 25, 26, 28, 33, 34, 36]. We have recently demonstrated that the duct alterations in benign lymphoepithelial lesion/M.Sjögren do not derive from myoepithelial cells (formerly called "epimyoepithelial lesion" [9, 12, 35]) but from basal cells and have proposed the term "lymphoepithelial MP" [19, 20]. In general, little information exists in the literature concerning the formal pathogenesis of salivary duct MP especially with respect to the site and cells of origin [11, 21, 25].

To understand the development of MP, the cellular composition and regenerative properties of the salivary duct have to be considered: as schematically illustrated in Fig. 2a, the four duct segments, i.e., acinus, intercalated duct, striated duct (all intralobular), and excretory duct (extralobular), are composed of five different cell types: acinar, intercalated duct, oxyphilic, myoepithelial, and basal cells [5, 11, 14, 15]. We have recently summarized the morphological and functional differences between the two abluminal cell types: myoepithelial and basal (reserve) cells [19].

i. Myoepithelial cells, characterized by co-expression of basal type cytokeratin (CK) 14, α-actin, and S-100, represent a presumably long-living epithelial–mesenchymal hybrid with functional specialization for the propulsion of saliva. They are mainly restricted to acini and intercalated ducts and rarely occur in the distal part of striated ducts.

Table 1 Monoclonal mouse antibodies (MAb) used in this study applied to antigens listed. *CK* cytokeratin, *MW* microwave, *TRS 6* target retrieval solution pH 6, *ABC-E* avidin–biotin complex method Elite, *APAAP* alkaline phosphatase anti-alkaline phosphatase

Antigen	MAb clone	Source	Pre-treatment	Dilution of MAb	Method
CK 14	MCA890	Serotec	MW 30 min TRS 6	1:200	ABC-E[b]
CK 13	Ks13.1	Progen	30 min protease XXIV	1:80	APAAP
CK 10	DE-K10	Progen	MW 30 min TRS 6	1:10	APAAP
CK Ks8.12	Ks8.12	Sigma	MW 30 min TRS 6	1:100	APAAP
CK 18	Ks18.04	Progen	MW 30 min TRS 6	1:200	ABC-E[b]
CK 7	Ks7.18	Progen	30 min protease XXIV	1:60	APAAP
α-Actin	Asm-1	Roche Diagnostics	MW 30 min TRS 6	1:100	ABC[a,b]
Bcl-2	124.	Dako	MW 30 min TRS 6	1:30	ABC-E[b]
Ki 67	MIB-1	Dianova	MW 30 min TRS 6	1:50	APAAP

[a] Secondary antibody rabbit anti-mouse immunoglobulin, biotinylated, $F(ab')_2$ and streptavidin complex
[b] With biotin blocking system

ii. Basal cells of striated/excretory ducts demonstrate co-expression of CK 14, CK K_s8.12, and Bcl-2. Basal cells have only recently been unequivocally accepted as a special cell type with a putative reserve cell function [5, 10, 14, 15, 30]. This complex cellular structure of the salivary duct with three distinctly composed segments differs profoundly from ducts of other glandular organs with a more uniform cellular composition, i.e., the mammary and prostate gland [3, 4].

The cell populations responsible for the physiological regeneration of the different segments of the salivary duct have not yet been definitely determined [11]. In the present study, the implementation of double immunohistochemical labeling for the proliferation-associated antigen Ki 67 and for different CK subtypes or for α-actin, respectively, was a prerequisite for the precise localization and quantification of cellular proliferation. This enabled us to identify those cell types responsible for the physiological regeneration of the salivary duct and the development of the different types of MP. While in several organs MP is considered to be involved in precursor stages of carcinogenesis [23], surprisingly little information is available concerning the relationship between MP and the complex tumorigenesis in salivary glands. An improved insight into regenerative and metaplastic processes of the salivary duct may provide a better understanding at least of the formal carcinogenesis in the salivary glands.

Materials and methods

Forty-five surgical salivary gland specimens (parotid gland *n*=34; submandibular gland *n*=7; minor salivary gland *n*=4; 24 males; 21 females; age 23–81 years) were retrieved from the archives of the Institute of Pathology, Ludwig-Maximilians-University, Munich. The diagnoses comprised benign lymphoepithelial lesion/M.Sjögren (*n*=6), human immunodeficiency virus-associated cystic lymphoepithelial lesion (*n*=5), sporadic lymphoepithelial cyst (*n*=5), chronic sialadenitis with/without silalolithiasis (*n*=6), postirradiation sialadenitis (*n*=3), chronic-sclerosing sialadenitis of submandibular gland/Küttner tumor (*n*=4), necrotizing sialo-MP (*n*=5), multifocal oncocytosis (*n*=3), and regular parenchyma (*n*=8). The following types of MP were recorded: lymphoepithelial MP (*n*=13), squamous cell MP (*n*=8), sebaceous MP (*n*=5), mucous (goblet) cell MP (*n*=11), oncocytic MP (*n*=7), and necrotizing sialo-MP (*n*=5). Oncocytic MP was restricted to specimens with small oncocytic proliferation, excluding cases with Whartin tumor or oncocytoma. Additionally, cases with basal cell hyperplasia were included, representing a reactive alteration with aspects of MP (*n*=12). In 11 cases, combinations of different types of MP were manifest (mostly lymphoepithelial MP, squamous cell MP, and basal cell hyperplasia). Necrotizing sialo-MP was mostly found in minor salivary glands, lymphoepithelial and sebaceous MP exclusively in parotid glands, while the other types of MP were encountered both in parotid and submandibular glands.

Each specimen was fixed in buffered formaldehyde (4%; pH 7), embedded in paraffin wax (low melting part paraffin; Vogel, Germany) and cut into 4-µm-thick serial sections. Commercially available monoclonal mouse antibodies were applied to a panel of CK subtypes as well as to α-smooth muscle actin, Ki 67(MIB-1), and Bcl-2 (Table 1). Modifications of the avidin–biotin complex (ABC) method and the alkaline phosphatase anti-alkaline phosphatase (APAAP) method were used as described previously [19]. Due to the high degree of endogenous biotin, especially in oxyphilic cells, an avidin–biotin blocking system (Dako Biotin Blocking System X0590) was added to the ABC method. The extent of cytoplasmic immunoreactivity was evaluated semi-quantitatively using the following grading system: no expression –; weak expression +; moderate expression ++; strong expression +++. Regular salivary parenchyma, mucosa, and vessels were used as internal positive controls.

A double immunohistochemical labeling technique was developed for the evaluation of the proliferation index in specific cell types: briefly, deparaffinized slides were subjected to microwave pre-treatment (750 W) with target retrieval solution (TRS 6; pH 6; 30 min). Endogenous peroxidase was blocked with oxygen peroxide solution (7.5%; 10 min). For staining for CK 14 and CK 7, an ABC method was applied (ABC kit; Vector). The slides were incubated with normal serum (horse) for 20 min after avidin–biotin blocking slides were incubated (room temperature; 60 min) for either monoclonal anti-CK 14 (1:200 dilution) or anti-CK 7 (1:250 dilution). Biotinylated universal antibody was applied as a secondary antibody according to the manufacturer's protocol; ABC method (Elite; 30 min each) was also applied. DAB+ (Dako; 3 min) was used as chromogen. For staining with Ki 67, the APAAP method was used (APAAP-ChemMate; Dako). The monoclonal anti-Ki 67 (1:80 dilution) was applied at room temperature for 60 min. Visualization of the bound anti-Ki 67 was obtained with a secondary antibody mouse immunoglobulin and APAAP immunocomplex (30 min each), followed by a repetition of both incubations (10 min each). Fast Red (Sigma) was used as the chromogen (10 min) and Vector hematoxylin (Gill's formula) as counterstain.

Table 2 Immunohistochemical characterization of the epithelial cytoskeleton and of the cellular proliferation in the regular salivary duct and in metaplasia of the central and peripheral duct segments. Cytoplasmic staining intensity: no expression –, mild expression +, moderate expression ++, strong expression +++. *SE* standard error

	CK 14	CK K_s 8.12	CK 13	CK 10	CK 18	CK 7	Bcl-2	α-Actin	Proliferative index [f] (±SE)
Basal cell [a, d]	+++	++(+)	–	–	–/+	–/+	+(+)	–	3.2% (±1.3) *n*=8
Myoepithelial cell [a]	++	–	–	–	–	–	–	+++	0.2% (±0.1) *n*=8
Oxyphilic cell [a]	–	–/(+)	–	–	+(+)	++(+)	–/(+)	–	0.2% (±0.2) *n*=8
Intercalated duct cell [a]	–	–	–	–	+++	+++	–	–	0.8% (±0.3) *n*=8
Acinar cell [a]	–	–	–	–	++(+)	–	–	–	2.0% (±0.9) *n*=8
Mucous cell metaplasia [b, d, e]	–/(+)	–/(+)	–	–	+(+)	++(+)	–/(+)	–	B 6.6% (±3.0) *n*=6 L 1.4% (±0.4)
Oncocytic metaplasia [b, d, e]	–/(+)	–/(+)	–	–	+(+)	+(+)	–/(+)	–	B 2.9% (±0.8) *n*=5 L 0.8% (±0.2)
Sebaceous metaplasia [b, d, e]	+++	–/(+)	–	+	–	–	–/(+)	–	B 5.0% (±0.9) S 1.2% (±0.5) *n*=5 L 0.1% (±0.2)
Basal cell hyperplasia [b, d, e]	+(+)	+++	+++	–	–/+	–/+	–/(+)	–	B 5.5% (±1.7) S 15.4% (±3.8) *n*=7 L 0.9% (±0.6)
Lymphoepithelial metaplasia [b, d, e]	++	+++	+++	–/(+)	–/+	–/+	–/(+)	–	B 3.1% (±0.9) S 4.7% (±1.6) *n*=6 L 0.4% (±0.4)
Squamous cell metaplasia [b, d, e]	+(+)	+++	+++	++(+)	–	–	–/(+)	–	B 8.4% (±3.4) S 17.5% (±4.5) *n*=6 L 0.7% (±0.5)
Necrotizing sialometaplasia[c]	++(+)	++(+)	–/+	–	–	–	–	–	27.1% (±5.5) *n*=5

[a] In the regular salivary duct
[b] In metaplasia of the central duct segment
[c] In metaplasia of the peripheral duct segment
[d] Basal cells of the regular striated/excretory duct including all types of metaplasia of the central duct segment
[e] Expression regarding suprabasal and luminal epithelial layers each
[f] Mean percentage of Ki 67 positive nuclei in 400 cells within the following cell layers of metaplasia: *B* basal cell layer, *S* suprabasal cell layers, *L* luminal cell layer

For double staining with α-actin and Ki 67, the same procedure was used as outlined above with the following exceptions: a labeled streptavidin biotin kit was applied (LSAB kit, Dako); instead of normal serum (horse), the slides were incubated with protease for 10 min. The monoclonal anti-α-actin was used at a dilution of 1:1500.

The labeling index was determined by calculating the percentage of cycling (Ki 67-positive) cells within a total of 400 cells each of specific cell types, identified by either positivity or negativity for CK 14, CK 7, or α-actin (only 100–200 cells each in sebaceous MP and necrotizing sialo-MP due to minor numbers of involved cells). The mean percentage was calculated as well as the standard error of the mean (SEM).

Results

Regular salivary duct

Our previous results of the CK profiles of the salivary duct have been recently published [19]. As a basis for further analysis of cellular proliferation, these findings are included in the upper part of Table 2 and schematically illustrated in Fig. 2a. Instead of the previously used CK 19 (with positive reaction both in basal and luminal cells; [19]), CK 7 is employed in the present study due to a more restricted expression in oxyphilic and intercalated duct cells (Fig. 1c). In the luminal layer of striated and excretory ducts, 4.2±1.3% of cells exhibit a transitional phenotype with cytological characteristics of oxyphilic cells and a reaction pattern equivalent to basal cells (CK 14, CK K_s8.12, and Bcl-2+, CK 7/18–; Fig. 1a, b).

Quantitative measurements of the Ki 67-index using double immunohistochemical staining show relatively high proliferation rates in basal cells (3.2±1.3%), acinar cells (2.0±0.9%), and intercalated duct cells (0.8±0.3%), contrasting with low proliferation rates in oxyphilic cells (0.2±0.2%) and myoepithelial cells (0.2±0.1%; Table 2; Fig. 1a, c, d; Fig. 2a).

Reactive/metaplastic alterations in striated and excretory ducts

Mucous cell, oncocytic, lymphoepithelial, sebaceous, and squamous cell MP as well as basal cell hyperplasia manifest in striated and excretory ducts, as schematically summarized in Fig. 2b. Basal type CK 14 and K_s8.12 are intensely expressed in basal cells of all these MPs and additionally in suprabasal layers of lymphoepithelial and squamous cell MP and of basal cell hyperplasia (Fig. 1e, f, g, i). CK 14 without CK K_s8.12 is expressed in supra-

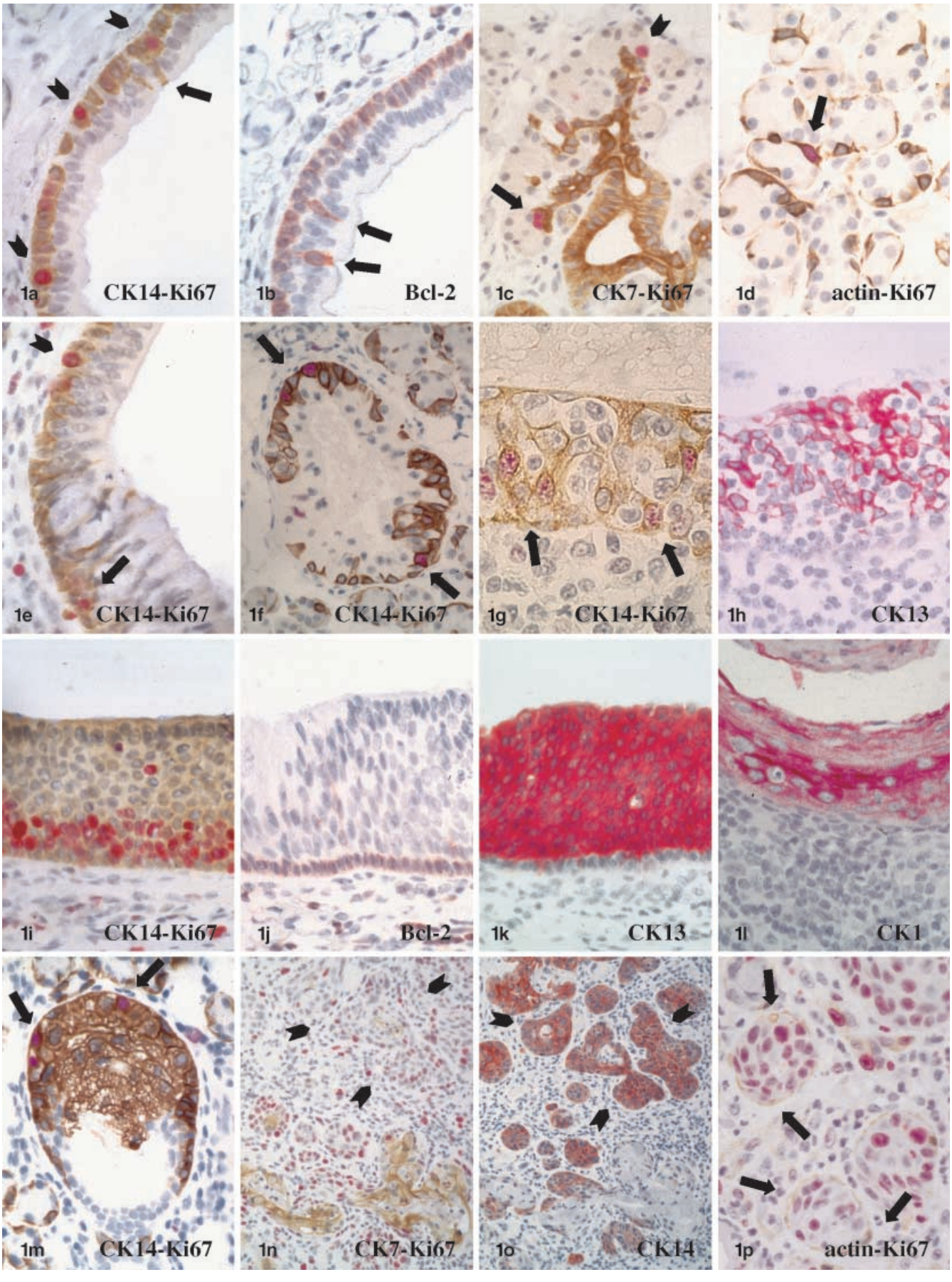
1a CK14-Ki67
1b Bcl-2
1c CK7-Ki67
1d actin-Ki67
1e CK14-Ki67
1f CK14-Ki67
1g CK14-Ki67
1h CK13
1i CK14-Ki67
1j Bcl-2
1k CK13
1l CK1
1m CK14-Ki67
1n CK7-Ki67
1o CK14
1p actin-Ki67

basal layers of sebaceous MP (Fig. 1m). Mucosa-type CK 13 is seen in suprabasal layers of lymphoepithelial and squamous cell MP and of basal cell hyperplasia (Fig. 1h, k). Expression of epidermis-type CK 10 is restricted to suprabasal layers of squamous cell MP (Fig. 1l) and, to a minor degree, of sebaceous MP. Co-expression of simple epithelium-type CK 7 and CK 18 in luminal cells is preserved only in oncocytic and mucous cell MP. Bcl-2 staining is seen moderately in all basal cells and faintly in few interspersed suprabasal cells of all types of MP (Fig. 1j). Expression of α-actin is absent in all MPs.

In the bi-layered epithelium of mucous cell and oncocytic MP as well as in sebaceous MP, the proliferative activity in basal cells (2.9–6.6%; Fig. 1e, f, m) intensely surpasses that in luminal cells (0.1–1.4%). In the stratified epithelium of lymphoepithelial MP, squamous cell MP and basal cell hyperplasia proliferation ranges from 3.1% to 8.4% in the basal cell layer, from 4.7% to 17.5% in suprabasal layers, and from 0.4% to 0.9% in the luminal layer (Table 2; Fig. 1g, i; Fig. 2b).

Reactive/metaplastic alterations in the acinus and intercalated duct

Necrotizing sialo-MP develops in the peripheral duct segment with preserved lobular architecture. Affected ducts show increased proliferative activity (Ki 67 rate 27.1±5.5%) of luminal acinar and intercalated duct cells with progressive loss of CK 7 and CK 18 (Fig. 1n) and intense gain of CK 14 and K_s8.12 (Fig. 1o). Occasional mild expression of CK 13 is restricted to few luminal cells. Actin-positive myoepithelial cells do not participate in the cellular proliferation and gradually disappear in the development of necrotizing sialo-MP (Fig. 1p; Table 2; Fig. 2c). Oncocytic MP, in addition to major manifestation in striated ducts, rarely occurs in acini and intercalated ducts, identified by abluminal myoepithelial cells (Fig. 2b).

Longstanding chronic inflammation of varying causes is associated with parenchymal atrophy, characterized by (sub)-total loss of CK 18-positive/CK 7-negative acinar cells. In comparison with regular parenchyma, cellular proliferation in areas with inflammation is increased in luminal intercalated duct cells (3.1±0.6), in myoepithelial cells (1.7±0.5%) and, as far as preserved, in acinar cells (4.0±1.2%; Fig. 1c; data not shown in Table 2).

In general, different types of MP are not found to be specific for distinct diagnoses. In 11 of 45 cases, two or more types of MP are combined in a given specimen. Relevant differences in the CK profiles or in proliferative activity are not seen in the same type of MP in specimens with different diagnoses.

◀ **Fig. 1** Immunohistochemical characterization of cytoskeletal proteins and cellular proliferation in the regular salivary duct (**a–d**) and in metaplasia (MP) of the central (**e–m**) and peripheral (**n–p**) duct segments. Immunohistochemical double labeling for cytokeratin (CK) 14 and Ki 67 (**a, e, f, g, i, m**), CK 7 and Ki 67 (**c, n**), and α-actin and Ki 67 (**d, p**). Original magnification: **a, b, d–f, h–m** ×160; **c**, **p** ×140; **g** ×190; **n, o,** ×120. **a, b** In the central duct segment (striated/excretory duct), Ki 67-associated proliferation is largely confined to CK 14-positive basal cells (**a** *arrowheads*). Few luminal cells demonstrate a transitional phenotype with preserved reactivity for CK 14 (**a** *arrow*). **b** Bcl-2 is confined to basal cells and to the few luminal cells with transitional phenotype (*arrows*). **c, d** In the peripheral duct segment, proliferation is mainly located in CK 7-negative acinar cells (**c** *arrowhead*) and CK 7-positive luminal intercalated duct cells (**c** *arrow*), while α-actin-positive abluminal myoepithelial cells exhibit a very low proliferative activity (**d** *arrow*). **e** In mucous cell MP, proliferation is largely confined to basal cells (*arrow*) in accordance with adjacent regular striated duct (*arrowhead*). **f** In oncocytic MP, proliferation is also largely confined to CK 14-positive basal cells (*arrows*). **g, h** In lymphoepithelial MP, proliferation manifests in CK 14-positive basal and lower suprabasal cell layers (**g** *arrows*), paralleled by suprabasal gain of CK 13 (**h**). **i, j, k** In basal cell hyperplasia also, proliferation is located in basal and lower suprabasal layers (**i**), while Bcl-2 expression (**j**) is largely restricted to basal cells, and CK 13 (**k**) is gained in all suprabasal cell layers. **l** Squamous cell MP, in addition to the findings in basal cell hyperplasia, exhibits suprabasal gain of epidermis-type CK 10. **m** In sebaceous MP, all cell layers are CK 14-positive, and proliferation is largely confined to basal cells (*arrows*). **n, o, p** Necrotizing sialo-MP develops by proliferation of intercalated duct and acinar cells characterized by loss of CK 7 (**n** *arrowheads*) and intense gain of CK 14 (**o** *arrowheads*), while α-actin-positive abluminal myoepithelial cells (**p** *arrows*) do not participate in the intense proliferation of luminal secretory cells

Discussion

Salivary duct regeneration

The exact mechanisms of the physiological regeneration of the salivary duct as a finely tuned balance of proliferation and differentiation have not yet been fully established, although regeneration from a putative uncommitted stem cell population has long been favored ("pluripotential unicellular reserve cell theory"; [11]). In an immunohistochemical study in a rat model, Burgess et al. [7] postulated a baseline cellular proliferation in all different cell types of the salivary duct including myoepithelial cells. In many investigations concerning ductal regeneration, however, basal cells, generally, have not been taken into account [7, 25, 37].

In this study, for the first time, an exact topographical localization and quantification of Ki 67-associated cellular proliferation in the regular human salivary gland was made possible by means of double immunohistochemical labeling. In summary, our data demonstrate a low baseline proliferative activity in the three cell types – basal, intercalated duct, and acinar cells – contrasting with a very low proliferative rate in myoepithelial and oxyphilic cells. Taking into account our previous results of the cellular composition [19], these proliferation indices imply diverse principles in the renewal of the central and peripheral duct segment.

i. In the central duct segment, basal cells (3.2%) demonstrate a 16-fold higher proliferative activity than lu-

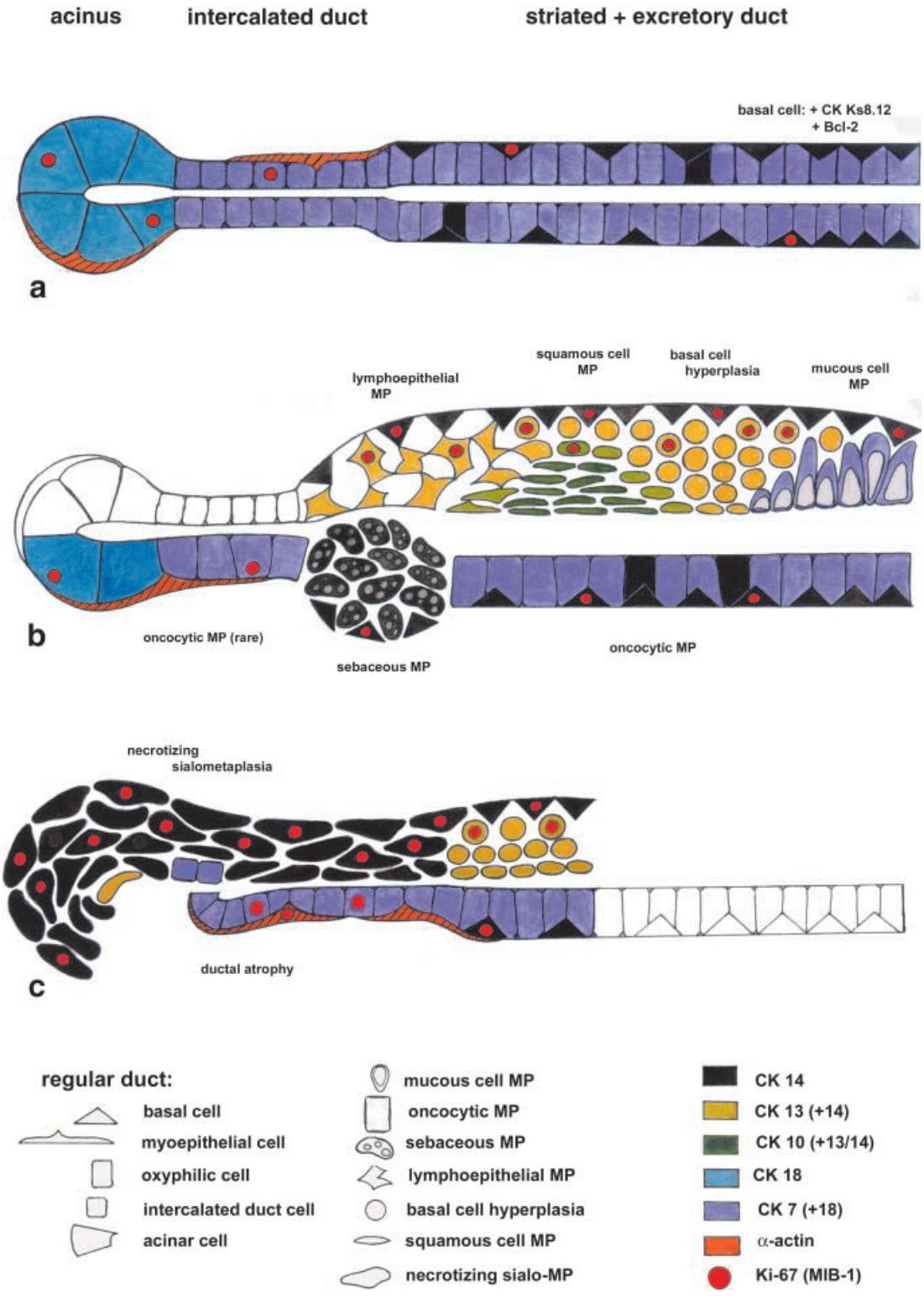

Fig. 2 Schematic illustration of the cellular composition and regeneration (Ki-67) of the regular salivary duct (**a**) and of reactive/metaplastic changes in the central (**b**) and peripheral (**c**) duct segments

minal oxyphilic cells (0.2%). Moreover, the exclusive Bcl-2 expression of basal cells exerts an anti-apoptotic effect and an important potential for cellular differentiation and morphogenesis [19, 24, 31]. The evidence of cells with a mixed phenotype furthermore suggests a transition and differentiation from basal to oxyphilic cells. These findings, altogether, strongly

imply that basal cells serve as a reserve cell pool and the progenitor for oxyphilic cells in striated and excretory ducts.

ii. In the peripheral duct segment, luminal intercalated duct (0.8%) and acinar cells (2.0%) exhibit a 4- to 10-fold higher proliferative activity than abluminal myoepithelial cells (0.2%). There is no evidence for a separate basal cell compartment or a transition between myoepithelial cells and luminal cell types. Altogether, as schematically illustrated in Fig. 2a, these arguments indicate that the regeneration of luminal secretory cells is exclusively maintained by self-renewal of acinar and intercalated duct cells, without any contribution from myoepithelial cells.

The highly specialized myoepithelial cells have been considered to be terminally differentiated cells with an extremely low proliferative activity [1, 14, 22, 25], even to the extent that they were regarded as amitotic [2]. In the present study, a very low baseline proliferative capacity is proven in myoepithelial cells of regular human parenchyma (0.2%), while in chronic sialadenitis the proliferative index is moderately increased up to 1.7% on average. In the experimental setting of duct ligation in the rat parotid gland, Burgess et al. [7] demonstrated an enormously increased proliferation in myoepithelial cells of up to 23.1%, obviously representing a maximal stimulation to overcome the experimental ductal blockage.

Salivary duct metaplasia

Salivary glands show a great variety of metaplastic epithelial alterations [6, 13, 18, 19, 28, 30, 32, 33, 34, 36]. The identification of characteristic CK profiles served as a basis for the analysis of the proliferation in MPs. In sebaceous MP, suprabasal gain of CK 14 and, to a minor degree, of CK 10 is consistent with adnexal differentiation. In lymphoepithelial MP, squamous cell MP, and basal cell hyperplasia, suprabasal gain of mucosa-type CK 13, CK 14, and K_s8.12 and parallel loss of secretory-type CK 7 and CK 18 indicate an increased mechanical stability, being intensified in squamous cell MP by additional gain of epidermis-type CK 10 [23, 27]. With respect to these findings, basal cell hyperplasia fulfils all relevant criteria to be regarded as a metaplastic process [23].

The following points argue in favor of an outstanding role of basal cells in the development of MP. All MPs, with exception of necrotizing sialo-MP and rare oncocytic MP in acini, are restricted to striated/excretory ducts, harboring basal cells. Moreover, the proliferation rate of basal cells in MP generally is increased relative to the regular duct. Most important, the exclusive Bcl-2 expression in basal cells, as discussed above, exerts a potential for pluridirectional differentiation. As in the regular duct, Bcl-2 positivity is immediately downregulated in suprabasal cell layers of MP once the cells have entered terminal differentiation [24, 31]. As illustrated in Fig. 2b, these arguments indicate that all MPs of the central duct segment develop from uncommitted basal cells with documented capacity for pluridirectional morphogenetic differentiation.

The main metaplastic process encountered in the peripheral duct segment is necrotizing sialo-MP, manifesting in areas of extreme, almost lethal tissue damage, accompanied by partial duct necrosis [6, 13, 33, 36]. Our findings demonstrate a development from intensely proliferating luminal acinar and intercalated duct cells, acquiring an epidermoid phenotype with a CK pattern equivalent to basal cells. There is no finding in favor of basal cells migrating from the striated duct into the peripheral duct segment. In contrast to conventional squamous cell MP developing in striated/excretory ducts, the lack of additional gain of CK 13 and CK 10 in necrotizing sialo-MP presumably is due to a more restricted morphogenetic capacity in the differentiated and Bcl-2-negative acinar and intercalated duct cells. Despite the documented proliferative capacity of myoepithelial cells in the regular duct and especially in chronic sialadenitis or ductal blockage, myoepithelial cells are involved neither in necrotizing sialo-MP nor in any other form of MP [16, 29].

In summary, our study proves a baseline proliferative capacity in all five cell types of the salivary duct. This implies that all cell types, including myoepithelial cells, principally have to be considered as potential progenitor cells for salivary gland tumors. While, in the peripheral segment, luminal secretory cells and myoepithelial cells regenerate independently without cellular transition, the renewal of luminal oxyphilic cells in striated/excretory ducts by large is maintained by proliferation and differentiation of Bcl-2 positive basal cells. These uncommitted basal cells, in addition, play the central role for a pluridirectional morphogenetic differentiation in the majority of ductal MP. It is tempting to assume that the great diversity of salivary gland tumors is a sequel of the complex cellular composition of the different ductal segments with divergent principles of regeneration and MP each. In this respect, our findings might contribute to a better understanding of the formal tumorigenesis. Further studies will have to investigate, whether distinct forms of MP might represent precursor lesions of certain tumors.

Acknowledgements This study was supported by a grant from the Editorial Board of the "Münchner Medizinische Wochenschrift e.V." (Grant no. 822356-2). The assistance of Mrs. Stefanie Wagner in reviewing the manuscript is gratefully acknowledged.

References

1. Aigner T, Neureiter D, Völker U, Belke J, Kirchner T (1998) Epithelial-mesenchymal transdifferentiation and extracellular matrix gene expression in pleomorphic adenomas of the parotid salivary gland. J Pathol 186:178–185
2. Batsakis JG, Regezi JA, Luna MA, El-Naggar A (1989) Histogenesis of salivary gland neoplasms: a postulate with prognostic implications. J Laryngol Otol 103:939–944

3. Böcker W, Bier B, Freytag G, Brömmelkamp B, Jarasch E-D, Edel G, Dockhorn-Dworniczak B, Schmid KW (1992) An immunohistochemical study of the breast using antibodies to basal and luminal keratins, alpha-smooth muscle actin, vimentin, collagen IV and laminin. Virchows Arch 421:315–322
4. Bonkhoff H, Remberger K (1998) Morphogenetic concepts of normal and abnormal growth in the human prostate. Virchows Arch 433:195–202
5. Born IA, Schwechheimer K, Maier H, Otto HF (1987) Cytokeratin expression in normal salivary glands and in cystadenolymphomas demonstrated by monoclonal antibodies against selective cytokeratin polypeptides. Virchows Arch 411:583–589
6. Brannon RB, Fowler CB, Hartmann KS (1991) Necrotizing sialometaplasia. A clinicopathologic study of sixty-nine cases and review of the literature. Oral Surg Oral Med Oral Pathol 72:317–325
7. Burgess KL, Dardick I, Cummings MM, Burford-Mason AP, Bassett R, Brown DH (1996) Myoepithelial cells actively proliferate during atrophy of rat parotid gland. Oral Surg Oral Med Oral Pathol 82:674–680
8. Cattoretti G, Becker MHG, Key G, Duchrow M, Schlüter C, Galle J, Gerdes J (1992) Monoclonal antibodies against recombinant parts of the Ki-67 antigen (MIB 1 and MIB 3) detect proliferating cells in microwave-processed formalin-fixed paraffin sections. J Pathol 168:357–363
9. Dardick I, Peter van Nostrand AM, Rippstein P, Skimming L, Hoppe D, Dairkee SH (1988) Characterisation of epimyoepithelial islands in benign lymphoepithelial lesions of major salivary gland: an immunohistochemical and ultrastructural study. Head Neck Surg 10:168–178
10. Dardick I, Parks WR, Little J, Brown DL (1988) Characterisation of cytoskeletal proteins in basal cells of human parotid salivary gland ducts. Virchows Arch 412:525–532
11. Dardick I, Byard RW, Carnegie A (1990) A review of the proliferative capacity of major salivary glands and the relationship to current concepts of neoplasia in salivary glands. Oral Surg Oral Med Oral Pathol 69:53–67
12. Donath K, Seifert G (1972) Ultrastructure and pathogenesis of the myoepithelial sialadenitis. On the occurrence of myoepithelial cells in the benign lymphoepithelial lesion. Virchows Arch 356:315–329
13. Donath K, Seifert G (1997) Tumour-simulating squamous cell metaplasia (SCM) in necrotic areas of salivary gland tumours. Pathol Res Pract 193:689–693
14. Draeger A, Nathrath WBJ, Lane B, Sundström BA, Stigbrand TI (1990) Cytokeratins, smooth muscle actin and vimentin in human normal salivary gland and pleomorphic adenomas. APMIS 99:405–415
15. Geiger S, Geiger B, Leitner O, Marshak G (1987) Cytokeratin polypeptides expression in different epithelial elements of human salivary glands. Virchows Arch 410:403–414
16. Harrison JD, Badir MS (1998) Chronic submandibular sialadenitis: ultrastructure and phosphatase histochemistry. Ultrastr Pathol 22:431–437
17. Hartwick RWJ, Batsakis JG (1990) Pathology consultation: non-Whartin's tumour oncocytic lesions. Ann Otol Rhinol Laryngol 99:674–677
18. Ihrler S, Zietz C, Riederer A, Diebold J, Löhrs U (1996) HIV-related parotid lymphoepithelial cysts. Immunohistochemistry and 3-D reconstruction of surgical and autopsy material with special reference to formal pathogenesis. Virchows Arch 429:139–147
19. Ihrler S, Zietz C, Sendelhofert A, Riederer A, Löhrs U (1999) Lymphoepithelial duct lesions in Sjögren-type sialadenitis. Virchows Arch 434:315–323
20. Ihrler S, Baretton G, Menauer F, Blasenbreu-Vogt S, Löhrs U (2000) Sjögren's syndrome and MALT-lymphomas of salivary glands – a DNA-cytometric and interphase-cytogenetic study. Mod Pathol 13:4–12
21. Kjörell U, Östberg Y (1984) Distribution of intermediate filaments and actin microfilaments in parotid autoimmune sialoadenitis of Sjögren syndrome. Histopathology 8:991–1011
22. Lee SK, Hwang JO, Chi JG, Yamada K, Mori M (1993) Prenatal development of myoepithelial cell of human submandibular gland observed by immunohistochemistry of smooth muscle actin and rhodamine-phalloidin fluorescence. Pathol Res Pract 189:332–341
23. Leube RE, Rustad TJ (1991) Squamous cell metaplasia in the human lung: molecular characteristics of epithelial stratification. Virchows Arch 61:227–253
24. Lu Qi-Long, Abel P, Foster CS, Lalani El-Nasir (1996) Bcl-2: role in epithelial differentiation and oncogenesis. Hum Pathol 27:102–110
25. Martinez-Madrigal F, Micheau C (1989) Histology of the major salivary glands. Am J Surg Pathol 13:879–899
26. Matthews TW, Dardick I (1988) Morphological alterations of salivary gland parenchyma in chronic sialadenitis. J Otolaryngol 17:385–394
27. Moll R (1988) Differenzierungsprogramme des Epithels und ihre Änderungen. Verh Dtsch Ges Pathology 72:102–114
28. Müller-Höcker J (1998) Oncocytic metaplasia/neoplasia – morphology, biochemistry, and molecular genetics. Pathologe 19:104–114
29. Palmer RM, Eveson JW (1987) Chronic sialadenitis. An immunohistochemical study in humans. Virchows Arch 412:73–78
30. Palmer RM, Eveson JW, Gusterson BA (1986) "Epimyoepithelial" islands in lymphoepithelial lesions. Virchows Arch 408:603–609
31. Pammer J, Horvat R, Weninger W, Ulrich (1995) Expression of bcl-2 in salivary glands and salivary gland adenomas. A contribution to the reserve cell theory. Pathol Res Pract 191:35–41
32. Seifert G, Waller D (1982) Klassifikation der Parotiszysten. Differentialdiagnose der Speichelgangzysten und lymphoepithelialen Zysten. Laryngorhinootologie 61:78–86
33. Sneige N, Batsakis JG (1992) Pathology consultation: necrotizing sialometaplasia. Ann Otol Rhinol Laryngol 101:282–284
34. Takeda Y (1993) Oncocytic hyperplasia in the human minor salivary glands: a post-mortem study. Virchows Arch 423: 105–109
35. Ulirsch RC, Jaffe ES (1987) Sjögren's syndrome-like illness associated with the acquired immunodeficiency syndrome-related complex. Hum Pathol 18:1064–1068
36. Ußmüller J, Donath K, Hartwein J (1992) The histological differentiation and differential diagnosis of squamous metaplasia in the parotid gland. HNO 40:334–338
37. Walker NI, Gobe GC (1987) Cell death and cell proliferation during atrophy of the rat parotid gland induced by duct obstruction. J Pathol 153:333–344

Virchows Arch (2002) 440:527–535
DOI 10.1007/s00428-001-0555-z

ORIGINAL ARTICLE

Christoph Röcken · Hartmut Kronsbein
Knut Sletten · Albert Roessner · Roland Bässler

Amyloidosis of the breast

Received: 8 May 2001 / Accepted: 3 September 2001 / Published online: 24 October 2001
© Springer-Verlag 2001

Abstract We report on three cases of amyloidosis of the breast, two of which coincided with breast cancer. Patient no. 1, a 60-year-old woman, presented with two mass lesions measuring 2 cm in diameter, one in each breast. Histologically, a tubulo-lobular carcinoma was found in the left breast accompanied by vascular, interstitial, and periductal amyloid deposits; the lesion in the right breast consisted of amyloid deposits only. Patient no. 2, an 86-year-old woman, presented with an ulcerated breast tumor measuring 5 cm in diameter on the left side. A poorly differentiated invasive ductal carcinoma was found in the mastectomy specimen, and it coincided with interstitial and vascular amyloid deposits. In both patients, tumor cells had invaded the amyloid deposits. Patient no. 3, a 73-year-old woman, presented with a mass measuring 5×3×3 cm in her left breast. Fibrocystic changes, as well as interstitial and periductal amyloid deposits, were found histologically. In each case electron microscopy showed rigid, non-branching fibrils of indefinite length and measuring 10–12 nm in diameter; these were consistent with amyloid fibrils. Clinical data, immunohistochemistry, and/or amino acid sequencing of the fibril proteins extracted from formalin-fixed and paraffin-embedded tissue specimens provided evidence that the amyloid deposits were of immunoglobulin light chain origin in all three cases. A review of the literature revealed that κ-light chain has been described more frequently than λ-light chain in the breast and that there are no specific clinical or radiological symptoms of amyloidosis affecting the breast; a diagnosis can be achieved only by histology.

C. Röcken (✉) · A. Roessner
Department of Pathology, Otto-von-Guericke-University,
Leipziger Str. 44, 39120 Magdeburg, Germany
e-mail: christoph.roecken@medizin.uni-magdeburg.de
Tel.: +49-391-6713179, Fax: +49-391-67190188

H. Kronsbein · R. Bässler
Department of Pathology, Klinikum Fulda, Germany

K. Sletten
Biotechnology Center of Oslo, University of Oslo, Norway

Keywords Amyloid · Breast · Carcinoma

Introduction

In surgical pathology, the diagnosis of amyloidosis may be unexpected clinically, and it is the pathologist who recognizes the deposits histologically [34, 41]. This is particularly the case for light chain-associated amyloidoses (AL amyloidoses), which may initially present with unspecific clinical symptoms such as carpal tunnel syndrome, proteinuria, or a tumor-like mass lesion [12]. The surgical pathologist may miss amyloid deposits if the deposits are very discrete, or they may be misinterpreted if further special stains are not requested. For example, subepithelial amyloid deposits in biopsies from the large intestine may be misinterpreted as collagenous colitis [16, 34], and amyloid deposits in the breast may be misinterpreted as fibrosis or elastosis [2, 38, 42]. Recognition of amyloid deposits is even more difficult when other pathological conditions coincide (e.g., breast cancer) that are not usually expected to be associated with amyloidosis. However, recognition and appropriate classification of amyloid deposits in biopsy specimens is mandatory [34], independent of whether amyloidosis is local, organ-limited, or generalized [13, 14] since its presence can be "the tip of the iceberg"; deposition of amyloid may be associated with a serious underlying disease, such as malignant B-cell or plasma cell proliferation or familial amyloid syndrome, and it can potentially cause disruption of organ function and/or organ failure [13, 14].

We describe three patients with amyloidosis of the breast, none of which had been expected clinically. In each patient breast cancer was suspected and was subsequently confirmed histologically in two of them. The third patient suffered from an amyloid tumor without coincidental breast cancer.

Case reports

Patient no.1

A 60-year-old woman presented with a 2-cm diameter mobile mass in the left breast near the nipple. Mammography indicated a possible malignant neoplastic lesion, and the entire breast and axillary lymph nodes were resected after a biopsy had been taken. In addition, an induration measuring 2 cm in diameter was found in the upper right quadrant of the right breast; this showed no evidence of malignancy on mammography or ultrasound, and it was resected and submitted for histological examination. Postoperatively, serum electrophoresis showed monoclonal gammopathy of IgG κ-light chain. Bence-Jones protein and proteinuria were not found in the urine. Osteolytic lesions were found in the right ileosacral joint, and these were interpreted as metastases. Two years previously the patient had been diagnosed with Sjögren's syndrome. The clinical history of this case has been described in more detail elsewhere [4].

Patient no. 2

An 86-year-old woman presented with a 5-cm diameter ulcerated tumor of the left breast, which had been observed by the patient for at least 2 years. The breast was amputated. Monoclonal gammopathy was not found by serum electrophoresis. A bone marrow biopsy showed no evidence of plasmacytoma. The patient died 6 months after surgery due to cardiac failure, and an autopsy was not performed.

Patient no. 3

A 73-year-old woman presented with a mass measuring 5×3×3 cm in the left breast. The tumor was excised. Biopsies from the stomach (antrum and corpus), duodenum, terminal ileum, and large intestine showed no amyloid deposits. Monoclonal gammopathy was not found by serum electrophoresis. X-ray films of the chest, abdomen, and hands showed no osteolytic lesions. The patient was discharged and is well 8 months after breast tumor resection.

Materials and methods

All specimens were fixed in formalin and embedded in paraffin. Deparaffinized sections were stained with hematoxylin and eosin and van Gieson's elastic stain. The presence of amyloid was demonstrated by the appearance of green birefringence due to alkaline, alcoholic Congo Red staining under polarized light [33, 41].

Immunostaining was performed with monoclonal antibodies directed against IgA (1:15), IgG (1:50), IgM (1:30), and AA amyloid (1:500). Further immunostaining was performed using polyclonal antibodies directed against amyloid P component (1:1600), transthyretin (1:600), β2-microglobulin (1:2000), λ-light chain (1:7500), and κ-light chain (1:7500; all the preceding from Dako, Denmark). Prior to immunostaining, the specimens were pre-treated with 10 mM ethylene diamine tetraacetate (2×10 min, 450 W microwave oven; transthyretin), 0.5 U/ml Protease I (16 min, λ- and κ-light chain, Ventana, Strasbourg) or 0.1% papain (8 min, β2-microglobulin). Immunostaining with anti-AA amyloid did not require specimen pre-treatment. Immunoreaction was visualized using the avidin–biotin complex method applying a Vectastain ABC alkaline phosphatase kit (distributed by Camon, Wiesbaden, Germany) or an UltraTech HRP Streptavidin-Biotin Universal Detection System (Immunotech, Marseilles, France). Neufuchsin and 3,3-diaminobenzidine-tetrahydrochloride, respectively, served as chromogens. The specimens were counterstained with hematoxylin. The specificity of immunostaining was controlled using specimens containing known classes of amyloid (AA amyloid, transthyretin, β2-microglobulin), using positive controls recommended by the manufacturers for the remaining antibodies, and by omitting the primary antibodies.

For electron microscopy, formalin-fixed specimens were fixed in a mixture of 2% formalin/2.5% glutaraldehyde (pH 7.2, overnight, 4°C) and then in 3.125% glutaraldehyde (7 h, 4°C). Following standard procedures of tissue processing for electron microscopy, the specimens were finally embedded in Epon-supplemented with 2% 2,4,6-tris(dimethylaminomethyl)phenol-30. Polymerization took place over 24 h at 60°C. Semi-thin sections (1 µm) were stained with toluidine blue. Ultra-thin sections (80–120 nm) were mounted on copper grids and counterstained with 3% aqueous uranyl acetate (30 min, RT) and contrasted with 1% aqueous lead citrate (15 min, RT).

The preparation of amyloid fibril proteins from formalin-fixed specimens was performed as described by Layfield et al. [25]. The extracted protein was resolved by sodium dodecyl sulfate–polyacrylamide gel electrophoresis as described elsewhere [35]. For amino acid sequencing, proteins on unstained polyacrylamide gels were transferred onto polyvinylidine–difluoride membrane (PVDF, Immobilon-P^{SQ}, pore size 0.1 µm; Millipore, Bedford, Mass.) using the tank-blotting system from Bio-Rad Laboratories (München, Germany) according to the manufacturer's instructions. Transferred proteins were visualized by Coomassie blue staining. For amino acid sequencing, the PVDF-electroblotted bands were cut out and placed into a 477A protein sequencer connected to a 120A PTH amino acid analyzer (Applied Biosystems, Foster City, Calif.). The samples were analyzed for seven to eleven cycles. The protein was identified using the "BLAST Sequence Similarity Searching" program devised by the National Center for Biotechnology Information.

Results

Patient no. 1

The biopsy and resection specimens from the left breast showed an invasive lobular and tubulo-lobular carcinoma of the breast (Fig. 1A–C). Metastases were found in two out of fifteen regional lymph nodes. Amyloid was found as extensive vascular, interstitial, and periductal deposits (Fig. 1C), which occasionally formed large confluent patches in both breasts. The resection specimens of the right breast showed amyloid deposits only, with no evidence of cancer. The amyloid deposits were immunoreactive for amyloid P component only; the other antibodies did not stain the amyloid deposits. Multinucleated giant cells (MGCs) were present within and adjacent to the amyloid deposits (Fig. 1B). On the left side the amyloid deposits were infiltrated by carcinoma cells, and vital tumor cells were occasionally enclosed by amyloid deposits

Fig. 1 **A** Invasive lobular carcinoma of the breast infiltrating interstitial amyloid deposits. **B** Multinucleated giant cells were found within or near amyloid deposits. **C** Periductal and interstitial amyloid deposits of the breast showed characteristic green birefringence (**A**–**C** specimens from case no. 1). **D** Ductal carcinoma of the breast infiltrating interstitial amyloid deposits. **E** Tumor cells of ductal carcinoma showing immunostaining for amyloid P component. **F** Amyloid deposits were occasionally associated with calcifications. **G** Amyloid deposits immunostain for IgM and (**H**) λ-light chain. (**D**–**H** specimens from case no. 2). Hematoxylin and eosin (**A**, **B**, **D**, **F**); Congo red staining in polarized light (**C**); anti-amyloid P component (**E**); anti-IgM (**G**), anti-λ-light chain (**H**), hematoxylin counterstain; Original magnifications: ×200 (**A**, **C**, **D**, **G**, **H**), ×400 (**B**, **E**, **F**)

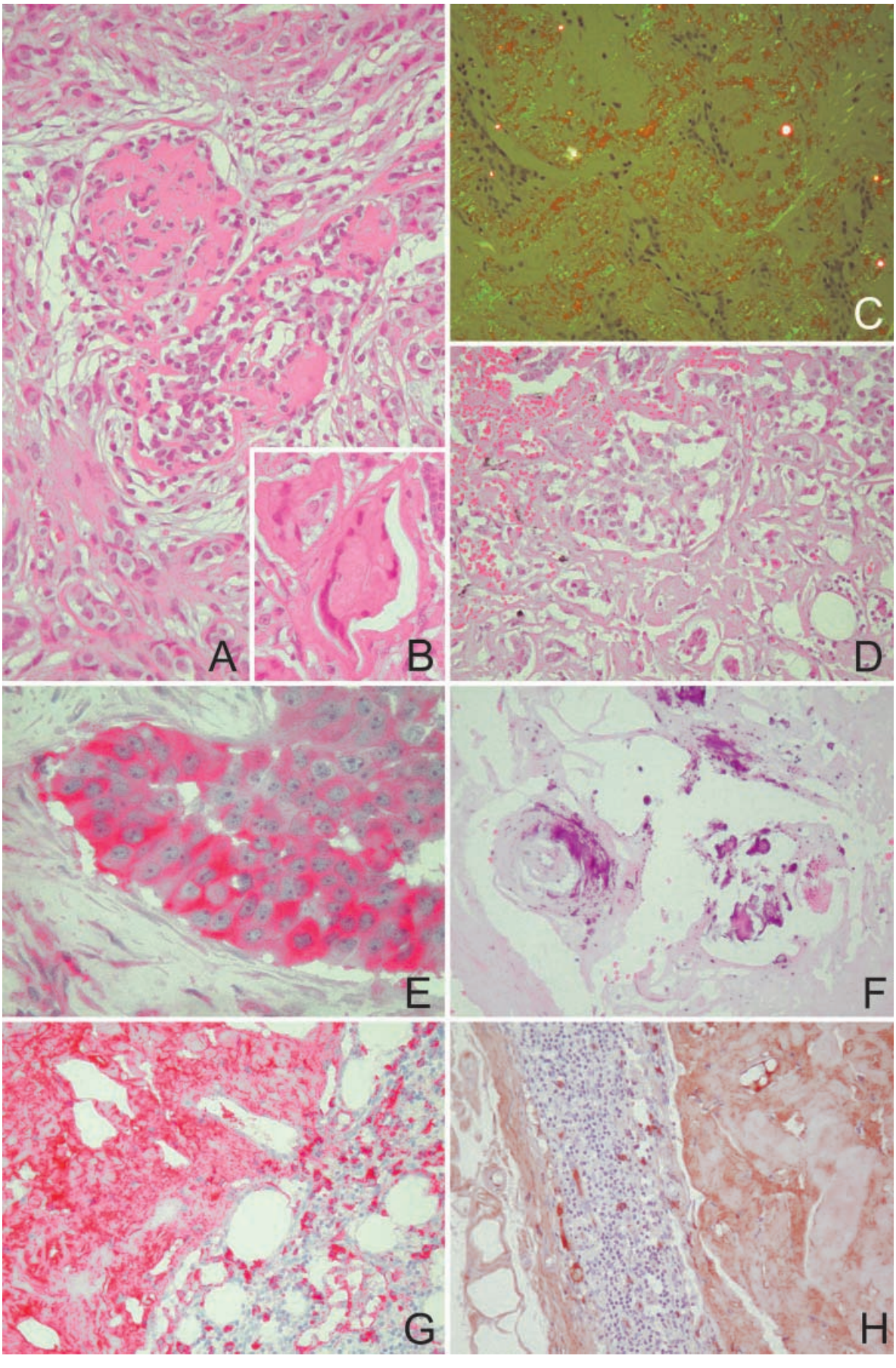
A
B
C
D
E
F
G
H

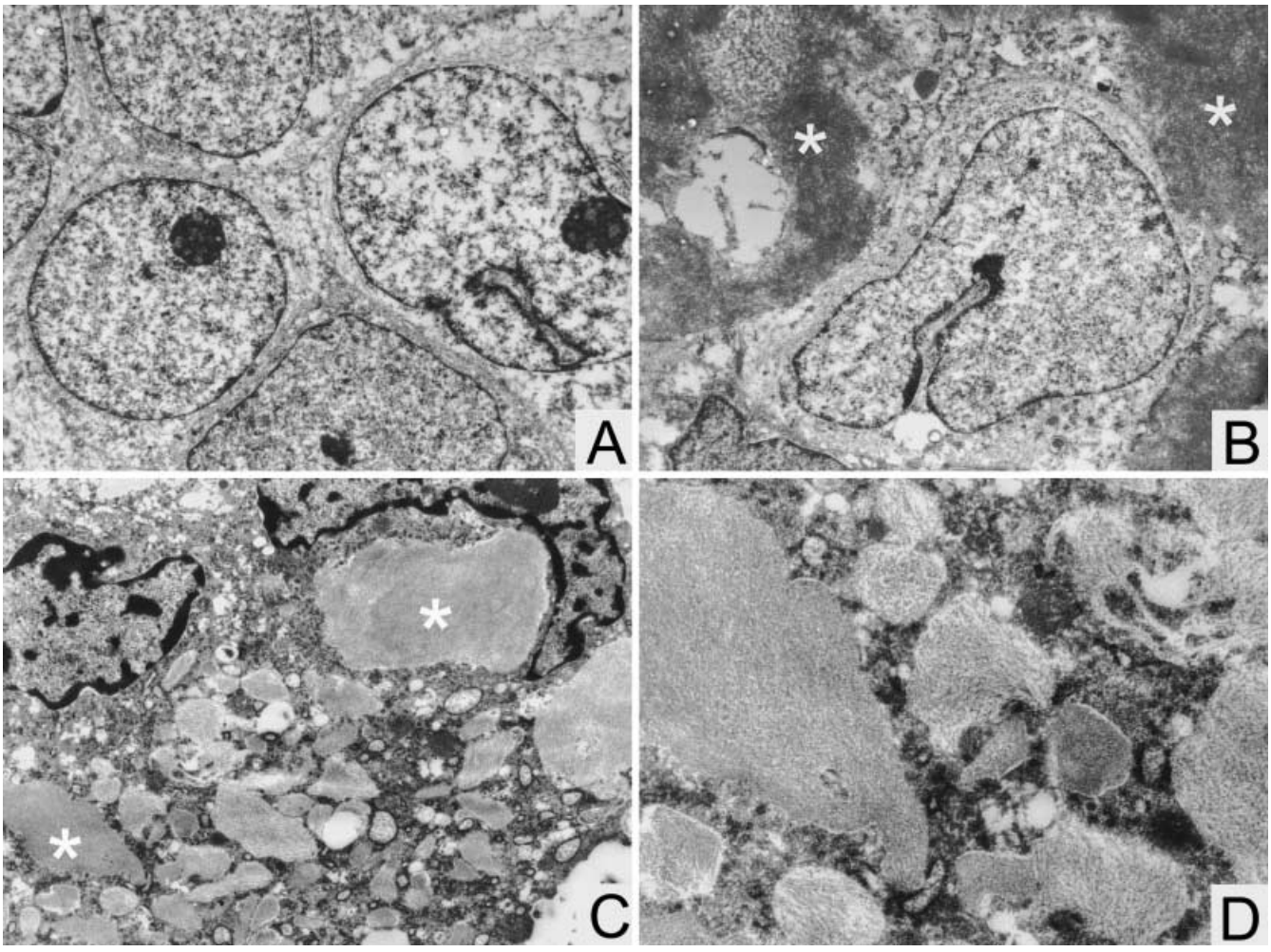

Fig. 2 Invasive lobular carcinoma of the breast (**A**) infiltrating interstitial amyloid deposits (**B**, *asterisk*). Occasional intracellular amyloid (C, *asterisk*) was found in multinucleated giant cells (**C**, **D**); Original magnifications: ×3000 (**A**, **F**, **G**), ×4400 (**C**), ×12,000 (**D**)

(Fig. 1A). Calcifications were present within the carcinoma and also within amyloid deposits where they were without surrounding neoplastic or non-neoplastic epithelium. Focal aggregates of lymphocytes and plasma cells were also found. Immunohistochemically the plasma cells showed no restriction to λ- or κ-light chain. Electron microscopy showed that the amyloid deposits consisted of rigid, non-branching fibrils of indefinite length and measuring 10–12 nm in diameter (Fig. 2). Occasionally intracellular amyloid was found in MGCs (Fig. 2). The formalin-fixed and paraffin-embedded material was subjected to amyloid fibril preparation according to Layfield et al. [25]. However, it was not possible to extract sufficient material to allow amino acid sequencing.

Patient no. 2

In the second patient, a poorly differentiated invasive ductal carcinoma was found (Fig. 1D) accompanied by

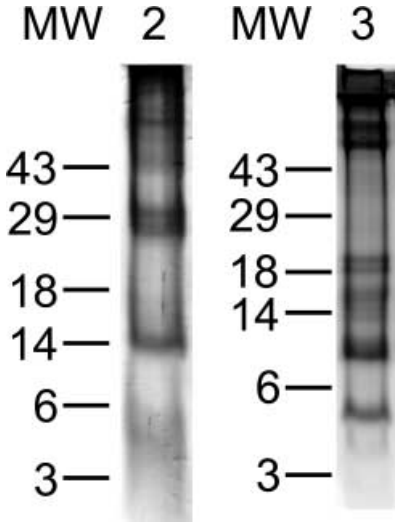

Fig. 3 Sodium dodecyl sulfate–polyacrylamide gel electrophoresis. *Lane 2* Fibril proteins extracted from formalin-fixed and paraffin-embedded breast tissue of patient no 2. *Lane 3* Fibril proteins extracted from formalin-fixed and paraffin-embedded breast tissue of patient no. 3. *MW* molecular weight standards in kDa

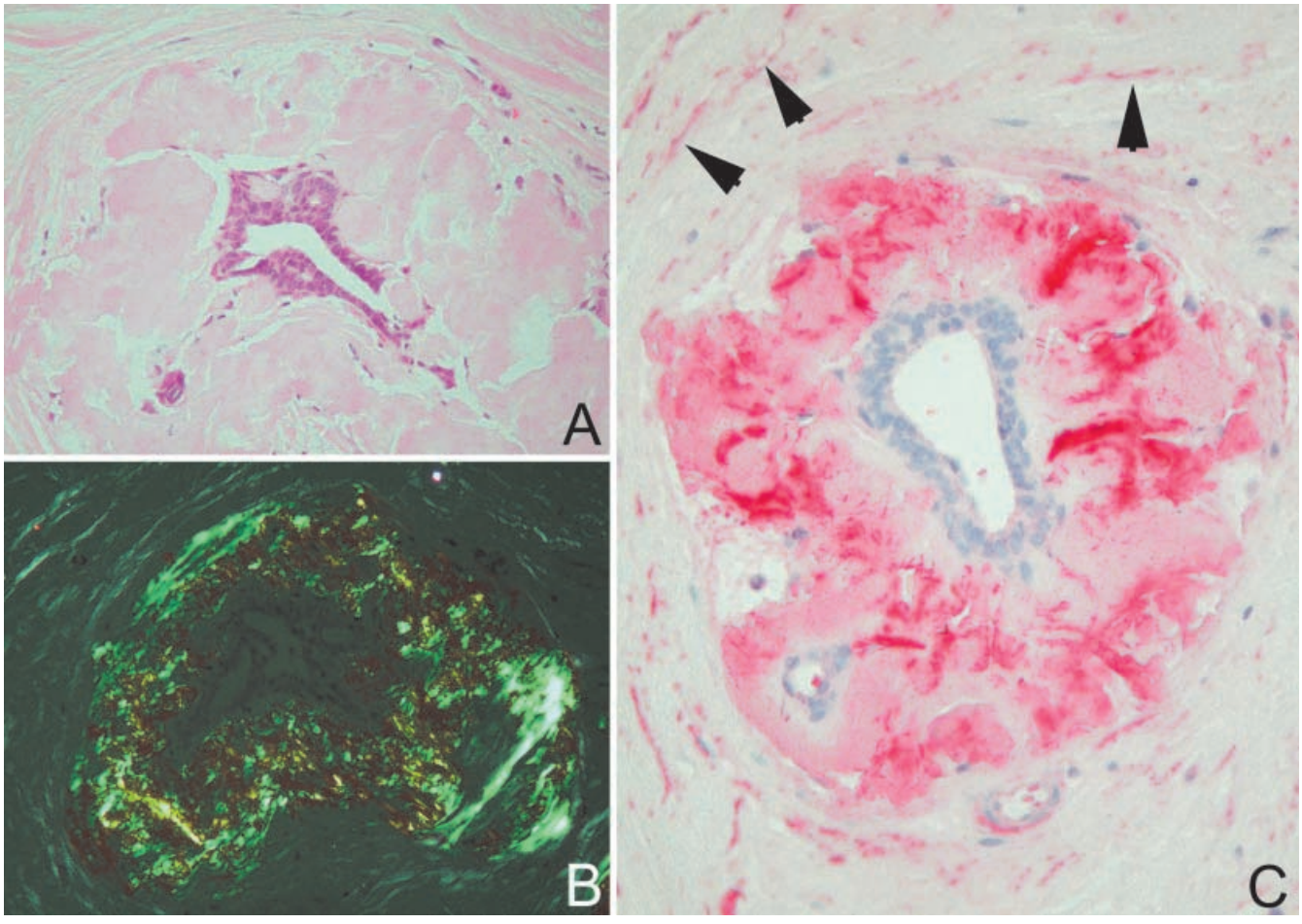

Fig. 4 **A** Periductal amyloid deposits of patient no. 3. **B** Congo red staining in polarized light showed green birefringence. **C** The amyloid deposits are immunoreactive for amyloid P component. Additional immunostaining was found outside amyloid deposits in the interstitium (*arrowheads*). Hematoxylin and eosin (**A**), Congo red staining in polarized light (**B**), anti-amyloid P component (**C**), hematoxylin counterstain. Original magnifications ×200

an intransit metastasis of 3.5 cm diameter and further metastases in three out of sixteen axillary lymph nodes. Extensive interstitial and vascular amyloid deposits were present in the breast, axillary lymph nodes, and surrounding adipose tissue (Fig. 1D, F). Again the deposits were partially infiltrated and surrounded by the invading carcinoma (Fig. 1D). Calcifications were found within amyloid deposits only (Fig. 1F). MGCs were present within and adjacent to the amyloid deposits. The amyloid deposits were immunoreactive for amyloid P component, IgM (Fig. 1G), and λ-light chain (Fig. 1H). Antibodies directed against AA-, ATTR-, and Aβ2M-amyloid, and against κ-light chain, IgA, and IgG did not stain the deposits. In addition, the tumor cells occasionally showed strong cytoplasmic immunostaining for amyloid P component (Fig. 1E). Electron microscopy showed rigid, non-branching fibrils of indefinite length and measuring 10–12 nm in diameter. Amyloid fibril proteins were extracted from formalin-fixed and paraffin-embedded specimens and separated using gel electrophoresis (Fig. 3). Two bands of approximately 14 kDa and 29 kDa were identified and subjected to N-terminal amino acid sequencing. Sequence data were not obtained for the 14-kDa band. Cleavage was performed with 3-bromo-3-methyl-2-(2-nitrophenylthio)3H-indole assuming the presence of at least one tryptophan residue in the protein, and this gave a slightly higher yield of phenylthiohydantoin amino acids, but these could not be interpreted due to high background. N-terminal analysis of the 29 kDa band did not yield a sequence, even after cyanogen bromide cleavage.

Patient no. 3

The breast specimen showed marked fibrocystic changes. In addition, amyloid was present as confluent interstitial and extensive periductular deposits associated with atrophy of the lobules and lactiferous ducts (Fig. 4A–B). Tiny calcifications were noted, and, again, MGCs were present within and adjacent to the amyloid deposits. The amyloid deposits were immunoreactive for amyloid P component only (Fig. 4C); the other antibodies did not stain the amyloid deposits. Immunostaining for amyloid P component was also found outside the amyloid in the non-tumorous and non-amyloidotic breast (Fig. 4C, ar-

rowheads). Electron microscopy showed rigid, non-branching fibrils of indefinite length and measuring 10–12 nm in diameter. Amyloid fibril proteins were extracted from formalin-fixed and paraffin-embedded specimens and separated using gel electrophoresis (Fig. 3). Two bands of approximately 5 kDa and 9 kDa in size were identified and subjected to N-terminal amino acid sequencing. This yielded the same sequence for both bands: IVMTQSPVTSVV. This sequence corresponds to immunoglobulin fragments of κ-light chain origin.

Discussion

We describe three female patients with amyloidosis of the breast. In each case the clinical suspicion was breast cancer, but histological examination confirmed malignancy in only two of the patients. The third patient was suffering from an amyloid tumor only. As described here, amyloid deposits in the breast may present as either periductal, interstitial, or vascular deposits. While periductal amyloidosis may lead to obstruction and atrophy of the lactiferous ducts, and vascular deposits may be quite extensive, no symptoms attributable to periductal or vascular amyloid depositions have been described for the breast [1, 2, 5, 7, 8, 9, 10, 11, 15, 17, 18, 19, 20, 23, 24, 26, 27, 28, 29, 30, 32, 37, 39, 43]. Clinically, amyloidosis of the breast presents as either a mass lesion, general tenderness, peau d'orange, or without any symptoms [1, 2, 5, 7, 8, 9, 10, 11, 15, 17, 18, 19, 20, 23, 24, 26, 27, 28, 29, 30, 32, 37, 39, 43]. Calcifications may be found by mammography and raise suspicion of fibrocystic change or malignancy [5, 7, 10, 17, 18, 20, 39, 43]. However, as yet no clinical or radiological symptoms have been described that are specific for amyloid affecting the breast. Diagnosis can be achieved by histological examination only, and clinically occult amyloid deposits of the breast may be detected only at autopsy [3].

Amyloid may affect either the right, the left, or both breasts without showing any preference (Table 1). It may occur as local and organ-limited deposits or as part of a generalized disease [3]. If there is an initial diagnosis of amyloidosis in breast tissue specimens, then the presence of a generalized amyloid disease needs to be excluded, either by biopsies from other organs and special sites (e.g., gastrointestinal tract or abdominal adipose tissue) or by elaborate clinical investigations. In patient no. 3, we were able to exclude generalized amyloidosis. In patient no. 2, the presence of vascular and interstitial amyloid deposits in axillary lymph nodes suggests the presence of a more generalized disease, but this patient escaped further investigations and an autopsy was not performed. Patient no. 1 may be suffering from generalized amyloidosis, but so far the evidence is lacking; during a 2-year follow-up period the patient has not developed any clinical signs of a generalized amyloidosis.

Amyloidosis of the breast may affect both genders (Table 1), but to date it has been described more commonly in women. The mean age at diagnosis is 63 years (range 43–86 years; Table 1), and malignancy or fibrocystic changes are often included in the differential diagnosis. In fact, amyloidosis of the breast may be related to non-malignant and malignant diseases. Rheumatoid arthritis is a non-malignant disease that has been described in association with amyloidosis of the breast [28]. Patient no. 1 had suffered from Sjögren's syndrome, but amyloidosis was probably unrelated to this. Immunohistochemical analysis showed that the deposits were not AA amyloid, and no clinical evidence was found for Morbus Waldenström, which may be associated with Sjögren's syndrome. Malignant diseases associated with breast amyloidosis are of diverse origin. Invasive ductal carcinoma of the breast was found to be associated with amyloidosis, as in our patient no. 2 [1, 2, 23, 37]. Lobular breast carcinomas coinciding with amyloid deposits (as in our patient no. 1) have not been described previously. Also, malignant non-Hodgkin's lymphomas may cause deposition of amyloid in the breast [17, 24, 32, 43]. The fibril proteins deposited in the breast have been classified as AA amyloid fibril proteins [23, 28] or as immunoglobulin of light chain origin [9, 19, 20, 24, 29, 30, 32, 39, 43]; κ-light chain was found more frequently than λ-light chain in breast amyloid (Table 1). It is unclear whether this is coincidental or reflects a particular tropism of κ-light chains for the breast [40]. The amyloid deposits of our first patient did not stain with any of the antibodies used, therefore excluding AA-, ATTR-, and Aβ2M-amyloidosis. However, AL amyloidosis cannot be excluded since the commercially available antibodies used herein show only occasional staining of AL amyloid deposits. However, in patient no. 1, AL amyloidosis is most likely because monoclonal gammopathy (IgG κ-light chain) was found in the serum. The deposits of our second and third patients were shown to be of light chain origin using immunohistochemical analysis and/or protein sequencing. Thus, all three patients studied suffered from AL amyloidosis affecting the breast, which, to date, is the most common type of amyloidosis to be described in the breast (Table 1).

AL amyloidosis is a member of the monoclonal immunoglobulin deposition diseases that involve the deposition of monoclonal proteins in organs and tissue with the potential to disrupt organ function and/or to cause organ failure [13, 14, 40]. The diseases are the result of a clonal B-cell or plasma cell proliferation. Thus the amyloid fibril proteins deposited in the breasts of our patients were not of epithelial origin. Nevertheless, one may suggest a pathophysiological link between breast cancer and deposition of amyloid deposits in breast carcinomas. Breast cancer may be associated with stromal changes, such as elastosis [3, 31, 38, 42]. Microfibrils of elastic tissue and amyloid fibrils share structural homologies [21, 22] since both are composed of a central core of amyloid P component covered with ribbons of highly sulfated glycosaminoglycans [21, 22]. Thus, stromal changes may serve as a scaffold for fibril proteins to be deposited locally. Amyloid P component was found even in non-

Table 1 Review of the literature. *MGCs* multinucleated giant cells, *AL* light chain-associated, *ND* not determined, *R* right site, *L* left site

Authors	Year	No. of cases	Sex	Age (years)	Size (cm)	Site	Amyloid type	Associated disease/clinical diagnosis	Calcifi-cations	MGCs
Fernandez and Hernandez	1973	1	Female	62	3	R	ND	No data	+	–
Baptist et al.	1973	5	Female	44–72	No data	No data	ND	Ductal carcinoma	–	–
Case et al.	1974	1	Female	52	4	L	ND	Plasma cell mastitis	+	–
Gavrilita and Laba	1976	5	No data	No data	No data	No data	No data	Breast cancer ("medullary type")	–	–
Bässler	1978	1	Female	60	Diffuse	R+L	ND	Generalized amyloidosis, plasmacytosis in bone marrow	No data	No data
		1	Male	69	Diffuse	R+L	ND	Generalized amyloidosis	No data	No data
		1	Male	76	Diffuse	R+L	ND	Generalized amyloidosis, plasmacytoma	No data	No data
Lipper and Kahn	1978	1	Female	47	3	R	ND	Amyloid tumor	–	+
Hardy et al.	1979	1	Female	53	Multiple 1	R+L	κ-Light chain	Generalized amyloidosis	–	+
McMahon et al.	1984	1	Female	54	1	R	κ-Light chain	Amyloid tumor	–	+
O'Connor et al.	1984	1	Female	56	Multiple	R+L	λ-Light chain	Generalized AL amyloidosis	–	–
		1	Female	52	Multiple	R+L	κ-light chain	Generalized AL amyloidosis	–	–
		1	Female	56	2	ND	κ-Light chain	Morbus Waldenström	–	–
		1	Female	61	Diffuse	R+L	λ-Light chain	Generalized AL amyloidosis	–	–
		1	Female	52	Diffuse	R+L	λ-Light chain	Generalized AL amyloidosis	–	–
Lew and Seymour	1985	1	Female	63	2	R	ND	Amyloid tumor	–	–
Cheung et al.	1986	1	Female	82	ND	R+L	ND	Amyloid tumors	–	+
Silverman et al.	1986	1	Female	67	5 3	L R	IgA	Amyloid tumors	–	–
		1	Female	79	2	L	λ-Light chain	Amyloid tumor	+	+
Lamovec and Jancar	1987	1	Female	63	6	L	κ-Light chain	Non-Hodgkins lymphoma	–	+
McMahon and Connolly	1987	1	Female	54	3.5	R	κ-Light chain	Amyloid tumor	–	–
Goonatillake and Allsop	1988	1	Female	55	2	R	ND	Rheumatoid arthritis	–	+
Hecht et al.	1991	1	Female	68 7×5	6×5 L	R	κ-Light chain	Generalized AL amyloidosis	+	–
Santini et al.	1992	1	Female	75	25	L	ND	Ductal carcinoma	–	+
Bisceglia et al.	1995	1	Female	53	1.5	R	ND	Amyloid tumor	+	–
Symonds et al.	1995	1	Female	69	5×5	R	κ-Light chain	Plasmacytosis in bone marrow	+	–
Gupta and Dowle	1996	1	Female	43	5	L	ND	Amyloid tumor	+	–
Alujevic et al.	1997	1	Female	71	1.5	L	ND	Ductal carcinoma	–	+
Luo and Rotterdam	1997	1	Female	82	2	R	AA amyloid	Amyloid tumor	–	+
Krüger et al.	1998	1	Female	75	–	–	AA amyloid	Ductal carcinoma	–	–
Echevarria et al.	2000	1	Female	43	3	R	κ-Light chain	Generalized AL amyloidosis	–	–
Gupta et al.	2000	1	Female	64	2.5×2 6×4	R L	AA^-, AP^+	MALT-lymphoma	+	+
Röcken et al. (present cases)		1	Female	60	2	R	AA^-, $ATTR^-$,	Lobular carcinoma, monoclonal	–	+
					2	L	$Aβ2M^-$	Gammopathy κ-light chain		
		1	Female	86	5	L	λ-Light chain	Ductal carcinoma	+	+
		1	Female	73	5×3×3	L	κ-light chain	Amyloid tumor	+	+

neoplastic and non-amyloidotic tissue from our patients, but most intriguing is the detection of amyloid P component in tumor cells of the second patient. This leads to speculation that tumor cells of ductal carcinomas are capable of synthesizing and secreting amyloid P component, thereby facilitating the deposition of amyloid. Further studies are needed to substantiate this hypothesis.

In each patient we found MGCs within or adjacent to amyloid deposits; MGCs may represent a tissue response, and they have been described previously in amyloidosis of the breast (Table 1). Previous animal studies provided evidence that MGCs might be involved in the resorption of amyloid deposits [44] since they synthesize a broad range of proteases, some of which are able to degrade amyloid fibril proteins [6, 36].

In summary, we describe three cases of AL amyloidosis affecting the breast, two of which were associated with breast cancer. There are no specific clinical or radiological symptoms of amyloidosis affecting the breast, and a diagnosis can be achieved only by histological examination. Local tissue factors may promote the deposition of amyloid, but this hypothesis needs further investigation.

Acknowledgements The specimens were donated to the "Mamma-Register Fulda" from case no. 1 by Dres. Schuleri and Gerlach, Institute of Pathology, Leopoldina Hospital Schweinfurt, and from case no. 3 by Prof. Dr. Wierich and Dr. Schmidt, Institute of Pathology Recklinghausen. The authors thank Dr. Barbara Stix and Sophie Mansfeld for their excellent technical assistance.

References

1. Alujevic A, Juric G, Separovic V, Kruslin B (1997) Invasive breast carcinoma with granulomatous stromal response. Zentralbl Gynakol 119:343–345
2. Baptist SJ, Thomas JA, Kothare SN (1973) Hyaline material in mammary cancer – a study of five cases. Indian J Cancer 10:317–321
3. Bässler R (1978) Pathologie der Interzellularsubstanz. Doerr W, Seifert G, Uehlinger E (eds) Pathologie der Brustdrüse. Springer, Berlin Heidelberg New York, pp 229–236
4. Bässler R, Würstlein R, Röcken C, Christ F (2000) Tumorförmige bilaterale Amyloidose der Mamma assoziiert mit einem invasiven lobulären Karzinom und Sjögren-Syndrom. Kasuistik und Literaturübersicht. Geburtshilfe und Frauenheilkunde 60:645–650
5. Bisceglia M, Carosi I, Murgo R, Giuliani F, Caluori D (1995) Primary amyloid tumor of the breast. Case report and review of the literature. Pathologica 87:162–167
6. Bühling F, Reisenauer A, Gerber A, Krüger S, Weber E, Brömme D, Roessner A, Ansorge S, Welte T, Röcken C (2001) Cathepsin K – a marker of macrophage differentiation? J Pathol 195:375–382
7. Case TC, Gillooley J, Madrazo AA, Ortiz VN (1974) Plasmacell mastitis: case report. J Am Geriatr Soc 22:39–42
8. Cheung PSY, Yan KW, Alagaratnam TT, Collins RJ (1986) Bilateral amyloid tumours of the breast. Aust N Z J Surg 56:375–377
9. Echevarria JJ, Lopez JA, Alvarez JA, Astigarraga E (2000) Breast involvement in a case of primary systemic amyloidosis: mammographic, US, and MR appearances. J Comput Assist Tomogr 24:451–453
10. Fernandez BB, Hernandez FJ (1973) Amyloid tumor of the breast. Arch Pathol 95:102–105
11. Gavrilita L, Laba E (1976) Breast cancer and amyloid stroma. Morphol Embryol 22:29–32
12. Gertz MA, Kyle RA (1989) Primary systemic amyloidosis – a diagnostic primer. Mayo Clin Proc 64:1505–1519
13. Glenner GG (1980) Amyloid deposits and amyloidosis. The β-fibrilloses. N Engl J Med 302:1333–1343
14. Glenner GG (1980) Amyloid deposits and amyloidosis. The β-fibrilloses. N Engl J Med 302:1283–1292
15. Goonatillake HD, Allsop JR (1988) Amyloid tumour of the breast simulating carcinoma. Aust N Z J Surg 58:589–590
16. Gradwell E (1998) Amyloid colitis mimicking collagenous colitis. Histopathology 32:383–383
17. Gupta D, Shidham V, Zemba-Palko V, Keshgegian A (2000) Primary bilateral mucosa-associated lymphoid tissue lymphoma of the breast with atypical ductal hyperplasia and localized amyloidosis. Arch Pathol Lab Med 124:1233–1236
18. Gupta RK, Dowle CS (1996) Cytodiagnosis of amyloid deposition within the breast. Cytopathology 7:136–140
19. Hardy TJ, Myerowitz RL, Bender BL (1979) Diffuse parenchymal amyloidosis of lungs and breast. Its association with diffuse plasmacytosis and κ-chain gammopathy. Arch Pathol Lab Med 103:583–585
20. Hecht AH, Tan A, Shen JF (1991) Case report: primary systemic amyloidosis presenting as breast masses, mammographically simulating carcinoma. Clin Radiol 44:123–124
21. Inoue S, Kisilevsky R (1996) A high resolution ultrastructural study of experimental murine AA amyloid. Lab Invest 74:670–683
22. Inoue S, Kisilevsky R (1999) In situ electron microscopy of amyloid deposits in tissues. Methods Enzymol 309:496–509
23. Krüger S, Kreft B, Heide W, Siebel U, Djonlagic H, Reusche E (1998) Sensorimotor polyneuropathy and systemic amyloidosis as paraneoplastic symptoms of a carcinoid-like well differentiated carcinoma of the breast. Dtsch Med Wochenschr 123:179–184
24. Lamovec J, Jancar J (1987) Primary malignant lymphoma of the breast. Lymphoma of the mucosa-associated lymphoid tissue. Cancer 60:3033–3041
25. Layfield R, Bailey K, Lowe J, Allibone R, Mayer RJ, Landon M (1996) Extraction and protein sequencing of immunoglobulin light chain from formalin-fixed cerebrovascular amyloid deposits. J Pathol 180:455–459
26. Lew W, Seymour AE (1985) Primary amyloid tumor of the breast. Case report and literature review. Acta Cytol 29:7–11
27. Lipper S, Kahn LB (1978) Amyloid tumor. A clinicopathologic study of four cases. Am J Surg Pathol 2:141–145
28. Luo JH, Rotterdam H (1997) Primary amyloid tumor of the breast: a case report and review of the literature. Mod Pathol 10:735–738
29. McMahon RFT, Connolly CE (1987) Amyloid breast tumor. Am J Surg Pathol 11:488
30. McMahon RFT, Waldron D, Given HF, Connolly CE (1984) Localised amyloid tumour of breast – a case report. Isr J Med Sci 153:323–324
31. Mera SL, Davies JD (1987) Elastosis in breast carcinoma: I. Immunohistochemical characterization of elastic fibres. J Pathol 151:103–110
32. O'Connor CR, Rubinow A, Cohen AS (1984) Primary (AL) amyloidosis as a cause of breast masses. Am J Med 77:981–986
33. Puchtler H, Sweat F, Levine M (1962) On the binding of Congo red by amyloid. J Histochem Cytochem 10:355–364
34. Röcken C, Schwotzer E, Linke RP, Saeger W (1996) The classification of amyloid deposits in clinicopathological practice. Histopathology 29:325–335
35. Röcken C, Hegenbarth V, Schmitz M, Stix B, Schade G, Mohnert A, Roessner A (2000) Plasmacytoma of the tonsil with secondary AL amyloidosis and osseous metaplasia. Virchows Arch 436:336–344
36. Röcken C, Stix B, Brömme D, Ansorge S, Roessner A, Bühling F (2000) A putative role for cathepsin K in degradation of AA and AL amyloidosis. Am J Pathol 158:1029–1038

37. Santini D, Pasquinelli G, Alberghini M, Martinelli GN, Taffurelli M (1992) Invasive breast carcinoma with granulomatous response and deposition of unusual amyloid. J Clin Pathol 45:885–888
38. Schiodt T, Jensen H, Nielsen M, Ranlov P (1972) On the nature of amyloid-like duct wall changes in carcinoma of the breast. A light microscopic, histochemical and electron microscopic study. Acta Pathol Microbiol Scand A 233:151–157
39. Silverman JF, Dabbs DJ, Norris HT, Pories WJ, Legier J, Kay S (1986) Localized primary (AL) amyloid tumor of the breast. Cytologic, histologic, immunocytochemical and ultrastructural observations. Am J Surg Pathol 10:539–545
40. Solomon A, Weiss DT (1995) Protein and host factors implicated in the pathogenesis of light chain amyloidosis (AL amyloidosis). Amyloid 2:269–279
41. Steensma DP (2001) "Congo" red – Out of Africa. Arch Pathol Lab Med 125:250–252
42. Sümegi I (1973) Elastase digestion of the amyloid-like substance surrounding mammary cancer and basal cell carcinoma of the skin. Acta Derm Venereol 53:99–104
43. Symonds DA, Eichelberger MF, Sager GL (1995) Calcifying amyloidoma of the breast. South Med J 88:1169–1172
44. Wright JR, Ozdemir AI, Matsuzaki M, Binette P, Calkins E (1972) Amyloid resorption: possible role of multinucleated giant cells. The apparent failure of penicillamine treatment. Johns Hopkins Med J 130:278–288

Virchows Arch (2002) 440:536–542
DOI 10.1007/s00428-001-0585-6

ORIGINAL ARTICLE

Maria P. Foschini · Gianluca Marucci
Vincenzo Eusebi

Low-grade mucoepidermoid carcinoma of salivary glands: characteristic immunohistochemical profile and evidence of striated duct differentiation

Received: 22 October 2001 / Accepted: 6 November 2001 / Published online: 9 February 2002
© Springer-Verlag 2002

Abstract The purpose of the present study is to determine the presence and distribution of epithelial and myoepithelial cells in mucoepidermoid carcinoma (MEC) of salivary glands and to compare them with normal salivary gland tissue and other primary carcinomas. This is in order to establish novel diagnostic criteria and to better understand MEC histogenesis. Formalin-fixed paraffin-embedded tissues from ten well-differentiated MECs, three adenoid cystic carcinomas (ACC), four acinic cell carcinomas (AC), and three epithelial-myoepithelial carcinomas (EMCC) of salivary glands were studied with immunohistochemistry using antibodies that recognise antigens indicative of epithelial and myoepithelial cell differentiation. An anti-mitochondrial antibody was also employed. Normal salivary tissue was present for comparative study in non-tumorous areas of the same section from 12 cases. MEC contained numerous keratin-positive cells. Anti mitochondrial antibody was diffusely positive in all ten of these tumours. Smooth muscle actin, h-caldesmon, and smooth muscle heavy chain myosin, which are indicative of myoepithelial cell differentiation, were negative. Rare cells in only one case were stained by calponin. Cytokeratin 14 (CK14) and anti mitochondrial antibody stained cells located mainly at the periphery of neoplastic nests and cystic spaces, while CK7 was mainly present in cells bordering gland lumina (zoning pattern). The immunohistochemical cell profile was similar to that seen in striated normal ducts. All others tumours studied showed a different immunohistochemical pattern, mostly consisting of a lack of mitochondrion-rich cells and the presence of myoepithelial cells in ACC and EMCC. Immunoreactivity in MEC for CK7, CK14 and mitochondrial antibodies appears as a peculiar pattern of staining, different from that of other salivary gland tumors; this seems helpful for diagnostic purposes. In addition, a differentiation of the "striated duct phenotype" is suggested.

Keywords Myoepithelial cell · Basal cell · Cytokeratin · Salivary gland · Mucoepidermoid carcinoma

M.P. Foschini (✉) · G. Marucci · V. Eusebi
Department of Oncology, Section of Anatomic Pathology,
"M. Malpighi", University of Bologna, Ospedale Bellaria,
Via Altura 3, 40139 Bologna, Italy
e-mail: mariapia.foschini@ausl.bologna.it
Tel.: +39-051-6225523, Fax: +39-051-6225759

Introduction

Mucoepidermoid carcinoma (MEC) of salivary glands is a tumor composed of several cell types. According to the accurate original description of Stewart et al. [29], MEC is mainly composed of mucous secreting, basaloid, intermediate, and epidermoid cells. In addition, these authors found that clear and columnar cells can be present. After comparing MEC morphological features with those of non-neoplastic salivary glands involved by chronic inflammatory processes, they suggested an origin from salivary gland ducts [29]. Most of the morphological information about cellular differentiation of MEC resides in ultrastructural observations [3, 7, 8,]. Dardick et al. [7, 8] indicated that MECs consisted of two types of cells similar to those located along the acinar-intercalated ducts. Ultrastructural and immunohistochemical studies have demonstrated the presence of occasional myoepithelial cells in MEC [9, 17, 19, 24]. Recently, proteins related to the contractile function of smooth muscle cells, such as calponin, caldesmon, and smooth muscle heavy chain myosin have been demonstrated to be present in normal and neoplastic myoepithelial cells [5, 15, 23, 26, 30].

The purpose of the present study is to determine the presence and distribution of epithelial and myoepithelial cells in MEC and to compare these findings with normal salivary gland tissue and other primary carcinomas of the salivary glands. This was undertaken in order to establish further diagnostic criteria and to better understand MEC histogenesis.

Table 1 Source and dilution of the antibodies

Antibody	Clone	Source	Dilution
Cytokeratin 7	OV-TL 12/30	Dako	1:100
Cytokeratin 14	LL002	Biogenex	1:100
Cytokeratin 17	E 3	Dako	1:20
Cytokeratin 19	RCK108	Dako	1:50
Cytokeratin 20	KS 20.8	Dako	1:40
Cytokeratin 8	EAB 902	Ortho	1:1000
Smooth muscle actin	1A4	Dako	1:100
Calponin	Calp	Biogenex	1:80
H-caldesmon	h-CD	Biogenex	1:80
Smooth muscle myosin – heavy chain	SmmS-1	Biogenex	1:300
Apocrine	D6	DBA	1:300
Mitochondria	113–1	Biogenex	1:500

Table 2 Clinical data. *F* female, *M* male

	Site (*n*)	M/F	Age
Mucoepidermoid carcinoma	Parotid (1) Hard palate (3) Soft palate (1) Retromolar pad (4) Cheek (1)	4/6	33–71 (mean 48)
Adenoid cystic carcinoma	Hard palate (2) Parotid (1)	1/2	48–55 (mean 51)
Acinic carcinoma	Parotid (4)	3/1	35–78 (mean 54)
Epithelial-myoepithelial carcinoma	Parotid (3)	1/2	70–86 (mean 78)

Materials and methods

Ten cases of low-grade (well-differentiated) MEC were selected as the basis of the present study. MEC cell types were assessed according to previously described criteria [7, 13, 29]. Immunohistochemical results obtained in MEC were compared with those obtained in normal salivary tissue and in other types of primary carcinomas of salivary glands. Accordingly, three cases of ACC, four of AC, and three of EMCC were included in the study. Tumours were diagnosed according to the WHO classification [27]. Normal salivary gland tissue for comparative study was present in the sample at a suitable distance from tumour tissue in 12 cases.

All cases were retrieved from the files of the Section of Anatomic Pathology, of the Department of Oncology, University of Bologna, at Ospedale Bellaria, Bologna,Italy. Tissues were formalin fixed and routinely processed to paraffin. Selected blocks were serially cut and stained with haematoxylin-eosin (H&E) and in accord with a routine ABC immunohistochemical method as described elsewhere [6, 11]. An epitope retrieval method was employed as follows: before immunostaining sections were steamed in citrate buffer for 25 min and cooled for 5 min. Sources and dilutions of the antisera used are listed in Table 1. The number of immunohistochemically positive cells in each tumour was semiquantitatively assessed as follows:

- +++ >75% Positive cells
- ++ 75–25% Positive cells
- + <25% Positive cells
- +\- Rare positive cells

Results

Clinical data of the patients are summarized in Table 2.

Mucoepidermoid carcinoma

Four cases were predominantly cystic; six cases showed cystic and solid areas. Neoplastic cells of MEC were divided into luminal and non luminal cells. Luminal cells were those lining cystic spaces and comprised mucous secreting cells (MS) and flat to columnar eosinophylic cells (C) (Fig. 1). Non-luminal cells comprised basaloid (B), intermediate (I) and epidermoid (E) cells (Figs. 2, 3). B cells were small, oval, and located near the basal membrane. I cells had a larger amount of eosinophylic cytoplasm and oval nuclei. E cells were large, polygonal, had eosinophylic cytoplasm and a round to oval nucleus. In addition, clusters of cells with abundant empty cytoplasm (clear cells) were focally seen in two cases. MECs were graded according to the grading system of Auclair et al [1].

Almost all the CKs as well as the mitochondrial antigen were expressed to varying degrees in all cases (Table 3). The only exception was that CK20 was negative in most of the cases and stained only rare I cells in three cases. Each single cell type presented a characteristic CK profile (Table 4). CK7 was the most represented epithelial marker and was mainly observed in the central part of the neoplastic nests and cystic spaces where luminal cells are located (Fig. 4). In contrast, CK14 and mitochondrial antigen predominated in the outer rim of the neoplastic nests and cysts where basaloid cells are seen (the distinct affinities of the separate CKs thus constituting a “zoning pattern”) (Figs. 5, 6).

As seen in Table 4 the immunohistochemical profile of the single cells was as follows: B cells mainly stained with CK14 and CK17 and focally with CK8. I cells showed a wider range of CK expression, being positive for CKs 7, 8, 17, 19 and focally for CK14. E cells presented only high-molecular-weight keratins, being positive with CKs 14 and 17. MS cells expressed low-molecular-weight CKs, 7, 8, and 19. C cells showed a CK expression similar to that of I cells, being positive for high- and low-molecular-weight cytokeratins.

The clear cells focally observed in two cases presented the same CK profile as I cells.

Non-luminal cells, B, I, and E cells additionally showed a finely granular cytoplasmic positivity with anti-mitochondrial antibody.

Smooth muscle actin (SMA), calponin (CALP), caldesmon (CALD), and smooth muscle (heavy-chain) myosin (SMM) were mostly negative, the only exception being in Case 1, which showed very rare intermediate cells positive with calponin. Apocrine marker was negative in all cases.

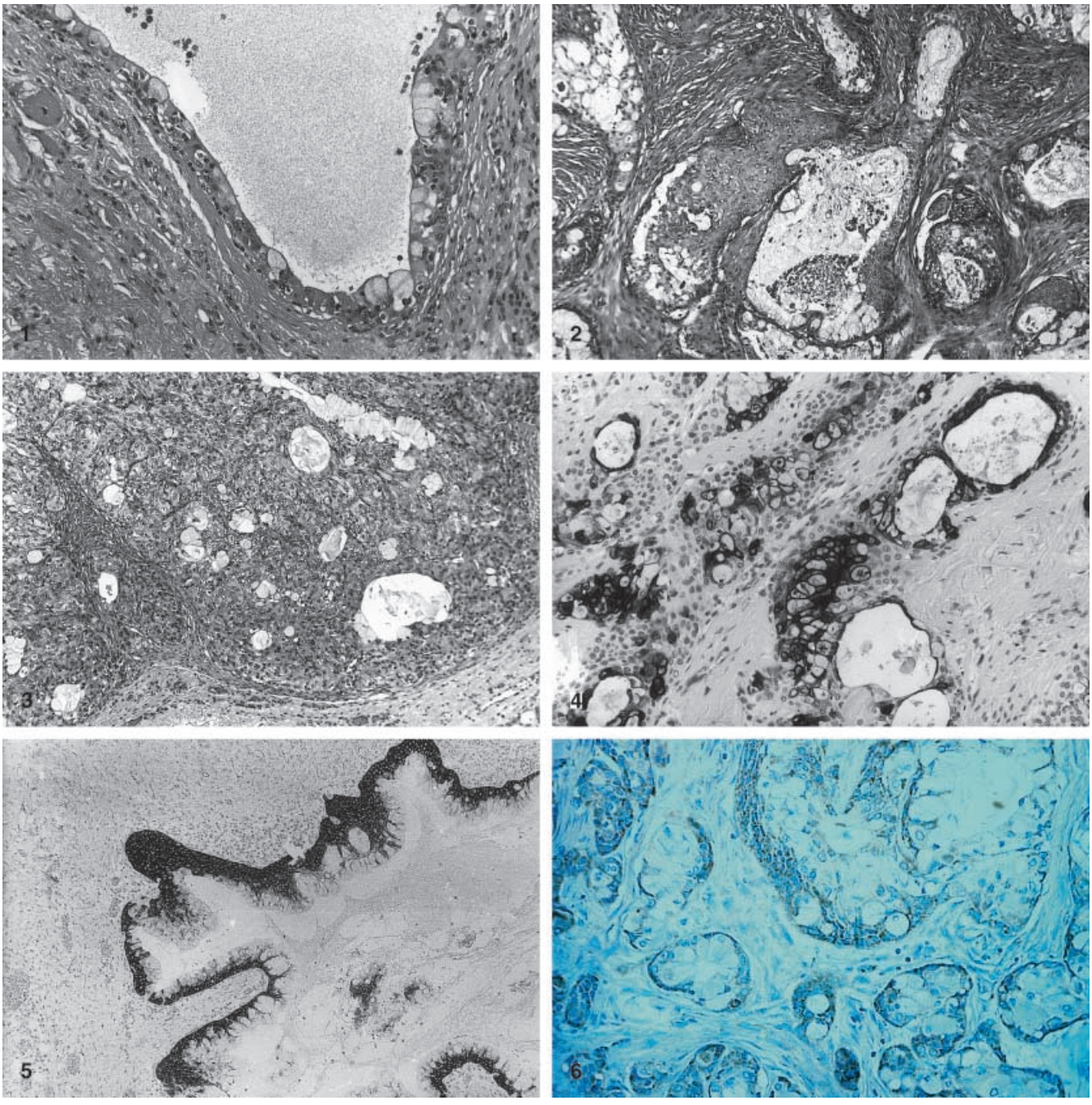

Fig. 1 Cystic spaces are lined by mucous secreting cells and by flat to columnar eosinophilic cells

Fig. 2 Basaloid cells are those small, oval cells located at the periphery of the neoplastic nests. Epidermoid cells are large, with eosinophilic cytoplasm

Fig. 3 Mucoepidermoid carcinoma with solid areas, mainly composed of intermediate cells

Fig. 4 CK7 is strongly positive in the neoplastic cells located in the central part of the neoplastic nests and cysts

Fig. 5 CK14 is mainly positive in the neoplastic cells located at the periphery of the neoplastic nests and cysts

Fig. 6 Mitochondrial antigen disclosed a granular positivity in the cells located at the periphery of the neoplastic nests and cysts

Normal salivary glands

Normal salivary glands (Table 5), (parotideal [1] and minor salivary gland) tissues [11] were studied. Luminal ductal cells (LDC) of striated and intercalated ducts were mostly positive for CKs 7, 8, and 19 (Fig. 7a). In addition LDC of striated ducts were shown to be positive for anti-mitochondrial antibody (Fig. 7b). CK14 in these same ducts demonstrated numerous basal cells (Fig. 7c). Luminal acinar cells (LAC) showed a diffuse positivity for CK7 and a focal positivity for CK19. As it appears in Fig. 7a, cytokeratin positivity in LACs was less intense than that observed in LDCs. On occasion,

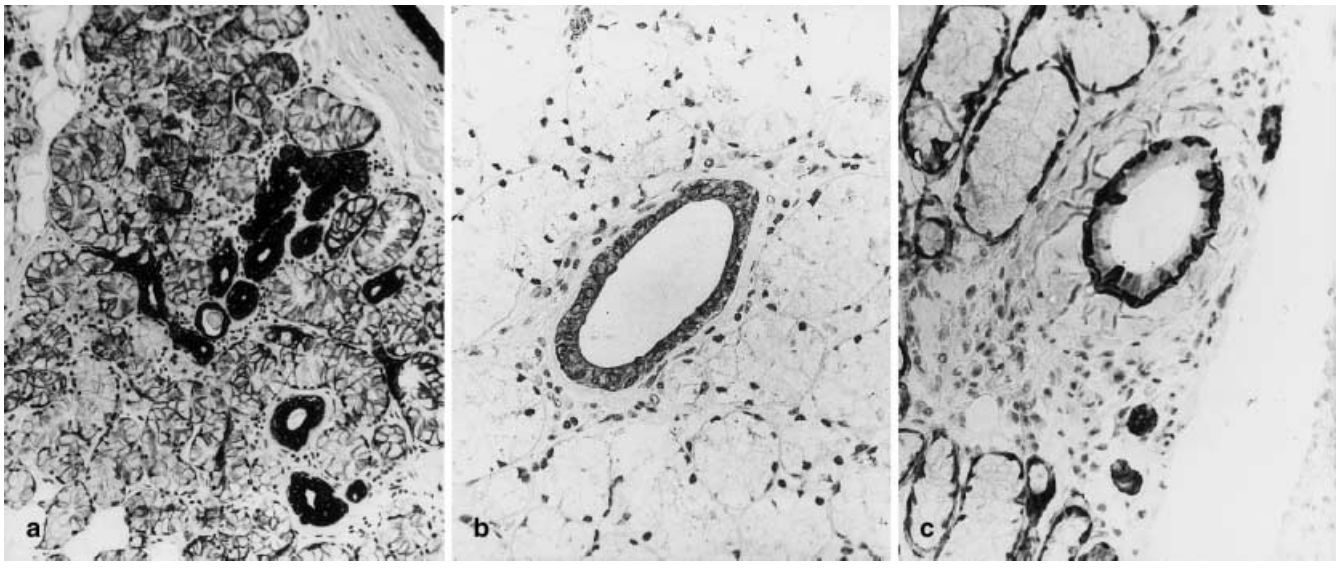

Fig. 7a–c Luminal ductal cells of striated ducts are positive with CK7 (**a**) and mitochondrial antigen (**b**). Basal cells are easily evident with CK14 (**c**)

Table 3 Immunohistochemical results in mucoepidermoid carcinoma. *CK7* cytokeratin 7, *CK8* cytokeratin 8, *CK14* cytokeratin 14, *CK 17* cytokeratin 17, *CK19* cytokeratin 19, *CK20* cytokeratin 20, *Mit* mitochondrial antigen, *SMA* smooth muscle actin, *SMM* smooth muscle myosin, *Calp* calponin, *Cald* caldesmon

Antisera	N°1	N°2	N°3	N°4	N°5	N°6	N°7	N°8	N°9	N°10
CK7	+++	++	+++	+++	+++	+++	+++	+++	+++	+++
CK8	++	+++	+++	++	++	++	++	+++	+++	++
CK14	+	+++	+++	+++	++	+++	++	++	+++	++
CK17	++	+	++	++	++	++	++	++	++	++
CK19	++	+++	++	++	+	++	+	+++	++	++
CK20	–	+/–	+/–	–	–	–	–	+	–	–
SMA	–	–	–	–	–	–	–	–	–	–
Calp	+	–	–	–	–	–	–	–	–	–
Cald	–	–	–	–	–	–	–	–	–	–
SMM	–	–	–	–	–	–	–	–	–	–
Apocrine	–	–	–	–	–	–	–	–	–	–
Mit	+	+++	+	++	+	+	++	+	+	+++

Table 4 Immunohistochemical profile of mucoepidermoid carcinoma cells. *B* Basal cell, *I* intermediate cell, *E* epidermoid cell, *MS* mucous-secreting cell, *C* columnar cell, *MIT* antimitochondrial antibody, *CK* cytokeratin

	B	I	E	MS	C
CK 7	–	+++	–	+++	+
CK 8	+\–	+	–	+++	+
CK 14	+	+\–	++	–	–
CK 17	+	+	+\–	–	++
CK 19	–	+	–	+	+
CK 20	–	+\– [a]	–	–	–
MIT	+	++	+	–	–

[a] Rare I cells were positive in 3\10 cases

positivity for apocrine marker was present. Basal and myoepithelial cells were strongly positive with CK14 and focally positive with CK17. CK17-positive cells were more evident in striated and intercalated ducts of salivary glands involved in inflammatory processes. There was no immunoreactivity for CK20 in normal salivary gland tissue.

Table 5 Immunohistochemical results in salivary glands. *LAC* luminal acinar cells, *MAC* myoepithelial acinar cells, *LDC* luminal ductal cells, *MDC* myoepithelial ductal cells, *BC* basal cells, *CK* cytokeratin, *Mit* mitochondria, *SMA* smooth muscle actin, *SMM* smooth muscle myosin, *Calp* calponin, *Cald* caldesmon

Antisera	LAC	MAC	LDC	MDC	BC
CK7	+++	+	+++	+	+
CK8	–	+	+	+	+
CK14	–	+	–	+	+
CK17	–	+	–	+	+
CK19	+	–	++	–	-
CK20	–	–	–	–	–
SMA	–	++	–	++	–
Calp	–	++	–	++	–
Cald	–	++	–	++	–
SMM	–	++	–	++	–
Apocrine	+/–	–	–	–	–
Mit	–	–	+++ [a]	–	–

[a] Positivity is limited to LDC of striated ducts.

Myoepithelial cell markers (SMA, CALD, CALP, SMM) stained cells located around acini and along intercalated ducts, as previously described [15]. Myoepithelial cells were not found around striated ducts.

Table 6 Summary of immunohistochemical results in salivary gland carcinomas. *CK7* cytokeratin 7, *CK8* cytokeratin 8, *CK14* cytokeratin 14, *CK17* cytokeratin 17, *CK19* cytokeratin 19, *CK20* cytokeratin 20, *SMA* smooth muscle actin,*CALP* calponin, *CALD* caldesmon, *SMM* smooth muscle myosin, *MIT* mitochondrial antigen, *APO* apocrine marker

	CK7	CK8	CK14	CK17	CK19	CK20	SMA	CALP	CALD	SMM	MIT	APO
MEC	10/10	10/10	10/10	10/10	10/10	2/10	0/10	1/10	0/10	0/10	10/10	0/10
ACC	3/3	3/3	3/3	3/3	3/3	0/3	3/3	3/3	1/3	2/3	2/3	0/3
EMCC	3/3	3/3	3/3	3/3	2/3	0/3	2/3	1/3	0/3	1/3	0/3	0/3
AC	4/4	4/4	0/4	0/4	4/4	0/4	0/4	0/4	0/4	0/4	1/4	1/4

Other primary salivary gland carcinomas

Adenoid cystic carcinoma (ACC) and epithelial-myoepithelial cell carcinoma (EMCC) in addition to keratins always presented positivity for at least one myoepithelial cell marker (Table 6). Acinic cell carcinomas stained only with low-molecular-weight CK7 and CK8. All other antibodies were negative, including the other myoepithelial cell markers. Apocrine marker stained rare neoplastic cells in one of the three cases of acinic cell carcinoma studied.

Anti-mitochondrial antibody outlined very rare positive cells in the various non-MEC tumours. CK20 was negative in all cases tested.

Discussion

MEC is a tumour that contains several types of cells. In the present series of well-differentiated MECs, the CK profile of the single cell types differed from one another. This was mostly evident as neoplastic nests and cystic spaces were outlined at the periphery by CK14 and by anti-mitochondrial antibody, while in the central part of the nests and along the cystic spaces most of the cells were distinctly positive with CK7 antibody (zoning pattern).

CKs in MEC have been previously characterized by Regezi et al. [24] who used as antibodies anti- generic high- and low-molecular-weight cytokeratins and found a diffuse positivity for both types of antibodies without the zoning pattern as seen in the present cases. This is probably a consequence of the different sources of the antibodies employed: as generic anti- high-molecular-weight keratin antibody recognizes a wide spectrum of keratins, thus probably staining different cell types. Similarly, the anti-low-molecular-weight keratin antibody used by Regezi et al. [24] recognised CK8, which in the present series was the type of CK that stained the highest number of neoplastic cells, failing to demonstrate any particular type of distribution.

Results here obtained are consistent with previous studies that employed antibodies recognizing a single type of CK [2, 20, 21]. Specifically, a similar distribution of CK was described by Luchtrath et al. [21] in a case of mammary MEC. They found low-molecular-weight CKs in the “non squamous cells” and high-molecular-weight CKs in the “squamoid cells”.

In the present series MEC neoplastic cells were consistently stained with anti-mitochondrial antibody. The anti-mitochondrial antibody in use in the present study recognizes a protein located in the inner surface of the mitochondrial membrane, and therefore this protein is present in all cells [22]. Immunostaining is detectable at light microscopic level only when the number of mitochondria increases [14], especially in oncocytomas [4, 22] including rare cases of MEC with oncocytic features [10, 16, 18, 28]. In the present series none of the tumours showed oncocytic features by H&E examination, namely abundant granular eosinophylic cytoplasm, central vesicular nuclei, and prominent nucleoli. Immunostaining with anti-mitochondrial antibody revealed up to 25% of neoplastic cells rich in mitochondria.

As elaborated by Damiani et al. [4], oncocytic tumours are defined not only by the quality of mitochondrion rich cells, but also by the number of such cells being greater than 70% of the total neoplastic population. In this respect the MEC described here cannot be included in the group of oncocytic tumours. Our series would seem to be better defined as one of “mitochondrion rich” tumours.

Myoepithelial cell differentiation is a frequent finding in salivary gland tumours and this differentiation has also been demonstrated in MEC [7, 9]. Ultrastructural similarities between intermediate cells of MEC and myoepithelial cells of pleomorphic adenoma have been described [9]. In addition, immunohistochemical positivity of intermediate cells for myoepithelial cell markers such as S-100 protein [17, 19], myosin, and Azophloxine GA [17] has been reported in MEC. Regezi et al. [24], who semiquantitatively evaluated immunostaining for myoepithelial markers, stated that myoepithelial cell differentiation in MEC is limited to rare cells. This view is in keeping with the present data as the newly identified myoepithelial markers, CALP, CALD, and SMM disclosed scattered intermediate cells positive with CALP in only one case. These findings thus indicate that myoepithelial cells are rare in MEC and constitutes a further similarity between MEC and striated ducts, rich in basal cells, and in which myoepithelial cells are occasionally found.

In the present series a different CK profile was obtained in the different cell types composing MEC (Table 4). Basaloid cells were mainly rich in high-molecular-weight CK, intermediate cells presented both high- and low-molecular-weight CK, mucous secreting cells

mainly contained low-molecular-weight CK, and epidermoid cells mainly contained high-molecular-weight CK. The different CK profiles suggest the existence of a spectrum of differentiation among the cell types. Specifically, basaloid cells probably transform into intermediate cells, and these latter further differentiate in a divergent manner into either mucous secreting or epidermoid cells.

In normal salivary glands, each cell type composing the acinar duct system was found to have a specific immunohistochemical profile (Table 5). Results we obtained in normal ductal, luminal, basal, and myoepithelial cells are comparable to those previously obtained by Draeger et al. [12]. The only difference was in the positivity for CK7 in numerous luminal acinar cells found in the present cases; Draeger et al [12] described such positivity as weak or absent. This apparent discrepancy might be explained by the use of an antigen retrieval method that probably enhanced CK7 positivity in our cases.

In comparing immunohistochemical positivity in MEC with that obtained in normal salivary glands, it is evident that MEC most resembles striated ducts. These latter are composed of basal cells and LDC that are rich in mitochondria and that show a wide spectrum of cytokeratin expression. In addition, myoepithelial cells are rare in striated ducts. It is pertinent to note that Stewart et al. [29] found similarities between the cells of MEC and those of striated ducts of salivary glands involved in inflammatory processes. Interestingly, MECs are rich in CK17, which is poorly expressed in normal salivary glands, but which became evident in those areas with inflammatory infiltration in the salivary glands we studied. These findings support the concept elaborated by Dardick [7] that MEC originates from cells located along the basal membrane of the salivary ducts.

The pattern of positivity obtained in MEC with anti-CKs 7 and 14, and anti-mitochondrial antibody can be helpful in the differential diagnosis of primary salivary gland tumors. Absence or rarity of myoepithelial cell markers is helpful in distinguishing MEC from carcinomas showing myoepithelial cell differentiation, such as ACC and epithelial–myoepithelial carcinoma. Acinic cell carcinomas were also found to be devoid of myoepithelial cells, but no CKs 14 or 17 were found in them.

In conclusion, MEC shows a specific type of immunohistochemical profile, characterized by presence of CK14 and anti-mitochondrial antibody in the peripheral cell layers of the neoplastic nests and cystic spaces and by CK7 immunoreactivity in the central portion of the same structure (zoning pattern). This pattern of positivity is here proposed as a help in diagnosis. Finally, MECs neoplastic cells share a immunohistochemical profile with striated duct cell components, suggesting differentiation toward those structures.

References

1. Auclair PL, Goode RK, Ellis GL (1992) Mucoepidermoid carcinoma of intraoral salivary gland. Evaluation and application of grading criteria in 143 cases. Cancer 69:2021–2030
2. Cavalcanti de Araujo V, Orsini Machado de Sousa S, Rodarte Carvalho Y, Soares de Araujo N (2000) Application of imunohistochemistry to the diagnosis of salivary gland tumors. Appl Immunohistochem Mol Morphol 8:195–202
3. Chaudry AP, Cutler LS, Leifer C, Labay G, Satchidanand S, Yamane GM (1989) Ultrastructural study of the histogenesis of salivary gland mucoepidermoid carcinoma. J Oral Pathol Med 18:400–409
4. Damiani S, Eusebi V, Losi L, D'Adda T, Rosai J (1998) Oncocytic carcinoma (malignant oncocytoma) of the breast. Am J Surg Pathol 22:221–230
5. Damiani S, Ludvikova M, Tomasic G, Bianchi S, Gown AM, Eusebi V (1999) Myoepithelial cells and basal lamina in poorly differentiated in situ duct carcinoma of the breast. Virchows Arch 434:227–234
6. Damiani S, Pasquinelli G, Lamovec J, Peterse JL, Eusebi V (2000) Acinic cell carcinoma of the breast: an immunohistochemical and ultrastructural study. Virchows Arch 437:74–81
7. Dardick I (1996) Salivary gland tumor pathology. Igaku – Shoin, New York, pp 163–177
8. Dardick I, Daya D, Hardie J, van Nostrand AW (1984) Mucoepidermoid carcinoma: ultrastructural and histogenetic aspects. J Oral Pathol 13:342–358
9. Dardick I, Gliniecki MR, Heathcote JG, Burford-Mason A (1990) Comparative histogenesis and morphogenesis of mucoepidermoid carcinoma and pleomorphic adenoma. An ultrastructural study. Virchows Arch A Pathol Anat Histopathol 417:405–417
10. Deveci MS, Deveci G, Gunhan O, Finci R (2000) Oncocytic mucoepidermoid carcinoma of the parotid gland: report of a case with DNA ploidy analysis and review of the literature. Pathol Int. 50(11):905–909
11. Di Tommaso L, Scarpellini F, Salvi F, Ragazzini T, Foschini MP (2000) Progesterone receptor expression in orbital cavernous hemangioma. Virchows Arch 436:284–288
12. Draeger A, Nathrath WB, Lane EB, Sundrstrom BE, Stigbrand TI (1991) Cytokeratins, smooth muscle actin and vimentin in human salivary gland and pleomorphic adenomas. APMIS 99:405–415
13. Ellis GL, Auclair PL (1996) Tumors of the salivary glands, 3rd series. In: Atlas of tumor pathology, Fascicle 17. Armed Forces Institute of Pathology, Washington, pp 155–175
14. Foschini MP, Macchia S, Losi L, Dei Tos AP, Pasquinelli G, Di Tommaso L, Del Duca S, Roncaroli F, DalMonte PR (1998) Identification of mitochondria in liver biopsies. A study by immunohistochemistry, immunogold and Western blot analysis. Virchows Arch 433:267–273
15. Foschini MP, Scarpellini F, Gown A, Eusebi V (2000) Differential expression of myoepithelial markers in salivary, sweat and mammary glands. Int J Surg Pathol 8(1):29–37
16. Hamed G, Shmookler BM, Ellis GL, Punja U, Feldman D (1994) Oncocytic mucoepidermoid carcinoma of the parotid gland. Arch Pathol Lab Med 118:313–314
17. Hassanin MB, Ghosh L, Das AK, Waterhouse JP (1989) Immunohistochemical and fluorescent microscopic study of histogenesis of salivary mucoepidermoid carcinoma. J Oral Pathol Med 18(5):291–298
18. Jahan-Parwar B, Huberman RM, Donovan DT, Schwartz MR, Ostrowski ML (1999) Oncocytic mucoepidermoid carcinoma of the salivary glands. Am J Surg Pathol 23(5):523–529
19. Kahn HJ, Baumal R, Marks A, Dardick I, van Nostrand AW (1985) Myoepithelial cells in salivary gland tumors. An immunohistochemical study. Arch Pathol Lab Med 109:190–195
20. Loyola AM, de Sousa SO, Araujo NS, Araujo VC (1998) Study of minor salivary gland mucoepidermoid carcinoma differentiation based on immunohistochemical expression of cytokeratins, vimentin and muscle-specific actin. Oral Oncol 34:112–118

21. Luchtrath H, Moll R (1989) Mucoepidermoid mammary carcinoma. Immunohistochemical and biochemical analyses of intermediate filaments. Virchows Archiv A Pathol Anat 416: 105–113
22. Papotti M, Gugliotta P, Forte G, Bussolati G (1994) Immunocytochemical identification of oxyphilic mitochondrion-rich cells. Appl Immunohistochem 2:261–267
23. Prasad AR, Savera AT, Gown AM, Zarbo RJ (1999) The myoepithelial immunophenotype in 135 benign and malignant salivary gland tumors other than pleomorphic adenoma. Arch Pathol Lab Med 123:801–806
24. Regezi JA, ZarboRJ, Batsakis JG (1991) Immunoprofile of mucoepidermoid carcinomas of minor salivary glands. Oral Surg Oral Med Oral Pathol 71:189–192
25. Roncaroli F, Riccioni L, Cerati M, Capella C, Calbucci F, Trevisan C, Eusebi V (1997) Oncocytic meningioma. Am J Surg Pathol 21:375–382
26. Savera AT, Gown AM, Zarbo RJ (1997) Immunolocalization of three novel smooth muscle-specific proteins in salivary gland pleomorphic adenoma: assessment of the morphogenetic role of myoepithelium. Mod Pathol 10(11):1093–1100
27. Seifert G, Sobin LH (1991) Histological typing of salivary gland tumours. World Health Organization international histological classification of tumours, 2nd edn. Springer, New York
28. Sidhu GS, Waldo ED (1975) Oncocytic change in mucoepidermoid carcinoma of the parotid gland. Arch Pathol 99:663–666
29. Stewart FW, Foote FW, Becker WF (1945) Mucoepidermoid tumors of salivary glands. Ann Surg 122:820–844
30. Wang NP, Wan BC, Skelly M, Frid M, Glukhova MA, Koteliansky VE, Gown AM (1997) Antibodies to novel myoepithelium-associated proteins distinguish between benign lesions and carcinoma in situ from invasive carcinoma of the breast. Appl Immunohistochem 5:141–151

Virchows Arch (2002) 440:543–546
DOI 10.1007/s00428-001-0580-y

ORIGINAL ARTICLE

Giuseppe Pelosi · Fausto Maffini · Nicola Decarli
Giuseppe Viale

Progesterone receptor immunoreactivity in minute meningothelioid nodules of the lung

Received: 30 July 2001 / Accepted: 24 October 2001 / Published online: 22 January 2002
© Springer-Verlag 2002

Abstract Meningothelioid nodules (MNs) are not uncommon lesions of the pulmonary interstitium composed of monomorphic round to spindle cells, likely reactive in nature. Their origin is unsettled, though a derivation from arachnoid-like cells in conditions of perturbed perfusion of the pulmonary tissue has been proposed. Here we confirm the consistent occurrence of intense progesterone-receptor immunoreactivity in MNs fortuitously detected in surgical specimens of lung carcinomas. This finding corroborates the view that these proliferations exhibit arachnoid cell-like differentiation and suggests a role for sex-steroid hormones in the control of their growth.

Keywords Meningothelioid nodule · Lung · Progesterone receptors · Immunohistochemistry

Introduction

Meningothelial nodules (MNs) of the lung, formerly known as multiple minute chemodectomas (chemodectomatosis), are tiny perivenular, interstitial nodules composed of small, oval to spindle cells arranged in nests without contact with the air spaces [5, 20]. These small lesions were first described by Korn et al. in 1960 as multiple minute pulmonary tumours resembling chemodectomas [10]. The authors reported 19 cases, mostly encountered in women, in which these "bodies" were incidentally found during routine histological examination. Only one case was grossly discernible. In the past, these lesions have been considered to be miniature carotid body tumours, due to their close association with pulmonary veins [9, 10]. Electron microscopy, however, has failed to show the characteristic dense-core granules of chemoreceptor cells, having instead demonstrated prominent desmosomes, cytoplasmic tangles of fibrils and complex interdigitating cell processes [5]. Accordingly, an origin from smooth muscle cells or myofibroblasts [4, 19] or from arachnoid-like cells of the lung has been suggested [3, 7]. Recently, the occasional occurrence of progesterone receptors in pulmonary MNs incidentally found in patients undergoing surgery for lung cancer has been reported [13]. In the current study, we document that pulmonary MNs are consistently immunoreactive for progesterone receptors, reinforcing their close resemblance to arachnoid cells and suggesting a role for sex-steroid hormones in their development.

G. Pelosi (✉) · F. Maffini · N. Decarli · G. Viale
Department of Pathology and Laboratory Medicine,
European Institute of Oncology and
University of Milan School of Medicine, Via G. Ripamonti, 435,
20141, Milan, Italy
e-mail: giuseppe.pelosi@ieo.it
Tel.: +39-02-57489414, Fax: +39-02-57489417

Materials and methods

Six patients with pulmonary MNs have been identified among 540 patients who underwent surgery for lung cancer at the European Institute of Oncology in Milan. All patients were smokers, but with no history of previous pulmonary infectious disease. Laboratory findings were unremarkable, and computed tomography (CT) scan did not contribute to the detection of these small pulmonary lesions. Four patients suffered either local (i.e. cough, thoracic pain and haemoptysis) or systemic (i.e. fever, asthenia and weight loss) symptoms related to the primary lung cancer. At follow-up control after 2 months to 11 months, all patients were alive and well with no signs of tumour recurrence.

Formalin-fixed and paraffin-embedded sections were stained with haematoxylin-eosin for routine examination, whereas additional sections were immunostained using the panel of antibodies listed in Table 1. A commercially available detection kit (Dako EnVision Plus-HRP, Dako, Glostrup, Denmark) was used, according to the manufacture's instructions. Reactions were developed with 3–3′-diaminobenzidine-nickel chloride (Sigma Chemical Co., St. Louis, Mo., USA) as a chromogen substrate to obtain a brown–black end product. Finally, slides were lightly counterstained with 1% Harris' haematoxylin. Appropriate positive and negative controls for each antibody were simultaneously run with the test cases and resulted in the expected staining pattern.

Table 1 Antibodies used in the study. *EMA* epithelial membrane antigen, *M* monoclonal, *P* polyclonal, *MW* microwave oven pre-treatment in citrate buffer pH 6 for 10 min. Dako (Glostrup, Denmark); Immunotech (Marseilles, France)

Antibodies	Clone	M/P	Source	Dilution	Antigen retrieval
Cytokeratin pool	AE1–AE3	M	Dako	1:50	MW
EMA	E29	M	Dako	1:200	MW
Progesterone receptor	1A6	M	Dako	1:800	MW
Estrogen receptor	1D5	M	Dako	1:200	MW
Vimentin	V9	M	Dako	1:50	MW
Desmin	D33	M	Dako	1:150	MW
Smooth muscle actin	1A4	M	Dako	1:200	–
HMB-45	HMB-45	M	Dako	1:50	MW
Ki-67	MIB1	M	Immunotech	1:400	pepsin
Synaptophysin	SY38	M	Dako	1:20	MW
Chromogranin A	LK2H10	M	Dako	1:40	–
S-100 protein	S-100	P	Dako	1:1600	–

Table 2 Results of the immunohistochemical study. *EMA* epithelial membrane antigen

Case no.	1	2	3	4	5	6
Number of nodules	2	1	1	1	1	5
Gender	Female	Female	Male	Male	Female	Female
Age (years)	56	83	72	62	45	61
Vimentin	+	+	+	+	+	+
EMA	+	+	+	+	+	+
Progesterone receptor	+	+	+	+	+	+
Cytokeratin pool	–	–	–	–	–	–
Smooth muscle actin	–	–	–	–	–	–
Desmin	–	–	–	–	–	–
Estrogen receptor	–	–	–	–	–	–
HMB-45	–	–	–	–	–	–
Synaptophysin	–	–	–	–	–	–
Chromogranin A	–	–	–	–	–	–
S-100 protein	–	–	–	–	–	–
Ki-67 antigen (%)	0.5	0.3	0.5	0.3	0.4	0.3

Results

The six patients with MNs accounted for about 1% of all lung carcinoma patients treated at the same institution. There were two males and four females, ranging in age from 56 years to 83 years (mean 63.2 years). The patients were treated with lobectomy and mediastinal lymph node dissection for adenocarcinoma (three cases), squamous cell carcinoma (two cases) or typical carcinoid.

Four patients had a single MN, whereas the other two patients had two and five nodules, respectively. All eleven MNs were incidental findings during routine pathological examination. The nodules were located in subpleural position, far from the primary tumour, appearing like ill-defined nodules, 0.5–1.5 mm in diameter. The right side (seven from middle or lower and three from upper lobes) was much more commonly affected than the left one.

Microscopically, the lesions were composed of interstitial round to spindle cells distributed in a perivascular network, with faintly eosinophilic cytoplasm and uniform nuclei with finely granular chromatin (Fig. 1a). The nodules were centred on veins, without a significant arterial supply and without plexus arrangement. Mitotic figures were not seen.

Immunohistochemically, MNs showed a diffuse and intense immunoreactivity for vimentin, epithelial membrane antigen and progesterone receptors (Fig. 1b), whereas the immunoreactions for cytokeratins, smooth muscle actin, desmin, synaptophysin, chromogranin A and oestrogen receptors were consistently negative (Table 2). The proliferative fraction assessed by Mib-1 immunostaining ranged from 0.3% to 0.5%. In two patients, the MNs were associated with neuroendocrine tumourlets, arising in the context of multiple bronchiectasies with lung scarring.

Discussion

In this study we report on the consistent occurrence of progesterone receptors in 11 pulmonary MNs. This is at variance with the findings of Niho et al., who previously reported that only 50% of these lesions showed definite immunoreactivity for these receptors [13]. Because the monoclonal antibody used in both studies is the same, the discrepant results could be due to differences in the immunohistochemical procedures. We used a highly sensitive detection kit based on the dextran polymer technology, whereas Niho et al. used a standard avidin–biotin complex method [13].

Fig. 1 a Meningothelioid nodule composed of small spindled cells with bland appearance arising within the pulmonary interstitium. Haematoxylin and eosin ×250. **b** Meningothelioid cells show even and intense nuclear immunoreactivity for progesterone receptors. ×200 ▶

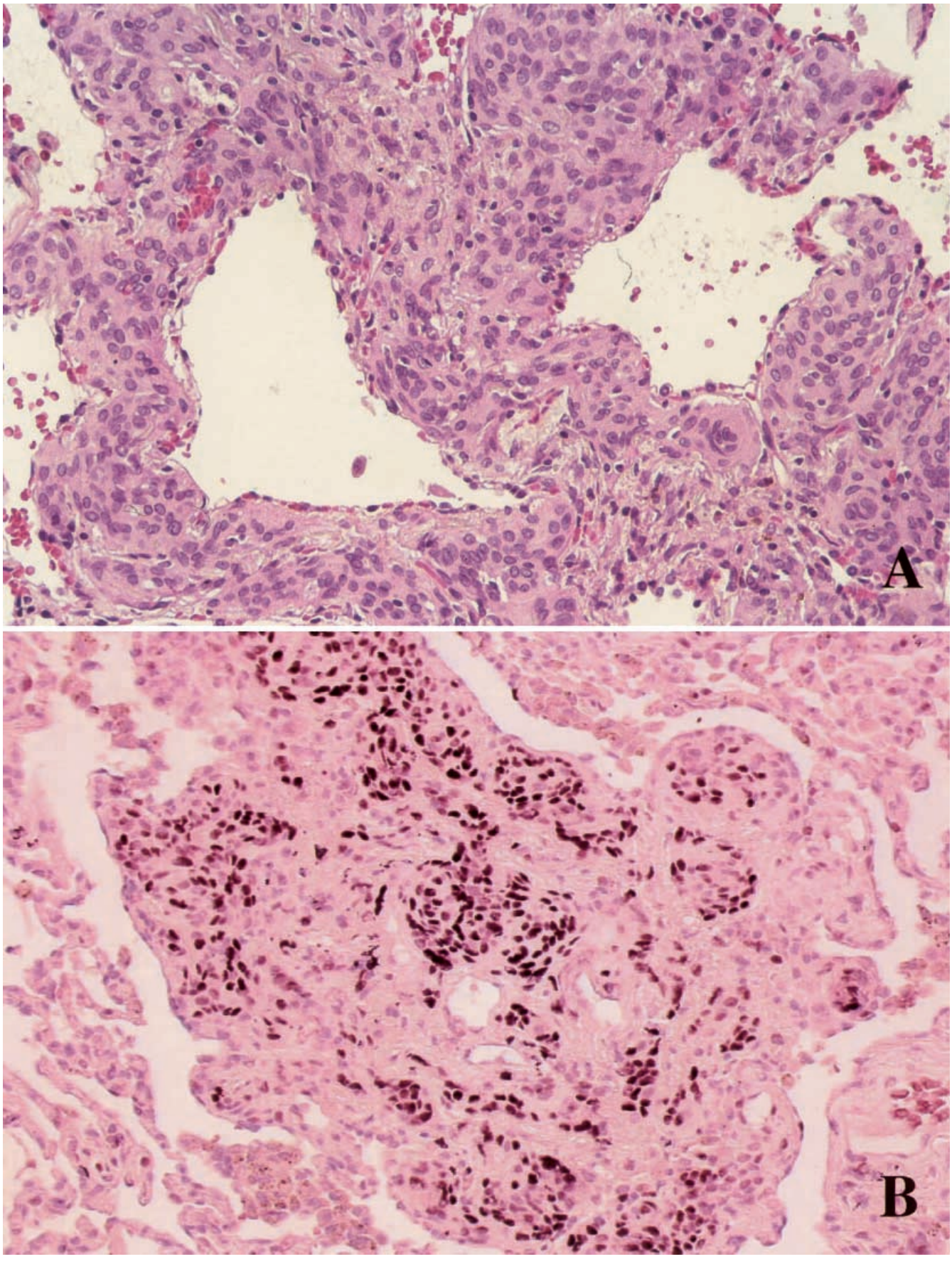
A
B

The occurrence of progesterone receptor immunoreactivity in MNs re-emphasises their close resemblance to arachnoid and meningioma cells. In fact, the abundant expression of progesterone receptors in normal arachnoid cells and human meningiomas is now well established [1, 14], and tumour cells immunoreactive for progesterone receptors have also been found in pulmonary meningiomas [15]. Furthermore, a close association between primary meningiomas of the lung and MNs distributed throughout the pulmonary parenchyma has been reported, suggesting that these small lesions may be the forerunners of pulmonary meningiomas [17]. Also the immunophenotype of the rare reported cases of primitive pulmonary meningiomas [11, 15] – showing consistent immunoreactivity for vimentin and epithelial membrane antigen – is similar to that of MNs. This indicates that pulmonary meningiomas may be tumours derived from or differentiating towards arachnoid cells of the lung.

The consistent expression of progesterone receptors also suggests a sex-steroid hormone-mediated control of the growth of MNs from arachnoid cells of the pulmonary interstitium. Although a female preponderance of about 5:1 has been reported [5], the occurrence of these lesions and the retention of their progesterone receptor immunoreactivity also in males suggest that the receptorial status is independent of gender and oestrogen control, as previously reported for meningiomas [18], normal endocrine cells and derived tumours [6] and solid-cystic tumours of the pancreas [21].

Arachnoid-like cells likely are a normal constituent of the lung, where they may affect the return of interstitial fluid to the pulmonary veins in a similar manner as for the arachnoid granulations of the meninges [8]. The expression of progesterone receptors may add selective advantages for the growth of the arachnoid-like cells of the pulmonary interstitium in conditions of perturbated vascular perfusion, as may occur in the neoplastic lung.

The occurrence of meningothelial proliferations outside the skull is well known [2, 12]. The low proliferative fraction and the lack of mitotic figures or cellular atypia suggest that these lesions are benign, slow-growing proliferations of arachnoid-like cells, although their reactive of neoplastic nature is still debated. A polyclonal origin of MNs has been recently proposed [13], and their higher prevalence in patients with thromboembolic disease, cardiac failure and various chronic pulmonary diseases with scarring, as well as in inhabitants of high-altitude regions, support the view that these lesions may represent hyperplastic growths induced by local hypoxia rather than true neoplasms [5, 9, 16]. Epidemiological data also support a reactive nature for pulmonary MNs. In fact, a prevalence of one MN in every 200–300 unselected autopsies has been reported [3, 10], and our findings of 11 such nodules in 6 of 540 patients with lung cancer is consistent with the above figures. The prevalence of MNs can still increase significantly to approximately one in 25 autopsies, if a specific search is made, especially in case of pulmonary embolism, cardiovascular disease and lung cancer [3, 9, 16]. Unfortunately, the invariable expression of progesterone receptors does not help clarifying whether these lesions are reactive or neoplastic in nature.

References

1. Blankenstein MA, Verheijen FM, Jacobs JM, Donker TH, Van Duijnhoven NV, Thijssen JH (2000) Occurrence, regulation, and significance of progesterone receptors in human meningioma. Steroids 65:795–800
2. Brinck U, Gunawan B, Schulten HJ, Pinzon W, Fischer U, Fuzesi L (2001) Clear-cell odontogenic carcinoma with pulmonary metastases resembling pulmonary meningothelial-like nodules. Virchows Arch 438:412–417
3. Churg AM, Warnock ML (1976) So-called minute pulmonary chemodectoma: a tumor not related to paragangliomas. Cancer 37:1759–1769
4. Cole SR, Pedersen CA, Kryzmowski GA, Knibbs DR, Cartun RW (1988) Histogenesis of so-called minute pulmonary chemodectomas. A study of 18 tumors by immunocytochemistry (abstract). Lab Invest 58:19A
5. Corrin B (2000) Pathology of the lungs. Churchill Livingstone, London, pp 540–541
6. Doglioni C, Gambacorta M, Zamboni G, Coggi G, Viale G (1990) Immunocytochemical localization of progesterone receptors in endocrine cells of the human pancreas. Am J Pathol 137:999–1005
7. Gaffey MJ, Mills SE, Askin FB (1988) Minute pulmonary meningothelial-like nodules. A clinicopathologic study of so-called minute pulmonary chemodectoma. Am J Surg Pathol 12:167–175
8. Heath D, Williams D (1993) Arachnoid nodules in the lung of high altitude Indians. Thorax 48:743–745
9. Ichinose H, Hewitt RL, Drapanas T (1971) Minute pulmonary chemodectoma. Cancer 28:692–700
10. Korn D, Bensch K, Liebow AA, Castleman B (1960) Multiple minute pulmonary tumors resembling chemodectomas. Am J Pathol 37:641–672
11. Lockett L, Chiang V, Scully N (1997) Primary pulmonary meningioma. Report of a case and review of the literature. Am J Surg Pathol 21:453–460
12. Michal M (2001) Meningeal nodules in teratoma of the testis. Virchows Arch 438:198–200
13. Niho S, Yokose T, Nishiwaki Y, Mukai K (1999) Immunohistochemical and clonal analysis of minute pulmonary meningothelial-like nodules. Hum Pathol 30:425–429
14. Perrot-Applanat M, Grojer-Picard MT, Kujas M (1992) Immunocytochemical study of progesterone receptor in human meningioma. Acta Neurochir (Wien) 115:20–30
15. Prayson RA, Farver CF (1999) Primary pulmonary malignant meningioma. Am J Surg Pathol 23:722–726
16. Spain DM (1967) Intrapulmonary chemodectomas in subjects with organising pulmonary thromboemboli. Am Res Respir Dis 96:1158–1164
17. Spinelli M, Claren R, Colombi R, Sironi M (2000) Primary pulmonary meningioma may arise from meningothelia-like nodules. Adv Clin Path 4:35–39
18. Tilzer LL, Plapp FB, Evans JP, Stone D, Alward K (1982) Steroid receptor proteins in human meningiomas. Cancer 49:633–636
19. Torikata C, Mukai M (1990) So-called minute chemodectoma of the lung. An electron microscopic and immunohistochemical study. Virchows Arch 417:113–118
20. Travis WD, Colby TV, Corrin B, Shimosato Y, Brambilla E (1999) Hystological typing of lung and pleural tumours. Springer Verlag, Berlin Heidelberg New York, pp 62
21. Zamboni G, Bonetti F, Scarpa A, Pelosi G, Doglioni C, Iannucci A, Castelli P, Balercia G, Aldovini D, Bellomi A (1993) Expression of progesterone receptors in solid-cystic tumour of the pancreas: a clinicopathological and immunohistochemical study of ten cases. Virchows Arch A Pathol Anat Histopathol 423:425–431

Virchows Arch (2002) 440:547–548
DOI 10.1007/s00428-001-0565-x

LETTER TO THE EDITOR

Fumio Ide · Kaoru Kusama

Sebaceous differentiation in basal cell adenocarcinoma of the submandibular gland

Received: 4 September 2001 / Accepted: 4 October 2001 / Published online: 26 March 2002
© Springer-Verlag 2002

Sir,

Basal cell adenocarcinoma (BCAC) is a malignant counterpart of basal cell adenoma occurring almost exclusively in the parotid glands [2]. Although large series have been published on BCAC [2, 3, 6], the presence of sebaceous cells in these carcinomas has been documented only once [9].We report the first case of BCAC of the submandibular gland with sebaceous differentiation.

A 41-year-old woman presented with a 2-year history of a well-delineated 6×5×5 cm mass in the left submandibular gland. The tumor and enlarged lymph nodes were resected. Six years after operation the patient is well, without recurrence or metastases. The tumor consisted of solid lobules of basaloid cells set in hyalinized stroma (Fig. 1 A). These cells were monotonous, without pleomorphism, significant mitotic activity, or atypia. No squamous or ductal differentiation was found. The lesion was nonencapsulated and invasive of both the surrounding salivary gland and muscular tissue (Fig. 1 B). Perineural invasion was identified (Fig. 2 A) but intravascular growth was not apparent. The lymph nodes were free of metastases. In certain areas there were focal collections of sebaceous cells within the tumor nests. Except for a single cell (Fig. 2 B), they were negative for periodic acid-Schiff, mucicarmine, and Alcian blue.

Basaloid cells were positive for AE1/AE3 (monoclonal; DAKO Glostrup, Denmark; 1:50) and 34βE12 (monoclonal; DAKO; 1:50). Sebaceous cells showed positive reaction with cytokeratin (CK) 14 (LL002; DAKO; 1:50) and epithelial membrane antigen (E29; DAKO; 1:100; Fig. 2 C). Both were immunonegative for CK10 (DE-K10), 10/13(DE-K13), 18(DC-10) and 19(RCK108; all from DAKO; 1:50). S-100 protein (polyclonal; DAKO; 1:100), α-smooth muscle actin (1A4; Sigma, St. Louis, Mo., USA; 1:2000), glial fibrillary acidic protein (6F-2; DAKO; 1:100), Vimentin (V9; DAKO; 1:100) and CD68 (KP-1; DAKO; 1:200) were negative in tumor cells.

Sebaceous cells have been found in a wide variety of salivary gland tumors such as Warthin's tumor, basal cell adenoma, pleomorphic adenoma, oncocytoma, adenoid cystic carcinoma, and mucoepidermoid carcinoma [2, 7]. However, it develops in BCAC only very rarely; in the critical commentary to "unusual differentiation of a combination tumor of the parotid gland," authored by Rühl and Morgenroth [9], a brief description of a parotid lesion was given together with two illustrations. Sebaceous adenocarcinoma itself is a rare tumor [2, 4, 7] and only two cases have been reported in the submandibular gland [7]. In contrast to pure sebaceous adenocarcinomas, our tumor was composed primarily of basaloid cells and had limited sebaceous cells; therefore we designated this case as BCAC with focal sebaceous differentiation.

With regard to the differential diagnosis, three types of clear, vacuolated cells are important: glycogen-rich or mucin-filled epithelial cells and macrophage-derived foam cells. The negativity of the periodic acid-Schiff reaction and of mucicarmine and Alcian blue stains rules out the possibility that clear cells contain glycogen or mucin. The lack of immunoreactivity for CD68 also confirm that these cells are not of histiocytic lineage [1]. Although we could not perform fat stains in the absence of wet tissue, immunopositivity for CK14 and epithelial membrane antigen supports the sebaceous nature [5, 8, 10].

Unlike previously reported cases of salivary and mammary tumors with sebaceous differentiation [4, 5, 7, 8], our tumor showed no association with squamous or myoepithelial cells. Therefore, it seems likely that immature basaloid cells in BCAC have a latent potentiality to differentiate toward sebaceous cells.

F. Ide · K. Kusama (✉)
Department of Oral Pathology,
Meikai University School of Dentistry, 1-1 Keyakidai, Sakado,
Saitama 350-0283, Japan
e-mail: kusama@dent.meikai.ac.jp
Tel.: +81-492-79-2773, Fax: +81-492-86-6101

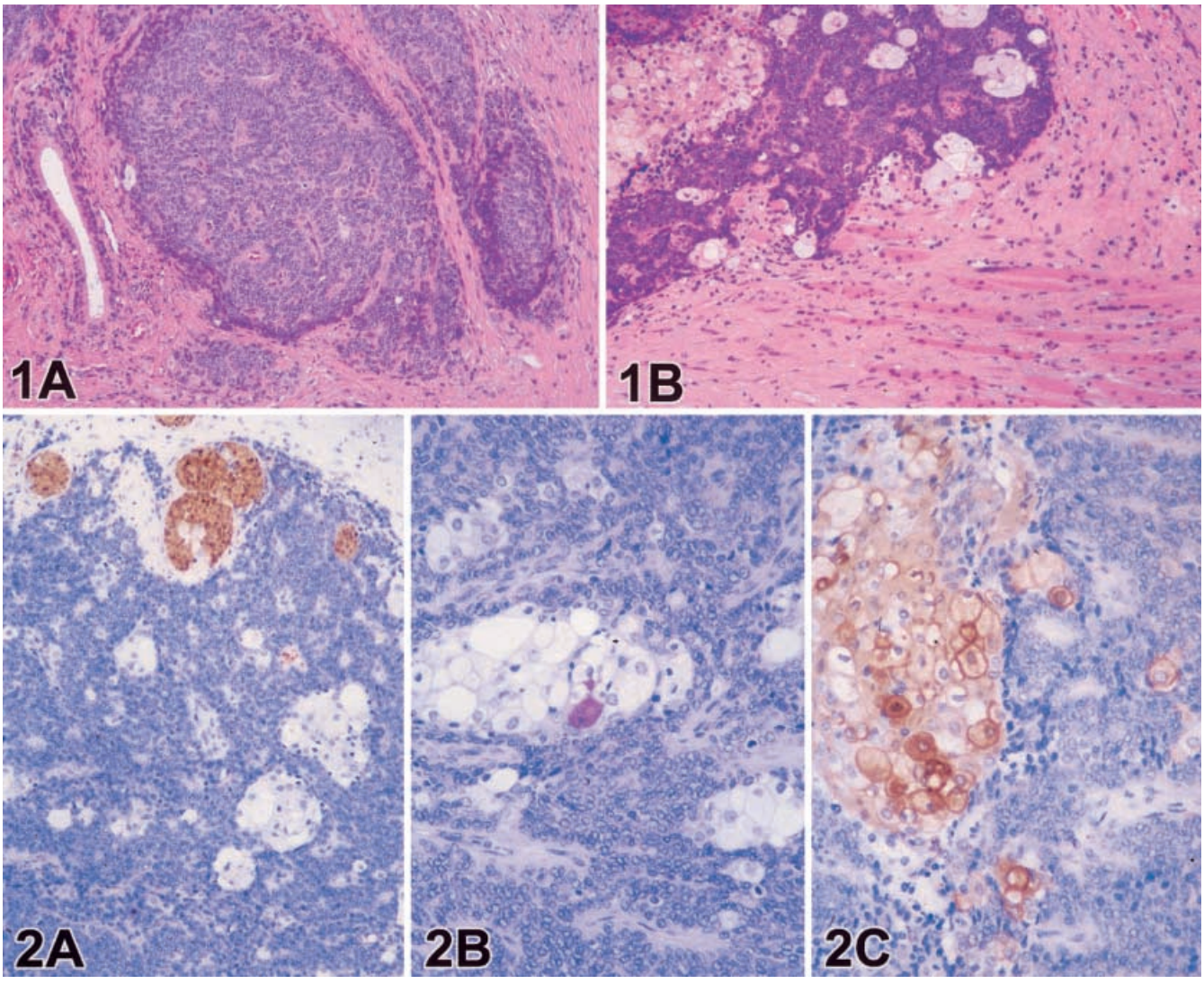

Fig. 1 A Solid nests of uniform basaloid cells segregated by hyaline septa (Hematoxylin & eosin, ×100). **B** Lobules with foci of sebaceous differentiation, infiltrating into periglandular muscule (Hematoxylin & eosin, ×100)

Fig. 2 A Perineural invasive growth. Both basaloid and sebaceous cells are negative for S-100 protein. Immunostaining, ×100). **B** Except for a single cell, sebaceous cells are negative for mucin (Mucicarmine, ×200). **C** Sebaceous cells are positive for epithelial membrane antigen (Immunostaining, ×200)

References

1. Damiani S, Cattani MG, Buonamici L, Eusebi V (1998) Mammary foam cells. Characterization by immunohistochemistry and in situ hybridization. Virchows Arch 432:433–440
2. Ellis GL, Auclair PL (eds) (1996) Tumors of the salivary glands. Armed Forces Institute of Pathology, Washington DC
3. Fonseca I, Soares J (1996) Basal cell adenocarcinoma of minor salivary and seromucous glands of the head and neck region. Semin Diagn Pathol 13:128–137
4. Gnepp DR (1983) Sebaceous neoplasms of salivary gland origin: a review. Pathol Annu 18:71–102
5. Jiao YF, Nakamura S, Oikawa T, Sugai T, Uesugi N (2001) Sebaceous gland metaplasia in intraductal papilloma of the breast. Virchows Arch 438:505–508
6. Nagao T, Sugano I, Ishida Y, Hasegawa M, Matsuzaki O, Konno A, Kondo Y, Nagao K (1998) Basal cell adenocarcinoma of the salivary glands. Comparison with basal cell adenoma through assessment of cell proliferation, apoptosis, and expression of p53 and bcl-2. Cancer 82:439–447
7. Ohara N, Taguchi K, Yamamoto M, Nagao T, Akagi T (1998) Sebaceous carcinoma of the submandibular gland with high-grade malignancy: report of a case. Pathol Int 48:287–291
8. Prescott RJ, Eyden BP, Reeve NL (1992) Sebaceous differentiation in a breast carcinoma with ductal, myoepithelial and squamous elements. Histopathology 21:181–184
9. Rühl GH, Morgenroth K (1993) Critical commentary to "unusual differentiation of a combination tumor of the parotid gland." Pathol Res Pract 189:581–584
10. Varga Z, Kolb SA, Flury R, Burkhard R, Caduff R (2000) Sebaceous carcinoma of the breast. Pathol Int 50:63–66

Virchows Arch (2002) 440:573–582
DOI 10.1007/s00428-002-0634-9

REVIEW ARTICLE

Christina Scheel · Christopher Poremba

Telomere lengthening in telomerase-negative cells: the ends are coming together

Received: 20 November 2001 / Accepted: 11 February 2002 / Published online: 9 April 2002
© Springer-Verlag 2002

Abstract Telomeres are crucial for chromosomal stability and cell viability. Activation of telomerase, a specialized reverse transcriptase, is the predominant mechanism for maintaining telomere length and function in yeasts and human cells. Telomere maintenance is regarded as a key element in the immortalization of cells and hence in oncogenesis. Although more than 90% of all malignant tumors display telomerase activity, there appear to be alternatives to this mechanism. Alternative lengthening of telomeres (ALT) in the absence of telomerase has been described in various organisms and recently also in immortalized and transformed human cells. This article will discuss how ALT is detected and how it affects telomere morphology. It will review the frequency and relevance of ALT in in vitro immortalized cell lines, tumor-derived cell lines, and primary tumors. We have only begun to link mechanisms by means of which ALT may act in immortalized human cells to the growing knowledge about telomeres, and we can look forward to further fascinating insights into telomere biology. Our review will also emphasize recent advances in our understanding of the induction and repression of ALT and the demonstration of ALT in cancer cells in the light of new treatment strategies targeted against telomere maintenance mechanisms.

Keywords Telomeres · Telomerase · ALT · Cancer

Introduction

The functional complex of telomeres and telomerase

Telomeres (τελομερ: Greek for end part or end piece), the physical ends of eukaryotic chromosomes, are crucial for maintaining chromosomal stability and cell viability. Telomeres protect chromosome ends from accidental chromosome breakage that would trigger DNA damage response mechanisms and promote cell-cycle arrest and DNA repair. Functional telomeres prevent aberrant chromosomal recombination and end-to-end fusions. They also promote proper segregation of chromosomes during cell division [24]. The telomeric sequence is composed of tandem repeats containing a block of neighboring guanine nucleotides. In humans, this sequence is 5′-TTAGGG-3′ [40].

In most organisms complete replication of telomeres is accomplished by telomerase, a specialized reverse transcriptase that was first isolated from the ciliate *Tetrahymena* [20]. Telomerase synthesizes repeats of telomeric DNA onto the guanine (G)-rich 3′ end of telomeres, thus creating a single-stranded 3′ end-overhang. In telomerase-null yeast, dysfunctional telomeres increase the mutation rate and genomic instability, suggesting that telomerase can prevent chromosomal instability [24].

Most somatic cells do not display telomerase activity. Telomeres shorten progressively in a stochastic manner, partly due to the inability of the DNA-dependent DNA polymerases to completely synthesize the 5′ end of the strand, because they lack a docking sequence as maintained by the primase product RNA. This has been referred to as the "end-replication problem" [43, 62]. Moreover, cell-cycle regulated 5′ to 3′ nuclease processing of the cytosine (C)-rich strand occurs [35]. Decrease in telomere length ultimately leads to proliferative failure in most dividing normal human cells [26]. In emerging immortalized cells, telomeres are usually maintained by activation of telomerase [11, 65].

In most transformed cells, immortalization is also associated with telomerase activation [25]. Previous investigations revealed telomerase activity in approximately 90% of human malignant tumors but not in normal human tissues (reviewed in [14]). Detection of telomerase activity can be used as a molecular marker. For example, it can serve as a prognostic molecular parameter in neuroblastoma [49, 50] or as a sensitive

C. Scheel · C. Poremba (✉)
Gerhard-Domagk Institute of Pathology,
Westfälische Wilhelms University, Domagkstrasse 17,
48149 Münster, Germany
e-mail: poremba@uni-muenster.de
Tel.: +49-251-8355449, Fax: +49-251-8355460

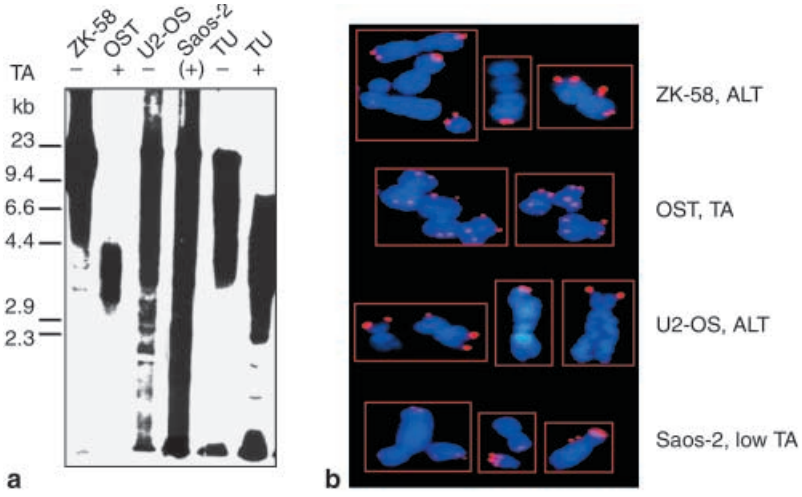

Fig. 1 Telomere length and morphology. **a** Telomere restriction fragment (TRF) analysis, telomere lengths of four osteosarcoma cell lines (ZK-58, OST, U2-OS, Saos-2) and two primary osteoblastic osteosarcomas (Tu). Genomic DNA was digested with restriction enzymes *Hin*fIII and *Rsa*I, separated on a 0.8% agarose gel, blotted onto a nylon membrane and hybridized with a telomere-specific biotinylated oligonucleotide probe. *kb* kilobases. Cell line Saos-2 displayed marginal telomerase activity in the telomere repeat amplification protocol assay and the elongated alternative lengthening of telomeres (ALT) telomeres in TRF analysis, we therefore termed Saos-2 to be of intermediate ALT type. **b** Telomere fluorescence in situ hybridization (t-FISH), details of metaphase spreads of four osteosarcoma cell lines (ZK-58, OST, U2-OS, Saos-2), *TA* telomerase activity

diagnostic marker for malignancy in fine-needle aspirates of breast tissue [47, 48]. A recent review lists the diagnostic value of telomerase activity as a marker of malignancy in a large number of tumor entities [31].

However, the specific association of telomerase activity with cancer progression has been challenged. The frequency and biologic importance of telomerase activity seem to vary, depending on the tumor type [67].

Telomere length regulation in telomerase-negative cells – alternative lengthening of telomeres

Other mechanisms of telomere regulation besides telomerase have been found in several eukaryotes. *Drosophila melanogaster* and related dipterans employ retrotransposons in telomere length regulation [36]. Homologous recombination is used for telomere elongation in the mosquito *Anopheles gambiae* [55]. In the case of telomerase-defective yeast, rare survivors are able to elongate their telomeres via recombination events that are dependent on the DNA double-strand break repair gene RAD52 and are initiated either in the subtelomeric Y′ regions or directly within the terminal telomere repeats [34, 60].

In human cells, there is at least one mechanism of telomere lengthening that apparently does not require telomerase activity. It has been termed alternative lengthening of telomeres (ALT). The existence of ALT has been deduced from the observation of heterogeneous and elongated telomeres in the absence of detectable telomerase [42]. ALT has been found in a subset of in vitro immortalized and tumor-derived cell lines as well as in spontaneous human tumors (reviewed in [52]). Telomere morphology and functionality in ALT cells appear to differ significantly from cells with telomerase activity [18, 46, 56]. So far, the molecular mechanisms underlying ALT have been investigated mainly in in vitro immortalized and tumor-derived cell lines [5, 6].

In in vitro immortalized human cell lines, ALT can occur by means of homologous recombination and copy switching of telomeric sequences [16]. ALT as a mechanism appears to be adequate to compensate for the lack of telomerase activity in telomerase-deficient yeast and in human cells during immortalization. However, we are only beginning to understand the molecular circumstances that allow telomere lengthening without telomerase activity [44, 53].

Detection of ALT in human cells

Studies of simian virus 40 (SV40) large-T antigen-induced transformation of human somatic cells revealed that telomeres progressively shorten in the course of continued cell divisions. Eventually, cells reached a state termed “crisis”, which is accompanied by massive apoptosis and a peak in the number of dicentric chromosomes resulting from end-to-end fusions, indicating chromosomal instability and telomere dysfunction [11, 15]. An increase in anaphase bridges was seen in primary cultures as they approached crisis. It was associated with extremely short telomeres [11]. Rare surviving immortalized cells emerging from crisis usually display activation of telomerase as detected with the PCR-based telomere repeat amplification protocol (TRAP) assay. Telomere length is eventually stabilized by telomerase around a mean optimized length that varies from cell type to cell type (usually 4–10 kb in human cells; reviewed in [4]).

However, a subset of post-crisis cells were found to have no detectable telomerase activity. Their mean

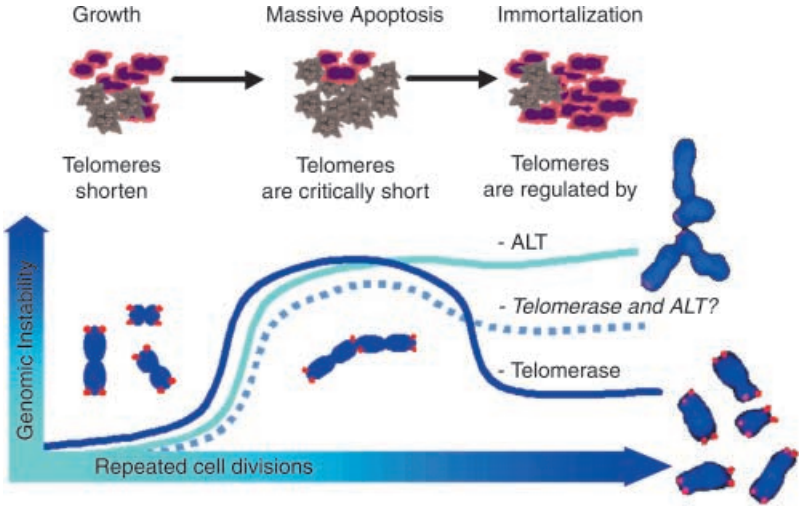

Fig. 2 Growth and telomere dynamics in cells during immortalization. With progressive telomere shortening, genomic instability, and the apoptosis rate increase, reaching a peak at crisis. Dependent on precedent mutations, immortalized survivor cells regulate telomere length either by telomerase activity or alternative lengthening of telomeres (ALT). A coexistence of both mechanisms may be possible as well. Dependent on the telomere elongation mechanism, cells may continue to proliferate with different tolerances and levels of genomic instability

telomere length was longer than in their pre-crisis counterparts, indicating that net telomere elongation had occurred in the absence of telomerase activity [5, 6, 42]. Southern blot-based telomere restriction fragment (TRF) analysis revealed telomere lengths ranging from very short (approximately 2 kb) to extremely long (≥23 kb) (Fig. 1a). This characteristic pattern was maintained over many hundreds of population doublings, indicating that ALT may be an efficient bypass for telomere maintenance by telomerase [54]. When the telomere on chromosome 13 of an in vitro immortalized ALT cell line was tagged by integration of transfected plasmid DNA, progressive shortening of this marked telomere, punctuated by rapid increases in length and resumption of telomere attrition was observed [42]. This cyclical behavior suggests that ALT acts on telomeres that reach a critically short length. Although there are differences in telomere lengths in cell populations with telomerase, they are relatively subtle. Telomerase stabilizes telomeres around an optimized length by elongating the shortest telomere in a dynamic balance between elongation and shortening [27].

Telomere morphology in ALT cells reflects compromised telomere function and chromosomal instability

Telomere morphology can be analyzed using telomere fluorescence in situ hybridization (t-FISH) with a telomere-specific peptide nucleic acid (PNA) probe. The intensity of the fluorescent signal at the telomere correlates directly with telomere length [33]. Analysis using t-FISH revealed that the heterogeneity of telomere length in ALT cells appears to reflect an intracellular phenomenon not due to mixed cell populations with very short and very long telomeres. Moreover, signal-free ends and interchromosomal telomeric signals could be detected within single metaphases and even between sister chromatids of the same chromosome [18, 33, 46, 56] (Fig. 1b). The occurrence of elongated and shortened telomeres and signal-free chromosome ends could give rise to chromosomal end-to-end associations and breakage-fusion-bridge cycles, resulting in an increased number of complex non-reciprocal chromosomal rearrangements [37]. Indeed, analysis by means of 24-color multiplex fluorescence in situ hybridization (M-FISH) in three osteosarcoma cell lines with telomerase activity or ALT, respectively, provides evidence supporting this hypothesis. It revealed a significantly higher proportion of complex rearranged chromosomes (with 3–6 chromosomes involved) and a higher overall number of rearrangements in cells with the ALT phenotype [56]. In these cells, ALT is associated with chromosomal instability. As a corollary, it can be assumed that ALT reflects a state of compromised telomere function. ALT cells do not appear to expand their proliferative potential under telomere-stabilizing conditions (Fig. 2).

Frequency and relevance of ALT in human cells

ALT can be observed in telomerase-negative tumor-derived cell lines and in primary tumors. Notably, not all tumors without telomerase activity have ALT-like telomeres [6]. Perhaps some of these findings reflect tumors that presented clinically before immortalization. Therefore, not all of the approximately 10% telomerase-negative tumors [14, 31] display the telomere morphology characteristic of ALT. However, the possibility that there are other mechanisms independent of telomerase and that do not exhibit the ALT pattern of telomere morphology cannot be excluded. Some telomerase-positive tumors were shown to have elongated and heterogeneous telomeres, which could indicate a coexistence of ALT and telomerase activity [6, 52]. Coexistence of ALT and telomerase seems to be biologically possible. It has been described in three recent studies on in vitro immortalized ALT cell lines in which telomerase activity was restored by means of ectopic expression of the enzyme [9, 22, 46]. So far, no extensive surveys for ALT have been carried out, but a variety of malignant human tumors

Table 1 Primary tumors that were shown to exhibit the alternative lengthening of telomeres (ALT) phenotype

Tumor type	Reference
Adrenocortical carcinoma	[6]
Breast carcinoma, Li-Fraumeni syndrome	[6]
Malignant melanoma	[6]
Lung carcinoma	[6]
Ovarian carcinoma	[6]
Osteosarcoma	[6, 56]
Renal carcinoma	[39]

may exhibit ALT [6, 39, 56] (Table 1). The rates of ALT activation are higher in in vitro immortalized cell lines than in tumor-derived cell lines (Table 2). Possibly, the incidence of ALT is higher in some cell types than in others. Most of the in vitro immortalized cell lines are of mesenchymal origin. Low-level telomerase activity is present in normal epithelial cells [68] but not in fibroblasts [30]. Epithelial cells may be simply more "competent" at telomerase activation. Since approximately 80% of solid tumors are carcinomas, this may be a reason why ALT has been found so infrequently (also refer to [6]).

A morphological marker of ALT

Recently, a potentially useful morphological marker of ALT was described – ALT-associated promyelocytic leukemia (PML) bodies (APBs) [69]. PML protein was so named for its involvement in fusion events in promyelocytic leukemia [13]. APBs are donut-shaped structures that can be found in interphase nuclei and contain PML protein, telomeric DNA and the double-stranded telomere-binding proteins human telomere repeat factors (TRF) 1 and 2. Furthermore, they contain proteins involved in DNA synthesis and recombination (replication factor A, RAD51 and RAD52). In one in vitro immortalized fibroblast cell line, APBs were detected at the time of immortalization, concomitant with the appearance of ALT. Furthermore, xenografted ALT tumors in nude mice were positive for APBs [69]. To test cells for ALT it is currently necessary to collect fresh frozen tissue samples for whole cell lysates to be used in the TRAP assay or genomic DNA for TRF analysis and/or to prepare metaphases for t-FISH. APBs can be found in 5% of interphase nuclei and it would therefore appear feasible to detect them by immunohistochemistry in paraffin-embedded tumor tissue. Evidence of APBs is provided by colocalization of PML with either TRF1 and/or TRF2 [69]. These findings should render it possible to analyze a wide panel of archival tumor tissue for the presence of ALT. It has not yet been determined why APBs are only found in a subset of interphase nuclei. Their appearance has been observed to be related to the cell cycle phase. The frequency of APB-positive cells increases in cultures enriched for cells in the G_2 phase [66]. One explanation could be a putative involvement in apoptosis, with APBs marking cells that are destined to undergo cell death [69]. While their function is still obscure, detection of APBs could prove a useful morphological marker for ALT.

ALT by recombination

Telomerase-negative yeast survivors

In single-celled organisms, such as ciliates and yeast, telomerase expression is constitutive. Although in the budding yeast *Saccharomyces cerevisiae* most mutant cells defective for the telomerase catalytic subunit die after approximately 60 cell divisions, a small subset of survivors is able to repopulate the culture [34]. Their survival was shown to be dependent on the DNA double-strand break repair gene RAD52. This is interesting, because APBs in human cells also contain the DNA repair component RAD52 [69]. Analysis of the telomeres in *Saccharomyces* survivor cells suggests that there are two different types of recombination events contributing to telomere elongation [34, 60]. Type-I survivors arise by recombination events in the telomere-adjacent Y′ sequence elements, have very short terminal telomere repeats, and grow slowly. Type-II survivors, in contrast, have long hypervariable tracts of telomere repeats, which are reminiscent of the telomere morphology in human ALT cells and are possibly due to recombination initiated within the telomere-repeat sequences [61]. Type-II survivor yeast cells grow at a rate similar to wild-type cells. Their

Table 2 Frequency of the alternative lengthening of telomeres (ALT) phenotype in human cell lines [5, 6, 56, 58]

	No. of samples	Telomerase activity (TRAP)		Elongated and heterogeneous telomere restriction fragments	
		Telomerase positive (%)	Telomerase negative (%)	Telomerase negative	Telomerase positive
In vitro immortalized cell lines	50	31 (62)	19 (38)	19	0
Tumor-derived cell lines[a]	57	52 (91)	5 (9)	5	1
Total	107	83 (78)	24 (22)	24	1

[a] The osteosarcoma cell line Saos-2 has been reported to be telomerase negative previously [6]. We found marginal telomerase in the telomere repeat amplification protocol (TRAP) assay. Since Saos-2 has the elongated and heterogeneous ALT telomeres in telomere restriction fragment analysis, we termed it an intermediate ALT cell line

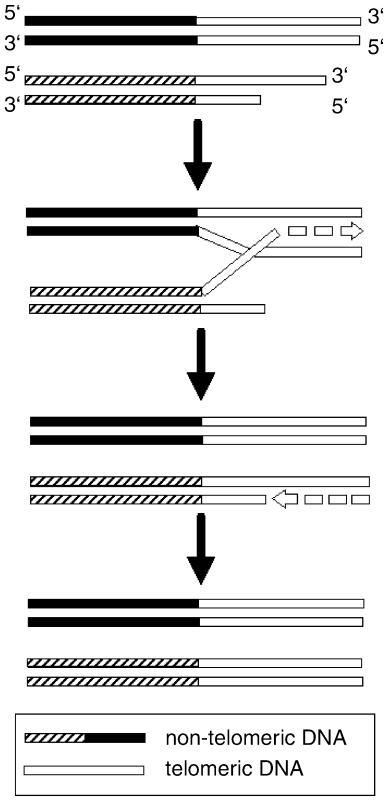

Fig. 3 Recombination in telomere elongation. Intertelomeric homologous recombination and copy switching, adapted from [22]

stability and growth rate suggest that the addition of telomeric repeats by recombination is a sufficient bypass for telomerase activity.

ALT by recombination in in vitro immortalized human cells

It was recently demonstrated that in human cells, ALT can occur by means of homologous recombination and copy switching [16] (Fig. 3). A plasmid tag was placed in the subtelomeric region and within the telomeric repeats of immortalized human ALT or telomerase-positive cell lines. Copying of DNA sequences from telomere to telomere was seen in the ALT cell line, but not in the cell line with telomerase activity. Since this assay was not designed to detect intratelomeric copying, it is possible that such events occurred in addition to intertelomeric copying. In this context, it appears important to note that the G-rich 3′ single-stranded overhang of telomeres in mammalian cells and *Trypanosoma* is tucked far back into the telomeric tract, forming a loop in vitro (the “T-loop”, Fig. 4) [21, 41]. The distal single-stranded overhang “invades” the proximal double-stranded telomeric sequence forming a displacement loop (“D-loop”). Possibly, this region itself can be used as a template for elongation of the distal 3′ single strand in ALT cells [52]. The T-loop resembles the D-loop, a functional intermediate in DNA replication. It can be viewed as a stalled D-loop requiring special circumstances to overcome its inactivation.

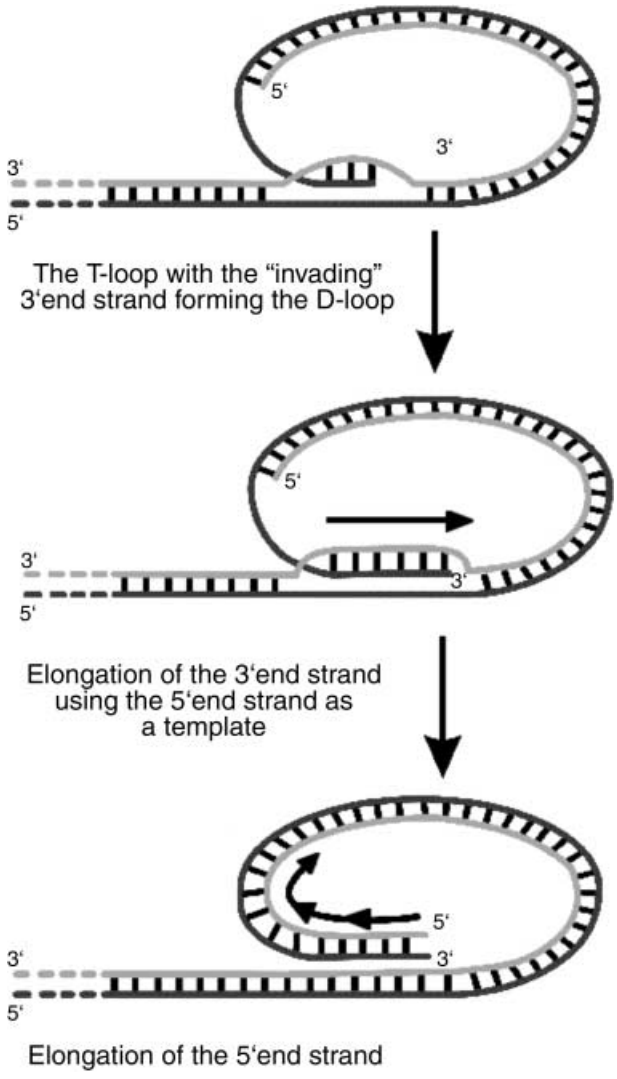

Fig. 4 Intratelomeric recombination. Intratelomeric recombination, the T-loop structure of the telomere may provide a template region for the G-rich 3′end single strand within the D-loop

Finally, the extrachromosomal telomeric DNA (ECTR) present in some ALT cells may be used as a template in recombination [69].

The barrier to homologous recombination

Interestingly, it was recently demonstrated that defects in the DNA mismatch repair (MMR) machinery in telomerase-defective budding yeast promote telomerase-independent proliferation [53], indicating that the anti-recombination activity of the MMR machinery might have an inhibitory effect on the ability of telomerase-defective cells to proliferate. Rizki and Lundblad showed that removal of this barrier may, under certain conditions, promote telomerase-independent cell proliferation, even-

tually eliminating the requirement for telomerase activity altogether.

Repression and induction of ALT

ALT appears to be an adequate mechanism for telomere length regulation to assure continued growth in single-celled organisms such as yeast as well as in certain in vitro immortalized and transformed human cells under certain conditions. Considering the abundance of telomeric sequences that could serve as a template for telomere elongation by a recombinational mechanism, the questions arise why and how ALT is repressed in normal human cells and in most in vitro immortalized and transformed human cells and how ALT is induced.

Involvement of telomerase

Many reports on ALT deal with the involvement of telomerase. They pose the following questions: (a) how is telomerase activity suppressed in ALT cells and could there be an atypical telomerase acting in ALT cells that escapes detection by the TRAP assay; (b) how is ALT repressed in telomerase-positive cells and can telomerase-deficient or telomerase-inhibited cells switch to ALT as a back-up mechanism; and (c) what effects does reconstituted telomerase activity have on ALT cells?

Telomerase is a multi-subunit enzyme. Essential for enzymatic activity are the reverse transcriptase protein catalytic subunit hTERT (TERT, hTRT, hEST) [59] and the endogenous RNA template hTR (TERC, TER) [17]. Expression of hTERT appears to be the rate-limiting step in telomerase activity [3]. However, we are only beginning to understand the regulation of telomerase. hTERT has several alternatively spliced transcripts [8], among them a deletion variant lacking conserved residues from the catalytic core of the protein [32]. This hTERT alpha splice variant has been identified as a dominant negative inhibitor of telomerase activity [10]. It is expressed in normal and developing human tissues [32] and it appears conceivable that it may also be expressed in some ALT cell lines or tumor tissue.

Importantly, in vitro telomerase activity is not necessarily synonymous with in vivo enzyme activity. A carboxyl terminus-modified hTERT that induced telomerase activity in the TRAP assay did not result in telomere maintenance when expressed in telomerase-negative mortal cells [12].

One could hypothesize that an atypical telomerase that escapes detection by TRAP may be involved in ALT. However, some ALT cells do not express any hTR, although the hTR sequence is wild type [7]. The promoter of the telomerase RNA gene has been found to be methylated in ALT cell lines that are characterized by a total absence of hTR expression [29]. Hence, the participation of an atypical telomerase in these cells can be excluded unless there is another RNA template that can be used.

Lessons from somatic cell hybrids and chromosome transfer

Studies employing somatic cell fusion imply that one or more repressors of ALT exist in normal, telomerase-negative and tumor-derived telomerase-positive cells and that repression of ALT in hybrid cells may not be mediated by telomerase [45]. Somatic fusion of an ALT cell line with a normal fibroblast cell line led to repression of ALT, as evidenced by a rapid attrition of telomere length and induction of senescence after approximately 30 population doublings [45]. Rare escapees from senescence reverted to ALT, as demonstrated by TRAP and TRF analysis. Interestingly, during repression of ALT, telomeres shortened at a rate that is approximately ten times as high [45] as that observed in normal somatic cells (which is 50–200 bp; reviewed in [4]). This rapid attrition was not observed in hybrid cells resulting from fusion of an in vitro immortalized ALT cell with tumor-derived cell lines displaying telomerase activity. In these hybrids ALT was repressed and telomeres shortened at a rate comparable to normal cells. Further studies are required to determine whether ALT occurs due to a dominant activating mutation or due to loss of repressors that are present in normal and telomerase-positive cells.

Restoration of telomerase activity in ALT cells: different effects

In telomerase-deficient strains of *Saccharomyces cerevisiae* containing long telomeres, the reintroduction of telomerase by ectopic expression of the enzyme results in reversion to wild-type telomere lengths [60]. Overall, the findings in human ALT cell lines differ from those in telomerase-negative yeast survivors.

It was initially demonstrated that telomerase activity can be restored by transient transfection of the DNA encoding the enzyme's catalytic subunit hTERT in ALT cell lines expressing the RNA subunit hTR and by double transfection with both hTERT and hTR in ALT cell lines lacking hTR expression [63]. Several recent studies have looked at the consequences of restoration of telomerase activity in human in vitro immortalized and tumor-derived ALT cell lines [9, 18, 22, 46]. All studies analyzed telomere morphology by means of t-FISH. In three of these studies, restoration of telomerase activity did not alter the characteristic features of ALT [9, 22, 46]; whereas, in the fourth report, ALT was suppressed in two of the derived cell lines [18]. In these cells, suppression of ALT was accompanied by rapid telomere attrition at a rate approximately ten times that expected in normal telomerase-negative cells. In addition, the authors concluded that telomerase activation was accompanied by greater chromosomal stability, a lower apoptosis rate and a decrease in the number of APBs. The three other studies reported coexistence of ALT and telomerase. While telomerase apparently elongated the shortest chromosomes, greatly elongated ALT-specific telomeres

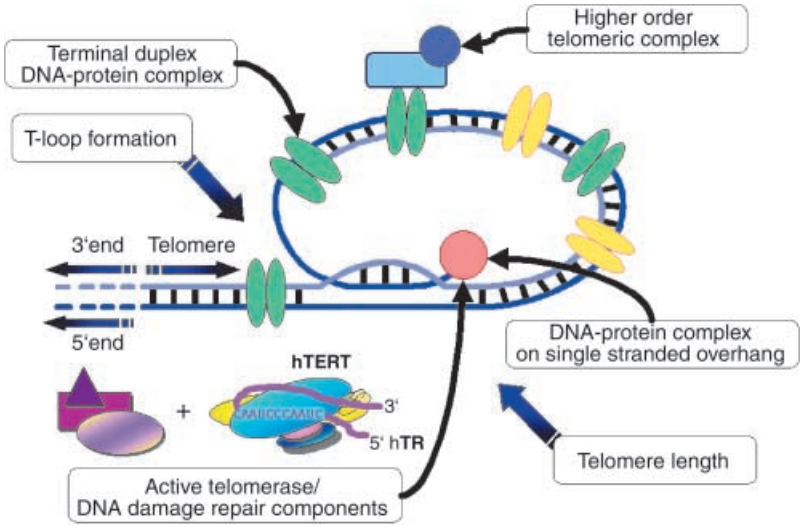

Fig. 5 Telomere maintenance: a complex picture. Some factors influencing telomere maintenance in human cells that are candidates to be altered in order to let alternative lengthening of telomeres take place

persisted, and the frequency of APBs remained essentially constant. These reports are important with regard to ALT as a possible back-up mechanism in telomerase-deficient or telomerase-inhibited cells. However, three studies demonstrating that telomerase inhibition leads to cell death in human cancer cells did not report the emergence of escapees utilizing ALT [10, 28, 70].

Reconstitution of mutant telomerase in ALT cells

Mutant telomerase activity could be detected in ALT cell lines transiently transfected with hTERT and modified hTRs harboring different mutations in the template region [63]. However, TRF analysis failed to show incorporation of mutant telomeric repeats. In a recent study, expression of mutant telomerase activity in ALT cells was shown to be lethal after a few population doublings, lethality being dependent on biologically and catalytically active telomerase [23]. The toxicity resulting from the synthesis of mutated sequences might be due to alteration of telomere structure or inhibition of efficient recombination.

Telomeric structure and signaling

Some recent studies on the higher order telomeric protein–DNA structure and signaling pathways have contributed to a more complete understanding of the ALT mechanism(s) and their significance in telomere maintenance.

Roles of telomerase apart from net-telomere lengthening: telomere capping

Why is there an additional enzyme that replicates telomere ends in the first place? Answers may lie in the many functions of telomerase apart from net telomere lengthening. Recent findings have uncovered contributions of active telomerase to telomere capping (reviewed in [2]). Ectopic hTERT expression extends the life span of T cells without net telomere lengthening [51]. In the aforementioned in vitro immortalization experiments, activation of telomerase in SV40-transformed fibroblasts led to the stabilization of telomeres at a shorter length than in their pre-crisis counterparts [15]. The prevalent end-to-end fusions, indicating loss of telomere function when cells enter crisis, are reduced both by ectopic expression of hTERT and by a hypomorphic mutant [71]. Moreover, telomerase is capable of inhibiting chromosomal instability [24]. Possibly, active telomerase itself prevents recombination in telomeric regions. In telomerase-deleted mutants of the yeast species *Kluyveromyces lactis*, recombination events between the telomeric tracts increase in frequency even in cells that still have relatively long telomeres [38]. It appears that, in many ways, introduction of telomerase is a tool used by dividing cells to carefully monitor complete replication of telomeric DNA in a cell-cycle dependent manner in order to guarantee telomere function and therefore chromosomal integrity (reviewed in [2, 19]). Consequently, T-loop formation and therefore capping of the telomere are at least partly dependent on telomere length. Shortening telomeres may continually undergo regulated degrees of temporary unfolding and uncapping, providing access for telomerase to elongate the shortest telomeres within a population [2, 27]. Cooperation of telomerase with components of the DNA damage machinery in gaining access to the telomere possibly allows cell cycle checkpoint control of telomere replication [19]. In a conceivable scenario, when telomeres shorten and neither telomerase nor certain inhibitory mechanisms (such as components of the MMR) are acting on the unfolding telomeres, recombination like in ALT may take place. Thus, all factors contributing to form the DNA–protein complex at the telomere (Fig. 5) are candidates for alteration in order for ALT to proceed.

ALT-promoting signaling pathways

Genetic changes known to promote ALT activation include transformation of cells with SV40 or human papillomavirus (HPV) oncogenes and spontaneous loss of the tumor suppressors p53 and $p16^{INK4a}$; however, to a greater degree, these changes result in activation of telomerase [56, 54]. Transformation by both SV40 and HPV is dependent on disruption of p53 and the retinoblastoma protein (pRb) (reviewed in [64]). The key role of p53 makes it difficult to dissociate specific executors of immortalization. pRb, $p16^{INK4a}$ and other proteins such as cyclin D1 are all linked in a common pathway that is disrupted in most cancers. Active pRb inhibits cell cycle progression; active cyclin D1 is part of the complex inhibiting pRb and, finally, $p16^{INK4a}$ inhibits cyclin D1 action. Proliferative potential can be increased by disruption of either pRb or $p16^{INK4a}$ [57]. It could be assumed that overexpression of cyclin D1 could have a similar effect, and this was recently demonstrated [44].

Oral-esophageal carcinomas are a model system in which to investigate the molecular mechanisms underlying squamous carcinogenesis. They frequently overexpress cyclin D1 and inactivate the p53 tumor suppressor. Opitz et al. demonstrated that cyclin D1 overexpression alone extended the replicative life span of normal oral keratinocytes. A combination of cyclin D1 and inactivation of p53 led to their immortalization by activation of ALT. It is likely that these changes contribute to an environment allowing mutations that promote the activation of ALT, for example by fostering genetic instability.

Perspectives

Even though the presence of telomerase activity has a strong diagnostic or prognostic impact, this does not automatically imply that inhibition of telomerase will prove to be a successful therapeutic strategy. ALT does not appear to be an avenue for telomere replication in normal cells in higher eukaryotes, as it would probably be an illegitimate recombinational event. However, ALT has been shown to occur alone and in coexistence with telomerase in in vitro immortalized cell lines, tumor-derived cell lines, and possibly in primary tumors. In view of new approaches to cancer therapy targeting telomere maintenance, the existence of ALT needs to be carefully evaluated [1]. Telomerase inhibitors will likely be less effective or even ineffective for tumors containing ALT cells. The corollary is that inhibition of telomerase may increase the selection pressure to activate ALT in previously telomerase-positive tumors. The association of ALT with chromosomal instability and telomere dysfunction may have major implications for tumor biology. The somewhat higher degree of telomere stabilization required for tumor progression may be dependent on preceding mutations during tumorigenesis that promote chromosomal instability. Elucidation of the molecular circumstances under which ALT is repressed and induced will be important not only for a more complete understanding of signaling at the telomere, but also to help advance the newest strategies in cancer therapy aiming at generally disrupting telomere maintenance and function.

Acknowledgements The authors would like to heartily thank all members of our molecular pathology research group, Karl-Ludwig Schäfer, Daniel Wai, Raihanatou Diallo, Yvonne Braun, Claudia Lanvers, Andreas Schuck, Bernd Frodermann, Helmut Görtz, Tanja Stümpler, and Marion Wobser for their contributions to a fruitful discussion. We are very grateful to Barbara Dockhorn-Dworniczak (Institute of Pathology, Kempten, Germany) for her constructive comments. We would also like to thank Andreas Scheel for his useful advice. We sincerely apologize to all authors whose primary references we had to omit due to space limitations. This work was supported in part by the IZKF Muenster, grant no. IKF3H2.

References

1. Bearss DJ, Hurley LH, Von Hoff DD (2000) Telomere maintenance mechanisms as a target for drug development. Oncogene 19:6632–6641
2. Blackburn EH (2001) Switching and signaling at the telomere. Cell 106:661–673
3. Bodnar AG, Ouellette M, Frolkis M, Holt SE, Chiu CP, Morin GB, Harley CB, Shay JW, Lichtsteiner S, Wright WE (1998) Extension of life-span by introduction of telomerase into normal human cells. Science 279:349–352
4. Broccoli D, Cooke H (1993) Aging, healing, and the metabolism of telomeres. Am J Hum Genet 52:657–660
5. Bryan TM, Englezou A, Gupta J, Bacchetti S, Reddel RR (1995) Telomere elongation in immortal human cells without detectable telomerase activity. EMBO J 14:4240–4248
6. Bryan TM, Englezou A, Dalla-Pozza L, Dunham MA, Reddel RR (1997) Evidence for an alternative mechanism for maintaining telomere length in human tumors and tumor-derived cell lines. Nat Med 3:1271–1274
7. Bryan TM, Marusic L, Bacchetti S, Namba M, Reddel RR (1997) The telomere lengthening mechanism in telomerase-negative immortal human cells does not involve the telomerase RNA subunit. Hum Mol Genet 6:921–926
8. Cabuy E, de Ridder L (2001) Telomerase activity and expression of telomerase reverse transcriptase correlated with cell proliferation in meningiomas and malignant brain tumors in vivo. Virchows Arch 439:176–184
9. Cerone MA, Londono-Vallejo JA, Bacchetti S (2001) Telomere maintenance by telomerase and by recombination can coexist in human cells. Hum Mol Genet 10:1945–1952
10. Colgin LM, Wilkinson C, Englezou A, Kilian A, Robinson MO, Reddel RR (2000) The hTERTalpha splice variant is a dominant negative inhibitor of telomerase activity. Neoplasia 2:426–432
11. Counter CM, Avilion AA, LeFeuvre CE, Stewart NG, Greider CW, Harley CB, Bacchetti S (1992) Telomere shortening associated with chromosome instability is arrested in immortal cells which express telomerase activity. EMBO J 11:1921–1929
12. Counter CM, Hahn WC, Wei W, Caddle SD, Beijersbergen RL, Lansdorp PM, Sedivy JM, Weinberg RA (1998) Dissociation among in vitro telomerase activity, telomere maintenance, and cellular immortalization. Proc Natl Acad Sci USA 95: 14723–14728
13. de The H, Lavau C, Marchio A, Chomienne C, Degos L, Dejean A (1991) The PML-RAR alpha fusion mRNA generated by the t(15;17) translocation in acute promyelocytic leukemia encodes a functionally altered RAR. Cell 66:675–684
14. Dhaene K, Van Marck E, Parwaresch R (2000) Telomeres, telomerase and cancer: an up-date. Virchows Arch 437:1–16

15. Ducray C, Pommier JP, Martins L, Boussin FD, Sabatier L (1999) Telomere dynamics, end-to-end fusions and telomerase activation during the human fibroblast immortalization process. Oncogene 18:4211–4223
16. Dunham MA, Neumann AA, Fasching CL, Reddel RR (2000) Telomere maintenance by recombination in human cells. Nat Genet 26:447–450
17. Feng J, Funk WD, Wang SS, Weinrich SL, Avilion AA, Chiu CP, Adams RR, Chang E, Allsopp RC, Yu J, et al (1995) The RNA component of human telomerase. Science 269: 1236–1241
18. Ford LP, Zou Y, Pongracz K, Gryaznov SM, Shay JW, Wright WE (2001) Telomerase can inhibit the recombination-based pathway of telomere maintenance in human cells. J Biol Chem 276:32198–32203
19. Gasser SM (2000) A sense of the end. Science 288:1377–1379
20. Greider CW, Blackburn EH (1985) Identification of a specific telomere terminal transferase activity in Tetrahymena extracts. Cell 43:405–413
21. Griffith JD, Comeau L, Rosenfield S, Stansel RM, Bianchi A, Moss H, de Lange T (1999) Mammalian telomeres end in a large duplex loop. Cell 97:503–514
22. Grobelny JV, Kulp-McEliece M, Broccoli D (2001) Effects of reconstitution of telomerase activity on telomere maintenance by the alternative lengthening of telomeres (ALT) pathway. Hum Mol Genet 10:1953–1961
23. Guiducci C, Cerone MA, Bacchetti S (2001) Expression of mutant telomerase in immortal telomerase-negative human cells results in cell cycle deregulation, nuclear and chromosomal abnormalities and rapid loss of viability. Oncogene 20: 714–725
24. Hackett JA, Feldser DM, Greider CW (2001) Telomere dysfunction increases mutation rate and genomic instability. Cell 106:275–286
25. Hahn WC, Counter CM, Lundberg AS, Beijersbergen RL, Brooks MW, Weinberg RA (1999) Creation of human tumour cells with defined genetic elements. Nature 400:464–468
26. Harley CB, Futcher AB, Greider CW (1990) Telomeres shorten during ageing of human fibroblasts. Nature 345:458–460
27. Hemann MT, Strong MA, Hao LY, Greider CW (2001) The shortest telomere, not average telomere length, is critical for cell viability and chromosome stability. Cell 107:67–77
28. Herbert B, Pitts AE, Baker SI, Hamilton SE, Wright WE, Shay JW, Corey DR (1999) Inhibition of human telomerase in immortal human cells leads to progressive telomere shortening and cell death. Proc Natl Acad Sci U S A 96:14276–14281
29. Hoare SF, Bryce LA, Wisman GB, Burns S, Going JJ, van der Zee AG, Keith WN (2001) Lack of telomerase RNA gene hTERC expression in alternative lengthening of telomeres cells is associated with methylation of the hTERC promoter. Cancer Res 61:27–32
30. Hsiao R, Sharma HW, Ramakrishnan S, Keith E, Narayanan R (1997) Telomerase activity in normal human endothelial cells. Anticancer Res 17:827–832
31. Keith WN, Evans TRJ, Glasspool RM (2001) Telomerase and cancer: time to move from a promising target to a clinical reality. J Pathol 195:404–414
32. Kilian A, Bowtell DD, Abud HE, Hime GR, Venter DJ, Keese PK, Duncan EL, Reddel RR, Jefferson RA (1997) Isolation of a candidate human telomerase catalytic subunit gene, which reveals complex splicing patterns in different cell types. Hum Mol Genet 6:2011–2019
33. Lansdorp PM, Poon S, Chavez E, Dragowska V, Zijlmans M, Bryan T, Reddel R, Egholm M, Bacchetti S, Martens U (1997) Telomeres in the haemopoietic system. Ciba Found Symp 211: 209–218
34. Lundblad V and Blackburn EH (1993) An alternative pathway for yeast telomere maintenance rescues est1- senescence. Cell 73:347–360
35. Makarov VL, Hirose Y, Langmore JP (1997) Long G tails at both ends of human chromosomes suggest a C strand degradation mechanism for telomere shortening. Cell 88:657–666
36. Mason JM, Biessmann H (1995) The unusual telomeres of Drosophila. Trends Genet 11:58–62
37. McClintock B (1941) The stability of broken ends of chromosomes in Zea Mays. Genetics 26:234–282
38. McEachern MJ, Blackburn EH (1996) Cap-prevented recombination between terminal telomeric repeat arrays (telomere CPR) maintains telomeres in Kluyveromyces lactis lacking telomerase. Genes Dev 10:1822–1834
39. Mehle C, Piatyszek MA, Ljungberg B, Shay JW, Roos G (1996) Telomerase activity in human renal cell carcinoma. Oncogene 13:161–166
40. Moyzis RK, Buckingham JM, Cram LS, Dani M, Deaven LL, Jones MD, Meyne J, Ratliff RL, Wu JR (1988) A highly conserved repetitive DNA sequence $(TTAGGG)_n$, present at the telomeres of human chromosomes. Proc Natl Acad Sci USA 85:6622–6626
41. Munoz-Jordan JL, Cross GA, de Lange T, Griffith JD (2001) t-Loops at trypanosome telomeres. EMBO J 20:579–588
42. Murnane JP, Sabatier L, Marder BA, Morgan WF (1994) Telomere dynamics in an immortal human cell line. EMBO J 13:4953–4962
43. Olovnikov AM (1971) Principles of marginotomy in template synthesis of polynucleotides. Dokl Akad Nauk 201:1496–1499
44. Opitz OG, Suliman Y, Hahn WC, Harada H, Blum HE, Rustgi AK (2001) Cyclin D1 overexpression and p53 inactivation immortalize primary oral keratinocytes by a telomerase-independent mechanism. J Clin Invest 108:725–732
45. Perrem K, Bryan TM, Englezou A, Hackl T, Moy EL, Reddel RR (1999) Repression of an alternative mechanism for lengthening of telomeres in somatic cell hybrids. Oncogene 18:3383–3390
46. Perrem K, Colgin LM, Neumann AA, Yeager TR, Reddel RR (2001) Coexistence of alternative lengthening of telomeres and telomerase in hTERT-transfected GM847 cells. Mol Cell Biol 21:3862–3875
47. Poremba C, Bocker W, Willenbring H, Schafer KL, Otterbach F, Burger H, Diallo R, Dockhorn DB (1998) Telomerase activity in human proliferative breast lesions. Int J Oncol 12: 641–648
48. Poremba C, Shroyer KR, Frost M, Diallo R, Fogt F, Schäfer K, Bürger H, Shroyer AL, Dockhorn-Dworniczak B, Boecker W (1999) Telomerase is a highly sensitive and specific molecular marker in fine-needle aspirates of breast lesions. J Clin Oncol 17:2020–2026
49. Poremba C, Willenbring H, Hero B, Christiansen H, Schafer KL, Brinkschmidt C, Jurgens H, Bocker W, Dockhorn-Dworniczak B (1999) Telomerase activity distinguishes between neuroblastomas with good and poor prognosis. Ann Oncol 10:715–721
50. Poremba C, Scheel C, Hero B, Christiansen H, Schaefer KL, Nakayama J, Berthold F, Juergens H, Boecker W, Dockhorn-Dworniczak B (2000) Telomerase activity and telomerase subunits gene expression patterns in neuroblastoma: a molecular and immunohistochemical study establishing prognostic tools for fresh-frozen and paraffin-embedded tissues. J Clin Oncol 18:2582–2592
51. Reddel RR (2000) The role of senescence and immortalization in carcinogenesis. Carcinogenesis 21:477–484
52. Reddel RR, Bryan TM, Colgin LM, Perrem KT, Yeager TR (2001) Alternative lengthening of telomeres in human cells. Radiat Res 155:194–200
53. Rizki A, Lundblad V (2001) Defects in mismatch repair promote telomerase-independent proliferation. Nature 411: 713–716
54. Rogan EM, Bryan TM, Hukku B, Maclean K, Chang AC, Moy EL, Englezou A, Warneford SG, Dalla PL, Reddel RR (1995) Alterations in p53 and p16INK4 expression and telomere length during spontaneous immortalization of Li-Fraumeni syndrome fibroblasts. Mol Cell Biol 15:4745–4753
55. Roth CW, Kobeski F, Walter MF, Biessmann H (1997) Chromosome end elongation by recombination in the mosquito Anopheles gambiae. Mol Cell Biol 17:5176–5183

56. Scheel C, Schaefer KL, Jauch A, Keller M, Wai D, Brinkschmidt C, van Valen F, Boecker W, Dockhorn-Dworniczak B, Poremba C (2001) Alternative lengthening of telomeres is associated with chromosomal instability in osteosarcomas. Oncogene 20: 3835–3844
57. Shapiro GI, Edwards CD, Rollins BJ (2000) The physiology of p16(INK4A)-mediated G1 proliferative arrest. Cell Biochem Biophys 33:189–197
58. Sprung CN, Bryan TM, Reddel RR, Murnane JP (1997) Normal telomere maintenance in immortal ataxia telangiectasia cell lines. Mutat Res 379:177–184
59. Takakura M, Kyo S, Kanaya T, Hirano H, Takeda J, Yutsudo M, Inoue M (1999) Cloning of human telomerase catalytic subunit (hTERT) gene promoter and identification of proximal core promoter sequences essential for transcriptional activation in immortalized and cancer cells. Cancer Res 59:551–557
60. Teng SC, Zakian VA (1999) Telomere–telomere recombination is an efficient bypass pathway for telomere maintenance in Saccharomyces cerevisiae. Mol Cell Biol 19:8083–8093
61. Teng SC, Chang J, McCowan B, Zakian VA (2000) Telomerase-independent lengthening of yeast telomeres occurs by an abrupt Rad50p-dependent, Rif-inhibited recombinational process. Mol Cell 6:947–952
62. Watson JD (1972) Origin of concatemeric T7 DNA. Nat New Biol 239:197–201
63. Wen J, Cong YS, Bacchetti S (1998) Reconstitution of wild-type or mutant telomerase activity in telomerase-negative immortal human cells. Hum Mol Genet 7:1137–1141
64. Whitaker NJ, Bryan TM, Bonnefin P, Chang AC, Musgrove EA, Braithwaite AW, Reddel RR (1995) Involvement of RB-1, p53, p16INK4 and telomerase in immortalisation of human cells. Oncogene 11:971–976
65. Wright WE, Pereira SO, Shay JW, et al (1989) Reversible cellular senescence: implications for immortalization of normal human diploid fibroblasts. Mol Cell Biol 9:3088–3092
66. Wu G, Lee WH, Chen PL (2000) NBS1 and TRF1 colocalize at promyelocytic leukemia bodies during late S/G2 phases in immortalized telomerase-negative cells. Implication of NBS1 in alternative lengthening of telomeres. J Biol Chem 275:30618–30622
67. Wynford-Thomas D (1999) Cellular senescence and cancer. J Pathol 187:100–111
68. Yasumoto S, Kunimura C, Kikuchi K, Tahara H, Ohji H, Yamamoto H, Ide T, Utakoji T (1996) Telomerase activity in normal human epithelial cells. Oncogene 13:433–439
69. Yeager TR, Neumann AA, Englezou A, Huschtscha LI, Noble JR, Reddel RR (1999) Telomerase-negative immortalized human cells contain a novel type of promyelocytic leukemia (PML) body. Cancer Res 59:4175–4179
70. Zhang X, Mar V, Zhou W, Harrington L, Robinson MO (1999) Telomere shortening and apoptosis in telomerase-inhibited human tumor cells. Genes Dev 13:2388–2399
71. Zhu J, Wang H, Bishop JM, Blackburn EH (1999) Telomerase extends the lifespan of virus-transformed human cells without net telomere lengthening. Proc Natl Acad Sci USA 96: 3723–3728

Virchows Arch (2002) 440:583–588
DOI 10.1007/s004280100458

ORIGINAL ARTICLE

Toni Valković · Frane Dobrila · Mauro Melato
Franco Sasso · Clara Rizzardi · Nives Jonjić

Correlation between vascular endothelial growth factor, angiogenesis, and tumor-associated macrophages in invasive ductal breast carcinoma

Received: 14 December 2000 / Accepted: 11 March 2001 / Published online: 16 May 2001
© Springer-Verlag 2001

Abstract Angiogenic and anti-angiogenic factors, secreted by tumor, inflammatory, and stromal cells play an important role in regulation of neovascularization. Among the most important of these is vascular endothelial growth factor (VEGF), a specific mitogen for endothelium, which increases vascular permeability and induces proteolytic enzymes necessary for vascular remodeling. Tumor-associated macrophages (TAMs) can express complex functions related to tumor biology, including growth, proliferative rate, stroma formation and dissolution, and neovascularization. The aim of this study was to define, using immunohistochemical analysis, the microvessel density (MVD), VEGF expression, and TAMs level in 97 human invasive ductal breast carcinomas not otherwise specified (NOS), investigate a possible relationship between them and then correlate their values with tumor grade, mitotic activity index (MAI), tumor size and lymph-node status. Statistical analysis showed a strong positive relationship between MVD and VEGF expression ($P<0.001$). Furthermore, both MVD and VEGF expression were significantly correlated with tumor grade and lymph-node status, and TAMs infiltration with MAI. TAM level showed a significant positive connection with VEGF expression and MVD. These in situ observations suggest that VEGF stimulates angiogenesis in human invasive ductal breast carcinoma NOS and attracts macrophages to the tumor locus, which then may be involved in angiogenesis promotion. The expression of this angiogenic molecule, and MVD and TAM level, can provide additional prognostic significance and help in the identification of patients who need postoperative adjuvant therapy.

Keywords Breast carcinoma · Angiogenesis · Vascular endothelial growth factor · Tumor-associated macrophages

T. Valković · N. Jonjić (✉)
Department of Pathology, Medical Faculty, University of Rijeka, B. Branchetta 20, 51000 Rijeka, Croatia
e-mail: nives@medri.hr
Tel.: +385-51-336566, Fax: +385-51-336776

F. Dobrila
Department of Surgery, Clinical Hospital Center of Rijeka, Croatia

M. Melato · C. Rizzardi
Department of Pathology of the University of Trieste, Italy

F. Sasso
Institute of Semeiotica Chirurgica, University of Trieste, Italy

Introduction

Angiogenesis, the formation of new capillaries, is an important component of tumor growth and probably takes place in the cascade of biological events involved in tumor metastasis [15]. A majority of studies have shown that more vascular tumors are associated with an increased risk of metastasis and less favorable prognosis [17, 47].

However, the mechanism whereby the tumor induces neovascularization is still questionable. Our understanding of the angiogenesis process has been enhanced significantly by the identification and characterization of a variety of angiogenic and antiangiogenic cytokines and their receptors. Alteration in the balance among them may determine angiogenic process in the tumor and the progression of neoplasia.

Vascular endothelial growth factor (VEGF) is a multifunctional glycoprotein involved in endothelial cell proliferation and migration [14], vasculogenesis [37], vascular permeability [34] and stromal degradation by activation of some proteolytic enzymes involved in tumor invasiveness and angiogenesis [13]. Four isoforms generated by alternative splicing with different affinities for heparin but with equal activity have been identified [18], the two larger ones remaining cell associated, whereas the two smaller isoforms are secreted as soluble molecules [28]. These effects are mediated on endothelial cells via two high affinity tyrosine kinase receptors, Flt-1 [10] and KDR [39]. The VEGF is expressed in different human tumors or tumor cell lines, including breast [7], brain [36], colon [6], kidney [7], ovary [3], cervix [16], lung [25], lymph node [11], melanoma [32], and esophagus [20].

The role of inflammatory cells in malignant tumors is of uncertain significance. The studies assessing the association between inflammation and prognosis have produced controversial results, even with multivariate analysis [29, 33, 35]. One of the most interesting and functionally diverse inflammatory cells are reactive macrophages which infiltrate tumors, the so-called tumor associated macrophages (TAMs). TAMs can destroy tumor cells [49], but they can also promote tumor proliferation [48], progression [27], and angiogenesis [31].

The aim of this study was to analyze a possible relationship among microvessel density (MVD), VEGF expression, and TAM level in invasive ductal breast carcinoma not otherwise specified (NOS) and to correlate these parameters with some established prognostic factors in breast cancer, namely tumor size and grade, lymph-node status, and mitotic activity index (MAI). This analysis can provide further information, which could be of interest for the numerous recently developed strategies of anti-angiogenic and other alternative therapies.

Materials and methods

Clinicopathological parameters

Ninety-seven cases of human invasive ductal breast carcinomas NOS, according to the World Health Organization (WHO) classification scale, with lymph-node tissues were considered after formalin fixation, paraffin embedding, and staining with hematoxylin and eosin. Breast and lymph-node tissues were obtained from specimens submitted to the Pathology Department, Medical Faculty of Rijeka.

Among them, 46 cases had negative and 51 cases had positive lymph nodes. Tumors were divided into three groups according to size, i.e., less then l cm, between 1 cm and 2 cm, and more than 2 cm. In all cases, MAI was considered, and carcinomas were grouped into two categories, i.e., tumors with MAI lower than ten and higher than ten. One pathologist using Bloom and Richardson's method modified by Elston and Elis [12] histologically graded all invasive carcinomas.

Immunohistological analysis

A total of 97 cases were processed for immunohistological analysis to determine the MVD, VEGF expression, and TAM level using a standard immunoperoxidase ABC (avidin–biotin–peroxidase complex) technique on paraffin-embedded sections. Small blood vessels were visualized by staining endothelial cells for CD 31 (Dako, Copenhagen, Denmark; clone JC/70A). Areas of the highest neovascularization (hot spot) were found in each tumor by scanning the section at low power, and then individual microvessels were counted on a 200× field (area of 0.785 mm^2). Within each hot spot, the highest single field values were recorded. The microvessel counts per field were converted to microvessel per square millimeters for subsequent statistical analysis. Any endothelial cells or endothelial cell cluster positive for CD31 and separate from an adjacent cluster was considered a single countable microvessel.

Anti-VEGF polyclonal antibody (BioGenex Laboratories, Inc., San Ramon, Calif.; code PU360-UP) was used to determine VEGF expression in the breast carcinomas. The smooth muscle in the sections served as an internal positive control, because these cells have been shown to express VEGF constitutively. Immunoreactivity was graded using the slightly modified method of Kimitoshi [20], as follows: *VEGF "–"* tumor cells were stained less intensely than smooth muscle; *VEGF "–/+"* <30% of parenchymal cells were stained similarly or more intensely than smooth muscle cells; and *VEGF "+"* >30% of parenchymal cells were stained similarly or more intensely than smooth muscle cells. VEGF immunoreactivity was not graded on the stromal elements of tumors.

To detect TAMs, sections of invasive ductal breast carcinomas NOS were stained using monoclonal CD68 antibodies (Dako, code KP1). The entire sections were evaluated and a semiquantitative estimate, used in our previous investigation [19], was performed as follows: (1) no macrophages in tumoral stroma; (2) small foci of macrophages in tumoral stroma; (3) large foci of macrophages in tumoral stroma; and (4) diffuse infiltration of CD68 positive cells in tumoral stroma. Statistical analysis was performed using SPSS Package Release 6.0 for PC using $\chi 2$ and *F* tests.

Table 1 Clinicopathological characteristics, microvessel density (MVD), vascular endothelial growth factor (VEGF) expression, and tumor-associated macrophages (TAMs) of patients studied

	No. of cases	MVD (mean)	VEGF			TAMs			
			–	–/+	+	1	2	3	4
Histological grade									
I	23	78.74	14	2	7	8	6	4	5
II	59	84.29	38	11	10	17	10	21	11
III	15	100.20	4	7	4	2	2	6	5
Mitotic activity index									
<10	59	83.88	38	8	13	22	15	13	9
≥10	38	87.73	18	12	8	5	3	18	12
Tumor size									
≤10 mm	11	79.36	8	1	2	7	1	1	2
11–20 mm	40	85.83	24	8	8	8	7	13	12
>20 mm	46	86.54	24	11	11	12	10	17	7
Lymph-node status									
Negative	46	75.22	33	5	8	15	10	13	8
1–3 Positive lymph nodes	29	97.48	13	7	9	8	4	9	8
>3 Positive lymph nodes	22	90.91	10	8	4	4	4	9	5

Results

The clinicopathological parameters of the 97 patients included in this study with the results of immunohistochemical analysis are summarized in Table 1. The microvessel density in the 97 cases of invasive ductal breast carcinomas ranged from 36/mm^2 to 161/mm^2 (median 85/mm^2, SD 25.6). The hot spots occurred anywhere in the tumor but most frequently at the invasive edge of the tumor.

Of the 97 breast carcinomas, 56 (57.7%) were in VEGF "–" group, 20 (20.6%) were in VEGF "–/+" group and 21 (21.6%) were in VEGF "+" group. Positive tumoral and stromal (smooth muscle, endothelium, fibroblasts, and macrophages) cells showed diffuse cytoplasmic immunoreactivity, ranging in intensity from weak to strong (Fig. 1). Many tumors showed a heterogeneous distribution of VEGF staining, and tumor cells that stained for VEGF were observed more often in the invasive front than in the tumor center.

With regard to TAMs, 27 (27.8%) tumors had no macrophages in the stroma, 18 (18.6%) had small foci, 31 (32%) had large foci, and 21 (21.6%) had diffuse infiltration of TAMs in the tumoral stroma (Fig. 2). Immunoreactivity was cytoplasmic, moderate or strong, granular or diffuse in nature. CD68-positive cells were observed in the stroma, very often on the invasive margins of the tumor or around the foci of necrosis. Furthermore, in the same specimen, we frequently noticed the concomitance between the "hot spot" and the areas of the highest TAM level and VEGF expression.

The average values of MVD showed significant differences in the different VEGF groups of tumors. Namely, the mean value of MVD was 76.2 for VEGF "–"; 102.2 for VEGF "–/+", and 94.2 for VEGF "+" group (P<0.001; Table 2). Further statistical analysis showed that lymph-node positive (P<0.001) and poorly differen-

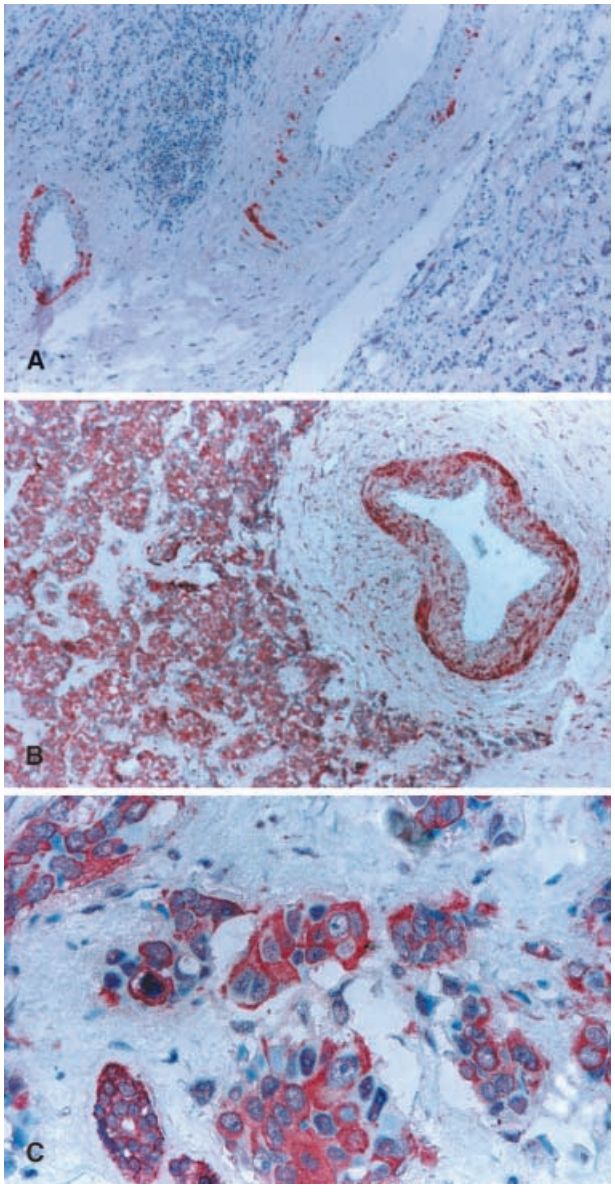

Fig. 1 Immunohistochemical staining for vascular endothelial growth factor (VEGF) in invasive breast carcinoma. **A** Positive vascular smooth muscle cells with surrounding negative tumor cells, ×10. **B** Tumor cells stained similarly to smooth muscle cells, ×10. **C** Strong expression of VEGF in tumor cells, ×40

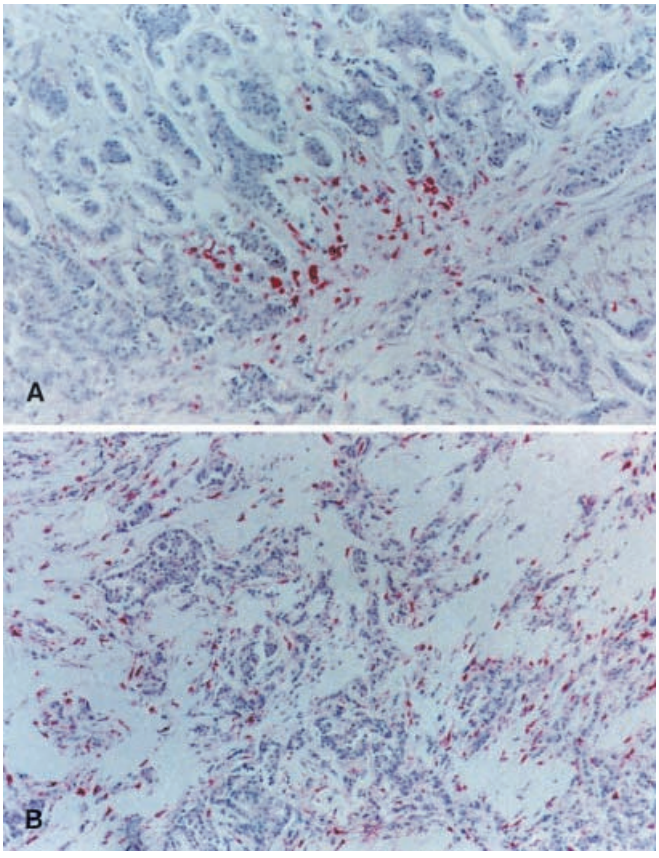

Fig. 2 Staining with anti-CD68 in invasive breast carcinoma not otherwise specified (NOS). **A** A smaller focus of tumor-associated macrophages (TAM) in tumoral stroma, ×10. **B** A diffuse infiltration of CD68-positive cells (TAM) in tumoral stroma, ×10

Table 2 Correlations between vascular endothelial growth factor (VEGF) expression, tumor-associated macrophage (TAM) infiltrations, and microvessel density (MVD)

	TAM 1	TAM 2	TAM 3	TAM 4	MVD, mean
VEGF –	21	15	14	6	76.16
VEGF –/+	2	1	10	7	102.15
VEGF +	4	2	7	8	94.24
MVD, mean	74.11	81.39	89.13	98.00	

Table 3 Correlation and *P* values between microvessel density (MVD) values, vascular endothelial growth factor (VEGF) expression, tumor-associated macrophage (TAM) level and established prognostic factors in breast carcinoma. *MAI* mitotic activity index, *NS* not significant

	VEGF expression[a]	Microvessel density[b]	TAM level[c]
Histological grade	P=0.024	P=0.03	NS
MAI	NS	NS	P<0.001
Tumor size	NS	NS	NS
Lymph-node status	P=0.047	P<0.001	NS

[a] $\chi 2$ test [b] F test [c] $\chi 2$ test

tiated (P=0.03) tumors have significantly higher MVD than those without lymph node infiltration and well- or moderately differentiated carcinomas.

The VEGF expression was significantly positively correlated with TAM infiltration (P=0.003) and lymph node involvement (P=0.047). Thus, VEGF-negative breast carcinomas (VEGF "–'' group) tended to have "no macrophages" or "small foci" of TAMs in the tumoral stroma and negative lymph nodes, while tumors that express VEGF (VEGF "–/+'' and "+'' groups) generally showed "large foci" or "diffuse infiltration" of TAMs and involved lymph nodes.

VEGF-negative tumors tended to be grade II, whereas VEGF-positive carcinomas were generally grade I. The grade-III breast cancers showed an intermediary level of VEGF expression. This difference was significant (P=0.024).

Tumors with diffuse macrophage infiltration had significantly higher MVD than breast cancers with no macrophages in the tumoral stroma (P=0.008). Finally, invasive ductal breast cancers with a great amount of TAMs (TAMs 3 and 4 groups) had significantly higher MAI than tumors with no or just a small focus of macrophages (TAMs 1 and 2 groups; P<0.001). Table 3 shows the correlation and significant P values between MVD, VEGF expression, TAMs level, and established prognostic parameters in breast cancer.

Discussion

In this study, we demonstrated a clear positive correlation between parenchymal VEGF expression, MVD, and TAM level in invasive ductal breast carcinoma NOS. The results of this investigation confirmed that VEGF is, probably, the most important and independent angiogenic pathway in human invasive ductal breast cancer, which is consistent with some studies published previously [21, 41, 42, 43]. Although some recent investigation did not find any correlation between VEGF and increased angiogenesis [23], their sample also included invasive lobular and other histological types of breast carcinoma which, according to other authors, pointed to a significant difference in VEGF expression in comparison with ductal carcinoma [21]. Furthermore, in this investigation, no association between VEGF and histological type was found; however, the number of included lobular carcinomas may well have been too small for such a conclusion.

It has been reported that VEGF has other protumoral effects, such as induction of plasminogen activator [30] and interstitial collagenase [44] expression, which may alter the tumoral extracellular matrix and facilitate tumor progression and spread to lymph nodes. One of these protumoral functions is also the chemotactic effect of VEGF on monocytes/macrophages [1, 8] that our analysis confirmed. We found a significant positive relationship between increased parenchymal VEGF expression and TAMs infiltration. Prior to our report, only Leek and his collaborator [23] investigated this association in vivo, and our finding is in agreement with their results.

Some authors, including ourselves, have discovered a positive relationship between TAMs and tumor cell proliferation, and a recent study showed the identical result [19, 48]. This suggests a reciprocal interaction between TAMs and tumor cells. The tumor produces VEGF (and other chemokines) which may facilitate an attraction of macrophages to the tumor locus, and TAMs in turn may provide optimal conditions for tumor proliferation and growth.

Furthermore, this investigation showed that the high VEGF expression was significantly associated with the metastases in the regional lymph nodes, which indicates that VEGF expression is associated with tumor progression, spread, and poor prognosis, probably by stimulating angiogenesis, macrophage infiltration, and remodeling of tumor tissue. These findings are consistent with some studies published previously [40, 41].

Quantitative histological studies have suggested that angiogenesis, as assessed using density of microvessels, correlates with prognosis in breast carcinoma [4, 41]; however, other studies have disputed this point [26, 38, 46], and this dilemma is still without a clear answer.

In our previous investigation, we failed to establish any significant correlation between MVD and some traditional prognostic parameters, such as tumor size, histological grade, mitotic activity, and lymph-node status [19], which was the reason why we attempted to redefine

these correlations with a larger sample population using anti-CD31 antibody to identify the microvessels.

This study reveals a significant positive correlation between the MVD and lymph node involvement in histological sections of invasive ductal breast carcinomas NOS. Namely, the density of microvessels within a tumor is not only a possible measure of the size of the vascular window through which tumor cells pass to spread to distant body sites but also, according to our results, a predictor of lymphogenous spread and metastatic disease in regional lymph nodes. Tumor cells can penetrate to adjacent lymphatics that form concomitantly with blood capillaries or, hypothetically, malignant cells can pass from the blood stream into the lymphatic via lymphaticovenous junctions [2, 24], which can explain our results.

In our sample, the tumor grade correlates with vascularization, i.e., with a significant increase in the number of small blood vessels in grade III. However, we cannot find any significant association between angiogenesis and the proliferation rate or tumor growth (expressed by MAI and tumor size), which indicates that biological phenomena of neovascularization, tumor proliferation, and growth are not permanently mutually dependent processes. It is obvious that the growth of solid tumors depends on angiogenesis (especially in the early phase of tumor development when stabile vascular network is forming), because newly formed blood vessels supply the tumor with nutrients and oxygen and dispose of its metabolic waste product. However, in a later period of tumor existence, other factors co-influence tumor proliferation and growth, which do not require, according to our results, the same cytokines as those for angiogenesis, at least in invasive ductal breast cancer NOS.

We found that MVD correlated with the TAM level, being significantly higher in ductal carcinomas with diffuse macrophage infiltration than tumors without TAMs in the stroma. This indicates an important role of TAMs (and probably other stromal cells) in angiogenesis. After all, VEGF immunoreactivity in our breast carcinomas was revealed not only in carcinoma cells but also in tumor-associated macrophages, vascular endothelial cells, and fibroblast, which indicates that tumoral stroma can also be a source of angiogenic impulses. This observation concurs with some findings published previously [22, 45].

The results of this investigation confirm a strong connection between parenchymal VEGF expression, angiogenesis, and macrophage infiltration, which represents an important synergistic inter-relation between tumor cells and stroma in the micro-ecosystem of human invasive ductal breast carcinoma NOS. TAMs, which can comprise up to one-half of the mass of breast carcinoma, are biologically extremely important stromal cells.

Moreover, these parameters can provide additional prognostic information and guidance in the identification of patients without involvement of regional lymph nodes who need postoperative adjuvant therapy. However, since a broad panel of angiogenic and anti-angiogenic peptides may be produced by breast cancer [9], further investigations should be carried out in order to define the best target for anti-angiogenic therapies.

References

1. Barleon B, Sozzani S, Zhou D, et al (1996) Migration of human monocytes in response to vascular endothelial growth factor (VEGF) is mediated via the VEGF receptor flt-1. Blood 87:3336–3343
2. Blood CH, Zetter BR (1990) Tumor interactions with the vasculature: angiogenesis and tumor metastasis. Biochem Biophys Acta 1032:89–118
3. Boocock CA, Charnock-Jones S, Sharkey AM, et al (1995) Expression of vascular endothelial growth factor and its receptors flt and KDR in ovarian carcinoma. J Natl Cancer Inst 87:506–516
4. Bosari S, Lee AK,DeLellis RA, et al (1992) Microvessel quantitation and prognosis in invasive breast carcinoma. Hum Pathol 23:755–761
5. Brown LF, Berse B, Jackman RW, et al (1993) Increased expression of vascular permeability factor (vascular endothelial growth factor) and its receptor in kidney and bladder carcinomas. Am J Pathol 143:1255–1262
6. Brown LF, Berse B, Jackman RW, et al (1993) Expression of vascular permeability factor (vascular endothelial growth factor) and its receptors in adenocarcinomas of the gastrointestinal tract. Cancer Res 53:4727–4735
7. Brown LF, Berse B, Jackman RW, et al (1995) Expression of vascular permeability factor (vascular endothelial growth factor) and its receptors in breast cancer. Hum Pathol 26:86–91
8. Claus M, Gerlach M, Gerlach H, et al (1990) Vascular permeability factor: a tumor-derivated polypeptide that induces endothelial cell and monocyte procoagulant activity, and promotes monocyte migration. J Exp Med 172:1535–1545
9. De Jong JS, Van Diest PJ, Van der Valk P, et al (1998) Expression of growth factors, growth inhibiting factors, and their receptors in invasive breast cancer. I: an inventory in search of autocrine and paracrine loops. J Pathol 184:44–52
10. DeVries C, Escobedo JA, Ueno H, et al (1992) The fms-like tyrosine kinase, a receptor for vascular endothelial growth factor. Science 255:989–991
11. Dvorak HF, Sioussat TM, Brown LF, et al (1991) Distribution of vascular permeability factor (vascular endothelial growth factor) in tumors: concentration in tumor blood vessels. J Exp Med 174:1275–1278
12. Elston CW, Ellis IO: (1991) Pathological prognostic factors in breast cancer. The value of histological grade in breast cancer: experience from a large study with long-term follow up. Histopathology 19:403–410
13. Ferrara N (1996) Vascular endothelial growth factor. Eur J Cancer 32A:2413–2422
14. Ferrara N, Carver-Moore K, Chen H, et al (1996) Heterozygous embryonic lethality induced by targeted inactivation of the VEGF gene. Nature 380:439–442
15. Fidler IJ, Ellis LS (1984) The implications of angiogenesis for the biology and therapy of cancer metastasis. Cell 79:l85–188
16. Guidi AJ, Abu JG, Berse B, et al (1995) Vascular permeability factor (vascular endothelial growth factor) expression and angiogenesis in cervical neoplasia. J Natl Cancer Inst 87:1237–1245
17. Horak ER, Leek R, Klenk N, et al (1992) Angiogenesis, assessed by platelet/endothelial cell adhesion molecule antibodies, as an indicator of node metastases and survival in breast cancer. Lancet 340:1120–1224
18. Houck KA, Ferrara N, Winer J, et al (1991) The vascular endothelial growth factor family: identification of a fourth molecular species and characterization of alternative splicing of RNA. Mol Endocrinol 5:1806–1814

19. Jonjić N, Valković T, Lučin K, et al (1998) Comparison of microvessel density with tumor associated macrophages in invasive breast carcinoma. Anti Cancer Res 18:3767-3770
20. Kimitoshi I, Yuichi O, Suganuma T, et al (1997) Vascular endothelial growth factor expression in primary esophageal squamous cell carcinoma. Cancer 79:206–213
21. Lee AHS, Dublin EA, Bobrow LG, et al (1998) Invasive lobular and invasive ductal carcinoma of the breast show distinct patterns of vascular endothelial growth factor expression and angiogenesis. J Pathol 185:394–401
22. Leek RD, Lewis CE, Whitehouse R, et al (1996) Association of macrophage infiltration with angiogenesis and prognosis in invasive breast carcinoma. Cancer Res 56:4625–4629
23. Leek RD, Hunt NC, Landers RJ, et al (2000) Macrophage infiltration is associated with VEGF and EGFR expression in breast cancer. J Pathol 190:430–436
24. Liotta LA, Stracke ML (1988) Tumor invasion and metastasis: biochemical mechanisms. In: Lippman ME, Dickson RB (eds) Breast cancer: cellular and molecular biology. Kluwer Academic Publishers, Boston, pp 223–238
25. Mattern J, Koomagi R, Volm M (1995) Vascular endothelial growth factor expression and angiogenesis in non-small cell lung carcinomas. Int J Oncol 6:1059–1062
26. Mayers MM, Seshadri R, Raymond W, et al (1998) Tumor microvascularity has no independent prognostic significance for breast cancer. Pathology 30:105–110
27. Musoni L, Riganti M, Acero R, et al (1988) Macrophages associated with murine tumor express plasminogen activator activity. Int J Cancer 41:227–230
28. Park JE, Keller GA, Ferrara N (1993) The vascular endothelial growth factor (VEGF) isoforms: differential deposition into the subepithelial extracellular matrix and bioactivity of extracellular matrix-bound VEGF. Mol Biol Cell 4:1317–1326
29. Parl FF, Dupont WD (1982) A retrospective cohort study of histologic risk factors in breast cancer patients. Cancer 50: 2410–2416
30. Pepper MS, Ferrara N, Orci L, et al (1991) Vacular endothelial growth factor (VEGF) induces plasminogen activators and plasminogen activator inhibitor-1 in microvascular endothelial cells. Biochem Biophys Res Commun 181:902–906
31. Polverini PJ, Leibovich SJ (1984) Induction of neovascularisation in vivo and endothelial proliferation in vitro by tumor associated macrophages. Lab Invest 51:635–642
32. Potgens AJG, Lubsen NH, Van Altena MC, et al (1995) Vascular permeability factor expression influences tumor angiogenesis in human melanoma lines xenografted to nude mice. Am J Pathol 146:197–209
33. Rilke F, Colnaghi MI, Cascinelli N, et al (1991) Prognostic significant of HER-2/neu expression in breast cancer and its relationship to other prognostic factors. Int J Cancer 49:44–49
34. Roberts WG, Palade GE (1995) Increased microvascular permeability and endothelial fenestration induced by vascular endothelial growth factor. J Cell Sci 108:2369–2379
35. Roses DF, Bell DA, Flotte TJ, et al (1982) Pathologic predictors of recurrence in stage I (T1N0M0) breast cancer. Am J Clin Pathol 78:817–820
36. Samoto K, Ikezaki K, Ono M, et al (1995) Expression of vascular endothelial growth factor and its possible relation with neovascularisation in human brain tumors. Cancer Res 55: 1189–1193
37. Senger DR, Van de Water L, Brown LF et al (1993) Vascular permeability factor (VPF, VEGF) in tumor biology. Cancer Metastasis Rev 12:303–324
38. Sightler HE, Borowsky AD, Dupont WD, et al (1994) Evaluation of tumor angiogenesis as a prognostic marker in breast cancer (abstract). Mod Pathol 7:22
39. Terman BI, Dougher VM, Carrion ME, et al (1992) Identification of the KDR tyrosine kinase as a receptor for vascular endothelial cell growth factor. Biochem Biophys Res Commun 187:989–991
40. Toi M, Hoshina S, Takayanagi T, et al (1994) Association of vascular endothelial growth factor expression with tumor angiogenesis and with early relapse in primary breast cancer. Jpn J Cancer Res 85:1045–1049
41. Toi M, Inada K, Hoshina S, et al (1995) Vascular endothelial growth factor and plated-derivated endothelial cell growth factor are frequently coexpressed in highly vascularized human breast cancer. Clin Cancer Res 1:961–964
42. Toi M, Inada K, Suzuki H, et al (1995) Tumor angiogenesis in breast cancer: its importance as a prognostic indicator and the association with vascular endothelial growth factor expression. Breast Cancer Res Treat 36:193–204
43. Toi M, Kondo S, Suzuki H, et al (1996) Quantitative analysis of vascular endothelial growth factor in primary breast cancer. Cancer 77:1101–1106
44. Unemory EN, Ferrara N, Bauer EA, et al (1992) Vascular endothelial growth factor induces interstitial collagenase expression in human endothelial cells. J Cell Physiol 153:557–562
45. Vacca A, Ribatti D, Ruco L, et al (1999) Angiogenesis extent and macrophage density increase simultaneously with pathological progression in B-cell non-Hodgkin's lymphoma. Br J Cancer 79:965–970
46. VanHoef MEHM, Knox WF, Dhesi SS (1993) Assessment of tumor vascularity as a prognostic factor in lymph node negative invasive breast cancer. Eur J Cancer 29A:1141–1145
47. Weidner N, Folkman J, Pozza F, et al (1992) Tumor angiogenesis: a new significant and independent prognostic indicator in early-stage breast carcinoma. J Natl Cancer 84:1875–1887
48. Wu S, Boyer CM, Whitaker RS (1993) Tumor necrosis factor-alpha as an autocrine and paracrine growth factor for ovarian cancer: monokine induction of tumor cell proliferation and tumor necrosis factor-alpha expression. Cancer Res 53:1939–1944
49. Zeigler-Heitbrock HEL, Theil C, Haas JG et al (1988) Tumor necrosis factor in human monocyte-mediated anti tumor cytotoxicity. Net Immun Cell Growth Regul 7:280–286

Virchows Arch (2002) 440:589–593
DOI 10.1007/s00428-002-0639-4

ORIGINAL ARTICLE

Keiichi Iwaya · Hitoshi Ogawa · Miki Izumi
Masahiko Kuroda · Kiyoshi Mukai

Stromal expression of CD10 in invasive breast carcinoma: a new predictor of clinical outcome

Received: 24 September 2001 / Accepted: 28 January 2002 / Published online: 13 April 2002
© Springer-Verlag 2002

Abstract CD10 is a cell surface neutral endopeptidase that is not consistently expressed in the stromal cells of the normal breast. Expression of CD10 is sometimes observed in the stromal cells of invasive ductal carcinoma, but its clinical significance has never been studied. Immunohistochemical examination of CD10 was performed in 123 cases of breast cancer. The median follow-up period of all patients was 8.0 years, and univariate and multivariate analyses were performed to evaluate the prognostic significance of stromal CD10 expression. There was no staining in the stromal cells of 13 non-invasive ductal carcinomas or normal breast tissue. Of 110 invasive ductal carcinomas, 20 cases (18%) in which more than 10% of the stromal cells stained positive throughout the cancer tissue were judged "positive". The frequency of positive stromal staining was significantly higher in the cases with axillary lymph-node metastasis (P=0.038), but there were no correlations between stromal CD10 expression and age, tumor size, histologic grade, or clinical stage. The patients whose tumors contained CD10-positive stromal cells had a shorter metastasis-free interval (P=0.0008). Univariate analysis demonstrated that patients with lymph-node metastasis also had a significantly shorter metastasis-free interval (metastasis vs no metastasis; P=0.0318). In the multivariate analysis, only CD10 remained a significant predictor for time to recurrence (P=0.0059), and CD10 was the single significant prognostic factor for overall survival in the univariate analysis (P=0.0021). These results suggest that stromal expression of CD10 in breast cancer is an important novel prognostic factor.

Keywords Breast carcinoma · CD10 · Stromal cell · Prognosis · Invasion

The manuscript was presented at the 90th annual meeting of United States and Canadian Academy of Pathology on 5 March 2001 in Atlanta.

K. Iwaya · H. Ogawa · M. Izumi · M. Kuroda · K. Mukai (✉)
First Department of Pathology, Tokyo Medical University,
160-8402 Shinjuku 6-1-1, Shinjuku-ku, Tokyo, Japan
e-mail: kmukai@tokyo-med.ac.jp
Tel.: +81-33351-6141, Fax: +81-33352-6335

Introduction

CD10 is a 90- to 110-kDa cell surface zinc-dependent metalloprotease that has been called "common acute lymphoblastic leukemia antigen" (CALLA). It has also been referred to as "neutral metalloendopeptidase" in the kidney and "enkephalinase" in the brain, and has been found to be expressed on the cell surface of most acute lymphoblastic leukemias [18, 19]. These enzymes, present in a variety of cell types, are now known to be virtually identical to CD10 or neutral endopeptidase 24.11 [20]. Although CD10 has been very useful in classifying the acute leukemias and subclassifying malignant lymphomas [10], frequent expression has been found in renal cell carcinoma, hepatocellular carcinoma, and carcinoma of the urinary bladder and prostate [4, 7, 14]. By contrast, the breast, stomach, and colon carcinoma cells express CD10 at much lower rates.

CD10 is constantly expressed by the myoepithelial cells of the human breast during its development and after its maturation, and it is considered a specific marker of the myoepithelial cells, because other components of adult breast, including the inner lining epithelial cells and surrounding fibroblasts, are negative for CD10 [11]. There are no CD10-positive stromal cells in the majority of developing breast tissue, but in a small percentage of women a minor population of stromal cells with fibroblast-like morphology has been shown to express CD10 [2].

Although most human breast tumors are negative for CD10, proliferating stromal cells in fibroadenoma and phyllodes tumors express CD10 [16]. CD10 is also expressed in the epithelium exhibiting apocrine metaplasia and in the fluid of breast cysts lined by apocrine epithelium. Such cysts have been reported to be associated with a higher risk of breast carcinoma [1, 9]. A minority of breast carcinoma cells have been shown to be weakly focally positive, supporting other data indicating that myoepithelial differentiation is not a common feature of malignant mammary tumors [11]. CD10 has recently been demonstrated on the stromal cells of some breast carcinomas, and CD10 has been suggested to be upregu-

lated in association with breast cancer cells [3]. However, the origin and function of CD10-positive stromal cells in breast cancer are unknown. The aim of the present study was to clarify the clinical significance of CD10 expression by the stromal cells in breast carcinomas.

Materials and methods

The subjects of this study were 123 Japanese women who underwent modified radical mastectomy for breast cancer at the Tokyo Medical University Hospital. The median follow-up period for all patients was 8.0 years, and that for the living patients was 9.2 years (range 3.3–13.3 years). Blocks of formalin-fixed, paraffin-embedded tissue from these patients were retrieved from the Diagnostic Pathology Division, and clinicopathological data, such as age at the time of diagnosis, tumor size, axillary lymph-node status, and clinical stage, were obtained from the medical records.

To confirm the presence of sufficient tumor tissue and to ensure contemporary uniform grading, paraffin-embedded tissue blocks were sectioned, stained with hematoxylin-eosin, reviewed for the presence of tumor, and graded by a single pathologist, as outlined previously [8]. Deparaffinized sections for immunostaining were subjected to heat-induced antigen retrieval with a pressure sterilizer. The sections were heated in 0.01 M sodium citrate buffer (pH 6.0) for 10 min in a conventional pressure sterilizer (ALP KT-2322, Alp Industry, Tokyo, Japan). After cooling, they were incubated with 10% normal swine serum in phosphate-buffered saline (PBS) for 10 min, then with an anti-CD10 monoclonal antibody (56C6, Novo Castra, Newcastle, UK) diluted to 1:100 overnight [13]. An LSABC kit (Dako Japan, Kyoto, Japan) was used as the detection system. After incubation with the secondary antibody and ABC reagent, the color reaction was developed in 0.02%, 3′-diaminobenzidine, and 0.02% H_20_2 in Tris buffer pH 8.0. Hematoxylin was used for counterstaining. When more than 10% of the stromal cells around breast cancer cells were positive for CD10, the expression was judged to be positive.

Correlation between stromal CD10 expression and clinicopathologic factors was evaluated using the χ^2 tests, and a P value less than 0.05 was considered significant. Univariate and multivariate survival analyses were performed to evaluate the prognostic significance of CD10 expression and the effect of other factors, such as age, tumor size, axillary lymph-node status, clinical stage, and histologic grade, on the clinical outcome. Briefly, the Kaplan-Meier method was applied to estimate survival probabilities. The logrank test was used for the univariate analysis to assess the statistical differences between the categories of each prognostic factor. Cox's proportional hazards regression model was applied to the multivariate analysis to assess the relationship between each prognostic factor and clinical outcome adjusted for the possible confounding effect of all other factors included in the same model. The statistical significance of each model and each factor was evaluated using the likelihood ratio test. Asymptotic standard errors of coefficients were used to calculate 95% confidence intervals (95% CI) for hazard ratios. All statistical significance levels (P value) were two-tailed. Survival data were analyzed using the SAS statistical package (Stat View 5.0, SAS Institute Inc., Cary, N.C.).

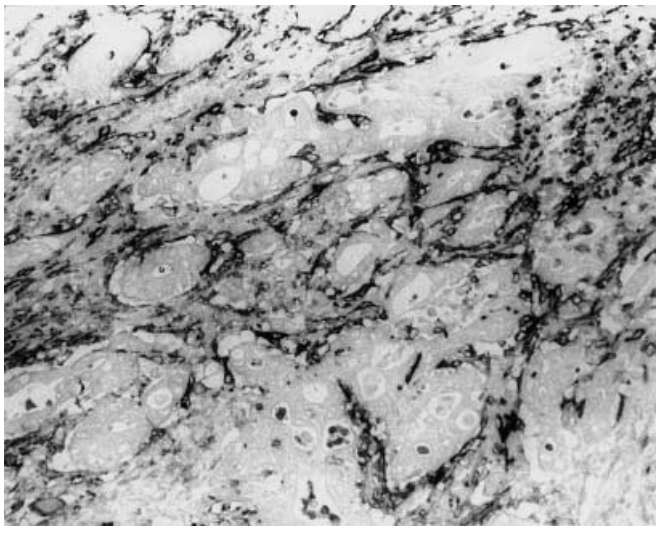

Fig. 1 Expression of CD10 in stromal cells within invasive ductal carcinoma tissue. CD10 is expressed in the stromal cells around the invasive ductal carcinoma cells. The intensity of positive CD10 staining is stronger in the areas of stroma close to cancer cells. Immunohistochemistry of CD10 (×400)

Table 1 Association between clinicopathologic factors and stromal cell staining of CD10

	No.	CD10		*P* value
		+	–	
Age				
<40 years	17	3 (15%)	14 (16%)	0.950
≥40 years	93	17 (85%)	76 (84%)	
Tumor size				
<5 cm	86	16 (80%)	70 (78%)	0.826
≥5 cm	24	4 (20%)	20 (22%)	
Axillary lymph-node status				
Metastasis	60	15 (75%)	45 (50%)	0.038
No metastasis	50	5 (25%)	45 (50%)	
Clinical stage				
1	27	4 (20%)	23 (26%)	0.896
2a	31	5 (25%)	26 (29%)	
2b	33	7 (35%)	26 (29%)	
3a	19	4 (20%)	15 (17%)	
Histologic grade				
1	4	0 (0%)	4 (4%)	0.488
2	84	17 (85%)	67 (74%)	
3	22	3 (15%)	19 (21%)	

Results

No stromal expression of CD10 was detected in the normal breast or in 16 intraductal carcinomas, although the non-neoplastic myoepithelial cells, used as a built-in positive control in this study constantly expressed CD10. There was no expression of CD10 in ductal cells, fibroblasts, and adipose cells, except in one case in which the fibroblasts of a suture granuloma that developed after excisional biopsy stained positive for CD10. Expression of CD10 by cancer cells was not analyzed in this study.

CD10 was judged to be positive in 20 (18%) of 110 invasive ductal carcinomas. The CD10-positive stromal cells were distributed around the cancer cells. The intensity of positive CD10 staining was stronger in the areas of stroma close to cancer cells (Fig. 1). Of the 20 CD10-positive cases, 15 (75%) were associated with axillary lymph-node metastasis. CD10-positive stromal cells

Table 2 Frequency of tumor recurrence and death among 110 breast cancer patients according to clinicopathologic factors

	No.	Recurrence	Death
Tumor size			
<5 cm	86	21 (24%)	14 (16%)
≥5 cm	24	6 (25%)	5 (21%)
Age			
<40 years	17	5 (29%)	3 (17%)
≥40 years	93	22 (24%)	16 (17%)
Axillary lymph-node status			
Metastasis	60	20 (33%)	13 (22%)
No metastasis	50	7 (14%)	6 (12%)
Clinical stage			
1	27	4 (15%)	3 (11%)
2a	31	6 (19%)	5 (16%)
2b	33	10 (30%)	5 (15%)
3a	19	7 (37%)	6 (32%)
Histologic grade			
1	4	0 (0%)	0 (0%)
2	84	20 (24%)	15 (18%)
3	22	7 (32%)	4 (18%)
CD10			
+	20	11 (55%)	8 (40%)
–	90	16 (18%)	11 (12%)

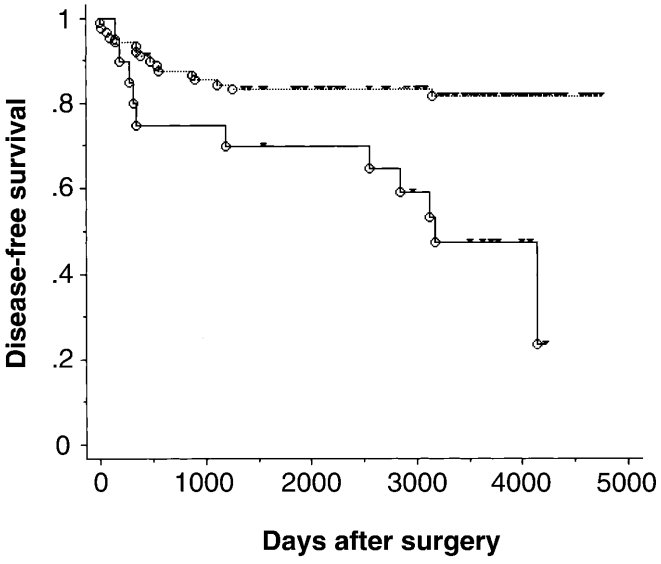

Fig. 2 Disease-free survival curves for 110 patients with invasive ductal breast carcinoma according to whether the stromal cell was CD10 positive. The disease-free survival curve in the cases with CD10-positive stroma is represented by the *solid line*, and the survival curve for patients with CD10-negative stroma by the *dotted line*. A significant difference between the two curves was demonstrated using the logrank method (P=0.0008)

Table 3 Univariate and multivariate analyses of the prognostic value of tumor size, age, lymph-node status, histologic grade, clinical stage, and stromal CD10 for disease-free survival. Results of the univarite analysis were estimated using the logrank test. *CI* confidence interval

Factor	Univariate *P*	Multivariate		
		Hazard rate	95%CI	*P*
Tumor size, <5 cm vs ≥5 cm	0.9728			
Age, <40 years vs ≥40 years	0.6398			
Lymph-node status, positive vs negative	0.0318	1.946	0.838–4.518	0.1213
Histologic grade, grades 1 & 2 vs grade 3	0.1613			
Clinical stage, stage 3a vs stages 1 & 2a & 2b	0.1947			
CD10, positive vs negative	0.0008	3.069	1.408–6.693	0.0048

Table 4 Association between outcome and stromal staining of CD10 in 60 node-positive patients

	No.	CD10		Logrank test
		+	–	
Recurrence	20	10 (67%)	10 (22%)	0.0028
No recurrence	40	5 (33%)	35 (78%)	
Dead	13	7 (47%)	6 (13%)	0.0042
Alive	47	8 (53%)	39 (87%)	

were present in two metastatic lymph nodes examined immunohistochemically. The rate of metastasis by CD10-negative tumors was 50%, and the difference between CD10-positive and CD10-negative tumors was significant (P=0.038). No significant correlations were found between CD10 positivity and other clinicopathologic factors, such as the age, tumor size, clinical stage, or histologic grade (Table 1).

Table 2 lists the frequency of tumor recurrence and death in 110 breast cancer patients according to clinicopathologic factors. Among the 20 CD10-positive cases, 11 (55%) patients developed recurrent disease, and eight (40%) died of their disease. In the CD10-negative cases, however, 16 of 90 (18%) patients experienced recurrence, and 11 (12%) patients died. Figure 2 shows the Kaplan-Meier disease-free survival curves for patients with tumors having CD10-positive stromal cells and without CD10-positive stromal cells, and the difference was significant (P=0.0008). A significant difference in disease-free survival curves was observed between the cases with positive and negative axillary lymph nodes (P=0.0318), according to the results of univariate analyses estimated by the logrank test, but other factors had no affect on the disease-free survival curves (Table 3). Among the 60 patients with lymph-node metastasis, a shorter metastasis-free interval was found in patients whose tumor contained CD10-positive stromal cells (P=0.0028; Table 4). Although there was a difference in survival in the 50 patients without lymph-node metastasis, according to whether their tumors contained CD10-positive stroma, it did not reach statistical significance

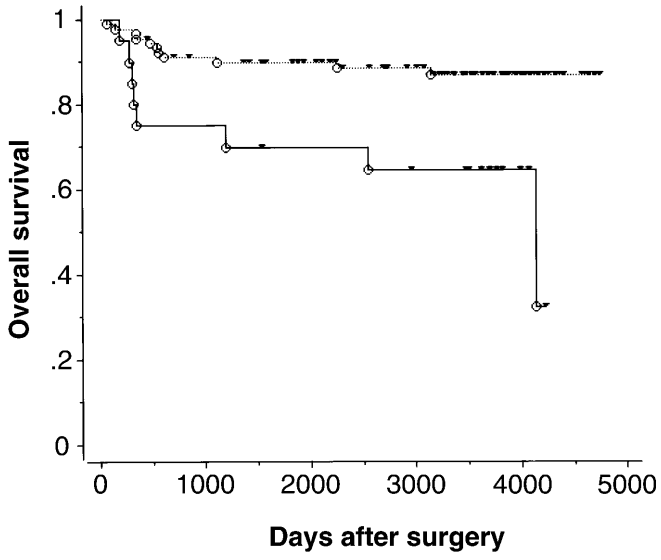

Fig. 3 Overall survival curves for 110 patients with invasive ductal breast carcinoma according to whether the stroma was CD10 positive. The overall survival curve for patients with CD10-positive stroma is represented by the *solid line*, and the survival curve for the patients with CD10-negative stroma by the *dotted line*. The difference was significant using the logrank method (P=0.0021)

Table 5 Association between outcome and stromal staining of CD10 in 50 node-negative patients

	No.	CD10		Logrank test
		+	–	
Recurrence	7	1 (20%)	6 (13%)	0.6821
No recurrence	43	4 (80%)	39 (87%)	
Dead	6	1 (20%)	5 (11%)	0.4557
Alive	44	4 (80%)	40 (89%)	

Table 6 Univariate analysis of the prognostic value of tumor size, age, lymph-node status, histologic grade, clinical stage, and stromal CD10 for overall survival. Results of univariate analyses were estimated using the logrank test

Factor	Univariate P
Tumor size, <5 cm vs ≥5 cm	0.6133
Age, <40 years vs ≥40 years	0.9604
Lymph-node status, positive vs negative	0.2265
Histologic grade, grades 1 & 2 vs grade 3	0.5624
Clinical stage, stage 3a vs stages 1 & 2a & 2b	0.0860
CD10, positive vs negative	0.0021

because a smaller number of tumors unassociated with lymph-node metastasis contained CD10-positive stromal cells, and the numbers were not sufficient to reach significance (Table 5). Multivariate analysis, including lymph-node status and stromal CD10 expressions, was performed in order to identify the independent factors affecting patient outcome, and the results showed that stromal CD10 expression was the only significant prognostic value for disease-free survival (P=0.0059; Table 3).

A significant difference was also found between the overall survival curves of patients with tumors having a CD10-positive stroma and those that did not (P=0.0021; Fig. 3). Table 6 shows that CD10 was the only significant prognostic valuable for overall survival in the univariate analysis, and that none of the other characteristics were significant.

Discussion

Proliferation of stromal cells is commonly seen when cancer cells invade and metastasize. The invasive and/or metastatic potential of several types of cancer cells is regulated by interactions with stromal cells, which involve stimulatory and inhibitory factors that regulate such functions as cellular adhesion, migration, and gene expression [6, 21, 23]. Abundant stromal cells or formation of fibrotic focus is a predictor of clinical aggressiveness [12]. Although the proliferation of stromal cells is thought to be induced by the cancer cells, the morphological phenotype distinguishing cancer-specific stromal proliferation from normal mesenchymal cells has not been studied extensively. We immunohistochemically demonstrated that CD10 is expressed by the stromal cells within the area of invasive ductal carcinoma, but not in the stromal cells of normal breast or non-invasive carcinoma. The fact that CD10-positive stromal cells are frequently seen at the invasive front suggests that tumor-stromal interaction exists between breast cancer cells and CD10-positive stromal cells. Because CD10 belongs to the group of metalloprotease family, CD10 may be induced by the cancer cells through soluble factors similar to other members of metalloprotease family. CD10-positive stromal cells were also detected in the metastatic lymph nodes, and significantly more frequent nodal involvement was found in carcinomas with CD10-positive stromal cells. We believe that expression of CD10 by stromal cells is tumor specific and that it facilitates the invasion and metastasis of breast carcinoma.

Prognostically, stromal CD10 expression is a new and strong predictor of tumor recurrence and death. Cox's proportional hazards regression model revealed that stromal CD10 expression had superior predictive power for predicting the outcome of the patients than lymph-node status, tumor size, histologic grade, or clinical stage. Although other independent retrospective and prospective studies will be necessary before clinical application, our data strongly suggest that stromal CD10 expression is closely linked to the aggressive biological behaviors including invasion and metastasis of breast carcinoma.

The question of how CD10-positive stromal cells increase the aggressiveness of breast carcinoma remains completely unresolved. Since CD10 is structurally similar to matrix metalloproteinase and stromelysin, it may

create a microenvironment that facilitates cancer cell invasion and/or metastasis [5, 22]. In normal bone marrow, CD10-positive stromal cells induce preB cells and myeloblasts to differentiate into B-cell lineage and to accelerate cell proliferation and cell motility [17, 15]. CD10-positive stromal cells in breast cancer may also interact with cancer cells to accelerate the cell cycle and to activate cell locomotion.

Finally, our data may be applied to new cancer therapy that blocks the induction of CD10-positive stromal cells in breast cancer tissue. This approach may reduce the role of CD10-positive stromal cells, which accelerate tumor aggressiveness. Further studies on the molecular basis of CD10 expression in stromal/cancer interaction will be necessary to envisage new therapeutic strategies.

Acknowledgments We acknowledge the cooperation of all those pathologists and clinicians who have contributed specimens and follow-up information for this series. In particular, we thank Professor Yasuhisa Koyanagi, Dr. Mikihiro Kusama, Dr. Hiroshi Kaise of third division of surgery, and Dr. Hiromi Serizawa of division of surgical pathology at Tokyo Medical University. This study was supported in part by Grants in Aid for Cancer Research and for the Second-term Comprehensive Strategy for Cancer Control from the Ministry of Health, Labour and Welfare.

References

1. Armstrong K, Banerjee N, Ghilchick M, Reed MJ, Parish DC (1996) Neutral endopeptidase activity in breast cysts. Biochem Soc Trans 24:337S
2. Atherton AJ, Anbazhagan R, Monaghan P, Bartek J, Gusterson BA (1994) Immunolocalisation of cell surface peptidases in the developing human breast. Differentiation 56:101–106
3. Atherton AJ, O'Hare MJ, Buluwela L, Titley J, Monaghan P, Paterson HF, et al (1994) Ectoenzyme regulation by phenotypically distinct fibroblast sub-populations isolated from the human mammary gland. J Cell Sci 107:2931–2939
4. Avery AK, Beckstead J, Renshaw AA, Corless CL (2000) Use of antibodies to RCC and CD10 in the differential diagnosis of renal neoplasms. Am J Surg Pathol 24:203–210
5. Basset P, Wolf C, Rouyer N, Bellocq JP, Rio MC, Chambon P (1994) Stromelysin-3 in stromal tissue as a control factor in breast cancer behavior. Cancer 74:1045–1049
6. Bemis LT, Schedin P (2000) Reproductive state of rat mammary gland stroma modulates human breast cancer cell migration and invasion. Cancer Res 60:3414–3418
7. Chu P, Arber DA (2000) Paraffin-section detection of CD10 in 505 nonhematopoietic neoplasms. Frequent expression in renal cell carcinoma and endometrial stromal sarcoma. Am J Clin Pathol 113:374–382
8. Fisher ER, Redmond C, Fisher B (1980) Histologic grading of breast cancer. Pathol Annu 15:239–251
9. Frame KL, Patton K, Reed MJ, Ghilchik MW, Parish DC (1996) Angiotensin-converting enzyme and enkephalinase in human breast cyst fluid. Br J Cancer 74:807–813
10. Greaves MF, Hariri G, Newman RA, Sutherland DR, Ritter MA, Ritz J (1983) Selective expression of the common acute lymphoblastic leukemia (gp 100) antigen on immature lymphoid cells and their malignant counterparts. Blood 61:628–639
11. Gusterson BA, Monaghan P, Mahendran R, Ellis J, O'Hare MJ (1986) Identification of myoepithelial cells in human and rat breasts by anti-common acute lymphoblastic leukemia antigen antibody A12. J Natl Cancer Inst 77:343–349
12. Hasebe T, Tsuda H, Hirohashi S, Shimosato Y, Iwai M, Imoto S, et al (1996) Fibrotic focus in invasive ductal carcinoma: an indicator of high tumor aggressiveness. Jpn J Cancer Res 87:385–394
13. Kaufmann O, Flath B, Spath-Schwalbe E, Possinger K, Dietel M (1999) Immunohistochemical detection of CD10 with monoclonal antibody 56C6 on paraffin sections. Am J Clin Pathol 111:117–122
14. Koiso K, Akaza H, Ohtani M, Miyanaga N, Aoyagi K (1994) A new tumor marker for bladder cancer. Int J Urol 1:33–36
15. Makrynikola V, Bianchi A, Bradstock K, Gottlieb D, Hewson J (1994) Migration of acute lymphoblastic leukemia cells into human bone marrow stroma. Leukemia 8:1734–1743
16. Mechtersheimer G, Kruger KH, Born IA, Moller P (1990) Antigenic profile of mammary fibroadenoma and cystosarcoma phyllodes. A study using antibodies to estrogen- and progesterone receptors and to a panel of cell surface molecules. Pathol Res Pract 186:427–438
17. Moreau I, Duvert V, Caux C, Galmiche MC, Charbord P, Banchereau J, et al (1993) Myofibroblastic stromal cells isolated from human bone marrow induce the proliferation of both early myeloid and B-lymphoid cells. Blood 82:2396–2405
18. Mumford RA, Pierzchala PA, Strauss AW, Zimmerman M (1981) Purification of a membrane-bound metalloendopeptidase from porcine kidney that degrades peptide hormones. Proc Natl Acad Sci U S A 78:6623–6627
19. Patey G, De La Baume S, Schwartz JC, Gros C, Roques B, Fournie-Zaluski MC, et al (1981) Selective protection of methionine enkephalin released from brain slices by enkephalinase inhibition. Science 212:1153-1155
20. Shipp MA, Vijayaraghavan J, Schmidt EV, Masteller EL, D'Adamio L, Hersh LB, et al (1989) Common acute lymphoblastic leukemia antigen (CALLA) is active neutral endopeptidase 24.11 ("enkephalinase"): direct evidence by DNA transfection analysis. Proc Natl Acad Sci U S A 86:297-301
21. Sternlicht MD, Lochter A, Sympson CJ, Huey B, Rougier JP, Gray JW, et al (1999) The stromal proteinase MMP3/stromelysin-1 promotes mammary carcinogenesis. Cell 98:137-146
22. Talvensaari-Mattila A, Paakko P, Hoyhtya M, Blanco-Sequeiros G, Turpeenniemi-Hujanen T (1998) Matrix metalloproteinase-2 immunoreactive protein: a marker of aggressiveness in breast carcinoma. Cancer 83:1153-1162
23. Tran NL, Nagle RB, Cress AE, Heimark RL (1999) N-Cadherin expression in human prostate carcinoma cell lines. An epithelial-mesenchymal transformation mediating adhesion with stromal cells. Am J Pathol 155:787-798

Virchows Arch (2002) 440:594–597
DOI 10.1007/s00428-002-0616-y

ORGINAL ARTICLE

Jutta Renkonen · Henrik Wolff · Timo Paavonen

Expression of cyclo-oxygenase-2 in human tongue carcinoma and its precursor lesions

Received: 4 September 2001 / Accepted: 9 January 2002 / Published online: 21 February 2002
© Springer-Verlag 2002

Abstract The expression of Cox-2 protein was studied by immunohistochemistry in normal oral mucosa and in mucosa with various lesions of oral leukoplakia, including hyperplasia and dysplasia of squamous epithelium and frank invasive squamous carcinoma. A gradient of Cox-2 staining was found: the expression of Cox-2 was lowest in normal epithelium, somewhat increased in hyperplastic epithelium, further increased in dysplastic epithelium, and highest in invasive squamous cell carcinomas. The presence of Cox-2 in squamous cell carcinomas of the oral mucosa and its precursor lesions indicate that Cox-2 could participate in the carcinogenic process of these oral malignancies.

Keywords Cyclo-oxygenase-2 · Oral dysplasia · Oral carcinoma · Carcinogenesis · Immunohistochemistry · Leukoplakia

Introduction

Idiopathic leukoplakia is a clinical term which includes hyperplastic, dysplastic, and carcinomatous changes, usually related to the use of tobacco [24, 27]. Some leukoplakias are known to develop into squamous carcinoma. Rates of transformation vary considerably from study to study [14, 16]. Oral cavity cancer account for 4% at all malignancies in men and 2% in women. Practically all cancers of oral cavity are squamous cell (epidermoid) carcinomas and 16% of the tumors in oral cavity are tongue carcinomas. Oral cavity cancers have been associated with tobacco and alcohol. Most cases occur in men over the age of 50 years [16]. Intraoral squamous cell carcinomas are usually moderately or poorly differentiated. Those located at the base of the tongue tend to be particularly undifferentiated and solid. The epithelium adjacent to the invasive tumor often shows carcinoma in situ or dysplastic changes. The main prognostic factors in carcinomas of the oral cavity are the stage of the disease, location, and microscopic grading. The overall 5-year survival rates are about 60% for tumors of the anterior tongue and 40% of the posterior tongue.

Several epidemiological studies have shown that prolonged use of aspirin is associated with reduced risk of colorectal cancer [5, 22]. In addition, a large prospective mortality study found the use of aspirin to be associated with reduced risk of esophagus, gastric, and colorectal cancers but not of those outside the gastrointestinal tract [22]. However, more recent studies suggest that aspirin also reduces the incidence of lung and breast cancers [7, 18]. The best known target of nonsteroid anti-inflammatory drugs, including aspirin, is cyclo-oxygenase (Cox), the rate-limiting enzyme in the conversion of arachidonic acid to prostanoids (Cox is also called prostaglandin endoperoxide synthase). Two Cox genes have been cloned (Cox-1 and Cox-2) that share over 60% identity at amino acid level and have similar enzymatic activities [8, 20, 25]. Cox-1 is considered a housekeeping gene, and prostanoids synthesized via the Cox-1 pathway are thought to be responsible for cytoprotection of the stomach, for vasodilation in the kidney, and for production of a proaggregatory prostanoid, thromboxane, by platelets. In contrast, Cox-2 is an inducible immediate-early gene, and its pathophysiological role has been connected to inflam-

Financial support was received from the State Subsidy of the Helsinki University Central Hospital and from the Cancer Organizations of Finland.

J. Renkonen
Transplantation Laboratory,
Haartman Institute and Helsinki University Central Hospital,
P.O. Box 21, Haartmaninkatu 3, 00014 Helsinki, Finland

J. Renkonen · T. Paavonen (✉)
Department of Pathology,
Haartman Institute and Helsinki University Central Hospital,
P.O. Box 400, Haartmaninkatu 3, 00029 Helsinki, Finland
e-mail: paavonen@helsinki.fi
Tel.: +358-9-19126333, Fax: +358-9-19126329

H. Wolff
Pathology Laboratory, Finnish Institute of Occupational Health,
Topeliuksenkatu 41, 00250 Helsinki, Finland

H. Wolff
Department of Pathology, Kymenlaakso Central Hospital,
Kotkantie 41, 48210 Kotka, Finland

mation, ovulation, and carcinogenesis, i.e., cellular growth and differentiation. Cox-2 expression seems to be especially prominent in gastrointestinal tumors [4, 10, 15, 17, 21], and it plays an important role in the development of intestinal adenomas and carcinomas in experimental animal models [6]. However, expression of Cox-2 has not been extensively studied outside the gastrointestinal tract, although recent studies suggest that it is present in skin, breast, and lung carcinomas [1, 9, 11, 26]. Cox-2 expression is also increased in squamous carcinoma of the esophagus, nasopharynx, and skin [2, 13, 19, 28]. We have now studied Cox-2 expression in human tongue carcinomas and in precursor lesions leading to this malignancy.

Materials and methods

Patient samples

Human tongue tissue samples, removed surgically because of cancer, were collected from the archives of Department of Pathology in Helsinki University Central Hospital from the years 1987–1988 and 1990–1992, and they were fixed in 10% neutral-buffered formalin and then embedded in paraffin. We had 38 normal tongue tissue samples, 41 tongue tissue samples with hyperplastic epithelium, 23 dysplastic tongue tissue samples, and 73 tongue carcinoma samples. All cancers were primary tongue tumors, and they were classified by the same pathologist according to WHO typing (T.P.) [12].

Immunohistochemistry

Tissue samples were embedded in paraffin, sectioned (4–5 μm), deparaffinized, and microwaved for 4×5min in 0.01 M Na-citrate buffer (pH 6.0). The slides were first immersed in 1.6% hydrogen peroxide in methanol for 30 min and then in blocking solution (0.01 M Tris, 0.1 M $MgCl_2$, 0.5% Tween-20, 1% bovine serum albumin, 5% normal goat serum) for 1 h to block endogenous peroxidase activity and unspecific binding sites, respectively. Immunostaining was performed with a rabbit polyclonal immunoglobulin G against a mouse Cox-2 peptide (Cayman Chemical, Ann Arbor, Mich., USA) in a dilution of 1:600 in the blocking solution at 4°C overnight. The sections were thereafter treated with biotinylated secondary antibodies in a dilution of 1:250 (Vectastain ABC kit, Vector Laboratories, Burlingame, Calif., USA), and antibody binding sites were finally visualized by avidin-biotin peroxidase complex solution (ABComplex, Vectastain, Vector Laboratories) and 3,3′-diaminobenzidine. As a control nonspecific rabbit IgG (Santa Cruz Biotechonology, Santa Cruz, Calif., USA) at concentration corresponding to that of the Cox-2 antibody (1:200) was used to stain all sections using an identical protocol.

Evaluation

The tongue samples were divided into four groups, namely normal, hyperplasia, dysplasia, and cancer by J.R. and T.P. The epithelial Cox-2 staining was quantitated on a scale from 0 (none) to 4 (very high staining) in consensus of two investigators (J.R. and T.P.). The final staining score took into account both the intensity of the staining and the number of positive cells according to the following scheme: both were quantitated from 1 to 4 and the sum of 1 or 2 received the final score 1 and the sum of 3 or 4 the final score of 2, etc.

Results

To investigate the expression of Cox-2 protein in benign and malignant tongue epithelium we used immunohistochemistry on a large number of patient samples. Our material was formalin-fixed and paraffin-embedded tissues, normal tongue epithelium (n=38), hyperplastic epithelium (n=41), dysplastic epithelium (n=23), and the squamous cell carcinoma epithelium (n=73). The degree of staining was semiquantitated with a scale from negative (0) to strong positivity (4).

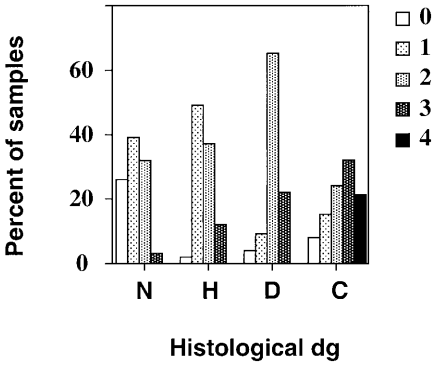

Fig. 1 The distribution of immunohistochemical epithelial Cox-2 expression in tongue samples as determined by degree of staining with a score from negative (*0*) to strong positivity (*4*). Normal epithelium (*N*), hyperplastic epithelium (*H*), dysplastic epithelium (*D*), invasive carcinoma (*C*)

Figure 1 presents the distribution of epithelial Cox-2 expression in different types of epithelial changes as determined by degree of staining with a score from negative (0) to strong positivity (4). The normal lesions do not express substantial quantities of Cox-2 and over 25% of the samples are totally negative. The level of Cox-2 expression increased when leukoplakias were investigated. The distribution of Cox-2 expression levels in hyperplastic samples was greater than normal. When the lesions studied were of dysplastic epithelium the expression of Cox-2 was further increased. No significant differences were between low and severe dysplasia, although the score in severe dysplasia was higher (data not shown). The highest levels of expression were seen in invasive carcinomas. Representative immunoperoxidase stainings are shown in Fig. 2.

The mean values of the intensity of Cox-2 expression in tongue epithelium are shown in Fig. 3. The mean value of the Cox-2 staining intensity increased gradually from normal epithelium (0.97) to hyperplastic lesions (1.58) and more to dysplastic lesions (2.04). The highest mean expression was in squamous cell cancer (2.42). The difference between Cox-2 expression in the normal epithelium and that in the hyperplastic epithelium is statistically significant (P=0.0041, paired t test) and the difference between normal and dysplastic epithelium highly significant (P=0.0011), as is that between normal and cancerous epithelium (P=0.0001).

Cancer material was further divided into histological grade I (n=22), grade II (n=30), and grade III (n=21) carcinomas. The mean ±SE Cox-2 staining scores in the different grades (I, II, III) were 2.14±0.23, and 2.24±0.27, and 3.05±0.22, respectively. The differences were significant between grades I and III (P<0.01) and between grades II and III (P<0.05).

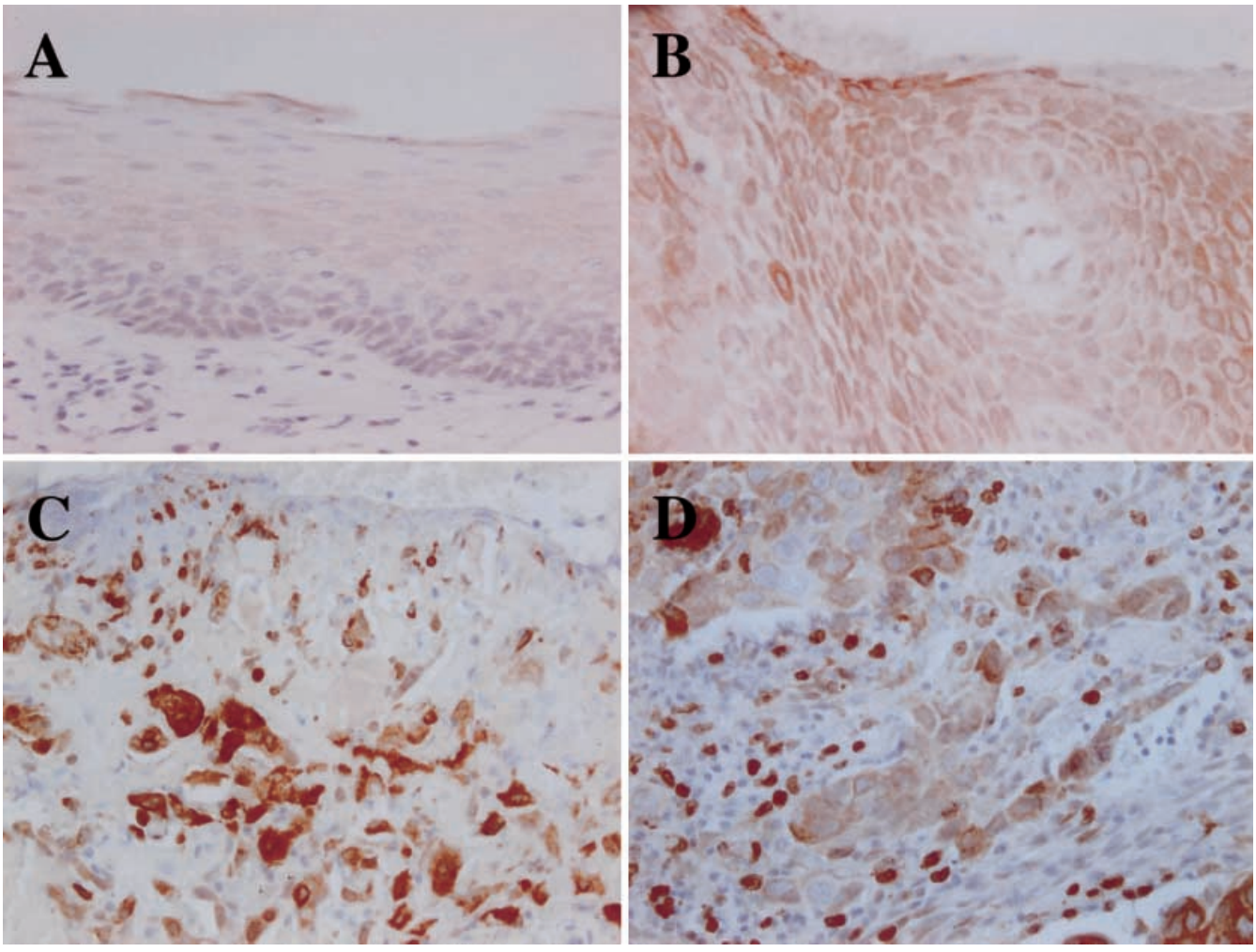

Fig. 2 Immunohistochemical Cox-2 stainings in normal (**A**), hyperplastic (**B**)„ and dysplastic tongue squamous epithelium (**C**) and in invasive tongue carcinoma (**D**). There is hardly any positivity in normal epithelium, but gradually increasing Cox-2 expression is seen during the progressive change in tongue epithelium from hyperplastic to malignant invasive carcinoma

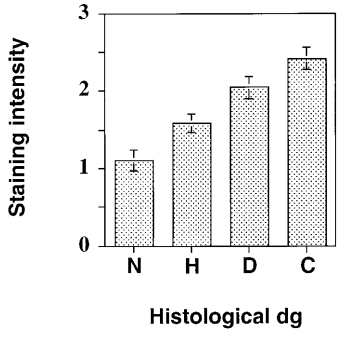

Fig. 3 The mean values of the immunohistochemical staining intensity of Cox-2 expression in tongue samples: normal epithelium (*N*), hyperplastic epithelium (*H*), dysplastic epithelium (*D*), invasive carcinoma (*C*) *Bars* mean ±SD

Discussion

We found higher levels of Cox-2 protein in malignant human tongue epithelial lesions than in benign lesions. Immunohistochemical staining of Cox-2 protein showed the lowest positivity in human normal tongue tissues. In hyperplastic tongue tissue samples we found slightly higher levels of Cox-2 expressions than in normal epithelium, but significantly higher levels in dysplastic tongue tissues. The most prominent expression of Cox-2 expression was found in invasive squamous cell carcinoma. The Cox-2 protein was localized primary in the cytoplasm of the epithelial cells. A similar pattern of Cox-2 protein localization has been shown in adenocarcinomas. Our studies indicate that the immunohistochemical expression of Cox-2 is especially prominent in malignant lesions compared to nonmalignant epithelium.

Increased Cox-2 expression is associated with the dedifferentiation of human squamous epithelium. The gradually increasing Cox-2 expression detected during the progressive change in tongue epithelium from normal to malignant invasive carcinoma via hyperplasia and dysplasia shows that the Cox-2 protein can have an important role in both the early and the later stages of squamous epithelial carcinogenesis. Similarly Shamma et al. [19] have reported that high-grade dysplasia in esopha-

gus contains significantly higher immunohistochemical staining of Cox-2 than normal epithelium.

Ristimäki et al. [15] have studied human gastric adenocarcinoma tissues and found that carcinomas contained significantly higher levels of Cox-2 than in paired gastric mucosal specimens devoid of cancer cells. In parallel to our results, they also found an elevated expression in hyperplastic gastric glands. In human colorectal cancer Tsuijii et al. [23] demonstrated that constitutive expression of Cox-2 can lead to phenotypic changes that alter the metastatic potential of colorectal cancer cells. In a recent review, Crofford et al. [3] postulated that Cox-2 is dramatically upregulated during inflammation. For example, synovial tissues in patients with rheumatoid arthritis express increased levels of Cox-2. Cox-2 is also increased in many types of human cancers, as noted above. Altogether, there is considerable evidence that inflammation or other causes of hyperplasia leads to increased Cox-2 expression, which in turn seems to have a causal relationship to cancers.

In a report on Cox-2 expression in lung cancer the most prominent expression was seen in highly developed subtypes, and the most poorly differentiated tumors lost their expression [26]. In our study the more undifferentiated carcinomas (histological grade III) had significantly stronger Cox-2 expression than grade I or II cases.

In conclusion, we report that tongue epithelial tumors and precursor lesions leading to these malignancies express Cox-2 in progressive manner toward more malignant lesions, suggesting a role for Cox-2 in the carcinogenesis of these tumors. The association of Cox 2 expression with the carcinogenic progression suggests that Cox-2 expression has a prognostic value. To our knowledge this is the first report of Cox-2 in tongue carcinomas.

Acknowledgements We thank Dr. Ari Ristimäki and Dr. Jouni Lauronen for valuable discussions.

References

1. Brueggemeier RW, Quinn AL, Parrett ML, Joarder FS, Harris RE, Robertson FM (1999) Correlation of aromatase and cyclooxygenase gene expression in human breast cancer specimens. Cancer Lett 140:27–35
2. Chan G, Boyle JO, Yang EK, Zhang F, Sacks PG, Shah JP, Edelsten D, Soslow RA, Koki AT, Woerner BM, Masferrer JL, Dannenberg AJ (1999) Cyclooxygenase-2 expression is upregulated in squamous cell carcinoma of the head and neck. Anticancer Res 59:991–994
3. Crofford LJ, Lipsky PE, Brooks P, Abramson SB, Simon LS, van de Putte LB (2000) Basic biology and clinical application of specific cyclooxygenase-2 inhibitors. Arthritis Rheum 43:4–13
4. Eberhart CE, Coffey RJ, Radhika A, Giardiello FM, Ferrenbach S, DuBois RN (1994) Up-regulation of cyclooxygenase 2 gene expression in human colorectal adenomas and adenocarcinomas. Gastroenterology 107:1183–1188
5. Giardiello FM, Offerhaus GJ, DuBois RN (1995) The role of nonsteroidal anti-inflammatory drugs in colorectal cancer prevention. Eur J Cancer 31A:1071–1076
6. Gupta RA, DuBois RN (1998) Aspirin, NSAIDs, and colon cancer prevention: mechanisms? Gastroenterology 114:1095–1098
7. Harris RE, Namboodiri KK, Farrar WB (1996) Nonsteroidal anti-inflammatory drugs and breast cancer. Epidemiology 7:203–205
8. Herschman HR (1996) Prostaglandin synthase 2. Biochim Biophys Acta 1299:125–140
9. Huang M, Stolina M, Sharma S, Mao JT, Zhu L, Miller PW, Wollman J, Herschman H, Dubinett SM (1998) Non-small cell lung cancer cyclooxygenase-2-dependent regulation of cytokine balance in lymphocytes and macrophages: up-regulation of interleukin 10 and down-regulation of interleukin 12 production. Cancer Res 58:1208–1216
10. Kargman SL, O'Neill GP, Vickers PJ, Evans JF, Mancini JA, Jothy S (1995) Expression of prostaglandin G/H synthase-1 and -2 protein in human colon cancer. Cancer Res 55:2556–2559
11. Leong J, Hughes-Fulford M, Rakhlin N, Habib A, Maclouf J, Goldyne ME (1996) Cyclooxygenases in human and mouse skin and cultured human keratinocytes: association of COX-2 expression with human keratinocyte differentiation. Exp Cell Res 224:79–87
12. Pindborg J, Reichart P, Smith C (1997) (WHO) World Health Organization. Histological typing of cancer and precancer of the oral mucosa. Springer, Berlin Heidelberg New York
13. Ratnasinghe D, Tangrea J, Roth MJ, Dawsey S, Hu N, Anver M, Wang QH, Taylor PR (1999) Expression of cyclooxygenase-2 in human squamous cell carcinoma of the esophagus; an immunohistochemical survey. Anticancer Res 19:171–174
14. Regezi JA, Sciubba J (1993) Oral pathology: clinical-pathologic correlations, 2nd edn. Saunders, Philadelphia
15. Ristimaki A, Honkanen N, Jankala H, Sipponen P, Harkonen M (1997) Expression of cyclooxygenase-2 in human gastric carcinoma. Cancer Res 57:1276–1280
16. Rosai J (1999) Ackerman's surgical pathology, 8th edn. Mosby, St. Louis
17. Sano H, Kawahito Y, Wilder RL, Hashiramoto A, Mukai S, Asai K, Kimura S, Kato H, Kondo M, Hla T (1995) Expression of cyclooxygenase-1 and -2 in human colorectal cancer. Cancer Res 55:3785–3789
18. Schreinemachers DM, Everson RB (1994) Aspirin use and lung, colon, and breast cancer incidence in a prospective study. Epidemiology 5:138–146
19. Shamma A, Yamamoto H, Doki Y, Okami J, Kondo M, Fujiwara Y, Yano M, Inoue M, Matsuura N, Shiozaki H, Monden M (2000) Up-regulation of cyclo-oxygenase-2 in squamous carcinogenesis of the esophagus. Clin Cancer Res 6:1229–1238
20. Smith WL, Garavito RM, DeWitt DL (1996) Prostaglandin endoperoxide H synthases (cyclooxygenases)-1 and -2. J Biol Chem 271:33157–33160
21. Soydan AS, Gaffen JD, Weech PK, Tremblay NM, Kargman S, O'Neill G, Bennett A, Tavares IA (1997) Cytosolic phospholipase A2, cyclo-oxygenases and arachidonate in human stomach tumours. Eur J Cancer 33:1508–1512
22. Thun MJ (1994) Aspirin, NSAIDs, and digestive tract cancers. Cancer Metastasis Rev 13:269–277
23. Tsujii M, Kawano S, DuBois RN (1997) Cyclooxygenase-2 expression in human colon cancer cells increases metastatic potential. Proc Natl Acad Sci U S A 94:3336–3340
24. Waal I van der, Schepman KP, van der Meij EH, Smeele LE (1997) Oral leukoplakia: a clinicopathological review. Oral Oncol 33:291–301
25. Williams CS, Luongo C, Radhika A, Zhang T, Lamps LW, Nanney LB, Beauchamp RD, DuBois RN (1996) Elevated cyclooxygenase-2 levels in Min mouse adenomas. Gastroenterology 111:1134–1140
26. Wolff H, Saukkonen K, Anttila S, Karjalainen A, Vainio H, Ristimäki A (1999) Expreession of cyclooxygenase-2 in human lung carcinoma. Cancer Res 99:111–222
27. Wright JM (1994) Oral precancerous lesions and conditions. Semin Dermatol 13:125–131
28. Zimmermann KC, Sarbia M, Weber AA, Borchard F, Gabbert HE, Schror K (1999) Cyclooxygenase-2 expression in human esophageal carcinoma. Cancer Res 59:198–204

Virchows Arch (2002) 440:598–603
DOI 10.1007/s00428-002-0629-6

ORIGINAL ARTICLE

Arafumi Maeshima · Michiie Sakamoto
Setsuo Hirohashi

Mixed mucinous-type and non-mucinous-type adenocarcinoma of the lung: immunohistochemical examination and K-*ras* gene mutation

Received: 13 August 2001 / Accepted: 6 February 2002 / Published online: 26 April 2002
© Springer-Verlag 2002

Abstract Mucinous-type adenocarcinoma and non-mucinous-type adenocarcinoma are known to be the representative histological subtypes of bronchioloalveolar carcinoma. Mucinous-type adenocarcinoma is also known to carry abnormalities of the K-*ras* gene at high frequency. However, the mixed subtype of the both mucinous-type and non-mucinous-type adenocarcinoma (mixed-type) has not been analyzed in detail, although its existence has been reported in a few papers. In this study we carried out immunohistochemical and molecular biological analyses of 15 examples of the mixed-type, in comparison with 11 cases of mucinous-type and 21 cases of non-mucinous-type adenocarcinoma. Immunohistochemically, lysozyme – one of the specific markers of mucinous-type adenocarcinoma – was not stained in the mucinous component of the mixed-type. K-*ras* gene mutations were detected only in mucinous-type (73%) and non-mucinous-type (10%) adenocarcinomas and not in either the mucinous or non-mucinous component of the mixed-type (0%). Therefore, although mixed-type adenocarcinomas consist of tumor cells showing both mucinous and non-mucinous morphology, the mucinous component of this type differs from mucinous-type adenocarcinoma in terms of immunohistochemical features and K-*ras* gene alteration.

Keywords Lung adenocarcinoma · Mucinous type · Non-mucinous type · Lysozyme · K-*ras* gene

Introduction

Lung adenocarcinoma presents various histological appearances. The World Health Organization (WHO) classification [30] divides conventional adenocarcinomas into five major subtypes according to their growth pattern and the structure of the tumor nest: bronchioloalveolar carcinoma (BAC), composed of tumor cells merely replacing the alveolar wall without stromal invasion; papillary adenocarcinoma, composed of predominantly invasive papillary components; acinar adenocarcinoma, showing tubule formation; solid adenocarcinoma with mucin formation, composed of solid component and mucus-producing cells; adenocarcinoma with mixed subtypes show a mixture of the above histological subtypes. According to this classification, non-mucinous-type adenocarcinoma is BAC and composed of mixed Clara-cell-like and type-II-pneumocyte-like tumor cells. Mucinous-type adenocarcinoma is also BAC, but is composed of tall columnar cells, similar to bronchial goblet cells, showing marked mucin production [24]. In mucinous-type adenocarcinoma, the K-*ras* gene is frequently mutated [9, 14, 15, 31] and lysozyme is expressed (unlike other cytological subtypes of lung adenocarcinoma) [8, 15, 18, 19, 24]. Mixed mucinous-type and non-mucinous-type (mixed-type) adenocarcinoma is classified as BAC. To our knowledge, there have been few studies of this mixed-type adenocarcinoma: only five cases have been reported by Manning et al. [17] and two cases by Clayton [5]. In this paper, we have evaluated 15 cases of mixed-type adenocarcinoma and compared these with mucinous-type and non-mucinous-type adenocarcinoma.

A. Maeshima · M. Sakamoto · S. Hirohashi (✉)
Pathology Division, National Cancer Center Research Institute,
5-1-1, Tsukiji, Chuo-ku, Tokyo 104-0045, Japan
e-mail: shirohas@ncc.go.jp
Tel.: +81-3-35422511, Fax: +81-3-32482463

Materials and methods

Forty-seven lung adenocarcinoma specimens were collected from surgically resected cases at the National Cancer Center Hospital, Tokyo, between 1980 and 1993. These samples comprised mixed-type adenocarcinoma (Fig. 1a–c, 15 cases), mucinous-type adenocarcinoma (Fig. 1d, 11 cases), and non-mucinous-type adenocarcinoma (Fig. 1e, 21 cases). The specimens were histologically subclassified according to the WHO classification [30].

The ages of the 15 patients with mixed-type adenocarcinoma ranged from 45 years to 80 years (mean 62 years), with ten females and five males. The tumor size of the mixed-type adenocarcinomas ranged from 1.8 cm to 5.0 cm (mean 3.3 cm). Although mixed-type adenocarcinomas are classified as BAC according to the WHO, in this study only one mixed-type adenocarcinoma was diagnosed as BAC, and the remaining 14 cases were categorized

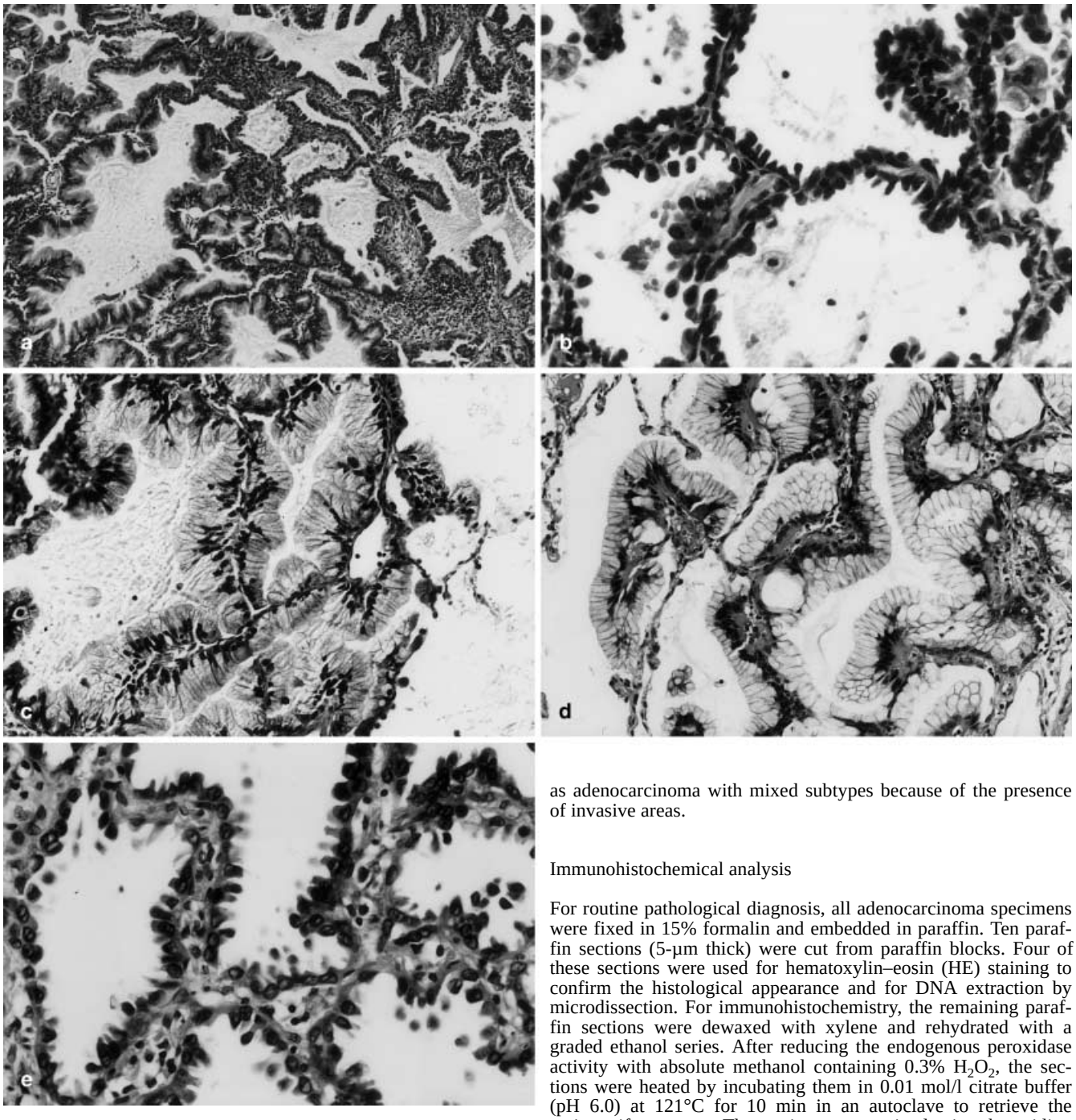

Fig. 1 Histology of mixed-type adenocarcinoma (**a–c**), mucinous-type adenocarcinoma (**d**), and non-mucinous-type adenocarcinoma (**e**). **a** The mucinous (*left*) and the non-mucinous (*right*) components are adjacent (low-power view). **b** The non-mucinous component with a bronchioloalveolar growth pattern (high-power view). **c** The mucinous component with a bronchioloalveolar and papillary growth pattern (high-power view). **d** A mucinous-type adenocarcinoma showing tall columnar tumor cells with cytoplasmic mucin lining the alveolar walls. **e** A non-mucinous-type adenocarcinoma, peg-shaped with low columnar tumor cells growing along the alveolar walls

as adenocarcinoma with mixed subtypes because of the presence of invasive areas.

Immunohistochemical analysis

For routine pathological diagnosis, all adenocarcinoma specimens were fixed in 15% formalin and embedded in paraffin. Ten paraffin sections (5-µm thick) were cut from paraffin blocks. Four of these sections were used for hematoxylin–eosin (HE) staining to confirm the histological appearance and for DNA extraction by microdissection. For immunohistochemistry, the remaining paraffin sections were dewaxed with xylene and rehydrated with a graded ethanol series. After reducing the endogenous peroxidase activity with absolute methanol containing 0.3% H_2O_2, the sections were heated by incubating them in 0.01 mol/l citrate buffer (pH 6.0) at 121°C for 10 min in an autoclave to retrieve the antigen, if necessary. The sections were stained using the avidin–biotin–peroxidase complex (ABC) method: sections were incubated overnight at 4°C with the first antibodies listed in Table 1, then the second antibody and the ABC solution were sequentially applied, each for 1 h at room temperature according to the manufacturer's instructions (Vector Laboratories, Burlingame, Calif). Finally, the sections were stained with benzidine and lightly counterstained with hematoxylin for light microscopy. Lesions with more than 10% tumor cells stained were considered positive.

Laser-capture microdissection and DNA extraction

The HE-stained slides were used for microdissection using a PixCell laser-capture microscope (LCM) with an infrared diode laser (Arcturus Engineering, Santa Clara, Calif) as previously re-

Table 1 List of the first antibodies. *CEA* carcinoembryonic antigen, *SP-A* surfactant apoprotein A, *CC-10* Clara cell 10 protein, *TTF-1* thyroid transcription factor-1, *A/C* autoclaved to retrieve antigen

Antibody	Dilution	Type	Pretreatment	Source
Lysozyme	1:1600	Polyclonal	None	Dako (Glostrup, Denmark)
CEA	1:200	Monoclonal	None	Dako
CA19-9	1:25	Monoclonal	None	Dako
SP-A (PE-10)	1:200	Monoclonal	None	Dako
CC-10 (C-20)	1:100	Polyclonal	A/C	Santa Cruz Biotechnology Inc. (Santa Cruz, Calif.)
TTF-1	ready-to-use	Monoclonal	A/C	NeoMarkers (Fremont, Calif.)

Table 2 Primer sets of exon 1 and 2 of the K-*ras* gene

Primer set	Forward	Reverse
First of exon 1	5′-ACTGGTGGAGTATTTGATAGTGTATTAACC-3′	5′-CTCATGAAAATGGTCAGAGAAACCTTTATC-3′
Second of exon 1	5′-GGCCTGCTGAAAATGACTGA-3′	5′-GTCCTGCACCAGTAATATGC-3′
First of exon 2	5′-TTTTCAGGTGCTTAGTGGCCA-3′	5′-ACAAAGAAAGCCCTCCCCAGT-3′
Second of exon 2	5′-TGTCCGTCATCTTTGGAGCAG-3′	5′-TGTACTGGTCCCTCATTGCACT-3′

Table 3 Summary of immunohistochemical studies. *CEA* carcinoembryonic antigen, *SP-A* surfactant apoprotein A

Tumor type	Lysozyme (%)	CEA (%)	CA19-9 (%)	SP-A (%)	CC-10 (%)	TTF-1 (%)
Mixed						
Mucinous component	1/15 (7)	5/15 (33)	7/15 (47)	2/15 (13)	5/15 (33)	9/15 (60)
Non-mucinous component	1/15 (7)	5/15 (33)	3/15 (20)	9/15 (60)	12/15 (80)	15/15 (100)
Mucinous	8/11 (73)	5/11 (45)	7/11 (64)	0/11 (0)	1/11 (9)	2/11 (18)
Non-mucinous	1/21 (5)	10/21 (48)	5/21 (24)	13/21 (62)	13/21 (62)	21/21 (100)

ported [3, 6, 7, 20]. Tumor cells were microdissected one sample per case in mucinous-type and non-mucinous-type adenocarcinoma, and two samples were separately extracted for the mucinous and the non-mucinous components in every mixed-type adenocarcinoma case. In all microdissected samples, about 2000 tumor cells were transferred to the film on the cap by irradiation with the laser using a spot size of 15 µm and a laser power of 25 mW for 2 ms. Tumor DNA was extracted from these cells using a QIAamp DNA miniprep kit (Qiagen, Hilden, Germany), according to the manufacturer's protocol. To increase the final DNA concentration, all samples were eluted in 100 µl nuclease-free water (Promega Corporation, Madison, Wis.).

Nested polymerase chain reaction and sequencing

To detect K-*ras* gene point mutations, we used nested polymerase chain reaction (PCR) specific for both exon 1 and exon 2, using oligonucleotide primer sets as outlined in Table 2. For the first PCR, a total volume of 20 µl contained 10 µl template DNA solution (from approximately 200 cells), 1 µM each primer, 200 µM dNTPs, 2 µl 10× Expand HF Buffer with 15 mM $MgCl_2$ and 0.52 U Expand High Fidelity PCR System enzyme mix (Roche Diagnostics, Basel, Switzerland). The mixture was incubated in a DNA Thermal Cycler (GeneAmp PCR System 9600, Perkin-Elmer Cetus, Norwalk, Conn.) for 30 cycles each at 94°C for 15 s, 58°C for 30 s, and 72°C for 1 min, after a single initial denaturation at 94°C for 2 min. The second PCR used the same conditions, with 2 µl of the first PCR mixture as template DNA. After the second PCR, 4 µl 10× Loading Buffer (Takara Shuzo Co. Ltd., Kyoto, Japan) was added to each PCR reaction, and the mixture was electrophoresed on a 3% low-melting-temperature agarose gel (NuSieve GTG agarose, FMC Bioproducts, Rockland, Me.) at 100 V for 30 min at room temperature, using a mini horizontal electrophoresis unit (Mupid-2, Cosmo Bio Co. Ltd., Tokyo, Japan). After the gel had been stained with ethidium bromide (Gibco BRL, Grand Island, N.Y.), it was examined under ultraviolet light, and any bands of the expected molecular weight were excised. This DNA was extracted from the agarose gel using a QIAquick PCR Purification Kit (Qiagen) according to the manufacturer's protocol. The purified DNA was then directly sequenced using an ABI PRISMTM 310 Genetic Analyzer (Applied Biosystems Inc., Foster, Calif.), according to the manufacturer's instructions. The complete process, from nested PCR to direct sequencing, was repeated at least twice for each sample.

Results

Immunohistochemical studies

The results of the immunohistochemical studies are shown in Table 3. Immunoreactivity for lysozyme, a good marker of mucinous-type adenocarcinoma [8, 15, 18, 19, 24], was present in many cases of mucinous-type adenocarcinoma (Fig. 2a), but was absent in almost all cases of both the mucinous (Fig. 2b) and the non-mucinous component of mixed-type and non-mucinous-type adenocarcinoma. The tumor markers carcinoembryonic antigen (CEA) and CA19-9 stained positively in 20–64% of cases of every adenocarcinoma subtype we studied. Surfactant apoprotein A (SP-A), Clara cell 10 protein (CC-10), and thyroid transcription factor-1 (TTF-1), all known characteristic markers of lung adenocarcinoma [1, 2, 11, 13, 18, 24, 25, 26, 27, 29], were all immunoreactive in many cases both of non-mucinous-type adenocarcinoma (Fig. 2c) and in the non-mucinous component

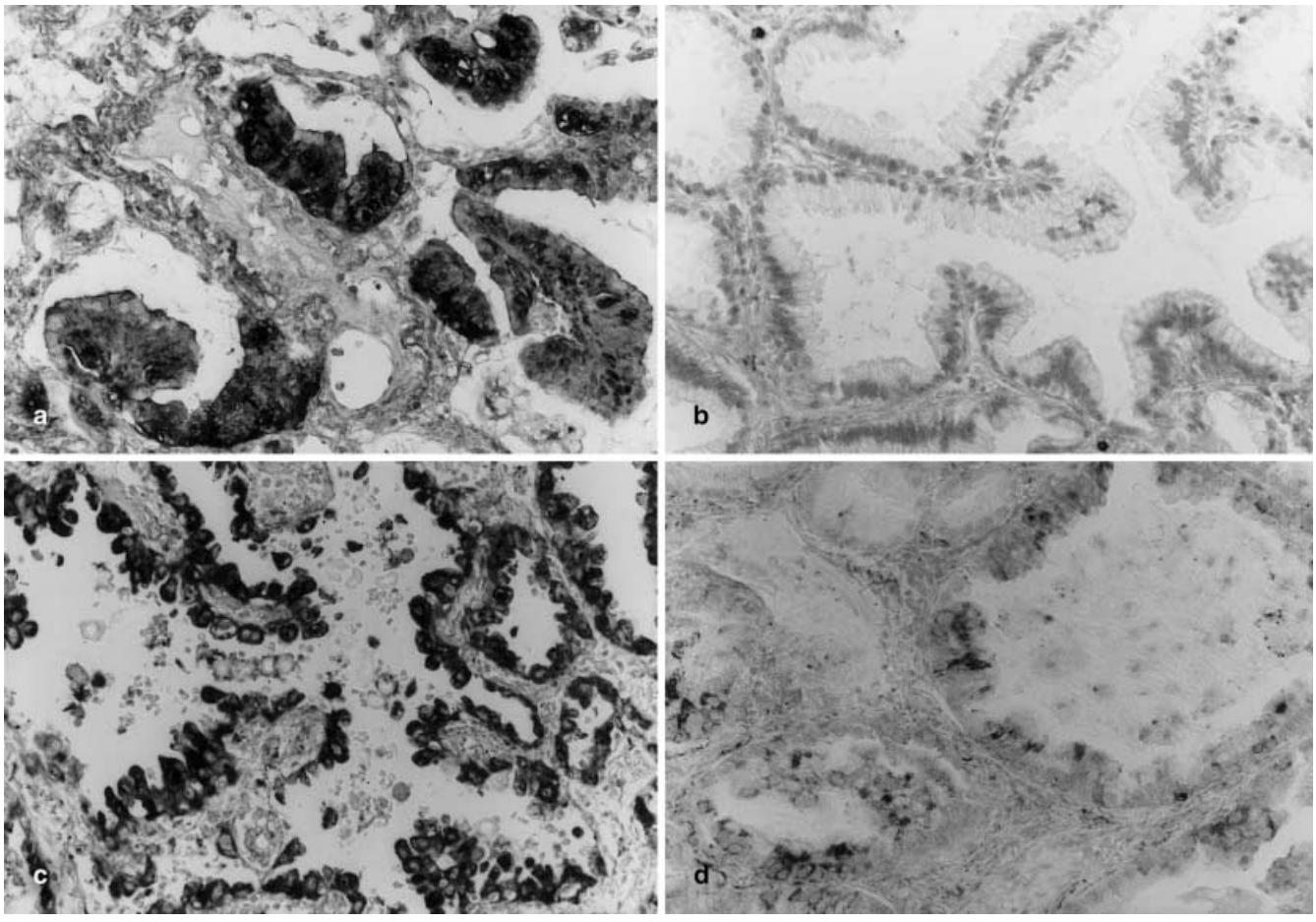

Fig. 2 Immunohistochemical staining of lysozyme (**a**, **b**) and surfactant apoprotein A (SP-A, **c**, **d**). **a** A mucinous-type adenocarcinoma is positive, and (**b**) the mucinous component of mixed-type adenocarcinoma is negative. Both the non-mucinous (**c**) and the mucinous (**d**) components of mixed-type adenocarcinoma show SP-A immunoreactivity in the cytoplasm

Table 4 Summary of molecular analysis of the K-*ras* gene

Tumor type	Exon 1	Exon 2
Mixed		
Mucinous component	0/15 (0%)	0/15 (0%)
Non-mucinous component	0/15 (0%)	0/15 (0%)
Mucinous	8/11 (73%)	0/11 (0%)
Non-mucinous	2/21 (10%)	0/21 (0%)
Total	10/47 (21%)	0/47 (0%)

of mixed-type adenocarcinoma, in some cases in the mucinous component of mixed-type adenocarcinoma (Fig. 2d), but only in very rare cases in mucinous-type adenocarcinoma.

K-ras gene mutation

The bands of nested PCR products on an agarose gel are shown in Fig. 3; the results of sequencing these bands are summarized in Table 4. *K-ras* gene mutations were detect-

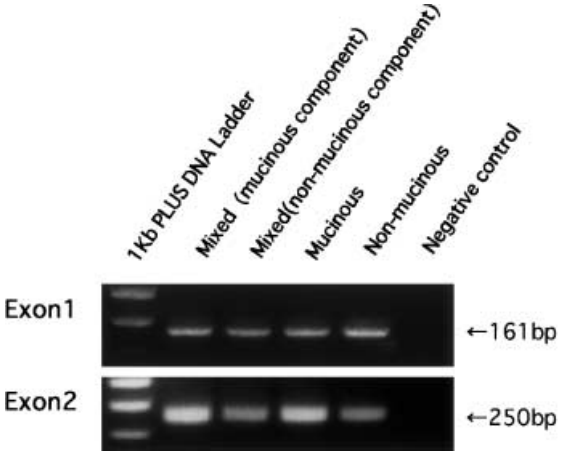

Fig. 3 Nested polymerase chain reaction of the K-*ras* gene. The *upper row* is a result of exon 1-specific polymerase chain reaction (PCR), and the *lower row* is a result of exon 2-specific PCR. The lanes sequentially show (from the left): 1 Kb PLUS DNA Ladder markers (Gibco BRL, Grand Island, N.Y.); the mucinous component of mixed-type adenocarcinoma; the non-mucinous component of mixed-type adenocarcinoma; mucinous-type adenocarcinoma; non-mucinous-type adenocarcinoma; and a negative control containing no DNA template

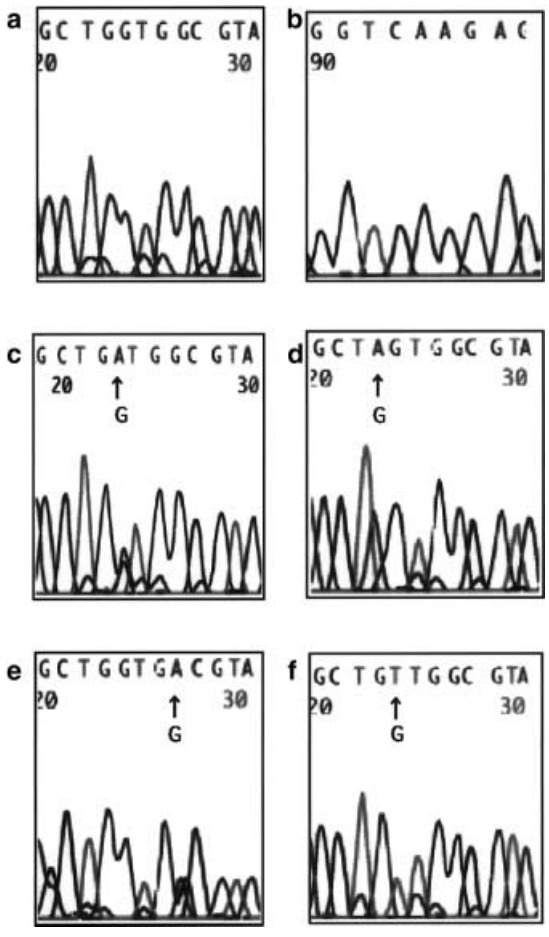

Fig. 4 Sequencing of the K-*ras* gene. **a** Thirty-seven cases had no mutation in exon 1, and (**b**) all cases had no mutations in exon 2. **c** Four mucinous-type adenocarcinomas and one non-mucinous-type adenocarcinoma had a point mutation in codon 12 (GGT to GAT). **d** Two cases of mucinous-type adenocarcinoma had a point mutation in codon 12 (GGT to AGT). **e** One mucinous-type and one non-mucinous-type adenocarcinoma had a point mutation in codon 13 (GGC to GAC). **f** One case of mucinous-type adenocarcinoma had a point mutation in codon 12 (GGT to GTT)

ed only in mucinous-type and non-mucinous-type adenocarcinomas. Point mutations were found in codon 12 or 13 of exon 1 in all cases of mutation (Fig. 4). In mucinous-type adenocarcinoma, K-*ras* gene mutations were found in 8 of 11 (73%) tumors. These mutations consisted of G to A transitions in the second position of codon 12 (GGT to GAT) in four tumors (Fig. 4c); in the first position of codon 12 (GGT to AGT) in two tumors (Fig. 4d); in the second position of codon 13 (GGC to GAC) in one tumor (Fig. 4e); and G to T transversion in the second position of codon 12 (GGT to GTT) in one tumor (Fig. 4f). In non-mucinous-type adenocarcinoma, alterations of the K-*ras* gene were found in 2 of 21 (10%) tumors. This mutation consisted of G to A transitions in the second position of codon 12 (GGT to GAT) in one tumor (Fig. 4c) and in the second position of codon 13 (GGC to GAC) in one tumor (Fig. 4e). In mixed-type adenocarcinoma we did not find any mutations of the K-*ras* gene.

Discussion

This report, to our knowledge, is the first immunohistochemical and K-*ras* gene-mutation analysis of mixed mucinous-type and non-mucinous-type adenocarcinoma. Studies of mixed-type adenocarcinoma have been reported only twice previously: Manning et al. [17] described five cases, with tumors containing areas simulating mucinous-type BAC and different areas simulating non-mucinous-type BAC; and Clayton [5] described two cases as bronchioloalveolar carcinomas with mixed non-mucinous and mucinous differentiation. Lysozyme stained positively in many cases of mucinous-type adenocarcinoma reported to date [15], but it has been negative in all but one case of the mucinous component of mixed-type adenocarcinoma. Moreover, SP-A, CC-10, and TTF-1, assumed to be peculiar to lung adenocarcinoma or pulmonary epithelial cells [1, 2, 11, 13, 18, 24, 25, 26, 27, 29], were positive in both non-mucinous-type adenocarcinoma, in the non-mucinous component of mixed-type adenocarcinoma, and in some of the mucinous component of mixed-type adenocarcinoma, while being negative in most mucinous-type adenocarcinomas. These findings suggested that the mucinous component of mixed-type adenocarcinoma and mucinous-type adenocarcinoma actually have some different immunohistochemical characteristics, despite resembling each other morphologically in HE-stained slides. In addition to those immunohistochemical findings, K-*ras* gene mutation was not observed in mixed-type adenocarcinoma, unlike mucinous-type adenocarcinoma. This suggests that, in lung adenocarcinoma composed of goblet cell-shaped tumor cells, there may be a difference in the mechanism of tumorigenesis between mucinous-type adenocarcinoma and mixed-type adenocarcinoma.

Since the tumor cells are goblet cell-shaped, it is possible that goblet cell hyperplasia underlies mixed-type adenocarcinoma. However, because we have not found K-*ras* gene mutation in goblet cell hyperplasia (0%; 0 of 36) [16] and mixed-type adenocarcinoma (0%; 0 of 15), we have not proved this hypothesis. Mutations of the K-*ras* gene obtained from ten samples (21%, eight samples of mucinous-type adenocarcinoma and two samples of non-mucinous-type adenocarcinoma) consisted mainly of G to A transitions. Generally, K-*ras* gene mutations were seen in 10% of cases of lung adenocarcinoma [10, 23]. Moreover, most cases showed G to A transitions of the K-*ras* gene, as we have reported previously [15]. Although there are many reports that a G to T transversion is the most frequent mutation in lung adenocarcinoma [4, 14, 21, 22, 23, 28, 31], a G to A transition seems to be predominant in pancreatic and colon cancer [4, 12, 32]. Thus, there may be a common mechanism in mucinous-type lung adenocarcinoma and pancreatic adenocarcinoma, because they are similar in terms of both mucin-producing tumor-cell morphology and their K-*ras* gene mutation pattern.

Mixed-type adenocarcinoma, containing both mucinous and non-mucinous components, is described as one type of BAC in the WHO classification. It is thought that the origin of mixed-type adenocarcinoma correlates

with both that of mucinous-type adenocarcinoma and non-mucinous-type adenocarcinoma; however, we have found no supportive evidence that mixed-type adenocarcinoma and mucinous-type adenocarcinoma have related origins. Although it is our guess, the origin of the mucinous component of mixed-type adenocarcinoma may be mucous metaplasia of non-mucinous-type adenocarcinoma. In conclusion, the non-mucinous component of mixed-type adenocarcinoma and non-mucinous-type adenocarcinoma certainly show marked similarity in immunohistochemical staining characteristics, but the mucinous component of mixed-type adenocarcinoma and mucinous-type adenocarcinoma show differences in both immunohistochemical reactivity and the rate of K-*ras* gene mutation. Thus, we suggest that these types of adenocarcinoma differ in their tumorigenesis and biological characteristics.

References

1. Bejarano PA, Baughman RP, Biddinger PW, Miller MA, Fenoglio-Preiser C, al-Kafaji B, DiLauro R, Whisett JA (1996) Surfactant proteins and thyroid transcription factor-1 in pulmonary and breast carcinomas. Mod Pathol 9:445–452
2. Bernard A, Roels H, Lauwerys R, Witters R, Gielens C, Soumillion A, Van Damme J, De Ley M (1992) Human urinary protein 1: evidence for identity with the Clara cell protein and occurrence in respiratory tract and urogenital secretions. Clin Chim Acta 207:239–249
3. Bonner RF, Emmert-Buck MR, Cole K, Pohida T, Chuaqui R, Goldstein SR, Liotta LA (1997) Laser capture microdissection: molecular analysis of tissue. Science 278:1481–1483
4. Bos JL (1989) *Ras* oncogenes in human cancer: a review. Cancer Res 49:4682–4689
5. Clayton F (1986) Bronchioloalveolar carcinomas: cell types, patterns of growth, and prognostic correlates. Cancer 57:1555–1564
6. Emmert-Buck MR, Bonner RF, Smith PD, Chuaqui R, Zhuang Z, Goldstein SR, Weiss RA, Liotta LA (1996) Laser capture microdissection. Science 274:998–1001
7. Fend F, Emmert-Buck MR, Chuaqui R, Cole K, Lee J, Liotta LA, Raffeld M (1999) Immuno-LCM: laser capture microdissection of immunostained frozen sections for mRNA analysis. Am J Pathol 154:61–66
8. Gemma A, Noguchi M, Hirohashi S, Tsugane S, Tsuchiya R, Niitani H, Shimosato Y (1991) Clinicopathologic and immunohistochemical characteristics of goblet cell type adenocarcinoma of the lung. Acta Pathol Japonica 41:737–743
9. Hayashi H, Kitamura H, Nakatani Y, Inayama Y, Ito T, Kitamura H (1999) Primary signet-ring cell carcinoma of the lung: histochemical and immunohistochemical characterization. Hum Pathol 30:378–383
10. Holst VA, Finkelstein S, Yousem SA (1998) Bronchioloalveolar adenocarcinoma of lung. Am J Surg Pathol 22:1343–1350
11. Holzinger A, Dingle S, Bejarano PA, Miller MA, Weaver TE, DiLauro R, Whitsett JA (1996) Monoclonal antibody to thyroid transcriptional factor-1: production, characterization, and usefulness in tumor diagnosis. Hybridoma 15:49–53
12. Hruban RH, van Mansfeld AD, Offerhaus GJ, van Weering DH, Allison DC, Goodman SN, Kensler TW, Bose KK, Cameron JL, Bos JL (1993) Ki-*ras* oncogene activation in adenocarcinoma of the human pancreas. A study of 82 carcinomas using a combination of mutant-enriched polymerase chain reaction analysis and allele-specific oligonucleotide hybridization. Am J Pathol 143:545–554
13. Khoor A, Gray ME, Singh G, Stahlman MT (1996) Ontogeny of Clara cell-specific protein and its mRNA: their association with neuroepithelial bodies in human fetal lung and in bronchopulmonary dysplasia. J Histochem Cytochem 44:1429–1438
14. Kobayashi T, Tsuda H, Noguchi M, Hirohashi S, Shimosato Y (1990) Association of point mutation in c-Ki-*ras* oncogene in lung adenocarcinoma with particular reference to cytologic subtypes. Cancer 66:289–294
15. Maeshima A, Miyagi A, Hirai T, Nakajima T (1997) Mucin-producing adenocarcinoma of the lung, with special reference to goblet cell type adenocarcinoma: immunohistochemical observation and Ki-*ras* gene mutation. Pathol Int 47:454–460
16. Maeshima AM, Maeshima A, Kawashima O, Nakajima T (1999) K-ras gene point mutation in neogenetic lesions of subpleural fibrotic lesions: either an early genetic event in lung cancer development or a non-specific genetic change during the inflammatory reparative process. Pathol Int 49:411–418
17. Manning JT, Spjut HJ, Tschen JA (1984) Bronchioloalveolar carcinoma: the significance of two histologic types. Cancer 54:525–534
18. Mizutani Y, Nakajima T, Morinaga S, Gotoh M, Shimosato Y, Akino T, Suzuki A (1988) Immunohistochemical localization of pulmonary surfactant apoproteins in various lung tumors. Cancer 61:532–537
19. Nakajima T, Kodama T, Tsumuraya M, Shimosato Y, Kameya T (1985) S-100 protein-positive Langerhans cells in various human lung cancers, especially in peripheral adenocarcinomas. Virchows Arch A 407:177–189
20. Paradis V, Dargere D, Bonvoust F, Rubbia-Brandt L, Bâ N, Bioulac-Sage P, Bedossa P (2000) Clonal analysis of micronodules in virus c-induced liver cirrhosis using laser capture microdissection (LCM) and HUMARA assay. Lab Invest 80:1553–1559
21. Rodenhuis S, van de Wetering ML, Mooi WJ, Evers SG, van Zandwijk N, Bos JL (1987) Mutational activation of the K-*ras* oncogene: a possible pathogenetic factor in adenocarcinoma of the lung. N Engl J Med 317:929–935
22. Rodenhuis S, Slebos RJ, Boot AJ, Evers SG, Mooi WJ, Wagenaar SS, van Bodegom PC, Bos JL (1988) Incidence and possible clinical significance of K-*ras* oncogene activation in adenocarcinoma of the human lung. Cancer Res 48:5738–5741
23. Rodenhuis S, Slebos RJC (1992) Clinical significance of *ras* oncogene activation in human lung cancer. Cancer Res 52:2665S–2669S
24. Shimosato Y (1999) Pulmonary neoplasms. In: Sternberger SS (ed) Diagnostic surgical pathology, 3rd edn. Lippincott Williams and Wilkins, Philadelphia, pp 1069–1115
25. Singh G, Katyal SL, Torikata C (1981) Carcinoma of type II pneumocytes: immunodiagnosis of a subtype of "bronchioloalveolar carcinoma." Am J Pathol 102:195–208
26. Singh G, Scheithauer BW, Katyal SL (1986) The pathologic features of carcinomas of type II pneumocytes: an immunocytologic study. Cancer 57:994–999
27. Singh G, Katyal SL, Whitsett JA (1992) Cis-acting elements that confer lung epithelial cell expression of the CC10 gene. J Biol Chem 267:14703–14712
28. Sugio K, Ishida T, Yokoyama H, Inoue T, Sugimachi K, Sasazuki T (1992) *Ras* gene mutations as a prognostic marker in adenocarcinoma of the human lung without lymph node metastasis. Cancer Res 52:2903–2906
29. Szabo E, Goheer A, Witschi H, Linnoila RI (1998) Overexpression of CC10 modifies neoplastic potential in lung cancer cells. Cell Growth Differ 9:475–485
30. Travis WD, Colby TV, Corrin B, Shimosato Y, Brambilla E (1999) Histological typing of lung and pleural tumors (WHO). Springer, Berlin Heidelberg New York
31. Tsuchiya E, Furuta R, Wada N, Nakagawa K, Ishikawa Y, Kawabuchi Y, Sugano H (1995) High K-*ras* mutation rates in goblet-cell-type adenocarcinomas of the lung. J Cancer Res Clin Oncol 121:577–581
32. Vogelstein B, Fearon ER, Hamilton SR, Kern SE, Preisinger AC, Leppert M, Nakamura Y, White R, Smits AM, Bos JL (1988) Genetic alterations during colorectal-tumor development. N Engl J Med 319:525–553

Virchows Arch (2002) 440:604–609
DOI 10.1007/s004280100519

ORIGINAL ARTICLE

R.-P. Henke · A. Erbersdobler

Numerical chromosomal aberrations in papillary renal cortical tumors

Relationship with histopathologic features

Received: 27 April 2001 / Accepted: 30 July 2001 / Published online: 5 September 2001
© Springer-Verlag 2001

Abstract Previous studies have indicated that a combined trisomy of chromosomes 7 and 17 is a constant finding in papillary renal cortical adenomas and that papillary renal cell carcinomas are marked by additional trisomies such as trisomy 12, 16, and 20. The aim of our study was to compare this cytogenetic classification of papillary renal cortical tumors with conventional histopathologic classification. We performed interphase cytogenetics with enumeration probes for chromosomes 7, 12, 16, 17, and 20 on 41 papillary tumors found in 21 nephrectomy and 10 autopsy kidneys. A total of 38 tumors harbored gains of chromosomes 7 or 17, and most of these showed a trisomic signal distribution. The three tumors with normal copy numbers for chromosomes 7 and 17 were a papillary grade-2 carcinoma, a small adenoma (both with distinctive oxyphilic cytoplasm), and a papillary carcinoma with focally clear cells. Gains for chromosomes 12, 16, or 20 were found in 21 tumors and were significantly associated with the presence of histologic criteria of malignancy ($P<0.0001$). Histopathologic and cytogenetic features of malignancy were found in eight tumors smaller than 10 mm. There is a good agreement of cytogenetic and histopathologic criteria of malignancy in papillary renal cell tumors. Interphase cytogenetics might give useful additional information in cases of doubt or when only small biopsy specimens are available.

Keywords Kidney · Papillary renal cell tumors · Interphase cytogenetics · Chromosomes

R.-P. Henke
Institute of Pathology, Taubenstrasse 28,
26122 Oldenburg, Germany

A. Erbersdobler (✉)
Institute of Pathology, University of Hamburg,
Martinistrasse 52, 20246 Hamburg, Germany
e-mail: erbersdobler@uke.uni-hamburg.de
Tel.: +49-40-428036513, Fax: +49-40-428034961

Introduction

Attempts to define a benign epithelial kidney tumor that can be clearly distinguished from renal cell carcinoma (RCC) have a long history. Bell, in his classical autopsy studies, reported an increased risk of metastasis in association with an increase in tumor diameter. Although he had found metastases in 3 of 65 tumors less than 30 mm in diameter and admitted that no certain histologic distinctions could be made between adenomas and carcinomas, he established renal cell adenoma defined by size as a nosologic entity [1, 2]. This classification was based on an arbitrary parameter and remained unsatisfactory. Bennington, reviewing the topic in 1973, concluded that there are neither gross, microscopic, nor histochemical features that reliably allow distinction between so-called cortical adenomas and renal adenocarcinomas [3]. Consequently, he and others suggested classifying small (<30 mm) neoplastic nodules of the kidney as renal adenocarcinoma of low metastatic potential [3, 27]. The diagnostic nihilism of this pragmatic approach stimulated others to refine the original size-based classification by adding cytologic grading as a modifier [28]. However, the repeated notion that low-grade tumors smaller than 30 mm are able to metastasize hampered widespread acceptance of this classification proposal [10]. In the third series fascicle of the Armed Forces Institute of Pathology (AFIP) and in the tumor classification of the World Health Organization (WHO) [24, 26], renal adenomas have been classified as tubulopapillary tumors lacking cytologic anaplasia and peritumoral fibrosis. Thus, clear-cell tumors have been excluded and size is no longer a criterion.

The findings of Kovacs and coauthors, proposing a clear-cut cytogenetic definition of renal cell adenoma, suggest a definite solution to the diagnostic dilemma [21]. These authors reported that papillary renal tumors are characterized by trisomies of chromosomes 7 and 17 and that carcinomas, in contrast to adenomas, are marked by additional numerical chromosomal gains, especially gains of chromosomes 12, 16, and 20 [18, 21]. However,

chromosomal analyses are expensive, time consuming, and restricted to specialized laboratories. Furthermore, very small papillary renal lesions that are incidentally found in paraffin-embedded material are hardly suitable for conventional cytogenetic studies. For routine diagnostics, it would be important to know whether morphologic and cytogenetic criteria of malignancy are congruent.

The aims of this study were to further investigate the relationship between trisomies of chromosomes 7 and 17 and papillary histology, and to compare the current morphologic classification of papillary renal cortical tumors with the cytogenetic classification of Kovacs and coworkers [18, 21]. Our findings confirm the frequent overrepresentation of chromosomes 7 and 17 in papillary renal tumors and document that the appearance of nuclear atypia and peritumoral fibrosis is closely correlated with the detection of gains of chromosomes 12, 16, or 20.

Materials and methods

We examined 21 nephrectomy specimens and 10 autopsy kidneys, in which papillary renal cell tumors had been identified during the routine pathological work-up. The tumors were classified as adenoma or carcinoma after examination of hematoxylin and eosin stained tissue sections. Criteria for the diagnosis of renal cortical adenoma were used as published by the AFIP and the WHO [24, 26]. In short, adenomas consisted of densely packed tubules or papillary structures lined by small, regular, cuboidal cells with rounded, uniform nuclei lacking cytologic anaplasia. Mitoses were absent or rare (<1 per 25 high-power fields of 0.19 mm^2). The tumors were circumscribed but not encapsulated, there were no significant inflammatory cells at the interface with the normal renal parenchyma, and a stromal reaction was absent. Grading of carcinomas was performed according to the Fuhrmann system [11]. Histologic classification and grading were performed by one of us (R.-P.H.) without knowledge of the results of interphase cytogenetics.

The following biotinylated nucleic acid probes of the alphoid satellite family were used: chromosome 7 (D7Z1), 12 (D12Z1), 16 (D16Z1), 17 (D17Z1), and 20 (D20Z1) (Oncor, Gaithersburg, Md.). The probes were selected on the basis of previous reports on numerical chromosomal changes in papillary renal tumors [18]. Details of our hybridization method are reported elsewhere [12, 13]. Briefly, 6-µm paraffin sections were adhered to silanized glass slides and air-dried. Sections were dewaxed, heated by exposure to microwaves in citric acid monohydrate, and treated with sodium thiocyanate, followed by a pepsin digest. Each section was covered with 0.1 ng/µl biotinylated probe in freshly prepared hybridization solution. Sections were covered with coverslips and were denatured for 10 min in a 78°C water bath. Hybridization was performed overnight at 37°C. Labeled DNA was detected with subsequent incubations with a mouse monoclonal anti-biotin antibody, a biotinylated goat anti-mouse antibody, peroxidase-conjugated streptavidin, and diaminobenzidine. The slides were counterstained with hematoxylin, dehydrated, and then permanently mounted.

Evaluation was performed by one of us (A.E.), blinded for the final histologic classification and grading. Slides were evaluated according to accepted criteria [14]. Hybridization signals were counted in sections that had signals in at least 90% of cells. Between 104 and 315 nuclei (mean 187; standard deviation 42; 5th percentile 119) were evaluated per chromosome and tumor in nephrectomy specimens. Due to smaller tumor size, the number of nuclei for evaluation in the autopsy cases was somewhat lower, ranging from 66 to 291 (mean 173; standard deviation 45; 5th percentile 101). The distribution of signal numbers in normal-appearing renal parenchyma, adjacent to the neoplastic foci, was also determined and served as an internal control. In these non-neoplastic controls, three hybridization signals were found with a mean of 1.0% of nuclei (range 1–3%; standard deviation 0.8%). To ensure a high specificity, a conservative cut-off level of 10% was chosen for the diagnosis of chromosomal gains.

A commercially available software package (SPSS version 6.1.3, SPSS Inc., Chicago, Ill.) was used for the statistical calculations. Two-by-two contingency tables were analyzed with Fisher's exact test. Significance of differences between groups with nonparametric distribution of data was analyzed with the Mann-Whitney test. A P value of less than 0.05 was considered to reflect significant differences between groups. All tests were two-sided.

Results

From 35 distinct tumor foci found in the 21 nephrectomy specimens, 19 were classified as papillary carcinomas and nine as papillary adenomas (Table 1). The other seven tumors were conventional carcinomas of clear-cell type and were not included in the study. Fourteen of the papillary tumors were incidental findings. Four of these were classified as carcinomas and ten as adenomas. Two were found in hydronephrotic end-stage kidneys, six were detected in addition to larger clear-cell carcinomas, and six were found in kidneys removed for larger papillary carcinomas. From 13 papillary tumors detected in 10 autopsy kidneys, 4 were classified as carcinomas and nine as adenomas (Table 2). In the whole series, necroses were restricted to carcinomas. A moderate intratumoral, mostly peritubular fibrosis was seen in three adenomas. A slight inflammatory infiltration of mixed cellularity was seen intratumorally in one and focally peritumoral in another adenoma. All but one carcinoma and 11 of the adenomas in this series showed at least 50% papillary architecture. The eight tumors with a predominant tubular pattern were small and measured from 1 mm to 8 mm. All of the four papillary tumors found in autopsy kidneys and 8 of the 19 classified as carcinomas in nephrectomy specimens were smaller than 30 mm. Of the 23 carcinomas, 8 (35%) were smaller than 10 mm.

In 30 of the 41 tumors, interphase cytogenetics showed a trisomic signal distribution for chromosomes 7 and 17 (Table 1 and Table 2). Figure 1 illustrates nephrectomy case 21a with a trisomy 7 and Fig. 2 shows nephrectomy case 1 with a trisomy 17. Gains of chromosomes 12, 16, or 20 were found in 21 cases and were significantly associated with the presence of peritumoral fibrosis or nuclear atypia (Fisher's exact test, $P<0.0001$).

The three cases with a disomic signal distribution for chromosome 17 showed a normal copy number for chromosomes 7, 12, 16, and 20, as well. Reexamination of these tumors revealed special histologic features: one tumor (nephrectomy case 8) was a papillary grade-2 carcinoma with distinctive eosinophilic and granular cytoplasm (Fig. 3a, b). This tumor also showed a moderate degree of intra- and peritumoral inflammation and fibrosis. Some of the papillary cores contained foamy macro-

Table 1 Pathologic examination and interphase cytogenetics of 28 papillary tumors in 21 nephrectomy specimens

Case no.	Size (mm)	Pathological diagnosis	Grade	Interphase cytogenetics*				
				p7	p12	p16	p17	p20
1	50.0	Tubulopapillary carcinoma	2	3	1	3	3	2
2a	60.0	Tubulopapillary carcinoma	2	4	2	2	3	2
2b	9.0	Papillary adenoma		3	2	2	2(3)	2
2c	50.0	Papillary carcinoma	2	3	3	2(3)	2(3)	2
2d	9.0	Tubulopapillary carcinoma	1	3	2	2	2(3)	2
3	50.0	Tubulopapillary carcinoma	2	3	3	2	3	2
4	7.0	Papillary carcinoma	2	3	2(3)	2(3)	3	2
5	1.5	Papillary adenoma		3	2	2	3	2
6	10.0	Papillary carcinoma	1	3(4;>4)	2(3)	3	2(3)	2(3)
7	45.0	Papillary carcinoma	2	2(3)	2	2	2(3)	3(4;>4)
8	20.0	Papillary carcinoma	2	2	2	2	2	2
9	80.0	Papillary carcinoma	2	3	2	2(3)	2(3)	2(3)
10	0.5	Papillary adenoma		2(3)	2	2	2(3)	2
11	50.0	Papillary carcinoma	2	3(4)	3	2(3)	2(3)	2(3)
12a	30.0	Papillary carcinoma	2	2(3)	2	2(3)	2(3)	2(3)
12b	3.0	Papillary adenoma		2(3)	2	2	2(3)	2
13	29.0	Tubulopapillary carcinoma	2	2(3)	2(3)	2(3)	2(3;4)	2
14	115.0	Tubulopapillary carcinoma	2	3	2	2	2(3)	2(3)
15	1.0	Tubular adenoma		2(3)	2	2	2(3)	2
16	8.0	Tubulopapillary carcinoma		2(3)	2(3)	2(3)	3	2(3)
17	16.0	Papillary carcinoma	1	3	3	2	2(3)	2
18	30.0	Papillary carcinoma	2	2(3;4)	3(4)	2(3)	2(3)	2(3)
19a	6.0	Tubular adenoma		2(3)	2	2	2(3)	2
19b	2.0	Papillary adenoma		2	2	2(3)	2(3)	2
20	6.0	Tubular adenoma		3	2	2	2(3)	2
21a	70.0	Tubulopapillary carcinoma	2	3	2	2(3)	3	2
21b	7.0	Papillary adenoma		2	2	2	4	2
21c	3.0	Papillary carcinoma	1	3(4)	2(3)	2(3)	3(4)	2(3;4)

* p is chromosome probe; values indicate counts of hybridization signals most frequently observed; values in parentheses indicate higher signal counts when observed in more than 10% of tumor cells

Table 2 Pathologic examination and interphase cytogenetics of 13 papillary tumors in 10 autopsy specimens

Case no.	Size (mm)	Pathological diagnosis	Grade	Interphase cytogenetics*				
				p7	p12	p16	p17	p20
1	8.0	Tubular adenoma		2	3	2	2(3)	2
2	2.0	Tubulopapillary adenoma		2(3)	2	2	2(3)	2
3a	3.0	Tubular adenoma		2(3)	2	2	2(3)	2
3b	1.0	Tubular adenoma		2(3)	2	2	2(3)	2
4a	5.0	Tubulopapillary carcinoma	2	3	2(3)	2(3)	3	2(3)
4b	6.0	Papillary carcinoma	2	3	2(3)	2(3)	3	2(3)
4c	2.5	Papillary adenoma		2(3)	2	2	2(3)	2
5	1.0	Papillary adenoma		2(3)	2	2	2(3)	2
6	3.0	Papillary carcinoma	2	2	2	2	2	2
7	1.5	Tubular adenoma		2(3)	2	2	2(3)	2
8	3.0	Tubulopapillary adenoma		2(3)	2	2	2(3)	2
9	2.0	Tubular carcinoma	2	3	2(3)	2	2(3)	2
10	3.0	Papillary adenoma		2	2	2	2	2

* p is chromosome probe; values indicate counts of hybridization signals most frequently observed; values in parentheses indicate higher signal counts when observed in more than 10% of tumor cells

phages. A broad eosinophilic and granular cytoplasm was also found in the second tumor with only normal chromosome numbers, an incidental 3-mm adenoma in an autopsy kidney (autopsy case 10). The third tumor in the group with normal chromosome numbers had been classified as low-grade carcinoma due to peritumoral fibrosis. This 3-mm tumor, which was found incidentally at autopsy (autopsy case 6), showed a papillary architecture throughout; however, in further step sections foci of cells with clear cytoplasm appeared. Thus, all three papillary tumors, which lacked the characteristic trisomy 17, were cytologically variant from the usual types of papillary renal tumors.

There were four tumors that showed discrepancies between cytogenetic and histologic assessment of malignancy. Two tumors, classified as carcinoma, did not show the expected chromosomal gains in addition to alterations of chromosomes 7 and 17, and two tumors, classified as adenomas by histologic criteria, displayed gains of chromosomes 12, 16, or 20, in addition to trisomy 17. The first two tumors were from the same patient (nephrectomy cases 2a and 2d), one measuring 60 mm, the other 9 mm. Reexamination of these tumors did not reveal any special histologic features. A third carcinoma from the same patient disclosed the expected pattern of trisomies 12 and 16 in addition to trisomies 7

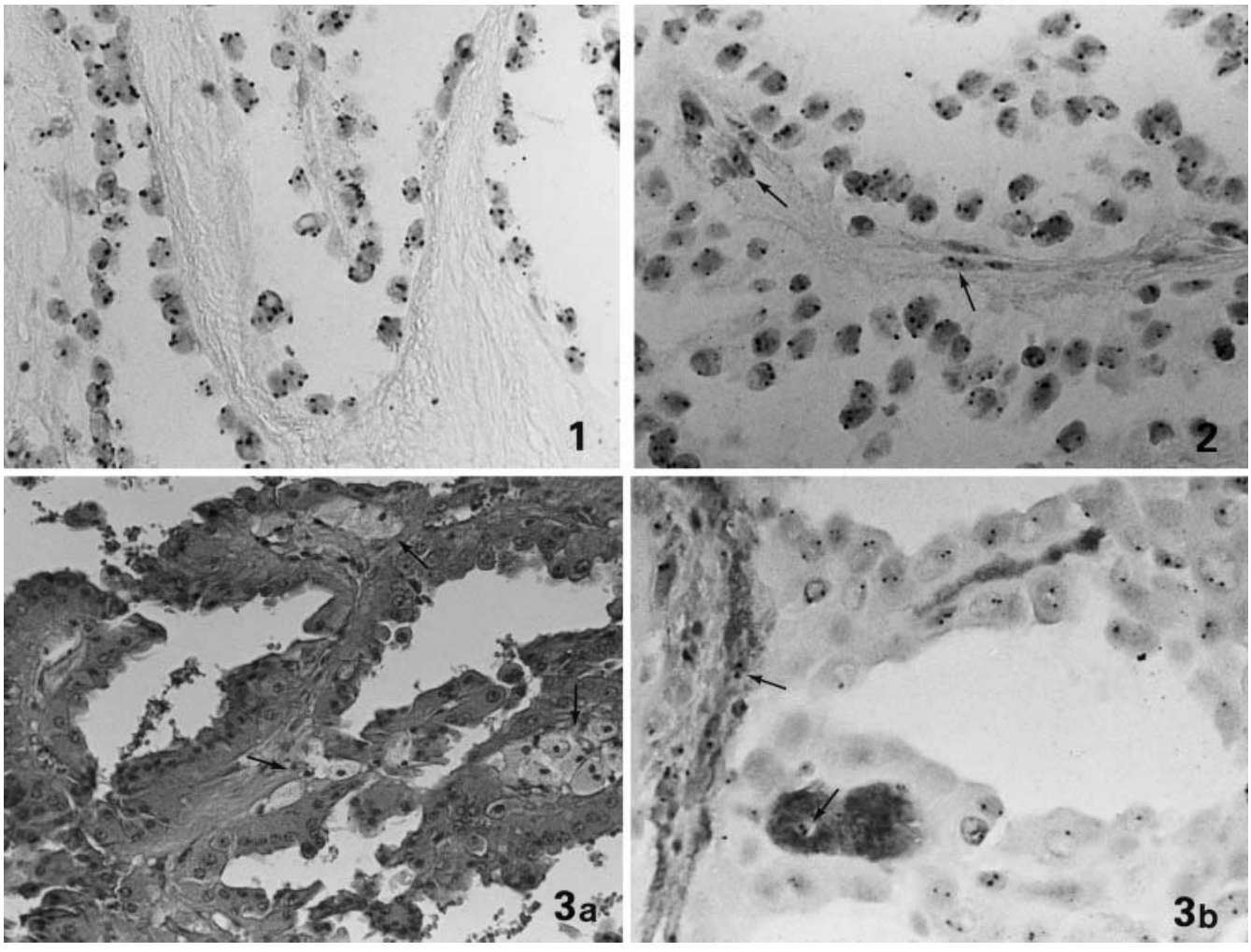

Fig. 1 Nephrectomy case 21a. Tubulopapillary renal cell carcinoma. In situ hybridization with a probe for chromosome 7 on a paraffin section reveals a trisomic signal distribution. Original magnification ×400

Fig. 2 Nephrectomy case 1. Papillary renal cell carcinoma. In situ hybridization with a probe for chromosome 17 on a paraffin section reveals a trisomic signal distribution for chromosome 17. Note non-neoplastic stromal cells with one and two signals (*arrows*). Original magnification ×400

Fig. 3 **a** Nephrectomy case 8. Papillary renal cell carcinoma with distinct oxyphilia of cytoplasm. Foamy macrophages can be seen in the papillary cores (*arrows*). Hematoxylin and eosin, original magnification ×160. **b** Same case as **a**. In situ hybridization with a probe for chromosome 17 on a step section shows a disomic signal distribution within the tumor cell population. Non-neoplastic stromal cells with a similar signal distribution are denoted by *arrows*. Original magnification, ×400

and 17. The latter two tumors (nephrectomy case 19b and autopsy case 1) were two adenomas measuring 2 mm and 8 mm, respectively. The only histologic peculiarity was a moderate intratumoral fibrosis in the larger of the two tumors, but the same pattern and degree of fibrosis was also noted in two other small adenomas, where histologic and cytogenetic classification were concordant.

Tumors with hypertriploid numbers of chromosomes 7, 17 or one of the other chromosomes did not show statistically significant differences regarding the variables tumor grade, size, age of patient, presence of necrosis, or pattern of inflammation or fibrosis.

Discussion

We have demonstrated that in papillary renal tumors with a trisomy of chromosome 17, the additional identification of gains of chromosomes 12, 16, or 20 was paralleled by the appearance of histologic features of malignancy, such as peritumoral fibrosis and nuclear atypia. Three tumors that lacked the characteristic gain of chromosome 17 showed particular cytologic features.

Since Bell's classical study of 149 renal cell tumors from the records of 30,000 autopsies [1], size has been a major criterion for the working definition of benign cortical tumors, neglecting the fact that small renal tumors are able to metastasize, although infrequently [1, 2, 10]. Later classification proposals tried to improve diagnostic accuracy by adding cytologic grading [28], but the categorization of small renal tumors has remained a diagnostic dilemma, and diagnostic criteria have further changed

over the years. Comparison and interpretation of these classification proposals is hampered by the fact that histologic and cytologic typing were applied differently. In Bell's study, tumors of all histologic types were included. In fact, the tumor illustrated as a "carcinoma of kidney" in the second figure of his classic paper is indistinguishable from an oncoytoma [1]. These tumors are categorized as benign (oncocytic adenoma) according to modern classification [24]. Murphy and Mostofi restricted their study of renal cell adenomas to tumors with a papillary, tubular, or alveolar pattern [25]. However, they describe "29 clear-cell carcinomas originating in adenoma". Cytogenetic data suggest that these adenomas probably were variants of conventional clear-cell carcinoma from the beginning and would not be classified as adenoma according to modern classification systems [22, 24, 26].

Papillary renal tumors of chromophilic cell type exhibit a set of chromosomal gains, characteristically including trisomies of chromosomes 7 and 17 [6, 17, 19, 20]. Trisomy of chromosomes 12, 16, and 20 has been associated with the progression from the adenoma into the carcinoma stage [18, 21]. For this reason we have focused our studies of renal tumors with papillary histology on chromosomes 7, 12, 16, 17, and 20, with the goal of further characterizing the relationship between histologic and cytogenetic classification criteria on paraffin-embedded material.

Gains of chromosome 7 were always combined with gains of chromosome 17 in our series, but 6 of the 41 tumors showed a normal disomic signal distribution for chromosome 7. Trisomy 7 is a very common anomaly in human neoplasms [23] and has been demonstrated in otherwise normal somatic cells of kidneys involved or not involved in RCC [4, 9]. In the latter context, trisomy 7 possibly indicates cells going through a unique stage that in time could make the cell more susceptible to abnormal proliferation [23]. Our data suggest that trisomy 7 is not as closely related to papillary tumors of the kidney as trisomy 17 is. Three tumors in our series did not show the expected gain of chromosome 17. Two of these tumors displayed a distinctly eosinophilic and granular, nearly oncocytic cytoplasm. Similar cytoplasmic changes are usually seen in chromophilic papillary RCC with increasing tumor grade, but the nuclei in our cases lacked significant atypia. The histologic reexamination of the third tumor confirmed a typical papillary architecture. However, additional step sections revealed areas in which the cytoplasm of many of the tumor cells appeared clear. Similar clear cell features have been described in at least three papillary RCCs exhibiting an X;1 translocation without trisomy 17 [8, 29]. It is tempting to speculate that our papillary tumor with clear cell features might also belong to this special subtype. However, probing its characteristic breakpoint on the X chromosome (Xp11.2) was beyond the scope of this study; so we cannot rule out that our tumor would be better classified as clear-cell RCC with an unusual papillary growth pattern.

The observation that lack of trisomy 17 in papillary renal neoplasms can be associated with a distinctive morphology has also been reported by Corless and co-authors, who found characteristic sclerosis of papillary cores and an absence of foamy macrophages in three of seven papillary RCCs that did not yield a consistent pattern of excess chromosome-17 signals [5]. Tumors with sclerotic papillary cores were not present among our cases. In accordance with our data, Kattar and co-authors found characteristic eosinophilic cells in three of the five tumors that lacked a trisomy 17 [16]. Papillary tumors with these cytologic characteristics – large cells and eosinophilic cytoplasm – have been subtyped as type 2 by Delahunt and Eble [7], and in another study it has been shown that only a minority of these tumors show the expected gains of chromosomes 7 and 17 [15]. Obviously, trisomy 17 is not mandatory for the development of a papillary phenotype in renal cell tumors, but is more related to a certain cell type. Analysis of additional cases with unusual features will be necessary to find out whether these tumors represent a true histogenetic variant of papillary RCC. Other deviations from the classical trisomy 7/17 pattern of papillary renal tumors were described previously by Corless and co-authors. They found four or five chromosome-17 signals per nucleus in seven of 28 low-grade tumors and in six of eight high-grade tumors [5]. High-grade and high-stage tumors showed a tendency toward four and five signals per nucleus. Whether this has any functional meaning or merely reflects increasing chromosomal instability in cancer progression remains to be solved. In accordance with our results, the distribution of gains of chromosome 7 did not perfectly parallel those for chromosome 17 in the same tumors. Thus, we agree with the conclusion that gains and/or secondary losses of chromosomes 7 and 17 in papillary renal cell tumors probably occur independently.

In a study using comparative genomic hybridization, Jiang and coworkers investigated a series of 25 papillary renal carcinomas. They disclosed frequent gains at chromosomes 7, 12q, 16q, 17, and 20q, as well as losses at chromosomes 1p, 4q, 6q, 9p, 13q, X, and Y. In concordance with our results, gains at chromosomes 7 and 17 were not found in a subset of papillary carcinomas with eosinophilic cytoplasm [15]. Interestingly, in the same study, one tumor with a completely papillary architecture displayed a deletion at 3p, which is usually found in clear-cell carcinomas. A papillary tumor with focal clear cells was also found in the present study, and, beside the possibility of the X;1 translocation discussed above, this tumor might at least focally have also contained a 3p-deletion.

The major advantage of interphase cytogenetics is the fact that it can be performed on routinely processed material, and morphologic details are well preserved. Incidental small papillary neoplasms are sometimes found in biopsies performed for the diagnosis of inflammatory glomerular or tubulointerstitial diseases or prior to transplantation. In these cases, interphase cytogenetics might

give useful additional information about chromosomal aberrations. The detection of gains of chromosomes 12, 16, or 20 in our series correlated well with a histologic diagnosis of malignancy based on nuclear atypia and/or peritumoral fibrosis, although the congruity between histologic and cytogenetic classification was not perfect. Each of these approaches has classified two tumors as carcinomas that have shown no signs of malignancy using the alternative approach. Reexamination of the histologic slides and the in situ hybridization did not disclose any special features in these four tumors.

We conclude that the histologic criteria defined by the AFIP and WHO classifications for the transition of renal adenoma into papillary (chromophilic) RCCs are in good agreement with cytogenetic hallmarks of this oncogenic sequence. However, the question of malignancy with a papillary renal neoplasm in very small biopsy specimens where morphologic features cannot be reliably assessed will continue to pose a diagnostic problem.

Acknowledgements This study was supported by a grant from the Hamburger Stiftung zur Förderung der Krebsbekämpfung, Hamburg, Germany. We thank N. Gürses and S. Schnöger for expert help with the in situ hybridization.

References

1. Bell ET (1938) A classification of renal tumors with observations on the frequency of the various types. J Urol 39:238–243
2. Bell ET (1950) Tumors of the kidney. In: Bell ET (ed) Renal diseases. Lea and Febiger, Philadelphia, p 411
3. Bennington JL (1973) Cancer of the kidney – etiology, epidemiology, and pathology. Cancer 32:1017–1029
4. Casalone R, Granata Casalone P, Minelli E, Portentoso P, Righi R, Meroni E, Giudici A, Donati D, Riva C, Salvatore S, et al (1992) Significance of the clonal and sporadic chromosome abnormalities in non-neoplastic renal tissue. Hum Genet 90:71–78
5. Corless CL, Aburatani H, Fletcher JA, Housman DE, Amin MB, Weinberg DS (1996) Papillary renal cell carcinoma. Quantitation of chromosomes 7 and 17 by FISH, analysis of chromosome 3p for LOH, and DNA ploidy. Diagn Mol Pathol 5:53–64
6. Dal Cin P, Gaeta J, Huben R, Li FP, Prout GR, Sandberg AA (1989) Renal cortical tumors. Am J Clin Pathol 92:408–414
7. Delahunt B, Eble JN (1997) Papillary renal cell carcinoma: a clinicopathologic and immunohistochemical study of 105 tumors. Mod Pathol 10:537–551
8. Dijkhuizen T, van den Berg E, Wilbrink M, Weterman M, Geurts van Kessel A, Störkel S, Folkers RP, Braam A, de Jong B (1995) Distinct Xp11.2 breakpoints in two renal cell carcinomas exhibiting X; autosome translocations. Genes Chromosomes Cancer 14:43–50
9. Emanuel A, Szucs S, Weier HUG, Kovacs G (1992) Clonal aberrations of chromosomes X, Y, 7 and 10 in normal kidney tissue of patients with renal cell tumors. Genes Chromosomes Cancer 4:75–77
10. Eschwege P, Saussine C, Steichen G, Delepaul B, Drelon L, Jacqmin D (1996) Radical nephrectomy for renal cell carcinoma 30 mm or less: Long-term followup results. J Urol 155: 1196–1199
11. Fuhrmann SA, Lasky LC, Limas C (1982) Prognostic significance of morphologic parameters in renal cell carcinoma. Am J Surg Pathol 6:655–663
12. Henke R-P, Ayhan N (1994) Enhancement of hybridization efficiency in interphase cytogenetics on paraffin-embedded tissue sections by microwave treatment. Anal Cell Pathol 6:319–325
13. Henke R-P, Krüger E, Ayhan N, Hübner D, Hammerer P (1994) Frequency and distribution of numerical chromosomal aberrations in prostatic cancer. Hum Pathol 25:476–484
14. Hopman AHN, Ramaekers FCS, Vooijs GP (1990) Interphase cytogenetics of solid tumours. In: Polak JM, McGee JO (eds) In situ hybridization. Principles and practice. Oxford University Press, Oxford New York Tokyo, pp 165–186
15. Jiang F, Richter J, Schraml P, Bubendorf L, Gasser T, Sauter G, Mihatsch MJ, Moch H (1998) Chromosomal imbalances in papillary renal cell carcinoma. Genetic differences between histological subtypes. Am J Pathol 153:1467–1473
16. Kattar MM, Grignon DJ, Wallis T, Haas GP, Sakr WA, Pontes JE, Visscher DW (1997) Clinicopathologic and interphase cytogenetic analysis of papillary (chromophilic) renal cell carcinoma. Mod Pathol 10:1143–1150
17. Kovacs G (1989) Papillary renal cell carcinoma: a morphologic and cytogenetic study of 11 cases. Am J Pathol 134:27–34
18. Kovacs G (1993) Molecular differential pathology of renal cell tumours. Histopathol 22:1–8
19. Kovacs G, Frisch S (1989) Clonal chromosome abnormalities in tumor cells from patients with sporadic renal cell carcinomas. Cancer Res 49:651–659
20. Kovacs G, Wilkens L, Papp T, DeRiese W (1989) Differentiation between papillary and nonpapillary renal cell carcinomas by DNA analysis. J Natl Cancer Inst 81:527–530
21. Kovacs G, Füzesi L, Emanuel A, Kung H (1991) Cytogenetics of papillary renal cell tumors. Genes Chromosomes Cancer 3:249–255
22. Kovacs G, Akhtar M, Beckwith BJ, Bugert P, Cooper CS, Delahunt B, Eble JN, Fleming S, Ljungberg B, Medeiros LJ, Moch H, Reuter VE, Ritz E, Roos G, Schmidt D, Srigley JR, Störkel S, van den Berg E, Zbar B (1997) The Heidelberg classification of renal cell tumours. J Pathol 183:131–133
23. Meloni AM, Bridge J, Sandberg AA (1992) Reviews on chromosome studies in urological tumors. I. Renal tumors. J Urol 148:253–265
24. Mostofi FK, Davis CJ (eds) (1998) Histological typing of kidney tumours. Springer, Berlin Heidelberg New York
25. Murphy GP, Mostofi FK (1970) Histologic assessment and clinical prognosis of renal adenoma. J Urol 103:31–36
26. Murphy WM, Beckwith JB, Farrow GM (eds) (1994) Tumors of the kidney, bladder, and related urinary structures. Armed Forces Institute of Pathology, Washington
27. Petersen RO (ed) (1986) Urologic pathology. Lippincott, Philadelphia
28. Thoenes W, Störkel S, Rumpelt HF (1986) Histopathology and classification of renal cell tumors (adenomas, oncocytomas and carcinomas). Pathol Res Pract 181:125–143
29. Tomlinson GF, Nisen PD, Timmons GF, Schneider NR (1991) Cytogenetics of a renal cell carcinoma in a 17-month-old child. Evidence for Xp11.2 as a recurring breakpoint. Cancer Genet Cytogenet 57:11–17

Virchows Arch (2002) 440:610–615
DOI 10.1007/s00428-001-0550-4

ORIGINAL ARTICLE

Christian Mawrin · Elmar Kirches · Carsten Boltze
Knut Dietzmann · Albert Roessner
Regine Schneider-Stock

Immunohistochemical and molecular analysis of p53, RB, and PTEN in malignant peripheral nerve sheath tumors

Received: 31 May 2001 / Accepted: 5 September 2001 / Published online: 16 November 2001
© Springer-Verlag 2001

Abstract The molecular basis of both sporadic and neurofibromatosis type 1 (NF1)-associated malignant peripheral nerve sheath tumors (MPNSTs) is yet largely undetermined. Therefore, we analyzed a series of 12 MPNSTs – including two cases which arose in the setting of NF1 – for molecular alterations in the *p53*, retinoblastoma (*Rb*), and *PTEN* tumor suppressor genes. Furthermore, the immunohistochemical expression of p53, RB, and PTEN protein was examined in these tumors. One mutation (8%), an A to T transversion leading to an amino acid exchange, was found in exon 5 of the *p53* gene in a sporadic MPNST. In two other sporadic tumors (20%), loss of heterozygosity (LOH) of the *p53* gene occurred. Nuclear overexpression of p53 protein was observed in ten tumors (83%). Loss of RB protein expression was seen in two MPNSTs (17%), and LOH of the *Rb* gene was detected in four tumors (44%), including the two NF1-associated MPNSTs, one of them showing concomitant loss of RB protein expression. No mutation in the *PTEN* gene was detected, and cytoplasmic immunoreactivity for the PTEN protein was maintained in eight MPNSTs (67%). We suggest that alterations in the p53 and RB pathway, both are essential in controlling the cell-cycle progression, are critical points in the tumorigenesis of sporadic and NF1-associated MPNSTs, whereas the *PTEN* gene seems to play no significant role in this process.

C. Mawrin · E. Kirches · K. Dietzmann
Department of Neuropathology, Otto-von-Guericke-University, Magdeburg, Germany

C. Boltze · A. Roessner · R. Schneider-Stock (✉)
Department of Pathology,
Otto-von-Guericke-University, Leipziger Strasse 44,
39120, Magdeburg, Germany
e-mail: regine.schneider-stock@medizin.uni-magdeburg.de
Tel.: +49-0391-6715060, Fax: +49-0391-6715060

C. Mawrin
Department of Psychiatry, Otto-von-Guericke-University, Magdeburg, Germany

Keywords Peripheral nerve sheath tumors · p53 · Rb · PTEN

Introduction

Malignant peripheral nerve sheath tumors (MPNSTs) are rare neoplasms accounting for about 5% of malignant tumors of soft tissue [18]. In MPNSTs, tumor cells can show differentiation of any cell of the nerve sheath, including the Schwann cell, perineural fibroblast, or fibroblast [1]. Almost two-thirds result from the malignant transformation of a neurofibroma (NF), often of the plexiform type and in the setting of neurofibromatosis type 1 (NF1) [12]. Only rare examples also develop from conventional schwannomas or ganglioneuromas [28, 40].

The molecular alterations contributing to MPNST tumorigenesis are at present largely undetermined. In patients with NF1, an inactivation of both NF1 alleles has been found, implicating a significant role of this gene in MPNST formation [15]. Additionally, there is a growing body of evidence that alterations in genes controlling cell-cycle regulation do contribute to MPNST tumorigenesis. The *p53* tumor suppressor gene that is mutated in more than half of human cancers [17] seems to play an important role in MPNSTs, because deletions and mutations affecting the *p53* gene locus, as well as nuclear accumulation of p53 protein, have been identified in these tumors [11, 23]. Furthermore, the recent demonstration of homozygous deletions of the CDKN2A gene [14, 25], together with alterations in the expression of p27Kip1 [13], are additional evidence of an altered cell-cycle control in MPNSTs.

However, it is likely that additional genes would play a role in the development of MPNSTs, and the karyotypic complexity seen in these tumors gives support for this notion [24]. Recently, a novel candidate tumor suppressor gene, the *PTEN* (phosphatase and tensin homologue deleted on chromosome ten) gene, also named MMAC1 or TEP1, has been identified on chromosome 10q23.3 [20]. *PTEN* has been reported to be frequently deleted or

to have point mutations in malignant gliomas, breast, and prostate cancer [34]. It was shown that PTEN mediates G1 cell-cycle arrest and/or apoptosis via the phosphoinositol-3-kinase-Akt pathway [9]. In this signaling process, one critical target is the cyclin-dependent kinase inhibitor p27(KIP1) [19]. Recruitment of p27(KIP1) to cyclin E immunocomplexes correlates to cell-cycle arrest and leads to a reduction in the cyclin-dependent kinase 2 (cdk2) activity and subsequent decrease in the levels of endogenous phosphorylated retinoblastoma (RB) protein [6]. Because RB is known to play a central role in the regulation of the cell cycle [2], functional inactivation due to inappropriate phosphorylation of the RB protein resulting from deregulation of upstream effectors in the RB pathway (e.g., p16 inactivation or cyclin overexpression [33]) or due to mutations in the *Rb* gene itself may result in a malignant phenotype.

We wanted to contribute to a growing number of MPNST cases screened for *p53* mutations and immunohistochemical expression, since only conflicting results have so far been reported in the literature, ranging from no mutations to high frequencies in NF1-associated as well as in sporadic cases [16, 23, 27, 31, 36, 38]. The molecular analysis of loss of heterozygosity (LOH) in the *Rb* gene region was motivated by a few reports suggesting a role of the RB pathway in MPNSTs, but leaving open the question of direct allelic losses of the gene. However, these reports described frequent chromosomal rearrangements affecting other components of the RB pathway in familial cases [4] or a loss of immunocytochemically detectable RB protein in a fraction of MPNSTs [13]. Although no hints from the literature suggested a role of PTEN, our study was supplemented by a screening for PTEN alterations. This tumor suppressor protein plays a role in other tumors of the nervous system and was recently suggested to exert a crosstalk with the RB pathway [26].

Given the need to shed more light into the molecular alterations associated with the development of MPNSTs, in the present study we performed immunohistochemical and molecular analysis of the *p53*, *Rb*, and *PTEN* tumor suppressor genes in a series of MPNSTs.

Materials and methods

We investigated a total of 12 MPNSTs, which were selected from the files of the Departments of Pathology and Neuropathology, Medical Faculty, Otto-von-Guericke-University Magdeburg, Germany. The diagnoses were based on clinical information, review of hematoxylin and eosin-stained tissue sections, and previous immunocytochemical staining results. All of the MPNSTs were spindle-cell tumors and none was epithelioid in type. The clinical details of the cases are given in Table 1. Two patients had a known history of NF1 (cases no. 1 and no. 3).

The tumor specimens were routinely formalin fixed and paraffin embedded. In addition, surgical specimens from all tumors were snap frozen and stored in liquid nitrogen at –80°C. All samples were routinely stained with hematoxylin and eosin to determine the histological diagnosis. For immunohistochemistry, 4-µm-thick sections were deparaffinized with xylene for 15 min and dehydrated through a series of graded alcohols. Sections were pre-

Table 1 Clinicopathological data, genetic findings, and immunostaining results in malignant peripheral nerve sheath tumors. *IH* immunohistochemistry, *mut.* mutation, *NI* non-informative, *LOH* loss of heterozygosity, *NA* not available, *DOD* died of disease. The age at diagnosis is shown

Case	Sex	Age (years)	Localization	Grade	Clinical outcome	Metastasis	Duration of follow-up (months)	*Rb* LOH	p53 LOH	p53 mut.	PTEN mut.	RB IH	p53 IH	PTEN IH	MIB-1 IH
1*	Male	46	Retroperitoneal	G2	DOD	Lung, liver	14	+	–	–	–	–	+	+	++
2	Male	47	Retroperitoneal	G3	NA	NA	NA	+	–	–	–	++	+	+	++
3*	Female	49	Gluteal	G1	Alive	–	45	+	–	–	–	++	+	+	++
4	Male	78	Thoracic wall	G2	Alive	-	56	NI	–	–	–	++	++	+	++
5	Female	57	Mesenteric	G1	Alive	Liver, lymph node	93	NI	+	–	–	++	++	+++	++
6	Male	44	Thoracic wall	G2	Alive	Thoracic wall	74	–	–	–	–	++	++	+	++
7	Male	39	Back	G2	Alive	–	29	–	NI	+	–	++	++	++	++
8	Male	37	Retroperitoneal	G2	Alive	Lung, lymph node	27	+	NI	–	–	++	++	–	++
9	Female	57	Elbow	G2	Alive	–	33	NI	–	–	–	++	++	++	++
10	Male	21	Shoulder	G2	NA	NA	NA	–	+	–	–	–	–	–	++
11	Male	47	Inguinal	G2	DOD	Lung	17	–	–	–	–	++	++	–	+++
12	Male	73	Forearm	G2	Alive	–	12	–	–	–	–	++	–	–	++

*Cases with known neurofibromatosis type 1

treated in a microwave oven using 0.01 M citrate buffer (pH 6.0) for three 10-min periods; for RB immunohistochemistry, sections were pretreated in glyca buffer (Biogenex, pH 3.0) for 15 min. Endogenous peroxidase activity was blocked by incubation (30 min) in 0.3% H_2O_2 in methanol. The sections were gently rinsed with Tris-buffered saline (TBS) and then incubated with bovine serum albumin for 30 min to reduce non-specific antibody binding. Sections were incubated with monoclonal antibodies against MIB-1 (clone Ki-S5; Dako, Hamburg, Germany; dilution 1:50), p53 (clone DO-7, Dako, 1:50), PTEN (clone A2b1, Chemicon, 1:800), and a polyclonal antibody against RB (Biogenex, 1:15) for 60 min at 37°C in a humified chamber. As a positive control, a colon carcinoma overexpressing RB protein (more than 80% of glandular cells were positive) and a glioblastoma multiforme with strong expression of PTEN protein and without mutation in all nine exons of the *PTEN* gene confirmed using polymerase chain reaction–single-strand conformation polymorphism (PCR-SSCP) analyses were used. Negative controls included omission of the primary antibody and its substitution with an irrelevant mouse monoclonal antibody. The signal was detected using the streptavidin-biotin-peroxidase complex method (LSAB) according to the manufacturer's recommendation (Dako). The RB signal was detected using the Vectastain ABC system according to the manufacturer's recommendation (Vector Lab., Burlingame, Calif.). DAB (3,3′ diaminobenzidine hydrochloride containing 0.08% hydrogen peroxidase) was used as a chromogen to visualize the peroxidase activity for PTEN, MIB-1, and p53; whereas neofucsin was used as a chromogen for RB immunostaining. Finally, the sections were counterstained with hematoxylin.

Immunohistochemical reactions for p53, pRB, and MIB-1 were scored according to the following categories: – definitely negative, + not more than 10% of the tumor cells were stained, ++ 10–50% of the neoplastic cells were stained, +++ more than 50% of the tumor cells were stained. Only a distinct nuclear immunoreaction was judged as positive for p53, pRB, and MIB-1. The immunoreaction for the PTEN protein was graded semi-quantitatively as follows: – no immunoreaction, + weak, ++ moderate, +++ strong immunoreaction.

DNA preparation

DNA from frozen tissues was prepared using the standard phenol–chloroform extraction method according to a protocol by Sambrook et al. [29].

PCR-SSCP analysis

For the *p53* gene, exons 5–8 were analyzed by means of the PCR-SSCP technique. A methodological description and primer sequences are given in detail by Schneider-Stock et al. [30, 31]. In brief, for SSCP analysis, an aliquot of the PCR product (7 µl) was denatured in formamide buffer at 95 C for 5 min, chilled on ice, and loaded onto ultrathin mutation detection enhancement (MDE) gels (AT Biochem, Malvern, Pa.).

For the *PTEN* gene, amplification of the protein coding region of all nine exons was performed with primers that have previously been reported [37, 39]. For exon 2, 3, 5, and 9, some additional primer pairs were used to generate shorter fragments for SSCP analysis. All primers were 20 bp in length, and their designations were chosen according to their 5′-end in the Genbank reference sequence of the *PTEN* gene (GI 4240386). All reverse (R)- primers correspond to the reverse reference sequence: exon 2 2F51937/2R52147; exon 3 3F83441/3R83560; exon 5 5F91051/5R91200; exon 9 9F123211/9R123409; exon 9 9F123301/9R123540. Four glioblastoma DNA samples with sequenced *PTEN* point mutations were kindly provided by Dr. G. Reifenberger (Institute of Neuropathology, University of Bonn, Germany). Together with a point mutation in the glioma cell line U87MG (ATCC), they served as positive controls.

Gels were stained by means of a modified silver-staining protocol introduced by Goldman and Merril [10]. PCR fragments showing mobility shifts of their single strands were directly sequenced on an automated fluorescence sequencer (ALF Express, Pharmacia Biotech) using the T7 sequenase protocol.

LOH analysis

Four intragenic *Rb* markers [three with restriction fragment-length polymorphism (RFLP) at introns 1, 17, and 25, and one with variable-number tandem repeat (VNTR) polymorphism at intron 20] and two intragenic p53 markers (VNTR intron 1; RFLP exon 4) were analyzed by means of PCR as recently described [32]. *Rb* markers and the intron 1 polymorphic region in the *p53* gene were amplified as follows: 95°C for 5 min, 20 cycles of 95°C for 10 s, 66°C for 10 s, and 72°C for 20 s, with a stepwise decrease of 2°C in each fifth cycle, and finally 30 cycles at 95°C for 45 s, 58°C for 1 min, and 72°C for 1 min. Amplification of exon 4 of the *p53* gene was performed with 35 cycles of 94°C for 1 min, 56°C for 1 min, and 72°C for 1 min.

We added 100 ng DNA, 20 mM Tris/HCl, 1.5 mM $MgCl_2$, 25 pmol each primer, 150 µM each dNTP, and 0.2 U *Taq* polymerase (Gibco, BRL) to a total reaction volume of 50 µl. Amplification was performed in an automated thermocycler (Maxicycler PTC 100, Watertown, Mass.). Restriction-fragment analyses were done using the following endonucleases: intron 1 *Bam*HI; intron 17 *Xba*I; intron 25 *Dra*I; exon 4 *Bsh*I. All restriction enzymes were obtained from AGS (Heidelberg, Germany). PCR fragments were run on native 8% polyacrylamide gels, cross-linked with piperazine diacrylamide, and visualized using a silver-staining method described by Budowle et al. [5].

An allelic loss was considered in cases when, in comparison with reference DNA, the signal of a tumor band disappeared or signal intensity was reduced by more than 50%. Evaluation was done twice – visually or by densitometry (VDS, Pharmacia Biotech) – in ambiguous cases.

Results

All MPNSTs examined by means of immunohistochemistry were characterized by an extraordinary high proliferative activity with MIB-1 labeling indices between 10% and 50%; in one case (no. 11 in Table 1), more than 50% of the nuclei were immunopositive for the MIB-1 proliferation marker (Fig. 1a).

Positive immunoreactions for the p53 protein were observed in 10 of 12 MPNSTs [83%; + 3 (25%); ++ 7 (58%); +++ 0 (0%)]. In 1 of 12 MPNSTs (8%; tumor 7 in Table 1), an A→T transversion at codon 155 in exon 5 of the *p53* gene was found, which resulted in an amino acid change from Thr to Ser. In this tumor, between 10% and 50% of the tumor cell nuclei were immunoreactive for the p53 protein (Fig. 1b). In two other tumors (no. 5 and no. 10 in Table 1; Fig. 2), allelic loss of the *p53* gene occurred (20%). This *p53* alteration was accompanied by positive immunostaining for p53 protein in the first case, while in the other case no nuclear accumulation of p53 protein was found.

Loss of pRb expression was observed in 2 of 12 MPNSTs (17%). In the remaining cases, between 10% and 50% of the neoplastic cells demonstrated a heterogeneous nuclear staining for the RB protein. LOH analysis demonstrated an allelic loss of the *Rb* gene in four of the informative tumors (44%; Fig. 2), including the two cases with known NF1 (Table 1). This alteration of the

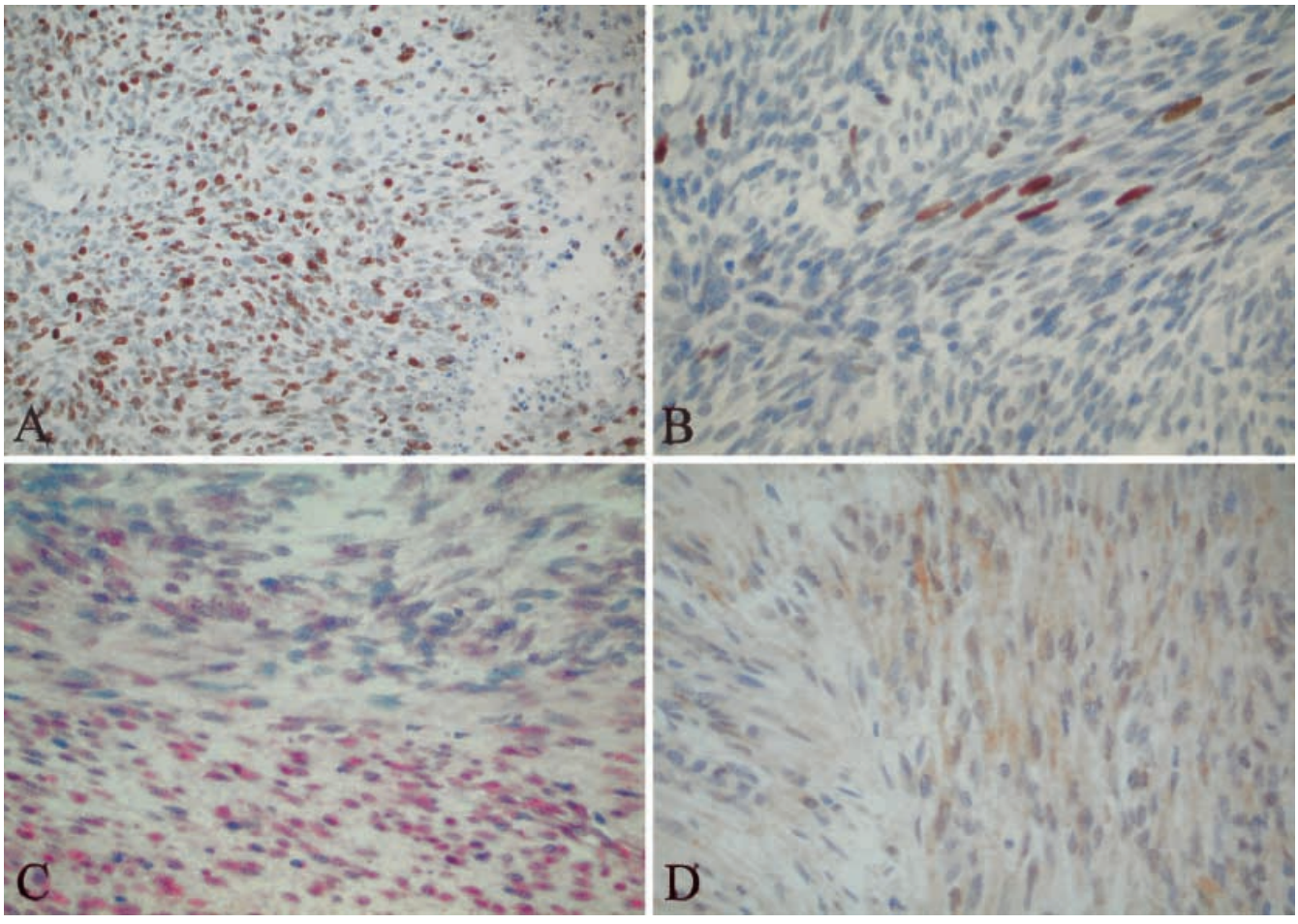

Fig. 1 Malignant peripheral nerve sheath tumor. **a** Highly proliferative tumor with more than 50% of the tumor cell nuclei immunoreactive for MIB-1 (×200). **b** Nuclear accumulation of p53 protein in the case with a mutation in exon 5 of the *p53* gene (case no. 7 in Table 1; ×400). **c** Immunoexpression of RB protein in a case with neurofibromatosis type 1 and allelic loss in the *Rb* gene (case no. 2 in Table 1; ×400). **d** Cytoplasmic immunoreactivity for the PTEN protein are detected mainly in fascicles composed of densely packed spindled tumor cells (×400)

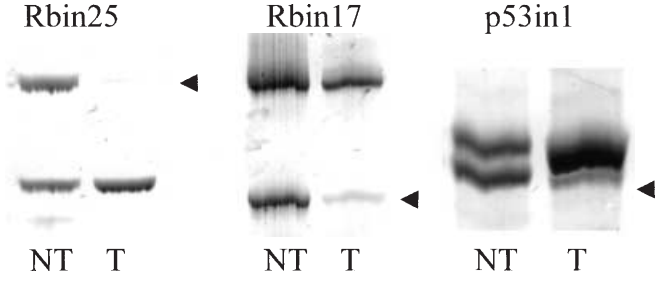

Fig. 2 Loss of heterozygosity (LOH) in the *Rb* gene (introns 25 and 17) in two malignant peripheral nerve sheath tumor (MPNST) cases (no. 1* and no. 2 in Table 1) and LOH in the p53 gene (intron 1) in another MPNST (no. 10 in Table 1). *NT* no tumor, *T* tumor; Allelic losses are marked by *arrows*

Rb gene was associated with a loss of *Rb* expression in one tumor (case no. 1). In the other three tumors with a LOH of the *Rb* gene, strong expression of the RB protein was maintained (Fig. 1c).

Expression of the PTEN protein was found in 8 of 12 MPNSTs [67%; + 5 (42%); ++ 2 (17%); +++ 1 (8%)]. The immunoreaction was generally observed within the cytoplasm of the neoplastic schwann cells; no staining of the nuclei was seen (Fig. 1d). In some tumors, there was a heterogeneous distribution of immunoreactive cells, with distinct areas without positive staining. However, in the 12 tumors examined, SSCP analysis failed to demonstrate aberrantly migrating single strands within the complete protein coding region of the *PTEN* gene.

There was no correlation between *p53*, *Rb*, and *PTEN* protein expression and tumor grading, localization and demographic data, respectively (Table 1).

Discussion

We studied the molecular alterations and immunohistochemical expression of the *p53*, *Rb*, and *PTEN* tumor suppressor genes in a series of 12 MPNSTs and determined the proliferative activity of the tumors using the MIB-1 labeling index.

P53 is the most commonly mutated tumor suppressor in human cancer and is found to be disrupted in more than 50% of tumors [17]. In our series, among 12 tumors, we identified one mutation (8%) of the *p53* gene in a sporadic MPNST. This is a much lower frequency than with the recent observations of Schneider-Stock et al. [31] who identified four mutations among 12 sporadic MPNSTs (33%), although in two other single cases [36, 38] no mutations in sporadic MPNSTs were found. In the setting of NF1, the reported frequency of p53 mutations in these tumors ranged from three of four (75%, [15]) and two of seven (29%, [23]) to no detectable mutation in five MPNSTs [27] and in the two NF 1 cases in the present study. In addition, although we did not find a LOH for p53 in the NF1-associated tumors in our series, this alteration has been recently reported in three of five NF1-associated MPNSTs [27], as well as in two single case reports including one malignant triton tumor, which is a rare variant of MPNST with muscle differentiation [21, 35]. However, because all these findings are largely based on a few cases, the differences in the frequency of both LOH for the *p53* gene, as well as *p53* mutational status, may be due to sampling error and therefore have to be determined more exactly in larger series.

In contrast to the limited information concerning the molecular alterations of p53, nuclear accumulation of the p53 protein in a significant proportion of MPNSTs has been repeatedly observed [11, 13]. Based on the observation that wild-type p53 has a very short half-life, in contrast to mutated p53 protein [8], immunodetection of p53 has been interpreted as the presence of p53 mutation. However, besides studies showing a good correlation between immune reaction and mutational analysis, others found a lack of such correlation [3]. In line with the latter, in the present study we observed a high proportion of cases with positive p53 immunostaining which lacked for detectable mutations in the p53 gene. This may be due to the fact that mutations may have occurred outside the sequenced region, although the mutational rate outside this region seems to be low [36]. Alternatively, staining could be facilitated by activating the expression of other genes encoding proteins that might interact with or stabilize p53, e.g., MDM2 [7].

The *Rb* gene represents another tumor suppressor with a central role in regulating the cell cycle [2], but molecular alterations of this gene in MPNSTs have not been investigated extensively. In the present study, we found LOH for the *Rb* gene in a substantial proportion (44%) of MPNSTs, including the two cases with NF1. This alteration was associated with a loss of expression of RB protein in one case, and in another case we observed loss of pRb without LOH. Our findings are further evidence of the important role of the *Rb* gene product in MPNST tumorigenesis. Recently, Berner et al. [4] reported frequent cytogenetic aberrations in the CDKN2A and *Rb* gene and suggested that disruption of the RB pathway may be common in MPNST. In another study, Kourea et al. [13] described a loss of immunohistochemical expression of RB in 11% of MPNSTs; this loss of RB protein was found to be significantly associated with tumor recurrence. The same researchers demonstrated a frequent occurrence of homozygous deletions of the *CDKN2A* gene in these tumors [14], which may precede the transformation from benign neurofibroma to MPNST in NF1 [25]. Because the CDKN2A gene and its gene product p16 are intimately linked to the RB pathway by preventing RB protein phophorylation (and subsequent inactivation allowing cell division) via inactivating cyclin-dependent kinases 4 and 6, a loss of RB function either due to allelic or protein loss or both may further encourage cell-cycle deregulation resulting in the highly malignant phenotype of MPNSTs.

The phosphorylation status of the RB protein has been shown to be controlled in part by the *PTEN* tumor suppressor gene [6]. Although the *PTEN* gene has been shown to be mutated in various human cancers, we failed to demonstrate mutations within the complete coding region of this gene in MPNSTs. Therefore, one can argue that there is probably no significant role for PTEN in these tumors. This is underlined by the presence of PTEN protein in the majority of the tumors. The lack of PTEN immunostaining seen in four cases may be either due to post-translational modification, rapid degradation of the protein, or lower transcriptional activity (promoter methylation). Although no details about the cellular distribution of PTEN immunoreaction in peripheral nerves can be obtained from the literature, we observed PTEN expression in the schwann cell cytoplasm in benign schwannomas, traumatic neuromas, as well as normal human sural nerve specimens (unpublished data). These observations suggest a constitutive expression of PTEN in non-neoplastic schwann cells, which is maintained in benign schwann cell neoplasms. Therefore, PTEN expression of MPNSTs, seen in the present study, probably reflect the schwann cell origin of these malignant tumors. This kind of progression was recently shown by McMenamin et al. [22].

In summary, we suggest that the *p53* and *Rb* tumor suppressor genes play an important role for the malignant phenotype in a significant subset of both sporadic and NF1-associated MPNSTs, whereas alterations in the *PTEN* tumor suppressor seem to play no role in these tumors. Our findings underline the notion of a disturbed cell-cycle control as a critical step in the development of MPNSTs.

References

1. Enzinger FM, Weiss SW (eds) (1995) Malignant tumors of the peripheral nerves. In: Soft tissue tumors. Mosby, St. Louis, pp 889–893
2. Bartek J, Bartkova J, Lukas J (1997) The retinoblastoma protein pathway in cell cycle control and cancer. Exp Cell Res 237:1–6
3. Battifora H (1994) p53 immunohistochemistry: a word of caution (editorial). Hum Pathol 25:435–437
4. Berner JM, Sorlie T, Mertens F, Henriksen J, Saeter G, Mandahl N, Brogger A, Myklebost O, Lothe RA (1999) Chromosome band 9p21 is frequently altered in malignant peripheral nerve sheath tumors: studies of CDKN2A and other genes of the pRB pathway. Genes Chromosomes Cancer 26:151–160

5. Budowle B, Chakraborty R, Giusti AM, Eisenberg AJ, Allen RC (1991) Analysis of the variable number of tandem repeats locus D1S80 by the polymerase chain reaction followed by high resolution polyacrylamide gel electrophoresis. Am J Hum Genet 48:137–144
6. Cheney IW, Neuteboom ST, Vaillancourt MT, Ramachandra M, Bookstein R (1999) Adenovirus-mediated gene transfer of MMAC1/PTEN to glioblastoma cells inhibits S phase entry by the recruitment of p27Kip1 into cyclin E/CDK2 complexes. Cancer Res 59:2318–2323
7. Cordon-Cardo C, Latres E, Drobnjak M, Oliva MR, Pollack D, Woodruff JM, Marechal V, Chen J, Brennan MF, Levine A (1994) Molecular abnormalities of mdm2 and p53 in adult soft tissue sarcomas. Cancer Res 54:794–799
8. Finlay C, Hinds P, Levine A (1989) The p53 proto-oncogene can act as a suppressor of transformation. Cell 57:1083–1093
9. Furnari FB, Huang HJ, Cavenee WK (1998) The phosphoinositol phosphatase activity of PTEN mediates a serum- sensitive G1 growth arrest in glioma cells. Cancer Res 58:5002–5008
10. Goldmann D, Merril CR (1982) Silver staining of DNA in polyacrylamide gels: linearity and effect of fragment size. Electrophoresis 3:24–26
11. Kindblom LG, Ahlden M, Meis-Kindblom JM, Stenman G (1995) Immunohistochemical and molecular analysis of p53, MDM 2, proliferating cell nuclear antigen and Ki67 in benign and malignant peripheral nerve sheath tumours. Virchows Arch 427:19–26
12. Kourea HP, Bilsky MH, Leung DH, Lewis JJ, Woodruff JM (1998) Subdiaphragmatic and intrathoracic paraspinal malignant peripheral nerve sheath tumors: a clinicopathologic study of 25 patients and 26 tumors. Cancer 82:2191–2203
13. Kourea HP, Cordon-Cardo C, Dudas M, Leung D, Woodruff JM (1999) Expression of p27(kip) and other cell cycle regulators in malignant peripheral nerve sheath tumors and neurofibromas: the emerging role of p27(kip) in malignant transformation of neurofibromas. Am J Pathol 155:1885–1891
14. Kourea HP, Orlow I, Scheithauer BW, Cordon-Cardo C, Woodruff JM (1999) Deletions of the INK4A gene occur in malignant peripheral nerve sheath tumors but not in neurofibromas. Am J Pathol 155:1855–1860
15. Legius E, Marchuk DA, Collins FS, Glover TW (1993) Somatic deletion of the neurofibromatosis type 1 gene in a neurofibrosarcoma supports a tumour suppressor gene hypothesis. Nat Genet 3:122–126
16. Legius E, Dierick H, Wu R, Hall BK, Marynen P, Cassiman JJ, Glover TW (1994) TP53 mutations are frequent in malignant NF1 tumors. Genes Chromosomes Cancer 10:250–255
17. Levine AJ (1997) p53, the cellular gatekeeper for growth and division. Cell 88:323–331
18. Lewis JJ, Brennan MF (1996) Soft tissue sarcomas. Curr Probl Surg 33:817–872
19. Li DM, Sun H (1998) PTEN/MMAC1/TEP1 suppresses the tumorigenicity and induces G1 cell cycle arrest in human glioblastoma cells. Proc Natl Acad Sci U S A 95:15406–15411
20. Li J, Yen C, Liaw D, Podsypanina K, Bose S, Wang SI, Puc J, Miliaresis C, Rodgers L, McCombie R, Bigner SH, Giovanella BC, Ittmann M, Tycko B, Hibshoosh H, Wigler MH, Parsons R (1997) PTEN, a putative protein tyrosine phosphatase gene mutated in human brain, breast, and prostate cancer Science 275:1943–1947
21. Lothe RA, Saeter G, Danielsen HE, Stenwig AE, Hoyheim B, O'Connell P, Borresen AL (1993) Genetic alterations in a malignant schwannoma from a patient with neurofibromatosis (NF1). Pathol Res Pract 189:465–471
22. McMenamin ME, Fletcher CD (2001) Expanding the spectrum of malignant change in schwannomas. Epithelioid malignant change, epithelioid malignant peripheral nerve sheath tumor, and epithelioid angiosarcoma: a study of 17 cases. Am J Surg Pathol 25:13–25
23. Menon AG, Anderson KM, Riccardi VM, Chung RY, Whaley JM, Yandell DW, Farmer GE, Freiman RN, Lee JK, Li FP (1990) Chromosome 17p deletions and p53 gene mutations associated with the formation of malignant neurofibrosarcomas in von Recklinghausen neurofibromatosis. Proc Natl Acad Sci U S A 87:5435–5439
24. Mertens F, Dal Cin P, De W, I, Fletcher CD, Mandahl N, Mitelman F, Rosai J, Rydholm A, Sciot R, Tallini G, van Den BH, Vanni R, Willen H (2000) Cytogenetic characterization of peripheral nerve sheath tumours: a report of the CHAMP study group. J Pathol 190:31–38
25. Nielsen GP, Stemmer-Rachamimov AO, Ino Y, Moller MB, Rosenberg AE, Louis DN (1999) Malignant transformation of neurofibromas in neurofibromatosis 1 is associated with CDKN2A/p16 inactivation. Am J Pathol 155:1879–1884
26. Paramio JM, Navarro M, Segrelles C, Gomez-Casero E, Jorcano JL (1999) PTEN tumour suppressor is linked to the cell cycle control through the retinoblastoma protein. Oncogene 18:7462–7468
27. Rasmussen SA, Overman J, Thomson SA, Colman SD, Abernathy CR, Trimpert RE, Moose R, Virdi G, Roux K, Bauer M, Rojiani AM, Maria BL, Muir D, Wallace MR (2000) Chromosome 17 loss-of-heterozygosity studies in benign and malignant tumors in neurofibromatosis type 1. Genes Chromosomes Cancer 28:425–431
28. Ricci A Jr, Parham DM, Woodruff JM, Callihan T, Green A, Erlandson RA (1984) Malignant peripheral nerve sheath tumors arising from ganglioneuromas. Am J Surg Pathol 8:19–29
29. Sambrook J, Fritsch EF, Maniatis T (1989) Molecular cloning. A laboratory manual. Cold Spring Harbor Laboratory Press, Cold Spring Harbor, MA
30. Schneider-Stock R, Haeckel C, Radig K, Pein CD, Roessner A (1997) Improved detection of p53 mutations in soft tissue tumors using new gel composition for automated nonradioactive analysis of single-strand conformation polymorphism. Electrophoresis 18:2849–2851
31. Schneider-Stock R, Radig K, Oda Y, Mellin W, Rys J, Niezabitowski A, Roessner A (1997) p53 gene mutations in soft-tissue sarcomas–correlations with p53 immunohistochemistry and DNA ploidy. J Cancer Res Clin Oncol 123:211–218
32. Schneider-Stock R, Walter H, Radig K, Rys J, Bosse A, Kuhnen C, Hoang-Vu C, Roessner A (1998) MDM 2 amplification and loss of heterozygosity at Rb and p53 genes: no simultaneous alterations in the oncogenesis of liposarcomas. J Cancer Res Clin Oncol 124:532–540
33. Sherr CJ (1996) Cancer cell cycles. Science 274:1672–1677
34. Steck PA, Pershouse MA, Jasser SA, Yung WK, Lin H, Ligon AH, Langford LA, Baumgard ML, Hattier T, Davis T, Frye C, Hu R, Swedlund B, Teng DH, Tavtigian SV (1997) Identification of a candidate tumour suppressor gene, MMAC1, at chromosome 10q23.3 that is mutated in multiple advanced cancers. Nat Genet 15:356–362
35. Strauss BL, Gutmann DH, Dehner LP, Hirbe A, Zhu X, Marley EF, Liapis H (1999) Molecular analysis of malignant triton tumors. Hum Pathol 30:984–988
36. Toguchida J, Yamaguchi T, Ritchie B, Beauchamp RL, Dayton SH, Herrera GE, Yamamuro T, Kotoura Y, Sasaki MS, Little JB (1992) Mutation spectrum of the p53 gene in bone and soft tissue sarcomas. Cancer Res 52:6194–6199
37. Tohma Y, Gratas C, Biernat W, Peraud A, Fukuda M, Yonekawa Y, Kleihues P, Ohgaki H (1998) PTEN (MMAC1) mutations are frequent in primary glioblastomas (de novo) but not in secondary glioblastomas. J Neuropathol Exp Neurol 57:684–689
38. Wadayama B, Toguchida J, Yamaguchi T, Sasaki MS, Yamamuro T (1993) p53 expression and its relationship to DNA alterations in bone and soft tissue sarcomas. Br J Cancer 68:1134–1139
39. Watanabe K, Peraud A, Gratas C, Wakai S, Kleihues P, Ohgaki H (1998) p53 and PTEN gene mutations in gemistocytic astrocytomas. Acta Neuropathol (Berl) 95:559–564
40. Woodruff JM, Selig AM, Crowley K, Allen PW (1994) Schwannoma (neurilemoma) with malignant transformation. A rare, distinctive peripheral nerve tumor. Am J Surg Pathol 18:882–895

Virchows Arch (2002) 440:616–626
DOI 10.1007/s00428-001-0595-4

ORIGINAL ARTICLE

**Jyoji Yamate · Tomoko Kuriyama · Maki Kawashima
Masako Nakanishi · Mika Ide · Mitsuru Kuwamura
Yasuhiro Tsukamoto · Takao Kotani
Shunji Nakatsuji**

Establishment and characterization of transplantable tumor line (KB) and cell lines (KB-P and KB-D8) from a rat thymus-derived dendritic cell sarcoma

Received: 3 August 2001 / Accepted: 27 November 2001 / Published online: 13 February 2002
© Springer-Verlag 2002

Abstract A transplantable tumor line (KB) was established in syngeneic rats from a naturally occurring sarcoma that had arisen in the thymus of a 24-month-old male F344 rat. Further, a cell line (KB-P) was induced from KB and a cloned cell line (KB-D8) was isolated from KB-P. The primary thymic tumor and KB tumors showed heterogeneous histological growth patterns such as sheet-like, ill-defined bundle, fascicular and interwoven fashions, consisting of spindle cells, oval cells and histiocytic large round cells. Immunohistochemically, neoplastic cells in KB tumors and KB-P and KB-D8 cultures reacted to vimentin and were labeled with antibodies of OX6 (for rat major histocompatibility complex class-II antigens), ED5 (for rat follicular dendritic cells; FDCs) and RED-1 (for interdigitating dendritic cells) in varying degrees, indicating that neoplastic cells exhibited the immunophenotypes of rat dendritic cells. In addition, neoplastic cells were immunoreactive to ED1 (for rat monocytes/macrophages) and ED2 (for rat tissue macrophages), and also showed positive reactions to histiocytic lysosomal enzymes such as acid phosphatase and nonspecific esterase. Ultrastructurally, neoplastic cells had cell surface projections, cisterna-like structures and variously developed lysosomes in the cytoplasm. Based on these findings, the present tumor was regarded as dendritic cell-derived sarcoma capable of expressing macrophage-like and histiocytic nature. A reverse-transcription polymerase chain reaction method revealed that the addition of lipopolysaccharide dose dependently increased the expression of mRNA of transforming growth factor-β1, a proinflammatory factor, in KB-D8 cells. The transplantable line (KB) and cell lines (KB-P and KB-D8) may become useful tools for studying the histogenesis and pathobiological functions of dendritic cells.

Keywords Macrophage-like nature · Rat dendritic cell-sarcoma · Rat MHC class-II antigens · Transforming growth factor-β1 · Transplantable tumor

J. Yamate (✉) · T. Kuriyama · M. Kawashima · M. Nakanishi
M. Ide · M. Kuwamura · T. Kotani
Department of Veterinary Pathology,
Graduate School of Agriculture and Biological Sciences,
Osaka Prefecture University, Gakuencho 1-1, Sakai,
Osaka 599-8531, Japan
e-mail: yamate@vet.osakafu-u.ac.jp
Tel.: +81-72-2549482, Fax: +81-72-2507208

Y. Tsukamoto
Department of Veterinary Anatomy,
Graduate School of Agriculture and Biological Sciences,
Osaka Prefecture University, Gakuencho 1-1, Sakai,
Osaka 599-8531, Japan

S. Nakatsuji
Department of Pathology, Toxicologic Research Laboratories,
Fujisawa Pharmaceutical Co., Ltd., Kashima 2-chome,
Yodogawa-ku, Osaka 532-8514, Japan

Introduction

Dendritic cells consist of interstitial dendritic cells in non-lymphoid tissues, interdigitating cells/follicular dendritic cells (FDCs) in lymphoid tissues, as well as Langerhans' cells of the epidermis [33, 38, 40]. Ontogenetically, dendritic cells are considered to develop from the hematopoietic stem cells, and the precursor cells at the immature stage spread over the tissues in the whole body [33, 40]. The dendritic cells play an important role in immune responses as potent antigen-presenting cells [4, 35, 41]. With the exception of Langerhans' cell histiocytosis [12], neoplasms of dendritic cell origin are extremely rare in humans [1, 17, 26]; the main site of involvement is the lymph node, and a few extranodal cases have been reported [9, 21, 25]. To our knowledge, there have been no papers describing dendritic cell sarcomas in the lymphoid tissue of rats [39].

F344 rats are an inbred strain with genetically homogeneous nature and have been widely used in chronic toxicity and carcinogenicity studies. We have attempted to establish various transplantable tumor lines from

spontaneous tumors found in F344 rats to study biological behaviors, morphological characteristics, and paraneoplastic manifestation relative to neoplasia [31, 43, 45, 48, 49]. In the attempt, we established a transplantable tumor line (KB) from a spontaneous sarcoma arising in the thymus of an aged F344 rat. The immunohistochemical examination of KB tumors revealed that neoplastic cells strongly reacted with an antibody (OX6) against rat major histocompatibility complex (MHC) class-II (Ia) antigens. The OX6 has been widely used to detect antigen-presenting cells such as dendritic cells in rat pathological lesions [18, 46, 52, 53]. The positive reactions to OX6 thus suggested that cells constituting KB tumors might show immunophenotypes of dendritic cells. We further succeeded in establishing an in vitro cell line (KB-P) from KB and in isolating a cloned cell line (KB-D8) from KB-P. In the present study, besides the primary tumor, KB tumors and cultured cells of KB-P and KB-D8 were characterized by light/electron microscopy and enzyme/immunohistochemistry. Further, possible productions of proinflammatory cytokines, such as transforming growth factor-β1 (TGF-β1) and tumor necrosis factor-α (TNF-α), were investigated by treating KB-D8 cells with lipopolysaccharide (LPS) because dendritic cells are considered to be macrophage-related [7, 33, 34, 40] and LPS is a major modulator of macrophage functions [2, 51].

Materials and methods

A tissue fragment 2 mm in diameter was cut from the primary thymic tumor and transplanted subcutaneously into a syngeneic male rat through a trochar under light anesthesia with ether. Serial transplantations then were made at 6-week interval until the eighth generation by implanting a tumor tissue fragment [48]. In each passage, one to four F344 male rats were used. The transplantable tumor line was designated KB.

Tissue fragments from KB tumor at passage three were dispersed with 0.1% trypsin and 0.02% ethylene diamine tetraacetic acid in phosphate-buffered saline (PBS). The dispersed cells were incubated in plastic tissue culture flasks at 37°C in a humidified 5% CO_2 atmosphere. The growth medium was Eagle's minimum essential medium (MEM; Nissui, Tokyo, Japan) containing 10% fetal bovine serum (Bioserum, UBL, Japan), 0.03% L-glutamine (Nissui), penicillin (100 U/ml), and streptomycin (100 μg/ml). The cultured cells, named KB-P, were serially passaged at 5-day to 7-day intervals until the 30th generation. KB-P cells at passage 20 were cloned twice consecutively using a limiting dilution technique [43, 45, 48]. A cloned cell line (KB-D8) was serially subcultured until the 25th passage. To examine tumorigenecity, 10^6 cells of KB-P or KB-D8 at different passages were inoculated into the subcutaneous tissue of syngeneic male rats.

According to our institutional guideline for animal care, F344 rats (Charles River Japan, Hino, Shiga, Japan) used were housed in an animal room controlled at 22±3°C, with a 12-h/12-h light/dark cycle, and were euthanized under ether anesthesia.

The primary tumor was fixed in 10% neutral buffered formalin. Besides the fixation, KB tumors and KB-P- or KB-D8-induced tumors were fixed in Zamboni's solution [50]. Tissue sections were stained with hematoxylin-eosin (HE), periodic acid Schiff (PAS), Watanabe's silver impregnation, azan-Mallory method, and phosphotungstic acid hematoxylin (PTAH). Frozen sections from the formalin-fixed tissues were stained with oil red O.

The immunohistochemical analyses were performed using the avidin-biotin complex method (ABC method; LSAB kit; Dako Corp., Carpinteria, Calif.) with primary antibodies listed in Table 1. Formalin-fixed, deparaffinized sections were used for pankeratin, vimentin, desmin, ED1 and α-smooth muscle actin (α-SMA), and Zamboni's solution-fixed, deparaffinized sections for ED2, ED5, RED-1, and OX6. The immunohistochemical methods were described [31, 50, 52]; briefly, after pretreatments as described below, sections were incubated with 1.5% skimmed milk and incubated with each primary antibody for 14 h at 4°C. A 1-h incubation with biotinylated goat anti-mouse antibody for monoclonal antibodies followed. Final incubation was carried out for 1 h with an avidin-horseradish peroxidase complex, and positive reactions were visualized with 3,3′-diaminobenzidine. Sections were counterstained with hematoxylin. Non-immunized mouse and rabbit serum served as negative controls. The pretreatments were made to quench endogenous peroxidase; sections for OX6, ED1, ED2, ED5, RED-1, and α-SMA antibodies were treated with 0.1% trypsin for 15–30 min at 37°C and then 3%H_2O_2; sections for pankeratin, vimentin, and desmin antibodies were treated by microwave and then incubated with 3% H_2O_2. Enzymehistochemically, frozen sections from fresh tumor tissues were stained for acid phosphatase (ACP), nonspecific esterase (NSE), and alkaline phosphatase (ALP) [48]; each method used is described in Table 1. For electron microscopy, small blocks from tumors were fixed in 2.5% buffered glutaraldehyde and post-fixed in 1% buffered osmium tetroxide. The ultra-thin sections from epoxy resin-embedded samples were stained with uranyl acetate and lead citrate, and examined under an electron microscope (Hitachi, H-600) at 75 kV.

For KB-P and KB-D8, doubling time was determined from viable cell numbers counted at 1 day and 5 days after seeding 10^4 cells [43, 48]. Chromosome numbers were counted in 100 cells by methods described elsewhere [43, 48]. Cells grown for 24–48 h on tissue culture glass slides were fixed in cold acetone for 5 min, and stained for ACP, NSE, and ALP. The acetone-fixed cells were also immunostained using the ABC method with the primary antibodies (Table 1). Cultured cells fixed in Bouin's solution were stained with HE. For electron microscopy, pelleted cells collected from KB-P and KB-D8 cultures were processed and examined using the same methods as described above.

The effects of LPS on KB-D8 cells were investigated with regard to OX6-immunophenotype modulation, and mRNA expressions of TGF-β1 and TNF-α. After washing in PBS, KB-D8 cells grown in slide chambers were incubated in serum-free medium for 24 h. Then, 1 ml MEM containing LPS (*Escherishia Coli*, 0127; Bacto, Detroit, Mich.) at concentrations of 0, 10, and 50 μg/ml was added. After 24-h incubation, the cells were fixed in acetone and stained immunohistochemically with OX6 using the ABC method. The expressions of TGF-β1 and TNF-α mRNAs were examined by means of reverse-transcription polymerase chain reaction (RT-PCR). The RT-PCR method was conducted as described previously [31, 43, 52]. From KB-D8 cells incubated with LPS (0, 10, and 50 μg/ml) for 24 h, total RNA was isolated [52]. The single-stranded cDNA was synthesized from total RNA (5 μg/ml) [31, 43] and was amplified by means of PCR with *Taq* DNA polymerase (Takara Shuzou, Kyoto, Japan) and each of the specific primers (sense and antisense) for rat TGF-β1, TNF-α, or β-actin (control). The following conditions were used for the amplification:

- For TGF-β1, 24 cycles of 1 min denaturation at 94°C, 1 min annealing at 62°C, and 1 min synthesis at 72°C [42]
- For TNF-α, 27 cycles of 1 min denaturation at 94°C, 1 min annealing at 57°C, and 1 min synthesis at 72°C [13]

The oligonucleotides used were as follows: the TGF-β1 sense primer 5′-CTTCAGCTCCACAGAGAAGAACTGC-3′ and antisense primer 5′-CACGATCATGTTGGACAACTGCTCC-3′ [42]; the TNF-α sense primer 5′-TGTCTACTGAACTTCGGGGTG-3′ and antisense primer 5′-GAGGCTGACTTTCTCCTGGTA-3′ [14]; the β-actin sense primer 5′-TAAAGACCTCTATGCCAACAC-3′ and antisense primer 5′-CTCCTGCTTGCTGATCCACAT-3′ [43, 52]. The PCR products were subjected to electropho-

Table 1 Primary antibodies used and results in the enzyme/immunohistochemical examinations. *KB tumors* thymic dendritic cell sarcoma-derived transplantable tumors examined at passages 1–8, *KB-P* KB-derived cultured cells examined at passages 10, 20, and 30, *KB-D8* a cloned cell line from KB-P examined at passages 5 and 20. KB-P tumors examined were induced by inoculation with KB-P at passages 10, 20, and 30. KB-D8 tumors examined were induced by inoculation with KB-D8 at passages 10 and 20. *α-SMA* alpha smooth muscle actin, *OX6* rat MHC class-II antigen-specific antibody, *ED1* and *ED2* rat macrophage/histiocyte-specific antibodies, *ED5* rat follicular dendritic cell-specific antibody, *RED-1* rat Langerhans' cell/interdigitating dendritic cell-specific antibody, *ACP* acid phosphatase, *NSE* nonspecific esterase, *ALP* alkaline phosphatase, *MFH* rat malignant fibrous histiocytoma [49, 50], *HS-P* rat histiocytic sarcoma-derived cell line [47, 48], – negative, ± very faint staining, + faint staining, *2+* moderate staining, *3+* strong staining

	Dilution	Rat tissues used as positive control	Staining results in the following materials					
			Original tumor	KB tumors	Cultured cells		Induced tumors	
					KB-P	KB-D8	KB-P	KB-D8
Monoclonal antibodies (source[a])								
Pankeratin (Dako)	×200	Epidermis	–	–	–	–	–	–
Vimentin (Dako)	×200	MFH	2+	2+	3+	3+	2+	2+
Desmin (Dako)	×200	Intestinal smooth muscle	–	–	–	–	–	–
α-SMA (Dako)	×100	Vascular smooth muscle	+	+	+	+	+	+
OX6 (Serotec)	×100	Spleen/HS-P	NE	3+	–	–	+	2+
ED1 (Chemicon)	×1000	Spleen/HS-P	NE	2+	+	+	+	+
ED2 (Serotec)	×1000	Spleen/HS-P	NE	2+	+	2+	+	+
ED5 (Serotec)	×100	Thymus/lymph node	NE	+	±	±	–	–
RED-1 (Serotec)	×100	Thymus	NE	+	2+	2+	+	+
Enzymatic staining (method)								
ACP (Gomori's method, pH 5.0)		MFH	NE	2+	+	+	2+	2+
NSE (α-naphthyl acetate, pH 7.4)		MFH	NE	2+	+	+	2+	2+
ALP (naphthol AS, pH 9.0)		MFH	NE	–	–	–	–	–

[a] Dako Corp, Carpinteria, Calif.; Serotec, Tokyo, Japan; Chemicon Int. Inc., Temecula, Calif.

resis in agarose gel. DNA was stained with ethidium bromide. The sizes of the amplification bands of TGF-β1, TNF-α, and β-actin were 310, 365, and 214 bp, respectively. The bands were semiquantitatively evaluated using image analysis software (NIH Image, Bethesda, Md.), and the intensity for TGF-β1 or TNF-α was normalized by that for β-actin [44]. To confirm the specificity of the bands, we used samples that had been treated without RT reaction or digested with DNAse as negative controls.

Results

A neoplastic nodule, firm, gray in color, and 1 cm in diameter, was found in the left lobus of thymus of a 24-month-old male F344 rat. The primary tumor was encapsulated by fibrous tissues, and there was neither infiltrative growth into surrounding tissues nor metastasis to distant organs. Histologically, the primary tumor consisted entirely of oval and spindle cells arranged in ill-defined bundles, and the remnants of thymic tissues were entrapped in the tumor tissue (Fig. 1). The cells had oval or elongated nuclei with hyperchromatin. Cell borders were indistinct, and mitotic figures were occasionally seen. Immunohistochemically, neoplastic cells reacted moderately to vimentin, indicating mesenchymal nature, and occasional cells were positive for α-SMA (Table 1). There were no neoplastic cells reacting with antibodies to pankeratin and desmin. A small amount of collagen fibers stained blue by azan-Mallory stain were present among neoplastic cells, and Silver stain showed the presence of thin reticular fibers surrounding occasional neoplastic cells. PAS-positive basement membrane-like materials were not seen. PTAH stains failed to demonstrate intracytoplastmic cross-striations or longitudinal striations.

Serial transplantations of KB tumors until the eighth passage produced a 100% take rate. There was no difference in tumor growth after implant between different passages; tissue fragments 2 mm in diameter grew into nodules of 6-cm diameter 6 weeks after the subcutaneous implantation. The subcutaneous KB tumors were well demarcated by fibrous capsule, and the cut surface was gray in color and often had necrotic areas in the center. Invasive growth was not seen, but there were a few metastatic lesions in the lungs of KB-transplanted rats. KB tumors showed various growth patterns. In addition to an ill-defined bundle pattern, as seen in the primary tumor, there were interwoven fascicles and compact-sheet growth patterns; the former consisted mainly of spindle-shaped cells (Fig. 2), whereas the latter was formed exclusively by round or oval cells (Fig. 3). Apart from the high-cellularity areas showing such growth patterns, there were low-cellularity areas consisting of solitary neoplastic cells and myxomatous intercellular materials (Fig. 4); these neoplastic cells possessed abundant, eosinophilic cytoplasm and a pale nucleus, and occasional cells were binucleated; these cells gave an appearance of histiocytic morphology (Fig. 4). Mitotic figures were frequently seen throughout tumor tissues of KB. A small amount of collagen fibers were present among neoplastic cells, and individual cells or clusters of several neoplastic cells were surrounded by reticular fibers. PAS-positive or oil red O-positive mate-

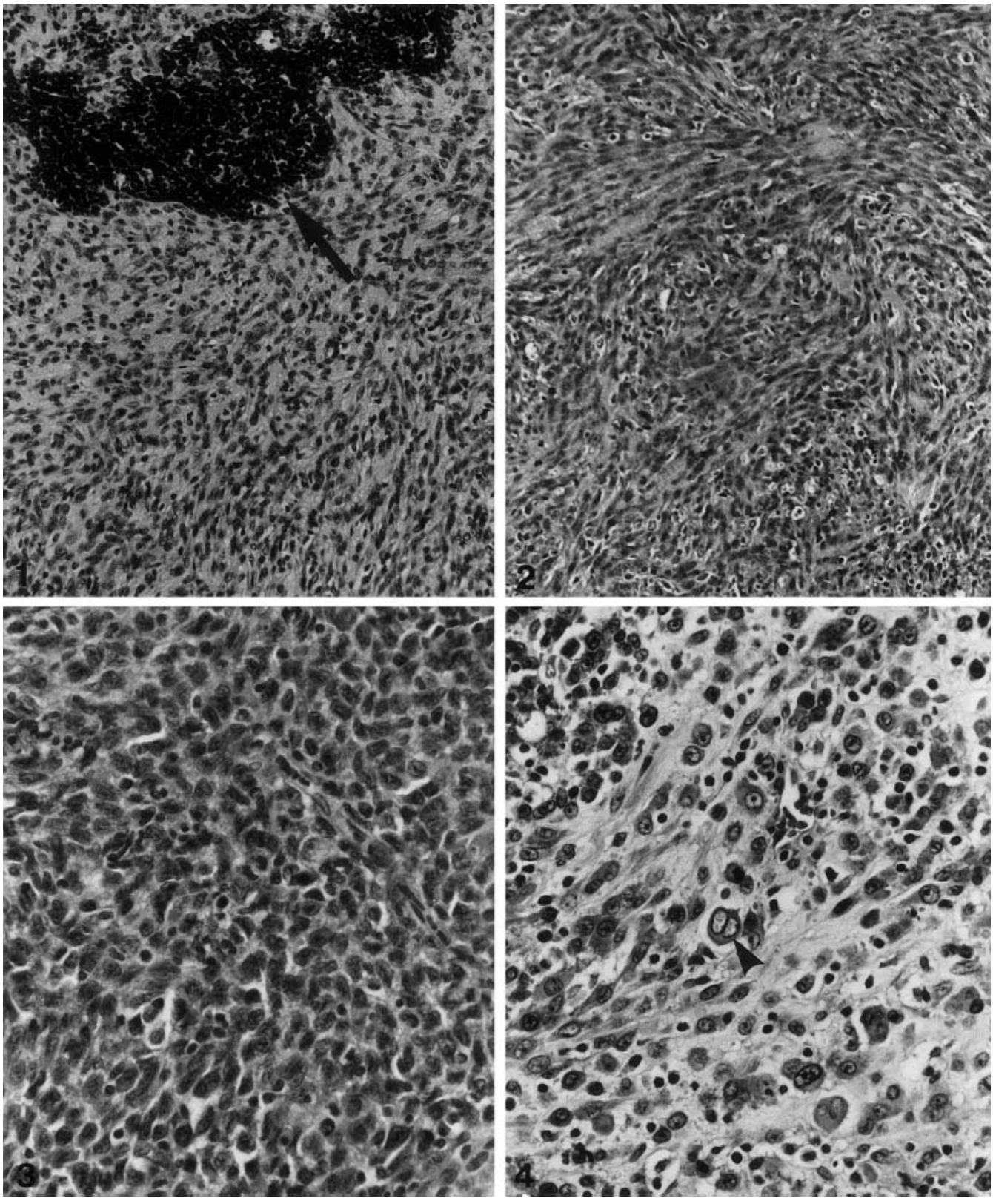

Fig. 1 The primary dendritic cell sarcoma arisen in a rat thymus consists entirely of oval and spindle cells arranged in ill-defined bundles. *Arrow* indicates the remnants of thymic tissues entrapped in the tumor tissue. Hematoxylin and eosin, ×250

Fig. 2 The dendritic cell sarcoma-derived transplantable tumor line (KB). KB tumor shows interwoven fascicles consisting of oval and spindle cells with hyperchromatic nuclei. Hematoxylin and eosin, ×250

Fig. 3 KB tumor consisting of round or oval cells arranged in a compact sheet. Cell borders are indistinct. Hematoxylin and eosin, ×350

Fig. 4 KB tumor consisting of solitary neoplastic cells and myxomatous intercellular materials. Neoplastic cells possess abundant cytoplasm and a pale nucleus, and occasional cells are binucleated (*arrowhead*); they give an appearance of histiocytic morphology. Hematoxylin and eosin, ×350

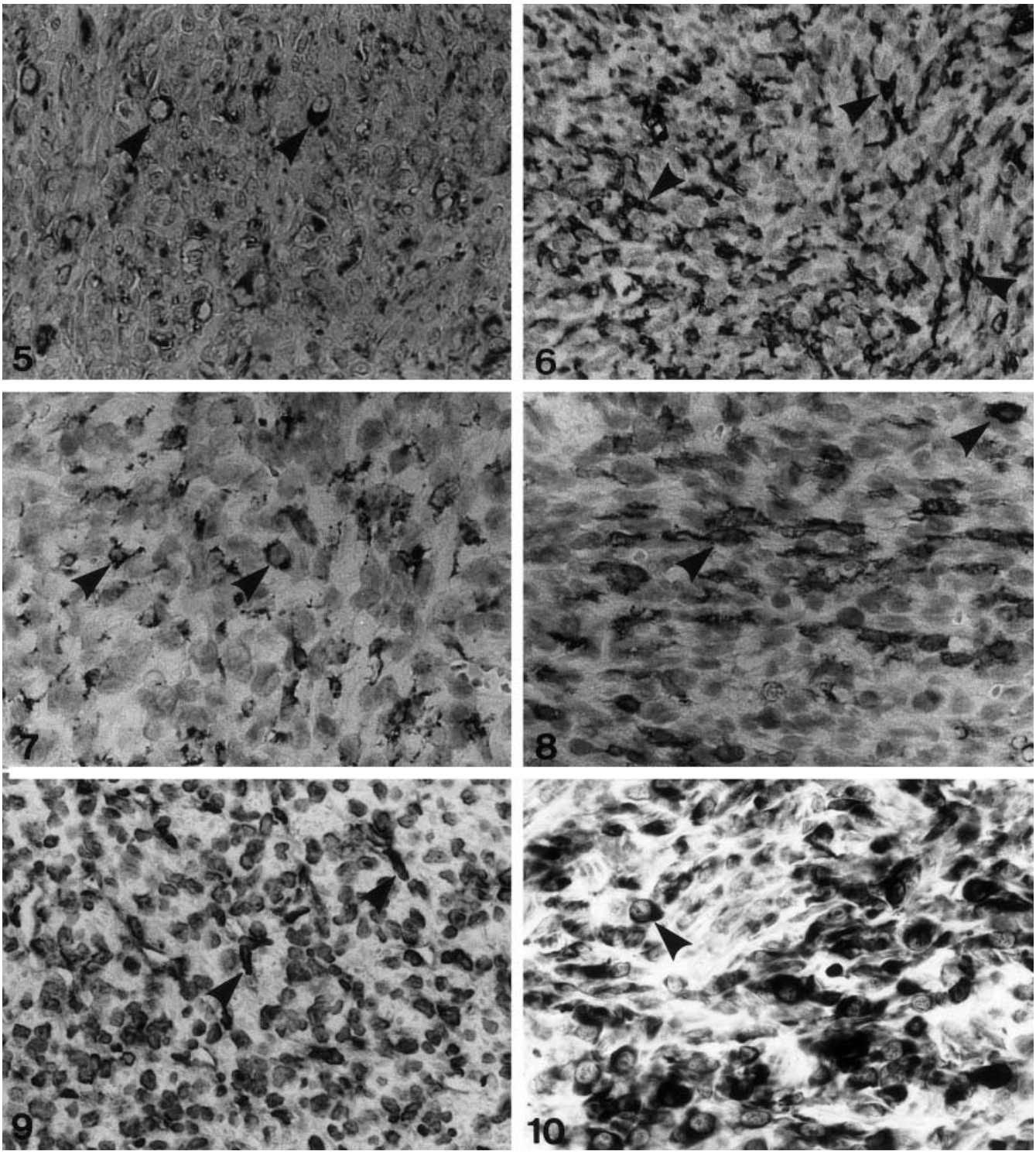

Fig. 5 Neoplastic cells in KB tumor show a moderate reaction to vimentin (*arrowheads*). Immunohistochemistry, ×250

Fig. 6 The vast majority of neoplastic cells in KB tumor react to OX6 (specific for rat MHC class-II antigens; *arrowheads*). Immunohistochemistry, ×280

Fig. 7 Many neoplastic cells in KB tumor are labeled with ED1 (specific for rat monocytes/macrophages; *arrowheads*). Because ED1 recognizes antigens on the membrane of lysosomal granules, the positive products appear granular. Immunohistochemistry, ×350

Fig. 8 Many neoplastic cells in KB tumor react to ED2 (specific for rat tissue macrophages; *arrowheads*). Immunohistochemistry, ×350

Fig. 9 Occasional neoplastic cells in KB tumor show a positive reaction to ED5 (specific for rat follicular dendritic cells; *arrowheads*). Immunohistochemistry, ×300

Fig. 10 Neoplastic cells positive to acid phosphatase are seen in KB tumor (*arrowhead*). Enzyme histochemistry, ×300

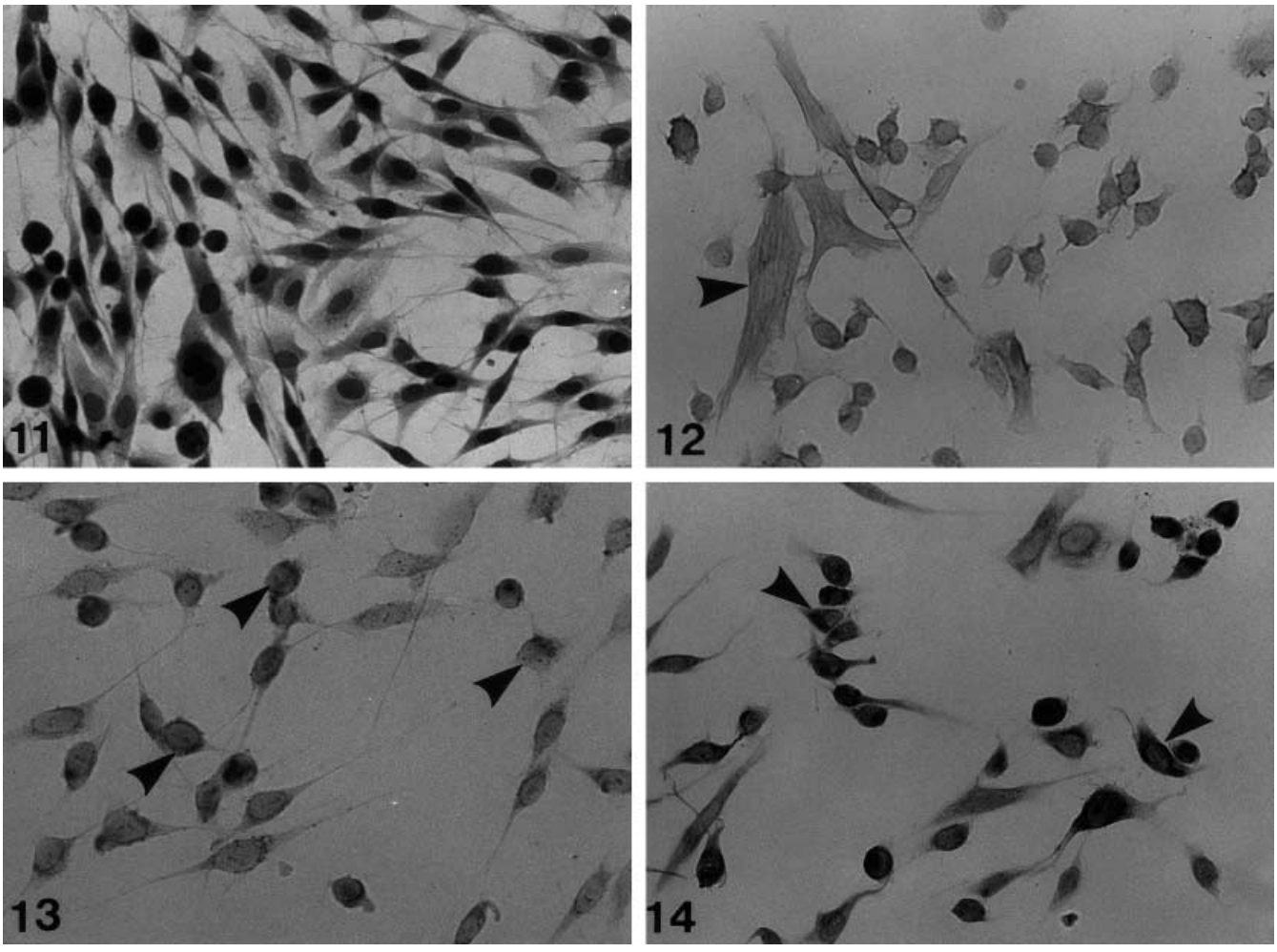

Fig. 11 Monolayer culture of cloned cell line (KB-DB) consisting of oval, spindle-shaped or polygonal cells with hyperchromatic nuclei. Hematoxylin and eosin, ×250

Fig. 12 Occasional cells in KB-D8 culture react with an antibody against α-smooth muscle actin; the positive products appear filamentous in the cytoplasm (*arrowhead*). Immunohistochemistry, ×250

Fig. 13 ED2-positive cells (*arrowheads*) are seen in KB-P culture. Immunohistochemistry, ×250

Fig. 14 Neoplastic cells reacting to RED-1 (specific for rat interdigitating dendritic cells) are seen in KB-D8 culture (*arrowheads*). Immunohistochemistry, ×250

rials were not seen in the cytoplasm of neoplastic cells. Immunohistochemically, neoplastic cells showed a moderate reaction to vimentin (Fig. 5), and occasional cells were positive for α-SMA (Table 1). Interestingly, tumor cells gave positive reactions for OX6, ED1, ED2, ED5, and RED-1 in varying degrees; in particular, almost all the neoplastic cells reacted strongly to OX6 (Fig. 6); there were also a number of cells positive to ED1 (Fig. 7) and ED2 (Fig. 8); ED5- (Fig. 9) or RED-1-postive cells were sporadically observed (Table 1). Enzymehistochemically, neoplastic cells gave a positive reaction for ACP and NSE (Fig. 10) but were negative for ALP (Table 1).

There were no marked differences in doubling time, modal chromosomal number, and cell morphology between KB-P and KB-D8. The average doubling times of KB-P (examined at passages 10, 20, and 30) and KB-D8 (examined at passages 10 and 20) were 20.3 h and 19.1 h, respectively. The modal chromosomal number of KB-P (examined at passages 20 and 30) and KB-D8 (examined at passages 10 and 20) was 48; the results indicated numerical aberration in chromosomal number of KB-P and KB-D8, since that in normal rat cells is 42 [43]. Monolayer cultures of KB-P and KB-D8 consisted of oval or spindle-shaped cells with hyperchromatic nuclei, and some cells showed polygonal configuration (Fig. 11). All the cultured cells were strongly positive for vimentin, but negative for pankeratin and desmin. Cells reacting with an α-SMA antibody were occasionally seen; the positive products appeared filamentous in the cytoplasm (Fig. 12). ED1-, ED2-, ED5-, and RED-1-positive cells were seen both in KB-P and KB-D8 in varying degrees, as shown in Table 1; particularly, cells reacting to ED2 (Fig. 13) and RED-1 (Fig. 14) were frequently observed; ED1-positive cells developed granular appearance in the cytoplasm; ED5-immunoreactivity was very faint. There were no cells reacting to OX6 in both KB-P and KB-D8. ACE- and NSE-positive cells were occa-

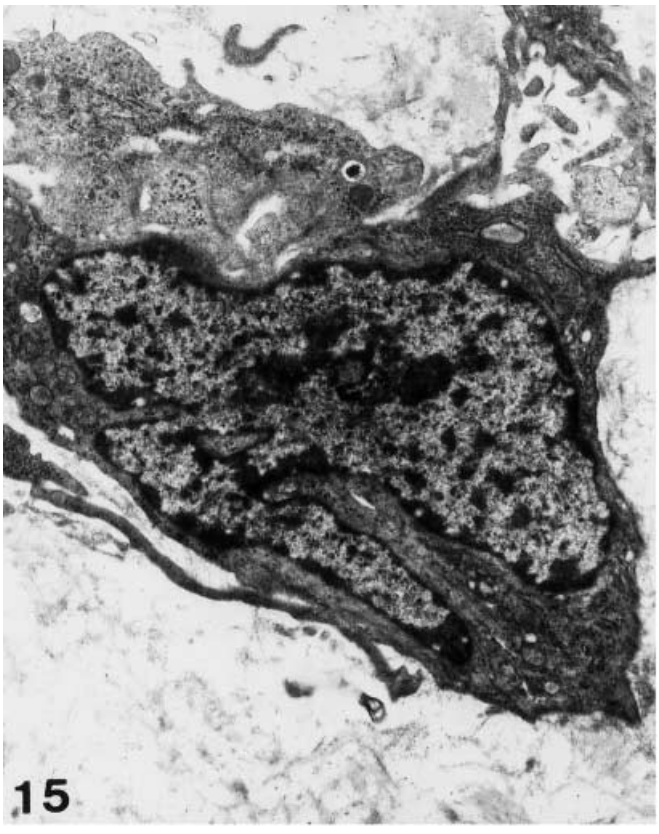
15

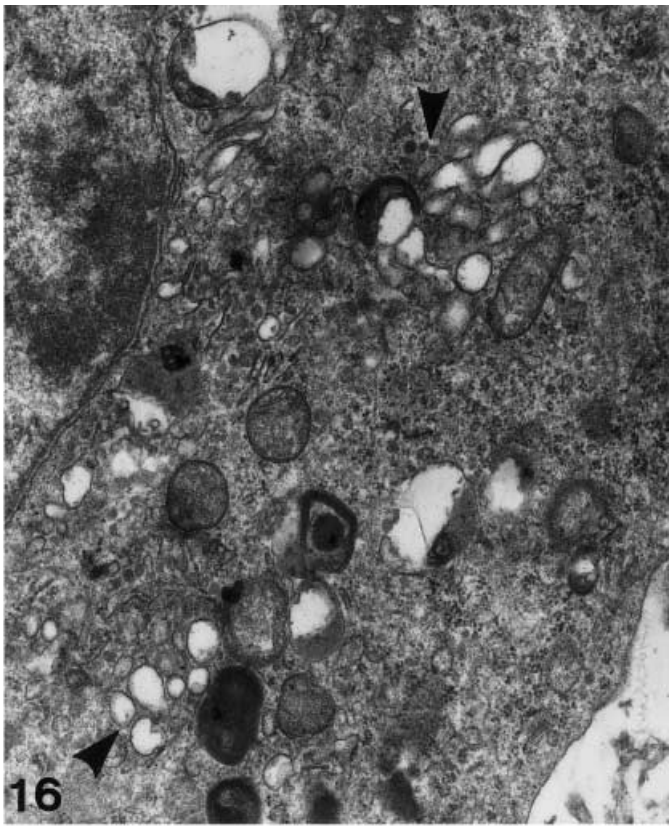
16

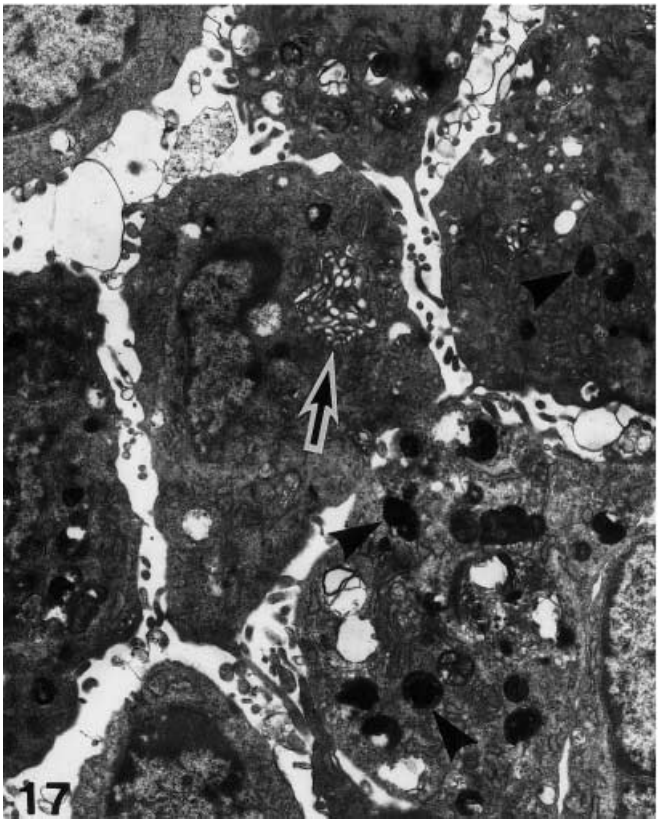
17

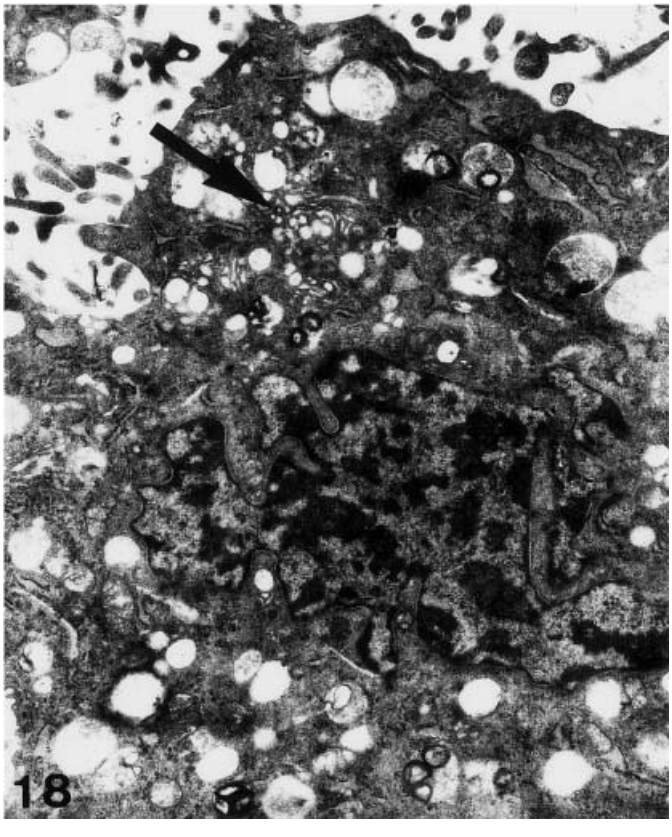
18

sionally seen, but cells reactive for ALP were not present (Table 1).

All rats inoculated subcutaneously with KB-P or KB-D8 cells developed tumors at the inoculation site. The induced tumors exhibited heterogeneous growth patterns as seen in the transplantable KB tumors. As shown in Table 1, neoplastic cells in the induced tumors reacted to vimentin, α-SMA, OX6, ED1, ED2, RED-1, ACP, and NSE in varying degrees, in agreement with immunohistochemical findings seen in KB tumors. However, ED5-immunopositive cells were not seen in the induced tumors.

Ultrastructural findings of KB tumors and tumors induced by KB-P and KB-D8 resembled each other. Neoplastic cells revealed oval or elongated configuration with some cytoplasmic projections, and their nuclei were often indented, having diffusely distributed chromatin condensations. There were numerous free ribosomes and some mitochondria in the cytoplasm, but cytoplasmic organelles such as endoplasmic reticulum and Golgi complex were poorly developed in many neoplastic cells examined (Fig. 15). Interestingly, there were occasional cells that possessed some lysosomes and unique structures consisting of dilated cisternae and some vesicles in the cytoplasm (Fig. 16). The cisterna-like structures were also seen in cultured KB-P and KB-D8 cells (Fig. 17 and Fig. 18). Besides the structure, KB-P and KB-D8 cells characteristically had variously developed lysosomal granules of varying sizes and prominent cell surface projections (Fig. 17); their nuclei occasionally showed deep invaginations (Fig. 18). There were no junctional structures such as desmosomes between neoplastic cells.

As shown in Fig. 19, the expression of TGF-β1 mRNA was detected by the RT-PCR in both LPS-untreated (0 μg/ml) and -treated (10 μg/ml and 50 μg/ml) KB-D8 cells, and the expression levels were dose dependently increased. However, no expression of TNF-α mRNA occurred in LPS-untreated and -treated KB-D8 cells. There were no cells reacting to OX6 in the presence of LPS, indicating that the exposure of LPS did not induce OX6-recognizing MHC class-II antigens in KB-D8 cells in vitro.

◀ **Fig. 15** Electron micrograph of a neoplastic cell in KB tumor. The cell has some cytoplasmic projections, and a deeply indented nucleus; there are numerous free ribosomes and some mitochondria in the cytoplasm, but cytoplasmic organelles are poorly developed. ×8000

Fig. 16 Electron micrograph of a neoplastic cell in KB tumor. The cell possesses some lysosomes and cisterna-like structures consisting of sacks and vesicles (*arrowheads*) in the cytoplasm. ×12000

Fig. 17 Electron micrograph of neoplastic cells in KB-P. The cisterna-like structures (*arrow*) and variously developed lysosomal granules of varying sizes (*arrowheads*) are seen; cell surface projections are prominent. ×6000

Fig. 18 Electron micrograph of a neoplastic cell in KB-D8. The cell shows cisterna-like structures (*arrows*) and a deeply invaginated nucleus. ×9000

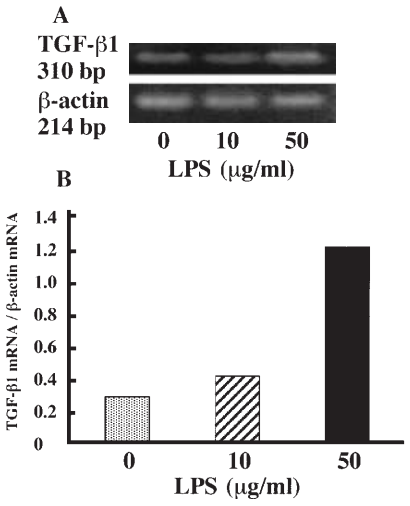

Fig. 19 Expressions of transforming growth factor (TGF)-β1 mRNA (**a**) in KB-D8 using reverse transcription polymerase chain reaction and their intensity relative to those of β-actin mRNA (**b**). The expression levels of TGF-β1 mRNA in KB-D8 cells were dose dependently increased by lipopolysaccharide (LPS) addition (0, 10, and 50 μg/ml)

Discussion

FDCs are present in the germinal center (B cell-rich areas) of lymphoid follicles in the spleen and lymph node, whereas interdigitating dendritic (reticulum) cells (IDCs) are normally localized in the T-cell-rich areas of all lymphoid tissues including the thymus [17, 37, 41]. In humans, neoplasms of dendritic cell origin are extremely rare [1, 17]. According to a review article in 1998 by Fonseca et al. [17], 51 cases of FDC sarcomas and 21 cases of IDC sarcomas have been well documented so far; most of them occurred in lymph nodes. Although preexisting hyaline-vascular type Castleman's disease has been reported in some patients with FDC sarcomas, the pathogenesis of dendritic cell sarcomas is unknown [17, 25]. Human dendritic cell sarcomas were characterized histologically by growth patterns such as compact sheet-like, fascicular, storiform, and interwoven fashions, consisting of oval and spindle cells immunoreactive to vimentin [1, 10, 17, 25, 26, 30]. Areas comprising of large, round histiocytic cells with oval or round nuclei and abundant cytoplasm were also observed in human cases [26, 30]. The present primary tumor and its derivative, KB tumors, showed heterogeneous histological growth patterns, being in keeping with those reported in human FDC and IDC sarcomas [10, 17, 25, 26, 30]. Normal dendritic cells are characterized by fine structures such as prominent cytoplasmic projections, tubulovesicular system (consisting of vesicles, sacs, and tubules) and deeply indented nucleus [28, 30, 40, 41]. Although cytoplasmic organelles were poorly developed in the present tumor cells, there were cells with cytoplasmic projections and cisterna-like structures reminiscent of the tubulovesicular

system. Such cisterna-like structures and cell projections were more evident in KB-P and KB-D8 cells; KB-P and KB-D8 cells showed also marked nuclear indentation. Birbeck's granules, a fine structure characteristic of Langerhans' cells [12, 40], were not seen in the present tumor cells.

OX6 labels dendritic cells expressing rat MHC class-II antigens [18, 46, 53]. Although the antigens may not be expressed in normal human FDCs, neoplastic cells in human FDC and IDC sarcomas are immunolabeled in common with an antibody against HLA-DR; thus, the immunostaining with the antibody is available in distinguishing dendritic cell sarcomas from other mesenchymal tumors [17]. In particular, human dendritic cell sarcoma is often confused with fibrosarcoma and malignant fibrous histiocytoma (MFH) [17, 21, 28]. We previously established transplantable tumor lines from fibrosarcoma [48] and MFH [45, 47], both which were derived from spontaneous F344 rat tumors. No cells reacting to OX6 were seen in either tumor (data not shown), whereas the vast majority of KB tumor cells reacted strongly to OX6. Additionally, there were cells positive to ED5 and RED-1 in KB tumors. ED5 labeled rat FDCs [24], and RED-1 recognized IDCs and Langerhans' cells in rats [29]. Greater immunoreactivity to RED-1 was seen in KB-P and KB-D8 cells. These findings indicated that the present tumor cells exhibited immunophenotypes of rat dendritic cells. In humans, there are some marker antibodies (CD21, CD35, and R4/23) specific for FDCs, and Langerhans' cells and IDCs appeared to react characteristically to CD1a and S-100 protein [1, 17, 26]. These antibodies have been used to distinguish FDC sarcomas from IDC sarcomas. However, it appears difficult to differentiate these sarcomas from each other by morphological review [9, 17], and dendritic cells in lymphoid tissues show heterogeneous immunophenotypes depending on the maturation or differentiation [41]. In rats, there are not so many useful marker antibodies specific for FDCs or IDCs. Based on the anatomical location of the primary tumor and on the pathological findings of KB tumors and KB-P and KB-D8 cultures, therefore, the present tumor was diagnosed as dendritic cell sarcoma.

It is interesting to note that neoplastic cells in KB tumors were labeled with ED1 and ED2. There were also cells reacting to ED1 and ED2 in KB-P and KB-D8 cultures and their induced tumors. ED1 stained cytoplasmic antigens of blood monocytes and exudate macrophages in rats, and antigens recognized by ED1 were on the membrane of cytoplasmic granules, especially phagolysosomes [11, 16, 46, 53]. ED2 reacted with cell membrane antigens of rat resident macrophages (Kupffer cells in the liver) [16, 46]. ACP and NSE are lysosomal enzymes that have been used as markers for histiocytic sarcomas [13, 22]. Positive reactions to ACP and NSE were seen in KB tumor cells, KB-P and KB-D8 cells, and cells constituting tumors induced by KB-P and KB-D8. In addition, KB-P and KB-D8 cells possessed variously developed lysosomal structures in the cytoplasm. These findings indicated that the present neoplastic cells revealed histiocytic or macrophage-like nature. Human FDC and IDC sarcomas expressed antigens recognized by monocyte/macrophage-specific antibodies such as CD14 and CD68 [1, 17, 25, 26, 28]. It has been considered that monocytes/macrophages and dendritic cells have a common origin evolving from hematopoietic stem cells in the bone marrow, and they can transdifferentiate between them [7, 33, 34, 40]. The present findings also imply the close relationship between rat dendritic cells and macrophages/histiocytes.

Alpha-SMA-immunopositive cells are present in human FDC sarcomas, although the expression is controversial [1, 9, 28]. Similar cells were intermingled in the present primary tumor, KB tumors, KB-P and KB-D8 cultures and tumors induced by KB-P and KB-D8 cells. The induction of actin filaments has been observed in myofibroblastic cells in fibrotic lesions [5, 36]. The derivation of myofibroblastic cells from pre-existing fibroblasts seems established in skin wound healing [15]. Besides, macrophages in xanthogranulomas and peritoneal macrophages around free-floating intraperitoneal blood clots have been reported to develop myofibroblastic characteristics [3, 6]. We recently reported that rat histiocytic sarcoma-derived cells (HS-P) reacted with α-SMA antibody, suggesting a possible modulation of macrophages towards myofibroblastic cells [51, 52]. It is likely that dendritic cells may also exhibit myofibroblastic immunophenotype. Desmin is a kind of cytoskeleton seen in myofibroblastic cells appearing in fibrotic lesions [36]. Desmin immunoreactivity was not seen in the present neoplastic cells.

MHC class-II antigens are enhanced during the transition from immature to mature dendritic cells, and the maturation process is induced by various inflammatory stimuli [8, 19, 23, 27, 32, 33]. Because cultured cells of KB-P and KB-D8 did not react to OX6, immunophenotypic change of OX6-recognizing MHC class-II antigens was investigated by addition of LPS. However, the expression of the antigens was not seen in LPS-treated KB-D8 cells. Since neoplastic cells in KB tumors and tumors induced by KB-P and KB-D8 cells reacted to OX6, microenvironmental conditions evoked in vivo by complicated mechanisms might be attributable to MHC class-II antigen expression [4, 54]. Interestingly, the RT-PCR method revealed that LPS addition dose dependently enhanced expression of TGF-β1 mRNA in KB-D8 cells, suggesting a likely production of TGF-β1 under the LPS stimulus. TGF-β1 inhibits the maturation of dendritic cells, particularly Langerhans' cells, in response to LPS [19]. It is interesting to pursue the relationship of acquisition of dendritic immunophenotypes with inflammatory cytokines such as TGF-β1. Recently, we reported that the treatment with LPS increased TNF-α mRNA expression in HS-P cells with macrophage-like nature [52]. On the contrary, the addition of LPS to KB-D8 cells failed to induce TNF-α mRNA expression. Although it has been considered that some dendritic cells might be generated from blood monocytes [7, 34], there appears to be a dif-

ference in responses to LPS between dendritic cells (KB-D8) and macrophages (HS-P).

In conclusion, we succeeded in establishing transplantable tumor line (KB) and cell lines (KB-P and KB-D8) from a rat thymus-derived dendritic cell sarcoma. Dendritic cells have heterogeneous functions to initiate primary and secondary immune responses as an antigen-presenting cell [20, 32]. The derivation, differentiation lineage and exact roles of dendritic cells in the immune system remain to be fully investigated [20, 33, 40, 41]. Newly established tumor lines (KB, KB-P, and KB-D8) may prove to be a useful tool for studies on the histogenesis and pathobiological functions of dendritic cells; in particular, it is intriguing to investigate the mechanisms of down- or upregulation of MHC class-II antigen expression.

Acknowledgements This study was supported in part by Grant-in-Aid (no. 12660287) for Scientific Research C, the Ministry of Education, Science, Sports and Culture, Japan.

References

1. Andriko JW, Kaldjian EP, Tsokos M, Abbondanzo SL, Jaffe ES (1998) Reticulum cell neoplasms of lymph nodes: a clinicopathologic study of 11 cases with recognition of a new subtype derived from fibroblastic reticular cells. Am J Surg Pathol 22:1048–1058
2. Benahmed M, Heymann D, Pilet P, Bienvenu J, Daculsi G (1997) LPS increases biomaterial degradation by human monocytes in vitro. J Biomed Mater Res 34:115–119
3. Bhawan J, Majno G (1989) The myofibroblast. Possible derivation from macrophages in xanthogranuloma. Am J Dermatopathol 11:255–258
4. Boczkowski D, Nair SK, Snyder D, Gilboa E (1996) Dendritic cells pulsed with RNA are potent antigen-presenting cells in vitro and in vivo. J Exp Med 184:465–472
5. Boukhalfa G, Desmouliere A, Rondeau E, Gabbiani G, Sraer JD (1996) Relationship between alpha-smooth muscle actin expression and fibrotic changes in human kidney. Exp Nephrol 4:241–247
6. Campbell GR, Ryan GB (1983) Origin of myofibroblasts in the avascular capsule around free-floating intraperitoneal blood clots. Pathology 15:253–264
7. Cavanagh LL, Saal RJ, Grimmett KL, Thomas R (1998) Proliferation in monocyte-derived dendritic cell cultures is caused by progenitor cells capable of myeloid differentiation. Blood 92:11598–11607
8. Cella M, Engering A, Pinet V, Pieters J, Lanzavecchia A (1997) Inflammatory stimuli induce accumulation of MHC class II complexes on dendritic cells. Nature 388:782–787
9. Chan JK, Tsang WY, Ng CS, Tang SK, Yu HC, Lee AW (1994) Follicular dendritic cell tumors of the oral cavity. Am J Surg Pathol 18:148–157
10. Choi PC, To KF, Lai FM, Lee TW, Yim AP, Chan JK (2000) Follicular dendritic cell sarcoma of the neck. Report of two cases complicated by pulmonary metastases. Cancer 89:664–672
11. Damoiseaux JG, Döpp EA, Calame W, Chao D, MacPherson GG, Dijkstra CD (1994) Rat macrophage lysosomal membrane antigen recognized by monoclonal antibody ED1. Immunology 83:140–147
12. De Graaf JH, Tamminga RY, Dam-Meiring A, Kamps WA, Timens W (1996) The presence of cytokines in Langerhans' cell histiocytosis. J Pathol 180:400–406
13. Delabie J, De Wolf-Peeters C, De Vos R, Vandenberghe E, Kennes K, De Jonge I, Desmet V (1991) True histiocytic neoplasm of Langerhans' cell type. J Pathol 163:217–223
14. Demetris AJ, Murase N, Ye Q, Galvao FHF, Richert C, Saad R, Pham S, Duquesnoy RJ, Zeevi A, Fung JJ, Starzl TE (1997) Analysis of chronic rejection and obliterative arteriopathy. Possible contributions of donor antigen-presenting cells and lymphatic disruption. Am J Pathol 150:563–578
15. Desmouliere A, Redard M, Darby I, Gabbiani G (1995) Apoptosis mediates the decrease in cellularity during the transition between granulation tissue and scar. Am J Pathol 146:56–66
16. Dijkstra CD, Dopp EA, Joling P, Kraal G (1985) The heterogeneity of mononuclear phagocytes in lymphoid organs. Distinct macrophage subpopulations in the rat recognized by monoclonal antibodies ED1, ED2 and ED3. Immunology 54:589–599
17. Fonseca R, Yamakawa M, Nakamura S, van Heerde P, Miettinen M, Shek TW, Myhre Jensen O, Rousselet MC, Tefferi A (1998) Follicular dendritic cell sarcoma and interdigitating reticulum cell sarcoma: a review. Am J Hematol 59:161–167
18. Fukumoto T, McMaster WR, Williams AF (1982) Mouse monoclonal antibodies against rat major histocompatibility antigens. Two Ia antigens and expression of Ia and class I antigens in rat thymus. Eur J Immunol 12:237–243
19. Geissmann F, Revy P, Regnault A, Lepelletier Y, Dy M, Brousse N, Amigorena S, Hermine O, Durandy A (1999) TGF-β1 prevents the noncognate maturation of human dendritic Langerhans cells. J Immunol 162:4567–4575
20. Gilboa E, Nair SK, Lyerly HK (1998) Immunotherapy of cancer with dendritic-cell-based vaccines. Cancer Immunol Immunother 46:82–87
21. Hollowood K, Stamp G, Zouvani I, Fletcher CD (1995) Extranodal follicular dendritic cell sarcoma of the gastrointestinal tract. Morphologic, immunohistochemical and ultrastructural analysis of two cases. Am J Clin Pathol 103:90–97
22. Hsu SM, Ho YS, Hsu PL (1991) Lymphomas of true histiocytic origin. Expression of different phenotypes in so-called true histiocytic lymphoma and malignant histiocytosis. Am J Pathol 138:1389–1404
23. Hubert P, van der Brule F, Giannini SL, Franzen-Detrooz E, Boniver J, Delvenne P (1999) Colonization of in vitro-formed cervical human papillomavirus-associated (pre)neoplastic lesions with dendritic cells. Role of granulocyte/macrophage colony-stimulating factor. Am J Pathol 154:775–784
24. Jeurissen SH, Dijkstra CD (1986) Characteristics and functional aspects of nonlymphoid cells in rat germinal centers, recognized by two monoclonal antibodies ED5 and ED6. Eur J Immunol 16:562–568
25. Katano H, Kaneko K, Shimizu S, Saito T, Irie T, Mori S (1997) Follicular dendritic cell sarcoma complicated by hyaline-vascular type Castleman's disease in a schizophrenic patient. Pathol Int 47:703–706
26. Liu SM, Huang PH, Liu JM (1998) Interdigitating reticulum cell tumor of lymph node: a case report and literature review. Pathol Int 48:974–980
27. Lutz MB, Assmann CU, Girolomoni G, Ricciardi-Castagnoli P (1996) Different cytokines regulate antigen uptake and presentation of a precursor dendritic cell line. Eur J Immunol 26:586–594
28. Masunaga A, Nakamura H, Katata T, Furubayashi T, Kanayama Y, Yamada A, Shiroko Y, Itoyama S (1997) Follicular dendritic cell tumor with histiocytic characteristics and fibroblastic antigen. Pathol Int 47:707–712
29. Mizoguchi S, Takahashi K, Takeya M, Naito M, Morioka T (1992) Development, differentiation, and proliferation of epidermal Langerhans cells in rat ontogeny studied by a novel monoclonal antibody against epidermal Langerhans cells, RED-1. J Leukoc Biol 52:52–61
30. Monda L, Warnke R, Rosai J (1986) A primary lymph node malignancy with features suggestive of dendritic reticulum cell differentiation. A report of 4 cases. Am J Pathol 122:562–572
31. Nakanishi M, Yamate J, Nakatsuji S, Ide M, Sawamoto O, Kuwamura M, Kotani T, Sakuma S (2001) Establishment of a transplantable tumour line (IP) derived from rat pulmonary carcinoma, developing humoral hypercalcaemia of maligancy in IP-bearing rats. Virchows Arch (in press)

32. Pierre P, Turley SJ, Gatti E, Hull M, Meltzer J, Mirza A, Inaba K, Steinman RM, Mellman I (1997) Developmental regulation of MHC class II transport in mouse dendritic cells. Nature 388:787–792
33. Rescigno M, Winzler C, Delia D, Mutini C, Lutz M, Ricciardi-Castagnoli P (1997) Dendritic cell maturation is required for initiation of the immune response. J Leukoc Biol 61:415–421
34. Romani N, Gruner S, Brang D, Kampgen E, Lenz A, Trochenbacher B, Konwalinka G, Fritsch PO, Steinman RM, Schuler G (1994) Proliferating dendritic cell progenitors in human blood. J Exp Med 180:83–93
35. Sallusto F, Cella M, Danieli C, Lanzavecchia A (1995) Dendritic cells use macropinocytosis and the mannose receptor to concentrate macromolecules in the major histocompatibility complex class II compartment. Downregulation by cytokines and bacterial products. J Exp Med 182:389–400
36. Sappino AP, Schurch W, Gabbiani G (1990) Differentiation repertoire of fibroblastic cells. Expression of cytoskeletal proteins as marker of phenotypic modulations. Lab Invest 63:144–161
37. Saunders D, Lucas K, Ismaili J, Wu L, Maraskovsky E, Dunn A, Shortman K (1996) Dendritic cell development in culture from thymic precursor cells in the absence of granulocyte/macrophage colony-stimulating factor. J Exp Med 184:2185–2196
38. Spencer SC, Fabre JW (1990) Characterization of the tissue macrophage and the interstitial dendritic cell as distinct leukocytes normally resident in the connective tissue of rat heart. J Exp Med 171:1841–1851
39. Stefanski SA, Elwell MR, Stromberg PC (1990) Spleen, lymph nodes, and thymus. In: Boorman GA, Eustis SL, Elwell MR, Montogomery CA Jr, MacKenzie WF (eds) Pathology of the Fischer rat. Academic Press, San Diego, pp 369–393
40. Takahashi K, Naito M, Takeya M (1996) Development and heterogeneity of macrophages and their related cells through their differentiation pathways. Pathol Int 46:473–485
41. Takahashi K, Asagoe K, Zaishun J, Yanai H, Yoshino T, Hayashi K, Akagi T (1998) Heterogeneity of dendritic cells in human superficial lymph node. In vitro maturation of immature dendritic cells into mature or activated interdigitating reticulum cells. Am J Pathol 153:745–755
42. Tanuma N, Kojima T, Shin T, Aikawa Y, Kohji T, Ishihara Y, Matsumoto Y (1997) Competitive PCR quantification of pro- and anti-inflammatory cytokine mRNA in the central nervous system during autoimmune encephalomyelitis. J Neuroimmunol 73:197–206
43. Tsujino K, Yamate J, Tsukamoto Y, Kumagai D, Kannan Y, Jippo T, Kuwamura M, Kotani T, Takeya M, Sakuma S (1997) Establishment and characterization of cell lines derived from a transplantable rat malignant meningioma. Morphological heterogeneity and production of nerve growth factor. Acta Neuropathol (Berl) 93:461–470
44. Tsujiuchi T, Sasaki Y, Tsutsumi M, Konishi Y (2000) Mutations and reduced expression of the transforming growth factor-β receptor II gene in rat lung adenocarcinoma induced by N-nitrosobis-(2-hydroxypropyl)amine. Jpn J Cancer Res 91:1090–1095
45. Yamate J, Tajima M, Togo M, Shibuya K, Ihara M, Kudow S (1991) Heterogeneity of cloned cell lines established from a transplantable rat malignant fibrous histiocytoma. Jpn J Cancer Res 82:298–307
46. Yamashiro S, Takeya M, Nishi T, Kuratsu J, Yoshimura T, Ushio Y, Takahashi K (1994) Tumor-derived monocyte chemoattractant protein-1 induces intratumoral infiltration of monocyte-derived macrophage subpopulation in transplanted rat tumors. Am J Pathol 145:856–867
47. Yamate J, Tajima M, Shibuya K, Saitoh T (1994) Enhancement of lipid phagocytosis by cloned cells derived from rat malignant fibrous histiocytoma under hyperlipemic conditions. Pathol Int 44:735–744
48. Yamate J, Iwaki M, Kumagai D, Tsukamoto Y, Kuwamura M, Nakatsuji S, Tsunenari I, Kotanai T, Sakuma S (1997) Characteristics of a rat fibrosarcoma-derived transplantable tumour line (SS) and cultured cell lines (SS-P and SS-A3–1) showing myofibroblastic and histiocytic phenotypes. Virchows Arch 431:431–440
49. Yamate J, Tsujino K, Kumagai D, Nakatsuji S, Kuwamura M, Kotani T, Sakuma S (1997) Morphological characteristics of a transplantable histiocytic sarcoma (HS-J) in F344 rats and appearance of renal tubular hyaline droplets in HS-J-bearing rats. J Comp Pathol 116:73–86
50. Yamate J, Yoshida H, Tsukamoto Y, Ide M, Kuwamura M, Ohashi F, Miyamoto T, Kotani T, Sakuma S, Takeya M (2000) Distribution of cells immunopositive for AM-3 K, a novel monoclonal antibody recognizing human macrophages, in normal and diseased tissues of dogs, cats, horses, cattle, pigs, and rabbits. Vet Pathol 37:168–176
51. Yamate J, Maeda M, Benn SJ, Laithwaite JE, Allan A, Ide M, Kuwamura M, Kotani T, Sakuma S, LaMarre J (2001) Effects of lipopolysaccharide on a macrophage-like cell line (HS-P) from a rat histiocytic sarcoma. J Comp Pathol 125:15–24
52. Yamate J, Maeda M, Tsukamoto Y, Benn,SJ, Laithwaite JE, Allan A, Kannan Y, Ide M, Kuwamura M, Kotani T, Sakuma S, LaMarre (2001) Macrophage-like cell line (HS-P) from a rat histiocytic sarcoma. J Comp Pathol 124:183–191
53. Zhang J, Herman EH, Ferrans VJ (1993) Dendritic cells in the hearts of spontaneously hypertensive rats treated with doxorubicin with or without ICRF-187. Am J Pathol 142:1916–1926
54. Zitvogel L, Mayordomo JI, Tjandrawan T, DeLeo AB, Clarke MR, Lotze MT, Storkus WJ (1996) Therapy of murine tumors with tumor peptide-pulsed dendritic cells. Dependence on T cells, B7 costimulation, and T helper cell 1-associated cytokines. J Exp Med 183:87–97

Virchows Arch (2002) 440:627–634
DOI 10.1007/s00428-001-0597-2

ORIGINAL ARTICLE

**Jörg Eberhard · Søren Jepsen · Markus Tiemann
Ralph Krause · Yahya Açil · Hans-Karl Albers**

Leukotriene A_4-hydrolase expression and leukotriene B_4 levels in chronic inflammation of bacterial origin

Immunohistochemistry and reverse-phase high-performance liquid chromatography analysis of oral mucosal epithelium

Received: 5 October 2001 / Accepted: 5 December 2001 / Published online: 19 February 2002
© Springer-Verlag 2002

Abstract Chronic inflammation of the oral epithelium of bacterial origin is associated with elevated leukotriene B_4 (LTB_4) levels. We investigated leukotriene A_4 (LTA_4)-hydrolase expression and LTB_4 levels in oral epithelium in relation to the clinical disease manifestation and immunohistopathology and LTA_4-hydrolase expression in cultured oral keratinocytes. In 11 patients, three different types of biopsy specimens of the oral mucosa tissues were examined. Each sample was divided, and one-half was analysed using immunohistochemistry with antibodies to LTA_4-hydrolase, CD1a, CD3, CD19, macrophages/monocytes and granulocytes. The other half of the sample was homogenised and analysed using reverse-phase high-performance liquid chromatography to determine LTB_4 levels. We found strong LTA_4-hydrolase expression in basal cells of the oral epithelium from tissue samples that appeared clinically healthy; however, histologically a mild chronic inflammation was observed. In contrast, patients with symptoms of an inflammation of the oral mucosa showed only weak LTA_4-hydrolase staining of the epithelial cell layers, but strong immunoreactivity in endothelial and invading inflammatory cells. LTB_4 levels were elevated in inflamed tissues compared with non-inflamed controls. Most significantly, there was a strong association between the immunohistochemical detection of the enzyme, LTB_4 levels, cellular infiltration and the clinical disease manifestations. In vitro experiments indicated that LTA_4-hydrolase expression may be induced by bacterial contamination. This study suggests that LTA_4-hydrolase expression and elevated LTB_4 levels in oral mucosal epithelium are integral parts of the induction and progression of chronic inflammatory reactions. Epithelial cells may participate in early stages of inflammation as a source of LTB_4.

Keywords Leukotrienes · Mouth mucosa · Keratinocytes · Bacterial infection · Gingivitis

J. Eberhard (✉) · S. Jepsen · R. Krause · H.-K. Albers
Department of Operative Dentistry and Periodontology,
University of Kiel, Arnold-Heller-Strasse 16,
24105 Kiel, Germany
e-mail: eberhard@konspar.uni-kiel.de
Tel.: +49-431-5972950, Fax: +49-431-5972795

M. Tiemann
Department of Hematopathology and Lymph Node Registry,
University of Kiel, Germany

Y. Açil
Department of Oral and Maxillofacial Surgery,
University of Kiel, Germany

Introduction

The oral mucosa is lined by a stratified squamous epithelium that is attached to the surface of the teeth. The epithelium protects against pathogenic microorganisms in dental plaques [1]. The continuous bacterial contamination of the oral mucosa leads to a weak inflammation even in clinically healthy-appearing tissues [27]. Essential for this subclinical chronic inflammation is the careful regulation of pro-inflammatory mediator synthesis capable of inducing an immune response to eliminate bacterial pathogens, but keeping the cellular infiltration so low that tissue damage is minimised. An increase in mediator levels or the induction of distinct mediators leads to an increase in cellular infiltration and progression to chronic gingival inflammation, which finally becomes clinically apparent. Based on its leukocyte chemoattractant potential [8, 10, 28, 35], the pro-inflammatory eicosanoid mediator leukotriene B_4 (LTB_4) is an important mediator in inflammatory disease, and its synthesis may be crucial for the maintenance of oral health. Consequently, the upregulation of LTB_4 synthesis may also be critical for the progression of inflammation. The synthesis of LTB_4 is a three-step biosynthetic pathway, of which the final step is the conversion of unstable LTA_4 to LTB_4 by LTA_4-hydrolase, underlining the regulatory role of this enzyme for LTB_4 synthesis [13, 26]. Although it is quite obvious that

the expression of the enzyme LTA_4-hydrolase is important for the amplification, regulation and/or resolution of the inflammatory response, the expression of LTA_4-hydrolase in chronic inflammatory disease of bacterial origin has not yet been studied. In particular, no information is available about the expression of this enzyme in subclinical stages of chronic inflammation. The following investigation therefore attempted to identify the source of LTA_4-hydrolase in oral mucosal epithelium and to measure the levels of LTB_4 in early and advanced phases of chronic inflammation. Information on the histopathological and clinical status of the tissues in relation to LTA_4-hydrolase expression and LTB_4 levels may also be relevant for other chronic inflammatory diseases in which eicosanoids are involved.

Materials and methods

Oral biopsy specimens

A total of 31 human oral biopsy specimens were obtained from 11 patients (age 28–74 years) undergoing routine oral surgery procedures at the Department of Maxillofacial Surgery of the University of Kiel. Informed consent was obtained from all patients. Specimens were taken from gingiva without any clinical signs of inflammation (n=9), from gingiva with signs of inflammation (n=11) and from gingiva of the retromolar region (n=11). The oral retromolar region is generally not subject to bacterial infection due to plaque accumulation and was used as control. The diagnosis of the inflammatory status was made according to the clinical parameters redness, swelling and bleeding on gentle probing. All three biopsies were taken from the same patient. From two patients no gingiva without any clinical signs of inflammation could be harvested. The oral epithelium was infiltrated with local anaesthetic (ultracain 1%) during removal. The patients had not received any topical or systemic anti-inflammatory treatment for at least 3 weeks prior to biopsy. The oral biopsy specimens were gently washed in phosphate-buffered saline (PBS, 50 mM, pH 7.4) to remove contaminating blood and were stored immediately in formaldehyde (10%) or shock frozen in liquid nitrogen. The tissue specimens were divided into two halves, one for immunohistochemistry and the other for reverse-phase high-performance liquid chromatography (RP-HPLC) analysis.

Preparation of tissue specimens

Tissue samples were fixed in 4% formaldehyde, dehydrated in alcohol and embedded in paraffin. Four-micron-thin sections were cut and treated with 1.5% H_2O_2 in ice-cold methanol for 20 min. The slides were subsequently immersed in 0.01 mol/l citrate buffer, pH 6.0, and incubated for 15 min at 90°C in a steam bath. Slides were washed in PBS and incubated with 2% mouse non-immune serum for 20 min to block non-specific binding. Antibodies (Table 1) were used at a final concentration of 10 µg/ml in 4% normal human serum. The primary antibody was detected with rabbit anti-mouse peroxidase (Dako, Hamburg, Germany).

The frozen tissues were placed on a tissue holder, and sections of approximately 5 µm were cut on a cryostat (2800 Frigocut E, Reichert-Jung, Arnsberg, Germany) at –20°C. For immunohistochemistry, endogenous peroxidase activity was inhibited by 1% H_2O_2 in methanol for 15 min, followed by blocking with normal horse serum for 10 min. After each step the sections were washed with PBS for 10 min. The specimens were incubated with the anti-LTA_4-hydrolase antibody (6 µg/ml) for 18 h at 4°C in a humid air chamber. Labelled streptavidin–biotin reagents were used for the detection of the antibody (Biologo, Kronshagen, Germany).

Specific staining was verified by substituting normal rabbit IgG (6 µg/ml) for the primary rabbit IgG anti-LTA_4-hydrolase antibody. Positive controls were made parallel to every new staining procedure using specimens of human psoriasis lesions. After washing with PBS the sections were counterstained with Mayer's hemalum (1:5, 45 s) and mounted in an aqueous Kaiser's glycerol gelatin medium (Merck, Darmstadt, Germany).

In vitro expression of LTA_4-hydrolase in cultured human oral epithelial cells

Human immortalised oral keratinocyte cell line HOK-18A was grown in keratinocyte growth medium, supplemented with 30 µl/ml bovine pituitary extract, 0.1 ng/ml human epidermal growth factor, 5 µg/ml bovine insulin, 0.5 µg/ml hydrocortisone, 50 µg/ml gentamicin and 50 ng/ml amphotericin-B until confluent. The cell density was 7×10^4 cells/cm^2.

The preparation of bacteria was as follows. *Haemophilus actinomycetemcomitans* was grown in trypticase soy broth in an anaerobic chamber (Campy Pac, Becton Dickinson, Heidelberg, Germany) until an optical density of 0.2 at 495 nm was reached. Bacteria were washed three times and resuspended in the keratinocyte growth medium at concentrations to obtain 100:1 and 1000:1 multiplicities of infection. Bacteria were added in 200-µl volumes to monolayers and were co-cultured at 37°C for 2 h to allow interactions between bacteria and epithelial cells. After incubation time, monolayers were washed three times to remove extracellular bacteria, and cells were fixed in ice-cold acetone for 10 min. Staining of LTA_4-hydrolase was performed as described previously.

RP-HPLC analysis

The LTB_4 concentrations of the oral biopsy specimens were determined by means of RP-HPLC analysis as previously described [10]. Briefly, the specimens were cut into small pieces and homogenised in a 200-µl Micro-Tissue-Grinder (Wheaton, Millville, N.J.) in 100 µl PBS. Subsequently the samples were homogenised with a Sonopuls HD 200 (Bandelin, Berlin, Germany) for 4 s. During these procedures the specimens were cooled with liquid nitrogen and ice. The mixture was kept at –20°C for 10 min before centrifugation at 1000 *g* (10 min, 4°C). The resulting supernatant was collected and equilibrated with 75 µl methanol, 325 µl aqua bidest and 25 µl trifluoroacetic acid. The samples were centrifuged at 1000 *g* for 10 min at 4°C, and the supernatant was analysed us-

Table 1 Antibodies used to recognise leukotriene A_4 (LTA_4), hydrolase and inflammatory cells in this study

Antigen	Antibody	Reference/source
LTA_4-hydrolase	Anti-LTA_4-hydrolase	[24]
CD1a antigen	Anti-CD1a	Dako, Hamburg
CD3 antigen	Anti-CD3	Dako, Hamburg
CD19 antigen	Anti-CD19	Dianova, Hamburg
Macrophages/monocytes	Ki-M1p	Dept. of Hematophatology, University of Kiel
Myeloid cells/granulocytes	Ki-My2	Dept. of Hematophatology, University of Kiel
Cytokeratin	KL-l	Dianova, Hamburg
Ki67 antigen	Ki-S5	Dept. of Hematophatology, University of Kiel

ing RP-HPLC. Two continually degassed solvents were used: (A) 0.018% (v/v) trifluoroacetic acid (TFA) in water/acetonitrile (25/75 v/v %) and (B) 0.018% (v/v) TFA in water/acetonitrile/methanol (7.5/38.5/54 v/v %). The columns were equilibrated with 50/50 (v/v %) solvent A and B for 5 min prior to the application of the sample. The gradients were as follows: (1) from 50% B to 100% B in 25 min, (2) 100% solvent B for another 5 min for washing and (3) from 100% B to 50% B in 2 min. Column equilibration was performed for 3 min (50/50% A/B).

Statistical analysis

The means and standard deviations of the LTB_4 concentrations were computed for the different groups and differences analysed using the Wilcoxon signed-rank test. The significance level was set at $P<0.05$.

Results

Histopathology of oral mucosal epithelium

The epithelium of the non-inflamed gingiva and the retromolar gingiva was stratified and parakeratinised. The connective tissue was composed of fibroblast-like cells oriented along collagenous fibres. Collagen fibres were the most abundant component of the connective tissue with only a few fibroblasts visible. A minor cellular infiltrate was observed in the connective tissue of biopsy specimens that appeared clinically healthy, while extensive infiltrates of inflammatory cells were seen in close proximity to the epithelium of biopsy specimens from patients with symptoms of gingivitis. The subepithelial connective tissue had reduced collagen content and multiple signs of microabscess formation. The epithelium varied in thickness from several cell layers to long epithelial extensions into the inflamed connective tissue. Parakeratinisation was partly lost, and epithelial cell necrosis was apparent.

Distribution of cytokeratin and Ki-S5

The immunolocalisation of cytokeratin (KL-1) clearly identified the cells covering the oral mucosa as epithelial cells in all tissue specimens, regardless of whether inflammation was present or not. The staining was apparent in nearly every cell of the epithelium, except for single cells in the inflamed specimens. Very few cells of the basal cell layer were positive for Ki-S5 in the weakly inflamed gingiva and the gingiva of the retromolar region. In the heavily inflamed samples, the cells of the basal layer were highly irregular in shape and size and showed high proliferative activity, as indicated by a positive staining for Ki-S5 in a large number of cells.

Localisation of LTA_4-hydrolase

Figure 1A–D shows the immunohistochemical staining with affinity-purified rabbit IgG antibody to LTA_4-hydrolase. The stratified and parakeratinised gingival epithelium of the retromolar area did not show any positive staining for LTA_4-hydrolase in epithelial or connective tissue cells. LTA_4-hydrolase in clinically healthy oral gingiva was predominantly immunolocalised in epithelial cells of the basal and spinous cell layers. In the basal cell layer staining was equally distributed throughout the layer, whereas staining of the spinous cell layer was limited to single cells (Fig. 1A). Staining of similar intensity but of limited frequency was seen in perivascular mononuclear cells and some fibroblast-like cells adjacent to the basal cell layer (Fig. 1B). In clinically inflamed tissues LTA_4-hydrolase activity was detected in epithelial cells and in the subepithelial connective tissue infiltrates. In addition to the basal and spinous cell layers, cells of the granular cell layer were also LTA_4-hydrolase positive (Fig. 1C). The staining of the basal cell layer appeared more intense in epithelial cells of non-inflamed tissues than in clinically inflamed samples (Fig. 1A, C). In the connective tissue LTA_4-hydrolase was localised in fibroblast-like cells in close proximity to the epithelial cells and distributed in single cells around blood vessels. Some infiltrates also showed focal expression of LTA_4-hydrolase, which was more intense than in epithelial and subepithelial localisations (Fig. 1D). Staining was specific in all samples, because only faint diffuse background staining was obtained with rabbit serum. Skin biopsy specimens from psoriasis lesions were used as positive controls.

Immunohistochemistry of cellular infiltrates

No apparent staining was detectable with any of the antibodies in oral gingiva of the retromolar region. Although the tissue samples of the gingiva appeared healthy on clinical inspection, locally restricted infiltrations of CD3, CD19, Ki-My2-positive granulocytes and Ki-M1P-positive macrophages were observed in the connective tissue (Fig. 1E, G). The histological appearance of the fibre and cellular components of the connective tissue of the retromolar gingiva were similar to clinically non-inflamed gingiva. In contrast to the non-inflamed specimens, the connective tissue of inflamed specimens was infiltrated by masses of cells with an obvious loss of connective tissue structure (Fig. 1G–H). T-lymphocytes, macrophages and granulocytes were observed in the connective tissue and in the epithelium (Fig. 1E–I). In healthy samples single cells were observed in all strata of the epithelium, while in inflamed tissues more cells infiltrated into the epithelial cell layers with subsequent epithelial cell necrosis (Fig. 1E, F). CD1a-positive Langerhans' cells with long cytoplasmic processes were located between epithelial cells of the stratum basale and were also scattered among the spinous and granular cell layers. The detection of Langerhans' cells was limited to the epithelium, while no cells were recognised in the connective tissue. The amount of Langerhans' cells did not differ between clinically healthy and inflamed tissues.

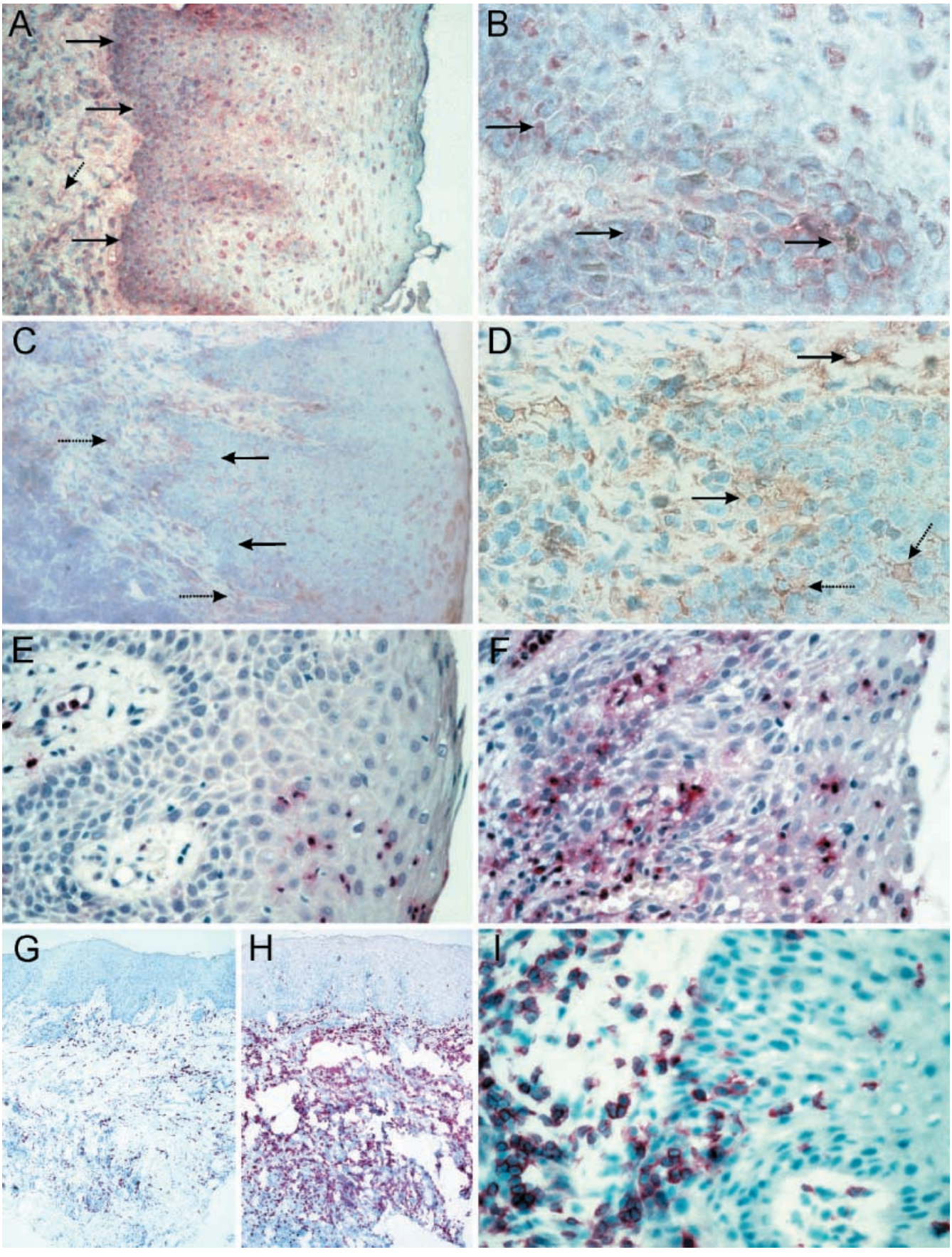
A
B
C
D
E
F
G
H
I

Based on immunolocalisation T-lymphocytes, macrophages/monocytes and granulocytes were abundant in the cellular infiltrates of all samples, while this was not regularly true for CD19-positive B cells.

In vitro expression of LTA_4-hydrolase in cultured keratinocytes

Figure 2 shows the immunohistochemical staining with rabbit IgG antibody to LTA_4-hydrolase. LTA_4-hydrolase was expressed at low levels by unstimulated keratinocytes (Fig. 2A), and expression was significantly increased by bacterial contamination with *H. actinomycetemcomitans* at infection rates of 100:1 and 1000:1 (Fig. 2B, C). Staining was specific in all samples, because only faint diffuse background staining was obtained with rabbit serum.

RP-HPLC analysis of LTB_4

A typical reverse-phase high-performance liquid chromatogram is presented in Fig. 3. No LTB_4 was detected in oral mucosal epithelium of the retromolar area. The mean concentration of LTB_4 was 0.39±0.31 ng/g wet tissue in non-inflamed tissues and 2.48±1.48 ng/g in inflamed tissues (Fig. 4). The differences in LTB_4 concentration were statistically significant ($P<0.05$).

◀ **Fig. 1** The immunohistochemical distribution of leukotriene A_4 (LTA_4) hydrolase in inflamed and non-inflamed oral gingival epithelium as revealed by an immunoperoxidase reaction using an antiserum against human LTA_4-hydrolase (**A**, **C** ×20; **B**, **D** ×63). All figures were from cryostat serial sections and counterstained with hemalum. **A** Sample from clinically healthy gingiva. Regular distribution of strong immunoreactivity in the basal cell layer (*arrows*) and positive staining of single epithelial cells in the spinous and granular cell layers. Subepithelial small blood vessels show positivity in endothelial cells (*dotted arrows*). **B** Clinically healthy gingiva. Higher magnification of the basal cell layer shows strong positive staining of LTA_4-hydrolase located in the cytoplasm (*arrows*). **C** Clinically inflamed gingiva. In contrast to clinically healthy tissues the basal cell layers show only weak staining (*arrows*), and immunoreactivity is distributed unevenly throughout the epithelial cell layers. An intensive immunoreactivity in the subepithelial cells is located in endothelial and inflammatory cells (*dotted arrows*). **D** Higher magnification of the clinically inflamed gingival tissues shows strong immunoreactivity in subepithelial venules and cells of the inflammatory infiltrate (*arrow*). In contrast to the healthy gingival tissues, epithelial basal cell layers do not show strong immunoreactivity, instead positivity is limited to invading inflammatory cells (*dotted arrows*). **E**–**I** The immunolocalisation of inflammatory cells in inflamed and non-inflamed oral gingival epithelium as revealed using an immunoperoxidase reaction. All figures were from paraffin-embedded serial sections and counterstained with hemalum (**E**, **F** ×40). **E** Ki-My2-positive neutrophils in clinically non-inflamed oral mucosal epithelium. Single cells migrate through the epithelial cell layers. **F** Ki-My2-positive neutrophils in inflamed tissues. The migration of granulocytes is more intense than in healthy samples. Single cell necrosis is apparent especially in the basal cell layers. **G** Ki-M1p-positive macrophages in clinically non-inflamed gingiva. Locally restricted infiltrations beneath the epithelium (**G** ×5). **H** Ki-M1p-positive macrophages in inflamed tissues demonstrate intensive staining throughout the connective tissue (**H** ×5). **I** CD3-positive T-lymphocytes invading the epithelial cell layers in inflamed tissues (**I** ×40)

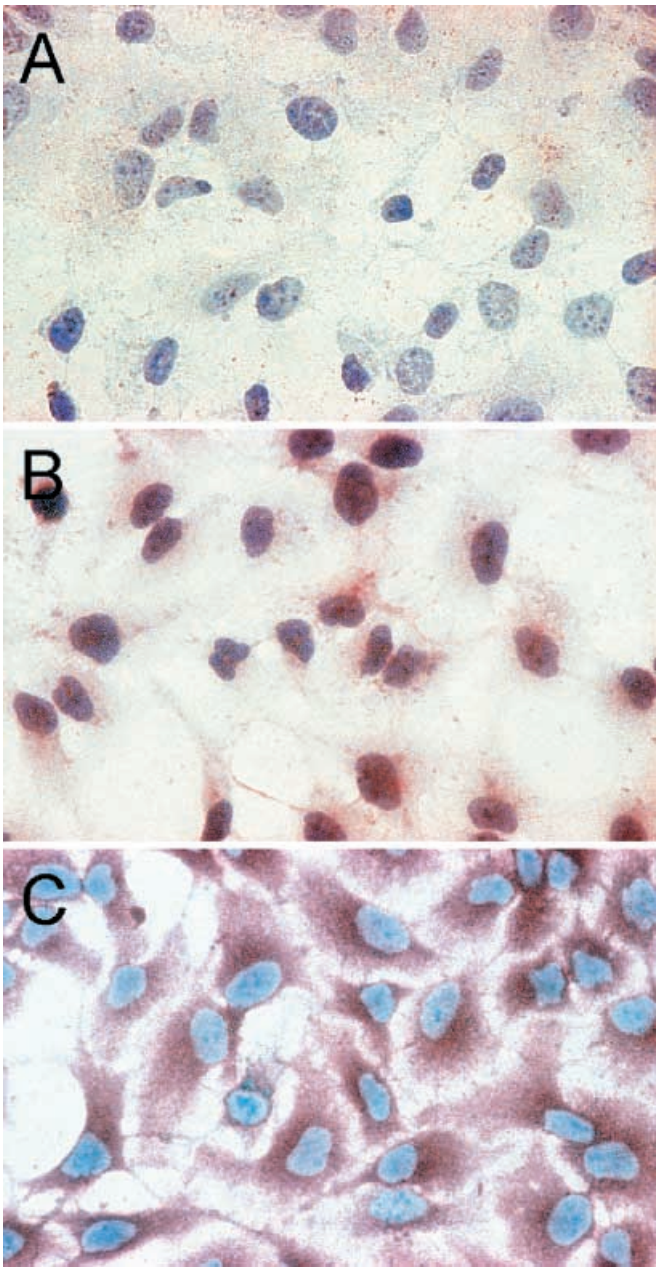

Fig. 2 Expression of LTA_4-hydrolase in cultured human oral epithelial cells (**A**–**C** ×63). **A** LTA_4-hydrolase expression in unstimulated oral keratinocytes. **B**, **C** LTA_4-hydrolase expression in keratinocytes after 2 h of bacterial contamination with *Haemophilus actinomycetemcomitans* at infection rates of 100:1 (**B**) and 1000:1 (**C**)

Discussion

The data presented here demonstrate for the first time the expression of LTA_4-hydrolase in oral mucosa biopsies from gingiva without and with symptoms of gingivitis.

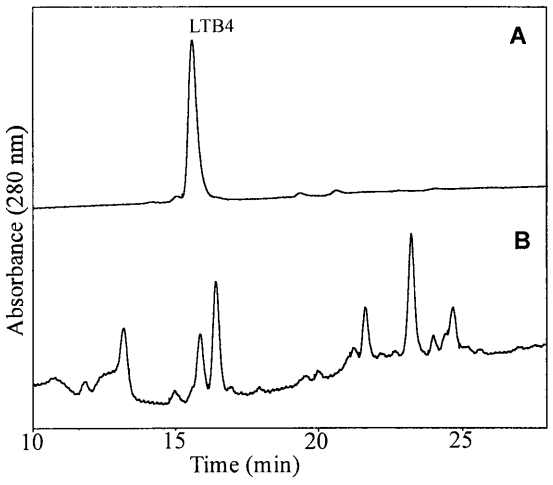

Fig. 3 Typical reverse-phase high-performance liquid chromatograms (RP-HPLC). **A** Standard leukotriene B_4 (LTB_4). **B** Representative oral biopsy in a volume of 200 µl. The ultraviolet (UV) absorbance intensity was measured using an UV diode-array detector with measurements at 280 nm

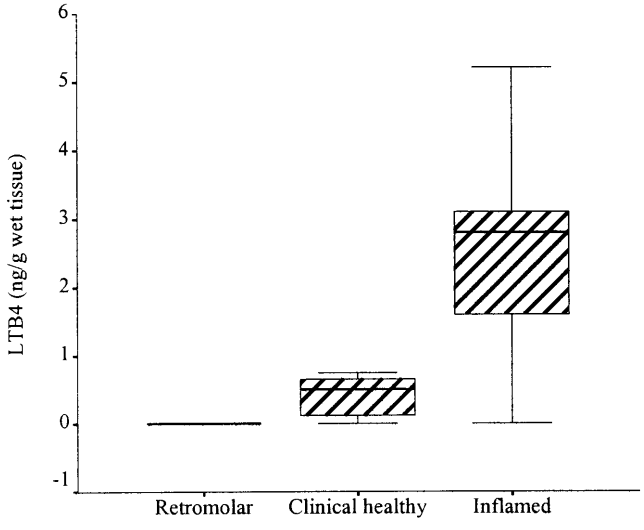

Fig. 4 Box plots of leukotriene B_4 (LTB_4) levels (ng/g wet tissue) in the three different gingival tissues

Most significantly, there was a strong association between the immunohistochemical detection of the enzyme and LTB_4 tissue levels on one hand and the histomorphologic appearance and clinical diagnosis of inflammation on the other hand. We were able to distinguish three clinically classified stages of oral mucosal inflammation using the expression of LTA_4-hydrolase, LTB_4 levels and cellular infiltration. Healthy retromolar oral epithelium, according to clinical and histological criteria, was not associated with LTA_4-hydrolase expression or detectable LTB_4 levels. In contrast, gingival tissues that appeared clinically healthy and were histologically characterised by a small infiltrate of T-lymphocytes, Langerhans' cells, macrophages/monocytes and granulocytes showed LTA_4-hydrolase expression. In these tissues LTA_4-hydrolase expression was observed in epithelial cells, which are therefore the most likely source of the elevated LTB_4 levels in these samples. We suggest that during the early stage of chronic inflammation epithelial cells might be the major source of LTB_4, because very limited immunoreactivity to the enzyme was observed in the infiltrate. However, the higher amount of LTA_4-hydrolase in epithelial cells may not necessarily account for their capacity to synthesise LTB_4. This may be the case if different isoforms of LTA_4-hydrolase exist in lymphocytes and epithelial cells, as shown for the human skin [16]. Clinically overt gingivitis was characterised by bleeding, increased levels of LTB_4 and massive inflammatory infiltration. We used bleeding on probing as a parameter to determine the disease status of the gingiva. This is a reliable and accepted clinical indicator to determine the inflammatory status [18], as confirmed by previous histological investigations [7, 11, 36]. LTA_4-hydrolase staining was observed in the epithelial cells and in inflammatory cells, the intensity being higher in the latter cells. Thus, during intense and clinically overt gingivitis LTB_4 may predominantly originate from infiltrating leukocytes rather than from the epithelial cells. This mechanism appeared likely in light of the observed tissue damage in inflamed samples caused by increased infiltration of T-lymphocytes, monocytes/macrophages and granulocytes into the epithelium, affecting the epithelial cells.

The tooth surface and adjacent gingival tissues are constantly exposed to bacteria [31]. It is reasonable to assume that these bacteria cause the induction of LTA_4-hydrolase expression and the elevated LTB_4 levels observed in this study in the clinically healthy oral gingiva surrounding the teeth. The in vitro stimulation of cultured oral keratinocytes by bacteria and the consequent increase in LTA_4-hydrolase expression supports this view. The chemoattractant nature of LTB_4 may therefore induce the invasion of relatively small numbers of inflammatory cells in the connective tissue, characterising this early chronic inflammatory disease stage. The infiltration of antigen-presenting Langerhans' cells supports this view [30], because infiltration of this cell type was also observed when gingival inflammation developed as a result of experimental plaque accumulation or naturally occurring gingival inflammation [4, 22]. The results indicate that the expression of LTA_4-hydrolase in epithelial cells is able to induce an immune response capable of LTB_4 synthesis to control bacterial infection of the gingival region without obvious tissue destruction. In consequence, the transition from local host–parasite equilibrium on one side and tissue injury associated with increased infiltration on the other side may be associated with elevated levels of LTA_4-hydrolase expression and LTB_4 levels in gingival tissues. The results are in agreement with other studies that have associated gingival health with minor cellular infiltration [27]. Because of the expression of LTA_4-hydrolase in epithelial cells, the epithelium may contribute to a significant extent to the regulation of the early inflammatory reaction by synthesis of LTB_4 and may actively participate in the pathogenesis of gingival inflammation. Other examples exist that

clearly show mechanisms by which epithelial cells contribute to the initiation of host defence [17].

The infiltrate is mainly composed of T-lymphocytes, macrophages/monocytes and granulocytes, confirming the chronic inflammatory character of the tissue changes and corroborating the results of other workers [2, 32, 41]. Because LTB_4 chemoattracts T-lymphocytes and granulocytes [3, 19, 40], it is quite likely that elevated LTB_4 levels caused the observed infiltration of these and other cells, but an indirect induction of lymphocyte migration via a second mediator cannot be excluded. LTB_4 is also a potent chemoattractant for granulocytes and macrophages [28], which were also observed in the inflamed tissue. These cells promote inflammation and cause direct tissue injury via surface adhesion and production of cytotoxic agents [37], leading to the tissue destruction observed in some samples.

A large body of work on the immunoregulation of chronic gingival and periodontal diseases has focused on T-lymphocytes, and it is increasingly evident that T-lymphocytes are involved in the control of these lesions [20, 33, 39]. Although some of the histologically observed tissue changes of the advanced chronic inflammatory reaction could be attributed directly to the action of LTB_4, such as the induction of epithelial cell proliferation or the induction of epithelial microabscesses [5, 6], the expression of LTA_4-hydrolase and consequent LTB_4 production in epithelial cells may be an important regulator for the immune response of gingival inflammation mediated by T-lymphocyte infiltration [9, 23, 34, 38].

Elevated levels of LTA_4-hydrolase and its products have been found in human diseases of chronic inflammatory character, such as atopic dermatitis [12, 25], psoriasis lesions [16], inflammatory bowel disease [15], membranous nephropathy [21] or chronic inflammation that is characteristic of asthma and allergic rhinitis [29]. This report is to our knowledge the first to describe the relationship between LTA_4-hydrolase expression, LTB_4 levels and clinical and histological appearance of a chronic disease of bacterial origin. With respect to results presented previously [14] and in this study, it is likely that these changes are induced by the accumulation of bacterial pathogens. The chronic gingival lesion analysed in the present study, which is extremely widespread in humans, may remain stable for years or decades or it may become converted into a progressive destructive periodontal lesion. The association between eicosanoid synthesis and disease progression displayed in this study may be relevant for the disease progression of other chronic inflammatory diseases irrespective of the causative agent.

In summary, this study indicates that the expression of LTA_4-hydrolase and elevated levels of LTB_4 in oral mucosal epithelium are integral parts of the induction and progression of chronic inflammatory reactions associated with the infiltration of inflammatory cells caused by pathogenic microorganisms. Epithelial cells participate in early stages of chronic inflammation and may act as a source of LTB_4, which may have diverse effects on immunoregulation.

Acknowledgements The authors thank Prof. R. Parwaresch, Christian-Albrechts-University of Kiel, Germany, for the helpful discussion during preparation of this work and Prof. G. Klöppel, Christian-Albrechts-University of Kiel, Germany, for the critical reading of the manuscript. We wish to thank Prof. T. Shimizu, University of Tokyo, Japan, for the LTA_4-hydrolase antibody.

References

1. Abiko Y, Suraweera AK, Nishimura M, Arakawa T, Takuma T, Mizoguchi I, Kaku T (2001) Differential expression of human beta-defensin 2 in keratinized and non-keratinized oral epithelial lesions: immunohistochemistry and in situ hybridization. Virchows Arch 438:248–453
2. Alcoforado GA, Kristoffersen T, Johannessen AC, Nilsen R (1990) The composition of gingival inflammatory cell infiltrates in children studied by enzyme histochemistry. J Clin Periodontol 17:335–340
3. Bacon KB, Camp RD, Cunningham FM, Woollard PM (1988) Contrasting in vitro lymphocyte chemotactic activity of the hydroxyl enantiomers of 12-hydroxy-5, 8, 10, 14-eicosatetraenoic acid. Br J Pharmacol 95:966–974
4. Baelum V, Fejerskov O, Dabelsteen E (1989) Langerhans cells in oral epithelium of chronically inflamed human gingiva. J Periodontal Res 24:127–136
5. Bauer FW, van de Kerkhof PC, Maassen-de Grood RM (1986) Epidermal hyperproliferation following the induction of microabscesses by leukotriene B4. Br J Dermatol 114:409–412
6. Camp R, Jones R, Brain S, Woolard P, Greaves M (1984) Production of intradermal microabscesses by topical application of leukotriene B4. J Invest Dermatol 82:202–204
7. Cooper PG, Caton JG, Polson AM (1983) Cell populations associated with gingival bleeding. J Periodontol 54:497–502
8. Czarnetzki B, Rosenbach T (1986) Chemotaxis of human neutrophils and eosinophils towards leukotriene B4 and its omega-oxidation products in vitro. Prostaglandins 31:851–858
9. Dasari VR, Jin J, Kunapuli SP (2000) Distribution of leukotriene B4 receptors in human hematopoetic cells. Immunopharmacology 48:157–163
10. Eberhard J, Jepsen S, Albers HK, Açil Y (2000) Quantification of arachidonic acid metabolites in small tissue biopsies by reversed-phase high-performance liquid chromatography. Anal Biochem 280:258–263
11. Engelberger T, Hefti A, Kallenberger A, Rateitschak KH (1983) Correlations among papilla bleeding index, other clinical indices and histologically determined inflammation of gingival papilla. J Clin Periodontol 10:579–589
12. Fogh K, Herlin T, Kragballe K (1989) Eicosanoids in skin of patients with atopic dermatitis: prostaglandin E2 and leukotriene B4 are present in biologically active concentrations. J Allergy Clin Immunol 83:450–455
13. Haeggstrom JZ (2000) Structure, function, and regulation of leukotriene A4 hydrolase. Am J Respir Crit Care Med 161: 25–31
14. Holm-Pedersen P, Agerbaek N, Theilade E (1975) Experimental gingivitis in young and elderly individuals. J Clin Periodontol 2:14–24
15. Ikehata A, Hiwatashi N, Kinouchi Y, Yamazaki H, Ito K, Toyota T (1995) Altered leukotriene B4 metabolism in colonic mucosa with inflammatory bowel disease. Scand J Gastroenterol 30:44–49
16. Iversen L, Deleuran B, Hoberg AM, Kragballe K (1996) LTA4 hydrolase in human skin: decreased activity, but normal concentration in lesional psoriatic skin. Evidence for different LTA4 hydrolase activity in human lymphocytes and human skin. Arch Dermatol Res 288:217–224
17. Kagnoff MF, Eckmann L (1997) Epithelial cells as sensors for microbial infection. J Clin Invest 100:6–10
18. Lang NP, Nyman S, Senn C, Joss A (1991) Bleeding on probing as it relates to probing pressure and gingival health. J Clin Periodontol 18:257–261

19. Leppert D, Hauser SL, Kishiyama JL, An S, Zeng L, Goetzl EJ (1995) Stimulation of matrix metalloproteinase-dependent migration of T cells by eicosanoids. FASEB J 9:1473–1481
20. Mathur A, Michalowicz BS (1997) Cell-mediated immune system regulation in periodontal diseases. Crit Rev Oral Biol Med 8:76–89
21. Menegatti E, Roccatello D, Fadden K, Piccoli G, de Rosa G, Sena LM, Rifai A (1999) Gene expression of 5-lipoxygenase and LTA4 hydrolase in renal tissue of nephritic syndrome patients. Clin Exp Immunol 116:347–353
22. Newcomb GM, Seymour GJ, Powell RN (1982) Association between plaque accumulation and Langerhans cell numbers in the oral epithelium of attached gingiva. J Clin Periodontol 9:297–304
23. Nickoloff BJ, Mitra RS, Green J, Shimizu Y, Thompson C, Turka LA (1993) Activated keratinocytes present bacterial-derived superantigens to T lymphocytes: relevance to psoriasis. J Dermatol Sci 6:127–133
24. Ohishi N, Minami M, Kobayashi J, Seyama Y, Hata J, Yotsumoto H, Takaku F, Shimizu T (1990) Immunological quantification and immunohistochemical localization of leukotriene A4 hydrolase in guinea pig tissues. J Biol Chem 265: 7520–7525
25. Okano-Mitani H, Ikai K, Imamura S (1996) Leukotriene A4 hydrolase in peripheral leukocytes of patients with atopic dermatitis. Arch Dermatol Res 288:168–172
26. Orning L, Gierse J, Fitzpatrick F (1994) The bifunctional enzyme leukotriene A4 hydrolase is an arginine aminopeptidase of high efficiency and specificity. J Biol Chem 269:11269–11273
27. Page RC, Schroeder HE (1976) Pathogenesis of inflammatory periodontal disease. A summary of current work. Lab Invest 34:235–249
28. Palmblad J, Malmsten C, Uden A, Radmark O, Endstedt L, Samuelsson B (1981) Leukotriene B4 is a potent and stereospecific stimulator of neutrophil chemotaxis and adherence. Blood 58:658–661
29. Rachelefsky G (1997) Childhood asthma and allergic rhinitis: the role of leukotrienes. J Pediatr 131:348–355
30. Reibel J, Dabelsteen E, Kenrad B, Buschard K (1985) Pattern of distribution of T lymphocytes, Langerhans cells and HLA-DR bearing cells in normal human oral mucosa. Scand J Dent Res 93:513–521
31. Ronstrom A, Attstrom R, Egelberg J (1975) Early formation of dental plaque on plastic films. 1. Light microscopic observations. J Periodontal Res 10:28–35
32. Seguier S, Godeau G, Brousse N (2000) Immunohistological and morphometric analysis of intra-epithelial lymphocytes and Langerhans cells in healthy and diseased human gingival tissues. Arch Oral Biol 45:441–452
33. Seymour GJ, Gemmell E, Reinhardt RA, Eastcott J, Taubman MA (1993) Immunopathogenesis of chronic inflammatory periodontal disease: cellular and molecular mechanisms. J Periodontal Res 28:478–486
34. Suchett-Kaye G, Morrier JJ, Barsotti O (1998) Interactions between non-immune host cells and the immune system during periodontal disease: role of the gingival keratinocyte. Crit Rev Oral Biol Med 9:292–305
35. Ternowitz T, Herlin T, Fogh K (1987) Human monocyte and polymorphonuclear leukocyte chemotaxis and chemokinetic response to leukotriene B4 and FMLP. Acta Pathol Microbiol Immunol Sect C 95:47–54
36. Thilo BE, Caton JG, Polson AM, Espeland MA (1986) Cell populations associated with interdental bleeding. J Clin Periodontol 13:324–329
37. Weiss SJ (1989) Tissue destruction by neutrophils. N Engl J Med 320:365–376
38. Yamaoka KA, Kolb JP (1993) Leukotriene B4 induces interleukin-5 generation from human T lymphocytes. Eur J Immunol 23:2392–2398
39. Yamazaki K, Nakajima T, Hara K (1995) Immunohistological analysis of T cell functional subsets in chronic inflammatory periodontal disease. Clin Exp Immunol 99:384–391
40. Zachariae C, Ternowitz T, Larsen CG, Nielsen V, Thestrup-Pedersen K (1988) Epidermal lymphocyte chemotactic factor specifically attracts OKT4-positive lymphocytes. Arch Dermatol Res 280:354–357
41. Zachrisson BU, Schultz-Haudt SD (1968) A comparative histological study of clinically normal and chronically inflamed gingiva from the same individuals. Odontol Tidskr 76:179–192

Virchows Arch (2002) 440:635–639
DOI 10.1007/s00428-002-0607-z

ORIGINAL ARTICLE

**Juliana Fariña · Concepción Millana
M. Jesús Fdez-Aceñero · Vicente Furió
Paloma Aragoncillo · Victorino G. Martín
Jerónimo Buencuerpo**

Ultrasonographic autopsy (echopsy): a new autopsy technique

Received: 18 September 2001 / Accepted: 12 December 2001 / Published online: 31 January 2002
© Springer-Verlag 2002

Abstract Autopsy has been one of the most important techniques for the development of modern medicine, mainly during the nineteenth century and the first half of last century. However, in the last few years, the number of autopsies performed in hospitals has dramatically decreased all over the world. This loss of interest can be attributed both to important advances in other diagnostic and therapeutic techniques and to the fear of malpractice suits. Several groups have tried to overcome this problem, developing different autopsy techniques, one of which is needle autopsy. Most authors using this technique have acknowledged that it is difficult to obtain material from certain organs and lesions, which makes its diagnostic reliability worse than that of conventional autopsy. To overcome this drawback, our team has recently developed a modification of needle autopsy, called ultrasonographic autopsy or echopsy, in which samples are obtained under ultrasonographic control. We report the results of the first 100 cases of echopsy performed in our hospital, comparing this technique with conventional autopsy performed on all the corpses. The concordance rate for the cause of death and the main pathological diagnosis between echopsy and classical autopsy was 83% in our series, which makes echopsy a feasible and reliable alternative to conventional autopsy in cases in which families refuse to give their consent for classical autopsy or in cases of infectious diseases.

Keywords Autopsy · Echopsy · Ultrasonographic autopsy · Needle autopsy

This work was performed at the Department of Surgical Pathology II, Hospital Clínico Madrid, Spain. It was supported by a grant from the Spanish Sanitary Investigation Fund.

J. Fariña · C. Millana · M.J. Fdez-Aceñero (✉) · V. Furió
P. Aragoncillo
Department of Pathology II, Hospital Clínico, Madrid, Spain
e-mail: mgg10167@teleline.es
Tel.: +34-91-3303035, Fax: +34-91-3303504

V.G. Martín
Department of Pathology, Saad Medical Center,
Al-Khobar, Saudi Arabia

J. Buencuerpo
Department of Medicine, Hospital Clínico, Madrid, Spain

M.J. Fdez-Aceñero
c/Hilarión Eslava 28, 60-A, 28015 Madrid, Spain

Introduction

Autopsy has been one of the most important techniques for the development of modern medicine, mainly during the nineteenth and twentieth centuries. However, during the last few decades, there has been a dramatic decrease in the number of autopsies being performed all over the world [7], even though this technique continues to reveal major unexpected findings in over 30% of cases [6, 8].

Several authors have developed modifications of the autopsy technique in an attempt to increase the number performed. One such modification is needle autopsy, introduced in 1955 [9]; this technique is used to obtain material from the organs with a tru-cut needle without opening the corpse [12]. However, it has not gained widespread acceptance due to its relatively low diagnostic reliability. Our team has developed a modification of needle autopsy that tries to overcome this problem by obtaining samples under ultrasonographic control: ultrasonographic autopsy or echopsy [2].

The objective of this paper is to report the results of the first 100 corpses in which this new type of autopsy was performed and to compare our results with those obtained by conventional autopsy, which was subsequently performed on all the corpses.

Material and methods

We performed ultrasonographic autopsy on 100 corpses (19 children and 81 adults). Ultrasonography was performed using a Siemens Sonoline SI-250 ultrasonograph. In adults, we studied the heart, liver, lungs, kidneys, spleen, pancreas, the gastrointestinal and urogenital tracts and the pleural and peritoneal cavities using a 3.5-MHz sectorial probe; the breasts, testes, thyroid gland, other

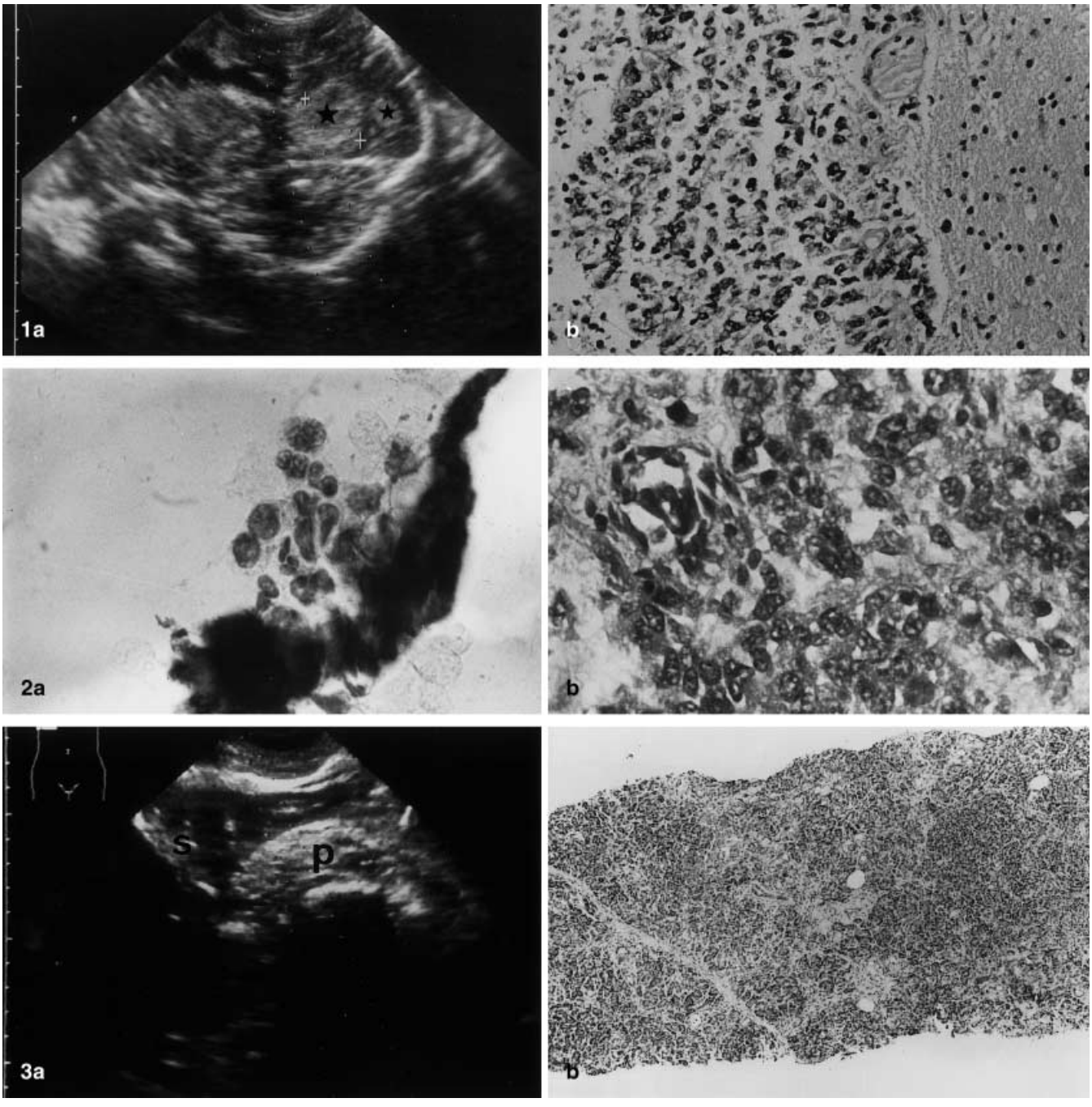

superficial structures and all the organs in children were studied using a multi-frequency 5-, 6- and 7.5-MHz sectorial probe. First we measured the organs and noted any lesions. A 14-gauge tru-cut needle (Baxter, 2N2704X, Healthcare Corporation, Deerfield, Illinois, USA) was used to obtain material for histological analysis from these organs and lesions under direct ultrasonographic vision. During this step, two people worked at the same time: the ultrasonographist, who located the lesion, and the autopsy technician, who aspirated the samples. We generally obtained five samples from normal organs and more from lesions or from organs in which disease had been suspected while the patient was alive. All the samples were immediately placed in buffered formalin in a container labelled with the name of the patient and the organ. We also aspirated effusions and other fluids for cytological analysis with a spinal needle connected to a syringe under sonographic control. These samples can also be sent for microbiological studies, but in this case the skin should be thoroughly disinfected

Fig. 1 **a** Echopsy image obtained from a 3×3 cm window opened in the skull. Ultrasonographic section taken with a 3.5-MHz probe in which two supratentorial metastases are seen (*asterisks*). **b** Histological image of one of these metastases. Material obtained by echopsy, corresponding to a small cell lung carcinoma. HE, ×200

Fig. 2 **a** Echopsy of peritoneal dissemination of a malignant mixed müllerian tumour. Specimen aspirated with a spinal needle. Papanicolaou. ×400. **b** Histological image of a carcinomatous area of the tumour shown in Fig. 2A. Material obtained from the uterus by echopsy. HE, ×400

Fig. 3 **a** Echopsy of a transverse section of the pancreas with a 3.5-MHz probe on the epigastric area. The pancreas (*P*) is seen under the stomach (*S*). **b** Histological image of the pancreas seen in Fig. 3A. There are no pathological abnormalities in the sample obtained by echopsy. HE, ×50

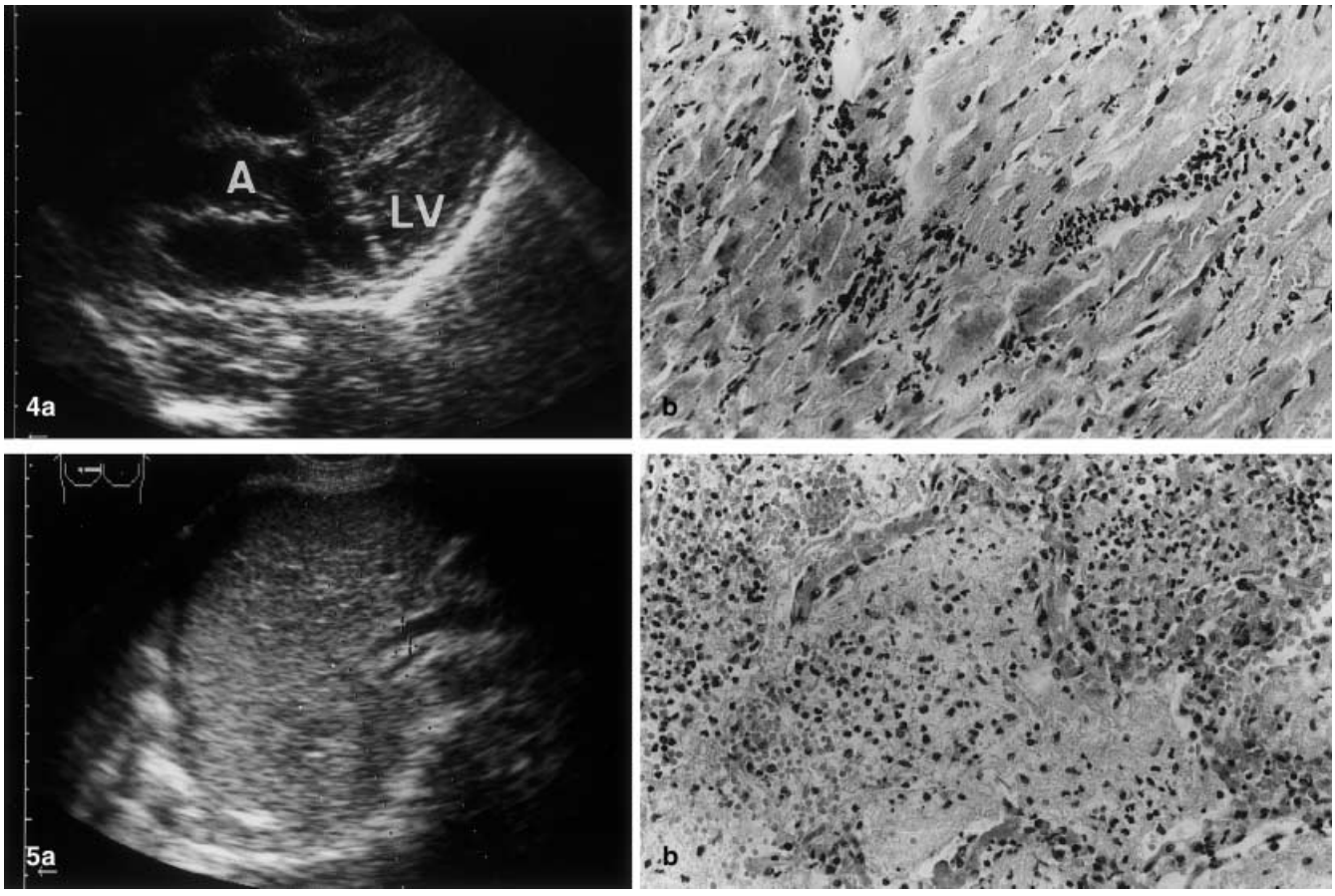

Fig. 4 **a** Ultrasonographic image of the four cardiac chambers and the root of the aorta (*A*). The 3.5-MHz probe is placed on the left parasternal area. The tru-cut needle has passed through the heart and is taking samples from the left ventricle (*LV*). **b** Histological image of an acute myocardial infarct in the corpse shown in Fig. 4A. HE, ×200

Fig. 5 **a** Transverse section of the right lung with a 3.5-MHz probe on the right parasternal area, showing a pulmonary condensation. The *crosses* indicate the bronchus. **b** Histological image of a pneumonia in the corpse shown in Fig. 5A. HE, ×200

before the sample is obtained. In order to analyse the adult brain, we either opened a 3-cm window in the skull or placed the corpse in a prone position and studied the brain through the foramen magnum; the same approaches were used to obtain samples for histological analysis. The brain of newborns and infants was easy to study through the fontanelles.

After echopsy was completed, other pathologists on the team performed conventional autopsy. They were only given information from the patients' medical records, but had no knowledge of the ultrasonographic findings.

The results of the two techniques were compared after the final report had been drawn up using a double-blind technique. We compared these techniques, estimating the concordance rate for the cause of death and the main pathological findings in both cases. We did not analyse the concordance rate for minor pathological findings. We also analysed the concordance rate between the two techniques and the clinical diagnosis.

Results

After a short training period in a radiology department, echopsy can be performed in 1–1.5 h. Echopsy was used to obtain samples suitable for histological analysis from the liver, the spleen, the lungs, the kidneys and the brain in 100% of the corpses. The heart was correctly sampled in 92% of corpses. We also obtained samples in 100% from the effusions and the cystic lesions diagnosed ultrasonographically. The success rate for other organs ranged from 21% for the gastrointestinal tract to 76% for the thyroid and the breast (Figs. 1, 2, 3, 4, 5).

Ultrasonography can visualize either cystic or solid lesions measuring more than 4 mm. Diffuse diseases affecting an organ can be diagnosed in almost 100% of cases. The samples obtained for histological analysis using the tru-cut needle measure up to 3×0.3 cm and can be used for conventional histological analysis and for immunohistochemistry, genetic and other diagnostic techniques.

The concordance rate between echopsy and conventional autopsy regarding the cause of death and the main pathological findings reached 83% in our series. In 61 corpses (61%), both techniques showed similar findings in agreement with the medical diagnosis made while the patient was alive. In 22 corpses, both techniques revealed important diseases that had contributed to the death of the patient, but had not been diagnosed while the patient was

Table 1 Cases in which the clinical diagnosis could only be confirmed by conventional autopsy

Case no.	Age (years)	Sex	Important data found on autopsy
1	55	m	Pulmonary thromboembolism
2	70	m	Rheumatic aortic stenosis
3	40	m	Recent myocardial infarct; thrombosis of the angioplasty stent
4	64	m	Acute subendocardial infarct
5	64	m	Endocarditis of bioprosthetic valve

Table 2 Case in which relevant diseases were diagnosed by conventional autopsy but not diagnosed while the patient was alive

LLL, left lower lobe; MALT, mucosa-associated lymphoid tissue

Case no.	Age (years)	Sex	Important data found on autopsy
1	72	f	Pulmonary thromboembolism
2	60	m	2.5-cm bronchial carcinoma in LLL
3	75	m	Marasmatic bacterial endocarditis
4	87	m	30-cm transmural ileal infarct
5	88	f	Mitral endocarditis
6	88	f	Colonic infarct; cecal MALT lymphoma; pulmonary thromboembolism

Table 3. Cases in which only some of the diseases diagnosed by conventional autopsy were revealed by echoscopy

Case no.	Age (years)	Sex	Clinical data	Pathologic findings found using both techniques	Pathologic findings only found on autopsy
1	67	m	Peritoneal tuberculosis	Micronodular cirrhosis and ascites	Marasmatic endocarditis
2	85	m	Agranulo-citosis due to drugs or infection	Pulmonary aspergillosis	Infrarenal aortic aneurysm
3	75	m	COPD, obesity. rheumatic mitral and aortic stenosis	Massive pulmonary atelectasis	1.8-cm bronchial cancer, rheumatic mitral and aortic stenosis
4	58	m	Chronic alcoholism	Micronodular cirrhosis	Aspiration broncho-pneumonia
5	79	m	Possible rupture of aortic aneurysm	Sepsis due to acute left pyelonephritis with abscess formation	Latent prostatic carcinoma
6	45 years M. Pulmonary thromboembolism			Gastric haemorrhage	Pulmonary thrombo-embolism

COPD, chronic obstructive pulmonary disease.

alive. The 17 cases in which the results of echopsy and conventional autopsy were in disagreement are summarized in Tables 1, 2 and 3. Table 1 includes five cases in which the clinical diagnosis was only confirmed by conventional autopsy; Table 2 summarizes six cases in which classical autopsy found important diseases not diagnosed either while the patient was still alive or on echopsy. Table 3 includes six additional cases in which echopsy only demonstrated some of the main diseases contributing to death which were not diagnosed while the patient was alive. In these cases, the reliability of classical autopsy was better than that of echopsy.

In summary, conventional autopsy revealed diseases contributing to death that were not suspected while the patient was alive in 34% of our series; this figure was only 28% for echopsy. No false-positive results were obtained using echopsy.

Discussion

The number of autopsies has been steadily decreasing in recent years all over the world. However, the number of clinicopathological discordances remains unchanged over 30% [8], a fact that confirms the importance of autopsies for medical teaching and the improvement of the clinical practice. New autopsy techniques with a higher level of acceptance among both clinicians and relatives might help to solve this problem, at least partially.

Needle autopsy was introduced by Terry [9] in 1955. However, its results have generally been discouraging, as most organs cannot be adequately sampled. Reports on needle autopsy have shown a 67%, 48% and 43% sensitivity rate for the diagnosis of the cause of death compared with conventional autopsy [3, 5, 12]. In 1969, Wellman [11] reported the results of 394 needle autop-

sies; he only obtained adequate samples from the liver (92%), the heart (55%), the lung (46%) and the kidney (34%), and all the remaining organs were only accidentally sampled. This author was only able to confirm 54% of the tumours diagnosed while the patient was alive using the samples obtained, and the diagnostic reliability was therefore low. Although these figures have remained unchanged in more recent reports [11], interest in this technique has recently been renewed by the appearance of new infectious diseases that pose too high a risk for the pathologist performing the autopsy. Some authors have advocated the use of needle autopsy to confirm the clinical diagnosis in this type of patient [1, 4, 10].

Our team had been using needle autopsy with similarly discouraging results. In an attempt to increase the reliability of the technique, we decided to introduce an imaging technique to help obtain samples. Ultrasonography appeared to be the most adequate technique, because it is easy and cheap and most pathologists are familiar with its use in fine-needle aspiration cytology. In addition, this technique is also well-known among patients' relatives and is considered to be quick and painless; we therefore thought that we could increase the acceptance of this postmortem technique.

The results reported here seem to confirm the improvement of needle autopsy using ultrasonographic control. We increased the adequacy of the samples obtained from most organs. The worst results were obtained in the gastrointestinal tract, from which we only obtained representative samples in 21%–25% of the corpses. We are currently working on the design of new needles to overcome this problem.

We confirmed the cause of death in 83% of our cases and revealed important diseases not diagnosed while the patient was alive in 28%; this technique is therefore not only suitable for confirming diseases diagnosed while the patient was alive, but can also discover unsuspected ones, retaining the role of conventional autopsy. In addition, we also obtained adequate samples from most organs and from all lesions larger than 4 mm. Most of the diagnostic pitfalls were diseases of the cardiovascular system and the tracheobronchial tree. Four of the 17 cases in which echopsy failed to yield the correct diagnosis were massive thromboembolisms, 4 were endocarditis either on native or on prosthetic valves, 2 were anatomical lesions of the cardiac valves and 2 were small endoluminal bronchial carcinomas (see Tables 1, 2, 3). The diagnostic accuracy of echopsy was much better for diffuse parenchymatous lung lesions (pneumonia, adult distress respiratory syndrome) and for myocardial infarct (we only missed two small subendocardial infarcts). We are trying to increase our experience with sonography of the cardiovascular system and the tracheobronchial tree after death in an attempt to improve our diagnostic accuracy in these systems. We have had trouble obtaining a good acoustic window that allows ventricular thickness to be measured reliably, especially as measurements while the patient is alive are made at the peak of the QRS complex, which is obviously lacking after death. We have also found it difficult to visualize the coronary arteries and the pathology affecting them (mainly rupture or thrombosis on atheromatous plaques), because while patients are alive these lesions are usually only observed from a transoesophagic approach and are difficult to see transthoracically. We are trying to improve our experience in these areas, but echopsy currently seems to have limitations in the diagnosis of this kind of pathology.

In summary, we report here on a new postmortem technique we have developed that overcomes some of the problems associated with needle autopsy. This technique seems to be better accepted by relatives, and its reliability (83% concordance rate with conventional autopsy) might make it the ideal technique in cases in which families refuse to give their consent for conventional autopsy and for infectious cases in order to reduce the risk of exposure of the pathologist.

Acknowledgements The authors are indebted to the participating pathologists and clinicians at Hospital Clínico, especially to the autopsy technicians, Ricardo J. Salto, Juan C. Iglesias and Rosa Caballé.

References

1. Baumgart KW, Quin JW, Gatenby PA (1990) The limited (needle biopsy) autopsy: a prospect for revival (letter). Med J Aust 153:301
2. Fariña J (1996) Ultrasound autopsy (in Spanish). Rev Clin Esp 196:49–51
3. Foroudi F, Cheung K, Duflou J (1995) A comparison of needle biopsy postmortem with the conventional autopsy. Pathology 27:79–82
4. Geller SA (1990) The needle autopsy in acquired immunodeficiency syndrome. Arch Pathol Lab Med 114:324–329
5. Huston BM, Malouf NN, Azar HA (1996) Percutaneous needle autopsy sampling Mod Pathol 9:1101–1107
6. Kingsfor DP (1995) A review of diagnostic inaccuracy. Med Sci Law 35:347–351
7. Roe FJC (1992) Let's have a postmortem. Indoor Environ 1:179–181
8. Sarode VR, Datta BN, Banerjee AK, Banerjee CK, Joshi K, Bhusnurmath B, Radotra BD (1993) Autopsy findings and clinical diagnosis: a review of 1000 cases. Hum Pathol 24: 194–198
9. Terry R (1955) Needle necropsy. J Clin Pathol 8:38–41
10. Underwood JCE, Slater DN, Parson MA (1983) The needle autopsy. Br Med J 286:1632–1634
11. Wellmann KF (1969) The needle autopsy. A retrospective evaluation of 294 consecutive cases. Am J Clin Pathol 52:441–444
12. West M, Chomet B (1957) An evaluation of needle necropsies. Am J Med Sci 234:554–560

Virchows Arch (2002) 440:640–647
DOI 10.1007/s00428-001-0549-x

ORIGINAL ARTICLE

A.W. Bates · S.I. Baithun

The significance of secondary neoplasms of the urinary and male genital tract

Received: 8 May 2001 / Accepted: 5 September 2001 / Published online: 19 Oktober 2001
© Springer-Verlag 2001

Abstract Secondary neoplasms account for some 1.6–3.0% of solid malignancies encountered in surgical specimens from the genitourinary tract. At autopsy the proportion is higher, largely due to sampling bias. The peak incidence occurs around the seventh decade, and male and female incidences are approximately equal at all sites except the kidney, which shows a male preponderance owing to an excess of metastatic lung cancer. Adenocarcinomas are the most common histological type of secondary neoplasm and may be histologically and immunohistochemically indistinguishable from primary neoplasms arising from colonic-type epithelial metaplasia. Seeding of tumour along the urinary passages does not appear to be a significant mechanism of metastasis, and spread from one part of the genitourinary tract to another is uncommon. Clinical information and ancillary investigations are more helpful than special histological techniques in differential diagnosis.

Keywords Neoplasia · Metastasis · Bladder · Kidney · Testis · Prostate

Introduction

The differential diagnosis of primary and secondary genito-urinary neoplasia is rarely emphasised in pathological texts: the genito-urinary tract is not regarded as a favoured site for metastatic neoplasia, and, with the exception of the bladder, is relatively inaccessible to direct tumourous invasion. The possibility of a secondary origin for malignancy in biopsies from genito-urinary sites must be considered in the differential diagnostic process, and this review aims to summarise information on the relative incidence, origin, localisation and histological appearances of secondary tumours in order to highlight potential diagnostic difficulties.

A.W. Bates (✉) · S.I. Baithun
Department of Histopathology and Morbid Anatomy,
Institute of Pathology, The Royal London Hospital,
London E1 1BB, UK
e-mail: A.Bates@bartsandthelondon.nhs.uk
Tel.: +44-207-3777347, Fax: +44-207-3777030

Incidence of secondary genito-urinary neoplasia

Some of the most complete series of secondary genito-urinary neoplasms, largely based on autopsy material, were reported in the late 1940s and early 1950s. Klinger produced a valuable overview of secondary tumours of the genito-urinary tract [46], partly to counter the impression that 'metastatic invasion of the urinary tract is a unique and rarely encountered phenomenon'. Most of his cases, drawn from 5000 autopsies, involved the kidney [1]. Ganem and Batal [31] reported a single case of carcinoma metastatic to the bladder, accompanied by a review of 79 similar cases in the literature, many of which came from Melicow's study of histological types of over 2500 surgical and autopsy cases of primary and secondary neoplasms of the bladder [55]. Later series of secondary bladder tumours include those of Goldstein [34] and Roberts [72].

Sir Rupert Willis identified some 50 cases of tumours metastatic to the testis in the literature prior to 1936 [93]. The perceived rarity of testicular secondary tumours often led to their misdiagnosis, as Melicow has described [54]: his own series comprised 13 cases, almost all of which were lymphomas. Price and Mostofi [68] reported a series of 38 secondary tumours of the testis from the files of the American Armed Forces Institute of Pathology, and later Pienkos and Jablokow [65] added a series of 15 new cases and reviewed 90 others from the literature. Blefari et al. [19] have identified some 200 cases in the international literature since 1935.

Zein et al. [94] reported 185 secondary neoplasms of the prostate from 6000 autopsies over 25 years, all but 58 of which were leukaemias or lymphomas. Johnson et al. [44] described 18 new cases of solid tumours metastatic to the prostate, with a further 25 from a review of the literature. Presman and Ehrlich [67] reported two cases of metastases to the ureter and identified 35 previ-

ously published cases, a total increased to 99 cases by Lucké and Schlumberger in 1957 [50]. A further series has since appeared identifying 37 cases in over 11,000 autopsies [6]. Secondary neoplasms of the penis have been the subject of a number of case reports [64] and a review of the Western literature in 1985 [66] identified a total of 219 cases. There have been only two reported series, of seven and five cases [30, 39].

These series have been augmented by a number of case reports of secondary neoplasms encountered in surgical material and remarkable for their being the presenting feature of malignancy, histological mimics of primary tumours, or for their rarity. Comparison between studies is hampered by their differing criteria; for example, some series include all secondary tumours and others only metastases. The inclusion of lymphomas and leukaemias is also variable: not only are these not metastatic in the conventional sense, they are seldom distinguished from primary lymphomas of the genito-urinary tract, a group better recognised, and more often diagnosed, since the development of the mucosa-associated lymphoid tissue (MALT) concept [14, 42]. Distinction between primary and secondary neoplasms can be difficult when it depends on differentiating between contiguous and non-contiguous involvement, the latter perhaps the result of "field change", for example, in transitional-cell carcinoma of the prostate [43]. This distinction is not merely semantic: contiguous and non-contiguous pT4a bladder cancers behave differently (the former have a worse prognosis) and should be separately staged [60].

Another way of looking at patterns of tumour metastasis is to record all identifiable metastases in patients with cancer at autopsy. The kidney is the fifth most common site for metastatic solid tumours following the lungs, liver, bones and adrenals [53, 63], and renal metastases are found at autopsy in some 9–20% of subjects dying of malignancy [52, 93] or 1.8–7.2% of all autopsies [21, 91]. Lymphomas and leukaemias involve the kidneys in 25–50% of cases [70, 86]. Secondary neoplasms of the prostate were found in 0.5–5.6% of patients who died from neoplasia [44, 94], and testicular secondaries in 0.5% [32]. Of 1000 cadavers with carcinoma of the breast, 167 had macroscopic metastases, in only four cases involving the bladder [2]. Some general studies of tumour metastases do not mention specific genito-urinary sites [22, 74] and in retrospect it is difficult, as in all retrospective autopsy series, to be certain of the thoroughness of examination. Differing incidences of secondary tumours at the various sites within the genito-urinary system may reflect the mix of surgical and autopsy cases, the age and sex distribution of the population, or other demographic variables in the sample. The proportion of secondary vesical tumours, for example, has been estimated at anything from 0.1–33% [34, 78], due partly to variability in the proportion of autopsy and surgical cases [29, 78], although the often-quoted lower figure of 0.1% derives from a misinterpretation of Dean and Ash's [29] figures, which do not in fact distinguish primary from secondary neoplasms.

Table 1 Incidence of secondary genito-urinary neoplasms in surgical and autopsy material [12, 13, 25, 30]

Site	Total cases	Malignant tumours (surgical, %)	Malignant tumours (autopsy, %)
Bladder	282	2.3	20
Testis	31	1.6	4
Kidney	443	3.0	30
Prostate	51	2.1	N.A.

Incidences of secondary neoplasms obtained from autopsy studies including all causes of death are, not surprisingly, low: Pienkos and Jablokow for example found an overall post-mortem incidence of secondary testicular tumours of 0.06% [65]. Klinger's table of relative incidences [46] derived from 5000 autopsies showed that metastases to the kidneys (118 cases) are much more numerous than those to bladder (33), prostate (10) and testis (3). Of 1000 autopsies of deaths due to malignancy, Abrahams et al. [2] found metastases to the kidney in 130, bladder in 36 and testis in 3 cases: many of these involved multiple genito-urinary sites and most were lymphomas. The data were drawn from a single autopsy series and so permit comparison between different sites.

For the surgical pathologist, more important than the overall incidence of a particular tumour type is the proportion of all malignant neoplasms encountered in surgical material that are secondary in origin. Despite large differences in overall incidence, studies on surgical material from the Royal London Hospital show that this proportion does not differ greatly between the different parts of the genito-urinary tract [12, 13, 25, 30]. Table 1 lists both the absolute numbers and proportions (as a percentage of all malignant neoplasms in surgical specimens and autopsies) of secondary tumours at sites in the urinary and male genital tract. Ureteric neoplasms have been included with those of the kidney. In no case were the seminal vesicles involved, except for direct infiltration by prostatic adenocarcinoma, a not uncommon finding in radical prostatectomy specimens. There were no cases of spread to the seminal vesicles from outwith the genito-urinary tract in this series, and there appear to be no case reports of metastasis to the seminal vesicles in surgical specimens in the literature. For all sites, the frequency of secondary tumours as a proportion of all tumours is higher in autopsy material: autopsy cases are more likely to have disseminated disease, there is a sampling bias towards unusual lesions, secondary neoplasms invading the outer layers of hollow organs are not amenable to diagnosis on endoscopy, and it is simpler to make a diagnosis of secondary neoplasia at autopsy than on the basis of a biopsy [12].

The excess of secondary tumours of the kidney in males (2.3:1) is attributable to the numerical significance of metastatic lung cancer. One might therefore expect the male to female ratio to approximate to unity as gender differences in cigarette smoking diminish. In the bladder,

Table 2 Primary sites of secondary neoplasms of the genito-urinary tract [12, 13, 25, 30]

Kidney	Prostate	Bladder	Testis
Lung 44%	Bladder 57%	Colon 21%	Prostate 27%
Stomach 9%	Lung 16%	Prostate 19%	Stomach 23%
Breast 7%	Rectum 10%	Rectum 12%	Lung 14%
Colo-rectum 7%	Pancreas 4%	Cervix 11%	Skin* 14%
Oesophagus 4%		Stomach 4%	
Pancreas 4%		Skin* 4%	
Uterus 2%		Lung 3%	

* Malignant melanoma

however, the slight male preponderance (1.2:1) is due to cases of direct invasion by colorectal carcinoma [12], a much less likely occurrence in the female. The overall incidence of secondary tumours may be set to increase as survival after an initial diagnosis of malignancy is prolonged [17].

Diagnosis of secondary neoplasia

Clinical history is the most important factor in correct interpretation of secondary genito-urinary neoplasia in biopsy material: known malignancy in a contiguous organ will suggest the possibility of direct spread, whereas metastases to the genito-urinary tract are almost invariably part of generalised carcinomatosis. Sites of origin of secondary neoplasia differ in prevalence throughout the urinary tract (Table 2). Disseminated malignancy first presenting as secondary neoplasia in the genito-urinary tract is infrequent, particularly in the proximal parts of the urinary tract, but occasional cases have been described in the kidney [73], and, more often, in the bladder, for example from gastric carcinoma (Fig. 1) [48], breast carcinoma [80] and malignant melanoma [24]. In malignant melanoma, sufficient pigment may be released to darken the urine [8]. Very rarely, carcinomatosis presents with a penile metastasis [4]. Problems of diagnosis may also arise when the interval between diagnosis of the primary tumour and discovery of the metastasis is very long [87]. Haematuria and/or pelvic pain are the most frequent symptoms of secondary genito-urinary involvement [46], especially in the prostate [82] and bladder [3].

Macroscopic features may be helpful in suggesting the correct diagnosis: secondary neoplasms of the kidney are usually multiple, bilateral, and cortical in location [25], while secondary neoplasms of the bladder are, unlike primary vesical tumours, almost always solitary [10], although it is often not possible to distinguish them on the basis of their cystoscopic appearance, even when the history of neoplasia elsewhere is known [79]. Since the majority of secondary neoplasms reach the bladder by direct spread, anatomical localisation of a secondary tumour may suggest its primary site: prostatic cancer commonly infiltrates the bladder neck, cervical cancer the trigone, rectal carcinoma the posterior wall and colonic cancer the fundus [12]. Primary squamous-cell carcinomas are reported to be most common in the trigone [85], although the validity of this observation depends on the rigour with which secondary tumours from the cervix were excluded. Pelvic computed tomography or magnetic resonance imaging are sensitive techniques, found to be as good as cystoscopy at detecting bladder involvement by secondary carcinoma [47].

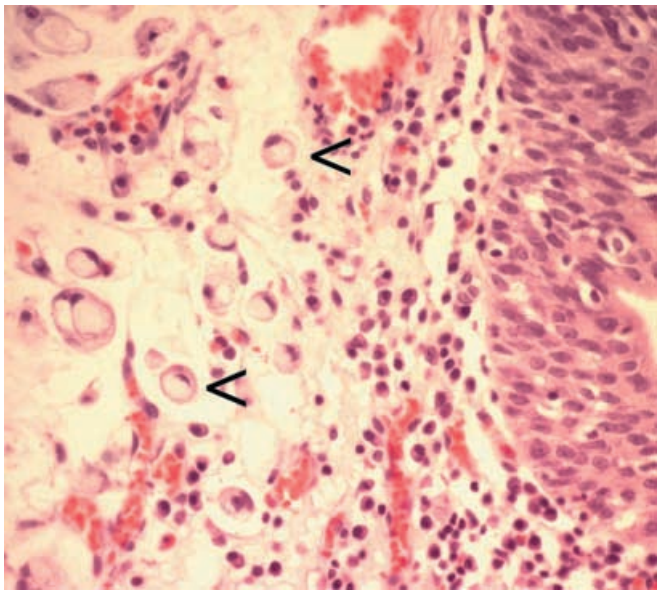

Fig. 1 Diffuse infiltration of the lamina propria of the bladder by signet ring cells of metastatic gastric adenocarcinoma (*arrowheads*). Note the non-dysplastic bladder mucosa to the right. Haematoxylin and eosin

Histology

Histopathological examination of biopsy material should be conducted with the possibility of secondary neoplasia in mind. Although the kidney is the most common genito-urinary site for secondary tumour (due to a high proportion of metastases), these neoplasms are rarely biopsied (only 16 of a series of 435 secondary renal tumours were from surgical material [25]) and are not normally a source of diagnostic difficulty, although occasionally metastases are inappropriately treated owing to mistaken diagnosis as a primary tumour [62]. Glomerular and tubular micrometastases occur in carcinomatosis and, although present in some 6% of cases if well sampled [91], are seldom seen in biopsies (Fig. 2). Cytologic examination of fine-needle aspiration specimens has been described to confirm the secondary nature of tumours visualised in the kidney [65] and may be useful in bilateral renal tumours, 20% of which are metastatic in nature [15]. A transjugular biopsy approach has been described for this purpose [77].

The most problematic sites are the bladder [12] and the testis, especially in children [30]. The incidence of

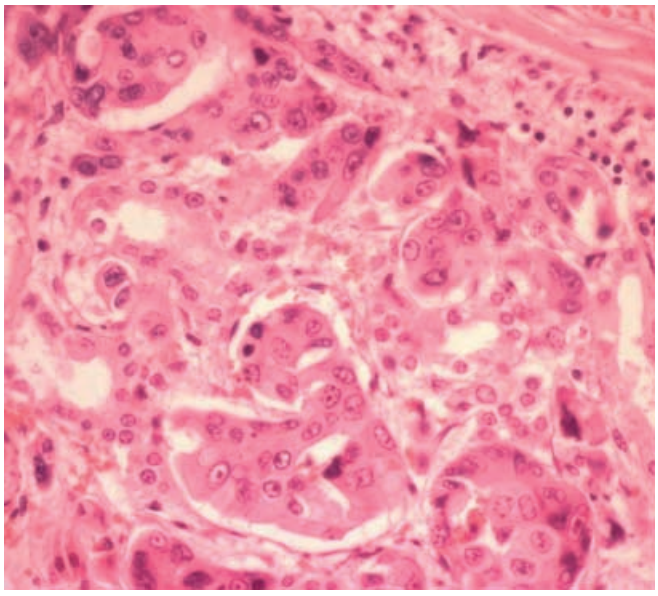

Fig. 2 Micrometastases of squamous-cell carcinoma within renal tubules. Haematoxylin and eosin

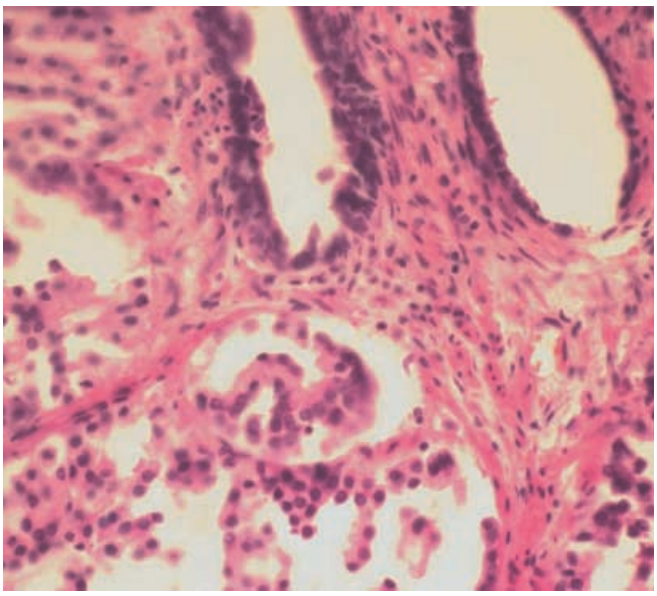

Fig. 3 Well-differentiated adenocarcinoma of the pancreas metastatic to prostate. Non-neoplastic prostate glands are present in the *upper part* of the figure. Haematoxylin and eosin

Table 3 Histological types of secondary neoplasms of the genito-urinary tract [12, 13, 25, 30]

Kidney		Prostate	
Adenocarcinoma	30%	Transitional cell carcinoma	57%
Squamous-cell carcinoma	28%	Adenocarcinoma	20%
Small-cell carcinoma	8%	Small-cell carcinoma	8%
Malignant melanoma	6%	Malignant melanoma	4%
Bladder		**Testis**	
Adenocarcinoma	54%	Adenocarcinoma	59%
Squamous-cell carcinoma	13%	Small round blue cell tumours (paediatric)	27%
Small-cell carcinoma	0.5%	Malignant melanoma	14%

secondary tumours in the bladder is approximately the same as that of non-transitional-cell primary tumours, the majority of which are adenocarcinomas or squamous-cell carcinomas, but which include such rare entities as malignant melanoma, small-cell carcinoma and primitive neuroectodermal tumour (PNET) [10]. Extensive lymphatic or vascular invasion is always suggestive of secondary tumour [38], but these features are seen only in a minority of surgical specimens from secondary neoplasms.

Adenocarcinomas are a numerically important group of secondary tumours at all genito-urinary sites (Table 3), especially the bladder, where it may closely resemble primary neoplasms (Fig. 3) [12]. Primary adenocarcinomas of the bladder are somewhat rarer than secondary ones [12, 33]: some are derived from urachal remnants and some from intestinal metaplasia elsewhere in the bladder; but, in either case, the mucosa is 'true' colonic type and expresses a unique colonic epithelial epitope [61]. Histological evidence of concomitant intestinal-type metaplasia or cystitis glandularis is suggestive of primary adenocarcinoma, and the proportion of primary vesical adenocarcinomas showing these features ranges from 14% to 66% [1], although both are relatively common incidental findings and not specific for primary origin unless adenocarcinoma-in-situ is also found [10]. Squamous-cell carcinoma shows less of a propensity to metastasise to the genito-urinary tract. Though rare, primary small-cell carcinoma is well described in the bladder and prostate [90] and is normally histologically indistinguishable from a metastasis, although the presence of polytopic metastases or disproportionate hormonal effects may suggest disseminated disease (Fig. 4) [51, 82]. The co-existence of transitional-cell carcinoma with small-cell carcinoma may reflect a common cell of origin [20], and the finding of mixed small-cell and transitional-cell carcinoma of the bladder, even in-situ, is strong evidence of a primary tumour [56].

Because of the rarity of primary melanoma in the bladder (only seven have been reported) and the possibility of misdiagnosis of a secondary deposit if the primary lesion has regressed, there are stringent criteria for its diagnosis before proceeding to radical surgery in the case of a primary lesion [84]. Unusual primary bladder

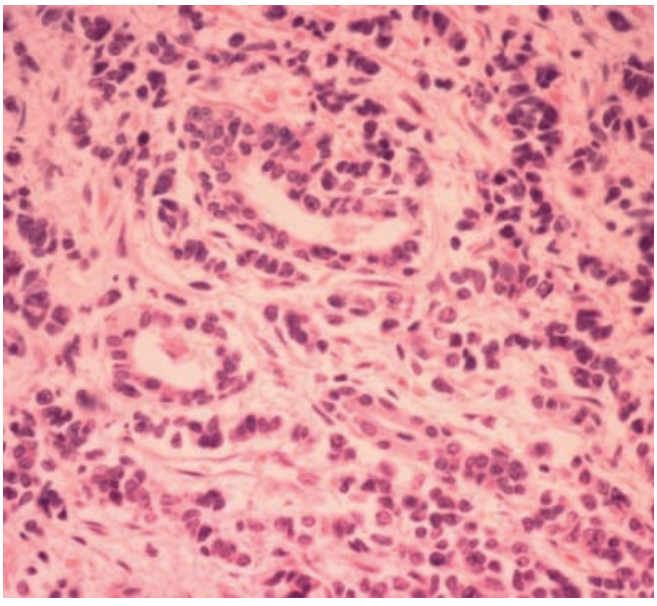

Fig. 4 Diffuse infiltration of prostatic stroma by small-cell (oat cell) carcinoma of pulmonary origin. Haematoxylin and eosin

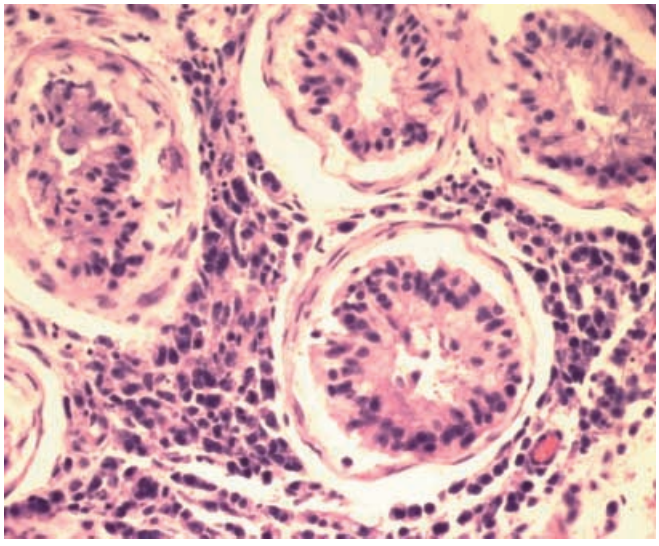

Fig. 6 A focus of small-cell (oat cell) carcinoma metastatic to the testis, showing a typical intertubular distribution. Haematoxylin and eosin

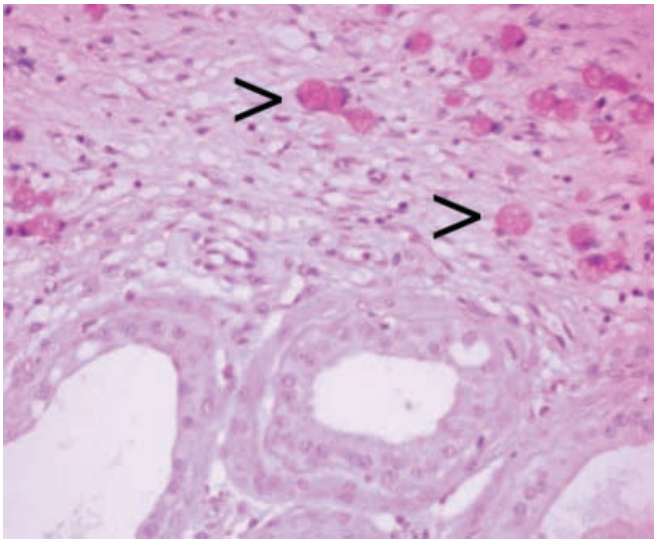

Fig. 5 Infiltration of the testis by cells of poorly differentiated gastric adenocarcinoma (*arrowheads*). Diastase Periodic acid–Schiff

neoplasms, such as osteochondrosarcoma [75, 89], mean that even lesions with bizarre histology cannot be assumed to be metastatic, and almost every type of metastatic tumour is mimicked by a more or less rare histological type of primary tumour [10]. In general, however, histomorphology remains the best way to assess the origin and prognosis of a bladder tumour [10]. There is little published work on cytological diagnosis of secondary genito-urinary tumours, but one study found that, in experienced hands, 90% of colonic adenocarcinomas involving the bladder were correctly diagnosed on urinary cytology [7]. Uncommon non-neoplastic conditions, e.g. prostatic melanosis, are theoretical sources of diagnostic difficulty [83], as are rare tumour-to-tumour metastases [35].

Secondary neoplasms of the testis are usually a late manifestation of disseminated disease (Fig. 5), although occasionally a tumour may present with a testicular metastasis [96], a diagnostic problem that can be exacerbated by a raised serum human chorionic gonadotrophin, mimicking a primary tumour [59]. Occasional misinterpretation of metastatic adenocarcinoma as embryonal carcinoma [38] or metastatic carcinoid as primary [16] has been reported, but generally secondary tumours in the adult testis do not resemble primary ones histologically (Fig. 6) [30]. In children, metastatic neuroblastoma, retinoblastoma [36], or even medulloblastoma (post surgery [30]) must be distinguished from equally rare primary "small round blue cell" tumours of the testis [27, 81] on the basis of the history and immunophenotype.

The value of immunohistochemistry

The distinction between primary and secondary adenocarcinoma of the bladder is one of the most common diagnostic problems in this area [88], and one with therapeutic significance, as primary carcinoma, especially if urachal in origin, is amenable to treatment by cystectomy [28]. Unfortunately, immunohistochemical methods are only marginally more useful than mucin histochemistry for distinguishing adenocarcinomas of the bladder and colon [37, 57, 92]. The immunohistochemical profiles of vesical and colonic adenocarcinomas are similar [88] except that a significant minority of vesical adeno-

carcinomas do not express carcinoembryonic antigen (CEA), while colonic adenocarcinomas almost invariably do [49]. Endometrial adenocarcinoma can be distinguished from a bladder primary in the majority of cases by its vimentin positivity [88].

Prostate-specific antigen (PSA) stains most primary prostatic adenocarcinomas, although a minority of these, often those that are atypical histologically, for example primary signet ring cell carcinoma, are PSA negative [76]. These tumours may be histologically indistinguishable from secondary carcinoma [71]. Poorly differentiated transitional-cell carcinoma can also be distinguished from prostate cancer by expression of cytokeratins 7 and 20 [9]. Prostatic small-cell carcinoma may also present differential diagnostic problems and has been reported in a patient as young as 23 years [51]: it is typically PSA and prostatic acid phosphatase (PAP) negative [40] but may be accompanied by areas of 'typical' prostatic adenocarcinoma, evidence of divergent differentiation.

Thyroid transcription factor-1 (TTF-1) immunostaining, normally positive in small-cell lung carcinoma, has been suggested as a means of differentiating small-cell lung carcinomas (the most common primary site of small-cell carcinoma metastatic to the prostate) from other small-cell carcinomas [58], although it is unhelpful in separating primary from secondary prostatic small-cell carcinomas as TTF-1 is expressed by at least some primary small-cell prostatic carcinomas [5]. The same appears to be true of primary small-cell carcinomas from other genito-urinary sites [23].

Routes of metastasis

In addition to the usual lymphatic and vascular routes of metastatic spread, there has been discussion of the possibility of tumour seeding within the genitourinary tract along the urinary passages, a concept which seems first to have been proposed by Ganem and Batal [31]. This remains a theoretical possibility, but the rarity of metastases from renal-cell carcinoma to bladder [11, 69, 95] or prostate [26] indicates that this mode of spread is probably not significant for this tumour. The comparative rarity of secondary tumours of the testis has often been commented upon [19]. This may be due in part to sampling bias, as this organ is not always examined at autopsy unless the history suggests testicular involvement, and clearly its remote anatomical location does not favour direct tumour spread. Kay et al. [45] postulated that metastases may reach the testis by retrograde extension through the vas deferens. This mode of spread was favoured by Hanash et al. [36] on the grounds that metastases of prostatic adenocarcinoma to the testis are relatively frequent and that in such cases palpation of the spermatic cord often suggests tumourous involvement. Of course all tumour metastatic to the testis must arrive via the spermatic cord, unless there is a congenital hydrocoele, but no tumour has yet been shown to metastasise along the vas and the apparent excess of prostatic secondaries which the theory seeks to explain may be accounted for by reporting bias: metastases are routinely sought in therapeutic orchidectomy specimens. Tumour emboli are, however, commonly seen within lymphatic and vascular channels in the vas [18], and we agree with Hunter and Hutcheson [41] that metastases reach the testes predominantly through the vascular system. Vascular spread also seems to be the route of metastases to the penis, although their rarity in so vascular an organ suggests that it is an unpermissive environment for tumour growth [30].

Conclusion

Secondary solid neoplasms comprise some 1.6–3.0% of all malignant neoplasms encountered in surgical specimens from the genito-urinary tract. Direct spread accounts for most of these: the majority of metastases occur in patients with widely disseminated malignancy. Many secondary neoplasms are histologically distinctive, but some, particularly secondary neoplasms of the bladder, are histologically indistinguishable from primary tumours in biopsy material. Immunohistochemistry, preferably in comparison with the primary lesion, plays only a minor role in certain cases. A proper clinical history and an appropriate index of suspicion may be the most important factors in suggesting the true diagnosis.

References

1. Abenoza P, Manivel C, Fraley EE (1987) Primary adenocarcinoma of urinary bladder. Clinicopathologic study of 16 cases. Urology 29:9–14
2. Abrahams HL, Spiro R, Goldstein N (1950) Metastases in carcinoma; analysis of 1000 autopsied cases. Cancer 3:74–85
3. Acino SM, Hampel N (1988) Renal cell carcinoma presenting with gross haematuria from a solitary bladder metastasis. Eur Urol 15:294–296
4. Adjiman S, Flam TA, Zerbib M, Debre B, Steg A (1989) Delayed nonurothelial metastatic lesions to the penis. A report of two cases. Eur Urol 16:391–392
5. Agoff SN, Lamps LW, Philip AT, Amin MB, Schmidt RA, True LD, Folpe AL (2000) Thyroid transcription factor-1 is expressed in extrapulmonary small cell carcinomas but not in other extrapulmonary neuroendocrine tumours. Mod Pathol 13:238–242
6. Babaian RJ, Johnson DE, Ayala AG, Sie ET (1979) Secondary tumors of ureter. Urology 14:341–343
7. Bardales RH, Pitman MB, Stanley MW, Korourian S, Suhrland MJ (1998) Urine cytology of primary and secondary urinary bladder adenocarcinoma. Cancer 84:335–343
8. Bartone FF (1964) Metastatic melanoma of the bladder. J Urol 91:151–155
9. Bassily NH, Vallorosi CJ, Akdas G, Montie JE, Rubin MA (2000) Coordinate expression of cytokeratins 7 and 20 in prostate adenocarcinoma and bladder urothelial carcinoma. Am J Clin Pathol 113:383–388
10. Bates AW, Baithun SI (1998) The differential diagnosis of secondary and unusual primary tumours of the bladder. Curr Diagnost Pathol 5:188–197
11. Bates AW, Baithun SI (1999) Renal cell carcinoma metastatic to bladder. Report of three cases. J Urol Pathol 10:71–76

12. Bates AW, Baithun SI (2000) Secondary neoplasms of the bladder are histological mimics of nontransitional cell primary tumours: clinicopathological and histological features of 282 cases. Histopathology 36:32–40
13. Bates AW, Baithun SI (2001) Secondary solid neoplasms of the prostate: a clinico-pathological series of 51 cases. Virchows Arch (in press) DOI 10.1007/s004280100505
14. Bates AW, Norton AJ, Baithun SI (2000) Malignant lymphoma of the urinary bladder: a clinicopathological study of 11 cases. J Clin Pathol 53:458–461
15. Benoit G, Boccon-Gibod L, Evrard P, Steg A (1983) Tumeurs secondaires du rein. Semin Hop 59:3127–3129
16. Berdjis CC, Mostofi FK (1977) Carcinoid tumours of the testis. J Urol 118:777–782
17. Berger Y, Nissenblatt M, Salwitz J, Lega B (1992) Bladder involvement in metastatic breast carcinoma. J Urol 147:137–139
18. Bhasin SD, Shrikhande SS (1990) Secondary carcinoma of testis – a clinicopathologic study of 10 cases. Int J Cancer 27:83–90
19. Blefari F, Risi O, Pino P (1992) Secondary tumors of the testis: two rare cases and review of the literature. Urol Int 48:469–470
20. Blomjous CEM, Vos W, de Voogt HJ, Gerald KB (1989) Small cell carcinoma of the urinary bladder: a clinicopathologic, morphometric, immunohistochemical, and ultrastructural study of 18 cases. Cancer 64:1347–1357
21. Bracken RB, Chica G, Johnson DE, Luna M (1979) Secondary renal neoplasms: an autopsy study. South Med J 72:806–807
22. Budinger JM (1958) Untreated bronchogenic carcinoma. A clinico-pathological study of 250 autopsied cases. Cancer 11:106–116
23. Cheuk W, Chan JKC (2001) Thyroid transcription factor-1 is of limited value in practical distinction between pulmonary and extrapulmonary small cell carcinomas. Am J Surg Pathol 25:545
24. Chin JL, Sales JL, Silver MM, Sweeney JP (1982) Melanoma metastatic to the bladder and bowel: an unusual case. J Urol 127:541–542
25. Chin Aleong J, Bates AW, Baithun SI (2000) Secondary neoplasms of the kidney: a clinico-pathological review of 443 cases. J Pathol 190[Suppl]:42A
26. Cihak RW, Haas R, Koenen CT, Chinchinian H (1980) Metastatic renal carcinoma to the prostate gland: presentation as prostatic hypertrophy. J Urol 123:791–792
27. Cummings OW, Ulbright TM, Young RH, Del Tos AP, Fletcher CDM, Hull MT (1997) Desmoplastic small round cell tumours of the paratesticular region. A report of six cases. Am J Surg Pathol 21:219–225
28. Dandekar NP, Dalal AV, Tongaonkar HB, Kamat MR (1997) Adenocarcinoma of the bladder. Eur J Surg Oncol 23:157–160
29. Dean AL, Ash JE (1950) Study of the bladder tumors in the registry of the American urological association. J Urol 63:618–621
30. Dutt N, Bates AW, Baithun SI (2000) Secondary neoplasms of the male genital tract with different patterns of involvement in adults and children. Histopathology 37:323–331
31. Ganem EJ, Batal JT (1956) Secondary malignant tumours of the urinary bladder metastatic from primary foci in distant organs. J Urol 75:965–972
32. Garcia-Gonzalez R, Pinto J, Val-Bernal JF (2000) Testicular metastases from solid tumors: an autopsy study. Ann Diagn Pathol 4:59–64
33. Gill HS, Dhillon HK, Woodhouse CR (1989) Adenocarcinoma of the urinary bladder. Br J Urol 64:138–142
34. Goldstein AG (1967) Metastatic carcinoma to the bladder. J Urol 98:209–215
35. Grignon DJ, Ro JY, Ayala AG (1989) Malignant melanoma with metastasis to adenocarcinoma of the prostate. Cancer 63:196–198
36. Hanash KA, Carney JA, Kelalis PP (1969) Metastatic tumors to testicles: routes of metastasis. J Urol 102:465–468
37. Hasegawa R, Fukushima S, Hirose M, Seki K, Takahashi M, Furukawa F, Toyoda K, Ito N (1987) Histochemical demonstration of colonic type mucin in glandular metaplasia and adenocarcinoma of the human urinary bladder. Acta Pathol Jpn 37:1097–1103
38. Haupt HM, Mann RB, Trump DL, Abeloff MD (1984) Metastatic carcinoma involving the testis. Clinical and pathologic distinction from primary testicular neoplasms. Cancer 10:592–595
39. Hayes WT, Young JM (1967) Metastatic carcinoma of the penis. J Chron Dis 20:891–895
40. Helpap B, Köllermann J (2001) Immunohistochemical analysis of the proliferative activity of neuroendocrine tumors from various organs. Are there indications for a neuroendocrine tumor – carcinoma sequence? Virchows Arch 438:86–91
41. Hunter DT, Hutcheson JB (1959) Krukenberg tumor of the testicle, report of a second case. J Urol 81:305–308
42. Isaacson PG, Norton AJ (1994) Extranodal lymphomas. Churchill Livingstone, Edinburgh
43. Ito T, Wada T, Furusato M, Aizawa S (1997) Prostatic involvement of bladder carcinoma. Nippon Hinyokika Gakkai Zasshi 88:677–683
44. Johnson DE, Chalbaud R, Ayala AG (1974) Secondary tumours of the prostate. J Urol 112:507–508
45. Kay S, Hennigar GR, Hooper JW (1954) Carcinoma of the testis metastatic from carcinoma of the prostate. A M A Arch Pathol 57:121–129
46. Klinger ME (1951) Secondary tumors of the genito-urinary tract. J Urol 65:144–153
47. Krestin GP, Hauser M, Eichenberger A, Kochli OR (1997) Blasen und Rektuminfiltration durch Uteruskarzinome: Treffsicherheit der CT und der MRT im Vergleich zu endoskopischen Verfahren. Rofo Fortschr Geb Rontgenstr Neuen Bildgebenden Verfahr 167:125–131
48. Leddy FF, Peterson NE, Ning TC (1992) Urogenital linitis plastica metastatic from the stomach. Urology 39:464–467
49. Lopez-Beltran A, Martin J, Garcia J, Toro M (1988) Squamous and glandular differentiation in urothelial bladder carcinomas. Histopathology, histochemistry and immunohistochemical expression of carcinoembryonic antigen. Histol Histopathol 3:63–68
50. Lucké B, Schlumberger H (1957) Tumors of the kidney, renal pelvis and ureter. Fascicle 30, atlas of tumor pathology. Armed Forces Institute of Pathology, Washington
51. Maddersbacher S, Schatzl G, Susani M, Maier U (1994) Prostatic metastasis of small cell lung cancer in a young male. Eur Urol 26:267–269
52. Maeda N, Yoshida T (1999) Metastatic tumour of renal pelvis and ureter from prostatic cancer: a case report. Hinyokika Kiyo 45:273–275
53. Matsushita Y, Katoh T, Isurugi K, Obara W, Suzuki T, Tamura T, Tanji S, Fujioka T (1998) Metastatic renal tumour originating from oesophageal carcinoma: a case report. Hinyokika Kiyo 44:591–594
54. Melicow MM (1955) Classification of tumours of testis: a clinical and pathological study based on 105 primary and 13 secondary cases in adults, and 3 primary and 4 secondary cases in children. J Urol 73:547–574
55. Melicow MM (1955) Tumours of the urinary bladder: a clinico-pathological analysis of over 2500 specimens and biopsies. J Urol 74:498–521
56. Mills SE, Wolfe JT, Weiss MA, Swanson PE, Wick MR, Fowler JE, Young RH (1987) Small cell undifferentiated carcinoma of the urinary bladder. A light-microscopic, immunocytochemical, and ultrastructural study of 12 cases. Am J Surg Pathol 11:606–617
57. Newbould M, McWilliam LJ (1990) A study of vesical adenocarcinoma, intestinal metaplasia and related lesions using mucin histochemistry. Histopathology 17:225–230
58. Ordónez NG (2000) Value of thyroid transcription factor-1 immunostaining in distinguishing small cell lung carcinomas from other small cell carcinomas. Am J Surg Pathol 24:1217–1223

59. Ota T, Shinohara M, Tanaka M, Date Y, Itakura H, Munakata A, Kinoshita K, Hishima T, Koike M, Kitamura M (2000) Spermatic cord metastases from gastric cancer with elevation of serum hCG-beta: a case report. Jpn J Clin Oncol 30:239–240
60. Pagano F, Bassi P, Ferrante GL, Piazza N, Abatangelo G, Pappagallo GL, Garbeglio A (1996) Is stage pT4a (D1) reliable in assessing transitional cell carcinoma involvement of the prostate in patients with a concurrent bladder cancer? A necessary distinction for contiguous or noncontiguous involvement. J Urol 155:244–247
61. Pantuck AJ, Bancila E, Das KM, Amenta PS, Cummings KB, Marks M, Weiss RE (1997) Adenocarcinoma of the urachus and bladder expresses a unique colonic epithelial epitope: an immunohistochemical study. J Urol 158:1722–1727
62. Parsi B, Beylot J, Turner K, Risch M, Lacoste D, Chomy P, Le Treut A, Grelet P (1989) Diagnostic des tumeurs secondaires bilaterales du rein. Apport de la cytologie. A propos de deux observations. Ann Med Interne (Paris) 140:368–371
63. Payne RA (1960) Metastatic renal tumours. Br J Surg 48:310–315
64. Perez-Mesa C, Oxenhandler R (1989) Metastatic tumours of the penis. J Surg Oncol 42:11–15
65. Pienkos EJ, Jablokow VR (1972) Secondary testicular tumours. Cancer 30:481–485
66. Powell BL, Craig JB, Muss HB (1985) Secondary malignancies of the penis and epididymis: a case report and review of the literature. J Clin Oncol 3:110–116
67. Presman D, Ehrlich L (1948) Metastatic tumours of the ureter. J Urol 59:312–325
68. Price EB, Mostofi FK (1957) Secondary carcinoma of the testis. Cancer 10:592–595
69. Remis RE, Halverstadt DB (1986) Metastatic renal cell carcinoma to the bladder: a case report and review of the literature. J Urol 16:1294–1296
70. Richmond J, Sherman RS, Diamond HD, Craver LF (1962) Renal lesions associated with malignant lymphomas. Am J Med 32:184–207
71. Ro JY, El-Nagger A, Ayala AG, Mody DR, Ordonez NG (1988) Signet-ring-cell carcinoma of the prostate: electron-microscopic and immunohistochemical studies of eight cases. Am J Surg Pathol 12:453–460
72. Roberts DI (1978) Secondary neoplasms of the genito-urinary tract. Br J Urol 50:68
73. Roy JB, Walton KN (1970) Secondary tumors of the kidney. J Urol 103:411–413
74. Saphir O, Parker ML (1941) Metastasis of primary carcinoma of the breast. With special reference to spleen, adrenal glands and ovaries. Arch Surg 42:1003–1018
75. Schutze U (1986) Osteosarcom der Harnblase mit einem Prostatakarzinom als Zweittumor. Zentralbl Allg Pathol 131:423–427
76. Segawa T, Kakehi Y (1993) Primary signet ring cell adenocarcinoma of the prostate: a case report and literature review. Hinyokika Kiyo 39:565–568
77. Seifert AL, Pearse HD, Keller FS (1979) Secondary tumors of the kidney: a new diagnostic procedure. J Urol 122:542–543
78. Sheehan EE, Greenberg SD, Scott R (1963) Metastatic neoplasms of the bladder. J Urol 90:281–284
79. Silver SA, Epstein JI (1993) Adenocarcinoma of the colon simulating primary urinary bladder neoplasia. A report of nine cases. Am J Surg Pathol 17:171–178
80. Silverstein LI, Plaine L, Davis JE, Kabakow B (1987) Breast carcinoma metastatic to bladder. Urology 29:544–547
81. Simpson TE, Lynn HB, Lynn SD (1969) Congenital neuroblastoma in the scrotum. Clin Pediatr 8:174–175
82. Smedley HM, Brown C, Turner A (1983) Ectopic ACTH-producing lung cancer presenting with prostatic metastasis. Postgrad Med J 59:371–372
83. Sofras F, Vlassopoulos G, Sakkas G, Daimonakou M (1993) Prostatic melanosis. Int Urol Nephrol 25:375–377
84. Stein BS, Kendall AR (1984) Malignant melanoma of the urinary tract. J Urol 132:859–868
85. Stephenson WT, Holmes FF, Noble MJ, Gerald KB (1990) Analysis of bladder carcinoma by subsite. Cystoscopic location may have prognostic value. Cancer 66:1630–1635
86. Sternby NH (1955) Studies in enlargement of leukaemic kidneys. Acta Haematol 14:354–362
87. Takehara K, Koga S, Nishikido M, Kanetake H, Hayashi T, Hara S, Ayabe H, Saito Y (1999) Breast cancer metastatic to the kidney. Anticancer Res 19:5571–5573
88. Torenbeek R, Lagendijk JH, Van Diest PJ, Bril H, Van de Molengraft FJJM, Meijer CJLM (1998) Value of a panel of antibodies to identify the primary origin of adenocarcinomas presenting as bladder carcinoma. Histopathology 32:20–27
89. Tzakas K, Ioannidis S, Dimitriadis G, Kotakidou R, Kalinderis A (1994) Primary osteochondrosarcoma of the urinary bladder. Br J Urol 73:320–321
90. Van Ahlen H, Nicolas V, Lenz W, Boldt I, Bockish A, Vahlensieck W (1992) Primary melanoma of urinary bladder. Urology 40:550–554
91. Wagle DG, Moore RH, Murphy GP (1975) Secondary carcinomas of the kidney. J Urol 114:30–32
92. Wells M, Anderson K (1985) Mucin histochemistry of cystitis glandularis and primary adenocarcinoma of the urinary bladder. Arch Pathol Lab Med 109:59–61
93. Willis RA (1952) The spread of tumours in the human body, 2nd edn. Butterworth and Co. London
94. Zein TA, Huben R, Lane W, Pontes JE, Englander LS (1955) Secondary tumours of the prostate. J Urol 133:615–616
95. Ziade J, Cipolla B, Robert I, Staerman F, Corbel L, Guillé F, Lobel B (1994) Métastase vésicale synchrone d'un adénocarcinome du rein à cellules claires. Acta Urol Belg 62:45–48
96. Zuk RJ, Trotter SE, Baithun SI (1989) 'Krukenberg' tumour of the testis. Histopathology 14:214–216

Virchows Arch (2002) 440:648–654
DOI 10.1007/s00428-001-0559-8

ORIGINAL ARTICLE

**Johannes Waiser · Stefan Schwaar · Torsten Böhler
Birgit Rudolph · Kerstin Dell · Klemens Budde
Manfred Dietel · Hans-Hellmut Neumayer**

Immunohistochemical double-staining of renal allograft tissue: critical assessment of three different protocols

Received: 15 March 2001 / Accepted: 18 September 2001 / Published online: 16 November 2001
© Springer-Verlag 2001

Abstract Quantitative analyses of renal allograft tissue using immunohistochemical double-staining could be a useful tool to extend the existing knowledge on renal allograft immunopathology. Due to technical reasons, this method has been only rarely applied in the past. The use of indirect immunohistochemistry for double-staining bears the risk of nonspecific cross reactions between the two staining sequences. To date, various procedures have been refined to avoid such cross reactions. Here we assessed the validity of three different protocols for indirect immunohistochemical double-staining on frozen sections of renal transplant biopsies (*n*=12). Both colocalized antigens and antigens with a non-overlapping distribution were stained according to each of the three protocols. Differentiation between the two staining sequences was achieved by employing different colored substrates of alkaline phosphatase (protocol 1), different enzymes (peroxidase and alkaline phosphatase) together with the use of 3,3′-diaminobenzidine-tetrahydrochloride substrate in the first staining sequence (protocol 2), or primary antibodies from different species (protocol 3). Sensitivity and specificity of each protocol were determined by quantitative comparison with control single-stainings of adjacent sections. Sensitivity of the first staining sequence was about 100% with each of the three protocols investigated. In the second staining sequence, sensitivities of protocols 1 (50%) and 2 (54–66%) were much lower than of protocol 3 (100%). Specificity of the second staining sequence was only 44% with protocol 1 compared with 98% with protocol 2 and 100% with protocol 3. In conclusion, protocols 1 and 2 are not recommended for quantitative double-staining analyses. In contrast, protocol 3 provided maximum sensitivity and specificity, even for antigens that are colocalized on the same cell type. Thus, the use of primary antibodies from different species is by far the most reliable technique for quantitative double-staining analyses in renal allograft tissue.

Keywords Double-staining · Immunohistochemistry · Renal transplantation

J. Waiser (✉) · S. Schwaar · T. Böhler · K. Dell · K. Budde
H.-H. Neumayer
Department of Internal Medicine-Nephrology,
University Hospital Charité, Campus Mitte, Humboldt-University,
Schumannstrasse 20/21, 10117 Berlin, Germany
e-mail: johannes.waiser@charite.de
Tel.: +49-30-450514044, Fax: +49-30-450514902

B. Rudolph · M. Dietel
Institute of Pathology, University Hospital Charité,
Campus Mitte, Humboldt-University, Schumannstrasse 20/21,
10117 Berlin, Germany

J. Waiser
Medizinische Klinik mit Schwerpunkt Nephrologie,
Universitätsklinikum Charité, Campus Charité Mitte,
Schumannstraße 20/21, 10117 Berlin, Germany

Introduction

Staining of renal allograft tissue with conventional immunohistochemistry is a well-established technique. The use of immunohistochemical double-staining would certainly help to extend the existing knowledge of renal allograft immunopathology. Especially concerning the expression of cellular antigens, this method offers a wide range of possible applications. To date, several double-staining protocols have been described. However, there are only a few studies in which renal allograft tissue was investigated using immunohistochemical double-staining [6, 7, 16, 18, 20].

Generally, the most simple way to achieve immunohistochemical double-staining would be to use two primary antibodies directly linked to two different detection systems (one-step method). This procedure offers considerable advantages in terms of simplicity and clarity, as it is fully independent of animal species or immunoglobulin isotype or subclass. These advantages are shared by double-staining protocols in which indirect immunohistochemistry is followed by direct immunohistochemistry in the second staining sequence. However, because the double-staining procedure itself reduces the amount of antigen present, more sensitive two- or three-step methods are recommended [26]. In pilot experiments (data

not shown), we confirmed that single-staining of renal allograft tissue with one-step protocols results in insufficient or negative staining, especially in case of low amounts of antigen. In comparison, a three-step protocol, which combined indirect immunohistochemistry with the avidin-biotin-complex (ABC) system [8, 9], provided the highest sensitivity and signal intensity.

Unfortunately, the use of indirect immunohistochemistry for double-staining sharply increases the risk of cross reactions between the two staining sequences and thus may result in nonspecific double-staining, especially when both primary antibodies have been raised in the same species. To date, various procedures have been refined in order to avoid nonspecific cross reactions. Here we assessed the validity of three indirect immunohistochemical double-staining protocols, differing at different levels of the staining sequence, on frozen sections from renal allograft biopsies. Cellular antigens with a non-overlapping distribution, as well as antigens that are colocalized on the same cell type, were investigated. Sensitivity and specificity of each of the three protocols were evaluated by comparison with single-stainings from adjacent sections.

Methods

Tissue preparation

Ultrasound-guided core needle biopsy in renal allograft recipients (n=12) was performed using Bard Biopty-Cut (C.R. Bard Inc., Covington, Ga.). Biopsy cylinders (17×1.7 mm) embedded in Tissue-Tek medium (Sakura Finetek, Torrance, Calif.) were snap frozen in liquid nitrogen and stored at –80 C. Cryostat sections (4 µm) were cut from biopsy specimens, placed on microslides (Superfrost Plus, Menzel GmbH, Braunschweig, Germany), air dried at room temperature (RT), and fixed in acetone (4 C, 15 min). Afterward, sections were either stained immediately or wrapped in aluminum foil and stored dry at –80 C until further processing.

Antibodies

All primary and secondary antibodies are listed in Table 1. For the validation of double-stainings, antibody pairs were selected according to their cellular distribution and their commercial availability. In order to assess specificity, pairs consisting of two antibodies directed toward antigens that are usually not colocalized on the same cell type were selected (CD4/CD8 and CD3/CD20). In order to assess sensitivity, we additionally used pairs of two antibodies directed toward antigens that may occur on the same cell type ($CD3^+/CD4^+$) or not ($CD3^-/CD4^+$).

The optimal concentration for each of antibody was evaluated using dilution experiments. A mouse monoclonal antibody directed toward *Aspergillus niger* glucose-oxidase, an enzyme that is neither present nor inducible in mammalian tissue, was used in the appropriate concentration as negative control (Dako Diagnostica GmbH, Hamburg, Germany). Primary antibodies were diluted in Dulbecco's phosphate-buffered saline (PBS, Biochrom, Berlin, Germany), 10% normal horse serum (Vector Laboratories, Burlingame, Calif.). Secondary antibodies were diluted in PBS, 2% normal horse serum.

General staining procedures

All incubation steps were performed in a humidity chamber at RT. Between each step, sections were washed twice in PBS (2×2.5 min). Following rehydration with PBS (5 min), endogenous biotin activity was blocked by incubation with avidin (15 min, Vector) and biotin (15 min, Vector). Nonspecific binding sites for secondary antibodies were saturated by incubation with normal horse serum (10% in PBS) for 15 min.

Because the alkaline phosphatase (AP) substrates Vector Blue Substrate Kit (Vector) and Vector Red Substrate Kit tend to produce a widespread precipitate over the entire section, both reagents were freshly prepared and micropore filtered (0.2 µm, Schleicher & Schuell, Dassel, Germany) immediately before application to the tissue. No nuclear counterstain was used in order to avoid difficulties in interpreting three-color tissue preparations. After staining, sections were air dried and mounted in aqueous medium (Dako). Controls included omission of primary antibodies, substitution of primary antibodies by unspecific antibodies directed toward *Aspergillus niger* glucose-oxidase, as well as stainings with a reversed color combination. Additionally, single-stainings of adjacent sections were performed in order to assess sensitivity and the specificity of double-staining.

Development of alkaline phosphatase with two different substrates (protocol 1)

For the first sequence, sections were incubated with primary antibodies (mouse IgG) for 60 min, biotinylated secondary antibodies (horse anti-mouse IgG) for 30 min, AP–ABC (Vector) for 30 min, and substrate solution (5–10 min under microscopic control) consisting of Vector Blue Substrate Kit and levamisole (Vector). For the

Table 1 List of antibodies. *ICAM-1* intercellular adhesion molecule-1, *M* monoclonal, *P* polyclonal

Antibody	Source	Type	Isotype	Concentration (µg/ml)	Main cellular expression	Manufacturer
Primary antibodies						
Anti-human CD3	Mouse	M	IgG	4	T-cells	Dako Diagnostica GmbH
Anti-human CD3	Goat	P	IgG	1	T-cells	Santa Cruz Biotechnology Inc.
Anti-human CD4	Mouse	M	IgG	4	T-helper cells, macrophages	Dako Diagnostica GmbH
Anti-human CD8	Mouse	M	IgG	1	T-cytotoxic cells	Dako Diagnostica GmbH
Anti-human CD18 (β_2 integrin)	Mouse	M	IgG	3	Leukocytes	Dako Diagnostica GmbH
Anti-human CD20	Mouse	M	IgG	8	B-cells	Dako Diagnostica GmbH
Anti-human CD54 (ICAM-1)	Mouse	M	IgG	4	Leukocytes, endothelial cells, glomerular cells	Dako Diagnostica GmbH
Secondary antibodies						
Anti-goat IgG, biotinylated	Horse	P	IgG	7.5		Vector Laboratories
Anti-mouse IgG, biotinylated	Horse	P	IgG	7.5		Vector Laboratories

second sequence, any unbound biotin activity resulting from the first sequence was blocked by incubation with excess of avidin (15 min) and biotin (15 min). Afterward, sections were incubated with primary antibodies (mouse IgG) for 60 min, biotinylated secondary antibodies (horse anti-mouse IgG) for 30 min, AP-ABC for 30 min, and substrate solution (5–10 min under microscopic control) consisting of Vector Red Substrate Kit and levamisole (Vector). Single-positive cells stained blue (Vector Blue Substrate Kit) or red (Vector Red Substrate Kit), while double-positive cells stained violet.

Use of two unrelated enzymes as antibody labels (protocol 2)

For the first sequence, sections were incubated with primary antibodies (mouse IgG) for 60 min and biotinylated secondary antibodies (horse anti-mouse IgG) for 30 min. Then, endogenous peroxidase (POD) was blocked by incubation with H_2O_2 (3% in PBS, Merck, Darmstadt, Germany) for 3 min. After incubation with ABC–POD (Vector) for 30 min, the brown color-developing substrate 3,3′-diaminobenzidine-tetrahydrochloride (DAB, Vector) was added (2–3 min under microscopic control). For the second sequence, any unbound biotin activity resulting from the first step was blocked by incubation with excess of avidin (15 min) and biotin (15 min). Subsequently, sections were incubated for 60 min with primary antibodies (mouse IgG) and biotinylated secondary antibodies (horse anti-mouse IgG) for 30 min. Following incubation with AP–ABC for 30 min, substrate solution consisting of Vector Blue Substrate Kit and levamisole was added (5–10 min under microscopic control). Single-positive cells stained brown (DAB) or blue (Vector Blue Substrate Kit), while double-positive cells stained gray.

Use of two primary antibodies raised in different species (protocol 3)

For the first sequence, sections were incubated with primary antibodies (monoclonal mouse IgG) for 60 min and biotinylated secondary antibodies (horse anti-mouse IgG) for 30 min. Afterward, sections were incubated with AP–ABC for 30 min, followed by substrate solution consisting of Vector Blue Substrate Kit and levamisole (5–10 min under microscopic control). For the second sequence, any unbound biotin activity resulting from the first step was blocked by incubation with excess of avidin (15 min) and biotin (15 min). Then, sections were incubated for 60 min with primary antibodies from a different species (polyclonal goat IgG), followed by incubation with biotinylated secondary antibodies (horse anti-goat IgG) for 30 min. Subsequently, endogenous POD was blocked by incubation with H_2O_2 (3% in PBS) for 3 min. After incubation with ABC–POD for 30 min, DAB-substrate was added (2–3 min under microscopic control). Single-positive cells stained blue (Vector Blue Substrate Kit) or brown (DAB), while double-positive cells stained gray.

Quantification and statistical analysis

Using an ocular grid with a total area of 0.0625 mm², we counted the number of positively stained cells of each section in ten randomly selected fields, at a total magnification of 400×. Results are expressed as mean±SEM.

Sensitivity and specificity of double-staining were assessed by comparison with single-stainings of adjacent sections. Sensitivity of the first staining sequence was assessed by dividing the total number of cells stained in the first staining sequence by the number of cells stained with the same primary antibody in single-staining experiments. Sensitivity of the second staining sequence was calculated by dividing the number of all true positive cells stained in the second staining sequence (colocalized antigens: single-positive + double-positive cells; non-colocalized antigens: single-positive cells) by the number of cells stained with the same primary antibody in single-staining experiments. Specificity of the second staining sequence was calculated by employing the following algorithm: [1 – (number of false double-positive cells in double-stainings of non-colocalized antigens divided by the number of positive cells in single-staining experiments, stained with same the primary antibody, which was used in the first sequence of double-staining)].

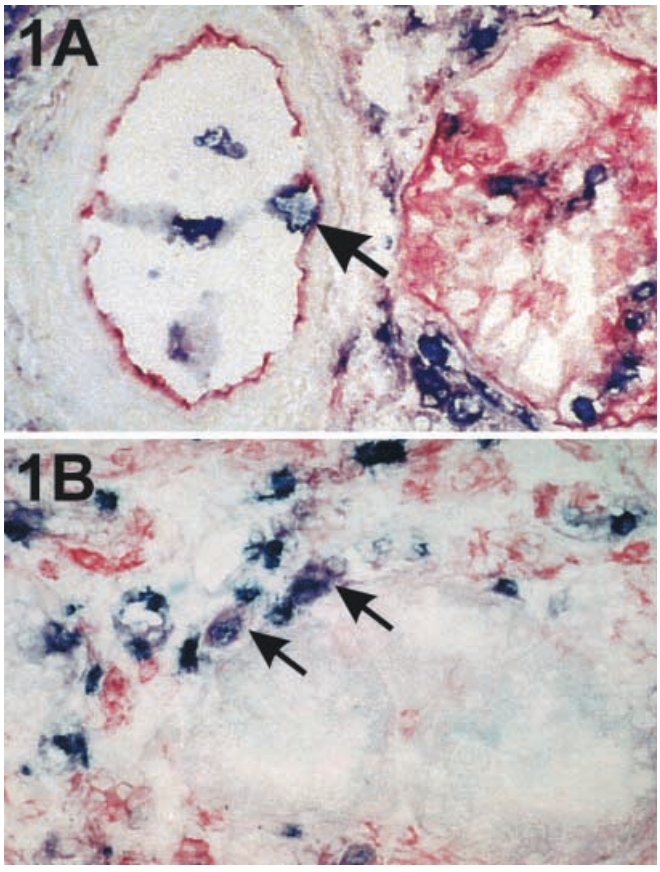

Fig. 1 a Double-staining (avidin-biotin-complex–alkaline phosphatase + avidin-biotin-complex–alkaline phosphatase) with monoclonal antibodies directed toward CD18 (β_2 integrin: blue, leukocytes) and CD54 (intercellular adhesion molecule-1=ICAM-1: red, endothelial cells and glomerular cells) (original magnification×400). *Arrow* indicates adherent leukocyte. **b** Double-staining (avidin-biotin-complex–alkaline phosphatase + avidin-biotin-complex–alkaline phosphatase) with monoclonal antibodies directed toward CD4 (red, T-helper cells and macrophages) and CD8 (blue, T-cytotoxic cells) (original magnification ×400). *Arrow* indicates false double-positive stained cells (violet)

Results

Development of alkaline phosphatase with two different substrates (protocol 1)

According to the manufacturer, proper development of the reaction product from AP prevents subsequent antibodies and ABC reagent from interacting with components used to stain the first antigen. This would enable multiple staining with primary antibodies raised in the same species. We found that this system (AP–ABC + AP–ABC) generally allowed double-staining of cellular antigens expressed on different cells (Fig. 1a). Quantita-

tive comparison with single-stainings from adjacent sections showed that the sensitivity of the first staining sequence was 100%. In contrast, the sensitivity of the second staining sequence was markedly reduced (Table 2). Double-staining with primary antibodies against two antigens that are usually not colocalized on the same cell type (CD4 and CD8) revealed that a large number of cells also stained false double-positive (Fig. 1b) resulting in a low specificity (Table 2). These findings were independent of the applied staining sequence. Omission of the second primary antibody, as well as substitution by a nonspecific antibody, confirmed our results (data not shown).

Use of two unrelated enzymes as antibody labels (protocol 2)

The use of DAB as substrate for POD in the first staining sequence was shown to enable labeling of the second antigen with immunohistochemical methods that generate a different-colored reaction product [19]. In agreement with protocol 1, the number of cells stained during the first sequence of double-staining was comparable to single-staining results (sensitivity 100%). In contrast to protocol 1, the number of false double-positive cells ($CD4^+CD8^+$) was very low, indicating a high specificity (Table 2). However, quantitative comparison with single-stainings from adjacent sections revealed that the sensitivity of the second staining sequence was markedly reduced (Table 2). This effect was detectable when non-colocalized antigens (CD4 and CD8 or CD3 and CD20) were investigated (Table 2 and Fig. 2), and even more pronounced when two antigens that can be colocalized on the same cell type were stained (CD3 and CD4) (Table 2). As before, the presented results were independent of the applied antibody sequence.

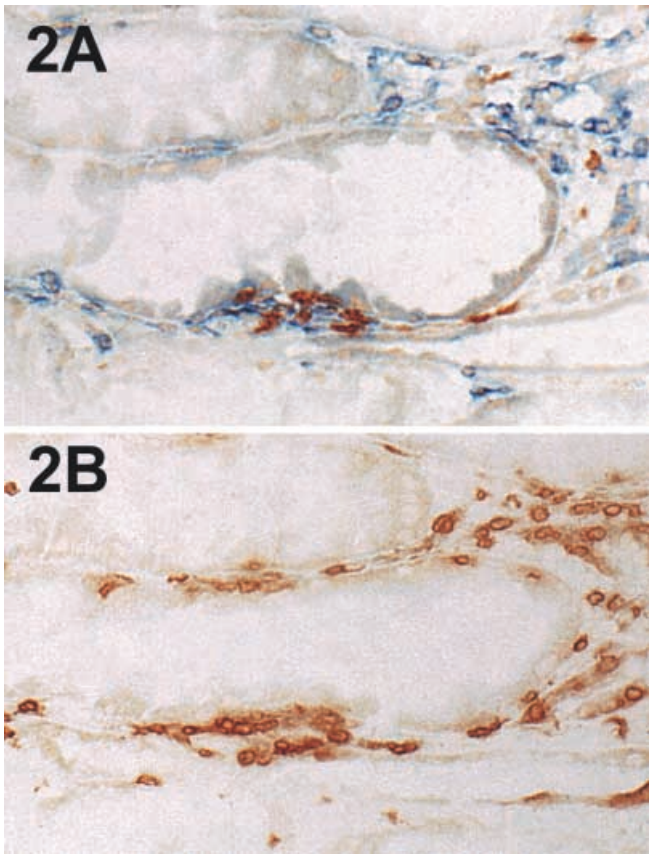

Fig. 2 a Double-staining (avidin-biotin-complex–peroxidase + avidin-biotin-complex–alkaline phosphatase) with monoclonal antibodies directed toward CD20 (brown, B-cells) and CD3 (blue, T-cells) (original magnification ×400). No false double-positive cells are detectable. **b** Single-staining (avidin-biotin-complex–peroxidase) of an adjacent section with a primary antibody directed toward CD3 (brown, all T-cells) (original magnification ×400). Compared with double-staining (**a**), a larger number of T-cells stained positive

Table 2 Sensitivity and specificity of the second staining sequence. On frozen sections from renal allograft biopsies (n=12) colocalized and non-colocalized antigens were stained according to three different double-staining protocols. The order of antigens reflects the sequence of primary antibody application in double-staining experiments. The ratio between double-staining and single-staining results (mean±SEM), as well as sensitivity and specificity of the 2nd staining sequence of double-staining are shown. Sensitivity was calculated by dividing the number of all true positive cells in double-stainings (CAg: $Ag1^+Ag2^+$+$Ag1^-Ag2^+$, NCAg: $Ag1^-Ag2^+$) by the number of positive cells ($Ag2^+$) in single-stainings. Specificity was assessed by employing the following algorithm: [1 – (number of false positive cells in double-stainings of non-colocalized antigens ($Ag1^+Ag2^+$) divided by the number of positive cells ($Ag1^+$) in single-stainings)]. *Ag* antigen, *Ag1* antigen stained in the first sequence of double-staining, *Ag2* antigen stained in the second sequence of double-staining, *CAg* colocalized antigen, *DS* double-staining, *n.a.* not applicable, *NCAg* non-colocalized antigen, *SS* single-staining

Protocol	CAg	NCAg	DS ($Ag1^+Ag2^+$):SS ($Ag2^+$)	DS ($Ag1^-Ag2^+$):SS ($Ag2^+$)	Sensitivity	DS ($Ag1^+Ag2^+$):SS ($Ag1^+$)	Specificity
1		+		$CD4^-CD8^+$:$CD8^+$ (0.50±0.06)	50%	$CD4^+CD8^+$:$CD4^+$ (0.56±0.08)	44%
2		+		$CD4^-CD8^+$:$CD8^+$ (0.66±0.06)	66%	$CD4^+CD8^+$:$CD4^+$ (0.02±0.006)	98%
2	+	+	$CD3^+CD4^+$:$CD4^+$ (0.20±0.02)	$CD3^-CD4^+$:$CD4^+$ (0.34±0.06)	54%	$CD3^+CD4^+$:$CD3^+$ (0.37±0.06)	n.a.
3		+		$CD20^-CD3^+$:$CD3^+$ (1.05±0.08)	100%	$CD20^+CD3^+$:$CD20^+$ (0.0±0.004)	100%
3	+	+	$CD4^+CD3^+$:$CD3^+$ (0.55±0.05)	$CD4^-CD3^+$:$CD3^+$ (0.51±0.05)	100%	$CD4^+CD3^+$:$CD3^+$ (0.42±0.03)	n.a.

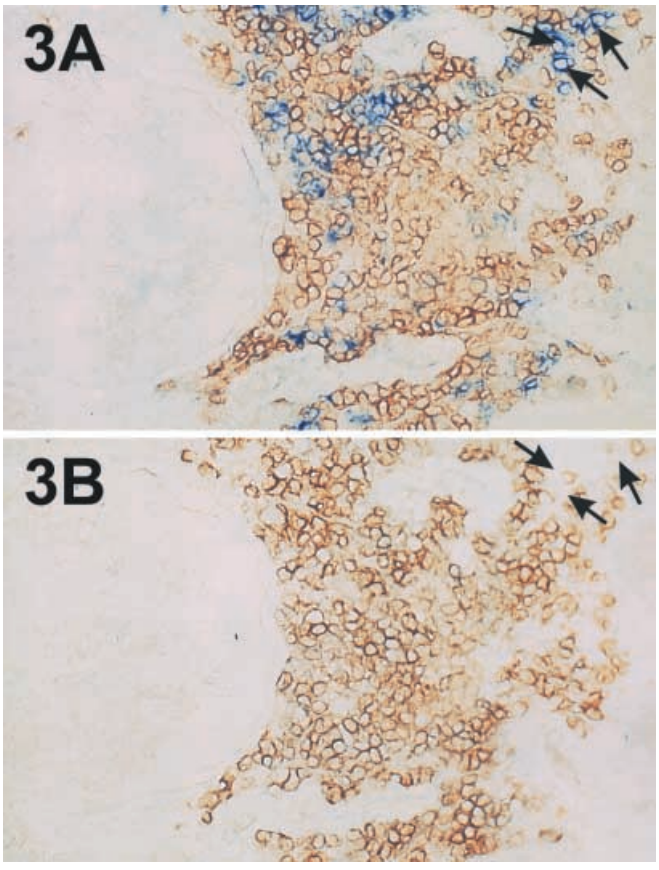

Fig. 3 a Double-staining (avidin-biotin-complex–alkaline phosphatase + avidin-biotin-complex–peroxidase) with two primary antibodies from different species directed toward CD20 (blue, all B-cells) and CD3 (brown, all T-cells) (original magnification ×400). No false double-positive cells were detectable. *Arrows* indicate corresponding cells (B-cells) staining positive (blue) in double-staining and negative in single-staining (**b**). **b** Single-staining (avidin-biotin-complex–peroxidase) of an adjacent section with a primary antibody directed toward CD3 (brown, all T-cells) (original magnification ×400). Compared with double-staining (**a**), the number of T-cells stained positive was equal

Use of two primary antibodies raised in different species (protocol 3)

This method sharply reduces the risk of interactions between the two sets of antibodies. In accordance with both other protocols described, comparison with single-stainings of adjacent sections confirmed that the first staining sequence is highly sensitive (100%). In contrast to protocols 1 and 2, the sensitivity of the second staining sequence also turned out to be high, no matter whether non-colocalized (CD20 and CD3) (Table 2 and Fig. 3) or potentially colocalized antigens (CD4 and CD3, Table 2) were investigated. In addition, double-staining of two antigens that are not colocalized on the same cell type (CD20 and CD3) revealed no false double-positive cells (Fig. 3), indicating a high specificity (Table 2).

Discussion

We assessed the validity of three indirect immunoenzyme double-staining protocols, differing at different levels of the staining sequences, by staining two cellular antigens with a non-overlapping distribution (CD4/CD8 and CD20/CD3), as well as two antigens that can be colocalized on the same cell type (CD3/CD4), on frozen sections from renal allograft biopsies (n=12). Sensitivity and specificity of each of the three protocols were evaluated by comparison with single-stainings from adjacent sections.

Protocol 1

Differentiation between the two staining sequences at substrate level was achieved using two different substrates of AP, resulting in blue (Vector Blue Substrate Kit) or red (Vector Red Substrate Kit) single-positive cells and in violet double-positive cells [28]. According to the manufacturer, cross reactions between the two staining sequences are prevented by substrate development. We found that staining of two different cellular antigens according to this protocol resulted in nonspecific double-staining of a considerable percentage of cells. Thus, the reaction product of the first substrate did not sufficiently prevent nonspecific binding. In addition, sensitivity of the second staining sequence turned out to be low. The lack of specificity and sensitivity renders this method useless for quantitative double-staining analyses of renal allograft tissue.

Protocol 2

Differentiation at enzyme level was achieved using POD together with DAB-substrate in the first and AP in the second staining sequence. In 1979, Sternberger and Joseph observed that double-staining is possible when POD and DAB-substrate are applied in the first staining sequence [19]. The DAB reaction product acts as a barrier that masks the antigenic sites of the first staining sequence and thus allows staining of two different antigens with antibodies of the same species. To date, this system has been applied in various fields [3, 7, 17, 29]. Investigating antigens with a non-overlapping distribution, we found almost no double-positive cells, indicating a high specificity. Concerning antigens that are colocalized on the same cell type, single- and double-positive cells were well distinguishable. The use of Vector Blue Substrate Kit as AP-substrate provided the best results for colocalized antigens, resulting in blue (Vector Blue Substrate Kit) or brown (DAB) single-positive and gray double-positive cells. However, comparison with single-stainings of adjacent sections showed that DAB not only masked the complexes of the first staining sequence, but also unrelated antigens. This effect was even more pronounced when both antigens were located on the same

cell type. In agreement with others [5, 23, 24], we conclude that the masking effect of DAB reduces sensitivity, especially when two antigens that may be localized on the same cell type are investigated. Therefore, this protocol is also not recommended for quantitative double-staining analyses of renal allograft tissue.

Protocol 3

Differentiation at antibody level was achieved using primary antibodies from different species. This technique has been employed in several studies in combination with immunohistochemistry [6, 18] or immunofluorescence [4, 14]. Our results clearly underline that this is the most reliable protocol for quantification of two different cellular antigens on frozen sections of renal allograft tissue. Comparison of this protocol with both other protocols revealed that only this technique ensures a maximum grade of sensitivity and specificity for both antigens that are colocalized on the same cell type and antigens with a non-overlapping distribution. Unfortunately, widespread application of this protocol is limited by the fact that most available anti-human antibodies have been raised in mouse.

Apart from the three protocols assessed here, several other indirect immunoenzyme double-staining procedures have been described. Tidman and Bastin reported that reproducible double-staining without cross reactions is possible using primary monoclonal antibodies from the same species that differ in their immunoglobulin subclass [2, 22]. However, controversial reports indicate that this method is not useful for immunohistochemical double-labeling, because subclass-specific sites on the primary antibody are fewer in number than non-subclass-restricted antibodies, thus resulting in low sensitivity and weak staining intensity [1, 5]. Van der Loos et al. introduced several multistep double-labeling protocols that include the sequential use of indirect immunohistochemistry during the first staining sequence followed by a second primary antibody attached to biotin [25] or other staining systems [27]. However, this protocol is limited by the number of commercially available biotin or otherwise labeled antibodies. In 1991, Krenács et al. introduced an interesting technique called “one-step double immunolabeling” [10]. By employing two preformed complexes of primary antibodies together with their specific secondary antibodies labeled with different enzymes, they were able to avoid nonspecific binding of secondary antibodies. In addition, this method provided the possibility of a relatively rapid antigen detection. Nakane et al. prevented cross reactivity by washing with a low-pH buffer between the first and the second incubation sequences [12]. The so-called “acid-elution technique” caused disruption of the first primary antibody complex, leaving the insoluble histochemical product in place. In contrast, Allen et al. found that acid elution did not allow acceptable double-staining [1]. They observed that inadequate acid elution only partially removed the initial antibody complexes, thus revealing many antigenic sites of the first primary antibody and increasing the level of cross reactions. In addition, very low pH buffers were required to achieve complete dissociation of high-affinity antibodies. These buffers obviously caused tissue damage, resulting in poor localization of the second primary antibody. Heating in sodium citrate in a microwave oven after the first incubation sequence was also used to denature bound antibody and to augment antigen retrieval [11, 13, 15, 21]. However, this procedure also seems to bear the risk of altering antigen integrity.

In conclusion, the success of indirect immunoenzyme double-staining for quantitative analyses of cellular antigens in renal allograft tissue strongly depends on the sensitivity and specificity of the second staining sequence. Our results make clear that the use of two primary antibodies from different species offers significant advantages with respect to both parameters and therefore is highly recommended. Unfortunately, this approach is restricted by the limited availability of primary antibodies raised in species different from mouse. In future, an expanding availability of primary antibodies from other species than mouse will substantially facilitate the use of this technique.

Acknowledgement This work was supported by a grant from the Else Kröner-Fresenius Foundation.

References

1. Allen MH, Markey AC, MacDonald DM (1991) The development of a reproducible immunocytochemical technique for demonstrating colocalized cutaneous antigens. Am J Dermatopathol 13:221–227
2. Bastin JM, Granger S, Tidman N, Janossy G, McMichael AJ (1981) Recognition of a human T-lymphocyte differentiation antigen by an IgM monoclonal antibody. Clin Exp Immunol 46:597–606
3. Cai W, Devaux B, Schaper W, Schaper J (1997) The role of Fas/APO 1 and apoptosis in the development of human atherosclerotic lesions. Atherosclerosis 131:177–186
4. De Vries TJ, Verheijen JH, de Bart AC, Weidle UH, Ruiter DJ, van Muijen GN (1996) Decreased expression of both the low-density lipoprotein receptor-related protein/alpha(2)-macroglobulin receptor and its receptor-associated protein in late stages of cutaneous melanocytic tumor progression. Cancer Res 56:1432–1439
5. Falini B, Abdulaziz Z, Gerdes J, Canino S, Ciani C, Cordell JL, Knight PM, Stein H, Grignani F, Martelli MF, Mason DY (1986) Description of a sequential staining procedure for double immunoenzymatic staining of pairs of antigens using monoclonal antibodies. J Immunol Methods 93:265–273
6. Goebeler M, Roth J, Burwinkel F, Vollmer E, Bocker W, Sorg C (1994) Expression and complex formation of S100-like proteins MRP8 and MRP14 by macrophages during renal allograft rejection. Transplantation 58:355–361
7. Grau V, Herbst B, Steiniger B (1998) Dynamics of monocytes/macrophages and T lymphocytes in acutely rejecting rat renal allografts. Cell Tissue Res 291:117–126
8. Hsu SM, Raine L (1981) Protein A, avidin, and biotin in immunohistochemistry. J Histochem Cytochem 29:1349–1353
9. Hsu SM, Raine L, Fanger H (1981) Use of avidin-biotin-peroxidase complex (ABC) in immunoperoxidase techniques: a comparison between ABC and unlabeled antibody (PAP) procedures. J Histochem Cytochem 29:577–580

10. Krenacs T, Uda H, Tanaka S (1991) One-step double immunolabeling of mouse interdigitating reticular cells: simultaneous application of pre-formed complexes of monoclonal rat antibody M1–8 with horseradish peroxidase-linked anti-rat immunoglobulins and of monoclonal mouse anti-Ia antibody with alkaline phosphatase-coupled anti-mouse immunoglobulins. J Histochem Cytochem 39:1719–1723
11. Lan HY, Mu W, Nikolic-Paterson DJ, Atkins RC (1995) A novel, simple, reliable, and sensitive method for multiple immunoenzyme staining: use of microwave oven heating to block antibody crossreactivity and retrieve antigens. J Histochem Cytochem 43:97–102
12. Nakane PK (1968) Simultaneous localization of multiple tissue antigens using the peroxidase-labeled antibody method: a study on pituitary glands of the rat. J Histochem Cytochem 16:557–560
13. Nikolic-Paterson DJ, Jun Z, Tesch GH, Lan HY, Foti R, Atkins RC (1996) De novo CD44 expression by proliferating mesangial cells in rat anti-Thy-1 nephritis. J Am Soc Nephrol 7:1006–1014
14. Oxholm A, Diamant M, Oxholm P, Bendtzen K (1991) Interleukin-6 and tumour necrosis factor alpha are expressed by keratinocytes but not by Langerhans cells. APMIS 99:58–64
15. Pardo J, Diaz L, Errasti P, Idoate M, de Alava E, Sola I, Lozano L, Panizo A (2000) Mast cells in chronic rejection of human renal allografts. Virchows Arch 437:167–172
16. Penfield JG, Wang Y, Li S, Kielar MA, Sicher SC, Jeyarajah DR, Lu CY (1999) Transplant surgery injury recruits recipient MHC class II-positive leukocytes into the kidney. Kidney Int 56:1759–1769
17. Printseva OJ, Peclo MM, Tjurmin AV, Faerman AI, Danilov SM, Repin VS, Smirnov VN (1989) A 90-kd surface antigen from a subpopulation of smooth muscle cells from human atherosclerotic lesions. Am J Pathol 134:305–313
18. Robertson H, Wheeler J, Thompson V, Johnson JS, Kirby JA, Morley AR (1995) In situ lymphoproliferation in renal transplant biopsies. Histochem Cell Biol 104:331–334
19. Sternberger LA, Joseph SA (1979) The unlabeled antibody method. Contrasting color staining of paired pituitary hormones without antibody removal. J Histochem Cytochem 27: 1424–1429
20. Takeda I, Horimi T, Okabayashi T, Kaneda M, Shimoyama H, Chohno S, Tanaka I, Miyake N, Orita K (1988) Double-staining analysis of mononuclear cells infiltrating rejected kidney. Transplant Proc 20:211–213
21. Tesch GH, Yang N, Yu H, Lan HY, Foti R, Chadban SJ, Atkins RC, Nikolic-Paterson DJ (1997) Intrinsic renal cells are the major source of interleukin-1 beta synthesis in normal and diseased rat kidney. Nephrol Dial Transplant 12:1109–1115
22. Tidman N, Janossy G, Bodger M, Granger S, Kung PC, Goldstein G (1981) Delineation of human thymocyte differentiation pathways utilizing double-staining techniques with monoclonal antibodies. Clin Exp Immunol 45:457–467
23. Valnes K, Brandtzaeg P (1982) Comparison of paired immunofluorescence and paired immunoenzyme staining methods based on primary antisera from the same species. J Histochem Cytochem 30:518–524
24. Valnes K, Brandtzaeg P (1984) Paired indirect immunoenzyme staining with primary antibodies from the same species. Application of horseradish peroxidase and alkaline phosphatase as sequential labels. Histochem J 16:477–487
25. Van der Loos CM, van den Oord JJ, Das PK, Houthoff HJ (1988) Use of commercially available monoclonal antibodies for immunoenzyme double staining. Histochem J 20:409–413
26. Van der Loos CM, Becker AE, van den Oord JJ (1993) Practical suggestions for successful immunoenzyme double-staining experiments. Histochem J 25:1–13
27. Van der Loos CM, Naruko T, Becker AE (1996) The use of enhanced polymer one-step staining reagents for immunoenzyme double-labeling. Histochem J 28:709–714
28. Wagner L, Worman CP (1988) Color-contrast staining of two different lymphocyte subpopulations: a two-color modification of alkaline phosphatase monoclonal anti-alkaline phosphatase complex technique. Stain Technol 63:129–136
29. Yamazaki K, Nakajima T, Hara K (1995) Immunohistological analysis of T cell functional subsets in chronic inflammatory periodontal disease. Clin Exp Immunol 99:384–391

Virchows Arch (2002) 440:655–659
DOI 10.1007/s00428-002-0615-z

CASE REPORT

**Ryoji Kushima · Manfred Stolte · Klaus Dirks
Michael Vieth · Hidetoshi Okabe · Franz Borchard
Takanori Hattori**

Gastric-type adenocarcinoma of the duodenal second portion histogenetically associated with hyperplasia and gastric-foveolar metaplasia of Brunner's glands

Received: 19 September 2001 / Accepted: 9 January 2002 / Published online: 21 February 2002
© Springer-Verlag 2002

Abstract We report a case of a pedunculated polyp with a focus of gastric-type adenocarcinoma arising in the opposite side of the papilla Vater of the duodenal second portion. The carcinoma was surrounded by lobules of hyperplastic Brunner's glands. Immunohistochemically the carcinoma tissue showed both gastric foveolar-type mucin (*MUC5AC*) and pyloric/Brunner's gland-type mucin (*MUC6*), in which proliferating cells positive for MIB-1 (Ki-67) were scattered diffusely. Most of the hyperplastic Brunner's glands were positive for *MUC6*, while cells toward the lumen in the superficial layer were positive for *MUC5AC* and MIB-1. This directional pattern of differentiation of Brunner's glands has recently been demonstrated by our group in the histogenetic course of gastric metaplasia originating directly from Brunner's glands. Therefore the present carcinoma is thought to have developed under induction of gastric-foveolar differentiation in a manner very similar to that of gastric metaplasia in hyperplastic Brunner's glands.

Keywords Brunner's glands · Duodenum · *MUC* gene · Hyperplasia · Gastric metaplasia

R. Kushima (✉) · H. Okabe
Department of Clinical Laboratory Medicine,
Shiga University of Medical Science,
Seta, Otsu, Shiga 520-2192 Japan
e-mail: kushima@belle.shiga-med.ac.jp
Tel.: +81-77-5482603, Fax: +81-77-5482407

M. Stolte · M. Vieth
Institute of Pathology, Klinikum Bayreuth, Bayreuth, Germany

K. Dirks
Department of Internal Medicine, Klinikum Bayreuth, Bayreuth, Germany

F. Borchard
Institute of Pathology, Klinikum Aschaffenburg, Aschaffenburg, Germany

T. Hattori
Department of Pathology, Shiga University of Medical Science, Otsu, Shiga, Japan

Introduction

Duodenal adenocarcinoma in the extra-ampullary region is rare, and usually consists of intestinal-type adenocarcinoma with tubular or villous adenomas akin to that of the colon. Adenocarcinomas very rarely arise in Brunner's glands [4, 5, 8, 9, 16, 22, 23, 29], gastric metaplasia, or heterotopic gastric mucosa [3, 13, 19, 21]. Most Brunner's gland tumors, so-called Brunner's gland adenomas or brunneriomas, are not true neoplasms but rather hyperplasia or hamartomas, which are composed of lobules of mature Brunner's glands surrounded by bands of smooth muscle [18, 24, 29]. There have been only five well documented cases of carcinoma with neoplastic transformation of the underlying Brunner's glands [5, 8, 9, 16, 29]. However, little is known about gastric-type differentiation in Brunner's gland tumors. We have recently shown a histogenetic pathway of gastric metaplasia in close association with a reparative lineage of Brunner's glands [12]. With special reference to MUC gene expression, this report documents an extremely rare case of adenocarcinoma that has findings relevant to the discussion of the differentiation, proliferation, and dysplastic progression of Brunner's glands.

Case report

Clinical history, endoscopic, and biopsy findings

An 85-year-old woman was referred to our hospital for evaluation of Mirizzi syndrome with choledocholithiasis. Upper gastrointestinal endoscopy revealed a pedunculated and lobulated polyp on the opposite side of the papilla of Vater of the duodenal second portion (Fig. 1a). Invasive carcinoma was suspected by histological investigation of the biopsy specimens (Fig. 1b), and polypectomy was performed in March 1999. There were no signs of recurrence in August 2001.

Materials and methods

The tumor specimen (2.0×1.5×1.0 cm) was fixed in 10% formalin, sliced into three sections, and embedded in paraffin. Paraffin blocks were cut into serial sections for routine histology and im-

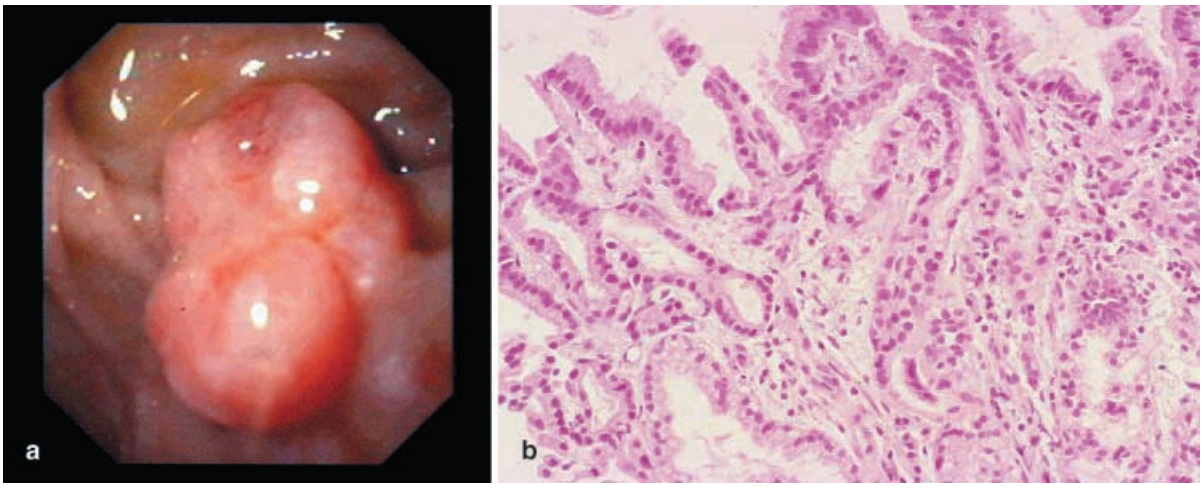

Fig. 1 a Endoscopic picture shows a pedunculated polyp with lobulation at the opposite side of the papilla of Vater of the second portion of the duodenum. **b** Biopsy section shows budding of glands and a trabecular pattern suggestive of invasion into the lamina propria, which is classified into "category 4.3: suspicion of invasive carcinoma" according to the Vienna classification of gastrointestinal neoplasia [20]

munohistochemical studies. In addition to hematoxylin and eosin staining, immunohistochemical staining was performed using the following monoclonal antibodies (MAbs): *MUC2* (Ccp58; 1:100, Novocastra, UK); *MUC5AC* (CLH2; 1:100, Novocastra), *MUC6* (CLH5; 1:100, Novocastra), CD10 (56C6; 1:50, Novocastra) and Ki-67 (MIB1; 1:100, Immunotech, France). More than ten distinct epithelial mucin genes (*MUC1*, *MUC2*, *MUC3*, *MUC4*, *MUC5AC*, *MUC5B*, *MUC6*, *MUC7*, *MUC8*, *MUC11*, *MUC12*, *MUC13*, and *MUC16*) have recently been identified [14, 26, 27, 28]. Among these, *MUC5AC*, *MUC6*, and *MUC2* are specifically expressed in gastric-foveolar cells, pyloric gland cells, and intestinal goblet cells of the mature gastrointestinal tract, respectively [17]. *MUC6* is also expressed in mucus neck cells of the stomach and Brunner's gland cells [10]. MAb CD10 was used to detect the brush border of small intestinal absorptive cells [15] and MAb MIB-1 to detect proliferating cells. For immunohistochemistry the streptavidin-biotin method was performed using the Histofine-kit (Nichirei, Japan). Peroxidase binding sites were visualized using the diaminobenzidine method, and the sections were lightly counterstained with hematoxylin.

Histological findings

As the polypoid tumor consisted mostly of lobules of Brunner's glands showing no cellular atypia, a diagnosis of Brunner's gland hyperplasia was made. Cystically dilated glands were also noted. A severely dysplastic focus, 6 mm at the longest diameter, was discovered to be surrounded completely by the hyperplastic area (Fig. 2a). The dysplastic lesion consisted of atypical cuboidal to low columnar cells with clear cytoplasm resembling cells of Brunner's glands. Not only prominent cellular and structural atypia but also focal invasion into the muscularis mucosae was noticed in this lesion (Fig. 2b), which was interpreted as an adenocarcinoma.

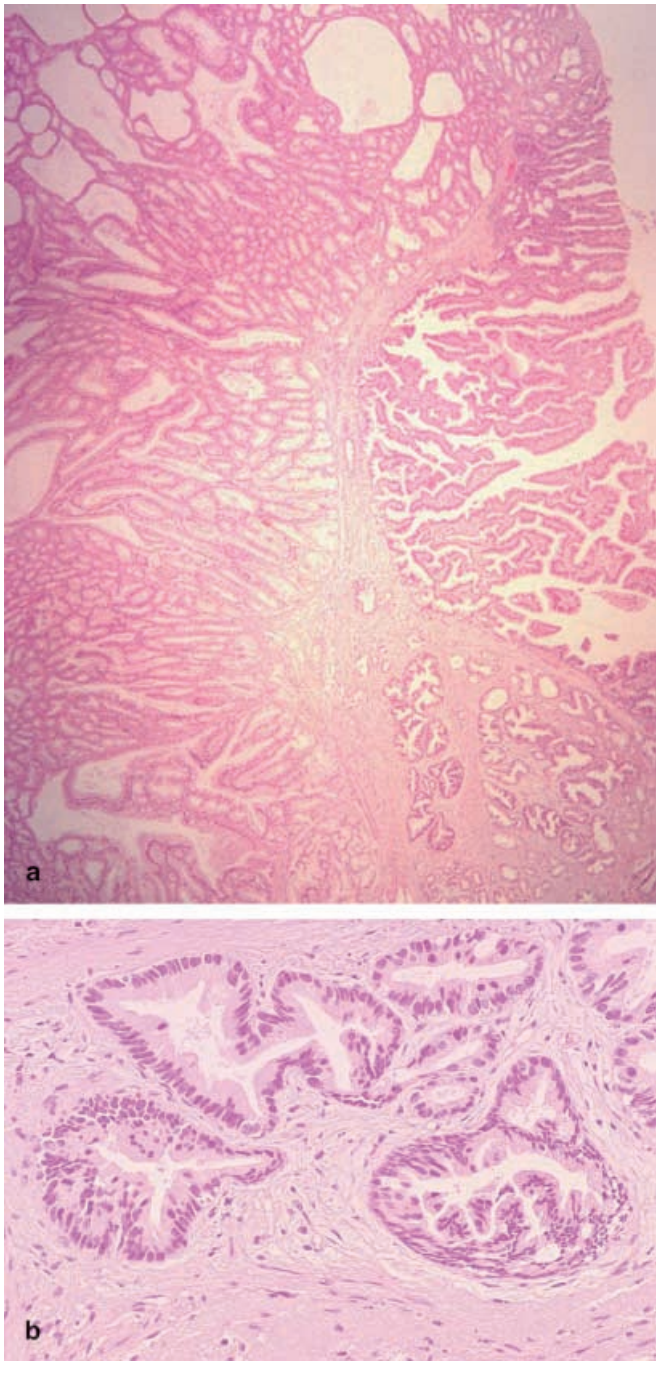

Fig. 2 a The tumor consists primarily of hyperplastic lobules of Brunner's glands showing no cellular atypia. A severely dysplastic focus is seen to be adjacent to hyperplastic Brunner's glands. **b** Detail of **a**, showing invasion into the muscularis mucosae with stromal reaction. Therefore this lesion is interpreted as adenocarcinoma

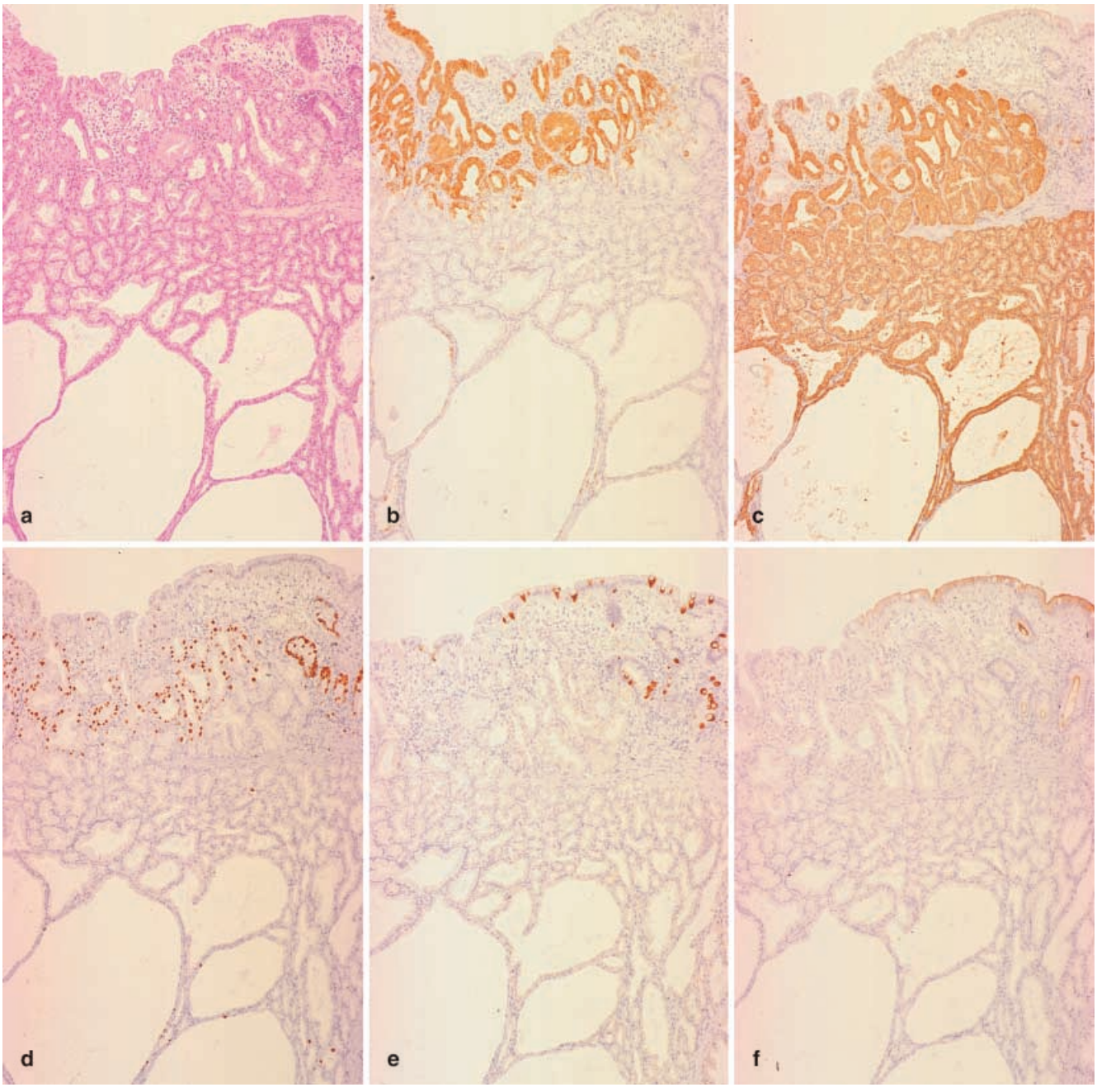

Fig. 3 Histological (**a**) and immunohistochemical (**b**–**f**) findings of the hyperplastic area. Toward the duodenal lumen, gastric-foveolar type cells expressing *MUC5AC* (**b**) extend continuously from hyperplastic lobules of Brunner's glands positive for *MUC6* (**c**). Proliferating cells positive for MIB-1 are densely located at the luminal surface forming generative cell zones (neo-G zones; **d**), above which *MUC5AC*-positve cells are evident towards the lumen. In neo-G zones cells positive for both *MUC5AC* and *MUC6* are evident. Normal G zones of duodenal crypts are seen in the upper right area. Positivity for *MUC2* (**e**) and CD10 (**f**) is detected only in the normal duodenal mucosa

Immunohistochemical findings of the hyperplastic area

At the luminal surface of the hyperplastic area, columnar cells with clear cytoplasm resembling gastric-foveolar cells positive for *MUC5AC* extended continuously from hyperplastic lobules of Brunner's glands positive for *MUC6*, whereas goblet and absorptive cells of the normal duodenal mucosa were evident in foci (Fig. 3). Although proliferating cells positive for MIB-1 were sporadically scattered within the lobules, they were densely located at the luminal surface forming generative cell zones (G zones), above which *MUC5AC*-positve cells were seen towards the lumen. In the G zones cells positive for both *MUC5AC* and *MUC6* were also observed. *MUC2* and CD10 were expressed in goblet cells and absorptive cells, respectively, in the normal duodenal mucosa.

Immunohistochemical findings of the adenocarcinoma

MUC5AC and *MUC6* were coexpressed in most of cells in the carcinomatous areas where proliferating cell positive for MIB-1 were distributed diffusely (Fig. 4). A few MUC-2 positive cells were scattered, but CD10 positivity was not detected.

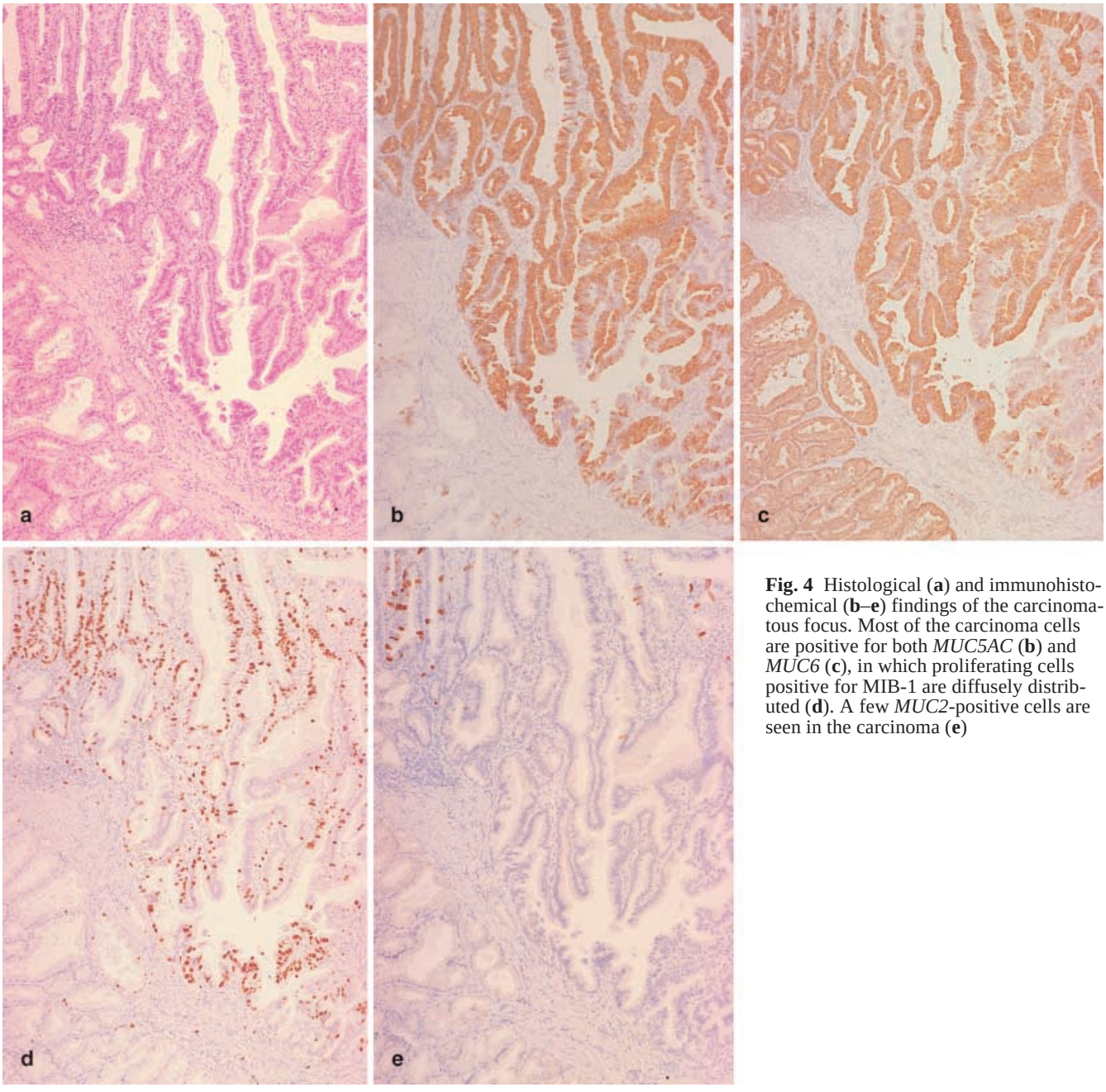

Fig. 4 Histological (**a**) and immunohistochemical (**b**–**e**) findings of the carcinomatous focus. Most of the carcinoma cells are positive for both *MUC5AC* (**b**) and *MUC6* (**c**), in which proliferating cells positive for MIB-1 are diffusely distributed (**d**). A few *MUC2*-positive cells are seen in the carcinoma (**e**)

Discussion

Brunner's glands are mucus-secreting lobular glands ocated in the deep mucosa and submucosa of the duodenum. Mucus-secreting adenocarcinomas in the duodenum with lobular structures are thought to be Brunner's gland carcinomas [4, 22, 23]. However, identifying the exact site of origin of these carcinomas by conventional staining is difficult. Until now four cases of adenocarcinomas have been demonstrated to originate from Brunner's glands with class III mucin staining using concanavalin A, which is specific for Brunner's glands, pyloric glands, and mucus neck cells of the stomach [5, 8, 9, 16]. Class III mucin is thought to be the product of the *MUC6* gene [10]. The site of origin of the present carcinoma is also thought to be Brunner's glands due to the localization and *MUC6* reactivity.

Moreover, *MUC5AC* of the gastric-foveolar type was extensively expressed in the present carcinoma, which can be diagnosed as adenocarcinoma of the exclusively gastric phenotype by our recently proposed criteria [25]. Kawamoto et al. [9] has also demonstrated differentiation to gastric-foveolar cells in a case of Brunner's gland carcinoma, using the galactose oxidase-cold thionin Schiff method.

However, proliferation and gastric-foveolar differentiation of the Brunner's glands are not fully understood. Some experimental studies suggest that Brunner's gland cells, which are widely believed to be functioning mature cells, can easily be stimulated to divide and proliferate [6, 7]. We recently demonstrated a histogenetic pathway of gastric metaplasia in close association with a reparative lineage of Brunner's glands following duodenal ulcer [12]. The generative cell zone newly established in Brunner's glands (neo-G zone) next to the ulcerated surface produces gastric foveolar-type cells positive for human gastric mucin (M1) [12], which is encoded by the *MUC5AC* gene [2]. It is thus suggested that enhanced proliferation activity within the lobules seem to have important role on the development of hyperplasia with gastric-foveolar metaplasia as shown in erosive condition.

In summary, we report a case of gastric-type adenocarcinoma arising in Brunner's glands, which provides important information about the proliferation and differentiation of Brunner's glands. The present carcinoma very likely developed in the neo-G zone of hyperplastic Brunner's glands under induction of gastric-foveolar differentiation. In addition, a few intestinal-type cells positive for *MUC2* were scattered in the carcinoma; indicating that such a kind of intestinal metaplasia occurred in the carcinoma as has been demonstrated in progressing gastric-type carcinomas of the stomach [1, 11].

References

1. Bamba M, Sugihara H, Kushima R, Okada K, Tsukashita S, Horinouchi M, Hattori T (2001) Time-dependent expression of intestinal phenotype in signet ring cell carcinomas of the human stomach. Virchows Arch 438:49–56
2. Bara J, Chastre E, Mahiou J, Singh RL, Forgue-Lafitte ME, Hollande E, Godeau F (1998) Gastric M1 mucin, an early oncofetal marker of colon carcinogenesis, is encoded by the MUC5AC gene. Int J Cancer 75:767–773
3. De Vita O, Bondi A, Euse-Bi V, Bordi C (1984) Simultaneous polypoid tumors of the stomach and duodenum with composite cell population (mucous, argyrophil, and lysozyme-containing cells): a case report. Am J Gastroenterol 79:606–610
4. Dixon CF, Lichtman AL, Weber HM, McDonald JR (1946) Malignant lesions of the duodenum. Surg Gynec Obstet 83:83–93
5. Dorandeu A, Raoul JL, Landemore G, Rioux-Leclercq N, Loget P, Taouji S, Launois B, Martin E, Ramee MP (1995) Adenocarcinoma of Brunner's glands: an entity exceptionally described (in French). Report of a case. Ann Pathol 15:211–215
6. Florey HW, Harding HE (1935) The healing of artificial defects of the duodenal mucosa. J Pathol Bacteriol 40:211–218
7. Fuse Y, Tsuchihashi Y, Sugihara H, Kodama T, Takino T, Fujita S (1988) Autoradiographic study on healing process of cysteamine-induced duodenal ulcer in rat. Possible importance of Brunner's glands in ulcer healing. Dig Dis Sci 33:1081–1088
8. Itsuno M, Makiyama K, Omagari K, Tanaka T, Hara K, Tsuda N, Ajioka Y, Watanabe H (1993) Carcinoma of duodenal bulb arising from the Brunner's gland. Gastroenterol Jpn 28:118–125
9. Kawamoto K, Motooka M, Hirata N, Masuda K, Ueyama T, Yasukouchi A, Iwashita A, Matsuzawa K, Katsuyama T (1994) Early primary carcinoma of the duodenal bulb arising from Brunner's glands. Gastrointest Endosc 40:233–236
10. Krause WJ (2000) Brunner's glands: a structural, histochemical and pathological profile. Prog Histochem Cytochem 35:259–367
11. Kushima R, Jancic S, Hattori T (1993) Association between expression of sialosyl-Tn antigen and intestinalization of gastric carcinomas. Int J Cancer 55:904–908
12. Kushima R, Manabe R, Hattori T, Borchard F (1999) Histogenesis of gastric foveolar metaplasia following duodenal ulcer: a definite reparative lineage of Brunner's gland. Histopathology 35:38–43
13. Kushima R, Ruthlein HJ, Stolte M, Bamba M, Hattori T, Borchard F (1999) 'Pyloric gland-type adenoma' arising in heterotopic gastric mucosa of the duodenum, with dysplastic progression of the gastric type. Virchows Arch 435:452–457
14. Lesuffleur T, Zweibaum A, Real FX (1994) Mucins in normal and neoplastic human gastrointestinal tissues. Crit Rev Oncol Hematol 17:153–180
15. McIntosh GG, Lodge AJ, Watson P, Hall AG, Wood K, Anderson JJ, Angus B, Horne CH, Milton ID (1999) NCL-CD10–270: a new monoclonal antibody recognizing CD10 in paraffin-embedded tissue. Am J Pathol 154:77–82
16. Miyamoto T, Matsuba S, Yokoyama Y, Ito M, Takeuchi T, Sugimura M, Nakamura T, Tatematsu M (1991) Early duodenal cancer supposedly arising from the Brunner's gland, report of case (in Japanese). Stomach Intestine 26:1395–1399
17. Reis CA, David L, Correa P, Carneiro F, de Bolos C, Garcia E, Mandel U, Clausen H, Sobrinho-Simoes M (1999) Intestinal metaplasia of human stomach displays distinct patterns of mucin (MUC1, MUC2, MUC5AC, and MUC6) expression. Cancer Res 59:1003–1007
18. Rotterdam H, Shehan DG, Sommers S (1993) Biopsy diagnosis of the digestive tract, 2nd edn. Raven, New York
19. Russin V, Krevsky B, Caroline DF, Tang CK, Ming SC (1986) Mixed hyperplastic and adenomatous polyp arising from ectopic gastric mucosa of the duodenum. Arch Pathol Lab Med 110:556–558
20. Schlemper RJ, Riddell RH, Kato Y, Borchard F, Cooper HS, Dawsey SM, Dixon MF, Fenoglio-Preiser CM, Flejou JF, Geboes K, Hattori T, Hirota T, Itabashi M, Iwafuchi M, Iwashita A, Kim YI, Kirchner T, Klimpfinger M, Koike M, Lauwers GY, Lewin KJ, Oberhuber G, Offner F, Price AB, Rubio CA, Shimizu M, Shimoda T, Sipponen P, Solcia E, Stolte M, Watanabe H, Yamabe H (2000) The Vienna classification of gastrointestinal epithelial neoplasia. Gut 47:251–255
21. Shimizu N, Tanaka S, Morikawa J, Yorioka S, Fukuda S, Yamashita S, Bamba M, Hattori T, Hosoda S (1989) Early duodenal cancer of the bulb-report of a case (in Japanese). Gan No Rinsho 35:100–106
22. Shorrock K, Haldane JS, Kersham MJ, Leach RD (1986) Obstructive jaundice secondary to carcinoma arising in Brunner's glands. J R Soc Med 79:173–174
23. Stewart HL Lieber MM (1937) Carcinoma of the suprapapillary portion of the duodenum. Arch Surg 35:99–129
24. Strutynsky N, Posniak R, Mori K (1982) Obstructing hamartoma of Brunner's glands of the duodenum. Dig Dis Sci 27:279–282
25. Tsukashita S, Kushima R, Masamichi B, Sugihara H, Hattori T (2001) MUC gene expression and histogenesis of adenocarcinoma of the stomach. Int J Cancer 94:166–170
26. Williams SJ, McGuckin MA, Gotley DC, Eyre HJ, Sutherland GR, Antalis TM (1999) Two novel mucin genes down-regulated in colorectal cancer identified by differential display. Cancer Res 59:4083–4089
27. Williams SJ, Wreschner DH, Tran M, Eyre HJ, Sutherland GR, McGuckin MA (2001) Muc13, a novel human cell surface mucin expressed by epithelial and hemopoietic cells. J Biol Chem 276:18327–18336
28. Yin BW, Lloyd KO (2001) Molecular cloning of the CA125 ovarian cancer antigen: identification as a new mucin, MUC16. J Biol Chem 276:27371–27375
29. Zanetti G, Casadei G (1981) Brunner's gland hamartoma with incipient ductal malignancy. Report of a case. Tumori 67:75–78